Durham University

Durham E-Theses

Investigating the mode of action and antileishmanial activity of 5-nitrothiophene-2-carboxamides

VANESSA JANE LYNE

How to cite:

LYNE, VANESSA JANE (2022) Investigating the mode of action and antileishmanial activity of 5-nitrothiophene-2-carboxamides. Doctoral thesis, Durham University.

Use policy

The full-text may be used and/or reproduced, and given to third parties in any format or medium, without prior permission or charge, for personal research or study, educational, or not-for-profit purposes provided that:

- a full bibliographic reference is made to the original source
- a https://etheses.durham.ac.uk/id/eprint/14323/ is made to the metadata record in Durham E-Theses
- the full-text is not changed in any way

The full-text must not be sold in any format or medium without the formal permission of the copyright holders.

Please consult the full Durham E-Theses policy for further details.

Academic Support Office, The Palatine Centre, Durham University, Stockton Road, Durham, DH1 3LE
e-mail: e-theses.admin@durham.ac.uk Tel: +44 0191 334 6107
https://etheses.durham.ac.uk

Investigating the mode of action and antileishmanial activity of 5-nitrothiophene-2-carboxamides

A thesis submitted in partial fulfilment of the requirements for the degree of Doctor of Philosophy in Chemical Biology from Durham University by

Vanessa Jane Lyne
December 2021
Department of Chemistry

Supervisors:
Professor Patrick G. Steel (Durham University)
Professor Paul W. Denny (Durham University)
Dr Andy Merritt (LifeArc)

Abstract

Two hit 5-nitrothiophene-2-carboxamides (5N2Cs), **16** and **17**, were identified in a high-throughput screen (HTS) of 1.8 million compounds from GlaxoSmithKline (GSK) that showed promising antileishmanial activity.[1] However, poor aqueous solubility and bioavailability limited their potential. A structure-activity relationship (SAR) campaign was carried out to optimise antileishmanial activity, reduce mammalian cell toxicity and improve aqueous solubility. The 5N2C functionality was found to be important for antileishmanial activity, however the right hand amino thiophene PAINS motif could be exchanged for an anthranilamide (**140** and **141**) with no loss of activity. Furthermore, introduction of a basic nitrogen in the form of a morpholine ring gave lead compounds **252** and **253**, with significantly improved aqueous solubility compared to the hits and retained potent antileishmanial activity and selectivity over HepG2 cells.

The 5N2C series are bioactivated by a type I nitroreductase in *Leishmania* (*Lmj*NTR1) to give two major metabolites: M+2 and 2M-98, where M is the mass of the parent nitro. The M+2 metabolite is proposed to be the 4,5-dihydrothiophene (**307a**), formed by direct reduction on the aromatic ring. The 2M-98 metabolite is proposed to be the thieno[2,3-*b*]pyridyl species (**309a**), formed by reaction of the postulated hydroxylamine (**311**) and α,β-unsaturated open chain nitrile (**312**) metabolites. The 2M-98 metabolite is an end point of bioactivation that results in detoxification of the transient electrophilic α,β-unsaturated open chain nitrile (**312**) intermediate.

Mitochondrial damage and ROS accumulation are both observed upon 5N2C treatment of *L. major* promastigotes. Moreover, the synthesis of probe **251**, based off the 5N2C scaffold, revealed that multiple protein targets are covalently modified upon *in cellulo* bioactivation. iTRAQ proteomics confirmed that most proteins affected are ribosomal proteins involved in translation. Crucially, this suggests that disruption of protein translation is one of the major modes of action for the 5N2C series.

Acknowledgements

I would like to firstly thank the multitude of collaborators that helped with this project. Thanks to Dr James Morris at Clemson University for the assaying of compounds against *T. brucei*. I would also like to thank Dr Susan Wyllie and Dr Juliana Pacheco at the University of Dundee for the testing of compounds against *L. donovani* promastigotes including wild type and overexpressing NTR1 and NTR2 lines. Without this initial work, I would not have known that nitroreductase was an important mode of bioactivation for the 5N2C series. Thanks to Professor Guillermo Labadie at the National University of Rosario for his ongoing testing against *T. cruzi* and Professor Nahid Ali at the CSIR-Indian Institute of Chemical Biology for her ongoing *L. donovani* intramacrophage testing. I would also like to thank Professor Ashwini Nangia at the University of Hyderabad and Dr Michael Hall at Newcastle University for their work in obtaining crystal structures for difficult samples. Thanks to Dr Exequiel Porta for your initial probe experiments and help with the 2M-98 metabolite identification. Further thanks go to Dr Kalesh Karunakaran at Durham University for the iTRAQ™ proteomics work and gene ontological analysis.

Thanks to the analytical services at Durham University for their help and assistance over the course of my PhD. Special thanks go to Dr Jackie Mosely and Mr Peter Stokes for their help with the mass spectrometry analysis of metabolites, Dr Juan Aguilar Malavia for his assistance with the NMR experiments for the 2M-98 metabolite, Dr Dmitri Yufit for analysing my X-ray crystallography samples, Mrs Christine Richardson for transmission electron microscopy sample preparation and imaging, and Dr Mark Fox for his assistance and training in cyclic voltammetry.

Thanks to my funding body, the Medical Research Council, for their financial support, without which this work would not have been possible. Thanks to my primary supervisor Professor Patrick Steel for his unwavering support and guidance throughout the 4 years of my PhD. You let me run with the project and take it in lots of different directions that weren't originally planned, which gave me the opportunity to explore so many amazing areas of science. Thanks for the ideas and

for pushing me to achieve my full potential. Further thanks go to my other supervisors Dr Paul Denny, who helped set me up in the world of parasitology and microbiology, and Dr Andy Merritt, who gave me amazing ideas and interesting discussions as well as an important industrial insight.

Thanks to Daniel Bruce, your love and support kept me grounded and I wouldn't be where I am today without your help both in the lab and at home. Big thanks also go to my family, in particular my parents who reminded me to take breaks and looked after me from afar.

Final thanks go to current and past members of the Steel group, who I bounced countless ideas off and who brightened up my days. Thanks to Dr Exe Porta for your amazing ideas and help over the years, for knowing the answer to every question I ever asked and for always making time for me in your busy schedule. Special thanks go to Michaela Buerdsell, Dr Rebecca Charlton, Dr Courtney Covington, Victor Agostino and Dr Kath Norman; you all kept me sane and well caffeinated throughout! Thanks to you all for your friendship and support, as well as your (hopefully) awesome proofreading abilities!

Declaration

The work in this thesis was carried out by the author in the Department of Chemistry at Durham University between October 2017 and December 2021, except for work carried out by collaborators who are acknowledged below and where relevant in the text. No part of this work has been submitted for any other degree at this or another university.

Collaborator contributions:

Microsomes enriched in *Lmj*IPCS were provided by Dr John Mina, Durham University. DMPK studies were carried out by LifeArc in collaboration with GVK BIO Sciences Pvt Ltd Hyderabad, India. Crystals and crystal structure of compound **17** were obtained by Dr Ashwini Nangia at the University of Hyderabad, India. Crystals and crystal structure of compound **206** were obtained by Dr Ronnie Ragbirsingh and Dr Michael Hall, Newcastle University. Antipromastigote toxicity assays against *Leishmania donovani* overexpressing NTR1, NTR2 and wild type were carried out by Dr Susan Wyllie and Dr Juliana Pacheco at the University of Dundee. *T. brucei* dose-response studies were carried out by Professor Jim Morris, Clemson (SC). pTrcHis*Lmj*NTR1 plasmids were supplied by Dr Shane Wilkinson, QMUL. Wiley ^{13}C NMR Data Checker analysis and preliminary whole cell probe experiments were carried out by Dr Exequiel Porta, Durham University. LeishBox 5N2C compounds were donated by Dr Silvia Gonzalez, GSK Tres Cantos. Probe-protein sample pulldown, iTRAQ proteomics, data interpretation and gene ontological analysis were carried out by Dr Kalesh Karunakaran-Nair-Ana, Durham University. TEM sample post fixation, resin embedding and TEM imaging was carried out by Dr Christine Richardson, Durham University.

Statement of Copyright

The copyright of this thesis rests with the author. No quotation from it should be published without the author's prior written consent and information derived from it should be acknowledged.

Table of Contents

Abstract……i

Acknowledgements……ii

Declaration……iv

Statement of Copyright……v

Table of Contents……vi

List of Abbreviations……xiii

1. Resynthesis and validation of hit 5N2Cs

1.1 Introduction 1

1.11 Project overview 1

1.12 Leishmaniasis 1

1.12.1 *Leishmania* parasitology 4

1.12.2 Treatments for Leishmaniasis 6

1.12.3 Ideal drug candidate profile 8

1.2 Previous work 10

1.21 IPCS as a drug target 10

1.22 High throughput screen to identify inhibitors of *Lmj*IPCS 12

1.3 Initial project aims 17

1.4 Results and discussion 18

1.41 Resynthesis and antileishmanial activity of original hits **16** and **17** 18

1.42 Investigation of IPCS activity for hits **16** and **17** 22

1.43 DMPK studies for hits **16** and **17** 26

1.5 Summary 28

2. Identification of 5N2C lead antileishmanial compounds

2.1 Introduction 29

2.11 Drugs to treat trypanosomatid diseases 29

2.12 Drug discovery for leishmaniasis – LeishBox 30

2.13 Nitro drugs 32

2.13.1 5-Nitrothiophenes 34

2.13.1.1 5-Nitrothiophenes reaching clinical trials 34

2.13.1.2 5-Nitrothiophenes to treat trypanosomatid disease 34

2.13.2 5-Nitrothiophene-2-carboxamides (5N2Cs) 39

2.13.2.1 5N2Cs to treat wider diseases 39
2.13.2.2 5N2Cs to treat trypanosomatid disease 40
2.14 Toxicity issues 42
2.14.1 Nitro group 42
2.14.2 Thiophene 43
2.14.3 2-Aminothiophene 43
2.2 Revised project aims 45
2.3 Results and discussion 46
2.31 Removing areas of toxicity concerns 46
2.31.1 Removing the 5-nitrothiophene group 46
2.31.1.1 Removing the nitro group 46
2.31.1.2 Replacing the nitrothiophene ring 48
2.31.1.3 Conclusions 50
2.31.2 Removal of the 2-aminothiophene PAINS motif 53
2.31.2.1 Cyclopentane series 53
2.31.2.2 Phenyl series 56
2.31.2.3 Conclusions 58
2.32 Exploring right-hand ring substituents 60
2.32.1 C-2 pendant substituents on right-hand phenyl ring 60
2.32.1.1 Conclusions 65
2.32.2 Additional substituents on right-hand phenyl ring 65
2.32.2.1 Conclusions 68
2.32.3 Conclusions 69
2.33 Improving aqueous solubility 71
2.33.1 Aqueous solubility in FBS supplemented PBS and biorelevant media 72
2.33.2 Investigating structural changes to improve aqueous solubility (generation 2) 76
2.33.2.1 Changing the central amide to improve aqueous solubility 78
2.33.2.2 Exploiting the 5-position to improve aqueous solubility 84
2.34 Broad spectrum antileishmanial activity 100
2.35 Antitrypanosomatid activity 104
2.4 Summary 105

3. Mode of action of 5N2C series

3.1 Introduction 107
3.11 Mode of action of antitrypanosomatid nitro drugs 107
3.11.1 Nifurtimox (**37**) 107

3.11.2 Benznidazole (**38**) 107
3.11.3 Fexinidazole (**39**) 108
3.12 Nitroreductase 108
3.12.1 NTR1 bioactivation of anti-trypanosomatid drugs 111
3.12.2 NTR2 bioactivation of antileishmanial compounds 114
3.12.3 5-Nitrothiophene bioactivation by NTRs 115
3.2 Aims 117
3.3 Results and Discussion 118
3.31 Bioactivation by nitroreductase 118
3.31.1 Reduction potential of the 5N2C series 119
3.31.1.1 Discussion 136
3.31.1.2 Conclusion 136
3.31.2 *Ldon*NTR1/NTR2 overexpressor model 138
3.31.3 Expression and purification of *Lmj*NTR1 144
3.31.3.1 Thermal shift assay using Durham Screens 147
3.31.4 Attempted purification of *Ldon*NTR1 151
3.31.4.1 Generation of pTrcHis*Ldon*NTR1 152
3.31.4.2 Attempted purification of *Ldon*NTR1 from T7.pTrcHis*Ldon*NTR1 153
3.31.5 *Lmj*NTR1 kinetics of 5N2C reduction 156
3.31.5.1 Discussion 161
3.31.5.2 Conclusion 163
3.31.6 Metabolomics of *Lmj*NTR1 bioactivation 164
3.31.6.1 Assay standardisation using nifurtimox (**37**) 164
3.31.6.2 5N2C series 167
3.31.6.3 Discussion 197
3.31.7 GSK LeishBox 5N2C reduction by *Lmj*NTR1 199
3.31.7.1 2M-98 metabolite is observed for 14 out of 15 LeishBox compounds 201
3.31.7.2 2M-14 metabolite is observed for 9 LeishBox 5N2Cs 203
3.31.7.3 All LeishBox 5N2Cs form M+2 metabolite after *Lmj*NTR1 bioactivation 204
3.31.7.4 Discussion 206
3.31.8 Probe design and synthesis 209
3.31.8.1 Preliminary *in cellulo* and *in vitro* experiments 210
3.31.8.2 Experiment optimisation 212
3.31.8.3 Reproducibility 214
3.31.8.4 Competition experiments 215
3.31.8.5 Probe studies against 3 *Leishmania* species 222

3.31.8.6 Conclusions 223
3.31.9 Proteomics 224
3.32 Global mode of action studies 232
3.32.1 Mitochondrial dysfunction 232
3.32.2 ROS accumulation 234
3.32.3 Transmission electron microscopy 237

4. Discussion 243

5. Future work

5.11 Chemistry future work 248
5.11.1 Scale up of lead compound **252** and **253** 248
5.11.2 Synthesis of alternative analogues 249
5.11.2.1 4,5-Disubstituted analogue **334** 249
5.11.2.2 Varying the nature of the morpholine group to reduce toxicity 251
5.12 Biological future work 252
5.12.1 5N2Cs to treat further trypanosomatid diseases 252
5.12.2 Progression of lead compounds **252** and **253** as new antileishmanial drugs 253
5.12.3 Mode of action of 5N2Cs 254
5.12.3.1 Disruption of translation 254
5.12.3.2 Cytocidal vs cytostatic nature of 5N2C treatment 254
5.12.3.3 DNA damage 255
5.12.3.4 Reduction in free thiols 255
5.12.3.5 Autophagy 256

6. Experimental

6.1 Chemistry experimental 257
6.11 Materials and methods 257
6.12 General procedures 259
6.13 Synthetic procedures 261
6.14 Biocatalysis 339
6.15 X-ray crystallography 340
6.2 Biological experimental 341
6.21 Reagents and equipment 341
6.21.1 General reagents 341
6.21.1.1 Chemicals 342
6.21.1.2 Genes and Primers 342

6.21.2 General equipment 342
6.21.3 Cell lines 343
6.21.4 Buffers and media 343
6.21.5 SDS-PAGE 346
6.22 Biological procedures 347
6.22.1 Cell culture and assays 347
6.22.1.1 *Leishmania* promastigote cell culture 347
6.22.1.2 HepG2 cell culture 347
6.22.1.3 Dose response assays 348
6.22.2 *Lmj*IPCS enriched microsome assays 350
6.22.2.1 HPTLC assay 350
6.22.2.2 96-Well filter plate assay 351
6.22.3 DMPK studies 352
6.22.4 Protein purification and biochemistry 352
6.22.4.1 Purification of *Lmj*NTR1 352
6.22.4.2 Subcloning of pTrcHis*Ldon*NTR1 354
6.22.4.3 Thermal shift assay 355
6.22.4.4 *Lmj*NTR1 kinetics of bioactivation 356
6.22.4.5 *Lmj*NTR1 metabolomics 356
6.22.5 Probe studies 357
6.22.5.1 Lysate generation 357
6.22.5.2 Fluorescence probe experiments 358
6.22.6 Proteomics 359
6.22.6.1 Sample preparation 359
6.22.6.2 iTRAQ proteomics 360
6.22.6.3 Gene Ontology analysis 362
6.22.7 Whole cell mode of action 362
6.22.7.1 Mitochondrial dysfunction (JC-1) 362
6.22.7.2 ROS accumulation (H2DCFDA) 363
6.22.7.3 Transmission electron microscopy 364
6.3 Physicochemical experimental 365
6.31 Materials and methods 365
6.32 Procedures 365
6.32.1 Kinetic solubility 365
6.32.2 Cyclic voltammetry 365

7. References……367

8. Appendices

8.1 Appendix 1: Biological data table……380

8.2 Appendix 2: DNA sequencing of *Lmj*NTR1 and *Ldon*NTR1……384

8.3 Appendix 3: Protein digest MS (*Lmj*NTR1 two bands)……386

8.4 Appendix 4: Proteomics results output……388

8.5 Appendix 5: NMR data for 2M-98 metabolite……393

8.6 Appendix 6: NMR spectra……396

8.7 Appendix 7: Electronic supplementary information……524

List of Abbreviations

5N2C	5-nitrothiophene-2-carboxamide
ALDH2	Aldehyde dehydrogenase
AM	Amastigote
Ar	Aromatic
ASAP	Atmospheric solids analysis probe
ATP	Adenosine triphosphate
ATR	Attenuated total reflection
BCA	Bicinchoninic acid
BL21(+)	*E. coli* BL21-CodonPlus DE3-RIPL
br	Broad
BSA	Bovine serum albumin
CC_{50}	Half maximal cytotoxic concentration
CCCP	Carbonyl cyanide 3-chlorophenylhydrazone
CHAPS	3-[(3-cholamidopropyl)dimethylammonio]-1-propanesulfonate
CL	Cutaneous leishmaniasis
CMW	Chloroform methanol water
CoA	Coenzyme A
Conc	Concentration
COSY	Correlated spectroscopy
d	Doublet
Da	Dalton
DAG	Diacylglycerol
DCF	Dichlorofluorescein
DCM	Dichloromethane
DMEM	Dulbecco's Modified Eagle Medium
DMF	Dimethylformamide
DMPK	Drug metabolism and pharmacokinetics
DMSO	Dimethylsulfoxide

DNDi	Drugs for Neglected Diseases initiative
E^0	Reduction potential
EC_{50}	Half maximal effective concentration
EDTA	Ethylenediaminetetraacetic acid
Enz	Enzyme
E_{pa}	Peak anode potential
E_{pc}	Peak cathode potential
ER	Endoplasmic reticulum
ESI	Electrospray ionisation
EWG	Electron withdrawing group
FAD	Flavin adenine dinucleotide
FASSGF	Simulated gastrointestinal fluid upon fasting
FASSIF	Simulated intestinal fluid upon fasting
FBS	Fetal bovine serum
FESSIF	Simulated intestinal fluid upon feeding
FMN	Flavin mononucleotide
FT-IR	Fourier-transform infrared spectroscopy
GCMS	Gas chromatography mass spectrometry
GenPurp	General purpose
GFP	Green fluorescent protein
GO	Gene Ontology
GSK	GlaxoSmithKline
H2DCFDA	2',7'-dichlorodihydrofluorescein diacetate
HBSS	Hank's balanced salt solution
HMBC	Heteronuclear Multiple Bond Correlation
HPLC	High-performance liquid chromatography
HPTLC	High performance thin-layer chromatography
hr	Hour
HRMS	High resolution mass spectrometry
HTS	High throughput screen
I_a	Current at peak anode potential

I_c	Current at peak cathode potential
IC_{50}	Half maximal inhibitory concentration
InMac	Intramacrophage
IP	Intraperitoneal
IP	Immunoprecipitation
IPC	Inositol phosphorylceramide
IPCS	Inositol phosphoryl ceramide synthase
iTRAQ	Isobaric Tag for Relative and Absolute Quantitation
IV	Intravenous
J	Coupling constant
k_{obs}	Observed rate constant
LC-MS	Liquid chromatography mass spectroscopy
M	Mass of parent nitro
m	Multiplet
m/z	Mass to charge ratio
MAC	Macrophage
MCL	Mucocutaneous leishmaniasis
min	Minute
MS/MS	Tandem mass spectrometry
MWI	Microwave irradiation
NADH	Nicotinamide adenine dinucleotide
NADPH	Nicotinamide adenine dinucleotide phosphate
NBD	Nitrobenzoxadiazole
ND	Not determined
NHE	Normal hydrogen electrode
Ni-NTA	Nickel nitrilotriacetic acid
NMR	Nuclear magnetic resonance
NOESY	Nuclear Overhauser Effect Spectroscopy
NTD	Neglected tropical disease
NTR	Nitroreductase
O.E.	Overexpressing cell line

PAINS	Pan-assay interference compounds
PBS	Phosphate buffered saline
PCR	Polymerase chain reaction
PDB	Protein Data Bank
pEC_{50}	$-\log_{(10)}(EC_{50})$
PEG	Polyethylene glycol
PenStrep	Penicillin-streptomycin
PES	Polyethersulfone
PI	Phosphatidyl inositol
PKDL	Post-kala-azar dermal leishmaniasis
q	Quartet
RFU	Relative fluorescence units
Rh-N_3	Rhodamine azide
ROS	Reactive oxygen species
R_t	Retention time
RT	Room temperature
s	Singlet
SAR	Structure activity relationship
SDS	Sodium dodecyl sulfate
SDS-PAGE	Sodium dodecyl sulfate- polyacrylamide gel electrophoresis
SEC	Size exclusion chromatography
SILAC	Stable Isotope Labelling of Amino acids in Culture
SPT	Serine palmitoyl transferase
t	Triplet
T7	T7 Express Competent *E. coli*
TAMRA	5-Carboxytetramethylrhodamine
TBTA	Tris(benzyltriazolylmethyl)amine
TCEP	Tris(2-carboxyethyl)phosphine
TEAB	Triethylammonium bicarbonate
TEM	Transmission electron microscopy

THF	Tetrahydrofuran
TLC	Thin layer chromatography
T_m	Melt temperature
TSA	Thermal shift assay
TUNEL	Terminal deoxynucleotidyl transferase dUTP nick-end labelling
UPLC	Ultra-performance liquid chromatography
UV-Vis	Ultraviolet-visible
VL	Visceral leishmaniasis
w	Weak
WHO	World Health Organisation
WT	Wild type

1 Resynthesis and validation of hit 5N2Cs

1.1 Introduction

1.11 Project overview

The work presented in this thesis aims to explore 5-nitrothiophene-2-carboxamides (5N2C) as potential new antileishmanial compounds. Previous work by Denny *et al.* identified inositol phosphorylceramide synthase (IPCS) as a promising drug target due to its lack of mammalian orthologue and important role in sphingolipid biosynthesis in *Leishmania*.[2] Following the discovery of IPCS, Norcliffe *et al.* identified two 5N2Cs from a high-throughput screen of 1.8 million compounds aiming to identify inhibitors of IPCS.[1] Throughout this work, the biological activity and mode of action of these 5N2Cs and a range of analogues will be assessed to identify new potent and selective lead antileishmanial compounds.

This thesis is subdivided into three main chapters. Chapter 1 describes the resynthesis of the original hit structures and validation of the results from the HTS. Chapter 2 explores a variety of different analogues to explore the structure-activity relationship (SAR) of the hits and identify potent new lead antileishmanial compounds with improved physicochemical properties and low mammalian cytotoxicity. Chapter 3 discusses the mode of action of the synthesised 5N2C library by investigating nitroreductase bioactivation.

1.12 Leishmaniasis

Leishmaniasis is a neglected tropical disease (NTD) with an estimated 700,000-1 million new cases occurring annually.[3] It is endemic across 98 countries, spanning Africa, Asia, the Middle East, India and the Mediterranean (Old World) and central and south America (New World).[4] There are four main clinical manifestations of the disease: visceral leishmaniasis (VL), cutaneous leishmaniasis (CL), mucocutaneous leishmaniasis (MCL) and post-kala-azar dermal leishmaniasis (PKDL). PKDL and MCL

occur as complications of VL and CL respectively.[3,5] CL is the most common disease manifestation whereas VL is almost always fatal if left untreated.[3] Leishmaniasis is a trypanosomatid disease caused by over 20 species of *Leishmania* parasite, which vary according to geographical location and cause different disease manifestations. The global endemicity of CL and VL is represented in Figure 1.12-1.

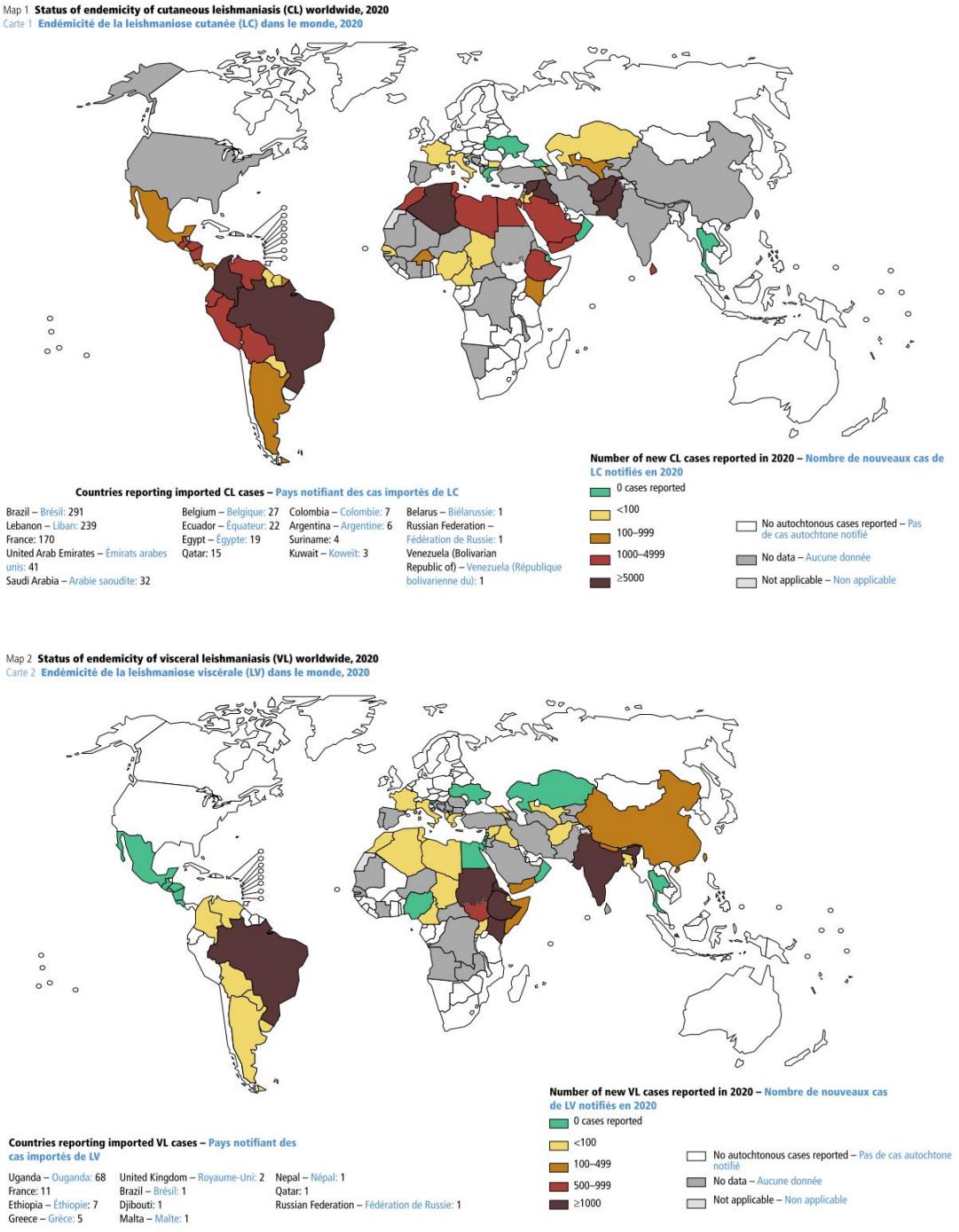

Figure 1.12-1 Global endemicity of cutaneous leishmaniasis (above) and visceral leishmaniasis (below). Figure obtained from WHO, 2021.[4]

1.12.1 *Leishmania* parasitology

Kinetoplastids, such as *Leishmania*, are flagellated unicellular eukaryotes with many unique features compared to most other eukaryotic cells (Figure 1.12-2B-C).[6] Firstly, they have a single extended mitochondrion along the length of the parasite which connects to the kinetoplast; a unique organelle containing interlocked circular DNA called kinetoplast DNA. Kinetoplastids also contain glycosomes, which are absent in mammalian cells. Glycosomes are believed to have evolved from peroxisomes and are the site of glycolysis and purine salvage in the cell.[7,8]

Leishmania exist in two morphological forms: promastigote and amastigote.[9] The promastigote form is injected into the host from the bite of an infected female phlebotomine sandfly during a blood meal. Phagocytosis of the *Leishmania* promastigote by host macrophages enables the transformation from the promastigote to the amastigote. Rapid division of the amastigotes within infected cells eventually leads to cell lysis, which releases the amastigotes into the bloodstream. These amastigotes can now infect other macrophages and also be ingested by an uninfected sandfly during a blood meal to continue the infectious cycle (Figure 1.12-2A).[6]

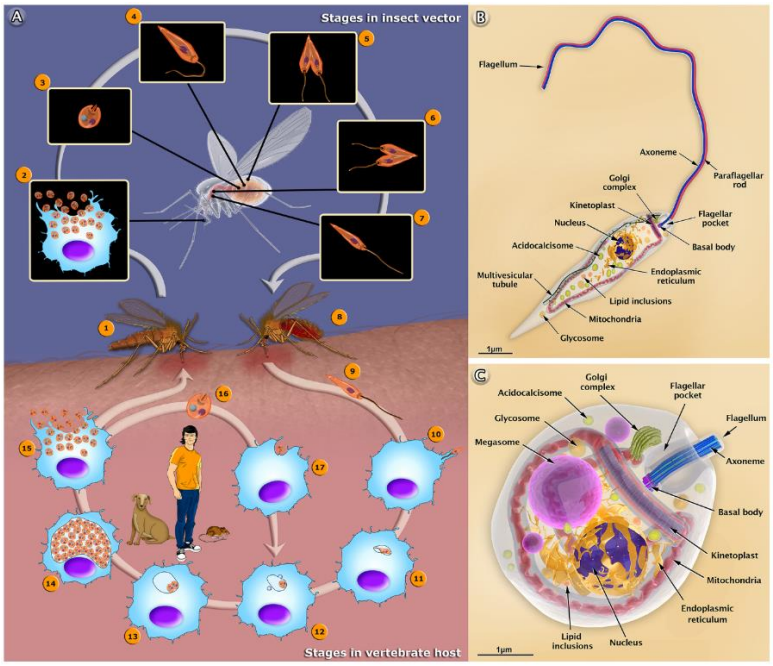

Figure 1.12-2: A lifecycle of the *Leishmania* parasite. B-C Structural organisation of the *Leishmania* parasite as the promastigote (B) and amastigote (C) form. Figure obtained from Teixeira, PLOS, 2013.[6]

1.12.2 Treatments for Leishmaniasis

The landscape of antileishmanial drugs is limited, with only a few examples that provide a cure for patients (Figure 1.12-3). Treatment preferences vary with location and *Leishmania* species and are limited by toxic side effects, cost, and mode of administration. Furthermore, leishmanial resistance to many current drugs makes the search for new therapeutics a necessary area of research to attempt to control the disease.[9]

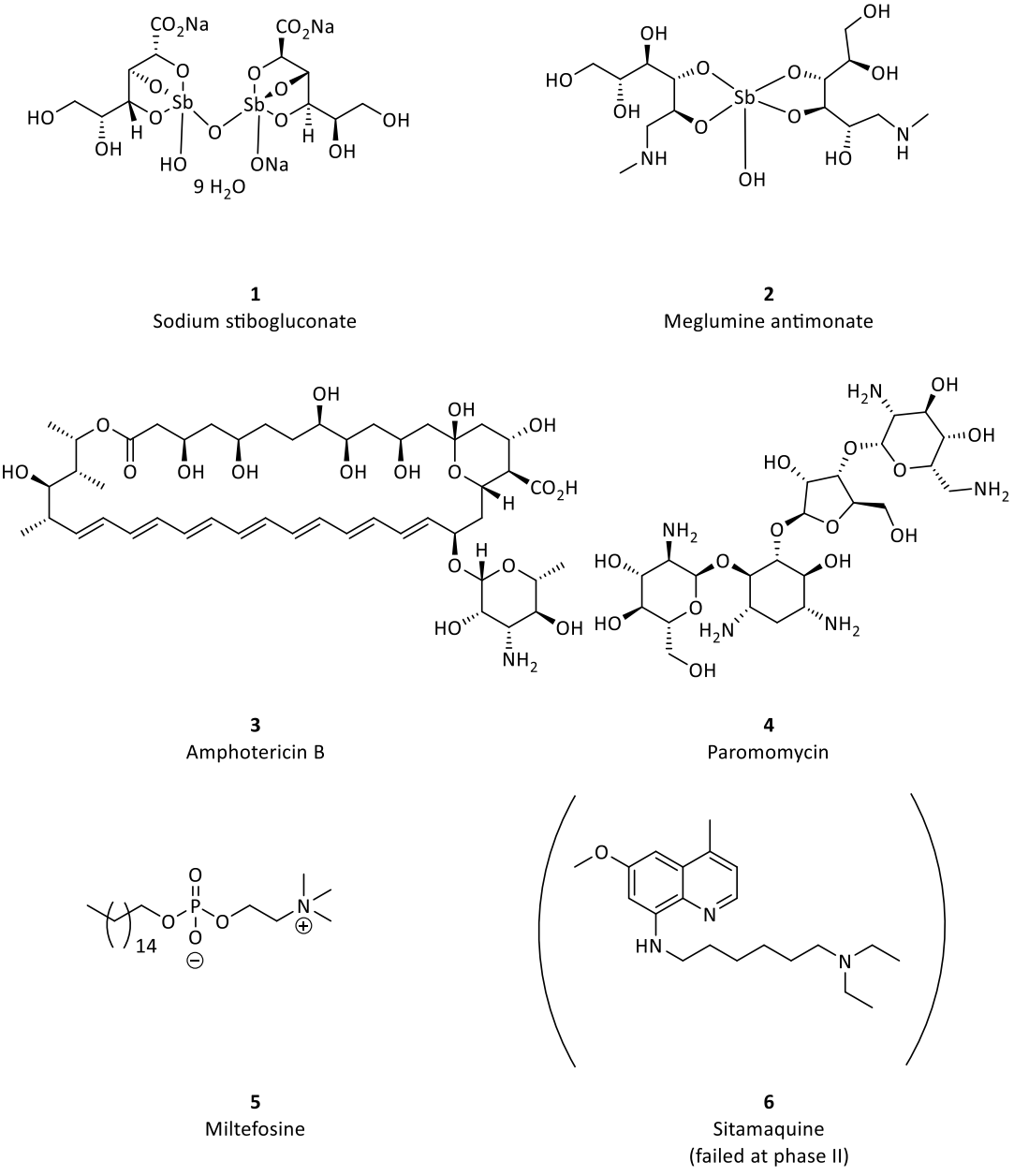

Figure 1.12-3 Common antileishmanial drugs used today. Sitamaquine (**6**) is included as an example of a new potential antileishmanial drug that failed at phase II clinical trials.[10,11]

Pentavalent antimonials (**1** and **2**) were introduced in 1945 to treat leishmaniasis and remain the first line of defence for treating leishmaniasis today. The mechanism of antimonial action against *Leishmania* is unknown, but it is generally accepted that antimonials induce apoptosis-like cell death through oxidative stress and increased levels of intracellular calcium.[12] However, antimonials have a range of limitations which restrict their usage. These include the need for invasive and time-consuming parenteral administration, widespread resistance and significant toxicity issues including patient fatality.[13]

Another parenterally administered drug is amphotericin B (**3**), which has since been formulated into a liposomal formulation to reduce toxicity and enable its use as a safer and more effective drug in areas with widespread antimonial resistance. Amphotericin B (**3**) is thought to increase the permeability of *Leishmania* cell membranes to small molecules by affecting essential membrane sterols.[12] However, high cost, parenteral administration and the emergence of resistance remain an issue. [9]

Alternative treatments include paromomycin (**4**) which is administered intramuscularly for VL or as an ointment for localised CL. This alkaloid drug works by inhibiting protozoan protein synthesis by binding to the 30S ribosomal subunit leading to the misreading of mRNA.[14] Paromomycin (**4**) is cheap, at $15 per adult course, and less invasive than parenterally administered drugs making it an attractive alternative treatment for leishmaniasis.[9]

The only orally available antileishmanial drug currently on the market is miltefosine (**5**). Miltefosine (**5**) is translocated across the parasitic cell membrane by aminophospholipid translocase enzymes, such as *Leishmania* P-type ATPase, resulting in an apoptosis-like cell death.[15,16] Although miltefosine (**5**) has milder side effects and more convenient oral administration, problems with the emergence of resistance remain a concern.

Currently, research is ongoing to find new antileishmanial treatment options. The Drugs for Neglected Diseases initiative (DNDi) is currently investigating four new

antileishmanials at phase I clinical trials for the treatment of VL.[17] Furthermore, sitamaquine (**6**) is an example of a compound that recently reached phase II clinical trials. [11] It is a quinoline derivative that induces oxidative stress and an apoptosis-like cell death by inhibition of succinate dehydrogenase. However, it did not progress to phase III trials due to significant toxicity issues observed in phase II clinical trials.[11]

The case of sitamaquine (**6**) illustrates the challenges facing researchers attempting to develop a new antileishmanial drug. However, the high toxicity, emergence of resistance and difficult parenteral administration issues present for most current antileishmanial drugs reiterates the need for effective new treatments for leishmaniasis. In addition to new treatments, it is important to discover and investigate promising new drug targets to facilitate new drug discovery programmes.

1.12.3 Ideal drug candidate profile

The aim of this work was to develop a new potent, non-toxic and orally available drug for the treatment of leishmaniasis. Antipromastigote activity can be initially used to assess the antileishmanial potency of candidate compounds. Potential lead compounds should have submicromolar antipromastigote activity across multiple species of *Leishmania* and low toxicity (CC_{50} (HepG2) > 10 µM) and high selectivity (S.I. > 30) over human liver cells. One of the major problems with current antileishmanial treatments is their limited oral bioavailability, of which only miltefosine (**5**) is orally available. New lead compounds should show good oral bioavailability, which can be initially assessed by high solubility in aqueous buffer (solubility (PBS) > 10 µM) and biorelevant buffers (solubility (FESSIF/FASSIF/FASSGF) > 30 µM). [18]

Potential new clinical candidates should have equivalent or better activity and toxicity profiles than the current clinical treatments for leishmaniasis. New candidates should have a less than 10-fold potency variation against a panel of clinical isolates and have single micromolar antileishmanial activity against intramacrophage amastigotes (EC_{50} < 5 µM). [18] Furthermore, compounds should have low THP-1 toxicity (CC_{50} > 50 µM and/or S.I. > 10), low genotoxicity and high

microsomal and hepatocyte stability (CL_{int} < 25 µL/min/mg).[19] Candidate compounds should show good bioavailability in a mouse model, where free plasma concentration should be maintained at around 4 times the EC_{50} for at least 4 hours, and animals should show a high tolerance of the drug at and above the recommended dosage (for example at and above 25 mg/kg/day). [19]

For proof of concept, a new treatment should be able to reduce parasite burden in an *in vivo* model by at least 70 % at 25 mg/kg with twice daily dosing for 10 days. However, a promising new clinical candidate should show over 90 % clearance under the same regime, with a comparable *in vivo* ED_{90} to miltefosine (**5**) (ED_{90} 27 mg/kg when dosed once daily). [18]

1.2 Previous work

1.21 IPCS as a drug target

Early work by Denny *et al*. found that sphingolipids were essential for differentiation in *Leishmania*, which confirmed earlier hypotheses by Zhang *et al*.[20,21] Investigation into the sphingolipid biosynthetic pathway of trypanosomatids by Denny *et al.* led to the identification of inositol phosphorylceramide synthase (IPCS) as the final enzyme in the sphingolipid biosynthetic pathway.[2]

The first two steps of the sphingolipid biosynthetic pathway of eukaryotes are shared across plants, fungi, mammals and trypanosomatids. Condensation of cytosolic L-serine (**8**) and palmitoyl CoA (**7**) is achieved using the heterodimeric serine palmitoyl transferase (SPT) to give 3-ketosphinganine. Both subunits of SPT (LCB1 and LCB2) are required for catalytic activity.[22] Subsequent reduction by 3-ketosphinganine reductase gives dihydrosphingosine (**9**). A divergence between plants and fungi, and mammals and trypanosomatids then occurs, resulting in ceramide (**10**, animals and trypanosomatids) or phytoceramide (plants and fungi) formation within the endoplasmic reticulum (ER). Ceramide (**10**) is then transported to the Golgi apparatus to be converted to sphingomyelin (**13**), using sphingomyelin synthase in mammals, or inositol phosphorylceramide (IPC, **14**), using IPCS in trypanosomatids such as *Leishmania* (Figure 1.21-1).[2,23] Similarly, plants and fungi convert phytoceramide to IPC using a plant or fungal orthologue of IPCS.

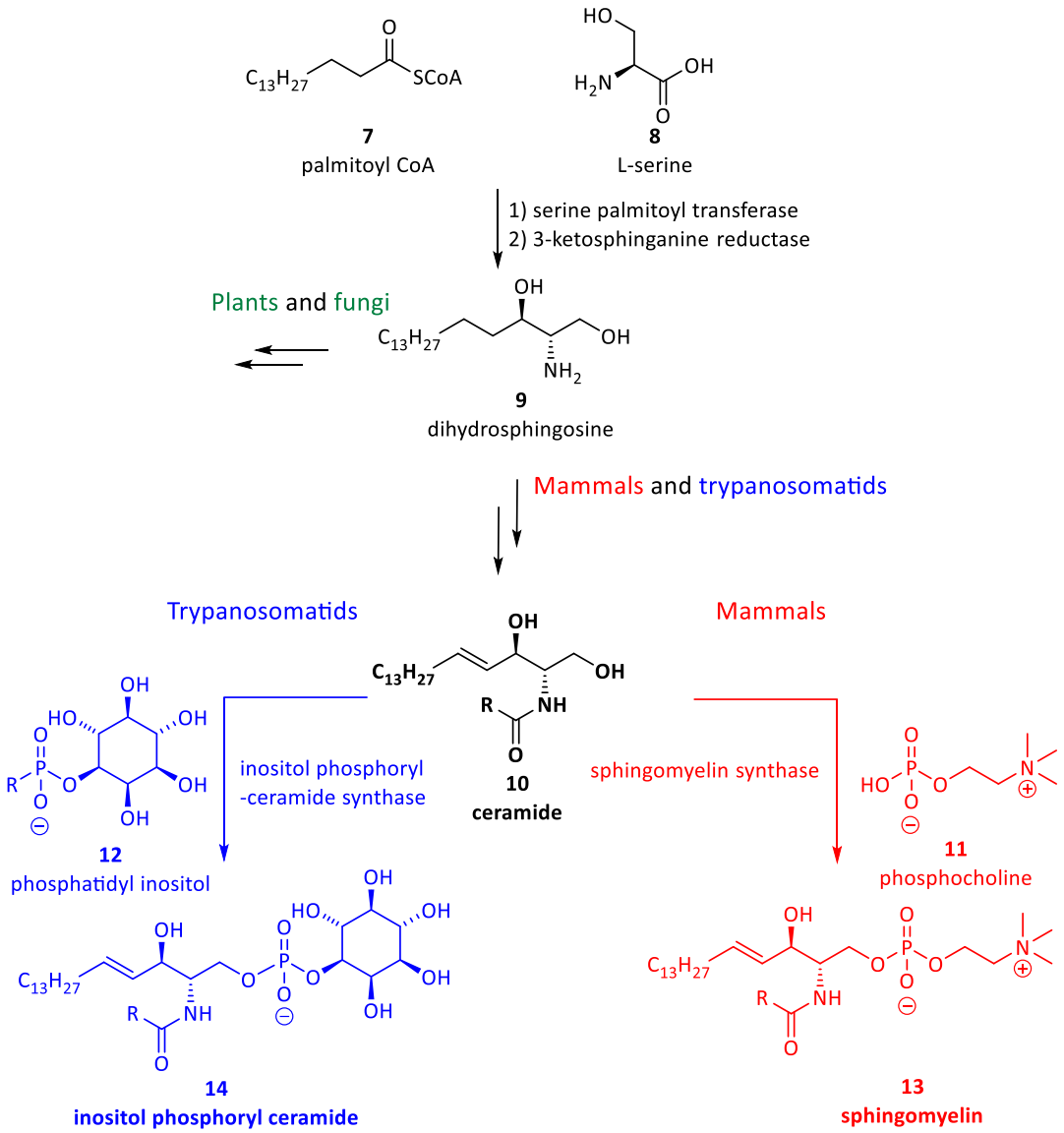

Figure 1.21-1 A branch of the sphingolipid biosynthetic pathway found in trypanosomatids, plants, fungi and mammals.

IPCS is responsible for maintaining the equilibrium between mitogenic diacylglycerol (DAG, **15**) and pro-apoptotic ceramide (**10**). [24] IPCS transfers a phosphoinositol group from phosphatidyl inositol (PI, **12**) to ceramide (**10**) to produce IPC (**14**) and DAG (**15**), facilitated by the histidine-histidine-aspartate catalytic triad. The biochemical reaction occurs through a ping-pong bi-bi, or double displacement, mechanism (Figure 1.21-2). [24,25]

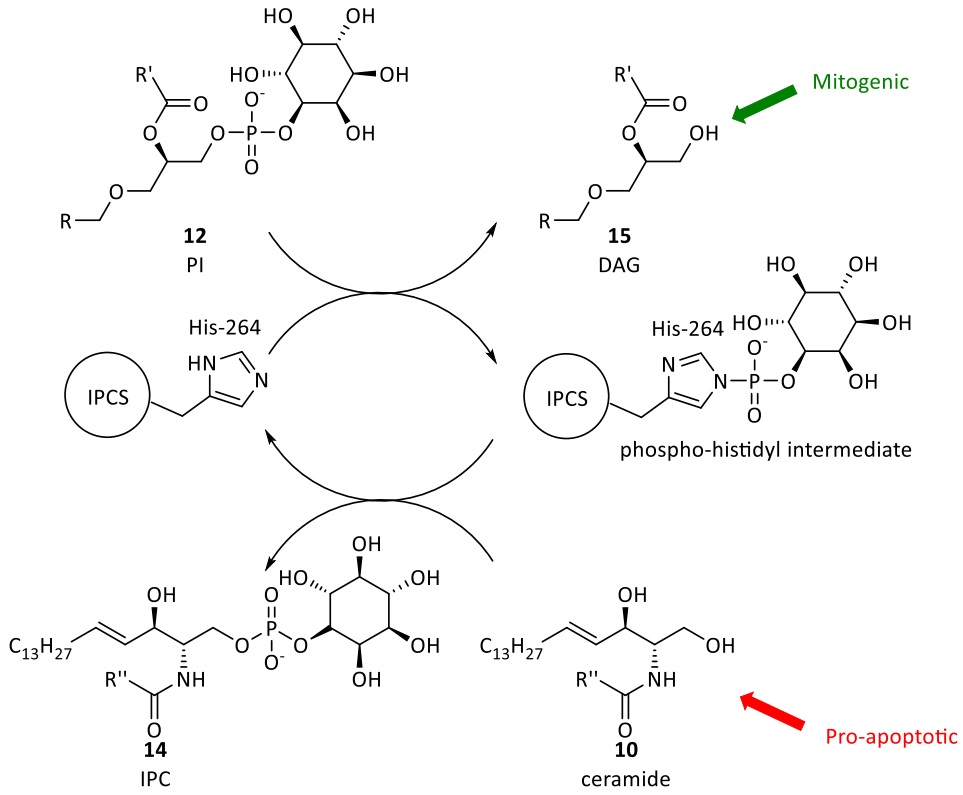

Figure 1.21-2 Ping-pong bi-bi mechanism for the biosynthesis of IPC (**14**). [25]

The divergence in the final step between mammals and trypanosomatids makes IPCS an attractive drug target due to the lack of mammalian orthologue. Inhibition of IPCS leads to a decrease in essential sphingolipid IPC (**14**) and mitogenic DAG (**15**), which is essential for cell growth.[26] Whilst inhibiting cell growth, a build-up of pro-apoptotic ceramide (**10**) also induces apoptosis.[27] The damaging effects caused by IPCS inhibition, in addition to the divergence in the final step of sphingolipid biosynthesis between mammals and trypanosomatids, makes IPCS an attractive drug target.

1.22 High throughput screen to identify inhibitors of *Lmj*IPCS

Following the identification of IPCS as a potential new drug target in *Leishmania* by Denny, efforts turned towards finding inhibitors of this enzyme as prospective new antileishmanial drugs.[28] Consequently, Norcliffe carried out a high throughput screen (HTS) of 1.8 million GSK compounds, to find inhibitors of *Lmj*IPCS that also showed high antileishmanial activity and low mammalian cell toxicity (Figure 1.22-1). [1,29]

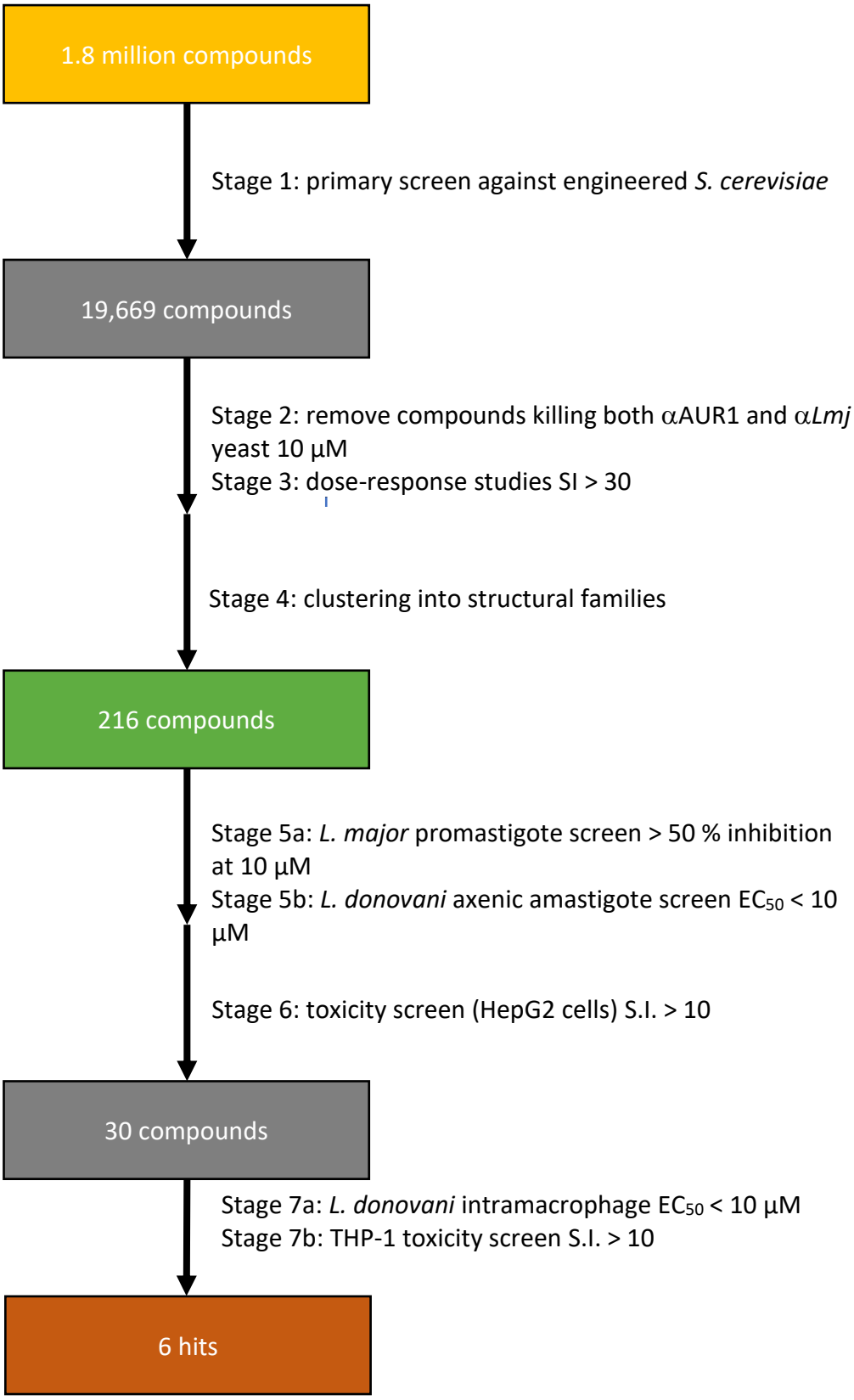

Figure 1.22-1 HTS carried out by Norcliffe *et al.* to identify inhibitors of *Lmj*IPCS that showed potent antileishmanial activity and low mammalian cell toxicity. [1]

Initially, a target-based approach was used to identify inhibitors of *Lmj*IPCS. 1.8 million compounds were screened against a genetically engineered strain of *S. cerevisiae* (α*Lmj*) which has no fungal IPCS but expresses *Lmj*IPCS, as genomic *Sc*AUR1 is knocked out and replaced by the gene for *Lmj*IPCS on a plasmid. The 19,669 compounds that showed activity against α*Lmj* were then screened against *Sc*AUR1 knockouts where the gene for fungal IPCS (AUR1) was replaced on a plasmid (αAUR1). This identified compounds that inhibit *Lmj*IPCS and not *Sc*AUR1. Subsequent dose-response studies and structural clustering identified 216 compounds with a selectivity index (αAUR1/α*Lmj*) > 30. [1]

The high throughput screen then switched to a phenotypic approach to ensure that the inhibitors of *Lmj*IPCS also had high antileishmanial activity. When testing new antileishmanial drugs, the most clinically relevant system would be intramacrophage amastigotes as this is the morphological form of the parasite in the host. However, these assays can often be difficult, low throughput and time consuming. As such, simpler promastigote assays are often used to broadly determine the antileishmanial activity of new compounds. As such, the 216 compounds were initially assayed against *L. major* promastigotes and *L. donovani* axenic amastigotes due to the high-throughput nature of these assays. Compounds were also screened for toxicity against HepG2 cells which led to the identification of 30 active and selective antileishmanial compounds. Intramacrophage amastigote and macrophage toxicity screens were then carried out on this more manageable number of compounds. This led to the identification of a series of 6 hit compounds, as shown in Figure 1.22-2. [1]

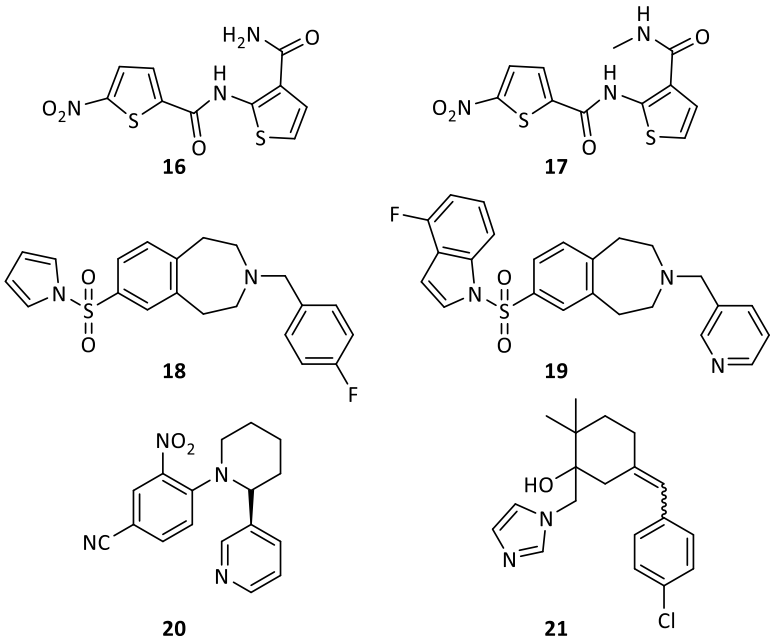

Figure 1.22-2 Identity of the 6 hit compounds identified by the HTS performed by Norcliffe.[1]

Following the HTS, Norcliffe carried out a secondary screening to confirm on-target *Lmj*IPCS activity of the 216 compounds identified using the yeast-based assay. Compounds were tested at 10 µM for inhibitory effects against *Lmj*IPCS enriched microsomes. Surprisingly, only benzazepines (**18**-**19**) and singleton **21** showed inhibitory effects, while nitro singleton **20** and 5-nitrothiophene-2-carboxamides (**16**-**17**) showed no inhibition (Figure 1.22-3).

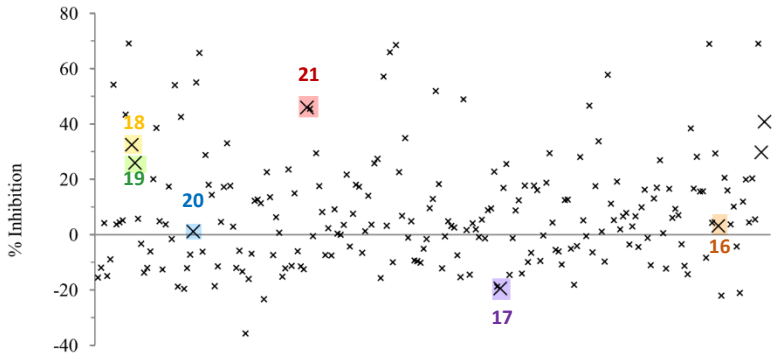

Figure 1.22-3 Secondary screening of 216 compounds for activity against *Lmj*IPCS enriched microsomes. The six hit compounds are highlighted as follows: orange (**16**), purple (**17**), yellow (**18**), green (**19**), blue (**20**), red (**21**). Figure obtained from the thesis of Norcliffe.[29]

This thesis concentrates on the exploration of the two 5-nitrothiophene-2-carboxamide (5N2C) hits (**16** and **17**), and their analogues, as potential new

antileishmanial drugs. The antileishmanial activity and mammalian cell toxicity of these hits from the HTS is presented in Table 1.22-1.

Table 1.22-1: Biological activity and physical properties of 5N2Cs **16** and **17** from the HTS.

Compound	*L.mj* % inh. at 10 μM	Axenic *L.don* pEC_{50}	InMac *L.don* pEC_{50}	HepG2 pEC_{50}	THP-1 pEC_{50}	PFI	#Ar
16	105.9	6.6	5.9	4.0	4.9	4.0	2
17	104.2	5.7	5.8	4.0	4.3	4.6	2

1.3 Initial project aims

Two potent 5N2C hit antileishmanial compounds (**16** and **17**) were identified by Norcliffe *et al*. However, ambiguity remained around their mode of action as secondary screening against a microsomal formulation of *Lmj*IPCS did not show the necessary inhibition. Subsequently, the initial aims of the project were to:

1. Resynthesise the original 5N2C hits (**16** and **17**);
2. Validate the antileishmanial activity and mammalian cell toxicity of **16** and **17**;
3. Investigate whether **16** and **17** inhibit *Lmj*IPCS.

1.4 Results and discussion

1.41 Resynthesis and antileishmanial activity of original hits 16 and 17

As discussed in section 1.2, previous work by Norcliffe identified two antileishmanial 5N2C hit compounds (**16** and **17**) from a HTS looking to identify inhibitors of *Lmj*IPCS.[1,29] The hits showed good antileishmanial activity and low toxicity against THP-1 and HepG2 cells (Table 1.22-1). However, neither compound showed significant levels of inhibition against a microsomal preparation of *Lmj*IPCS during secondary screening.[29] This was somewhat surprising given the basis of the HTS and merited further investigation. Subsequently, an initial goal of the project was to resynthesise the original hits and validate their antileishmanial activity, lack of mammalian cell toxicity and *Lmj*IPCS activity.

To obtain sufficient quantities of hit compounds **16** and **17** for validation of the HTS results, an efficient synthetic strategy had to be devised. Classically, 2-aminothiophenes with electron withdrawing substituents in the 3- position are synthesised using the Gewald reaction.[30] Following this literature precedent, resynthesis of original hit compound **17** was achieved by firstly reacting methylcyanoacetate (**24**) with methylamine in THF. This was followed by a modified Gewald synthesis to give amine **30**. The final product was subsequently obtained after amide coupling of **30** with 5-nitrothiophene-2-carbonyl chloride (**23**) (Scheme 1.41.1).[31] Successful synthesis of **17** was validated by the characteristic presence of the central amide in the proton NMR (δ_H 13.61 ppm). Exploiting the commercial availability of the required nitriles enabled the simple synthesis of three derivatives varying in the nature of the C-3 substituent on the right-hand ring (**34-36**). Again, each analogue had a characteristic central amide signal in the proton NMR at δ_H 11.74-12.28 ppm. The low solubility of the high sp^2 nature hit compounds and their simple analogues led to precipitation from the THF reaction solvent. This simplified purification as analytically pure product was obtained by filtration and trituration with water.

Although this route successfully generated hit compound **17** and analogues **34-36**, it failed to deliver hit compound **16** due to dehydration of the desired primary amide to nitrile **36**.

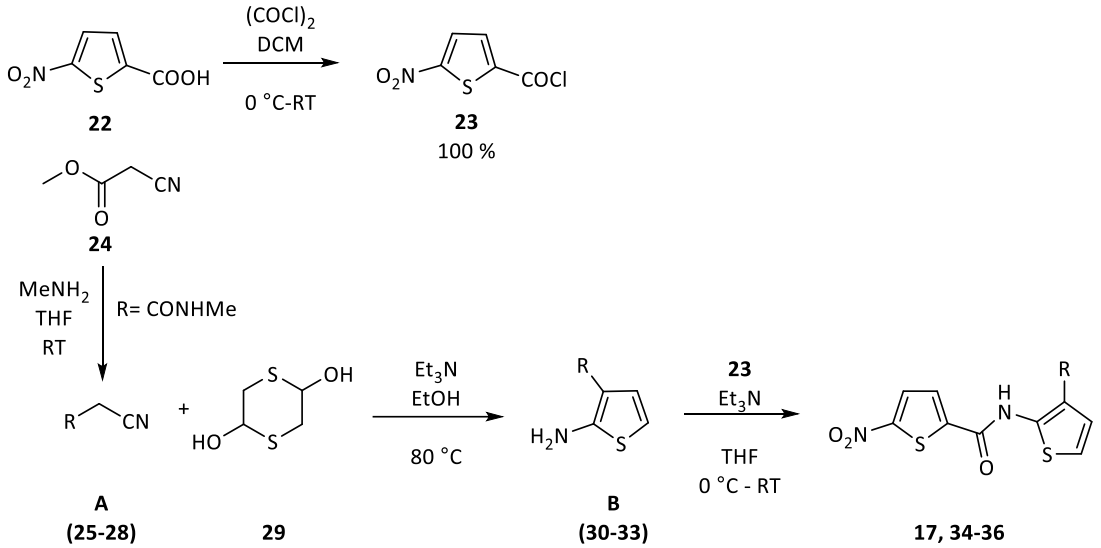

R	Intermediate ID (yield %)		Product ID (yield %)
	A	B	
CONHMe	**25** (100 %)	**30** (61 %)	**17** (52 %)
COOMe	**26**	**31** (55 %)	**34** (41 %)
COOEt	**27**	**32** (79 %)	**35** (28 %)
CN	**28**	**33** (59 %)	**36** (50 %)

Scheme 1.41.1 Synthetic route towards original hit compound **17** and further bisthiophene analogues **34-36**.[31] Where no yield is quoted the intermediate was commercially sourced.

Subsequently, an alternative route had to be investigated to obtain hit compound **16**. Acid catalysed hydration of nitrile **36** gave the desired product **16** in 80 % yield (Scheme 1.41.2). Synthesis of hit compound **16** was validated by the loss of the nitrile peak in the carbon NMR of **36** (δ_C 114.5 ppm) and the gain of a second carbonyl peak which was absent in the starting material at δ_C 167.2 ppm.

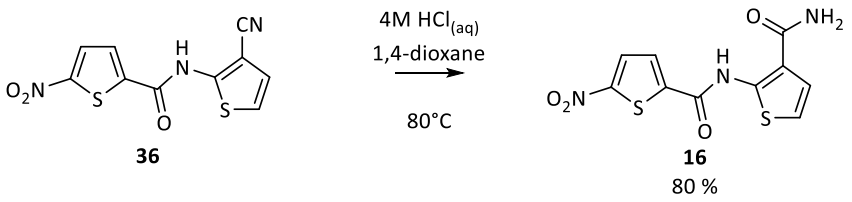

Scheme 1.41.2 Synthesis of original hit **16** was achieved through acidic hydration of nitrile **36**.

The three-pot synthetic route detailed in Scheme 1.41.1 was suitable for small scale preparations of hit compound **17** but would not allow for multi-gram scale synthesis, due to the prohibitory costs of the methylamine in THF required to access nitrile starting material **25**. Subsequently, alternative routes were also investigated to enable compound **17** to be synthesised in larger quantities. Successful multigram synthesis was achieved using a two-pot synthesis. Firstly, aqueous methylamine was added to methylcyanoacetate (**24**) in ethanol (1:1 water: ethanol). Following consumption of the starting material by TLC, the Gewald reaction components were added before heating at 80 °C for 1 hr. This enabled the efficient 1-pot synthesis of intermediate amine **30**. Following purification, **30** was coupled with 5-nitrothiophene-2-carbonyl chloride (**23**) to give product **17** in comparable yields to the previous route (Scheme 1.41.3).

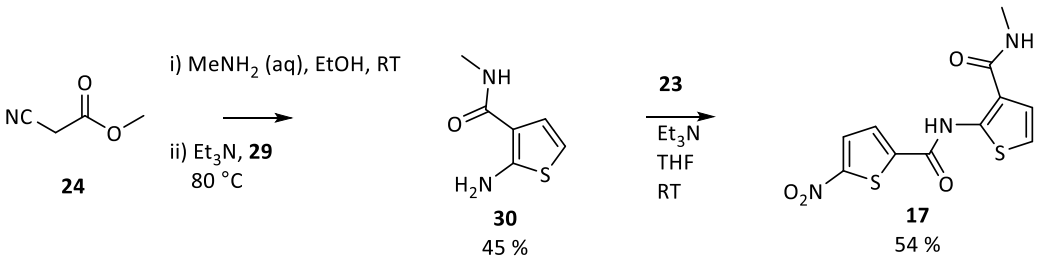

Scheme 1.41.3 Two-pot synthetic route to access hit compound **17** in multigram scale.

With the resynthesised hit compounds **16** and **17** and simple analogues **34-36** in hand, an initial goal was to validate their antileishmanial activity. This was achieved by dose-response antipromastigote assays, in which 1 x 10^6 parasites mL^{-1} were incubated with a 3-fold dilution series of compound for 48 hrs in Schneiders insect media (pH 7.2, 15 % FBS, 1% PenStrep). Cell viability was assessed colorimetrically using the well-reported alamarBlue® or resazurin reagent.[32] All analogues (**16-17, 34-36**) showed sub to single micromolar activity against *L. major* promastigotes (Figure

1.41-1), supporting the HTS results and showing that the right hand ring 3-substituent can be varied. The high reproducibility and observed potency of the hits and simple derivatives against *L. major* promastigotes warranted the use of this assay as a quick and easy indicator of antileishmanial activity rather than using more clinically relevant but time consuming intramacrophage amastigote assays. These results provided the rationale to continue investigating the series as potential antileishmanial agents.

With antileishmanial activity revalidated, the next goal was to verify mammalian cell toxicity using HepG2 cells. 1.2 x 10^4 cells $well^{-1}$ were seeded into a 96-well plate 24 hrs in advance, before incubating with a 3-fold dilution series of compound in fresh *Dulbecco's Modified Eagle Medium* (DMEM, pH 7.4, 10 % FBS, 1 % PenStrep) for 48 hrs. Cell viability was assessed using Alamar Blue® or resazurin in a similar manner to the antipromastigote assays described above. Both hit compounds **16** and **17** and ester derivatives **34** and **35** showed low HepG2 toxicity and high selectivity index when comparing HepG2 toxicity with *L. major* antipromastigote activity. However, nitrile **36** displayed significant HepG2 toxicity (Figure 1.41-1). Whilst macrophage cytotoxicity is also an important metric as this is the site of *Leishmania* infection *in vivo*, HepG2 toxicity was used as the primary cytotoxicity screen due to the ease of propagation of the cells and ability to use these results to give an indication of potential liver cell toxicity *in vivo*. This is important as the liver is primarily responsible for the metabolism and clearance of most drugs and as such, is the place where most toxic effects are initially observed.[33] The observed low HepG2 toxicity and high selectivity index of the hits supports the HTS results and suggests that these compounds deserve further investigation as antileishmanial agents.

A

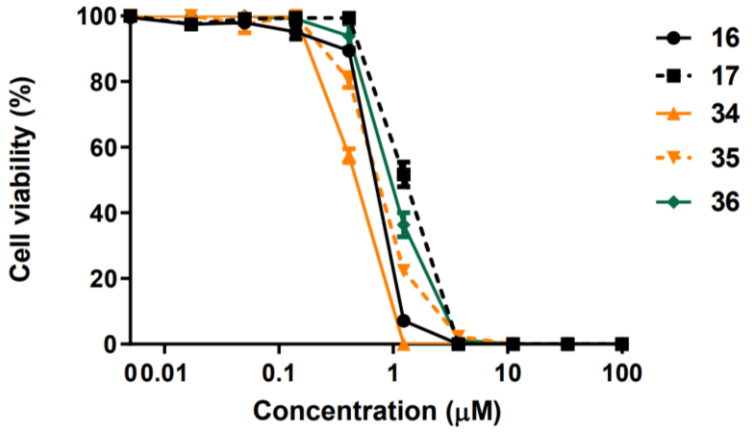

B

Compound	16	17	34	35	36
EC_{50}(*L. major*) / μM	0.52 ± 0.05	0.99 ± 0.09	0.59 ± 0.05	0.93 ± 0.09	1.1 ± 0.1
CC_{50} (HepG2) / μM	24 ± 1	96 ± 4	>100	>100	8.0 ± 0.7
S.I. (HepG2/*L. major*)	46	97	>100	>100	7.2

Figure 1.41-1 A. Dose-response curve for *L. major* promastigotes treated with the original hit compounds, and ester and nitrile analogues (generated using GraphPad Prism 8). B. EC_{50} values for original hit compounds (**16** and **17**), ester (**34** and **35**), and nitrile (**36**) derivatives against *L. major* promastigotes. CC_{50} values against HepG2 cells are also provided. Antileishmanial activity and HepG2 cytotoxicity are reported as the mean of three repeats, with errors representing standard error.

1.42 Investigation of IPCS activity for hits 16 and 17

With the resynthesised hits validated as potent and non-toxic antileishmanial agents, the next steps were to reinvestigate their *Lmj*IPCS activity.[1] Previously, Norcliffe showed that neither **16** or **17** inhibited *Lmj*IPCS at 10 μM (section 1.2).[29] It was decided to repeat these assays at 100 μM to verify whether **16** or **17** show any inhibition of *Lmj*IPCS at a higher concentration. These experiments were carried out using high performance thin-layer chromatography (HPTLC) to visualise the enzymatic turnover of a fluorescent analogue of the *Lmj*IPCS substrate ceramide (NBD-C_6-ceramide) to the fluorescent product NBD-C_6-IPC by microsomes enriched

in *Lmj*IPCS, as previously described by Mina *et al.* (see footnote[1]). [34,35] IPCS inhibition was defined by the absence of the fluorescent product inositol phosphoryl ceramide (NBD-C_6-IPC). Clemastine, a validated IPCS inhibitor, was used as a positive control and showed the necessary depletion of NBD-C_6-IPC.[36] However, both **16** and **17** showed a significant amount of NBD-C_6-IPC, indicating that both compounds do not inhibit IPCS at 100 µM (Figure 1.42-1).

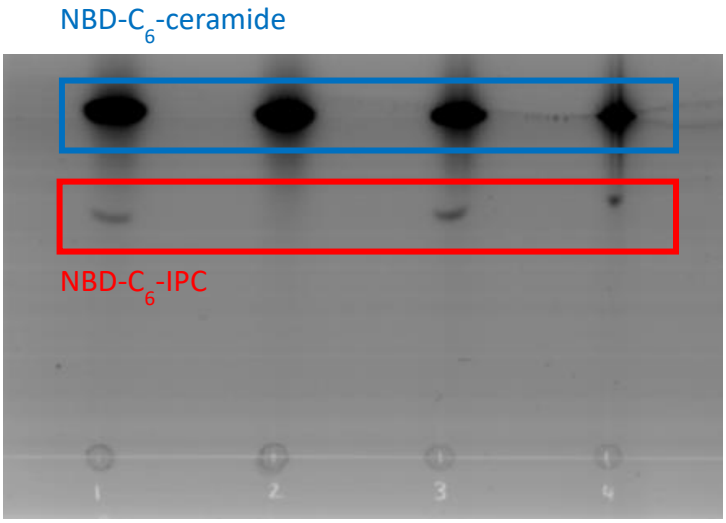

DMSO Clemastine **16** **17**

Figure 1.42-1 The original hit compounds do not inhibit IPCS, as shown by the presence of IPC when compound (100 µM) was incubated with IPCS substrates and microsomes enriched with IPCS. HPTLC was used to separate the reaction components using a solvent system of 45:55:10 methanol:chloroform:0.25 % KCl $_{(aq)}$ before visualisation at λ_{ex} 480/ λ_{em} 540nm.

One factor that challenged this assay was the lack of solubility of the hits, consistent with the low solubility observed during the synthesis. To eliminate the possibility that low solubility led to the null results, the assay was repeated in buffers in which the hits show higher solubility (FESSIF and 15 mM sodium taurocholate, discussed in section 2.33.1). However, in both buffers one or both positive control(s) (clemastine and tamoxifen) did not inhibit *Lmj*IPCS activity (Figure 1.42-2).[36,37] This could be explained by the presence of bile salts which act as biosurfactants and interfere with the lipid bilayers, potentially leading to membrane disruption and impacting the activity of *Lmj*IPCS.[38]

[1] Microsomes enriched in *Lmj*IPCS were provided by J. Mina.

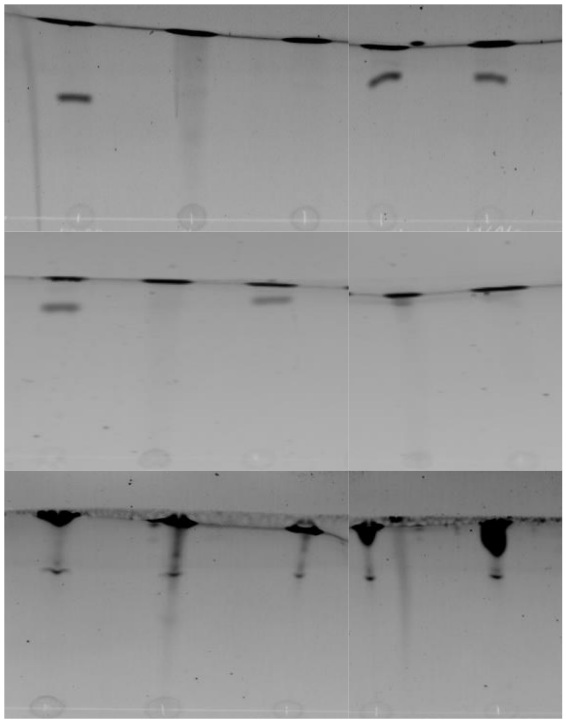

Figure 1.42-2 *Lmj*IPCS enriched microsomal HPTLC assay testing alternative buffers 15 mM sodium taurocholate and FESSIF. In both cases, *Lmj*IPCS is not inhibited by validated inhibitors clemastine (clem) and tamoxifen (tam), as such, these buffers cannot be used for microsomal assays.

Following the observed lack of activity of hits **16** and **17** in the HPTLC based assay, an analogous technique was investigated where *Lmj*IPCS enriched microsomes were used in a plate-based assay developed by Mina *et al.* to allow for the quantification of inhibition. [34,35] It was proposed that this dose-response experiment would identify any partial inhibition of *Lmj*IPCS by the hits more clearly than the previous HPTLC experiments. Briefly, the desired compounds were incubated with NBD-C_6-ceramide, PI (**12**) and *Lmj*IPCS enriched microsomes in a 3-fold serial dilution before applying to a filter plate with an anion exchange resin (AG4-X4), which binds to the negatively charged NBD-C_6-IPC. This allows excess NBD-C_6-ceramide to be washed off before elution of the anionic NBD-C_6-IPC with potassium formate and quantification using fluorescence spectroscopy (λ_{ex} 480/ λ_{em} 540nm). [34,35] This fluorescence output can be corrected according to the controls to give % activity of IPCS at each concentration, from which an IC_{50} can be calculated. No enzyme inhibition was observed at any concentration across three biological replicates for original hits **16**

and **17**, while clemastine caused 98 % inhibition at 50 µM (Figure 1.42-3). It can subsequently be concluded that the hit compounds do not inhibit IPCS in a microsomal model.

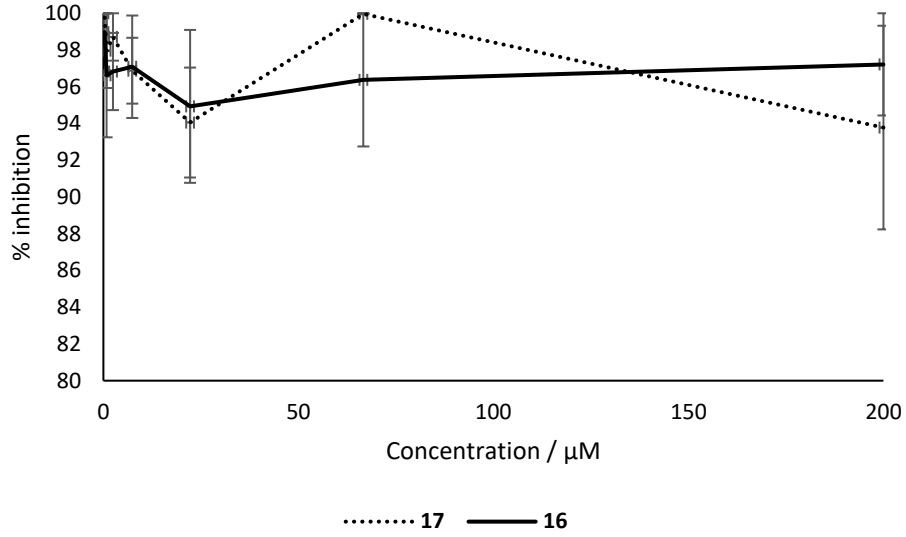

Figure 1.42-3 Plate based assay developed by Mina *et al.* shows no IPCS inhibition at any concentration (< 200 µM) for hits **16** and **17**. [34,35] Averages and errors are calculated from three biological replicates.

Following the lack of inhibition of *Lmj*IPCS by the hits in microsomal experiments, an orthogonal technique was employed. The antileishmanial activity of hits **16** and **17** was assessed for genetic mutants of *L. major* in which the LCB2 subunit of the serine palmitoyl transferase (SPT) was removed (*lcb2*$^{-}$) and added back on a plasmid (px).[21] SPT is the first enzyme in the sphingolipid biosynthetic pathway and its removal renders *Lmj*IPCS non-functional.[2] A comparison of activity of the hits against the *lcb2*$^{-}$ mutant to the px addback or wild type can be used to determine whether parasitic cell death was caused by *Lmj*IPCS inhibition. This method is attractive over microsomal experiments as compound solubility issues are negated due to the much-improved solubility of the hits in media supplemented with FBS compared to aqueous buffers (discussed in section 2.33.1).

Clemastine, a validated *Lmj*IPCS inhibitor, was used as a positive control and showed the expected decrease in activity against the *lcb2*$^{-}$ mutant.[36] However, no difference was observed between the cytotoxicity of hits **16** and **17** against the *lcb2*$^{-}$ mutant compared to the WT or px cell lines (Figure 1.42-4). This suggests that the

antipromastigote activity of hits **16** and **17** is not due to *Lmj*IPCS inhibition, or that there is significant polypharmacology for this series which renders any leishmanicidal effects due to *Lmj*IPCS inhibition insignificant.

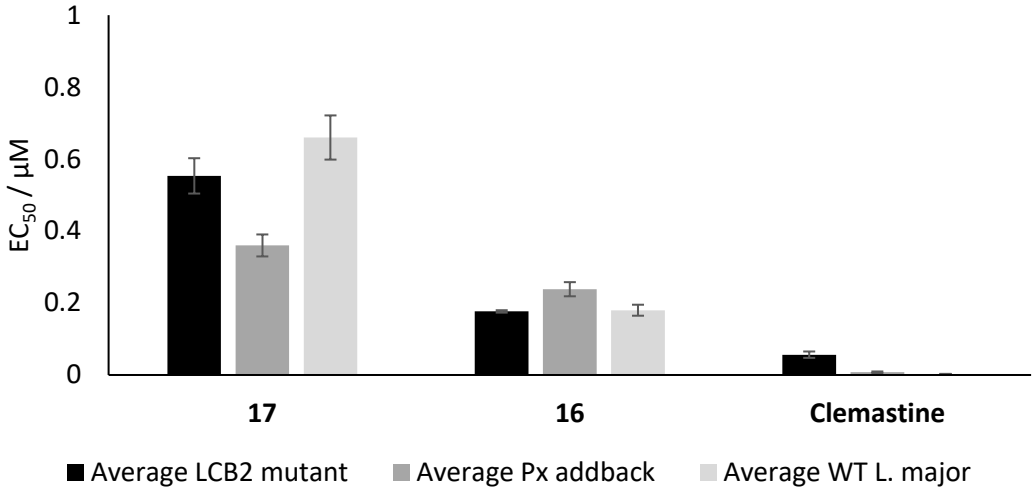

Figure 1.42-4 Inhibition of cell growth of WT and mutant (LCB2 and px) cell lines by original hits **16** and **17**. Clemastine, a validated *Lmj*IPCS inhibitor was used as a positive control. Averages are calculated from at least three biological repeats and errors are standard errors from three repeats.

The lack of *Lmj*IPCS inhibition, discussed above, supported the secondary screening results obtained by Norcliffe.[29] In summary, compounds **16** and **17** are potent antileishmanial compounds with low mammalian cell toxicity, but have an unknown mode of action and pharmacokinetic profile.

1.43 DMPK studies for hits 16 and 17

The low solubility of compounds **16** and **17** observed during synthesis raised concerns around the potential bioavailability of these compounds *in vivo* (section 1.41). Subsequently, it became important to explore the bioavailability of these compounds in a mouse model, to investigate whether the compounds would be druggable in their current form. This was achieved by drug metabolism and pharmacokinetic (DMPK) studies, in which the blood plasma concentration of **16** and **17** was measured

at various timepoints after either oral administration or intraperitoneal injection (Figure 1.43-1, see footnote[2]).

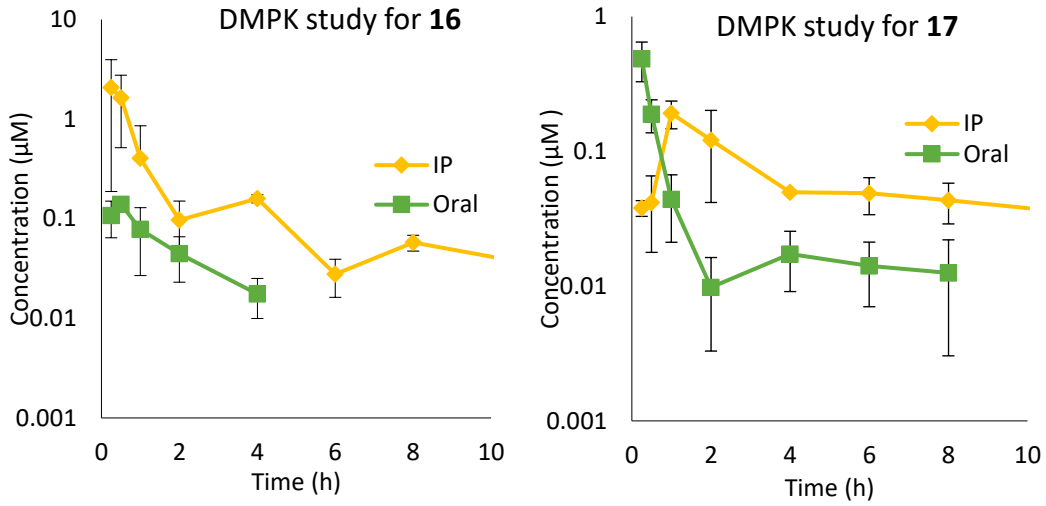

Figure 1.43-1 DMPK study assessing the plasma bioavailability of the original hit compounds upon IP and oral administration to a mouse model. Averages and errors are calculated from 3 individual mice repeats.

Oral administration is preferred as it enables ease of administration and overcomes one of the major issues with the current drugs used to treat leishmaniasis, of which only miltefosine (**5**) is available orally.[39] All other current antileishmanial drugs are administered by intraperitoneal (IP) or intravenous (IV) infusion or injection, with the exception of paromomycin (**4**) which can be administered topically for CL infections. As such, it was also important to monitor the performance of the hits by IP injection to allow comparisons to be drawn with current antileishmanial treatment options. After IP injection, it was found that at 1 hr blood plasma concentration was only 0.4 ± 0.4 µM for **16** and 0.19 ± 0.04 µM for **17**. Blood plasma concentrations were even lower after oral administration with values of 0.08 ± 0.05 µM for **16** and 0.04 ± 0.02 µM for **17** after 1 hr. The average blood plasma concentrations were calculated from 3 mice, which showed a wide variation and lack of reproducibility indicative of solubility challenges. Kinetic solubility experiments were conducted to verify these results. This was achieved by incubating a DMSO stock solution of compound in PBS

[2] DMPK studies were carried out by LifeArc in collaboration with GVK BIO Sciences Pvt Ltd Hyderabad, India

(< 5 % DMSO) for 2 hr before centrifugation to remove any undissolved material. The concentration of the supernatant was determined using UV-Vis by comparing the absorbance maximum of the sample with a calibration curve of the same compound. This confirmed that the original hits **16** and **17** and simple analogues **34** and **35** were insoluble as they could not be detected, indicating that the solubility was lower than the detection limit (i.e. solubility (PBS) < 7.4 μM).

1.5 Summary

In summary, compounds **16** and **17** showed promising antileishmanial activity and low mammalian cell toxicity. However, an unknown mode of action, poor solubility and poor pharmacokinetic profile limited progression in their current formulation.

2 Identification of 5N2C lead antileishmanial compounds

2.1 Introduction

As discussed in Chapter 1, there is a pressing need for new antileishmanial drugs with well-understood and distinct modes of action.

2.11 Drugs to treat trypanosomatid diseases

As discussed in section 1, *Leishmania* is a trypanosomatid parasite, along with *Trypanosoma cruzi* and *Trypanosoma brucei*, causative agents of Chagas disease and African sleeping sickness, respectively. *T. cruzi* and *T. brucei* exist as epimastigotes in the vector salivary gland and transform into metacyclic trypomastigotes for infection. Once in the host, *T. cruzi* infects cells to form amastigotes whereas *T. brucei* remains as bloodstream trypomastigotes.[40,41] Following *T. brucei* inoculation, the disease starts in the more treatable and less severe haemo-lymphatic stage. However, once the parasites cross the blood-brain barrier the disease enters the fatal neurological stage, which is complicated to treat.[42]

All current treatments for Chagas disease contain nitroheterocycles (nifurtimox (**37**) and benznidazole (**38**)), whilst fexinidazole (**39**) is the only treatment for African sleeping sickness suitable for both disease stages (Figure 2.11-1). [42,43] The similarities between *Leishmania*, *T. brucei* and *T. cruzi* opens the possibility for one universal drug to treat all three diseases. Indeed, fexinidazole (**39**) has been explored for repurposing to treat VL, and nifurtimox (**37**) has been explored to treat African sleeping sickness. [44,45] Subsequently, the nitroheterocycle present in many drugs used to treat *T. brucei* and *T. cruzi* infections suggests that nitroheterocyclic drugs should also be explored for the treatment of leishmaniasis.

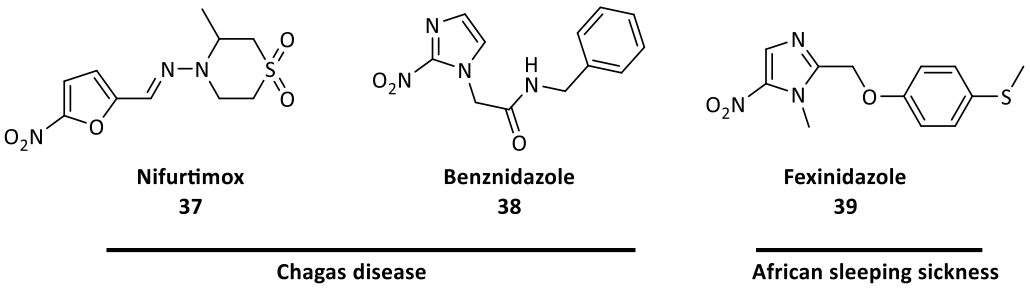

Figure 2.11-1 Current nitroheterocyclic drugs used to treat trypanosomatid diseases.

2.12 Drug discovery for leishmaniasis – LeishBox

GlaxoSmithKline (GSK) created three collections of hit compounds to accelerate the drug discovery process for trypanosomatid diseases: ChagasBox, HATBox and LeishBox. These libraries were generated through a series of phenotypic HTS of 1.8 million compounds to identify compounds with promising activity against *T. cruzi*, *T. brucei* and *L. donovani* respectively. The LeishBox is a library of 192 compounds that show potent activity in a THP-1 intramacrophage model, which were identified as outlined in Figure 2.12-1. [46]

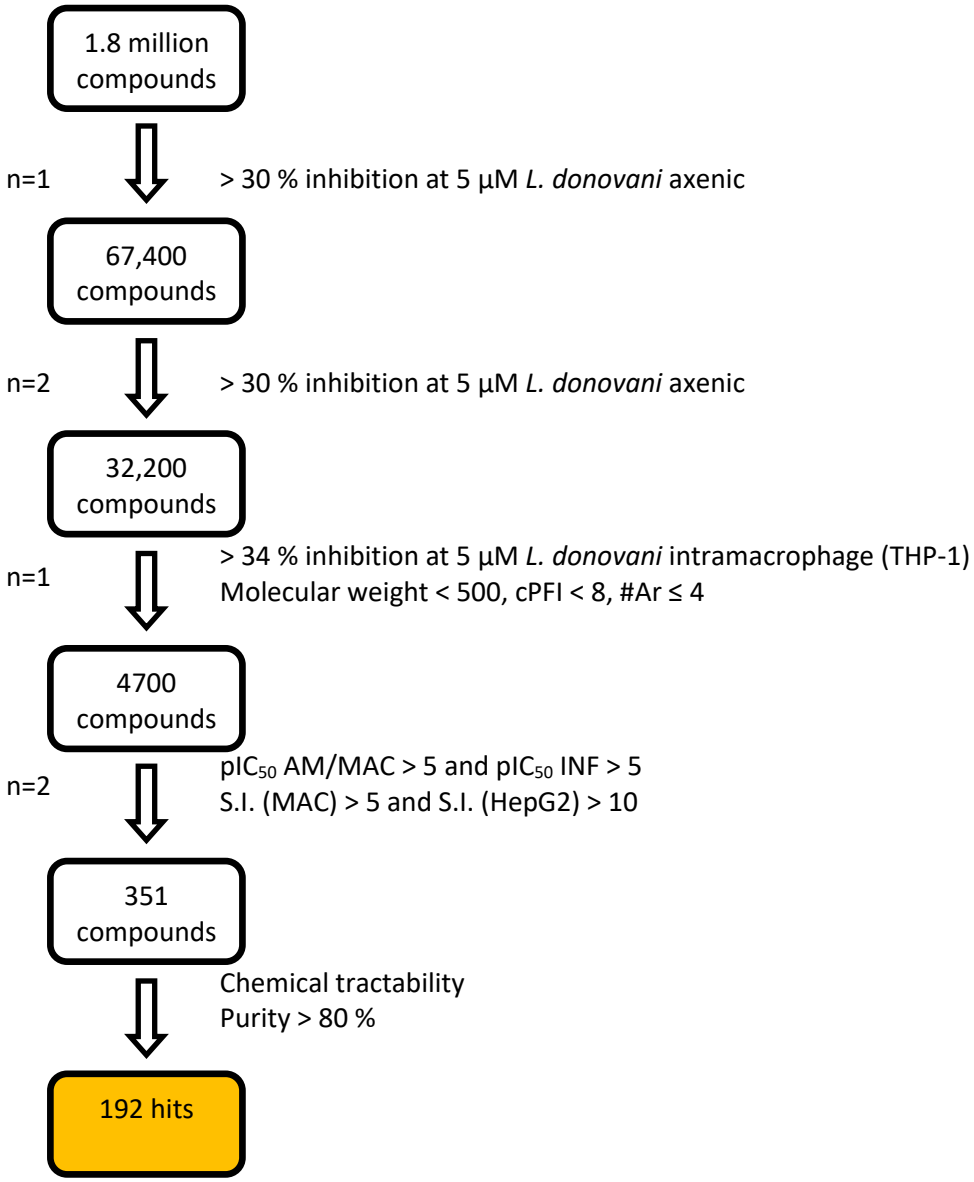

Figure 2.12-1 HTS of 1.8 million compounds from GSK for antileishmanial activity against *L. donovani*. *Ld* bob and THP-1 macrophages were used throughout. n=number of repeats, cPFI = calculate property forecast index, #Ar = number of aromatic rings, AM/MAC = fluorescence assay counting amastigote (AM) per macrophage (MAC) ratio, INF = fluorescence assay counting percentage of infected cells. Figure adapted from Pena *et al.*, 2015.[46]

Significantly, 61 out of the 192 LeishBox compounds contain a nitro group, outlining the importance of this functionality for future treatments of leishmaniasis. The prevalence of the nitro group in the LeishBox taken together with the successful use of nitroheterocyclic drugs for the treatment of trypanosomatid diseases poses the following question: why are there no nitro drugs to treat leishmaniasis?

2.13 Nitro drugs

There are approximately 40 currently approved nitro containing drugs on the market for the treatment of cancer as well as bacterial, neurological and parasitic diseases (Table 2.13-1). [47,48] This includes the trypanosomatid diseases discussed in section 2.11 (entry 5-7, Table 2.13-1). Other drugs, such as delaminid (**44**, entry 8, Table 2.13-1), have shown promise for repurposing to treat leishmaniasis.[49] Nitro drugs are especially useful for treating trypanosomatid and bacterial diseases due to the presence of type I nitroreductase enzymes (NTR). This, in principle, allows for the selective bioactivation and toxification of prodrugs within the parasite, which provides the rationale to continue exploring new nitro drugs for the treatment of other trypanosomatid diseases such as leishmaniasis.

Table 2.13-1: A selection of marketed nitro containing drugs used to treat parasitic diseases or with potential for repurposing (DrugBank 5.0).[47,48,50]

Entry	Approved drug	Structure	Disease
1	Nitazoxanide (**40**)	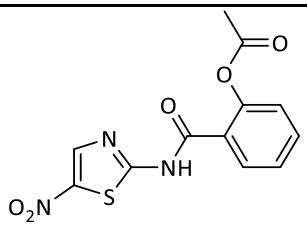	Giardiasis and cryptosporidiosis
2	Metronidazole (**41**)	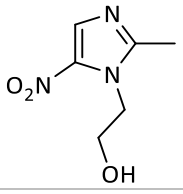	Trichomoniasis, giardiasis and amebiasis
3	Tinidazole (**42**)	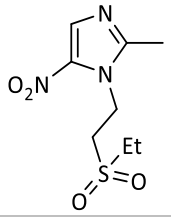	Giardiasis and amebiasis
4	Ornidazole (**43**)	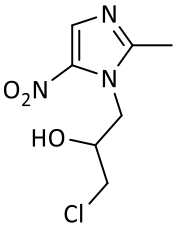	Trichomoniasis, giardiasis and amebiasis
5	Nifurtimox (**37**)	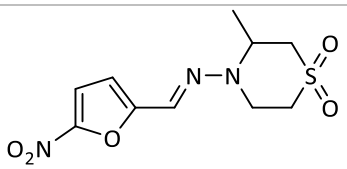	Chagas disease
6	Benznidazole (**38**)	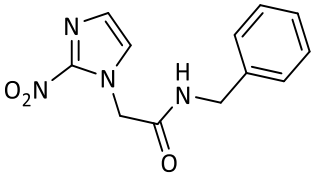	Chagas disease
7	Fexinidazole (**39**)	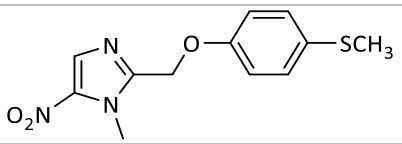	African sleeping sickness
8	Delaminid (**44**)	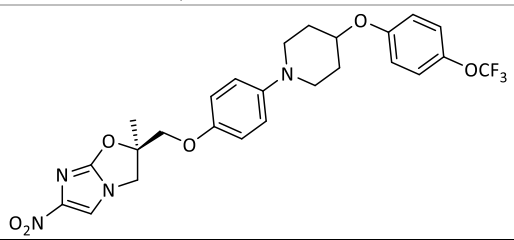	Tuberculosis (repurposing for leishmaniasis)

2.13.1 5-Nitrothiophenes

Of the 61 nitro containing drugs in the LeishBox, 14 are 5-nitrothiophenes.[46] The progression of this functionality to clinical trial for wider diseases (section 2.13.1.1) as well as its potential to treat trypanosomatid disease (section 2.13.1.2) is discussed below.

2.13.1.1 5-Nitrothiophenes reaching clinical trials

Only two drugs containing the 5-nitrothiophene functionality have reached clinical trials for any disease, both of which are experimental drugs (DrugBank 5.0).[47] The first is SR-9009 (**45**, drug bank ID DB14013), which is involved in circadian rhythm modulation (Figure 2.13-1). SR-9009 (**45**) was originally developed to treat sleep disorders and metabolic disease, but recent studies have also shown promise for the use of SR-9009 (**45**) as an experimental anti-cancer drug. [51,52] There are currently no pharmaceutical preparations of SR-9009 (**45**) but it has been misused in illicit doping products.[53] The second nitrothiophene containing and only 5N2C containing drug in the DrugBank is Nifurzide (**46**, DrugBank ID DB13325), an antibiotic developed to treat gastrointestinal infections (Figure 2.13-1). [54] The drug was explored in phase I clinical trials, but did not progress further due to poor solubility.[55,56]

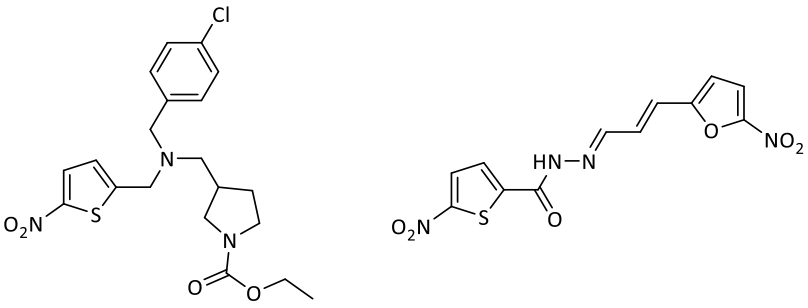

SR-9009
45

Nifurzide
46

Figure 2.13-1: Structures of the only two nitrothiophene containing experimental drugs (DrugBank 5.0). [47]

2.13.1.2 5-Nitrothiophenes to treat trypanosomatid disease

Nitroimidazoles and nitrofurans are currently some of the gold standards for treating trypanosomatid disease. Other nitroheterocycles such as nitrothiophenes have been

briefly explored as potential antileishmanial drugs but have never progressed to clinical trials.

Often, drug discovery campaigns arise from exploring the SAR of known drugs. This technique led Rando *et al.* to exchange the nitrofuran in nifuroxazide (**47**) for nitrothiophene (**48**), which gave an improvement in antileishmanial activity. [57] However, similar attempts by Chauvière to replace the nitroimidazole in megazol (**49**) for nitrothiophene (**50**) gave analogues with much poorer antitrypanosomatid activity. [58] Using a slightly different approach, Pacheco *et al.* investigated the antileishmanial activity of 5-nitrofuran-2-nitrones (**51**) and 5-nitrothiophene-2-nitrones (**52**) that were inspired by nifurtimox (**37**) (Figure 2.13-2). These analogues showed promising antileishmanial activity against both promastigote and amastigote forms of *L. amazonensis* and *L. infantum*.[59]

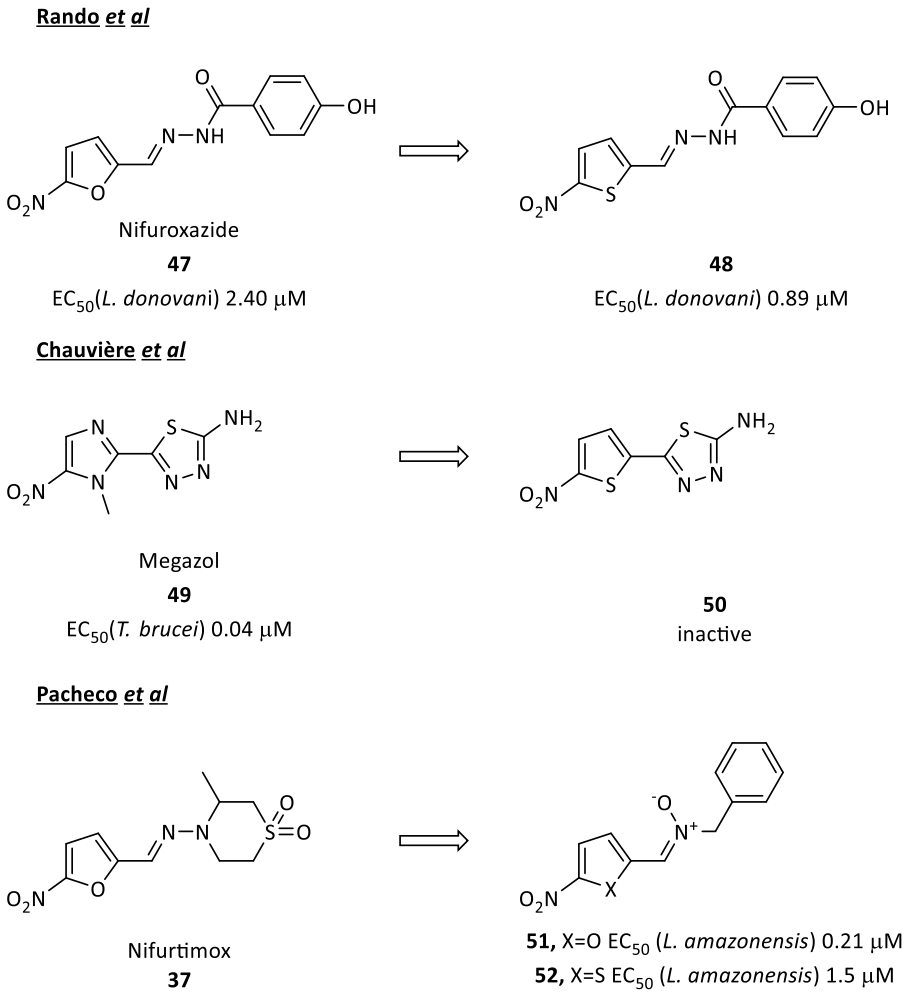

Figure 2.13-2 Literature examples of 5-nitrothiophene incorporation into currently existing drugs in an attempt to make more potent antitrypanosomal compounds.[57–59]

Drug discovery campaigns can also arise by adapting a natural product or a particular scaffold which is predicted to give a specific mode of action. Manda *et al.* incorporated a 5-nitrothiophene group onto a tetrahydro-β-carboline core (**53**), inspired by the high antileishmanial activity of β-carboline alkaloids such as harmane **54**. This led to a marginal improvement in antipromastigote activity compared to the original alkaloid.[60] A more successful attempt came from Romero *et al.* who incorporated furan (**55**), nitrofuran (**56**) and nitrothiophene (**57**) groups onto a quinazolinone core (**58**) in the hope of generating superoxide dismutase inhibitors. In this case, incorporation of the nitro group in both nitrothiophene (**57**) and nitrofuran (**56**) analogues introduced antileishmanial activity to this previously inactive scaffold. [61,62] A large body of research was carried out by the Foroumadi group based around 2-amino (**59**) and 2-thio-1,3,4-thiadiazoles (**60**), which showed

promising antileishmanial activity. These functionalities were combined with 5-nitrothiophene (**61-62**) and 5-nitrofuran (**63-64**) groups in attempt to improve activity further. [63–67] The most active 2-amino analogues were from the 5-nitrothiophene (**62**) series, which showed 5-fold more potent antileishmanial activity than the corresponding 5-nitrofuran (**64**).[67] Conversely, the 5-nitrofuran (**65**) series showed a marginal improvement in antileishmanial activity over the 5-nitrothiophenes (**66**) for 2-thiol analogues (Figure 2.13-3).[66]

Manda *et al.*

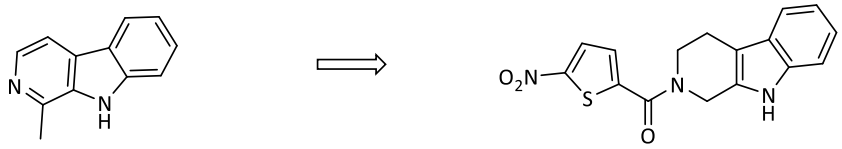

Harmane

54

EC_{50} (*L. donovani*) 19.2 μM

53

EC_{50} (*L. donovani*) 12 μM

Romero *et al.*

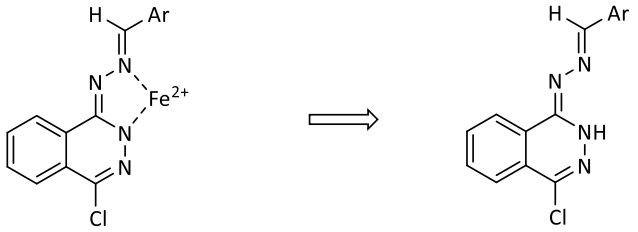

58

55, Ar = furan EC_{50}(*L. braziliensis*) > 20 μM

56, Ar = 5-nitrofuran EC_{50}(*L. braziliensis*) 0.12 μM

57, Ar = 5-nitrothiophene EC_{50}(*L. braziliensis*) 3.20 μM

Foroumadi group

Mina Behrouzi-fardmoghadam *et al.*

Tahghighi *et al.*

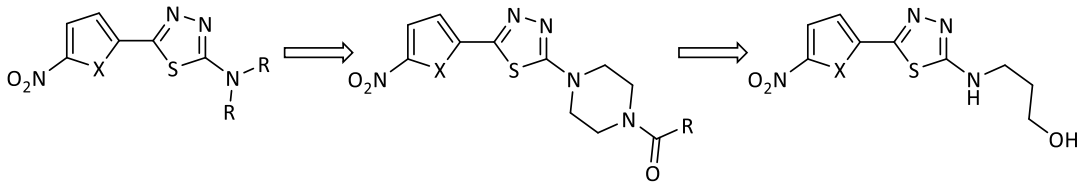

59

61, X=S EC_{50}(*L. major*) 23.8->50 μM

63, X=O EC_{50}(*L. major*) 10.7-26 μM

62, X=S EC_{50}(*L. major*) 3 μM

64, X=O EC_{50}(*L. major*) 18 μM

Alipour *et al.*

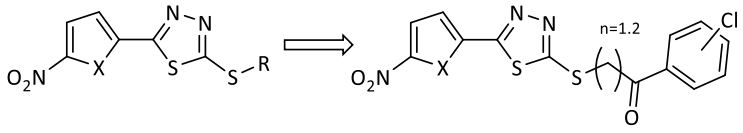

60

65, X=O EC_{50}(*L. major*) 1.1-1.8 μM

66, X=S EC_{50}(*L. major*) 1.3-2.6 μM

Sadat-Ebrahimi *et al.*

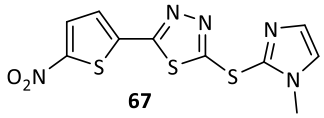

67

EC_{50}(*L. major)* 34 μM

Figure 2.13-3 Literature examples of 5-nitrothiophene incorporation onto scaffolds of interest.[60–63,65–67]

2.13.2 5-Nitrothiophene-2-carboxamides (5N2Cs)

Further analysis of the 14 LeishBox 5-nitrothiophenes revealed that all 14 analogues, including original hit **16**, contain the extended 5-nitrothiophene-2-carboxamide (5N2C) functionality. [46] The exploration of this functionality for the treatment of wider diseases (section 2.13.2.1) as well as a focussed discussion of its use to treat trypanosomatid disease (section 2.13.2.2) is presented below.

2.13.2.1 5N2Cs to treat wider diseases

5N2Cs have been relatively underexplored for the treatment of disease, with examples being mainly limited to antibacterials such as Nifurzide (**46**), which provide an alternative mode of action compared to classic antibiotics.[68] Hameed *et al.* showed that 5N2Cs (**68-70**) have potent activity against 75 clinical *E. coli* isolates and that nitroreductase bioactivation is essential for activity.[69] Further notable studies by Wang *et al.* and Samala *et al.* successfully incorporated 5N2C to capsaicin (**71**) to give derivatives **72-74**, and in a molecular hybridisation approach to give **75**. These studies provided drugs that were active against multi-resistant *S. aureus* and *M. tuberculosis* respectively (Figure 2.13-4). [70–72]

Hameed *et al.*

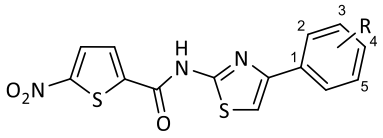

68, R= 2-F & 4-F, MIC (*E. coli* average) 2.5 μg mL^{-1}

69, R= 4-F, MIC (*E. coli* average) 1.25 μg mL^{-1}

70, R= 4-C & 5-OMe MIC (*E. coli* average) 5.0 μg mL^{-1}

Wang *et al.*

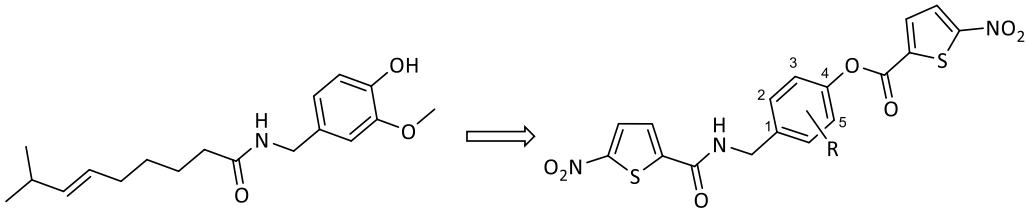

Capsaicin

71

MIC (*S. aureus*) 256 μg mL^{-1}

72, R=3-CH_3, MIC (*S. aureus*) 0.39-0.78 μg mL^{-1}

73, R=H, MIC (*S. aureus*) 0.78-1.56 μg mL^{-1}

74, R=3-Cl, MIC (*S. aureus*) 0.78-1.56 μg mL^{-1}

Samala *et al.*

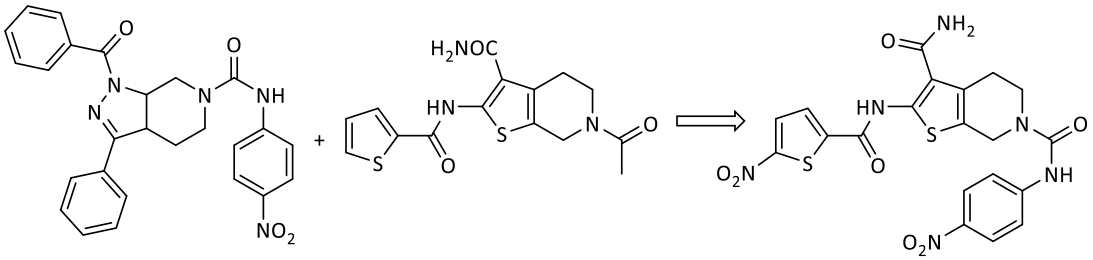

76
MIC (*M. tuberculosis*) 26.7 μM

77
MIC (*M. tuberculosis*) 9.15 μM

75
MIC (*M. tuberculosis*) 9.28 μM

Figure 2.13-4 Notable studies where 5N2C functionality has been introduced to generate antibacterial compounds active against *E. coli*, multi-resistant *S. aureus* and *M. tuberculosis*. [69–72]

2.13.2.2 5N2Cs to treat trypanosomatid disease

The untapped potential of the 5N2C functionality to treat trypanosomatid disease was reiterated by secondary screening of 188 LeishBox compounds against clinical isolates, lesion-derived amastigotes and bone marrow derived macrophages. [73,74] Lamotte *et al.* showed that only 5 LeishBox compounds retained activity against both *L. donovani* and *L. amazonensis* in this clinically relevant model. A comparison of their, strutcures revealed that 4 compounds contained a 5-nitrothiophene-2-

carboxamide (5N2C) moiety, outlining this as a structural motif of interest to treat leishmaniasis.[74]

Despite its prevalence in the LeishBox and promising activity in clinically relevant models, the 5N2C scaffold has received little attention for the treatment of trypanosomatid disease. [58–61] There are only limited examples of successful incorporation of 5N2Cs to give potent antitrypanosomatid compounds. Golden *et al.* showed that replacing 5-nitrofuran-2-carboxamide (**78**) with 5N2C (**79**) resulted in an 8-fold improvement in activity against *T. brucei*. [76–78] Similar improvements in activity were observed by Ogungbe *et al.* by substitution of the quinoline ring in rhodesain (**80**) for 5N2C (**81**) (Figure 2.13-5). [75,79]

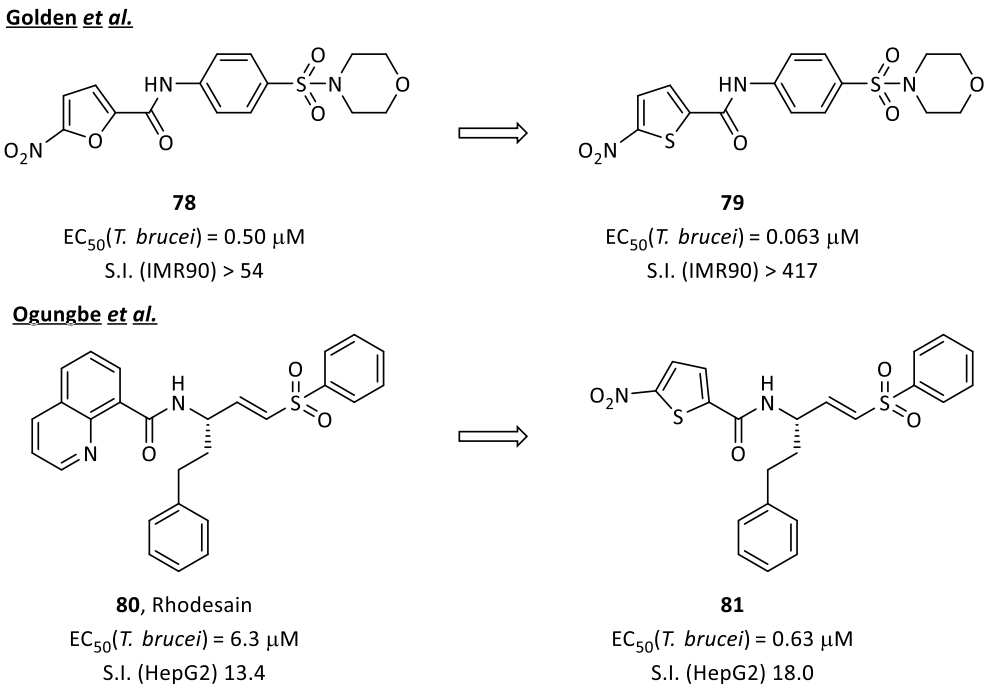

Figure 2.13-5 Literature examples by Golden *et al.* and Ogungbe *et al.* illustrating successful incorporation of the 5-nitrothiophene-2-carboxamide group to create more potent antitrypanosomal compounds. [75,77]

The high antitrypanosomatid activity of 5N2Cs and the ability to treat clinically relevant strains makes further exploration of this functionality of paramount importance in the attempt to find new antileishmanial drugs.

2.14 Toxicity issues

The original hit compounds **16** and **17** discussed in Chapter 1 have great potential for the treatment of trypanosomatid disease due to the promising antileishmanial properties of the 5N2C scaffold in the literature. However, the hits contain multiple functionalities typically avoided by the pharmaceutical industry. Toxicity concerns associated with the nitro, thiophene and 2-aminothiophene groups are discussed below.

2.14.1 Nitro group

Nitro containing drugs are classically avoided by the pharmaceutical industry due to potential side effects including carcinogenicity, neurotoxicity, hepatotoxicity, mutagenicity and bone-marrow suppression.[80,81] These side effects often arise due to unwanted bioactivation in the host by microsomal reductases, and as such nitro-containing molecules are often removed from screening programmes as structural alerts.[82,83] This caution is not without reason, as multiple nitro-containing drugs have been removed from the market due to severe adverse side effects. Tolcapone (**82**) was a marketed drug approved in 1998 for the treatment of Parkinson disease. However, it was withdrawn due to several cases of acute liver injury and at least three deaths from acute liver failure.[84] Nimesulide (**83**), a non-steroidal anti-inflammatory drug and nitrefazole (**84**), an alcohol sensitiser, were both also withdrawn due to serious liver damage and fatalities (Figure 2.14-1).[85,86]

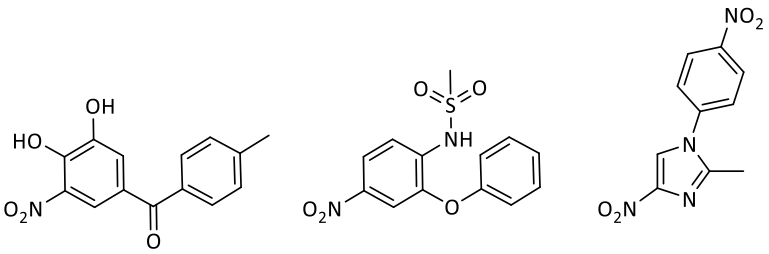

Tolcapone **82** Nimesulide **83** Nitrefazole **84**

Figure 2.14-1 Nitro containing drugs withdrawn from the market due to associated toxicity issues.

However, the presence of a nitro group does not necessarily result in toxic side effects. Often, the nitro group is essential for a drugs mode of action, as is the case

for many bactericidal and antitrypanosomatid drugs. In summary, the presence of a nitro group in a new potential drug does not necessarily mean that it is not worth pursuing, however it is important to thoroughly assess any potential toxic effects before progression towards animal or human studies.

2.14.2 Thiophene

Thiophene may also be considered a structural alert in drug discovery campaigns due to its metabolism by cytochrome P450s in the liver to highly reactive thiophene epoxide and S-oxides.[87,88] For example, tienilic acid (**85**), used for the treatment of hypertension, and suprofen (**86**), a non-steroidal anti-inflammatory drug, were both withdrawn due to hepatotoxicity (Figure 2.14-2).[89,90]

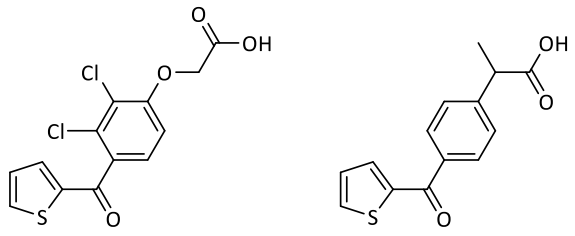

Figure 2.14-2 Thiophene containing drugs withdrawn from the market due to toxicity issues.

However, thiophene remains an essential constituent of many drugs and multiple alternative metabolic pathways can detoxify thiophene containing drugs and not lead to detrimental side effects.[87] Furthermore, the substitution pattern of thiophene containing drugs can alter their potential for reactive metabolite formation. For example, Hu *et al.* showed that 2,5-diamino thiophenes are bioactivated by rat and human liver microsomes to reactive metabolites, whereas 2-amino or 2,4-diamino thiophenes did not form these reactive metabolites.[91]

2.14.3 2-Aminothiophene

2-Aminothiophenes are known pan-assay interference compounds (PAINS) and are often removed from screening libraries due to their promiscuity.[92] This promiscuity presents a concern for possible host toxicity through multiple mechanisms. Nevertheless, 2-aminothiophenes have been incorporated extensively in medicinal

chemistry, ranging from anticancer to antiparasitic compounds. Efforts should be made to avoid 2-aminothiophene functionality in new drug discovery programmes where possible. However, compounds that rely on this functionality for activity should not be immediately disregarded as there are numerous examples showing the successful incorporation of this functionality in marketed drugs.

2.2 Revised project aims

The original hits **16** and **17** show promising antileishmanial activity but are limited by poor aqueous solubility and bioavailability. Furthermore, the presence of groups associated with host toxicity, in addition to the unknown mode of action of the hits, remained a concern. As such, the aims of the project were redefined as follows:

- To explore removing areas of toxicity concern including the nitro group, left hand thiophene and 2-amino thiophene PAINS motif (section 2.31);
- To explore chemical space to improve antileishmanial activity and identify areas where hit structures can be manipulated (section 2.322.32);
- To improve aqueous solubility (section 2.33);
- To ensure broad spectrum antileishmanial activity (section 2.34);
- To explore the mode of action of the hits and any synthesised analogues (Chapter 3).

2.3 Results and discussion

2.31 Removing areas of toxicity concerns

In Chapter 1, the original hits **16** and **17** and simple analogues **34-36** were investigated as potential antileishmanial compounds. As discussed in the previous section, the two hits contain multiple structural motifs that are potential toxicity issues. Therefore, initial attempts were made to explore the 5-nitrothiophene ring and the 2-amino thiophene group (Figure 2.31-1). [93]

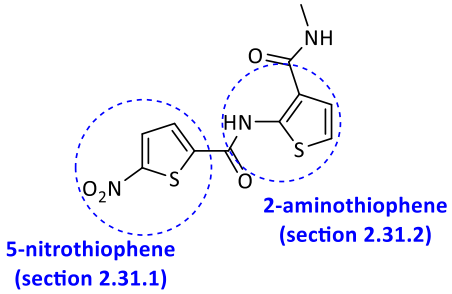

Figure 2.31-1 Structural elements of the original hits of concern due to associated toxicity connotations.

2.31.1 Removing the 5-nitrothiophene group

2.31.1.1 Removing the nitro group

A series of analogues was generated in which the nitro group was replaced with hydrogen (**107**), bromine (**108**) and amine (**120**) functionalities. These and multiple analogues were synthesised using an analogous synthetic route to original hit **17**. Where the relevant acid chloride was not commercially available, it was synthesised from the acid using oxalyl chloride. This was followed by simple amide coupling to give various analogues **107-119** (Scheme 2.31.1, Route i). The successful synthesis of these analogues was validated by the presence of the characteristic signal for the central amide by proton NMR (δ_H 12.66-13.60 ppm). Amine **120** was synthesised by H_2/Pd reduction of the nitro group of original hit **17** (Scheme 2.31.1, Route ii), as characterised by the molecular ion peak in LC-MS (282.2 $[M+H]^+$).

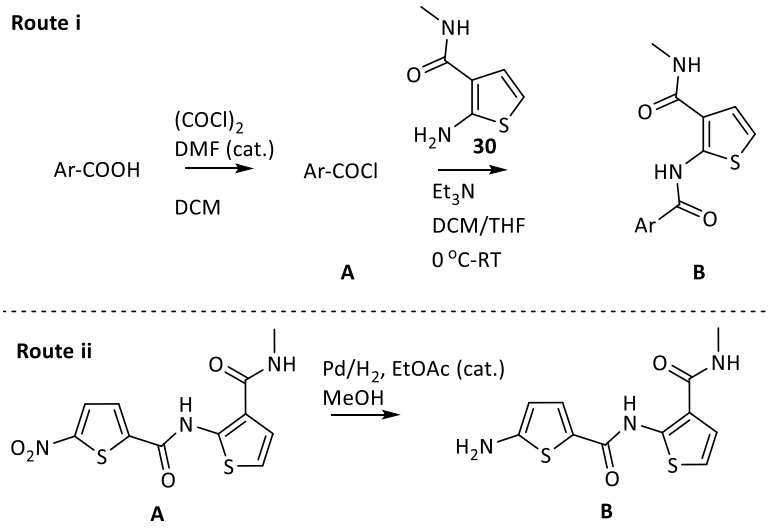

Route	Ar-	ArCOOH ID	Intermediate (A) ID (yield %)	Product (B) ID (yield %)
i	Thiophene-2-	-	**94**	**107** (40 %)
	5-Bromothiophene-2-	**87**	**95** (99 %)	**108** (23 %)
	5-Nitrofuran-2-	**88**	**96** (100 %)	**109** (10 %)
	4-Nitrophenyl-2-CF_3-	**89**	**97** (100 %)	**110** (65 %)
	Thiazole-2-	**90**	**98** (ND)	**111** (21 %)
	Thiazole-5-	**91**	**99** (ND)	**112** (30 %)
	Thiazole-4-	**92**	**100** (ND)	**113** (38 %)
	2,1,3-Benzoxadiazole-5-	**93**	**101** (100 %)	**114** (20 %)
	Phenyl-	-	**102**	**115** (20 %)
	Pyridyl-4-	-	**103**	**116** (26 %)
	Pyridyl-3-	-	**104**	**117** (10 %)
	4-Nitrophenyl-1-	-	**105**	**118** (3 %)
	3-Nitrophenyl-1-	-	**106**	**119** (9 %)
ii	-	-	**17** (32 %)*	**120** (42 %)

Scheme 2.31.1 Synthetic routes towards derivatives (**107-120**) where the 5-nitrothiophene group was changed. *overall yield for synthesis of starting material **17**. ND = not determined, intermediate moved immediately on.

Analysis of each analogue against *L. major* promastigotes revealed that replacing the nitro group with hydrogen (**107**), bromine (**108**) or an amine (**120**) resulted in a complete loss of antileishmanial activity (EC_{50} (*L. major*) >100 μM). Following this observation, attempts were made to replace the 5-nitrothiophene ring with various other aromatic substituents including phenyl (**115**), pyridyl (**116-117**), thiazole (**111-113**) and benzoxadiazole (**114**) (Scheme 2.31.1). Analogously to the thiophene series, introduction of these alternative aromatic rings lacking a nitro group also failed to

give potent antileishmanial compounds (EC_{50} (*L. major*) 33 to >100 μM). This suggests that the nitro group is essential for antileishmanial activity, and that any possible *in cellulo* reduction of the nitro group to an amine does not lead to toxic effects.

2.31.1.2 Replacing the nitrothiophene ring

Having identified the need for the nitro group, it was of interest to survey the requirements of the left-hand (hetero)aromatic ring. Consequently, analogues were synthesised in which the heterocycle was replaced with other aromatics that retained a nitro group. The 4- and 3-nitro phenyl analogues (**118-119**) were synthesised as above (Scheme 2.31.1). However, neither analogue showed any antileishmanial activity (EC_{50} (*L. major*) >100 μM). Introduction of an additional electron withdrawing trifluoromethyl group (**110**) improved antileishmanial activity (EC_{50} (*L. major*) 16.6 ± 0.2 μM), however this was still less effective than hits **16** and **17**. The increase in activity upon addition of an electron withdrawing group suggests that the electronics of the left-hand ring may be critical for antileishmanial activity. However, the lower activity of **110** compared to hits **16** and **17** indicates that a 5-membered nitro heterocycle is optimal for antileishmanial activity.

However, it was still of interest to attempt to replace the thiophene ring due to its associated toxicity issues. [87,88,94] Subsequently, attempts were made to replace the 5-nitrothiophene ring with a 2-nitrothiazole group (**125**). Literature precedent for the synthesis of thiazoles with two electron withdrawing groups is limited. However, one account by Woelk *et al.* reported the successful synthesis of 2-nitrothiazole-2-carboxylic acid (**122**) from 2-aminothiazole-5-carboxylic acid (**121**) using sodium nitrite, tetrafluoroboric acid and copper. [95] This synthesis was successfully replicated as proved by a molecular ion in the LC-MS trace (m/z 173.1 $[M-H]^-$). However, all attempts to convert **122** to the acid chloride resulted in substitution of the nitro group with chlorine (**123**), which was reacted with amine **30** to give chlorothiazole analogue **124**. Similarly, attempts to react **122** with amine **30** using EDCl/HOBt also failed to give any desired product (Scheme 2.31.2A). Attempts to reverse the order of the synthesis were then explored. However, although Boc protection on the amino group of 2-aminothiazole-5-carboxylic acid (**121**) successfully gave **126**, proved by the

presence of a 9-proton Boc group singlet in the proton NMR spectrum (δ_H 1.49 ppm), further conversion to the acid chloride (**127**) was unsuccessful (Scheme 2.31.2B). Due to these challenges, attempts to synthesise the nitrothiazole derivative (**125**) were abandoned.

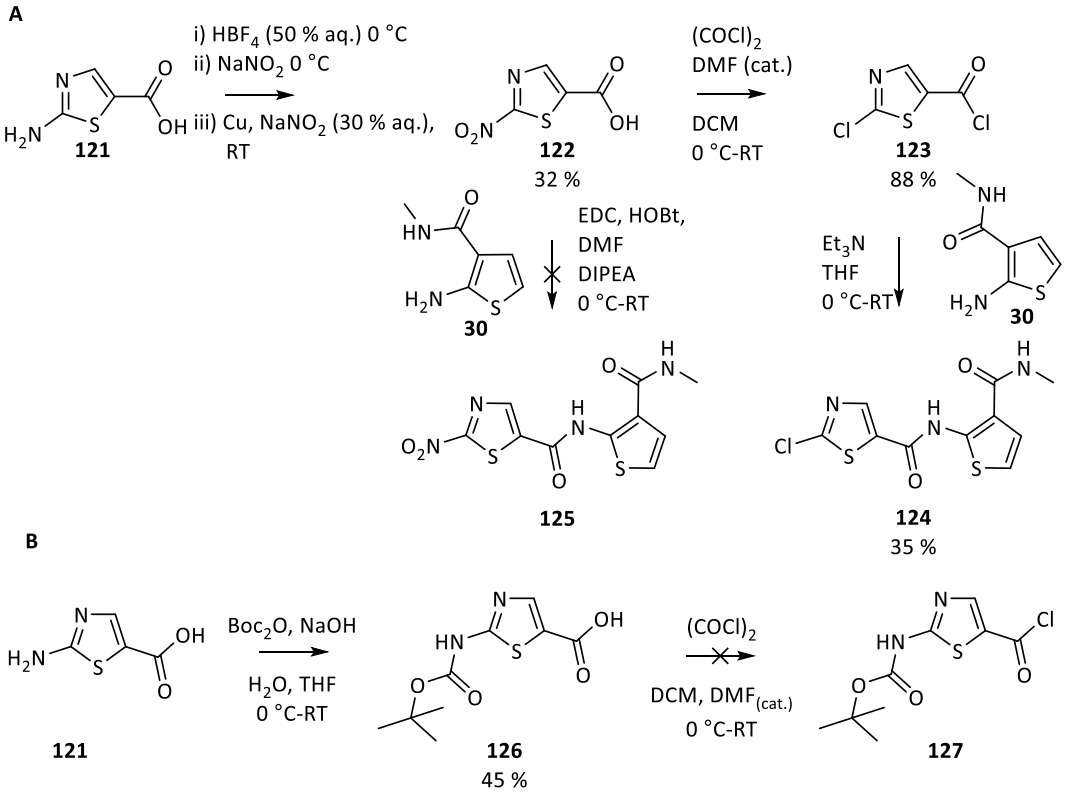

Scheme 2.31.2 A. Synthetic route towards **124** formed instead of desired nitrothiazole product (**125**). B. Further attempts to access the desired Boc protected acid chloride (**127**) failed.

Undeterred by the lack of successful synthesis of the 2-nitrothiazole derivative (**125**), attempts were made to substitute the 5-nitrothiophene for a 5-nitrofuran (**109**). Synthesis of **109** was achieved according to Scheme 2.31.1. Following successful synthesis, antipromastigote dose-response experiments showed that the 5-nitrofuran ring is well tolerated, with no loss of antileishmanial activity (EC_{50} (*L. major*) 0.37 ± 0.009 µM) compared to the hits.

With **109** available, it was of interest to determine its mammalian cell toxicity. Unfortunately, significant mammalian cell toxicity was observed (CC_{50} (HepG2) 2.0 ± 0.2 µM) rendering this derivative unsuitable for progression. It is widely reported that nitrofuran containing compounds can act as substrates for human aldehyde

dehydrogenase 2 (ALDH2) in the liver, resulting in toxicity issues. [96] To test whether this contributes to the observed toxicity of **109**, HepG2 cells were incubated with the ALDH2 inhibitor daidzin and dose-response analyses were carried out. A 5-fold decrease in HepG2 toxicity was observed for **109** when administered with daidzin, which shows that HepG2 toxicity is caused by ALDH2 activity for **109** (Figure 2.31-2). Nifurtimox (**37**) is a 5-nitrofuran drug that was used as a negative control due to its low HepG2 toxicity. No significant difference in HepG2 toxicity was observed for nifurtimox (**37**) when administered with daidzin, which suggests that ALDH2 activity is not responsible for any toxicity observed in this case.

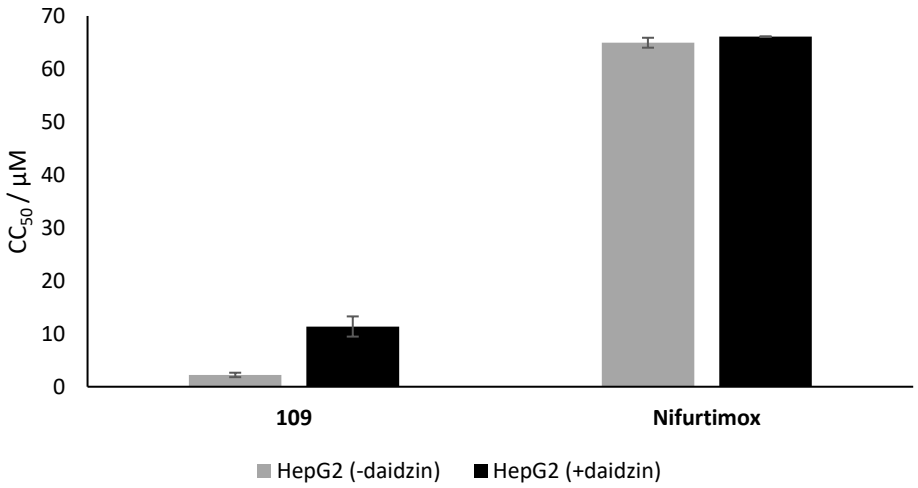

Figure 2.31-2 HepG2 toxicity in the presence or absence of the ALDH2 inhibitor daidzin shows that toxicity is caused by ALDH2 activity for 5-nitrofuran **109** but not nifurtimox (**37**). HepG2 toxicity is reported as the mean of three repeats, with errors representing standard error.

2.31.1.3 Conclusions

In conclusion, removing the nitro group and/or incorporation of 6-membered aromatics resulted in complete loss of antileishmanial activity. This suggested that the left-hand ring is better left as a 5-nitrothiophene to maintain antileishmanial activity (Figure 2.31-3). 5-Nitrofuran (**109**) retained antileishmanial activity but showed significant HepG2 toxicity. It is unknown whether this trend extends further to other 5-membered heteroaromatics as synthesis was either unsuccessful (e.g. thiazole (**125**)) or not attempted (e.g. oxazole). Overall, no benefit could be found by replacing the 5-nitrothiophene from the original hits. Although concerns surrounding

the toxicity associated with this functionality remained, reassurance came from the observation that many current trypanosomatid drugs, such as nifurtimox (**37**), benznidazole (**38**) and fexinidazole (**39**), contain nitro groups. Subsequently, investigation into the 5N2C series continued whilst retaining the 'essential' 5-nitrothiophene group.

A

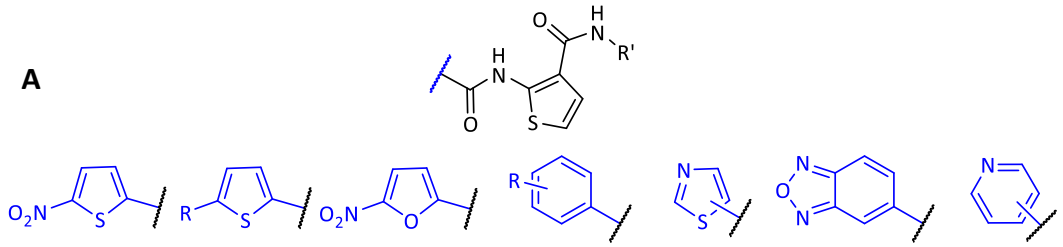

R'=
H (**16**)
Me (**17**)

R' = Me
R=
H (**107**)
Br (**108**)
NH_2 (**120**)

R' = Me (**109**)

R' = Me
R=
2-CF_3-4-NO_2 (**110**)
H (**115**)
4-NO_2 (**118**)
3-NO_2 (**119**)

R' = Me
Position=
-2 (**111**)
-5 (**112**)
-4 (**113**)
-5 2-chloro (**124**)

R' = Me (**114**)

R' = Me
R=
-4 (**116**)
-3 (**117**)

B

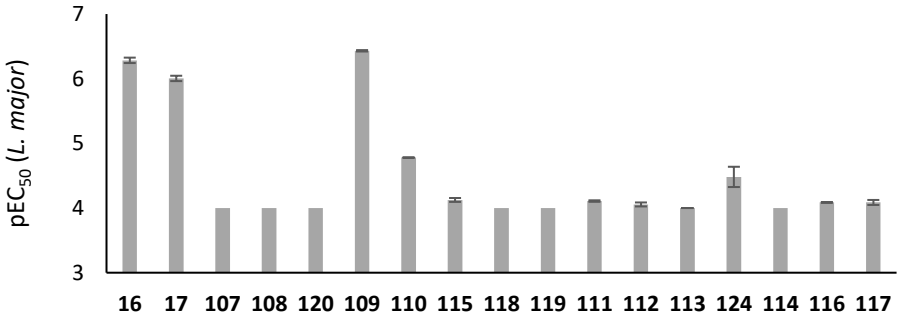

C

Compound	EC_{50} (*L. major*) / µM	CC_{50} (HepG2) / µM
16	0.52 ± 0.05	24 ± 1
17	0.99 ± 0.09	96 ± 4
107	>100	-
108	>100	-
120	>100	-
109	0.37 ± 0.009	2.0 ± 0.2
110	16.6 ± 0.2	-
115	75 ± 5	-
118	>100	-
119	>100	-
111	78 ± 2	-
112	88 ± 6	-
113	>100	-
124	33 ± 10	-
114	>100	-
116	82 ± 1	-
117	82 ± 7	-

Figure 2.31-3 A. Structures of altered 5-nitrothiophene series. B. Bar chart displaying the structural effects of altering the 5-nitrothiophene ring on the antileishmanial activity of the compounds. The only tolerated change is to a 5-nitrofuran (**109**). C. Table of EC_{50} and CC_{50} values against *L. major* and HepG2 cells for altered 5-nitrothiophene series. Antileishmanial activity and HepG2 toxicity reported as a mean of three biological repeats, with errors representing standard error.

2.31.2 Removal of the 2-aminothiophene PAINS motif

Following the unsuccessful removal of the 5-nitrothiophene ring from the original hits in section 2.31.1, attention turned to the other regions of toxicity concerns. 2-Aminothiophene is a known PAIN and compounds containing it may be expected to exhibit undesired polypharmacology within the host.[93] Therefore, it was desirable to remove this moiety to avoid any potential associated toxicity issues.

2.31.2.1 Cyclopentane series

Initially, it was of interest to investigate whether an isosteric aliphatic cyclopentane substituent would be tolerated in place of the right-hand thiophene. This would increase sp^3 character and potentially improve on the poor aqueous solubility observed for the original hits. Synthesis of the cyclopentane series began with enamine (**129**) formation on the 1,3-dicarbonyl starting material **128** followed by reduction using sodium cyanoborohydride.[97,98] The resulting amine **130** was coupled with 5-nitrothiophene-2-carboxylic acid (**22**) using EDCl/HOBt to give esters **131** and **132** which were separated by column chromatography. The esters were subsequently hydrolysed using LiOH to give acids **133** and **134**. Only the anti-diastereomer, **133**, was isolated in sufficient quantities to carry out the final PyBOP catalysed amide formation with methylamine to give **135** (Scheme 2.31.3).

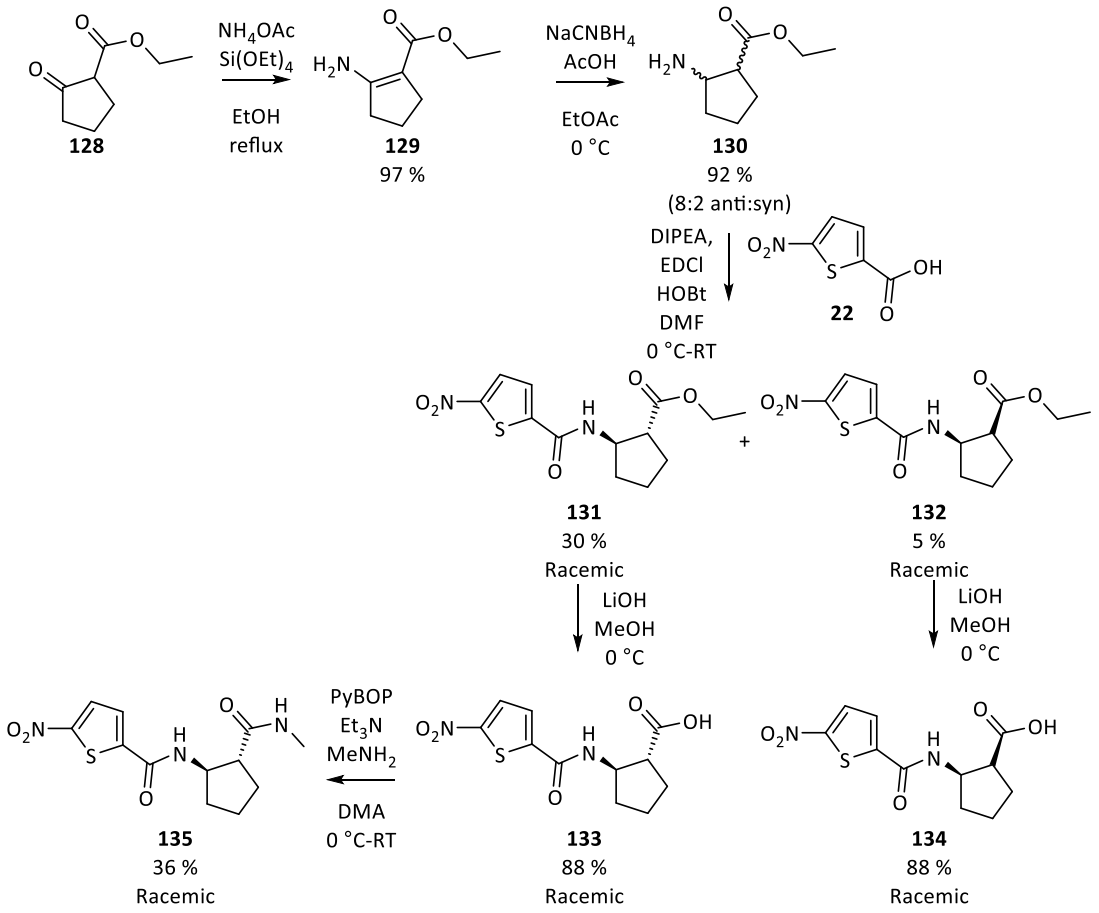

Scheme 2.31.3 Synthetic route towards cyclopentane derivatives. [97,98]

In the case of compound **135**, the characteristic central amide proton peak is shifted significantly upfield in the proton NMR (δ_H 8.84 ppm) compared to bisthiophene hits **16** and **17** due to the lack of delocalisation into the right-hand ring. Confirmation of the desired structure was obtained from analysis of the proton NMR spectrum which revealed the presence of a doublet with an integral of 3 protons (δ_H 2.25 ppm), caused by the pendant amide CH_3 group.

Upon testing compound **135** and various intermediates (**131-134**) for antipromastigote activity against *L. major* it became clear that the sp^3 rich cyclopentane ring is not tolerated in this position. Compound **135** has 20-fold lower antileishmanial activity than hit **17**. In addition, little difference in antileishmanial activity was observed between syn- and anti- conformations for the ester and acid

derivatives (**131-134**). In summary, an aliphatic cyclopentane ring is not tolerated as a replacement of the right-hand thiophene ring (Figure 2.31-4).

A

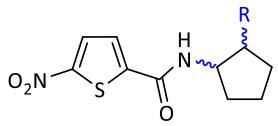

R = COOEt (anti) (**131**) COOEt (syn) (**132**) | R = COOH (anti) (**133**) COOH (syn) (**134**) | R = CONHMe (anti) (**135**)

B

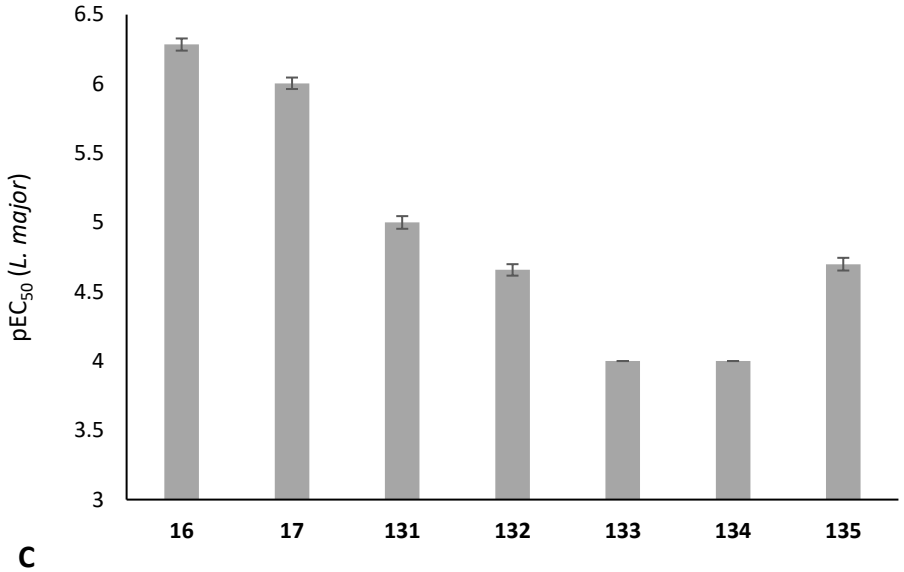

C

Compound	16	17	131	132	133	134	135
EC_{50} (*L. major*) / µM	0.52 ± 0.05	0.99 ± 0.09	10 ± 1	22 ± 2	>100	>100	20 ± 2

Figure 2.31-4 A. Structures of the cyclopentane ring series. B. Barchart displaying the effect of structural changes to the cyclopentane ring on antileishmanial activity. C. EC_{50} values for the original hits (**16** and **17**), cyclopentane esters (**131** and **132**), cyclopentane acids (**133** and **134**) and cyclopentane amide (**135**) against *L. major* promastigotes. Antileishmanial activity is reported as the mean of three repeats, with errors representing standard error.

Following the lack of observed activity for cyclopentane derivatives **131**-**135**, it became of interest to introduce a cyclopentene ring in the same position. This would enable delocalisation of the central amide into the pendant electron withdrawing group whilst maintaining the higher sp^3 character of the molecule compared to the original hits. Cyclopentene derivative **136** was synthesised by reaction of

cyclopentene intermediate **129** with 5-nitrothiophene-2-carbonyl chloride (**23**) (Scheme 2.31.4). The characteristic central amide proton for **136** is shifted significantly downfield in the proton NMR (δ_H 11.49 ppm) when compared to cyclopentanes **131-135**, consistent with the proposed increase in delocalisation.

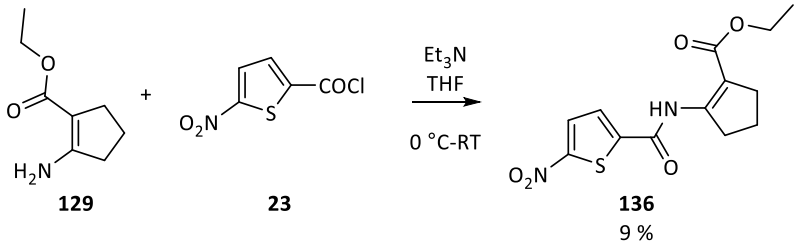

Scheme 2.31.4 Synthesis of cyclopentene derivative **136**.

Antileishmanial activity was retained for **136** compared to the original hits (EC_{50}(*L. major*) 0.46 ± 0.03 μM), suggesting that the delocalisation of the central amide into the pendant electron withdrawing group is important for activity. However, high HepG2 toxicity (CC_{50}(HepG2) 2.9 ± 0.4 μM) limited the further progression of this compound.

2.31.2.2 Phenyl series

Upon concluding that the delocalisation of the central amide into the pendant group is important for antileishmanial activity in section 2.31.2.1, attempts were made to substitute the right hand thiophene for a phenyl ring. The synthesis of the primary and methyl amide phenyl analogues (**140** and **141**) was achieved by direct amide coupling of commercially sourced anthranilamide (**139**) with 5-nitrothiophene-2-carbonyl chloride (**23**) to give **140** in an analogous route to hit **17**. Anthranilamide **138** was prepared by a simple ring opening of isatoic anhydride (**137**) using methylamine, before coupling with **23** to give product **141** (Scheme 2.31.5). Proof of synthesis of phenyl analogues **140** and **141** came from the presence of the characteristic central amide proton (δ_H 13.37 and 13.11 ppm respectively) in an analogous manner to the bisthiophenes discussed in section 1.41.

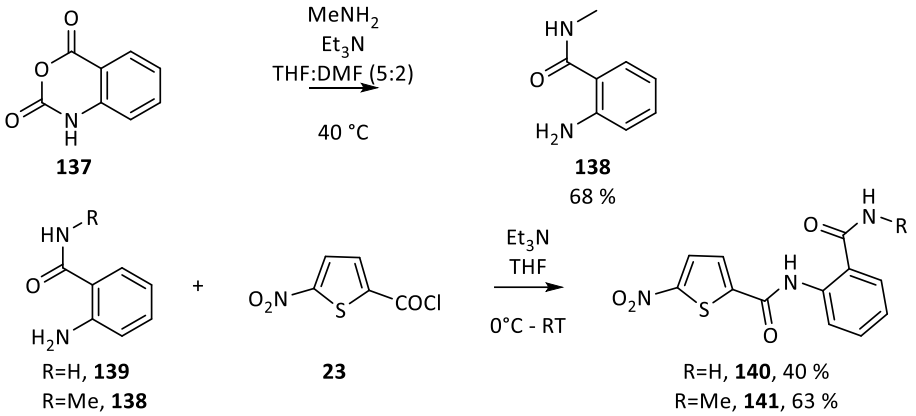

Scheme 2.31.5 Synthetic route to access phenyl analogues **140** and **141**.

On testing against *L. major* promastigotes, phenyl analogues **140** and **141** proved to be equipotent to the two original hits (Figure 2.31-5A). Whilst both compounds retained antileishmanial activity, this was challenged by significant HepG2 toxicity (Figure 2.31-5B). However, in contrast to the thiophene series it was speculated that the ease of analogue synthesis and ability to explore chemical space based on the phenyl ring could enable analogues to be generated with improved HepG2 toxicity.

A

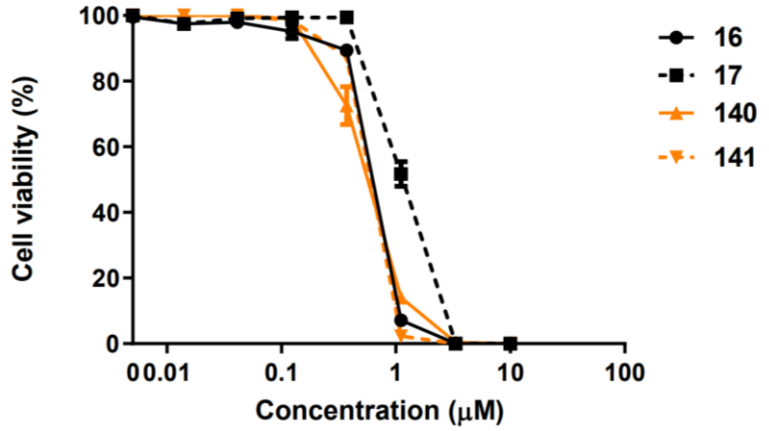

B

Compound	16	17	140	141
EC_{50}(*L. major*) / μM	0.52 ± 0.05	0.99 ± 0.09	0.47 ± 0.04	0.65 ± 0.05
CC_{50} (HepG2) / μM	24 ± 1	96 ± 4	4.7 ± 0.5	5.0 ± 0.6

Figure 2.31-5 A. Dose-response curve for *L. major* promastigotes treated with the original hit compounds and phenyl analogues. B. EC_{50} values for original hit compounds (**16** and **17**) and phenyl analogues (**140** and **141**) against *L. major* promastigotes. Antileishmanial activity and HepG2 toxicity are reported as the mean of three repeats, with errors representing standard error.

2.31.2.3 Conclusions

In conclusion, the right-hand thiophene cannot be exchanged for an aliphatic cyclopentane ring. Although reintroducing a double bond to give cyclopentene derivative **136** showed promising antileishmanial activity, it also showed significant toxicity to HepG2 cells. Introduction of a phenyl ring in exchange for the right-hand thiophene gave two equipotent compounds **140** and **141**, also with significant HepG2 toxicity (Figure 2.31-6). However, the potent activity and synthetic tractability of the phenyl series suggested that further exploration was possible, to find compounds with improved antileishmanial activity and low HepG2 toxicity. Work towards this goal is discussed in the following section.

A

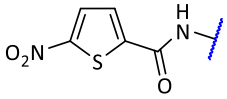

R=
H (**16**)
CH_3 (**17**)

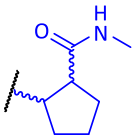

135 (anti, racemic)

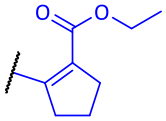

136

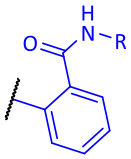

R=
H (**140**)
CH_3 (**141**)

B

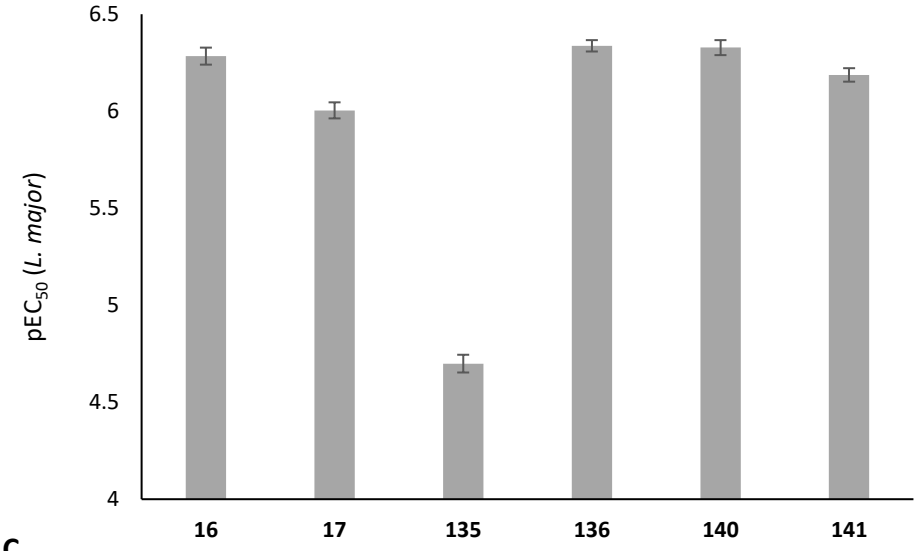

C

Compound	16	17	135	136	140	141
EC_{50} (*L. major*) / µM	0.52 ± 0.05	0.99 ± 0.09	20 ± 2	0.46 ± 0.03	0.47 ± 0.04	0.65 ± 0.05
CC_{50} (HepG2) / µM	24 ± 1	96 ± 4	-	2.9 ± 0.4	4.7 ± 0.5	5.0 ± 0.6

Figure 2.31-6 A. Structures of altered right hand ring series. B. Bar chart displaying the structural effects of altering the right-hand ring on the antileishmanial activity of the compounds. Change to a phenyl (**140-141**) or cyclopentene (**136**) is tolerated. C. Table of EC_{50} values against *L. major* for altered right hand ring series. Antileishmanial activity and HepG2 toxicity are reported as the mean of three repeats, with errors representing standard error.

2.32 Exploring right-hand ring substituents

As discussed in the previous section, it was of interest to explore the chemical space around the phenyl ring of analogue **141** to both enhance activity and reintroduce selectivity over HepG2 cells. This would be explored by changing the nature of the pendant amide group and adding substituents around the ring (Figure 2.32-1).

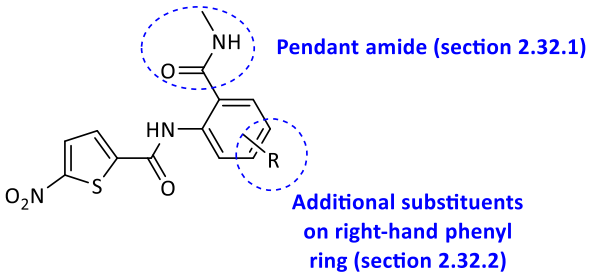

Figure 2.32-1 Regions of interest to explore around the right-hand ring to improve antileishmanial activity and reduce mammalian cell toxicity.

2.32.1 C-2 pendant substituents on right-hand phenyl ring

The pendant amide in the original hits could be exchanged for esters without loss of antileishmanial activity or selectivity (section 1.41). Subsequently, it was of interest to explore the importance of this group for the phenyl series. Investigation began by incorporating an acid as a key intermediate to generate C-2 substituted analogues. Acid analogue **143** was synthesised by the amide coupling of anthranilic acid (**142**) with 5-nitrothiophene-2-carbonyl chloride (**23**) (Scheme 2.32.1A). However, this only resulted in low yields of the desired acid (**143**), with an alternative cyclic byproduct (**144**), as confirmed by X-ray crystallography, also being isolated in small quantities (Scheme 2.32.1B). Acid **143** showed poor antipromastigote activity analogous to that observed for cyclopentane acid analogues **133** and **134** (section 2.31.2.1). This suggests that the negative charge present in acid analogues at physiological pH is detrimental to antileishmanial activity. Interestingly, byproduct **144** shares equipotent activity with acid **143**, suggesting that the two structures may be interconvertible under biological conditions (Figure 2.32-2).

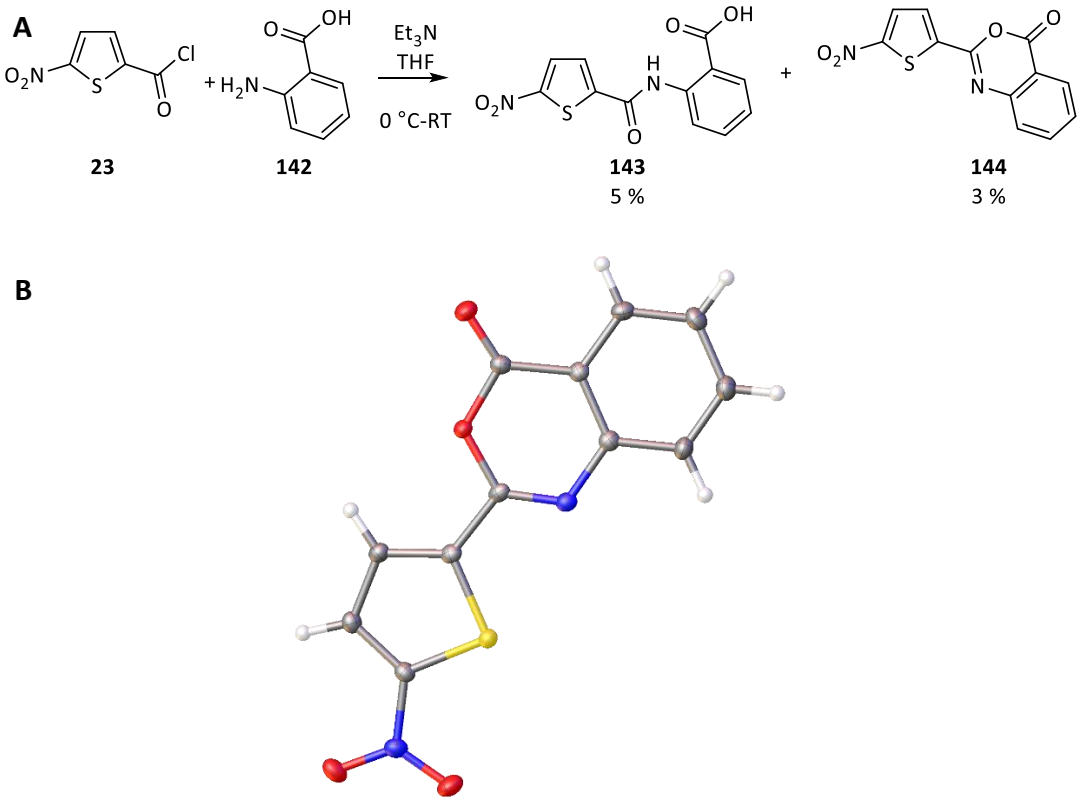

Scheme 2.32.1 A. Synthetic route towards acid derivative **143** resulting in byproduct **144** formation. B. Crystal structure verifying the structure of byproduct **144**.

In summary, the synthetic difficulties surrounding **143** suggested that alternative routes would be necessary to access different C-2 functionalised analogues.

A series of analogues were successfully synthesised by amide coupling of commercially available anilines with 5-nitrothiophene-2-carbonyl chloride (**23**), akin to phenyl analogue **140** (Scheme 2.32.2, Route i, **155-162**). Where the aniline was not commercially available, synthesis was achieved by reacting the relevant aliphatic amine with isatoic anhydride (**137**) before amide coupling (Scheme 2.32.2, Route ii, **163**) or by utilising byproduct **144** to react with the relevant aliphatic amines (Scheme 2.32.2 Route iii, **164-165**).

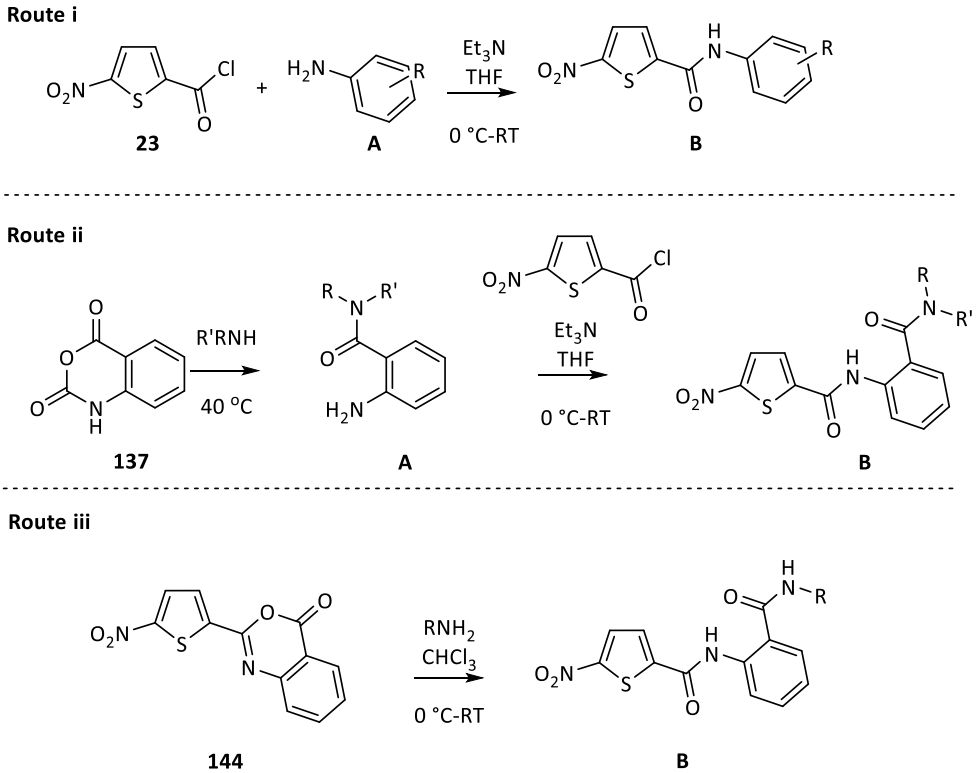

Route	R	R’	ID of A (yield %)	Product ID (B) (yield %)
i	2-$CONH_2$	-	**145**	**140** (40 %)
	3-CONHMe	-	**146**	**155** (62 %)
	2-H	-	**147**	**156** (15 %)
	2-OMe	-	**148**	**157** (15 %)
	3-OMe	-	**149**	**158** (9 %)
	4-OMe	-	**150**	**159** (13 %)
	2-CF_3	-	**151**	**160** (41 %)
	3-CF_3	-	**152**	**161** (94 %)
	2-$COCH_3$	-	**153**	**162** (62 %)
ii	CH_3	H	**138** (68 %)	**141** (63 %)
	CH_3	CH_3	**154** (99 %)	**163** (24 %)
iii	$CH_3(CH_2)_{12}$	-	-	**164** (82 %)
	iPr	-	-	**165** (100 %)

Scheme 2.32.2 Synthetic routes towards phenyl analogues involving simple amide coupling of commercially available anthranilamides (route i), synthesis of anthranilamides from isatoic anhydride (**137**) and amide coupling (route ii) or derivatisation from intermediate **144** (route iii).

Firstly, it was of interest to discover whether the pendant primary or methyl amide was important for antileishmanial activity. Simply replacing this group with hydrogen (**156**) led to a 7-fold drop in antileishmanial activity compared to **141**. Similarly,

substitution for more bulky amide substituents, including isopropyl amide (**165**), dimethyl amide (**163**) or long aliphatic chain (C_{13}) amide (**164**), led to a similar decrease in antileishmanial activity (Figure 2.32-2).

Secondly, the importance of the position of the pendant amide group was investigated. Moving the pendant amide group to the 3-position (**155**) removed the possibility for delocalisation into the pendant group. This led to a 5-fold drop in antileishmanial activity compared to phenyl analogue **141** (Figure 2.32-2).

Thirdly, the importance of the nature of the pendant amide was investigated. Replacing the pendant amide group with electron donating 2-, 3- or 4- methoxy groups (**157-159**) led to a decrease in antileishmanial activity. Replacement with an electron withdrawing 2- or 3- CF_3 substituent (**160-161**) led to a 5- to 13-fold decrease in activity compared to **141** (Figure 2.32-2).

A

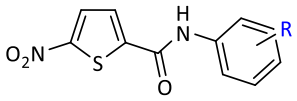

R = 2-$CONH_2$ (**140**) 2-CONHMe (**141**) | R = 2-COOH (**143**) 3-CONHMe (**155**) | R = 2-H (**156**) | R = 2-OMe (**157**) 3-OMe (**158**) 4-OMe (**159**) | R = 2-CF_3 (**160**) 3-CF_3 (**161**) | R = 2-$COCH_3$ (**162**) | R = 2-$CONMe_2$ (**163**) 2-$CONH(CH_2)_{12}CH_3$ (**164**) 2-$CONH^iPr$ (**165**)

B

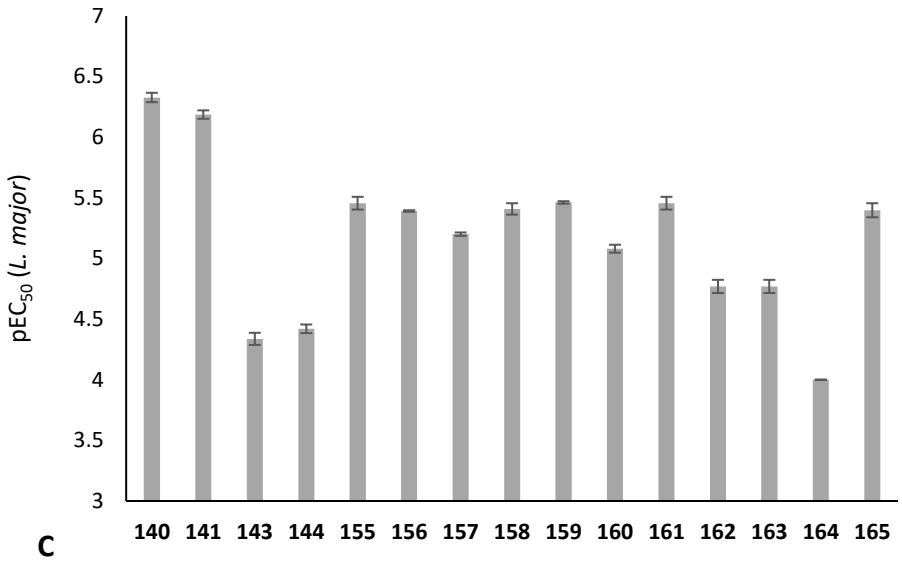

C

Compound	EC_{50} (*L. major*) / µM
140	0.47 ± 0.04
141	0.65 ± 0.05
143	46 ± 5
144	38 ± 3
155	3.5 ± 0.4
156	4.06 ± 0.06
157	6.3 ± 0.2
158	3.9 ± 0.4
159	3.45 ± 0.08
160	8.3 ± 0.6
161	3.5 ± 0.4
162	17 ± 2
163	17 ± 2
164	>100
165	4.0 ± 0.5

Figure 2.32-2 A. Structures of the altered right hand ring series. B. Barchart displaying structural changes to the right-hand ring and the effect on antileishmanial activity. C. EC_{50} values for phenyl derivatives (**140** and **141**), derivatives with no C-2 amide (**155-162**) and derivatives with bulky C-2 amide (**163-165**) against *L. major* promastigotes. Antileishmanial activity is reported as the mean of three repeats, with errors representing standard error.

2.32.1.1 Conclusions

In conclusion, no benefit could be found by replacing or moving the C-2 amide group present in phenyl analogue **141**. Subsequently, all further analogues were generated whilst retaining this amide.

2.32.2 Additional substituents on right-hand phenyl ring

Having identified the C-2 amide as activity enhancing it was of interest to explore chemical space around the remainder of the right-hand phenyl ring whilst retaining the C-2 pendant amide. Initial approaches for functionalisation around the right-hand aromatic ring involved a series of analogues with methyl or methoxy substituents at the 3-, 4- or 5- positions (**193-197**). The relevant anthranilamides were synthesised by a triphosgene mediated cyclisation of the anthranilic acid followed by a methylamine ring opening. The substituted final products were then made by an amide coupling with 5-nitrothiophene-2-carbonyl chloride (**23**) in an analogous manner to that described above (Scheme 2.32.3). As before, each desired analogue was confirmed by the central amide signal in the proton NMR (δ_H 10.39-13.70 ppm).

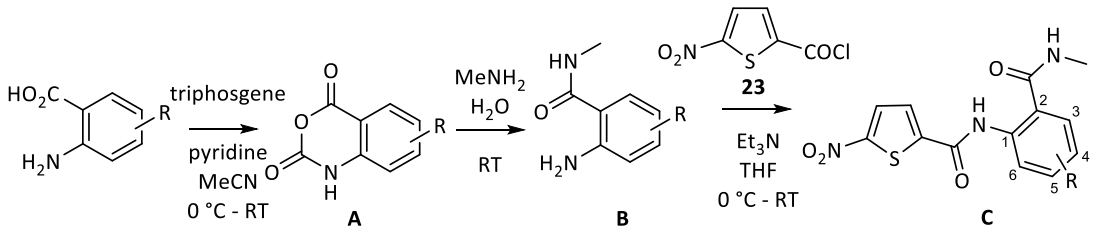

R	Starting material	Intermediate ID (A or B) (yield %)		Product ID (C) (yield %)
		A	B	
3-Me	**166**	**175** (63 %)	**184** (10 %)	**193** (34 %)
4-OMe	**167**	**176** (54 %)	**185** (42 %)	**194** (68 %)
4-Me	**168**	**177** (90 %)	**186** (46 %)	**195** (70 %)
5-OMe	**169**	**178** (54 %)	**187** (63 %)	**196** (57 %)
5-Me	**170**	**179** (85 %)	**188** (54 %)	**197** (64 %)
5-CF_3	**171**	**180** (44 %)	**189** (65 %)	**198** (18 %)
5-Br	**172**	**181** (80 %)	**190** (68 %)	**199** (23 %)
6-OMe	**173**	**182** (94 %)	**191** (50 %)	-
6-Me	**174**	**183** (85 %)	**192** (57 %)	-

Scheme 2.32.3 Synthetic route towards substituted analogues **193-199**.

Attempts to synthesise the 6-substituent resulted in cyclisation of the final product to give **200** and **201** as shown in Scheme 2.32.4.

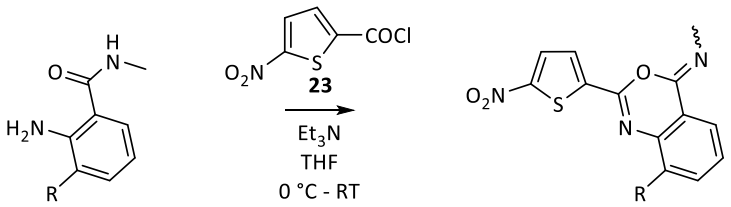

R =
OMe (**191**)
Me (**192**)

R =
OMe (**200**), 8 %
Me (**201**), 12 %

Scheme 2.32.4 Alternative product (**200-201**) formed when 6-substituted amino 2-benzamides are reacted with 5-nitrothiophene-2-carbonyl chloride (**23**).

Pleasingly, the addition of a 5- substituent (**196** and **197**) resulted in a 2-fold improvement in antileishmanial activity. However, addition of a 3- (**193**) or 4- (**194** and **195**) substituent decreased antileishmanial activity by between 5- and 50-fold compared to non-substituted analogue **141** (Figure 2.32-3).

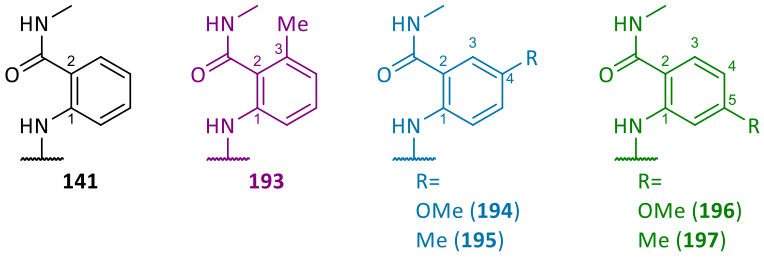

141 **193**

R=
OMe (**194**)
Me (**195**)

R=
OMe (**196**)
Me (**197**)

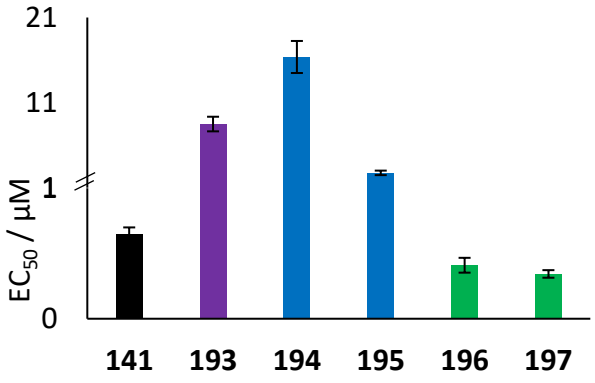

Figure 2.32-3 EC_{50} values against *L. major* promastigotes for substituted phenyl series **(193-197**) in comparison to unsubstituted phenyl analogue **141**. Antileishmanial activity is reported as the mean of three repeats, with errors representing standard error.

In contrast to unsubstituted phenyl analogue **141**, both 5-substituted compounds **196** and **197** showed low HepG2 toxicity (Figure 2.32-4). The high antipromastigote activity and low HepG2 toxicity observed for 5-substituted phenyl analogues **196** and **197** warranted further investigation into this position. 5-Trifluoromethyl and 5-bromo analogues (**198** and **199**) were synthesised using the same synthetic strategy outline in Scheme 2.32.3. Both trifluoromethyl (**198**) and bromo (**199**) 5-substituted analogues retained decent antileishmanial activity. However, significant HepG2 toxicity was observed for both (Figure 2.32-4).

A

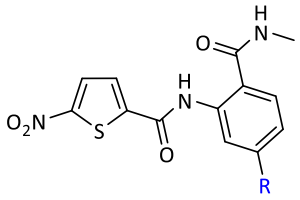

R = H (**141**) R = OMe (**196**) Me (**197**) R = CF_3 (**198**) Br (**199**)

B

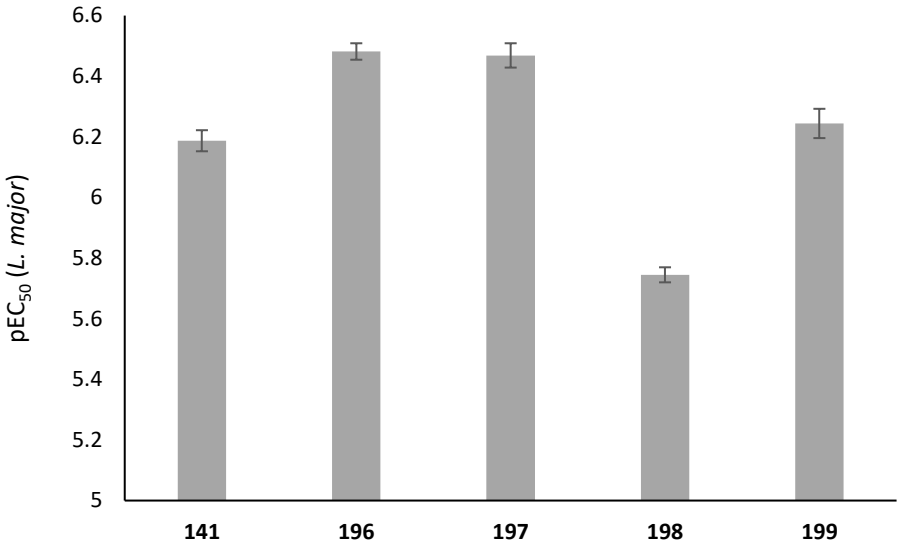

C

Compound	141	196	197	198	199
EC_{50} (*L. major*) / µM	0.65 ± 0.05	0.33 ± 0.02	0.34 ± 0.03	1.8 ± 0.1	0.57 ± 0.06
CC_{50} (HepG2) / µM	5.0 ± 0.6	>100	31 ± 4	13 ± 3	7.2 ± 0.5

Figure 2.32-4 A. Structures of the 5- substituted phenyl series. B. Bar chart displaying the effect of structural changes to the 5- substituent on the phenyl ring on antileishmanial activity. C. EC_{50} values for the phenyl analogue (**141**) and 5-substituted analogues (**196**-**199**) against *L. major* promastigotes. Antileishmanial activity and HepG2 toxicity are reported as the mean of three repeats, with errors representing standard error.

2.32.2.1 Conclusions

In summary, adding a 5-OMe or 5-Me substituent to the phenyl series gives highly potent and selective antileishmanial lead compounds (**196** and **197**) (Figure 2.32-5).

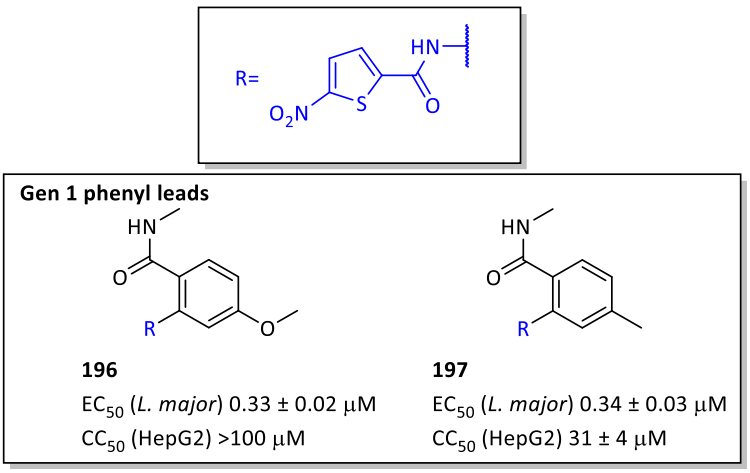

Figure 2.32-5 Generation 1 phenyl series lead compounds that show high antileishmanial activity and low mammalian cell toxicity. Antileishmanial activity and HepG2 toxicity are reported as the mean of three repeats, with errors representing standard error.

2.32.3 Conclusions

In conclusion, the 5-nitrothiophene group in the original hits is important to retain high antileishmanial activity and low HepG2 toxicity. In the previous chapter, ester derivatives **34** and **35** showed potent antileishmanial activity and low HepG2 toxicity and as such can be identified as generation 1 lead compounds (Figure 2.32-6). The right hand 2-aminothiophene PAINS motif can be exchanged for an aniline derivative whilst retaining antileishmanial activity (**140** and **141**), however HepG2 toxicity is observed. The pendant amide on the right-hand phenyl ring is important for potent antileishmanial activity, however introduction of a 5-OMe or 5-Me substituent (**196** and **197**) whilst retaining this group results in a 2-fold improvement in antileishmanial activity. Furthermore, **196** and **197** show low HepG2 toxicity and as such are promising generation 1 lead compounds. Analogue **196** is especially interesting as it provides a handle to add more complex substituents to explore chemical space further and improve antileishmanial activity and physicochemical properties. In total, four new generation 1 lead compounds have been identified that show improved or equipotent antileishmanial activity and high selectivity over HepG2 cells (Figure 2.32-6).

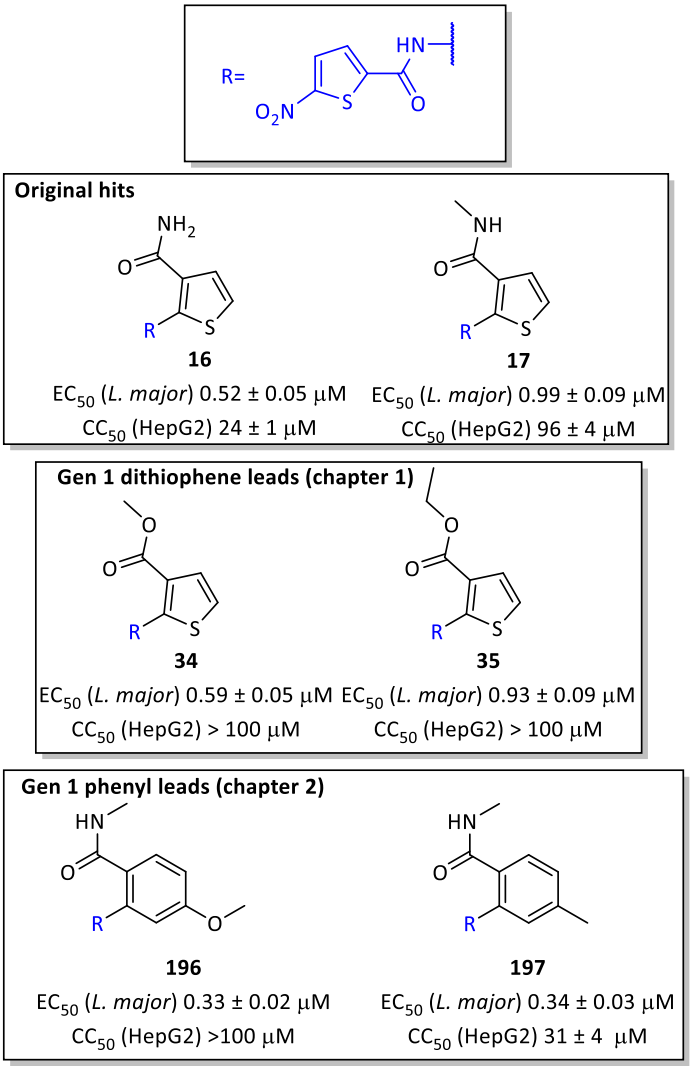

Figure 2.32-6 Generation 1 lead compounds that show high antileishmanial activity and low mammalian cell toxicity. Antileishmanial activity and HepG2 toxicity are reported as the mean of three repeats, with errors representing standard error.

2.33 Improving aqueous solubility

One of the major issues with the original hit compounds is their lack of aqueous solubility, as discussed in Chapter 1. Four new potential lead compounds were identified throughout previous sections which showed promising antileishmanial activity and low mammalian cell toxicity (Figure 2.32-6). However, none of these active and selective compounds showed an improvement in aqueous solubility compared to the original hits, with solubility in PBS (pH 7.4) being less than the detection limit in all cases (Figure 2.33-1). As a result, none of the first generation of lead compounds were suitable as potential new antileishmanial compounds.

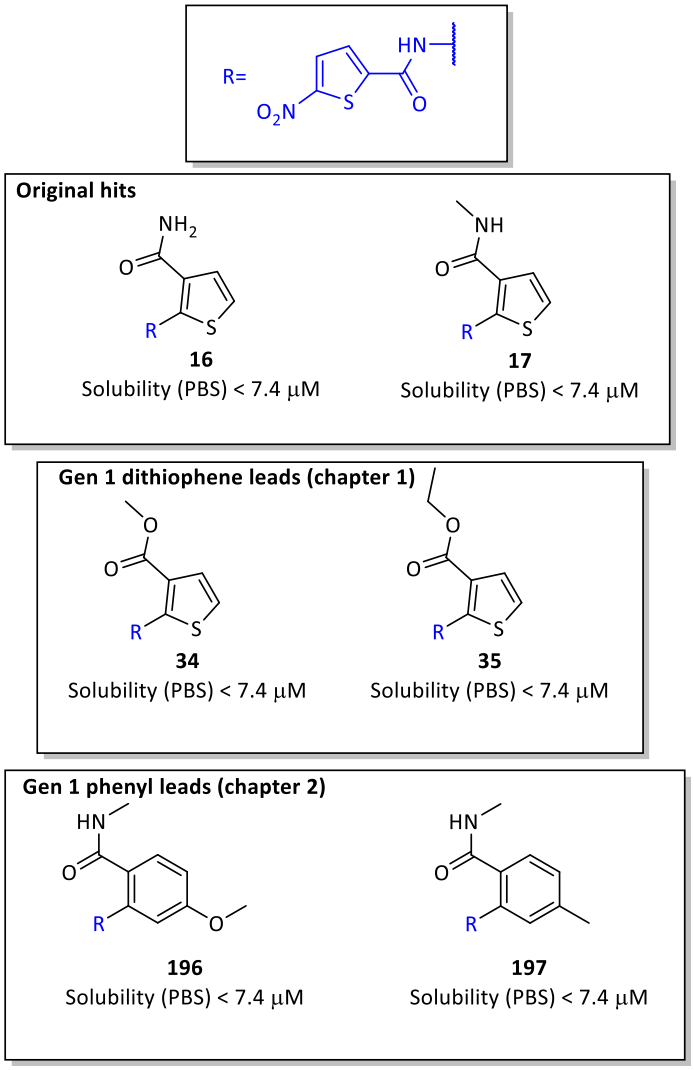

Figure 2.33-1 Generation 1 lead compounds that showed good antileishmanial activity and low mammalian cell toxicity have poor aqueous solubility. Solubility is reported as the mean of three repeats, with errors representing standard error.

2.33.1 Aqueous solubility in FBS supplemented PBS and biorelevant media

The high antileishmanial activity of the generation 1 lead analogues proved difficult to rationalise considering their lack of aqueous solubility. Literature precedent suggested that the improvement in solubility observed in the dose-response assays could be attributed to the fetal bovine serum (FBS) in the media, specifically the serum protein content; including bovine serum albumin (BSA) and lipoproteins.[99–101] Subsequently, the aqueous solubility of the generation 1 analogues was assessed in PBS supplemented with 15 % FBS to simulate media conditions. All solubility experiments were carried out in an analogous way to the PBS solubility experiments described previously. In each case, solubility was drastically improved in PBS supplemented FBS in agreement with the literature precedent (Figure 2.33-2).

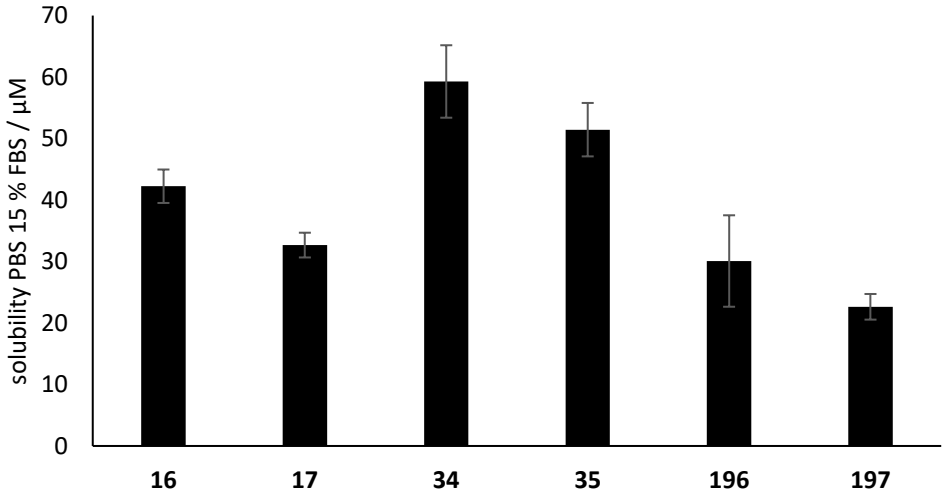

	16	17	34	35	196	197
Solubility PBS (pH 7.4) / µM	< 7.4	< 7.4	< 7.4	< 7.4	< 7.4	< 7.4
Solubility PBS 15 % FBS / µM	42 ± 3	33 ± 2	59 ± 6	51 ± 4	30 ± 7	23 ± 2

Figure 2.33-2 Solubility of generation 1 lead compounds in PBS supplemented with 15 % FBS. Solubilities are reported as the mean of three repeats, with errors representing standard error.

Following the improvement in solubility observed in PBS supplemented with FBS, the solubility of the original hits and generation 1 lead compounds was assessed in biorelevant buffers. Biorelevant buffers (Table 2.33-1) simulate biological conditions in the intestinal fluid upon feeding (FESSIF) and fasting (FASSIF) and gastrointestinal

fluid upon fasting (FASSGF). As such, biorelevant buffers can be used in conjunction with aqueous solubility to predict how well an oral drug may behave *in vivo*.

Table 2.33-1 Composition of biorelevant buffers FESSIF, FASSIF and FASSGF.[102]

	FASSIF	FESSIF	FASSGF
pH	6.5	5.0	1.6
Taurocholate / mM	3	15	0.08
Phospholipids / mM	0.75	3.75	0.02
Sodium / mM	148	319	34
Chloride / mM	106	203	59
Phosphate / mM	29	-	-
Acetic acid / mM	-	144	-

The solubility of the four generation 1 lead compounds and two original hits was first assessed in FESSIF. Each compound showed significantly enhanced solubility in FESSIF compared to PBS. The solubility of the two original hits (**16** and **17**) was also assessed in FASSIF and FASSGF. Solubility decreased at least 2-fold in FASSIF and 10-fold in FASSGF compared to FESSIF (Figure 2.33-3). Not only does FESSIF have a lower pH than FASSIF (pH 5.0 vs pH 6.5), but it also has higher concentrations of bile salts (taurocholate) and phospholipids (Table 2.33-1). Original hits **16** and **17** show significantly poorer solubility at low pH (e.g. in FASSGF) and as such, the improvement in solubility in FESSIF vs FASSIF was predicted to be due to the higher bile salt (taurocholate) and phospholipid content in FESSIF. [103]

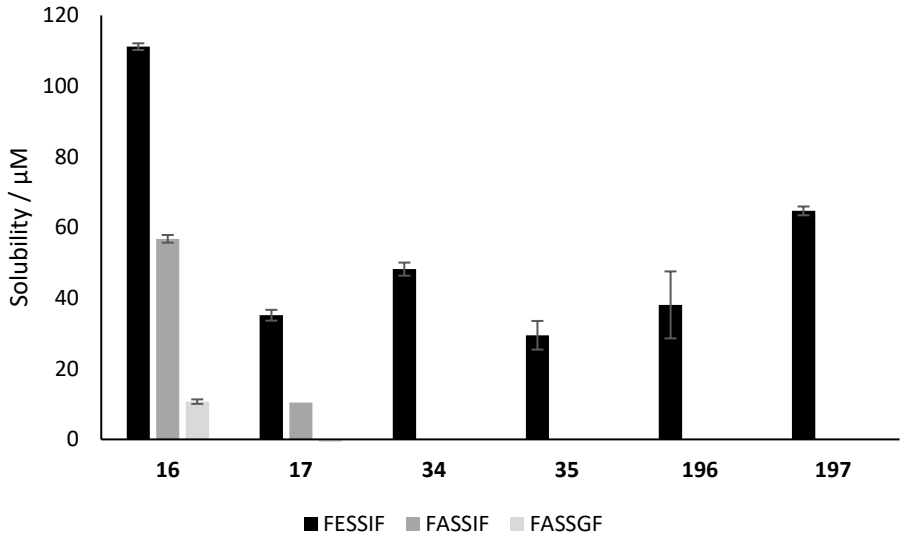

		16	17	34	35	196	197
Solubility / µM	**FESSIF**	111 ± 2	35.1 ± 0.9	48 ± 2	29 ± 2	38 ± 4	65 ± 9
	FASSIF	57 ± 2	10 ± 1	ND	ND	ND	ND
	FASSGF	10.6 ± 0.3	< 7.4	ND	ND	ND	ND

Figure 2.33-3 Solubility of generation 1 lead compounds in biorelevant buffers (FESSIF, FASSIF and FASSGF). Solubilities are reported as the mean of three repeats, with errors representing standard error. ND means not determined.

To investigate whether bile salts cause the improvement in hit solubility, the two original hits (**16** and **17**) were assessed in PBS spiked with 15 mM sodium taurocholate (**202**). An improvement in solubility was observed for both hits compared to PBS (Figure 2.33-4). Sodium taurocholate (**202**) forms micelles at 15 mM which, taken alongside its surfactant properties, may improve solubility by forming favourable interactions with the hit compounds and disrupting the crystal packing.[103]

A

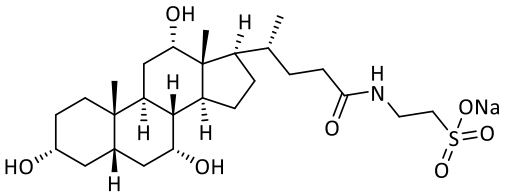

Sodium taurocholate (**202**)

B

	Solubility / µM	
Compound	**PBS**	**15 mM sodium taurocholate in PBS**
16	<7.4	107 ± 6
17	<7.4	22.1 ± 0.7

Figure 2.33-4 A. Structure of sodium taurocholate. B. Solubility of the two original hit compounds (**16** and **17**) in PBS compared to PBS spiked with sodium taurocholate (**202**). Solubilities are reported as the mean of three repeats, with errors representing standard error.

The improvement in aqueous solubility of the generation 1 lead compounds in PBS supplemented with FBS and FESSIF helped to rationalise their high antileishmanial activity. However, the low aqueous solubility in PBS remained a major concern as it suggested that there may be difficulties in administering the drug.

2.33.2 Investigating structural changes to improve aqueous solubility (generation 2)

Given the challenges remaining for the generation 1 lead compounds, efforts turned to a second generation of analogues. These analogues were designed and synthesised in a direct attempt to improve aqueous solubility, whilst retaining good antileishmanial activity and low mammalian cell toxicity.

Firstly, it was noted that the lack of aqueous solubility of the original hits could be attributed to the rigidity and planarity of the hit structures. Previous attempts to introduce flexibility by introducing a cyclopentane ring (**131-135**) failed to retain antileishmanial activity (section 2.31.2.1). It was suggested that the main cause of this lack of solubility was the intramolecular hydrogen bond which forms a 6-membered ring in the original hits. This was confirmed by a single crystal X-ray structure of original hit **17** which showed the presence of this hydrogen bond (see footnote[3]) and the tight packing of monomer units (Figure 2.33-5).

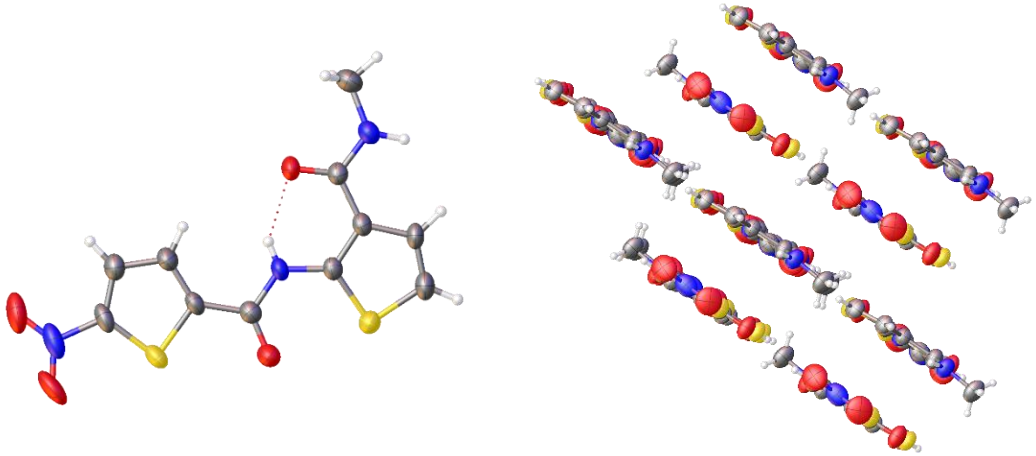

Figure 2.33-5 Crystal structures of hit **17** (space group P_{-1}) showing intramolecular hydrogen bonding resulting in planarity (see footnote[1]).

As efforts to remove the intramolecular hydrogen bonding by changing the nature of the carbonyl containing pendant group failed to give potent antileishmanial compounds (section 2.32.1), alternative approaches were needed. Firstly, efforts focussed on changing the nature of the central amide (section 2.33.2.1) and secondly,

[3] Crystals and crystal structure of **17** was obtained by members of the Ashwini Nangia group at the University of Hyderabad, India.

alternative substituents were added to the 5-position on the right-hand phenyl ring (section 2.33.2.2).

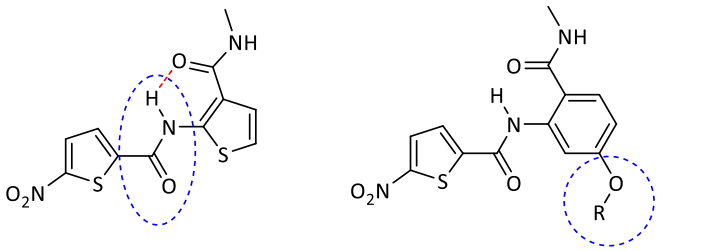

Figure 2.33-6 Areas of interest to change to improve aqueous solubility of the 5N2C series.

2.33.2.1 Changing the central amide to improve aqueous solubility

It was postulated that the lack of solubility for the compounds tested to date could be attributed to the rigidity and planarity afforded by the 6-membered intramolecular hydrogen bond observed in the crystal structure of **17** (Figure 2.33-5). Consequently, attempts were made to disrupt this hydrogen bonding by changing the nature of the central amide.

Firstly, a methyl group was introduced to replace the central amide proton to give compound **206**. Synthesis of **206** was achieved by hydrolysis of methyl-2-aminothiophene-3-carboxylate (**31**) to the acid followed by cyclisation with triphosgene.[104] The resulting thienooxazine-2,4-dione (**203**) was methylated using methyl iodide to give **204** before ring opening with methylamine to give the secondary amine intermediate **205**. Amide coupling with 5-nitrothiophene-2-carbonyl chloride (**23**) yielded the desired product **206** (Scheme 2.33.1). Successful synthesis was proved by the loss of the secondary amine proton signal from precursor **205** (δ_H 7.90 ppm) and the presence of the 3-proton singlet (δ_H 3.45 ppm) in the proton NMR corresponding to the central amide methyl group of **206**.

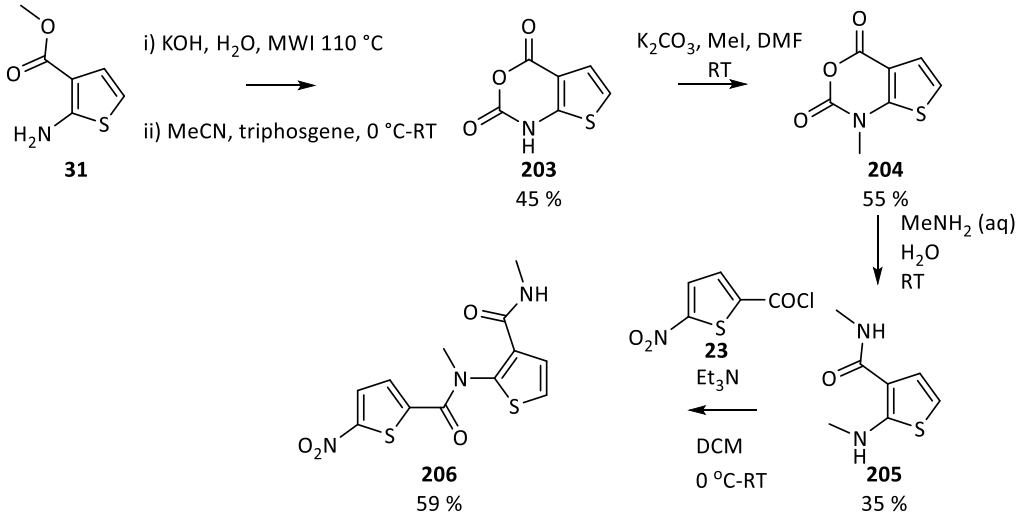

Scheme 2.33.1 Synthetic route towards methylated central amide analogue **206**.

As predicted, incorporation of a methyl group into the central amide broke up the intramolecular hydrogen bonding and resulted in an alternative folded geometry, as

verified by the crystal structure (Figure 2.33-7, see footnote[4]). This altered geometry led to a drastic improvement in aqueous solubility for **206** compared to the original hits (solubility (PBS) 190 ± 20 µM).

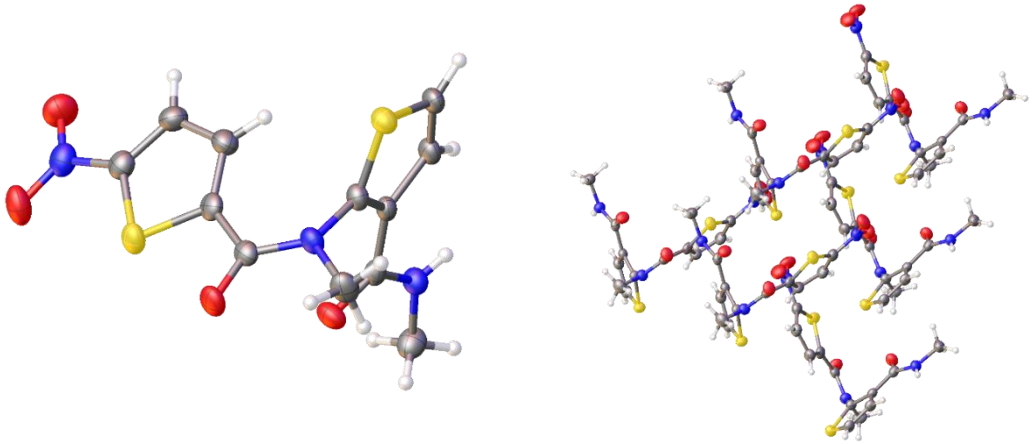

Figure 2.33-7 Crystal structures of methyl capped analogue **206** showing loss of intramolecular hydrogen bonding and an alternative folded geometry (see footnote[2]).

However, introduction of a methyl cap on the central amide (**206**) resulted in an approximately 10-fold loss in antileishmanial activity compared to the original hits (Figure 2.33-7). This suggests that the rigidity caused by the intramolecular hydrogen bonding holds the hit compounds in a favoured geometry for their mode of action.

Undeterred by the loss of activity for **206**, other changes to the central amide were explored to improve compound flexibility and solubility. A tetrahydroquinoline group (**208**) was introduced to increase sp^3 character whilst tethering the central amide to the right-hand aromatic ring. Synthesis was achieved by simple amide coupling of 1,2,3,4-tetrahydroquinoline (**207**) with 5-nitrothiophene-2-carbonyl chloride (**23**) in analogy with the synthesis of compound **17** (Scheme 2.33.2), proved by the molecular ion signal in LC-MS (*m/z* 289.2 $[M+H]^+$). Aqueous solubility was improved for **208** compared to the original hits, however, this was again accompanied by a 10-fold loss in antileishmanial activity (Figure 2.33-8). Following this, a methylene linker was added between the central amide and right-hand ring to give **210** in an analogous

[4] Crystals and crystal structure for **206** was obtained by Ronnie Ragbirsingh in the Michael Hall group at Newcastle University.

route to **208** and **17** (Scheme 2.33.2). A comparable increase in PBS solubility was observed, accompanied with a 20-fold drop in antileishmanial activity (Figure 2.33-8).

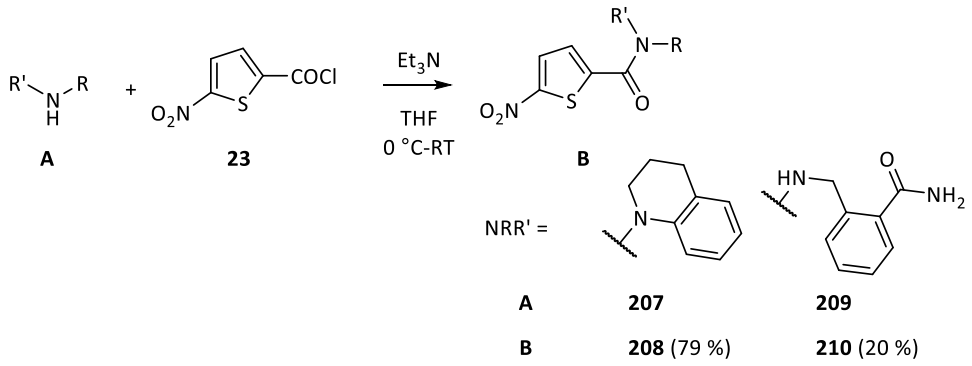

Scheme 2.33.2 Synthetic route towards CH_2 extended linker (**210**) and tetrahydroquinoline (**208**) analogues.

Following the observation that the introduction of flexibility to the central amide through compounds **206**, **208,** and **210** led to a decrease in antileishmanial activity, an alternative approach was adopted. The central amide of hit **2** was replaced with an imine (**212**) to maintain rigidity but introduce a new geometry due to a possible alternative hydrogen bond. Synthesis of **212** was achieved by reacting amine **30** with 5-nitrothiophene-2-carboxaldehyde (**211**) (Scheme 2.33.3). Proof of synthesis came from the imine singlet peak in the proton NMR (δ_H 8.90 ppm).

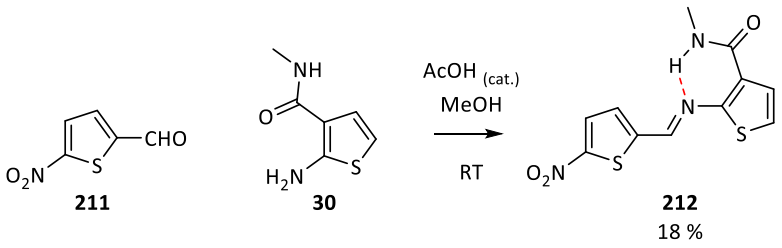

Scheme 2.33.3 Synthetic route towards imine **212** with predicted alternative hydrogen bond shown in red.

An improvement in aqueous solubility was observed for **212** compared to hit **17**, accompanied by retention of antileishmanial activity (Figure 2.33-8). However, synthetic difficulties prevented effective purification past 80 %, which limited the progression of this compound due to potential toxicity issues associated with the contaminating species.

Following the successful improvement in solubility and retention of antileishmanial activity observed for imine **212**, attempts were made to synthesise an analogue with a reversed central amide (**213**). This was predicted to maintain some rigidity whilst removing the intramolecular hydrogen bonding. Taking a retrosynthetic approach, it was clear that 2-amino-5-nitrothiophene (**214**) and 2-(methylcarbamoyl)benzoic acid (**215**) were key synthetic equivalents (Scheme 2.33.4).

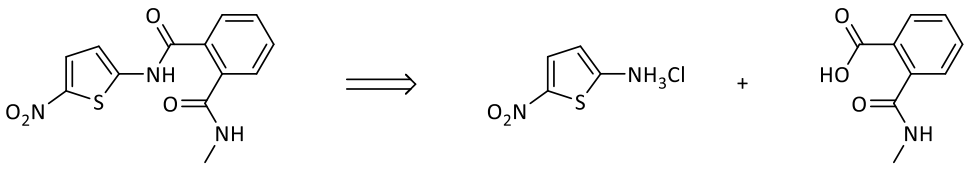

213 **214** **215**

Scheme 2.33.4 Retrosynthetic strategy identified 2-amino-5-nitrothiophene (**214**) and 2-(methylcarbamoyl)benzoic acid (**215**) as key synthetic equivalents in attempts to synthesise the reversed amide derivative **213**.

Synthesis of 2-amino-5-nitrothiophene (**214**) was achieved following the precedent of Galvez *et al*. [105] The first step of the synthesis involved generating 5-nitrothiophene-2-carbonyl azide (**216**) from **23** using sodium azide. The azide product was then refluxed with t-butanol resulting in a Curtius rearrangement via the isocyanate intermediate. This was an indirect route towards the Boc protected 2-amino-5-nitrothiophene (**217**), which was subsequently deprotected to give 2-amino-5-nitrothiophene (**214**) (Scheme 2.33.5, Route A). Successful synthesis was proved by the presence of the amine broad singlet in the proton NMR (δ_H 8.64 ppm).

Once 2-amino-5-nitrothiophene (**214**) had been successfully synthesised, attention turned towards the synthesis of 2-(methylcarbamoyl)benzoic acid (**215**). This was achieved by reaction of phthalic anhydride (**218**) with methylamine followed by acidification (Scheme 2.33.5, Route B).

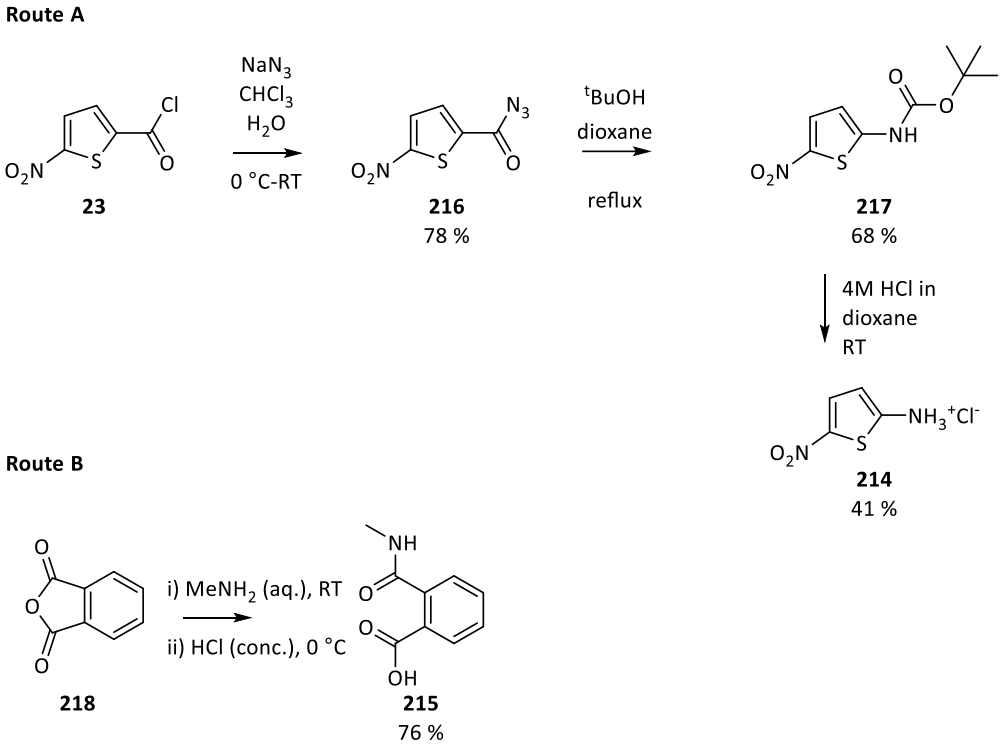

Scheme 2.33.5 Synthetic routes towards 2-amino-5-nitrothiophene intermediate **214** and 2-(methylcarbamoyl) benzoic acid intermediate **215**.

However, any attempts at amide coupling of the two synthetic equivalents failed to give any desired product. Efforts to generate the acid chloride also failed, resulting in an inseparable mixture of acid **215** and N-methylphthalimide (**219**) byproduct. Attempts to directly react 2-amino-5-nitrothiophene (**214**) with **219** also failed to give any desired product even under forcing conditions (120 °C, MWI). As such, attempts to synthesise the reversed amide were abandoned.

A

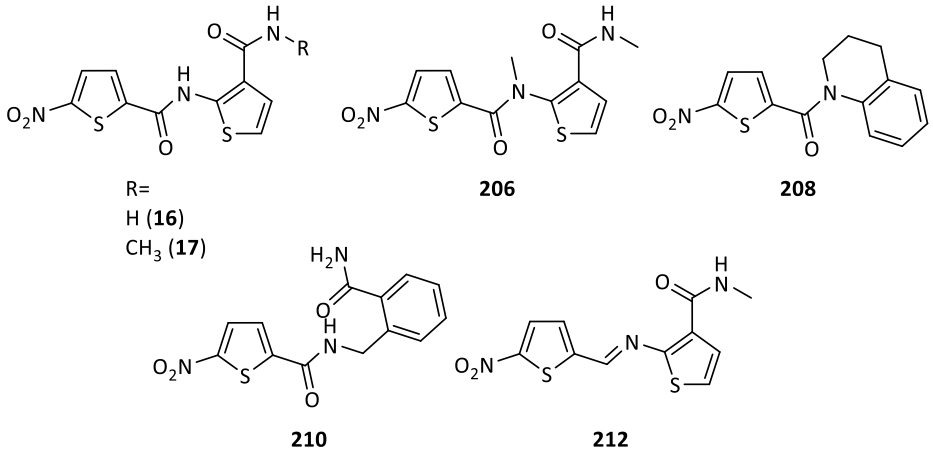

B

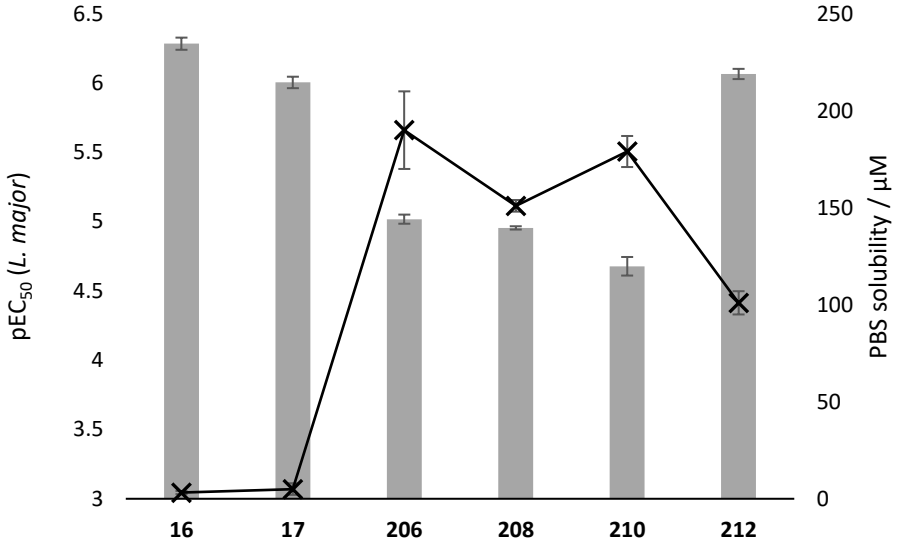

C

Compound	16	17	206	208	210	212
EC_{50} (*L. major*) / µM	0.52 ± 0.05	0.99 ± 0.09	9.6 ± 0.7	11.1 ± 0.3	21 ± 3	0.86 ± 0.07
Aqueous solubility (PBS / µM)	3.2 ± 0.8	5 ± 3	190 ± 20	151 ± 3	179 ± 8	101 ± 6

Figure 2.33-8 A. Structures of altered central amide series. B. Bar chart displaying the structural effects of altering the central amide on the antileishmanial activity of the compounds. The only tolerated change is to an imine (**212**). Crosses represent aqueous solubility. C. Table of EC_{50} values against *L. major* for altered central amide series. Solubility and antileishmanial activity are reported as the mean of three repeats, with errors representing standard error.

2.33.2.1.1 Summary

In summary, almost all attempts to introduce flexibility by changing the nature of the central amide resulted in a significant loss of antileishmanial activity (**206, 208, 210** & **212**). The only tolerated change was to replace the central amide with an imine (**212**), which retained antileishmanial activity and improved aqueous solubility relative to the original hits. However, difficulties during purification of this analogue prevent its progression due to potential toxicity issues that may arise from the impurities present. In conclusion, no benefit could be found by changing the nature of the central amide. As such, any desired improvement in solubility must be achieved by alternative methods.

2.33.2.2 Exploiting the 5-position to improve aqueous solubility

As discussed previously, aqueous solubility could not be improved by introducing sp^3 character into the core of the molecule, changing the central amide or removing or replacing the pendant amide group in **140** and **141.** However, the successful incorporation of various groups in the 5-position whilst retaining the pendant amide (**196-199**) suggested that this position could be exploited to add more complex groups to improve aqueous solubility. Initial efforts centred around synthesis of 5-^{t}Bu analogue **226** as the additional bulk may help to prevent tight crystal packing and improve aqueous solubility.

Synthesis of tert-butyl analogue **226** was achieved as follows (Scheme 2.33.6). Nitration of 4-tertbutyltoluene (**220**) selectively gave the 2-nitro substituted product **221**. This was followed by potassium permanganate oxidation of the methyl group to give acid **222**, which was subsequently converted to the acid chloride (**223**) using oxalyl chloride. The methyl amide (**224**) was then simply made by reaction of this intermediate with methylamine. Hydrogenation of the nitro group using hydrogen gas and palladium on carbon yielded the desired amine (**225**), which was subsequently coupled with 5-nitrothiophene-2-carbonyl chloride (**23**) to give product **226**. Proof of synthesis was again provided by the central amide proton in the proton NMR (δ_H 12.87 ppm).

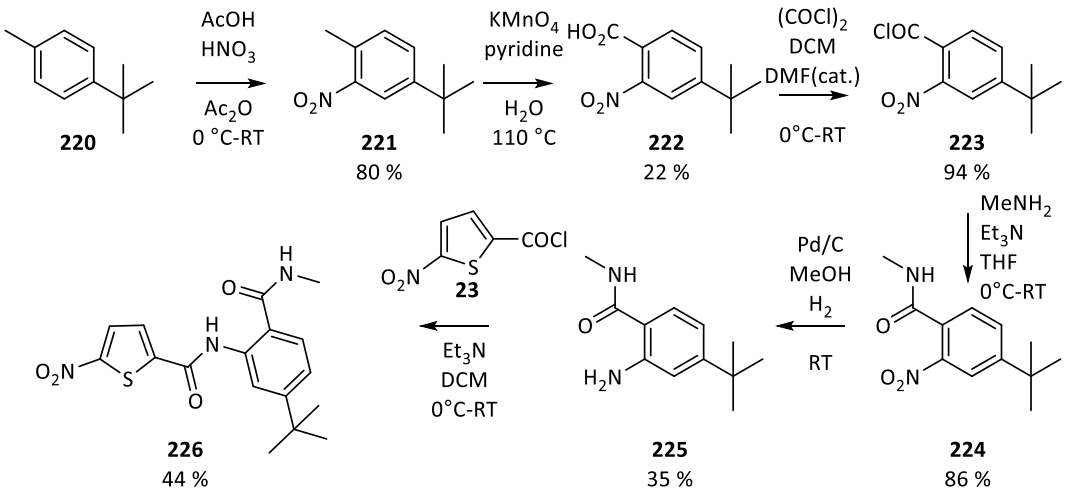

Scheme 2.33.6 Synthetic route towards tert-butyl substituted analogue **226**.

Tert-butyl analogue **226** retained decent antileishmanial activity (EC_{50}(*L. major*) 1.35 ± 0.07 µM) and low HepG2 toxicity (CC_{50} (HepG2) > 100 µM) but did not have improved solubility compared to hit **17** (solubility(PBS) < 2.5 µM). A single crystal X-ray structure of **226** showed that there is an expansion of the lattice to accommodate solvent of crystallisation, however this was insufficient to improve solubility (Figure 2.33-9).

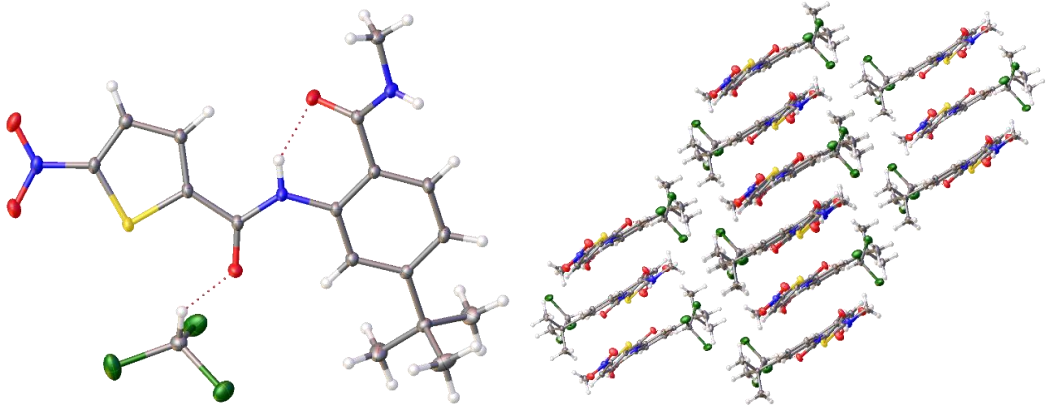

Figure 2.33-9 Crystal structure of **226** shows expansion by accommodating solvent of crystallisation.

Following the lack of improvement in solubility for **226**, efforts refocussed on introducing a flexible PEG substituent (**232**), which was predicted to disrupt crystal packing by forcing apart the layers within the lattice. The first attempted synthesis of **232** involved alkylation of 4-bromo-3-nitrophenol (**227**) with PEG bromide (**228**) to give intermediate **229** followed by Fe/NH_4Cl mediated nitro reduction to give

intermediate amine **230**.[106] Coupling of amine **230** with 5-nitrothiophene-2-carbonyl chloride (**23**) resulted in an inseparable mixture containing the desired intermediate product **231**, confirmed by the molecular ion peak in LC-MS (*m/z* 443 & 445 $[M-H]^-$). Subsequently, this crude mixture was moved forwards for a palladium(II) catalysed amidation described by Sawant *et al*.[107] However, no final product mass was observed by LC-MS and as such, the route was abandoned (Scheme 2.33.7).

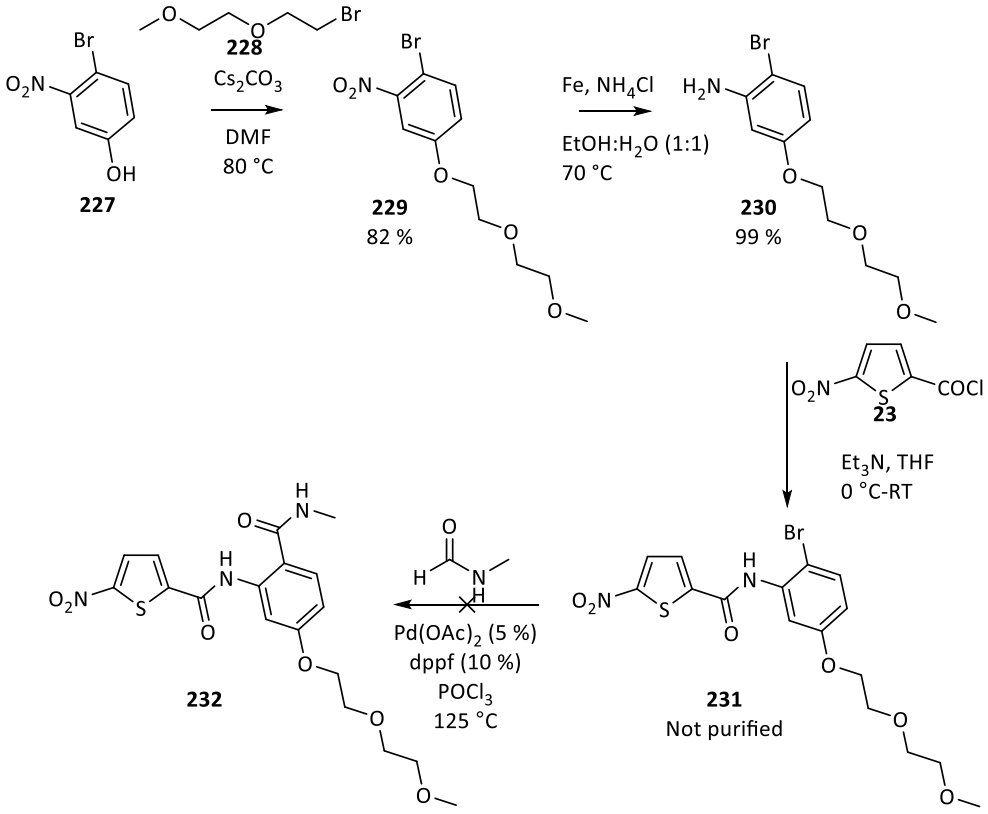

Scheme 2.33.7 First attempted synthesis of PEG analogue **232** from 4-bromo-3-nitrophenol (**227**).

Given the difficulties experienced in the previous route, the order of the steps was reversed and aminocarbonylation was attempted on nitro intermediate **229**. However, the aminocarbonylation conditions resulted in an *in situ* nitro reduction and an unusual carbonylation to give an alternative quinazolinone product (**233**) (Scheme 2.33.8). [107,108] This presents an interesting route to access quinazolinone heterocycles, as it enables utilisation of an alternative starting material to generate the necessary anthranilamide *in situ*. However, the reaction conditions were clearly not compatible with the functionalities present in the molecule to enable the desired

aminocarbonylation. As such, no further attempts were made to utilise the Sawant aminocarbonylation conditions.[107]

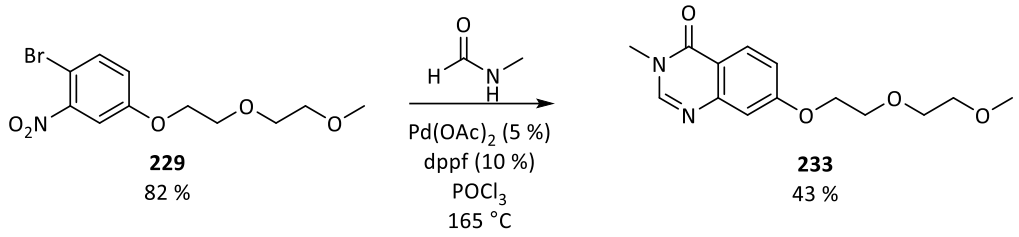

Scheme 2.33.8 Aminocarbonylation on **229** gave an alternative quinazolinone byproduct (**233**). [107,108]

An alternative route was explored in which 3-nitro-4-methylphenol (**234**) was alkylated with PEG bromide (**228**) to give intermediate **235**. However, subsequent attempts to oxidise the methyl group to an acid failed to give the desired product (**236**) (Scheme 2.33.9A). Attempts at lithium halogen exchange followed by carbon dioxide trapping on intermediate **229** (Scheme 2.33.9B), or Boc protection of 4-methoxyanthranilic acid (**169**) also failed (Scheme 2.33.9C). [109]

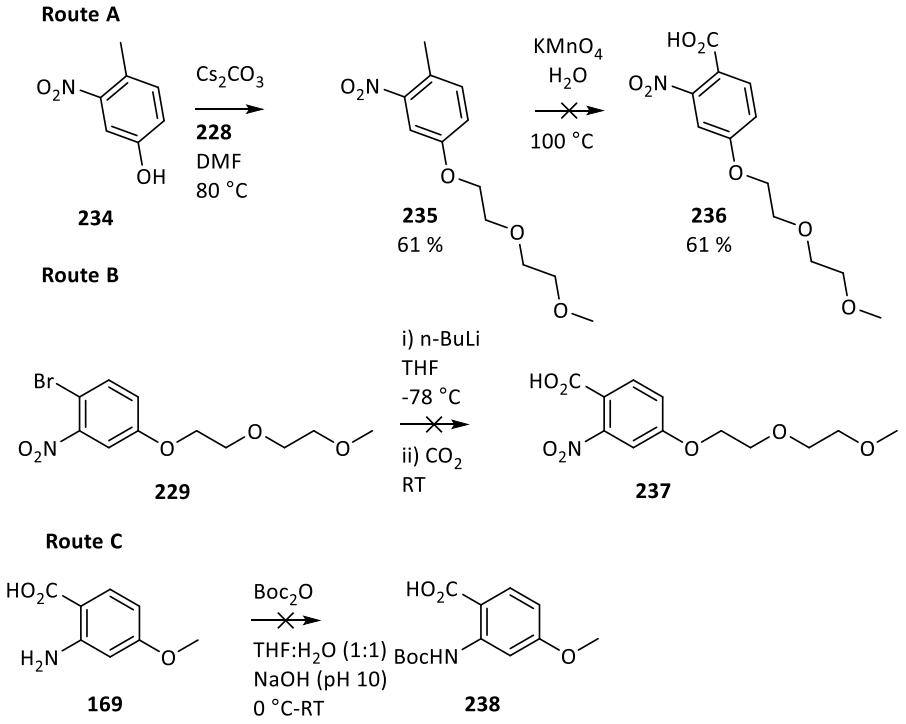

Scheme 2.33.9 A. Permanganate oxidation of the methyl group in **234** failed to give the desired product. B. Lithium halogen exchange and CO_2 trapping on **229** failed to give the desired acid. C. Boc protection of 4-methoxyanthranilic acid (**169**) failed.

Subsequently, a different approach was attempted using chemistry previously validated in the synthesis of 5-methoxy analogue **196** (section 2.32.2). Firstly, a triphosgene mediated cyclisation was used to generate intermediate **178**, in an analogous fashion to the first step in the synthesis of **196**. In contrast to the synthetic route towards **196**, this was followed by demethylation using BBr_3 to give intermediate alcohol (**239**), as proved by the loss of the CH_3 peak from the starting material in the proton NMR (δ_H 3.85 ppm). However, a complex mixture was obtained under various conditions upon deprotonation of the alcohol. This was attributed to deprotonation followed by reaction with intermediate (**239**) itself rather than the desired PEG bromide electrophile (Scheme 2.33.10).

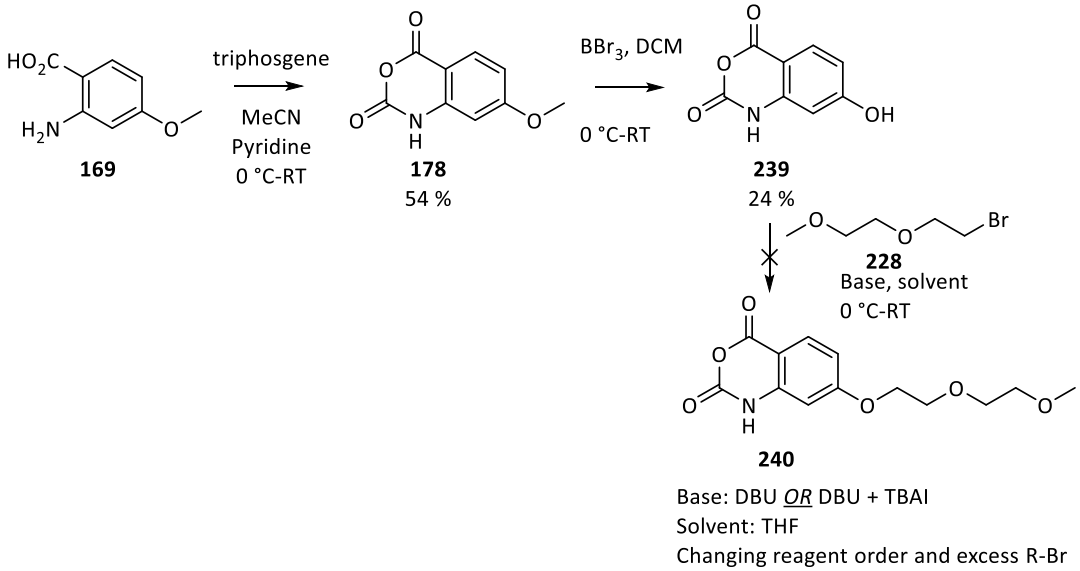

Scheme 2.33.10 BBr_3 demethylation appeared promising, however intermediate **239** reacted with itself preferentially over the desired PEG-bromide electrophile.

Following the success of the BBr_3 demethylation in Scheme 2.33.10, the order of the steps was reversed to circumvent the difficulties upon deprotonation of this species. The synthetic route of **196** was utilised up to and including ring opening of the benzoxazine-2,4-dione intermediate **178** with methylamine to give amino-5-hydroxy-*N*-methyl-2-benzamide (**187**). Methoxy intermediate **187** was successfully demethylated using BBr_3 to give alcohol **241**, validated by the loss of the methyl signal in the proton NMR (δ_H 2.95 ppm). Alcohol **241** was subsequently deprotonated by sodium hydride and alkylated with **228**. The following substituted ether product

246 was then coupled with 5-nitrothiophene-2-carbonyl chloride (**23**) to give the desired 5-substituted PEG analogue (**232**, Scheme 2.33.11), confirmed by the presence of the characteristic central amide NH signal in the proton NMR (δ_H 13.16 ppm).

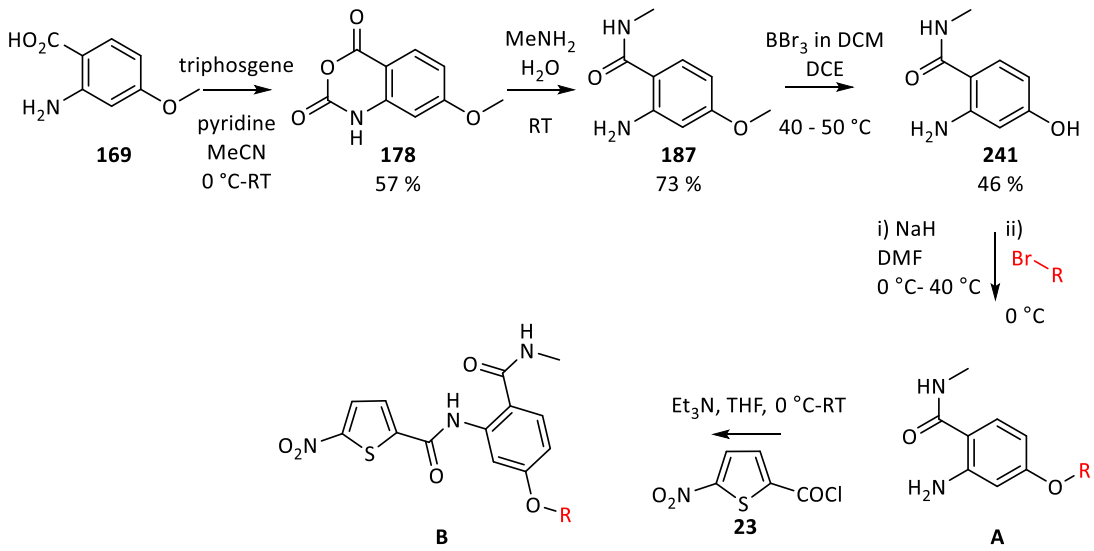

R	Reactant RBr ID	Intermediate A ID (yield %)	Product (B) ID (yield %)
$(C_2H_4)O)_2CH_3$	**228**	**246** (27 %)	**232** (75 %)
$(C_2H_4)O)_2C{\equiv}CH$	**242**	**247** (67 %)	**251** (29 %)
(C_2H_4)morpholin-4-yl	**243**	**248** (18 %)	**252** (31 %)
(C_3H_6)morpholin-4-yl	**244**	**249** (57 %)	**253** (48 %)
(C_2H_4)oxan-4-yl	**245**	**250** (85 %)	**254** (57 %)

Scheme 2.33.11 Synthetic route towards extended 5-substituted analogues.

PEG analogue **232** showed equipotent antileishmanial activity when compared to 5-methoxy compound **196** and low HepG2 cytotoxicity (Figure 2.33-12). However, the aqueous solubility of **232** was only marginally improved compared to the original hits (solubility (PBS) 2.27 ± 0.05 µM). A crystal structure of **232** was obtained to rationalise the lack of improvement in solubility (Figure 2.33-10).

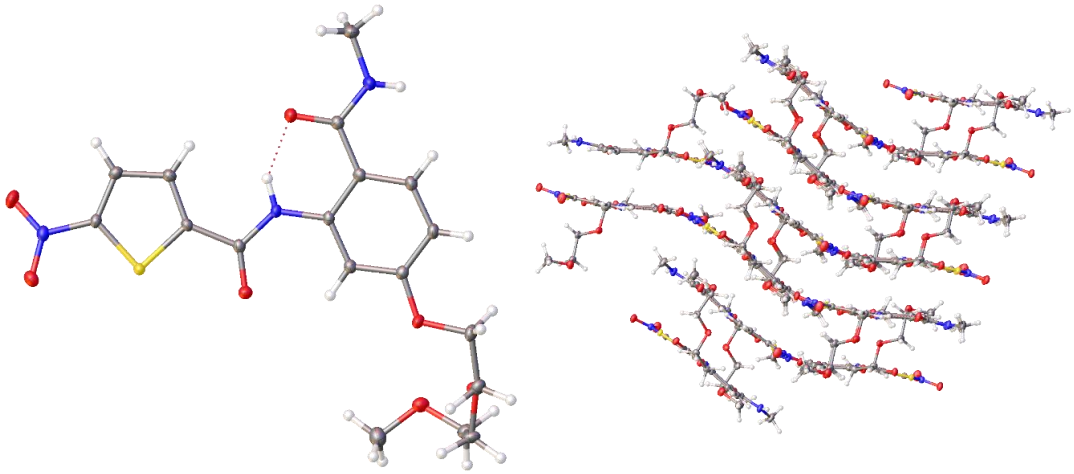

Figure 2.33-10 Crystal structure of **232** ($P2_{1/c}$) showing interlacing of PEG chains between the layers.

232 displays an alternative space group to original hit **17** ($P2_{1/c}$ vs. P_{-1}). However, the crystal lattice reveals tight packing of monomer units caused by the PEG chains interlacing between the monomer units and lattice layers. In conclusion, the addition of a PEG chain did not achieve the desired goal of reducing the density of crystal packing, which in turn accounts for the lack of improved aqueous solubility.

Following the promising antileishmanial activity and low mammalian cell toxicity observed for PEG substituted analogue **232**, it was proposed that alternative groups could be added to the 5- position to improve aqueous solubility. The solubility of a compound is reliant on the interplay between its lattice enthalpy contribution, determined by the interaction between the monomer units in the solid form, and the enthalpy of solvation contribution, determined by the energy of interactions between the monomer units and solvent upon dissolution. As such, a derivative was designed to improve solubility by incorporating a morpholine ring into the 5-substituent (**252**). The addition of a basic nitrogen will introduce charge at physiological pH to increase the enthalpy of solvation whilst the additional steric bulk

may interfere with crystal packing to reduce the lattice enthalpy. **252** was synthesised in an analogous manner to **232** (Scheme 2.33.11). The alkyl bromide reagent necessary for the formation of **252**, in addition to those necessary for further analogues **251** and **253-254**, were synthesised according to Scheme 2.33.12. Successful synthesis of **252** was validated by the presence of the characteristic central amide signal in the proton NMR (δ_H 13.18 ppm). Compound **252** showed high antileishmanial activity (EC_{50} (*L. major*) 0.440 ± 0.006 µM), low mammalian cell toxicity (CC_{50} (HepG2) 24 ± 1 µM) and improved aqueous solubility (solubility (PBS) 19.3 ± 0.6 µM) compared to the original hits (Figure 2.33-12).

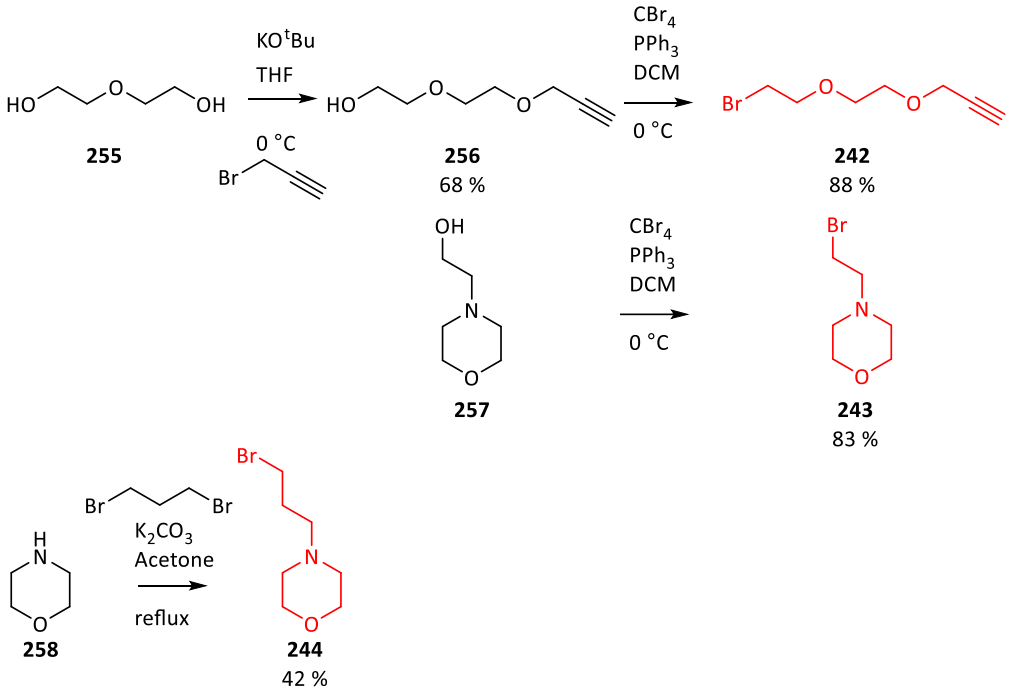

Scheme 2.33.12 Synthesis of R-Br (**242-244**), when not commercially available, used during the synthesis of **251**-**254**.

A single crystal X-ray crystal structure was obtained for **252**, which reveals an increase in free space within the lattice, shown by a 0.11 g cm^{-3} lower predicted density than original hit **17** (Figure 2.33-11).

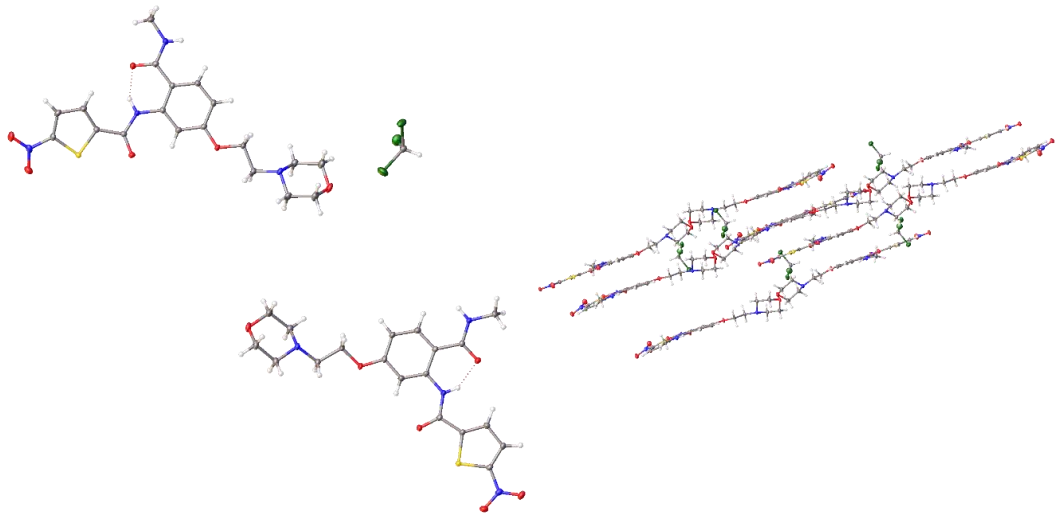

Figure 2.33-11 Crystal structure of **252** (P_{-1}) showing increase in crystal lattice spacing apparent due to presence of solvent of crystallisation.

The increase in free space in the crystal lattice of **252** caused by the additional bulk of the morpholine ring could account for the increase in solubility. However, this does not account for the contribution of the electrostatic interactions between the basic nitrogen and water at physiological pH. As such, a control compound was synthesised in which the basic nitrogen from **252** was replaced with carbon to give tetrahydroquinoline derivative **254**. Synthesis was achieved using the same route as **232** (Scheme 2.33.11). In this case, antileishmanial activity was retained and mammalian cell toxicity was reduced compared to **252** (Figure 2.33-12). However, aqueous solubility was much reduced compared to **252** (solubility (PBS) 3.7 ± 0.9 µM), suggesting that the improvement in solubility observed for **252** is mainly due to the additional basic nitrogen.

Although **252** seemed like a promising new lead compound, issues surrounding the low 18 % yield obtained in the alkylation of phenol **241** with alkyl bromide **243** limited the ability to efficiently scale up the synthesis (Scheme 2.33.11). It was speculated that **243** may react as a nitrogen mustard to form the aziridine, resulting in two potential products which could account for the low yield. Subsequently, analogue **253** was synthesised with a propyl linker attached to the morpholine ring to reduce this side reaction. Synthesis was again achieved using the same route as **232** (Scheme 2.33.11). As anticipated, the yield of the alkylation step was improved to 57 %. Furthermore, antileishmanial activity was retained and mammalian cell toxicity was

comparable to **252**. In addition, aqueous solubility was improved slightly for analogue **253** compared to **252** (Figure 2.33-12).

A

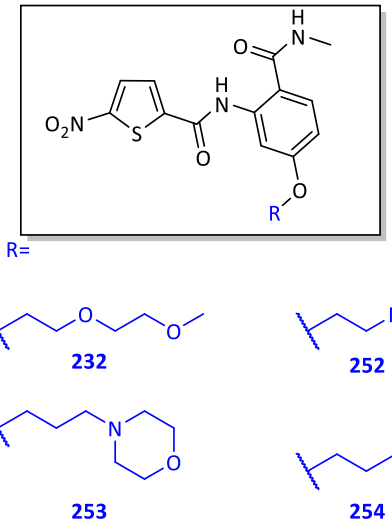

B

Compound	232	252	253	254
EC_{50} (*L. major*) / µM	0.32 ± 0.02	0.44 ± 0.006	0.30 ± 0.02	0.33 ± 0.06
CC_{50} (HepG2) / µM	>100	24 ± 1	13 ± 2	>100
Solubility (PBS) / µM	2.27 ± 0.05	19.3 ± 0.6	29 ± 3	3.7 ± 0.9

Figure 2.33-12 Structures of the extended 5- substituted phenyl series. B. EC_{50} values for the extended 5-substituted analogues (**232** and **252-254**) against *L. major* promastigotes, CC_{50} values against HepG2 cells and aqueous solubility (PBS). Solubility, antileishmanial activity and HepG2 toxicity are reported as the mean of three repeats, with errors representing standard error.

Following the success of morpholine analogues **252** and **253**, attempts were made to introduce a piperazine ring and a second basic nitrogen. Firstly, attempts were made to synthesise the $(CH_2)_2$-N-methyl-piperazine derivative **259**. Neither alkylation of N-methylpiperazine (**260**) (Scheme 2.33.13A) or an Appel reaction on 4-(2-hydroxylethyl)-1-methyl-piperezine (**262**) (Scheme 2.33.13B) successfully gave the desired 4-(2'-bromoethyl)-1-methyl-piperezine (**261**) product by LC-MS or ^{1}H NMR even though both reactions went to completion. Synthesis of the alternative crude mesylate intermediate **263** was successful and went to completion (Scheme 2.33.13B), as confirmed by Atmospheric Solids Analysis Probe (ASAP) mass spectrometry (*m/z* 223.1 $[M+H]^+$). However, the reaction failed at the next stage upon alkylation of phenol **241**, with the desired product only observed in the crude reaction mixture. Upon purification, only the starting alcohol **241** and 1-methyl-1,4-

diazabicyclo[2,2,2]octane (**264**) were observed, suggesting inherent instability of the resulting product (Scheme 2.33.13C).

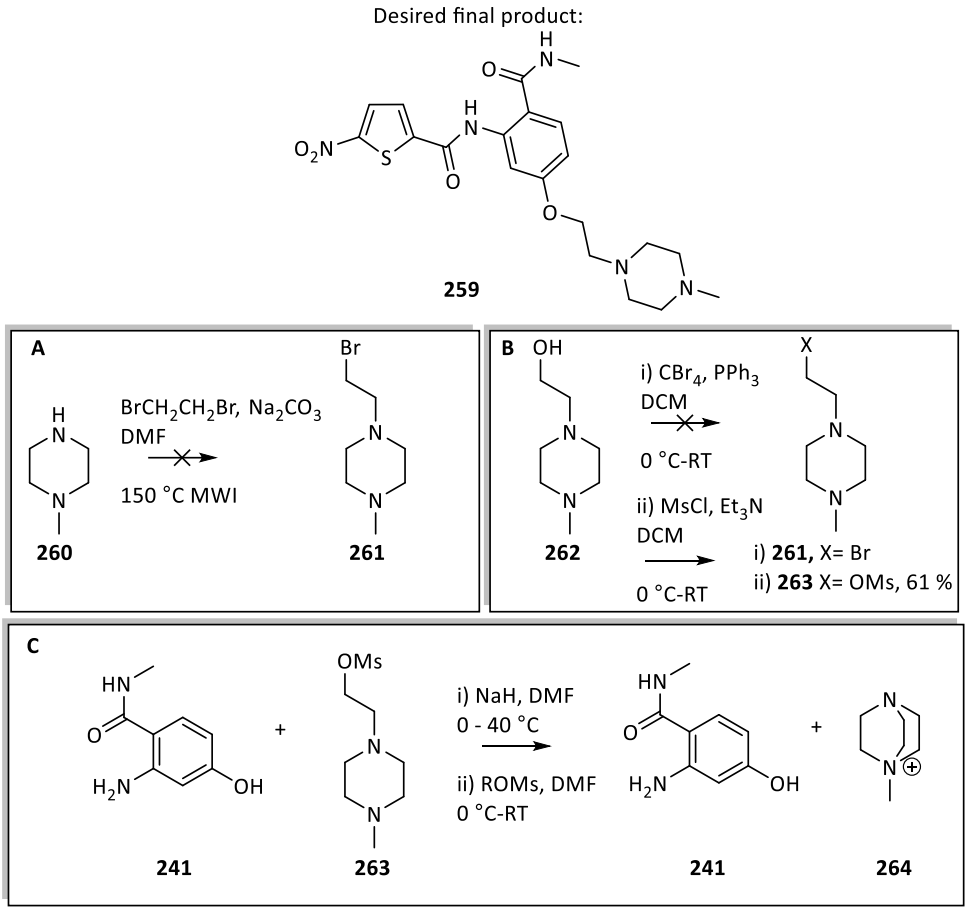

Scheme 2.33.13 Attempted synthesis of $(CH_2)_2$N-methyl-piperazine derivative **259**.

Synthetic difficulties could be associated with the piperazine acting as a mustard resulting in the formation of the 1-methyl-1,4-diazabicyclo[2,2,2]octane byproduct (**264**), similar to that predicted during the synthesis of **252**. Subsequently, attempts were made to synthesise the $(CH_2)_3$-*N*-methylpiperazine derivative (**265**). Initial attempts to alkylate *N*-methylpiperazine (**260**) with 1-bromo-3-chloropropane resulted in dialkylation (**266**) (Scheme 2.33.14A). Alternative attempts to alkylate phenol intermediate (**241**) with 1,3-dibromopropane gave desired product **267**, which coeluted with elimination product **268** (Scheme 2.33.14B). This crude mixture was taken forwards and successfully reacted with *N*-methylpiperazine (**260**) to give the desired intermediate **271**, as confirmed by the *N*-methylpiperazine methyl signal in the proton NMR (δ_H 2.30 ppm). However, **271** coeluted with the elimination

product (**268**) leading to very small yields which were not sufficient for further conversion (Scheme 2.33.14B). Alternatively, alkylation of the phenol intermediate (**241**) with 3-bromopropan-1-ol enabled pure alkylated product (**269**) to be isolated. Subsequent mesylation afforded the crude mesylate (**270**) in 80 % yield with trace amounts of alcohol **269** remaining, as confirmed by ASAP (m/z 303.1 $[M+H]^+$). This crude product was then reacted with *N*-methylpiperazine (**260**) to yield small quantities of the desired product **271** which couldn't be purified sufficiently by normal or reverse phase chromatography to be useful for further reactions (Scheme 2.33.14B).

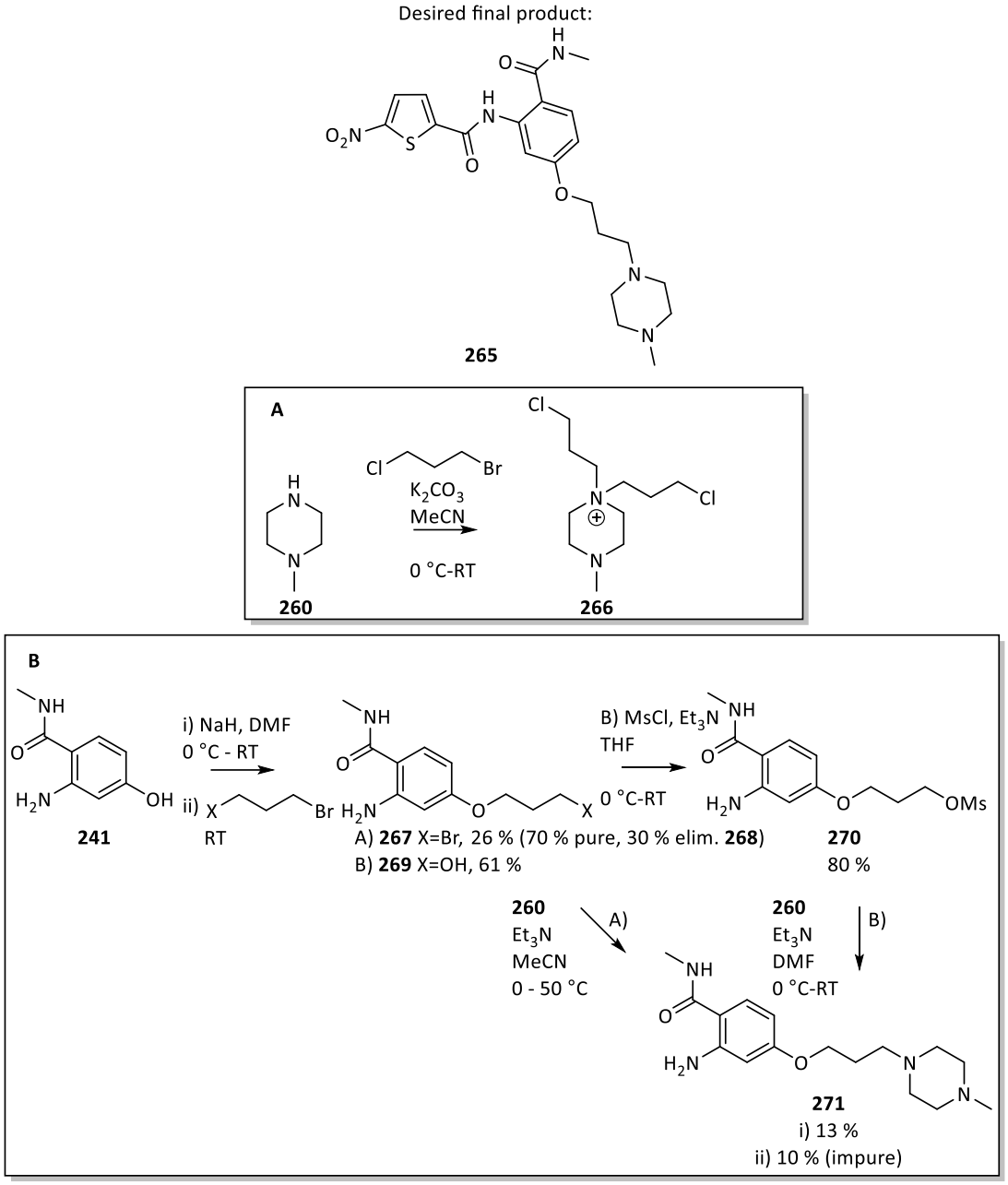

Scheme 2.33.14 Attempts to synthesise $(CH_2)_3$-N-methylpiperazine derivative **265**.

Subsequently, no further attempts were made to synthesise N-methylpiperazine derivatives **259** and **265**.

2.33.2.2.1 Generation 2 lead compound solubility in Biorelevant buffers

Overall, **252** and **253** were identified as generation 2 lead compounds as they showed high antileishmanial activity, high selectivity over HepG2 cells and high aqueous

solubility. However, it was of interest to investigate the solubility of these lead compounds in biorelevant buffers FESSIF, FASSIF and FASSGF in an analogous manner to generation 1 lead compounds outlined in section 2.33.1. Millimolar levels of solubility were observed for both new lead compounds (**252** and **253**) in both FESSIF and FASSGF, with hundreds of micromolar solubility observed in FASSIF and PBS supplemented with 15 mM sodium taurocholate (Figure 2.33-13). The relatively low solubility of the two lead compounds (**252** and **253**) in 15 mM taurocholate suggests that the high solubility observed in FESSIF and FASSGF is mainly due to the lower pH of these buffers in comparison to FASSIF and PBS rather than due to bile salt concentration. Overall, the solubility of the lead compounds in biorelevant buffers represented a drastic improvement compared to the original hits. Subsequently, morpholine derivatives **252** and **253** were confirmed as new lead antileishmanial compounds.

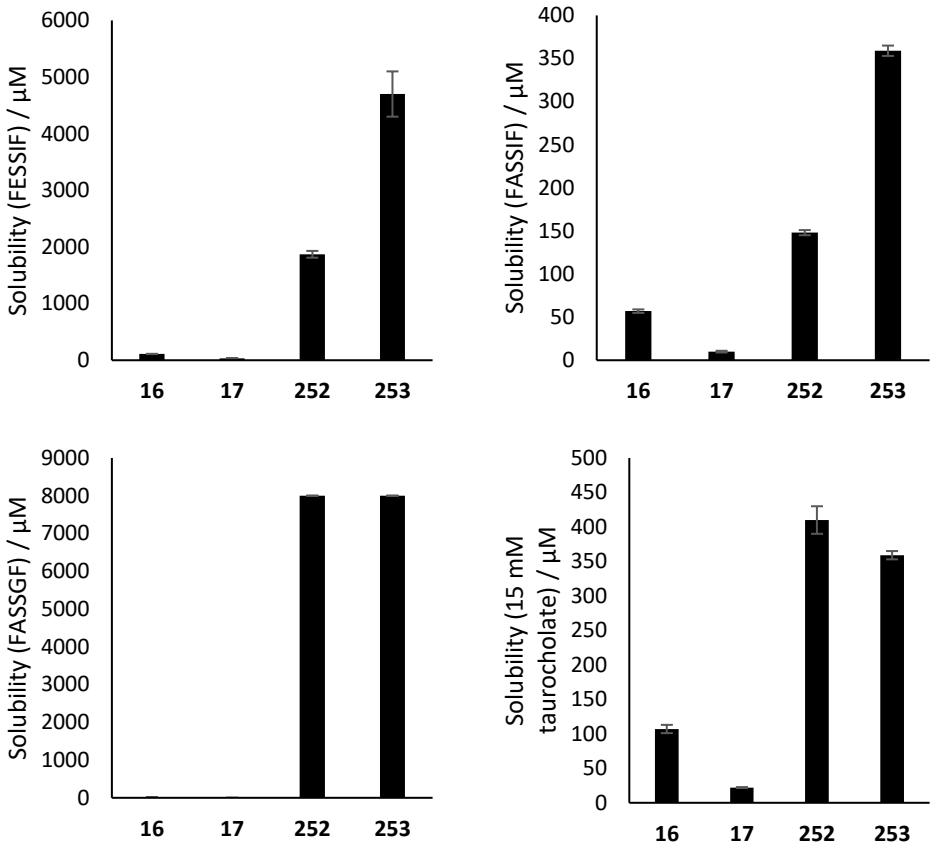

Compound	16	17	252	253
Solubility PBS / µM	< 7.4	< 7.4	19.3 ± 0.6	29 ± 3
Solubility FESSIF / µM	111 ± 2	35 ± 1	1870 ± 60	4700 ± 400
Solubility FASSIF / µM	57 ± 2	10 ± 1	148 ± 3	359 ± 6
Solubility FASSGF / µM	10.7 ± 0.3	< 7.4	>8000	>8000
Solubility 15 mM taurocholate / µM	107 ± 6	22.1 ± 0.7	410 ± 20	359 ± 6

Figure 2.33-13 Comparison of the solubility of generation 2 lead compounds (**252-253**) with the original hit compounds (**16-17**) in biorelevant buffers and 15 mM taurocholate. Solubility is reported as the mean of three repeats, with errors representing standard error.

2.33.2.2.2 Summary

In summary, two morpholine-containing compounds, **252** and **253**, have been identified as having retained or improved antileishmanial activity and high selectivity over HepG2 cells when compared to the original hits **16** and **17**. In addition, compounds **252** and **253** show improved aqueous solubility compared to the original

hits (Figure 2.33-14), addressing one of the main aims outlined in section 2.2. Both compounds are promising new lead compounds, however, **253** has more potential at this stage due to higher yields in the synthetic route which enables slightly easier scale up compared to **252**.

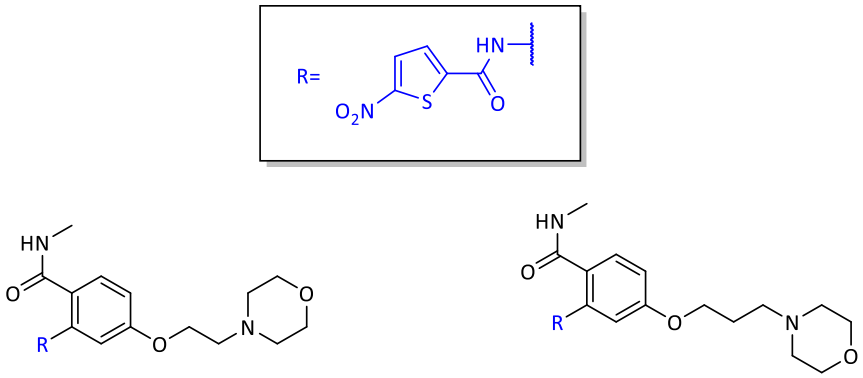

252
EC_{50} (*L. major*) 0.44 ± 0.006 μM
CC_{50} (HepG2) 24 ± 1 μM
Solubility (PBS) 19.3 ± 0.6 μM

253
EC_{50} (*L. major*) 0.20 ± 0.02 μM
CC_{50} (HepG2) 13 ± 2 μM
Solubility (PBS) 29 ± 3 μM

Figure 2.33-14 Generation 2 lead compounds **252** and **253** which show high antileishmanial activity, low mammalian cell toxicity and high aqueous solubility. Solubility, antileishmanial activity and HepG2 toxicity are reported as the mean of three repeats, with errors representing standard error.

2.34 Broad spectrum antileishmanial activity

Leishmaniasis is a disease caused by over 20 species of *Leishmania* which vary based on disease manifestation and geographical location. It is important to ensure that potential new antileishmanial drugs are active across a variety of *Leishmania* species. To this end, *L. amazonensis*, a representative new-world strain responsible for cutaneous leishmaniasis and *L. donovani*, a representative old-world strain responsible for visceral leishmaniasis, were used in addition to *L. major* to ensure broad spectrum activity.

A total of 19 compounds discussed across Chapter 1 and Chapter 2 showed potent antipromastigote activity against *L. major* (EC_{50} < 2 µM). These compounds can be split into three classes: bisthiophenes, phenyl series and singletons (Figure 2.34-1).

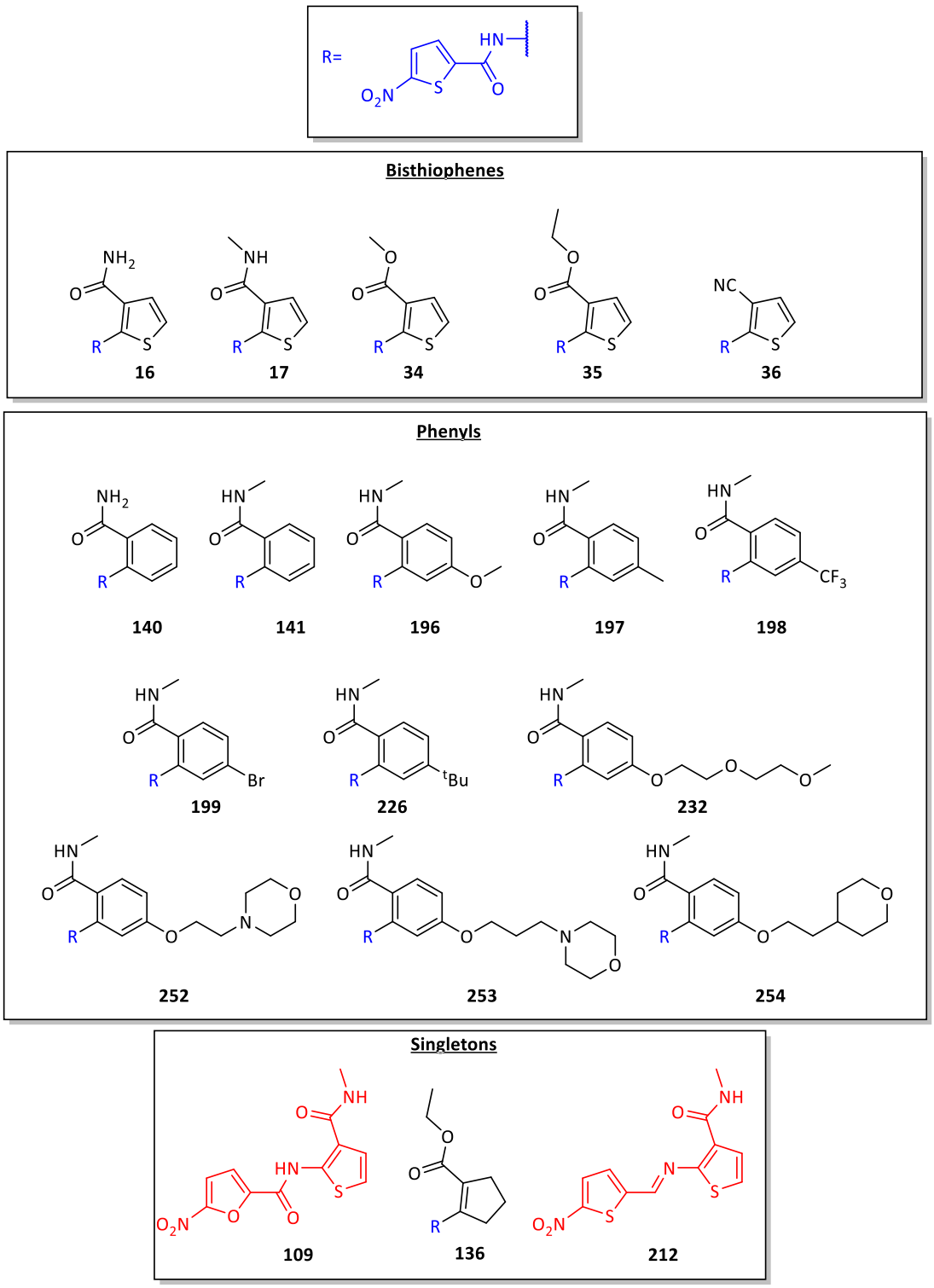

Figure 2.34-1 19 most active antileishmanial compounds. Compounds in red are singletons not represented by the blue general structure.

The 19 compounds were tested against *L. amazonensis* and a selection against *L. donovani* promastigotes. Antipromastigote dose-response assays were carried out as per *L. major* (section 1.41) where 0.5 x 10^6 cells mL^{-1} were incubated with compound

for 48 hrs for *L. amazonensis* and 1 x 10^5 cells mL^{-1} for 72 hrs for *L. donovani* (see footnote[5]). 17 of 19 compounds showed potent antipromastigote activity against all three species of *Leishmania* (EC_{50} < 2 μM), with some compounds showing single nanomolar potency against *L. donovani* promastigotes (Figure 2.34-2). Pleasingly, generation 2 lead compounds **252** and **253** showed submicromolar activity against both *L. major* and *L. amazonensis* promastigotes.

[5] *L. donovani* antipromastigote assays were carried out by members of the Dr Susan Wyllie group, University of Dundee.

A

Class	Product ID	EC_{50} / µM		
		L. major	*L. amazonensis*	*L. donovani*
Bisthiophenes	**16**	0.52 ± 0.05	0.042 ± 0.004	0.0040 ± 0.0002
	17	0.99 ± 0.09	0.29 ± 0.03	0.033 ± 0.002
	34	0.59 ± 0.05	0.91 ± 0.09	0.30 ± 0.006
	35	0.93 ± 0.09	1.85 ± 0.05	-
	36	1.1 ± 0.1	2.1 ± 0.2	1.12 ± 0.03
Phenyl	**140**	0.47 ± 0.04	0.070 ± 0.001	-
	141	0.65 ± 0.05	0.052 ± 0.002	0.012 ± 0.0005
	196	0.33 ± 0.02	0.021 ± 0.002	0.006 ± 0.0002
	197	0.34 ± 0.03	0.027 ± 0.002	0.005 ± 0.0002
	198	1.84 ± 0.1	0.24 ± 0.01	-
	199	0.57 ± 0.06	0.048 ± 0.004	-
	226	1.35 ± 0.07	2.5 ± 0.3	-
	232	0.32 ± 0.02	0.22 ±0.03	-
	252	0.44 ± 0.008	0.27 ± 0.01	-
	253	0.30 ± 0.02	0.080 ± 0.01	-
	254	0.33 ± 0.06	0.46 ± 0.04	-
Singletons	**109**	0.37 ± 0.009	0.33 ± 0.03	0.20 ± 0.001
	136	0.46 ± 0.03	0.72 ± 0.03	-
	212	0.86 ± 0.07	0.56 ± 0.06	0.040 ± 0.001

B

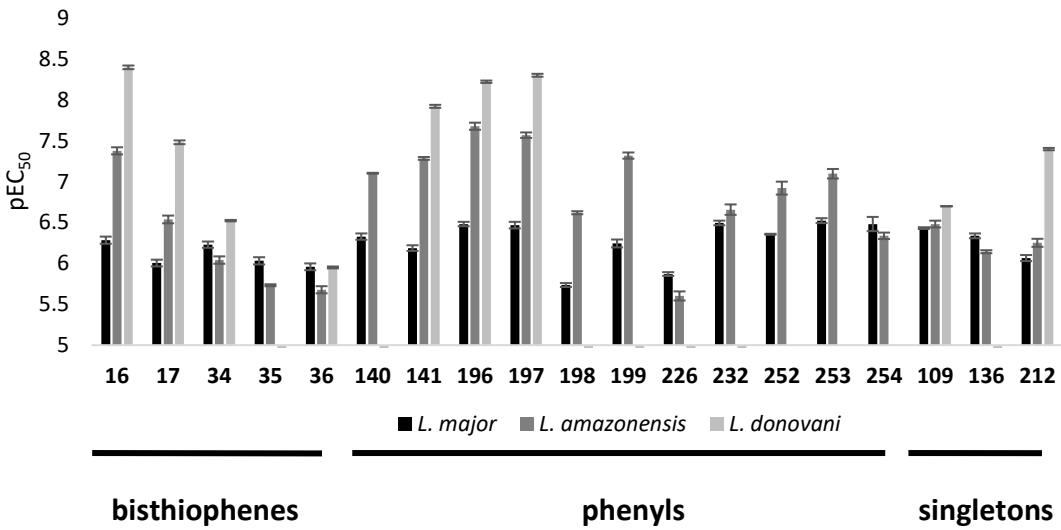

Figure 2.34-2 A. EC_{50} values for 19 compounds against 3 *Leishmania* species. B. Bar chart showing the antileishmanial activity of 19 compounds against 3 *Leishmania* species. Antileishmanial activities are reported as the mean of three repeats, with errors representing standard error.

2.35 Antitrypanosomatid activity

Leishmania spp. are trypanosomatids along with *T. cruzi* and *T. brucei*, which share many biological similarities. Leishmaniasis, Chagas disease and African sleeping sickness all pose global health challenges and require new treatments to combat them. Due to the similarities between the trypanosomatids, it is possible that drug therapies could be developed with broad spectrum anti-trypanosomatid activity to potentially treat all three diseases. To explore whether the 5N2C series could fit this role, a selection of the most active and selective antileishmanial compounds were also tested against *T. brucei.* In short, *T. brucei* bloodstream trypomastigotes (1×10^5 cells mL^{-1}) were incubated with a dilution series of compound in HMI-9 (10 % FBS) for 48 hrs at 37 °C, 5 % CO_2 before assessing cell viability using CellTiter Blue (see footnote[6]). The antitrypanosomatid activity of the selected compounds is given in Table 2.35-1.

Table 2.35-1: Activity of 6 potent and selective antileishmanial compounds against *T. brucei*. Antitrypanosomal activity is reported as the mean of three repeats, with errors representing standard error.

Compound	EC_{50} (*T. brucei*)/ µM
16	0.33 ± 0.29
17	2.78 ± 0.81
226	0.51 ± 0.12
252	0.78 ± 0.38
253	0.29 ± 0.13
254	1.36 ± 1.26

Each compound showed potent activity against *T. brucei* bloodstream trypomastigotes. Lead compounds **252** and **253** showed submicromolar activity, which taken alongside their high aqueous solubility and relatively low HepG2 toxicity, could allow progression into future medicinal chemistry campaigns towards African sleeping sickness.

[6] *T brucei* dose-response studies were carried out by lab members in the J. Morris group, Clemson (SC).

2.4 Summary

The original hit compounds **16** and **17** were discounted as new antileishmanial drugs due to their poor aqueous solubility and bioavailability. Furthermore, both hits contained multiple structural alerts that pose potential toxicity concerns in the host. Consequently, a range of analogues were synthesised to explore the structure-activity relationship of the hits to generate new lead compounds with fewer areas of toxicity concerns and improved aqueous solubility (Figure 2.4-1).

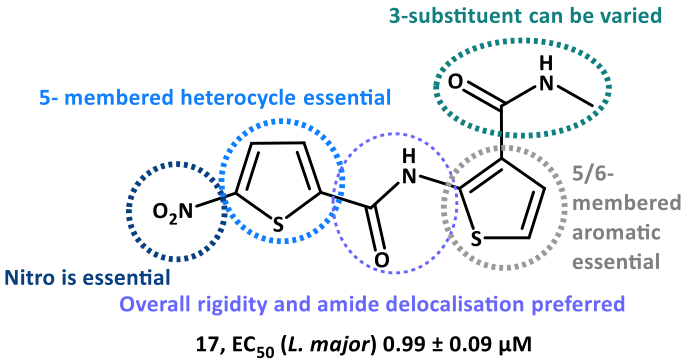

Figure 2.4-1 Summary of the SAR campaign based off the original hit **17** structure.

Initially, efforts focussed around replacing the 5-nitrothiophene group. However, removing the nitro group, or replacing the 5-nitrothiophene with other nitro aromatics resulted in a complete loss of antileishmanial activity in all but one case. 5-Nitrofuran analogue **109** retained high antileishmanial activity but showed significant HepG2 toxicity and was therefore not a suitable replacement for the 5-nitrothiophene ring.

Once the 5-nitrothiophene ring had been identified as important for potent antileishmanial activity and selectivity, efforts turned to removing the 2-aminothiophene PAINS motif. Delocalisation of the central amine nitrogen lone pair into an electron withdrawing ortho- substituent was identified as important for antileishmanial activity, as removing this delocalisation in cyclopentane analogue **135** led to a 20-fold decrease in antileishmanial activity. However, when delocalisation was reintroduced in cyclopentene analogue **136**, antileishmanial activity was restored. Following the successful replacement of the 2-aminothiophene with cyclopentene in **136**, efforts turned to incorporating an anthranilamide in the

same position. Anthranilamides **140** and **141** retained potent antileishmanial activity and offered more opportunities to explore chemical space around the right-hand phenyl ring. Multiple substituents including OMe (**196**), Me (**197**), CF_3 (**198**), Br (**199**) and ^{t}Bu (**226**) were tolerated in the 5-position on the right-hand anthranilamide ring, opening this position for potential further derivatisation.

Once toxicity concerns had been addressed, efforts turned to improving aqueous solubility. The lack of aqueous solubility of the hits was attributed to the hydrogen bond between the central amide and pendant amide group. However, changing the central amide to introduce flexibility or removing and replacing the pendant amide led to a drop in antileishmanial activity. Consequently, it was proposed that solubility enhancing groups could be incorporated into the 5-position of the right hand anthranilamide. Addition of bulky ^{t}Bu (**226**) and PEG (**232**) substituents did not improve aqueous solubility. However, addition of a basic nitrogen through a morpholine group in analogues **252** and **253** gave a significant improvement in aqueous solubility. This was attributed to the basic nitrogen increasing the enthalpy of hydration contribution and favouring dissolution rather than the bulk of the group disrupting the crystal lattice, as tetrahydroquinoline derivative **254**, where the nitrogen from **252** is replaced with a carbon, shows much poorer aqueous solubility.

Morpholine compounds **252** and **253** were identified as new lead compounds due to their high activity against *L. major* promastigotes, *L. amazonensis* promastigotes and *T. brucei* trypomastigotes, high selectivity index over HepG2 cells and improved aqueous solubility.

3 Mode of action of 5N2C series

3.1 Introduction

3.11 Mode of action of antitrypanosomatid nitro drugs

As previously discussed in Chapter 1, the 5N2C series in this work do not inhibit *Lmj*IPCS. To search for alternative modes of action for this series, the mode of action of other nitro containing antitrypanosomatid drugs was first investigated.

3.11.1 Nifurtimox (37)

Initial investigations into the mode of action of nifurtimox (**37**) suggested that cell death was associated with radical damage due to the production of H_2O_2, potentially via single electron reduction by trypanothione reductase or lipoamide dehydrogenase.[110–112] Similar radical metabolites were also observed in the liver upon nifurtimox (**37**) treatment.[113] Further early studies showed that nifurtimox (**37**) also caused lipid alterations and damaged kinetoplast DNA in *T. cruzi*. [114,115] Muelas-Serrano *et al.* also showed that nifurtimox (**37**) caused alterations to the mitochondria, nucleus and ribosomes in *T. cruzi*.[116] However, the discovery of a type I nitroreductase (NTR1) in *T. cruzi*, *T. brucei* and *Leishmania* by the 'TriTryp' genome sequencing project in 2005 proved to be key for understanding the antitrypanosomatid activity of nifurtimox (**37**).[117–119] The activity of nifurtimox (**37**) was reduced 4-fold against a single knockout of NTR1 in *T. cruzi* compared to wild type, proving that NTR1 bioactivation is important for the biological activity of nifurtimox (**37**).[120] Later, the identification of a second type I nitroreductase, NTR2 by Wyllie *et al.* (2016), revealed a second mode of bioactivation for nifurtimox (**37**).[49] However, in this case a double knockout of NTR2 only decreased sensitivity to nifurtimox (**37**) by 3.5-fold, suggesting that NTR2 bioactivation contributes to the toxicity of nifurtimox (**37**) but is not the primary toxification mechanism.[49]

3.11.2 Benznidazole (38)

Unlike nifurtimox (**37**), the mode of action of benznidazole (**38**) does not involve the generation of reactive oxygen species.[112] Early studies suggested that *T. cruzi*

bioactivates benznidazole (**38**) to reactive species which bind to DNA, lipids, thiols and proteins.[114,121,122] A 2014 study by Rajão *et al.* found that *T. cruzi* treated with benznidazole (**38**) overexpress DNA repair proteins, supporting the early hypotheses that bioactivated benznidazole (**38**) binds to DNA.[123] This bioactivation was confirmed to be NTR1 mediated following its discovery in trypanosomatids. [117–119] NTR1 bioactivates benznidazole (**38**) to cytotoxic electrophilic species that can react with cell components.[124] Unlike nifurtimox (**37**), benznidazole (**38**) is not bioactivated by NTR2 in trypanosomatids. [49]

3.11.3 Fexinidazole (39)

Fexinidazole (**39**) was first investigated as a treatment for African sleeping sickness in 1983, but only progressed to phase II clinical trials in 2009.[125,126] The mode of action of fexinidazole (**39**) is similar to nifurtimox (**37**), as it was found that *T. brucei* resistant to nifurtimox (**37**) were also 27-fold more resistant to fexinidazole (**39**) than wild type.[127] This common mode of action was later shown by Wyllie *et al.* to be mediated by NTR1 bioactivation. [44]

3.12 Nitroreductase

The principal mode of action of current nitro containing anti-trypanosomatid drugs centres around bioactivation by nitroreductases. Members of the nitroreductase family fall into two classes: type I and type II nitroreductases.[128] Type I nitroreductase use nicotinamide adenine dinucleotide (NADH) or nicotinamide adenine dinucleotide phosphate (NADPH) to elicit two electron reductions via a flavin mononucleotide (FMN) cofactor. This process is oxygen insensitive and does not generate reactive oxygen species. In general, type I NTRs reduce nitro containing compounds to the nitroso, hydroxylamine and potentially amine metabolites (Scheme 3.12.1A). However, the exact metabolite profile for each nitro compound depends on the stability and reactivity of each metabolite. In the case of drugs, type I NTR bioactivation often results in toxification of a prodrug to cytotoxic metabolites. Type II nitroreductase enzymes contain either an FMN or flavin adenine dinucleotide (FAD) cofactor and catalyse a one-electron reduction of the nitro group to generate a

radical. This reacts with oxygen to regenerate the parent nitro and produce superoxide anions which causes oxidative stress (Scheme 3.12.1B).[113]

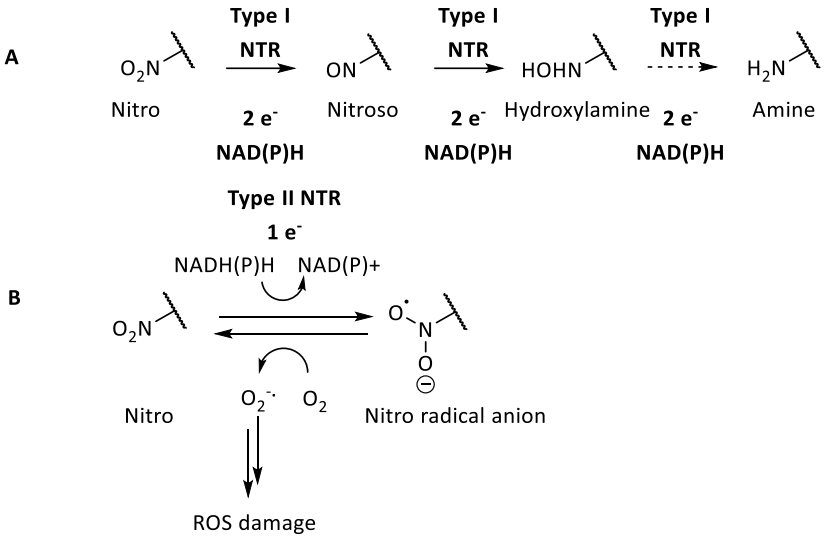

Scheme 3.12.1 General products of type I (**A**) and type II (**B**) nitroreductase metabolism of a nitro compound (adapted from Patterson *et al.* (2014)).[48]

Type I nitroreductase enzymes are present in prokaryotes but absent in most eukaryotes, with the exception of some fungal species, such as *S. cerevisiae*, and protozoan parasites, such as trypanosomatids.[129] The lack of mammalian equivalent of type I NTRs makes them attractive for prodrug bioactivation to treat bacterial, fungal and trypanosomatid diseases. Indeed, type I NTR bioactivation is involved in the mode of action of the antibiotics including nitrofurazone (**272**) and nitrofurantoin (**273**), in addition to the current antitrypanosomatid drugs discussed previously.[130,131]

Type I nitroreductase enzymes are homodimeric with two FMN cofactors sitting in clefts at the dimeric interface, forming hydrogen bonds to one and hydrophobic interactions with both monomeric units. The reducing agent (NADH or NADPH) π-stacks with the FMN cofactor and transfers a reducing hydride equivalent to the FMN, with an associated conformational change. $NAD(P)^+$ then leaves the active site and the nitro substrate enters, accepting the two-electron reducing equivalent to regenerate the native nitroreductase-FMN dimeric complex (Figure 3.12-1).[132]

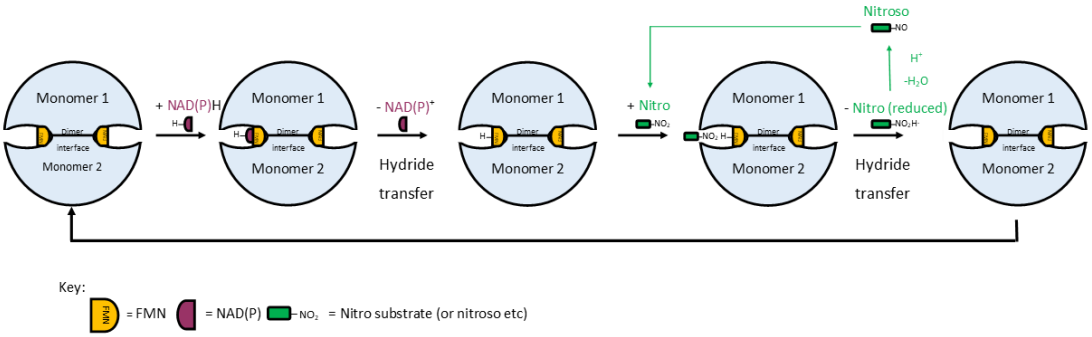

Figure 3.12-1 General mechanism of action of a type I nitroreductase.

Type I NTRs are promiscuous enzymes that bioactivate a range of nitro containing molecules. Haynes *et al.* obtained crystal structures of a type I nitroreductase from *E. cloacae* in the oxidised form with benzoate (PDB 1kqb, Figure 3.12-2) and acetate (PDB 1kqc) ligands as nitro substrate mimics. The crystal structure with the benzoate ligands revealed a flex in helix 6 to accommodate the larger ligand (Figure 3.12-2B).[133] This structural flexibility could account for the wide substrate scope of type I NTRs.

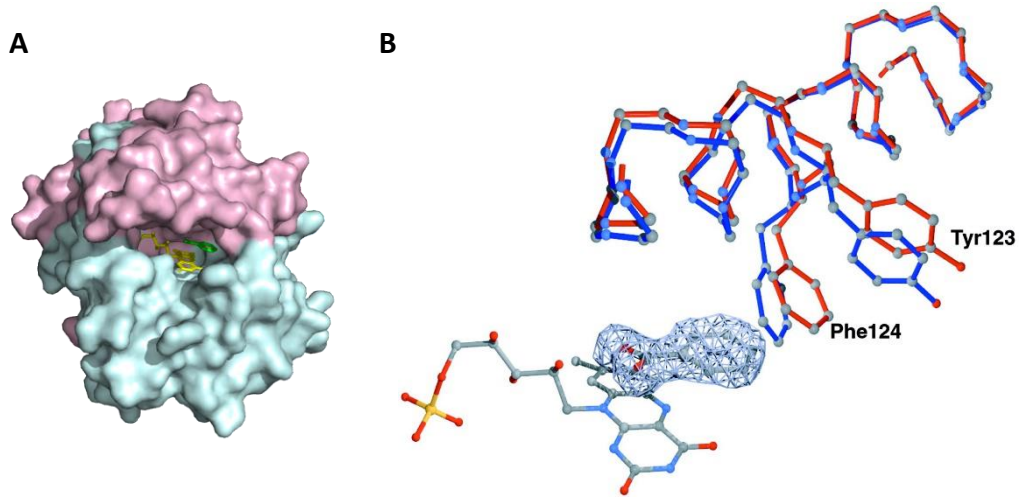

Figure 3.12-2 A. Type I NTR from *E. cloacae* crystal structure with co-crystalised benzoate ligand (PDB 1kqb). The FMN cofactor is highlighted in yellow, and the benzoate ligand is highlighted in green. Image generated using The PyMOL Molecular Graphics System, Version 2.0 Schrödinger, LLC. B. Flex in helix 6 to accommodate the bulkier benzoate ligand from comparison of the crystal structures with acetate (blue) and benzoate (red) ligands. Reproduced from Haynes *et al.* (2001).[133]

As previously discussed, *Leishmania* has two type I nitroreductase enzymes: NTR1 and NTR2. NTR1 is found in the mitochondria of all trypanosomatids including *Leishmania*, *T. cruzi* and *T. brucei*, sharing 57.8 – 65.7 % sequence identity with one another. Unlike NTR1, NTR2 is found in the cytosol of *Leishmania*.[49] No homologue

of NTR2 is present in *T. brucei*, however prostaglandin F2α synthase is a close homologue of *Ld*NTR2 found in *T. cruzi*, sharing 44 % sequence identity.[49,134] NTR1 is essential for parasite virulence as a double knockout of NTR1 cannot be generated in *L. donovani* or *T. brucei*.[49,120,135] The exact native function of NTR1 is uncertain, however nitroreductase enzymes are known to have roles in flavin fragmentation, ubiquinone biosynthesis, dehalogenation and dehydrogenation. [49,120,134–137] Furthermore, NTR1-null *T. cruzi* epimastigotes cannot differentiate, have retarded growth and reduced motility.[120]

Both NTR1 and NTR2 catalyse a series of two electron reductions on a wide substrate range. In general, NTR1 mediates the reduction of aromatic nitro compounds, such as nifurtimox (**37**), benznidazole (**38**) and fexinidazole (**39**), and NTR2 mediates the reduction of bicyclic nitro compounds, such as delaminid (**44**), DNDI-VL-2098 (**274**) and (*R*/*S*)- PA-824 (**275** and **276**) (Figure 3.12-3).[49]

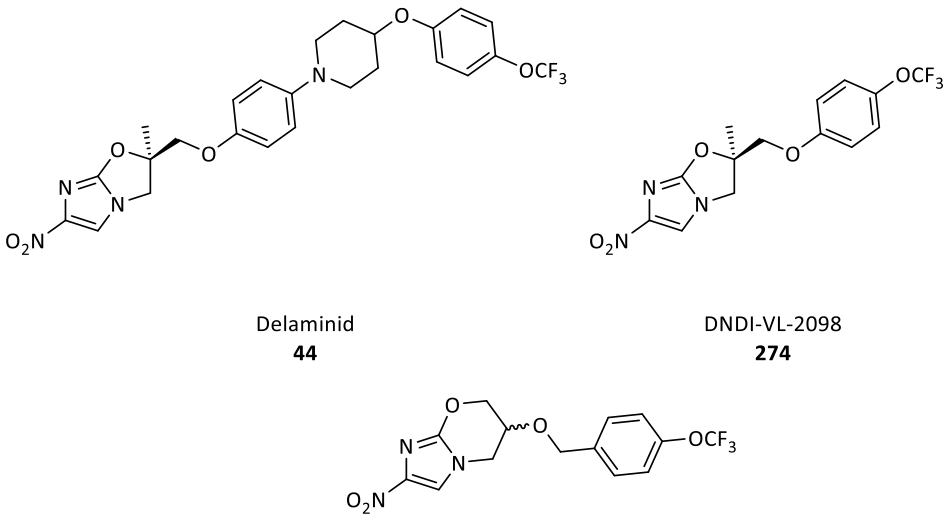

Figure 3.12-3 Substrates of NTR2 in trypanosomatids.

3.12.1 NTR1 bioactivation of anti-trypanosomatid drugs

As discussed previously, nifurtimox (**37**) can be bioactivated by both NTR1 and NTR2 in *Leishmania.* [49,120,135,138,139] Testing nifurtimox (**37**) against NTR1 and NTR2 overexpressing *L. donovani* parasites showed a 16-fold and 15-fold increase in

activity respectively compared to wild-type.[49,135] Nifurtimox (**37**) is metabolised by NTR1 to a cytotoxic α,β-unsaturated open chain nitrile (**279**), via nitroso (**277**) and hydroxylamine (**278**) metabolites. This is slowly reduced further by NTR1 to a non-toxic saturated open chain nitrile (**280**) (Figure 3.12-4). [138] Hall *et al.* showed that the α,β-unsaturated open chain nitrile metabolite had a greater than 5-fold increase in toxicity against THP-1 cells compared to nifurtimox (**37**), confirming it as a cytotoxic species.[140]

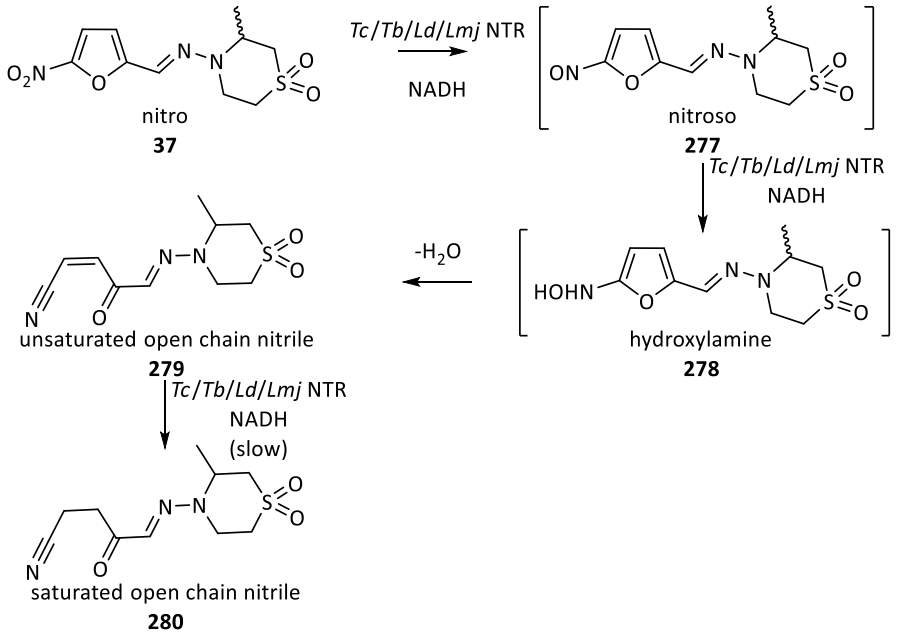

Figure 3.12-4 Nifurtimox (**37**) bioactivation by trypanosomatid NTRs adapted from Wilkinson *et al.* (2011). [141]

Benznidazole (**38**) undergoes bioactivation by NTR1 initially in a similar way to nifurtimox (**37**) to give the hydroxylamine (**282**) species. A series of dehydration and hydration steps converts the hydroxylamine (**282**) to the dihydro-dihydroxy species (**285**) which slowly releases cytotoxic glyoxal (**287**) and a guanidino species (**286**) (Figure 3.12-5).[124] Glyoxal (**287**) is a potent 1,2-dialdehyde electrophile that causes toxicity through reaction with amino acid side chains and nucleic acids, leading to protein inhibition and DNA damage respectively.[142]

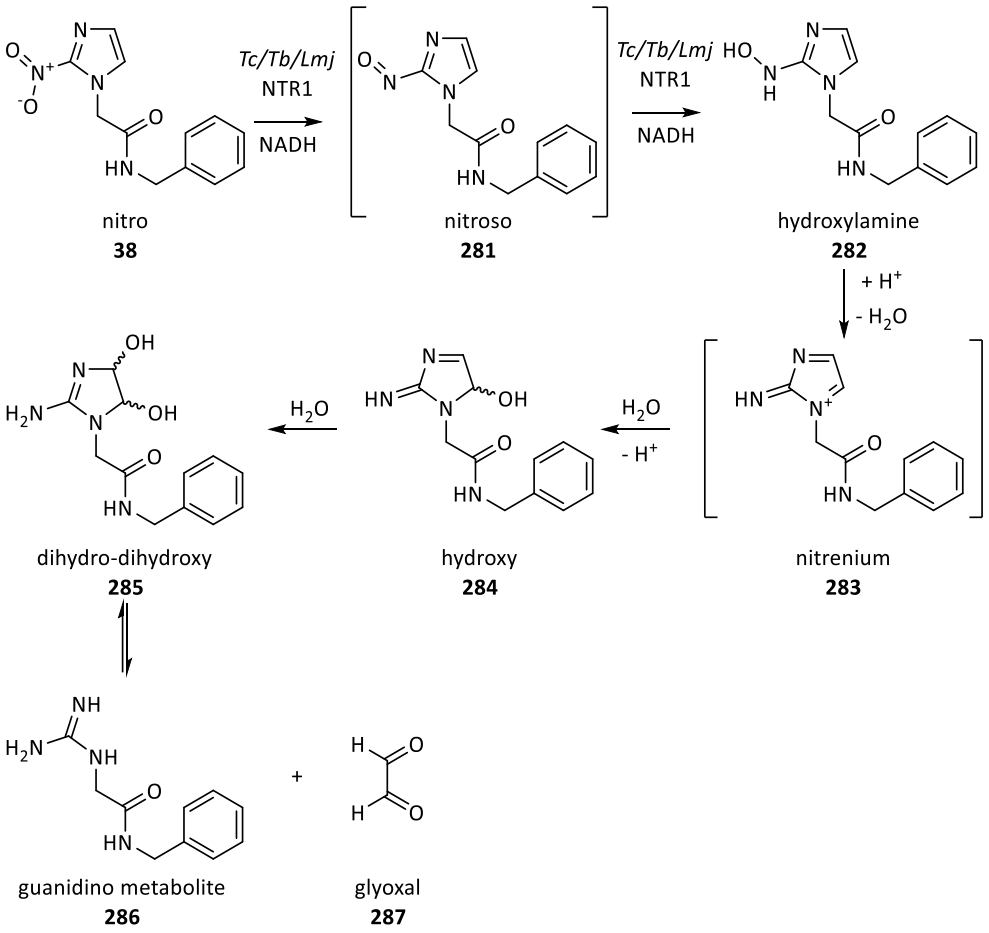

Figure 3.12-5 Bioactivation of benznidazole (**38**) by NTR1 in trypanosomatids, adapted from Hall *et al.* (2012). [124]

Fexinidazole (**39**) is oxidised *in vivo* to the sulfoxide (**288**) and sulfone (**289**) species (Figure 3.12-6).[143]

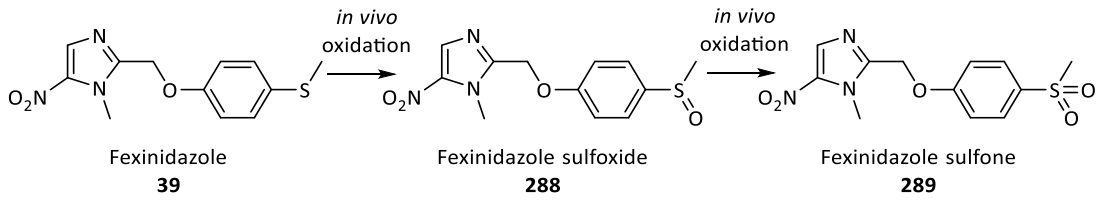

Figure 3.12-6 Oxidation of fexinidazole (**39**) *in vivo* to sulfoxide (**288**) and sulfone (**289**) metabolites. [143]

Both metabolites (**288** and **289**) are bioactivated by NTR1 in *Leishmania*, with fexinidazole sulfone (**289**) showing a 19-fold increase in toxicity against *L. major* axenic amastigotes overexpressing NTR1 compared to wild type.[44] However, the

metabolite profile of fexinidazole (**39**) following NTR1 bioactivation has not been reported to date.

3.12.2 NTR2 bioactivation of antileishmanial compounds

As discussed previously, NTR2 bioactivates bicyclic nitro compounds such as DNDI-VL-2098 (**274**), a potential VL treatment, and delaminid (**44**) and (*R*/*S*)-PA-824 (**275** & **276**), both originally developed as tuberculosis treatments with the potential for repurposing. [49,124,134,144,145] The metabolite profile following *Ld*NTR2 bioactivation of these bicyclic nitro compounds has not been reported. However, the metabolite profile of (*R*)- PA-824 (**275**) following bioactivation by *M. tuberculosis* deazaflavin (F_{420})-dependent nitroreductase (*Mtb*Ddn) has been investigated. This presents an interesting alternative bioactivation profile to the NTR1 substrates discussed previously. Instead of nitro reduction to nitroso and hydroxylamine species, the compound is reduced directly on the ring to give the 4,5-dihydroimidazole species (**291**), which loses its nitro group to generate nitrous acid and nitric oxide, resulting in respiratory poisoning and toxicity (Figure 3.12-7).[146–148]

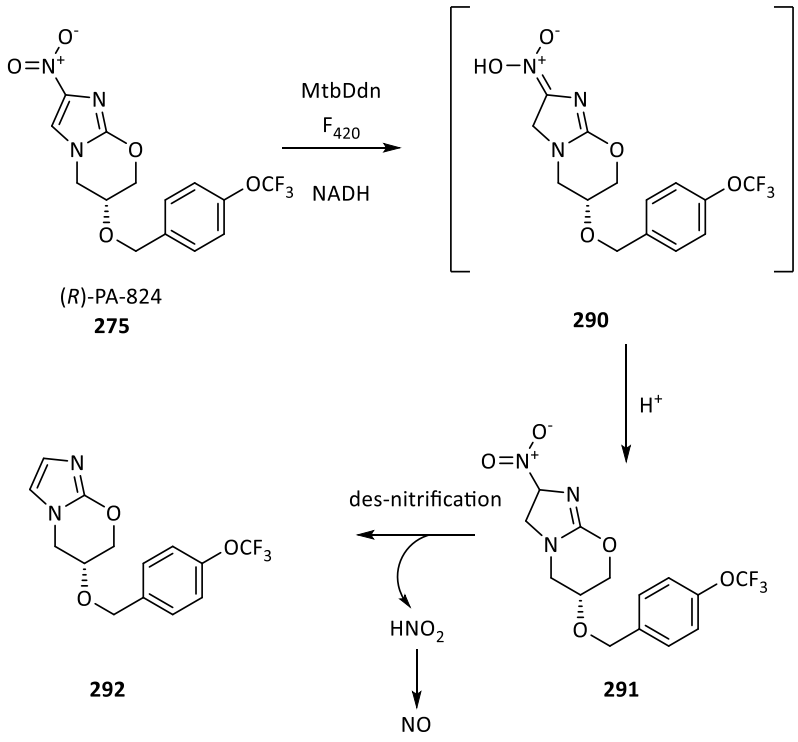

Figure 3.12-7 (*R*)- (**275**) or (*S*)- (**276**) PA-824 bioactivation by *Mtb*Ddn, adapted from Wyllie *et al*. (2014). [48]

Both (*R*)- and (*S*)- PA-824 (**275** and **276**) isomers are potent antileishmanial compounds, with the (*R*)- enantiomer (**275**) supressing *L. donovani* infection by 99.9 % *in vivo*.[134] (*R*)-PA-824 (**275**) also shows good *T. cruzi* activity against both epimastiogte and amastigote forms, potentially due to bioactivation by the NTR2 homologue prostaglandin F2α synthase. However, both isomers show poor activity against procyclic and bloodstream *T. brucei* parasites, which has no functional analogue of NTR2 (Table 3.12-1). [134]

Table 3.12-1: Anti trypanosomatid activity of (*R*) and (*S*)-PA-824 (**275** and **276**). Reproduced from Patterson *et al.* (2013). [134]

	Developmental stage	**(*S*)-PA-824 (276) / µM**	**(*R*)-PA-824 (275) / µM**
L. donovani	Promastigote	0.9 ± 0.1	0.16 ± 0.03
	Amastigote (InMac)	4.9 ± 0.3	0.93 ± 0.06
T. cruzi	Epimastigote	3.4 ± 0.03	0.70 ± 0.08
	Amastigote (InVero)	> 30	4.4 ± 0.5
T. brucei	Procyclic	37 ± 3	25.0 ± 0.2
	Bloodstream	38 ± 3	14.9 ± 0.7

3.12.3 5-Nitrothiophene bioactivation by NTRs

NTR bioactivation has only been briefly investigated for a selection of 5-nitrothiophenes in the literature. [59,62,149] Pacheco *et al.* showed that 5-nitrothiophene-2-nitrones (**293-295**) are bioactivated by *Ldon*NTR1 in an overexpressor model (Figure 3.12-8). [59,149]

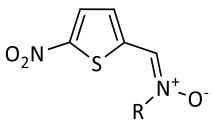

R= *t*-Bu (**293**), Me (**294**), Bn (**295**)

Figure 3.12-8 Literature example of a 5-nitrothiophene scaffold (**293-295**) that shows bioactivation by NTR in trypanosomatids.[59]

There are no current reports that investigate the metabolite profile of 5-nitrothiophenes after trypanosomatid NTR bioactivation. However, Hartkoorn *et al.*

showed that 5-nitrothiophene **296** is bioactivated by *Mtb*Ddn in *M. tuberculosis* to release nitric oxide. It was suggested that this was due to bioactivation of 5-nitrothiophene ring in a similar manner to (*R*)-PA-824 (**275**) resulting in des-nitrification (Figure 3.12-9). [150]

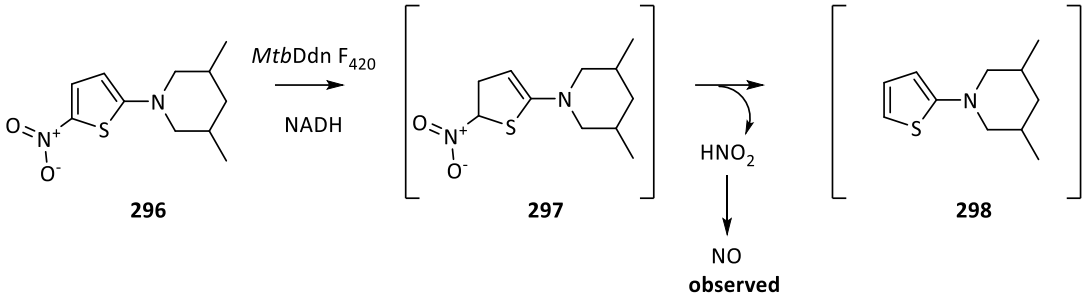

Figure 3.12-9 Postulated bioactivation of 5-nitrothiophene **296** by *Mtb*Ddn resulting in generation of NO. [150]

The compound series in this work are more specifically 5N2Cs. There is no literature precedent for the bioactivation of 5N2Cs by NTRs in trypanosomatids, but Hameed *et al.* did report that 5N2Cs are bioactivated by bacterial nitroreductases (nsfA and nsfB) in *E. coli.* [69] However, the metabolite profile following bioactivation in *E. coli* was not investigated.

Chapter 3 of this thesis will investigate the mode of action of 5N2Cs in *Leishmania* by first exploring the possibility for NTR bioactivation before assessing the wider mode of action of the series.

3.2 Aims

As previously discussed in Chapter 1, the 5N2C series do not inhibit *Lmj*IPCS. It was therefore of interest to explore the mode of action of the 5N2C series to achieve the following aims:

1. Explore the possibility for nitroreductase bioactivation (section 3.31);
2. Investigate any more global modes of action of the 5N2C series (section 3.32).

3.3 Results and Discussion

3.31 Bioactivation by nitroreductase

As previously discussed in section 2.1, *Leishmania* has a class of enzymes called nitroreductase (NTR) that are absent in humans. Subsequently, prodrugs that are substrates for NTRs have the potential to be bioactivated to cytotoxic species in the parasite whilst leaving the host unharmed. This makes nitro containing drugs a promising prospect to treat *Leishmania* infections. Significantly, nitro containing drugs such as nifurtimox (**37**), fexinidazole (**38**) and benznidazole (**39**), are bioactivated by nitroreductase (NTR1 or NTR2) in trypanosomatids. [44,49,124,129,138] Furthermore, a recent 2021 report from Pacheco *et al.* showed that 5-nitrothiophene-2-nitrones **293-295** are bioactivated by *Ldon*NTR1 in an overexpressor model.[59] Given this precedent, efforts focussed on nitroreductase as a mode of bioactivation for the 5N2C series in *Leishmania*.

3.31.1 Reduction potential of the 5N2C series

The ability of a compound to act as a nitroreductase substrate is dependent on its reduction potential. Pedron *et al.* observed that reduction potential correlates with antileishmanial activity for a series of nitroquinoline-2-ones. Compounds only showed activity when $E^{1/2} > -0.6$ V and a representative active compound ($E^{1/2}$ -0.45 V) subsequently showed bioactivation by *Ldon*NTR1.[151] Following this precedent, it was of interest to determine the reduction potential of a selection of 5N2Cs using cyclic voltammetry before nitroreductase activity could be assessed (Figure 3.31-1). In short, compounds were dissolved in dry DMSO with 0.1 M $(NBu_4)[PF_6]$ as a supporting electrolyte and purged with nitrogen for 3 minutes before a sweeping potential was applied using a potentiostat. Any redox transitions were corrected relative to an internal ferrocenium/ferrocene reference couple and reported vs normal hydrogen electrode (NHE). The exploration of reduction potentials for the 5N2C series will establish whether compounds could act as nitroreductase substrates and enable the analysis of any correlations with antileishmanial activity.

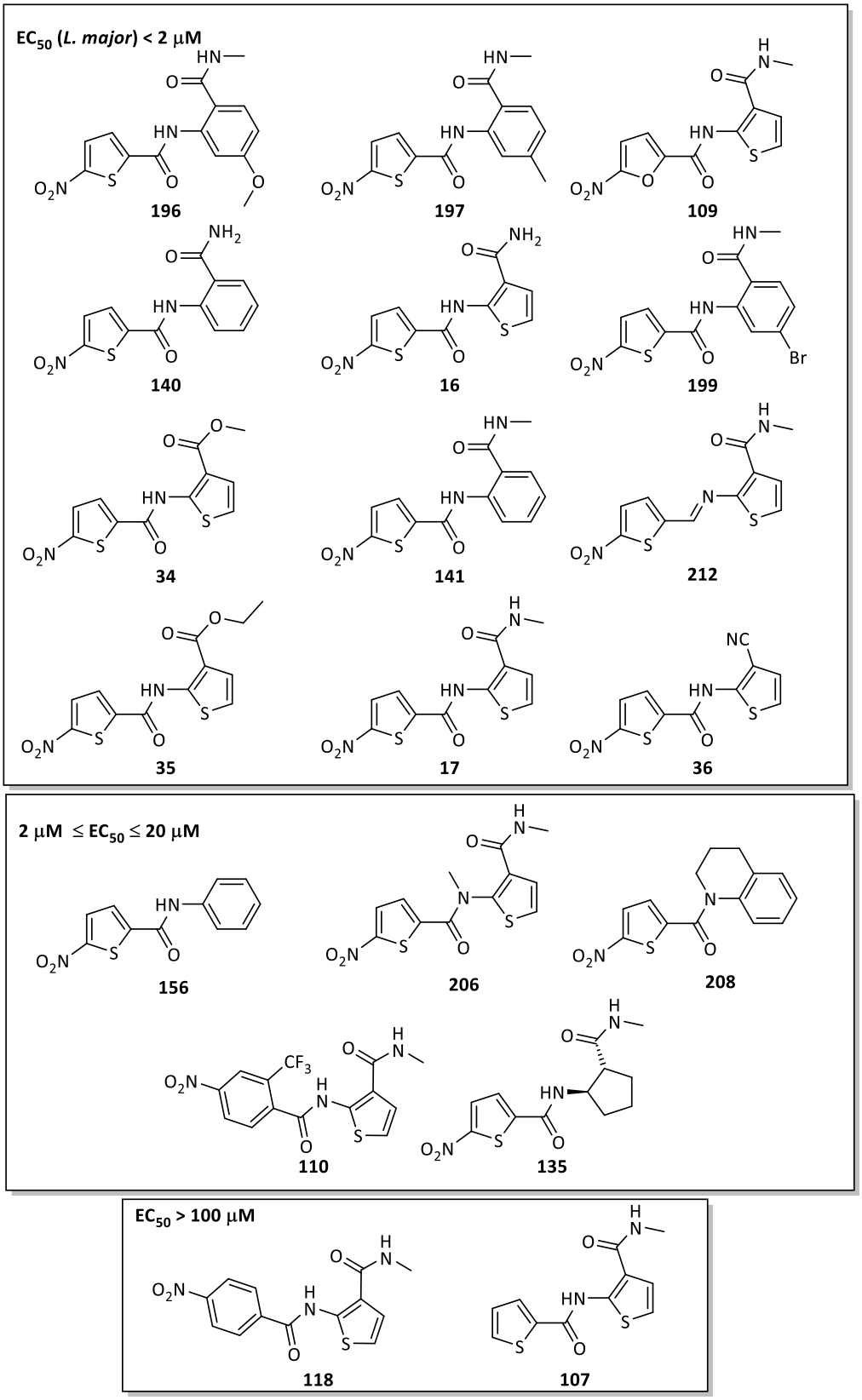

Figure 3.31-1 Selection of 5N2C compounds used for cyclic voltammetry with a range of antileishmanial activities.

Cyclic voltammetry is a technique where positive (oxidation) and negative (reduction) potentials are applied to a sample and the change in current upon redox processes is measured as an output (Figure 3.31-2A). If a redox process is electrochemically reversible, a mirror image of the reduction or oxidation wave will be replicated upon application of the opposite potential. In this case, the position of the peak cathode (E_{pc}) and peak anode (E_{pa}) potentials should be within 0.1 V of one another and the magnitude of the current for these peaks should be equal (Figure 3.31-2B). A transition may be defined as partially reversible if a peak is also observed when the reversed potential is applied but it does not fit the definition of a fully reversible transition (Figure 3.31-2C). Furthermore, transitions can be classed as irreversible if there is no peak when the reversed potential is applied (Figure 3.31-2C).

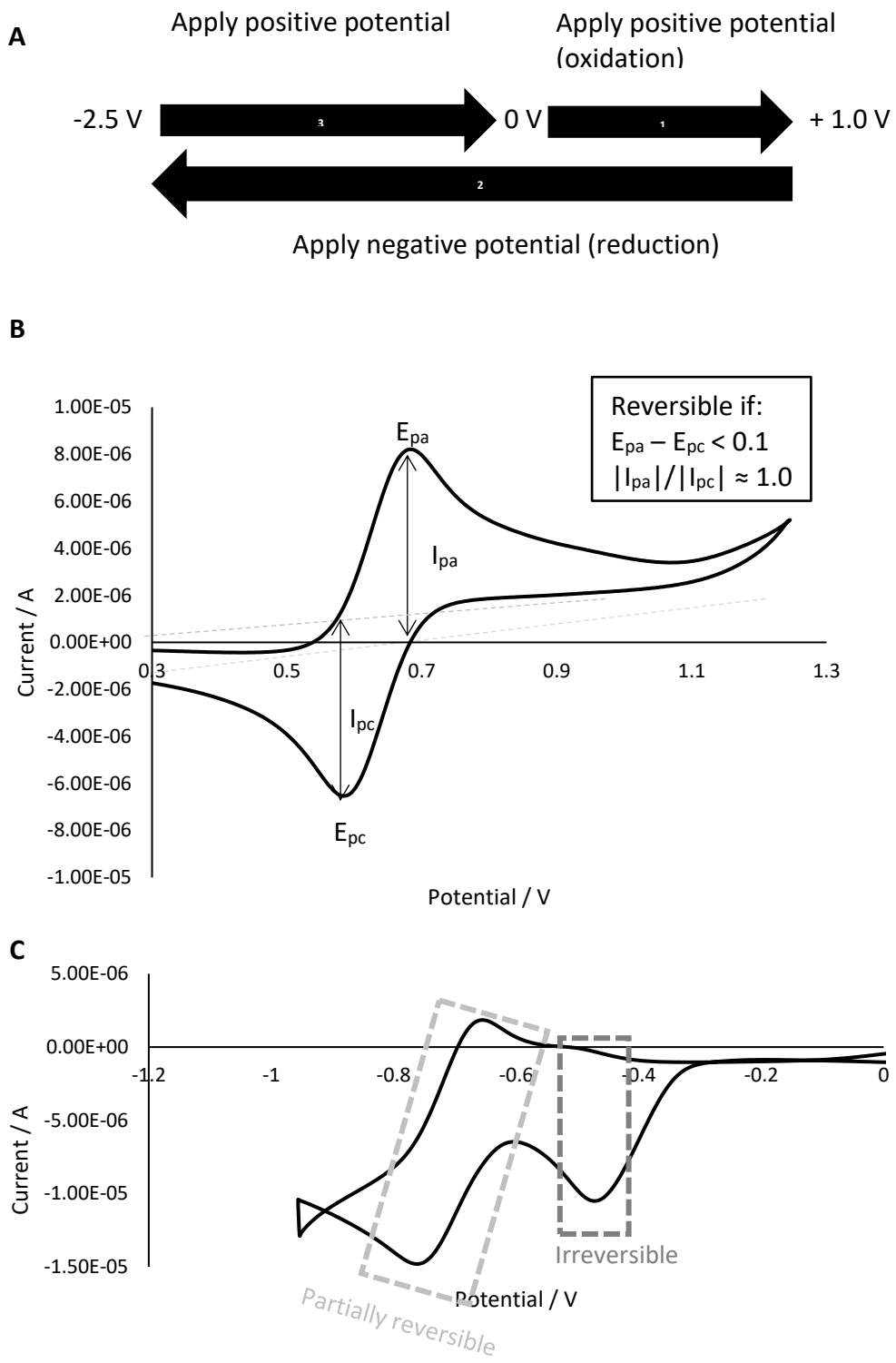

Figure 3.31-2 A. Representation of the potential changes used in cyclic voltammetry to measure reduction and oxidation potentials of a compound. B. Representative cyclic voltammogram for a reversible transition (the Fc^+/Fc standard couple is used as an illustrative example). C. Representative cyclic voltammogram for partially reversible and irreversible transitions (**17** used as an illustrative example).

Analysis of the reduction potentials for the series of 5N2Cs enabled clustering into 4 groups: bisheterocycles with an irreversible first transition and partially reversible second transition, 5N2C phenyl series with two partially reversible transitions, singletons with one reversible transition and *p*-nitrophenyl series with partially reversible transitions (Table 3.31-1).

Table 3.31-1 Values of peak cathodic and anodic potentials for the first two reduction waves for series 1-4 compounds. All values are stated vs. NHE. * peak current was low and barely visible. ND means I^{II}_a/I^{II}_c was not determined, take as a not truly reversible wave. Values reported as the average of three repeats.

Series	Compound number	E^{I}_{pc} / V	E^{I}_{pa} / V	$E^{0}(I)$/ V	I^{I}_a/I^{I}_c	E^{II}_{pc} / V	E^{II}_{pa} / V	$E^{0}(II)$/ V	I^{II}_a/I^{II}_c
1	**16**	-0.47	-	-	-	-0.77	-0.65	-0.71	ND
	17	-0.47	-	-	-	-0.76	-0.66	-0.71	ND
	109	-0.56	-	-	-	-0.85	-0.83	-0.84	ND
	35	-0.52	-	-	-	-1.13	-0.93	-1.03	ND
	34	-0.50	-	-	-	-0.86	-0.76	-0.81	ND
	36	-0.45	-	-	-	-0.76	-0.65	-0.71	ND
2	**140**	-0.53	-0.44	-0.49	ND	-0.72*	-0.67	-0.69	ND
	141	-0.55	-0.45	-0.50	ND	-0.76*	-0.68	-0.72	ND
	196	-0.52	-0.46	-0.49	ND	-0.79	-0.68	-0.74	ND
	197	-0.57	-0.46	-0.52	ND	-0.76	-0.71	-0.74	ND
	199	-0.53	-0.45	-0.49	ND	-0.75	-0.65	-0.70	ND
3	**212**	-0.28	-0.30	-0.29	0.86	-0.60	-0.58	-0.59	0.99
	206	-0.60	-0.52	-0.56	1.22	-	-	-	-
	135	-0.63	-0.50	-0.57	1.01	-	-	-	-
	156	-0.64	-0.59	-0.62	1.02	-	-	-	-
	208	-0.58	-0.48	-0.53	0.93	-	-	-	-
4	**118**	-0.65	-	-	-	-1.11	-1.03	-1.07	ND
	110	-0.61	-	-	-	-1.07	-0.94	-1.01	ND

Each of the compounds in series 1 (Figure 3.31-3) are bisheterocycles with a relatively acidic central amide proton, which share a common profile in the cyclic voltammogram. Hit nitrothiophene **17** showed a + 0.09 V higher reduction potential than corresponding nitrofuran **109**, potentially due to the ability of the sulfur to accommodate extra electrons from the reduced nitro group.[57]

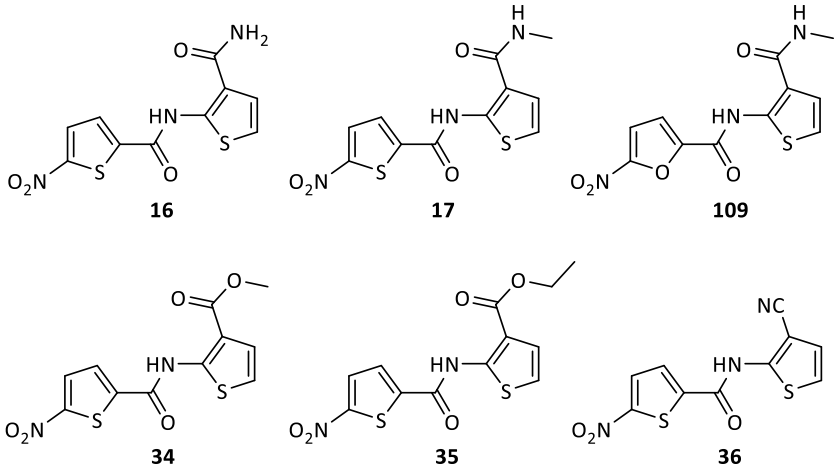

Figure 3.31-3 Series 1 compounds, each with an acidic central amide proton, sharing similar cyclic voltammograms.

Firstly, series 1 compounds undergo an irreversible reduction at E^{I}_{pc} values between -0.45 and -0.56 V. This wave is predicted to be due to a rapid 'father-son' type protonation where the acidic proton in the 'father' molecule (**300**) protonates the nitro radical 'son' molecule (**301**) (Figure 3.31-5A) to generate a neutral radical species (**302**) and an anionic species (**303**).[152] This process is almost instantaneous and results in an irreversible first reduction. A similar process also occurs in other nitro heteroaromatics containing an acidic proton such as megazol derivative **299**; a nitroimidazole with antitrypanosomatid activity (Figure 3.31-4).[152,153]

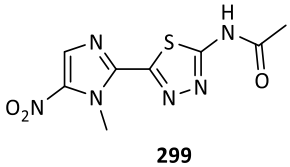

Figure 3.31-4 Megazol acetamide derivative **299** which shows a similar redox behaviour to series 1 compounds due to 'father-son' type protonation. [152,153]

Secondly, there is a partially reversible transition which involves reduction of the anionic species (**303**) to give a dianionic radical species (**304**) (Figure 3.31-5A). A representative cyclic voltammogram for series 1 is given in Figure 3.31-5B.

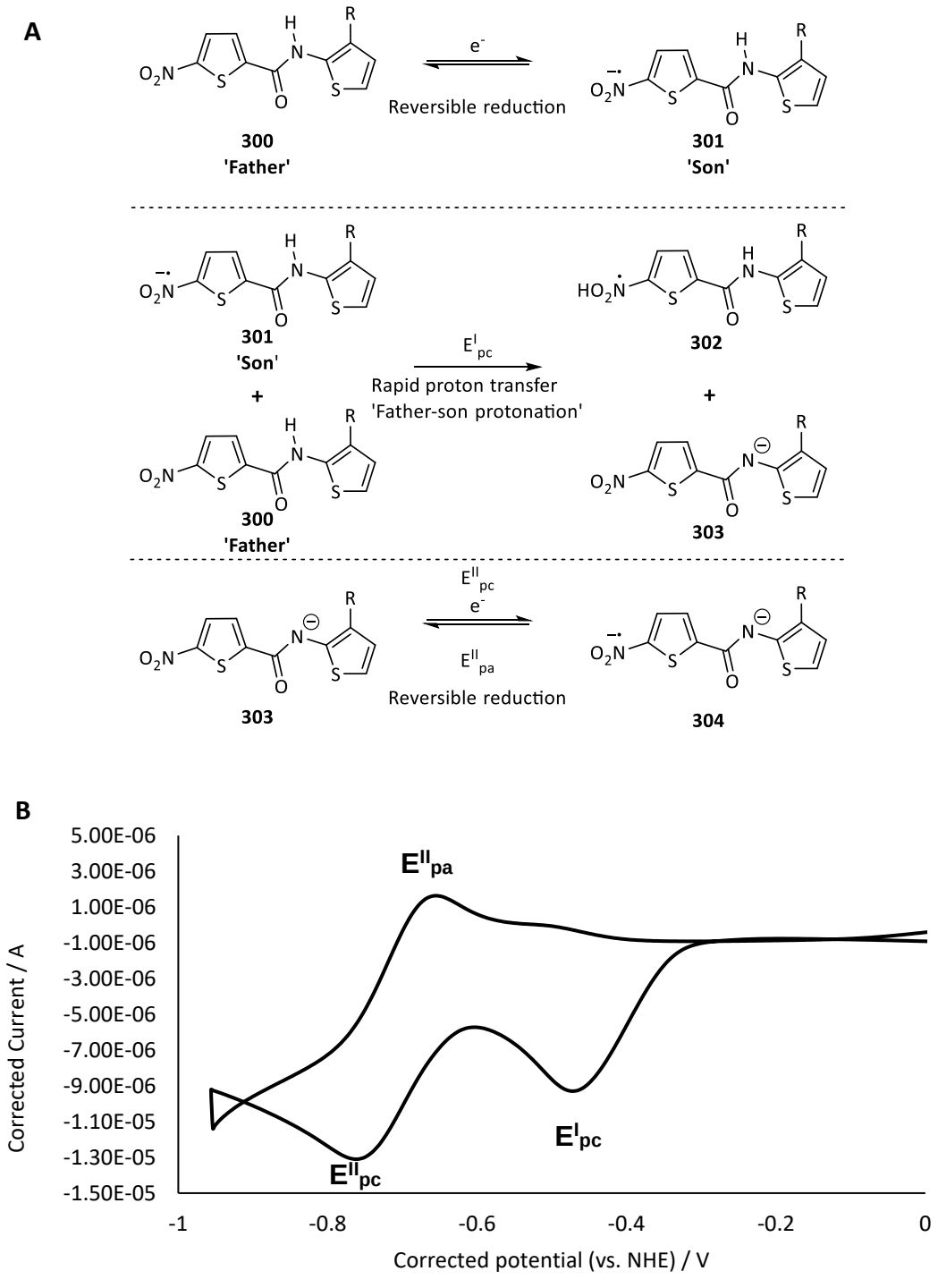

Figure 3.31-5 A. Proposed mechanism for single electron reduction of series 1 during cyclic voltammetry. B. Representative cyclic voltammogram for series 1 compounds (actual trace shown is for **17**).

Bonta *et al.* showed that adding sodium hydroxide to solutions of megazol derivative **299** resulted in loss of the first irreversible reduction peak due to removal of the acidic 'father' proton. [152] Following this precedent, sodium hydroxide was added to solutions of **17** in DMSO as a representative compound for series 1. In support of the proposed mechanism, E^{I}_{pc} decreases and eventually disappears upon addition of sufficient sodium hydroxide (> 0.3 μM) as only the anionic form (**303**), which is reduced to the dianionic radical (**304**) in E^{II}, is now present (Figure 3.31-6A). Upon addition of sodium hydroxide, E^{II} becomes more reversible as I_{pc}/I_{pa} tends towards 1.0 and $\Delta(E_{pc} - E_{pa}) \leq 0.1$ (Figure 3.31-6B-C). This shows that the reduction of the nitro anion (**303**) is reversible if all the compound exists as the anionic form.

A

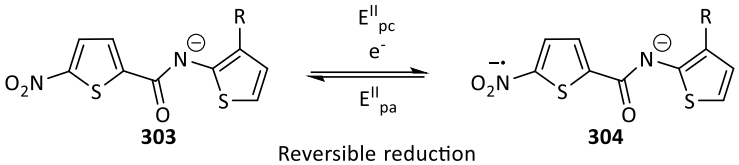

B

Concentration NaOH / μM	E^{I}_{pc} / V	E^{II}_{pc} / V	E^{II}_{pa} / V	$\Delta(E^{II}_{pc} - E^{II}_{pa})$ / V	E^{0} / V	I^{II}_{pc}	I^{II}_{pa}	I^{II}_{pa}/ I^{II}_{pc}
0.0	-0.45	-0.73	-0.65	0.08	-0.69	2.07	0.09	0.04
0.1	-0.46	-0.73	-0.65	0.08	-0.69	2.42	3.11	1.29
0.2	-0.46	-0.74	-0.64	0.10	-0.69	2.67	3.21	1.20
0.3	-	-0.74	-0.64	**0.10**	-0.69	3.06	3.03	**0.99**
0.5	-	-0.74	-0.64	**0.10**	-0.69	3.78	3.95	**1.04**

C

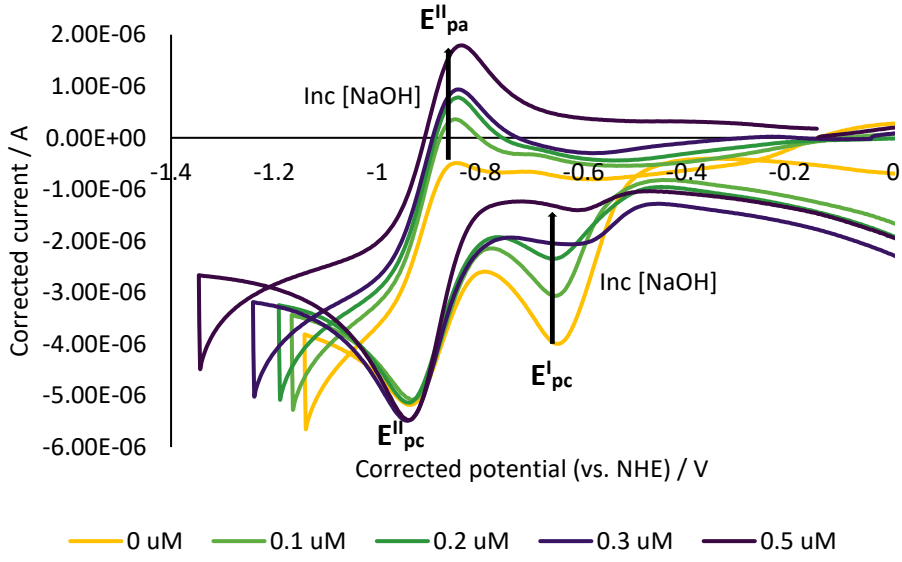

Figure 3.31-6 **A.** Overall equation showing the only reduction process possible upon addition of sufficient NaOH. **B.** Table of values for **17** showing how E^{I}_{pc} disappears and E^{II} becomes more classically reversible (bold) as NaOH concentration is increased. **C.** Cyclic voltammogram of **17** at different concentrations of NaOH.

In summary, the reduction potential of all series 1 compounds lie within the biological range of NTR (E^{I}_{pc} -0.47 to -0.56 V), as defined by Pedron *et al*.[151] The series

also show an interesting electrochemical profile caused by the 'father-son' protonation facilitated by the relatively acidic central amide proton. However, this is not directly relevant when applying these results to the type I nitroreductase model, as NTR reduction is a 2-electron process and as such this protonation is not biologically relevant.

A second series consists of 5N2C phenyl compounds with two partially reversible transitions (Figure 3.31-7).

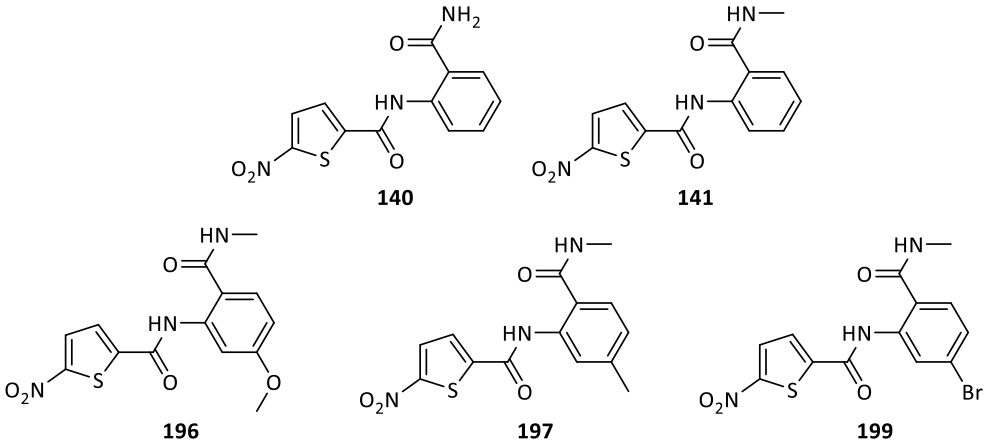

Figure 3.31-7 Series 2 compounds (each with a phenyl group as the right-hand ring) which were clustered due to similar cyclic voltammograms.

Series 2 compounds each show a first reduction (E^{I}_{pc} values between -0.52 and -0.57 V) with partially reversible character, as indicated by a small E^{I}_{pa} peak in the cyclic voltammogram. The transition is not truly reversible as I_{pa}/I_{pc} does not have the value of 1.0. As with series 1, this wave was predicted to be due to father-son type protonation due to the presence of an acidic proton in the molecule (Figure 3.31-5A).[152] However, the partially reversible character of this transition suggests that this protonation is not as rapid as for series 1. The second reduction is barely visible in this series, which could again be indicative of the much smaller concentration of the anionic form compared to series 1 (Figure 3.31-8).

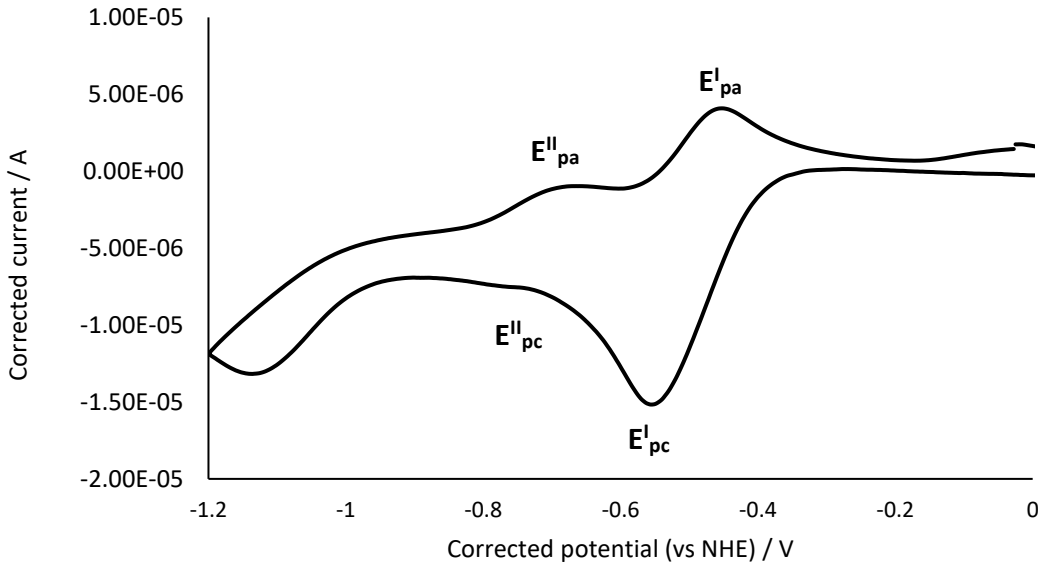

Figure 3.31-8 Representative cyclic voltammogram for series 2 compounds (actual trace shown is for **141**).

Analogously to series 1, sodium hydroxide was added to DMSO solutions of **141** as a representative compound for series 2 to rationalise the suggested mechanism. Although the results are less clear than for series 1, they still support the proposed mechanism. E^{I}_{pc} decreases and eventually disappears upon addition of sufficient sodium hydroxide (> 0.7 μM). Concurrently, the second reduction peak (E^{II}) increases in size and becomes more reversible as only the anionic form (**305**) is now present (Figure 3.31-9)

A

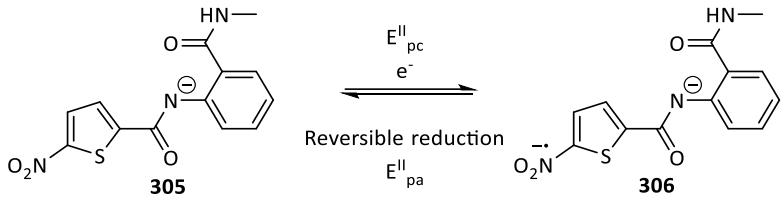

B

Concentration NaOH / μM	E^{I}_{pc} / V	E^{II}_{pc} / V	E^{II}_{pa} / V	$\Delta(E^{II}_{pc} - E^{II}_{pa})$ / V	E^{0} / V	I^{II}_{pc}	I^{II}_{pa}	I^{II}_{pa}/ I^{II}_{pc}
0.0	-0.59	-0.76*	-0.68	0.08	-0.72	-	-	-
0.3	-0.65	-0.92	-0.87	**0.05**	-0.90	2.26	2.12	**0.94**
0.7	-	-0.95	-0.95	**0.00**	-0.95	2.73	3.25	**1.19**

C

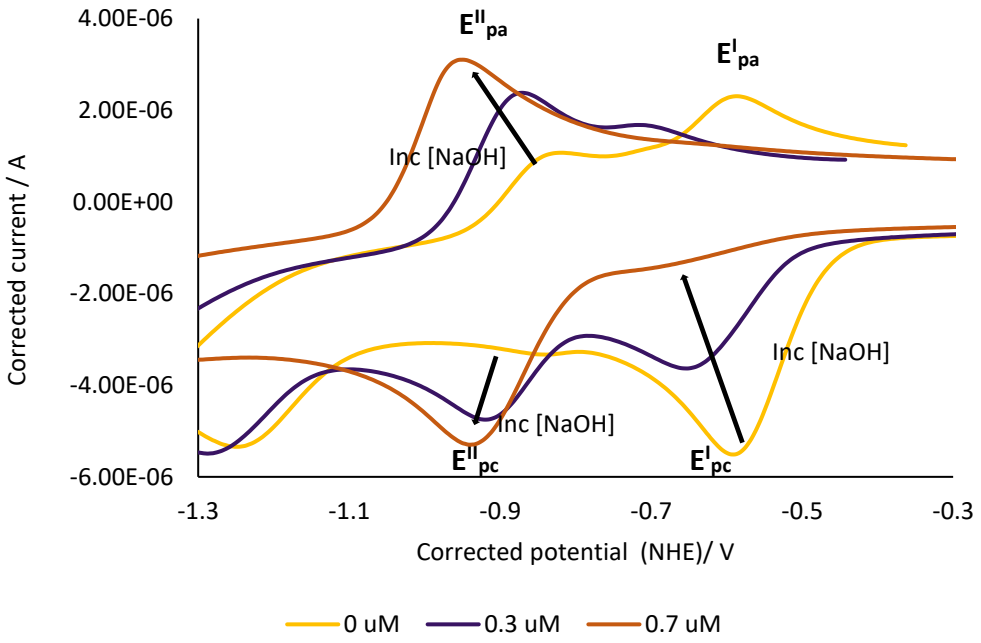

Figure 3.31-9 A. Overall equation showing the only reduction process possible upon addition of sufficient NaOH. B. Table of values for **141** showing how E^{II} becomes more classically reversible (bold) as sodium hydroxide concentration is increased. C. Cyclic voltammogram of **141** at different concentrations of sodium hydroxide.

In summary, the reduction potentials for series 2 compounds lie within the biological range of NTR (E^{i}_{pc} -0.52 to -0.57 V), in analogy with series 1. Series 2 compounds also share a similar electrochemical profile with series 1 due to the presence of the relatively acidic central amide proton.

A third series consists of singleton compounds with no acidic proton (Figure 3.31-10). Two compounds (**156** and **135**) do still have a central amide proton, however a negative charge in this position is not delocalised into an electron withdrawing group. Subsequently, this proton is much less acidic than those in series 1 and 2, as shown by a lower chemical shift in proton NMR (δ_H 10.64 and 8.84 ppm for **156** and **135** compared to 13.11 ppm for **141**). Subsequently, compounds **156** and **135** share electrochemical character with those with no central amide proton (**212**, **208** and **206**).

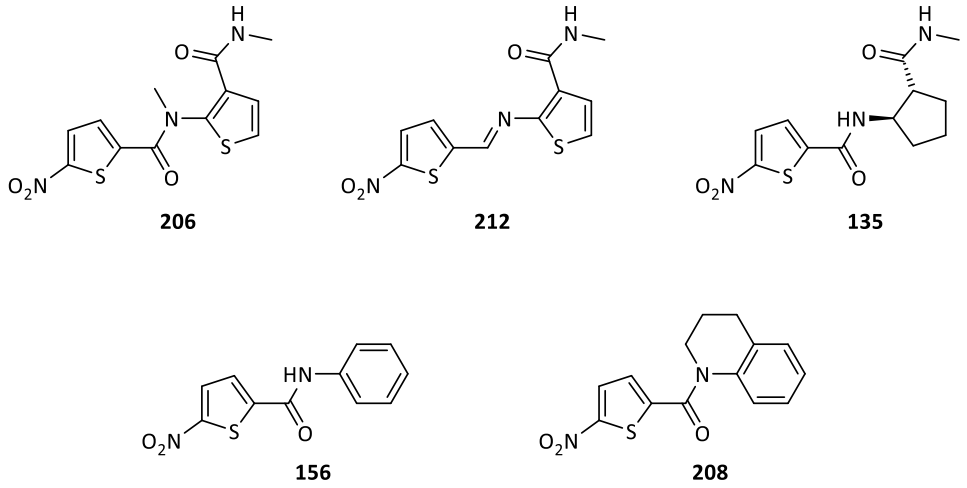

Figure 3.31-10 Series 3 compounds (each with no acidic proton) were clustered due to similar cyclic voltammograms.

Series 3 compounds each show an apparently reversible first reduction (E^{I}_{pc} values between -0.28 and -0.65 V). The first waves for **156** and **135** are fully reversible (Table 3.31-1). However, the first reduction waves for **212**, **208** and **206** are not truly reversible as I_{pa}/I_{pc} does not have the value of 1.0. The reversible nature of the first reduction transition and lack of second reduction (except for **212**) supports the proposed reduction mechanism for series 1 and 2. Series 3 compounds have no acidic proton and as such cannot undergo the 'father-son' protonation seen in series 1 and 2. This enables the first reduction to be reversible for series 3. Furthermore, the lack of second reduction peak for series 3 can be explained by the absence of deprotonated 'father' molecule, which is proposed to be reduced in the second

reduction wave for series 1 and 2. A representative cyclic voltammogram for series 3 is shown in Figure 3.31-11.

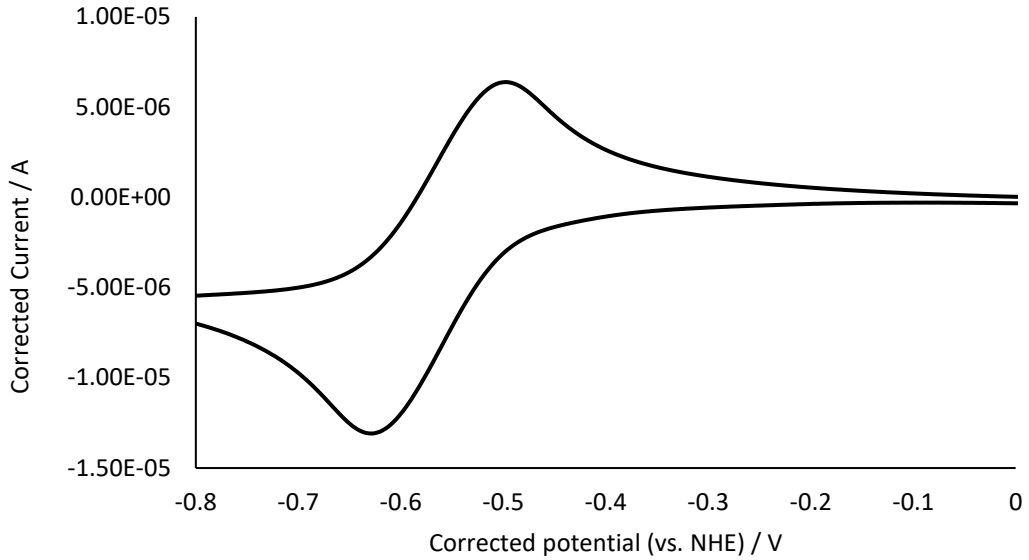

Figure 3.31-11 Representative cyclic voltammogram for series 3 compounds (actual trace shown is for **135**).

In summary, the reduction potentials of series 3 (except **212**) are lower than series 1 and 2 (E^{I}_{pc} -0.58 to -0.64 V), putting them at the limits of NTRs reducing capabilities.[151] Conversely, **212** is the only compound with two reduction potentials within the capabilities of NTR and as such may have a different bioactivation profile to the other 5N2Cs. Furthermore, the absence of the relatively acidic proton simplifies the cyclic voltammogram for series 3 compared to series 1 and 2.

A final series of p-nitrophenyl derivatives was identified whose redox behaviours do not relate to any other compounds (Figure 3.31-12).

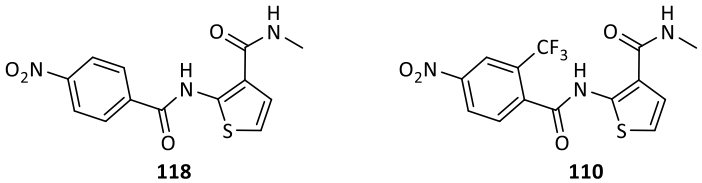

Figure 3.31-12 **118**, the p-nitrophenyl derivative and compound **110**, predicted to have a more positive first reduction potential.

118 shows no activity against *L. major* or *L. amazonensis* (EC_{50} > 100 µM). It has an E^{I}_{pc} value of -0.65 V, which is slightly more negative than the other compounds which have some activity against *Leishmania*. To investigate whether the more negative reduction potential causes the lack of antileishmanial activity, compound **110** was investigated. This has an additional electron withdrawing CF_3 group in the 2- position, which caused a shift of + 0.04 V in all peak cathodic reduction potentials when compared to **118** (Figure 3.31-13). An increase in antileishmanial activity to 16.6 µM is observed, which corresponds to the increase in reduction potential. This suggests that the activity of the nitrophenyl series could be attenuated by adding more electron withdrawing substituents. However, since **110** has such poor activity compared to the 5N2C series, this was not considered further.

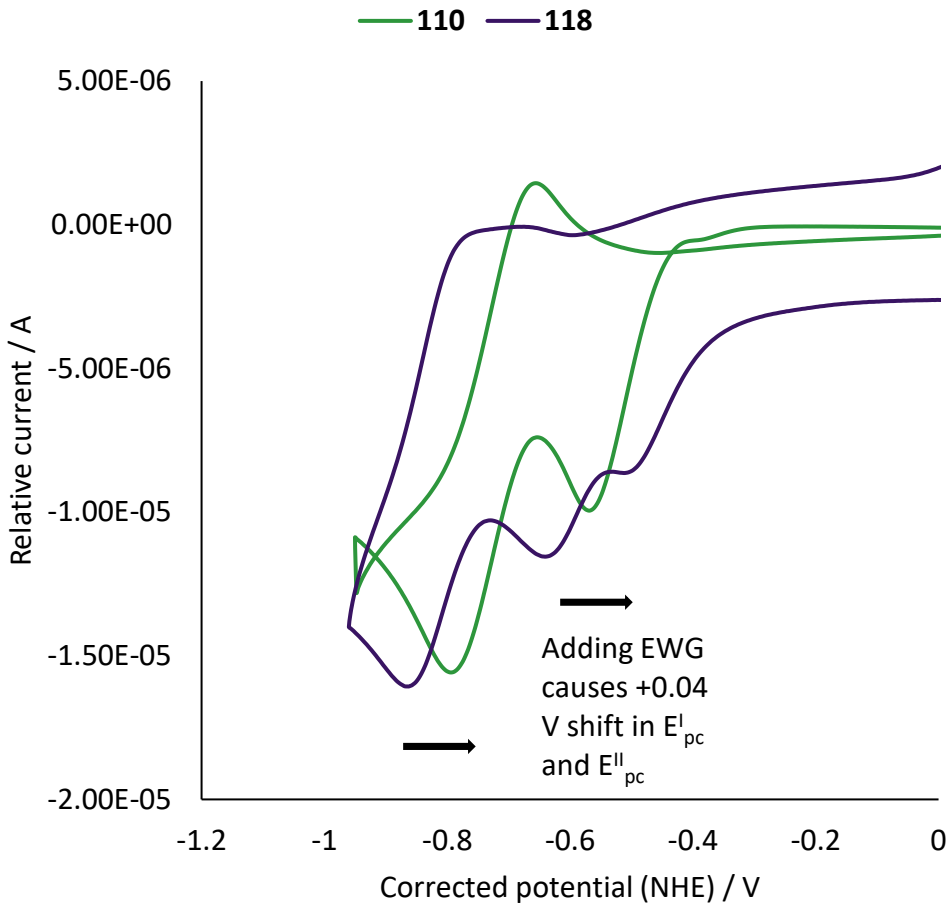

Figure 3.31-13 Cyclic voltammogram for *p*-nitro phenyl derivatives **118** and **110**.

In summary, series 4 compounds show that the electrochemical nature of the aromatic substituent significantly affects the reduction potential of the nitro group. **118** has a reduction potential outside of the capabilities of NTRs (E^{I}_{pc} -0.65 V) specified by Pedron *et al.*[151] This could explain the lack of antileishmanial activity seen for this analogue. Conversely, **110** has a reduction potential at the interface of NTRs capabilities (E^{I}_{pc} -0.61 V), which could enable bioactivation and hence explain the improvement in antileishmanial activity.

3.31.1.1 Discussion

In all cases (except **212**), the second reduction for the 5N2Cs is likely to be unimportant in a biological setting due to it being outside of the reducing abilities of *Leishmania* NTRs (< -0.60 V, Table 3.31-1).[151] As such, only the first reduction wave should be considered as being relevant for nitroreductase bioactivation. However, no direct correlation can be found between reduction potential and antileishmanial activity (Figure 3.31-14). It is apparent that the most active compounds have an acidic proton (i.e. are in series 1 and 2) and have E^{I}_{pc} > -0.57 V. Less active antileishmanial compounds are found in series 3 and 4 and have E^{I}_{pc} < -0.57 V. Subsequently, there appears to be a cut off in reduction potential for the 5N2C series at E^{I}_{pc} -0.57 V, below which activity is lost. However, above this limit there is no correlation between antileishmanial activity and the magnitude of E^{I}_{pc}.

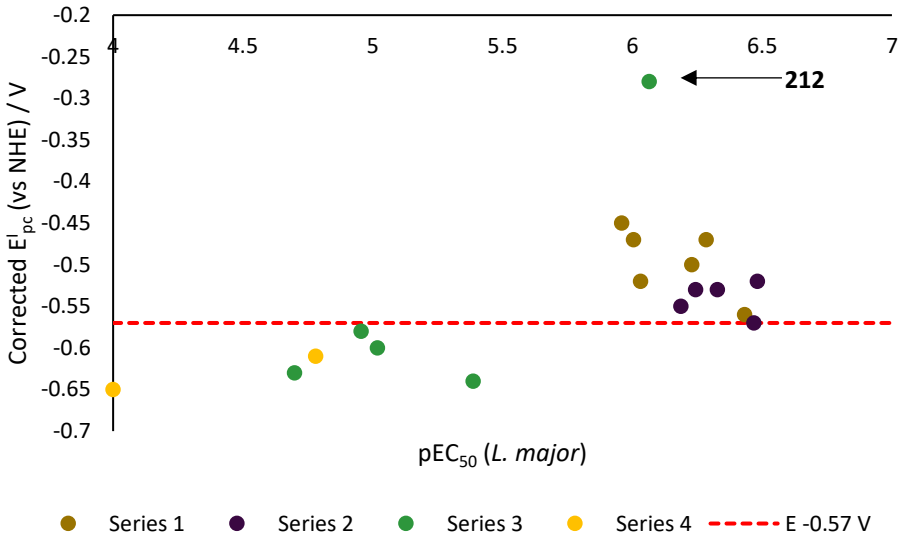

Figure 3.31-14 Correlation between E^{I}_{pc} and activity against *L. major* promastigotes. A cut-off of -0.57 V is found which separates compounds with good activity in series 1 and 2 from poor activity in series 3 and 4.

3.31.1.2 Conclusion

In conclusion, compounds with high antileishmanial activity (series 1 and 2, EC_{50} < 2 µM) have a first reduction potential that is within the capabilities of NTR (E^{I}_{pc} > -0.57). Conversely, compounds with lower antileishmanial activity (series 3 and 4, EC_{50} > 2

μM) have lower reduction potentials and subsequently may not act as NTR substrates (E^{I}_{pc} < -0.58 V). A reduction potential cut-off of -0.57 V can subsequently be drawn for the 5N2Cs, below which antileishmanial activity is diminished. However, no direct correlation can be found between antileishmanial activity and reduction potential.

3.31.2 *Ldon*NTR1/NTR2 overexpressor model

As discussed in the previous section, the reduction potentials for 5N2Cs with high antileishmanial activity fall within the biologically relevant range for trypanosomatid NTRs. Consequently, it became important to determine whether bioactivation of the 5N2Cs by *Leishmania* NTRs contributes to the observed antileishmanial activity.[151] Pacheco *et al.* showed that 5-nitrothiophene-2-nitrone derivatives (**293-295**) are bioactivated by both NTR1 and NTR2 in an *L. donovani* overexpressor model.[59] Subsequently, it was of interest to validate whether a selection of synthesised 5N2Cs are bioactivated by NTR1 and/or NTR2 using the same model (Figure 3.31-15).

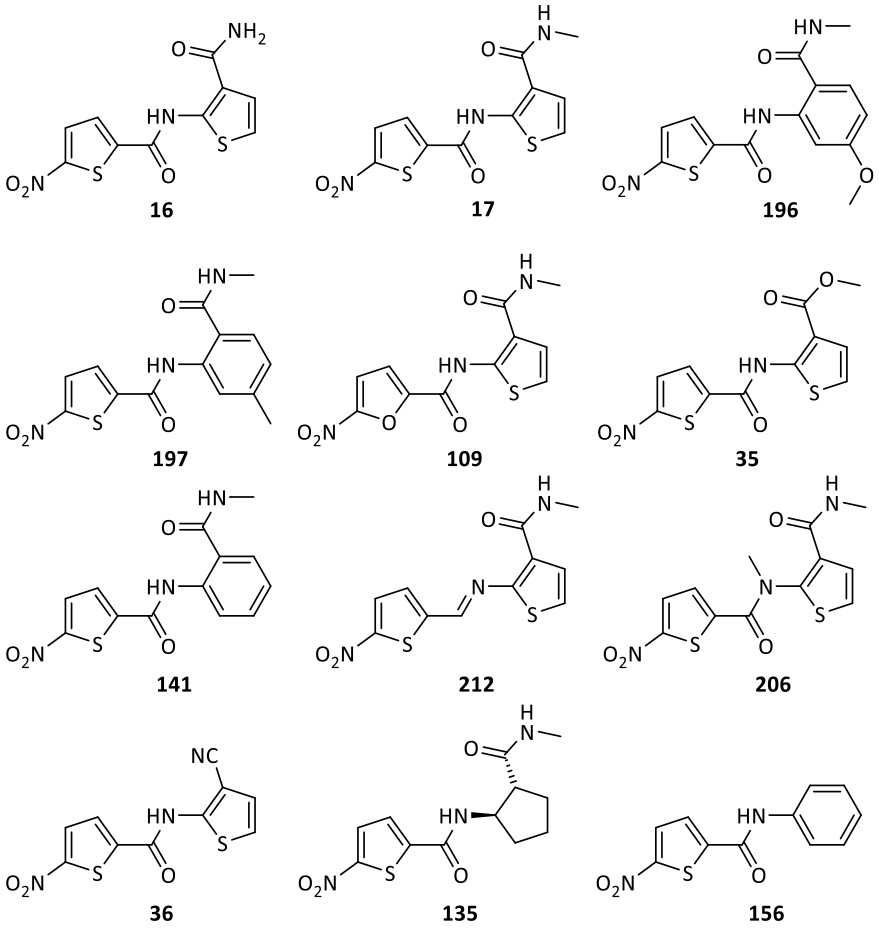

Figure 3.31-15 Selection of 5N2Cs tested against *Ldon* wild type and *Ldon*NTR1 and *Ldon*NTR2 overexpressor lines.

A selection of compounds was tested against three cell lines: *L. donovani* overexpressing NTR1, overexpressing NTR2 and wild type (see footnote[7]). In short, compound was incubated in a dilution series with 1 x 10^5 parasites mL^{-1} for 72 hrs before assessing cell viability using resazurin. Nifurtimox (**37**) and delaminid (**44**) were used as positive controls as nifurtimox (**37**) is a substrate of both NTR1 and NTR2 and delaminid (**44**) is an NTR2 substrate.[49,135] The antileishmanial activity of each compound against wild type *L. donovani* was compared to each of the NTR overexpressor lines to give fold change (Equation 3.31.1), which gives an indication of toxicity caused by NTR bioactivation.

$$\text{Fold change} = \frac{EC_{50}(\text{L. donovani WT})}{EC_{50}(\text{L. donovani NTR overexpressor})}$$

Equation 3.31.1 Calculation of fold change which gives an indication of the extent of antileishmanial activity caused by NTR bioactivation.

A compound with low fold change is either not bioactivated by NTR or the metabolites generated after bioactivation are non-toxic to the parasite and as such NTR bioactivation does not contribute to the toxicity caused by the compound. A summary of the fold changes observed for the 5N2C series is shown in Figure 3.31-16.

[7] The experiments described here were done by Juliana Pacheco and Susan Wyllie, Dundee.

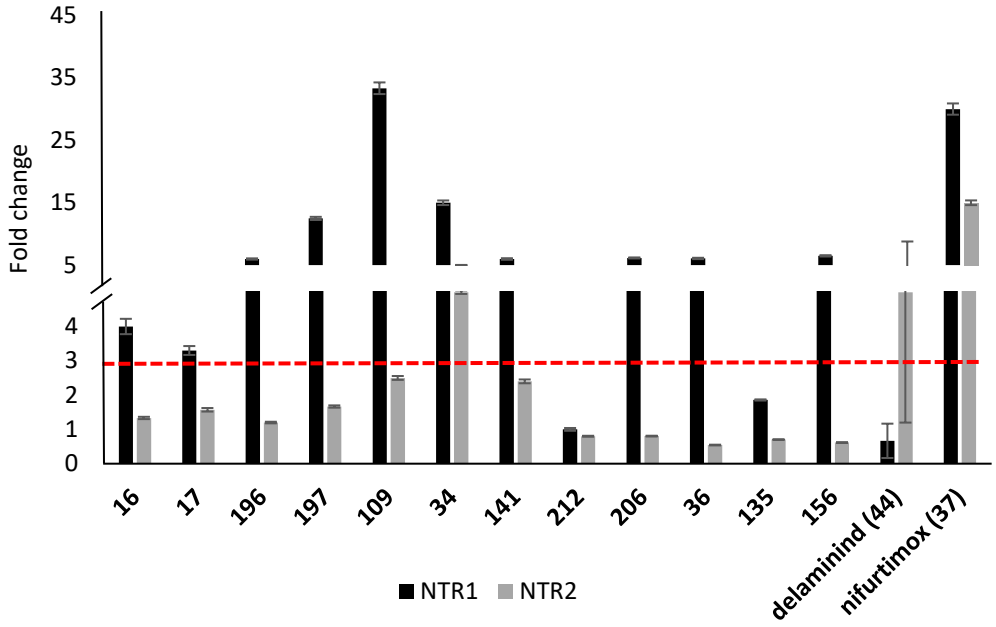

	L.don **(WT) EC_{50} / nM**	***L.don*** **NTR1 (O.E.) EC_{50} / nM**	**Fold change *Ld*NTR1**	***L.don*** **NTR2 (O.E.) EC_{50} / nM**	**Fold change *Ld*NTR2**
16	4.0 ± 0.2	1.0 ± 0.1	4	3.0 ± 0	1.3
17	33 ± 2	10.0 ± 0.5	3.3	21.0 ± 0.5	1.6
196	6.0 ± 0.2	1.0 ± 0	6	5.0 ± 0.1	1.2
197	5.0 ± 0.2	0.4 ± 0	12.5	3.0 ± 0	1.7
109	200 ± 9	6.0 ± 0.2	33.3	80.0 ± 0.3	2.5
34	300 ± 6	20.0 ± 0.9	15	60.0 ± 0.2	5
141	12.0 ± 0.5	2.0 ± 0	6	5.0 ± 0.1	2.4
212	40 ± 1	40 ± 3	1	50.0 ± 0.7	0.8
206	3700 ± 90	600 ± 6	6.2	4600 ± 60	0.8
36	1120 ± 30	184 ± 4	6.1	2060 ± 60	0.5
135	3400 ± 60	1830 ± 6	1.9	4800 ± 100	0.7
156	930 ± 30	143.0 ± 0.6	6.5	1510 ± 20	0.6
Delaminid (44)	2 ± 3	3.0 ± 0.2	0.67	0.4 ± 0.1	5
Nifurtimox (37)	1800 ± 90	60 ± 2	30	120.0 ± 0.7	15

Figure 3.31-16 A. The fold change between the EC_{50} of *L. donovani* wild type and *L. donovani* overexpressing either *Ldon*NTR1 or *Ldon*NTR2 for each compound. Compounds lying below the red line are not nitroreductase substrates. B. EC_{50} values for each substrate against WT *L. donovani*, and *Ldon*NTR1 and *Ldon*NTR2 overexpressing lines. Compounds highlighted in red are not nitroreductase substrates. Results are reported as the mean of three repeats, with errors representing standard error.

Based on discussions with Dr Wyllie, an arbitrary cut off in fold change of 3 was adopted, above which compounds may be classed as causing toxicity through NTR bioactivation. The majority of 5N2C compounds caused toxicity through NTR1 rather than NTR2 bioactivation. However, imine **212** and cyclopentane **135** proved to be exceptions with no or limited toxicity caused by NTR1 or NTR2 bioactivation (fold change < 3). Conversely, methyl ester derivative **34** causes toxicity upon both NTR1 and NTR2 bioactivation. Considering the trend for the majority of compounds, it was deduced that the toxicity of the 5N2C series was facilitated by NTR1 rather than NTR2 bioactivation and as such future efforts concentrated on the NTR1 enzyme.

The compound with the greatest fold change caused by NTR1 bioactivation is 5-nitrofuran (**109**), even though it has a 0.09 V lower reduction potential than the corresponding thiophene (**17**, section 3.31.1). This is not suprising as the compound used as a standard for *Ldon*NTR1 activity, nifurtimox (**37**), also contains a 5-nitrofuran group. However, the most easily chemically reduced compound, **212** (E^0 -0.29 V), which shares an imine in common with nifurtimox (**37**), shows no bioactivation by *Ldon*NTR1 or *Ldon*NTR2 (Figure 3.31-16).

The lack of correlation between reduction potential and fold change in the *Ldon*NTR1 overexpressor model is similar to that observed by Pachecho *et al.* for 5-nitrothiophene-2-nitrones (**293-295**). [59] Previous suggestions that compounds with E^{I}_{pc} < -0.57 V may not be bioactivated by NTRs have been proved incorrect as 2 out of 3 compounds in this category (blue box) show a fold change of greater than 3 (Figure 3.31-17). This suggests that factors other than reduction potential effect the extent of toxicity caused by *Ldon*NTR1 bioactivation.

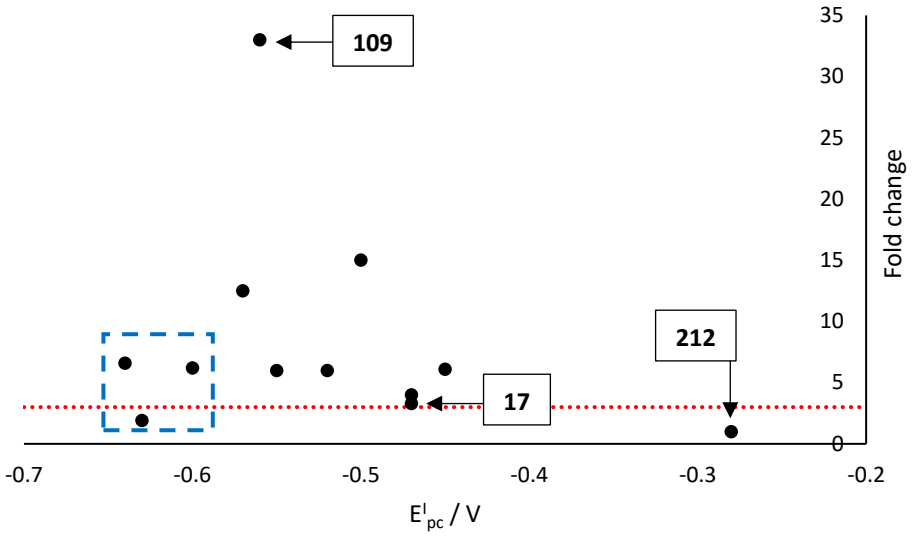

Figure 3.31-17 Scatter plot displaying the relationship between reduction potential and fold change in the *Ldon*NTR1 overexpressor model. The blue box highlights compounds previously assumed to not be NTR substrates due to E^{I}_{pc} < -0.57 V. Individual compounds that have been discussed in the text are also highlighted.

Furthermore, there appears to be little correlation between the fold change and the magnitude of antileishmanial activity against wild type *L. donovani* (Figure 3.31-18).

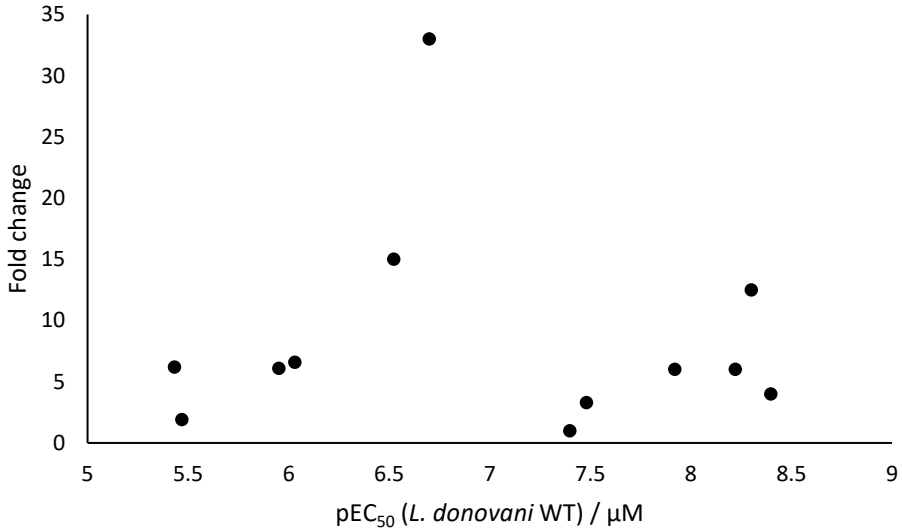

Figure 3.31-18 Comparison of fold change with wild type *L. donovani* antileishmanial activity.

The variety in fold-change within the 5N2C series is a complex issue, which does not directly relate to the magnitude of wild type antileishmanial activity. Many factors contribute to the observed fold change including the reduction potential of the nitro

group, the 3D structure of the compound which dictates how well it can 'fit' into the nitroreductase active site and the toxicity of the metabolite profile after bioactivation. Subsequently, the value of 'fold change' should be used with caution and only to identify compounds as nitroreductase substrates. As such, compounds that show a fold change of greater than 3 likely act as substrates for *Ldon*NTR1, however the magnitude of fold-change does not imply that a compound is a better substrate or that it is turned over more quickly. Likewise, compounds with a fold change of less than 3 may still be substrates for *Ldon*NTR1 if the major metabolites generated are non-toxic to the parasite. Subsequently, it was of interest to examine whether the rate of NTR bioactivation, or the metabolite profile following bioactivation, could help to explain the lack of correlation between fold change and antielishmanial activity for the 5N2C series.

3.31.3 Expression and purification of *Lmj*NTR1

As discussed in the previous section, a representative selection of 5N2Cs were bioactivated by *Ldon*NTR1 in an overexpressor model. However, a lack of correlation between fold change and reduction potential or antileishmanial activity was observed. Subsequently, it was of interest to verify the 5N2Cs as NTR substrates before investigating the mode of bioactivation more fully. To validate the 5N2Cs as NTR substrates, recombinant nitroreductase must be expressed and purified first. Following the literature procedure by Voak *et al.*, attempts were made to purify *Lmj*NTR1.[129]

E. coli BL21-CodonPlus DE3-RIPL (BL21(+)) cells were chosen to introduce unnatural codons (AGA, AGG, AUA, CCC, CUA) to *E. coli,* enabling the expression of *Lmj*NTR1 from *L. major* genomic DNA without the need to codon optimise the gene for *E. coli*. pTrcHis*Lmj*NTR1 contains a truncated version of the *Lmj*NTR1 gene amplified from genomic DNA, with the mitochondrial targeting sequence and pre-catalytic domain removed to improve protein solubility (see footnote[8]). [129] Features of the pTrcHisC plasmid introduce the 36 amino acid His_6 tag and Xpress epitope to the *N*-terminus of the *Lmj*NTR1 237 amino acid sequence for expression and purification purposes. The sequence alignment of the recombinant and native *Lmj*NTR1 protein is shown in Figure 3.31-19.

[8] pTrcHisC.*Lmj*NTR1 supplied by Dr Shane Wilkinson, QMUL.

```
L.major_nativ      1 MLRRSPRLLLVAAGARPAASTPRASEAAGTCGNEERHSNTSSGHGGFLAT     50
                                                .|....|.:    ||  :|:
L.major_recom      1 ------------------------------MGGSHHHHH----HG--MAS     14

L.major_nativ     51 L-------RHLV------AWNRTNAAAAASSSSVSCAETPACVSSSAALD     87
                     :       |.|.      .|                           .||
L.major_recom     15 MTGGQQMGRDLYDDDDKDRW---------------------------ILD     37

L.major_nativ     88 AVEAVVRDRWTCRQFDTAKPIDLDTLKRVLAATTRAPTGFNLQGWHAVVV    137
                     ||||||||||||||||||||||||||||||||||||||||||||||||||||
L.major_recom     38 AVEAVVRDRWTCRQFDTAKPIDLDTLKRVLAATTRAPTGFNLQGWHAVVV     87

L.major_nativ    138 TNEAVREQLFKAALGQPQVLQAPATVVFVGDTEPERNAPQALEMGLETGY    187
                     ||||||||||||||||||||||||||||||||||||||||||||||||||||
L.major_recom     88 TNEAVREQLFKAALGQPQVLQAPATVVFVGDTEPERNAPQALEMGLETGY    137

L.major_nativ    188 YSPLYGATYLRNIYYLMHGGPMQSMAAVKSVVSAWYSRAAGTPLISVPVS    237
                     ||||||||||||||||||||||||||||||||||||||||||||||||||||
L.major_recom    138 YSPLYGATYLRNIYYLMHGGPMQSMAAVKSVVSAWYSRAAGTPLISVPVS    187

L.major_nativ    238 RTGYAWKQTMIPATTFVNLCTAAGWETCMMEGIDEDAVKRALGVPAERYT    287
                     ||||||||||||||||||||||||||||||||||||||||||||||||||||
L.major_recom    188 RTGYAWKQTMIPATTFVNLCTAAGWETCMMEGIDEDAVKRALGVPAERYT    237

L.major_nativ    288 VPVIISVGYATATEAEKRQVCSSRFATPHTVRWNKF    323
                     ||||||||||||||||||||||||||||||||||||
L.major_recom    238 VPVIISVGYATATEAEKRQVCSSRFATPHTVRWNKF    273
```

Figure 3.31-19 Sequence alignment of native *Lmj*NTR1 and recombinant His_6-*Lmj*NTR1. In the native sequence, the black section contains the mitochondrial targeting and precatalytic domain. In the recombinant sequence, the 86 residue pre-catalytic domain is removed and replaced with the blue His_6-tag and Xpress Epitope region. Pairwise sequence alignment achieved using EMBOSS Needle.[154]

BL21(+) cells were transformed with the pTrcHis*Lmj*NTR1 plasmid. The transformed BL21(+).pTrcHis*Lmj*NTR1 cultures were selected and grown to a litre scale. Purification of *Lmj*NTR1 was then accomplished by slight modification of the procedure proposed by Voak *et al*.[129] Cell lysis was achieved by incubation with lysozyme (1 mg mL^{-1}) and CHAPS (1 % w/v) on ice followed by sonication. Affinity chromatography was first carried out at room temperature, however this led to significant protein precipitation on the Ni-NTA column. Subsequently, all purification steps were carried out on ice or at 4 °C, which rectified this problem. As an FMN containing protein, *Lmj*NTR1 purification was simplified by pooling the yellow protein containing fractions that eluted at 500 mM imidazole using Ni-NTA affinity chromatography (Figure 3.31-20B). The protein was then purified further by size exclusion chromatography (superdex 16/60 75 pg) to give the final *Lmj*NTR1 protein

sample, verified by SDS-PAGE (12.5 %) (Figure 3.31-20A). This process enabled purification of approximately 7 mg of *Lmj*NTR1.

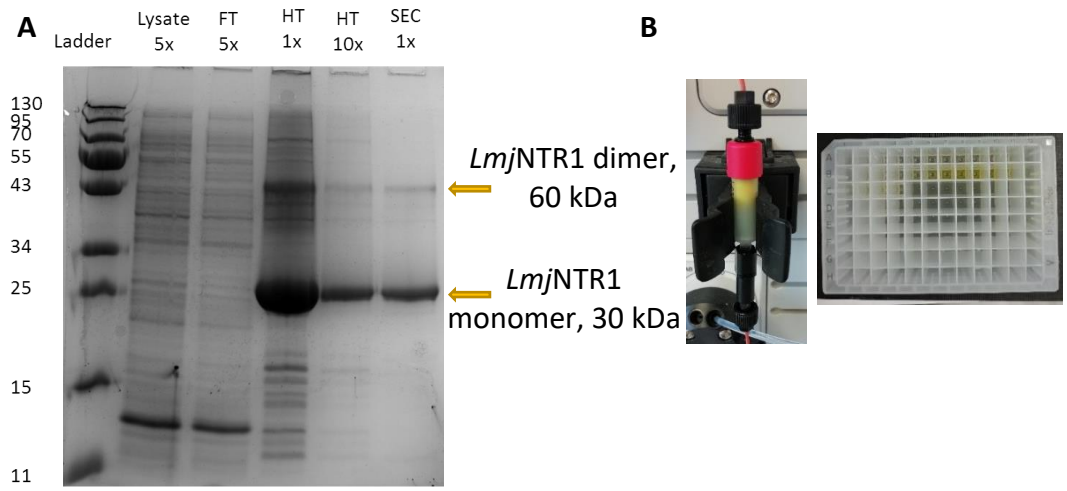

Figure 3.31-20 A. SDS-PAGE (12.5 %) gel showing *Lmj*NTR1 purification stages after Ni-NTA affinity (HT 1x and 10x diluted) and size exclusion (SEC) chromatography. B. Characteristic yellow colour observed for *Lmj*NTR1 as an FMN containing protein in both stages of purification (left: His-Trap, right: SEC).

The protein identity was confirmed by LC-MS (Figure 3.31-21). Furthermore, the two protein bands observed in the SDS-PAGE (12.5 %) gel of Figure 3.31-20A were confirmed to be the monomeric and dimeric species of *Lmj*NTR1 by protein digest mass spectrometry (appendix 8.3).

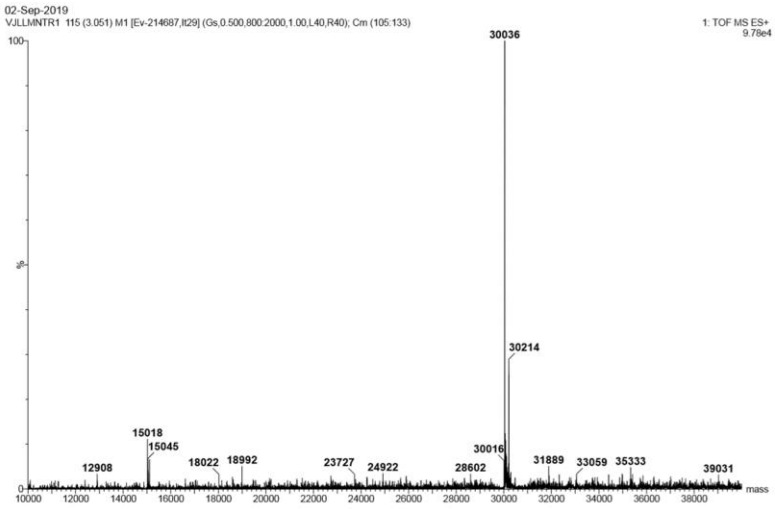

Expected protein mass / Da	30168
Observed protein mass / Da	30036
Mass difference / Da	132
Mass difference cause	N- terminal methionine cleavage

Figure 3.31-21 LC mass spectrum of *Lmj*NTR1 containing fractions, showing the mass [*Lmj*NTR1 – Met + H]$^+$, confirming the identity of the protein.

3.31.3.1 Thermal shift assay using Durham Screens

Previous efforts by the Wilkinson group to dialyse *Lmj*NTR1 out of high imidazole buffer resulted in protein precipitation (see footnote[9]). This high imidazole concentration is undesirable as it may result in bacterial contamination or have chaotropic effects. As such, following the successful purification of *Lmj*NTR1, it was of interest to investigate the stability of *Lmj*NTR1 in alternative buffers. Protein stability, homogeneity and solubility can be determined using thermal shift assay (TSA). SYPRO™ Orange binds to unfolded proteins and fluoresces to give an indication of the protein melt temperature (T_m), which increases in stabilising environments.[155] SYPRO™ Orange was added to *Lmj*NTR1 in buffer before TSA analysis. A variety of different buffer conditions were assessed using the Durham Salt and Durham pH screens to identify favourable conditions that cause an increase in protein stability (Figure 3.31-22 and Figure 3.31-23). [156]

[9] S. Wilkinson group, unpublished work.

	1	2	3	4	5	6	7	8	9	10	11	12
A	40.1	40.5	32.0	30.0	32.0	37.7	32.0	39.7	40.9	32.0	38.3	39.0
B	31.0	36.3	41.3	37.3	41.7	42.1	37.0	39.7	42.5	40.1	41.6	41.8
C	38.9	42.2	42.2	41.7	41.9	42.1	37.3	38.5	40.2	45.8	45.5	44.3
D	39.4	40.2	41.5	39.9	42.2	41.9	40.0	39.5	41.0	39.5	40.4	41.0
E	41.0	41.4	41.9	40.9	41.7	42.2	40.2	40.3	40.3	40.1	41.1	41.7
F	39.8	40.8	41.0	41.2	41.6	41.2	41.0	40.9	40.7	41.5	41.6	41.1
G	41.2	40.8	39.2	41.3	41.3	40.8	41.1	40.6	39.3	39.9	35.5	33.8
H	37.2	36.1	34.6	39.4	36.1	31.0	39.2	36.9	34.0	33.0	31.0	33.0

	1	2	3	4	5	6	7	8	9	10	11	12
A	water	water	4 M urea	100 mM citric acid pH 4.1	100 mM citric acid pH 4.6	100 mM citric acid pH 5.1	100 mM acetic acid pH 4.2	100 mM acetic acid pH 4.7	100 mM acetic acid pH 5.2	100 mM succinic acid pH 4.4	100 mM succinic acid pH 4.9	100 mM succinic acid pH 5.4
B	100 mM malic acid pH 4.3	100 mM malic acid pH 4.8	100 mM malic acid pH 5.3	100 mM tartaric acid pH 4.3	100 mM tartaric acid pH 4.8	100 mM tartaric acid pH 5.3	100 mM propionic acid pH 4.3	100 mM propionic acid pH 4.8	100 mM propionic acid pH 5.3	100 mM malonic acid pH 5.2	100 mM malonic acid pH 5.7	100 mM malonic acid pH 6.2
C	100 mM citric acid pH 5.5	100 mM citric acid pH 6.0	100 mM citric acid pH 6.5	100 mM succinic acid pH 5.6	100 mM succinic acid pH 6.1	100 mM succinic acid pH 6.6	100 mM MES pH 5.6	100 mM MES pH 6.1	100 mM MES pH 6.6	100 mM maleic acid pH 5.7	100 mM maleic acid pH 6.2	100 mM maleic acid pH 6.7
D	100 mM sodium cacodylate pH 5.7	100 mM sodium cacodylate pH 6.2	100 mM sodium cacodylate pH 6.7	100 mM ADA pH 6.1	100 mM ADA pH 6.6	100 mM ADA pH 7.1	100 mM bisTRIS pH 6.1	100 mM bisTRIS pH 6.6	100 mM bisTRIS pH 7.1	100 mM ACES pH 6.3	100 mM ACES pH 6.8	100 mM ACES pH 7.3
E	100 mM phosphate pH 6.3	100 mM phosphate pH 6.8	100 mM phosphate pH 7.3	100 mM PIPES pH 6.3	100 mM PIPES pH 6.8	100 mM PIPES pH 7.3	100 mM imidazole pH 6.6	100 mM imidazole pH 7.1	100 mM imidazole pH 7.6	100 mM MOPS pH 6.6	100 mM MOPS pH 7.1	100 mM MOPS pH 7.6
F	100 mM bisTRIS propane pH 6.6	100 mM bisTRIS propane pH 7.1	100 mM bisTRIS propane pH 7.6	100 mM HEPES pH 7.0	100 mM HEPES pH 7.5	100 mM HEPES pH 8.0	100 mM tricine pH 7.5	100 mM tricine pH 8.0	100 mM tricine pH 8.5	100 mM EPPS pH 7.5	100 mM EPPS pH 8.0	100 mM EPPS pH 8.5
G	100 mM TRIS pH 7.7	100 mM TRIS pH 8.2	100 mM TRIS pH 8.7	100 mM bicine pH 7.7	100 mM bicine pH 8.2	100 mM bicine pH 8.7	100 mM TAPS pH 7.9	100 mM TAPS pH 8.4	100 mM TAPS pH 8.9	100 mM bisTRIS propane pH 8.5	100 mM bisTRIS propane pH 9.0	100 mM bisTRIS propane pH 9.5
H	100 mM boric acid pH 8.6	100 mM boric acid pH 9.1	100 mM boric acid pH 9.6	100 mM CHES pH 8.8	100 mM CHES pH 9.3	100 mM CHES pH 9.8	100 mM glycine pH 9.2	100 mM glycine pH 9.7	100 mM glycine pH 10.2	100 mM CAPS pH 9.9	100 mM CAPS pH 10.4	100 mM CAPS pH 10.9

Figure 3.31-22 Durham pH screen TSA output data (T_m) for *Lmj*NTR1 (above) and screen contents (below). Data analysed using NAMI. [156,157]

The Durham pH screen showed that the protein is most stable around neutral pH but can be stabilised at lower pH by the presence of poly-carboxylic acid containing buffers such as maleic acid. [156] Interestingly, the presence of imidazole at 100 mM around neutral pH does not seem to improve the stability of *Lmj*NTR1, contrary to previous reports. [129,139] However, it must be noted that the protein in each of the

conditions above has 250 mM imidazole from the original protein sample. Subsequently, the only conclusion that can be safely drawn with respect to imidazole is that increasing its concentration past 250 mM does not improve protein solubility and stability further.

	1	2	3	4	5	6	7	8	9	10	11	12
A	40.7	41.2	32.0	51.7	31.0	32.0	34.4	37.7	39.7	40.6	49.4	44.8
B	57.7	53.5	52.1	49.2	46.5	43.6	52.1	48.8	47.8	45.2	43.6	41.9
C	44.8	43.6	43.1	42.9	42.6	41.9	39.5	40.2	41.0	41.2	41.6	41.9
D	44.5	43.6	43.1	43.0	43.0	50.3	49.8	48.2	45.4	43.2	42.2	41.9
E	41.5	41.5	42.4	41.3	41.3	41.1	45.1	42.2	44.8 64.2	42.8	41.4	35.3
F	39.7	38.9	41.6	46.4	43.3	39.9	40.3	45.0	46.0	43.6	41.4	44.8
G	43.1	33.0	35.0	34.0	41.1	41.0	41.3	42.8	42.8	43.2	43.4	43.5
H	43.5	43.7	44.1	43.0	43.0	41.2	40.2	41.0	41.2	41.6	41.3	41.8

	1	2	3	4	5	6	7	8	9	10	11	12
A	water	water	4 M urea	3.0 M Gu-HCl	1.0 M Gu-HCl	0.8 M Gu-HCl	0.6 M Gu-HCl	0.4 M Gu-HCl	0.2 M Gu-HCl	5 mM Gu-HCl	0.5 M Na_3 citrate	0.2 M Na_3 citrate
B	1.5 M Na_2 malonate	1.0 M Na_2 malonate	0.8 M Na_2 malonate	0.6 M Na_2 malonate	0.4 M Na_2 malonate	0.2 M Na_2 malonate	1.5 M $(NH_4)_2SO_4$	1.0 M $(NH4)_2SO_4$	0.8 M $(NH_4)_2SO_4$	0.6 M $(NH_4)_2SO_4$	0.4 M $(NH_4)_2SO_4$	0.2 M $(NH_4)_2SO_4$
C	1.5 M NaCl	1.0 M NaCl	0.8 M NaCl	0.6 M NaCl	0.4 M NaCl	0.2 M NaCl	1.5 M NH_4Cl	1.0 M NH_4Cl	0.8 M NH_4Cl	0.6 M NH_4Cl	0.4 M NH_4Cl	0.2 M NH_4Cl
D	1.0 M $MgSO_4$	0.8 M $MgSO_4$	0.6 M $MgSO_4$	0.4 M $MgSO_4$	0.2 M $MgSO_4$	1.0 M Na_2SO_4	0.8 M Na_2SO_4	0.6 M Na_2SO_4	0.4 M Na_2SO_4	0.2 M Na_2SO_4	0.5 M KCl	0.2 M KCl
E	0.5 M LiCl	0.2 M LiCl	0.5 M RbCl	0.2 M RbCl	0.5 M CsCl	0.2 M CsCl	0.4 M NaF	0.1 M NaF	1.5 M NaBr	0.4 M NaBr	0.1 M NaBr	0.4 M NaI
F	0.1 M NaI	0.4 M $MgCl_2$	5 mM $MgCl_2$	5 mM $CaCl_2$	5 mM $SrCl_2$	1 mM $ZnCl_2$	0.1 mM $ZnCl_2$	1 mM $NiCl_2$	0.1 mM $NiCl_2$	5 mM $MnCl_2$	0.5 mM $MnCl_2$	1 mM $CoCl_2$
G	0.1 mM $CoCl_2$	1 mM $CuSO_4$	0.1 mM $CuSO_4$	1 mM $CdSO_4$	5 mM EDTA pH 7.5	5 mM EGTA pH 7.5	2 mM magic triangle pH 7.0	2 mM $La(NO_3)_3$	2 mM $PrCl_3$	2 mM $NdCl_3$	2 mM $SmCl_3$	2 mM $EuCl_3$
H	2 mM $GdCl_3$	2 mM $DyCl_3$	2 mM $HoCl_3$	2 mM $YbCl_3$	2 mM $LuCl_3$	5 mM Na_2HPO_4	5 mM Na_3VO_4	5 mM Na_2WO_4	5 mM Na_2MoO_4	5 mM DTT	5 mM TCEP pH 7.0	5 mM β-mercapto ethanol

Figure 3.31-23 Durham salt screen output data for *Lmj*NTR1 (above) and screen contents (below).[156] Data analysed using NAMI. [156,157]

The Durham salt screen showed significant protein stabilisation in the presence of high concentrations of polycarboxylate salts such as sodium malonate and sodium citrate.[156] Further stabilisation was observed in the presence of sulfate anions, in the form of ammonium or sodium sulfate.

In conclusion, *Lmj*NTR1 could be dialysed into buffers containing sulfate, malonate or citrate in addition to 250 mM imidazole to improve protein stability and solubility.

3.31.4 Attempted purification of *Ldon*NTR1

Once *Lmj*NTR1 had been purified, efforts moved towards purifying *Ldon*NTR1. No literature precedent is available for this purification; however, its isolation was desirable as it would enable a direct comparison with the *Ldon*NTR1 overexpressor studies discussed in section 3.31.2. The high sequence identity (95.8 %) between *Lmj*NTR1 and *Ldon*NTR1 truncated protein sequence gave hope that purification of this protein would be possible (Figure 3.31-24).

A

%	*L. major*	*L. infantum*	*L. braziliensis*	*L. donovani*	*T. cruzi*	*T. brucei*
L. major	-	-	-	-	-	-
L. infantum	95.8	-	-	-	-	-
L. braziliensis	87.3	89.0	-	-	-	-
L. donovani	95.8	100	89.0	-	-	-
T. cruzi	57.4	57.4	57.0	57.4	-	-
T. brucei	57.8	58.6	59.1	58.6	65.7	-

B

```
LmjNTR1            1 DAVEAVVRDRWTCRQFDTAKPIDLDTLKRVLAATTRAPTGFNLQGWHAVV     50
                     ||||||||.||||||||||||||||||||||||||||||||||||||||||
LdonNTR1           1 DAVEAVVRARWTCRQFDTAKPIDLDTLKRVLAATTRAPTGFNLQGWHAVV     50

LmjNTR1           51 VTNEAVREQLFKAALGQPQVLQAPATVVFVGDTEPERNAPQALEMGLETG    100
                     |||.||||||||||||||||||||||||||||||||||||||||||||||||
LdonNTR1          51 VTNTAVREQLFKAALGQPQVLQAPATVVFVGDTEPERNAPQALEMGLETG    100

LmjNTR1          101 YYSPLYGATYLRNIYYLMHGGPMQSMAAVKSVVSAWYSRAAGTPLISVPV    150
                     ||||||||.|||||||.|||||||||||||||||:||||||||||||||||
LdonNTR1         101 YYSPLYGAAYLRNIYYFMHGGPMQSMAAVKSVVSAWYSQAAGTPLISVPV    150

LmjNTR1          151 SRTGYAWKQTMIPATTFVNLCTAAGWETCMMEGIDEDAVKRALGVPAERY    200
                     ||.||||||||||||||||.||||:||||||||||||||||||||||||||
LdonNTR1         151 SRAGYAWKQTMIPATTFVNLCAAAGWDTCMMEGIDEDAVKRALGVPAERY    200

LmjNTR1          201 TVPVIISVGYATATEAEKRQVCSSRFATPHTVRWNKF    237
                     ||||||||||||||.||||||||.|||||||||||||||
LdonNTR1         201 TVPVIISVGYATAAEAEKRQVGSSRFATPHTVRWNKF    237
```

Figure 3.31-24 A. Sequence identity between the truncated protein sequence of trypanosomatid NTR1s. B. Pairwise sequence alignment of the truncated protein sequence of *Lmj*NTR1 and *Ldon*NTR1. Both achieved using EMBOSS Needle.[154]

Firstly, purification was attempted directly from the pJoe.*Ldon*NTR1 expression vector purchased from GenScript. Following transformation of T7 Express Competent *E. coli* (T7), the protein purification procedure was carried out as previously discussed. However, the protein did not adhere to the Ni-NTA column and therefore no purification was achieved. Subsequently, efforts were made to subclone the

*Ldon*NTR1 truncated sequence into pTrcHisC, as this plasmid generated *Lmj*NTR1 protein that was known to adhere to the Ni-NTA column.

3.31.4.1 Generation of pTrcHis*Ldon*NTR1

Generation of pTrcHis*Ldon*NTR1 was achieved by Gibson cloning in a series of restriction digestion and PCR steps as outlined below. The pTrcHisC plasmid was linearised using the restriction enzymes BamHI and HindIII. The *Ldon*NTR1 gene was then amplified by PCR from pJoe.*Ldon*NTR1, purified and digested by BamHI and HindIII restriction digest. The DNA product after each stage was purified from the agarose gel (Figure 3.31-25).

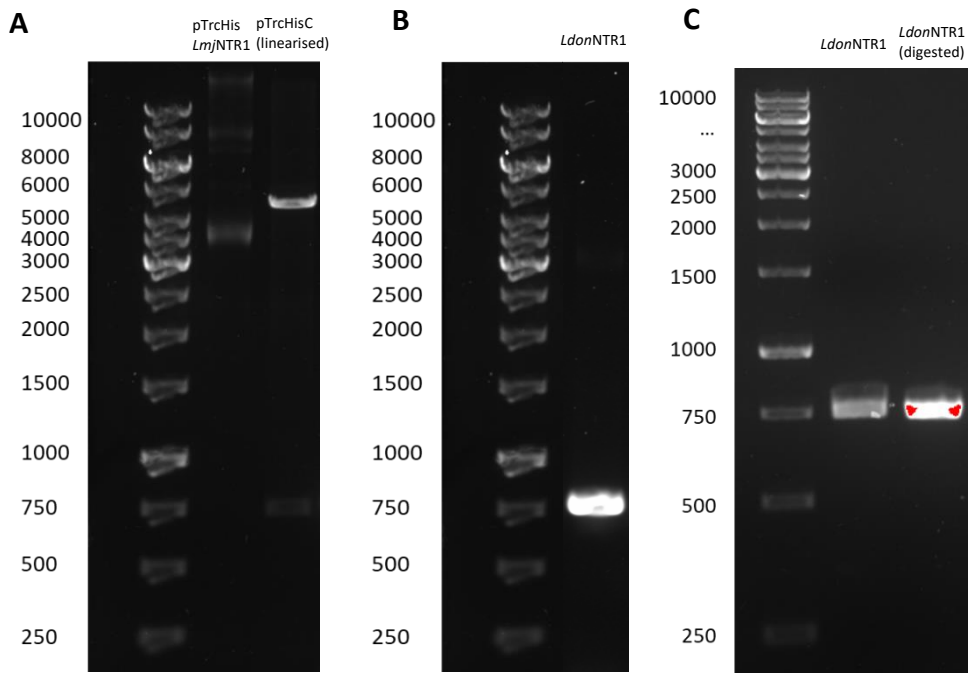

Figure 3.31-25 A. 1 % agarose DNA gel showing the BamHI/HindIII restriction digest of pTrcHis*Lmj*NTR1 (5126 bp) to generate the desired pTrcHisC linearised vector (4412 bp). B. 1 % agarose DNA gel following PCR amplification of the *Ldon*NTR1 insert (722 bp) from pJoe*Ldon*NTR1. C. 2 % agarose DNA gel showing the BamHI/HindIII restriction digest of the *Ldon*NTR1 insert to give 700 bp fragment.

The final step involved ligation of the digested *Ldon*NTR1 insert into the linearised pTrcHisC vector. The resulting plasmid was used to transform T7 competent *E. coli*, which were grown on NZCYM-Amp selection plates overnight. Successful ligation was proved by colony PCR, in which 8 out of 8 colonies showed successful transformation

(Figure 3.31-26). One of the successful colonies was selected at random to be grown overnight. The resulting pTrcHisLdonNTR1 plasmid was purified and the correct gene identity was confirmed by DNA sequencing (appendix 8.2).

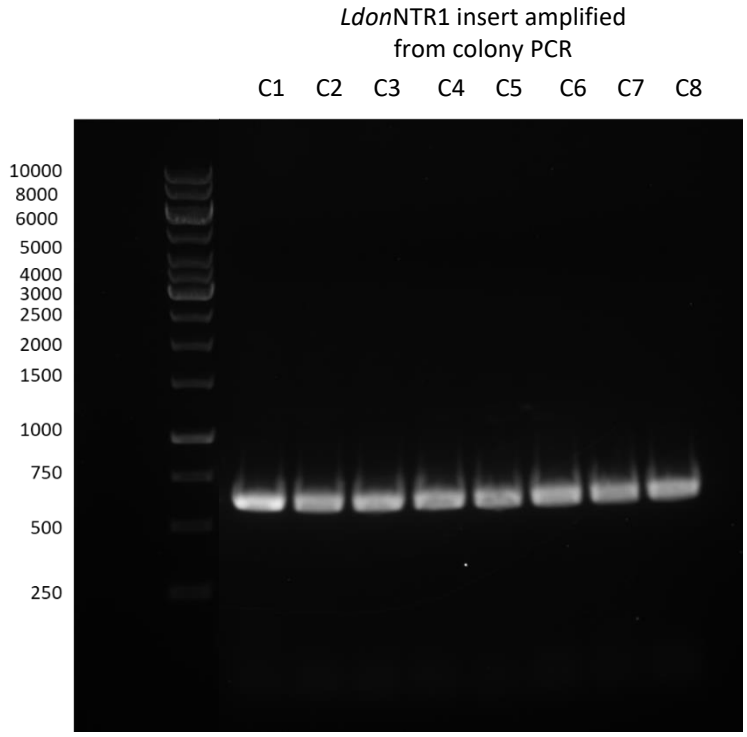

Figure 3.31-26 Colony PCR of 8 colonies (315-C8) showing successful transformation of T7 competent *E. coli* with pTrcHis*Ldon*NTR1.

3.31.4.2 Attempted purification of *Ldon*NTR1 from T7.pTrcHis*Ldon*NTR1

Following successful plasmid preparation and transformation of T7 competent *E. coli* with pTrcHis*Ldon*NTR1, attempts were made to purify *Ldon*NTR1. Purification was first attempted using the same conditions as were used for *Lmj*NTR1 (see section 3.31.3). However, protein precipitation occurred upon loading the lysate onto the Ni-NTA column. It was previously noted that *Lmj*NTR1 was stabilised by poly carboxylic acid containing salts (see section 3.31.3.1). Subsequently, it was inferred that *Ldon*NTR1 may also be stabilised in these conditions. As such purification was attempted in four different buffers, as described in Table 3.31-2.

Table 3.31-2 Buffer compositions scoped to purify *Ldon*NTR1.

Buffer N	Buffer components
Buffer 1	0.5 M Na_3 citrate, 0.1 M MOPS pH 7.6
Buffer 2	0.5 M Na_2 malonate, 0.1 M MOPS pH 7.6
Buffer 3	0.5 M Na_2 succinate, 0.1 M MOPS pH 7.6
Buffer 4	0.5 M Na_2 fumarate, 0.1 M MOPS pH 7.6

In addition to the change in buffer composition, 75 % less lysate was loaded onto each column to reduce the protein concentration and improve solubility. Each of the four new buffer conditions resulted in a significant improvement when compared to the original method and enabled loading of the lysate onto the column without precipitation. Upon elution from the column, protein was collected under the four new conditions (Figure 3.31-27).

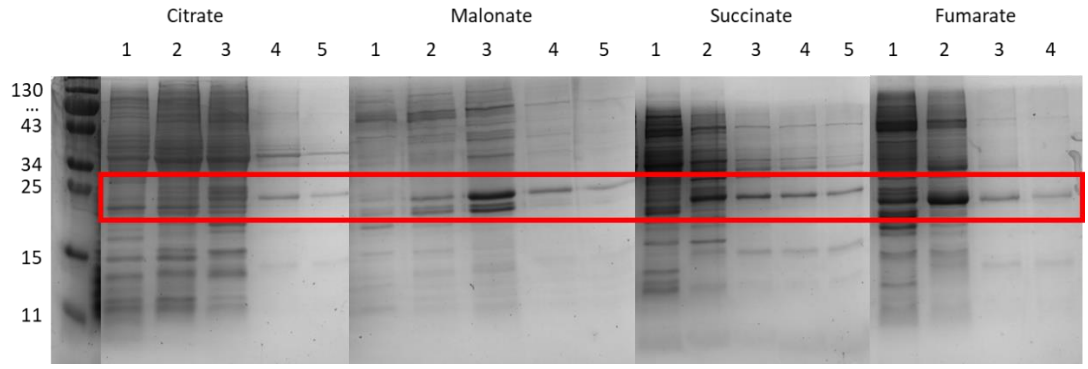

Figure 3.31-27 SDS-PAGE (12.5 %) gels from the four different *Ldon*NTR1 purification conditions. The red box indicates the region in which the *Ldon*NTR1 band should be observed. 1-n indicate fractions 1-n eluted from the Ni-NTA column.

However, the elution fractions from each condition lacked the characteristic yellow colour of FMN containing proteins and precipitated over a few hours at 4 °C. This suggested that the protein obtained had not folded correctly or dimerised, and as such had not bound to the FMN cofactor. This observation was verified by taking the cleanest protein sample which had not precipitated (fumarate fraction 4, Figure 3.31-27) and testing the activity by monitoring the consumption of known substrate nifurtimox (**37**) by UV-Vis in the presence of NADH (Figure 3.31-28).[129] No nifurtimox

(**37**) consumption was observed for *Ldon*NTR1 and subsequently the enzyme obtained was not active.

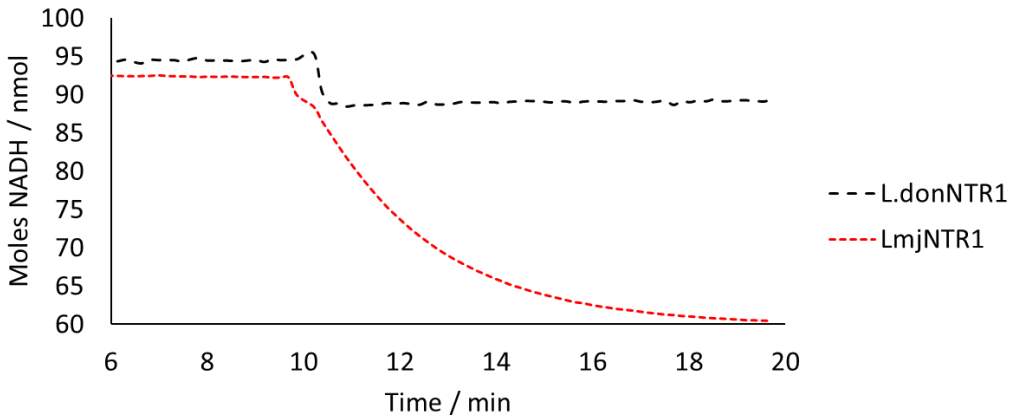

Figure 3.31-28 Kinetics experiment monitoring the consumption of NADH by *Ldon*NTR1 or *Lmj*NTR1 over time. Enzyme was added at 10 minutes.

The reasons for the protein misfolding and not dimerising or not binding to the FMN cofactor are unknown. Further attempts to purify *Ldon*NTR1 were abandoned and as such all future experiments were carried out using *Lmj*NTR1.

3.31.5 *Lmj*NTR1 kinetics of 5N2C reduction

As previously discussed, the 5N2C series are substrates for *Ldon*NTR1 in an overexpressor model (section 3.31.2). Various compounds showed differing degrees of toxicity facilitated by bioactivation, however this did not correlate with reduction potential or antileishmanial activity. Further investigation into the bioactivation of 5N2Cs by NTR1 was necessary to verify them as substrates and understand the mode of bioactivation more fully. One hypothesis was that the rate of bioactivation correlates with bioactivity. Subsequently, with purified *Lmj*NTR1 in hand, the kinetics of 5N2C bioactivation were investigated.

Adopting a protocol reported by Voak *et. al,* the kinetics of *Lmj*NTR1 bioactivation was determined by monitoring consumption of the NADH substrate by UV-Vis (λ_{abs} 340 nm) over time. [129] Consumption of NADH directly correlates to the consumption of nitro prodrug by *Lmj*NTR1 and can be used to determine the rate of substrate bioactivation. The gradient of the resulting decrease in absorbance intensity can be used to calculate the enzyme activity (k_{obs}) in nmol($NADH_{oxidised}$) $mg_{LmjNTR1}^{-1}$ min^{-1} (Figure 3.31-29).

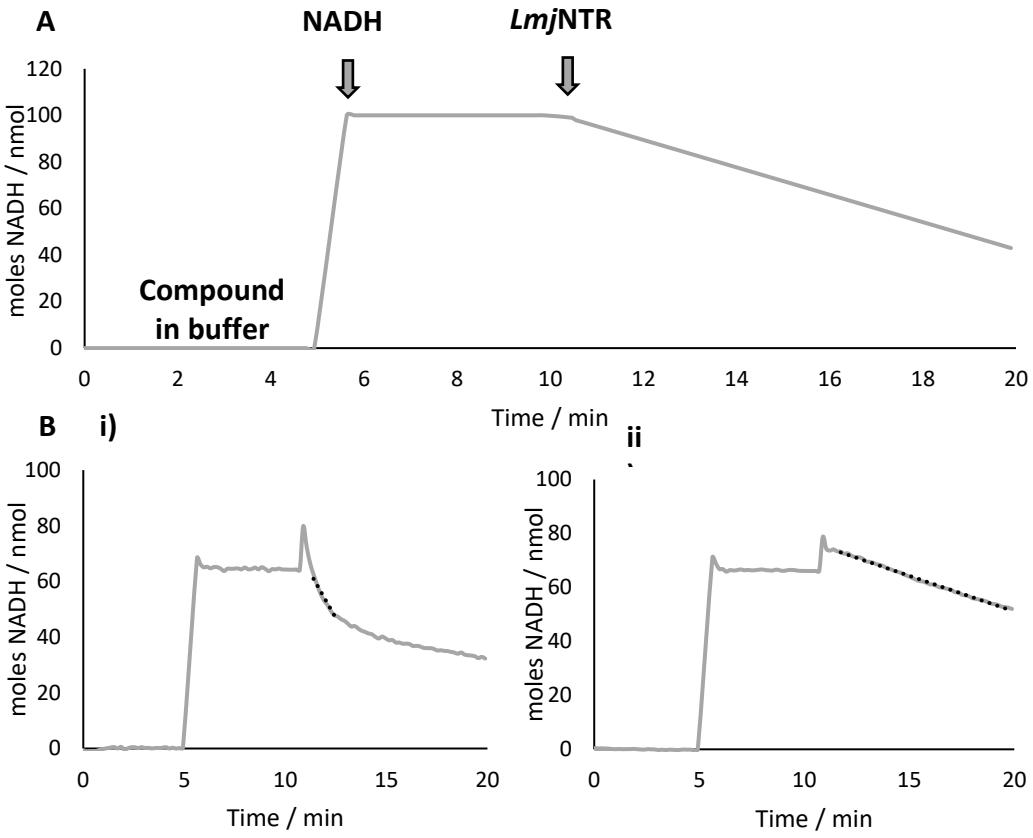

Figure 3.31-29 A. Model dataset used to outline the experiment and expected response. B. Consumption of NADH over time during the metabolism of **131** (i) and **17** (ii) by *Lmj*NTR1. The black dotted line indicates the region taken for calculation of the enzyme activity (in nmol mg^{-1} min^{-1}).

In order to avoid variation in activity over different repeats, nifurtimox (**37**), a validated *Lmj*NTR1 substrate, was used as a standard.[129] The ratio $k_{obs}/k_{nifurtimox}$ gives an indication of the rate of bioactivation compared to a known substrate and drug. Higher values of $k_{obs}/k_{nifurtimox}$ indicate an increased rate of 5N2C turnover, with compounds showing $k_{obs}/k_{nifurtimox} > 1$ being turned over faster than nifurtimox (**37**). The rate of bioactivation of a series of 24 representative compounds, including **107** which has no nitro group and was used as a negative control, is represented in Table 3.31-3, Figure 3.31-30 and Figure 3.31-31.

Most of the compounds tested (dithiophene 5N2Cs, phenyl 5N2Cs and 5-substituted 5N2Cs) show relatively slow rates of *Lmj*NTR1 bioactivation compared to nifurtimox (**37**) ($k_{obs}/k_{nifurtimox} < 0.5$, Table 3.31-3, entries 1-15 & 17-19). Compounds that are turned over the fastest include cyclopentanes **131** and **135** and extended CH_2 linker

210 (Table 3.31-3, entries 20-22), which suggests that increased flexibility and lack of delocalisation of the central amide into the right-hand ring increases the rate of *Lmj*NTR1 bioactivation. 5-nitrofuran **109** was turned over very slowly by *Lmj*NTR1 compared to nifurtimox (**37**) (Table 3.31-3, entry 7), potentially due to the increased delocalisation and rigidity of **109** compared to nifurtimox (**37**).

Table 3.31-3 Rate of *Lmj*NTR1 mediated bioactivation of selected compounds compared to antileishmanial activity, solubility, reduction potential and fold change. All values are calculated from at least 3 repeats and errors stated are standard errors.

Entry	Compound ID	$k_{obs}/k_{nifurtimox}$	pEC_{50} (*L. major*)	Kinetic solubility (PBS) / µM	E^{I}_{pc} / V	Fold change (EC_{50} *Ldon*NTR1 WT / EC_{50} *Ldon*NTR1 OE)
1	**107**	-0.01 ± 0.01	< 4	-	-	-
2	**16**	0.032 ± 0.003	6.3 ± 0.6	< 7.4	-0.47	4.0
3	**17**	0.113 ± 0.005	6.0 ± 0.5	< 7.4	-0.47	3.3
4	**34**	0.13 ± 0.01	6.3 ± 0.5	< 7.4	-0.50	15.0
5	**36**	0.028 ± 0.003	6.0 ± 0.5	228 ± 2	-0.45	6.1
6	**212**	0.032 ± 0.003	6.1 ± 0.5	101 ± 6	-0.28	1.0
7	**109**	0.0378 ± 0.0008	6.4 ± 0.2	-	-0.56	33.3
8	**140**	0.096 ± 0.002	6.3 ± 0.5	< 2.5	-0.53	-
9	**157**	0.0095 ± 0.003	5.2 ± 0.2	-	-	-
10	**195**	0.067 ± 0.002	5.6 ± 0.6	-	-	-
11	**199**	0.081 ± 0.005	6.2 ± 0.7	< 2.5	-0.53	-
12	**198**	0.0150 ± 0.0009	5.7 ± 0.3	6.5 ± 0.2	-	-
13	**232**	0.174 ± 0.003	6.5 ± 0.4	2.27 ± 0.05	-	-
14	**251**	0.041 ± 0.002	6.3 ± 0.6	1.8 ± 0.4	-	-
15	**252**	0.121 ± 0.006	6.36 ± 0.09	19.3 ± 0.6	-	-
16	**253**	0.509 ± 0.005	6.5 ± 0.4	29 ± 3	-	-
17	**254**	0.083 ± 0.002	6 ± 1	3.7 ± 0.9	-	-
18	**208**	0.26 ± 0.01	5.0 ± 0.1	151 ± 3	-0.58	-
19	**110**	0.37 ± 0.04	4.78 ± 0.06	-	-0.61	-
20	**131**	1.26 ± 0.06	5.0 ± 0.5	-	-	-
21	**135**	1.61 ± 0.07	4.7 ± 0.5	-	-0.63	1.9
22	**210**	1.43 ± 0.05	4.7 ± 0.7	179 ± 8	-	-
23	**Nifurtimox (37)**	1.00 ± 0.02	5.6 ± 0.3	-	-	30

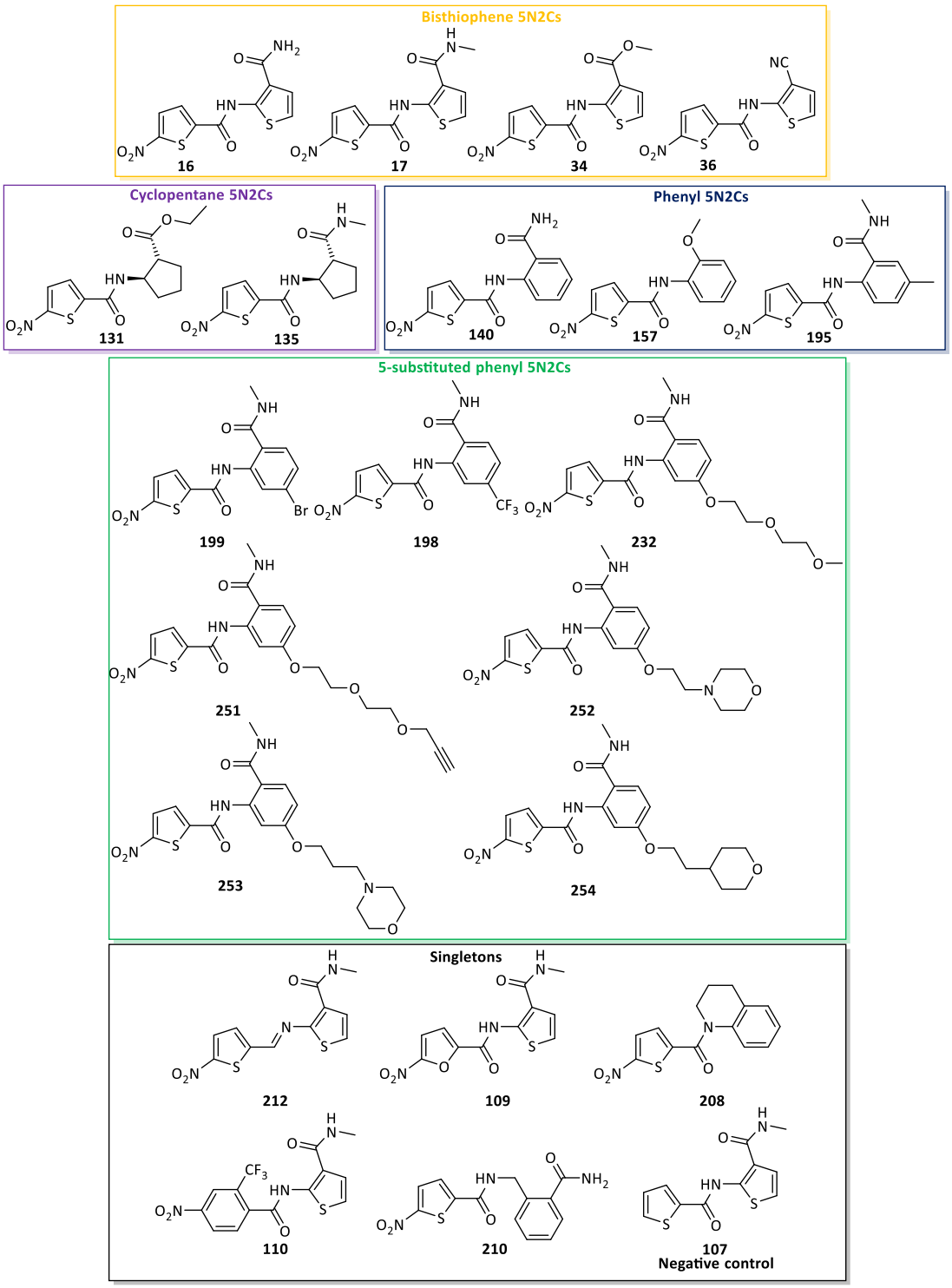

Figure 3.31-30 Representative compounds used for kinetics of LmjNTR1 turnover experiments.

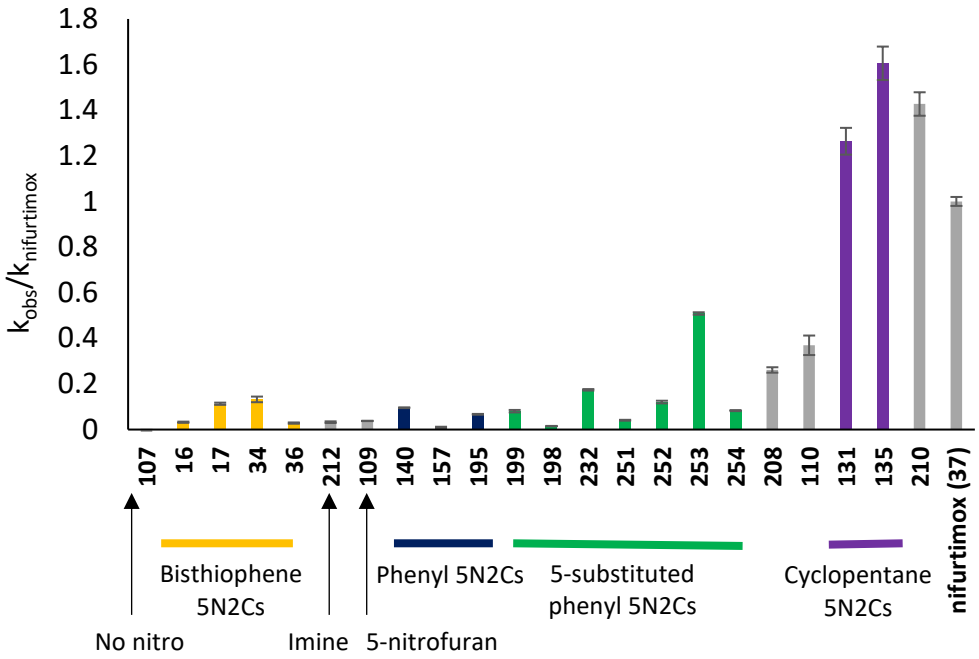

Figure 3.31-31 Rate of enzymatic turnover of various analogues by *Lmj*NTR (35 µg mL^{-1}) in the presence of 100 nmol NADH in Tris buffer (pH 7.5, 50 mM). Key compounds and families have been highlighted: yellow (bisthiophene 5N2Cs), blue (phenyl 5N2Cs), green (5-substituted phenyl 5N2Cs) and purple (cyclopentane 5N2Cs). Results are reported as the mean of three repeats, with errors representing standard error.

3.31.5.1 Discussion

The rate of bioactivation was compared to antileishmanial activity, aqueous solubility, fold change from *Ld*NTR1 overexpressor experiments and reduction potential to better understand the causes and effects of the observed rates of bioactivation (Figure 3.31-32).

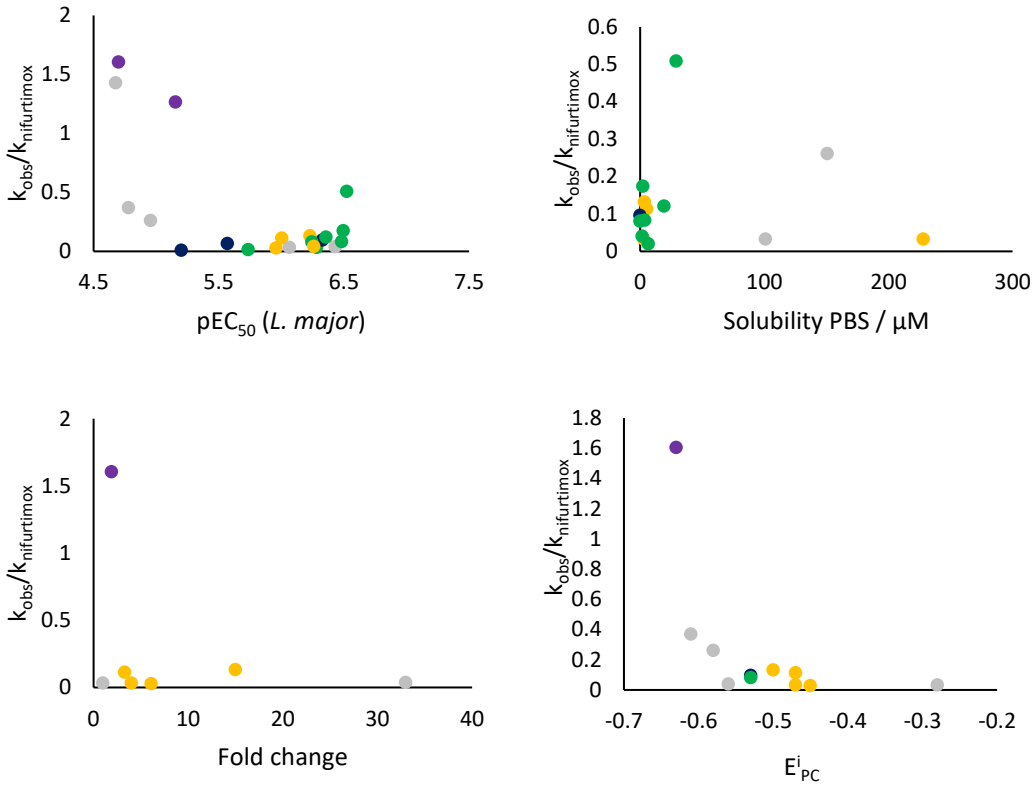

Figure 3.31-32 Correlation of rate of bioactivation ($k_{obs}/k_{nifurtimox}$) with pEC_{50} (*L. major*), aqueous solubility, fold change and reduction potential (E^{I}_{pc}). Key compounds and families have been highlighted: yellow (bisthiophene 5N2Cs), blue (phenyl 5N2Cs), green (5-substituted phenyl 5N2Cs) and purple (cyclopentane 5N2Cs).

There appears to be very little correlation between rate of bioactivation and any of the factors investigated, with multiple examples discussed below. Firstly, the lack of improved rate of turnover for nitrile **36** compared to the original hits is surprising as this analogue has a similar reduction potential but significantly improved solubility (Table 3.31-3, entry 2-3 & 5). This suggests that the enzymatic turnover is not limited by the poor aqueous solubility of the 5N2C series.

Secondly, imine **212** has a reduction potential + 0.19 V higher than the original hits, but has a similar or lower rate of turnover (Table 3.31-3, entry 2-3 & 6). This suggests that the ease of chemical reduction does not directly correlate with the rate of *Lmj*NTR1 bioactivation.

Thirdly, there appears to be no correlation between fold change from the phenotypic *Ld*NTR1 overexpressor system and rate of bioactivation for the majority of

compounds (Figure 3.31-32). Interestingly, cyclopentane **135** shows the fastest rate of bioactivation but one of the smallest fold changes in the overexpressor model (Table 3.31-3, entry 21). Likewise, 5-nitrofuran **109** shows the largest fold change in the overexpressor model but one of the slowest rates of bioactivation (Table 3.31-3, entry 7). This suggests that fast bioactivation results in detoxification of the parent 5N2C.

This insight is reiterated by studying the correlation between antileishmanial activity and rate of bioactivation (Figure 3.31-32). There appears to be an upper limit of antileishmanial activity that is reached when bioactivation by *Lmj*NTR1 is too fast, as when $k_{obs}/k_{nifurtimox} > 1.0$, antileishmanial activity is poor (Table 3.31-3, entry 20-22). However, when rate of bioactivation is low ($k_{obs}/k_{nifurtimox} \leq 0.5$), there seems to be little correlation with antileishmanial activity (Table 3.31-3, entry 2-19). This may appear counter-intuitive as a slower rate of bioactivation appears to give more active antileishmanial compounds. In contrast, the phenotypic overexpressor experiments showed that the same compounds show a general increase in toxicity upon overexpression of *Ld*NTR1 (section 3.31.2).

3.31.5.2 Conclusion

In conclusion, the lack of correlation between the kinetics of bioactivation and antileishmanial activity or fold change suggests that there is a more complex interplay taking place than the simple activation of a non-toxic prodrug to a cytotoxic metabolite. It is known that bioactivation is necessary for toxic effects, as compounds are more toxic against *L. donovani* overexpressing NTR1 (section 3.31.2). However, when bioactivation is too fast this appears to detoxify the drug (section 3.31.5). In order to investigate the lack of correlations, the metabolite profile after bioactivation could be investigated. This would elucidate whether a more complex bioactivation process is taking place, which could help to rationalise the lack of correlation between rate of bioactivation and antileishmanial activity or fold change.

3.31.6 Metabolomics of *Lmj*NTR1 bioactivation

The compound series synthesised in this work have been shown to be bioactivated by nitroreductase 1 in phenotypic *L. donovani* NTR1 overexpressor experiments (section 3.31.2) and biochemical kinetics experiments using recombinant *Lmj*NTR1 (section 3.31.5). However, no correlation was found between fold change and rate of bioactivation, or with antileishmanial activity in both cases. This suggests that there is a complex interplay occurring which is not explained by the simple bioactivation of a non-toxic prodrug to a cytotoxic metabolite. To investigate this further, the metabolite profile after *Lmj*NTR1 bioactivation of a range of 5N2Cs was investigated by LC-MS. Sample preparation for metabolomics experiments using recombinant *Lmj*NTR1 was achieved following a general method adapted from that reported by Hall *et al.* (see section 6.2).[138]

3.31.6.1 Assay standardisation using nifurtimox (37)

Nifurtimox (**37**) is a 5-nitrofuran drug that is bioactivated by trypanosomatid NTR1 and has a well-documented metabolite profile (section 3.12.1).[129,138] This was utilised to ensure that both the LC-MS method and sample generation procedure were suitable for the detection of nitroreductase metabolites. No parent nitro (**37**) compound could be observed after 10 minutes incubation and detection of the nitroso (**277**), unsaturated open chain nitrile (**279**) and saturated open chain nitrile (**280**) was possible. The hydroxylamine intermediate (**278**) was not detected, which suggests this species is short-lived. Each species was characterised by tandem mass spectrometry (MS/MS) and accurate mass, which supported the literature precedent (Figure 3.31-33).[138]

A

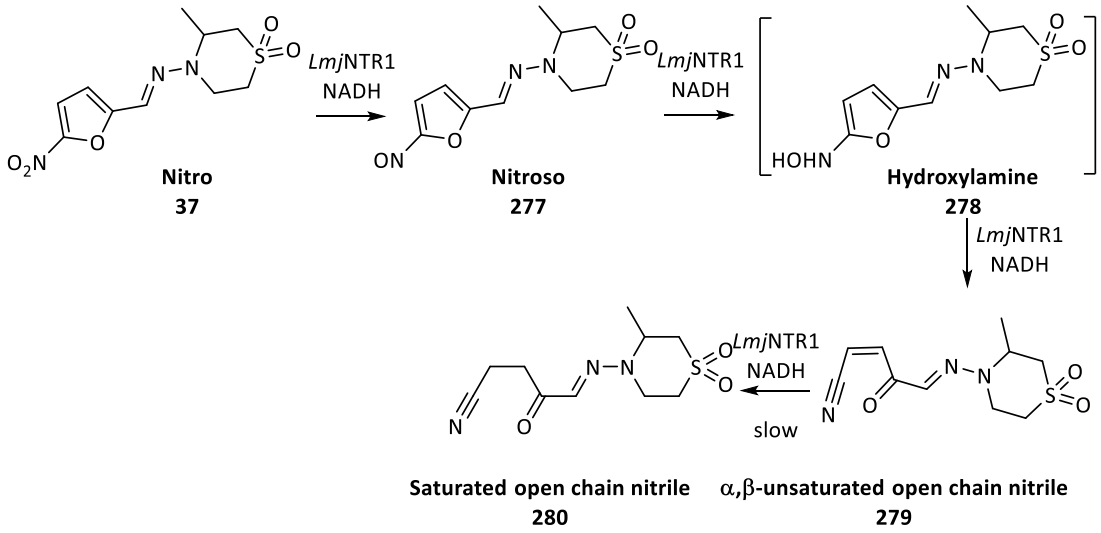

B

		Nitroso (277)	α,β-unsaturated open chain nitrile (279)	Saturated open chain nitrile (280)
LC-MS	Rt/ min	1.78	2.31	2.24
	ESI$^+$	272.07	256.08	258.09
Accurate mass	Formula [M+H]$^+$	C10H14N3O4S	C10H14N3O3S	C10H16N3O3S
	Desired mass ESI$^+$	272.0705	256.0756	258.0912
	Observed mass ESI$^+$	272.0696	256.0751	258.0908
MS/MS	Fragment 1 mass ESI$^+$	148.05	148.05	148.05
	Fragment 1 ID	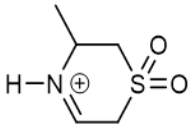		
	Fragment 2 mass ESI$^+$	125.03	109.04	-
	Fragment 2 ID	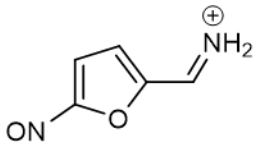	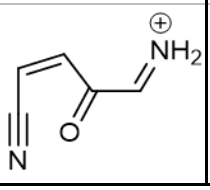	-

Figure 3.31-33 A. Bioactivation of nifurtimox (**37**) by *Lmj*NTR1 to observed metabolites. B. Accurate mass and MS/MS analysis of the observed metabolites.

When a limiting amount of NADH was used (0.7 eq), not all nifurtimox (**37**) was consumed and the reduction stopped at the unsaturated open chain nitrile (**279**), even after 18 hrs (Figure 3.31-34A). This suggested that the final reduction step was the slowest and was not achieved under limiting NADH conditions. However, in non-limiting NADH conditions (3.3 eq), the product distribution did not change between 10 minutes and 18 hrs, suggesting that all NADH had been used up after 10 minutes and the reaction was complete (Figure 3.31-34B-C). Consequently, a reaction time of 10 minutes and non-limiting NADH conditions were used for future experiments.

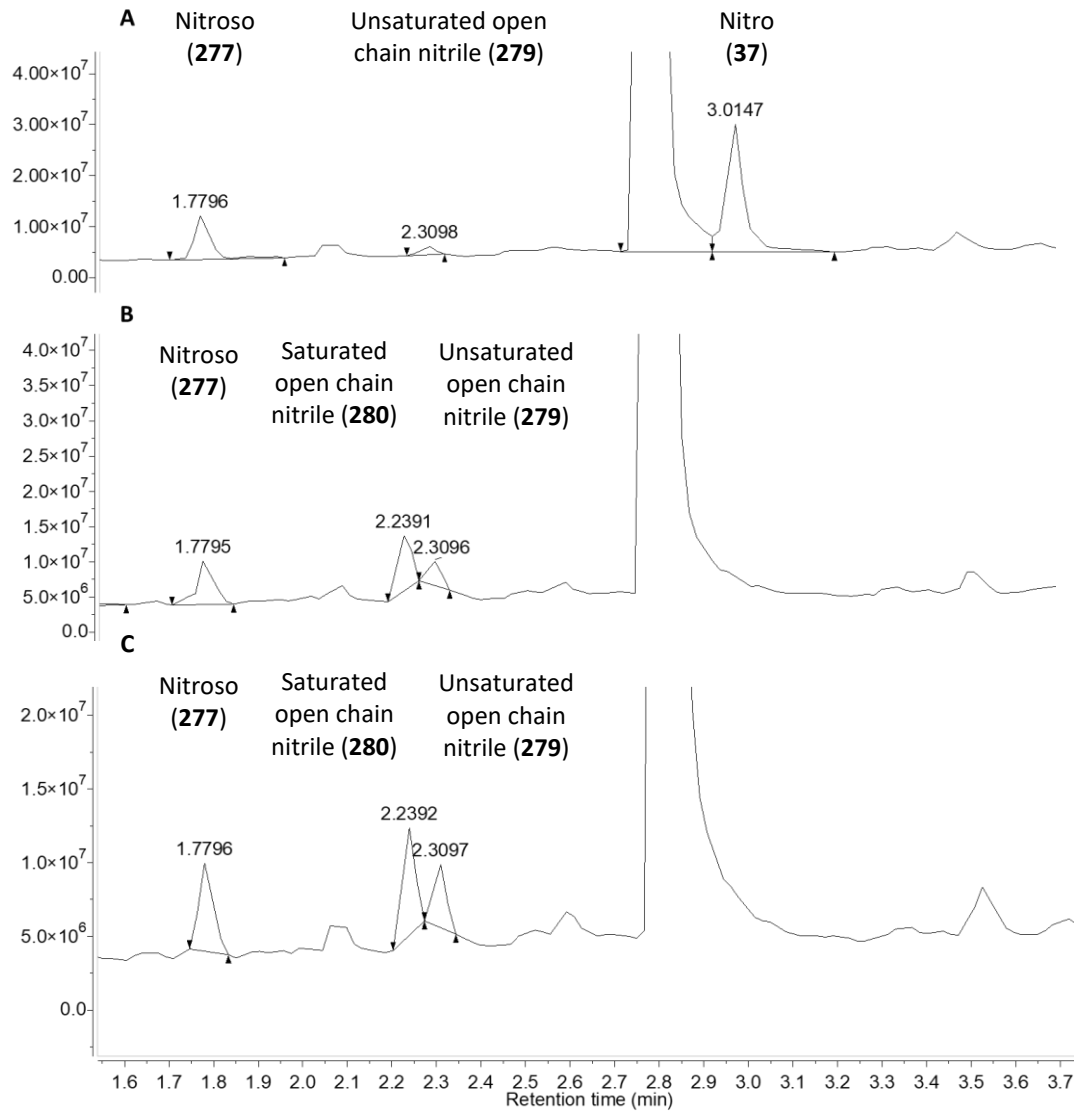

Figure 3.31-34 Nifurtimox (**37**) metabolism by recombinant *Lmj*NTR1 in limiting NADH conditions (66 µM) after 18 hr (A) and non-limiting NADH conditions (330 µM) after 10 minutes (B) and 18 hr (C).

3.31.6.2 5N2C series

Following validation of the sample generation and LC-MS methods using nifurtimox (**37**), attention turned to the synthesised 5N2C library. As discussed in section 3.12.3, nitrothiophenes have only been briefly explored as trypanosomatid NTR substrates.[59,62] There have been no reported investigations into the metabolite profile of 5-nitrothiophenes after trypanosomatid bioactivation. Consequently, it was of interest to investigate the metabolite profile of a series synthesised 5N2Cs with a variety of rates of *Lmj*NTR1 bioactivation to further explore the lack of correlation between rate of bioactivation and cytotoxicity (Figure 3.31-35).

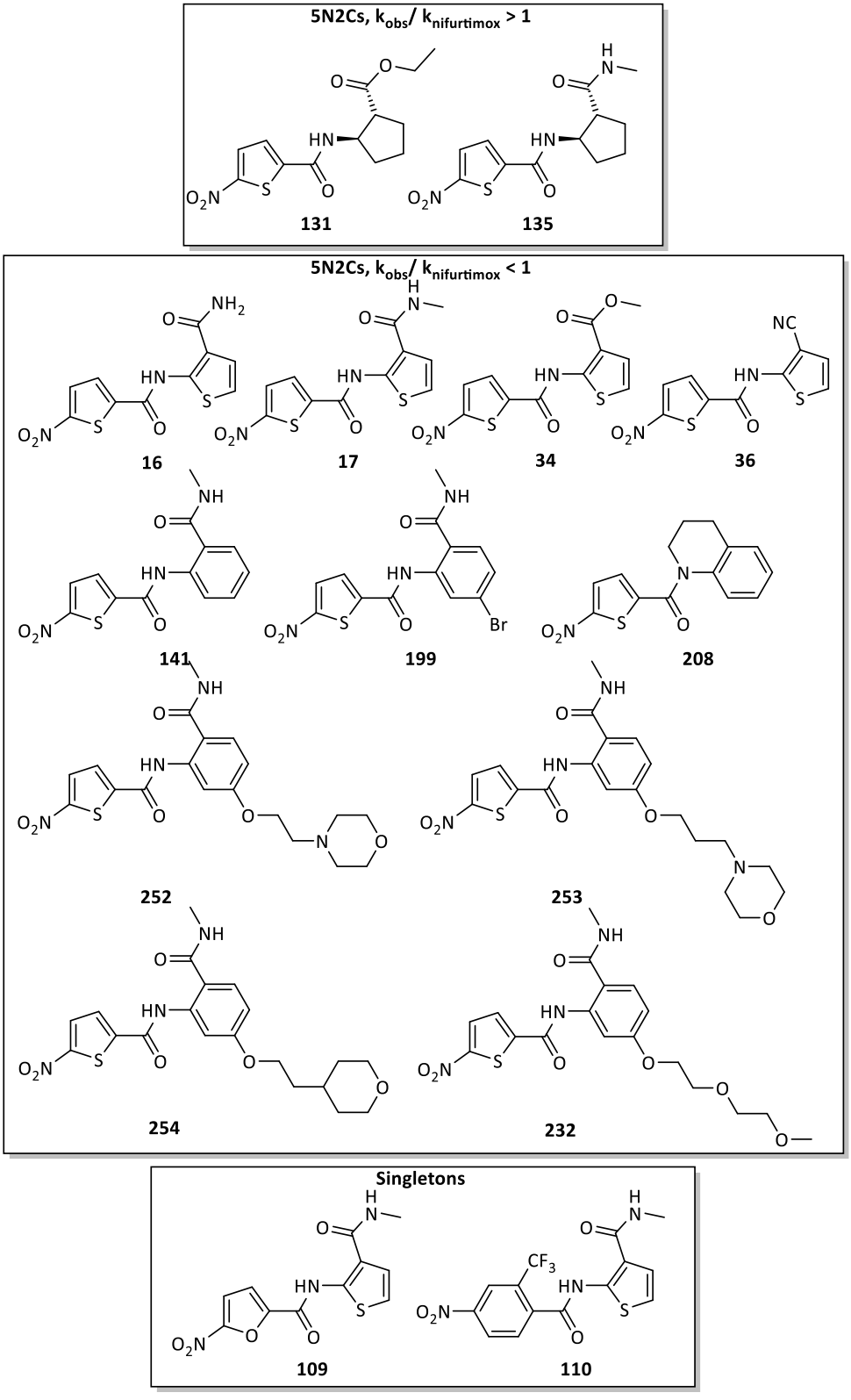

Figure 3.31-35 Structures of 13 5N2C compounds and 2 singletons used during metabolomics experiments.

3.31.6.2.1 Nitroso, hydroxylamine and open chain nitrile metabolites

As discussed in the previous section, bioactivation of nifurtimox (**37**) by *Lmj*NTR1 results in nitroso (**277**), hydroxylamine (**278**), α,β-unsaturated open chain nitrile (**279**) and saturated open chain nitrile (**280**) metabolites. Therefore, it was of interest to investigate whether a range of 5N2Cs, in addition to 5-nitrofuran **109** and nitrophenyl **110**, form similar metabolites.

Nitroso metabolites were observed upon *Lmj*NTR1 bioactivation in greater than trace quantities for 6/13 of the 5N2Cs tested, as verified by accurate mass (Table 3.31-4). However, each of these compounds also formed the nitroso metabolite in trace quantities in the absence of *Lmj*NTR1, which suggests that background NADH mediated reduction can occur. Hydroxylamine, open chain nitriles and amine metabolites are not observed in appreciable quantities for any of the 5N2Cs tested. Background reduction in the absence of enzyme is concerning, as it suggests that toxicity may be observed in reducing environments within the host. However, lead compounds **252** and **253** identified in Chapter 2 do not show any background reduction and therefore do not have these toxicity concerns.

.

Table 3.31-4 Identification of nitroso metabolites for a selection of 5N2Cs after *Lmj*NTR1 bioactivation. *trace quantities so accurate mass analysis is not possible. † = nitroso metabolites only observed in the absence of *Lmj*NTR1 at italicised retention times.

	Compound	LC-MS				Accurate mass		
		+ *Lmj*NTR1	– *Lmj*NTR1	Rt / min	m/z ESI$^-$	Nitroso formula [-H]$^-$	Desired mass ESI$^-$	Observed ESI$^-$
5N2C $k_{obs}/k_{nifurtimox}$ > 1	**131**	-	-	-	-	-	-	-
	135	+*	-	1.81	280.07	*	*	*
5N2C $k_{obs}/k_{nifurtimox}$ < 1	**16**	+	+	2.34	279.99	C10H6N3O3S2	279.9851	297.9848
	17	+	+	2.57	294.00	C11H8N3O3S2	294.0007	294.0009
	34	-	-	-	-	-	-	-
	36	+	†	2.59/*2.73*	261.97	C10H4N3O2S2	261.9745	261.9737
	141	-	-	-	-	-	-	-
	199	+	†	*3.15*/ 3.29/ *3.80*	365.95 / 367.95 (1:1)	C13H9N3O3S^{79}Br	365.9548	365.9545
	208	-	-	-	-	-	-	-
	232	+	+*	3.73	406.11	C18H20N3O6S	406.1073	406.1060
	252	-	-	-	-	-	-	-
	253	-	-	-	-	-	-	-
	254	+	+	3.16	416.13	C20H22N3O5S	416.1280	416.1275

Nitroso, hydroxylamine and amine metabolites were observed for nitrofuran **109**, as confirmed by accurate mass and MS/MS (Table 3.31-5). Nitroso and amine metabolites were observed exclusively in the presence of *Lmj*NTR1. However, trace amounts of hydroxylamine metabolite were observed in the absence of *Lmj*NTR1 suggesting that there was some background NADH reduction. In contrast, reduction stops at the nitroso species for nitrophenyl **110**, which was formed exclusively in the presence of *Lmj*NTR1.

Table 3.31-5: Nitroso, hydroxylamine and amine metabolites observed for **109** and **110**

			109	**110**
Nitroso	**LC-MS**	**Rt / min**	1.71	3.01
		m/z ESI$^-$	278.02	356.03
	Accurate mass	**Chemical formula [-H]$^-$**	C11H8N3O4S	C14H9N3O3F3S
		Desired mass ESI$^-$	278.0236	356.0317
		Observed mass ESI$^-$	278.0228	356.0315
	MS/MS	**Fragment m/z**	221.00	174.02
		Fragment ID	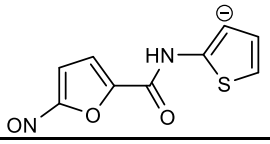	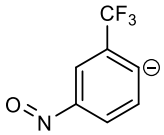
Hydroxylamine	**LC-MS**	**Rt / min**	1.92	
		m/z ESI$^-$	280.04	
	Accurate mass	**Chemical formula [-H]$^-$**	C11H10N3O4S	
		Desired mass ESI$^-$	280.0392	
		Observed mass ESI$^-$	280.0387	
	MS/MS	**Fragment m/z**	98.02	
		Fragment ID	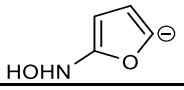	
Amine	**LC-MS**	**Rt / min**	2.59	
		m/z ESI$^-$	264.04	
	Accurate mass	**Chemical formula [-H]$^-$**	C11H10N3O3S	
		Desired mass ESI$^-$	264.0443	
		Observed mass ESI$^-$	264.0430	
	MS/MS	**Fragment m/z**	181.01	
		Fragment ID	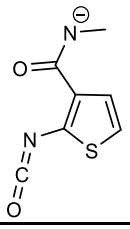	

The formation of large quantities of the nitroso metabolite for **110** suggests that this is the primary metabolism for this analogue. The identification of nitroso to amine metabolites for **109** shows that this reduction pathway is also significant for nitrofurans. In contrast, the lack of observable nitroso metabolites for 7/13 5N2Cs

suggests that another mechanism of bioactivation must be taking place for the 5N2C series.

*3.31.6.2.2 **131** as a model 5N2C compound*

Once nitroso, hydroxylamine and amine metabolites were found to be relatively insignificant for more than half of the series, attention turned towards identification of the major metabolites for the 5N2C series. Thus, the metabolite profile of **131** was studied as this 5N2C is turned over quickly by *Lmj*NTR1 and would generate the highest concentrations of metabolites to aid detection (section 3.31.5). Following LC-MS analysis of **131** incubated with and without *Lmj*NTR1 in non-limiting NADH conditions for 10 minutes, the mass spectrometry traces were compared to identify any peaks that correspond to metabolites that are formed by enzymatic bioactivation. Three major additional peaks were observed, which correspond to M+2 (**307**), 2M-14 or M+298 (**308**) and 2M-98 or M+214 (**309**) metabolites, where M is the mass of the parent nitro species (Figure 3.31-36). Upon detection of these metabolites, efforts turned to validating their identities and investigating whether the same metabolites are formed for the extended 5N2C series.

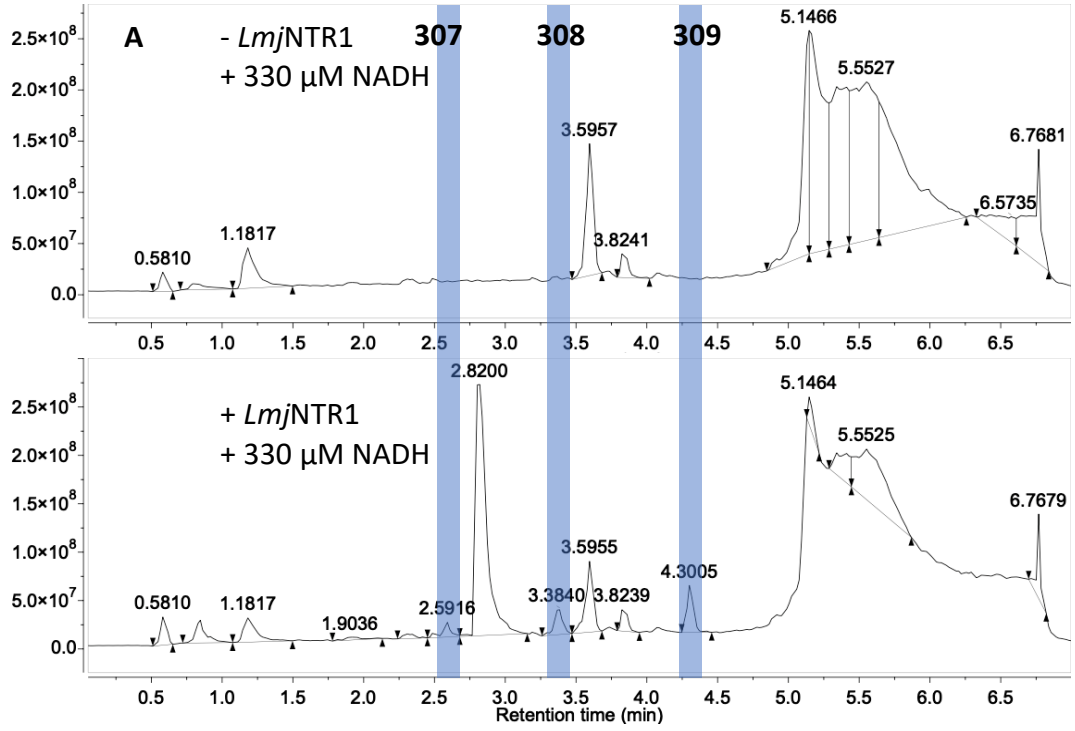

B

ID	Rt / min	m/z ESI$^-$	ID
Metabolite 1 (307)	2.59	313.09	M+2
Metabolite 2 (308)	3.38	609.17	M+298 OR 2M-14
Metabolite 3 (309)	4.30	525.18	M+214 OR 2M-98

Figure 3.31-36 A. Comparison of LC-MS trace upon incubation of **131** + NADH – *Lmj*NTR1 (above) and **131** + NADH + *Lmj*NTR1 (below). B. Three new peaks identified as M+2 (**307**), 2M-98 or M+214 (**308**) and 2M-14 or M+298 (**309**) metabolites. Peak at 2.82 mins is from the enzyme and can be disregarded.

3.31.6.2.3 Expanding model to wider 5N2C series

Following the detection of three major metabolites, it was important to validate their identities and significance for the wider 5N2C series. Each 5N2C compound (Figure 3.31-35) was incubated with 330 µM NADH and the metabolite profile assessed as described above. Metabolite 1 (M+2) was observed for all 5N2Cs tested. Furthermore, comparison of the accurate masses across the whole 5N2C series identified this metabolite as having the formula M+2H (Table 3.31-6). Metabolite 2 was identified as 2M-14 rather than M+298 and was observed for 11/13 of the 5N2Cs tested. Accurate mass was consistent with the formula 2M-O+2H (Table 3.31-7).

Finally, metabolite 3 was identified as 2M-98 rather than M+214 and was present across 12/13 of the 5N2Cs tested. 8 of the 5N2Cs showed two isomers of the 2M-98 metabolite, verified to have the same chemical formula (2M-H_2SO_4) by accurate mass (Table 3.31-8). All three metabolites were formed exclusively in the presence of *Lmj*NTR1, with the exception of 2M-98 which was also formed non-enzymatically for **36**. Testing across a range of 5N2C scaffolds identified the chemical formula of the metabolites and showed that a common metabolite profile is observed across the wider 5N2C series.

Table 3.31-6 LC-MS and accurate mass data for M+2 metabolite across a range of 5N2Cs providing the chemical formula M+2H.

		M+2 or M+H_2						
Kinetics category	**Compound ID**	**LC-MS**				**Accurate mass**		
		+ *Lmj*NTR1	**– *Lmj*NTR1**	**Rt / min**	**m/z ESI^-**	**M+2 formula $[-H]^-$**	**Desired mass ESI^-**	**Observed ESI^-**
5N2C $k_{obs}/k_{nifurtimox}$ > 1	**131**	+	-	2.59	313.09	C13H17N2O5S	313.0858	313.0859
	135	+	-	1.69	298.09	C12H16N3O4S	298.0862	298.0854
5N2C $k_{obs}/k_{nifurtimox}$ < 1	**16**	+	-	2.1	298	C10H8N3O4S2	297.9956	297.9947
	17	+	-	2.46	312.01	C11H10N3O4S2	312.0113	312.0102
	34	+	-	3.03	313	C11H9N2O5S2	312.9953	312.9941
	36	+	-	2.59	279.99	C10H6N3O3S2	279.9851	279.9846
	141	+	-	2.23	306.06	C13H12N3O4S	306.0549	306.0536
	199	+	-	2.79	383.96/385.96 (1:1)	C13H11N3O4S^{79}Br	383.9654	383.965
	208	+	-	3.03	289.06	C14H13N2O3S	289.0634	289.0647
	232	+	-	2.44	424.12	C18H22N3O7S	424.1178	424.117
	252	+	-	1.6	435.13	C19H23N4O6S	435.1338	435.1331
	253	+	-	1.69	449.15	C20H25N4O6S	449.1495	449.1489
	254	+	-	2.87	434.14	C20H24N3O6S	434.1286	434.1383
5-nitrofuran	**109**	+	-	1.89	296.03	C11H10N3O5S	296.0341	296.0341
4-nitro-2-trifluoromethyl phenyl	**110**	-	-	-	-	-	-	-

Table 3.31-7 LC-MS and accurate mass data for 2M-14 metabolite across a range of 5N2Cs providing the chemical formula 2M-O+H_2.

		2M-14 or 2M-O+H_2						
Kinetics category	**Compound ID**	**LC-MS**				**Accurate mass**		
		+ *Lmj*NTR1	**– *Lmj*NTR1**	**Rt / min**	**m/z ESI⁻**	**2M-14 formula [-H]⁻**	**Desired mass ESI⁻**	**Observed ESI⁻**
5N2C $k_{obs}/k_{nifurtimox} > 1$	**131**	+	-	3.37	609.17	C26H33N4O9S2	609.1689	609.1694
	135	+	-	2.13	579.17	C24H31N6O7S2	579.1696	579.1707
5N2C $k_{obs}/k_{nifurtimox} < 1$	**16**	+	-	2.61	578.98	C20H15N6O7S4	578.9885	578.9889
	17	-	-	-	-	-	-	-
	34	+	-	3.73	608.99	C22H17N4O9S4	608.9878	608.9872
	36	+	-	3.25	542.96	C20H11N6O5S4	542.9674	542.9662
	141	-	-	-	-	-	-	-
	199	+	-	3.48	752.93:754.93:756.93 (1:2:1)	$C26H21N6O7S2Br^{79}Br^{81}$	754.9239	754.9255
	208	+	-	3.82	561.13	C28H25N4O5S2	561.1266	561.126
	232	+	-	3.07	831.23	C36H43N6O13S2	831.233	831.233
	252	+	-	1.78	853.26	C38H45N8O11S2	853.2649	853.2643
	253	+	-	1.91	881.3	C40H49N8O11S2	881.2962	881.2968
	254	+	-	3.54	851.27	C40H47N6O11S2	851.2744	851.2733
5-nitrofuran	**109**	-	-	-	-	-	-	-
4-nitro-2-trifluoromethyl phenyl	**110**	-	-	-	-	-	-	-

Table 3.31-8 LC-MS and accurate mass data for 2M-98 metabolite across a range of 5N2Cs providing the chemical formula 2M-H_2SO_4. Bold = major peak when 2 isomers present. *= peak present in -*Lmj*NTR1 sample.

		2M-98 or 2M-H_2SO_4						
Kinetics category	**Compound ID**	**LC-MS**				**Accurate mass**		
		+ *Lmj*NTR1	**– *Lmj*NTR1**	**Rt / min**	**m/z ESI^-**	**2M-98 formula $[-H]^-$**	**Desired mass ESI^-**	**Observed ESI^-**
5N2C $k_{obs}/k_{nifurtimox} > 1$	**131**	+	-	4.3	525.18	$C_{26}H_{29}N_4O_6S$	525.1808	525.1807
	135	+	-	**2.64/2.72**	495.18	$C_{24}H_{27}N_6O_4S$	495.1814	495.1800
5N2C $k_{obs}/k_{nifurtimox} < 1$	**16**	+	-	2.94/**3.51**	495	$C_{20}H_{11}N_6O_4S_3$	495.0004	495.0005
	17	+	-	3.30/**4.00**	523.03	$C_{22}H_{15}N_6O_4S_3$	523.0317	523.031
	34	+	-	4.55/**5.21**	525	$C_{22}H_{13}N_4O_6S_3$	524.9997	524.9995
	36	+	+	3.59/**4.25***	458.98	$C_{20}H_7N_6O_2S_3$	458.9793	458.9786
	141	+	-	3.24/**4.02**	511.12	$C_{26}H_{19}N_6O_4S$	511.1184	511.1187
	199	+	-	4.06/**4.93**	666.94:668.94:670.94 (1:2:1)	$C_{26}H_{17}N_6O_4SBr^{79}Br^{81}$	668.9375	668.9394
	208	-	-	-	-	-	-	-
	232	+	-	3.35/**3.96**	747.24	$C_{36}H_{39}N_6O_{10}S$	747.2448	747.2444
	252	+	-	2.17	769.28	$C_{38}H_{41}N_8O_8S$	769.2768	769.2756
	253	+	-	2.27	797.31	$C_{40}H_{45}N_8O_8S$	797.3081	797.3074
	254	+	-	4.71	767.28	$C_{40}H_{43}N_6O_8S$	767.2863	767.2849
5-nitrofuran	**109**	"+ 2M-H2O25"	-	3.82	507.05	$C_{22}H_{15}N_6O_5S_2$	507.0545	507.0534
4-nitro-2-trifluoromethyl phenyl	**110**	-	-	-	-	-	-	-

With evidence that a similar metabolic pathway was present for all 5N2Cs on incubation with *Lmj*NTR1, it was of interest to verify whether the M+2, 2M-14 and 2M-98 metabolites are formed *in cellulo* and thus have biological relevance rather than just being an artifact of the biochemical experiment. To achieve this, the experiment was repeated using a whole cell system, as discussed in the next section.

3.31.6.2.4 Whole cell metabolomics

To investigate whether the observed metabolites are also formed *in cellulo*, whole cell metabolomics experiments were carried out. The whole cell metabolomics procedure was developed from Barrett *et al*.[158] In short, original hit compounds **16** and **17** were incubated with *L. major* promastigotes at 10 µM for 24 hrs. The treated parasites were harvested, and growth was terminated by briefly submerging in a dry ice /ethanol bath. The cells were pelleted, washed with PBS and lysed using chloroform:methanol:water (1:3:1). Following centrifugation, the supernatant was assessed by LC-MS. 2M-98 metabolites were observed for both **17** and **16** incubated samples, showing that this metabolite is biologically relevant (Figure 3.31-37). However, M+2 and 2M-14 metabolites were not observed in the whole cell metabolomics experiments. This either suggests that these metabolites are formed as an artifact of the biochemical experiment or that the metabolites are consumed by reacting with cell components and thus are not isolated from the whole cell environment.

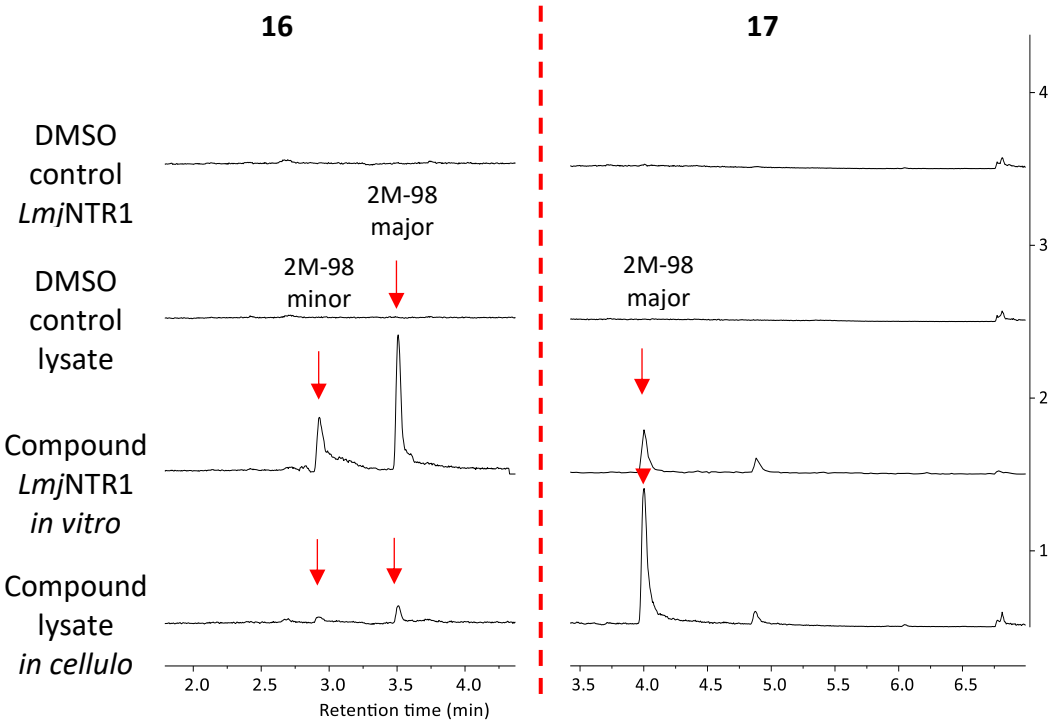

Figure 3.31-37 2M-98 metabolite can be observed for **16** and **17** both *in vitro* and *in cellulo* following incubation with *L. major* promastigotes (red arrows). Both major and minor metabolites can be observed *in cellulo* for **16**, whereas only trace amounts of the 2M-98 minor metabolite was observed for **17**.

3.31.6.2.5 Metabolite structure determination

Having ensured that the metabolic pathway was of relevance in a whole cell parasite context, it was of interest to identify the structure of each metabolite.

A. M+2 metabolite

The M+2 metabolite was present for all 5N2Cs tested in the biochemical metabolomics experiments. The analogous M+2 metabolite can also be identified for 5-nitrofuran **109** but not for nitrophenyl **110**, suggesting that the heterocycle is necessary for M+2 formation but its exact nature is not. The lack of M+2 peak in the whole cell metabolomics experiment could suggest that this metabolite is labile and reacts with cell components.

As discussed in section 3.1, only one literature example alludes to the metabolite profile of 5-nitrothiophenes after NTR bioactivation. Hartkoorn *et al.* discovered that 5-nitrothiophene compounds are bioactivated by F_{420} dependent *Mtb*Ddn to give the des-nitro species and release NO in a similar manner to (*R*)- and (*S*)- PA-824 (**275-276**) (Figure 3.12-9). [150] The final des-nitro species was not observed for any of the 5N2Cs tested. However, upon studying the mechanism of (*R*)-PA-824 (**275**) bioactivation, an unusual direct reduction on the aromatic ring is observed (Figure 3.31-38). [146,148] Subsequently, the M+2 metabolite observed for the 5N2C series was hypothesised to be the dihydrothiophene formed by direct reduction of the thiophene ring. This reduction is proposed to occur at the 4 position to give the 4,5-dihydrothiophene due to the increased electron withdrawing nature of the nitro group compared to the amide. However, the exact nature of the dihydrothiophene could not be proved for the 5N2C series.

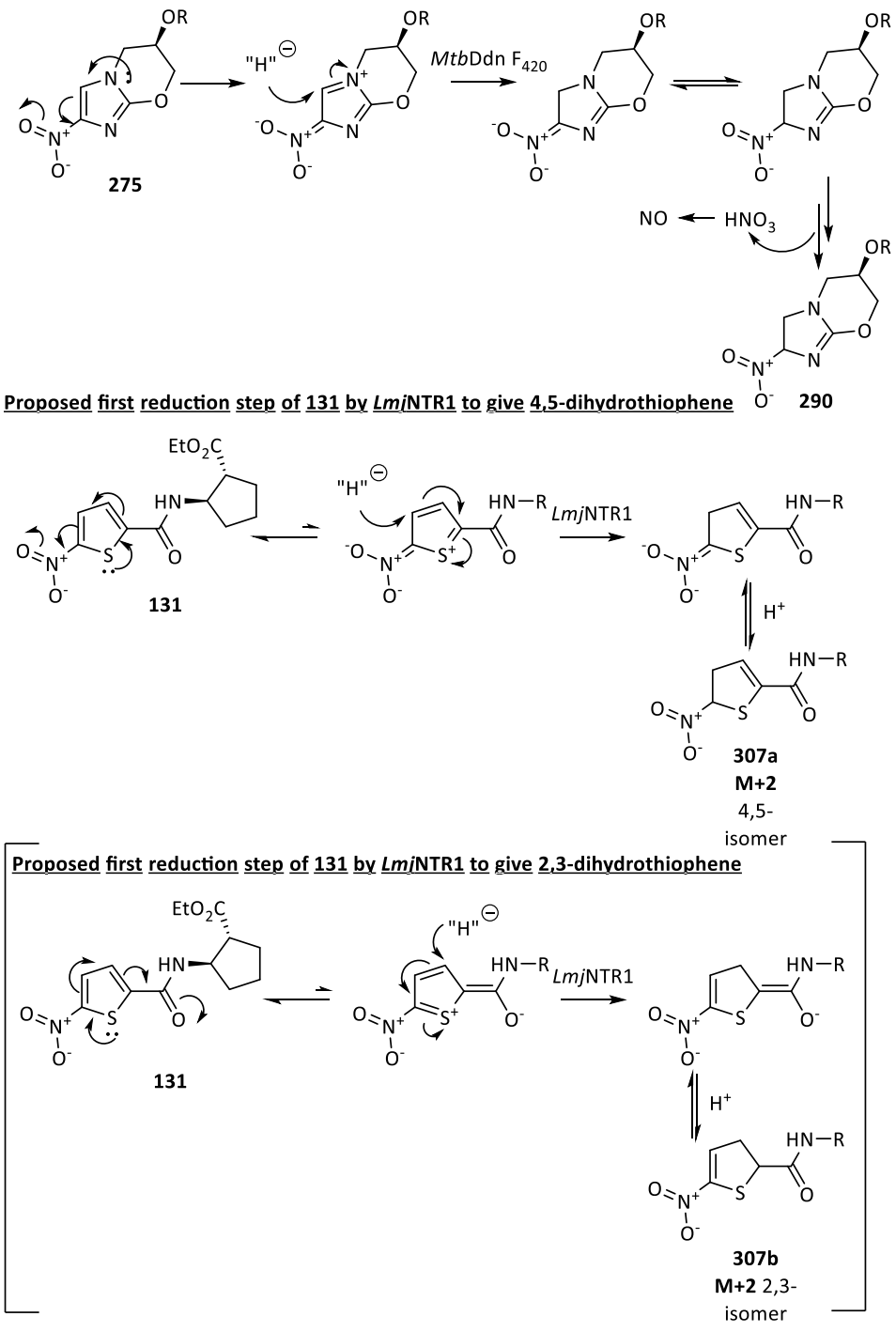

Figure 3.31-38 First step of the reduction of (*R*)-PA-824 (**275**) by *Mtb*Ddn to give the 4,5-dihydroimidazole intermediate (**290**) compared to the proposed reduction for representative 5N2C compound **131** by *Lmj*NTR1 to give 4,5-dihydrothiophene (**307a**). [146,148,150]

To verify the proposed M+2 metabolite structure, MS/MS experiments were carried out. Characteristic fragments were identified across much of the 5N2C M+2

metabolite series. A common fragment corresponding to the 5-nitrodihydrothiophene ring was observed for 9/13 of the 5N2Cs tested (fragment 1, Table 3.31-9), formed by fragmentation α- to the central amide carbonyl. The corresponding isocyanate formed by this fragmentation is also observed for 7/13 of the 5N2Cs (fragment 2, Table 3.31-9). Furthermore, the analogous 5-nitrodihydrofuran fragment (m/z 112.00) and isocyanate (m/z 181.01) were also observed for **109**, supporting the identity of the M+2 metabolite for the 5-nitrofuran-2-carboxamide scaffold. Furthermore, the bromine isotope pattern observed for the M+2 metabolite of 5-Br analogue **199** is again consistent with the formation of this species from the parent 5N2C.

Whilst collecting this data provided strong support for the proposed structure(s) of the M+2 metabolite, the position of the unsaturation could not be determined.

Table 3.31-9 Evidence for a dihydrothiophene as M+2H metabolite structure provided by MS/MS analysis. * Metabolite unstable or not present in high enough concentrations for successful MS/MS analysis.

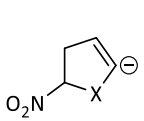

X=O
X=S

Fragment 1

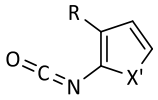

X'=S
X'=CHCH (phenyl)

Fragment 2

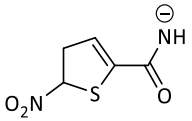

Fragment 3

Compound ID	LC-MS		MS/MS					
	Rt / min	m/z ESI$^-$	Fragment 1 present	Fragment 1 ESI$^-$	Fragment 2 present	Fragment 2 ESI$^-$	Fragment 3 present	Fragment 3 ESI$^-$
131	2.59	313.09	+	130.00	-	-	+	173.00
135	1.69	298.09	+	130.00	-	-	+	173.00
16	2.10	298.00	*	*	*	*	*	*
17	2.46	312.01	-	-	+	181.01	-	-
34	3.03	313.00	-	-	-	-	+	173.00
36	2.59	279.99	+	129.99	-	-	-	-
141	2.23	306.06	+	129.99	+	175.04	-	-
199	2.79	383.96/385.96 (1:1)	+	130.00	+	252.96/254.96	-	-
208	3.03	289.06	-	-	-	-	-	-
232	2.44	424.12	+	130.00	+	293.11	-	-
252	1.60	435.13	+	130.00	+	304.13	-	-
253	1.69	449.15	+	130.00	+	318.14	-	-
254	2.87	434.14	+	130.00	+	303.13	-	-
109	1.89	296.03	+	112.00	+	181.01	-	-
110	-	-	-	-	-	-	-	-

B. 2M-14 metabolite

The 2M-14 metabolite was observed for 11/13 of the 5N2Cs tested (Table 3.31-7). The general formula 2M-O+H_2 has similarities to the formula upon hydroxylamine formation (M-O+H_2). It can be predicted that the 2M-14 metabolite is formed by reaction of a hydroxylamine intermediate with the parent nitro species. Furthermore, this reaction must occur at the 3- or 4- position of the common 5-nitrothiophene portion of the parent molecule as the 2M-14 metabolite is formed for various 5N2Cs, independent of the nature of the right-hand ring. Two structures can be proposed for the 2M-14 metabolite, with the most likely structure being the 4-substituted thiophene due to the increased electron withdrawing effect of the nitro group, in analogy with that proposed for the M+2 metabolite (Figure 3.31-39).

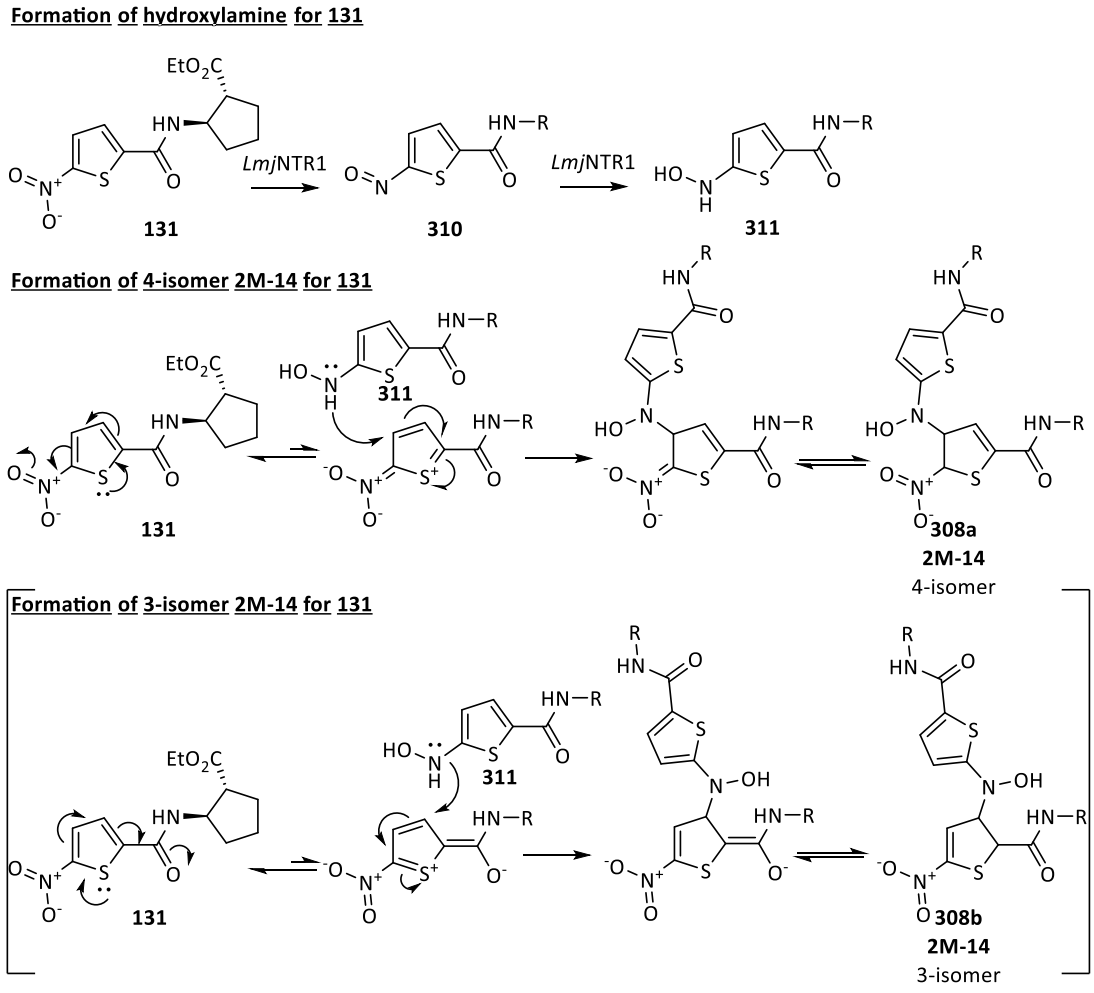

Figure 3.31-39 Proposed mechanism for the formation of the 2M-14 metabolite for representative 5N2C compound **131**.

MS/MS analysis was carried out for four of the 2M-14 metabolites (from 5N2Cs **36**, **34**, **131** and **135**). One common fragment was observed for all four 5N2Cs tested, corresponding to the fragmentation α to the carbonyl of the central amide (fragment 1, Table 3.31-10) in analogy with fragment 1 observed for M+2 metabolites. A second fragment was observed for cyclopentanes **131** and **135** corresponding to fragmentation across the hydroxylamine-thiophene bond (fragment 2, Table 3.31-10).

Table 3.31-10 Evidence of 2M-14 metabolite structure provided by MS/MS analysis.

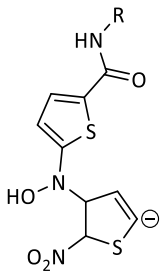

Fragment 1

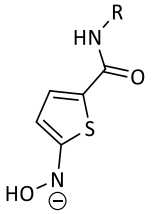

Fragment 2

Compound ID	LC-MS		MS/MS			
	Rt / min	m/z ESI^-	Fragment 1 present	Fragment 1 ESI^-	Fragment 2 present	Fragment 2 ESI^-
131	3.37	609.17	+	426.08	+	297.09
135	2.13	579.17	+	411.08	+	282.09
34	3.73	608.99	+	425.99	-	-
36	3.25	542.96	+	392.98	-	-

The limited MS/MS and accurate mass data supports the proposed structures of the 2M-14 metabolites. It is unlikely that the dimeric 2M-14 species is the cytotoxic agent as it likely results in detoxification of the hydroxylamine metabolite. The absence of this dimeric species from the whole cell experiment, unlike the M+2 metabolite discussed earlier, likely suggests that it is not biologically relevant and may form as an artifact of the biochemical experiment. As such, the 2M-14 metabolite was not investigated further.

C. 2M-98 metabolite

The 2M-98 metabolite was observed for 12/13 5N2Cs in the biochemical metabolomics experiments (Table 3.31-8). Only tetrahydroquinoline **208** did not form the 2M-98 metabolite, suggesting that an acyclic central amide bond is necessary for its formation. The analogous 2M-82 metabolite can also be identified for 5-nitrofuran **109**. However, no corresponding analogue is observed for nitrophenyl **110**. The presence of the 2M-98 peak for **17** and **16** *in cellulo* shows that it is biologically significant, justifying further investigation.

The 2M-98 metabolite must lose the necessary 'H_2SO_4' portion upon dimerization from the 5-nitrothiophene-2-carboxamide portion of the structures as this is the structural feature that is shared across the 5N2C series. Unlike the 2M-14 and M+2 metabolites, it was difficult to predict a rational chemical structure for the 2M-98 metabolite directly. The 2M-98 metabolite from 9/12 5N2Cs was subjected to MS/MS fragmentation and the results are summarised in Table 3.31-11 below.

Table 3.31-11 MS/MS data for 2M-98 major metabolite (bold) across a range of 5N2Cs showing a common fragmentation pattern. * Metabolite instability led to incoherent MS/MS spectrum. Bold= major metabolite peak when two isotopes observed.

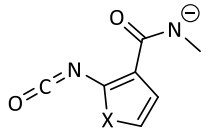

Fragment 1

2M-98 - Fragment 1
=
2M-98 - (M-128)
=
2M-98 - (M-$C_4H_2NO_2S$)

Fragment 2

Compound ID	LC-MS		MS/MS			
	Rt / min	m/z ESI^-	Fragment 1 present	Fragment 1 ESI^-	Fragment 2 present	Fragment 2 ESI^-
131	4.30	525.18	-	-	+	342.09
135	**2.64/2.72**	495.18	-	-	+	327.09
16	2.94/**3.51**	495.00	+	166.99	+	327.00
17	3.30/**4.00**	523.03	+	181.01	+	342.02
34	4.55/**5.21**	525.00	-	-	+	342.00
36	3.59/**4.25**	458.98	-	-	+	308.99
141	3.24/**4.02**	511.12	+	175.05	+	335.06
199 ($^{79}Br_2$)	4.06/**4.93**	666.94	+	252.96	+	412.97
232	3.35/**3.96**	747.24	*	*	*	*
252	2.17	769.28	+	304.12	+	464.15
253	2.27	797.31	*	*	*	*
254	4.71	767.28	*	*	*	*
109	3.82	507.05	+	181.01	+	325.04

Fragment 1 was observed for 6/9 analogues, resulting from fragmentation α to the carbonyl of the central amide in 2M-98 to give the isocyanate, in analogy with the M+2 metabolite. The low stability of fragment 1 for the remaining 3/9 5N2Cs could rationalise why it is not observed in these cases. However, fragment 2 is observed in all cases and results from the mass left over upon loss of fragment 1 from the 2M-98 metabolite. The common fragmentation profile observed suggests a common structure for all 2M-98 metabolites. Although the identity of fragment 2 remained unknown at this stage, MS/MS showed that the central amide and right-hand ring of each parent 5N2C remains untouched upon formation of the 2M-98 metabolite. Furthermore, MS/MS and accurate mass analysis proved that the central unknown core of the 2M-98 metabolite must have the chemical formula $C_8H_2N_2S$ (Figure 3.31-40).

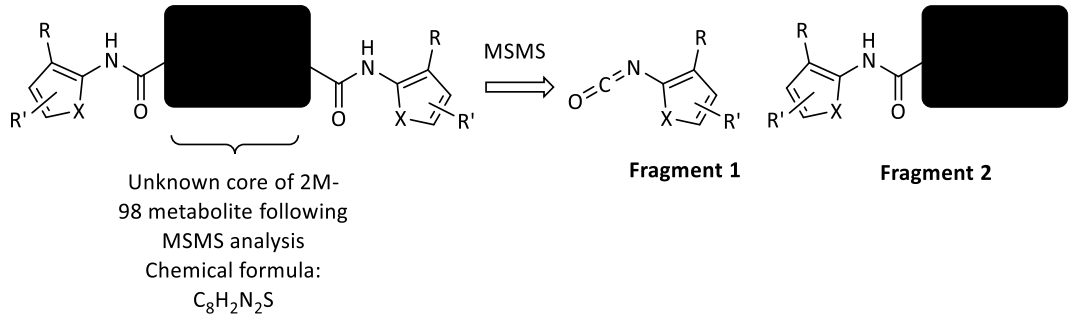

Figure 3.31-40: Conclusions drawn after MS/MS analysis of 2M-98 metabolite.

i) NMR analysis of 2M-98 metabolite

Following MS/MS analysis, attention turned to alternative ways to identify the 2M-98 metabolite. It was hypothesised that, provided sufficient NADH is supplied, *Lmj*NTR1 could be exploited to push the bioactivation of **131** to completion and isolate sufficient quantities of the 2M-98 metabolite (**309**) for further analysis. **131** was selected as it is turned over quickly by *Lmj*NTR1 and only one isomer of the 2M-98 metabolite was observed for this species, unlike **135**, thus increasing the possible yields obtained. Consequently, 10 mg of **131** was incubated with *Lmj*NTR1 and 6 eq. NADH in Tris buffer. Organic metabolites were extracted and purified by column chromatography to give 4 mg of the desired 2M-98 metabolite (**309**), as confirmed by LC-MS analysis (R_t 4.30 min, *m/z* 525.18 $[(2M-98)-H]^-$).

Following the successful synthesis and isolation of the 2M-98 metabolite (**309**), NMR analysis was used to investigate its identity. The proton NMR of the 2M-98 metabolite (**309**) revealed a mixture of diastereomers. The 2M-98 metabolite had 2 aromatic peaks and two distinct amide NH doublet proton signals in addition to the aliphatic signals expected for the two cyclopentane portions of the molecule (Figure 3.31-41).

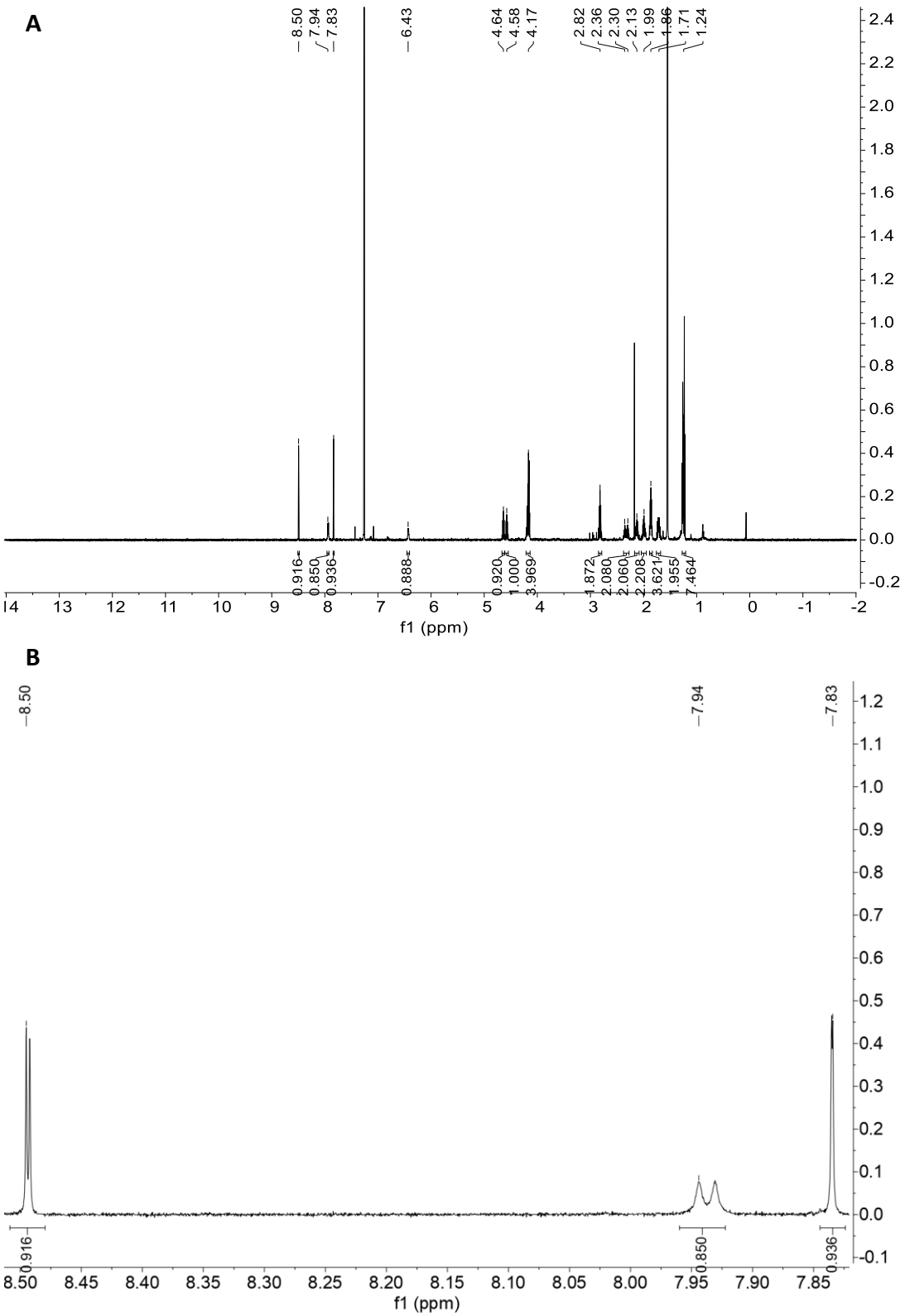

Figure 3.31-41: A. ^{1}H NMR spectrum of 2M-98 metabolite for **131**. B. Expansion of aromatic region showing distinct aromatic peaks for diastereomers.

At this stage, predictions could start to be made about the structure of the 2M-98 metabolite (**309**). Firstly, MS/MS showed that the unknown core of the 2M-98

metabolite (**309**) had the formula $C_8H_2N_2S$. Secondly, ^{1}H NMR showed that the two protons in the core of the 2M-98 metabolite (**309**) must be aromatic and distant from one another. Furthermore, the 2M-98 metabolite (**309**) is not symmetrical as two distinct amide proton environments are observed. Subsequently, two possible thieno[2,3-*b*]pyridyl 2M-98 isomeric structures were proposed (**309a** and **309b**, Figure 3.31-42). Due to the presence of two 2M-98 metabolite isomers for 8/12 5N2Cs, it is likely that both are formed following *Lmj*NTR1 bioactivation for most analogues. Both structures could be formed by the reaction of two rational metabolites, namely hydroxylamine (**311**) and α,β-unsaturated open chain nitrile (**312**), through a plausible mechanism (Figure 3.31-42). Furthermore, both intermediate species necessary to react to form the 2M-98 metabolite are observed during *Lmj*NTR1 bioactivation of nifurtimox (**37**) (Figure 3.31-33). It was hypothesised that similar intermediate metabolites could be formed following *Lmj*NTR1 bioactivation of the 5N2C series.

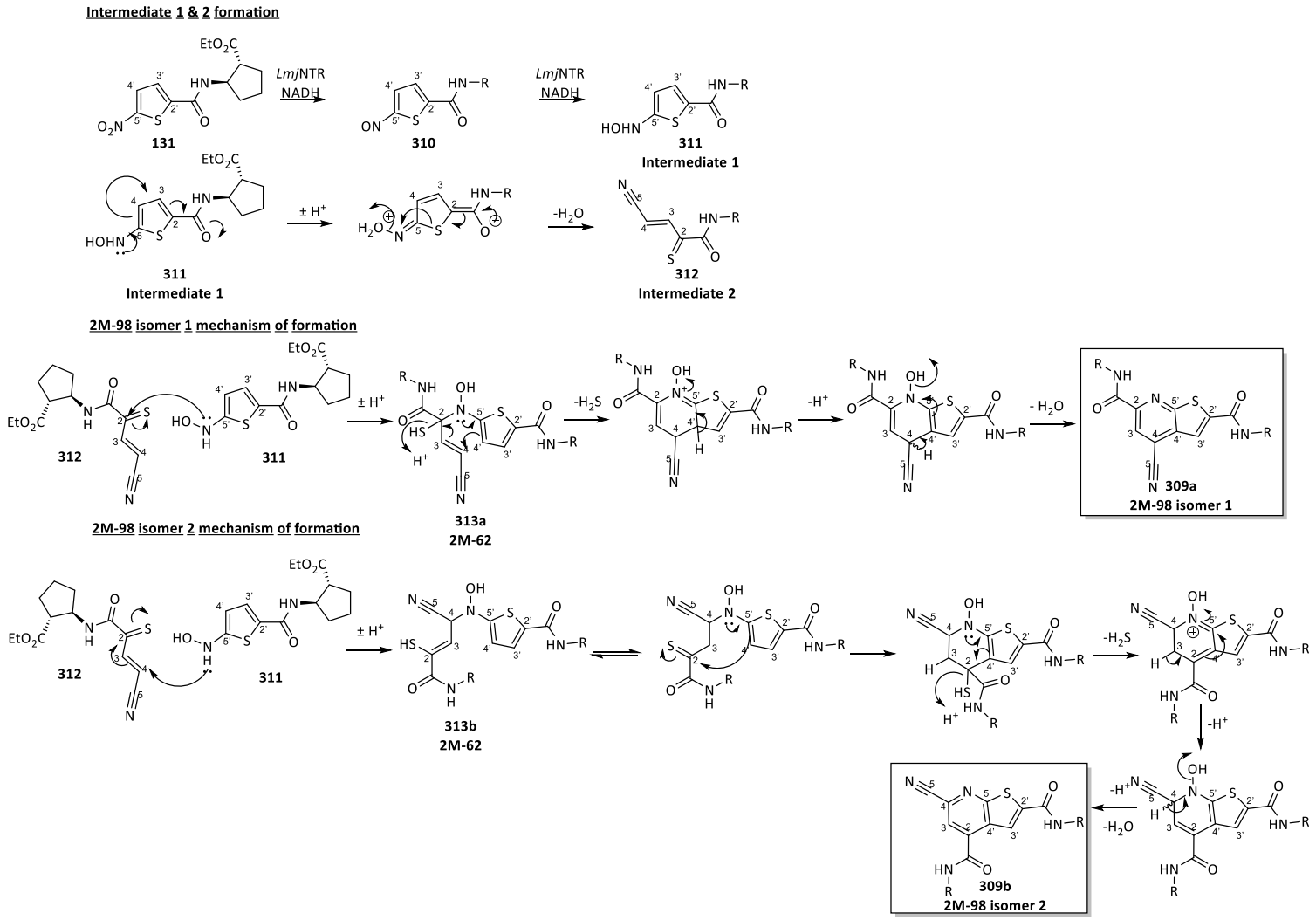

Figure 3.31-42 Mechanism of formation of the two 2M-98 isomers (**309a** and **309b**) from rational hydroxylamine (**311**) and α,β-unsaturated open chain nitrile (**312**) intermediates.

The observed ^{13}C NMR spectrum for the 2M-98 metabolite (**309**) was compared to predicted spectra for both isomers using Wiley ^{13}C NMR Data Checker software (see footnote[10]). Isomer 1 (**309a**) had a significant overlap between the predicted and observed spectrum and was predicted to be the major 2M-98 isomer formed after *Lmj*NTR1 bioactivation of the 5N2C series (Figure 3.31-43).

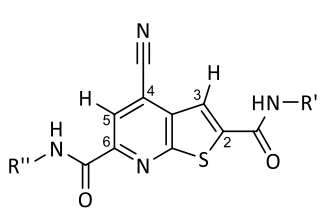

309a
2M-98 isomer 1

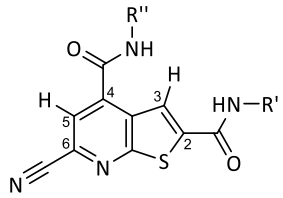

309b
2M-98 isomer 2

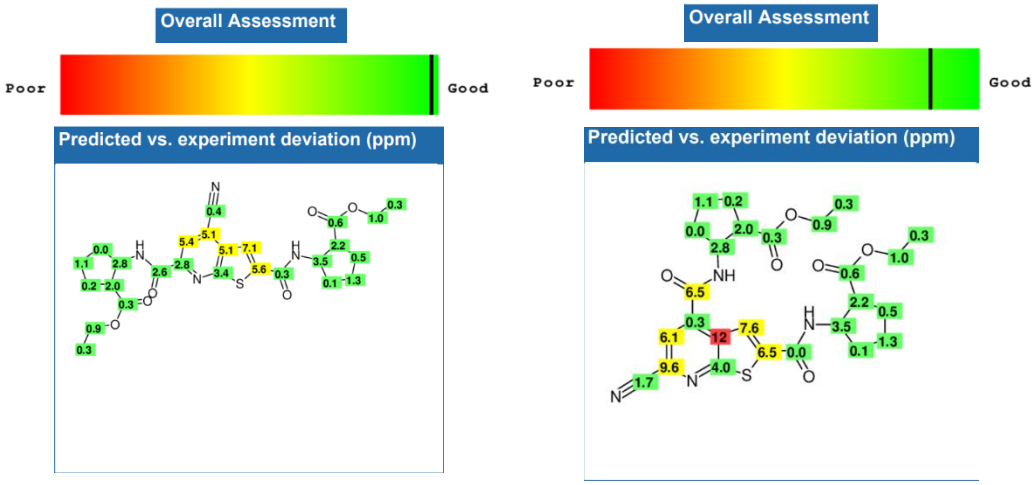

Figure 3.31-43: Overlap of calculated and observed ^{13}C NMR spectra suggesting that isomer 1 (**309a**) is the major 2M-98 isomer formed after *Lmj*NTR1 bioactivation. Green highlighted atoms = good agreement between calculated and observed spectra ($\Delta\delta_c$ < 5 ppm). Yellow highlighted atoms = moderate agreement between calculated and observed spectra (5ppm < $\Delta\delta_c$ < 10 ppm). Red highlighted atoms = poor agreement between calculated and observed spectra ($\Delta\delta_c$ > 10 ppm).

Structural assignment of the 2M-98 metabolite (**309a**) was achieved using a combination of the Wiley predicted assignment and 2D NMR experiments. The assignment of the aromatic protons was possible due to correlation of 5-H with CN in a Heteronuclear Multiple Bond Correlation (HMBC) experiment and 3-H with R'-NH in a Nuclear Overhauser Effect Spectroscopy (NOESY) experiment (appendix 8.5).

[10] Dr Exequiel Porta carried out the Wiley ^{13}C NMR Data Checker analysis.

To validate the antileishmanial activity of the 2M-98 metabolite (**309**), its antipromastigote activity against *L. major* was assessed. A three-fold decrease in activity is observed between the activity of the parent nitro (**131**) and the 2M-98 metabolite (**309**), suggesting that the 2M-98 metabolite is a non-toxic end point of bioactivation (Table 3.31-12).

Table 3.31-12: Antipromastigote activity of the parent nitro (**131**) compared to the 2M-98 metabolite (**309a**).

	Parent nitro (131)	**2M-98 (309a)**
EC_{50} (*L. major*) / µM	12 ± 3	33 ± 6

3.31.6.3 Discussion

LC-MS analysis was used to investigate the metabolite profile of a range of 5N2Cs bioactivated by *Lmj*NTR1. This led to the identification of three major metabolites: 2M-98, 2M-14 and M+2. However, only the 2M-98 metabolite was also observed by LC-MS analysis of the lysate generated from *L. major* treated with **16** or **17**. Successful isolation of the 2M-98 metabolite (**309a**) by scaling up the enzymatic bioactivation of **131** led to its identification as a thieno[2,3-*b*]pyridyl species. This species proved to be non-cytotoxic to *L. major* promastigotes, consistent with the 2M-98 metabolite being a non-toxic end point of bioactivation.

It was hypothesised that the transient electrophilic α,β- unsaturated open chain nitrile is the cytotoxic agent, as is the case for nifurtimox (**37**). Indeed, the absence of intermediate hydroxylamine and α,β- unsaturated open chain nitrile by LC-MS suggests that these species are highly labile and react before detection is possible. The α,β- unsaturated open chain nitrile intermediate is a highly potent electrophile with a Michael acceptor conjugated into both a nitrile group and a thioketone (Figure 3.31-42). It was hypothesised that this intermediate could react with nucleophilic cell components resulting in covalent inhibition of protein targets and cell death.

This complex metabolomic profile of 5N2Cs could explain the lack of correlation observed between the cytotoxicity of a compound and its rate of bioactivation (Scheme 3.31.1).

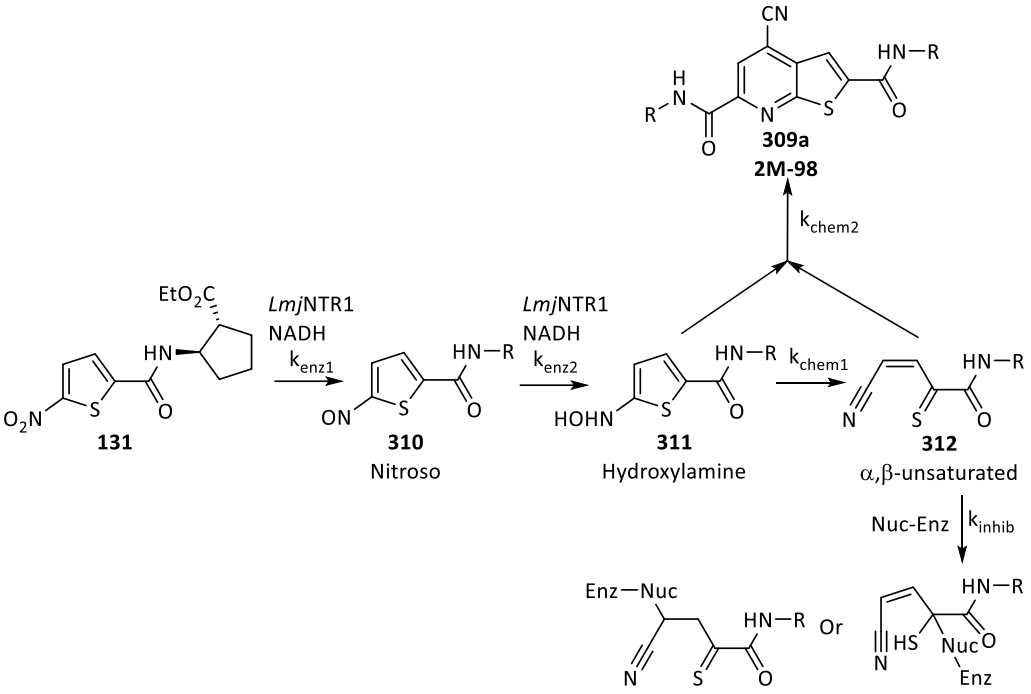

Scheme 3.31.1: Hypothesised route of bioactivation for representative 5N2C **131** by *Lmj*NTR1 results in either non-toxic 2M-98 (**309a**) formation ($k_{enz} > k_{chem1}$) or toxicity by covalent modification of protein targets ($k_{enz} \approx k_{chem1}$).

For compounds that are bioactivated very quickly by *Lmj*NTR1 ($k_{enz1/2}$ is large), it is predicted that the non-enzyme mediated ring opening of the hydroxylamine to the α,β- unsaturated open chain nitrile is rate determining ($k_{enz} > k_{chem1}$). Subsequently, whenever the electrophilic α,β- unsaturated open chain nitrile is formed, high concentrations of the hydroxylamine precursor result in efficient conversion to the non-toxic 2M-98 metabolite via k_{chem2}. However, compounds that are bioactivated slowly by *Lmj*NTR1 ($k_{enz1/2}$ is small) are likely to maintain low concentrations of the hydroxylamine intermediate ($k_{enz} \approx k_{chem1}$). Therefore, the cytotoxic α,β- unsaturated open chain nitrile has the chance to react with nucleophilic cell components resulting in toxic effects (k_{inhib}) rather than quenching by reaction with the hydroxylamine intermediate to give 2M-98. This hypothesis could help to rationalise the lack of correlation observed between rate of bioactivation and fold change or antileishmanial activity discussed in section 3.31.5.1.

3.31.7 GSK LeishBox 5N2C reduction by *Lmj*NTR1

In previous section, three major metabolites (M+2, 2M-98 and 2M-14) were identified across the synthesised 5N2C library. It was of interest to determine whether this metabolite profile also extends to more structurally diverse 5N2C antileishmanial compounds. As such, 13 antileishmanial compounds containing the 5N2C scaffold were obtained from the LeishBox and 2 from the HATBox (Figure 3.31-44, see footnote[11]). [46] Each compound was treated with excess NADH (3.3 eq.) in the presence and absence of *Lmj*NTR1 and the metabolite profile was analysed by LC-MS, accurate mass and MS/MS as previously described (section 3.31.6).

[11] LeishBox 5N2C compounds **16, 314-327** donated by Dr Silvia Gonzalez, GSK Tres Cantos

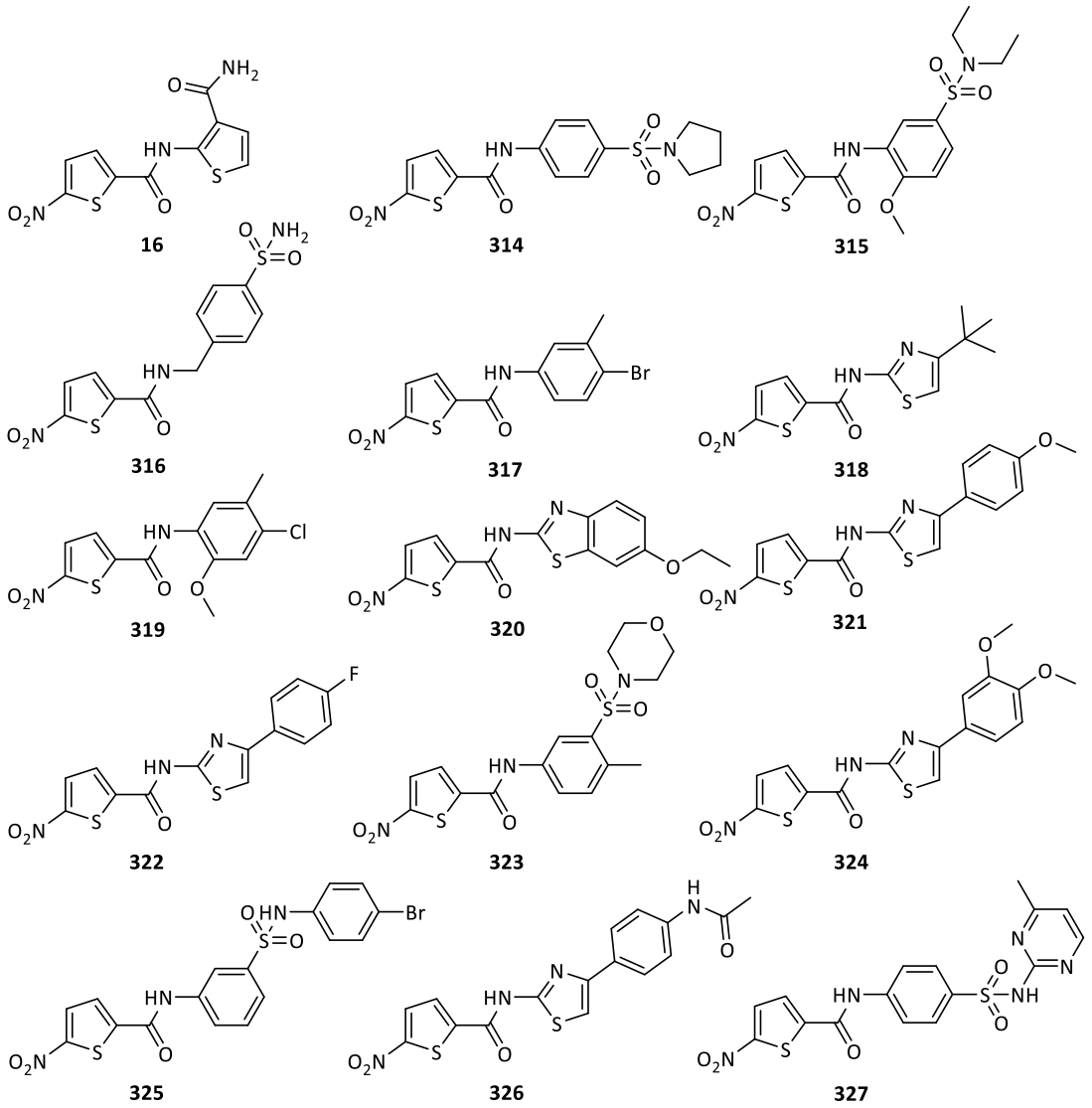

Figure 3.31-44 5N2C library obtained from the GSK LeishBox (see footnote) and HATBox (**315** and **327**).

3.31.7.1 2M-98 metabolite is observed for 14 out of 15 LeishBox compounds

One of the major metabolites for the synthesised 5N2C library observed after *Lmj*NTR1 bioactivation is the 2M-98 metabolite, formed by reaction of the hydroxylamine metabolite with the proposed cytotoxic α,β-unsaturated open chain nitrile metabolite (section 3.31.6). The presence of the 2M-98 metabolite can therefore be used to indirectly prove the presence of the α,β-unsaturated open chain nitrile intermediate.

The 2M-98 metabolite is observed for 14/15 of the LeishBox 5N2Cs tested, as confirmed by accurate mass and MS/MS (Figure 3.31-45). 9 of these 14 compounds, including all thiazole containing compounds (**318**, **321**, **322**, **324** and **326**), meta-substituted sulfonamides (**315**, **323** and **325**) and one para substituted sulfonamide (**314**), show at least trace bioactivation in the absence of *Lmj*NTR1 when NADH is present (entry 2-3, 6 & 9-14, Table 3.31-13). In these cases, NADH is still essential for this background reduction to occur, as in the absence of NADH no 2M-98 metabolite is observed in any case. The remaining 5 compounds, which include bisthiophene (**16**), electronically neutral phenyl (**316** and **317**), tetra-substituted analogue **319** and one para sulfonamide (**327**), show selective bioactivation to the 2M-98 metabolite in the presence of *Lmj*NTR1 (entry 1, 4-5 & 15, Table 3.31-13).

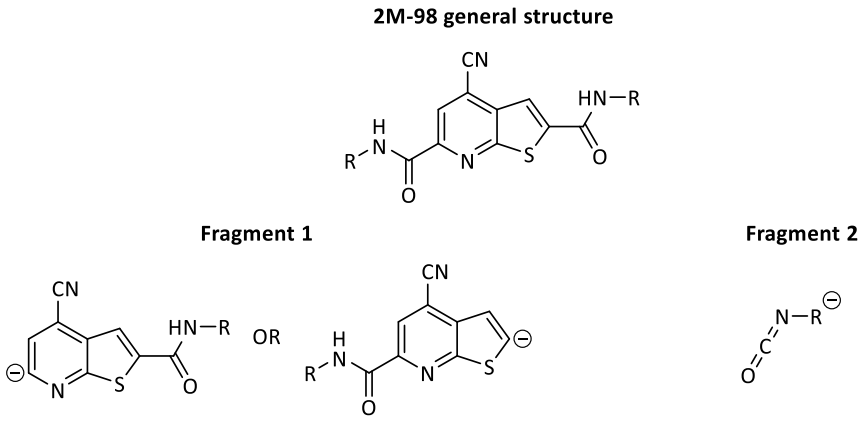

Figure 3.31-45 2M-98 metabolite general structure and key fragments observed by MS/MS.

Table 3.31-13 MS/MS and accurate mass data for the 2M-98 metabolite formed for the LeishBox 5N2Cs.

				LC-MS		Accurate mass			MS/MS			
Entry	**Compound ID**	**Present + NTR**	**Present - NTR**	Rt/ min	2M-98 ESI^-	2M-98 formula $[-H]^-$	Desired mass ESI^-	Observed mass ESI^-	Fragment 1 present	Fragment 1 mass ESI^-	Fragment 2 present	Fragment 2 mass ESI^-
1	**16**	+	-	3.45	495.00	C20H11N6O4S3	495.0003	495.0004	+	327	+	167
2	**314**	+	+	4.32	663.11	C30H27N6O6S3	663.1149	663.1154	+	411.06	-	-
3	**315**	+	+	4.72	727.17	C32H35N6O8S3	727.1677	727.1678	+	443.09	-	-
4	**316**	+	-	2.31	583.05	C24H19N6O6S3	583.0528	583.0528	+	371.03	+	211.02
5	**317**	+	-	5.55	580.93:582:93:584.92 (1:2:1)	C24H15Br2N4O2S	582.9258	582.9262	+	369.96	-	-
6	**318**	+	+	5.37/ 4.71	523.10	C24H23N6O2S3	523.104 OR 523.1031	523.1045	+	341.05	-	-
7	**319**	+	-	5.64	553.03: 555.03 : 557.02	C26H19Cl2N4O4S	553.0498	553.0504	+	356.02	-	-
8	**320**	-	-	-	-	-	-	-	-	-	-	-
9	**321**	+	+	5.06	623.06	C30H19N6O4S3	623.0623	623.063	+	391.03	-	-
10	**322**	+	+	5.20	599.02	C28H13F2N6O2S3	599.0234	599.023	+	379.01	-	-
11	**323**	+	+	4.28	723.14	C32H31N6O8S3	723.1369	723.1365	+	441.07	-	-
12	**324**	+	+	4.67	683.08	C32H23N6O6S3	683.0831	683.0841	+	421.04	-	-
13	**325**	+	+	4.78	862.90 : 864.90 : 866.90	C34H21Br2N6O6S3	864.9037	864.9031	+	510.97	-	-
14	**326**	+	+	3.86	677.08	C32H21N8O4S3	677.084	677.0848	+	418.04	-	-
15	**327**	+	-	3.30	739.10	C32H23N10O6S3	739.0963	739.0964	+	449.05	+	289.04

3.31.7.2 2M-14 metabolite is observed for 9 LeishBox 5N2Cs

During bioactivation of the synthesised 5N2C library by *Lmj*NTR1, a 2M-14 metabolite was also formed. Although this metabolite is not relevant in a whole cell model (section 3.31.6.2.4), it was still of interest to investigate whether this metabolite is also formed biochemically for the LeishBox 5N2Cs. The 2M-14 metabolite was observed for 10/15 LeishBox 5N2Cs (entry 1-5, 7, 9-12, Table 3.31-14). One compound (**314**, entry 2, Table 3.31-14) also shows bioactivation in the presence and absence of *Lmj*NTR1. Accurate mass for a representative sample (**316**, entry 4, Table 3.31-14) supports the 2M-14 identity proposed in the previous section.

Table 3.31-14 Accurate mass data for the 2M-14 metabolite formed for the LeishBox 5N2Cs.

				LC-MS		**Accurate mass**		
Entry	**Comp-ound ID**	**Pres-ent + NTR**	**Pres-ent - NTR**	Rt/ min	2M-14 ESI^-	2M-14 formula $[-H]^-$	Desired mass ESI^-	Observed mass ESI^-
1	**16**	-	-	2.59	578.99	-	-	-
2	**314**	+	+	3.44	747.10	-	-	-
3	**315**	+	-	3.82	811.16	-	-	-
4	**316**	+	-	2.17	667.04	C24H23N6O9S4	667.0422	667.0409
5	**317**	+	-	4.60	662.92: 664.92: 666.92 (1:2:1)	-	-	-
6	**318**	-	-	-	-	-	-	-
7	**319**	+	-	4.37	637.04	-	-	-
8	**320**	-	-	-	-	-	-	-
9	**321**	+	-	3.97	707.05	-	-	-
10	**322**	+	-	4.11	683.01	-	-	-
11	**323**	+	-	3.44	807.13	-	-	-
12	**324**	+	-	3.6	767.07	-	-	-
13	**325**	-	-	-	-	-	-	-
14	**326**	-	-	-	-	-	-	-
15	**327**	-	-	-	-	-	-	-

3.31.7.3 All LeishBox 5N2Cs form M+2 metabolite after *Lmj*NTR1 bioactivation

Bioactivation of the synthesised 5N2C library by *Lmj*NTR1 also gives a dihydrothiophene M+2 metabolite. This metabolite has a Michael acceptor like functionality and as such could act as an electrophile *in cellulo* resulting in toxic effects. However, unlike the transient proposed α,β-unsaturated open chain nitrile metabolite, this is stable enough to be analysed directly by LC-MS.

All LeishBox 5N2Cs form the M+2 dihydrothiophene metabolite upon incubation with NADH and *Lmj*NTR1 (Figure 3.31-46). The M+2 metabolite is formed only in the presence of *Lmj*NTR1 for 13/15 LeishBox 5N2Cs (entry 1, 3-10 & 12-15, Table 3.31-15). However, 2 compounds (**314** and **323**) also form trace amounts of the M+2 metabolite in the absence of *Lmj*NTR1 (entry 2 & 11, Table 3.31-15).

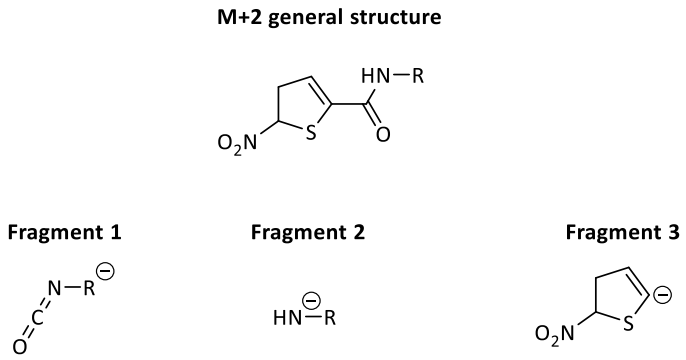

Figure 3.31-46 M+2 metabolite general structure and key fragments observed by MS/MS.

Table 3.31-15 MS/MS and accurate mass data for the M+2 metabolite formed for the LeishBox 5N2Cs.

				LC-MS		Accurate mass			MS/MS					
Entry	**Compound ID**	**Present + *Lmj*NTR 1**	**Present - *Lmj*NTR 1**	Rt/ min	M+2 ESI^-	M+2 formula $[-H]^-$	Desired mass ESI^-	Observed ESI^-	Fragment 1 present	Fragment 1 mass ESI^-	Fragment 2 present	Fragment 2 mass ESI^-	Fragment 3 present	Fragment 3 mass ESI^-
1	**16**	+	-	2.06	298.00	$C_{10}H_8N_3O_4S_2$	297.9958	297.9956	+	167.00	-	-	+	130.00
2	**314**	+	+	2.73	382.05	$C_{15}H_{16}N_3O_5S_2$	382.0528	382.0531	-	-	+	225.07	+	130.00
3	**315**	+	-	3.12	414.08	$C_{16}H_{20}N_3O_6S_2$	414.0794	414.0794	-	-	-	-	+	130.00
4	**316**	+	-	1.69	342.02	$C_{12}H_{12}N_3O_5S_2$	342.0219	342.0218	+	211.02	-	-	+	130.00
5	**317**	+	-	3.37	340.96: 342.96 (1:1)	$C_{12}H_{10}BrN_2O_3S$	342.957	342.9575	-	-	-	-	+	130.00
6	**318**	+	-	3.33	312.05	$C_{12}H_{14}N_3O_3S_2$	312.0477	312.0477	-	-	+	155.06	+	130.00
7	**319**	+	-	3.51	327.02: 329.02 (3:1)	$C_{13}H_{12}ClN_2O_4S$	327.0201	327.0206	-	-	-	-	+	130.00
8	**320**	+	-	3.19	350.03	$C_{14}H_{12}N_3O_4S_2$	350.0263	350.0269	-	-	+	193.04	-	-
9	**321**	+	-	3.23	362.03	$C_{15}H_{12}N_3O_4S_2$	362.0265	362.0269	-	-	+	205.04	+	130.00
10	**322**	+	-	3.33	350.01	$C_{14}H_9FN_3O_3S_2$	350.0073	350.0069	-	-	+	193.02	+	130.00
11	**323**	+	+	2.73	412.06	$C_{16}H_{18}N_3O_6S_2$	412.0632	412.0637	-	-	+	255.08	+	130.00
12	**324**	+	-	2.94	392.04	$C_{16}H_{14}N_3O_5S_2$	392.0372	392.0375	-	-	+	235.05	+	130.00
13	**325**	+	-	3.37	481.95: 483.95 (1:1)	$C_{17}H_{13}BrN_3O_5S_2$	483.9453	483.946	+	352.94	-	-	-	-
14	**326**	+	-	2.48	389.04	$C_{16}H_{13}N_4O_4S_2$	389.0367	389.0378	-	-	+	232.05	+	130.00
15	**327**	+	-	2.03	420.04	$C_{16}H_{14}N_5O_5S_2$	420.0436	420.0436	-	-	+	263.06	+	130.00

3.31.7.4 Discussion

The results from the metabolomic study of the LeishBox 5N2Cs show distinct parallels with those observed for the 5N2C library synthesised in this work, with M+2, 2M-98 and 2M-14 metabolites being identified in both the synthesised and LeishBox 5N2C series. The formation of 2M-14 metabolites is not considered further due to the absence of this metabolite in the whole cell metabolomics experiments.

Synthesised and LeishBox 5N2Cs form the M+2 metabolite only in the presence of *Lmj*NTR1, except for **314** and **323** which also form this metabolite under reducing non-enzymatic conditions. The 2M-98 metabolite was observed across the 5N2C family, except for **208** from the synthesised library and **320** from the LeishBox. 2M-98 formation is possible in the absence of *Lmj*NTR1 for nine of the LeishBox compounds and one synthesised 5N2C (**36**). The presence of this metabolite across the 5N2C series gives evidence for the formation of the labile α,β-unsaturated open chain nitrile, which could not be directly observed by LC-MS.

Non-enzymatic bioactivation is undesirable as it could lead to host cell toxicity. For example, the reducing conditions necessary to maintain electrochemical gradients could result in toxicity issues which are as yet unexplored.[159] To rationalise this, HepG2 toxicity was explored as a metric to discover any potential links between non-enzymatic bioactivation of 5N2Cs in reducing environments and host cell toxicity (Table 3.31-16). A selection of LeishBox and synthesised 5N2Cs that form metabolites non-enzymatically have relatively high HepG2 toxicities (entries 6, 8, 15-16 & 23-25 Table 3.31-16).[46] However, there are also multiple compounds that show non-enzymatic bioactivation but retain low HepG2 cytotoxicity (entries 3-4, 10, 13, 19, 22 & 26-27, Table 3.31-16). Furthermore, multiple compounds have high HepG2 toxicity but no background formation of metabolites in reducing conditions (entry 7, 17, 20-21 & 28, Table 3.31-16). As such, it is likely that there are multiple contributing factors to HepG2 toxicity which complicate the drawing of conclusions regarding the toxic effects of non-enzymatic bioactivation of 5N2Cs.

Table 3.31-16 Comparison of HepG2 toxicity and antileishmanial activity with non-enzymatic metabolite formation. †EC_{50} and S.I. for *L. major* promastigotes vs HepG2 reported for synthesised 5N2C and InMac *L. donovani* vs HepG2 for LeishBox library. *HATBox compounds. ND= not determined.

Series	Entry	Compound ID	Non-enzymatic formation of metabolite			Antileishmanial activity (EC_{50}) † / µM [46]	CC_{50} HepG2 / µM [46]	S.I †
			2M-98	M+2	Nitroso			
Synthesised	1	131	-	-	-	9.9	ND	ND
	2	135	-	-	-	20	ND	ND
	3	16	-	-	+	0.52	24	46
	4	17	-	-	+	0.99	96	97
	5	34	-	-	-	0.59	>100	>169
	6	36	+	-	+	1.1	8	7
	7	141	-	-	-	0.65	5	8
	8	199	-	-	+	0.57	7.2	13
	9	208	-	-	-	11.1	ND	ND
	10	232	-	-	+	0.32	>100	>303
	11	252	-	-	-	0.44	24	55
	12	253	-	-	-	0.30	12.7	42
	13	254	-	-	+	0.33	>100	>300
LeishBox	14	16	-	-	ND	1.3	> 100	> 79
	15	314	+	+	ND	1.0	6.3	6
	16	315*	+	-	ND	50	> 100	> 2
	17	316	-	-	ND	13	16	1
	18	317	-	-	ND	2.5	40	16
	19	318	+	-	ND	2.5	50	20
	20	319	-	-	ND	5.0	32	6
	21	320	-	-	ND	5.0	16	3
	22	321	+	-	ND	1.6	> 100	> 63
	23	322	+	-	ND	1.0	13	13
	24	323	+	+	ND	2.0	16	8
	25	324	+	-	ND	1.3	10	8
	26	325	+	-	ND	0.79	16	20
	27	326	+	-	ND	0.79	50	63
	28	327*	-	-	ND	5.0	16	3

Compounds that have a poor selectivity index over HepG2 cells or show any non-enzymatic bioactivation should be treated with caution when considering compounds for progression to future medicinal chemistry campaigns. Only three members of the synthesised compound library (**252**, **253**, **34**) and two LeishBox 5N2Cs (**317** and **319**) have potent antileishmanial activity, a high S.I. and do not undergo any non-enzymatic bioactivation (Figure 3.31-47). From these compounds, **252** and **253** remain the most promising lead compounds due to their additional high aqueous solubility, as discussed in Chapter 2.

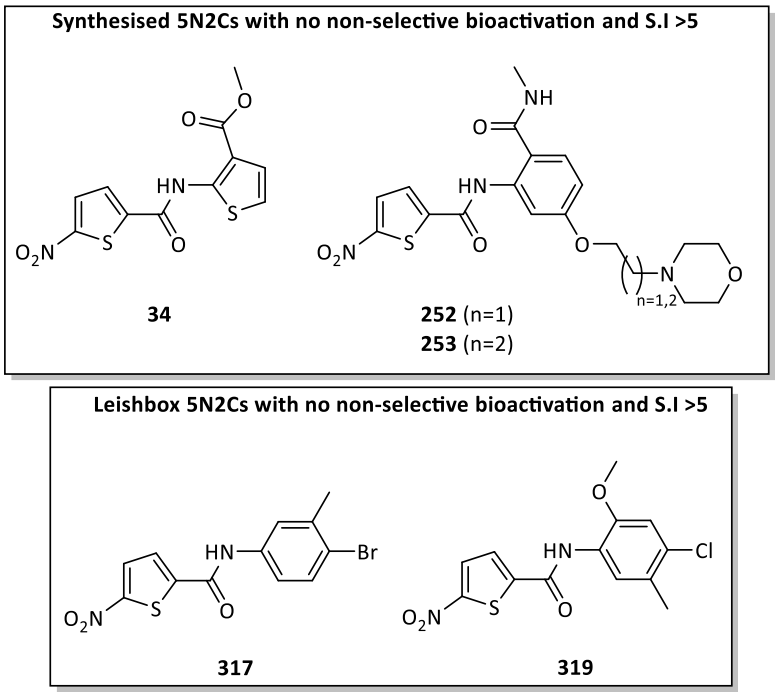

Figure 3.31-47 5N2C scaffolds showing selective bioactivation in the presence of *Lmj*NTR1, potent antileishmanial activity and low HepG2 toxicity.

3.31.8 Probe design and synthesis

The evidence discussed in section 3.31.6 suggests that transient electrophilic intermediates, such as the α,β- unsaturated open chain nitrile, are cytotoxic species which covalently modify nucleophilic cell components such as proteins, lipids, thiols and DNA. To investigate this hypothesis, a probe (**251**) was designed with a 5N2C prodrug warhead to bind to protein targets and a biorthogonal alkyne tag to enable visualisation and isolation of protein targets.[160] Reflecting on the good activity of the 5-methoxy (**196**) and 5-PEG (**232**) compounds discussed in Chapter 2, it was proposed that a propargyl group could be introduced to the end of a 5-PEG substituent to give **251** (Figure 3.31-48).

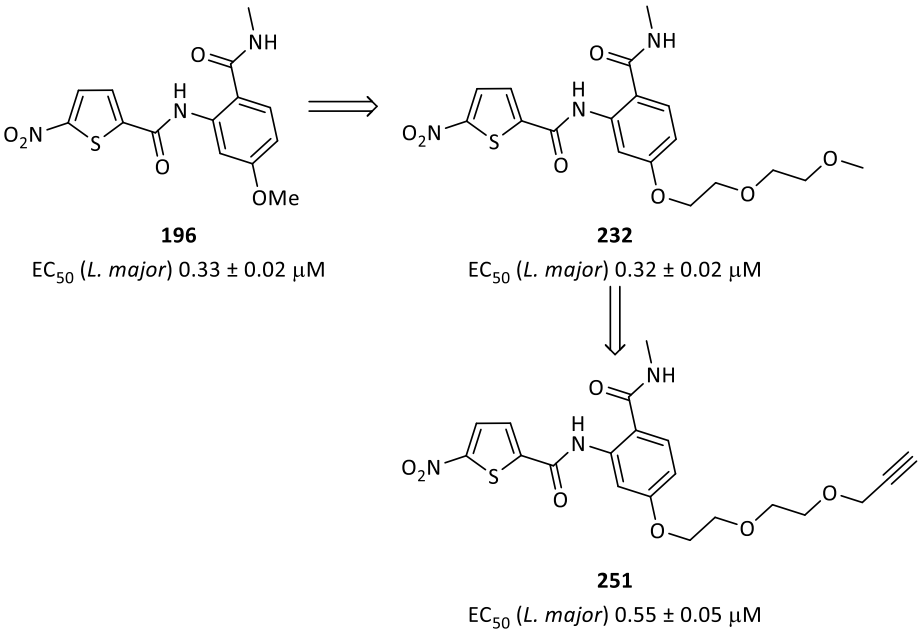

Figure 3.31-48 Compound evolution and development of probe **251**.

Synthesis of probe **251** was achieved in an analogous fashion to PEG **232** (Scheme 2.33.11). Pleasingly, probe **251** retained submicromolar antileishmanial activity and kinetics experiments showed that it is turned over, albeit slowly, by *Lmj*NTR1 (Table 3.31-17). Analysis of the metabolites formed by bioactivation using LC-MS showed the presence of the same three major metabolites discussed in section 3.31.6, 2M-98, 2M-14 and M+2, verified by accurate mass and MS/MS. Since probe **251** showed promising antileishmanial activity and shared a common metabolite profile after

*Lmj*NTR1 bioactivation with the wider 5N2C series, it was proposed that it could be used to identify protein targets covalently bound by the 5N2C series.

Table 3.31-17 Antileishmanial activity and rate of bioactivation by *Lmj*NTR1 of **251**.

	EC_{50} / µM		$k_{obs}/k_{nifurtimox}$
	L. major	***L. amazonensis***	
251	0.55 ± 0.05	0.77 ± 0.09	0.041 ± 0.002

The design of probe **251** was such that it has no inherently reactive nucleophilic or electrophilic groups. This was important to ensure that any binding to protein targets was due to *Lmj*NTR1 bioactivation *in cellulo* to a reactive intermediate species rather than inherent reaction of the parent probe (**251**).

3.31.8.1 Preliminary *in cellulo* and *in vitro* experiments

As an initial experiment, **251** was incubated with mid-late log phase *L. major* promastigotes for 4 hrs at 10 µM (see footnote[12]). The cells were lysed using IP lysis buffer (-EDTA + protease inhibitor) and click chemistry was performed on the resulting treated lysate using rhodamine azide (Rh-N_3, 1 eq.), copper sulfate (10 eq.), sodium ascorbate (10 eq.) and TBTA (10 eq.) for 1 hr. SDS-PAGE (12.5 %) and fluorescent imaging was used to visualise the results. Pleasingly, multiple fluorescent bands were observed suggesting that the probe, once bioactivated, covalently binds to multiple protein targets (Figure 3.31-49).

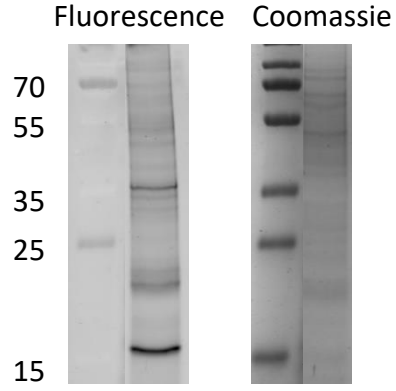

Figure 3.31-49 SDS-PAGE (12.5 %) fluorescent and Coomassie image of preliminary whole cell *L. major* probe incubation experiment.

[12] The initial whole cell probe scoping experiment was carried out by Dr Exequiel Porta.

In vitro experiments were also carried out to determine whether the probe binds to proteins when exogenous *Lmj*NTR1 and NADH was added. *Lmj*NTR1, bovine serum albumin (BSA) and NADH were incubated for 1hr with and without probe **251** to investigate whether bioactivation leads to probe binding to BSA, which can be visualised by subsequent click chemistry with rhodamine azide. Binding was observed for *Lmj*NTR1 itself and BSA after bioactivation. However, no difference was observed between the samples where probe **251** was present (+P) or absent (-P), which suggests that rhodamine azide itself is bioactivated by *Lmj*NTR1 and subsequently binds to protein targets (Figure 3.31-50).

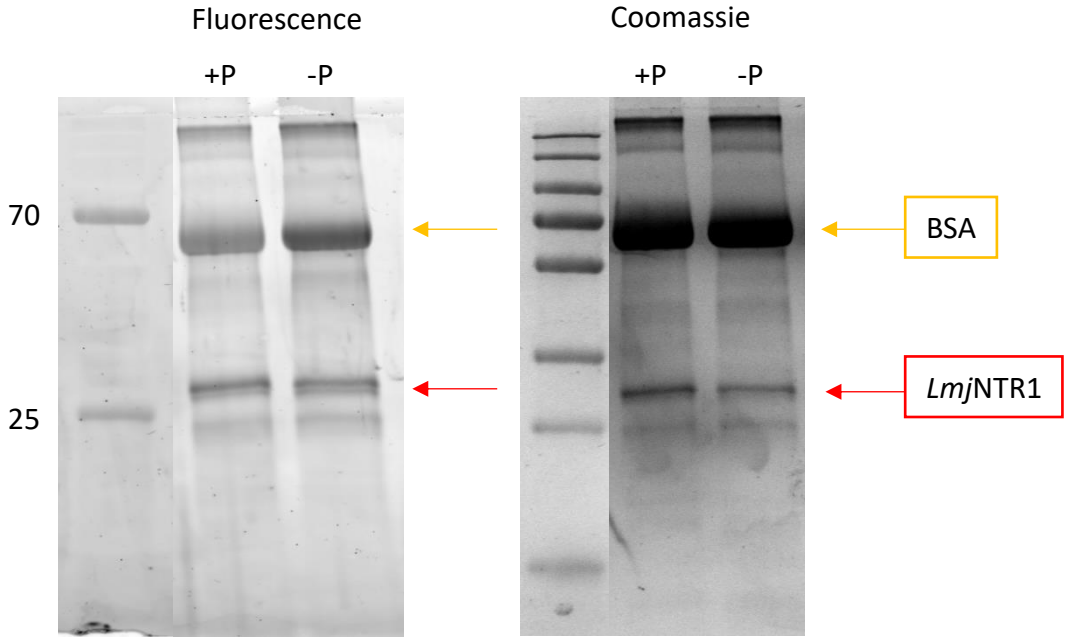

Figure 3.31-50 Binding to both *Lmj*NTR1 and BSA is observed in both the presence (+P) and absence (-P) of probe **251**. BSA (1 mg/mL) was incubated with probe **251** (50 µM) and *Lmj*NTR1 (33 µg mL^{-1}) for 1 hr at room temperature before click chemistry was performed using Rh-N_3 as previously described.

Further *in vitro* experiments where the amount of *Lmj*NTR1 was varied showed a decrease in fluorescence as the concentration of *Lmj*NTR1 was increased (Figure 3.31-51). This observation supports the prediction that the electrophilic intermediates are converted more efficiently to the non-active 2M-98 product when present in high concentrations.

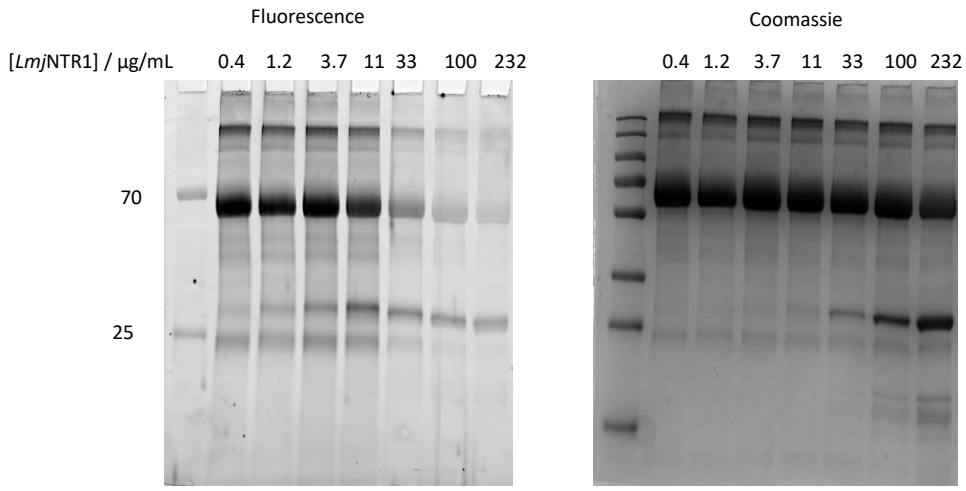

Figure 3.31-51 A decrease in binding to BSA is observed as concentration of *Lmj*NTR1 is increased. BSA (1 mg/mL) was incubated with probe **251** (50 µM) and *Lmj*NTR1 (various concentrations) for 1 hr at room temperature before click chemistry was performed using Rh-N_3 as previously described.

However, the observation of bioactivation and subsequent binding of rhodamine azide to proteins in the absence of probe made any *in vitro* experiments invalid. As such, only whole cell experiments were used to further investigate the binding of probe **251** to protein targets.

3.31.8.2 Experiment optimisation

Once preliminary whole cell results had been obtained, it became important to ensure that the optimal lysis, click and incubation conditions were being used.

3.31.8.2.1 Lysis conditions

Cell lysis was performed using both IP lysis buffer (-EDTA +protease inhibitor) and a 4 % SDS buffer. In general, IP lysis buffer gave cleaner fluorescent bands and was easier to quantify protein content through the BCA assay than the SDS based buffer. As such, IP lysis buffer was used for future experiments.

3.31.8.2.2 Fluorescent plate reader settings

The fluorescent plate reader (Typhoon 9400) has multiple filters that can be used to obtain high quality fluorescent images. During these studies the TAMRA (λ_{ex} 532/ λ_{em} 580 nm) and the GenPurp (λ_{ex} 532/ λ_{em} 560 nm) filters were assessed. It was found

that the GenPurp filter gave less background fluorescence than the TAMRA filter and enabled visualisation of the All-Blue protein ladder. As such, the GenPurp filter was used for all future experiments.

3.31.8.2.3 Click chemistry (CuAAC) conditions

Decreasing the amount of probe incubated with the whole cells prior to lysis in a 3-fold dilution series from 10 µM caused a decrease in overall fluorescence output and did not improve the resolution of the bands of interest significantly (Figure 3.31-52A). Subsequently, 10 µM probe was used throughout future experiments.

The concentration of Rh-N_3 could be reduced from 100 µM to 50 µM without loss of signal. However, it was found that the concentration of Rh-N_3 could not be decreased to 10 µM without loss of fluorescence intensity (Figure 3.31-52B). As such, 100 µM or 50 µM Rh-N_3 could be used. For consistency, 100 µM was used for all future experiments.

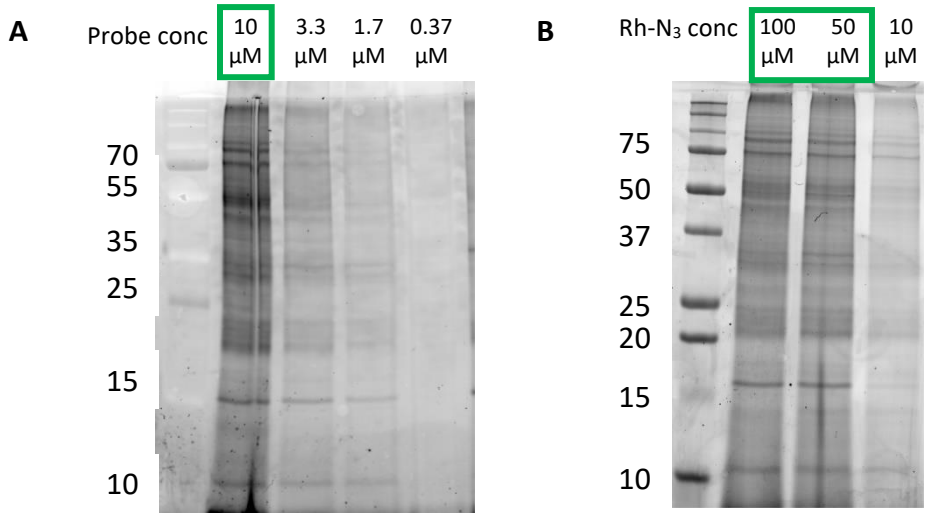

Figure 3.31-52 A. Fluorescent image showing the effect of decreasing the amount of **251** probe incubated with the whole cells prior to lysis. 10 µM probe (lane 2), 3.3 µM probe (lane 3) 1.1 µM (lane 4) 0.37 µM (lane 5). B. Fluorescent image showing the effect of decreasing the amount of Rh-N_3 from 100 µM (lane 2) to 50 µM (lane 3) and 10 µM (lane 4).

3.31.8.2.4 Time of incubation

Probe **251** was incubated with *L. major* promastigotes for 0.5, 1, 2 and 4 hrs to assess if any protein binding was time dependent and to find the shortest incubation time with the best results (Figure 3.31-53).

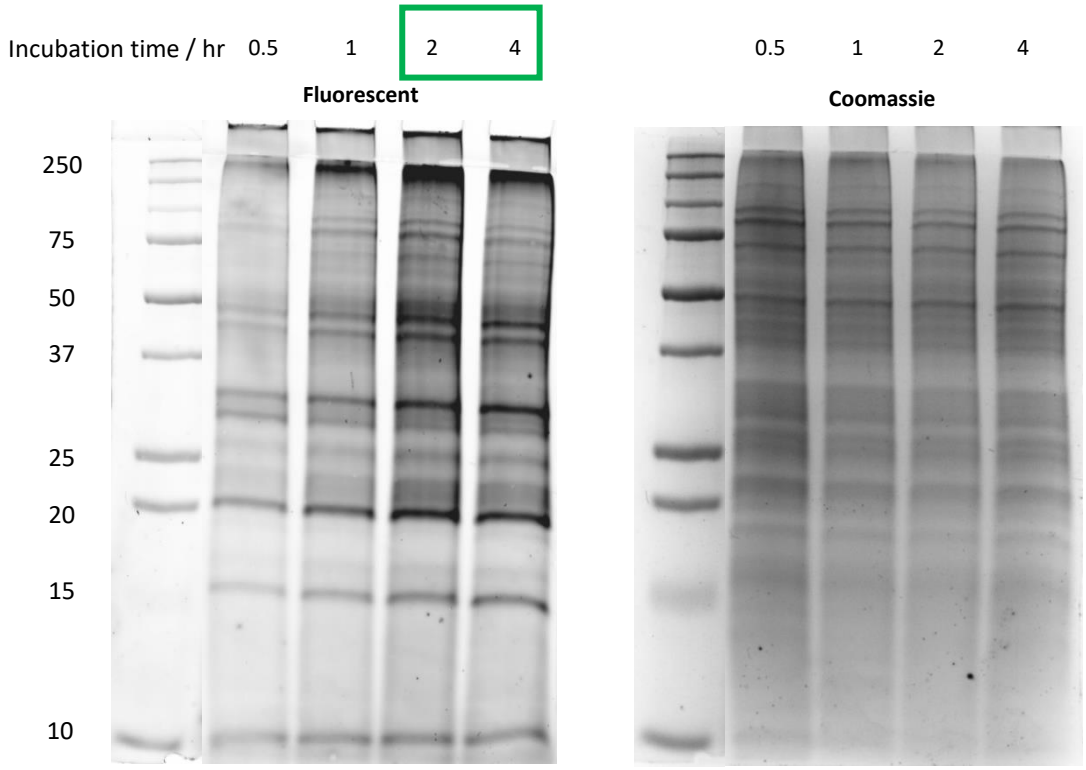

Figure 3.31-53 Fluorescence image of *L. major* incubated with 10 µM probe for 0.5, 1, 2 and 4 hrs. Coomassie stain showing constant protein concentration across all 4 lanes.

It was found that as incubation time was increased up to 2 hours, probe binding increased. However, this effect saturated after 2 hrs as no difference was observed between the 2 and 4 hr incubation samples. As such, an incubation time of 2 hrs was used for future experiments.

3.31.8.3 Reproducibility

Following optimisation of experimental conditions, it was necessary to ensure that probe binding was due to reproducible events inside the cell and not at random. Each whole cell incubation experiment was repeated at least 3 times to ensure reproducibility across multiple biological repeats. Inconsistency across repeats could

allude to non-selective binding of the probe to protein targets. It was found that many bands remained the same across multiple repeats, including three main bands that form a fingerprint across all replicates at approximately 10 kDa, 15 kDa and 20 kDa. However, multiple other bands are present which are not fully reproducible across repeats, such as bands at approximately 27 and 32 kDa (Figure 3.31-54). As such, it appears that the cytotoxic metabolite(s) have some selectivity for at least 3 proteins but will also react with multiple other protein targets.

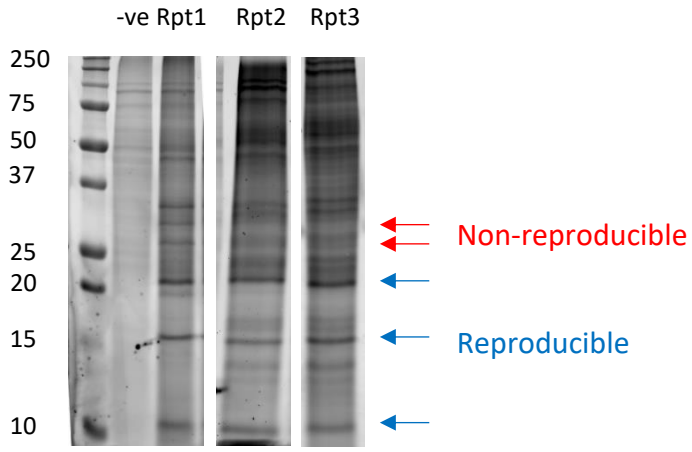

Figure 3.31-54 Biological repeats of *L. major* promastigotes incubated for 2 hrs with 10 µM **251** probe. -ve indicates negative control with no probe present.

3.31.8.4 Competition experiments

Competition experiments can be used to determine the binding selectivity of a probe. If a competitor compound binds to the same target proteins as the probe, a decrease in the fluorescence intensity of these bands is expected. Classically, a commercially available inhibitor would be used for these experiments based on the target protein class.[160] For example 3,4-dichloro-isocoumarin, a validated serine protease inhibitor, could be used in competition experiments if the probe is expected to bind to serine proteases.[161] However, the 5N2Cs have an unknown target protein profile so a commercial competitor would be unsuitable. Instead, three different competitors based off the 5N2C scaffold were used. The first competitor investigated was methoxy capped PEG analogue **232**, which shares the most structural similarity to probe **251**. Following on from this, original hit **17** and lead compound **253** were used

to investigate whether the target protein profile is shared across more structurally diverse 5N2Cs.

Each competition experiment was carried out as follows. Competitor was preincubated with whole *L. major* cells for 30 minutes before addition of the probe for a further 90 minutes. Lysate generation and click chemistry were carried out as discussed previously. The fingerprint bands at 10, 15 and 20 kDa were used to visualise the competition effects.

*3.31.8.4.1 Competition with most similar compound (**232**)*

Firstly, competition experiments were carried out using methoxy capped PEG analogue **232** (Figure 3.31-55). The structural similarity between **232** and probe **251** indicated that a common target protein profile was likely.

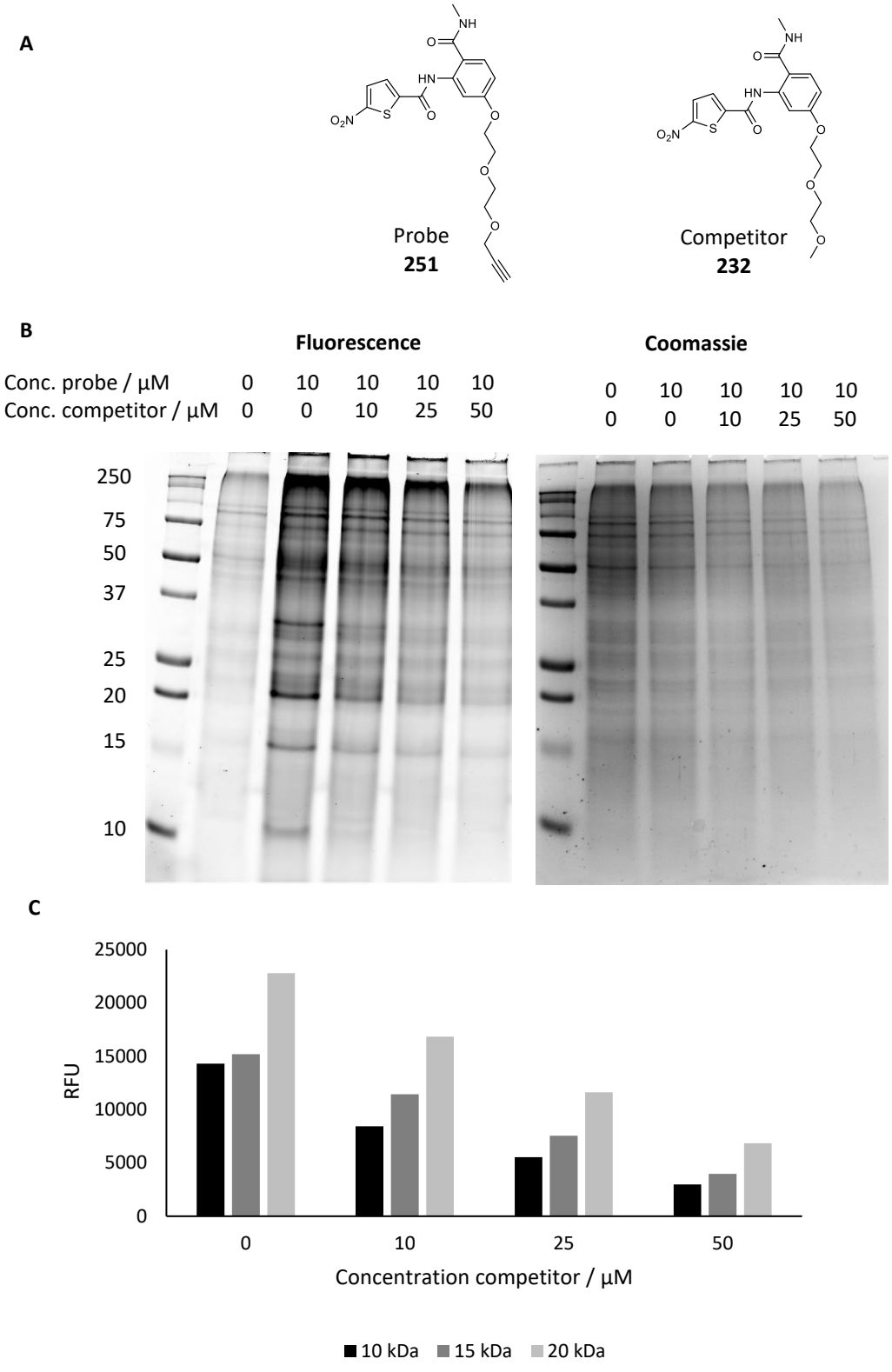

Figure 3.31-55 A. Structure of probe **251** and competitor **232**. B. Fluorescent image and Coomassie stain of representative competition experiment between probe **251** and the most structurally similar compound **232**. Three biological repeats were obtained for each experiment. C. Fluorescence intensity of the bands at approximately 10 kDa, 15 kDa and 20 kDa as concentration of competitor is increased, calculated from the one biological repeat shown above.

This competition experiment showed that the previously identified bands at approximately 10 kDa, 15 kDa and 20 kDa each involve some degree of selectivity when binding to the probe as the probe can be outcompeted by increasing amounts of structurally similar competitor **232**. Other bands at approximately 32 kDa and 47 kDa also appear to show the same decrease in fluorescence intensity across three repeats and warrant further investigation. However, the fluorescence of some background bands does not change with increasing competitor concentration, suggesting that these bands do not involve selective probe binding events.

In summary, the competition experiment above showed that probe **251** selectively binds to multiple protein targets, as evidenced by a decrease in fluorescence of these bands as the concentration of **232** is increased. However, the large number of bands observed, in addition to the presence of some non-selective binding suggests that the probe (**251**) displays significant polypharmacology.

*3.31.8.4.2 Competition with original hit (**17**)*

Once bands that suggest specific binding had been identified, it became important to validate whether the original hit **17** would also outcompete the probe (**251**). This would suggest a common mode of action between the probe (**251**) and hit **17**. It was found that the original hit (**17**) also outcompeted probe (**251**) binding for the 10, 15 and 20 kDa bands but to a much lower extent than **232**. This could either suggest that **17** has polypharmacology beyond the scope of the probe competition experiments, divergent activity or that the cytotoxic metabolite for the original hit is simply less bioavailable or has lower binding affinities for the identified enzymes. As such, it is not possible to confirm that the original hit **17** has the same target profile as probe **251** (Figure 3.31-56).

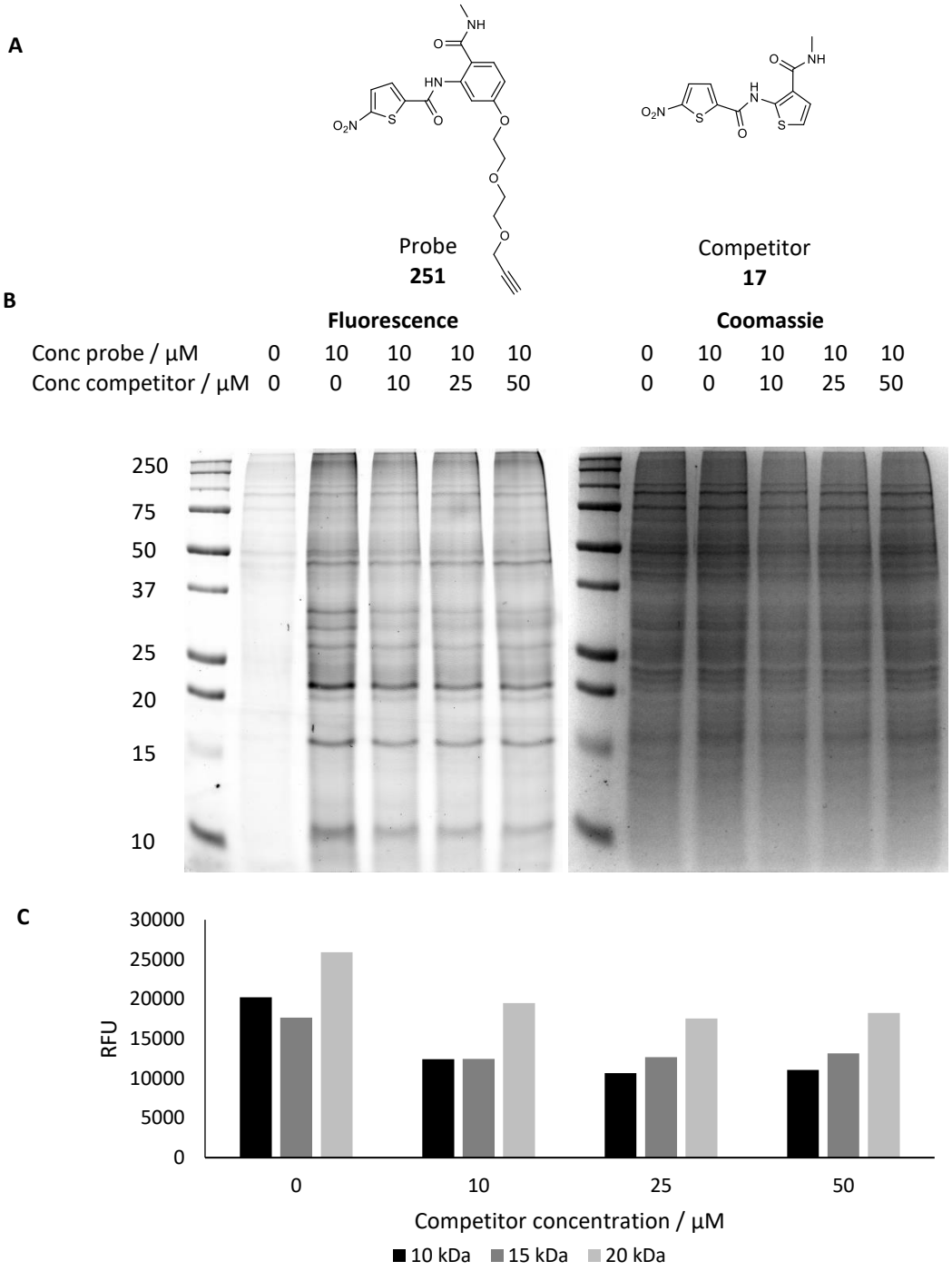

Figure 3.31-56 A. Structure of probe **251** and competitor **17**. B. Fluorescent image and Coomassie stain of representative competition experiment between probe **251** and the original hit compound **17**. Three biological repeats were obtained for each experiment. C. Fluorescence intensity of the bands at approximately 10 kDa, 15 kDa and 20 kDa as concentration of competitor is increased, calculated from the one biological repeat shown above.

3.31.8.4.3 Competition with lead compound (253)

In addition to validating the target profile of the original hit **17**, it was also of interest to validate the target profile of the lead compound (**253**) that shows the most promising biological activity and physicochemical properties (Figure 3.31-57).

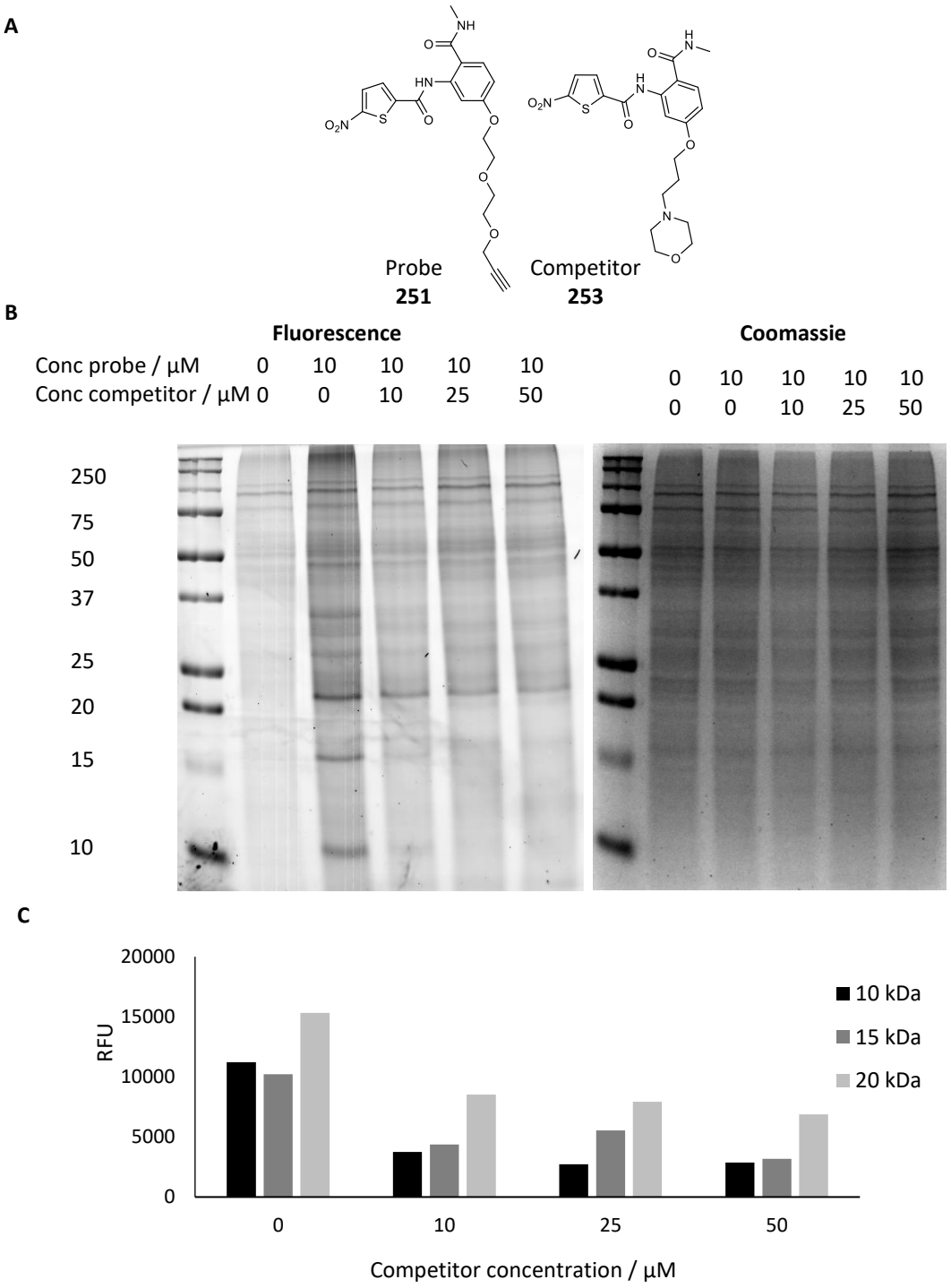

Figure 3.31-57 A. Structure of probe **251** and competitor **253**. B. Fluorescent image and Coomassie stain of representative competition experiment between probe **251** and lead compound **253**. Three biological repeats were obtained for each experiment. C. Fluorescence intensity of the bands at approximately 10 kDa, 15 kDa and 20 kDa as concentration of competitor is increased, calculated from the one biological repeat shown above.

It was found that **253** outcompetes probe **251** well for all three previously identified bands (10 kDa, 15 kDa and 20 kDa), but especially for bands at 10 kDa and 15 kDa where the probe is completely outcompeted by competitor at 25 µM. As in the case of **232**, it is possible to observe higher molecular weight bands decreasing in intensity as competitor concentration is increased. However, it is difficult to quantify this decrease due to the background signal observed above 20 kDa. This background fluorescence was observed for every replicate of each whole cell probe experiment, even though protein precipitation was used to remove excess rhodamine and other interfering substances. This suggests that the background fluorescence is due to the large number of protein targets bound by the probe, which separate more cleanly at lower molecular weights.

3.31.8.5 Probe studies against 3 *Leishmania* species

Once a large target profile had been identified for **251** in *L. major,* the investigation was extended to other species of *Leishmania*. Probe **251** was incubated at 10 µM with *L. amazonensis* and *L. mexicana* promastigotes for 2 hrs. Click chemistry with rhodamine azide was performed on the lysates and the results were visualised by SDS-PAGE (12.5 %) and fluorescence imaging. Since the *L. major* protein fingerprint had already been determined, this was ran alongside the other two species as a comparison (Figure 3.31-58).

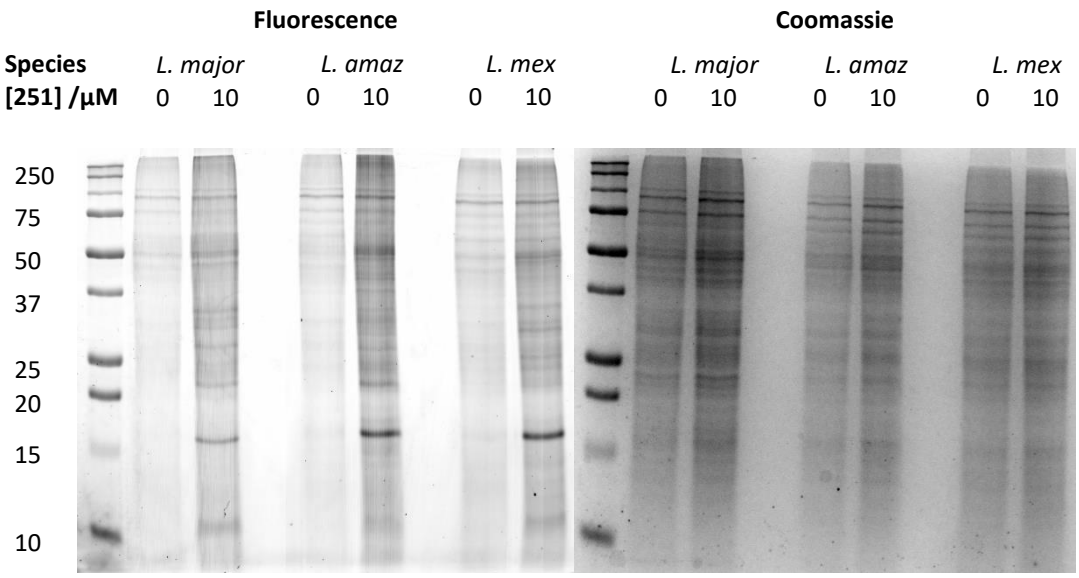

Figure 3.31-58 Fluorescence and Coomassie stained images of *L. major*, *L. amazonensis* and *L. mexicana* probe **251** treated and untreated cell lysates.

The 3 main bands at 10 kDa, 15 kDa and 20 kDa found in *L. major* were also reproducibly identified in both *L. amazonensis* and *L. mexicana* treated cell lysates, suggesting protein homologues are present across the three species. Analysis of other bands was not attempted due to the density of bands observed above 20 kDa. However, the commonality of the three identified bands suggests that there is a shared target protein profile across multiple species of *Leishmania*, alluding to a common mode of action.

3.31.8.6 Conclusions

Probe **251** covalently modifies multiple protein targets following bioactivation by *Lmj*NTR1 and subsequently displays significant polypharmacology. The similar antileishmanial activity of the probe to the wider 5N2C series considered alongside the competition experiments suggests that the 5N2C series share common covalent modifications of multiple protein targets. The covalent modification observed for the three main identifiable proteins involves specific binding, however further analysis of the multiple other protein targets present was not possible due to the density of the bands above 20 kDa. As such, alternative methods, such as proteomics, would be necessary to investigate higher molecular weight proteins and to identify the protein classes covalently modified following bioactivation.

3.31.9 Proteomics

In the previous section, probe **251** was found to covalently modify multiple protein targets. This must occur following bioactivation as the parent probe structure has no inherently reactive groups. Competition experiments with **232** showed that probe **251** binds both selectively, for example in a specific binding pocket or to a specific amino acid residue, and non-selectively, for example to exposed surface residues, to a multitude of protein targets. Non-selective binding is likely to be irrelevant for the mode of action of the 5N2Cs, as binding events are likely random and do not affect the functionality of proteins. As such, only proteins that are selectively covalently bound by the probe should be considered. The large number of bands observed following click chemistry with rhodamine azide made analysis through fluorescent imaging challenging. Subsequently, a gel-free quantitative parallel proteomics approach was also used.

Quantitative proteomics enables the identification of protein targets in addition to the relative amount of each protein in a single experiment. This enables proteins that are selectively covalently modified by a probe to be identified by comparing the quantities of each protein bound across two samples: cell cultures treated with probe only (**sample 1**) and cell cultures preincubated with competitor before probe incubation (**sample 2**).

Various quantitative proteomics approaches are available, including metabolic labelling approaches such as Stable Isotope Labelling of Amino acids in Culture (SILAC), and chemical labelling approaches such as Isobaric Tag for Relative and Absolute Quantitation (iTRAQ™).[160] SILAC incorporates light, medium or heavy isotopically labelled amino acids into different cell cultures over multiple generations. **Sample 1** and **sample 2** would then be generated using these prelabelled cell cultures. In contrast, iTRAQ™ involves the addition of different isobarically labelled iTRAQ™ reagents following pulldown of covalently modified proteins from treated wild type cell cultures (**sample 1** and **sample 2**). Following isotopic labelling of proteins by either approach, mass spectrometry analysis can be used to identify the covalently modified proteins and quantify the relative amounts

in each sample. Although both approaches would be possible for this application, iTRAQ™ (Applied Biosystems) proteomics was chosen due to the more confident protein identification offered at low concentration. This is because isobaric tagged peptides with the same identity from different samples have the same mass and subsequently appear as the same peak. This offers greater peptide concentration and greater MS/MS intensities for peptide identification, which is useful for this study due to the large number and low concentration of proteins covalently modified by **251**. [162,163]

iTRAQ™ reagents are made up of three sections: i) a charged reporter group with different masses due to different isotope incorporation, ii) a neutral balance group with different masses such that the mass of the balance group and reporter group together is equal for each reagent, iii) an amine specific peptide reactive group. A different iTRAQ™ reagent is added to each sample (e.g. reporter group-balance group 114-31 for **sample 1** and 115-30 for **sample 2**). The iTRAQ™ reagents subsequently react with lysine side chains and *N*-terminal amines, labelling peptides with the isobaric tag (Figure 3.31-59).[162]

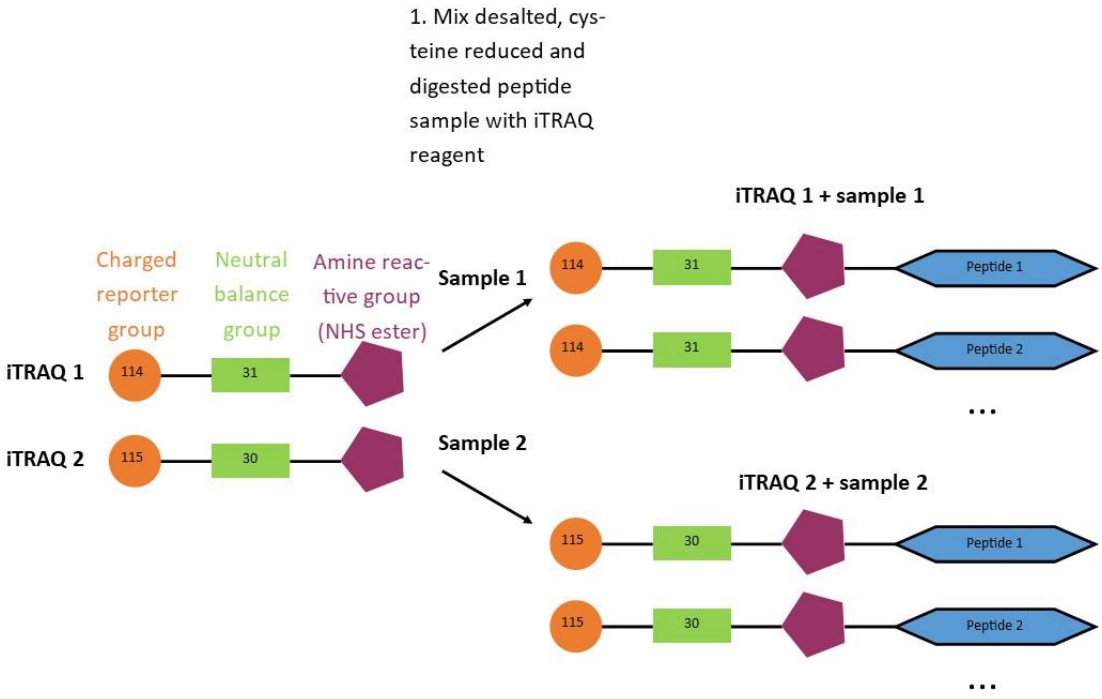

Figure 3.31-59 iTRAQ™ labelling of two protein samples to give isobaric tagged peptide fragments.

Isobaric tag labelled **sample 1** and **sample 2** would then be combined and LC-MS used to separate the peptide-iTRAQ™ masses. Each peptide peak would be subjected to MS/MS analysis, which cleaves the balance group liberating the small reporter group. The relative quantities of each reporter group can then be used for quantification of the 'fold-change' difference in the amount of peptide from each sample, which gives an indication of the selectivity of probe binding. MS/MS analysis of the liberated peptide enables protein identification by comparison with known *L. major* peptide sequences (Figure 3.31-60).

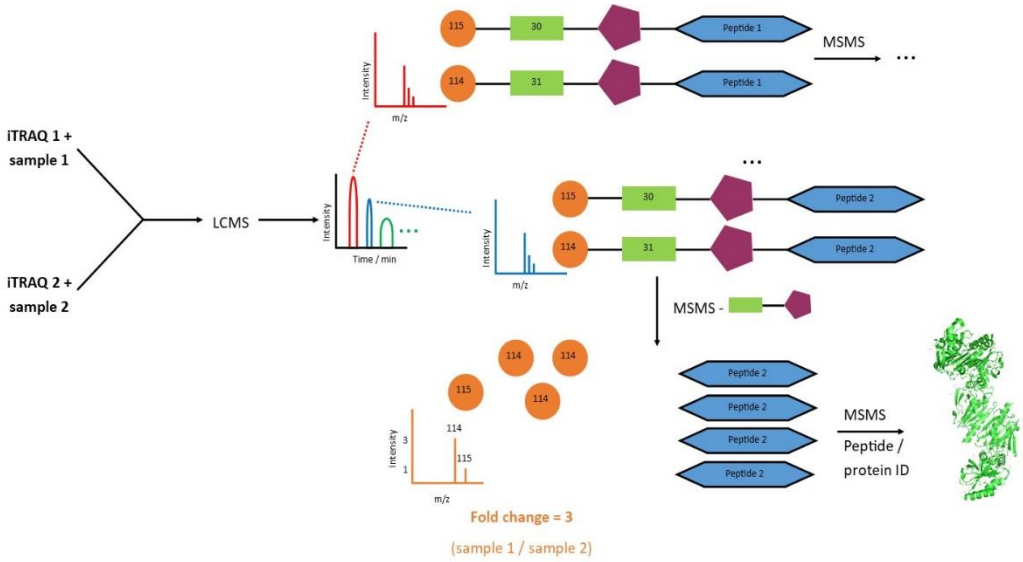

Figure 3.31-60 LC-MS and MS/MS analysis of isobaric tagged peptides enables quantification and identification of peptide fragments.

The samples for iTRAQ™ proteomics were prepared as follows: the first where whole cell *L. major* were incubated with 10 µM **251** probe for 2 hrs (**sample 1**) and the second where *L. major* were pre-incubated with 50 µM **232** competitor for 0.5 hr before 10 µM **251** probe incubation for 1.5 hrs (**sample 2**). Following cell lysis, click chemistry was used to attach a biotin group which enabled proteins that were covalently modified by the bioactivated probe to be isolated using NeutrAvidin-Agarose beads. Following on-bead isolation of the covalently modified proteins, disulphide bridges were fully reduced to free cysteine with TCEP, free cysteine were alkylated with chloroacetamide and the proteins were digested with trypsin. The free peptide solution was then desalted using a C-18 spin column, and the iTRAQ™

reagents were added. iTRAQ™ proteomics analysis was then carried out as discussed above (see footnote[13]).

Following this approach, 431 proteins were identified that were selectively bound by **251** (fold change > 2), 213 of which were present across three biological repeats and had fold change > 4. Proteins with the largest fold change (fold change > 50) include various ribosomal proteins, a putative SNARE protein, a phosphomannomutase like protein, tryparedoxin peroxidase, nucleoside diphosphate kinase and glyceraldehyde-3-phosphate dehydrogenase (appendix 8.4). The large number of proteins that are covalently modified by **251** suggests that the 5N2C series displays significant polypharmacology and therefore does not have a specific protein target following *Lmj*NTR1 bioactivation. As such, there was no merit to analysing the protein identities individually. Instead, it was of interest to investigate whether there were any trends between the identified proteins.

A more global approach was taken to investigate if any particular biological processes, protein cellular locations or protein molecular functions were over-represented. Gene ontology (GO) analysis enables interpretation of large data sets and clustering based on the individual's functional characteristics. The results from the GO analysis can be visualised in the bubble plots below. The x-axis of the bubble plots represents the extent of selective probe binding to proteins, with larger $\log_2$(fold change) values representing a greater extent of selective probe binding. The y-axis represents the significance of the observation, using a $-\log_{10}$ scale of the *p*-value. Higher y values have a much lower probability that the observed change occurred by chance. The size of the bubbles also represents the significance ($-\log_{10}$(*p*-value)), and the colour of the bubbles represents the number of proteins that contributed to that observation.

Initial hypotheses suggested that mostly mitochondrial proteins may be affected due to the presumed lability of the cytotoxic metabolites and the mitochondrial location of *Lmj*NTR1. Surprisingly, a significant majority of the proteins affected were found

[13] Kalesh Karunakaran-Nair-Ana carried out the sample pulldown, iTRAQ proteomics, data interpretation and gene ontological analysis.

in the ribosome (Figure 3.31-62), with many being structural constituents of the ribosome (Figure 3.31-63) involved in the biological process of translation (Figure 3.31-61). This showed that the cytotoxic metabolites are less labile than initially predicted as mitochondrial proteins were not over-represented. Other over-represented cellular locations include glycosomes and peroxisomes, whilst other biological processes affected include gene expression and various metabolic pathways. Significantly, this suggests that the 5N2C series act by bioactivation by *Lmj*NTR1 followed by inhibition of ribosomal proteins, in addition to multiple other pharmacologies. Drugs involved in the inhibition of translation generally result in the slowing of cell growth and proliferation. [164–167] Interestingly, many nitrofuran containing antibiotics, such as nitrofurazone (**272**) and nitrofurantoin (**273**), in addition to the nitrothiophene containing antiprotozoal and antiviral drug nitazoxanide (**40**), are also reduced by nitroreductase-like proteins resulting in disruption of ribosome synthesis and function. [130,131,168–173] This could suggest a common mode of action of nitro heterocycles across multiple kingdoms.

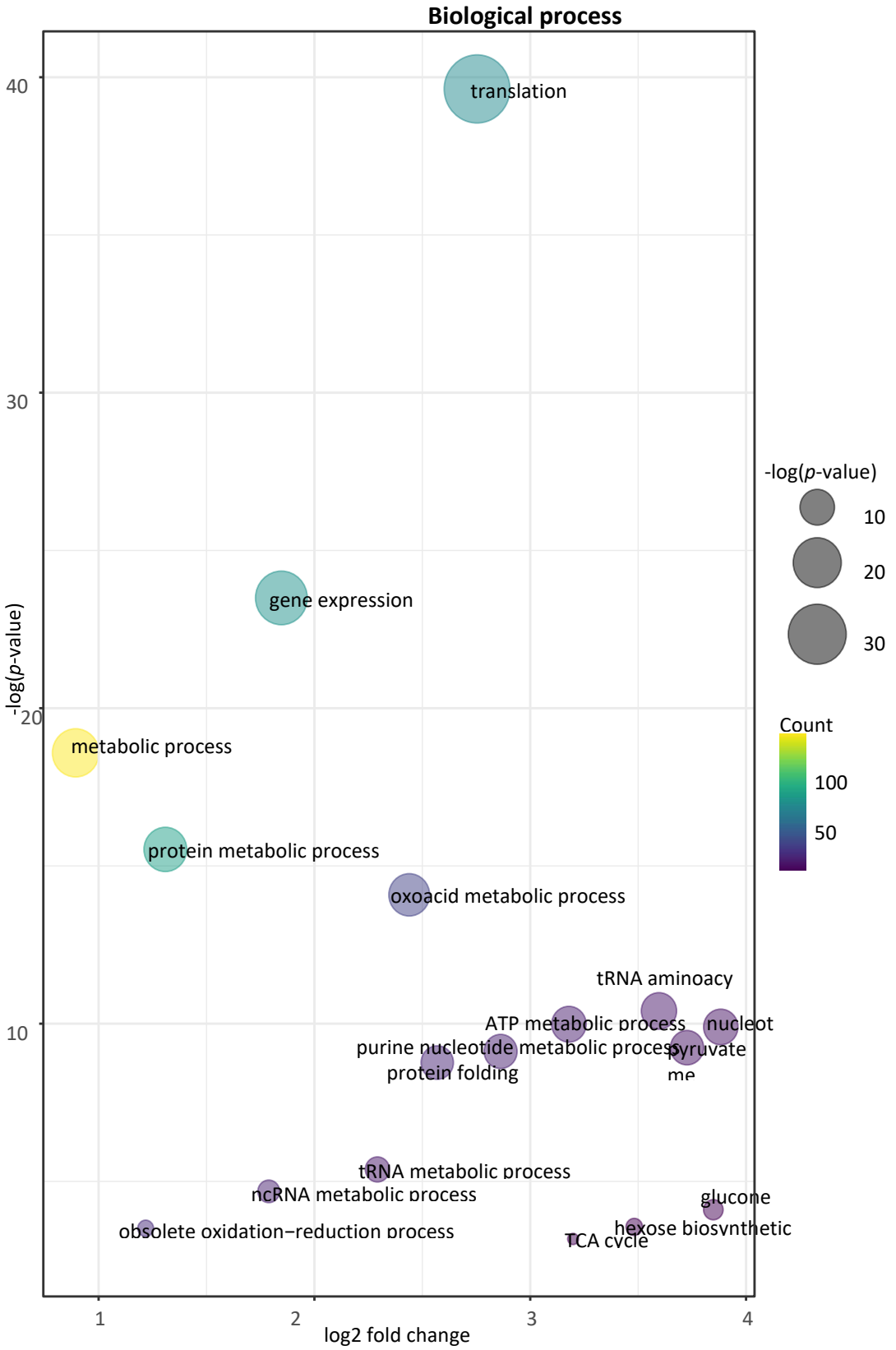

Figure 3.31-61: GO analysis showing that the major biological process affected by bioactivated 5N2Cs is translation.

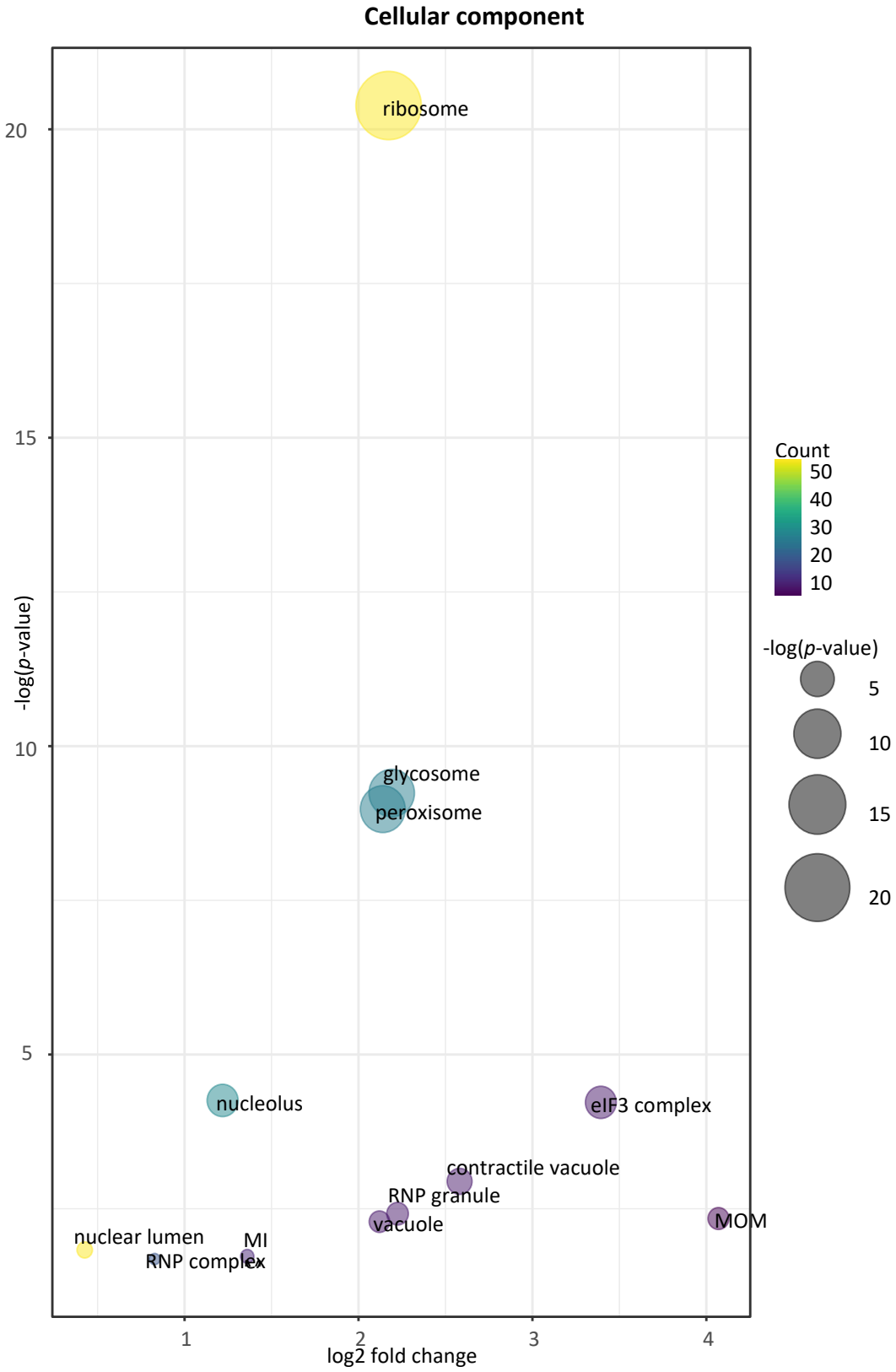

Figure 3.31-62 GO analysis showing that the major cellular component affected by bioactivated 5N2Cs are ribosomes, followed by peroxisomes and glycosomes.

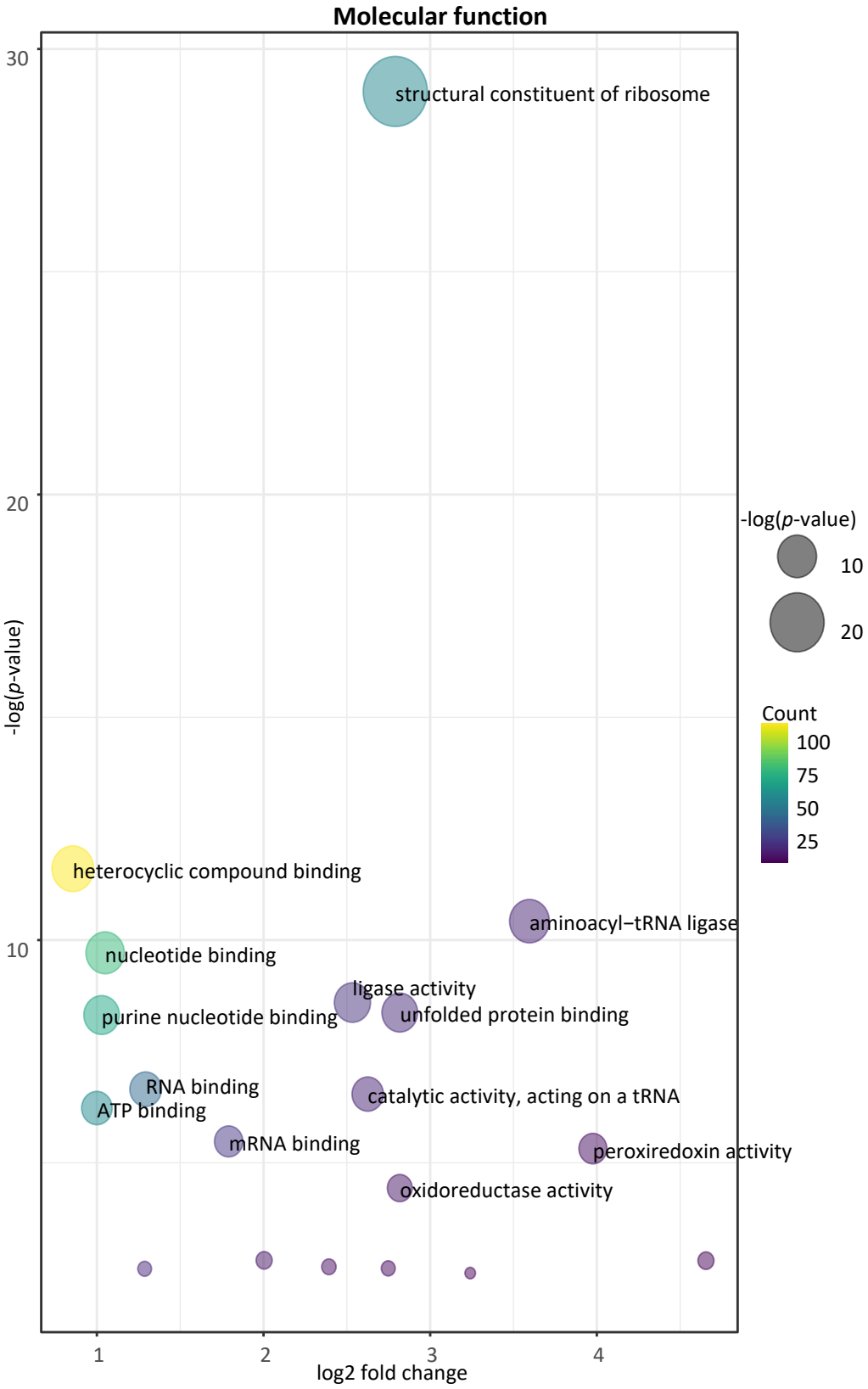

Figure 3.31-63 GO analysis showing that the molecular function affected by bioactivated 5N2Cs are structural constituents of ribosomes.

3.32 Global mode of action studies

In the previous sections, the 5N2C series were shown to be bioactivated by *Lmj*NTR1 to give a major 2M-98 metabolite. Although 2M-98 itself is relatively non-cytotoxic, the electrophilic intermediates generated throughout its synthesis have the potential to covalently inhibit multiple protein targets. iTRAQ™ proteomic studies were then used to identify the covalently modified proteins, which showed that inhibition of translation through binding to ribosomal proteins was a major mode of action for the 5N2Cs. However, many other proteins from different classes were also covalently modified by bioactivated 5N2Cs, suggesting that the 5N2C series displays significant polypharmacology. Consequently, a complementary phenotypic approach was taken to investigate other possible modes of action of the 5N2C series in *Leishmania* using a combination of techniques discussed below.

3.32.1 Mitochondrial dysfunction

The mitochondrial location of *Lmj*NTR1 suggested that the 5N2C series may function by disrupting the mitochondria. To investigate this hypothesis, mitochondrial function assays were carried out on treated whole cell *L. major* promastigotes. This was achieved using the mitochondrial JC-1 dye, which aggregates in functional mitochondria causing a shift in fluorescence from the monomer dye units (λ_{ex} 480 nm/ $\lambda_{em\ (monomer)}$ 530 nm or $\lambda_{em\ (aggregate)}$ 590 nm). Compounds that cause depolarisation of the mitochondria have a smaller ratio of $\lambda_{em\ (aggregate)}$ / $\lambda_{em\ (monomer)}$, which can be normalised to give percentage mitochondrial function.

Initially, the original hit compounds (**16** and **17**) and lead compound (**253**) were incubated with *L. major* promastigotes for 48 hrs at the EC_{50} and EC_{90} (Table 3.32-1).

Table 3.32-1 EC_{50} and EC_{90} values for hits **16** and **17** and lead **253**. EC_{90} values were calculated using a slope factor of 1.0 using GraphPad prism 8.

	16	**17**	**253**
EC_{50}(*L. major*) / µM	0.52	0.99	0.30
EC_{90}(*L. major*) / µM	4.68	8.91	2.70

The cells were then incubated with JC-1, washed and the fluorescence emission was measured (λ_{ex} 480/ λ_{em} 530 and 590 nm). Miltefosine (**5**) did not show any mitochondrial dysfunction at either the EC_{50} or EC_{90} and was used as a negative control. Hit compounds **16** and **17** started to show dysfunction at the EC_{90}, however lead **253** showed little dysfunction even at the EC_{90} (Figure 3.32-1).

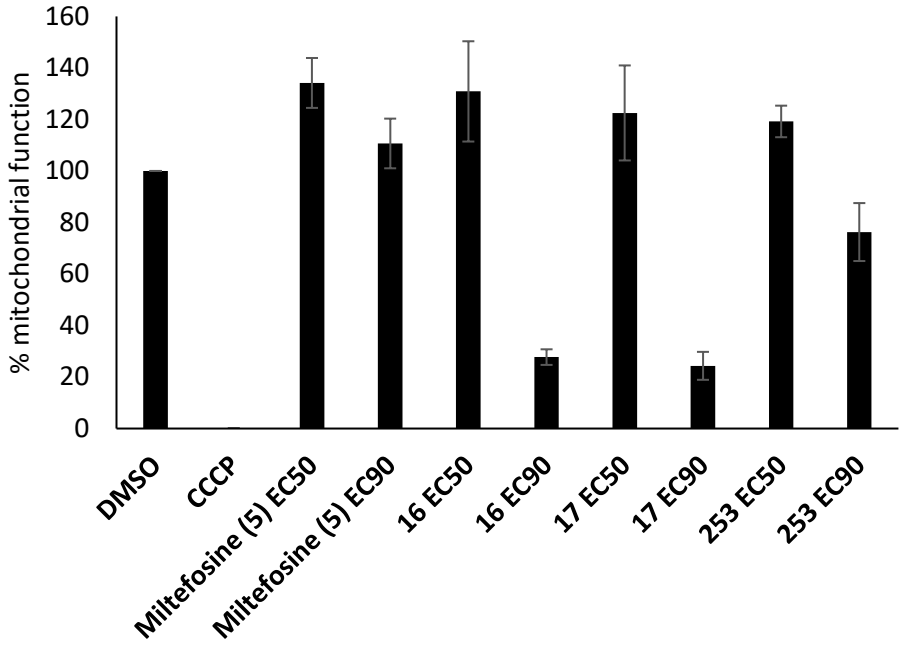

Figure 3.32-1: Mitochondrial dysfunction caused by 5N2C treatment at the EC_{50} and EC_{90} as determined by the JC-1 assay. Averages determined from at least three biological repeats. Error bars represent the standard error between these repeats.

The discrepancy between the mitochondrial dysfunction caused by the 5N2Cs suggests potential divergent modes of action between the original hits **16** and **17** and lead **253**. However, it is also possible that the effects observed are dose dependant (Table 3.32-1). To investigate this, the two hits **16** and **17** and lead **253** were assayed as above but using fixed concentrations of compound (1, 5 and 10 µM). Original hits **16** and **17** and lead **253** each showed a decrease in mitochondrial function as drug concentration was increased. However, unlike hits **16** and **17**, lead **253** did not show complete mitochondrial dysfunction, even at 10 µM (Figure 3.32-2).

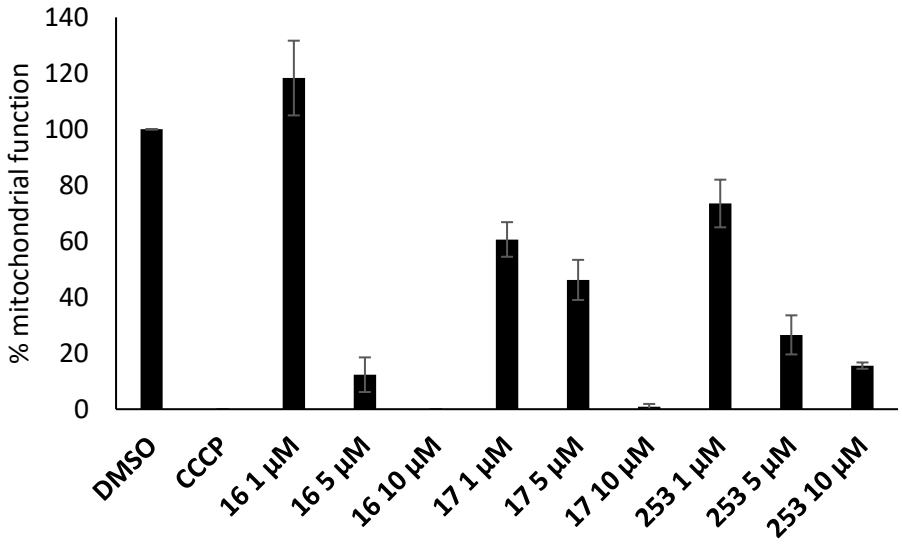

Figure 3.32-2 Mitochondrial dysfunction caused by 5N2C treatment at fixed concentrations of 1, 5 and 10 µM as determined by the JC-1 assay. Averages determined from at least three biological repeats. Error bars represent the standard error between these repeats.

In conclusion, the JC-1 assays described above show that original hits **16** and **17** result in mitochondrial dysfunction, albeit at high concentrations. However, this effect is less pronounced for lead **253**, which may suggest divergent modes of action between the hits **16** and **17** and lead **253**. Overall, the mitochondria appear to be affected by 5N2Cs, however this is likely to be only one of many polypharmacologies exhibited by the 5N2C series.

3.32.2 ROS accumulation

Type I nitroreductase bioactivation (e.g. *Lmj*NTR1) is classically oxygen insensitive and does not lead to the generation of reactive oxygen species (ROS).[129] However, some nitro containing drugs, such as nitazoxanide (**40**), have been shown to still generate ROS in *Leishmania*. [174] Consequently, it was of interest to investigate whether ROS accumulation is a downstream polypharmacology following 5N2C treatment. Classically, ROS accumulation is measured by incubating samples with the H2DCFDA (**328**) dye. H2DCFDA (**328**) is deacetylated by esterases *in cellulo* and subsequently oxidised by ROS to the fluorescent compound dichlorofluorescein (**330**) (DCF, λ_{ex} 507/ λ_{em} 530 nm, Figure 3.32-3). As such, compounds that cause ROS accumulation will give an increase in fluorescence.

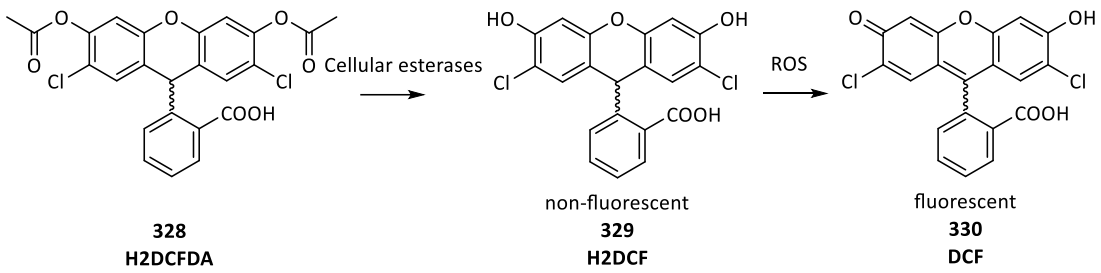

Figure 3.32-3 H2DCFDA (**328**) bioactivation in the cell followed by oxidation by ROS to give fluorescent DCF (**330**).

Hit compounds **16** and **17** and lead **253** were incubated at the EC_{50} and EC_{90} (Table 3.32-1) with *L. major* promastigotes for 48 hrs before incubation with H2DCFDA (**328**) and measuring the fluorescence emission (λ_{ex} 507/ λ_{em} 530 nm). Miltefosine (**5**) was used as a positive control as it is known to generate ROS in *Leishmania*.[175] All compounds (miltefosine, **16**, **17** and **253**) showed ROS accumulation when incubated at the EC_{90} (Figure 3.32-4).

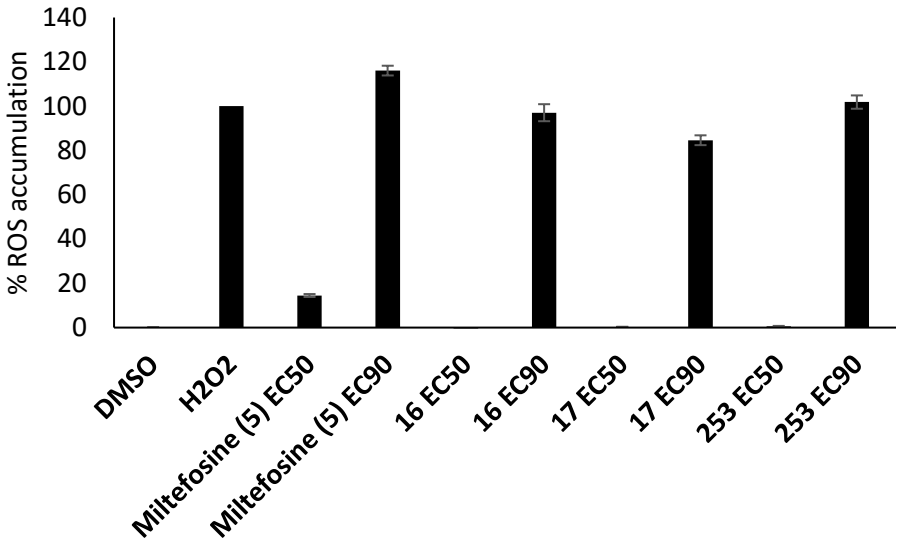

Figure 3.32-4 ROS accumulation caused by 5N2C treatment at the EC_{50} and EC_{90} as determined by the H2DCFDA assay. Averages determined from at least three biological repeats. Error bars represent the standard error between these repeats.

As before, each compound was also tested at fixed concentrations of 1, 5 and 10 µM to ensure that any observed effects were not exacerbated by dosage. All compounds showed an increase in ROS accumulation at 10 µM, with **16** and **253** also showing substantial ROS generation at 5 µM (Figure 3.32-5).

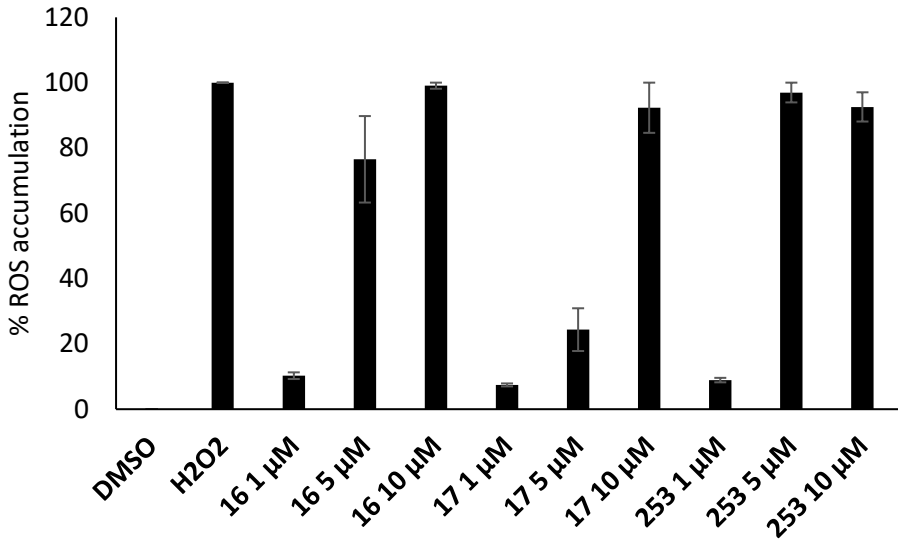

Figure 3.32-5 ROS accumulation caused by 5N2C treatment at fixed concentrations of 1, 5 and 10 µM as determined by the H2DCFDA assay. Averages determined from at least three biological repeats. Error bars represent the standard error between these repeats.

In summary, 5N2C treatment results in the generation of ROS, which could contribute to cell death. Although type I nitroreductase enzymes do not directly generate ROS, it is possible that the cytotoxic metabolites generated by *Lmj*NTR1 bioactivation diminish the parasite's ability to cope with oxidative stress.

3.32.3 Transmission electron microscopy

Throughout this chapter, the 5N2C series have been shown to exhibit significant polypharmacology including generation of ROS, some mitochondrial dysfunction and covalent modification of ribosomes. However, further modes of action were yet to be explored.

Transmission electron microscopy (TEM) has been used extensively in the literature to reveal ultrastructural changes before and after drug treatment. TEM was applied by Mesquita *et al.* and Muelas-Serrano *et al.* to study the mode of action of nitazoxanide (**40**) (Figure 3.32-6i) and nifurtimox (**37**) (Figure 3.32-6ii) respectively in trypanosomatids. In both cases, extensive cytoplasmic vacuolisation and mitochondrial and nuclear alterations were observed, with nifurtimox also causing ribosomal alterations. [116,174]

Figure 3.32-6 i) TEM of *L. infantum* parasites incubated with nitazoxanide (**40**) (60 µg mL^{-1}) after 1 hr (B), 3 hr (C) and 6 hr (D) compared to untreated parasites (A). Highlighted features include vacuoles (v), mitochondria (m), nucleus (n), flagellum (f), lipids (L) and kinetoplast (k). Reproduced from Mesquita *et al.* (2013) with permission from the publisher. [174] ii) TEM of *T. cruzi* epimastigotes upon nifurtimox (**37**) treatment (0.5 µg mL^{-1}) for 6 hr (B) and 24 hr (C) compared to untreated (A). Arrows indicate vacuoles, osmiophilic bodies and dense particles. Reproduced from Muelas Serrano *et al*. (2002).[116]

i)

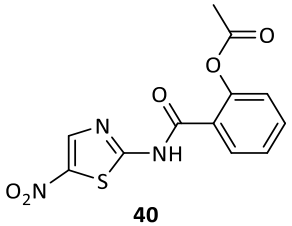

40
Nitazoxanide

ii)

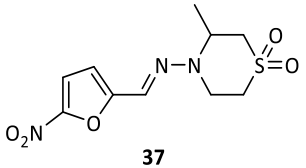

37
Nifurtimox

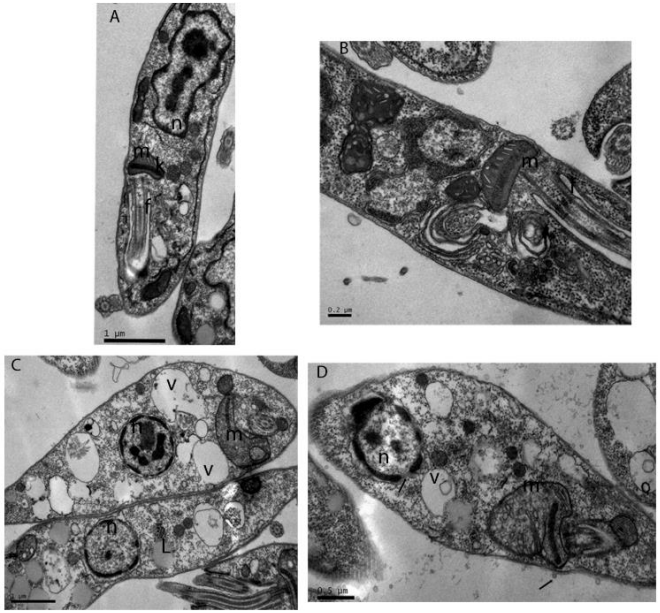

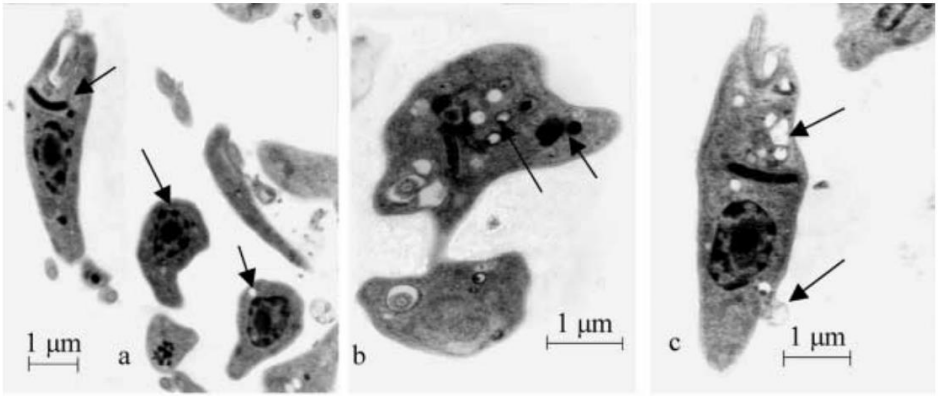

Following this precedent, it became of interest to study the ultrastructure of *L. major* cells upon treatment with **17** at the EC_{50} and EC_{90} as a representative 5N2C compound. Following compound treatment, cells were fixed using a glutaraldehyde-paraformaldehyde solution and post-fixed using an osmium tetroxide solution before alcohol dehydration, infiltration with propylene oxide and fixation onto Epon resin overnight (see footnote[14]). Imaging was achieved using a Hitachi H7600 transmission electron microscope. Using a DMSO only control as a reference, treated cells were analysed for ultrastructural changes upon drug treatment.

No changes to the Golgi apparatus, plasma membrane, kinetoplast, or flagellar pocket were observed at either the EC_{50} or EC_{90} compared to the negative control (Table 3.32-2, entries 1-5). However, some mitochondrial swelling was observed upon **17** treatment (Table 3.32-2, entry 6). Furthermore, concentric membrane structures, vacuolisation and chromatin condensation are all observed upon **17** treatment (Table 3.32-2, entries 7-9).

Table 3.32-2: Structural features observed by TEM upon treatment with **17** at the EC_{50} and EC_{90} for 12 hrs.

Ent -ry	Feature	DMSO (negative control)	17 EC_{50}	17 EC_{90}	Comment
No change observed upon 17 treatment					
1	Golgi apparatus		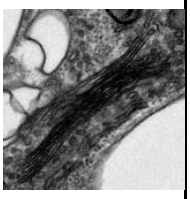	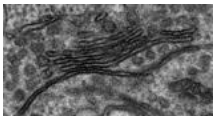	No change
2	Plasma membrane microtubules		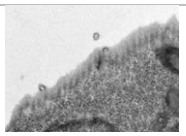		No change

[14] TEM sample post fixation, resin embedding and TEM imaging was carried out by Dr Christine Richardson, Durham University.

3	Plasma membrane (blebbing)	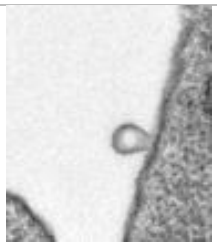		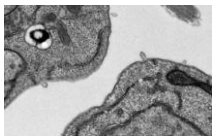	No change
4	Kinetoplast	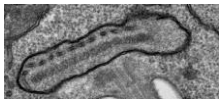		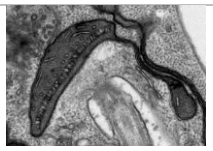	No change
5	Flagellar pocket		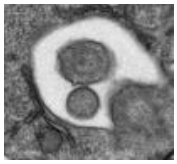	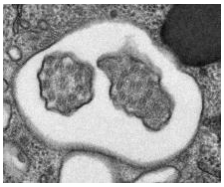	No change
Changes observed upon 17 treatment					
6	Mitochondria	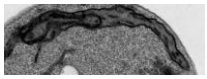	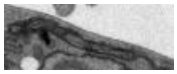	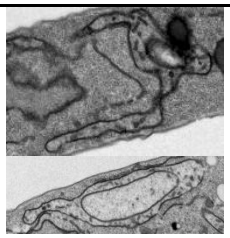	Mitochon-drial swelling upon treatment
7	Concentric membrane structures	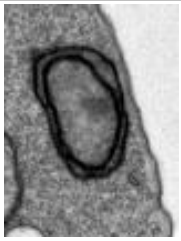	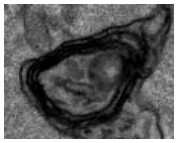	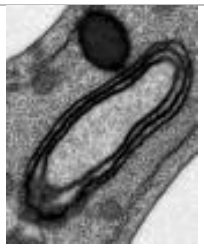	Increase upon treatment
8	Vacuolisation	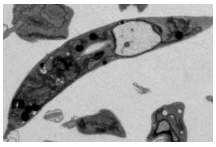	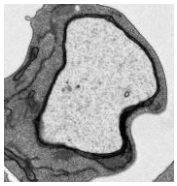		Increase in number and size on treatment
9	Nucleus	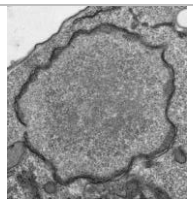		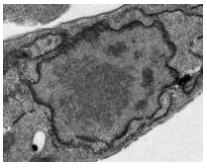	Chromatin condensa-tion upon treatment

Quantification of abnormal cell features in treated compared to control cells identified mitochondrial swelling, concentric membrane structures and vacuolisation as noteworthy (Figure 3.32-7).

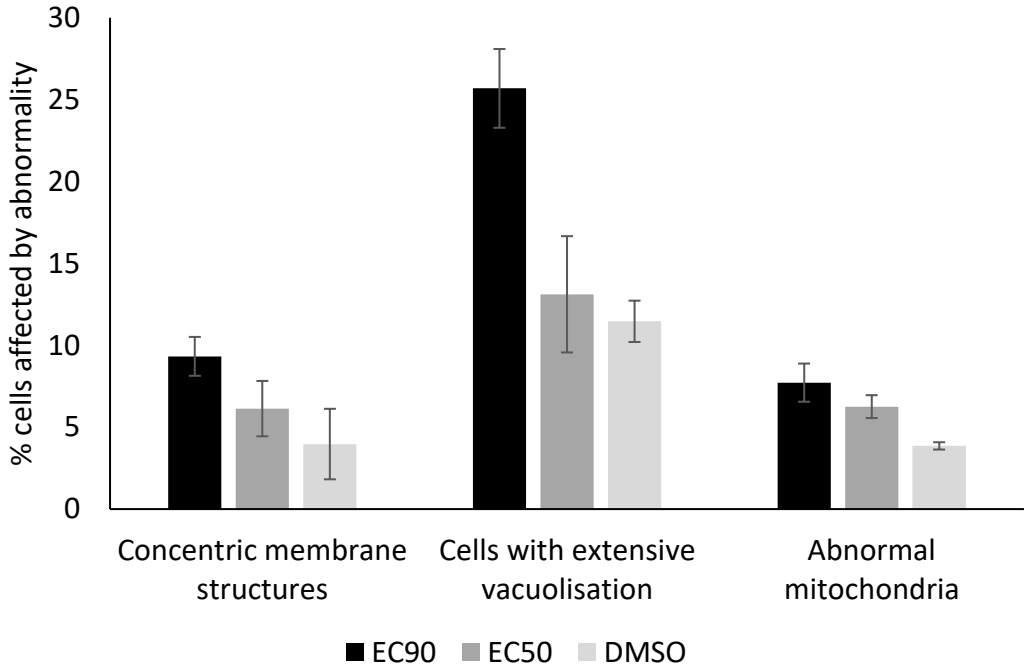

Figure 3.32-7 Abnormal feature counting for **17** treated samples compared to DMSO control. Averages calculated from three images. Error bars represent the standard error over three images.

The observed ultrastructural changes upon 5N2C treatment are consistent with the literature for nifurtimox (**37**) and nitazoxanide (**40**). [116,174] Some of these features could also be consistent with the onset of autophagy. Autophagy is essential during the cell cycle of trypanosomatids and is involved in differentiation, by enabling the recycling of old or damaged cellular components. [176–178] This is achieved by engulfing cell components into autophagosomes which mature and fuse with lysosomes resulting in hydrolysis of cell contents. Although autophagy is an essential process, it can result in cell death when unregulated.[179,180] In trypanosomatids, autophagy is characterised by the presence of concentric membrane structures[181], mitochondrial swelling[174], cytoplasmic vacuolisation[174,182] and autophagosome formation[181,183]. Many of these features were found in 5N2C treated cells (Table 3.32-2). Autophagosome-like bodies were potentially observed, but they appeared structurally distinct to autophagosomes observed in the literature (Figure 3.32-8). [181]

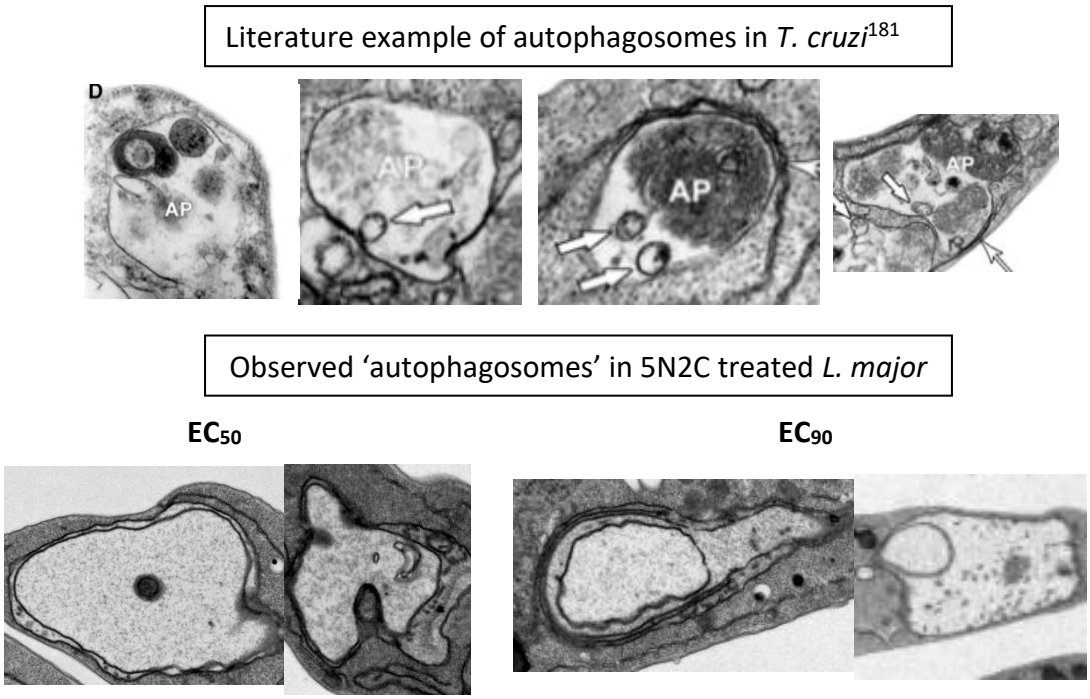

Figure 3.32-8 Autophagosome formation in *T. cruzi* epimastigotes compared to potential autophagosome formation after 5N2C treatment in *L. major*. Literature images are reproduced from Menna-Barreto (2009) with permission of the publisher.[181]

As no confirmed autophagosomes were observed, the onset of autophagy could not be proven.

4 Discussion

The original hit compounds **16** and **17**, identified by the HTS, showed promising antileishmanial activity and low HepG2 toxicity (Figure 4-1). However, low aqueous solubility and poor bioavailability limited their use as new antileishmanial drugs. The poor aqueous solubility of the hits was attributed to the rigid structure afforded by the 6-membered intramolecular hydrogen bonded ring. Removal of this hydrogen bonding led to a drastic improvement in aqueous solubility (**206**), however this was associated with a significant drop in antileishmanial activity. An extensive SAR campaign enabled the replacement of the potential PAINS 2-aminothiophene motif with an anthranilamide (**140** and **141**). It also showed that the 5N2C group was important for antileishmanial activity, as all attempts to remove the nitro group or left-hand heterocycle failed to give potent antileishmanial compounds (EC_{50}(*L. major*) > 16.6 μM). The essentiality of the nitroheterocycle is not surprising considering the nitroheterocycle present in many current antitrypanosomatid drugs including nifurtimox (**37**), benznidazole (**38**) and fexinidazole (**39**). Furthermore, the extensive presence of the 5N2C functionality in the LeishBox demonstrates its importance for the antileishmanial activity of many compounds.[46]

The limitation of aqueous solubility was removed whilst retaining antileishmanial activity by incorporating a basic nitrogen in the form of a morpholine ring to the 5-position of the phenyl ring to give **252** and **253**. Precedents to the use of a morpholine ring to improve aqueous solubility had been previously shown by Zafar *et al.*, who found that adding a morpholine ring to thieno[2,3-*b*]pyridine derivatives improved aqueous solubility by three orders of magnitude.[184] Ultimately, **252** and **253** were identified as new lead compounds due to their high antileishmanial activity, high selectivity index over HepG2 cells and significantly improved aqueous solubility (Figure 4-1). Whilst promising, the potential for host toxicity due to bioactivation of the nitro group, for example by host microsomal reductases, remained to be explored.[82,83]

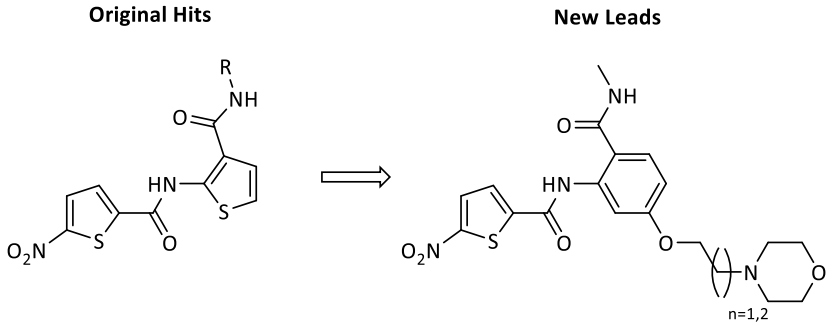

Compound ID	R	n	EC_{50} (*L. major*) / µM	CC_{50} (HepG2) / µM	Aqueous solubility (PBS) / µM
16	H	-	0.52 ± 0.05	24 ± 1	< 7.4
17	CH_3	-	0.99 ± 0.09	96 ± 4	< 7.4
252	-	1	0.44 ± 0.006	24 ± 1	19.3 ± 0.6
253	-	2	0.30 ± 0.02	13 ± 2	29 ± 3

Figure 4.1 Original hits (**16** and **17**) evolution to new lead compounds (**252** and **253**) with improved aqueous solubility. Antileishmanial activity, HepG2 toxicity and solubility values are reported as the mean of three biological repeats, with errors representing standard error.

Following the identification of two new lead antileishmanial compounds in Chapter 2, the mode of action of the 5N2C series was explored in Chapter 3.

All currently marketed nitro-containing drugs have complex and poorly understood modes of action. However, monocyclic nitrofurans and nitroimidazoles such as nifurtimox (**37**), benznidazole (**38**) and fexinidazole (**39**) are all anti-trypanosomatid prodrugs that require bioactivation by nitroreductase.[44,112] Similarly, the data discussed in Chapter 3 provides compelling evidence that 5N2Cs are bioactivated by NTR1 in *Leishmania*. The lack of a mammalian type I nitroreductase orthologue ensures that bioactivation is selective to the parasite and accounts for the observed selectivity index. The synthesised 5N2C library were bioactivated to two major metabolites: M+2 and 2M-98. The same two major metabolites were also observed for 15/15 and 14/15 5N2Cs obtained from the LeishBox respectively, which shows that these metabolites are relevant for more structurally diverse 5N2Cs and not limited to those investigated in this work.

The M+2 metabolite was predicted to be the 4,5-dihydrothiophene (**307a**), based on accurate mass and MS/MS data. This draws distinct parallels with the *Mtb*Ddn mediated bioactivation of nitroimidazoles (*R*)- and (*S*)- PA-824 (**275** and **276**), which are also bioactivated directly on the aromatic ring to give the 4,5-dihydroimidazole (**291**).[146] The 2M-98 metabolite was predicted to be a thieno[2,3-*b*]pyridyl species (**309a**), based on accurate mass, MS/MS and NMR data. Although the 2M-98 metabolite has not been observed for other nitroheterocycles in the literature, the proposed intermediate metabolites necessary for its formation are common to nifurtimox (**37**) upon bioactivation by trypanosomatid NTR1s.[138] In the case of nifurtimox (**37**), detoxification of the α,β-unsaturated open chain nitrile electrophilic intermediate (**279**) is achieved by a further slow reduction step to the saturated open chain nitrile (**280**). [138] In contrast, detoxification of the 5N2C α,β-unsaturated open chain nitrile electrophilic intermediate (**312**) can occur by reaction with the hydroxylamine intermediate (**311**). This leads to a complex bioactivation profile for 5N2Cs, where faster rates of bioactivation lead to detoxification of cytotoxic intermediates, consistent with the lack of correlation when comparing rates of bioactivation with fold change from the *Ldon*NTR1 overexpressor studies and antileishmanial activity.

In general, the electrophilic intermediates generated by nitroreductase bioactivation of nitroheterocycles such as nifurtimox (**37**) are predicted to covalently modify lipids, thiols, proteins and DNA. [114,115] Indirect evidence of lipid, kinetoplast and nuclear DNA damage upon nifurtimox (**37**) treatment supports the hypothesis of DNA and lipid covalent modification. [114–116] However, the covalent modification of protein targets has not been explored further for nifurtimox (**37**). Design of probe **251** followed by fluorescence and proteomics studies led to the identification of hundreds of proteins that are selectively covalently modified by bioactivated **251**. Crucially, most of these proteins were ribosomal proteins involved in translation. Interestingly, damage to ribosomes was also observed by Muelas-Serrano *et al* upon treatment of *T. cruzi* with nifurtimox (**37**). [116] This may suggest a common mode of action of the α,β-unsaturated open-chain nitrile electrophilic intermediate for both 5N2Cs (**312**) and nifurtimox (**279**).

The large number of proteins covalently modified by bioactivated **251** suggests that the 5N2C series exhibits significant polypharmacology. The mitochondria was expected to be the primary site of toxic effects for the 5N2C series, reflecting the mitochondrial location of NTR1 and presumed lability of the cytotoxic metabolites. Consistent with this, damage to the mitochondria was observed by Muelas-Serrano *et al.* in their TEM studies of *T. cruzi* treated with nifurtimox (**37**). [116] Similar TEM studies in this work showed mitochondrial swelling upon treatment of *L. major* with hit **17**. Furthermore, mitochondrial membrane depolarisation was observed in *L. major* treated with hits **16** and **17**, with less pronounced effects also observed upon **253** treatment. However, very few mitochondrial proteins were identified in the proteomics studies, which suggests that any mitochondrial dysfunction is likely a secondary effect rather than caused by direct covalent modification of essential mitochondrial proteins. Furthermore, this suggests that the predicted cytotoxic electrophilic intermediate metabolites are less labile than originally predicted, as they can diffuse or be transported from the mitochondria to distant locations before protein targets are covalently modified.

Another effect observed upon 5N2C treatment was ROS accumulation. Oxidative stress is a common mode of action of nitro containing drugs. For example, Mesquita *et al* showed that the nitrothiazole drug nitazoxanide (**40**) caused abnormal mitochondria, extensive vacuolisation and nuclear alterations in *L. infantum*. These ultrastructural changes were suggested to be induced by oxidative stress, justified by the elevated levels of ROS and mitochondrial depolarisation observed in parallel experiments. [174] In a similar fashion, many of the ultrastructural changes observed by TEM and the mitochondrial depolarisation detected upon 5N2C treatment of *L. major* could be caused by oxidative stress. Whilst type I nitroreductase are oxygen insensitive and do not generate ROS, ROS accumulation could be a downstream effect of metabolite action. In support of this, one of the major non-ribosomal proteins identified as covalently modified by **251** metabolites in the proteomics studies was tryparedoxin peroxidase, which could decrease the parasites ability to cope with oxidative stress leading to elevated levels of ROS. [185]

In summary, nitroheterocycles in the literature are suggested to bind to proteins, lipids, thiols and DNA upon NTR bioactivation. [114,115] Binding to DNA, thiols and lipids was not explored for the 5N2C series. However, oxidative stress and mitochondrial damage were observed for the 5N2C series, consistent with effects observed upon treatment with nitazoxanide (**40**) and nifurtimox (**37**) respectively. [174] Furthermore, hundreds of protein targets were covalently modified by 5N2Cs following bioactivation, most of which are ribosomal proteins. This suggests that inhibition of translation is one of the major modes of action of the 5N2Cs in trypanosomatids.

Inhibition of translation generally results in the slowing of cell growth and proliferation. [164–167] Significantly, this suggests that the 5N2C series may cause cytostatic rather than cytocidal effects. Cytostatic agents are generally considered to be less viable new drugs due to the lack of clearance of the disease and complications for immunocompromised patients, such as those with HIV coinfection.[186] However, a review of the effectiveness of bactericidal and bacteriostatic antibiotics from published, randomised clinical trials by Wald-Dickler *et al* showed that 49 out of 56 trials identified no difference in efficacy, with 6 out of 56 even showing superior efficacy for bacteriostatic compared to bactericidal agents.[187] Subsequently, the possibility of cytostatic behaviour for the 5N2Cs should not discourage further study. However, further validation of translational disruption and the cytostatic vs cyctocidal nature of the 5N2Cs is still required.

5 Future work

5.11 Chemistry future work

5.11.1 Scale up of lead compound 252 and 253

Before *in vivo* and DMPK studies are possible for lead compounds **252** and **253**, they need to be synthesised in large scales (100 mg- 1 g), which would be challenging with the current synthetic route. Some of the major problems with the current route are its linear, multistep and low yielding nature (overall linear yield 1.1 % and 5.2 % for **252** and **253**, respectively). As discussed in section 2.33.2.2, multiple different synthetic routes were assessed before extended 5-substituted analogues, such as **252** and **253**, were successfully synthesised. An alternative synthetic route could be devised to produce lead compounds **252** and **253** in higher yields. However, simple changes to the current route could be made to improve the overall yield.

The first two steps of the current route are triphosgene mediated cyclisation of anthranilic acid **169** to give intermediate **178**, followed by ring opening with methylamine to form anthranilamide **187**. Isolation of **178** is reliant on its precipitation upon addition of water, which was not always successful or high yielding. Any intermediate **178** left in solution reacts with water to give the anthranilic acid **169**. Subsequently, it may be possible to combine the first two steps of the synthesis and generate intermediate **187** directly by addition aqueous methylamine (40 %) to intermediate **178** (Scheme 5.11.1). This will decrease the number of steps and may also increase the overall yield of intermediate **187**. In turn, this may enable the isolation of sufficient quantities of lead compounds **252** and **253** to enable further testing such as *in vivo* analysis.

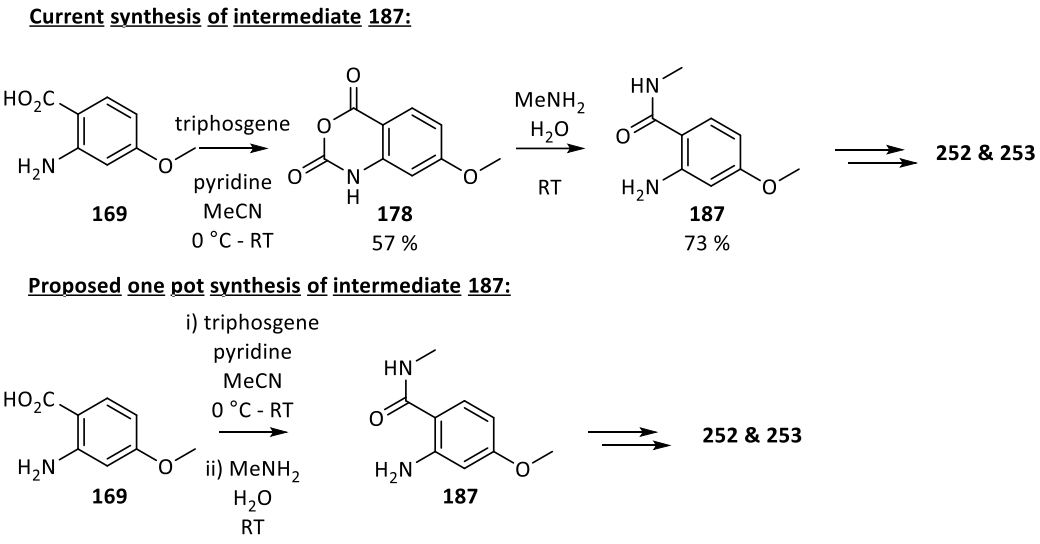

Scheme 5.11.1 Proposed alternative route towards intermediate **187**.

5.11.2 Synthesis of alternative analogues

The synthetic challenges encountered for lead compounds **252** and **253**, in addition to any potential toxicity issues, may prevent their progression into an *in vivo* model and further as potential new antileishmanial drugs. One of the key challenges was the introduction of the 5-hydroxy group in intermediate **241**. As such, alternative compounds have been proposed to enable the ease of scale up and to attempt to attenuate potential toxicity issues.

5.11.2.1 4,5-Disubstituted analogue 334

At the end of the project, 4,5-dimethoxyl analogue **334** was successfully synthesised in an analogous manner to **196** (Scheme 5.11.2).

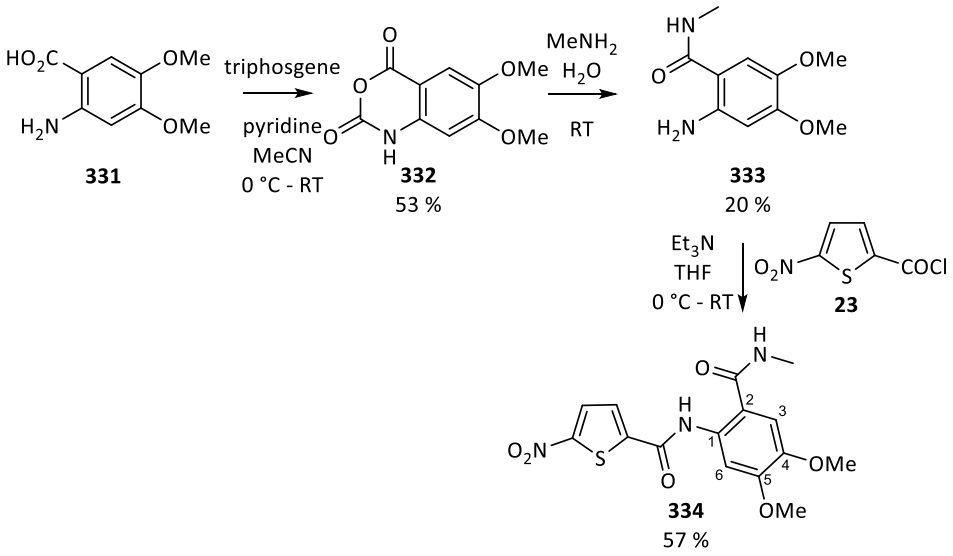

Scheme 5.11.2: Synthetic route towards 4,5-dimethoxy analogue **334**.

Dimethoxy analogue **334** retained single micromolar antipromastigote activity (EC_{50}(*L. major*) 1.2 ± 0.1 µM compared to 0.33 ± 0.02 µM for 5-methoxy analogue **196**), which suggests that the 4,5 disubstitution pattern is tolerated. This could be exploited to synthesise alternative morpholine analogue **335** (Figure 5.11-1).

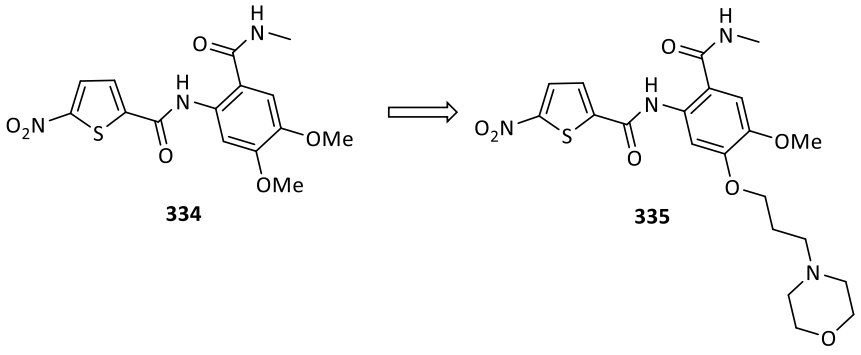

Figure 5.11-1 Proposal of alternative morpholine compound **335** based off the retained antileishmanial activity observed for **334**.

This is of interest as the substitution pattern of **335** is similar to that found in vanillin (**336**). This cheap and commercially available precursor may offer an alternative route to access **335** in larger scales than could be achieved for current lead compounds **252** and **253** (Scheme 5.11.3).

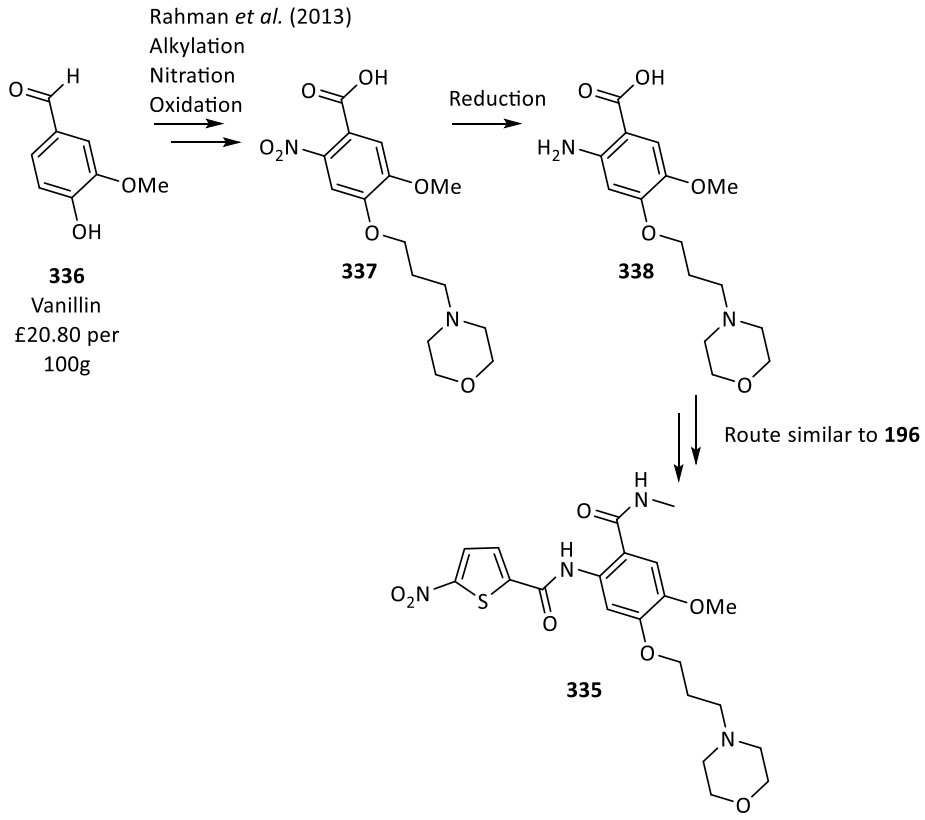

Scheme 5.11.3 Cheap and potentially scalable route to disubstituted morpholine analogue **335**. Price obtained from Merck, correct as of December 2021. Precedent for the first step(s) from Rahman *et al.* (2013).[188]

5.11.2.2 Varying the nature of the morpholine group to reduce toxicity

As previously discussed in section 2.33.2.2, multiple different substituents are tolerated in the 5- position, with morpholine compounds **252** and **253** emerging as new lead compounds due to their high aqueous solubility. However, the moderate HepG2 toxicity observed for **252** and **253** may become concerning depending on the dosage necessary to treat the intramacrophage form of the disease *in vivo*. Lower HepG2 toxicity was observed for tetrahydropyran analogue **254**, which suggests that changes could be made to the morpholine ring in lead compounds **252** and **253** to attenuate toxicity. Some suggestions of alternative groups that could be incorporated in the position of the morpholine ring are given in Figure 5.11-2.

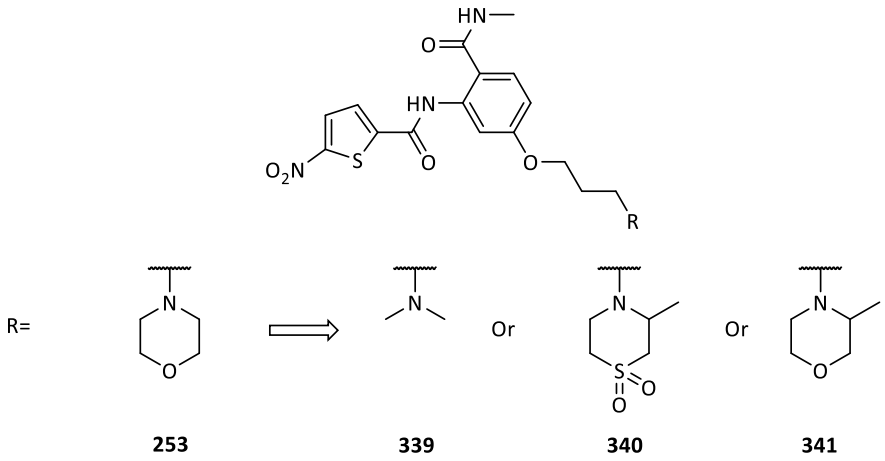

Figure 5.11-2 Suggested alternative analogues which could be synthesised in an attempt to attenuate HepG2 toxicity.

Firstly, the morpholine ring could be substituted for a simple dimethylamine group (**339**). Secondly, inspired by nifurtimox (**37**), a 3-methyl-1,1-dioxo-1,4-thiazinan-4-yl ring could be incorporated in place of the morpholine (**340**). Thirdly, the analogous 3-methylmorpholine compound (**341**) could be synthesised to explore the steric effect of the alpha methyl group on HepG2 toxicity. Although none of these substitutions guarantee a decrease in mammalian cell toxicity, they are worth exploring.

5.12 Biological future work

5.12.1 5N2Cs to treat further trypanosomatid diseases

Leishmaniasis is a trypanosomatid disease closely related to Chagas disease and African sleeping sickness. All three neglected tropical diseases require new and improved chemotherapeutic options. A selection of compounds that showed potent activity against a range of *Leishmania* spp. (section 2.34) also had similar efficacy against *T. brucei* trypomastigotes (section 2.35), the causative agent of African sleeping sickness. This suggests that the 5N2C series could be used as a new general treatment for both trypanosomatid diseases. To verify this, the activity of a range of active 5N2Cs against *T. cruzi*, the causative agent of Chagas disease, is currently being assessed by Professor Labadie, National University of Rosario, Argentina. Ultimately,

this will show whether the 5N2Cs could be used as broad spectrum antitrypanosomatid drugs.

5.12.2 Progression of lead compounds 252 and 253 as new antileishmanial drugs

Two lead compounds (**252** and **253**) were synthesised in this work that show promising antipromastigote activity, high selectivity index over HepG2 cells and high aqueous solubility. Although the selectivity index for **252** and **253** for *L. major* promastigotes over HepG2 cells is high (S.I. 55 and 65 respectively), the magnitude of the toxicity against HepG2 cells is still significant (CC_{50}(HepG2) 24 ± 1 μM and 13 ± 2 μM respectively). Antipromastigote activity gives a good indication of a compounds antileishmanial effects. However, the best model is the intramacrophage amastigote, as this is the form of the parasite within the mammalian host. Intramacrophage (InMac) *L. donovani* amastigote assays are currently being undertaken for a selection of the most active 5N2Cs by Professor Nahid Ali at the CSIR-Indian Institute of Chemical Biology, Kolkata, India. If InMac activity is in the single micromolar range, the selectivity index over HepG2 cells may drop below an acceptable limit. As such, it is necessary to expand the toxicology studies to different mammalian cell lines, such as THP-1 cells and bone marrow-derived macrophages, to explore any further potential toxicity issues.

Assuming high InMac activity and high selectivity over different mammalian cell lines can be established, it would then be of interest to explore bioactivation by microsomal reductases to determine whether any cytotoxic intermediate compounds may be generated in the host resulting in toxicity issues. [82,83] Success in these studies would then enable **252** and **253** to progress to DMPK studies and into an *in vivo* disease mouse model.

5.12.3 Mode of action of 5N2Cs

5.12.3.1 Disruption of translation

Proteomics studies (section 3.31.9) revealed that ribosomal proteins involved in translation are covalently modified by 5N2Cs following bioactivation. However, this still requires additional validation. Protein synthesis can be monitored by incorporating radioactive amino acids, such as ^{35}S-methionine, or clickable reagents, such as O-propargyl-puromycin, into nascent proteins in treated *Leishmania* cells.[189,190] *De novo* protein synthesis in a treated sample can then be compared to a negative control by monitoring the extent of radioactive marker incorporation or clicked with a fluorescent dye and monitored by fluorescence, respectively.

Alternatively, cell-free transcription-translation assays could be performed on commercially available S30 extracts of *L. tarentolae* (Jena Bioscience). The 5N2C of interest and *Lmj*NTR1 could be added to the S30 extract before incubation with pLEXSY-*invitro*2-EGFP (Jena Bioscience). Expression of EGFP in treated compared to control cells could then be used to determine the extent of inhibition of translation upon incubation with bioactivated 5N2Cs. [165] In a similar fashion, S30 extracts could be prepared from treated and control *L. major* cultures, before incubation with pLEXSY-*invitro*2-EGFP (Jena Bioscience).[165,191] Again, the extent of EGFP expression could be used to determine the inhibition of translation in treated vs untreated cells.

5.12.3.2 Cytocidal vs cytostatic nature of 5N2C treatment

Inhibition of translation generally results in the slowing of cell growth and proliferation. [164–167] Rate-of-kill assays can be used to determine whether a compound is cytostatic or cytocidal, and can indicate how long it takes for the compound to cause cell death.[192] Preliminary time-to-death analysis showed that 5N2C treatment slowed cell growth but did not result in cell death at the EC_{90} (Figure 5.12-1). However, further repeats would be required to fully investigate the effects of 5N2C treatment on cell proliferation.

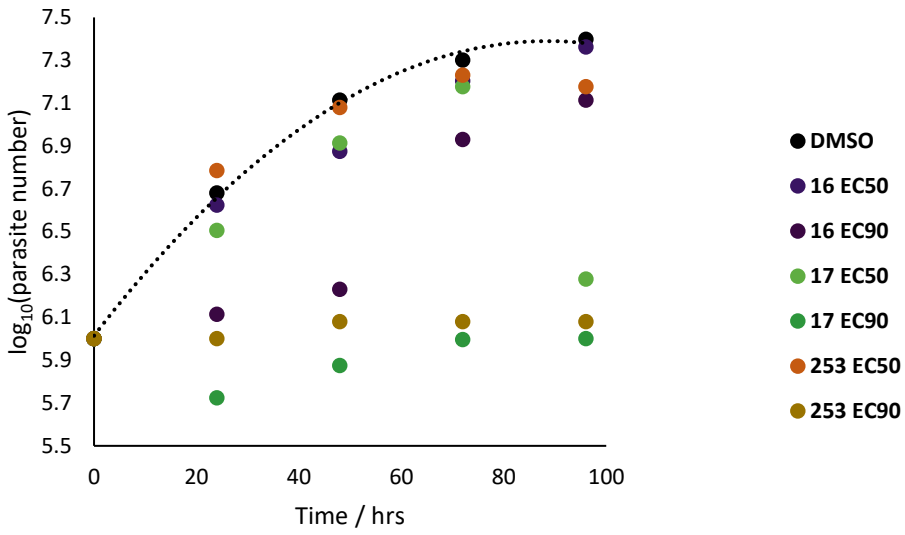

Figure 5.12-1 Preliminary rate of kill analysis for hits **16** and **17** and lead **253** from 1 biological repeat.

Furthermore, visual inspection of cell morphology following 5N2C treatment revealed elongated and immobile cells, indicative of stationary phase promastigotes. In contrast, if a compound caused cell death, cells would likely be rounded or overly fragmented. Subsequently, optical imaging or scanning electron microscopy could be useful to verify the cell morphology of *Leishmania* following 5N2C treatment.

5.12.3.3 DNA damage

Many nitroheterocyclic drugs, including nifurtimox (**37**) and benznidazole (**38**), cause damage to DNA as part of their mode of action.[116,121] Chromatin condensation was observed upon treatment of *L. major* with **17** by TEM, however this in itself is not sufficient evidence to claim DNA damage as a mode of action of the 5N2Cs. A terminal deoxynucleotidyl transferase dUTP nick-end labelling (TUNEL) assay could be performed to detect DNA degradation by labelling blunt ends of double stranded DNA breaks.[193]

5.12.3.4 Reduction in free thiols

A depletion in free thiol concentration is observed in *T. cruzi* treated with nifurtimox (**37**) and benznidazole (**38**).[194] Classically, this is caused by oxidative stress, however this was found to not be the case for nifurtimox.[195] A similar study could be carried

out in 5N2C treated *Leishmania* to determine whether thiol depletion is also caused by 5N2C treatment. For example, the concentration of free thiols from treated and control *L. major* promastigote cultures could be determined by reaction with monobromobimane and analysed by HPLC as reported by Fairlamb *et al*.[196]

5.12.3.5 Autophagy

Features observed by transmission electron microscopy could be consistent with the onset of autophagy upon 5N2C treatment. However, the identification of autophagosomes could not be verified and as such autophagy could not be confirmed. The onset of autophagy could be detected by monitoring the levels of Atg8, a protein marker for autophagosome formation. ATG8 levels in 5N2C treated *Leishmania* could be determined by immunofluorescence with an antibody against the Atg8.1 protein or using parasites expressing GFP-ATG8.[177,197]

6 Experimental Procedures

6.1 Chemistry experimental

6.11 Materials and methods

All reagents were purchased from commercial suppliers. All solvents were dry unless otherwise stated and were either dried in house or purchased from commercial suppliers. Reactions were monitored by thin layer chromatography (TLC), liquid chromatography mass spectrometry (LC-MS), gas chromatography mass spectrometry (GCMS) or atmospheric solids analysis probe (ASAP). TLC (silica gel aluminium sheet F254, Merck) plates were visualised under UV light (254 nm) using a UVP Mineralight® lamp or by staining with permanganate, ninhydrin, Mary's reagent or phosphomolybdic acid. Microwave reactions were carried out using a Persona Chemistry Emrys Optimizer Automated Multi-User Microwave Synthesizer. Flash column chromatography was achieved using CombiFlash® NextGen 300+ (Teledyne Isco) with RediSep® Rf normal phase and C-18 reverse phase columns (Teledyne). Nuclear magnetic resonance (NMR) spectra were recorded on the following instruments: Varian VNMRS-600 instrument with operating frequencies of 600.130 MHz for ^{1}H and 150.903 MHz for ^{13}C NMR, Varian VNMRS-700 with operating frequencies of 700.130 MHz for ^{1}H and 176.048 MHz for ^{13}C NMR, Avance III-HD-400, Bruker spectrometer-400 and Bruker Neo-400. Spectra were referenced relative to $CDCl_3$ (δ_H 7.26 ppm, δ_C 77.16 ppm), DMSO-d_6 (δ_H 2.50 ppm, δ_C 39.52 ppm) or CD_3OD (δ_H 4.87 ppm, δ_C 49.00 ppm). Chemical shifts are reported in parts per million (ppm), coupling constants (*J*) in hertz (Hz) and multiplicity as singlet (s), doublet (d), triplet (t), quartet (q), multiplet (m) or a combination thereof. All ^{1}H NMR and ^{13}C NMR spectral assignments were made with the aid of ^{1}H-^{1}H COSY, ^{1}H-^{1}H NOESY, ^{1}H-^{13}C HSQC and ^{1}H-^{13}C HMBC NMR experiments. Ar- refers to an aromatic carbon or proton that could not be assigned. Infra-red (IR) spectra were recorded on a PerkinElmer Paragon™ 1000 FT-IR spectrometer or a PerkinElmer Frontier™ FT-IR with Golden Gate Diamond ATR apparatus. IR assignments are reported in wavenumbers (cm^{-1}) and may be assigned as broad (br) or weak (w). Melting points

were recorded on Thermo Scientific Electrothermal IA9100 Digital Melting Point apparatus. High resolution mass spectrometry (HRMS) and LC-MS were recorded on either a Waters TQD mass spectrometer with Acquity UPLC (ESI-LC water (0.1 % formic acid): MeCN, flow rate 0.6 mL min^{-1} with a UPLC BEH C18 1.7 µm (2.1 mm x 50 mm) column), Waters QtoF Premier mass spectrometer with Acquity UPLC (ESI-LC water (0.1 % formic acid): MeCN, flow rate 0.2 mL min^{-1} with a UPLC BEH C18 1.7 µm (2.1 mm x 100 mm) column) or a Waters SQD mass spectrometer with Acquity UPLC (ESI-LC water (0.1 % formic acid): MeCN, flow rate 0.6 mL min^{-1} with a UPLC BEH C18 1.7 µm (2.1 mm x 50 mm) column). GCMS was carried out on a Shimadzu QP2010-Ultra with a temperature gradient 50 °C – 300 °C and a hold time of 5 mins, using a Rxi-17Sil MS (0.15 µm x 10 m x 0.15 mm) column. ASAP was carried out by dipping a melting point tube into sample solution. Samples are run isothermally at 350 °C on a Waters LCT Premier XE with Acquity UPLC or at 450 °C on a Waters Xevo QToF mass spectrometer.

6.12 General procedures

General procedure A

Oxalyl chloride (1.2 eq.) was added dropwise to a solution of carboxylic acid in dry dichloromethane (DCM, 1-2 mL per 1 mmol) under argon at 0 °C, followed by 1 drop of dimethylformamide (DMF). The reaction was stirred at room temperature (RT) for 2 hrs before volatiles were removed *in vacuo* to give the desired acid chloride.

General procedure B[30]

Triethylamine (2.5 eq.) was added to a solution of 1,3-substituted nitrile (1.0 eq.) and [1,4]-dithiane-2,5-diol (1.0 eq.) in absolute ethanol (EtOH, 1-2 mL per 1 mmol). The reaction mixture was refluxed for 2 hrs before cooling and filtering. Volatiles were removed *in vacuo* and the residue was dissolved in ethyl acetate (EtOAc), washed with 1M NaOH, water and brine and purified as specified to give the 3-substituted 2-aminothiophene.

General procedure C

5-Nitrothiophene-2-carbonyl chloride (**23**) (unless otherwise specified, 1.2 eq.) was dissolved in dry tetrahydrofuran (THF) or DCM (as specified) and added dropwise to a solution of substituted amine (1.0 eq.) and triethylamine (2.5 eq.) in dry THF or DCM at 0 °C under argon. The reaction mixture was stirred at RT for 2 hrs (unless otherwise specified). Product was filtered and triturated with water, unless otherwise stated, to give the title amide.

General procedure D

Pyridine (2.0 eq.) was added to a solution of substituted 2-amino benzoic acid (1.0 eq.) in dry acetonitrile (1.7 mL per 1 mmol). Triphosgene (0.33 eq.) was added gradually at 0 °C. The reaction was stirred at RT for 6 hrs, before dilution with water (5 mL). The suspension was then filtered to give the substituted benzoxazine-2,4-dione.

General procedure E

40 % Methylamine in water (5.0 eq.), was added to a stirred suspension of substituted benzoxazine-2,4-dione (1.0 eq.) in water (1.5 mL per 1 mmol). The resulting solution was stirred at RT for 2 hrs. The product was extracted into EtOAc and washed with saturated sodium carbonate, water and brine. The organic layer was dried over $MgSO_4$ and volatiles were removed *in vacuo* to give the substituted amino *N*-methyl-2-benzamide.

General procedure F[198]

Amino-5-hydroxy-*N*-methyl-2-benzamide (**241**) (1.0 eq.) in dry DMF was added to a stirred suspension of sodium hydride (60 % in mineral oil, 1.1 eq.) in DMF at RT. The suspension was heated to 40 °C over 30 minutes before addition of the specified alkyl bromide in dry DMF at RT. The reaction mixture was stirred at RT for 20 hrs (unless otherwise specified) before quenching with saturated sodium bicarbonate (general procedure **Fi**) or ammonium chloride (general procedure **Fii**). The reaction was extracted into EtOAc, washed with water, saturated sodium bicarbonate and brine and dried over $MgSO_4$, before volatiles were removed *in vacuo.* Further purification was achieved as specified to give the desired substituted ether product.

General procedure G

5-Nitrothiophene-2-carbonyl chloride (**23**) (1.2 eq.), unless otherwise stated, was dissolved in dry THF or DCM (stated) and added dropwise to a solution of substituted amine (1.0 eq.) and triethylamine (2.5 eq.) in dry THF or DCM at 0 °C under argon and stirred for 20 hr at RT. Volatiles were removed and the residue extracted into EtOAc, washed with saturated sodium bicarbonate (general procedure **Gi**) or 1M HCl (general procedure **Gii**), water and brine and purified as specified to afford the title product.

6.13 Synthetic procedures

5-Nitrothiophene-2-carbonyl chloride (23)

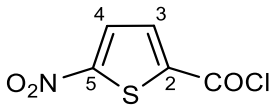

Following general procedure **A**, where the acid was 5-nitrothiophene-2-carboxylic acid (0.50 g, 2.9 mmol, 1 eq.) afforded 5-nitrothiophene-2-carbonyl chloride (**23**) as a pale yellow solid (0.56 g, 100 %) melting point 49-51 °C (lit. 52 °C).[105] ν_{max} (ATR) 1724 (C=O), 1513, 1336 cm^{-1}. δ_H (700 MHz, $CDCl_3$) 7.93 (1H, d, *J* 4.4, 4-*H*), 7.90 (1H, d, *J* 4.4, 3-*H*). δ_c (176 MHz, $CDCl_3$) 159.9 (*C*=O), 158.4 (*C*-2), 141.2 (*C*-5), 135.5 (*C*-3), 128.1 (*C*-4).

2-Amino-3-cyanothiophene (33)

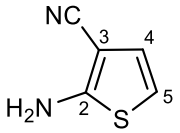

Following general procedure **B**, where the nitrile was malononitrile (2.31 g, 35 mmol, 1.0 eq.) afforded, without further purification, 2-amino-3-cyanothiophene (**33**) as an off white solid (2.66 g, 59 %) melting point 99 – 100 °C (lit. 103 – 105 °C).[199] ν_{max} (ATR) 3434 (N–H), 3336 (N–H), 2215 (C≡N) cm^{-1}. δ_H (700 MHz, $CDCl_3$) 6.72 (1H, d, *J* 5.7, 4-*H*), 6.34 (1H, d, *J* 5.7, 5-*H*), 4.83 (2H, s, NH_2). δ_C (176 MHz, $CDCl_3$) 162.5 (*C*-2), 125.8 (*C*-4), 115.6 (*C*≡N), 110.5 (*C*-5), 88.6 (*C*-3). *m/z* (LC-MS ES^+) 125.1 $[M+H]^+$.

***N*-(3-cyanothiophen-2-yl)-5'-nitrothiophene-2'-carboxamide (36)**

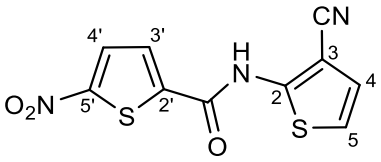

5-Nitrothiophene-2-carbonyl chloride (**23**) (0.61 g, 3.2 mmol, 1.0 eq.) was dissolved in dry THF (3 mL) and added dropwise to a solution of 2-amino-3-cyanothiophene (**33**) (0.50 g, 3.9 mmol, 1.2 eq.), DIPEA (0.67 mL, 3.8 mmol, 1.2 eq.) and DMAP (0.004

g, 0.03 mmol, 0.01 eq.) in dry THF (5 mL) under argon at 0 °C. The reaction mixture was stirred at RT for 22 hrs. Volatiles were removed *in vacuo* and the residue was purified by flash column chromatography (EtOAc:hexane) to give *N*-(3-cyanothiophen-2-yl)-5'-nitrothiophene-2'-carboxamide (**36**) as an orange/yellow solid (0.45 g, 50 %) melting point 251-253 °C (dec.). ν_{max} (ATR) 3266 (N–H), 2230 (C≡N), 1564 (C=O), 1501, 1285 cm^{-1}. δ_H (599 MHz, DMSO-d_6) 12.28 (1H, s, N*H*), 8.21 (1H, d, *J* 4.5 , 4'–*H*), 8.14 (1H, d, *J* 4.5, 3'–*H*), 7.37 (1H, d, *J* 5.8, 5–*H*), 7.28 (1H, d, *J* 5.8, 4–*H*). δ_C (151 MHz, DMSO-d_6) 158.3 (*C*=O), 154.2 (*C*-2'), 147.8 (*C*-2), 142.6 (*C*-5'), 130.4 (*C*-3'), 129.9 (*C*-4'), 125.9 (*C*-4), 121.3 (*C*-5), 114.5 (*C*≡N), 96.7 (*C*-3). *m/z* (LC-MS ES^-) 278.1 $[M-H]^-$. HRMS (ES^-) found $[M-H]^-$ 277.9682, $C_{10}H_4N_3O_3S_2$ requires *M* 277.9694. CHN found: C 50.17; H 5.23; N 9.05. $C_{10}H_5N_3O_3S_2$ requires C 49.99; H 5.16; N 8.97.

_N_-(3-carbamoylthiophen-2-yl)-5'-nitrothiophene-2'-carboxamide (16)

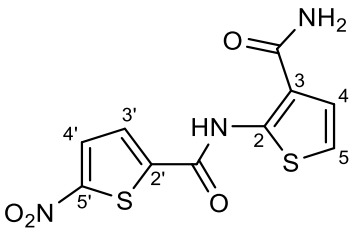

N-(3-cyanothiophen-2-yl)-5'-nitrothiophene-2'-carboxamide (**36**) (0.207 g, 0.72 mmol, 1 eq.) was dissolved in 1,4 dioxane (16 mL) and stirred with 4M $HCl_{(aq)}$ (5.6 mL, 22.3 mmol, 31 eq.) at 80 °C under argon for 72 hrs. The reaction mixture cooled on ice for 1 hr and the resulting precipitate was filtered and dried *in vacuo* to give *N*-(3-carbamoylthiophen-2-yl)-5'-nitrothiophene-2'-carboxamide (**16**) as an orange-yellow solid (0.17 g, 80 %) melting point 293-296 °C (dec.). ν_{max} (ATR) 3477 (N–H), 3376 (N–H), 1646 (C=O), 1593, 1508, 1338 cm^{-1}. δ_H (599 MHz, DMSO-d_6) 13.64 (1H, s, 2-N*H*), 8.20 (1H, d, *J* 4.4, 4'-*H*), 8.14 (1H, s, NH_2), 7.78 (1H, s, NH_2), 7.68 (1H, d, *J* 4.4, 3'-*H*), 7.51 (1H, d, *J* 5.8, 4-*H*), 7.13 (1H, d, *J* 5.8, 5-*H*). δ_C (151 MHz, DMSO-d_6) 167.2 (3-*C*=O), 155.9 (2'-*C*=O), 153.9 (*C*-2'), 144.9 (*C*-2), 142.9 (*C*-5'), 130.3 (*C*-4'), 128.2 (*C*-3'), 123.3 (*C*-4), 117.6 (*C*-5), 116.6 (*C*-3). *m/z* (LC-MS ES^+) 298.1 $[M+H]^+$. HRMS (ES^+) found

$[M+H]^+$ 297.9961, $C_{10}H_8N_3O_4S_2$ requires *M* 297.9956. CHN found: C 40.40; H 2.42; N 13.78. $C_{10}H_7N_3O_4S_2$ requires C 40.40; H 2.37; N 14.13.

2-Cyano-*N*-methylacetamide (25)

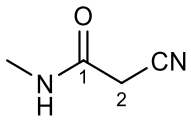

Methylamine in THF (2.0 M, 10 mL, 20 mmol, 2.0 eq.) was added to methyl cyanoacetate (1.0 mL, 10 mmol, 1.0 eq.) at RT. The reaction mixture was stirred for 1 hour before volatiles were removed *in vacuo* to yield 2-cyano-*N*-methylacetamide (**25**) as a white solid (0.96 g, 98 %) melting point 98-99 °C (lit. 99 °C).[200] ν_{max} (ATR) 3290 (N–H), 2268 (C≡N), 1655 (C=O) cm^{-1}. δ_H (700 MHz, $CDCl_3$) 6.26 (1H, s, N*H*), 3.38 (2H, s, CH_2), 2.88 (3H, d, *J* 4.8, CH_3). δ_C (176 MHz, $CDCl_3$) 161.6 (*C*=O), 114.9 (*C*≡N), 27.1 (*C*H_3), 25.8 (*C*H_2). *m/z* (GCMS EI) 98.1 $[M]^+$, 68.1 $[M - CH_3NH]^+$, 58.1 $[M - CH_2CN]^+$.

2-Amino-*N*-methylthiophene-3-carboxamide (30)

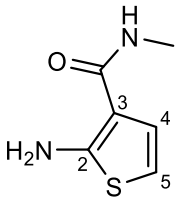

Following general procedure **B**, where the nitrile was 2-cyano-*N*-methylacetamide (**25**) (0.50 g, 5.1 mmol, 1.0 eq.) afforded, following work up with saturated $NaHCO_3$ and no further purification, 2-amino-*N*-methylthiophene-3-carboxamide (**30**) as a white solid (0.49 g, 61 %), melting point 150-151 °C. ν_{max} (ATR) 3440 (N–H), 3404 (N–H), 3354 (N–H), 1612 (C=O), 1532, 1415 cm^{-1}. δ_H (599 MHz, DMSO-d_6) 7.63 (1H, q, *J* 4.7, N*H*), 7.15 (2H, s, NH_2), 7.02 (1H, d, *J* 5.9, 4-*H*) 6.25 (1H, d, *J* 5.9, 5-*H*), 2.68 (3H, d, *J* 4.7, CH_3). δ_C (151 MHz, DMSO-d_6) 165.9 (*C*=O), 160.8 (*C*-2), 124.0 (*C*-4), 107.4 (*C*-3), 105.8 (*C*-5), 25.4 (*C*H_3). *m/z* (LC-MS ES^+) 157.5 $[M+H]^+$. HRMS (ES^+) found $[M+H]^+$ 157.0436, $C_6H_8N_2OS$ requires *M* 157.0436. CHN found: C 46.28; H 5.19; N 17.81. $C_6H_7N_2OS$ requires C 46.13; H 5.16; N 17.93.

_N_-Methyl-2-(5'-nitrothiophene-2'-amido)thiophene-3-carboxamide (17)

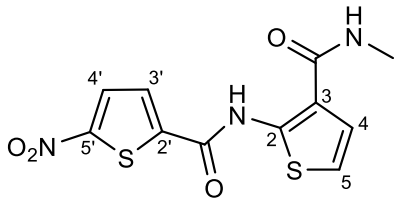

Following general procedure **C**, using THF (10 mL) as a reaction solvent, where the substituted amine was 2-amino-*N*-methylthiophene-3-carboxamide (**30**) (0.23 g, 1.5 mmol, 1.0 eq.) afforded *N*-methyl-2-(5'-nitrothiophene-2'-amido)thiophene-3-carboxamide (**17**) as a yellow solid (0.24 g, 52 %) melting point 248 °C (dec.). ν_{max} (ATR) 3442 (N–H), 3087 (N–H), 1657 (C=O), 1627 (C=O), 1541, 1335 cm^{-1}. δ_H (599 MHz, DMSO-d_6) 13.61 (1H, s, 2-N*H*), 8.62 (1H, s, CH_3-N*H*), 8.20 (1H, d, *J* 4.4, 4'-*H*), 7.72 (1H, d, *J* 4.4, 3'-*H*), 7.49 (1H, d, *J* 5.8, 4-*H*), 7.15 (1H, d, *J* 5.8, 5-*H*), 2.83 (3H, d, *J* 4.5, CH_3). δ_C (151 MHz, DMSO-d_6) 165.5 (3-*C*=O), 155.9 (2'-*C*=O), 153.9 (*C*-2'), 144.2 (*C*-2), 142.8 (*C*-5'), 130.3 (*C*-4'), 128.3 (*C*-3'), 122.5 (*C*-4), 117.9 (*C*-5), 116.6 (*C*-3), 25.8 (*C*H_3). *m/z* (LC-MS ES^+) 312.1 ($[M+H]^+$). HRMS (ES^+) found $[M+H]^+$ 312.0120, $C_{11}H_{10}N_3O_4S_2$ requires *M* 312.0113. CHN found: C 42.61; H 2.99; N 13.29. $C_{11}H_9N_3O_4S_2$ requires C 42.44; H 2.91; N 13.50.

Methyl 2-aminothiophene-3-carboxylate (31)

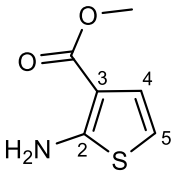

Following general procedure **B**, using 0.6 eq [1,4]-dithiane-2,5-diol for 0.5 hr, where the nitrile was methyl-2-cyanoacetate (2.0 mL, 20 mmol, 1.0 eq.) afforded, following removal of volatiles and purification by flash column chromatography (hexane: EtOAc), methyl 2-aminothiophene-3-carboxylate (**31**) as an off white solid (1.72 g, 55 %), melting point 80–81 °C (lit. 72–73 °C).[201] ν_{max} (ATR) 3431 (N–H), 3325 (N–H), 1658 (C=O) cm^{-1}. δ_H (700 MHz, DMSO-d_6) 7.24 (2H, s, NH_2), 6.81 (1H, d, *J* 5.8, 4-*H*), 6.26 (1H,

dd, *J* 5.8 *J* 0.7, 5-*H*), 3.69 (3H, s, C*H*$_3$). δ_C(151 MHz, DMSO-d$_6$) 164.8 (*C*=O), 164.0 (*C*-2), 125.0 (*C*-4), 106.5 (*C*-5), 103.7 (*C*-3), 50.5 (*C*H$_3$). *m/z* (LC-MS ES$^+$) 158.1 [M+H]$^+$.

Methyl 2-(5'-nitrothiophene-2'-amido)thiophene-3-carboxylate (34)

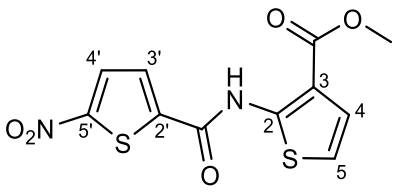

Following general procedure **C**, using DCM (10 mL) as a reaction solvent, where the substituted amine was methyl 2-aminothiophene-3-carboxylate (**31**) (0.50 g, 3.5 mmol, 1.0 eq.) afforded methyl 2-(5'-nitrothiophene-2'-amido)thiophene-3-carboxylate (**34**) as a yellow solid (0. 45 g, 41 %) melting point 228–229 °C. ν_{max} (ATR) 3220 (N–H), 3100 (N–H), 1675 (C=O), 1649 (C=O), 1566, 1335 cm^{-1}. δ_H(599 MHz, DMSO-d$_6$) 11.74 (1H, s, 2-N*H*), 8.22 (1H, d, *J* 4.4, 4'-*H*), 7.85 (1H, d, *J* 4.4, 3'-*H*), 7.28 (1H, d, *J* 5.8, 4-*H*), 7.21 (1H, d, *J* 5.8, 5-*H*), 3.90 (3H, s, C*H*$_3$). δ_C (151 MHz, DMSO-d$_6$) 165.2 (3-*C*=O), 157.2 (2'-*C*=O), 154.8 (*C*-2'), 146.9 (*C*-2), 142.7 (*C*-5'), 130.7 (*C*-4'), 129.6 (*C*-3'), 124.5 (*C*-4), 119.2 (*C*-5), 115.1 (*C*-3), 52.1 (*C*H$_3$). *m/z* (LC-MS ES$^+$) 313.1 [M+H]$^+$. HRMS (ES$^+$) found [M+H]$^+$ 312.9968, $C_{11}H_9N_2O_5S_2$ requires *M* 312.9953. CHN found: C 42.29; H 2.59; N 8.95. $C_{11}H_8N_2O_5S_2$ requires C 42.30; H 2.58; N 8.97.

2-Aminothiophene-3-ethanoate (32)

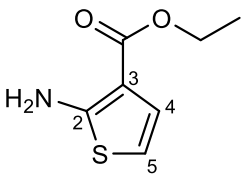

Following general procedure **B**, using 2 eq triethylamine, where the nitrile was ethyl-2-cyanoacetate (7.50 g, 66 mmol, 1 eq.) afforded, without further purification, 2-aminothiophene-3-ethanoate (**32**) as a brown solid (8.28 g, 79 %), melting point 43 – 44 °C (lit. 44 °C).[202] ν_{max} (ATR) 3445 (N–H), 3335 (N–H), 1663 (C=O) cm^{-1}. δ_H (599 MHz, DMSO-d$_6$) 7.22 (1H, s, N*H*$_2$), 6.82 (1H, d, *J* 5.8, 4-*H*), 6.26 (1H, d, *J* 5.8, 5-*H*), 4.17 (2H, q, *J* 7.2, C*H*$_2$), 1.24 (3H, t, *J* 7.1, C*H*$_3$). δ_C (151 MHz, DMSO-d$_6$) 164.4 (*C*=O), 164.0 (*C*-2),

125.0 (*C*-4), 106.4 (*C*-5), 104.0 (*C*-3), 58.9 (CH_2), 14.4 (CH_3). *m/z* (LC-MS ES^+) 172.5 $[M+H]^+$.

Ethyl 2-(5'-nitrothiophene-2'-amido)thiophene-3-carboxylate (35)

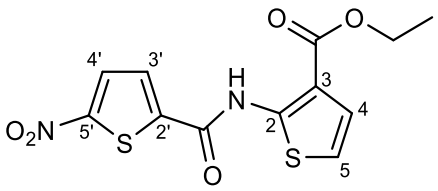

Following general procedure **Gi**, using DCM (5 mL) as a reaction solvent, where the substituted amine was 2-aminothiophene-3-ethanoate (**32**) (0.39 g, 2.3 mmol, 0.8) afforded, following work up with sodium hydroxide and purification using flash column chromatography (DCM: hexane), ethyl 2-(5'-nitrothiophene-2'-amido)thiophene-3-carboxylate (**35**) as a yellow solid (0.21 g, 28 %) melting point 212 – 213 °C. ν_{max} (ATR) 3119 (N–H), 1722 (C=O), 1646 (C=O), 1508, 1329 cm^{-1}. δ_H (700 MHz, $CDCl_3$) 12.14 (1H, s, N-*H*), 7.93 (1H, d, *J* 4.3, 4'-*H*), 7.65 (1H, d, *J* 4.3, 3'-*H*), 7.29 (1H, d, *J* 5.8, 4-*H*), 6.86 (1H, d, *J* 5.8, 5-*H*), 4.40 (2H, q, *J* 7.1, CH_2), 1.42 (3H, t, *J* 7.1, CH_3). δ_C (176 MHz, $CDCl_3$) 166.2 (O*C*=O), 156.8 (NH*C*=O), 155.6 (*C*-2'), 147.9 (*C*-2), 142.9 (*C*-5'), 128.4 (*C*-4'), 127.3 (*C*-3'), 124.3 (*C*-4), 117.4 (*C*-5), 114.5 (*C*-3), 61.4 (CH_2), 14.5 (CH_3). *m/z* (LC-MS ES^+) 327.2 $[M+H]^+$. HRMS (ES^+) found $[M+H]^+$ 327.0110, $C_{12}H_{11}N_2O_5S_2$ requires *M* 327.0109. CHN found: C 44.04; H 3.12; N 8.59. $C_{12}H_{10}N_2O_5S_2$ requires C 44.16; H 3.09; N 8.58.

***N*-methyl-2-(thiophene-2'-amido)thiophene-3-carboxamide (107)**

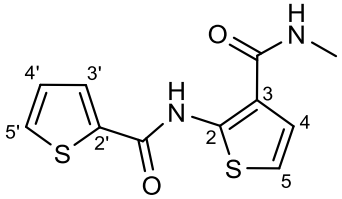

Following general procedure **C**, using THF (8 mL) as a reaction solvent for 7 hrs, where the acid chloride was thiophene-2-carbonyl chloride (0.23 g, 1.60 mmol, 1.25 eq.) and the substituted amine was 2-amino-*N*-methylthiophene-3-carboxamide (**30**) (0.20 g, 1.28 mmol, 1 eq.) afforded, following removal of volatiles from the filtrate

followed by flash column chromatography (hexane:EtOAc) and recrystallisation (hexane: DCM), *N*-methyl-2-(thiophene-2'-amido)thiophene-3-carboxamide (**107**) as a white crystalline solid (0.14 g, 40 %) melting point 191-192 °C. ν_{max} (ATR) 3445 (N–H), 3405 (N–H), 1651 (C=O), 1624 (C=O) cm^{-1}. δ_H (700 MHz, $CDCl_3$) 12.90 (1H, s, 2-N*H*), 7.81 (1H, dd, *J* 3.8, *J* 1.1, 5'-*H*), 7.60 (1H, dd, *J* 5.0, *J* 1.1, 3'-*H*), 7.15 (1H, dd, $J_{3',4'}$ 5.0, $J_{4',5'}$ 3.8, 4'-H), 6.95 (1H, dd, *J* 5.8, *J* 0.4, 4-*H*), 6.82 (1H, dd, *J* 5.8, *J* 0.8, 5-*H*), 5.99 (1H, s, CH_3-N*H*), 3.04 (3H, d, *J* 4.9, CH_3). δ_C (176 MHz, $CDCl_3$) 166.4 (3-*C*=O), 158.8 (2'-*C*=O), 147.2 (*C*-2), 137.7 (*C*-2'), 132.0 (*C*-3'), 129.6 (*C*-5'), 128.2 (*C*-4'), 120.4 (*C*-4), 117.1 (*C*-5), 114.6 (*C*-3), 26.5 (*C*H_3). *m/z* (LC-MS ES^+) 267.5 $[M+H]^+$. HRMS (ES^+) found $[M+H]^+$ 267.0265, $C_{11}H_{11}N_2O_2S_2$ requires *M* 267.0262. CHN found: C 49.58; H 3.70; N 10.43. $C_{11}H_{10}N_2O_2S_2$ requires C 49.61; H 3.78; N 10.52.

5-Bromothiophene-2-carbonyl chloride (95)

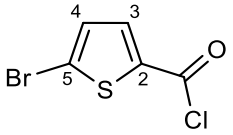

Following general procedure **A** where the acid was 5-bromothiophene-2-carboxylic acid (3.00 g, 14 mmol, 1.0 eq.) afforded 5-bromothiophene-2-carbonyl chloride (**95**) as an off-white semi-solid (3.14 g, 99 %). ν_{max} (ATR) 1747 (C=O) cm^{-1}. δ_H(400 MHz, $CDCl_3$) 7.72 (1H, d, *J* 9.4, Ar-*H*), 7.17 (1H, d, *J* 9.4, Ar-*H*). δ_C(101 MHz, $CDCl_3$) 164.4 (*C*=O), 158.6 (*C*-2), 138.1 (*C*-4) 132.0 (*C*-3), 126.7 (*C*-5).

5'-Bromo-*N*-[3-(methylcarbamoyl)thiophen-2-yl]thiophene-2'-carboxamide (108)

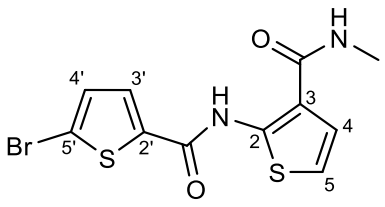

Following general procedure **C**, using THF (10 mL) as a reaction solvent for 15 hr, where the acid chloride was 5-bromothiophene-2-carbonyl chloride (**95**) (2.26 g, 10 mmol, 1.2 eq.) and the substituted amine was 2-amino-*N*-methylthiophene-3-carboxamide (**30**) (1.31 g, 8.3 mmol, 1.0 eq.) afforded, following removing volatiles

from the filtrate and purification by flash column chromatography (50:50 EtOAc:Hexane) followed by recrystallisation (EtOAc:Hexane), 5'-bromo-*N*-[3-(methylcarbamoyl)thiophen-2-yl]thiophene-2'-carboxamide (**108**) as an off-white solid (0.66 g, 23 %) melting point 171–172 °C. ν_{max} (ATR) 3382 (N–H), 1639 (C=O), 1629 (C=O), 1552, 1321. δ_H(599 MHz, $CDCl_3$) 12.92 (1H, s, 2-N*H*), 7.53 (1H, d, *J* 4.0, 4-*H*), 7.10 (1H, d, *J* 4.0, 5-*H*), 6.98 (1H, d, *J* 5.8, 4'-*H*), 6.81 (1H, dd, *J* 5.8 *J* 0.8, 1H), 6.15 (1H, d, *J* 4.7 CH_3-N*H*), 3.01 (3H, d, *J* 4.7, C*H*$_3$). δ_C(151 MHz, $CDCl_3$) 166.4 (2'-*C*=O), 157.6 (3-*C*=O), 146.8 (*C*-2'), 139.0 (*C*-2), 131.3 (*C*-5), 129.6 (*C*-4), 120.6 (*C*-4'), 120.1 (*C*-3), 117.2 (*C*-3'), 114.9 (*C*-5'), 26.5 (*C*H_3). *m/z* (LC-MS ES$^+$) 345.0 [M(^{79}Br)+H]$^+$ & 347.0 [M(^{81}Br)+H]$^+$. HRMS (ES$^+$) found [M+H]$^+$ 344.9380, $C_{11}H_{10}N_2O_2S_2Br$ requires *M* 344.9367. CHN found: C 38.13; H 2.60; N 8.10. $C_{11}H_9N_2O_2S_2Br$ requires C 38.27; H 2.63; N 8.11.

5-Nitrofuran-2-carbonyl chloride (96)

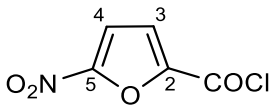

Following general procedure **A** where the acid was 5-nitrofuroic acid (0.50 g, 3.2 mmol, 1.0 eq.) afforded 5-nitrofuran-2-carbonyl chloride (**96**) as a pale yellow semi-solid (0.56 g, 100 %). ν_{max} (ATR) 1749 (C=O), 1543, 1348 cm^{-1}. δ_H(599 MHz, $CDCl_3$) 7.57 (1H, d, *J* 3.9, 3-*H*), 7.41 (1H, d, *J* 3.9, 4-*H*). δ_C(151 MHz, DMSO-d_6) 155.5 (*C*-5), 153.7 (*C*=O), 145.2 (*C*-2), 123.7 (*C*-3), 111.7 (*C*-4).

***N*-[3-(methylcarbamoyl)thiophen-2-yl]-5'-nitrofuran-2'-carboxamide (109)**

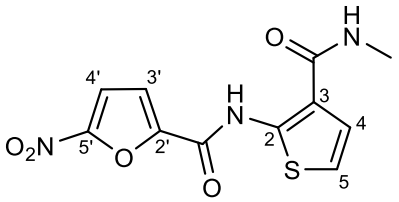

Following general procedure **C**, using THF (6 mL) as a reaction solvent, where the acid chloride was 5-nitrofuran-2-carbonyl chloride (**96**) (0.44 g, 2.5 mmol, 1.2 eq.) and the substituted amine was 2-amino-*N*-methylthiophene-3-carboxamide (**30**) (0.33 g, 2.1

mmol, 1.0 eq.) afforded, following recrystallisation (DCM:hexane), *N*-[3-(methylcarbamoyl)thiophen-2-yl]-5'-nitrofuran-2'-carboxamide (**109**) as a yellow solid (0.062 g, 10 %) melting point 233 – 234 °C. ν_{max} (ATR) 3466 (N–H), 3300 (N–H), 1671 (C=O), 1660 (C=O) 1556, 1355 cm^{-1}. δ_H(599 MHz, DMSO-d_6) 13.43 (1H, s, 2-N*H*), 8.55 (1H, d, *J* 4.6, CH_3-N*H*), 7.85 (1H, d, *J* 3.9, 4'-*H*), 7.58 (1H, d, *J* 3.9, 3'-*H*),7.49 (1H, d, *J* 5.8, 4-*H*), 7.16 (1H, d, *J* 5.8, 5-*H*), 2.84 (3H, d, *J* 4.6, CH_3). δ_C(151 MHz, DMSO-d_6) 165.2 (3-*C*=O), 152.5 (2'-*C*=O), 151.7 (*C*-5'), 146.3 (*C*-2'), 143.7 (*C*-2), 122.5 (*C*-4), 117.9 (*C*-3' & *C*-5), 116.9 (*C*-3), 113.8 (*C*-4'), 25.8 (*C*H_3). *m/z* (LC-MS ES^+) 296.1 $[M+H]^+$. HRMS (ES^+) found $[M+H]^+$ 296.0370, $C_{11}H_{10}N_3O_5S$ requires *M* 296.0341. CHN found: C 44.32; H 2.99; N 14.01. $C_{11}H_9N_3O_5S$ requires C 44.74; H 3.07; N 14.23.

4-Nitro-2-(trifluoromethyl)benzoyl chloride (97)

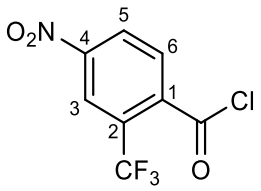

Following general procedure **A** where the acid was 4-nitro-2-(trifluoromethyl)benzoic acid (1.00 g, 4.25 mmol, 1.0 eq.) afforded 4-nitro-2-(trifluoromethyl)benzoyl chloride (**97**) as a yellow oil (1.08 g, 100 %). ν_{max} (ATR) 1795 (C=O), 1542, 1335 cm^{-1}. δ_H(700 MHz, $CDCl_3$) 8.64 (1H, d, *J* 2.2, 3-*H*), 8.56 (1H, dd, *J* 8.6 *J* 2.2, 5-*H*), 8.12 (1H, d, *J* 8.6, 6-*H*). δ_C(176 MHz, $CDCl_3$) 165.4 (*C*=O), 149.5 (*C*-4), 139.6 (q, *J* 1.9, *C*-1), 131.4 (*C*-6), 129.7 (q, *J* 34.9, *C*-2), 127.2 (*C*-5), 122.8 (q, *J* 5.3, *C*-3), 121.8 (q, *J* 274.8, *C*F_3). δ_F(376 MHz, $CDCl_3$) -59.4 (C*F*$_3$).

***N*-methyl-2-[4'-nitro-2'-(trifluoromethyl)benzamido]thiophene-3-carboxamide (110)**

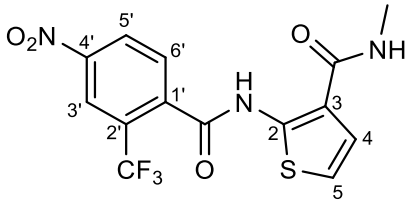

Following general procedure **Gi**, using THF (6 mL) as a reaction solvent, where the acid chloride was 4-nitro-2-(trifluoromethyl)benzoyl chloride (**97**) (0.49 g, 1.92 mmol, 1.2 eq.) and the substituted amine was 2-amino-*N*-methylthiophene-3-carboxamide (**30**) (0.49 g, 1.92 mmol, 1.2 eq.) afforded, following work up using chloroform and purification by flash column chromatography (EtOAc/hexane), *N*-methyl-2-[4'-nitro-2'-(trifluoromethyl)benzamido]thiophene-3-carboxamide (**110**) as a yellow solid (0.39 g, 65 %), melting point 170–172 °C. ν_{max} (ATR) 3442 (N–H),1682 (C=O), 1629 (C=O), 1553, 1351 cm^{-1}. δ_H(700 MHz, $CDCl_3$) 12.66 (1H, s, 2-N*H*), 8.64 (1H, d, *J* 2.2, 3'-*H*), 8.51 (1H, dd, *J* 8.3 *J* 2.2, 5'-*H*), 7.91 (1H, d, *J* 8.3, 6'-*H*), 7.00 (1H, d, *J* 5.9, 4-*H*), 6.93 (1H, dd, *J* 5.9, 5-*H*), 6.04 (1H, s, N*H*CH_3), 2.97 (3H, d, *J* 4.9, C*H*$_3$). δ_C(176 MHz, $CDCl_3$) 166.0 (3-*C*=O), 162.0 (1'-*C*=O). 148.7 (*C*-4'), 145.8 (*C*-2), 139.8 (*C*-1'), 130.5 (*C*-6'), 130.2 (q, *J* 34.2, *C*-2'), 127.2 (*C*-5'), 122.6 (q, *J* 5.1, *C*-3'), 122.3 (q, *J* 268.2, *C*F_3), 120.5 (*C*-4), 118.1 (*C*-5), 116.1 (*C*-3), 26.4 (*C*H_3). δ_F(376 MHz, $CDCl_3$) -59.4 (C*F*$_3$). *m/z* (LC-MS ES^+) 374.2 $[M + H]^+$. HRMS (ES^+) found $[M+H]^+$ 374.0422, $C_{14}H_{11}N_3O_4F_3S$ requires 374.0422. CHN found: C 45.17; H 2.75; N 11.16. $C_{14}H_{12}N_3O_4F_3S$ requires C 45.04; H 2.70; N 11.25.

N-[3-(methylcarbamoyl)thiophen-2-yl]-1',3'-thiazole-2'-carboxamide (111)

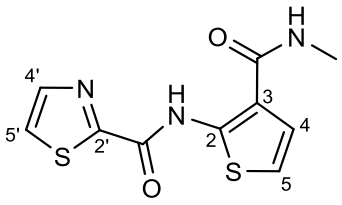

Following general procedure **A**, where the acid was 1,3-thiazole-2-cabroxylic acid (0.200 g, 1.5 mmol, 1.0 eq.), afforded 1,3-thiazole-2-carbonyl chloride (**98**) as a pale-yellow solid, which was used without purification or characterisation.

Following general procedure **C**, using THF (6 mL) as a reaction solvent, where the acid chloride was 1,3-thiazole-2-carbonyl chloride (**98**) (0.20 g, 1.35 mmol, 1.2 eq.) and the substituted amine was 2-amino-*N*-methylthiophene-3-carboxamide (**30**) (0.18 g, 1.13 mmol, 1.0 eq.) afforded, following removal of volatiles from the filtrate and purification of the residue by flash column chromatography (hexane:EtOAc) followed

by recrystallisation (hexane:EtOAc), N-[3-(methylcarbamoyl)thiophen-2-yl]-1',3'-thiazole-2'-carboxamide (**111**) as a pale yellow solid (0.073 g, 21 %) melting point 212–213 °C. ν_{max} (ATR) 3330 (N–H), 3228 (N–H), 3111 (N–H) 1666 (C=O), 1619 (C=O) cm^{-1}. δ_H(700 MHz, DMSO-d_6) 13.52 (1H, s, 2-N*H*), 8.48 (1H, d, *J* 4.7, CH_3-N*H*), 8.21 (1H, d, *J* 3.0, 5'-*H*), 8.17 (1H, d, *J* 3.0, 4'-*H*), 7.48 (1H, d, *J* 5.8, 4-*H*), 7.14 (1H, dd, *J* 5.8 *J* 0.8, 5-*H*), 2.82 (3H, d, *J* 4.7, CH_3). δ_C(176 MHz, DMSO-d_6) 165.0 (3-*C*=O), 161.2 (*C*-2'), 155.9 (2'-*C*=O), 144.6 (*C*-4'), 143.8 (*C*-2), 127.5 (*C*-5'), 122.6 (*C*-4), 117.5 (*C*-5), 117.0 (*C*-3), 25.7 (*C*H_3). *m/z* (LC-MS ES^+) 268.2$[M+H]^+$. HRMS (ES^+) found $[M+H]^+$ 268.0226, $C_{10}H_{10}N_3O_2S_2$ requires *M* 268.0214. CHN found: C 45.38; H 3.56; N 15.39. $C_{10}H_9N_3O_2S_2$ requires C 44.93; H 3.39; N 15.72.

N-[3-(methylcarbamoyl)thiophen-2-yl]-1',3'-thiazole-5'-carboxamide (112)

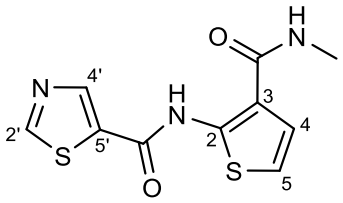

Following general procedure **A**, where the acid was 1,3-thiazole-5-cabroxylic acid (0.200 g, 1.5 mmol, 1.0 eq.), afforded 1,3-thiazole-5-carbonyl chloride (**99**) as an off white solid, which was used without purification or characterisation.

Followed general procedure **C**, using THF (6 mL) as a reaction solvent, where the acid chloride was 1,3-thiazole-5-carbonyl chloride (**99**) (0.20 g, 1.35 mmol, 1.2 eq.) and the substituted amine was 2-amino-*N*-methylthiophene-3-carboxamide (**30**) (0.18 g, 1.13 mmol, 1.0 eq.), afforded N-[3-(methylcarbamoyl)thiophen-2-yl]-1',3'-thiazole-5'-carboxamide (**112**) as an off-white solid (0.091 g, 30 %) melting point 277–278 °C. ν_{max} (ATR) 3308 (N–H), 3077 (N–H), 1660 (C=O), 1623 (C=O) cm^{-1}. δ_H(700 MHz, DMSO-d_6) 13.32 (1H, s, 2-N*H*), 9.39 (1H, s, 2'-*H*), 8.55 (1H, d, *J* 4.7, CH_3-N*H*), 8.47 (1H, s, 4'-*H*), 7.47 (1H, d, *J* 5.8, 4-*H*), 7.10 (1H, d, *J* 5.8, 5-*H*), 2.83 (1H, d, *J* 4.7, CH_3). δ_C(176 MHz, DMSO-d_6) 165.5 (3-*C*=O), 159.5 (*C*-2'), 156.3 (5'-*C*=O), 145.0 (*C*-4'), 144.6 (*C*-2), 133.0 (*C*-5'), 122.4 (*C*-4), 117.2 (*C*-5), 116.0 (*C*-3), 25.8 (*C*H_3). *m/z* (LC-MS ES^+) 268.1$[M+H]^+$.

HRMS (ES$^+$) found [M+H]$^+$ 268.0222, $C_{10}H_{10}N_3O_2S_2$ requires *M* 268.0214. CHN found: C 44.98; H 3.51; N 15.26. $C_{10}H_9N_3O_2S_2$ requires C 44.93; H 3.39; N 15.72.

N-[3-(methylcarbamoyl)thiophen-2-yl]-1',3'-thiazole-4'-carboxamide (113)

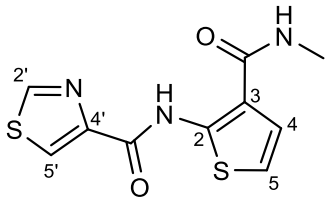

Following general procedure **A**, where the acid was 1,3-thiazole-4-cabroxylic acid (0.200 g, 1.5 mmol, 1.0 eq.), afforded 1,3-thiazole-4-carbonyl chloride (**100**) as an off white solid, which was used without purification or characterisation.

Following general procedure **C**, using THF (6 mL) as a reaction solvent, where the acid chloride was 1,3-thiazole-4-carbonyl chloride (**100**) (0.20 g, 1.35 mmol, 1.2 eq.) and the substituted amine was 2-amino-*N*-methylthiophene-3-carboxamide (**30**) (0.18 g, 1.13 mmol, 1.0 eq.), afforded N-[3-(methylcarbamoyl)thiophen-2-yl]-1',3'-thiazole-4'-carboxamide (**113**) as an off-white solid (0.13 g, 38 %) melting point 272–273 °C. ν_{max} (ATR) 3375 (N–H), 3111 (N–H), 1657 (C=O), 1639 (C=O) cm^{-1}. δ_H(599 MHz, DMSO-d$_6$) 13.40 (1H, s, 2-N*H*), 9.32 (1H, d, *J* 2.1, 2'-*H*), 8.60 (1H, d, *J* 2.1, 5'-*H*), 8.40 (1H, d, *J* 4.7, CH_3-N*H*), 7.45 (1H, d, *J* 5.9, 4-*H*), 7.07 (1H, d, *J* 5.9, 5-*H*), 2.80 (3H, d, *J* 4.7, C*H*$_3$). δ_C(151 MHz, DMSO-d$_6$) 165.0 (3-*C*=O), 157.3 (4'-*C*=O), 156.0 (*C*-2'), 148.6 (*C*-4'), 144.3 (*C*-2), 126.7 (*C*-5'), 122.5 (*C*-4), 117.0 (*C*-5), 116.3 (*C*-3), 25.7 (*C*H$_3$). *m/z* (LC-MS ES$^+$) 268.1[M+H]$^+$. HRMS (ES$^+$) found [M+H]$^+$ 268.0223, $C_{10}H_{10}N_3O_2S_2$ requires *M* 268.0214. CHN found: C 44.81; H 3.46; N 15.44. $C_{10}H_9N_3O_2S_2$ requires C 44.93; H 3.39; N 15.72.

2,1,3-Benzoxadiazole-5-carbonyl chloride (101)

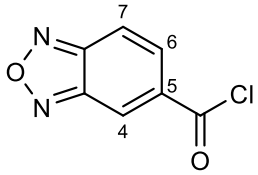

Following general procedure **A**, where the acid was 2,1,3-benzoxzdiazole-5-carboxylic acid (0.20 g, 1.2 mmol, 1.0 eq.), afforded 2,1,3-benzoxadiazole-5-carbonyl chloride (**101**) as a pale yellow solid (0.22g, 100 %) melting point 43–44 °C (lit. 55–58 °C).[203] ν_{max} (ATR) 1754 (C=O) cm^{-1}. δ_H (400 MHz, $CDCl_3$) 8.86 (1H, s, 4-*H*), 7.90-8.00 (2H, m, Ar-*H*). δ_C (101 MHz, $CDCl_3$) 166.9 (*C*=O), 149.6 (*C*-3), 148.8 (*C*-8), 136.4 (*C*-5), 129.7 (*C*-6), 124.9 (*C*-Ar), 117.8 (*C*-Ar).

N-[3-(methylcarbamoyl)thiophen-2-yl]-2,1,3-benzoxadiazole-5'-carboxamide (114)

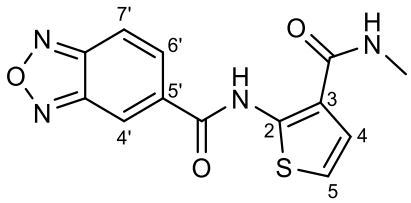

Following general procedure **C**, using THF (2 mL) as a reaction solvent, where the acid chloride was 2,1,3-benzoxadiazole-5-carbonyl chloride (**101**) (0.22 g, 1.2 mmol, 1.2 eq.) and the substituted amine was 2-amino-*N*-methylthiophene-3-carboxamide (**30**) (0.16 g, 1.13 mmol, 1.0 eq.), afforded N-[3-(methylcarbamoyl)thiophen-2-yl]-2,1,3-benzoxadiazole-5'-carboxamide (**114**) as a yellow solid (0.062 g, 20 %) melting point 248–249 °C. ν_{max} (ATR) 3410 (N–H), 3081 (N–H), 1661 (C=O), 1621 (C=O), 1555, 1311 cm^{-1}. δ_H(599 MHz, DMSO-d_6) 13.58 (1H, s, 2-N*H*), 8.56-8.59 (2H, m, 4'-*H* & N*H*-CH_3), 8.28 (1H, dd, *J* 9.4 *J* 1.1, 7'-*H*), 7.95 (1H, dd, *J* 9.4 *J* 1.5, 6'-*H*), 7.48 (1H, d, *J* 5.9, 4-*H*), 7.13 (1H, d, *J* 5.9, 5-*H*), 2.83 (3H, d, *J* 4.5, CH_3). δ_C(151 MHz, DMSO-d_6) 165.5 (3-*C*=O), 160.7 (5'-*C*=O), 149.2 (*C*-8'), 148.8 (*C*-3'), 144.8 (*C*-2), 136.2 (*C*-5'), 130.0 (*C*-6'), 122.5 (*C*-4), 117.6 (*C*-7'), 117.5 (*C*-5), 116.7 (*C*-4'), 116.5 (*C*-3), 25.8 (CH_3). *m/z* (LC-MS ES^+) 303.2 $[M+H]^+$. HRMS (ES^+) found $[M+H]^+$ 303.0556, $C_{13}H_{11}N_4O_3S$ requires *M* 303.0552. CHN found: C 51.21; H 3.40; N 18.05. $C_{13}H_{10}N_4O_3S$ requires C 51.65; H 3.33; N 18.53.

2-Benzamido-*N*-methylthiophene-3-carboxamide (115)

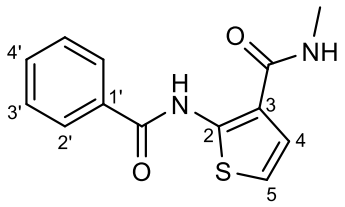

Following general procedure **Gi**, using THF (3 mL) as a reaction solvent, where the acid chloride was benzoyl chloride (0.10 mL 0.84 mmol, 1.2 eq.) and the substituted amine was 2-amino-*N*-methylthiophene-3-carboxamide (**30**) (0.11 g, 0.70 mmol, 1.0 eq.) afforded, following recrystallisation from DCM:hexane, 2-benzamido-*N*-methylthiophene-3-carboxamide (**115**) as an off white solid (0.037g, 20 %) melting point 183 – 184 °C. ν_{max} (ATR) 3374 (N–H), 3330 (N–H), 1661 (C=O), 1635 (C=O), 1555, 1405 cm^{-1}. δ_H (599 MHz, $CDCl_3$) 13.03 (1H, s, 2-N*H*), 8.05-8.08 (2H, m, 2'-*H*), 7.56-7.59 (1H, m, 4'-*H*), 7.50-7.54 (2H, m, 3'-*H*), 6.99 (1H, d, *J* 5.7, 4-*H*), 6.83 (1H, dd, *J* 5.7, *J* 0.8, 5-*H*), 6.07 (1H, s, CH_3-N*H*), 3.03 (3H, d, *J* 4.9, CH_3). δ_C (151 MHz, $CDCl_3$) 166.3 (3-*C*=O), 163.7 (1'-*C*=O), 147.3 (*C*-2), 132.5 (*C*-4'), 132.3 (*C*-1'), 128.9 (*C*-3'), 127.6 (*C*-2'), 120.4 (*C*-4), 116.9 (*C*-5), 114.7 (*C*-3), 26.3 (*C*H_3). *m/z* (LC-MS ES^+) 261.2 $[M+H]^+$. HRMS (ES^+) found $[M+H]^+$ 261.0682, $C_{13}H_{13}N_2O_2S$ requires *M* 261.0698. CHN found: C 59.23; H 4.70; N 10.69. $C_{13}H_{12}N_2O_2S$ requires C 59.98; H 4.65; N 10.76.

N-[3-(methylcarbamoyl)thiophen-2-yl]pyridine-4'-carboxamide (116)

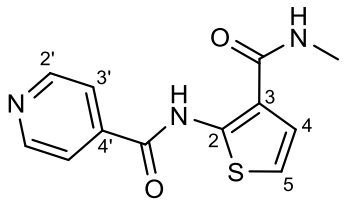

Isonicotinoyl chloride (0.11 g, 0.77 mmol, 1.2 eq.) dissolved in dry DMF (3 mL) was added to 2-amino-*N*-methylthiophene-3-carboxamide (**30**) (0.100 g, 0.64 mmol, 1.0 eq.) dissolved in dry THF (7 mL) and triethylamine (0.089 mL, 1.9 mmol, 2.5 eq.) at 0 °C under argon and the reaction was stirred at RT for 23 hr. Volatiles were removed *in vacuo* before extraction into EtOAc (20 mL) and washed with water (3 x 20 mL) and brine (20 mL) before drying over $MgSO_4$. Purification was achieved by flash column chromatography (EtOAc:hexane) followed by recrystallisation ($CHCl_3$/hexane) to give N-[3-(methylcarbamoyl)thiophen-2-yl]pyridine-4'-carboxamide (**116**) (0.043 g, 26 %) as an off white solid melting point 230–231 °C. ν_{max} (ATR) 3297 (N–H), 3088 (N–H), 1658 (C=O), 1627 (C=O) cm^{-1}. δ_H (599 MHz, $CDCl_3$) 13.28 (1H, s, C2-N*H*), 8.80-8.88 (2H, m, 2'-*H*), 7.88 (2H, d, *J* 5.9, 3'-*H*), 7.00 (1H, d, *J* 5.8, 4-*H*), 6.90 (1H, d, *J* 5.8, 5-*H*), 6.13 (1H, s, N*H*-CH_3), 3.04 (3H, d, *J* 4.9, C*H*$_3$). δ_C (151 MHz, $CDCl_3$) 166.4 (CH_3-*C*=O),

161.9 (4'-*C*=O), 151.1 (*C*-2'), 146.6 (*C*-2), 139.6 (*C*-4'), 121.2 (*C*-3'), 120.6 (*C*-4), 117.7 (*C*-5), 115.6 (*C*-3), 26.5 (*C*H_3). *m/z* (LC-MS ES^+) 262.2 $[M+H]^+$. HRMS (ES^+) found $[M+H]^+$ 262.0658, $C_{12}H_{12}N_3O_2S$ requires *M* 262.0650. CHN found: C 54.69; H 4.20; N 15.96. $C_{12}H_{11}N_3O_2S$ requires C 55.16 H 4.24; N 16.08.

N-[3-(methylcarbamoyl)thiophen-2-yl]pyridine-3'-carboxamide (117)

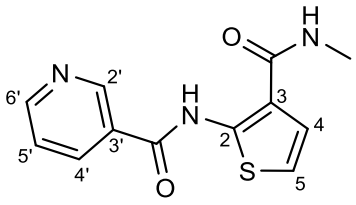

Pyridine-3-carbonyl chloride (0.11 g, 0.77 mmol, 1.2 eq.) dissolved in dry DMF (3 mL) was added to 2-amino-*N*-methylthiophene-3-carboxamide (**30**) (0.10 g, 0.64 mmol, 1.0 eq.) and triethylamine (0.089 mL, 1.9 mmol, 2.5 eq.) dissolved in dry THF (3 mL) at 0 °C under argon and the reaction was stirred at RT for 19 hrs. Volatiles were removed *in vacuo* and the residue was extracted into EtOAc (20 mL) and washed with water (4 x 20 mL) and brine (1 x 20 mL) before drying over $MgSO_4$. The solvent was removed *in vacuo* and the resulting solid was purified by trituration in DCM and water to give N-[3-(methylcarbamoyl)thiophen-2-yl]pyridine-3'-carboxamide (**117**) as an off-white semi-solid (0.016 g, 10 %). ν_{max} (ATR) 3315 (N–H), 3088 (N–H), 1656 (C=O), 1630 (C=O). δ_H(599 MHz, DMSO-d_6) 13.49 (1H, s, 2-N*H*), 9.10 (1H, d, *J* 2.3, 2'-*H*), 8.84 (1H, dd, *J* 4.8 *J* 1.8, 6'-*H*), 8.56 (1H, d, *J* 4.7, CH_3-N*H*), 8.26-8.28 (1H, m, 4'-*H*), 7.67 (1H, ddd, *J* 7.9 *J* 4.8 *J* 0.9, 5'-*H*), 7.48 (1H, d, *J* 5.8, 4-*H*), 7.11 (1H, d, *J* 5.8, 5-*H*), 2.83 (3H, d, *J* 4.7, C*H*$_3$). δ_C(176 MHz, DMSO-d_6) 165.6 (3-*C*=O), 161.1 (3'-*C*=O), 153.1 (*C*-6'), 148.1 (*C*-2'), 145.1 (*C*-2), 134.8 (*C*-4'), 128.0 (*C*-3'), 124.2 (*C*-5'), 122.4 (*C*-4), 117.1 (*C*-5), 116.1 (*C*-3), 25.8 (*C*H_3). *m/z* (LC-MS ES^+) 262.2 $[M+H]^+$. HRMS (ES^+) found $[M+H]^+$ 262.0660, $C_{12}H_{12}N_3O_2S$ requires *M* 262.0650.

***N*-methyl 2-(4'-nitrobenzamido)thiophene-3-carboxamide (118)**

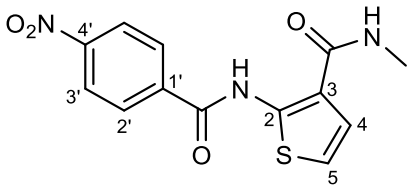

Following general procedure **C**, using THF (10 mL) as a reaction solvent for 72 hrs, where the acid chloride was 4-nitrobenzoyl chloride (0.29 g, 1.54 mmol, 1.2 eq.) and the substituted amine was 2-amino-*N*-methylthiophene-3-carboxamide (**30**) (0.20 g, 1.3 mmol, 1.0 eq.) afforded, following removal of volatiles from the filtrate, purification by flash column chromatography (EtOAc: hexane) and recrystallisation (EtOAc: hexane), *N*-methyl-2-(4'-nitrobenzamido)thiophene-3-carboxamide (**118**) as a yellow solid (0.013 g, 3 %) melting point 276 – 277 °C. ν_{max} (ATR) 3405 (N–H), 3117 (N–H), 1662 (C=O), 1619 (C=O), 1560, 1352 cm^{-1}. δ_H (700 MHz, DMSO- d_6) 13.59 (1H, s, 2-N*H*), 8.60 (1H, d, *J* 4.7, CH_3NH), 8.47 (2H, d, *J* 8.8, 3'-*H*), 8.17 (2H, d, *J* 8.8, 2'-*H*), 7.50 (1H, d, *J* 5.8, 4-*H*), 7.14 (1H, d, *J* 5.8, 5-*H*), 2.84 (3H, d, *J* 4.7, CH_3). δ_C (176 MHz, DMSO- d_6) 165.6 (3-*C*=O), 160.9 (1'-*C*=O), 149.7 (*C*-1'), 145.0 (*C*-2), 137.2 (*C*-4'), 128.6 (*C*-2'), 124.4 (*C*-3'), 122.4 (*C*-4), 117.2 (*C*-5), 116.2 (*C*-3), 25.8 (CH_3). *m/z* (LC-MS ES^+) 306.1 $[M+H]^+$. HRMS (ES^+) found $[M+H]^+$ 306.0552, $C_{13}H_{12}N_3O_4S$ requires *M* 306.0549.

***N*-methyl-2-(3'-nitrobenzamido)thiophene-3-carboxamide (119)**

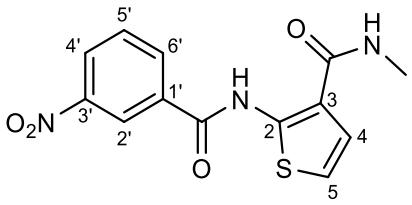

Following general procedure **C**, using THF (8 mL) as a reaction solvent for 3 hrs, where the acid chloride was 3-nitrobenzoyl chloride (0.29 g, 1.54 mmol, 1.3 eq.) and the substituted amine was 2-amino-*N*-methylthiophene-3-carboxamide (**30**) (0.20 g, 1.3 mmol, 1.0 eq.), afforded *N*-methyl-2-(3'-nitrobenzamido)thiophene-3-carboxamide (**119**) as a yellow solid (0.032 g, 9 %) melting point 260 – 261 °C. ν_{max} (ATR) 3449 (N–H), 3431 (N–H), 1660 (C=O), 1620 (C=O), 1550, 1357 cm^{-1}. δ_H (599 MHz, DMSO-d_6)

13.60 (1H, s, 2-N*H*), 8.65–8.68 (1H, m, 5'-*H*), 8.58 (1H, s, N*H*-CH_3), 8.50 (1H, d, *J* 8.2, 4'-*H*), 8.31-8.34 (1H, m, 6'-*H*), 7.92-7.97 (1H, m, 2'-*H*), 7.49 (1H, d, *J* 5.8, 4-*H*), 7.12 (1H, d, *J* 5.8, 5-*H*), 2.84 (3H, d, *J* 4.5, NH-CH_3). δ_C (151 MHz, DMSO-d_6) 165.6 (3-*C*=O), 160.4 (1'-*C*=O), 148.2 (*C*-1'), 145.0 (*C*-2), 133.6 (*C*-3'), 132.9 (*C*-6'), 131.1 (*C*-2'), 127.0 (*C*-4'), 122.4 (*C*-4), 121.9 (*C*-5'), 117.3 (*C*-5), 116.3 (*C*-3), 25.8 (*C*H_3). *m/z* (LC-MS ES^+) 306.1 $[M+H]^+$. HRMS (ES^+) found $[M+H]^+$ 306.0554, $C_{13}H_{12}N_3O_4S$ requires *M* 306.0549. CHN found: C 51.16; H 3.69; N 13.56. $C_{13}H_{11}N_3O_4S$ requires C 51.14; H 3.63; N 13.76.

5'-Amino-N-[3-(methylcarbamoyl)thiophen-2'-yl]thiophene-2-carboxamide (120)

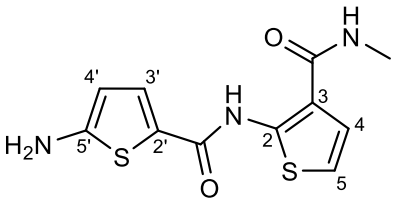

Pd/C (0.070 g, 0.6 mmol, 0.5 eq.) was wet with a catalytic amount of EtOAc and degassed before *N*-methyl-2-(5'-nitrothiophene-2'-amido)thiophene-3-carboxamide (**17**) (0.40 g, 1.3 mmol, 1.0 eq.) in MeOH (8 mL) was added. The reaction was stirred under a H_2 atmosphere (balloon pressure) for 27 hrs before filtering through Celite and removing volatiles *in vacuo*. Purification by flash column chromatography ($CHCl_3$:MeOH) gave 5'-amino-N-[3-(methylcarbamoyl)thiophen-2'-yl]thiophene-2-carboxamide (**120**) as a brown semi-solid (0.15 g, 42 %). ν_{max} (ATR) 3039-3463 (br, NH_2), 1624 (C=O), 1607 (C=O) cm^{-1}. δ_H(700 MHz, MeOD) 7.42 (1H, d, *J* 4.1, 3'-H), 7.23 (1H, d, *J* 5.9, 4-*H*), 6.82 (1H, d, *J* 5.9, 5-*H*), 6.08 (1H, d, *J* 4.1, 4'-H), 2.91 (3H, s, CH_3). δ_C(176 MHz, MeOD) 168.2 (3-*C*=O), 164.4 (2'-*C*=O), 160.7 (*C*-5'), 148.0 (*C*-2), 133.0 (*C*-3'), 122.7 (*C*-4), 118.3 (*C*-2'), 117.0 (*C*-5), 115.4 (*C*-3), 107.0 (*C*-4'), 26.3 (*C*H_3). *m/z* (LC-MS ES^+) 282.2 $[M+H]^+$. HRMS (ES^+) found $[M+H]^+$ 282.0377, $C_{11}H_{12}N_3O_2S_2$ requires *M* 282.0371.

2-Nitrothiazole-5-carboxylic acid (122)

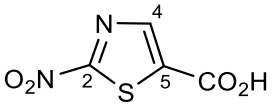

2-Aminothiazole-5- carboxylic acid (0.50 g, 3.5 mmol, 1.0 eq.) was dissolved in 50 % aqueous tetrafluoroboric acid (3.0 mL, 17.3 mmol, 5.0 eq.). The solution was cooled to 0 °C before sodium nitrite (0.24 g, 3.5 mmol, 1.0 eq.) was added gradually. This solution was stirred at 0 °C for 50 mins before being slowly added to a suspension of copper powder (0.80 g, 12.6 mmol, 3.6 eq.) in 30 % aqueous sodium nitrite (10 mL) at 25 °C. The reaction mixture was stirred at RT for 1 hr, filtered and diluted with water. [95] The water layer was washed with EtOAc before acidification with 3M HCl. The product was then extracted into EtOAc, dried over $MgSO_4$ and solvent was removed *in vacuo* to give 2-nitrothiazole-5-carboxylic acid (**122**) as a yellow solid (0.19 g, 32 %) melting point 142–143 °C (lit. 146–150 °C).[95] ν_{max} (ATR) 3101 (O–H),1690 (C=O), 1515, 1308 cm^{-1}. δ_H(400 MHz, CD_3OD) 8.38 (1H, s, 4-*H*). δ_C(101 MHz, CD_3OD) 169.7 (*C*=O), 162.1 (*C*-2), 147.0 (*C*-4), 138.6 (*C*-5). *m/z* (LC-MS ES^-) 173.1 [M – H]$^-$.

2-Chlorothiazole-5-carbonyl chloride (123)

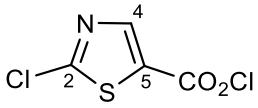

Following general procedure **A** for 4 hrs, where the acid was 2-nitrothiazole-5-carboxylic acid (**122**) (0.17 g, 0.98 mmol, 1.0 eq.) afforded, following filtering and removing volatiles, 2-chlorothiazole-5-carbonyl chloride (**123**) and an orange semi-solid (0.17 g, 88 %). ν_{max} (ATR) 1704 (C=O). δ_H(400 MHz, DMSO-d_6) 8.24 (1H, s, 4-*H*). δ_C(101 MHz, DMSO-d_6) 160.9 (*C*=O), 155.3 (*C*-2), 146.6 (*C*-4), 132.9 (*C*-5).

N-[3-(methylcarbamoyl)thiophen-2-yl]-2'-chloro-1',3'-thiazole-5'-carboxamide (124)

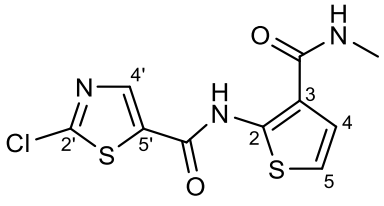

2-Chlorothiazole-5-carbonyl chloride (**123**) (0.17 g, 0.89 mmol, 1.1 eq.) in dry THF (1 mL) was added to a solution of 2-amino-*N*-methylthiophene-3-carboxamide (**30**) (0.13 g, 0.81 mmol, 1.0 eq.) and triethylamine (0.28 mL, 2.1 mmol, 2.5 eq.) in THF at 0 °C under argon and the reaction was stirred at RT for 20 hrs. Volatiles were removed *in vacuo* and the residue was extracted into EtOAc, washed with 1 M HCl and then extracted into 1M NaOH. The basic layer was washed with EtOAc and reacidified to pH 5 and extracted into EtOAc. The organic layer was washed with brine and dried over $MgSO_4$. Volatiles were removed *in vacuo* and the crude product was purified by flash column chromatography (EtOAc/hexane) followed by recrystallisation ($CHCl_3$/hexane) to give N-[3-(methylcarbamoyl)thiophen-2-yl]-2'-chloro-1',3'-thiazole-5'-carboxamide (**124**) as a yellow solid (0.008 g, 3 %) melting point 210 – 211 °C. ν_{max} (ATR) 3337 (N–H), 1667 (C=O), 1621 (C=O) cm^{-1}. δ_H(700 MHz, $CDCl_3$) 13.07 (1H, s, 2-N*H*), 8.18 (1H, s, 4'-*H*) 6.97 (1H, d, *J* 5.9, 4-*H*), 6.87 (1H, dd, *J* 5.9, *J* 0.8, 5-*H*), 6.01 (1H, s, CH_3-N*H*), 3.04 (3H, d, *J* 4.9, CH_3). δ_C(176 MHz, $CDCl_3$) 166.3 (3-*C*=O), 156.9 (*C*-2'), 156.2 (5'-*C*=O), 146.2 (*C*-2), 142.8 (*C*-4'), 135.7 (*C*-5'), 120.5 (*C*-4), 117.7 (*C*-5), 115.3 (*C*-3), 25.5 (*C*H_3). *m/z* (LC-MS ES^+) 302.2 $[M+H]^+$. HRMS (ES^+) found $[M+H]^+$ 301.9828, $C_{10}H_9N_3O_2S_2Cl$ requires 301.9825.

2-{[(Tert-butoxy)carbonyl]amino}-1,3-thiazole-5-carboxylic acid (126)

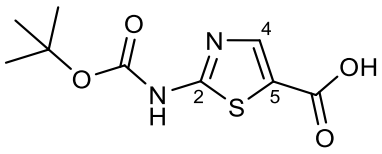

2-Aminothiazole-5-carboxylic acid (1.00 g, 6.9 mmol, 1.0 eq.) was dissolved in 2M NaOH (5.2 mL, 8.3 mmol, 1.5 eq.) and water (10 mL) before addition of Boc_2O (1.82 g, 8.3 mmol, 1.2 eq.) in THF (10 mL) at 0 °C. The mixture was stirred at RT for 24 hrs before acidification with 1M HCl to pH 4. The resulting suspension was stirred for 1hr before filtering to give 2-{[(tert-butoxy)carbonyl]amino}-1,3-thiazole-5-carboxylic acid (**126**) as an off-white solid (0.99 g, 58 %) melting point 220 – 221 °C. ν_{max} (ATR) 2356 – 3180 (N-H, O-H), 1732 (C=O), 1669 (C=O) cm^{-1}. δ_H(700 MHz, DMSO-d_6) 13.03 (1H, s, N*H* or O*H*), 11.89 (1H, s, N*H* or O*H*), 7.94 (1H, s, 4-*H*), 1.49 (9H, s, CH_3). δ_C(176

MHz, DMSO-d_6) 164.0 (*C*=ONH), 162.8 (*C*=OOH), 152.9 (*C*-5), 144.9 (*C*-4), 121.9 (*C*-2), 81.9 (*C*-CH_3), 27.8 (*C*H_3). *m/z* (LC-MS ES^+) 245.3 $[M+H]^+$.

Ethyl 2-aminocyclopent-1-ene-1-carboxylate (129) [97]

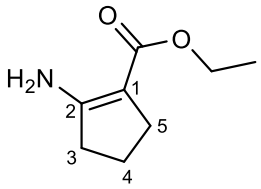

Ammonium acetate (7.70 g, 100 mmol, 5 eq.) was added to a solution of ethyl 2-oxocyclopentanecarboxylate (3.0 mL, 20 mmol, 1 eq.) and tetraethylorthosilicate (8.9 mL, 40 mmol, 2 eq.) in absolute EtOH (100 mL). The reaction mixture was refluxed under argon for 5 hours. Volatiles were removed *in vacuo* and the residue was purified by flash column chromatography (8:2 hexane: EtOAc, 1 % triethylamine) to give ethyl 2-aminocyclopent-1-ene-1-carboxylate (**129**) as a pale yellow solid (3.01 g, 97 %) melting point 50-51 °C (lit. 48 – 49 °C)[204]. ν_{max} (ATR) 3444 (N–H), 3331 (N–H), 1649 (C=O), 1625 (C=C). δ_H (700 MHz, $CDCl_3$) 4.16 (2H, q, *J* 7.1, OCH_2), 2.52 (2H, tt, *J* 7.1, *J* 1.1, 5-*H*), 2.48 (2H, tt, *J* 7.4, *J* 1.1, 3-*H*), 1.80-1.84 (2H, m, 4-*H*), 1.27 (3H, t, *J* 7.1, CH_3). δ_C (176 MHz, $CDCl_3$) 168.3 (*C*=O), 161.7 (*C*-2), 95.8 (*C*-1), 58.8 (O*C*H_2), 35.3 (*C*-3), 29.7 (*C*-5), 20.9 (*C*-4), 14.9 (*C*H_3). *m/z* (LC-MS ES^+) 156.8 $[M+H]^+$.

± Ethyl 2-aminocyclopentane-1-carboxylate (130) [98]

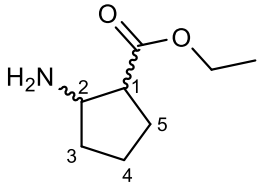

Sodium cyanoborohydride (1.21 g, 19.3 mmol, 3 eq.) and glacial acetic acid (1.1 mL, 19.3 mmol, 3 eq.) were added to a solution of ethyl 2-aminocyclopent-1-ene-1-carboxylate (**129**) (1.00 g, 6.4 mmol, 1 eq.) in EtOAc (20 mL) at 0 °C. The reaction mixture was stirred at 0 °C for 1 hr before dilution with EtOAc (100 mL). The organic extract was washed with 10 % sodium carbonate solution (3 x 30 mL) and dried over $MgSO_4$ before solvent was removed *in vacuo* to give a 8:2 anti:syn mixture of ethyl

2-aminocyclopentane-1-carboxylate (**130**) as an orange oil (0.92 g, 92 %). ν_{max} (ATR) 2992 (N–H), 2961 (N–H), 1720 (C=O) cm^{-1}. δ_H (anti, 700 MHz, $CDCl_3$) 4.16 (2H, q, *J* 7.3, CH_3-C*H*$_2$), 3.40-3.44 (1H, m, 2-*H*), 3.04 (2H, s, N*H*$_2$), 2.46-2.49 (1H, m, 1-*H*), 2.03-2.07 (2H, m, 4-*H*), 1.81-1.87 (2H, m, 5-*H*), 1.41-1.47 (2H, m, 3-*H*), 1.27 (3H, t, *J* 7.3, C*H*$_3$). δ_C (anti, 176 MHz, $CDCl_3$) 175.8 (*C*=O), 61.2 (CH_3-*C*H_2), 56.7 (*C*-2), 52.5 (*C*-1), 35.1 (*C*-3), 28.1 (*C*-4), 22.6 (*C*-5), 14.3 (*C*H_3). *m/z* (LC-MS ES^+) 158.2 $[M+H]^+$.

± Ethyl-2-(5'-nitrothiophene-2'-amido)cyclopentane-1-carboxylate (131 & 132)

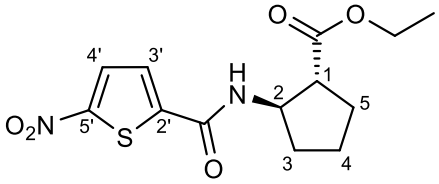

131
racemic

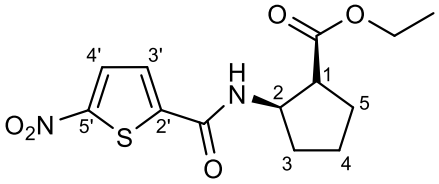

132
racemic

DIPEA (3.0 mL, 16.9 mmol, 3.0 eq.) was added to a solution of 5-nitrothiophene-2-carboxylic acid (0.99 g, 5.7 mmol, 1.0 eq.) in DMF (8 mL). The solution was cooled to 0 °C and treated with EDCI (2.17 g, 11.3 mmol, 2.0 eq.), HOBt (1.73 g, 11.3 mmol, 2.0 eq.) and a mixture of anti:syn (8:2) ethyl 2-aminocyclopentane-1-carboxylate (**130**) (1.09 g, 6.9 mmol, 1.2 eq.). The reaction mixture was stirred at RT for 20 hours before dilution with EtOAc (70 mL) and washing with water (3 x 50 mL). The EtOAc layer was dried over $MgSO_4$ and purified by flash column chromatography (hexane: EtOAc) to give *anti*-ethyl-2-(5'-nitrothiophene-2'-amido)cyclopentane-1-carboxylate (**131**) as a yellow solid (0.53 g, 30 %) melting point 111-112 °C. ν_{max} (ATR) 3325 (N–H), 1731 (C=O), 1634 (C=O), 1511, 1338 cm^{-1}. δ_H (599 MHz, $CDCl_3$) 7.83 (1H, d, *J* 4.4, 4'-*H*), 7.41 (1H, d, *J* 4.4, 3'-*H*), 6.69 (1H, s, N*H*), 4.48-4.53 (1H, m, 2-*H*), 4.13 (2H, q, *J* 7.2, CH_3-C*H*$_2$), 2.74-2.78 (1H, m, 1-*H*), 2.21-2.26 (1H, m, 3-*H*), 2.04-2.08 (1H, m, 5-*H*), 1.89-1.95 (1H, m, 5-*H*), 1.76-1.81 (2H, m, 4-*H*), 1.61-1.67 (1H, m, 3-*H*), 1.22 (3H, t, *J* 7.2, C*H*$_3$). δ_C (151 MHz, $CDCl_3$) 174.4 (O*C*=O), 160.0 (NH*C*=O), 154.2 (*C*-2'), 145.2 (*C*-5'), 128.4 (*C*-4'), 126.2 (*C*-3'), 61.0 (CH_3-*C*H_2), 55.6 (*C*-2), 50.5 (*C*-1), 32.8 (*C*-3), 28.5 (*C*-5), 23.2 (*C*-4), 14.3 (*C*H_3). *m/z* (LC-MS ES^+) 313.2 $[M+H]^+$. HRMS (ES^+) found $[M+H]^+$ 313.0862, $C_{13}H_{17}N_2O_5S$ requires *M* 313.0858. CHN found: C 50.17; H 5.23; N 9.05. $C_{13}H_{16}N_2O_5S$ requires C 49.99; H 5.16; N 8.97. Flash column chromatography followed by

recrystallisation (DCM: hexane) also gave *syn*-ethyl-2-(5'-nitrothiophene-2'-amido)cyclopentane-1-carboxylate (**132**) as an off-white solid (0.096 g, 5 %) melting point 109 – 110 °C. ν_{max} (ATR) 3333 (N–H), 1730 (C=O), 1640 (C=O), 1511, 1341 cm^{-1}. δ_H (700 MHz, $CDCl_3$) 7.84 (1H, d, *J* 4.3, 4'-*H*), 7.35-7.36 (1H, m, N*H*), 7.33 (1H, d, *J* 4.3, 3'-*H*), 4.55-4.59 (1H, m, 2-*H*), 4.12-4.19 (2H, m, C*H*$_2$–CH_3), 3.03 (1H, dt, *J* 8.4, *J* 6.7, 1-*H*), 2.12-2.14 (1H, m, 3-*H*), 2.00-2.09 (2H, m, 4-*H*), 1.86-1.89 (1H, m, 5-*H*), 1.79-1.83 (1H, m, 3-*H*), 1.67-1.73 (1H, m, 5-*H*), 1.26 (3H, t, *J* 7.1, C*H*$_3$). δ_C (176 MHz, $CDCl_3$) 175.5 (O*C*=O), 159.6 (NH*C*=O), 154.3 (*C*-2'), 145.4 (*C*-5'), 128.3 (*C*-4'), 125.8 (*C*-3'), 61.2 (CH_3-*C*H_2), 52.7 (*C*-2), 46.0 (*C*-1), 32.3 (*C*-3), 29.1 (*C*-4), 22.5 (*C*-5), 14.3 (*C*H_3). *m/z* (LC-MS ES^+) 313.1 $[M+H]^+$. HRMS (ES^+) found $[M+H]^+$ 313.0863, $C_{13}H_{17}N_2O_5S$ requires *M* 313.0858. CHN found: C 49.11; H 5.08; N 8.73. $C_{13}H_{16}N_2O_5S$ requires C 49.99; H 5.16; N 8.97.

± Anti 2-(5'-nitrothiophene-2'-amido)cyclopentane-1-carboxylic acid (133)

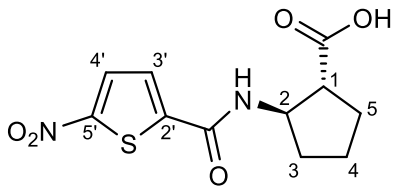

racemic

± Anti ethyl-2-(5'-nitrothiophene-2'-amido)cyclopentane-1-carboxylate (**131**) (0.11 g, 0.35 mmol, 1.0 eq.) was dissolved in MeOH (3 mL) before 1M LiOH (1.8 mL, 1.76 mmol, 5.0 eq.) was added at 0 °C under argon. The reaction mixture was stirred at 0 °C for 7 hours, before acidification to pH 7. MeOH was removed *in vacuo* and the remaining solution was acidified further to pH 2, before extraction into EtOAc (3 x 30 mL). The organic layer was washed with brine (2 x 30 mL) and dried over $MgSO_4$. Solvent was removed *in vacuo* to give ± anti 2-(5'-nitrothiophene-2'-amido)cyclopentane-1-carboxylic acid (**133**) (0.080 g, 88 %) as an off white solid, melting point 229–230 °C. ν_{max} (ATR) 3314 (O–H), 1702 (C=O), 1628 (C=O), 1508, 1314 cm^{-1}. δ_H (700 MHz, CD_3OD) 7.96 (1H, d, *J* 4.3, 4'-*H*), 7.68 (1H, d, *J* 4.3, 3'-*H*), 4.54-4.57 (1H, m, 2-*H*), 2.81-2.85 (1H, m, 1-*H*), 2.14-2.18 (1H, m, 3-*H*), 2.08-2.13 (1H, m, 5-*H*), 1.89-1.93 (1H, m, 5-*H*), 1.76-1.87 (2H, m, 4-*H*), 1.65-1.71 (1H, m, 3-*H*). δ_C (176 MHz,

CD_3OD) 178.2 (O-*C*=O), 162.0 (N-*C*=O), 155.4 (*C*-2'), 146.7 (*C*-5'), 129.8 (*C*-4'), 128.1 (*C*-3'), 56.4 (*C*-2), 51.0 (*C*-1), 33.5 (*C*-3), 30.0 (*C*-5), 24.4 (*C*-4). *m/z* (LC-MS ES^+) 285.2 $[M+H]^+$. HRMS (ES^+) found $[M+H]^+$ 285.0560, $C_{11}H_{13}N_2O_5S$ requires *M* 285.0545. CHN found: C 46.66; H 4.49; N 9.35. $C_{11}H_{12}N_2O_5S$ requires C 46.47; H 4.25; N 9.85.

± Syn 2-(5'-nitrothiophene-2'-amido)cyclopentane-1-carboxylic acid (134)

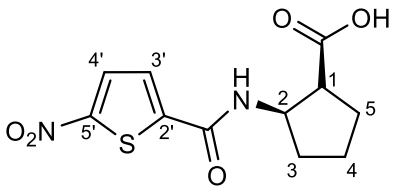

racemic

± Syn ethyl-2-(5'-nitrothiophene-2'-amido)cyclopentane-1-carboxylate (**132**) (0.055 g, 0.2 mmol, 1.0 eq.) was dissolved in MeOH (2 mL) before 1M LiOH (1.1 mL, 1.1 mmol, 5.0 eq.) was added at 0 °C under argon. The reaction mixture was stirred at 0 °C for 5 hours, before acidification to pH 7. MeOH was removed *in vacuo* and the remaining solution was acidified further to pH 2, before extraction into EtOAc (3 x 30 mL). The organic layer was washed with brine (2 x 30 mL) and dried over $MgSO_4$. Volatiles were removed *in vacuo* to give ± syn 2-(5'-nitrothiophene-2'-amido)cyclopentane-1-carboxylic acid (**134**) (0.05 g, 88 %) as an off white solid, melting point 201–202 °C. ν_{max} (ATR) 3316 (O–H), 3097 (N–H), 1698 (C=O), 1620 (C=O), 1558, 1344 cm^{-1}. δ_H(599 MHz, CD_3OD) 7.95 (1H, d, *J* 4.4, 4'-*H*), 7.68 (1H, d, *J* 4.4, 3'-*H*), 4.60 (1H, q, *J* 7.6, 2-*H*), 3.11 (1H, q, *J* 7.6, 1-*H*), 2.05–2.11 (2H, m, aliph-*H*), 1.84–2.00 (3H, m, aliph-*H*), 1.62–1.70 (1H, m, aliph-*H*). δ_C(151, CD_3OD) 177.2 (HO-*C*=O), 162.1 (5'-*C*=O), 155.3 (*C*-2'), 146.6 (*C*-5'), 129.7 (*C*-4'), 128.3 (*C*-3'), 54.6 (*C*-2), 48.4 (*C*-1), 31.9 (*C*-aliph), 28.8 (*C*-aliph), 23.5 (*C*-aliph). *m/z* (LC-MS ES^+) 285.5 $[M+H]^+$. HRMS (ES^+) found $[M+H]^+$ 285.0557, $C_{11}H_{13}N_2O_5S$ requires 285.0545.

N-[± 2'-(methylcarbamoyl)cyclopentyl]-5'-nitrothiophene-2-carboxamide (135)

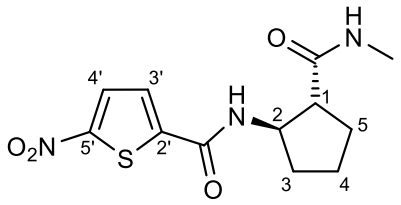

racemic

± Anti 2-(5'-nitrothiophene-2'-amido)cyclopentane-1-carboxylic acid (**133**) (0.100 g, 0.35 mmol, 1.0 eq.), methylamine (2.0 M in THF, 0.3 mL, 0.62 mmol, 5.0 eq.) and triethylamine (0.05 mL, 0.25 mmol, 2.0 eq.) were dissolved in DMA (2 mL). PyBOP (0.078 g, 0.15 mmol, 1.2 eq.) was added and the reaction mixture was stirred at RT for 1.5 hrs. The reaction mixture was diluted with water (10 mL) and extracted into EtOAc (20 mL) and washed with water (3 x 20 mL), $NaHCO_3$ (3 x 20 mL) and brine (1 x 20 mL). The organic extract was dried over $MgSO_4$ and solvent was removed *in vacuo*. Trituration in EtOAc (1 mL) gave N-[± 2'-(methylcarbamoyl)cyclopentyl]-5'-nitrothiophene-2-carboxamide (**135**) as an off white solid (0.037 g, 36 %) melting point 251–252 °C. ν_{max} (ATR) 3355 (N–H), 3274 (N–H), 1638 (C=O), 1567 (C=O), 1506, 1315 cm^{-1}. δ_H (700 MHz, DMSO-d_6) 8.84 (1H, d, *J* 7.6, 2-N*H*), 8.13 (1H, d, *J* 4.4, 4'-*H*), 7.82 (1H, d, *J* 4.4, 3'-*H*), 7.72 (1H, d, *J* 4.7, CH_3-N*H*), 4.35 (1H, m, 2-*H*), 2.66 (1H, m, 1-*H*), 2.55 (3H, d, *J* 4.7, CH_3), 1.90–1.99 (2H, m, aliph-*H*), 1.58-1.74 (4H, m, aliph-*H*). δ_C(176 MHz, DMSO-d_6) 173.8 (1-*C*=O), 159.0 (5'-*C*=O), 152.8 (*C*-2'), 146.7 (*C*-5'), 130.1 (*C*-4'), 127.3 (*C*-3'), 54.5 (*C*-2), 50.2 (*C*-1), 32.4 (*C*-aliph), 29.4 (*C*-aliph), 25.6 (*C*H_3), 23.7 (*C*-aliph). *m/z* (LC-MS ES^+) 298.2 $[M+H]^+$. HRMS (ES^+) found $[M+H]^+$ 298.0871, $C_{12}H_{16}N_3O_4S$ requires *M* 298.0862. CHN found: C 48.38; H 5.15; N 13.97. $C_{12}H_{15}N_3O_4S$ requires C 48.47 H 5.08; N 14.13.

Ethyl 2-(5'-nitrothiophene-2'-amido)cyclopent-1-ene-1-carboxylate (136)

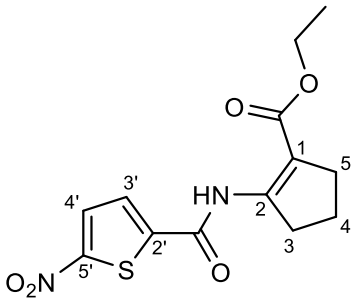

Following general procedure **Gi**, using THF (10 mL) as a reaction solvent for 44 hr, where the substituted amine was 2-aminocyclopent-1-ene-1-carboxylate (**129**) (0.40 g, 2.6 mmol, 1.0 eq.) afforded, following purification by flash column chromatography (EtOAc:hexane), ethyl 2-(5'-nitrothiophene-2'-amido)cyclopent-1-ene-1-carboxylate (**136**) as a yellow solid (0.072 g, 9 %), melting point 146-148 °C. ν_{max} (ATR) 3090 (N-H), 1673 (C=O), 1633 (C=O), 1534, 1333 cm^{-1}. δ_H (599 MHz, $CDCl_3$) 11.49 (1H, s, N*H*), 7.88 (1H, d, *J* 4.3, 4'-*H*), 7.55 (1H, d, *J* 4.3, 3'-*H*), 4.26 (2H, q, *J* 7.1, O*CH*$_2$), 3.23 (2H, tt, *J* 7.7 *J* 2.2, 3-*H*), 2.53-2.59 (2H, m, 5-*H*), 1.93-2.01 (2H, m, 4-*H*), 1.33 (3H, t, *J* 7.1, C*H*$_3$). δ_C (151 MHz, $CDCl_3$) 168.5 (1-*C*=O), 157.7 (2'-*C*=O), 155.3 (*C*-5'), 154.1 (*C*-2), 145.0 (*C*-2'), 128.4 (*C*-4'), 127.2 (*C*-3'), 110.5 (*C*-1), 60.6 (*C*H_2CH$_3$), 33.9 (*C*-3), 28.4 (*C*-5), 21.2 (*C*-4), 14.5 (*C*H_3). *m/z* (LC-MS ES^+) 311.3 $[M+H]^+$. HRMS (ES^+) found $[M+H]^+$ 311.0711, $C_{13}H_{15}N_2O_5S$ requires *M* 311.0702.

***N*-(2-carbamoylphenyl)-5'-nitrothiophene-2'-carboxamide (140)**

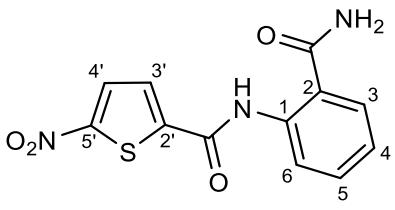

Following general procedure **C**, using THF (20 mL) as a reaction solvent, where the substituted amine is anthranilamide (0.21 g, 1.6 mmol, 1.0 eq.) afforded, following removal of volatiles from the filtrate and purification by flash column chromatography (EtOAc: hexane), *N*-(2-carbamoylphenyl)-5'-nitrothiophene-2'-carboxamide (**140**) as a yellow solid (0.18 g, 40 %) melting point 250 – 251 °C. ν_{max}

(ATR) 3494 (N-H), 3396 (N–H), 3058 (N–H), 1651 (C=O), 1617 (C=O), 1527, 1340 cm^{-1}. δ_H (599 MHz, DMSO-d_6) 13.37 (1H, s, 1-N*H*), 8.49-8.52 (2H, m, 3-*H* & 2-CON*H*), 8.21 (1H, d, *J* 4.4, 4'-*H*), 7.94 (2H, dd, *J* 7.9, *J* 1.4, 6-*H* & 2-CON*H*), 7.68 (1H, d, *J* 4.4, 3'-*H*), 7.58-7.61 (1H, m, 5-*H*), 7.23-7.25 (1H, m, 4-*H*). δ_C (151 MHz, DMSO-d_6) 171.0 (2-*C*=O), 157.6 (2'-*C*=O), 153.5 (*C*-2'), 146.1 (*C*-5'), 139.0 (*C*-1), 132.8 (*C*-4), 130.3 (*C*-4'), 128.8 (*C*-3), 127.3 (*C*-3'), 123.6 (*C*-5), 120.3 (*C*-6), 119.4 (*C*-2). *m/z* (LC-MS ES^+) 292.3 $[M+H]^+$. HRMS (ES^+) found $[M+H]^+$ 292.0412, $C_{12}H_{10}N_3O_4S$ requires *M* 292.0392. CHN found: C 49.60; H 3.09; N 14.33. $C_{12}H_9N_3O_4S$ requires C 49.48; H 3.11; N 14.43.

Amino-*N*-methyl-2-benzamide (138) [205]

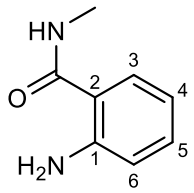

Methylamine (2.0 M in THF, 7.7 mL, 15.3 mmol, 5 eq.) and triethylamine (2.1 mL, 15.3 mmol, 5 eq.) were added to a solution of isatoic anhydride (0.50 g, 3.07 mmol, 1 eq.) in DMF (3 mL) at RT under argon. The reaction mixture was stirred at 40 °C for 2 hours, then quenched by pouring into water (10 mL). The product was extracted with EtOAc and washed with brine. The organic layer was dried over $MgSO_4$ and volatiles were removed *in vacuo* before purification by flash column chromatography (50:50 hexane: EtOAc) to yield amino-*N*-methyl-2-benzamide (**138**) as an off white solid (0.31 g, 68 %), melting point 78 – 79 °C (lit. 79 – 80 °C).[206] ν_{max} (ATR) 3454 (N–H), 3349 (N–H), 1624 (C=O) cm^{-1}. δ_H (700 MHz, $CDCl_3$) 7.29 (1H, dd, *J* 7.4, *J* 1.4, 6-*H*), 7.20 (1H, ddd, *J* 8.0, *J* 7.4, *J* 1.3, 5-*H*), 6.68 (1H, dd, *J* 7.9, *J* 1.3, 3-*H*), 6.64 (1H, ddd, *J* 8.0, *J* 7.9, *J* 1.4, 4-*H*), 6.05 (1H, s, N*H*-CH_3), 5.50 (2H, s, NH_2), 2.97 (3H, d, *J* 4.9, CH_3). δ_C (176 MHz, $CDCl_3$) 170.1 (*C*=O), 148.7 (*C*-1), 132.2 (*C*-5), 127.2 (*C*-6), 117.4 (*C*-3), 116.8 (*C*-4), 116.4 (*C*-2), 26.6 (*C*H_3). *m/z* (GCMS EI) 150.1 $[M]^+$.

***N*-[2-(methylcarbamoyl)phenyl]-5'-nitrothiophene-2'-carboxamide (141)**

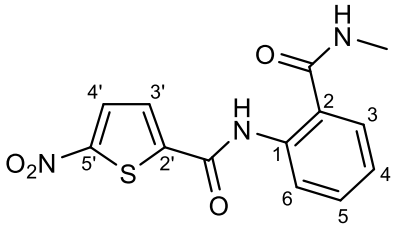

Following general procedure **C**, using DCM (8 mL) as a reaction solvent, where the substituted amine was *N*-[2'-(methylcarbamoyl)phenyl]-5'-nitrothiophene-2-carboxamide (**138**) (0.21 g, 1.4 mmol, 1.0 eq.) afforded, following trituration with water, EtOH and DCM, *N*-[2-(methylcarbamoyl)phenyl]-5'-nitrothiophene-2'-carboxamide (**141**) as a yellow solid (0.31 g, 63 %) melting point 228 – 229 °C. ν_{max} (ATR) 3428 (N–H), 3118 (N–H), 1666 (C=O), 1646 (C=O), 1507, 1325 cm^{-1}. δ_H (700 MHz, DMSO-d_6) 13.11 (1H, s, 1-N*H*), 8.94 (1H, d, *J* 4.7, CH_3N*H*), 8.46 (1H, dd, *J* 8.5, *J* 1.2, Ar-*H*), 8.21 (1H, d, *J* 4.3, 4'-*H*), 7.85 (1H, dd, *J* 7.8, *J* 1.5, Ar-*H*), 7.70 (1H, d, *J* 4.3, 3'-*H*), 7.58 (1H, ddd, *J* 8.5, *J* 7.5, *J* 1.5, Ar-*H*), 7.24 (1H, ddd, *J* 7.8, *J* 7.5, *J* 1.2, Ar-*H*), 2.83 (3H, d, *J* 4.7, C*H*$_3$). δ_c (176 MHz, DMSO-d_6) 168.8 (2-*C*=O), 157.6 (2'-C=O), 153.4 (*C*-2'), 146.0 (*C*-5'), 138.4 (*C*-Ar), 132.4 (*C*-Ar), 130.3 (*C*-4'), 128.1 (*C*-Ar), 127.3 (*C*-3'), 123.7 (*C*-Ar), 120.4 (*C*-Ar), 120.1 (*C*-Ar), 26.4 (*C*H_3). *m/z* (LC-MS ES$^+$) 306.1 $[M+H]^+$. HRMS (ES$^+$) found $[M+H]^+$ 306.0553, $C_{13}H_{12}N_3O_4S$ requires *M* 306.0549. CHN found: C 51.05; H 3.59; N 13.80 $C_{13}H_{11}N_3O_4S$ requires C 51.14; H 3.63; N 13.76.

2-(5'-Nitrothiophene-2'-amido)benzoic acid and 2-(5'-nitrothiophen-2'-yl)-4H-3,1-benzoxazin-4-one (143 & 144)

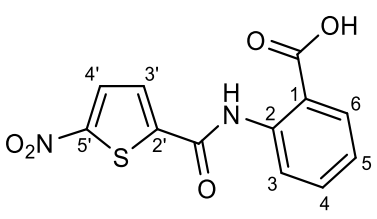

143

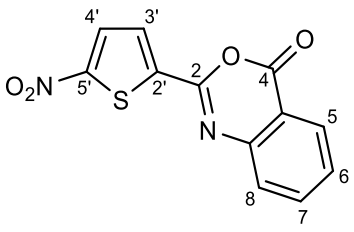

144

Following general procedure **Gi**, using THF (6 mL) as a reaction solvent, where the substituted amine was anthranilic acid (0.19 g, 1.4 mmol, 1.0 eq.) afforded, following work up with DCM and purification by flash column chromatography (DCM:MeOH),

the two title products. Fractions containing **143** were purified further by recrystallisation (MeOH) to give 2-(5'-nitrothiophene-2'-amido)benzoic acid (**143**) as an yellow solid (0.019 g, 5 %) melting point 239 – 240 °C. ν_{max} (ATR) 2700–3316 (O–H), 1679 (C=O), 1663 (C=O), 1538, 1255 cm^{-1}. δ_H(599 MHz, CD_3OD) 8.65 (1H, dd, *J* 8.3 *J* 1.4, 6-*H*), 8.14 (1H, dd, *J* 8.2 *J* 1.4, 3-*H*), 8.01 (1H, d, *J* 4.3, 4'-*H*), 7.70 (1H, d, *J* 4.3, 3'-*H*), 7.61 (1H, ddd, *J* 8.2 *J* 7.3 *J* 1.4, 4-*H*), 7.21 (1H, ddd, *J* 8.3 *J* 7.3 *J* 1.4, 5-*H*). δ_C(151 MHz, CD_3OD) 172.1 (1-*C*=O), 159.8 (2'-*C*=O), 155.9 (*C*-2'), 147.1 (*C*-5'), 141.9 (*C*-2), 135.5 (*C*-4), 132.8 (*C*-3), 130.0 (*C*-4'), 128.1 (*C*-3'), 124.7 (*C*-5), 121.2 (*C*-6), 117.7 (*C*-1). *m/z* (LC-MS ES^+) 293.1 $[M+H]^+$. HRMS (ES^+) found $[M+H]^+$ 293.0255, $C_{12}H_9N_2O_5S$ requires *M* 292.0232. CHN found: C 49.27; H 2.83; N 9.48. $C_{12}H_8N_2O_5S$ requires C 49.31; H 2.76; N 9.58. Fractions containing **144** were purified further by recrystallisation (DCM) to give 2-(5'-nitrothiophen-2'-yl)-4H-3,1-benzoxazin-4-one (**144**) as a yellow solid (0.010 g, 3 %) melting point 196-197 °C. ν_{max} (ATR) 1731–1780 (C=O, C=N), 1542, 1358 cm^{-1}. δ_H(599 MHz, $CDCl_3$) 8.25 (1H, ddd, *J* 8.0 *J* 1.3 *J* 0.6, 8-*H*), 7.93 (1H, d, *J* 4.3, 4'-*H*), 7.87 (1H, ddd, *J* 8.0 *J* 7.3 *J* 1.3, 7-*H*), 7.84 (1H, d, *J* 4.3, 3'-*H*), 7.69 (1H, ddd, *J* 8.0 *J* 1.3 *J* 0.6, 5-*H*), 7.59 (1H, ddd, *J* 8.0 *J* 7.3 *J* 1.3, 6-*H*). δ_C(151 MHz, $CDCl_3$) 158.1 (*C*-4), 155.3 (*C*-2'), 151.9 (*C*-2), 146.2 (6-*C*), 140.0 (*C*-5'), 137.2 (*C*-7), 129.7 (*C*-3'). 129.5 (*C*-6), 129.2 (*C*-8), 128.7 (*C*-4'), 127.6 (*C*-5), 117.2 (4-*C*). *m/z* (LC-MS ES^+) 275.2 $[M+H]^+$. HRMS (ES^+) found $[M+H]^+$ 275.0158, $C_{12}H_7N_2O_4S$ requires 275.0127.

_N_-methyl-3-[(5'-nitrothiophen-2'-yl)amino]benzamide (155)

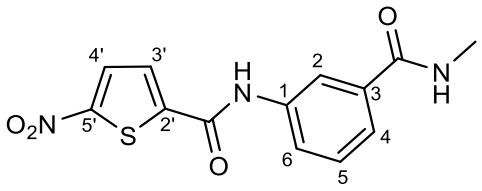

Following general procedure **C**, using THF (5 mL) as a reaction solvent, where the substituted amine was 3-amino-*N*-methyl benzamide (0.14 g, 0.94 mmol, 1.0 eq.), afforded *N*-methyl-3-[(5'-nitrothiophen-2'-yl)amino] benzamide (**155**) as a yellow solid (0.1076 g, 37 %) melting point 275-277 °C. ν_{max} (ATR) 3384 (N–H), 3258 (N–H), 1654 (C=O), 1639 (C=O), 1548, 1344 cm^{-1}. δ_H (700 MHz, DMSO-d_6) 10.79 (1H, s, 1-N*H*),

8.45-8.46 (1H, m, CH_3-N*H*), 8.22 (1H, d, *J* 4.5, 4'-*H*), 8.18-8.21 (1H, m, 2-*H*), 8.10 (1H, d, *J* 4.5, 3'-*H*), 7.93 (1H, ddd, *J* 8.2, *J* 2.3, *J* 1.1, 6-*H*), 7.61 (1H, ddd, *J* 7.9, *J* 2.5, *J* 1.1, 4-*H*), 7.46-7.48 (1H, m, 5-*H*), 2.79 (3H, d, *J* 4.5, C*H*$_3$). δ_c (176 MHz, DMSO-d_6) 166.2 (3-*C*=O), 158.3 (2'-*C*=O), 153.5 (*C*-2'), 146.1 (*C*-5'), 138.0 (*C*-1), 135.3 (*C*-3), 130.1 (*C*-4'), 128.8 (*C*-5), 128.5 (*C*-3'), 123.0 (*C*-6), 122.7 (*C*-4), 119.9 (*C*-2), 26.3 (*C*H_3). *m/z* (LC-MS ES$^+$) 306.1 $[M+H]^+$. HRMS (ES$^+$) found $[M+H]^+$ 306.0551, $C_{13}H_{12}N_3O_4S$ requires *M* 306.0549. CHN found: C 51.02; H 3.77; N 13.44 $C_{13}H_{11}N_3O_4S$ requires C 51.14; H 3.63; N 13.76.

5'-Nitro-*N*-phenylthiophene-2'-carboxamide (156)

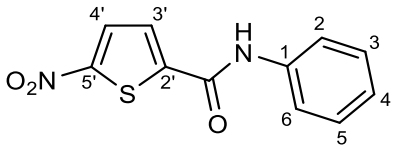

Following general procedure **C**, using THF (3 mL) as a reaction solvent, where the substituted amine was aniline (0.13 mL, 1.4 mmol, 1.0 eq.), afforded 5'-nitro-*N*-phenylthiophene-2'-carboxamide (**156**) as a yellow solid (0.053 g, 15 %) melting point 188 – 189 °C. ν_{max} (ATR) 3353 (N–H), 1656 (C=O), 1535, 1324 cm^{-1}. δ_H(700 MHz, DMSO-d_6) 10.64 (1H, s, N*H*), 8.21 (1H, d, *J* 4.4, 4'-*H*), 8.07 (1H, d, *J* 4.4, 3'-*H*), 7.72–7.73 (2H, m, 2-*H*), 7.38–7.40 (2H, m, 3-*H*), 7.17 (1H, tt, *J* 7.4 *J* 1.2, 4-*H*). δ_C(176 MHz, DMSO-d_6) 158.2 (*C*=O), 153.3 (*C*-2'), 146.4 (*C*-5'), 137.9 (*C*-1), 130.1 (*C*-4'), 128.8 (*C*-3), 128.3 (*C*-3') 124.6 (*C*-4), 120.6 (*C*-2). *m/z* (LC-MS ES$^+$) 249.2 $[M+H]^+$. HRMS (ES$^+$) found $[M+H]^+$ 249.0357, $C_{11}H_9N_2O_3S$ requires 249.0334. CHN found: C 53.19; H 3.29; N 11.19. $C_{12}H_{10}N_2O_4S$ requires C 53.22; H 3.25; N 11.28.

***N*-(2-methoxyphenyl)-5'-nitrothiophene-2'-carboxamide (157)**

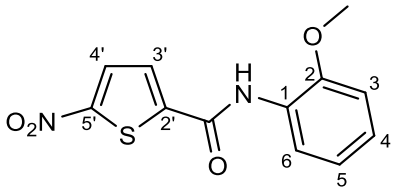

Following general procedure **C**, using THF (3 mL) as a reaction solvent, where the substituted amine was *o*-anisidine (0.25 mL, 2.2 mmol, 1.0 eq.), afforded *N*-(2-

methoxyphenyl)-5'-nitrothiophene-2'-carboxamide (**157**) as a yellow solid (0.092 g, 15 %) melting point 151 – 152 °C. ν_{max} (ATR) 3425 (N–H), 1662 (C=O), 1530, 1336 cm^{-1}. δ_H(700 MHz, DMSO-d_6) 10.13 (1H, s, N*H*), 8.19 (1H, d, *J* 4.4, 4'-*H*), 8.05 (1H, d, *J* 4.4, 3'-*H*), 7.54 (1H, dd, *J* 7.7 *J* 1.7, 6-*H*), 7.26 (1H, ddd, *J* 8.3 *J* 7.4 *J* 1.7, 4-*H*), 7.13 (1H, dd, *J* 8.3 *J* 1.3, 3-*H*), 6.99 (1H, ddd, *J* 7.7 *J* 7.4 *J* 1.3, 5-*H*), 3.83 (3H, s, C*H*$_3$). δ_C(176 MHz, DMSO-d_6) 158.3 (*C*=O), 153.2 (*C*-2'), 152.5 (*C*-2), 146.2 (*C*-5'), 130.1 (*C*-4'), 128.2 (*C*-3'), 127.2 (*C*-4), 126.1 (*C*-6), 125.1 (*C*-1), 120.2 (*C*-5), 111.8 (*C*-3), 55.7 (*C*H$_3$). *m/z* (LC-MS ES$^+$) 279.5 $[M+H]^+$. HRMS (ES$^+$) found $[M+H]^+$ 279.0466, $C_{12}H_{11}N_2O_4S$ requires 279.0440. CHN found: C 51.72; H 3.64; N 9.98. $C_{12}H_{10}N_2O_4S$ requires C 51.79; H 3.62; N 10.07

***N*-(3-methoxyphenyl)-5'-nitrothiophene-2'-carboxamide (158)**

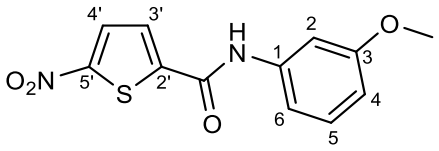

Following general procedure **C**, using THF (2 mL) as a reaction solvent, where the substituted amine was *m*-anisidine (0.11 mL, 0.95 mmol, 1.0 eq.), afforded *N*-(3-methoxyphenyl)-5'-nitrothiophene-2'-carboxamide (**158**) as a yellow solid (0.024 g, 9 %) melting point 180 – 181 °C. ν_{max} (ATR) 3335 (N–H), 1639 (C=O), 1539, 1342 cm^{-1}. δ_H(700 MHz, DMSO-d_6) 10.60 (1H, s, N*H*), 8.21 (1H, d, *J* 4.4, 4'-*H*), 8.06 (1H, d, *J* 4.4, 3'-*H*), 7.39 (1H, m, 2-*H*), 7.28–7.32 (2H, m, 5-*H* & 6-*H*), 6.75 (1H, ddd, *J* 7.7 *J* 2.5 *J* 1.4, 4-*H*), 3.76 (3H, s, C*H*$_3$). δ_C(176 MHz, DMSO-d_6) 159.5 (*C*-3), 158.2 (*C*=O), 153.4 (*C*-2'), 146.3 (*C*-5'), 139.1 (*C*-1), 130.1 (*C*-4'), 129.7 (*C*-5), 128.3 (*C*-3'), 112.8 (*C*-6), 110.2 (*C*-4), 106.3 (*C*-2), 55.1 (*C*H$_3$). *m/z* (LC-MS ES$^+$) 279.0 $[M+H]^+$. HRMS (ES$^+$) found $[M+H]^+$ 279.0471, $C_{12}H_{11}N_2O_4S$ requires 279.0440. CHN found: C 51.71; H 3.57; N 9.96. $C_{12}H_{10}N_2O_4S$ requires C 51.79; H 3.62; N 10.07.

***N*-(4-methoxyphenyl)-5'-nitrothiophene-2'-carboxamide (159)**

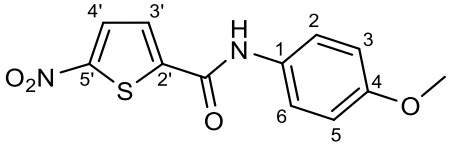

Following general procedure **C**, using THF (2 mL) as a reaction solvent, where the substituted amine was *p*-anisidine (0.12 g, 0.95 mmol, 1.0 eq.), afforded *N*-(4-methoxyphenyl)-5'-nitrothiophene-2'-carboxamide (**159**) as a yellow solid (0.035 g, 13 %) melting point 187 – 188 °C. ν_{max} (ATR) 3341 (N–H), 1634 (C=O), 1528, 1327 cm^{-1}. δ_H(599 MHz, DMSO-d_6) 10.55 (1H, s, N*H*), 8.20 (1H, d, *J* 4.5, 4'-*H*), 8.03 (1H, d, *J* 4.5, 3'-*H*), 7.62-7.64 (2H, m, 2-*H*), 6.95-6.97 (2H, m, 3-*H*), 3.75 (3H, s, CH_3). δ_C(151 MHz, DMSO-d_6) 157.8 (*C*=O), 156.2 (*C*-4), 153.1 (*C*-2'), 146.7 (*C*-5'), 130.9 (*C*-1), 130.1 (*C*-4'), 128.0 (*C*-3'), 122.3 (*C*-2), 114.0 (*C*-3), 55.2 (*C*H_3). *m/z* (LC-MS ES^+) 279.2 $[M+H]^+$. HRMS (ES^+) found $[M+H]^+$ 279.0441, $C_{12}H_{11}N_2O_4S$ requires 279.0440. CHN found: C 51.27; H 3.62; N 9.91. $C_{12}H_{10}N_2O_4S$ requires C 51.79; H 3.62; N 10.07.

5'-Nitro-*N*-[2-(trifluoromethyl)phenyl]thiophene-2'-carboxamide (160)

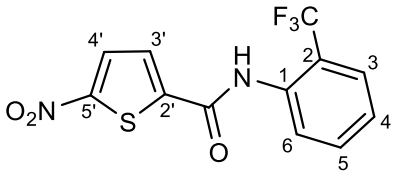

Following general procedure **Gi**, using DCM (4 mL) as a reaction solvent, where the substituted amine was 2-trifluoromethyl aniline (0.16 mL, 1.24 mmol, 1.0 eq.) afforded, following work up with DCM and purification by flash column chromatography (EtOAc:hexane), 5-amino-N-[2-(trifluoromethyl)phenyl]thiophene-2-carboxamide (**160**) as a yellow solid (0.16 g, 41 %), melting point 129–130 °C. ν_{max} (ATR) 3275 (N–H), 1647 (C=O), 1545, 1321 cm^{-1}. δ_H(700 MHz, $CDCl_3$) 8.30 (1H, d, *J* 8.2, 6-*H*), 8.10 (1H, s, N*H*), 7.92 (1H, d, *J* 4.3, 4'-*H*), 7.69 (1H, d, *J* 7.9, 3-*H*), 7.64 (1H, d, *J* 8.2 *J* 7.7, 5-*H*), 7.46 (1H, d, *J* 4.3, 3'-*H*), 7.34 (1H, dd, *J* 7.9 *J* 7.7, 4-*H*). δ_C(176 MHz, $CDCl_3$) 158.2 (*C*=O), 155.3 (*C*-2'), 144.4 (*C*-5'), 134.3 (*C*-1), 133.4 (*C*-5), 128.3 (*C*-4'), 126.6 (q, *J* 5.2, *C*-3), 126.5 (*C*-3'), 125.7 (*C*-4), 124.5 (*C*-6), 124.3 (q, *J* 273.0, *C*F_3), 120.6 (q, *J* 29.0, *C*-2). δ_F(376 MHz, $CDCl_3$) -60.1 (C*F*$_3$). *m/z* (LC-MS ES^+) 317.2 $[M+H]^+$. HRMS (ES^+) found $[M+H]^+$ 317.0210, $C_{12}H_8N_2O_3F_3S$ requires *M* 317.0208. CHN found: C 45.70; H 2.24; N 8.78. $C_{12}H_7N_2O_3F_3S$ requires C 45.57; H 2.23; N 8.86.

5'-Nitro-*N*-[3-(trifluoromethyl)phenyl]thiophene-2'-carboxamide (161)

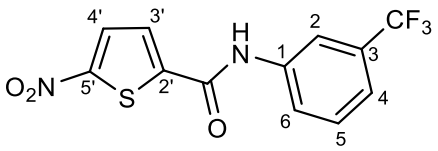

Following general procedure **C**, using DCM (4 mL) as a reaction solvent, where the substituted amine was 3-trifluoromethyl aniline (0.16 mL, 1.24 mmol, 1.0 eq.), afforded 5-amino-N-[3-(trifluoromethyl)phenyl]thiophene-2-carboxamide (**161**) as a yellow solid (0.37 g, 94 %), melting point 178–179 °C. ν_{max} (ATR) 3404 (N–H), 1683 (C=O), 1555, 1316 cm^{-1}. δ_H(700 MHz, DMSO-d_6) 10.90 (1H, s, N*H*), 8.22 (1H, d, *J* 4.4, 4'-*H*), 8.16 (1H, d, *J* 2.0, 2-*H*), 8.07 (1H, d, *J* 4.4, 3'-*H*), 8.01 (1H, ddd, *J* 8.1 *J* 2.0 *J* 1.0, 4-*H*), 7.64 (1H, dd, *J* 8.1 *J* 7.8, 5-*H*), 7.52 (1H, ddd, *J* 8.1 *J* 2.0 *J* 1.0, 6-*H*). δ_C(176 MHz, DMSO-d_6) 158.7 (*C*=O), 153.6 (*C*-2'), 145.5 (*C*-5'), 138.8 (*C*-1), 130.2 (*C*-5), 130.1 (*C*-4'), 129.5 (q, *J* 31.2, *C*-3), 128.8 (*C*-3'), 124.0 (q, *J* 274.3, *C*F_3), 124.0 (*C*-6), 120.9 (d, *J* 3.8, *C*-4), 116.6 (q, *J* 4.1, *C*-2). δ_F(376 MHz, $CDCl_3$) -62.8 (C*F_3*). *m/z* (LC-MS ES^+) 317.1 $[M+H]^+$. HRMS (ES^+) found $[M+H]^+$ 317.0216, $C_{12}H_8N_2O_3F_3S$ requires *M* 317.0208. CHN found: C 45.57; H 2.22; N 8.89. $C_{12}H_7N_2O_3F_3S$ requires C 45.57; H 2.23; N 8.86

***N*-(2-acetylphenyl)-5'-nitrothiophene-2'-carboxamide (162)**

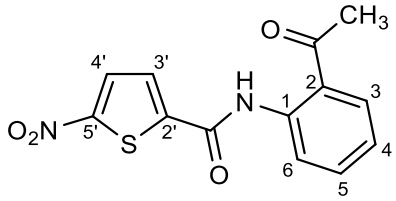

Following general procedure **C**, using DCM (3 mL) as a reaction solvent for 6 hrs, where the substituted amine was 2-aminoacetophenone (0.20 g, 1.5 mmol, 1.0 eq.), afforded *N*-(2-acetylphenyl)-5'-nitrothiophene-2'-carboxamide (**162**) as a yellow solid (0.268 g, 62 %) melting point 215-216 °C. ν_{max} (ATR) 3106 (N–H), 1664 (C=O), 1644 (C=O), 1518, 1316 cm^{-1}. δ_H(599 MHz, DMSO-d_6) 12.30 (1H, s, N*H*), 8.32 (1H, dd, *J* 8.3 *J* 1.2, 6-*H*), 8.23 (1H, d, *J* 4.4, 4'-*H*), 8.09 (1H, dd, *J* 8.2 *J* 1.5, 3-*H*), 7.84 (1H, d, *J* 4.4, 3'-*H*), 7.68–7.71 (1H, m, 5-*H*), 7.33-7.36 (1H, m, 4-*H*), 2.68 (3H, d, *J* 0.9, C*H_3*). δ_C(151 MHz, DMSO-d_6) 203.1 (2-*C*=O), 158.3 (2'-*C*=O), 153.7 (*C*-2'), 145.4 (*C*-5'), 137.7

(*C*-1), 134.4 (*C*-5), 131.8 (*C*-3), 130.3 (*C*-4'), 127.9 (*C*-3'), 125.3 (*C*-2), 124.4 (*C*-4), 121.3 (*C*-6), 28.7 (*C*H_3). *m/z* (LC-MS ES^+) 291.2 $[M+H]^+$. HRMS (ES^+) found $[M-H]^-$ 289.0262, $C_{13}H_9N_2O_4S$ requires 289.0283. CHN found: C 53.75; H 3.43; N 9.73. $C_{13}H_{10}N_2O_4S$ requires C 53.79; H 3.47; N 9.66.

2-Amino-N-dimethyl benzamide (154) [205]

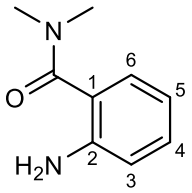

Dimethylamine (40 % in water, 3.5 mL, 30.7 mmol, 5 eq.) was added to isatoic anhydride (1.0 g, 6.1 mmol, 1.0 eq.) in water (4 mL). The reaction was stirred at RT for 20 hrs before dilution with EtOAc. The organic extract was washed with water, sodium carbonate and brine and dried over $MgSO_4$. Volatiles were removed *in vacuo*. Further product was recovered by removing the water from the aqueous layer *in vacuo* and extraction of the residue with EtOAc and removing volatiles *in vacuo*. The residues were combined to give 2-amino-N-dimethyl benzamide (**154**) as a pale yellow oil (1.00 g, 99 %). ν_{max} (ATR) 3452 (N-H), 3349 (N-H), 1616 (C=O) cm^{-1}. δ_H (599 MHz, $CDCl_3$) 7.14 (1H, ddd, *J* 7.7, *J* 1.6, 4-*H*), 7.09 (1H, dd, *J* 8.0 *J* 1.6, 6-*H*), 6.68-6.73 (2H, m, 3-*H* & 5-*H*), 4.12 (2H, s, NH_2), 3.05 (6H, s, CH_3). δ_C (151 MHz, $CDCl_3$) 171.2 (*C*=O), 145.6 (*C*-2), 130.6 (*C*-4), 128.1 (*C*-6), 120.3 (*C*-1), 117.5 (*C*-3 or *C*-5), 116.9 (*C*-3 or *C*-5), 39.6 & 35.3 (*C*H_3). *m/z* (LC-MS ES^+) 165.2 $[M+H]^+$. HRMS (ES^+) found $[M+H]^+$ 165.1045, $C_9H_{13}N_2O$ requires *M* 165.1028.

N-[2-(dimethylcarbamoyl) phenyl]-5'-nitrothiophene-2'-carboxamide (163)

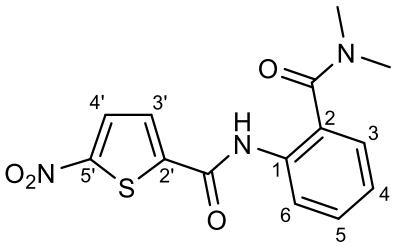

Following general procedure **Gii**, using THF (5 mL) as a reaction solvent for 6 hrs, where the substituted amine was 2-amino-N-dimethyl benzamide (0.26 g, 1.6 mmol, 1.0 eq.) afforded, following filtration and trituration of the crude solid and purification of the worked up filtrate by flash column chromatography (EtOAc:hexane), N-[2-(dimethylcarbamoyl) phenyl]-5'-nitrothiophene-2'-carboxamide (**163**) as a pale yellow solid (0.12 g, 24 %) melting point 214-216 °C. ν_{max} (ATR) 3230 (N-H), 1659 (C=O), 1618 (C=O), 1546, 1360 cm^{-1}. δ_H (599 MHz, DMSO-d_6) 10.68 (1H, s, 1-N*H*), 8.19 (1H, d, *J* 4.4, 4'-*H*), 7.92 (1H, d, *J* 4.4, 3'-*H*), 7.46-7.53 (2H, m, 3-*H* & 4-*H*), 7.38 (1H, dd, *J* 7.5 *J* 1.6, 6-*H*), 7.33 (1H, ddd, *J* 7.5, *J* 1.4, 5-*H*), 2.91 (3H, s, *C*H_3), 2.87 (3H, s, *C*H_3). δ_C (151 MHz, DMSO-d_6) 168.5 (2-*C*=O), 158.5 (*C*-2'), 153.3 (2'-*C*=O), 145.6 (*C*-5'), 133.8 (*C*-1), 131.6 (*C*-2), 130.2 (*C*-4'), 129.6 (*C*-3 or *C*-4), 128.3 (*C*-3'), 127.8 (*C*-6), 125.9 (*C*-3 or *C*-4 and *C*-5), 38.8 & 34.6 (*C*H_3). *m/z* (LC-MS ES^+) 320.3 $[M+H]^+$. HRMS (ES^+) found $[M+H]^+$ 320.0713, $C_{14}H_{14}N_3O_4S$ requires *M* 320.0705.

5'-Nitro-*N*-[2-(tridecylcarbamoyl)phenyl]thiophene-2'-carboxamide (164)

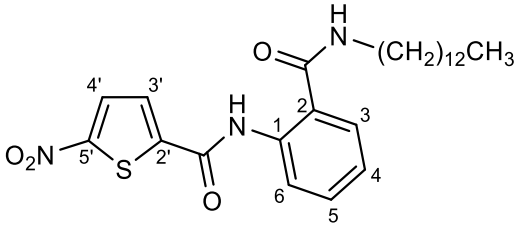

2-(5'-Nitrothiophen-2'-yl)-4H-3,1-benzoxazin-4-one (**144**) (0.02 g, 0.07 mmol, 1.0 eq.) was dissolved in dry chloroform (0.5 mL). Tridecylamine (0.048 g, 0.24 mmol, 3.2 eq.) in dry chloroform (0.5 mL) was added dropwise at 0 °C. The reaction mixture was stirred at RT for 1 hour. Volatiles were removed *in vacuo* before the crude solid was triturated in hexane to give 5'-nitro-*N*-[2-(tridecylcarbamoyl)phenyl]thiophene-2'-carboxamide (**164**) as a yellow solid (0.027 g, 82 %), melting point 112 – 113 °C. ν_{max} (ATR) 3336 (N–H), 1681 (C=O), 1626 (C=O), 1522, 1332 cm^{-1}. δ_H(599 MHz, $CDCl_3$) 12.72 (1H, s, 1-*N*H), 8.70 (1H, d, *J* 8.5, 6-*H*), 7.90 (1H, d, *J* 4.3, 4'-*H*), 7.65 (1H, d, *J* 4.3, 3'-*H*), 7.51–7.56 (2H, m, 3-*H* & 5-*H*), 7.16 (1H, d, *J* 7.4, 4-*H*), 6.36 (1H, s, 2-CON*H*), 3.45–3.49 (2H, m, NH-CH_2), 1.62–1.67 (2H, m, NHCH_2-CH_2), 1.25-1.41 (20H, m, CH_2), 0.88 (3H, t, *J* 7.0, CH_3). δ_C(151 MHz, $CDCl_3$) 169.2 (2-*C*=O), 158.4 (2'-*C*=O), 154.8 (*C*-

2'), 146.7 (*C*-5'), 139.4 (*C*-1), 133.2 (Ar-*C*), 128.6 (*C*-4'), 126.5 (*C*-3' & Ar-*C*), 123.8 (*C*-4), 121.6 (*C*-6), 119.9 (*C*-2), 40.4 (*C*H_2-NH), 32.1 (*C*H_2), 29.4–29.8 (C*H*$_2$), 27.1 (C*H*$_2$), 22.8 (C*H*$_2$),14.3 (*C*H_3). *m/z* (LC-MS ES$^+$) 474.3 $[M+H]^+$. HRMS (ES$^+$) found $[M+H]^+$ 474.2426, $C_{25}H_{36}N_3O_4S$ requires 474.2427. CHN found: C 63.57; H 7.56; N 8.40. $C_{25}H_{35}N_3O_4S$ requires C 63.40; H 7.45; N 8.87.

5'-Nitro-N-{[(propan-2-yl)carbamoyl]-2-phenyl}thiophene-2'-carboxamide (165)

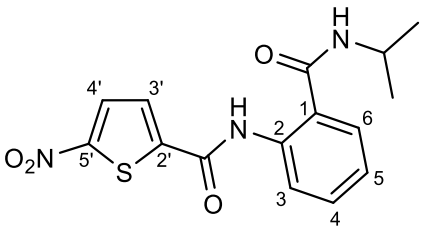

2-(5'-Nitrothiophen-2'-yl)-4H-3,1-benzoxazin-4-one (**144**) (0.013 g, 0.05 mmol, 1.0 eq.) was dissolved in dry chloroform (0.5 mL). Isopropylamine (0.02 mL, 0.22 mmol, 4.4 eq.) in dry chloroform (0.5 mL) was added dropwise at 0 °C. The reaction mixture was stirred at RT for 3 hrs. Volatiles were removed *in vacuo* to give 5'-nitro-N-{[(propan-2-yl)carbamoyl]-2-phenyl}thiophene-2'-carboxamide (**165**) as a yellow solid (0.016 g, 100 %), melting point 234 °C. ν_{max} (ATR) 3305 (N–H), 1679 (C=O), 1627 (C=O), 1513, 1340 cm^{-1}. δ_H(599 MHz, $CDCl_3$) 12.74 (1H, s, 2-N*H*), 8.70 (1H, dd, *J* 8.4 *J* 1.0, 3-*H*), 7.90 (1H, dd, *J* 4.3 *J* 0.9, 4'-*H*), 7.65 (1H, dd, *J* 4.3 *J* 0.9, 3'-*H*), 7.50-7.56 (2H, m, 4-*H* & 6-*H*), 7.16 (1H, ddd, *J* 8.6 *J* 7.5 *J* 1.1, 5-*H*), 6.16 (1H, d, *J* 7.2, CH-N*H*), 4.27-4.34 (1H, m, C*H*-NH), 1.31 (dd, *J* 6.6, *J* 0.9, C*H*$_3$). δ_C(151 MHz, $CDCl_3$) 168.4 (1-*C*=O), 158.4 (2'-*C*=O), 154.8 (*C*-2'), 146.8 (*C*-5'), 139.5 (*C*-2), 133.2 (*C*-4), 128.6 (*C*-4'), 126.5 (*C*-3' & *C*-6), 123.8 (*C*-5), 121.6 (*C*-3), 120.0 (*C*-1), 42.4 (*C*H-CH_3), 22.8 (*C*H_3). *m/z* (LC-MS ES$^+$) 334.8 $[M+H]^+$. HRMS (ES$^-$) found $[M-H]^-$ 332.0700, $C_{15}H_{14}N_3O_4S$ requires 332.0705.

5-Methyl-2,4-dihydro-1*H*-3,1-benzoxazine-2,4-dione (175)

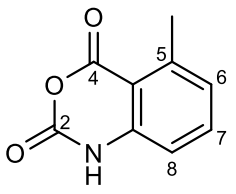

Following general procedure **D**, where the substituted 2-amino benzoic acid was 2-amino-6-methylbenzoic acid (0.50 g, 2.82 mmol, 1.0 eq.), afforded 5-methyl-2,4-dihydro-1*H*-3,1-benzoxazine-2,4-dione (**175**) as an off white solid (0.37 g, 63 %) melting point 220–221 °C (lit. 216–217 °C).[207] ν_{max} (ATR) 3106 (N–H), 1782 (C=O), 1715 (C=O) cm^{-1}. δ_H(700 MHz, DMSO-d_6) 11.60 (1H, s, 1-*H*), 7.58 (1H, dd, *J* 8.0 *J* 7.7, 7-*H*), 7.07 (1H, dd, *J* 7.7 *J* 1.0, Ar-*H*), 7.00 (1H, dd, *J* 8.0 *J* 0.9, Ar-*H*) 2.61 (3H, s, CH_3). δ_C(176 MHz, DMSO-d_6) 159.0 (*C*-4), 147.1 (*C*-2), 142.5 (1-*C*(Ar) & *C*-5), 135.8 (*C*-7), 126.0 (*C*-Ar), 113.3 (*C*-Ar) 108.7 (4-*C*), 21.7 (*C*H_3). *m/z* (LC-MS ES^+) 178.2 $[M+H]^+$.

6-Methoxy-2,4-dihydro-1*H*-3,1-benzoxazine-2,4-dione (176)

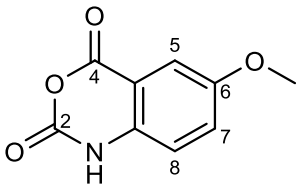

Following general procedure **D**, where the substituted 2-amino benzoic acid was 2-amino-5-methoxybenzoic acid (0.50 g, 2.99 mmol, 1.0 eq.) afforded, following purification by flash column chromatography (hexane:EtOAc), 6-methoxy-2,4-dihydro-1*H*-3,1-benzoxazine-2,4-dione (**176**) as a pale yellow solid (0.31 g, 54 %) melting point 253-255 °C (lit. 243 °C).[208] ν_{max} (ATR) 3094 (N–H), 1781 (C=O), 1716 (C=O) cm^{-1}. δ_H(700 MHz, DMSO-d_6) 11.60 (1H, s, 1-*H*), 7.38 (1H, dd, *J* 8.9 *J* 2.9, 7-*H*), 7.33 (1H, d, *J* 2.9, 5-*H*), 7.11 (1H, d, *J* 8.9, 8-*H*), 3.81 (3H, s, CH_3). δ_C(176 MHz, DMSO-d_6) 159.8 (*C*-4), 155.2 (*C*-6), 146.9 (*C*-2), 135.5 (1-*C*(Ar)), 125.7 (*C*-7), 116.9 (*C*-8), 110.7 (4-*C*), 109.8 (*C*-5), 55.7 (*C*H_3). *m/z* (LC-MS ES^+) 194.2 $[M+H]^+$.

6-Methyl-2,4-dihydro-1*H*-3,1-benzoxazine-2,4-dione (177)

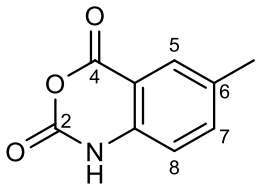

Following general procedure **D**, where the substituted 2-amino benzoic acid was 2-amino-5-methylbenzoic acid (0.50 g, 2.82 mmol, 1.0 eq.), afforded 6-methyl-2,4-

dihydro-1*H*-3,1-benzoxazine-2,4-dione (**177**) as an off white solid (0.53 g, 90 %) melting point 260-261 °C (lit. 249–250 °C).[209] ν_{max} (ATR) 3106 (N–H), 1773 (C=O), 1724 (C=O) cm^{-1}. δ_H(700 MHz, DMSO-d_6) 11.64 (1H, s, 1-*H*), 7.72 (1H, d, *J* 2.1, 5-*H*), 7.56 (1H, ddd, *J* 8.3 *J* 2.1 *J* 0.7, 7-*H*), 7.06 (1H, d, *J* 8.3, 8-*H*), 2.33 (3H, s, CH_3). δ_C(176 MHz, DMSO-d_6). 159.9 (*C*-4), 147.1 (*C*-2), 139.2 (1-*C*(Ar)), 137.9 (*C*-7), 132.9 (*C*-6), 128.3 (*C*-5), 115.3 (*C*-8), 110.0 (4-*C*), 20.0 (*C*H_3). *m/z* (LC-MS ES^+) 178.2 $[M+H]^+$.

7-Methoxy-2,4-dihydro-1*H*-3,1-benzoxazine-2,4-dione (178)

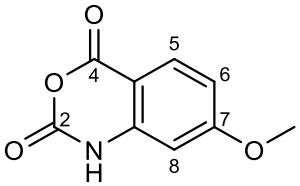

Following general procedure **D**, where the substituted 2-amino benzoic acid was 2-amino-4-methoxybenzoic acid (0.50 g, 2.99 mmol, 1.0 eq.) afforded, following purification by flash column chromatography (hexane:EtOAc), 7-methoxy-2,4-dihydro-1*H*-3,1-benzoxazine-2,4-dione (**178**) as a pale yellow solid (0.31 g, 54 %) melting point 219–220 °C (lit. 216–218 °C).[108] ν_{max} (ATR) 3206 (N–H), 1759 (C=O), 1705 (C=O) cm^{-1}. δ_H(700 MHz, DMSO-d_6) 11.64 (1H, s, 1-*H*), 7.84 (1H, d, *J* 8.8, 5-*H*), 6.84 (1H, dd, *J* 8.8 *J* 2.4, 6-*H*), 6.59 (1H, d, *J* 2.4, 8-*H*), 3.85 (3H, s, CH_3). δ_C(176 MHz, DMSO-d_6) 165.9 (*C*-4), 159.2 (*C*-7), 147.4 (*C*-2), 143.6 (1-*C*(Ar)), 131.0 (*C*-5), 111.6 (*C*-6), 102.9 (4-*C*), 98.5 (*C*-8), 55.9 (*C*H_3). *m/z* (LC-MS ES^+) 194.2 $[M+H]^+$.

7-Methyl-2,4-dihydro-1*H*-3,1-benzoxazine-2,4-dione (179)

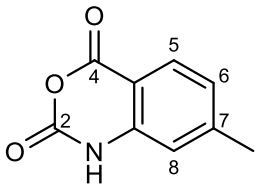

Following general procedure **D**, where the substituted 2-amino benzoic acid was 2-amino-4-methylbenzoic acid (0.50 g, 2.82 mmol, 1.0 eq.), afforded 7-methyl-2,4-dihydro-1*H*-3,1-benzoxazine-2,4-dione (**179**) as a pale yellow solid (0.50 g, 85 %) melting point 228–229 °C (lit. 228 °C).[210] ν_{max} (ATR) 3119 (N–H), 1755 (C=O), 1701

(C=O) cm^{-1}. δ_H(700 MHz, DMSO-d_6) 11.67 (1H, s, 1-*H*), 7.80 (1H, d, *J* 8.0, 5-*H*), 7.08 (1H, ddd, *J* 8.0 *J* 1.5 *J* 0.8, 6-*H*), 6.93 (1H, m, 8-*H*), 2.38 (3H, s, CH_3). δ_C(176 MHz, DMSO-d_6) 159.7 (*C*-4), 148.1 (1-*C*(Ar)), 147.3 (*C*-2), 141.5 (*C*-7), 128.9 (*C*-5), 124.8 (*C*-6), 115.1 (*C*-8), 107.7 (4-*C*), 21.6 (*C*H_3). *m/z* (LC-MS ES^+) 178.2 $[M+H]^+$.

7-Trifluoromethyl-2,4-dihydro-1*H*-3,1-benzoxazine-2,4-dione (180)

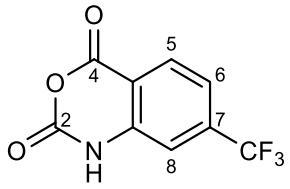

Following general procedure **D**, where the substituted 2-amino benzoic acid was 2-amino-4-trifluoromethylbenzoic acid (0.50 g, 2.44 mmol, 1.0 eq.) afforded, following recrystallisation from pyridine: hexane, 7-trifluoromethyl-2,4-dihydro-1*H*-3,1-benzoxazine-2,4-dione (**180**) as an off white solid (0.25 g, 44 %), melting point 247–249 °C (lit. 240–242 °C).[211] ν_{max}(ATR) 3199 (N–H), 1793 (C=O), 1777 (C=O) cm^{-1}. δ_H(700 MHz, DMSO-d_6) 11.96 (1H, s, 1-*H*), 8.12 (1H, dd, *J* 8.2 *J* 0.9, 5-*H*), 7.56 (1H, dd, *J* 8.2 *J* 1.7, 6-*H*), 7.40 (1H, dd, *J* 1.7 *J* 0.9, 8-*H*). δ_C(176 MHz, DMSO-d_6) 159.1 (*C*-4), 146.7 (*C*-2), 141.8 (1-*C*(Ar)), 135.5 (q, *J* 32.5, *C*-7), 130.5 (*C*-5), 123.1 (q, *J* 273.2, *C*F_3), 119.4 (d, *J* 3.6, C-6), 114.0 (4-*C*), 112.0 (d, *J* 4.2, *C*-8). δ_F(376 MHz, DMSO-d_6) -62.4 (C*F*$_3$). *m/z* (LC-MS ES^-) 230.1 $[M-H]^-$.

7-Bromo-2,4-dihydro-1*H*-3,1-benzoxazine-2,4-dione (181)

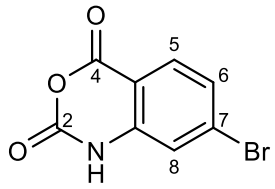

Following general procedure **D**, where the substituted 2-amino benzoic acid was 2-amino-4-trifluoromethylbenzoic acid (2.00 g, 9.3 mmol, 1.0 eq.) afforded, following purification by flash column chromatography (EtOAc: hexane), 7-bromo-2,4-dihydro-1*H*-3,1-benzoxazine-2,4-dione (**181**) as an off white solid (1.80 g, 80 %) melting point 284–285 °C (lit. 256 °C).[212] ν_{max}(ATR) 3184 (N–H), 1775 (C=O) cm^{-1}. δ_H(700 MHz,

DMSO-d_6) 11.81 (1H, s, 1-*H*), 7.83 (1H, d, *J* 8.4, 5-*H*), 7.43 (1H, dd, *J* 8.4 *J* 1.8, 6-*H*), 7.30 (1H, d, *J* 1.8, 8-*H*). δ_C(176 MHz, DMSO-d_6) 159.3 (*C*-4), 146.8 (*C*-2), 142.5 (1-*C*(Ar)), 130.8 (*C*-5), 130.2 (*C*-7), 126.5 (*C*-6), 117.7 (*C*-8), 109.8 (4-*C*). *m/z* (LC-MS ES$^-$) 240.0 [M(^{79}Br) – H]$^-$ & 242.0 [[M(^{81}Br) – H]$^-$.

8-Methoxy-2,4-dihydro-1*H*-3,1-benzoxazine-2,4-dione (182)

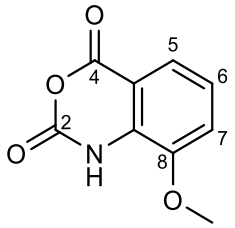

Following general procedure **D**, where the substituted 2-amino benzoic acid was 2-amino-3-methoxybenzoic acid (0.50 g, 2.99 mmol, 1.0 eq.), afforded 8-methoxy-2,4-dihydro-1*H*-3,1-benzoxazine-2,4-dione (**182**) as a white solid (0.54 g, 94 %) melting point 269 – 270 °C (lit. 255 – 260 °C).[213] ν_{max} (ATR) 3125 (N–H), 1782 (C=O), 1710 (C=O) cm^{-1}. δ_H(700 MHz, DMSO-d_6) 11.26 (1H, s, 1-*H*), 7.48 (1H, dd, *J* 8.1 *J* 1.2, 5-*H*), 7.40 (1H, dd, *J* 8.1 *J* 1.2, 7-*H*), 7.20 (1H, dd, *J* 8.1, 6-*H*), 3.89 (3H, s, C*H*$_3$). δ_C(176 MHz, DMSO-d_6) 159.8 (*C*-4), 146.8 (*C*-2), 146.2 (*C*-8), 131.6 (1-*C*(Ar)), 123.4 (*C*-6), 119.6 (*C*-5), 117.5 (*C*-7), 110.8 (4-*C*), 56.4 (*C*H$_3$). *m/z* (LC-MS ES$^+$) 194.2 [M+H]$^+$.

8-Methyl-2,4-dihydro-1*H*-3,1-benzoxazine-2,4-dione (183)

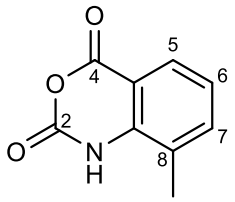

Following general procedure **D**, where the substituted 2-amino benzoic acid was 2-amino-3-methylbenzoic acid (0.50 g, 2.82 mmol, 1.0 eq.), afforded 8-methyl-2,4-dihydro-1*H*-3,1-benzoxazine-2,4-dione (**183**) as an off white solid (0.50 g, 85 %) melting point 293 – 294 °C (lit. 275 °C).[214] ν_{max} (ATR) 3207 (N–H), 1782 (C=O), 1715

(C=O) cm^{-1}. δ_H(700 MHz, DMSO-d_6) 11.02 (1H, s, 1-*H*), 7.78 (1H, ddd, *J* 7.7 *J* 1.6 *J* 0.7, 5-*H*), 7.59 (1H, ddd, *J* 7.5 *J* 1.6 *J* 0.8, 7-*H*), 7.16 (1H, dd, *J* 7.7 *J* 7.5, 6-*H*), 2.33 (3H, s, C*H*$_3$). δ_C(176 MHz, DMSO-d_6) 160.0 (*C*-4), 147.3 (*C*-2), 139.7 (1-*C*(Ar)), 137.9 (*C*-7), 126.7 (*C*-5), 124.4 (*C*-8), 123.2 (*C*-6), 110.4 (4-*C*), 17.0 (*C*H_3). *m/z* (LC-MS ES^+) 178.2 $[M+H]^+$.

2-Amino-6-methyl-*N*-methyl-1-benzamide (184)

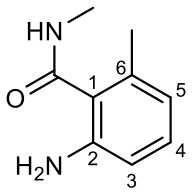

Following general procedure **E**, where the substituted benzoxazine-2,4-dione was 5-methyl-1*H*-3,1-benzoxazine-2,4-dione (**175**) (0.30 g, 1.69 mmol, 1.0 eq.), afforded 2-amino-6-methyl-*N*-methyl-1-benzamide (**184**) as an off-white solid (0.029 g, 10 %) melting point 120-121 °C. ν_{max} (ATR) 3560 (N–H), 3300 (N–H), 1611 (C=O) cm^{-1}. δ_H(700 MHz, $CDCl_3$) 7.03 (1H, dd, *J* 8.0 *J* 7.7, 4-*H*), 6.57 (1H, dd, *J* 7.7 *J* 0.9, 5-*H*), 6.53 (1H, dd, *J* 8.0 *J* 0.9, 3-*H*), 5.78 (1H, s, N*H*CH_3), 4.11 (2H, s, NH_2), 3.00 (3H, d, *J* 4.9, NHCH_3), 2.30 (3H, s, Ar-CH_3). δ_C(176 MHz, $CDCl_3$) 170.2 (*C*=O), 144.8 (*C*-2), 135.3 (*C*-6), 130.1 (*C*-4), 123.1 (*C*-1), 120.5 (*C*-5), 113.9 (*C*-3), 26.6 (*C*H_3NH), 20.2 (*C*H_3-Ar). *m/z* (LC-MS ES^+) 165.3 $[M+H]^+$.

2-Amino-5-methoxy-*N*-methyl-1-benzamide (185)

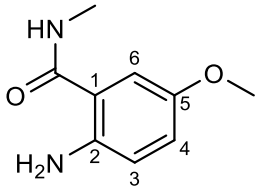

Following general procedure **E**, where the substituted benzoxazine-2,4-dione was 6-methoxy-1*H*-3,1-benzoxazine-2,4-dione (**176**) (0.11 g, 0.57 mmol, 1.0 eq.), afforded 2-amino-5-methoxy-*N*-methyl-1-benzamide (**185**) as an off white solid (0.043 g, 42 %) melting point 115–116 °C. ν_{max} (ATR) 3424 (N–H) 3283, (N–H_2), 3198 (N–H_2), 1637 (C=O) cm^{-1}. δ_H(700 MHz, $CDCl_3$) 6.85–6.87 (2H, m, 4-*H* & 6-*H*), 6.65–6.67 (1H, m, 3-*H*),

6.12 (1H, s, C=ON*H*), 5.04 (2H, s, NH_2), 3.75 (3H, s, O-CH_3), 2.97 (3H, d, *J* 4.9, NH-CH_3). δ_C(176 MHz, $CDCl_3$) 169.8 (*C*=O), 151.5 (*C*-5), 142.1 (*C*-2), 119.3 (*C*-4), 119.0 (*C*-3), 117.9 (*C*-1), 112.2 (*C*-6), 56.2 (O*C*H_3), 26.7 (N*C*H_3). *m/z* (LC-MS ES^+) 181.3 $[M+H]^+$.

2-Amino-5-methyl-*N*-methyl-1-benzamide (186)

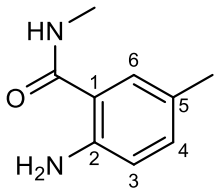

Following general procedure **E**, where the substituted benzoxazine-2,4-dione was 6-methyl-1*H*-3,1-benzoxazine-2,4-dione (**177**) (0.40 g, 2.26 mmol, 1.0 eq.), afforded 2-amino-5-methyl-*N*-methyl-1-benzamide (**186**) as an off white solid (0.17 g, 46 %) melting point 125-126 °C. ν_{max} (ATR) 3425 (N–H), 3295 (N–H_2), 1637 (C=O) cm^{-1}. δ_H(700 MHz, $CDCl_3$) 7.10 (1H, d, *J* 2.2, 6-*H*) 7.02 (1H, ddd, *J* 8.2 *J* 2.2 *J* 0.6, 4-*H*), 6.61 (1H, d, *J* 8.2, 3-*H*), 6.08 (1H, s, CH_3NH), 5.30 (1H, s, NH_2), 2.96 (3H, d, *J* 4.9, CH_3NH), 2.22 (3H, s, Ar-CH_3). δ_C(176 MHz, $CDCl_3$) 170.2 (*C*=O), 146.3 (*C*-2), 133.1 (*C*-4), 127.3 (*C*-6), 126.0 (*C*-5), 117.6 (*C*-3), 116.6 (*C*-1), 26.6 (*C*H_3-NH), 20.5 (*C*H_3-Ar). *m/z* (LC-MS ES^+) 165.3 $[M+H]^+$.

2-Amino-4-methoxy-*N*-methyl-1-benzamide (187)

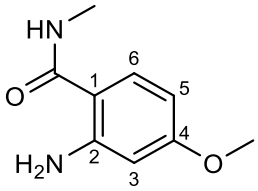

Following general procedure **E**, where the substituted benzoxazine-2,4-dione was 7-methoxy-1*H*-3,1-benzoxazine-2,4-dione (**178**) (0.48 g, 2.5 mmol, 1.0 eq.), afforded 2-amino-4-methoxy-*N*-methyl-1-benzamide (**187**) as an off white solid (0.28 g, 63 %) melting point 132–133 °C. ν_{max} (ATR) 3436 (N–H), 3345, (N–H_2), 3314 (N–H_2), 1646 (C=O) cm^{-1}. δ_H(700 MHz, $CDCl_3$) 7.22 (1H, d, *J* 8.7, 6-*H*), 6.21 (1H, dd, *J* 8.7 *J* 2.5, 5-*H*), 6.15 (1H, d, *J* 2.5, 3-*H*), 5.91 (1H, s, CH_3-N*H*), 5.69 (2H, s, NH_2), 3.77 (3H, s, O-CH_3), 2.95 (3H, d, *J* 4.8, NH-CH_3). δ_C(176 MHz, $CDCl_3$) 169.9 (*C*=O), 162.9 (*C*-4), 151.0 (*C*-2),

128.8 (*C*-6) 109.4 (*C*-1), 104.0 (*C*-5), 100.9 (*C*-3), 55.3 (O-*C*H_3), 26.6 (NH-*C*H_3). *m/z* (LC-MS ES$^+$) 181.5 $[M+H]^+$.

2-Amino-4-methyl-*N*-methyl-1-benzamide (188)

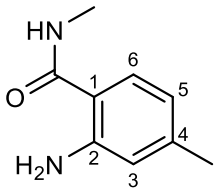

Following general procedure **E**, where the substituted benzoxazine-2,4-dione was 7-methyl-1*H*-3,1-benzoxazine-2,4-dione (**179**) (0.50 g, 2.82 mmol, 1.0 eq.), afforded 2-amino-4-methyl-*N*-methyl-1-benzamide (**188**) as an off white solid (0.25 g, 54 %) melting point 99–100 °C. ν_{max} (ATR) 3460 (N–H), 3337 (N–H_2), 1623 (C=O) cm^{-1}. δ_H(700 MHz, $CDCl_3$) 7.18 (1H, d, *J* 8.0, 6-*H*), 6.48 (1H, dd, *J* 1.7 *J* 0.9, 3-*H*), 6.45 (1H, ddd, *J* 8.0 *J* 1.7 *J* 0.9, 5-*H*), 6.05 (1H, s, CH_3-N*H*), 5.50 (2H, s, NH_2), 2.94 (3H, d, *J* 4.8, NH-CH_3), 2.24 (3H, d, *J* 0.9, Ar-CH_3). δ_C(176 MHz, $CDCl_3$) 170.1 (*C*=O), 148.9 (*C*-2), 142.8 (*C*-4), 127.1 (*C*-6), 117.9 (*C*-5), 117.7 (*C*-3), 113.7 (*C*-1), 26.6 (*C*H_3-NH), 21.5 (*C*H_3-Ar). *m/z* (LC-MS ES$^+$) 165.3 $[M+H]^+$.

2-Amino-4-trifluoromethyl-*N*-methyl-1-benzamide (189)

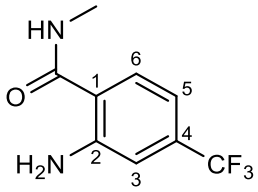

Following general procedure **E**, where the substituted benzoxazine-2,4-dione was 7-trifluoromethyl-1*H*-3,1-benzoxazine-2,4-dione (**180**) (0.20 g, 0.87 mmol, 1.0 eq.), afforded 2-amino-4-trifluoromethyl-*N*-methyl-1-benzamide (**189**) as an off white solid (0.12 g, 65 %) melting point 159-161 °C. ν_{max} (ATR) 3465 (N–H), 3365 (N–H_2), 3323 (N–H_2), 1725 (C=O) cm^{-1}. δ_H(700 MHz, $CDCl_3$) 7.38 (1H, d, *J* 8.1, 6-*H*), 6.90 (1H, s, 3-*H*), 6.85 (1H, ddd, *J* 8.1 *J* 1.7 *J* 0.7, 5-*H*), 6.11 (1H, s, N*H*-CH_3), 5.67 (2H, s, NH_2), 2.98 (3H, d, *J* 4.9, CH_3). δ_C(176 MHz, $CDCl_3$) 169.1 (*C*=O), 148.7 (*C*-2), 134.2 (q, *J* 32.1,

C-4), 127.8 (*C*-6), 123.8 (q, *J* 272.6, *C*F_3) 118.8 (*C*-1), 113.9 (q, *J* 4.0, *C*-3), 112.9 (q, *J* 3.7, *C*-5), 26.8 (*C*H_3). δ_F(376 MHz, $CDCl_3$) -63.6 (C*F*$_3$). *m/z* (LC-MS ES^+) 219.3 $[M+H]^+$.

2-Amino-4-bromo-*N*-methyl-1-benzamide (190)

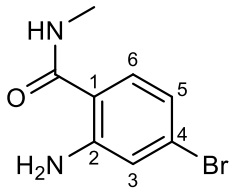

Following general procedure **E**, where the substituted benzoxazine-2,4-dione was 7-bromo-1*H*-3,1-benzoxazine-2,4-dione (**181**) (1.70 g, 7.0 mmol, 1.0 eq.), afforded 2-amino-4-bromo-*N*-methyl-1-benzamide (**190**) as an off white semi-solid (1.10 g, 68 %). ν_{max} (ATR) 3454 (N–H), 3346 (N–H_2), 1719 (C=O), cm^{-1}. δ_H(700 MHz, DMSO-d_6) 8.23 (1H, d, *J* 4.7, N*H*-CH_3), 7.38 (1H, d, *J* 8.4, 6-*H*), 6.90 (1H, d, *J* 2.0, 3-*H*), 6.63–6.65 (3H, m, NH_2 & 5-*H*), 2.71 (3H, d, *J* 4.7, CH_3). δ_C(176 MHz, DMSO-d_6) 168.5 (*C*=O), 151.0 (*C*-2), 129.8 (*C*-6), 124.9 (*C*-4), 118.1 (*C*-3), 117.0 (*C*-5), 113.7 (*C*-1), 25.9 (*C*H_3). *m/z* (LC-MS ES^+) 229.2 $[M(^{79}Br)+H]^+$ & 231.2 $[M(^{81}Br)+H]^+$.

2-Amino-3-methoxy-*N*-methyl-1-benzamide (191)

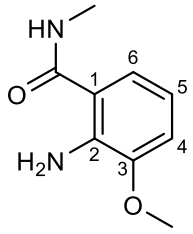

Following general procedure **E**, where the substituted benzoxazine-2,4-dione was 8-methoxy-1*H*-3,1-benzoxazine-2,4-dione (**182**) (0.30 g, 1.55 mmol, 1.0 eq.), afforded 2-amino-3-methoxy-*N*-methyl-1-benzamide (**191**) as an off white solid (0.14 g, 50 %) melting point 121–122 °C. ν_{max} (ATR) 3427 (N–H), 3346 (N–H), 3311 (N–H_2), 1629 (C=O) cm^{-1}. δ_H(700 MHz, $CDCl_3$) 6.92 (1H, dd, *J* 8.2 *J* 1.2, 6-*H*), 6.81 (1H, dd, *J* 8.2 *J* 1.2, 4-*H*), 6.59 (1H, dd, *J* 8.2, 5-*H*), 6.05 (1H, s, N*H*C=O), 5.78 (1H, s, NH_2), 3.86 (3H, s, O-CH_3), 2.97 (3H, s, NH-CH_3). δ_C(176 MHz, $CDCl_3$) 170.1 (*C*=O), 147.9 (*C*-3), 139.7 (*C*-2),

118.8 (*C*-6), 115.6 (*C*-1), 115.4 (*C*-5), 111.8 (*C*-4), 55.8 (O-*C*H_3), 26.6 (NH-*C*H_3). *m/z* (LC-MS ES$^+$) 181.3 $[M+H]^+$.

2-Amino-3-methyl-*N*-methyl-1-benzamide (192)

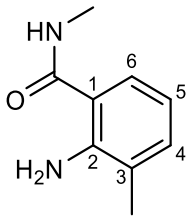

Following general procedure **E**, where the substituted benzoxazine-2,4-dione was 8-methyl-1*H*-3,1-benzoxazine-2,4-dione (**183**) (0.40 g, 2.26 mmol, 1.0 eq.), afforded 2-amino-3-methyl-*N*-methyl-1-benzamide (**192**) as an off white solid (0.21 g, 57 %) melting point 126-127 °C. ν_{max} (ATR) 3419 (N–H), 3342 (N–H_2), 1710 (C=O) cm^{-1}. δ_H(700 MHz, $CDCl_3$) 7.18–7.19 (1H, m, 6-*H*), 7.12 (1H, ddd, *J* 7.6 *J* 1.6 *J* 0.8, 4-*H*), 6.58 (1H, dd, *J* 7.6, 5-*H*), 6.06 (1H, s, N*H*-CH_3), 5.57 (2H, s, NH_2), 2.97 (3H, d, *J* 4.9, NH-CH_3), 2.16 (3H, d, *J* 0.8, Ar-CH_3). δ_C(176 MHz, $CDCl_3$) 170.6 (*C*=O), 147.0 (*C*-2), 133.2 (*C*-4), 125.0 (*C*-6), 123.9 (*C*-3), 116.1 (*C*-5), 115.9 (*C*-1), 26.7 (*C*H_3-NH), 17.6 (*C*H_3-Ar). *m/z* (LC-MS ES$^+$) 165.3 $[M+H]^+$.

***N*-[3-methyl-2-(methylcarbamoyl)phenyl]-5'-nitrothiophene-2'-carboxamide (193)**

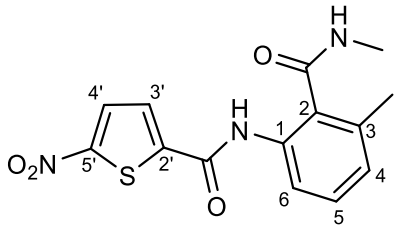

Following general procedure **C**, using DCM (7 mL) as a reaction solvent, where the substituted amine was amino-3-methyl-*N*-methyl-2-benzamide (**184**) (0.59 g, 3.59 mmol, 1.0 eq.), afforded *N*-[3-methyl-2-(methylcarbamoyl)phenyl]-5'-nitrothiophene-2'-carboxamide (**193**) as a yellow solid (0.39 g, 34 %) melting point 211–212 °C. ν_{max} (ATR) 3319 (N–H), 3268 (N–H), 1630 (C=O), 1608 (C=O), 1547, 1302 cm^{-1}. δ_H(700 MHz, DMSO-d_6) 10.39 (1H, s, 1-N*H*), 8.18 (1H, d, *J* 4.4, 4'-*H*), 8.14 (1H, m, CH_3-N*H*), 7.87 (1H, d, *J* 4.4, 3'-*H*), 7.43 (1H, d, *J* 7.9, 6-*H*), 7.34 (1H, dd, *J* 7.9 *J* 7.7, 5-

H), 7.17 (1H, d, *J* 7.7, 4-*H*), 2.72 (3H, d, *J* 4.6, NHC*H*$_3$), 2.30 (3H, s, Ar-C*H*$_3$). δ_C(176 MHz, DMSO-d$_6$) 167.2 (2-*C*=O), 158.6 (2'-*C*=O), 153.3 (*C*-2'), 145.8 (*C*-5'), 135.5 (*C*-1), 133.5 (*C*-3), 133.4 (*C*-2), 130.2 (*C*-4'), 128.8 (*C*-5), 128.1 (*C*-3' & *C*-4), 123.5 (*C*-6), 25.9 (*C*H$_3$NH), 19.5 (*C*H$_3$Ar). *m/z* (LC-MS ES$^+$) 320.3 [M+H]$^+$. HRMS (ES$^+$) found [M+H]+ 320.0703, $C_{14}H_{14}N_3O_4S$ requires 320.0705. CHN found: C 52.41; H 3.99; N 13.08. $C_{14}H_{13}N_3O_4S$ requires C 52.66; H 4.10; N 13.16.

_N_-[4-methoxy-2-(methylcarbamoyl)phenyl]-5'-nitrothiophene-2'-carboxamide (194)

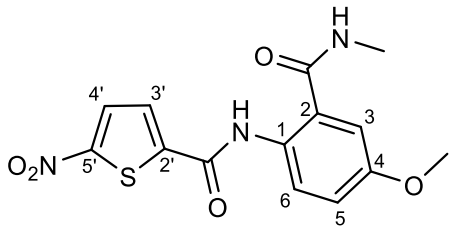

Following general procedure **C**, using DCM (1 mL) as a reaction solvent, where the substituted amine was amino-4-methoxy-*N*-methyl-2-benzamide (**185**) (0.032 g, 0.18 mmol, 1.0 eq.), afforded *N*-[4-methoxy-2-(methylcarbamoyl)phenyl]-5'-nitrothiophene-2'-carboxamide (**194**) as a yellow solid (0.040 g, 68 %) melting point 281–282 °C. ν_{max} (ATR) 3360 (N–H), 3085 (N–H), 1664 (C=O), 1597 (C=O), 1525, 1334 cm^{-1}. δ_H(700 MHz, DMSO-d$_6$) 12.69 (1H, s, 1-N*H*), 8.91 (1H, d, *J* 4.7, CH$_3$N*H*), 8.34 (1H, d, *J* 9.1, 6-*H*), 8.21 (1H, d, *J* 4.4, 4'-*H*), 7.70 (1H, d, *J* 4.4, 3'-*H*), 7.39 (1H, d, *J* 2.9, 3-*H*), 7.18 (1H, dd, *J* 9.1 *J* 2.9, 5-*H*), 3.82 (3H, s, O-C*H*$_3$), 2.83 (3H, d, *J* 4.7, NHC*H*$_3$). δ_C(176 MHz, DMSO-d$_6$) 168.4 (2-*C*=O), 157.2 (2'-*C*=O), 155.2 (*C*-4), 153.2 (*C*-2'), 146.3 (*C*-5'), 131.3 (*C*-1), 130.4 (*C*-4'), 127.0 (*C*-3'), 122.4 (*C*-6), 122.2 (*C*-2), 117.8 (*C*-5), 113.1 (*C*-3), 55.6 (O-*C*H$_3$), 26.4 (NH- *C*H$_3$). *m/z* (LC-MS ES$^+$) 336.3 [M+H]$^+$. HRMS (ES$^+$) found [M+H]+ 336.0657, $C_{14}H_{13}N_3O5S$ requires 336.0654. CHN found: C 49.22; H 3.81; N 12.21. $C_{14}H_{14}N_3O5S$ requires C 50.14; H 3.91; N 12.54.

***N*-[4-methyl-2-(methylcarbamoyl)phenyl]-5'-nitrothiophene-2'-carboxamide (195)**

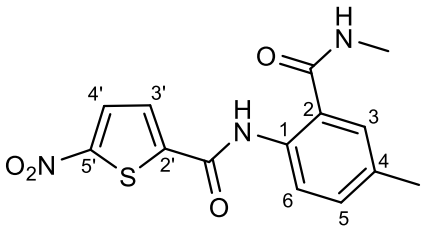

Following general procedure **C**, using DCM (4 mL) as a reaction solvent, where the substituted amine was amino-4-methyl-*N*-methyl-2-benzamide (**186**) (0.16 g, 0.97 mmol, 1.0 eq.), afforded *N*-[4-methyl-2-(methylcarbamoyl)phenyl]-5'-nitrothiophene-2'-carboxamide (**195**) as a yellow solid (0.22 g, 70 %) melting point 272-274 °C. ν_{max} (ATR) 3436 (N–H), 3115 (N–H), 1671 (C=O) 1643 (C=O), 1525, 1329 cm^{-1}. δ_H(700 MHz, DMSO-d_6) 12.98 (1H, s, 1-N*H*), 8.89 (1H, s, N*H*CH_3), 8.34 (1H, d, *J* 8.4, 6-*H*), 8.20 (1H, d, *J* 4.3, 4'-*H*), 7.67–7.69 (2H, m, 3'-*H* & 3-*H*), 7.38 (1H, dd, *J* 8.4 *J* 2.0, 5-*H*), 2.82 (3H, d, *J* 4.5, NH-CH_3), 2.33 (3H, s, Ar-CH_3). δ_C(176 MHz, DMSO-d_6) 168.8 (2-*C*=O), 157.3 (2'-*C*=O), 153.3 (*C*-2'), 146.2 (*C*-5'), 136.0 (*C*-1), 133.0 (*C*-4), 132.8 (*C*-5), 130.3 (*C*-4'), 128.4 (*C*-3), 127.1 (*C*-3'), 120.4 (*C*-6), 120.1 (*C*-2), 26.4 (*C*H_3-NH), 20.4 (*C*H_3-Ar). *m/z* (LC-MS ES^+) 320.3 $[M+H]^+$. HRMS (ES^+) found [M+H]+ 320.0703, $C_{14}H_{14}N_3O_4S$ requires 320.0705. CHN found: C 52.48; H 4.05; N 12.97. $C_{14}H_{13}N_3O_4S$ requires C 52.66; H 4.10; N 13.16.

***N*-[5-methoxy-2-(methylcarbamoyl)phenyl]-5'-nitrothiophene-2'-carboxamide (196)**

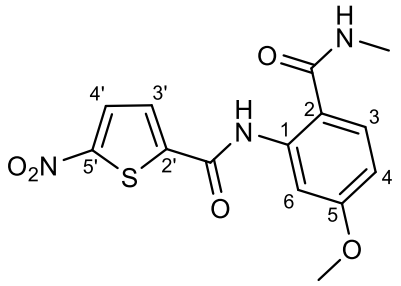

Following general procedure **C**, using DCM (1 mL) as a reaction solvent, where the substituted amine was amino-5-methoxy-*N*-methyl-2-benzamide (**187**) (0.039 g, 0.22 mmol, 1.0 eq.), afforded *N*-[5-methoxy-2-(methylcarbamoyl)phenyl]-5'-

nitrothiophene-2'-carboxamide (**196**) as a yellow solid (0.041 g, 57 %) melting point 230-231 °C. ν_{max} (ATR) 3210 (N–H), 1764 (C=O), 1705 (C=O) 1592, 1348 cm^{-1}. δ_H(700 MHz, DMSO-d_6) 13.70 (1H, s, 1-N*H*), 8.82 (1H, d, *J* 4.6, N*H*CH_3), 8.22 (1H, d, *J* 4.4, 4'-*H*), 8.18 (1H, d, *J* 2.7, 6-*H*), 7.87 (1H, d, *J* 8.9, 3-*H*), 7.69 (1H, d, *J* 4.4, 3'-*H*), 6.82 (1H, d, *J* 8.9 *J* 2.7, 4-*H*), 3.83 (3H, s, O-CH_3), 2.82 (3H, d, *J* 4.6, NHCH_3). δ_C(176 MHz, DMSO-d_6) 168.8 (2-*C*=O), 162.1 (*C*-5), 157.7 (2'-*C*=O), 153.5 (*C*-2'), 146.0 (*C*-5'), 140.7 (*C*-1), 130.4 (*C*-4'), 129.7 (*C*-3), 127.2 (*C*-3'), 111.6 (*C*-2), 109.2 (*C*-4), 105.1 (*C*-6), 55.5 (O-CH_3), 26.3 (NH-CH_3). *m/z* (LC-MS ES^+) 336.3 $[M+H]^+$. HRMS (ES^+) found [M+H]+ 336.0667, $C_{14}H_{14}N_3O_5S$ requires 336.0654. CHN found: C 49.61; H 3.88; N 12.31. $C_{14}H_{13}N_3O_5S$ requires C 50.14; H 3.91; N 12.54.

***N*-[5-methyl-2-(methylcarbamoyl)phenyl]-5'-nitrothiophene-2'-carboxamide (197)**

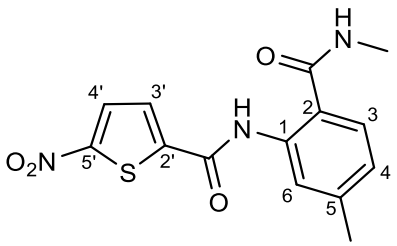

Following general procedure **C**, using DCM (6 mL) as a reaction solvent, where the substituted amine was amino-5-methyl-*N*-methyl-2-benzamide (**188**) (0.21 g, 1.28 mmol, 1.0 eq.), afforded *N*-[5-methyl-2-(methylcarbamoyl)phenyl]-5'-nitrothiophene-2'-carboxamide (**197**) as a yellow solid (0.26 g, 64 %) melting point 206–207 °C. ν_{max} (ATR) 3439 (N–H) 3118 (N–H), 1653 (C=O), 1586 (C=O), 1529, 1335 cm^{-1}. δ_H(599 MHz, DMSO-d_6) 13.29 (1H, s, 1-N*H*), 8.88–8.89 (1H, m, CH_3-N*H*), 8.35 (1H, d, *J* 1.8, 6-*H*), 8.21 (1H, d, *J* 4.4, 4'-*H*), 7.77 (1H, d, *J* 8.0, 3-*H*), 7.69 (1H, d, *J* 4.4, 3'-*H*), 7.06 (1H, ddd, *J* 8.0 *J* 1.8 *J* 0.9, 4-*H*) 2.82 (3H, d, *J* 4.5, NHCH_3), 2.36 (3H, s, Ar-CH_3). δ_C(151 MHz, DMSO-d_6) 168.9 (2-*C*=O), 157.5 (2'-*C*=O), 153.4 (*C*-2'), 146.2 (*C*-5'), 142.7 (*C*-5), 138.7 (*C*-1), 130.4 (*C*-4'), 128.0 (*C*-3), 127.2 (*C*-3'), 124.3 (*C*-4), 120.6 (*C*-6), 116.9 (*C*-2), 26.4 (NH-CH_3), 21.3 (Ar-CH_3). *m/z* (LC-MS ES^+) 320.3 $[M+H]^+$. HRMS (ES^+) found [M+H]+ 320.0697, $C_{14}H_{14}N_3O_4S$ requires 320.0705. CHN found: C 52.76; H 4.12; N 13.06. $C_{14}H_{13}N_3O_4S$ requires C 52.66; H 4.10; N 13.16.

N-[2-(methylcarbamoyl)-5-(trifluoromethyl)phenyl]-5'-nitrothiophene-2'-carboxamide (198)

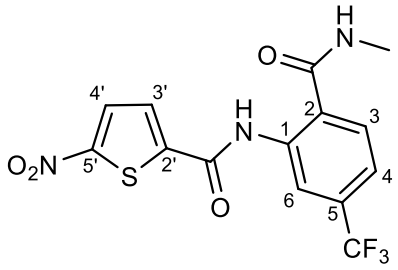

Following general procedure **Gi**, using THF (6 mL) as a reaction solvent, where the substituted amine was amino-5-trifluoromethyl-*N*-methyl-2-benzamide (**189**) (0.20 g, 0.92 mmol, 1.0 eq.) afforded, following work up in DCM and recrystallisation from chloroform: hexane, *N*-[2-(methylcarbamoyl)-5-(trifluoromethyl)phenyl]-5'-nitrothiophene-2'-carboxamide (**198**) as a yellow solid (0.060 g, 18 %) melting point 228 °C. ν_{max} (ATR) 3384 (N–H), 3123 (N–H), 1683 (C=O), 1650 (C=O), 1540, 1338 cm^{-1}. δ_H(400 MHz, DMSO-d_6) 12.99 (1H, s, 1-N*H*), 9.16 (1H, s, N*H*-CH_3), 8.79 (1H d, *J* 5.0 6-*H*), 8.24 (1H, d, *J* 4.4, 4'-*H*), 8.05 (1H, d, *J* 8.3, 3-*H*), 7.74 (1H, d, *J* 4.4, 3'-*H*), 7.65 (1H, m, 4-*H*), 2.85 (3H, d, *J* 4.4, CH_3). δ_C(101 MHz, DMSO-d_6) 167.6 (2-*C*=O), 158.7 (2'-*C*=O), 153.8 (*C*-2'), 145.2 (*C*-5'), 138.7 (*C*-1), 131.8 (*C*-5), 130.4 (*C*-4'), 129.5 (*C*-3), 127.9 (*C*-3'), 123.8 (*C*-2), 123.5 (q, *J* 272.7, *C*F_3), 120.4 (*C*-4), 117.1 (*C*-6), 26.6 (*C*H_3). δ_F(376 MHz, DMSO-d_6) -61.9 (C*F*$_3$). *m/z* (LC-MS ES^+) 374.2 $[M+H]^+$. HRMS (ES^+) found $[M+H]^+$ 374.0440, $C_{14}H_{11}N_3O_4F_3S$ requires *M* 374.0422. CHN found: C 44.83; H 2.77; N 11.08. $C_{14}H_{10}N_3O_4F_3S$ requires C 45.04; H 2.70; N 11.26.

***N*-[5-bromo2-(methylcarbamoyl)phenyl]-5'-nitrothiophene-2'-carboxamide (199)**

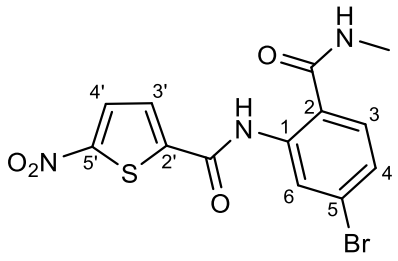

Followed general procedure **C**, using DCM (5 mL) as a reaction solvent, where the substituted amine was amino-5-bromo-*N*-methyl-2-benzamide (**190**) (1.03 g, 4.5

mmol, 1.0 eq.) afforded, following recrystallisation (pyridine/hexane), *N*-[5-bromo2-(methylcarbamoyl)phenyl]-5'-nitrothiophene-2'-carboxamide (**199**) (0.39 g, 23 %) as a yellow solid, melting point 238 °C. δ_H(700 MHz, DMSO-d_6) 13.22 (1H, s, 1-N*H*), 9.03 (1H, d, *J* 4.7, CH_3-N*H*), 8.70 (1H, d, *J* 2.1, 6-*H*), 8.22 (1H, d, *J* 4.4, 4'-*H*), 7.81 (1H, d, *J* 8.5, 3-*H*), 7.70 (1H, d, *J* 4.4, 3'-*H*), 7.48 (1H, dd, *J* 8.5 *J* 2.1, 4-*H*), 2.83 (3H, d, *J* 4.7, C*H*$_3$). δ_C(176 MHz, DMSO-d_6) 168.1 (2-*C*=O), 157.9 (2'-*C*=O), 153.7 (*C*-2'), 145.3 (*C*-5'), 139.7 (*C*-1), 130.3 (*C*-4'), 129.9 (*C*-3), 127.7 (*C*-3'), 126.4 (*C*-4), 125.5 (*C*-5), 122.7 (*C*-6), 118.9 (*C*-2), 26.4 (*C*H$_3$). *m/z* (LC-MS ES$^+$) 384.2 [M(^{79}Br)+H]$^+$ & 386.2 [M(^{81}Br)+H]$^+$. HRMS (ES$^+$) found [M+H]+ 383.9648, $C_{13}H_{11}N_3O_4SBr$ requires 383.9654. CHN found: C 40.51; H 2.61; N 10.92. $C_{14}H_{14}N_3O5S$ requires C 40.63; H 2.62; N 10.94.

N-[8-methoxy-2-(5'-nitrothiophen-2'-yl)-4*H*-3,1-benzoxazin-4-ylidene]methanamine (200)

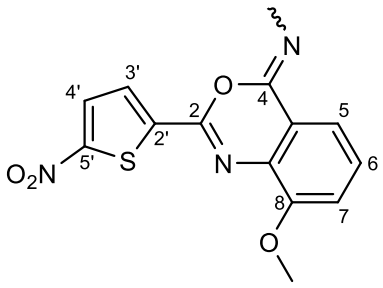

Following general procedure **C**, using DCM (3 mL) as a reaction solvent, where the substituted amine was amino-6-methoxy-*N*-methyl-2-benzamide (**191**) (0.14 g, 0.77 mmol, 1.0 eq.), afforded N-[(4Z)-8-methoxy-2-(5-nitrothiophen-2-yl)-4H-3,1-benzoxazin-4-ylidene]methanamine (**200**) as a yellow solid (0.020 g, 8 %) melting point 225-226 °C. ν_{max} (ATR) 1698 (C=N), 1617 (C=N), 1505, 1338 cm^{-1}. δ_H(400 MHz, DMSO-d_6) 8.18 (1H, d, *J* 4.4, 4'-*H*), 7.84 (1H, d, *J* 4.4, 3'-*H*), 7.55 (1H, dd, *J* 7.9 *J* 1.3, Ar-*H*), 7.41 (1H, dd, *J* 8.3 *J* 7.9, 6-*H*), 7.29 (1H, dd, *J* 8.3 *J* 1.3, Ar-*H*), 3.91 (3H, s, O-C*H*$_3$), 3.22 (3H, s, N-C*H*$_3$). See footnote[15]. *m/z* (LC-MS ES$^+$) 318.3 [M+H]$^+$. HRMS (ES$^+$) found [M+H]+ 318.0555, $C_{14}H_{12}N_3O_4S$ requires 318.0549. CHN found: C 52.42; H 3.43; N 12.87. $C_{14}H_{11}N_3O_4S$ requires C 52.99; H 3.50; N 13.25.

[15] Sample not sufficiently soluble to obtain a ^{13}C NMR spectrum.

N-[8-methyl-2-(5'-nitrothiophen-2'-yl)-4*H*-3,1-benzoxazin-4-ylidene]methanamine (201)

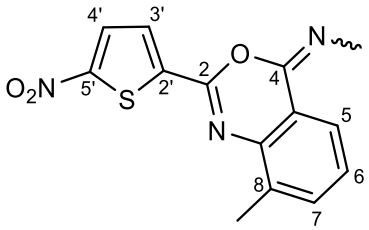

Following general procedure **C**, using DCM (3 mL) as a reaction solvent, where the substituted amine was amino-6-methoxy-*N*-methyl-2-benzamide (**192**) (0.14 g, 0.77 mmol, 1.0 eq.) afforded, following removing volatiles and purification of the filtrate by flash column chromatography (EtOAc:hexane), *N*-[6-methyl-2-(methylcarbamoyl)phenyl]-5'-nitrothiophene-2'-carboxamide (**201**) as a yellow solid (0.026, 12 %). ν_{max} (ATR) 1694 (C=N), 1624 (C=N), 1539, 1337 cm^{-1}. δ_H(700 MHz, DMSO-d_6) 8.20 (1H, d, *J* 4.4, 4'-*H*), 7.89 (1H, d, *J* 4.4, 3'-*H*), 7.83 (1H, dd, *J* 7.9 *J* 1.5, 5-*H*), 7.53 (1H, dd, *J* 7.5 *J* 1.5, 7-*H*), 7.35 (1H, dd, *J* 7.9 *J* 7.5, 6-*H*), 3.22 (3H, s, N-*C*H_3), 2.47 (3H, s, Ar-C*H*$_3$). δ_C(176 MHz, DMSO-d_6) 153.3 (*C*-2'), 149.1 (*C*-2), 145.3 (*C*-4), 140.7 (*C*-5'), 138.8 (1-*C*(Ar)), 134.8 (*C*-8), 134.2 (*C*-7), 130.3 (*C*-4'), 129.5 (*C*-3'), 128.5 (*C*-6), 123.1 (*C*-5), 119.7 (4-*C*(Ar)), 32.9 (*C*H_3-N), 16.4 (*C*H_3 (Ar)). *m/z* (LC-MS ES^+) 302.3 $[M+H]^+$. HRMS (ES^+) found [M+H]+ 302.0599, $C_{14}H_{12}N_3O_3S$ requires 302.0599.

1H,2H,4H-thieno[2,3-d][1,3]oxazine-2,4-dione (203)

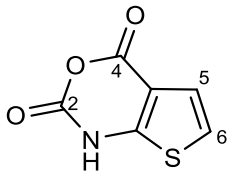

Methyl-2-aminothiophene-3-carboxylate (**30**) (2.00 g, 12.7 mmol, 1.0 eq.) was dispersed in 1M KOH (25.4 mL, 25.4 mmol, 2.0 eq.) and stirred under MWI (150 W, 110 °C, 15 min). The resulting solution was diluted with acetonitrile (12 mL) and cooled to 0 °C before addition of triphosgene (3.04 g, 10.2 mmol, 0.8 eq.). The reaction was left to stand at RT for 16 hrs before filtering to obtain 1H,2H,4H-thieno[2',3'-d][1,3]oxazine-2,4-dione (**203**) as a brown solid (0.97 g, 45 %) melting

point 212-214 °C (lit. 230–231 °C).[104] ν_{max} (ATR) 3224 (N–H), 1764 (C=O), 1710 (C=O) cm^{-1}. δ_H(700 MHz, DMSO-d_6) 12.58 (1H, s, N*H*), 7.20 (1H, dd, *J* 5.6 *J* 0.7, 6-*H*), 7.17 (1H, dd, *J* 5.6 *J* 0.7, 5-*H*). δ_C(176 MHz, DMSO-d_6) 155.7 (1-*C*), 155.2 (*C*-4), 147.6 (*C*-2), 122.3 (*C*-6), 118.4 (*C*-5), 110.0 (4-*C*). *m/z* (LC-MS ES^-) 168.1 $[M-H]^-$.

1-Methyl-1H,2H,4H-thieno[2,3-d][1,3]oxazine-2,4-dione (204)

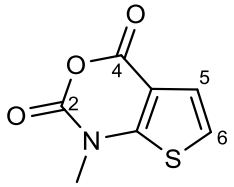

Potassium carbonate (0.95 g, 6.9 mmol, 1.2 eq.) was added to 1H,2H,4H-thieno[2',3'-d][1,3]oxazine-2,4-dione (**203**) (0.97 g, 5.7 mmol, 1.0 eq.) in dry DMF (5 mL). The mixture was stirred for 5 mins before iodomethane (1.1 mL, 17.2 mmol, 3 eq.) was added. The reaction was stirred at RT for 1 hr. Water was added until a precipitate formed, which was then filtered to give 1-methyl-1H,2H,4H-thieno[2',3'-d][1,3]oxazine-2,4-dione (**204**) as a brown solid (0.58 g, 55 %) melting point 145-146 °C (lit. 190 °C).[215] ν_{max} (ATR) 1773 (C=O), 1728 (C=O) cm^{-1}. δ_H (700 MHz, DMSO-d_6) 7.29–7.30 (2H, m, 5-*H* & 6-*H*), 3.44 (3H, s, CH_3). δ_C (176 MHz, DMSO-d_6) 158.7 (1-*C*), 154.4 (*C*-4), 148.0 (*C*-2), 123.6 (*C*-5/6), 119.1 (*C*-5/6), 110.3 (4-*C*), 35.2 (*C*H_3). *m/z* (LC-MS ES^+) 184.1 $[M+H]^+$.

***N*-methyl-2-(methylamino)thiophene-3-carboxamide (205)**

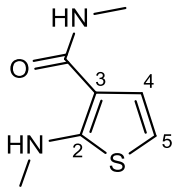

1-Methyl-1H,2H,4H-thieno[2',3'-d][1,3]oxazine-2,4-dione (**204**) (0.58 g, 3.2 mmol, 1.0 eq.) was dispersed in water (8 mL) before addition of 40 % aqueous methylamine (1.2 mL, 16.0 eq, 5 eq.). The reaction mixture was stirred at RT for 4 hrs before dilution with EtOAc. The organic layer was washed with sodium bicarbonate and brine and dried over $MgSO_4$. Volatiles were removed *in vacuo* and the residue

purified by flash column chromatography (EtOAc:hexane) to give *N*-methyl-2-(methylamino)thiophene-3-carboxamide (**205**) as an orange oil (0.19 g, 35 %). ν_{max} (ATR) 3318 (N–H), 1607 (C=O) cm^{-1}. δ_H(700 MHz, $CDCl_3$) 7.90 (1H, s, N*H*), 6.78 (1H, d, *J* 5.8, 4-*H*), 6.20 (1H, d, *J* 5.8, 5-*H*), 5.63 (1H, s, N*H*), 2.95 (3H, d, *J* 5.2, 2-NHC*H*$_3$), 2.90 (3H, d, *J* 4.9, CONHC*H*$_3$). δ_C(176 MHz, $CDCl_3$) 167.0 (*C*=O), 165.0 (*C*-2), 123.3 (*C*-4), 106.0 (*C*-5), 105.4 (*C*-3), 33.7 (2-NH-*C*H$_3$), 26.1 (CONH-*C*H$_3$). *m/z* (LC-MS ES^+) 171.3 $[M+H]^+$. HRMS (ES^+) found $[M+H]^+$ 171.0593, $C_7H_{11}N_2OS$ requires 171.0592.

_N_-methyl-2-(_N_-methyl-5'-nitrothiophene-2'-amido)thiophene-3-carboxamide (206)

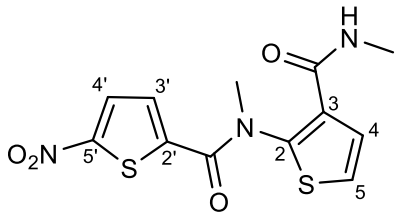

Followed general procedure **Gi**, using DCM (1.4 mL) as a reaction solvent for 1hr, where the substituted amine was *N*-methyl-2-(methylamino)thiophene-3-carboxamide (**205**) (0.12 g, 0.70 mmol, 1.0 eq.) afforded, following work up in DCM and purification by flash column chromatography (EtOAc:hexane), *N*-methyl-2-(*N*-methyl-5'-nitrothiophene-2'-amido)thiophene-3-carboxamide (**206**) as a pale yellow solid (0.13 g, 59 %) melting point 101-102 °C. ν_{max} (ATR) 3323 (N–H), 1630 (C=O), 1504, 1330 cm^{-1}. δ_H(599 MHz, $CDCl_3$) 7.64 (1H, d, *J* 4.4, 4'-*H*), 7.31 (1H, d, *J* 5.8, 5-*H*), 7.22 (1H, d, *J* 5.8, 4-*H*), 7.12 (1H, d, *J* 4.4, 3'-*H*), 6.15 (1H, s, N*H*), 3.45 (3H, s, 2-NC*H*$_3$), 2.88 (3H, d, *J* 4.9, NH-C*H*$_3$). δ_C(151 MHz, $CDCl_3$) 162.0 (3-*C*=O), 161.6 (2'-*C*=O), 154.6 (*C*-2'), 146.8 (*C*-2), 141.8 (*C*-5'), 132.7 (*C*-3), 131.1 (*C*-3'), 127.3 (*C*-4'), 126.0 (*C*-4), 125.2 (*C*-5), 40.2 (2-NCH$_3$), 26.7 (NH-*C*H$_3$). *m/z* (LC-MS ES^+) 326.2 $[M+H]^+$. HRMS (ES^+) found [M+H]+ 326.0262, $C_{12}H_{12}N_3O_4S_2$ requires 326.0269.

1-(5'-Nitrothiophene-2'-carbonyl)-1,2,3,4-tetrahydroquinoline (208)

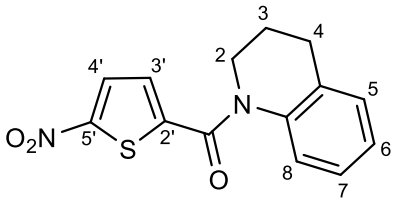

Following general procedure **Gi**, using DCM (4 mL) as a reaction solvent, where the substituted amine was 1,2,3,4-tetrahydroquinoline (0.19 mL, 1.50 mmol, 1.0 eq.) afforded, following work up with 1M NaOH, 1-(5'-nitrothiophene-2'-carbonyl)-1,2,3,4-tetrahydroquinoline (**208**) as a yellow solid (0.34 g, 79 %) melting point 97-98 °C. ν_{max} (ATR) 1632 (C=O), 1536, 1339 cm^{-1}. δ_H(700 MHz, $CDCl_3$) 7.62 (1H, d, *J* 4.3, 4'-*H*), 7.24 (1H, dd, *J* 7.5 *J* 1.2, 5-*H*), 7.16 (1H, ddd, *J* 8.0 *J* 7.8 *J* 1.2, 7-*H*), 7.03 (1H, dd, *J* 7.8 *J* 7.5, 6-*H*), 6.90 (1H, d, *J* 8.0, 8-*H*), 6.81 (1H, d, *J* 4.3, 3'-*H*), 3.92 (2H, t, *J* 6.8, 2-H_2), 2.81 (2H, t, *J* 6.6, 4-H_2), 2.07 (2H, dt, *J* 6.8 *J* 6.6, 3-H_2). δ_C(176 MHz, $CDCl_3$) 161.2 (*C*=O), 153.8 (*C*-2'), 144.8 (*C*-5'), 138.3 (1-*C*(Ar)) 133.7 (4-*C*(Ar)), 129.7 (*C*-3'), 128.8 (*C*-5), 127.3 (*C*-4'), 126.6 (*C*-7), 126.5 (*C*-6), 125.6 (*C*-8), 44.8 (*C*-2), 26.8 (*C*-4), 24.2 (*C*-3). *m/z* (LC-MS ES^+) 289.2 $[M+H]^+$. HRMS (ES^+) found $[M+H]^+$ 289.0657, $C_{14}H_{13}N_2O_3S$ requires *M* 289.0647. CHN found: C 58.16; H 4.20; N 9.57. $C_{12}H_7N_2O_3F_3S$ requires C 58.32; H 4.20; N 9.72.

N-(2-carbamoylbenzyl)-5'-nitrothiophene-2'-carboxamide (210)

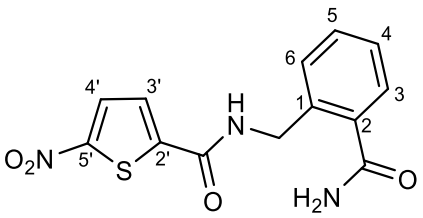

Following general procedure **Gi**, using THF (1 mL) as a reaction solvent and triethylamine (3.5 eq.) for 1hr, where the substituted amine was 2-aminomethylbenzamide hydrochloride (54 mg, 0.29 mmol, 1.0 eq.), afforded, without further purification, N-(2-carbamoylbenzyl)-5'-nitrothiophene-2'-carboxamide (**210**) as a yellow solid (18 mg, 20 %) melting point 185-186 °C. ν_{max} (ATR) 3080 (NH), 1654 (C=O), 1621 (C=O), 1509, 1334 cm^{-1}. δ_H (599 MHz, CD_3OD) 7.96

(1H, d, *J* 4.9, 4'-*H*), 7.65 (1H, d, *J 4.9*, 3'-*H*), 7.55 (1H, d, *J* 8.5, 3-*H*), 7.45-7.47 (2H, m, 5-*H* & 6-*H*), 7.34-7.38 (1H, m, 4-*H*), 4.72 (2H, s, 1-CH_2). δ_C (151 MHz, CD_3OD) 174.7 (2-*C*=O), 162.1 (2'-*C*=O), 155.5 (*C*-5'), 146.3 (*C*-2'), 137.4 (*C*-1), 136.6 (*C*-2), 131.7 & 130.3 (*C*-5 & *C*-6), 129.8 (*C*-4'), 128.9 (*C*-3), 128.7 (*C*-4), 128.2 (*C*-3'), 42.9 (1-*C*H_2). *m/z* (LC-MS ES^+) 306.3 $[M+H]^+$. HRMS (ES^+) found $[M+H]^+$ 306.0554, $C_{13}H_{12}N_3O_4S$ requires *M* 306.0549.

_N_-methyl-2-[(*E*)-[(5'-nitrothiophen-2'-yl)methylidene]amino]thiophene-3-carboxamide (212)

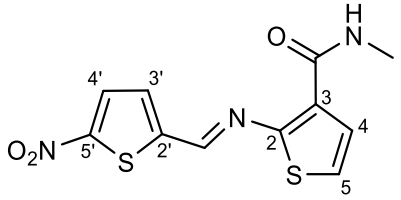

5-Nitrothiophene-2-carboxaldehyde (0.22 g, 1.4 mmol, 1.0 eq.) was dissolved in dry MeOH (2 mL) and added to a solution of 2-amino-*N*-methylthiophene-3-carboxamide (**30**) (0.27 g, 1.7 mmol, 1.2 eq.) and acetic acid (0.01 mL, 0.14 mmol, 0.1 eq.) in dry MeOH (2 mL). The reaction was stirred at RT for 4 hrs. The reaction mixture was filtered to give an orange solid, which was purified by flash column chromatography ($CHCl_3$:MeOH) to give *N*-methyl-2-[(*E*)-[(5'-nitrothiophen-2'-yl)methylidene]amino]thiophene-3-carboxamide (**212**) as an orange solid of 80 % purity (0.076 g, 14 %) melting point 183-187 °C. ν_{max} (ATR) 3310 (N–H), 1647 (C=N), 1582 (C=O), 1552, 1334 cm^{-1}. δ_H(700 MHz, DMSO-d_6) 8.90 (1H, s, C*H*N), 8.21 (2H, m, 4'-*H* & N*H*), 7.84 (1H, d, *J* 4.4, 3'-*H*), 7.48 (1H, d, *J* 5.6, 5-*H*), 7.35 (1H, d, *J* 5.6, 4-*H*), 2.88 (3H, d, *J* 4.8, CH_3). δ_C(176 MHz, DMSO-d_6) 162.1 (*C*=O), 153.2 (*C*-5'), 152.0 (2'-*C*HN), 151.0 (*C*-2), 147.0 (*C*-2'), 133.3 (*C*-3'), 132.5 (*C*-3), 130.6 (*C*-4'), 128.9 (*C*-4), 123.2 (*C*-5), 26.0 (*C*H_3). *m/z* (LC-MS ES^+) 296.1 $[M+H]^+$. HRMS (ES^+) found $[M+H]^+$ 296.0192, $C_{11}H_{10}N_3O_3S_2$ requires *M* 296.0164. CHN found: C 44.76; H 3.39; N 13.42. $C_{11}H_9N_3O_3S_2$ requires C 44.73; H 3.07; N 14.23.

5-Nitrothiophene-2-carbonyl azide (216) [105]

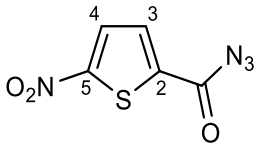

5-Nitrothiophene-2-carbonyl chloride (**23**) (1.88 g, 9.8 mmol, 1.0 eq.) was dissolved in chloroform and cooled to 0 °C. Sodium azide (1.07 g, 16.5 mmol, 1.7 eq.) was dissolved in water (3 mL) and added dropwise to the chloroform solution. The reaction was stirred at 0 °C for 0.5 hr and then at RT for 16 hrs. The organic layer was separated, washed with brine and dried over $MgSO_4$. Volatiles were removed *in vacuo* to give 5-nitrothiophene-2-carbonyl azide (**216**) as a yellow semi-solid (1.51 g, 78 %). ν_{max} (ATR) 3115, 2170, 2135 (N=N=N), 1683 (C=O), 1511, 1339 cm^{-1}. δ_H(700 MHz, $CDCl_3$) 7.88 (1H, d, *J* 4.3, 4-*H*), 7.73 (1H, d, *J* 4.3, 3-*H*). δ_C(176 MHz, $CDCl_3$) 166.0 (*C*=O), 156.7 (*C*-5), 139.2 (*C*-2), 132.5 (*C*-3), 128.3 (*C*-4). *m/z* (LC-MS ES^-) 172.1 [M - N_3 + OH - H]$^-$.

Tert-butyl *N*-(5-nitrothiophen-2-yl)carbamate (217) [216]

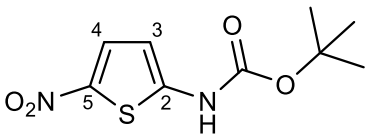

5-Nitrothiophene-2-carbonyl azide (**216**) (1.51 g, 7.6 mmol, 1.0 eq.) was dissolved in dry dioxane (7.5 mL) and t-BuOH was added (0.9 mL, 9.9 mmol, 1.3 eq.). The reaction was stirred at reflux for 2 hrs under argon. Volatiles were removed *in vacuo* and the resulting crude solid was purified by flash column chromatography (hexane: EtOAc) to give tert-butyl *N*-(5-nitrothiophen-2-yl)carbamate (**217**) as a yellow solid (1.26 g, 68 %) melting point 143 °C. ν_{max} (ATR) 3246 (N–H), 1719 (C=O), 1556, 1312 cm^{-1}. δ_H(700 MHz, DMSO-d_6) 11.61 (1H, s, N*H*), 7.95 (1H, d, *J* 4.8, 4-*H*), 6.53 (1H, d, *J* 4.8, 3-*H*), 1.50 (9H, s, CH_3). δ_C(176 MHz, DMSO-d_6) 152.3 (*C*=O), 150.8 (*C*-2), 140.3 (*C*-5), 130.5 (*C*-4), 109.7 (*C*-3), 82.2 (*C*$(CH_3)_3$), 27.8 (*C*H_3). *m/z* (LC-MS ES^+) 245.3 [M + H]$^+$.

5-Nitro-2-amino thiophene hydrochloride (214)

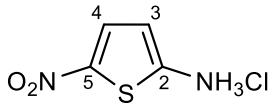

Tert-butyl *N*-(5-nitrothiophen-2-yl)carbamate (**217**) (0.10 g, 0.41 mmol, 1.0 eq.) was stirred with dry 4M HCl in dioxane (1.6 mL, 6.6 mmol, 16 eq.) under argon at RT for 26 hrs before filtering to give 5-nitro-2-amino thiophene hydrochloride (**214**) as an orange solid (0.030 g, 41 %) melting point 178 °C (dec). ν_{max} (ATR) 3401 (N–H), 3293 (N–H), 1528, 1330 cm^{-1}. δ_H(400 MHz, DMSO-d_6) 8.64 (2H, s, NH_2), 7.75 (1H, d, *J* 4.9, 4-*H*) 6.01 (1H, d, *J* 4.9, 3-*H*). δ_C(101 MHz, DMSO-d_6) 167.6 (*C*-2), 134.8 (*C*-4), 130.4 (*C*-5), 106.2 (*C*-3). *m/z* (LC-MS ES^+) 145.2 $[M + H]^+$.

2-(Methylcarbamoyl)benzoic acid (215)

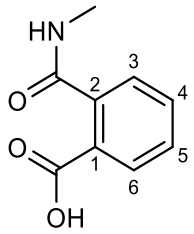

Phthalic anhydride (0.50 g, 3.3 mmol, 1 eq.) was stirred with 40 % aqueous methylamine (1.3 mL, 16.9 mmol, 5 eq.) at RT for 10 mins before acidification with conc. HCl and addition of EtOAc. The organic layer was washed with brine and dried over $MgSO_4$. Volatiles were removed *in vacuo* to give a colourless oil. Upon standing overnight a white solid formed which was triturated in EtOAc to give 2-(methylcarbamoyl)benzoic acid (**215**) as a white solid (0.46 g, 76 %) melting point 133.5 °C, which was taken forwards without further purification. ν_{max} (ATR) 3319 (N–H), 3016 (O–H), 1723 (C=O), 1602 (C=O) cm^{-1}. δ_H(700 MHz, DMSO-d_6) 13.00 (1H, s, O*H*), 8.18 (1H, s, N*H*), 7.74 (1H, ddd, *J* 7.6 *J* 1.4 *J* 0.5, 6-*H*), 7.55 (1H, dt, *J* 7.6 *J* 1.4, 4-*H*), 7.49 (1H, dt, *J* 7.6 *J* 1.3, 5-*H*), 7.39 (1H, ddd, *J* 7.6 *J* 1.3 *J* 0.5, 3-*H*), 2.71 (1H, d, *J* 4.6, CH_3). δ_C(176 MHz, DMSO-d_6) 168.9 (*C*O-NH), 168.0 (*C*O-OH), 138.5 (*C*-2), 131.1 (*C*-4), 130.8 (*C*-1), 129.1 (*C*-6 & *C*-5), 127.5 (*C*-3), 26.1 (CH_3). *m/z* (LC-MS ES^+) 180.2 $[M + H]^+$.

4-Tert-butyl-1-methyl-2-nitrobenzene (221) [217]

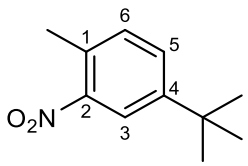

Acetic acid (7.1 mL, 124 mmol, 4.3 eq.) was added slowly to an ice cold 70 % nitric acid (5.7 mL, 95 mmol, 3.3 eq.), keeping the temperature below 15 °C. The mixture was added dropwise to a solution of 4-tertbutyltoluene (5.0 mL, 29 mmol, 1.0 eq.) in acetic anhydride (30 mL) over 1 hr. The reaction mixture was stirred for a further 2 hrs before pouring onto ice and extraction into DCM. The organic extracts were combined and treated with 2 M NaOH (160 mL) on ice. The organic layer was then washed with water and brine and dried over $MgSO_4$. Volatiles were removed *in vacuo* to give 4-tert-butyl-1-methyl-2-nitrobenzene (**221**) as an orange oil (4.47 g, 80 %). ν_{max} (ATR) 1534, 1342 cm^{-1}. δ_H(400 MHz, $CDCl_3$) 7.97-7.99 (1H, m, 3-*H*), 7.53 (1H, dd, *J* 8.0 *J* 1.5, 5-*H*), 7.27 (1H, d, *J* 8.0, 6-*H*), 2.57 (3H, s, 1-CH_3), 1.35 (9H, s, 4-C-CH_3). δ_C(101 MHz, $CDCl_3$) 150.8 (*C*-4), 149.1 (*C*-2), 132.6 (*C*-6), 130.7 (*C*-1), 130.4 (*C*-5), 121.6 (*C*-3), 34.8 (*C*-$(CH_3)_3$), 31.2 (C-(*C*$H_3)_3$), 20.1 (1-*C*H_3). *m/z* (LC-MS ES^+) 194.3 $[M+H]^+$.

4-Tert-butyl-2-nitrobenzoic acid (222) [217]

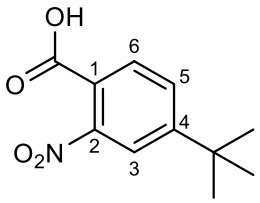

Potassium permanganate (16.6 g, 105 mmol, 5 eq.) was added to a solution of 4-tert-butyl-1-methyl-2-nitrobenzene (**221**) (4.05 g, 21.0 mmol, 1.0 eq.) in pyridine (30 mL) and water (30 mL) and heated to 110 °C for 2 hrs, before addition of further of potassium permanganate (16.6 g, 105 mmol, 5 eq.). The reaction was stirred at 110 °C for 16 hrs before cooling and filtering over celite. The filter cake was washed with 2 M NaOH (400 mL) and EtOAc (100 mL). The aqueous layer was acidified with concentrated HCl and extracted into EtOAc (3 x 100 mL). The organic extracts were

dried over $MgSO_4$ and volatiles were removed in vacuo to give 4-tert-butyl-2-nitrobenzoic acid (**222**) as an off white solid (1.01 g, 22 %) melting point 150–151 °C (lit. 152–154 °C).[218] ν_{max} (ATR) 2768–3187 (O–H), 1696 (C=O), 1530, 1368 cm^{-1}. δ_H(400 MHz, $CDCl_3$) 7.86 (1H, dd, *J* 8.1 *J* 1.0, 6-*H*), 7.79 (1H, d, *J* 1.4, 3-*H*), 7.68 (1H, dd, *J* 8.1 *J* 1.4, 5-*H*), 1.38 (9H, s, (CH_3)$_3$). δ_C(101 MHz, $CDCl_3$) 170.0 (*C*=O), 158.1 (*C*-4), 149.7 (*C*-2), 130.8 (*C*-6), 129.4 (*C*-5), 122.2 (*C*-1), 121.1 (*C*-3), 35.7 (*C*(CH_3)$_3$), 31.0 (C(*C*H_3)$_3$. *m/z* (LC-MS ES^+) 224.2 $[M+H]^+$.

4-Tert-butyl-2-nitrobenzoyl chloride (223)

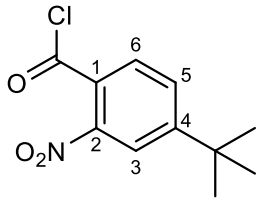

Following general procedure **A,** where the acid was 4-tert-butyl-2-nitrobenzoic acid (**222**) (0.50 g, 2.24 mmol, 1.0 eq.), afforded 4-tert-butyl-2-nitrobenzoyl chloride (**223**) as a yellow oil (0.51 g, 94 %). ν_{max} (ATR) 1796 (C=O), 1534, 1351 cm^{-1}. δ_H(400 MHz, $CDCl_3$) 8.01 (1H, d, *J* 1.4, 3-*H*), 7.71-7.77 (2H, m, 5-*H* & 6-*H*), 1.39 (9H, s, C(CH_3)$_3$). δ_C(101 MHz, $CDCl_3$) 165.7 (*C*=O), 158.2 (*C*-4), 146.4 (*C*-2), 130.6 (*C*-5/6), 129.2 (*C*-5/6), 129.0 (*C*-1), 121.8 (*C*-3), 35.8 (*C*(CH_3)$_3$), 31.0 (C(*C*H_3)$_3$).

4-Tert-butyl-N-methyl-2-nitrobenzamide (224)

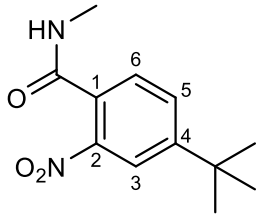

Methylamine (2.0 M in THF, 5.3 mL, 10.6 mmol, 5.0 eq.) was added to a solution of 4-tert-butyl-2-nitrobenzoyl chloride (**223**) (0.51 g, 2.11 mmol, 1.0 eq.) in THF (5 mL) at 0 °C before addition of triethylamine (0.70 mL, 5.28 mmol, 2.5 eq.). The reaction was stirred at RT for 0.5 hr before dilution with water. Volatiles were removed *in vacuo* and the resulting suspension was extracted with chloroform. The organic

fractions were collected and washed with water and brine, dried over $MgSO_4$ and volatiles removed *in vacuo* to give 4-tert-butyl-N-methyl-2-nitrobenzamide (**224**) as a yellow oil (0.43 g, 86 %). ν_{max} (ATR) 3290 (N–H), 1647 (C=O), 1534, 1356 cm^{-1}. δ_H(400 MHz, $CDCl_3$) 8.04 (1H, d, *J* 2.2, 3-*H*), 7.66 (1H, dd, *J* 8.0 *J* 2.2, 5-*H*), 7.43 (1H, dd, *J* 8.0 *J* 2.9, 6-*H*), 5.80 (1H, s, N*H*), 3.02 (3H, dd, *J* 4.9 *J* 2.9, NHCH_3), 1.36 (9H, s, C(CH_3)$_3$). δ_C(101 MHz, $CDCl_3$) 167.5 (*C*=O), 155.0 (*C*-4), 146.6 (*C*-2), 130.8 (*C*-5), 130.3 (*C*-1), 128.6 (*C*-6), 121.7 (*C*-3), 35.4 (*C*(CH_3)$_3$), 31.1 (C(*C*H_3)$_3$), 27.2 (NH*C*H_3). *m/z* (LC-MS ES^+) 237.0 $[M+H]^+$. HRMS (ES^+) found $[M+H]^+$ 237.1252, $C_{12}H_{17}N_2O_3$ requires *M* 237.1239.

2-Amino-4-tert-butyl-*N*-methylbenzamide (225)

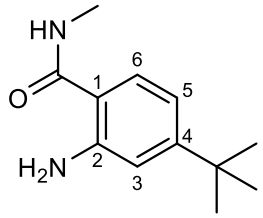

4-Tert-butyl-N-methyl-2-nitrobenzamide (**224**) (0.39 g, 1.65 mmol, 1.0 eq.) was dissolved in methanol (8 mL) and added to Pd/C pre-wetted with EtOAc and purged with nitrogen 3 times. The reaction mixture was stirred under an atmosphere of H_2 (balloon pressure) at RT for 3 hrs, when it was filtered over celite and volatiles were removed in vacuo. The residue was purified by flash column chromatography (EtOAc:hexane) to give 2-amino-4-tert-butyl-*N*-methylbenzamide (**225**) as a pale yellow oil (0.12 g, 35 %). ν_{max} (ATR) 3350 (N–H), 2965 (N–H), 1632 (C=O) cm^{-1}. δ_H(400 MHz, $CDCl_3$) 7.24–7.27 (1H, m, 6-*H*), 6.76 (1H, d, *J* 1.6, 3-*H*), 6.72 (1H, dd, *J* 8.3 *J* 1.6, 5-*H*), 6.13 (1H, s, N*H*CH_3), 2.94 (3H, d, *J* 4.8, NHCH_3), 1.27 (9H, s, C(CH_3)$_3$. δ_C(101 MHz, $CDCl_3$) 169.8 (*C*=O), 156.1 (*C*-4), 146.9 (*C*-2), 127.0 (*C*-6), 115.7 (*C*-3/5), 115.3 (*C*-3/5), 114.5 (*C*-1), 34.9 (4-*C*), 31.1 (C(*C*H_3)$_3$), 26.6 (NH*C*H_3). *m/z* (LC-MS ES^+) 207.0 $[M+H]^+$. HRMS (ES^+) found $[M+H]^+$ 207.1473, $C_{12}H_{19}N_2O$ requires *M* 207.1497.

***N*-[5-tert-butyl-2-(methylcarbamoyl)phenyl]-5'-nitrothiophene-2'-carboxamide (226)**

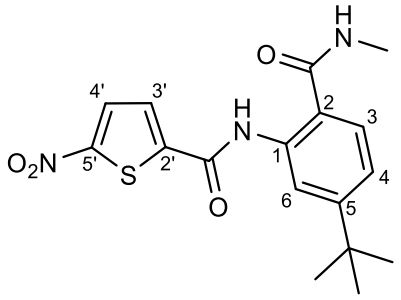

Following general procedure **C**, using DCM (2 mL) as a reaction solvent for 3 hrs, where the substituted amine was 2-amino-4-tert-butyl-*N*-methylbenzamide (**225**) (0.11 g, 0.53, 1.0 eq.) afforded, after dilution with DCM and washing with water and brine, removal of volatiles, trituration with water and recrystallisation from $CHCl_3$:hexane, *N*-[5-tert-butyl-2-(methylcarbamoyl)phenyl]-5'-nitrothiophene-2'-carboxamide (**226**) as a yellow solid (0.084 g, 44 %) melting point 242–243 °C. ν_{max} (ATR) 3384 (N–H), 2965 (N–H), 1654, 1642 (C=O), 1538, 1355 cm^{-1}. δ_H(400 MHz, $CDCl_3$) 12.87 (1H, s, 1-N*H*), 8.83 (1H, d, *J* 2.1, 6-*H*), 7.91 (1H, d, *J* 4.2, 4'-*H*), 7.68 (1H, d, *J* 4.2, 3'-*H*), 7.45 (1H, d, *J* 8.3, 3-*H*), 7.18 (1H, dd, *J* 8.3 *J* 2.1, 4-*H*), 6.37 (1H, s, N*H*-CH_3), 3.04 (3H, d, *J* 4.7, NH-C*H*$_3$), 1.36 (9H, s, C(C*H*$_3$)$_3$). δ_C(101 MHz, $CDCl_3$) 169.8 (2-*C*=O), 158.5 (2'-*C*=O), 157.5 (*C*-5), 154.7 (*C*-2'), 147.0 (*C*-5'), 139.5 (*C*-1), 128.7 (*C*-4'), 126.4 (*C*-3'), 126.3 (*C*-3), 121.0 (*C*-4), 118.6 (*C*-6), 116.6 (*C*-2), 35.5 (*C*(CH$_3$)$_3$), 31.1 (C(*C*H$_3$)$_3$), 27.1 (NH-*C*H$_3$). *m/z* (LC-MS ES$^+$) 362.3 $[M+H]^+$. HRMS (ES$^+$) found $[M+H]^+$ 362.1179, $C_{17}H_{20}N_3O_4S$ requires *M* 362.1175. CHN found: C 56.61; H 5.38; N 11.41. $C_{17}H_{19}N_3O_4S$ requires C 56.49; H 5.30; N 11.63.

5-[2'-(2''-Methoxyethoxy)ethoxy]-2-bromo-1-nitrobenzene (229)

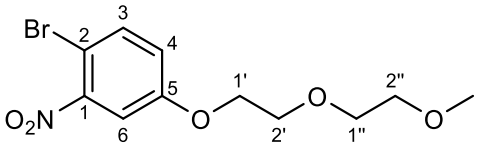

4-Bromo-3-nitrophenol (0.200 g, 0.92 mmol, 1.0 eq.) was dissolved in DMF (1 mL) before addition of cesium carbonate (0.32 g, 1.01mmol, 1.1 eq.) and 1-bromo-2-(2-

methoxyethoxy)ethane (0.13 mL, 1.01 mmol, 1.1 eq.). The reaction mixture was stirred at 80 °C for 1 hr before dilution with water (10 mL) and EtOAc (5 mL). The aqueous layer was back extracted with EtOAc (3 x 5 mL) and washed with water, sodium bicarbonate and brine. The combined organic extracts were dried over $MgSO_4$ and concentrated to give a yellow oil, which was purified by flash column chromatography (EtOAc: hexane 1:1) to give 5-[2'-(2''-methoxyethoxy)ethoxy]-2-bromo-1-nitrobenzene (**229**) as a yellow oil (0.24, 82 %). ν_{max} (ATR) 2800-3020 (C-H), 1539, 1351 cm^{-1}. δ_H (599 MHz, $CDCl_3$) 7.59 (1H, d, *J* 8.9, 3-*H*) 7.41 (1H, d, *J* 3.0, 6-*H*), 6.99-7.04 (1H, dd, *J* 8.9 *J* 3.0, 4-*H*), 4.15-4.20 (2H, m, 1'-H_2), 3.84-3.89 (2H, m, 2'-H_2), 3.68-3.73 (2H, m, 1''-H_2), 3.54-3.59 (2H, m, 2''-H_2), 3.38 (3H, s, CH_3). δ_C (151 MHz, $CDCl_3$) 158.6 (*C*-5), 150.2 (*C*-1), 135.6 (*C*-3), 120.6 (*C*-4), 111.8 (*C*-6), 104.9 (*C*-2), 72.1 (*C*-2''), 71.0 (*C*-1''), 69.6 (*C*-2'), 68.6 (*C*-1'), 59.2 (*C*H_3). *m/z* (LC-MS ES^+) 320.2 $[M(^{79}Br)+H]^+$ & 322.2 $[M(^{81}Br)+H]^+$. HRMS (ES^+) found $[M+H]^+$ 320.0140, $C_{11}H_{15}NO_5{}^{79}Br$ requires *M* 320.0134.

5-[2'-(2''-Methoxyethoxy)ethoxy]-2-bromo-1-aminobenzene (230) [106]

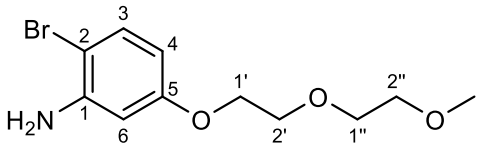

5-[2'-(2''-Methoxyethoxy)ethoxy]-2-bromo-1-nitrobenzene (**229**) (0.31 g, 0.97 mmol, 1.0 eq.), iron powder (0.27 g, 4.84 mmol, 5.0 eq.) and ammonium chloride (0.13 g, 2.42 mmol, 2.5 eq.) were dissolved in EtOH:H_2O (1:1, 6 mL) and heated to 70 °C for 30 minutes. The reaction mixture was hot filtered through celite and volatiles were removed *in vacuo*. 2N ammonia in MeOH :$CHCl_3$ (1:9) was added, followed by sonication and a further filtration through celite. Volatiles were removed *in vacuo* to give 5-[2'-(2''-methoxyethoxy)ethoxy]-2-bromo-1-aminobenzene (**230**) as a brown oil (0.28 g, 99 %). ν_{max} (ATR) 3347, 3460 (N-H) cm^{-1}. δ_H (599 MHz, $CDCl_3$) 7.24 (1H, d, *J* 8.8, 3-*H*), 6.35 (1H, d, *J* 2.8, 6-*H*), 6.23 (1H, dd, *J*8.8, *J*2.8, 4-*H*), 4.05-4.08 (2H, m, 1'-H_2), 3.79-3.82 (2H, m, 2'-H_2), 3.67-3.70 (2H, m, 1''-H_2), 3.54-3.58 (2H, m, 2''-H_2), 3.38 (3H, s, CH_3). δ_C (151 MHz, $CDCl_3$) 159.3 (*C*-5), 144.9 (*C*-1), 132.9 (*C*-3), 106.4 (*C*-4), 102.3 (*C*-6), 100.8 (*C*-2), 72.1 (*C*-2''), 70.8 (*C*-1''), 69.8 (*C*-2'), 67.7 (*C*-1'), 59.2 (*C*H_3).

m/z (LC-MS ES$^+$) 290.2 [M(^{79}Br)+H]$^+$ & 292.2 [M(^{81}Br)+H]$^+$. HRMS (ES$^+$) found [M+H]$^+$ 290.0401, $C_{11}H_{17}NO_3{}^{79}Br$ requires *M* 290.0392.

7-[2'-(2''-Methoxyethoxy)ethoxy]-3-methyl-3,4-dihydroquinazolin-4-one (233)[107]

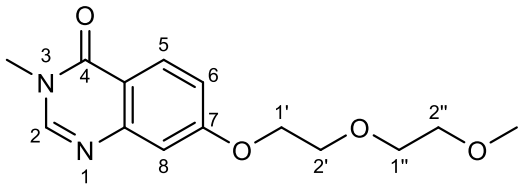

5-[2'-(2''-Methoxyethoxy)ethoxy]-2-bromo-1-nitrobenzene (**229**) (1.00g, 3.1 mmol, 1 eq.), dppf (0.17 g, 0.32 mmol, 0.1 eq.) and $Pd(OAc)_2$ (0.035 g, 0.16 mmol, 0.05 eq.) were dissolved in N-methylformamide (15 mL) and heated to 165 °C for 72 hrs under nitrogen. The reaction mixture was cooled and extracted into EtOAc. The organic layer was washed with water, sodium bicarbonate and brine before drying over $MgSO_4$. Volatiles were removed and the residue purified by flash column chromatography (9:1 DCM:MeOH) to give 7-[2'-(2''-methoxyethoxy)ethoxy]-3-methyl-3,4-dihydroquinazolin-4-one (**233**) as a brown oil (0.40 g, 43 %). ν_{max} (ATR) 2244 ((N)C=N), 1664 (C=O), 1604 (C=N) cm^{-1}. δ_H (599 MHz, $CDCl_3$) 8.19 (1H, d, *J* 8.8, 5-*H*), 8.02 (1H, s, 2-*H*), 7.10 (1H, dd, *J* 8.8 *J* 2.4, 6-*H*), 7.07 (1H, d, *J*2.4, 8-*H*), 4.21-4.29 (2H, m, 1'-H_2), 3.89-3.92 (2H, m, 2'-H_2), 3.72-3.74 (2H, m, 1''-H_2), 3.57-3.60 (2H, m, 2''-H_2), 3.56 (3H, s, 3-CH_3), 3.39 (3H, s, O-CH_3). δ_C (151 MHz, $CDCl_3$) 163.5 (*C*-7), 161.0 (*C*-4), 150.2 (1-*C*), 147.4 (*C*-2), 128.0 (*C*-5), 117.6 (*C*-6), 115.5 (4-*C*), 108.7 (*C*-8), 71.9 (*C*-2''), 70.8 (*C*-1''), 69.4 (*C*-2'), 67.7 (*C*-1'), 59.0 (O-*C*H_3), 33.9 (3-*C*H_3). *m/z* (LC-MS ES$^+$) 279.3 [M+H]$^+$. HRMS (ES$^+$) found [M+H]$^+$ 279.1367, $C_{14}H_{19}N_2O_4$ requires *M* 279.1345.

5-[2'-(2''-Methoxyethoxy)ethoxy]-2-methyl-1-nitrobenzene (235)

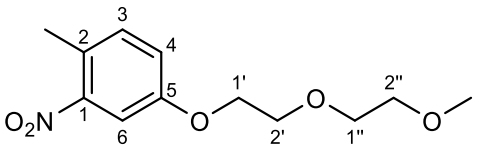

4-Methyl-3-nitrophenol (0.100 g, 0.65 mmol, 1.0 eq.) was dissolved in DMF before addition of caesium carbonate (0.23 g, 0.72 mmol, 1.1 eq.) and 1-bromo-2-(2-methoxyethoxy)ethane (0.089 g, 0.72 mmol, 1.1 eq.). The reaction mixture was

stirred at 80 °C for 45 minutes before dilution with water (10 mL) and EtOAc (5 mL). The aqueous layer was back extracted with EtOAc (3 x 5 mL) and washed with water, sodium bicarbonate and brine. The combined organic extracts were dried over $MgSO_4$ and concentraed to give a yellow oil, which was purified by flash column chromatography (EtOAc: hexane 2:3) to give 5-[2'-(2''-methoxyethoxy)ethoxy]-2-methyl-1-nitrobenzene (**235**) as a yellow oil (0.102, 61 %). ν_{max} (ATR) 2800-3000 (C-H), 1522, 1340 cm^{-1}. δ_H (599 MHz, $CDCl_3$) 7.51 (1H, d, *J* 2.8, 6-*H*), 7.21 (1H, dd, *J* 8.4 *J* 0.7, 3-*H*), 7.08 (1H, dd, *J* 8.4 *J* 2.8, 4-*H*) 4.14-4.19 (2H, m, 1'-H_2), 3.83-3.90 (2H, m, 2'-H_2), 3.67-3.74 (2H, m, 1''-H_2), 3.54-3.60 (2H, m, 2''-H_2), 3.37 (3H, s, OCH_3), 2.50 (3H, d, *J* 0.7, 2-CH_3). δ_C (151 MHz, $CDCl_3$) 157.4 (*C*-5), 149.4 (*C*-1), 133.5 (*C*-3), 125.8 (*C*-2), 120.6 (*C*-4), 110.1 (*C*-6), 72.0 (*C*-2'') 70.9 (*C*-1''), 69.6 (*C*-2'), 68.2 (*C*-1'), 59.2 (O-*C*H_3), 19.8 (2-*C*H_3). *m/z* (LC-MS ES^+) 256.27 $[M+H]^+$. HRMS (ES^-) found $[M+H]^+$ 256.1192, $C_{12}H_{17}NO_5$ requires *M* 256.1185.

7-Hydroxy-2,4-dihydro-1*H*-3,1-benzoxazine-2,4-dione (239)

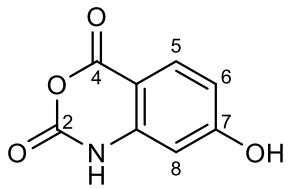

BBr_3 (1.0 M in DCM, 2.1 mL, 2.07 mmol, 4 eq.) was added dropwise to a solution of 7-methoxy-2,4-dihydro-1*H*-3,1-benzoxazine-2,4-dione (**178**) (0.10g, 0.52 mmol, 1.0 eq.) in dry DCM (2mL) at 0 °C. The reaction mixture was stirred at RT for 24 hrs and quenched by pouring onto ice. The resulting solid was filtered and washed with water to give 7-hydroxy-2,4-dihydro-1*H*-3,1-benzoxazine-2,4-dione (**239**) as a pale yellow solid (0.022 g, 24 %) melting point 264.2 °C. ν_{max} (ATR) 2871-3350 (N-H, O-H), 1742 (C=O), 1703 (C=O) cm^{-1}. δ_H (400 MHz, DMSO-d_6) 11.55 (1H, s, N*H*), 11.01 (1H, s, O*H*), 7.74 (1H, d, *J* 8.7, 5-*H*), 6.65 (1H, dd, *J* 8.7 *J* 2.2, 6-*H*), 6.51 (1H, d, *J* 2.2, 8-*H*). δ_C (101 MHz, DMSO-d_6) 165.1 (*C*-4), 159.3 (*C*-7), 147.6 (*C*-2), 143.7 (1-*C*(Ar)), 131.4 (*C*-5), 112.9 (*C*-6), 101.4 (4-*C*(Ar)), 100.2 (*C*-8). *m/z* (LC-MS ES^-) 178.29 $[M-H]^-$.

Amino-5-hydroxy-*N*-methyl-2-benzamide (241)

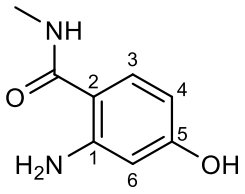

Boron tribromide in DCM (6.8 mL, 1.0 M, 6.8 mmol, 2.2 eq.) was added dropwise to amino-5-methoxy-*N*-methyl-2-benzamide (**187**) (0.56 g, 3.1 mmol, 1.0 eq.) in dry DCE (15 mL) at RT. The reaction was stirred at 40 °C for 20 hrs before addition of boron tribromide in DCM (6.8 mL, 1.0 M, 6.8 mmol, 2.2 eq.). The resulting mixture was stirred at 50 °C for 24 hrs before quenching with saturated sodium bicarbonate (20 mL). Volatiles were removed *in vacuo*, the residue was resuspended in MeOH, filtered and volatiles were removed before repeating. The resulting residue was purified by flash column chromatography (9:1 DCM:MeOH) to give amino-5-hydroxy-*N*-methyl-2-benzamide (**241**) as an off white solid (0.34 g, 66 %), melting point 174-175 °C. ν_{max} (ATR) 3092-3300 (O–H), 2986 (N–H), 1631 (C=O) cm^{-1}. δ_H (599 MHz, CD_3OD) 7.29 (1H, d, *J* 8.6, 3-*H*), 6.15 (1H, d, *J* 2.4, 6-*H*), 6.09 (1H, dd, *J* 8.6 *J* 2.4, 4-*H*), 2.83 (3H, s, C*H*$_3$). δ_C (151 MHz, CD_3OD) 172.5 (*C*=O), 162.1 (*C*-5), 152.6 (*C*-1), 130.7 (*C*-3), 109.6 (*C*-2), 105.9 (*C*-4), 103.4 (*C*-6), 26.5 (*C*H_3). *m/z* (LC-MS ES^+) 167.1 $[M+H]^+$. HRMS (ES^+) found $[M+H]^+$ 167.0840, $C_8H_{11}N_2O_2$ requires *M* 167.0821.

5-[2'-(2''-Methoxyethoxy)ethoxy]-1-amino-*N*-methyl-2-benzamide (246)

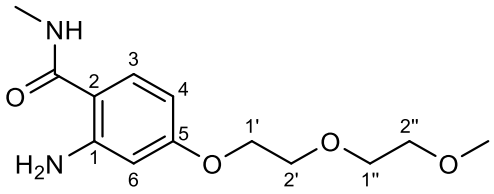

Following general procedure **Fi**, using DMF (0.9 mL) as a reaction solvent, where the alkyl bromide was 1-bromo-2-(2-methoxyethoxy)ethane (0.015 mL, 0.11 mmol, 1.0 eq.) afforded, after purification by flash column chromatography (hexane:EtOAc), 5-[2'-(2''-methoxyethoxy)ethoxy]-1-amino-*N*-methyl-2-benzamide (**246**) as a pale yellow solid (7.9 mg, 27 %) melting point 62-63 °C. ν_{max} (ATR) 3284-3513 (N–H), 1631 (C=O) cm^{-1}. δ_H (599 MHz, CD_3OD) 7.35 (1H, d, *J* 8.8, 3-*H*), 6.28 (1H, d, *J* 2.5, 6-*H*), 6.21

(1H, dd, *J* 8.8 *J* 2.5, 4-*H*), 4.05-4.11 (2H, m, 1'-H_2), 3.77-3.84 (2H, m, 2'-H_2), 3.64-3.70 (2H, m, 1''-H_2), 3.54-3.60 (2H, m, 2''-H_2), 3.36 (3H, s, OCH_3), 2.84 (3H, s, NHCH_3). δ_C (151 MHz, CD_3OD) 172.3 (*C*=O), 163.4 (*C*-5), 152.6 (*C*-1), 130.6 (*C*-3), 110.4 (*C*-2), 105.1 (*C*-4), 102.1 (*C*-6), 73.0 (*C*-2''), 71.5 (*C*-1''), 70.7 (*C*-2'), 68.3 (*C*-1'), 59.1 (O*C*H_3), 26.5 (NH*C*H_3). *m/z* (LC-MS ES^+) 269.3 $[M+H]^+$. HRMS (ES^+) found $[M+H]^+$ 269.1513, $C_{13}H_{21}N_2O_4$ requires *M* 269.1501.

N-{5-[2''-(2'''-methoxyethoxy)ethoxy]-2-(methylcarbamoyl)phenyl}-5'-nitrothiophene-2'-carboxamide (232)

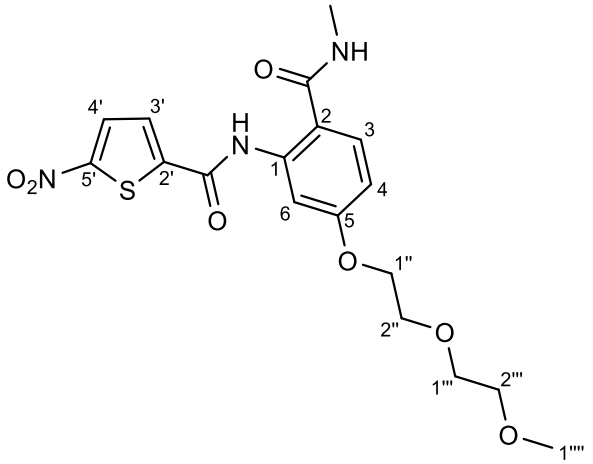

Following general procedure **Gii**, using THF (1 mL) as a reaction solvent, where the substituted amine was 5-[2'-(2''-methoxyethoxy)ethoxy]-1-amino-*N*-methyl-2-benzamide (**246**) (7.9 mg, 0.029 mmol, 1.0 eq.) afforded, without further purification, N-{5-[2''-(2'''-methoxyethoxy)ethoxy]-2-(methylcarbamoyl)phenyl}-5'-nitrothiophene-2'-carboxamide (**232**) as a yellow solid (9.3 mg, 75 %), melting point 204-205 °C. ν_{max} (ATR) 3414 (N–H), 3119 (N–H), 1652 (C=O), 1586 (C=O), 1527, 1334 cm^{-1}. δ_H (599 MHz, $CDCl_3$) 13.16 (1H, s, 1-N*H*), 8.39 (1H, d, *J* 2.6, 6-*H*), 7.91 (1H, d, *J* 4.3, 4'-*H*), 7.68 (1H, d, *J* 4.3, 3'-*H*), 7.43 (1H, d, *J* 8.8, 3-*H*), 6.70 (1H, dd, *J* 8.8 *J* 2.6, 4-*H*), 6.29 (1H, s, N*H*CH_3), 4.21-4.25 (2H, m, 1''-H_2), 3.87-3.90 (2H, m, 2''-H_2), 3.71-3.74 (2H, m, 1'''-H_2), 3.54-3.60 (2H, m, 2'''-H_2), 3.39 (3H, s, 1''''-*H*), 3.03 (3H, d, *J* 4.8, NHCH_3). δ_C (151 MHz, $CDCl_3$) 169.7 (2-*C*=O), 162.5 (*C*-5), 158.6 (2'-*C*=O), 154.8 (*C*-2'), 146.8 (*C*-5'), 141.7 (*C*-1), 128.6 (*C*-4'), 127.9 (*C*-3), 126.6 (*C*-3'), 111.7 (*C*-2), 111.2 (*C*-4), 105.9 (*C*-6), 72.1 (*C*-2'''), 70.9 (*C*-1'''), 69.6 (*C*-2''), 67.9 (*C*-1''), 59.2 (*C*-1''''), 27.0

($NHCH_3$). *m/z* (LC-MS ES^+) 424.4 $[M+H]^+$. HRMS (ES^+) found $[M+H]^+$ 424.1194, $C_{18}H_{22}N_3O_7S$ requires *M* 424.1178.

2-(2'-(Prop-2''-ynyloxy)ethoxy)ethanol (256) [219]

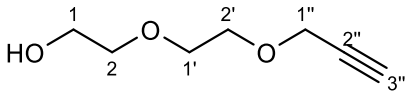

Diethylene glycol (3.53 g, 33.3 mmol, 1.98 eq.) was added to a suspension of potassium tertbutoxide (1.91 g, 17 mmol, 1.01 eq.) in dry THF (45 mL) under nitrogen at 0 °C. The reaction was stirred for 30 minutes before dropwise addition of propargyl bromide (80 % in toluene, 1.6 mL, 16.8 mmol, 1.00 eq.). The resulting mixture was stirred at RT for 20 hrs before dilution with THF and filtering through celite. Volatiles were removed *in vacuo* and the residue was purified by flash column chromatography (1:1 EtOAc: hexane) to give 2-(2'-(prop-2''-ynyloxy)ethoxy)ethanol (**256**) as a colourless oil (1.65 g, 68 %). ν_{max} (ATR) 3106-3490 (OH (br)) 2113 (C≡C (w)) cm^{-1}. δ_H (400 MHz, $CDCl_3$) 4.21 (2H, d, *J* 2.4, 1''-H_2), 3.72-3.77 (2H, m, 2-H_2), 3.68-3.72 (4H, m, 1'-H_2 & 2'-H_2), 3.57-3.64 (2H, m, 1-H_2), 2.44 (1H, t, *J* 2.4, 3''-*H*), 2.10 (1H, s(br), O*H*). δ_C (101 MHz, $CDCl_3$) 79.6 (*C*-3''), 74.8 (*C*-2''), 72.6 (*C*-1), 70.4 (*C*-1'), 69.3 (*C*-2'), 61.9 (*C*-2), 58.6 (*C*-1''). *m/z* (LC-MS ES^+) 167.3 $[M+Na]^+$.

1-Bromo-2-[2'-(prop-2''-ynyloxy)ethoxy]ethane (242)

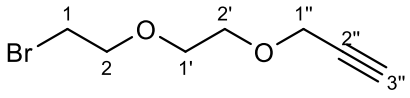

Triphenylphosphine (0.40 g, 1.53 mmol, 1.1 eq.) was added portionwise to a solution of tetrabromomethane (0.51 g, 1.53 mmol, 1.1 eq.) and 2-(2'-(prop-2''-ynyloxy)ethoxy)ethanol (**256**) (0.20 g, 1.39 mmol, 1.0 eq.) in dry DCM (4 mL) at 0 °C. The reaction was stirred at RT for 2 hrs, before volatiles were removed *in vacuo*. The residue was purified by flash column chromatography (9:1 hexane: EtOAc) to give 1-bromo-2-[2'-(prop-2''-ynyloxy)ethoxy]ethane (**242**) as a colourless oil (0.25 g, 88 %). ν_{max} (ATR) 3289 (C≡C-H), 2838-2957 (C-H (aliphatic)) cm^{-1}. δ_H (400 MHz, $CDCl_3$) 4.20 (2H, d, *J* 2.4, 1''-H_2), 3.80 (2H, t, *J* 6.3, 2-H_2), 3.70 (4H, m, 1'-H_2 & 2'-H_2), 3.47 (2H, t, *J*

6.3, 1-*H*$_2$), 2.43 (1H, t, *J* 2.4, 3''-*H*). δ_C (101 MHz, $CDCl_3$) 79.6 (*C*-3''), 74.7 (*C*-2''), 71.3 (*C*-2), 70.5 (*C*-1'), 69.2 (*C*-2'), 58.6 (*C*-1''), 30.3 (*C*-1). *m/z* (GCMS EI) 206.0 [M(^{79}Br)]$^+$ & 208.0 [M(^{81}Br)]$^+$, 137.0 [M(^{79}Br) – CH_2OCH_2CCH] & 139.0 M(^{81}Br) – CH_2OCH_2CCH]$^+$, 107.0 [M(^{79}Br) – $OCH_2CH_2OCH_2CCH$ & 109.0 [M(^{81}Br) – $OCH_2CH_2OCH_2CCH$]$^+$.

Amino-N-methyl-5-{2'-[2''-(prop-2'''-yn-1'''-yloxy)ethoxy]ethoxy}-2-benzamide (247)

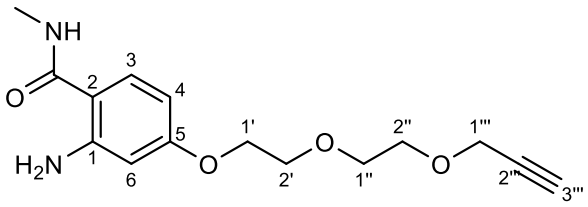

Following general procedure **Fi**, using DMF (0.9 mL) as a reaction solvent, where the alkyl bromide was 1-bromo-2-[2'-(prop-2''-ynyloxy)ethoxy]ethane (**242**) (66 mg, 0.32 mmol, 1.0 eq.) afforded, following purification by flash column chromatography (hexane:EtOAc), amino-N-methyl-5-{2'-[2''-(prop-2'''-yn-1'''-yloxy)ethoxy]ethoxy}-2-benzamide (**247**) as a white solid (62 mg, 67 %) melting point 96-98 °C. ν_{max} (ATR) 3338-3516 (N–H), 3307 (C≡C–H), 2014 (C≡C), 1632 (C=O) cm^{-1}. δ_H (599 MHz, CD_3OD) 7.36 (1H, d, *J* 8.8, 3-*H*), 6.28 (1H, d, *J* 2.5, 6-*H*), 6.21 (1H, dd, *J* 8.8 *J* 2.5, 4-*H*), 4.19 (2H, d, *J* 2.4, 1'''-*H*$_2$), 4.05-4.11 (2H, m, 1'-*H*$_2$), 2.76-3.85 (2H, m, 2'-*H*$_2$), 3.68-3.72 (4H, m, 1''-*H*$_2$ & 2''-*H*$_2$), 2.83-8.84 (4H, m, C*H*$_3$ & 3'''-*H*). δ_C (151 MHz, CD_3OD) 172.3 (*C*=O), 163.4 (*C*-5), 152.6 (*C*-1), 130.6 (*C*-3), 110.4 (*C*-2), 105.1 (*C*-4), 102.1 (*C*-6), 80.5 (*C*-2'''), 75.9 (*C*-3'''), 71.5 (*C*-1'' or *C*-2''), 70.7 (*C*-2'), 70.1 (*C*-1'' or *C*-2''), 68.3 (*C*-1'), 59.1 (*C*-1'''), 26.5 (*C*H$_3$). *m/z* (LC-MS ES$^+$) 293.3 [M+H]$^+$. HRMS (ES$^+$) found [M+H]$^+$ 293.1521, $C_{15}H_{21}N_2O_4$ requires *M* 293.1501.

N-[2-(methylcarbamoyl)-5-{2’’-[2’’’-(prop-2’’’’-yn-1’’’’-yloxy)ethoxy]ethoxy}phenyl]-5’-nitrothiophene-2’-carboxamide (251)

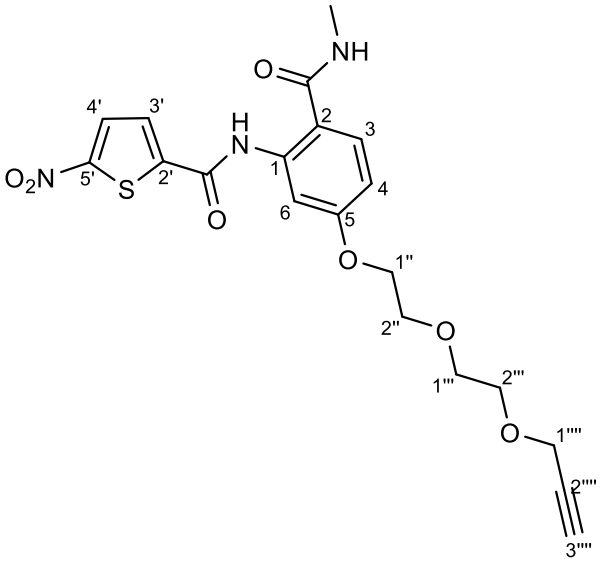

Following general procedure **Gii**, using THF (1 mL) as a reaction solvent, where the substituted amine was amino-N-methyl-5-{2’-[2’’-(prop-2’’’-yn-1’’’-yloxy)ethoxy]ethoxy}-2-benzamide (**247**) (0.045 g, 0.15 mmol, 1.0 eq.) afforded, following purification by flash column chromatography (EtOAc:hexane), N-[2-(methylcarbamoyl)-5-{2’’-[2’’’-(prop-2’’’’-yn-1’’’’-yloxy)ethoxy]ethoxy}phenyl]-5’-nitrothiophene-2’-carboxamide (**251**) as a yellow solid (0.020 g, 29 %), melting point 190-192 °C. ν_{max} (ATR) 3421 (N–H), 3077 (N–H), 3250 (C≡C–H), 2117 (C≡C), 1657 (C=O), 1584 (C=O), 1526, 1332 cm^{-1}. δ_H (599 MHz, DMSO-d_6) 13.68 (1H, s, 1-N*H*), 8.83 (1H, d, *J* 4.4, CH_3-N*H*), 8.24 (1H, d, *J* 4.4, 4’-*H*), 8.18 (1H, d, *J* 2.6, 6-*H*), 7.87 (1H, d, *J* 8.9, 3-*H*), 7.71 (1H, d, *J* 4.4, 3’-*H*), 6.84 (1H, dd, *J* 8.9 *J* 2.6, 4-*H*), 4.16-4.19 (2H, m, 1’’-H_2), 4.15 (2H, d , *J* 2.4, 1’’’’-H_2), 3.76-3.79 (2H, m, 2’’-H_2), 3.61-3.64 (2H, m, 1’’’-H_2), 3.57-3.61 (2H, m, 2’’’-H_2), 3.42 (1H, t, *J* 2.4, 3’’’’-*H*), 2.82 (3H, d, *J* 4.4, CH_3). δ_C (151 MHz, DMSO-d_6) 168.8 (2’-*C*=O), 161.3 (*C*-5), 157.7 (2’-*C*=O), 153.5 (*C*-2’), 146.0 (*C*-5’), 140.7 (*C*-1), 130.4 (*C*-4’), 129.7 (*C*-3), 127.3 (*C*-3’), 111.7 (*C*-2), 109.5 (*C*-4), 105.7 (*C*-6), 80.3 (*C*-2’’’’), 77.1 (*C*-3’’’’), 69.6 (*C*-1’’’), 68.7 (*C*-2’’), 68.5 (*C*-2’’’), 67.5 (*C*-1’’), 57.5 (*C*-1’’’’), 26.4 (*C*H_3). *m/z* (LC-MS ES^+) 448.4 $[M+H]^+$. HRMS (ES^+) found $[M+H]^+$ 448.1196, $C_{20}H_{22}N_3O_7S$ requires *M* 448.1178.

4-(2'-Bromoethyl)morpholine (243)

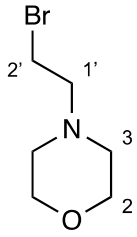

Triphenylphosphine (2.2 g, 8.4 mmol, 1.1 eq.) was added portionwise to a solution of tetrabromomethane (2.8 g, 8.4 mmol, 1.1 eq.) and 4-(2-hydroxyethyl)morpholine (1.00 g, 7.6 mmol, 1.0 eq.) in dry DCM (10 mL) at 0 °C. The reaction was stirred at RT for 2 hrs, before volatiles were removed *in vacuo*. The residue was dispersed in hexane, filtered and volatiles removed *in vacuo*. The residue was purified by flash column chromatography (8:2 EtOAc:hexane) to give 4-(2'-bromoethyl)morpholine (**243**) as colourless oil (1.22 g, 83 %). ν_{max} (ATR) 2810 (C–H), 2860 (C–H), 2968 (C–H), 663 cm^{-1}. δ_H (599 MHz, $CDCl_3$) 3.68-3.75 (4H, m, 2-*H*), 3.38-3.46 (2H, m, 2'-*H*), 2.74-2.82 (2H, m, 1'-*H*), 2.47-2.54 (4H, m, 3-*H*). δ_C (151 MHz, $CDCl_3$) 67.0 (*C*-2), 60.3 (*C*-1'), 53.5 (*C*-3), 28.7 (*C*-2). *m/z* (LC-MS ES^+) 194.1 $[M(^{79}Br)+H]^+$ & 196.1 $[M(^{81}Br)+H]^+$. HRMS (ES^+) found $[M+H]^+$ 194.0192, $C_6H_{13}NO^{79}Br$ requires *M* 194.0181.

Amino-N-methyl-5-[2'-(morpholin-4''-yl)ethoxy]-2-benzamide (248)

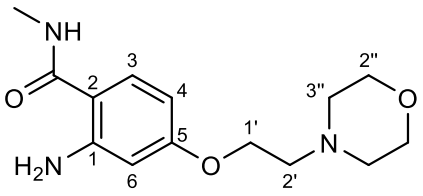

Following general procedure **Fii**, using DMF (0.9 mL) as a reaction solvent for 20hr, where the alkyl bromide was 4-(2'-bromoethyl)morpholine (**243**) (120 mg, 0.61 mmol, 1.01 eq.) afforded, after purification by flash column chromatography (9:1 DCM:MeOH), amino-N-methyl-5-[2'-(morpholin-4''-yl)ethoxy]-2-benzamide (**248**) as a white solid (30 mg, 18 %). ν_{max} (ATR) 3449 (N–H), 3347 (N–H), 1635 (C=O) cm^{-1}. δ_H (599 MHz, $CDCl_3$) 7.21 (1H, d, *J* 8.7, 3-*H*), 6.21 (1H, dd, *J* 8.7 *J* 2.5, 4-*H*), 6.15 (1H, d, *J* 2.5, 6-*H*), 5.91 (1H, s, CON*H*), 5.67 (2H, s, NH_2), 4.08 (2H, t, *J* 5.7, 1'-H_2), 3.66-3.77 (4H, m, 2''-H_2), 2.94 (3H, d, *J* 4.8, CH_3), 2.78 (2H, t, *J* 5.7, 2'-H_2), 2.54-2.58 (4H, m, 3''-H_2).

δ_C (151 MHz, $CDCl_3$) 169.8 (*C*=O), 162.0 (*C*-5), 151.0 (*C*-1), 128.8 (*C*-3), 109.5 (*C*-2), 104.4 (*C*-4), 101.6 (*C*-6), 67.1 (*C*-2''), 65.8 (*C*-1'), 57.7 (*C*-2'), 54.2 (*C*-3''), 26.6 (CH_3). *m/z* (LC-MS ES^+) 280.4 $[M+H]^+$. HRMS (ES^+) found $[M+H]^+$ 280.1670, $C_{14}H_{22}N_3O_3$ requires *M* 280.1661.

N-[2-(methylcarbamoyl)-5-[2''-(morpholin-4'''-yl)ethoxy]phenyl]-5'-nitrothiophene-2'-carboxamide (252)

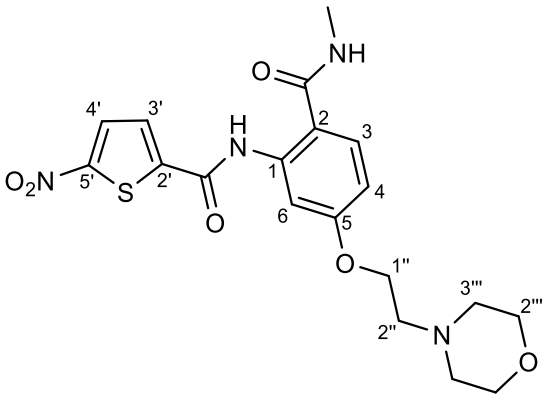

Following general procedure **Gi**, using THF (1 mL) as a reaction solvent, where the substituted amine was amino-N-methyl-5-[2'-(morpholin-4''-yl)ethoxy]-2-benzamide (**248**) (22 mg, 0.079 mmol, 1.0 eq.) afforded, after filtration and trituration with water of the crude precipitate and purification of the filtrate after work up by flash column chromatography (EtOAc:hexane), N-[2-(methylcarbamoyl)-5-[2''-(morpholin-4'''-yl)ethoxy]phenyl]-5'-nitrothiophene-2'-carboxamide (**252**) as a yellow solid (10.7 mg, 31 %), melting point 168-170 °C. ν_{max} (ATR) 3428 (N-H), 1650 (C=O), 1536, 1331 cm^{-1}. δ_H (599 MHz, $CDCl_3$) 13.18 (1H, s, 1-N*H*), 8.40 (1H, d, *J* 2.6, 6-*H*), 7.91 (1H, d, *J* 4.3, 4'-*H*), 7.69 (1H, d, *J* 4.3, 3'-*H*), 7.43 (1H, d, *J* 8.8, 3-*H*), 6.69 (1H, dd, *J* 8.8 *J* 2.6, 4-*H*), 6.27 (1H, s, N*H*Me), 4.20 (2H, t, *J* 5.6, 1''-H_2), 3.71-3.76 (4H, m, 2'''-H_2), 3.03 (3H, d, *J* 4.8, CH_3), 2.83 (2H, t, *J* 5.6, 2''-H_2), 2.59 (4H, *J* 4.8, 3'''-H_2). δ_C (151 MHz, $CDCl_3$) 169.7 (2-*C*=O), 162.5 (*C*-5), 158.7 (2'-*C*=O), 154.9 (*C*-5'), 146.7 (*C*-2'), 141.7 (*C*-1), 128.6 (*C*-4'), 127.9 (*C*-3), 126.6 (*C*-3'), 111.7 (*C*-2), 111.2 (*C*-4), 105.9 (*C*-6), 67.1 (*C*-2'''), 66.3 (*C*-1''), 57.6 (*C*-2''), 54.2 (*C*-3'''), 27.0 (CH_3). *m/z* (LC-MS ES^+) 435.3 $[M+H]^+$. HRMS (ES^+) found $[M+H]^+$ 435.1336, $C_{19}H_{23}N_4O_6S$ requires *M* 435.1338.

4-(3'-Bromopropyl)-morpholine (244)

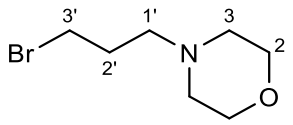

Potassium carbonate (6.35 g, 46 mmol, 4 eq.) was added to morpholine (1.0 mL, 11 mmol, 1.0 eq.) in acetone (10 mL), followed by 1,3-dibromopropane (4.7 mL, 46 mmol, 4 eq.). The reaction mixture was refluxed for 24 hrs, filtered and concentrated. The residue was extracted into DCM and washed with aqueous sodium bicarbonate and brine before drying over $MgSO_4$. Volatiles were removed and the residue purified by flash column chromatography (EtOAc:hexane) to give 4-(3'-bromopropyl)-morpholine (**244**) as a white semi-solid (0.99 g, 42 %). ν_{max} (ATR) 2863-2965 (C-H), 585 cm^{-1}. δ_H (599 MHz, DMSO-d_6) 4.30 (4H, m, *J* 8.3, 1'-H_2 & 3'-H_2), 3.80 (4H, t, *J* 4.8, 2-H_2), 3.55 (4H, t, *J* 4.8, 3-H_2), 2.51-2.54 (2H, m, 2'-H_2). δ_C (151 MHz, $CDCl_3$) 62.1 (*C*-1' & *C*-3'), 61.0 (*C*-2), 58.2 (*C*-3), 13.3 (*C*-2'). *m/z* (LC-MS ES^+) 208.0 $[M(^{79}Br)+H]^+$ & 210.0 $[M(^{81}Br)+H]^+$. HRMS (ES^+) found $[M+H]^+$ 208.0342, $C_7H_{15}NOBr$ requires *M* 208.0337.

Amino-N-methyl-5-[3'-(morpholin-4''-yl)propoxy]-2-benzamide (249)

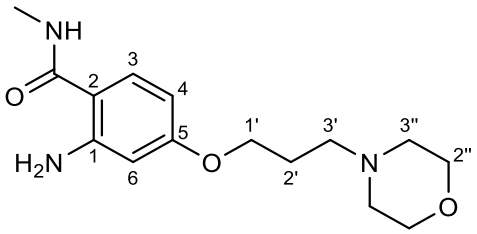

Following general procedure **Fii**, using DMF (0.9 mL) as a reaction solvent, where the alkyl bromide was 4-(3'-bromopropyl)morpholine (**244**) (126 mg, 0.61 mmol, 1.01 eq.) afforded, following purification by flash column chromatography (9:1 DCM:MeOH), amino-N-methyl-5-[3'-(morpholin-4''-yl)propoxy]-2-benzamide (**249**) as a white semi-solid (100 mg, 57 %). ν_{max} (ATR) 3316-3476 (N-H), 1620 (C=O) cm^{-1}. δ_H (599 MHz, $CDCl_3$) 7.21 (1H, d, *J* 8.7, 3-*H*), 6.19 (1H, dd, *J* 8.7 *J* 2.4, 4-*H*), 6.14 (1H, d, *J* 2.4, 6-*H*), 5.92 (1H, s, N*H*CH_3), 5.68 (2H, s, NH_2), 4.00 (2H, t, *J* 6.3, 1'-H_2), 3.74-3.79 (4H, m, 2''-H_2), 2.95 (3H, d, *J* 4.8, CH_3), 2.51-2.62 (6H, m, 3'-H_2 & 3''-H_2), 1.98-2.05 (2H, m, 2'-H_2). δ_C (151 MHz, $CDCl_3$) 169.9 (*C*=O), 162.2 (*C*-5), 151.0 (*C*-1), 128.8 (*C*-3),

109.4 (*C*-2), 104.4 (*C*-4), 101.4 (*C*-6), 66.7 (*C*-2''), 65.9 (*C*-1'), 55.7 (*C*-3'), 53.7 (*C*-3''), 26.6 (*C*H_3), 26.1 (*C*-2'). *m/z* (LC-MS ES$^+$) 294.7 $[M+H]^+$. HRMS (ES$^+$) found $[M+H]^+$ 294.1836, $C_{15}H_{24}N_3O_3$ requires *M* 294.1818.

N-[2-(methylcarbamoyl)-5-[3''-(morpholin-4'''-yl)propoxy]phenyl]-5'-nitrothiophene-2'-carboxamide (253)

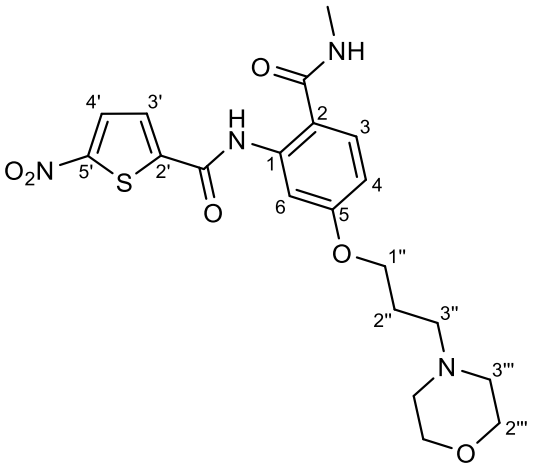

Following general procedure **Gi**, using THF (3 mL) as a reaction solvent, where the substituted amine was amino-N-methyl-5-[3'-(morpholin-4''-yl)propoxy]-2-benzamide (**249**) (0.100 g, 0.34 mmol, 1.0 eq.) afforded, without further purification, N-[2-(methylcarbamoyl)-5-[3''-(morpholin-4'''-yl)propoxy]phenyl]-5'-nitrothiophene-2'-carboxamide (**253**) as a yellow solid (73 mg, 48 %) melting point 206-208 °C. ν_{max} (ATR) 3391 (N-H), 3100 (N-H), 1661 (C=O), 1641 (C=O), 1521, 1331 cm^{-1}. δ_H (599 MHz, $CDCl_3$) 13.19 (1H, s, 1-N*H*), 8.37 (1H, d, *J* 2.6, 6-*H*), 7.91 (1H, d, *J* 4.3, 4'-*H*), 7.69 (1H, d, *J* 4.3, 3'-*H*), 7.44 (1H, d, *J* 8.8, 3-*H*), 6.66 (1H, dd, *J* 8.8 *J* 2.6, 4-*H*), 6.31 (1H, s, N*H*Me), 4.13 (2H, t, *J* 6.3, 1''-H_2), 3.73-3.79 (4H, m, 2'''-H_2), 3.02 (3H, d, *J* 4.8, CH_3), 2.46-2.62 (6H, m, 3''-H_2 & 3'''-H_2), 2.01-2.06 (2H, m, 2''-H_2). δ_C (151 MHz, $CDCl_3$) 169.7 (2-*C*=O), 162.7 (*C*-5), 158.7 (2'-*C*=O), 154.8 (*C*-5'), 146.8 (*C*-2'), 141.7 (*C*-1), 128.6 (*C*-4'), 127.9 (*C*-3), 126.6 (*C*-3'), 111.6 (*C*-2), 111.0 (*C*-4), 106.0 (*C*-6), 66.9 (*C*-2'''), 66.5 (*C*-1''), 55.5 (*C*-3'''), 53.8 (*C*-3''), 27.0 (*C*H_3), 26.1 (*C*-2''). *m/z* (LC-MS ES$^+$) 449.7 $[M+H]^+$. HRMS (ES$^+$) found $[M+H]^+$ 449.1489, $C_{20}H_{25}N_4O_6S$ requires *M* 449.1495.

Amino-N-methyl-5-[2'-(oxan-4''-yl))ethoxy]-2-benzamide (250)

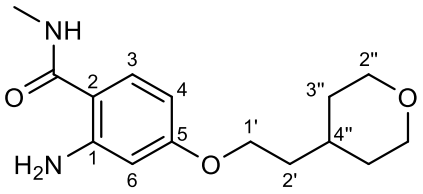

Following general procedure **Fii**, using DMF (0.9 mL) as a reaction solvent, where the alkyl bromide was 4-(2-bromoethyl)-tetrahydropyran (74 mg, 0.38 mmol, 1.01 eq.) afforded, after purification by flash column chromatography (EtOAc:hexane), amino-N-methyl-5-[2'-(oxan-4''-yl))ethoxy]-2-benzamide (**250**) as a white solid (90 mg, 85 %) melting point 144-146 °C. ν_{max} (ATR) 3289-3500 (N-H), 1634 (C=O) cm^{-1}. δ_H (599 MHz, $CDCl_3$) 7.21 (1H, d, *J* 8.7, 3-*H*), 6.18 (1H, dd, *J* 8.7, *J* 2.5, 4-*H*), 6.13 (1H, d, *J* 2.5, 6-*H*), 5.96 (1H, s, N*H*CH_3), 5.68 (2H, s, NH_2), 3.92-3.99 (4H, m, 1'-H_2 & 2''-H_2), 3.39 (2H, td, *J* 11.8 *J* 2.1, 2''-H_2), 2.94 (3H, d, *J* 4.8, CH_3), 1.68-1.81 (3H, m, 2'-H_2 & 4''-*H*), 1.62-1.67 (2H, m, 3''-H_2), 1.29-1.40 (2H, m, 3''-H_2). δ_C (151 MHz, $CDCl_3$) 169.9 (*C*=O), 162.3 (*C*-5), 151.0 (*C*-1), 128.8 (*C*-3), 109.3 (*C*-2), 104.4 (*C*-4), 101.4 (*C*-6), 68.1 (*C*-2''), 65.2 (*C*-1'), 36.2 (*C*-2'), 33.1 (*C*-3''), 32.0 (*C*-4''), 26.6 (*C*H_3). *m/z* (LC-MS ES^+) 279.2 $[M+H]^+$. HRMS (ES^+) found $[M+H]^+$ 279.1711, $C_{15}H_{23}N_2O_3$ requires *M* 279.1709.

N-[2-(methylcarbamoyl)-5-[2''-(oxan-4'''-yl)ethoxy]phenyl]-5'-nitrothiophene-2'-carboxamide (254)

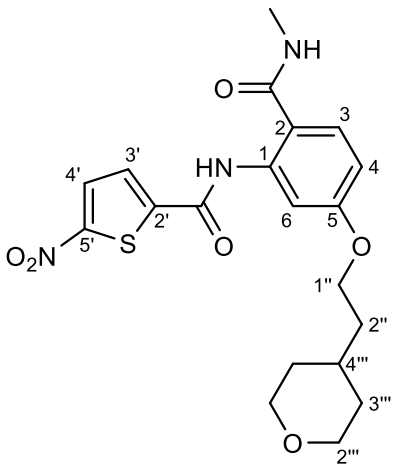

Following general procedure **Gi**, using THF (2 mL) as a reaction solvent, where the substituted amine was amino-N-methyl-5-[2'-(oxan-4''-yl))ethoxy]-2-benzamide

(**250**) (0.037 g, 0.13 mmol, 1.0 eq.) afforded, after purification by flash column chromatography (EtOAc:hexane), N-[2-(methylcarbamoyl)-5-[2''-(oxan-4'''-yl)ethoxy]phenyl]-5'-nitrothiophene-2'-carboxamide (**254**) as a yellow solid (33 mg, 57 %), melting point 144-146 °C. ν_{max} (ATR) 3433 (N-H), 1638 (C=O), 1659 (C=O), 1537, 1333 cm^{-1}. δ_H (599 MHz, $CDCl_3$) 13.20 (1H, s, 1-N*H*), 8.39 (1H, d, *J* 2.6, 6-*H*), 7.91 (1H, d, *J* 4.3, 4'-*H*), 7.69 (1H, d, *J* 4.3, 3'-*H*), 7.43 (1H, d, *J* 8.8, 3-*H*), 6.66 (1H, dd, *J* 8.8 *J* 2.6, 4-*H*), 6.28 (1H, s, CH_3-N*H*), 4.11 (2H, t, *J* 6.1, 1''-H_2), 3.94-4.01 (2H, m, 2'''-H_2), 3.41 (2H, td, *J* 11.9 *J* 2.1, 2'''-H_2), 3.02 (3H, d, *J* 4.7, CH_3), 1.73-1.84 (3H, m, 2''-H_2 & 4'''-*H*), 1.64-1.69 (2H, m, 3'''-H_2), 1.32-1.42 (2H, m, 3'''-H_2). δ_C (151 MHz, $CDCl_3$) 169.7 (2-*C*=O), 162.8 (*C*-5), 158.7 (2'-*C*=O), 154.8 (*C*-5'), 146.8 (*C*-2') 141.8 (*C*-1), 128.6 (*C*-4'), 127.9 (*C*-3), 126.6 (*C*-3'), 111.5 (*C*-2), 111.1 (*C*-4), 105.8 (*C*-6), 68.1 (*C*-2'''), 65.8 (*C*-1''), 36.1 (*C*-2''), 33.1 (*C*-3'''), 32.0 (*C*-4'''), 27.0 (*C*H_3). *m/z* (LC-MS ES^+) 434.6 $[M+H]^+$. HRMS (ES^+) found $[M+H]^+$ 434.1388, $C_{20}H_{24}N_3O_6S$ requires *M* 434.1386.

2-(4'-Methylpiperazin-1'-yl)ethyl methanesulfonate (263)

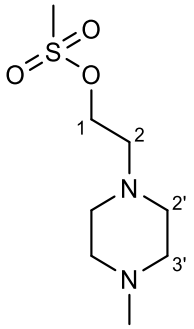

Triethylamine (0.33 mL, 2.5 mmol, 1.2 eq.) and mesyl chloride (0.18 mL, 2.3 mmol, 1.1 eq.) were added to 1-(2-hydroxyethyl)-4-methylpiperazine (0.30 g, 2.1 mmol, 1.0 eq.) in dry DCM (10 mL) at 0 °C under nitrogen. The reaction was slowly warmed to RT and stirred overnight. Saturated $NaHCO_3$ was added and the reaction stirred for 15 mins before extraction into DCM x 3. Organic extracts were combined, dried over MgSO4 and volatiles removed in vacuo to give 2-(4'-methylpiperazin-1'-yl)ethyl methanesulfonate (**263**) as a yellow semi solid (0.28 g, 61 %). The product was immediately used without further purification or characterisation. *m/z* ($ASAP^+$) 223.1 $[M+H]^+$.

Amino-N-methyl-5-[3'-bromopropoxy]benzamide (267)

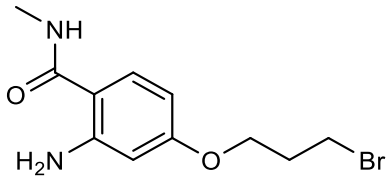

267
Desired product 70 %

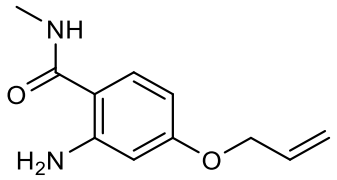

268
elimination product 30 %

Following general procedure **Fi** using DMF (0.9 mL) as a reaction solvent for 24 hr, where the alkyl bromide was 1,3-dibromopropane (0.12 mL, 1.2 mmol, 4.0 eq.) afforded, after purification by flash column chromatography (8:2 EtOAc:hexane), a 70:30 mixture of amino-N-methyl-5-[3'-bromopropoxy]benzamide (**267**): elimination product (**268**) which was used without further purification or characterisation (32 mg, 26 %). *m/z* (LC-MS ES^+) **268**; 207.2 $[M+H]^+$ & **267**; 287.3 $[M(^{79}Br) + H]^+$ & 289.3 $[M(^{81}Br) + H]^+$.

2-Amino-N-methyl-4-[3'-propoxy]benzamide (269)

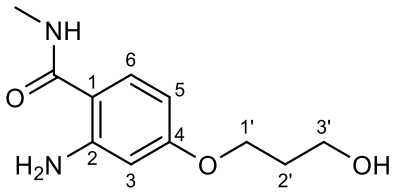

Following general procedure **Fii**, using DMF (0.9 mL) as a reaction solvent for 20 hr, where the alkyl bromide was 3-bromopropanol (0.030 mL, 0.33 mmol, 1.01 eq.) afforded, after high vacuum at 40 °C overnight, 2-amino-N-methyl-4-[3'-propoxy]benzamide (**269**) as a colourless oil (41 mg, 61 %). ν_{max} (ATR) 3301-3506 (O-H), 2927 (N-H), 2957 (N-H), 1626 (C=O) cm^{-1}. δ_H (599 MHz, CD_3OD) 7.35-7.41 (1H, m, 6-*H*), 6.28-6.30 (1H, m, 3-*H*), 6.20-6.24 (1H, m, 5-*H*), 4.05 (2H, t, *J* 6.3, 1'-H_2), 3.70-3.80 (2H, m, 3'-H_2), 2.84 (3H, s, CH_3), 1.96 (2H, tt, *J* 6.3, 2'-H_2). δ_C (151 MHz, CD_3OD) 172.3 (*C*=O), 163.7 (*C*-4), 152.2 (*C*-2), 130.5 (*C*-6), 110.5 (*C*-1), 105.4 (*C*-5), 102.3 (*C*-3), 65.5 (*C*-1'), 59.5 (*C*-3'), 33.3 (*C*-2'), 26.5 (*C*H_3). *m/z* (LC-MS ES^+) 225.3 $[M+H]^+$. HRMS (ES^+) found $[M+H]^+$ 225.1238, $C_{11}H_{17}N_2O_3$ requires *M* 225.1239.

2-Amino-N-methyl-4-[3'-methanesulfonatepropoxy]benzamide (270)

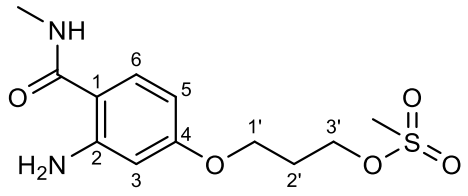

Triethylamine (0.026 mL, 0.19 mmol, 1.2 eq.) and mesyl chloride (0.014 mL, 0.18 mmol, 1.1 eq.) were added to 2-amino-N-methyl-4-[3'-hyrdoxypropoxy]benzamide (**269**) (0.036 g, 0.16 mmol, 1.0 eq.) in dry THF (2 mL) at 0 °C under nitrogen. The reaction was slowly warmed to RT and stirred overnight. Saturated $NaHCO_3$ was added and the reaction stirred for 15 mins before volatiles were removed *in vacuo*. The residue was extracted into EtOAc x 3 and washed with brine. Organic extracts were combined, dried over MgSO4 and volatiles removed in vacuo to give 2-amino-N-methyl-4-[3'-methanesulfonatepropoxy]benzamide (**270**) as a yellow oil (0.039 g, 80 %). The product was used without further purification or characterisation. *m/z* (ASAP$^+$) 303.1 $[M+H]^+$.

2-Amino-N-methyl-4-[3'-(4'-methylpiperazin-1'-yl)propoxy]benzamide (271)

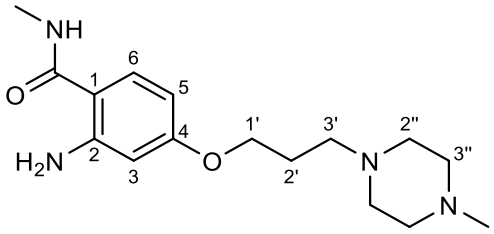

2-Amino-N-methyl-4-[3'-bromopropoxy]benzamide (**267**) (24 mg, 0.084 mmol, 1.0 eq.) in dry MeCN (0.5 mL) was added dropwise to a mixture of *N*-methylpiperazine (0.011 mL, 0.10 mmol, 1.2 eq.) and triethylamine (0.028 mL, 0.21 mmol, 2.5 eq.) in MeCN (0.5 mL) at 0 °C. The reaction was stirred at 50 °C for 20 hrs. Volatiles were removed and the residue purified by reverse phase flash column chromatography to give 2-amino-N-methyl-4-[3'-(4'-methylpiperazin-1'-yl)propoxy]benzamide (**271**) as a white semi-solid (3.5 mg, 14 %). ν_{max} (ATR) 3337 (N-H), 3440 (N-H), 1630 (C=O) cm^{-1}. δ_H (400 MHz, CD_3OD) 7.35 (1H, d, *J* 8.8, 6-*H*), 6.26 (1H, d, *J* 2.5, 3-*H*), 6.19 (1H, dd, *J* 8.8 *J* 2.5, 5-*H*), 3.99 (2H, t, *J* 6.1, 1'-H_2), 2.83 (3H, s, CONHCH_3), 2.35-2.75 (10H, m, 3''-

H$_2$ & 2''-*H*$_2$ & 3'-*H*$_2$), 2.30 (3H, s, 4''-C*H*$_3$), 1.92-1.99 (2H, m, 2'-*H*$_2$). δ_C (101 MHz, CD_3OD) 172.2 (*C*=O), 163.6 (*C*-4), 152.4 (*C*-2), 130.5 (*C*-6), 110.3 (*C*-1), 105.1 (*C*-5), 102.0 (*C*-3), 66.9 (*C*-1'), 56.2 (*C*-3'), 55.6 & 53.7 (*C*-2'' & *C*-3''), 45.9 (1''-*C*H$_3$), 27.4 (*C*-2'), 26.5 (CONH*C*H$_3$). *m/z* (LC-MS ES$^+$) 307.5 $[M+H]^+$. HRMS (ES$^+$) found $[M+H]^+$ 307.2114, $C_{16}H_{27}N_4O_2$ requires *M* 307.2134.

6,7-Dimethoxy-2,4-dihydro-1*H*-3,1-benzoxazine-2,4-dione (332)

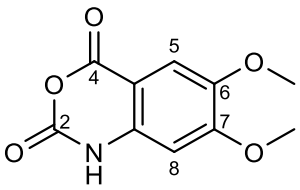

Following general procedure **D**, where the substituted 2-amino benzoic acid was 2-amino-4,5-dimethoxybenzoic acid (0.50 g, 2.99 mmol, 1.0 eq.), afforded, following purification by flash column chromatography (hexane:EtOAc), 6,7-dimethoxy-2,4-dihydro-1*H*-3,1-benzoxazine-2,4-dione (**332**) as a pale yellow solid (0.30 g, 53 %) melting point 258-260 °C (lit. 263-264 °C)[220]. ν_{max} (ATR) 3190 (N–H), 1783 (C=O), 1725 (C=O) cm^{-1}. δ_H (599 MHz, DMSO-d$_6$) 11.54 (1H, s, N*H*), 7.26 (1H, s, 5-*H*), 6.64 (1H, s, 8-*H*), 3.86 (3H, s, 7-OC*H*$_3$), 3.81 (3H, s, 6-OC*H*$_3$). δ_C (151 MHz, DMSO-d$_6$) 159.2 (*C*-4), 156.4 (*C*-7), 146.6 (*C*-2), 145.5 (*C*-6), 137.5 (NH-*C*), 108.5 (*C*-5), 101.1 (4-*C*), 97.9 (8-*C*), 56.0 (7-O*C*H$_3$), 55.8 (6-O*C*H$_3$). *m/z* (LC-MS ES$^+$) 224.2 $[M+H]^+$. HRMS (ES$^+$) found $[M+H]^+$ 224.0558, $C_{10}H_{10}NO_5$ requires *M* 224.0059.

Amino-4,5-dimethoxy-*N*-methyl-2-benzamide (333)

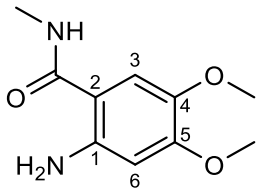

Following general procedure **E**, where the substituted benzoxazine-2,4-dione was 6,7-dimethoxy-1*H*-3,1-benzoxazine-2,4-dione (**332**) (0.30 g, 1.3 mmol, 1.0 eq.) afforded, following purification by flash column chromatography (EtOAc), amino-4,5-dimethoxy-*N*-methyl-2-benzamide (**333**) as a pale brown oil (0.083 g, 20 %). ν_{max} (ATR) 3426 (N-H), 3121 (N-H), 1659 (C=O) cm^{-1}. δ_H (599 MHz, $CDCl_3$) 6.80 (1H, s,

3-*H*), 6.20 (1H, s, 6-*H*), 5.94 (1H, s, N*H*CH_3), 5.37 (2H, s, NH_2), 3.85 (3H, s, 5-OCH_3), 3.81 (3H, s, 4-OCH_3), 2.96 (3H, d, *J* 4.8, NHCH_3). δ_C (151 MHz, $CDCl_3$) 169.8 (*C*=O), 153.3 (*C*-5), 144.8 (*C*-1), 141.0 (*C*-4), 111.1 (*C*-3), 107.5 (*C*-2), 101.0 (*C*-6), 57.2 (4-O*C*H_3), 55.9 (5-O*C*H_3), 26.7 (NH*C*H_3). *m/z* (LC-MS ES^+) 211.3 $[M+H]^+$. HRMS (ES^+) found $[M+H]^+$ 211.1080, $C_{10}H_{15}N_2O_3$ requires *M* 211.1083.

N-[4,5-dimethoxy-2-(methylcarbamoyl)]phenyl]-5'-nitrothiophene-2'-carboxamide (334)

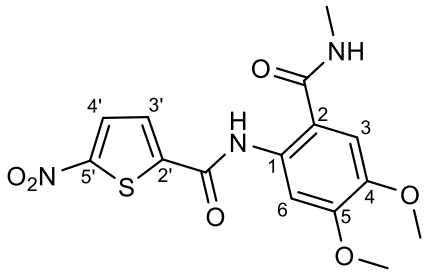

Following general procedure **C,** using THF (2 mL) as a reaction solvent for 20 hr, where the substituted amine was amino-4,5-dimethoxy-*N*-methyl-2-benzamide (**333**) (0.083 g, 0.40 mmol, 1.0 eq.) afforded N-[4,5-dimethoxy-2-(methylcarbamoyl)]phenyl]-5'-nitrothiophene-2'-carboxamide (**334**) as an orange solid (2.8 mg, 57 %)**.** ν_{max} (ATR) 3436 (N-H), 3129 (N-H), 1661 (C=O), 1640 (C=O), 1515, 1331 cm^{-1}. δ_H (599 MHz, DMSO-d_6) 13.56 (1H, s, 1-N*H*), 8.84 (1H, d, *J* 4.5, N*H*Me), 8.27 (1H, s, 6-*H*), 8.23 (1H, d, *J* 4.4, 4'-*H*), 7.68 (1H, d, *J* 4.4, 3'-*H*), 7.43 (1H, s, 3-*H*), 3.82-3.83 (6H, m, OCH_3), 2.85 (3H, d, *J* 4.5, NHCH_3). δ_C (151 MHz, DMSO-d_6) 168.7 (2-*C*=O), 157.2 (*C*-2'), 153.3 (2'-*C*=O), 151.5 (*C*-5), 146.4 (*C*-5'), 144.5 (*C*-4), 133.9 (*C*-1), 130.4 (*C*-4'), 127.0 (*C*-3'), 111.0 (*C*-3), 110.9 (*C*-2), 103.6 (*C*-6), 56.0 (O*C*H_3), 55.5 (O*C*H_3), 26.3 (NH*C*H_3). *m/z* (LC-MS ES^+) 366.3 $[M+H]^+$. HRMS (ES^+) found $[M+H]^+$ 366.0737, $C_{15}H_{16}N_3O_6S$ requires *M* 366.0760.

6.14 Biocatalysis

Ethyl 2'-(4-cyano-6-{[2''-(ethoxycarbonyl)cyclopentyl]carbamoyl}thieno[2,3-b]pyridine-2-amido)cyclopentane-1'-carboxylate (309a)

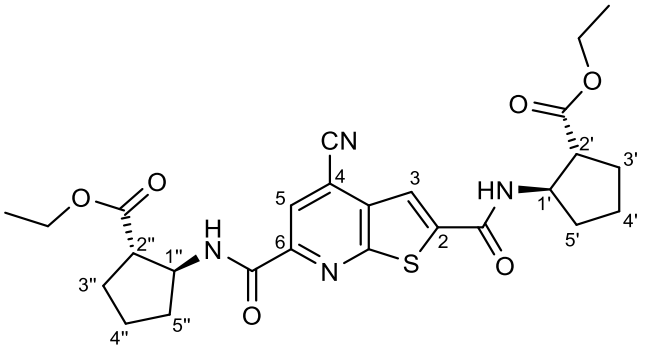

anti anti racemic

Anti-ethyl-2-(5'-nitrothiophene-2'-amido)cyclopentane-1-carboxylate (**131**) (10 mg, 0.032 mmol, 1 eq.) was incubated with NADH (128 mg, 0.19 mmol, 6 eq.) in tris buffer (50 mM, pH 7.5, 640 mL) with *Lmj*NTR1 (2 mg) for 16 hrs. The solution was extracted into EtOAc, washed with brine and volatiles removed *in vacuo*. The residue was purified by flash column chromatography (EtOAc: hexane) to give ethyl 2'-(4-cyano-6-{[2''-(ethoxycarbonyl)cyclopentyl]carbamoyl}thieno[2,3-*b*]pyridine-2-amido)cyclopentane-1'-carboxylate (**109a**) as a white solid which is a mixture of diastereomers (4 mg, 47 %). ν_{max} (ATR) 3332.7 (N-H), 2240 (w, CN), 1732 (C=O), 1657 (C=O) cm^{-1}. δ_H (599 Hz, $CDCl_3$) 8.49-8.50 (1H, m, 5-H), 7.94 (1H, d, *J* 8.0, 1''-N*H*), 7.83-7.84 (1H, m, 3-*H*), 6.43 (1H, d, *J* 7.2, 1'-N*H*), 4.61-4.67 (1H, m, 1''-*H*) 4.55-4.60 (1H, m, 1'-*H*), 4.13-4.22 (4H, m, OCH_2), 2.78-2.84 (2H, m, 2'-*H* & 2''-*H*), 2.27-2.36 (2H, m, 5''-H_a & 5'-H_a), 2.09-2.16 (2H, m, 3''-H_a & 3'-H_a), 1.95-2.03 (2H, m, 3''-H_b & 3'-H_b), 1.82-1.90 (4H, m, 4'-H_2 & 4''-H_2), 1.68-1.75 (2H, m, 5''-H_b & 5'-H_b), 1.21-1.29 (6H, m, OCH_2CH_3). δ_C (151 Hz, $CDCl_3$) 174.5 (2' or 2''-*C*=O), 174.2 (2' or 2''-*C*=O), 161.9 (6-*C*=O), 160.8 (2-*C*=O), 160.4 (1a-*C*), 148.9 (*C*-6), 146.0 (*C*-2), 134.2 (3/4-*C*), 121.7 (*C*-5), 118.9 (*C*-3), 116.8 (*C*-4), 115.1 (*C*≡N), 61.1 (O-CH_2), 61.0 (O-CH_2), 55.9 (*C*-1'), 55.1 (*C*-1''), 50.9 (*C*-2' or -2''), 50.7 (*C*-2' or -2''), 33.2 (*C*-5' or -5''), 33.0 (*C*-5' or -5''), 28.7 (*C*-3' or -3''), 28.4 (*C*-3' or -3''), 23.4 (*C*-4' or -4''), 23.2 (*C*-4' or -4''), 14.4 (CH_3), 14.3 (CH_3). *m/z* (LC-MS ES^-) 525.2 $[M-H]^-$. HRMS (ES^+) found $[M+H]^+$ 525.1807, $C_{26}H_{29}N_4O_6S$ requires *M* 525.1808.

6.15 X-ray crystallography

Single crystal X-ray diffraction (XRD) data was collected for the following samples using the following diffractometers: i) **17**, crystallised from DMSO/MeOH, using a Bruker SMART-APEX CCD diffractometer using Mo-Kα (λ = 0.71073 Å) radiation. Data reduction was performed using Bruker SAINT software and intensities corrected using SADABS (see footnote[16]). Structures solved using SHELX-97. ii) **185**, **192** and **214**, all crystallised from chloroform and **129** from DCM using a Bruker D8 Venture diffractometer using Mo-Kα (λ = 0.71073 Å) radiation. The structures were solved using Olex2 software with ShelXS structure solution programme and refined using ShelXL package (see footnote[17]). iii) **169**, crystallised in FYR oil from DMSO and 2-methyl-2,4-pentanediol according to a procedure by Tyler *et al*.[221] Samples were prepared using a mosquito® liquid handling robot. Diffraction data was collected using Rigaku Oxford Xcalibur, Atlas, Gemini ultra diffractometer using Mo-Kα (λ = 0.71073 Å) radiation. Data reduction and intensity correction was performed using CrysAlisPro. The structures were solved using Olex2 software with ShelXT structure solution programme and refined using ShelXL package (see footnote[18]).

[16] **17** was crystallised by members of the Professor Ashwini Nangia group and X-ray crystallography was carried out at University of Hyderabad, India.
[17] **185**, **192** and **214** crystals were analysed by Dr Dmitri Yufit, Durham University.
[18] **169** was crystallised by Ronnie Ragbirsingh in the Dr Michael Hall group and X-ray crystallography was carried out at Newcastle University.

6.2 Biological experimental

All biological results in this thesis are reported as the mean of three biological repeats, with errors representing standard error in each case.

6.21 Reagents and equipment

6.21.1 General reagents

Biological grade reagents, buffers and media were commercially sourced. Media and buffers were made up using purified water from a MilliQ® water purification system. Biorelevant buffers (FESSIF, FASSIF and FASSGF) were purchased from Biorelevant and made up according to manufacturer's instructions. PBS tablets were obtained from Fischer Scientific.

Schneider's media throughout refers to Schneiders insect media (Merck) supplemented with 15 % fetal bovine serum (FBS, heat inactivated, South American origin, ThermoFisher scientific) and 1 % Penicillin-Streptomycin (PenStrep, Gibco™, 10,000 U mL^{-1}, ThermoFisher scientific). DMEM refers to Dulbecco's Modified Eagle Medium (Gibco™ DMEM, high glucose, GlutaMAX™ Supplement, pyruvate, ThermoFisher scientific) supplemented with 10 % FBS and 1 % PenStrep. Schneider's media and DMEM were filter sterilised using sterile vacuum filter flasks (0.22 µm pore CA membrane, Merck) and stored at 4 °C.

E. coli cultures were grown in NZCYM media (Merck) which was sterilised by autoclave prior to supplementing with 100 µg mL^{-1} ampicillin (Merck).

SDS-PAGE gels were run alongside either Precision Plus Protein™ All Blue Prestained Protein Standards (BioRad) or Thermo Scientific™ PageRuler™ Plus Prestained Protein Ladder, 10 to 250 kDa (Fisher Scientific) as a reference. Agarose DNA gels were ran alongside Thermo Scientific™ GeneRuler 1 kb Plus DNA Ladder (Fisher Scientific) as a reference.

6.21.1.1 Chemicals

Clemastine fumarate, tamoxifen, resazurin, daidzin, miltefosine, amphotericin B and cycloheximide were purchased from Merck (formerly Sigma Aldrich). Rhodamine azide and biotin azide were synthesised in house by Dr Exequiel Porta. All synthesised compounds and controls were dissolved in biological grade DMSO (Fisher Bioreagents) to give 10 mM stocks unless otherwise stated.

6.21.1.2 Genes and Primers

The gene for NTR1 from *L. donovani* was obtained from UniProt (A0A3S5H5J0) and purchased from GenScript in pJOE5751 (4 µg). Primers were ordered from Merck (formerly Sigma Aldrich). DNA concentration was estimated using the nanodrop feature on a DeNovix DS-11+ Spectrophotometer. Primers used for PCR amplification (pJoe5751) and DNA sequencing (pTrcHis) are shown below:

Table 6.21-1 Primer design for PCR and DNA sequencing used throughout.

Plasmid	Primer name	Primer sequence
pJoe5751	Forward primer (*Ld*_fwd)	5'-taagcaggatcctcGACGCGGTTGAAGCGGTG-3'
	Reverse primer (*Ld*_rev)	5'-gcgggcaagcttTTAAAATTTGTTCCAACG-3'
pTrcHis	Forward Primer (pTrcHis_fwd)	5'-GAGGTATATATTAATGTATCG-3'
	Reverse primer (pTrcHis_rev)	5'-GATTTAATCTGTATCAGG-3'

6.21.2 General equipment

Centrifuge tubes, serological pipettes, microcentrifuge tubes, reagent reservoirs and pipette tips were obtained from Fisher Scientific or StarLab and autoclaved if non-sterile (121 °C, 5 mins).

Centrifugation steps were carried out using a Beckman Coulter centrifuge, Simga1-14 microfuge, Sorvall® Legend RT centrifuge, Sorvall® Legend Micro 17R centrifuge or Boeco U-320. Vortexing was performed using a Vortex Mixer MT20 Chiltern®.

6.21.3 Cell lines

All parasite and human cell cultures were grown and manipulated following biosafety level 2 instructions under sterile conditions. *L. major* FV1, *L. amazonensis* (MHOM/Br/75/JOSEFA), *L. donovani* BOB (derived from MHOM/SD/62/1S-CL2D), *L. mexicana* (strain 0157) and *T. brucei* (90-13, 427 strain) were used throughout. *Lcb2*$^{-}$ cells *(*Δ*Lmlcb2::HYG/* Δ*Lmlcb2::PAC*) and px addback cells (Δ*Lmlcb2::HYG/* Δ*Lmlcb2::PAC [px NEO LmLCB2]* were both derived from *L. major* FV1 strain and developed by Denny *et al*.[21] px addback cells were grown in the presence of 40 µL per 50 mL G418 (Gibco™). *Ld*NTR1 overexpressing cell lines (*Ld*BOB [pIR1SAT-*Lm*NTR]) were developed by Wyllie *et al*.[44] *Ld*NTR2 overexpressing cell lines (*Ld*BOB [pIR1SAT-*Lin*NTR2] or [pX63-3HA-*Lin*NTR2]) were developed by Wyllie *et al*.[49]

6.21.4 Buffers and media

Buffers and media were prepared as follows and made up to the specified volume using Milli-Q grade purified water. Where necessary, pH was adjusted using concentrated HCl, saturated sodium hydroxide solution, or dilutions thereof.

Table 6.21-2 Compositions of buffers used throughout. *Stable for weeks-months if stored at – 80 °C.

Buffer	Final volume / mL	Stock	Quantity	Final concentration
TAE X10	1000	Tris base Glacial acetic acid EDTA (500 mM, pH 8)	48.5 g 11.4 mL 20 mL	40 mM 20 mM
Storage buffer	50	Tris HCl (1 M) Glycerol (80 % w/v)	2.5 mL 6.25 mL	50 mM 20 % v/v 5 mM

		$MgCl_2.6H_2O$ (1 M) cOmplete™ EDTA-free Protease Inhibitor Cocktail tablets (Roche)	0.25 mL 1 tablet	
Phosphate buffer (pH 7.0)	1000	KH_2PO_4 K_2HPO_4	3.77 g 7.71 g	28 mM 44 mM
Buffer A (pH 7.8)	1000	NaH_2PO_4 NaCl	6.9 g 29.3 g	50 mM 500 mM
Lysis buffer A (pH 7.8)	50	Buffer A cOmplete™ EDTA-free Protease Inhibitor Cocktail tablets (Roche)	50 mL 1 tablet	
Wash buffer 1 (pH 7.8)	100	Imidazole Buffer A	0.34 g 100 mL	50 mM
Wash buffer 2 (pH 7.8)	100	Imidazole Buffer A	0.68 g 100 mL	100 mM
Elution buffer (pH 7.8)	100	Imidazole CHAPS Buffer A	3.4 g 1.0 g 100 mL	500 mM 1 % (w/v)
Tris buffer (pH 8.5)	50	Tris base	0.061 g	10 mM
Tris buffer (pH 7.5)	50	Tris base	0.30 g	50 mM
IP lysis buffer	50	Tris base NaCl Triton™ X-100 Glycerol cOmplete™ EDTA-free Protease	0.15 g 0.44 g 0.50 mL 2.50 mL 1 tablet	25 mM 150 mM 1 % (v/v) 5 % (v/v)

		Inhibitor Cocktail tablets (Roche)		
NADH (1 mM in Tris pH 8.5)*	10	NADH Tris buffer (pH 8.5)	7.1 mg 10 mL	1 mM
SDS electrophoresis running buffer (X10, pH 8.3)	1000	Tris base Glycine SDS	30.2 g 141.0 g 10 g	25 mM 250 mM 0.1 (w/v)
Resazurin solution	40	Resazurin sodium salt PBS	5 mg 40 mL	500 µM
Sodium cacodylate buffer	1000	Sodium cacodylate	42.8 g	0.2 M
Double strength fixative solution	50	Paraformaldehyde (16 %) Gluteraldehyde (25 %) 0.2 M sodium cacodylate buffer	12.5 mL 10 mL 25 mL	4 % 5 % 0.1 M
Post-fixative solution	20	Osmium tetroxide (2 %) 50 mM $CaCl_2$ Potassium ferrocyanide (5 %) 0.2 M sodium cacodylate buffer	10 mL 2 mL 3.2 mL Make up to 20 mL	1 % 5 mM 0.8 %

Table 6.21-3 Composition of media used throughout. *Ampicillin is added following autoclave sterilisation or microwaving.

Media	Final volume / mL	Stock solution	Quantity
Schneider's Insect Medium	1000	Schneider's Insect Medium $NaHCO_3$ $CaCl_2$	24.5 g 0.4 g 0.6 g
NZCYM-ampicillin media	1000	NZCYM powder Ampicillin (100 mg mL^{-1})*	22 g 1 mL
NZCYM-ampicillin agar	100	Agar NZCYM media Ampicillin (100 mg mL^{-1})*	1 g 99 mL 0.1 mL
Agarose gel (1 %)	100	TAE buffer Agarose	100 mL 1 g

6.21.5 SDS-PAGE

SDS-PAGE gels were made to 1 mm thickness with 12.5 % acrylamide. Protein samples were diluted with Invitrogen™ NuPAGE™ LDS Sample Buffer (4X) (Fisher Scientific) supplemented with 5 % β-mercaptoethanol (Fluorochem) to 1X NuPAGE™ LDS or protein pellets were dissolved in 1X NuPAGE™ LDS with 5 % β-mercaptoethanol and gels were ran in 1X SDS running buffer (diluted from 10X SDS running buffer with MilliQ grade purified water) using Bio-rad mini protein tetra system electrophoresis equipment at 200 V for 55 mins. SDS PAGE gels were made using the following recipe (Table 6.21-4).

Table 6.21-4 12.5 % acrylamide gel recipe

	2 x 1 mm		4 x 1 mm	
	Resolution/ µL	Stack/ µL	Resolution/ µL	Stack/ µL
Buffer	4800	2400	9600	4800
40 % BisAcrylamide	3750	1425	7500	2850
MilliQ H_2O	3150	2974	6300	5948
10 % APS	124.0	62.6	248.0	125.2
TEMED	12.5	6.3	25.0	12.5

4X resolving and 4X stacking buffers were obtained from Alfa Aesar, acrylamide:bis-acrylamide 29:1, 40 % solution was purchased from Fisher Bioreagents. Electrophoresis grade TEMED was purchased from MP Biomedicals and ammonium persulfate was purchased from Merck and made up to a 10 % solution using MilliQ grade purified water. SDS-PAGE gels were stained using Quick Coomassie Stain (Generon) overnight before destaining with MilliQ grade purified water and imaging using Bio-rad Molecular Imager Gel Doc XR+ with Image Lab (version 6.0.1) software.

6.22 Biological procedures

6.22.1 Cell culture and assays

6.22.1.1 *Leishmania* promastigote cell culture

All steps were carried out under sterile conditions. Frozen stocks of the relevant *Leishmania* promastigote species were thawed rapidly and added to Schneider's media. *L. major* px addback cells were grown in Schneider's media supplemented with 40 µL G418 (Gibco) per 50 mL Schneider's media. Promastigotes were grown at 26 °C in Nunc EasYFlask 25 cm^2 Nunclon Delta Surface (ThermoScientific) and frozen stocks were prepared on low passage cultures (p2-4) by pelleting the cells by centrifugation and resuspending in Schneider's media with 10 % DMSO. The cultures were aliquoted into cryovials (Starlab) and cooled slowly to - 150 °C for long term storage.

6.22.1.2 HepG2 cell culture

All steps were carried out under sterile conditions. HepG2 cells were thawed rapidly into DMEM. Cells were grown at 37 °C, 5 % CO_2 for > 5 days in T-75 CytoOne® Flask,

TC-Treated, Vented flasks (Starlab) in a Sanyo MCO-18M incubator. HepG2 cells were passaged by decanting media, washing with 3 x 5 mL pre-warmed sterile PBS and disrupting with pre-warmed Gibco™ TrypLE solution (Fisher Scientific) for 10 mins at 37 °C. The trypsin was deactivated by addition of DMEM. The cells were homogenised and 5 mL of cell culture was added to 20 mL fresh DMEM. Cells were split 1:4 every 3 days. Frozen stocks were prepared in the same way as the passage, but resuspended into DMEM with 10 % DMSO, aliquoted into cryovials (Starlab) and cooled slowly to - 150 °C for long term storage.

6.22.1.3 Dose response assays

6.22.1.3.1 L. major and L. amazonensis promastigote

All steps were carried out under sterile conditions. *Leishmania* promastigotes were incubated (1 x 10^6 parasites mL^{-1} for *L. major* and 0.5 x 10^6 parasites mL^{-1} for *L. amazonensis*) with a 3-fold serial dilution of compound in Schneider's media in Corning™ Costar™ 96-Well Flat-Bottom Microplates (Fisher Scientific) at 26 °C for 44 hrs. Cycloheximide or amphotericin B were used as positive controls and 2 % DMSO was used as a negative control. alamarBlue® (ThermoFisher scientific) or resazurin solution was added to each well and incubated for a further 4 hrs at 26 °C. Cell-viability was determined using a BioTek™ FLx800 microplate reader with Gen5® 1.08 data analysis software (BioTek) by monitoring fluorescence emission (λ_{ex} 560/ λ_{em} 590 nm). Dose response curves were fitted using sigmoidal regression analysis (GraphPad Prism 8 software) and used to calculate EC_{50} values.

6.22.1.3.2 L. major lcb2$^-$ mutant and px addback

All steps were carried out under sterile conditions. *L. major* lcb2$^-$, px addback and wild type promastigotes were assayed as described in section 6.22.1.3.1). In the case of the px addback, cells were grown and tested in Schneider's insect media supplemented with 40 µL G418 (Gibco) per 50 mL.

6.22.1.3.3 L. donovani promastigote

All steps were carried out under sterile conditions by Dr Juliana Pacheco, Wellcome centre for Anti-Infectives Research, Dundee. *L. donovani* promastigotes (1 x 10^5

parasites mL^{-1}) were incubated with a serial dilution of compound in modified M199 media for 72 hrs at 26 °C. Resazurin (50 µM) was added to each well and incubated for a further 3 hrs at 26 °C. Cell-viability was determined using a fluorescence plate reader λ_{ex} 528/ λ_{em} 590 nm. Dose response curves were fitted using GRAFIT (version 5.0.4, Erithacus software) and used to calculate EC_{50} values.

6.22.1.3.4 LdonNTR1 and L.donNTR2 overexpressor

All steps were carried out under sterile conditions by Dr Juliana Pacheco, Wellcome centre for Anti-Infectives Research, Dundee. *L. donovani* wild type and overexpressor NTR1 and NTR2 cell lines were incubated at 1 x 10^5 cells mL^{-1} with a serial dilution of compound in modified M199 media for 72 hrs at 26 °C. Resazurin (50 µM) was added to each well and incubated for a further 3 hrs at 26 °C. Cell-viability was determined using a fluorescence plate reader λ_{ex} 528/ λ_{em} 590 nm. Dose response curves were fitted using GRAFIT (version 5.0.4, Erithacus software) and used to calculate EC_{50} values. Fold change was calculated by dividing the EC_{50} against wild type promastigotes with the EC_{50} against the overexpressor cell line.

6.22.1.3.5 T. brucei trypomastigotes

All steps were carried out under sterile conditions by members of the Professor Jim Morris lab, Clemson, South Carolina. *T. brucei* bloodstream trypomastigotes (1 x 10^5 cells mL^{-1}) were incubated with a serial dilution of compound in HMI-9 (10 % FBS, 10 % NuSerum) in black 384-well polystyrene plates for 48 hrs (37 °C, 5 % CO_2). CellTiter Blue was added, and the plate incubated for 1 hr before removing the plate lid to allow pH to equilibrate across the plate and recording the fluorescence (λ_{ex} 546/ λ_{em} 585 nm). Dose response curves were fitted using sigmoidal regression analysis (GraphPad Prism 8 software) and used to calculate EC_{50} values.

6.22.1.3.6 HepG2

All steps were carried out under sterile conditions. 80 – 100 % confluent HepG2 were plated into Corning™ Costar™ 96-Well Flat-Bottom Microplates (Fisher Scientific) by adding 200 µL of a homogenous dispersion of cells at a concentration of 0.6 x 10^5 cells mL^{-1} before incubation at 37 °C, 5 % CO_2 overnight. The media was then removed and compounds, diluted in DMEM (10 % FBS, 1 % PenStrep) were added to the

prepared plates using a 3-fold serial dilution from 100 µM (DMSO < 2 %) to give a final well volume of 100 µL (see footnote[19]). The plates were incubated at 37 °C, 5 % CO_2 for 44 hrs in a Sanyo MCO-18M incubator. alamarBlue® (ThermoFisher scientific) or resazurin solution (10 µL) was added to each well and incubated for a further 4 hrs at 37 °C, 5 % CO_2. Cell-viability was determined using a BioTek™ FLx800 microplate reader with Gen5® 1.08 data analysis software (BioTek) by monitoring fluorescence emission (λ_{ex} 560/ λ_{em} 590 nm). Dose response curves were fitted using sigmoidal regression analysis (GraphPad Prism 8 software) and used to calculate EC_{50} values.

6.22.2 *Lmj*IPCS enriched microsome assays

6.22.2.1 HPTLC assay

The following steps were sufficient for 5 samples and 2 controls and were carried out according to a literature procedure by Mina *et al*.[34] Solution 1 was made by drying 30 µL of 1 mM phosphatidyl inositol in chloroform (PI, bovine liver, 1,2-Diacyl-sn-glycero-3-phospho-(1-D-myo-inositol) ammonium salt, Merck) into a microcentrifuge tube using an Eppendorf® centrifugal vacuum concentrator 5301. Then, 105 µL phosphate buffer (72 mM, pH 7.0), 30 µL CHAPS (Melford 3 mM) and 7.5 µL NBD-C_6-ceramide (Invitrogen, 200 µM) were added and solution 1 was stored on ice until use. Solution 2 was made by combining 105 µL phosphate buffer (72 mM, pH 7.0), 30 µL CHAPS (3 mM), 6 µL storage buffer (or appropriate) and 1.5 µL microsomes (or appropriate such that 0.6 U well-1 of enzyme activity) in a LoBind microcentrifuge tube (Merck). 23.75 µL of solution 2 was added to *n* LoBind microcentrifuge tubes, followed by 1 µL of a 5 mM DMSO stock of compound or control before incubation at 30 °C for 20 mins. 23.75 µL of solution 1 was added and the samples were incubated at 30 °C for a further 30 mins. The reaction was quenched with 150 µL 10:10:3 chloroform: methanol: water (CMW) and the layers separated by centrifugation (16.7 x g for 8 mins). The chloroform layer was dried using an Eppendorf® vacuum concentrator and redissolved in 20 µL 10:10:3 CMW. 3 x 3 µL were spotted onto a TLC silica gel aluminium sheet (F254, Merck). The reaction

[19] In the case of ALDH2 inhibition experiments, daidzin (100 µM) was incubated with HepG2 cells when compound was added.

products were separated using an eluent system of 55:45:10 methanol: chloroform:0.25 % KCl(aq) and visualised using FLA-3000 (Fujifilm) fluorescent imaging system with AIDA image analyser software (version 3.52).

6.22.2.2 96-Well filter plate assay

The following steps were carried out according to a literature procedure by Mina *et al*.[34] Solution 1 was made by drying 48 µL of 1 mM phosphatidyl inositol in chloroform (PI, bovine liver, 1,2-Diacyl-sn-glycero-3-phospho-(1-D-myo-inositol) ammonium salt, Merck) into a 10 mL vial before addition of 1680 µL phosphate buffer (72 mM, pH 7.0), 480 µL CHAPS (Melford 3 mM) and 120 µL NBD-C_6-ceramide (Invitrogen, 200 µM). Solution 2 was made by combining 1680 µL phosphate buffer (72 mM, pH 7.0), 480 µL CHAPS (3 mM), 72 µL storage buffer (or appropriate) and 48 µL microsomes (or appropriate such that 0.6 U well-1 of enzyme activity) in a glass vial. 19 µL of solution 1 was added to the necessary wells of a Corning® 96 Well Clear Polystyrene V-bottomed Microplate (Merck). A 3-fold dilution series of compound in DMSO (from 5 mM) was performed. 0.8 µL of control/test compound was added to the respective wells in triplicate (to give compound concentrations on the plate from 100 µM). The plate was stored at 0 °C until needed. 20 µL of solution 2 was added to the necessary wells of the chilled 96-well plate. The plate was incubated for 25 mins at 30 °C before quenching with 200 µL $well^{-1}$ MeOH. The well contents were transferred to a pre-prepared MultiScreen® Solvinert 96-well filter plate (100 µL $well^{-1}$ of a 0.2 g mL^{-1} suspension of AG-X4 resin (BioRad) in EtOH sedimented, activated with 50 µL $well^{-1}$ formic acid and washed with 100 µL $well^{-1}$ MilliQ grade purified water). The filter plate was centrifuged, and any remaining NBD-C_6-ceramide was eluted by washing each well with 5 x 200 µL MeOH. NBD-C_6-IPC was eluted using 4 x 50 µL 1M potassium formate into an OptiPlate-96 Black microplate (PerkinElmer) and the fluorescence (ex. 460 nm/ em. 540 nm) was read using a Synergy™ H4 plate readers with Gen5® 1.08 data analysis software (BioTek). Dose response curves were fitted using sigmoidal regression analysis (GraphPad Prism 8 software) and used to calculate IC_{50} values.

6.22.3 DMPK studies

DMPK studies were performed by GVK BIO Sciences Pvt Ltd Hyderabad, India, in collaboration with LifeArc. Three swiss albino mice per experiment were inoculated (IP or oral) with compound at 10 mg kg^{-1} in 10 % DMSO (2 mg mL^{-1}) on day 1. A small blood sample (50 µL) was taken after 15 minutes, 30 minutes, 1 hr, 2 hr, 4 hr, 6 hr, 8 hr and 24 hr. Proteins were precipitated in acetonitrile and the supernatant was diluted in 1:1 methanol: water and subject to LC-MS analysis. The concentration of compound in the blood was determined by comparing the peak area to a calibration curve.

6.22.4 Protein purification and biochemistry

6.22.4.1 Purification of *Lmj*NTR1

BL21-codon plus competent cells (BL21 (+), Agilent) were transformed with pTrcHis*Lmj*NTR1 according to the manufacturer's instructions. A BL21 (+).pTrcHis*Lmj*NTR1 colony was grown overnight in 20 mL NZCYM-ampicillin at 37 °C, 150 rpm in an SI500 (Stuart) orbital incubator before inoculating into 1 L NZCYM-ampicillin. The cell culture was shaken in a New Brunswick™ Excella® E25 shaker at 37 °C, 150 rpm until OD_{600} 0.8 (as determined using a DeNovix DS-11+ Spectrophotometer), then at 16 °C for 30 mins. Protein expression was initiated by adding 1 mL IPTG (1 M, Melford) with shaking at 16 °C overnight. Cells were harvested by centrifugation (4000 rpm, 30 mins, 4 °C) and the pellet resuspended in 50 mL lysis buffer A (Table 6.21-2) before adding lysozyme (50 mg, Melford) and CHAPS (0.5 g, Melford) and incubating on ice for 30 mins. All future steps were carried out at 4 ˚C or on ice. Cell lysis was achieved by sonication using Bandelin Sonopuls (3 x 1 min at frequency (3 x 10 %) and power 30 % with 1 min rest between cycles). The lysate was centrifuged (20,000 rpm, 30 mins, 4 ˚C) and the supernatant was filtered (0.22 µm Fisherbrand™ Sterile PES Syringe Filter, Fisher Scientific). The filtered lysate was applied to a HisTrap™ Fast Flow 1 column (GE healthcare) using a Gilson MINIPULS 3 Peristaltic Pump, pre-equilibrated with water and buffer A. The flowthrough was reapplied to the column and the column was washed with wash buffer 1 (buffer A + 50 mM imidazole) and wash buffer 2 (buffer A + 100 mM imidazole) before eluting

with elution buffer (buffer A + 500 mM imidazole, 1 % w/v CHAPS). Yellow protein containing fractions were collected and purified further by size exclusion chromatography (using superdex 16/60 75 pg and ÄKTA pure FPLC system (GE Healthcare). The sample was concentrated using a Vivaspin® 2 Ultrafiltration Device (Sartorius) and purity verified by SDS PAGE. Protein concentration was determined by Bradford assay (detailed below) or using Pierce™ Rapid Gold BCA Protein Assay Kit (ThermoFisher Scientific) following manufacturer's instructions. Protein aliquots were supplemented with 20 % glycerol and flash frozen in liquid nitrogen before long term storage at - 80 ˚C.

6.22.4.1.1 Bradford assay for protein quantification

A 2-fold dilution series of BSA (Merck) from 22 µg mL^{-1} was generated in buffer A and protein samples were diluted 100 to 1000-fold in buffer A (final volume 600 µL). 150 µL Bradford reagent (ThermoFisher) was added quickly to each sample before vortexing and plating in triplicate onto a 96-well plate (200 µL $well^{-1}$). UV absorbance (595 nm) was read using a Synergy™ H4 plate reader with Gen5® 1.08 data analysis software (BioTek) and corrected compared to a blank (buffer A + Bradford reagent). Protein concentration was determined by correlating unknown sample absorption with the linear region of the calibration curve.

6.22.4.1.2 Protein mass spectrometry

Protein mass spectrometry samples were prepared to approximately 1 mg mL^{-1} in ammonium acetate (10 mM, pH 5) using a Vivaspin® 2 Ultrafiltration Device (Sartorius) to swap buffers. Mass spectrometry samples were analysed by ESI-MS using a QToF Premier Mass Spectrometer (Waters Ltd) and an Aquity UPLC (Waters Ltd, UK), fitted with Waters MassPrep desalting cartridge, detecting positive ions with an Acquity photodiode array detector. The following MS method is used: 9 min Desalt pos V LM 800 2000 CV35. Protein data was processed using Masslynx 4.1 and deconvoluted using MaxEnt 1 to show the nominal neutral mass of the protein.

Protein digest mass spectrometry was carried out by Dr Adrian Brown, Durham university. This was achieved by elution of the protein from the excised band before

trypsin digestion and analysis using Sciex TripleTOF 6600 linked to Eksigent nanoLC 425 chromatography system using a flow rate of 5 µL min^{-1}. Peak lists were generated using MSConvert and proteins identified using the database search engine PEAKS X.

6.22.4.2 Subcloning of pTrcHis*Ldon*NTR1

6.22.4.2.1 Restriction digestion of pTrcHisCLmjNTR1

pTrcHis*Lmj*NTR1 (1 µg) was incubated with 5 µL FD buffer, 4 µL MilliQ grade purified water and 1 µL each of BamHI FD and HindIII FD (all from New England Biolabs) at 37°C for 30 mins. The reaction was quenched with DNA Gel Loading Dye (6X, ThermoFisher Scientific) and loaded onto a 1 % agarose gel with ethidium bromide (0.2-0.5 µg mL^{-1}). DNA gel electrophoresis was carried out in TAE buffer with ethidium bromide (0.2-0.5 µg mL^{-1}) for 1 hr at 100 V using a BioRad wide Mini-Sub® Cell GT Cell. The open chain pTrcHisC plasmid band was visualised using a Syngene GVM20 UV transilluminator and was cut from the gel and extracted using the QIAquick Gel Extraction kit (Qiagen) following manufacturer's instructions.

6.22.4.2.2 PCR amplification of LdonNTR1 gene insert

12.5 µL CloneAmp™ HiFi PCR Premix (Takara Biosciences) was combined with 20 ng template DNA (pJOE*Ldon*NTR1) and 70 ng Ld_fwd and Ld_rev primers (Table 6.21-1).The reaction volume was made up to 25 µL using MilliQ grade purified water and was subject to the PCR cycle described in Table 6.22-1 using Biometra Tone Gradient 96 Thermo Cycler (Analytik Jena).

Table 6.22-1: PCR cycle for amplification of *Ldon*NTR1 insert from pJOE*Ldon*NTR1.

Stage		**Temperature / °C**	**Time / sec**
Initial denaturation		98	30
Amplification (30 cycles)	Denaturation	98	10
	Annealing	55	15
	Extension	72	5
Final extension		72	300

Following PCR, using DNA Gel Loading Dye (6X, ThermoFisher Scientific) was added and loaded onto a 1 % agarose gel with ethidium bromide (0.2-0.5 µg mL^{-1}) and ran

in TAE buffer with ethidium bromide (0.2-0.5 µg mL^{-1}) for 1 hr at 100 V using a BioRad wide Mini-Sub® Cell GT Cell. The *Ldon*NTR1 band was visualised using a Syngene GVM20 UV transilluminator and was cut from the gel and extracted using the QIAquick Gel Extraction kit (Qiagen) following manufacturer's instructions.

6.22.4.2.3 Restriction digest of LdonNTR1 gene insert

Restriction digest of the *Ldon*NTR1 gene (1 µg) was achieved following the procedure detailed in section 6.22.4.2.1 using a 2 % agarose gel.

6.22.4.2.4 Ligation of LdonNTR1 insert into linearised pTrcHisLmjNTR1

Linearised pTrcHis (65 ng) was combined with the *Ldon*NTR1 digested insert (32 ng) in 1X T4 ligase buffer with 1 µL T4 DNA ligase (New England Biolabs) and incubated for 2 hrs at RT. T7-express competent *E. coli* (Thermo Fisher) were transformed with the resulting plasmid following manufacturer's instructions and grown on NZCYM-ampicillin selection plates overnight (Table 6.21-3).

6.22.4.2.5 Colony PCR and confirmation of LdonNTR1 identity

Eight colonies from the selection plates generated in section 6.22.4.2.4 were dispersed individually in 50 µL NZCYM-ampicillin media. 1 µL of each colony suspension was used as the template DNA and PCR was performed as previously described in section 6.22.4.2.2. Successful transformants were grown in NZCYM-ampicillin media overnight (37 °C, 150 rpm). pTrcHis*Ldon*NTR1 was extracted and purified using QIA prep spin miniprep kit (Qiagen) and DNA sequencing using the *Ldon*_rev and *Ldon*_fwd primers (Table 6.21-1) proved the correct gene identity (DBS genomics). Glycerol stocks (25 %) of T7.pTrcHis*Ldon*NTR1 were stored at – 80 °C until use.

6.22.4.3 Thermal shift assay

Protein samples were concentrated or diluted to approximately 2 mg mL^{-1} before incubation with SYPRO™ Orange (1 µL per 250 µL protein, ThermoFisher). 10 µL of

the protein SYPRO™ Orange mixture was combined with 10 µL of the corresponding Durham pH or Durham Salt screen (Molecular Dimensions) condition in a 96-well non-skirted PCR plate (Thermo Scientific™). The plates were sealed using StarSeal Advanced Polyolefin Film (Starlab), centrifuged (1000 rpm, 2min) and incubated for 30 mins. TSA analysis was achieved using 7500 Fast RT-PCR System (AppliedBiosystems), with fluorescence data collected between 25 and 95 °C at a temperature gradient of 1 °C min^{-1}. Data was analysed using NAMI software.[157]

6.22.4.4 *Lmj*NTR1 kinetics of bioactivation

This method was adapted from Voak *et al*.[129] For stage 1, compound (100 µM) was incubated in tris buffer (50 mM, pH 7.5) and absorbance at 340 nm was measured every 10 seconds for 5 minutes using Varian Cary® 100 UV-Vis Spectrophotometer with Cary WinUV kinetics software (version 3.00 (182)). For stage 2, 66 µM β-nicotinamide adenine dinucleotide, reduced disodium salt hydrate (NADH, Merck) was added and absorbance at 340 nm was measured every 10 seconds for 5 minutes. For stage 3, *Lmj*NTR1 (35 µg mL^{-1}) was added and absorbance at 340 nm was measured every 10 seconds for 10 minutes. The gradient of the stage 3 decay was corrected for any background reduction (stage 2) and used to calculated the rate of bioactivation in $nmol_{(NADH(ox))}$ $mg_{(enzyme)}^{-1}$ min^{-1}.

6.22.4.5 *Lmj*NTR1 metabolomics

6.22.4.5.1 Sample preparation

This method was adapted from Hall *et al*.[138] In general, 100 µM compound was incubated with 330 µM β-nicotinamide adenine dinucleotide, reduced disodium salt hydrate (NADH, Merck) and 35 µg mL^{-1} *Lmj*NTR1 in tris buffer (50 mM, pH 7.5) at a final volume of 100 µL for 10 minutes. The reaction was quenched by vortexing with 100 µL Ni Sepharose 6 Fast Flow resin suspension followed by centrifugation (14,500 rpm, 5 min). For soluble samples 100 µL of the supernatant was removed for LC-MS analysis. For less soluble samples, 100 µL of supernatant was removed and replaced with 100 µL DMSO followed by centrifugation (14,500 rpm, 5 min). 100 µL of the

supernatant was removed for LC-MS analysis using Waters Synapt G2-S (Waters Corp., UK).

6.22.4.5.2 LC-MS method

Synapt G2-S (Waters Corp., UK) was used to detect electrospray ionisation ions between m/z 100 and 2000 using a photodiode array detector (λ_{abs} 210-500 nm). Full scan data was collected in negative ion mode. 3 µL sample volumes were injected onto a UPLC C18 (1.7 µm 2.1x100mm) column for metabolite separation using a gradient of mobile phases (Table 6.22-2) at a flow rate of 0.4 mL min^{-1}. The mobile phases used were water (A1, 0.1 % formic acid) and acetonitrile (B1, 0.1 % formic acid). Collision induced dissociated tandem mass spectrometry (MS/MS) was achieved using a fragmentation energy of 15 eV in negative ion mode. All data was analysed using MassLynx version 4.1 software and MestReNova version 14.1.1. Accurate mass analysis of metabolites identified by LC-MS analysis was achieved using MassLynx version 4.1.

Table 6.22-2: LC-MS method used for *Lmj*NTR1 metabolite identification. Solvent A1 is water with 0.1 % formic acid, solvent B1 is acetonitrile with 0.1 % formic acid.

Time / min	Flow rate / mL min^{-1}	% A1	% B1
0	0.4	99	1.0
5	0.4	1.0	99
6	0.4	1.0	99
6.1	0.4	99	1.0
7	0.4	99	1.0

6.22.5 Probe studies

6.22.5.1 Lysate generation

The following procedure was carried out under sterile conditions. 10 mL of a rapidly dividing late log phase culture of *L. major* promastigotes was incubated with 10 µM probe **251** for 2 hrs on a Stuart See-Saw rocker SSL4. In the case of competition experiments, competitor **232**, **17** or **253** was preincubated with cells at 10, 25 or 50

µM for 30 minutes before addition of probe **251** (10 µM) for 1.5 hrs. Cells were pelleted by centrifugation (2000 x g, 5 min, 4 °C) and the pellet washed 3 times with PBS. 0.5 mL IP lysis buffer – EDTA (Table 6.21-2) was added to the washed cell pellet, which was resuspended and incubated on ice for 5 minutes with regular shaking or vortexing. Cell debris was pelleted (11000 rpm, 10 min, 4 °C) and the protein concentration of the supernatant was determined using the Pierce™ Rapid Gold BCA Protein Assay Kit (ThermoFisher Scientific) following manufacturer's instructions. Lysates were stored at – 80 °C until use.

6.22.5.2 Fluorescence probe experiments

6.22.5.2.1 Click chemistry conditions

Rhodamine azide (1 µL of 10 mM DMSO stock, 1 eq.) was added to 90.7 µL of treated cell lysate (1 mg mL^{-1}). $CuSO_4.5H_2O$ (Merck) solution (60 mM in water) was premixed with equal volumes of TBTA (Merck) solution (60 mM in DMSO) before addition of Cu:TBTA (3.3 µL, 10 eq.), a brief vortex and incubation at RT for 2 mins. Sodium ascorbate (Fluorochem, 1.7 µL of 60 mM stock in water, 10 eq.) was added and the click reaction was incubated at RT for 60 minutes. The reaction was quenched by addition of Na_4EDTA (Merck) solution (2 eq.).

6.22.5.2.2 Chloroform methanol water precipitation

Following quenching of the click reaction 400 µL ice cold methanol followed by 100 µL ice cold chloroform and 300 µL MilliQ grade purified water were added, with thorough vortexing between each addition. The samples were centrifuged (15000 rpm, 10 min). Most of the aqueous layer was removed, followed by the organic layer such that the protein wafer at the interface was undisturbed. All remaining liquid was discarded and the protein wafer washed with 400 µL ice cold methanol and air dried at RT. The protein wafer was redissolved in 20 µL of 1 x dilution of Invitrogen™ NuPAGE™ LDS Sample Buffer (4X) (Fisher Scientific) supplemented with 5 % β-mercaptoethanol (Fluorochem) and heated to 96 °C for 10 mins before loading onto an SDS PAGE gel (12.5 % acrylamide) and running using Bio-rad mini protein tetra system electrophoresis equipment at 200 V for 55 mins.

6.22.5.2.3 Gel imaging

Fluorescent gel images were obtained using the GenPurp filter (λ_{ex} 532/ λ_{em} 560 nm) on a Typhoon 9400 (Amersham Biosciences) with the programme ImageQuant (version 5.2). Fluorescent images were visualised and manipulated using Image Lab (version 6.0.1). Following fluorescence imaging, gels were stained using Quick Coomassie Stain (Generon) overnight before destaining with MilliQ grade purified water and imaging using Bio-rad Molecular Imager Gel Doc XR+ with Image Lab (version 6.0.1) software.

6.22.6 Proteomics

6.22.6.1 Sample preparation

Samples were prepared as previously described (6.22.5.1). Sample 1 was prepared by incubating *L. major* promastigotes with 10 µM probe **251** for 2 hrs prior to lysis, and sample 2 was prepared by incubating *L. major* promastigotes with 50 µM **232** competitor for 30 minutes followed by 10 µM **251** for 1.5 hrs prior to lysis.

6.22.6.1.1 Click chemistry

Click chemistry was performed on sample 1 and sample 2 following the general procedure outlined in section 6.22.5.1. Biotin azide (1 µL of 10 mM DMSO stock, 1 eq.) was used instead of rhodamine azide, and following this addition a final volume of 4 % SDS (Fisher Scientific) was added to each sample to aid protein solubilisation. Click chemistry was then performed as described in section 6.22.5.1.

6.22.6.1.2 Affinity enrichment

The following steps were carried out by Dr Kalesh Karunakaran-Nair-Ana, Durham university. The click chemistry reaction mixture proteins were precipitated using 4:3:1 methanol: chloroform: water as described in section 6.22.5.2.2. The air-dried protein pellets were dissolved in PBS with 2 % SDS to a concentration of 5 mg/mL before 20-fold dilution with PBS such that SDS final concentration was 0.1 %. The supernatant obtained following centrifugation (10,000 x g, 5 mins) was mixed with 50 µL freshly washed (3 times with PBS 0.1 % SDS) NeutrAvidin-Agarose beads for 1.5 hrs on an end-over-end shaker at RT. The beads were then washed three times with

1 % SDS in PBS, once with 6 M urea in PBS, three times with PBS and once with 25 mM TEAB buffer. Each washing step used 20 volumes of the relevant solution with centrifugation (2000 x g, 1 min) between each wash.

6.22.6.1.3 On-bead reduction, alkylation and tryptic digestion

The following steps were carried out by Dr Kalesh Karunakaran-Nair-Ana, Durham university. Washed beads were resuspended in 25 mM TEAB buffer (200 µL) and treated with 10 mM TCEP for 45 minutes at 30 °C. The beads were washed with 25 mM TEAB buffer and resuspended in 25 mM TEAB buffer (200 µL). 15 mM chloroacetamide was added, and the beads were incubated in the dark at RT for 20 mins. The beads were then washed with 25 mM TEAB buffer and resuspended in 200 µL fresh 50 mM TEAB buffer. Sequencing grade modified trypsin (5 µg) was added, and the samples incubated at 37 °C for 16 hrs. Following centrifugation (5000 x g, 5 min) the supernatant was collected, and the bead pellet was washed with 50 % acetonitrile containing 0.1 % formic acid. The bead washings were combined with the previous supernatant. This peptide solution was acidified to pH 3 with formic acid and evaporated to dryness. The peptides were redissolved in 0.1 % formic acid in water and desalted using Pierce C-18 Spin Columns (Thermo Scientific; CN: 89873) following manufacturer's instructions and the peptides were evaporated to dryness.

6.22.6.2 iTRAQ proteomics

6.22.6.2.1 iTRAQ labelling

The following steps were carried out by Dr Kalesh Karunakaran-Nair-Ana, Durham university. The dry desalted peptide pellet was resuspended in dissolution buffer (0.5 M TEAB, from iTRAQ Reagents Multiplex Kit, Merck). The iTRAQ reagent vials were warmed to RT and absolute EtOH (70 µL) was added to each. The iTRAQ reagent solutions were then added to the respective peptide digest vials (sample 1 or sample 2) and incubated at 25 °C for 1.5 hrs. The labelling reaction was quenched with 1 M Tris base solution (100 mM final concentration). Sample 1 and 2 were then combined in a fresh vial and concentrated on a speed-vac. The dried peptides were redissolved in water with 0.1 % formic acid and 2 % acetonitrile and desalted using a C-18 Sep-

Pak Classic cartridge (Waters; WAT051910) following manufacturer's instructions. The eluted peptides were concentrated on a speed-vac and further cleaned using HILIC TopTip (PolyLC; TT200HIL) solid-phase extraction tips following manufacturers instructions. Eluted peptides were concentrated on a speed-vac and redissolved in 0.1 % formic acid.

6.22.6.2.2 LC-MS/MS analysis

The following steps were carried out by Dr Kalesh Karunakaran-Nair-Ana and Dr Adrian Brown, Durham university. iTRAQ labelled peptides were resolved using an ekspert^{TM} nanoLC 425 with Low Micro Gradient Flow module (Eksigent) using a YMC-Triart C18 column (12 nm, S-3 µm, 150 x 0.3 mm ID, 1/32"; Part number: TA12S03-15H0RU). A C-18 trap column was connected prior to the main column (Trap-YMC-Triart 12 nm S-5 µm, 5 x 0.5 mm ID, 1/32"; Part number: TA12S05-E5J0RU). A 5 µL injection volume of iTRAQ labelled peptide sample was used, which were separated using solvent A (water with 0.1 % formic acid) and solvent B (acetonitrile with 0.1 % formic acid) with a flow rate of 5 µL min^{-1}. The following solvent gradient was used for resolution: 3% B to 5% B (0 to 2 min), 5% B to 30% B (2 to 68 min), 30% B to 35% B (68 to 73 min), 35% B to 80% B (73 to 75 min), constant at 80% (75 to 78 min), 80% B to 3% B (78 to 79 min), constant at 3% B (79 to 87 min). MS analysis of the eluting peaks from 0 to 85 mins was performed using TripleTOF 6600 (Sciex) in high resolution mode. MS1 analysis was performed for a mass range of 400-1600 m/z with 250 ns accumulation time per spectrum. Further fragmentation of each MS1 spectrum was achieved in high sensitivity mode with a maximum of 30 precursors per cycle and 33 ms minimum accumulation time for each precursor across the range of 100 to 1500 m/z (ion selection +2 to +5, 500 cps intensity threshold, and dynamic exclusion for 15 sec).

6.22.6.2.3 Proteomics data processing

The following steps were carried out by Dr Kalesh Karunakaran-Nair-Ana, Durham university and Adrian Brown, Proteomics Facility, Department of Biosciences, Durham University. MaxQuant (version 1.6.3.4) with integrated Andromeda database search engine was used to identify and quantify proteins from the .wiff files

obtained from the Sciex TripleTOF 6600 system. MS/MS spectra were queried against *L. major* sequences from UniProt KB. Database search used the following parameters: Reporter ion MS2 with multiplicity 2plex, trypsin digestion with maximum 2 missed cleavages, carbamidomethylation of cysteine as fixed modification, oxidation of methionine and acetylation of protein N-termini as variable modifications, maximum number of modifications per peptide set at 5, minimum peptide length of 6, and protein FDR 0.01. Correction factors for N-terminal and lysine iTRAQ labelling were also configured into the database search, following the iTRAQ Reagent Multiplex Kit instructions. The MaxQuant search output was processed using Perseus software (version 1.6.2.3). Potential contaminants, reverse sequences, sequences only identified by site, endogenous biotinylated proteins, and proteins with less than 2 unique peptides were removed. The ratio of reporter ion intensity for sample 1 (with probe only) compared to sample 2 (with competitor) gave fold change, which were converted to a log2 scale. Significant data points were determined by a permutation-based FDR calculation following a *t*-test on three replicated and volcano plot generation (FDR = 0.05, number of randomisations = 250).

6.22.6.3 Gene Ontology analysis

The following steps were carried out by Dr Kalesh Karunakaran-Nair-Ana, Durham university. The Gene Ontology Terms (Biological Process, Molecular Function and Cellular Component) that were over-represented for significant hits relative to the whole proteome of *L. major* were derived using Tritrypdb.org. Data visualisation was achieved using R (version 4.1.1) using the ggplot2 package.

6.22.7 Whole cell mode of action

6.22.7.1 Mitochondrial dysfunction (JC-1)

This procedure was adapted from Fonseca-Silva *et al* using Mitochondria Staining Kit (CS0390, Merck).[222] 5 mL of mid log phase *L. major* promastigotes (1 x 10^6 cells mL^{-1}) were incubated with the specified compound at the specified concentration, or DMSO for the untreated control, for 48 hrs at 26 °C. Cells were harvested by centrifugation (2000 x g, 5 min) and resuspended in 1 mL Hank's Balanced Salt Solution (HBSS, Merck). Cells were counted diluted into 0.5 mL aliquots at 2 x 10^6

cells mL^{-1}. For the positive control, carbonyl cyanide 3-chlorophenylhydrazone (CCCP, Merck) at a final concentration 20 µM was incubated with an aliquot of the untreated control for 20 mins. JC-1 dye (5 µL of 0.25 mg mL^{-1} stock) was added and samples were incubated for 10 mins at 37 °C. Cells were pelleted by centrifugation (2000 xg, 2 mins) and washed with HBSS twice. Cells were resuspended in HBSS and plated in triplicate (100 µL $well^{-1}$) onto a Corning™ Costar™ 96-Well Flat-Bottom Microplate (Fisher Scientific) and fluorescence emission was measured for monomer (λ_{ex} 480/ λ_{em} 530 nm) and aggregated (λ_{ex} 480/ λ_{em} 590 nm) dye units using a Synergy™ H4 plate reader with Gen5® 1.08 data analysis software (BioTek). A ratio of the fluorescence emission at 590 nm vs 530 nm was calculated to give the relative membrane potential. Data was corrected relative to the positive CCCP and negative untreated DMSO control to give % mitochondrial function.

6.22.7.2 ROS accumulation (H2DCFDA)

This procedure was adapted from Fonseca-Silva *et al*.[222] 5 mL of mid log phase *L. major* promastigotes (1 x 10^6 cells mL^{-1}) were incubated with compound at the specified concentration, or DMSO for the untreated control, for 48 hrs at 26 °C. Cells were harvested by centrifugation (2000 x g, 5 min) and resuspended in 1 mL Hank's Balanced Salt Solution (HBSS, Merck). Cells were counted before dilution into 0.5 mL aliquots at 2 x 10^6 cells mL^{-1}. For the positive control, hydrogen peroxide (Merck) at a final concentration of 0.01 % was incubated with an aliquot of the untreated control for 20 mins. 2',7'-dichlorofluorescin diacetate (H2DCFDA, Merck) was added to a final concentration of 20 µM and samples were incubated for 20 mins at 37 °C. Cells were plated in triplicate (100 µL $well^{-1}$) onto a Corning™ Costar™ 96-Well Flat-Bottom Microplate (Fisher Scientific) and fluorescence emission was measured (λ_{ex} 507/ λ_{em} 530 nm) using a Synergy™ H4 plate reader with Gen5® 1.08 data analysis software (BioTek). Data was corrected relative to the positive H_2O_2 control and negative untreated DMSO control to give % ROS accumulation.

6.22.7.3 Transmission electron microscopy

6.22.7.3.1 Preparation of treated L. major promastigote samples

The following steps were carried out under sterile conditions. 5 mL *L. major* promastigotes (1 x 10^6 cells mL^{-1}) were incubated with **17** at the EC_{50} and EC_{90} or DMSO (negative control) at 26 °C for 12 hrs.

6.22.7.3.2 Fixation of treated L. major promastigote samples

The following steps were carried out under sterile conditions. 5 mL double strength fixative (Table 6.21-2) was added and the cells were incubated for 5-10 mins at RT. The cells were harvested by centrifugation (800 x g, 10 min) and the pellet resuspended in 1 mL of single strength fixative solution (8 % paraformaldehyde, 12.5 % glutaraldehyde, 0.1 M sodium cacodylate). The cells were centrifuged (800 x g, 10 min) and the cell pellet was incubated in this fixative solution for 2 hrs.

6.22.7.3.3 Post-fixation and resin embedding of cells

The following steps were carried out under non-sterile conditions by Dr Christine Richardson, Department of Biosciences, Durham university. The supernatant fixative solution was removed from the cell pellet and the pellet washed with 3 x 5 mL 0.1 M sodium cacodylate buffer. The cell pellet was incubated with post-fixation solution (1 % osmium tetroxide, 0.8 % potassium ferrocyanide, 5 mM calcium chloride, 0.1 M sodium cacodylate) for 1 hr at RT. The supernatant was removed, and the pellet washed with 0.1 M sodium cacodylate buffer. The pellet was transferred to a glass vial and dehydrated using EtOH (3 x 50 %, 3 x 70 %, 3 x 95 % for 5 mins each, 3 x 100 % for 10 mins each). The dehydrated pellet was infiltrated with 3 x EtOH:propylene oxide (1:1) for 10 mins each time. The pellet was then infiltrated with 3 x propylene oxide for 10 mins each time, followed by propylene oxide:Epon resin (1:1) for 1 hr at 60 °C. Incubate on resin overnight, changing solution 1-2 times during the day. Embed the cell pellet and polymerise at 60 °C for 24 hrs. Thin slices of parasites embedded in Epon resin were imaged using a Hitachi H7600 transmission electron microscope with EMSIS Xarosa 20 Megapixel Bottom-mount CMOS camera.

6.3 Physicochemical experimental

6.31 Materials and methods

All chemicals and solvents were sourced from commercial suppliers. Buffers were made up using purified water from a MilliQ® water purification system. Biorelevant buffers (FESSIF, FASSIF and FASSGF) were purchased from Biorelevant and made up according to manufacturer's instructions. 15 % FBS (heat inactivated, South American origin, ThermoFisher scientific) in PBS (Fisher Scientific) was filter sterilised (0.22 μm Fisherbrand™ Sterile PES Syringe Filter, Fisher Scientific) before use. Sodium taurocholate was purchased from Merck.

6.32 Procedures

6.32.1 Kinetic solubility

λ_{max} was determined for each compound from the UV-Vis absorption spectrum of a 200 μM compound solution in buffer of interest using a Varian Cary® 100 UV-Vis Spectrophotometer. A calibration curve of λ_{max} vs concentration was obtained by serial dilution of compound from 200 μM in the buffer of interest, correcting for background buffer absorption. For each sample, a DMSO solution of compound was incubated in buffer of interest (< 5 % DMSO) for 2 hrs at RT. The solution was filtered (0.22 μm Fisherbrand™ Sterile PES Syringe Filter, Fisher Scientific) or centrifuged (14,500 rpm, 10 min) to remove undissolved debris and the supernatant was removed and diluted as required. The corrected UV absorption of the supernatant at λ_{max} was measured using a Varian Cary® 100 UV-Vis Spectrophotometer and compared to the calibration curve to determine compound solubility.

6.32.2 Cyclic voltammetry

Cyclic voltammetry measurements were made using an Autolab PGSTAT30 potentiostat, running with GPES 4.9 software from Eco-Chimie, Utrecht, Netherlands. Experiments were carried out at RT using a three-electrode cell connected to an argon line and equipped with a glassy carbon working electrode (3 mm diameter), Pt

wire counter electrode and Pt wire pseudo-reference electrode. The supporting electrolyte was $(NBu_4)[PF_6]$ made up to 0.1 M in anhydrous DMSO. Compound solutions were degassed under argon for 3 minutes prior to measurements being taken. Under these conditions the ferrocenium/ferrocene couple in DMSO was used as the internal reference. Experimental peak potentials are converted by -0.2 V with respect to the NHE reference when the ferrocenium/ferrocene couple is at 0 V.

7 References

1 J. L. Norcliffe, J. G. Mina, E. Alvarez, J. Cantizani, F. de Dios-Anton, G. Colmenarejo, S. G.-D. Valle, M. Marco, J. M. Fiandor, J. J. Martin, P. G. Steel and P. W. Denny, *Nat. Sci. reports*, 2018, **8**, 1–10.

2 P. W. Denny, H. Shams-eldin, H. P. Price, D. F. Smith and R. T. Schwarz, *J. Biol. Chem.*, 2006, **281**, 28200–28209.

3 Leishmaniasis fact sheet. Geneva: World Health Organization; 2021, https://www.who.int/news-room/fact-sheets/detail/leishmaniasis, (accessed 4 November 2021).

4 J. A. Ruiz-postigo, S. Jain, A. Mikhailov, A. N. Maia-Elkhoury, S. Valadas, S. Warusavithana, M. Osman, Z. Lin, A. Beshah, A. Yajima and E. Gasimov, *Wkly. Epidemological Rec.*, 2021, **35**, 401–419.

5 G. L. L. Machado-Coelho, W. T. Caiaffa, O. Genaro, P. A. Magalhães and W. Mayrink, *Trans. R. Soc. Trop. Med. Hyg.*, 2005, **99**, 55–61.

6 D. E. Teixeira, M. Benchimol, J. C. F. Rodrigues, P. H. Crepaldi, P. F. P. Pimenta and W. de Souza, *PLoS Pathog.*, 2013, **9**, 8–11.

7 M. Parsons, T. Furuya, S. Pal and P. Kessler, *Mol. Biochem. Parasitol.*, 2001, **115**, 19–28.

8 M. Parsons, *Mol. Microbiol.*, 2004, **53**, 717–724.

9 W. H. Organisation, WHO Expert Committee on the Control of the Leishmaniases & World Health Organization. (2010). Control of the leishmaniases: report of a meeting of the WHO Expert Commitee on the Control of Leishmaniases, Geneva, 22-26 March 2010, https://apps.who.int/iris/handle/10665/44412.

10 T. Garnier, M. B. Brown, M. J. Lawrence and S. L. Croft, *J. Pharm. Pharmacol.*, 2006, **58**, 1043–1054.

11 P. M. Loiseau, S. Cojean and J. Schrével, *Parasite*, 2011, **18**, 115–119.

12 A. K. Haldar, P. Sen and S. Roy, *Mol. Biol. Int.*, 2011, 1–23.

13 F. Chappuis, E. Alirol, D. T. Worku, Y. Mueller and K. Ritmeijer, *Antimicrob. Agents Chemother.*, 2011, **55**, 455–456.

14 S. Sundar and J. Chakravarty, *Expert Opin. Investig. Drugs*, 2008, **17**, 787–794.

15 C. Paris, P. M. Loiseau, C. Bories and J. Bréard, *Antimicrob. Agents Chemother.*, 2004, **48**, 852–859.

16 F. J. Pérez-Victoria, F. Gamarro, M. Ouellette and S. Castanys, *J. Biol. Chem.*, 2003, **278**, 49965–49971.

17 Visceral Leishmaniasis - what we have achieved, https://dndi.org/diseases/visceral-leishmaniasis/projects-achievements/, (accessed 19 November 2021).

18 S. Wyllie, M. Thomas, S. Patterson, S. Crouch, M. De Rycker, R. Lowe, S. Gresham, M. D. Urbaniak, T. D. Otto, L. Stojanovski, F. R. C. Simeons, S. Manthri, L. M. MacLean, F. Zuccotto, N. Homeyer, H. Pflaumer, M. Boesche, L. Sastry, P. Connolly, S. Albrecht, M. Berriman, G. Drewes, D. W. Gray, S. Ghidelli-Disse, S. Dixon, J. M. Fiandor, P. G. Wyatt, M. A. J. Ferguson, A. H. Fairlamb, T. J. Miles, K. D. Read and I. H. Gilbert, *Nature*, 2018, **560**, 192–197.

19 R. A. A. Ferreira, C. de O. R. Junior, P. D. G. Martinez, P. J. Koovits, B. M. Soares, L. L. G. Ferreira, S. Michelan-Duarte, R. C. Chelucci, A. D. Andricopulo,

M. K. Galuppo, S. R. B. Uliana, A. Matheeussen, G. Caljon, L. Maes, S. Campbell, J. M. Kratz, C. E. Mowbray and L. C. Dias, *PLoS Negl. Trop. Dis.*, 2021, **15**, 1–20.
20 K. Zhang, M. Showalter, J. Revollo, F. Hsu, J. Turk and S. M. Beverley, *Eur. Mol. Biol. Organ.*, 2003, **22**, 6016–6026.
21 P. W. Denny, D. Goulding, M. A. J. Ferguson and D. F. Smith, *Mol. Microbiol.*, 2004, **52**, 313–327.
22 M. R. Hojjati, Z. Li and X. C. Jiang, *Biochim. Biophys. Acta*, 2005, **1737**, 44–51.
23 C. R. Gault, L. M. Obeid and Y. A. Hannun, *Adv. Exp. Med. Biol.*, 2010, **688**, 1–23.
24 V. Mandlik, S. Shinde, A. Chaudhary and S. Singh, *Integr. Biol.*, 2012, **4**, 1130.
25 J. G. Mina, J. A. Mosely, H. Z. Ali, P. W. Denny and P. G. Steel, *Org. Biomol. Chem.*, 2011, **9**, 1823–1830.
26 F. G. Tafesse, K. Huitema, M. Hermansson, S. Van Der Poel, J. Van Den Dikkenberg, A. Uphoff, P. Somerharju and J. C. M. Holthuis, *J. Biol. Chem.*, 2007, **282**, 17537–17547.
27 E. E. Prieschl and T. Baumruker, *Immunol. Today*, 2000, **21**, 555–560.
28 P. W. Denny, H. Shams-Eldin, H. P. Price, D. F. Smith and R. T. Schwarz, *J. Biol. Chem.*, 2006, **281**, 28200–28209.
29 J. L. Norcliffe (PhD Thesis), University of Durham, 2015.
30 K. Gewald, *Chem. Heterocycl. Compd.*, 1977, **12**, 1077–1090.
31 S. Hesse, E. Perspicace and G. Kirsch, *Tetrahedron Lett.*, 2007, **48**, 5261–5264.
32 J. Mikus and D. Steverding, *Parasitol. Int.*, 2000, **48**, 265–269.
33 O. A. Almazroo, M. K. Miah and R. Venkataramanan, *Clin. Liver Dis.*, 2017, **21**, 1–20.
34 J. G. Mina, J. A. Mosely, H. Z. Ali, H. Shams-Eldin, R. T. Schwarz, P. G. Steel and P. W. Denny, *Int. J. Biochem. Cell Biol.*, 2010, **42**, 1553–1561.
35 J. M. Figueiredo, W. B. Dias, L. Mendonça-Previato, J. O. Previato and N. Heise, *Biochem. J.*, 2005, **387**, 519–529.
36 J. G. M. Mina, R. L. Charlton, E. Alpizar-Sosa, D. O. Escrivani, C. Brown, A. Alqaisi, M. P. G. Borsodi, C. P. Figueiredo, E. V de Lima, E. A. Dickie, W. Wei, R. Coutinho-Silva, A. Merritt, T. K. Smith, M. P. Barrett, B. Rossi-Bergmann, P. W. Denny and P. G. Steel, *ACS Infect. Dis.*, 2021, **7**, 47–63.
37 C. T. Trinconi, D. C. Miguel, A. M. Silber, C. Brown, J. G. M. Mina, P. W. Denny, N. Heise and S. R. B. Uliana, *Int. J. Parasitol. Drugs Drug Resist.*, 2018, **8**, 475–487.
38 M. C. Neves, H. A. L. Filipe, R. L. Reis, J. P. P. Ramalho, F. Coreta-Gomes, M. J. Moreno and L. M. S. Loura, *Front. Physiol.*, 2019, **10**, 1–11.
39 Paladin Labs Inc., Application for Inclusion of Emtricitabine On WHO Model List of Essential Medicines, https://www.who.int/selection_medicines/committees/expert/18/applications/Miltefosine_application.pdf, (accessed 4 October 2021).
40 African sleeping sickness - Biology, https://www.cdc.gov/parasites/sleepingsickness/biology.html, (accessed 4 November 2021).
41 Chagas disease- Biology, https://www.cdc.gov/parasites/chagas/biology.html, (accessed 4 November

2021).
42 Trypanosomiasis, human African (sleeping sickness), https://www.who.int/news-room/fact-sheets/detail/trypanosomiasis-human-african-(sleeping-sickness), (accessed 4 November 2021).
43 Chagas disease fact sheet, https://www.who.int/news-room/fact-sheets/detail/chagas-disease-(american-trypanosomiasis), (accessed 4 November 2021).
44 S. Wyllie, S. Patterson, L. Stojanovski, F. R. C. Simeons, S. Norval, R. Kime, K. D. Read and A. H. Fairlamb, *Sci. Transl. Med.*, 2012, **4**, 1–16.
45 G. Priotto, S. Kasparian, W. Mutombo, D. Ngouama, S. Ghorashian, U. Arnold, S. Ghabri, E. Baudin, V. Buard, S. Kazadi-Kyanza, M. Ilunga, W. Mutangala, G. Pohlig, C. Schmid, U. Karunakara, E. Torreele and V. Kande, *Lancet*, 2009, **374**, 56–64.
46 I. Pena, M. P. Manzano, J. Cantizani, A. Kessler, J. Alonso-padilla, A. I. Bardera, E. Alvarez, G. Colmenarejo, I. Cotillo, I. Roquero, F. De Dios-anton, V. Barroso, A. Rodriguez, D. W. Gray, M. Navarro, V. Kumar, A. Sherstnev, D. H. Drewry, J. R. Brown, J. M. Fiandor and J. J. Martin, *Nat. Sci. reports*, 2015, **5**, 1–12.
47 D. S. Wishart, Y. D. Feunang, A. C. Guo, E. J. Lo, A. Marcu, J. R. Grant, T. Sajed, D. Johnson, C. Li, Z. Sayeeda, N. Assempour, I. Iynkkaran, Y. Liu, A. Maciejewski, N. Gale, A. Wilson, L. Chin, R. Cummings, D. Le, A. Pon, C. Knox and M. Wilson, *Nucleic Acids Res.*, 2018, **46**, 1074–1082.
48 S. Patterson and S. Wyllie, *Trends Parasitol.*, 2014, **30**, 289–298.
49 S. Wyllie, A. J. Roberts, S. Norval, S. Patterson, J. Foth, M. Berriman, K. D. Read and A. H. Fairlamb, *PLoS Pathol.*, 2016, 1–22.
50 K. Nepali, H. Lee and J. Liou, *J. Medici*, 2019, **62**, 2851–2893.
51 L. A. Solt, Y. Wang, S. Banerjee, T. Hughes, D. J. Kojetin, T. Lundasen, Y. Shin, J. Liu, M. D. Cameron, R. Noel, S. H. Yoo, J. S. Takahashi, A. A. Butler, T. M. Kamenecka and T. P. Burris, *Nature*, 2012, **485**, 62–68.
52 G. Sulli, A. Rommel, X. Wang, M. J. Kolar, F. Puca, A. Saghatelian, M. V. Plikus, I. M. Verma and S. Panda, *Nature*, 2018, 553, 351–355.
53 L. Geldof, K. Deventer, K. Roels, E. Tudela and P. Van Eenoo, *Int. J. Mol. Sci.*, 2016, **17**, 1–16.
54 A. Delsarte, M. Faway, J. M. Frere, J. Coyette, C. M. Calberg-Bacq and E. Heinen, *Antimicrob. Agents Chemother.*, 1981, **19**, 477–486.
55 F. Leonard, A. Andremont and C. Tancrede, *J. Appl. Bacteriol.*, 1985, **58**, 545–553.
56 J. P. Labaune, J. P. Moreau and R. Byrne, *Biopharm. Drug Dispos.*, 1986, **7**, 431–441.
57 D. G. Rando, M. A. Avery, B. L. Tekwani, S. I. Khan and E. I. Ferreira, *Bioorganic Med. Chem.*, 2008, **16**, 6724–6731.
58 G. Chauvière, B. Bouteille, B. Enanga, C. De Albuquerque, S. L. Croft, M. Dumas and J. Périé, *J. Med. Chem.*, 2003, **46**, 427–440.
59 J. Da Silva Pacheco, D. D. S. Costa, E. F. Cunha-Júnior, V. V. Andrade-Neto, A. H. Fairlamb, S. Wyllie, M. O. F. Goulart, D. C. Santos, T. L. Silva, M. A. Alves, P. R. R. Costa, A. G. Dias and E. C. Torres-Santos, *ACS Med. Chem. Lett.*, 2021, **12**, 1405–1412.

60 S. Manda, S. I. Khan, S. K. Jain, S. Mohammed, B. L. Tekwani, I. A. Khan, R. A. Vishwakarma and S. B. Bharate, *Bioorganic Med. Chem. Lett.*, 2014, **24**, 3247–3250.
61 A. H. Romero, J. Núñez-Duran, X. Serrano-Martín, J. Leañez, R. Medina, A. Mijoba, A. Alcala, Y. García-Marchan, S. E. López and C. Ciangherotti, *Eur. J. Med. Chem.*, 2017, **127**, 606–620.
62 A. H. Romero, J. Rodríguez, Y. García-Marchan, J. Leañez, X. Serrano-Martín and S. E. López, *Bioorg. Chem.*, 2017, **72**, 51–56.
63 M. Behrouzi-Fardmoghadam, F. Poorrajab, S. K. Ardestani, S. Emami, A. Shafiee and A. Foroumadi, *Bioorganic Med. Chem.*, 2008, **16**, 4509–4515.
64 F. Poorrajab, S. K. Ardestani, A. Foroumadi, S. Emami, A. Kariminia, M. Behrouzi-Fardmoghadam and A. Shafiee, *Exp. Parasitol.*, 2009, **121**, 323–330.
65 S. E. Sadat-Ebrahimi, M. Mirmohammadi, Z. M. Tabatabaei, M. A. Arani, S. Jafari-Ashtiani, M. Hashemian, P. Foroumadi, A. Yahya-Meymandi, S. Moghimi, M. H. Moshafi, P. Norouzi, S. K. Ardestani and A. Foroumadi, *Iran. J. Pharm. Res.*, 2019, **18**, 1816–1822.
66 E. Alipour, S. Emami, A. Yahya-Meymandi, M. Nakhjiri, F. Johari, S. K. Ardestani, F. Poorrajab, M. Hosseini, A. Shafiee and A. Foroumadi, *J. Enzyme Inhib. Med. Chem.*, 2011, **26**, 123–128.
67 A. Tahghighi, S. Emami, S. Razmi, F. Rezazade Marznaki, S. Kabudanian Ardestani, S. Dastmalchi, F. Kobarfard, A. Shafiee and A. Foroumadi, *J. Enzyme Inhib. Med. Chem.*, 2013, **28**, 843–852.
68 D. Olender, J. Żwawiak and L. Zaprutko, *Pharm.* , 2018, 11.
69 S. Hameed P, N. Bharatham, N. Katagihallimath, S. Sharma, R. Nandishaiah, A. P. Shanbhag, T. Thomas, R. Narjari, M. Sarma, P. Bhowmik, P. Amar, R. Ravishankar, R. Jayaraman, K. Muthan, R. Subbiah, V. Ramachandran, V. Balasubramanian and S. Datta, *Sci. Rep.*, 2018, **8**, 1–18.
70 J. Qiu, X. Niu, J. Wang, Y. Xing, B. Leng, J. Dong, H. Li, M. Luo, Y. Zhang, X. Dai, Y. Luo and X. Deng, *PLoS One*, 2012, **7**, 1–10.
71 Z. C. Wang, B. Wei, F. N. Pei, T. Yang, J. Tang, S. Yang, L. F. Yu, C. G. Yang and F. Yang, *Eur. J. Med. Chem.*, 2020, **198**, 112352.
72 G. Samala, P. B. Devi, R. Nallangi, J. P. Sridevi, S. Saxena, P. Yogeeswari and D. Sriram, *Bioorganic Med. Chem.*, 2014, **22**, 1938–1947.
73 A. Hefnawy, J. Cantizani, I. Peña, P. Manzano, S. Rijal, J.-C. Dujardin, G. De Muylder and J. Martin, *Sci. Rep.*, 2018, **8**, 11765.
74 S. Lamotte, N. Aulner and G. F. Späth, *Nat. Sci. Reports*, 2019, **9**, 1–11.
75 H. Zhang, J. Collins, R. Nyamwihura, O. Crown, O. Ajayi and I. V. Ogungbe, *Bioorganic Med. Chem. Lett.*, 2020, **30**, 127217.
76 S. Khare, A. S. Nagle, A. Biggart, Y. H. Lai, F. Liang, L. C. Davis, S. W. Barnes, C. J. N. Mathison, E. Myburgh, M. Y. Gao, J. R. Gillespie, X. Liu, J. L. Tan, M. Stinson, I. C. Rivera, J. Ballard, V. Yeh, T. Groessl, G. Federe, H. X. Y. Koh, J. D. Venable, B. Bursulaya, M. Shapiro, P. K. Mishra, G. Spraggon, A. Brock, J. C. Mottram, F. S. Buckner, S. P. S. Rao, B. G. Wen, J. R. Walker, T. Tuntland, V. Molteni, R. J. Glynne and F. Supek, *Nature*, 2016, **537**, 229–233.
77 A. Hackler, S. L. Patrick, E. W. Kahney, D. P. Flaherty, E. R. Sharlow, J. C. Morris and J. E. Golden, *Bioorganic Med. Chem. Lett.*, 2017, **27**, 755–758.
78 D. P. Flaherty, J. R. Miller, D. M. Garshott, M. Hedrick, P. Gosalia, Y. Li, M.

Milewski, E. Sugarman, S. Vasile, S. Salaniwal, Y. Su, L. H. Smith, T. D. Y. Chung, A. B. Pinkerton, J. Aubé, M. U. Callaghan, J. E. Golden, A. M. Fribley and R. J. Kaufman, *ACS Med. Chem. Lett.*, 2014, **5**, 1278–1283.
79 H. Zhang, J. Collins, R. Nyamwihura, S. Ware, M. Kaiser and I. V. Ogungbe, *Bioorganic Med. Chem. Lett.*, 2018, **28**, 1647–1651.
80 M. J. Strauss, *Ind. Eng. Chem. Prod. Res. Dev.*, 1979, **18**, 158–166.
81 J. S. Walsh and G. T. Miwa, *Annu. Rev. Pharmacol. Toxicol.*, 2011, **51**, 145–167.
82 U. A. Boelsterli, H. K. Ho, S. Zhou and K. Y. Leow, *Curr. Drug Metab.*, 2006, **7**, 715–727.
83 Ching Yung Wang, Chung Wai Chiu and G. T. Bryan, *Biochem. Pharmacol.*, 1975, **24**, 1563–1568.
84 In *LiverTox: Clinical and Research Information on Drug- Induced Liver Injury [Internet]. Bethesda (MD): National Institute of Diabetes and Digestive and Kidney Diseases*, 2012.
85 M. Donati, A. Conforti, M. C. Lenti, A. Capuano, O. Bortolami, D. Motola, U. Moretti, A. Vannacci, C. Rafaniello, A. Vaccheri, E. Arzenton, R. Bonaiuti, L. Sportiello and R. Leone, *Br. J. Clin. Pharmacol.*, 2016, 238–248.
86 J. K. Aronson, in *Meyler's Side Effects of Drugs: The International Encyclopedia of Adverse Drug Reactions and Interactions*, 16th edn., 2015, p. 204.
87 D. Gramec, L. Peterlin Mašič and M. Sollner Dolenc, *Chem. Res. Toxicol.*, 2014, **27**, 1344–1358.
88 C. K. Jaladanki, N. Taxak, R. A. Varikoti and P. V. Bharatam, *Chem. Res. Toxicol.*, 2015, **28**, 2364–2376.
89 J. P. O'Donnell, D. K. Dalvie, A. S. Kalgutkar and R. S. Obach, *Drug Metab. Dispos.*, 2003, **31**, 1369–1377.
90 S. Lecoeur, E. Bonierbale, D. Challine, J. C. Gautier, P. Valadon, P. M. Dansette, R. Catinot, F. Ballet, D. Mansuy and P. H. Beaune, *Chem. Res. Toxicol.*, 1994, **7**, 434–442.
91 Y. Hu, S. Yang, F. B. Shilliday, B. R. Heyde, K. M. Mandrell, R. H. Robins, J. Xie, M. T. Reding, Y. Lai and D. C. Thompson, *Drug Metab. Dispos.*, 2010, **38**, 1522–1531.
92 J. B. Baell and G. A. Holloway, *J. Med. Chem.*, 2010, **53**, 2719–2740.
93 S. Jasial, Y. Hu and J. Bajorath, *J. Med. Chem.*, 2017, **60**, 3879–3886.
94 A. Dreiem and F. Fonnum, *Neurotoxicology*, 2004, **25**, 959–966.
95 T. N. Sokolova and N. A. Kravchenya, *Grodn. State Med. Inst.*, 1993, **27**, 36–37.
96 L. Zhou, H. Ishizaki, M. Spitzer, K. L. Taylor, N. D. Temperley, S. L. Johnson, P. Brear, P. Gautier, Z. Zeng, A. Mitchell, V. Narayan, E. M. Mcneil, D. W. Melton, T. K. Smith, M. Tyers, N. J. Westwood and E. E. Patton, *Chem. Biol.*, 2012, **19**, 883–892.
97 Y. Zhao, J. Zhao, Y. Zhou, Z. Lei, L. Li and H. Zhang, *New J. Chem.*, 2005, **29**, 769–772.
98 T. He, W. C. Gao, W. K. Wang and C. Zhang, *Adv. Synth. Catal.*, 2014, **356**, 1113–1118.
99 C. Y. Lin, C. S. Huang and M. L. Hu, *Br. J. Nutr.*, 2007, **98**, 226–232.

100 X. Cai, S. Madari, A. Walker, A. Paiva, Y. Li, J. Herbst, W. Shou and H. Weller, *SLAS Discov.*, 2019, **24**, 738–744.
101 S. A. Abouelmagd, B. Sun, A. C. Chang, Y. J. Ku and Y. Yeo, *Mol. Pharm.*, 2015, **12**, 997–1003.
102 FaSSIF/FeSSIF/FaSSGF, https://biorelevant.com/fassif-fessif-fassgf/buy/, (accessed 8 October 2021).
103 S. D. Mithani, V. Bakatselou, C. N. TenHoor and J. B. Dressman, *Pharm. Res.*, 1996, 13, 163–167.
104 P. Song, P. Peng, M. Han, X. Cao, X. Ma, T. Liu and Y. Zhou, *Bioorg. Med. Chem.*, 2014, **22**, 4882–4892.
105 C. Galvez and F. Garcia, *J. Heterocycl. Chem.*, 1981, **18**, 851–853.
106 Y. Liu, Y. Lu, M. Prashad, O. Repič and T. J. Blacklock, *Adv. Synth. Catal.*, 2005, **347**, 217–219.
107 D. N. Sawant, Y. S. Wagh, K. D. Bhatte and B. M. Bhanage, *J. Org. Chem.*, 2011, **76**, 5489–5494.
108 R. Cheng, T. Guo, D. Zhang-Negrerie, Y. Du and K. Zhao, *Synth.*, 2013, **45**, 2998–3006.
109 R. Shang, Y. Liu, Z. Xin, W. Guo, Z. Guo, B. Hao and L. Jianping, *Eur. J. Med. Chem.*, 2013, **63**, 231–238.
110 R. Docampo and A. O. M. Stoppani, *Arch. Biochem. Biophys.*, 1979, **197**, 317–321.
111 K. Blumenstiel, R. Schöneck, V. Yardley, S. L. Croft and R. L. Krauth-Siegel, *Biochem. Pharmacol.*, 1999, **58**, 1791–1799.
112 S. Patterson and A. H. Fairlamb, *Curr. Med. Chem.*, 2018, **26**, 4454–4475.
113 S. N. J. Moreno, R. P. Mason and R. Docampo, *J. Biol. Chem.*, 1984, **259**, 6298–6305.
114 S. G. Goijman, A. C. Frasch and A. O. Stoppani, *Biochem. Pharmacol.*, 1985, **34**, 1457–1461.
115 E. Barreto-Bergter, L. Hogge and F. Steele da Cruz, *Mol. Biochem. Parasitol.*, 1986, **21**, 221–226.
116 S. Muelas-Serrano, J. Pérez-Serrano, A. Gómez-Barrio, V. Arán and F. Rodríguez-Caabeiro, *Parasitol. Res.*, 2002, **88**, 97–101.
117 A. C. Ivens, C. S. Peacock, E. A. Worthey, L. Murphy, G. Aggarwal, M. Berriman, E. Sisk, M.-A. Rajandream, E. Adlem, R. Aert, A. Anupama, Z. Apostolou, P. Attipoe, N. Bason, C. Bauser, A. Beck, S. M. Beverley, G. Bianchettin, K. Borzym, G. Bothe, C. V Bruschi, M. Collins, E. Cadag, L. Ciarloni, C. Clayton, R. M. R. Coulson, A. Cronin, A. K. Cruz, R. M. Davies, J. De Gaudenzi, D. E. Dobson, A. Duesterhoeft, G. Fazelina, N. Fosker, A. C. Frasch, A. Fraser, M. Fuchs, C. Gabel, A. Goble, A. Goffeau, D. Harris, C. Hertz-Fowler, H. Hilbert, D. Horn, Y. Huang, S. Klages, A. Knights, M. Kube, N. Larke, L. Litvin, A. Lord, T. Louie, M. Marra, D. Masuy, K. Matthews, S. Michaeli, J. C. Mottram, S. Müller-Auer, H. Munden, S. Nelson, H. Norbertczak, K. Oliver, S. O'neil, M. Pentony, T. M. Pohl, C. Price, B. Purnelle, M. A. Quail, E. Rabbinowitsch, R. Reinhardt, M. Rieger, J. Rinta, J. Robben, L. Robertson, J. C. Ruiz, S. Rutter, D. Saunders, M. Schäfer, J. Schein, D. C. Schwartz, K. Seeger, A. Seyler, S. Sharp, H. Shin, D. Sivam, R. Squares, S. Squares, V. Tosato, C. Vogt, G. Volckaert, R. Wambutt, T. Warren, H. Wedler, J. Woodward, S. Zhou,

W. Zimmermann, D. F. Smith, J. M. Blackwell, K. D. Stuart, B. Barrell and P. J. Myler, *Science*, 2005, **309**, 436–442.

118 M. Berriman, E. Ghedin, C. Hertz-Fowler, G. Blandin, H. Renauld, D. C. Bartholomeu, N. J. Lennard, E. Caler, N. E. Hamlin, B. Haas, U. Böhme, L. Hannick, M. A. Aslett, J. Shallom, L. Marcello, L. Hou, B. Wickstead, U. C. M. Alsmark, C. Arrowsmith, R. J. Atkin, A. J. Barron, F. Bringaud, K. Brooks, M. Carrington, I. Cherevach, T.-J. Chillingworth, C. Churcher, L. N. Clark, C. H. Corton, A. Cronin, R. M. Davies, J. Doggett, A. Djikeng, T. Feldblyum, M. C. Field, A. Fraser, I. Goodhead, Z. Hance, D. Harper, B. R. Harris, H. Hauser, J. Hostetler, A. Ivens, K. Jagels, D. Johnson, J. Johnson, K. Jones, A. X. Kerhornou, H. Koo, N. Larke, S. Landfear, C. Larkin, V. Leech, A. Line, A. Lord, A. Macleod, P. J. Mooney, S. Moule, D. M. A. Martin, G. W. Morgan, K. Mungall, H. Norbertczak, D. Ormond, G. Pai, C. S. Peacock, J. Peterson, M. A. Quail, E. Rabbinowitsch, M.-A. Rajandream, C. Reitter, S. L. Salzberg, M. Sanders, S. Schobel, S. Sharp, M. Simmonds, A. J. Simpson, L. Tallon, C. M. R. Turner, A. Tait, A. R. Tivey, S. Van Aken, D. Walker, D. Wanless, S. Wang, B. White, O. White, S. Whitehead, J. Woodward, J. Wortman, M. D. Adams, T. M. Embley, K. Gull, E. Ullu, J. D. Barry, A. H. Fairlamb, F. Opperdoes, B. G. Barrell, J. E. Donelson, N. Hall, C. M. Fraser, S. E. Melville and N. M. El-Sayed, *Science*, 2005, **309**, 416–422.

119 N. M. El-Sayed, P. J. Myler, D. C. Bartholomeu, D. Nilsson, G. Aggarwal, A.-N. Tran, E. Ghedin, E. A. Worthey, A. L. Delcher, G. Blandin, S. J. Westenberger, E. Caler, G. C. Cerqueira, C. Branche, B. Haas, A. Anupama, E. Arner, L. Aslund, P. Attipoe, E. Bontempi, F. Bringaud, P. Burton, E. Cadag, D. A. Campbell, M. Carrington, J. Crabtree, H. Darban, J. F. da Silveira, P. de Jong, K. Edwards, P. T. Englund, G. Fazelina, T. Feldblyum, M. Ferella, A. C. Frasch, K. Gull, D. Horn, L. Hou, Y. Huang, E. Kindlund, M. Klingbeil, S. Kluge, H. Koo, D. Lacerda, M. J. Levin, H. Lorenzi, T. Louie, C. R. Machado, R. McCulloch, A. McKenna, Y. Mizuno, J. C. Mottram, S. Nelson, S. Ochaya, K. Osoegawa, G. Pai, M. Parsons, M. Pentony, U. Pettersson, M. Pop, J. L. Ramirez, J. Rinta, L. Robertson, S. L. Salzberg, D. O. Sanchez, A. Seyler, R. Sharma, J. Shetty, A. J. Simpson, E. Sisk, M. T. Tammi, R. Tarleton, S. Teixeira, S. Van Aken, C. Vogt, P. N. Ward, B. Wickstead, J. Wortman, O. White, C. M. Fraser, K. D. Stuart and B. Andersson, *Science*, 2005, **309**, 409–415.

120 S. R. Wilkinson, M. C. Taylor, D. Horn, J. M. Kelly and I. Cheeseman, *Proc. Natl. Acad. Sci.*, 2008, **105**, 5022–5027.

121 E. G. Díaz de Toranzo, J. A. Castro, B. M. Franke de Cazzulo and J. J. Cazzulo, *Experientia*, 1988, **44**, 880–881.

122 V. P. Torchilin, A. L. Klibanov, L. Huang, S. O'Donnell, N. D. Nossiff and B. A. Khaw, *J. FASEB*, 1992, **6**, 2716–2719.

123 M. A. Rajão, C. Furtado, C. L. Alves, D. G. Passos-Silva, M. B. de Moura, B. L. Schamber-Reis, M. Kunrath-Lima, A. A. Zuma, J. P. Vieira-da-Rocha, J. B. F. Garcia, I. C. Mendes, S. D. J. Pena, A. M. Macedo, G. R. Franco, N. C. de Souza-Pinto, M. H. G. de Medeiros, A. K. Cruz, M. C. M. Motta, S. M. R. Teixeira and C. R. Machado, *Environ. Mol. Mutagen.*, 2014, **55**, 309–321.

124 B. S. Hall and S. R. Wilkinson, *Antimicrob. Agents Chemother.*, 2012, **56**, 115–123.

125 F. W. Jennings and G. M. Urquhart, *Z. Parasitenkd.*, 1983, **69**, 577–581.
126 Drugs for Neglected Diseases initiative, *2008-2009 Annual Report: Delivering Innovation and Building a Robust Pipeline*, 2009.
127 A. Y. Sokolova, S. Wyllie, S. Patterson, S. L. Oza, K. D. Read and A. H. Fairlamb, *Antimicrob. Agents Chemother.*, 2010, **54**, 2893–2900.
128 F. Peterson, R. Mason, J. Hovsepian and J. Holtzman, *J. Biol. Chem.*, 1979, **254**, 4009–4014.
129 A. A. Voak, V. Gobalakrishnapillai, K. Seifert, E. Balczo, L. Hu, B. S. Hall and S. R. Wilkinson, *J. Biol. Chem.*, 2013, **288**, 28466–28476.
130 S. Zenno, H. Koike, A. N. Kumar, R. Jayaraman, M. Tanokura and K. Saigo, *J. Bacteriol.*, 1996, **178**, 4508–4514.
131 I. M. de Oliveira, J. A. P. Henriques and D. Bonatto, *Biochem. Biophys. Res. Commun.*, 2007, **355**, 919–925.
132 A. L. Lovering, E. I. Hyde, P. F. Searle and S. A. White, *J. Mol. Biol.*, 2001, **309**, 203–213.
133 C. A. Haynes, R. L. Koder, A. F. Miller and D. W. Rodgers, *J. Biol. Chem.*, 2002, **277**, 11513–11520.
134 S. Patterson, S. Wyllie, L. Stojanovski, M. R. Perry, F. R. C. Simeons, S. Norval, M. Osuna-Cabello, M. De Rycker, K. D. Read and A. H. Fairlamb, *Antimicrob. Agents Chemother.*, 2013, **57**, 4699–4706.
135 S. Wyllie, S. Patterson and A. H. Fairlamb, *Antimicrob. Agents Chemother.*, 2013, **57**, 901–906.
136 E. Akiva, J. N. Copp, N. Tokuriki and P. C. Babbitt, *Proc. Natl. Acad. Sci.*, 2017, **114**, E9549–E9558.
137 A. M. Mejia, B. S. Hall, M. C. Taylor, A. Gómez-Palacio, S. R. Wilkinson, O. Triana-Chávez and J. M. Kelly, *J. Infect. Dis.*, 2012, **206**, 220–228.
138 B. S. Hall, C. Bot, R. Shane, B. S. Hall, C. Bot and S. R. Wilkinson, *J. Biol. Chem.*, 2011, **286**, 13088–13095.
139 B. S. Hall, X. Wu, L. Hu and S. R. Wilkinson, *Antimicrob. Agents Chemother.*, 2010, **54**, 1193–1199.
140 B. S. Hall, E. L. Meredith and S. R. Wilkinson, *Antimicrob. Agents Chemother.*, 2012, **56**, 5821–5830.
141 S. R. Wilkinson, C. Bot, J. M. Kelly and B. S. Hall, *Curr. Top. Med. Chem.*, 2011, **11**, 2072–2084.
142 P. J. Thornalley, *Drug Metab. Drug Interact.*, 2008, **23**, 125–150.
143 E. Torreele, B. B. Trunz, D. Tweats, M. Kaiser, R. Brun, G. Mazué, M. A. Bray and B. Pécoul, *PLoS Negl. Trop. Dis.*, 2010, **4**, 1–15.
144 S. Gupta, V. Yardley, P. Vishwakarma, R. Shivahare, B. Sharma, D. Launay, D. Martin and S. K. Puri, *J. Antimicrob. Chemother.*, 2015, **70**, 518–527.
145 S. Patterson, S. Wyllie, S. Norval, L. Stojanovski, F. R. C. Simeons, J. L. Auer, M. Osuna-Cabello, K. D. Read and A. H. Fairlamb, *Elife*, 2016, **5**, 1–21.
146 R. Singh, U. Manjunatha, H. I. M. Boshoff, H. H. Young, P. Niyomrattanakit, R. Ledwidge, C. S. Dowd, Y. L. Ill, P. Kim, L. Zhang, S. Kang, T. H. Keller, J. Jiricek and C. E. Barry, *Science (80-.).*, 2008, **322**, 1392–1395.
147 M. Dogra, B. D. Palmer, G. Bashiri, M. D. Tingle, S. S. Shinde, R. F. Anderson, R. O'Toole, E. N. Baker, W. A. Denny and N. A. Helsby, *Br. J. Pharmacol.*, 2011, **162**, 226–236.

148 U. Manjunatha, H. I. M. Boshoff and C. E. Barry, *Commun. Integr. Biol.*, 2009, **2**, 215–218.
149 J. Da Silva Pacheco (PhD Thesis), Oswaldo Cruz Foundation, 2019.
150 R. C. Hartkoorn, O. B. Ryabova, L. R. Chiarelli, G. V. Riccardi, V. Makarov and S. T. Makarov, *Antimicrob. Agents Chemother.*, 2014, **58**, 2944–2947.
151 J. Pedron, C. Boudot, S. Hutter, S. Bourgeade-delmas, J. Stigliani, A. Sournia-saquet, A. Moreau, E. Boutet-robinet, L. Paloque, E. Mothes, M. Laget, L. Vendier, G. Pratviel, S. Wyllie, A. Fairlamb, N. Azas, B. Coutioux, A. Valentin and P. Verhaeghe, *Eur. J. Med. Chem.*, 2018, **155**, 135–152.
152 M. Bonta, J. Pe, L. J. Nu and J. A. Squella, *Electrochim. Acta*, 2002, **47**, 4045–4053.
153 M. A. C, R. Figueroa, C. Olea-azar and V. J. Arán, *J. Chill. Chem. Soc.*, 2010, **55**, 244–249.
154 F. Madeira, Y. M. Park, J. Lee, N. Buso, T. Gur, N. Madhusoodanan, P. Basutkar, A. R. N. Tivey, S. C. Potter, R. D. Finn and R. Lopez, *Nucleic Acids Res.*, 2019, **47**, W636—W641.
155 A. Chari, D. Haselbach, J.-M. Kirves, J. Ohmer, E. Paknia, N. Fischer, O. Ganichkin, V. Möller, J. J. Frye, G. Petzold, M. Jarvis, M. Tietzel, C. Grimm, J.-M. Peters, B. A. Schulman, K. Tittmann, J. Markl, U. Fischer and H. Stark, *Nat. Methods*, 2015, **12**, 859–865.
156 D. Bruce, E. Cardew, S. Freitag-Pohl and E. Pohl, *J. Vis. Exp.*, 2019, 1–11.
157 M. K. Grøftehauge, N. R. Hajizadeh, M. J. Swann and E. Pohl, *Acta Crystallogr. Sect. D Biol. Crystallogr.*, 2015, **71**, 36–44.
158 A. W. Pountain and M. P. Barrett, *Wellcome Open Res.*, 2019, **4**, 1–13.
159 F. Q. Schafer and G. R. Buettner, in *Signal Transduction by Reactive Oxygen and Nitrogen Species: Pathways and Chemical Principles*, eds. H. J. Forman, J. Fukuto and M. Torres, Springer Netherlands, Dordrecht, 2006, pp. 1–14.
160 S. Wang, Y. Tian, M. Wang, M. Wang, G. B. Sun and X. B. Sun, *Front. Pharmacol.*, 2018, **9**, 1–9.
161 E. V. Wolf, A. Zeissler and S. H. L. Verhelst, *ACS Chem. Biol.*, 2015, **10**, 2325–2333.
162 P. L. Ross, Y. N. Huang, J. N. Marchese, B. Williamson, K. Parker, S. Hattan, N. Khainovski, S. Pillai, S. Dey, S. Daniels, S. Purkayastha, P. Juhasz, S. Martin, M. Bartlet-Jones, F. He, A. Jacobson and D. J. Pappin, *Mol. Cell. Proteomics*, 2004, **3**, 1154–1169.
163 I. P. Shadforth, T. P. J. Dunkley, K. S. Lilley and C. Bessant, *BMC Genomics*, 2005, **6**, 1–6.
164 K. Kalesh, S. Sundriyal, H. Perera, S. L. Cobb and P. W. Denny, *mSystems*, 2021, **6**, 1–15.
165 M. Shalev-Benami, Y. Zhang, H. Rozenberg, Y. Nobe, M. Taoka, D. Matzov, E. Zimmerman, A. Bashan, T. Isobe, C. L. Jaffe, A. Yonath and G. Skiniotis, *Nat. Commun.*, 2017, **8**, 1–9.
166 S. Das, P. Shah, R. K. Baharia, R. Tandon, P. Khare, S. Sundar, A. A. Sahasrabuddhe, M. I. Siddiqi and A. Dube, *PLoS Negl. Trop. Dis.*, 2013, **7**, 1–11.
167 E. Bifeld, S. Lorenzen, K. Bartsch, J.-J. Vasquez, T. N. Siegel and J. Clos, *mSystems*, 2018, **3**, 1–18.

168 P. R. Race, A. L. Lovering, R. M. Green, A. Ossor, S. A. White, P. F. Searle, C. J. Wrighton and E. I. Hyde, *J. Biol. Chem.*, 2005, **280**, 13256–13264.
169 T. Kobori, H. Sasaki, W. C. Lee, S. Zenno, K. Saigo, M. E. P. Murphy and M. Tanokura, *J. Biol. Chem.*, 2001, **276**, 2816–2823.
170 Y. Tu and D. R. McCalla, *Chem. Biol. Interact.*, 1976, **14**, 81–91.
171 C. C. McOsker and P. M. Fitzpatrick, *J. Antimicrob. Chemother.*, 1994, **33**, 23–30.
172 S. Piacentini, S. La Frazia, A. Riccio, J. Z. Pedersen, A. Topai, O. Nicolotti, J. F. Rossignol and M. G. Santoro, *Sci. Rep.*, 2018, **8**, 1–14.
173 S. Xu and N. Yamamoto, *Genes and Genomics*, 2020, **42**, 915–926.
174 J. T. Mesquita, E. G. Pinto, N. N. Taniwaki, A. J. Galisteo and A. G. Tempone, *Acta Trop.*, 2013, **128**, 666–673.
175 W. Moreira, P. Leprohon and M. Ouellette, *Cell Death Dis.*, 2011, **2**, e201-8.
176 K. Vickerman and L. Tetley, *Ann. Soc. Belg. Med. Trop. (1920).*, 1977, **57**, 441–457.
177 M. C. Vanrell, A. D. Losinno, J. A. Cueto, D. Balcazar, L. V. Fraccaroli, C. Carrillo and P. S. Romano, *PLoS Negl. Trop. Dis.*, 2017, **11**, 1–23.
178 R. F. S. Menna-Barreto, K. Salomão, A. P. Dantas, R. M. Santa-Rita, M. J. Soares, H. S. Barbosa and S. L. de Castro, *Micron*, 2009, **40**, 157–168.
179 R. F. S. Menna-Barreto, *Cell Death Dis.*, 2019, **10**, 1–11.
180 B. Levine and J. Yuan, *J. Clin. Invest.*, 2005, **115**, 2679–2688.
181 R. F. S. Menna-Barreto, J. R. Corrêa, C. M. Cascabulho, M. C. Fernandes, A. V. Pinto, M. J. Soares and S. L. De Castro, *Parasitology*, 2009, **136**, 499–510.
182 A. Bera, S. Singh, R. Nagaraj and T. Vaidya, *Mol. Biochem. Parasitol.*, 2003, **127**, 23–35.
183 D. O. dos Anjos, E. S. Sobral Alves, V. T. Gonçalves, S. S. Fontes, M. L. Nogueira, A. M. Suarez-Fontes, J. B. Neves da Costa, F. Rios-Santos and M. A. Vannier-Santos, *Int. J. Parasitol. Drugs Drug Resist.*, 2016, **6**, 207–219.
184 A. Zafar, L. I. Pilkington, N. A. Haverkate, M. Van Rensburg, E. Leung, S. Kumara, W. A. Denny, D. Barker, A. Alsuraifi, C. Hoskins and J. Reynisson, *Molecules*, 2018, **23**, 1–14.
185 C. A. Henard, E. D. Carlsen, C. Hay, P. E. Kima and L. Soong, *PLoS Negl. Trop. Dis.*, 2014, **8**, 1–11.
186 J. A. L. Lindoso, M. A. Cunha, I. T. Queiroz and C. H. V. Moreira, *HIV/AIDS - Res. Palliat. Care*, 2016, **8**, 147–156.
187 N. Wald-Dickler, P. Holtom and B. Spellberg, *Clin. Infect. Dis. an Off. Publ. Infect. Dis. Soc. Am.*, 2018, **66**, 1470–1474.
188 K. M. Rahman, P. J. M. Jackson, C. H. James, B. P. Basu, J. A. Hartley, M. De La Fuente, A. Schatzlein, M. Robson, R. B. Pedley, C. Pepper, K. R. Fox, P. W. Howard and D. E. Thurston, *J. Med. Chem.*, 2013, **56**, 2911–2935.
189 O. Novac, A. S. Guenier and J. Pelletier, *Nucleic Acids Res.*, 2004, **32**, 902–915.
190 J. Liu, Y. Xu, D. Stoleru and A. Salic, *Proc. Natl. Acad. Sci. U. S. A.*, 2012, **109**, 413–418.
191 N. E. Gregorio, M. Z. Levine and J. P. Oza, *Methods Protoc.*, 2019, **2**, 1–34.
192 J. Cantizani, P. Gamallo, I. Cotillo, R. Alvarez-Velilla and J. Martin, *PLoS Negl. Trop. Dis.*, 2021, **15**, 1–21.
193 K. Kyrylkova, S. Kyryachenko, M. Leid and C. Kioussi, *Methods Mol. Biol.*,

2012, **887**, 41–47.
194 J. D. Maya, Y. Repetto, M. Agosín, J. M. Ojeda, R. Tellez, C. Gaule and A. Morello, *Mol. Biochem. Parasitol.*, 1997, **86**, 101–106.
195 M. Boiani, L. Piacenza, P. Hernández, L. Boiani, H. Cerecetto, M. González and A. Denicola, *Biochem. Pharmacol.*, 2010, **79**, 1736–1745.
196 A. H. Fairlamb, G. B. Henderson, C. J. Bacchi and A. Cerami, *Mol. Biochem. Parasitol.*, 1987, **24**, 185–191.
197 S. Besteiro, R. A. M. Williams, L. S. Morrison, G. H. Coombs and J. C. Mottram, *J. Biol. Chem.*, 2006, **281**, 11384–11396.
198 US2012/53176 A1, 2012.
199 J. Romiszewski, Z. Puterová-Tokarová, J. Mieczkowski and E. Gorecka, *New J. Chem.*, 2014, **38**, 2927–2934.
200 Z. Zhang, T. Song, X. Li, Z. Wu, Y. Feng, F. Xie, C. Liu, J. Qin and H. Chen, *Eur. J. Med. Chem.*, 2013, **59**, 141–149.
201 S. Bugge, S. J. Kaspersen, E. Sundby and B. H. Hoff, *Tetrahedron*, 2012, **68**, 9226–9233.
202 P. Rashmi, L. V. G. Nargund, K. Hazra and J. N. N. S. Chandra, *Arch. Pharm. Chem. Life Sci.*, 2011, **344**, 459–465.
203 L. Keurulainen, M. Heiskari, S. Nenonen, A. Nasereddin, D. Kopelyanskiy, T. O. Leino, J. Yli-Kauhaluoma, C. L. Jaffe and P. Kiuru, *Med. Chem. Commun.*, 2015, **6**, 1673–1678.
204 J. H. Kim, H. Shin and S. G. Lee, *J. Org. Chem.*, 2012, **77**, 1560–1565.
205 E. Sawatzky, A. Drakopoulos, M. Rölz, C. Sotriffer, B. Engels and M. Decker, *Beilstein J. Org. Chem.*, 2016, **12**, 2280–2292.
206 Z. Z. Wang and Y. Tang, *Tetrahedron*, 2016, **72**, 1330–1336.
207 A. G. Schultz, P. J. Mccloskey and J. J. Court, *Am. Chem. Soc.*, 1987, **109**, 6493–6502.
208 L. Yu, J. Ye, X. Zhang, Y. Ding and Q. Xu, *Catal. Sci. Technol.*, 2015, **5**, 4830–4838.
209 L. Yu, J. Ye, X. Zhang, Y. Ding and Q. Xu, *Catal. Sci. Technol.*, 2015, **5**, 4830–4838.
210 L. Mitscher, H. Gracey, G. Clark and T. Suzuki, *J. Med. Chem.*, 1978, **21**, 485–489.
211 F. Romana, V. Colotta, D. Catarzi, F. Varano, O. Lenzi, G. Filacchioni, C. Costagli and A. Galli, *Eur. J. Med. Chem.*, 2005, **40**, 897–907.
212 D. G. O'Sullivan and P. W. Sadler, *J. Chem. Soc.*, 1957, **0**, 2916–2920.
213 T. Nagasaka and Y. Koseki, *J. Org. Chem.*, 1998, **63**, 6797–6801.
214 C. Rui and S. Liu, *J. Agric. Food Chem.*, 2012, **60**, 10942–10951.
215 F. Fabis, S. Jolivet-Fouchet and S. Rault, *Tetrahedron Lett.*, 1999, **55**, 6167–6174.
216 WO2012/51450, 2012.
217 R. Reuter and H. A. Wegner, *Beilstein J. Org. Chem.*, 2012, **8**, 877–883.
218 D. L. Brydon, J. I. G. Cadogan, J. Cook, M. J. P. Harger and J. T. Sharp, *J. Chem. Soc. B*, 1971, 1996–2006.
219 V. Percec, P. Leowanawat, H. J. Sun, O. Kulikov, C. D. Nusbaum, T. M. Tran, A. Bertin, D. A. Wilson, M. Peterca, S. Zhang, N. P. Kamat, K. Vargo, D. Moock, E. D. Johnston, D. A. Hammer, D. J. Pochan, Y. Chen, Y. M. Chabre, T. C. Shiao,

M. Bergeron-Brlek, S. André, R. Roy, H. J. Gabius and P. A. Heiney, *J. Am. Chem. Soc.*, 2013, **135**, 9055–9077.
220 J. A. Grosso, D. E. Nichols, J. D. Kohli and D. Glock, *J. Med. Chem.*, 1982, **25**, 703–708.
221 A. R. Tyler, R. Ragbirsingh, C. J. McMonagle, P. G. Waddell, S. E. Heaps, J. W. Steed, P. Thaw, M. J. Hall and M. R. Probert, *Chem*, 2020, **6**, 1755–1765.
222 F. Fonseca-Silva, J. D. F. Inacio, M. M. Canto-Cavalheiro and E. E. Almeida-Amaral, *PLoS One*, 2011, **6**, 1–7.

8 Appendices

8.1 Appendix 1: Biological data table

Table 8.1-1 Compilation of antileishmanial activity, HepG2 toxicity and aqueous solubility for the compounds synthesised in this work. Compound structure can be determined using the common skeletons (column 2) and information in columns 3 and 4.

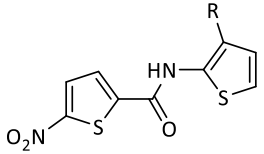

Skeleton 1

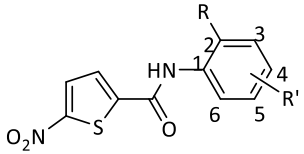

Skeleton 2

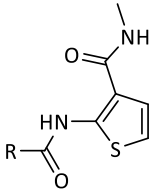

Skeleton 3

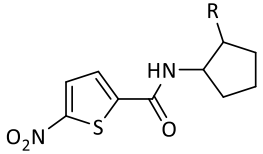

Skeleton 4

Compound ID	Skeleton	R	R'	Antipromastigote activity			Toxicity	Aqueous solubility					
				EC_{50} (*L. major*) / µM	EC_{50} (*L. amaz*) / µM	EC_{50} (*L. don*) / µM	CC_{50} (HepG2) / µM	PBS / µM	FESSIF / µM	FASSIF / µM	FASSGF / µM	PBS + 15 % FBS / µM	PBS + 15 mM taurocholate / µM
16	1	$CONH_2$	-	0.52 ± 0.05	0.042 ± 0.004	0.004 ± 0.0002	24 ± 1	< 7.4	111 ± 2	57 ± 2	10.7 ± 0.3	42 ± 3	107 ± 6
17	1	CONHMe	-	0.99 ± 0.09	0.29 ± 0.03	0.033 ± 0.002	96 ± 4	< 7.4	35.1 ± 0.9	10 ± 1	>7.4	33 ± 2	22.1 ± 0.7
34	1	COOMe	-	0.59 ± 0.05	0.91 ± 0.09	0.300 ± 0.006	>100	< 7.4	48 ± 2	-	-	59 ± 6	-
35	1	COOEt	-	0.93 ± 0.09	1.85 ± 0.05	-	>100	< 7.4	29 ± 2	-	-	51 ± 4	-
36	1	CN	-	1.1 ± 0.1	2.1 ± 0.2	1.12 ± 0.03	8 ± 0.7	228 ± 2	-	-	-	-	-
140	2	$CONH_2$	-	0.47 ± 0.04	0.079 ± 0.001	-	4.7 ± 0.5	< 2.5	90 ± 2	-	-	43 ± 7	-
141	2	CONHMe	-	0.65 ± 0.05	0.052 ± 0.002	0.0120 ± 0.0005	5.0 ± 0.6	8.5 ± 0.7	143 ± 0.5	-	-	-	-
143	2	COOH	-	46 ± 4	-	-	-	-	-	-	-	-	-
155	2	H	3-CONHMe	3.5 ± 0.4	0.26 ± 0.03	-	-	-	-	-	-	-	-
156	2	H	-	4.06 ± 0.06	3.6 ± 0.4	0.93 ± 0.03	-	15 ± 1	-	-	-	64 ± 4	-
157	2	OMe	-	6.3 ± 0.2	-	-	-	-	-	-	-	-	-
158	2	H	3-OMe	3.94 ± 0.4	-	-	-	-	-	-	-	-	-

159	2	H	4-OMe	3.45 ± 0.08	-	-	-	-	-	-	-	-	-
160	2	CF_3	-	8.3 ± 0.6	4.24 ± 0.1	-	-	-	-	-	-	-	-
161	2	H	3-CF_3	3.5 ± 0.4	2.22 ± 0.2	-	-	-	-	-	-	-	-
162	2	$COCH_3$	-	16 ± 2	-	-	-	-	-	-	-	-	-
164	2	$CONH(CH_2)_{12}CH_3$	-	>100	-	-	-	-	-	-	-	-	-
165	2	$CONH^iPr$	-	4.0 ± 0.5	-	-	-	-	-	-	-	-	-
193	2	CONHMe	3-Me	8.5 ± 0.8	-	-	-	-	-	-	-	-	-
194	2	CONHMe	4-OMe	16 ± 2	-	-	-	-	-	-	-	-	-
195	2	CONHMe	4-Me	2.7 ± 0.3	-	-	-	-	-	-	-	-	-
196	2	CONHMe	5-OMe	0.33 ± 0.02	0.021 ± 0.002	0.0060 ± 0.0002	>100	< 7.4	38 ± 4	-	-	30 ± 7	-
197	2	CONHMe	5-Me	0.34 ± 0.03	0.027 ± 0.002	0.0050 ± 0.0002	31 ± 4	< 7.4	65 ± 9	-	-	23 ± 2	-
198	2	CONHMe	5-CF_3	1.84 ± 0.1	0.24 ± 0.01	-	13 ± 3	6.5 ± 0.2	250 ± 10	-	-	53 ± 1	-
199	2	CONHMe	5-Br	0.57 ± 0.06	0.048 ± 0.004	-	7.2 ± 0.5	< 2.5	210 ± 10	-	-	20.0 ± 0.6	-
226	2	CONHMe	5-^{t}Bu	1.35 ± 0.07	2.5 ± 0.3	-	>100	< 2.5	260 ± 20	79 ± 2	23 ± 2	128 ± 8	38 ± 2
232	2	CONHMe	5-$O(CH_2CH_2O)_2Me$	0.32 ± 0.02	0.22 ± 0.03	-	>100	2.27 ± 0.05	7.26 ± 0.04	< 7.4	11 ± 1	42 ± 2	6.1 ± 0.1
251	2	CONHMe	5-$O(CH_2CH_2O)_2C{\equiv}CH$	0.55 ± 0.05	0.77 ± 0.09	-	-	<2.5	51 ± 8	< 2.5	< 2.5	-	-
252	2	CONHMe	5-$O(CH_2CH_2)$morpholin-4-yl	0.44 ± 0.006	0.27 ± 0.01	-	24 ± 1	19.2 ± 0.6	1870 ± 60	148 ± 3	>8000	-	410 ± 20
253	2	CONHMe	5-$O(CH_2CH_2CH_2)$morpholin-4-yl	0.30 ± 0.02	0.08 ± 0.01	-	13 ± 2	29 ± 3	4700 ± 400	359 ± 6	>8000	-	359 ± 6
254	2	CONHMe	5-$O(CH_2CH_2)$oxan-4-yl	0.33 ± 0.06	0.46 ± 0.04	-	>100	3.7 ± 0.9	47 ± 4	-	-	-	-
107	3	2-thiophene	-	>100	>100	-	-	-	-	-	-	-	-
108	3	5-bromothiophene-2-	-	>100	>100	-	-	-	-	-	-	-	-
109	3	5-nitrofuran-2-	-	0.37 ± 0.009	0.33 ± 0.03	0.2 ± 0.001	2 ± 0.2	-	-	-	-	-	-
110	3	4-NO_2-2-CF_3Ph	-	16.6 ± 0.2	38.7 ± 0.9	-	-	-	-	-	-	-	-
111	3	2-thiazole	-	78 ± 2	>100	-	-	-	-	-	-	-	-
112	3	5-thiazole	-	88 ± 6	53 ± 3	-	-	-	-	-	-	-	-
113	3	4-thiazole	-	>100	93 ± 7	-	-	-	-	-	-	-	-
114	3	2,1,3-benzoxadiazole-5-	-	>100	>100	-	-	-	-	-	-	-	-

115	3	Ph	-	75 ± 5	55 ± 5	-	-	-	-	-	-	-	-
116	3	4-pyridyl	-	82 ± 1	45 ± 5	-	-	-	-	-	-	-	-
117	3	3-pyridyl	-	82 ± 7	59 ± 2	-	-	-	-	-	-	-	-
118	3	4-NO_2Ph	-	>100	>100	-	-	-	-	-	-	-	-
119	3	3-NO_2Ph	-	>100	>100	-	-	-	-	-	-	-	-
120	3	5-aminothiophene-2-	-	>100	-	-	-	-	-	-	-	-	-
124	3	2-chlorothiazole-5-	-	33 ± 10	-	-	-	-	-	-	-	-	-
131	4	Anti-COOEt	-	10 ± 1	13 ± 1	-	-	-	-	-	-	-	-
132	4	Syn-COOEt	-	22 ± 2	9.7 ± 0.4	-	-	-	-	-	-	-	-
133	4	Anti-COOH	-	>100	>100	-	-	-	-	-	-	-	-
134	4	Syn-COOH	-	>100	>100	-	-	-	-	-	-	-	-
135	4	Anti-CONHMe	-	20 ± 2	8.0 ± 0.9	3.40 ± 0.06	-	-	-	-	-	-	-
136	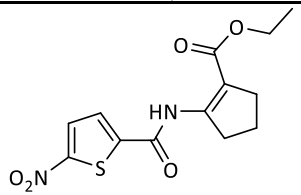			0.46 ± 0.03	0.72 ± 0.03	-	2.9 ± 0.4	<50	54 ± 4	-	-	-	-
144	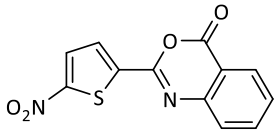			38± 3	-	-	-	-	-	-	-	-	-
206	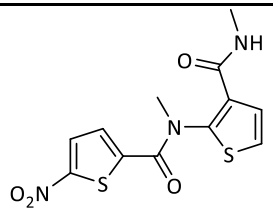			9.6 ± 0.7	15.9 ± 0.6	3.70 ± 0.09	38 ± 9	190 ± 20	-	-	-	-	-
208	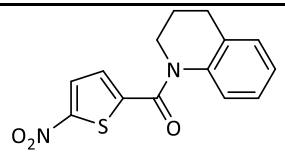			11.1 ± 0.3	-	-	-	151 ± 8	-	-	-	176 ± 3	-

210	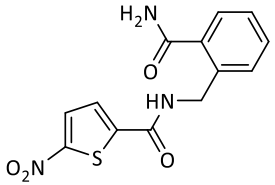	21± 3	-	-	-	179 ± 8	-	-	-	166 ± 5	-
212	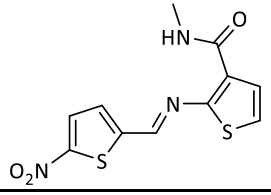	0.86 ± 0.07	0.56 ± 0.06	0.040 ± 0.001	18.8 ± 0.7	100 ± 6	137 ± 2	-	-	120 ± 10	-

8.2 Appendix 2: DNA sequencing of *Lmj*NTR1 and *Ldon*NTR1

```
Actual            1 ATGGGGGGTTCTCATCATCATCATCATCATGGTATGGCTAGCATGACTGG     50
                    ||||||||||||||||||||||||||||||||||||||||||||||||||
Theoretical       1 ATGGGGGGTTCTCATCATCATCATCATCATGGTATGGCTAGCATGACTGG     50

Actual           51 TGGACAGCAAATGGGTCGGGATCTGTACGACGATGACGATAAGGATCGAT    100
                    ||||||||||||||||||||||||||||||||||||||||||||||||||
Theoretical      51 TGGACAGCAAATGGGTCGGGATCTGTACGACGATGACGATAAGGATCGAT    100

Actual          101 GGATCCTCGACGCGGTTGAAGCGGTGGTTCGTGCGCGTTGGACCTGCCGT    150
                    ||||||||||||||||||||||||||||||||||||||||||||||||||
theoretical     101 GGATCCTCGACGCGGTTGAAGCGGTGGTTCGTGCGCGTTGGACCTGCCGT    150

Actual          151 CAGTTCGATACCGCGAAGCCGATCGACCTGGATACCCTGAAACGTGTGCT    200
                    ||||||||||||||||||||||||||||||||||||||||||||||||||
Theoretical     151 CAGTTCGATACCGCGAAGCCGATCGACCTGGATACCCTGAAACGTGTGCT    200

Actual          201 GGCGGCGACCACCCGTGCGCCGACCGGTTTTAACCTGCAAGGCTGGCACG    250
                    ||||||||||||||||||||||||||||||||||||||||||||||||||
Theoretical     201 GGCGGCGACCACCCGTGCGCCGACCGGTTTTAACCTGCAAGGCTGGCACG    250

Actual          251 CGGTGGTTGTGACCAACACCGCGGTGCGTGAACAGCTGTTCAAGGCGGCG    300
                    ||||||||||||||||||||||||||||||||||||||||||||||||||
Theoretical     251 CGGTGGTTGTGACCAACACCGCGGTGCGTGAACAGCTGTTCAAGGCGGCG    300

Actual          301 CTGGGTCAGCCGCAAGTTCTGCAAGCGCCGGCGACCGTTGTGTTTGTTGG    350
                    ||||||||||||||||||||||||||||||||||||||||||||||||||
Theoretical     301 CTGGGTCAGCCGCAAGTTCTGCAAGCGCCGGCGACCGTTGTGTTTGTTGG    350

Actual          351 TGACACCGAGCCGGAACGTAACGCGCCGCAGGCGCTGGAGATGGGTCTGG    400
                    ||||||||||||||||||||||||||||||||||||||||||||||||||
Theoretical     351 TGACACCGAGCCGGAACGTAACGCGCCGCAGGCGCTGGAGATGGGTCTGG    400

Actual          401 AAACCGGCTACTATAGCCCGCTGTACGGTGCGGCGTATCTGCGTAACATC    450
                    ||||||||||||||||||||||||||||||||||||||||||||||||||
Theoretical     401 AAACCGGCTACTATAGCCCGCTGTACGGTGCGGCGTATCTGCGTAACATC    450

Actual          451 TACTATTTCATGCATGGTGGCCCGATGCAGAGCATGGCGGCGGTTAAGAG    500
                    ||||||||||||||||||||||||||||||||||||||||||||||||||
Theoretical     451 TACTATTTCATGCATGGTGGCCCGATGCAGAGCATGGCGGCGGTTAAGAG    500

Actual          501 CGTTGTGAGCGCGTGGTACAGCCAGGCGGCGGGTACCCCGCTGATCAGCG    550
                    ||||||||||||||||||||||||||||||||||||||||||||||||||
Theoretical     501 CGTTGTGAGCGCGTGGTACAGCCAGGCGGCGGGTACCCCGCTGATCAGCG    550

Actual          551 TTCCGGTTAGCCGTGCGGGCTATGCGTGGAAACAGACCATGATTCCGGCG    600
                    ||||||||||||||||||||||||||||||||||||||||||||||||||
Theoretical     551 TTCCGGTTAGCCGTGCGGGCTATGCGTGGAAACAGACCATGATTCCGGCG    600

Actual          601 ACCACCTTTGTGAACCTGTGCGCGGCGGCGGGTTGGGATACCTGCATGAT    650
                    ||||||||||||||||||||||||||||||||||||||||||||||||||
Theoretical     601 ACCACCTTTGTGAACCTGTGCGCGGCGGCGGGTTGGGATACCTGCATGAT    650

Actual          651 GGAGGGCATTGACGAAGATGCGGTTAAACGTGCGCTGGGCGTGCCGGCGG    700
                    ||||||||||||||||||||||||||||||||||||||||||||||||||
Theoretical     651 GGAGGGCATTGACGAAGATGCGGTTAAACGTGCGCTGGGCGTGCCGGCGG    700

Actual          701 AGCGTTACACCGTTCCGGTGATCATTAGCGTGGGTTATGCGACCGCGGCG    750
                    ||||||||||||||||||||||||||||||||||||||||||||||||||
Theoretical     701 AGCGTTACACCGTTCCGGTGATCATTAGCGTGGGTTATGCGACCGCGGCG    750

Actual_         751 GAGGCGGAAAAGCGTCAAGTTGGCAGCAGCCGTTTTGCGACCCCGCACAC    800
                    ||||||||||||||||||||||||||||||||||||||||||||||||||
Theoretical     751 GAGGCGGAAAAGCGTCAAGTTGGCAGCAGCCGTTTTGCGACCCCGCACAC    800

Actual          801 CGTGCGTTGGAACAAATTTAAA    824
                    ||||||||||||||||||.||
Theoretical     801 CGTGCGTTGGAACAAATTTTAA    822
```

Figure 8.2-1 Pairwise alignment of combined forwards and reverse Sanger sequencing for pTrcHis*Ldon*NTR1 (actual) compared to the theoretical sequence (EMBOSS Needle). Purple regions represent the overlap between forward and reversed sequences. Orange bases were identified from the reverse sequence only. Green bases were observed from the forwards sequence only. Red bases represent disagreement between actual and theoretical sequences.

8.3 Appendix 3: Protein digest MS (*Lmj*NTR1 two bands)

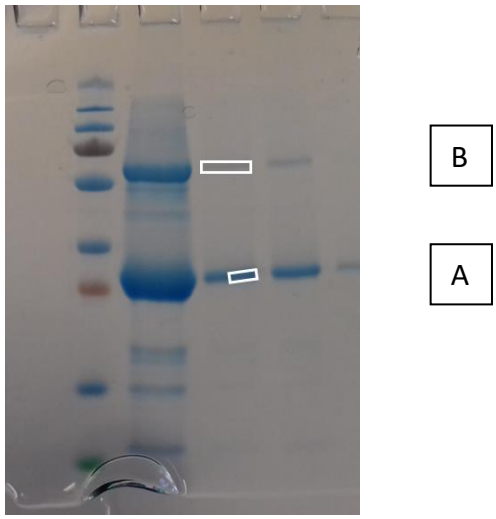

Figure 8.3-1 Regions excised from SDS-PAGE (12.5 %) gel for protein digest MS.

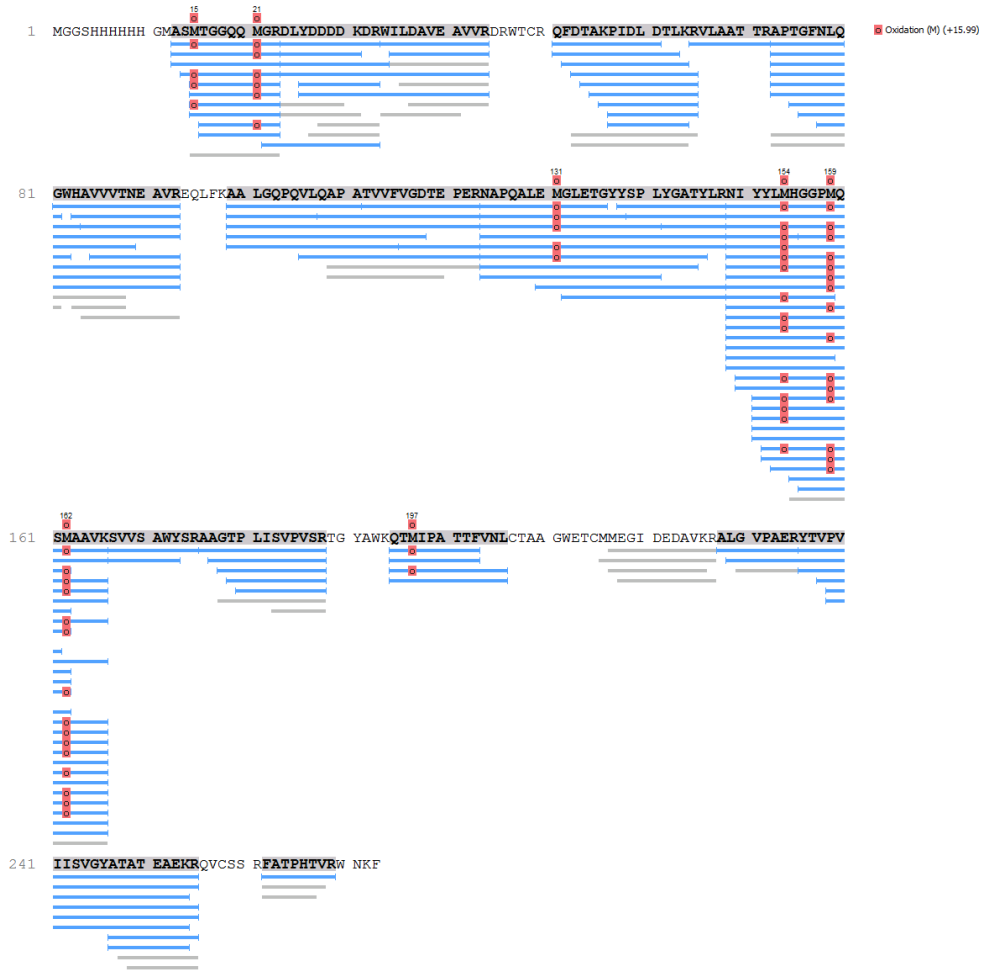

Figure 8.3-2 Peptides identified (blue lines) by protein digest MS for the lower band (A) compared to the theoretical sequence suggests that the protein sequence is correct. Grey bars are sequence tags. Red O represents oxidation of methionine.

Figure 8.3-3 Peptides identified (blue lines) by protein digest MS for the upper band (B) compared to the theoretical sequence suggests that the protein sequence is correct. This shows that the upper band is the dimeric form of the lower band. Grey bars are sequence tags. Red O represents oxidation of methionine.

8.4 Appendix 4: Proteomics results output

Table 8.4-1 Proteomics output results showing proteins with a Log2FC > 1. Log2FC gives the fold change difference between sample with probe only (**sample 1**) and sample with probe and competitor (**sample 2**) on a Log2 scale. '+' in the significance column represents a protein observed over 3 repeats.

	Significant	[-LOG(p-value)]	log2 FC	Majority protein IDs	Fasta headers	Unique peptides	Unique sequence coverage [%]	Mol. weight [kDa]
2	+	4.975188514	9.614343	Q4Q504	tr|Q4Q504|Q4Q504_LEIMA 60S ribosomal protein L27 OS=Leishmania major OX=5664 GN=LMJF_	11	49.3	15.434
3	+	5.824889837	9.004871	Q4FWX5	tr|Q4FWX5|Q4FWX5_LEIMA Putative 60S ribosomal protein L2 OS=Leishmania major OX=5664 G	9	38.8	28.272
4	+	2.280685179	8.909387	Q4Q9C5	tr|Q4Q9C5|Q4Q9C5_LEIMA Putative Qc-SNARE protein OS=Leishmania major OX=5664 GN=LMJ	1	6	28.122
5	+	4.22925995	8.787978	Q4QC91;Q4Q6V5	tr|Q4QC91|Q4QC91_LEIMA Putative 60S ribosomal protein L9 OS=Leishmania major OX=5664 G	8	50	21.556
6	+	1.030810248	8.509214	Q4Q2G5	tr|Q4Q2G5|Q4Q2G5_LEIMA Phosphomannomutase-like protein OS=Leishmania major OX=5664	1	2.4	65.235
7	+	4.517720721	7.934414	E9AEA9;E9AEA8	tr|E9AEA9|E9AEA9_LEIMA Putative 60S ribosomal protein L13 OS=Leishmania major OX=5664 G	10	48.6	24.775
8	+	2.229556521	7.896242	E9ADB9	tr|E9ADB9|E9ADB9_LEIMA 60S acidic ribosomal protein P0 OS=Leishmania major OX=5664 GN=	9	24.8	34.807
9	+	3.674347728	7.688556	Q4Q0Q0	sp|Q4Q0Q0|RSSA_LEIMA 40S ribosomal protein SA OS=Leishmania major OX=5664 GN=LmjF36.1	6	26	27.499
10	+	3.214716531	7.647546	P48157	sp|P48157|RL11_LEIMA 60S ribosomal protein L11 OS=Leishmania major OX=5664 GN=RPL11 PE	6	27.7	21.645
11	+	3.821910218	7.560961	Q4QF80;Q4QF76;Q4QF6	tr|Q4QF80|Q4QF80_LEIMA Tryparedoxin peroxidase OS=Leishmania major OX=5664 GN=TRYP1	2	16.6	22.099
12	+	3.737025881	7.483445	Q9NE83;E9AF23	sp|Q9NE83|RS6_LEIMA 40S ribosomal protein S6 OS=Leishmania major OX=5664 GN=RPS6 PE=1	8	37.8	28.304
13	+	2.421728089	7.461701	Q9U1E1	tr|Q9U1E1|Q9U1E1_LEIMA Nucleoside diphosphate kinase OS=Leishmania major OX=5664 GN=	6	49.7	16.64
14	+	3.772991929	7.367046	Q4Q6Z5;Q4Q6Z4	tr|Q4Q6Z5|Q4Q6Z5_LEIMA Glyceraldehyde-3-phosphate dehydrogenase OS=Leishmania major	15	44.9	39.166
15	+	3.784951142	6.664655	Q4Q2H9;Q4QEX4	tr|Q4Q2H9|Q4Q2H9_LEIMA Putative 60S ribosomal protein L21 OS=Leishmania major OX=5664	5	35.2	17.988
16	+	3.079581853	6.641365	E9AEE8;Q4Q2R6	tr|E9AEE8|E9AEE8_LEIMA 40S ribosomal protein S19-like protein OS=Leishmania major OX=566	4	31.7	18.12
17	+	2.960196922	6.629197	Q4QAC5	tr|Q4QAC5|Q4QAC5_LEIMA Putative 60S ribosomal protein L26 OS=Leishmania major OX=5664	3	16.8	16.176
18	+	3.360796041	6.619435	E9AEL4	tr|E9AEL4|E9AEL4_LEIMA Putative ATP-dependent DEAD-box RNA helicase OS=Leishmania maj	12	37.8	46.405
19	+	4.445130311	6.601764	E9ADW5	tr|E9ADW5|E9ADW5_LEIMA Putative ribosomal protein L1a OS=Leishmania major OX=5664 GN=	12	48.5	41.02
20	+	1.650448314	6.583232	O02614	tr|O02614|O02614_LEIMA Peptidyl-prolyl cis-trans isomerase OS=Leishmania major OX=5664 G	7	42.4	18.823
21	+	2.226028391	6.571029	Q4FX73	sp|Q4FX73|RS3A_LEIMA 40S ribosomal protein S3a OS=Leishmania major OX=5664 GN=LmjF.35	12	53	30.008
22	+	3.540461096	6.562333	Q4Q7Y7;O43943;A0A222	tr|Q4Q7Y7|Q4Q7Y7_LEIMA Guanine nucleotide-binding protein subunit beta-like protein OS=L	13	48.4	34.399
23	+	3.570876314	6.531597	Q4Q063	tr|Q4Q063|Q4Q063_LEIMA CCT-theta OS=Leishmania major OX=5664 GN=LMJF_36_6910 PE=3 SV	13	28.7	58.184
24	+	5.2648118	6.522629	Q4Q6S3;E9AF12	tr|Q4Q6S3|Q4Q6S3_LEIMA Ribosomal protein L15 OS=Leishmania major OX=5664 GN=LMJF_30_	7	29.4	24.435
25	+	3.316365602	6.4649	E9AFK3	tr|E9AFK3|E9AFK3_LEIMA Putative 60S ribosomal protein L23 OS=Leishmania major OX=5664 G	4	38.1	14.956
26	+	2.270098123	6.462841	Q4Q3M1	tr|Q4Q3M1|Q4Q3M1_LEIMA Putative 40S ribosomal protein S13 OS=Leishmania major OX=5664	6	42.4	17.445
27	+	1.876577211	6.432354	E9AC32	tr|E9AC32|E9AC32_LEIMA 40S ribosomal protein S7 OS=Leishmania major OX=5664 GN=LMJF_0	6	35.5	23.714
28	+	1.914540662	6.40469	Q4QJF1	tr|Q4QJF1|Q4QJF1_LEIMA ATPase alpha subunit OS=Leishmania major OX=5664 GN=LMJF_05_0	12	23.2	62.548
29	+	1.926683258	6.391688	Q4QI58;A0A2Z4EJ02;P9(	tr|Q4QI58|Q4QI58_LEIMA Stress-induced protein sti1 OS=Leishmania major OX=5664 GN=LMJF_	20	34.6	62.107
30	+	3.089359307	6.32162	Q4Q5P0;Q71LW5	tr|Q4Q5P0|Q4Q5P0_LEIMA 40S ribosomal protein S2 OS=Leishmania major OX=5664 GN=LMJF_	1	4.2	28.658
31	+	3.514220124	6.319661	A0A5J6E2G1;Q4QAQ6	tr|A0A5J6E2G1|A0A5J6E2G1_LEIMA Cytosolic malic enzyme (Fragment) OS=Leishmania major C	8	22.1	60.548
32	+	2.513426141	6.31401	Q4QBJ1	tr|Q4QBJ1|Q4QBJ1_LEIMA Putative 40S ribosomal protein L14 OS=Leishmania major OX=5664 G	7	32	19.9
33	+	2.08256744	6.294397	E9ACB9	tr|E9ACB9|E9ACB9_LEIMA Putative voltage-dependent anion-selective channel OS=Leishmani	8	31	29.959
34	+	1.898844181	6.283336	Q4Q1V0	tr|Q4Q1V0|Q4Q1V0_LEIMA Fructose-bisphosphate aldolase OS=Leishmania major OX=5664 GN	13	44.5	40.827
35	+	2.355019284	6.277712	E9ADF9;E9ADF8	tr|E9ADF9|E9ADF9_LEIMA Phosphoenolpyruvate carboxykinase (ATP) OS=Leishmania major OX	18	44.8	58.223
36	+	3.685453881	6.222671	Q4QBH2	tr|Q4QBH2|Q4QBH2_LEIMA Peroxidoxin OS=Leishmania major OX=5664 GN=LMJF_23_0040 PE=	6	31.4	25.342
37	+	1.257945133	6.192552	Q4Q4I0;Q4Q4I6	tr|Q4Q4I0|Q4Q4I0_LEIMA Heat shock protein 83-1 OS=Leishmania major OX=5664 GN=HSP83-8	31	45.1	80.405
38	+	4.490954213	6.187222	Q4Q1C4	tr|Q4Q1C4|Q4Q1C4_LEIMA Succinate--CoA ligase [ADP-forming] subunit beta, mitochondrial O	9	25.7	44.187
39	+	4.667180267	6.169379	E9ADX1;Q4Q2G4	tr|E9ADX1|E9ADX1_LEIMA Tryparedoxin-like protein OS=Leishmania major OX=5664 GN=LMJF_	1	1.9	41.373
40	+	2.085474393	6.163154	Q4QFG2;Q4Q3B9	tr|Q4QFG2|Q4QFG2_LEIMA Putative 60S ribosomal protein L13a OS=Leishmania major OX=5664	8	38.3	25.449
41	+	2.112707992	6.159117	E9AFJ4	tr|E9AFJ4|E9AFJ4_LEIMA Glycosomal membrane protein OS=Leishmania major OX=5664 GN=LM	8	36.9	24.899
42	+	3.744709512	6.156912	Q4QGW7	tr|Q4QGW7|Q4QGW7_LEIMA Putative 60S ribosomal protein L28 OS=Leishmania major OX=566	6	40.1	16.278
43	+	2.293312346	6.15049	Q4QG31	tr|Q4QG31|Q4QG31_LEIMA 40S ribosomal protein S4 OS=Leishmania major OX=5664 GN=RS4 PE	12	45.4	30.682
44	+	3.495163457	6.145238	Q4Q6E1	tr|Q4Q6E1|Q4Q6E1_LEIMA H(+)-exporting diphosphatase OS=Leishmania major OX=5664 GN=LI	9	12.6	83.564
45	+	4.65076873	6.123581	Q4QAX6;Q4Q5P2	tr|Q4QAX6|Q4QAX6_LEIMA Putative 60S ribosomal protein L17 OS=Leishmania major OX=5664	4	21.1	19.083
46	+	1.863476633	6.114374	Q4QGX9	tr|Q4QGX9|Q4QGX9_LEIMA Pyruvate, phosphate dikinase OS=Leishmania major OX=5664 GN=L	27	38.7	100.93
47	+	2.930553046	6.110094	E9AFK0	tr|E9AFK0|E9AFK0_LEIMA Putative 60S ribosomal protein L27A/L29 OS=Leishmania major OX=5	4	29	16.098
48	+	4.411130239	6.076613	Q4QFM2	tr|Q4QFM2|Q4QFM2_LEIMA Putative kinesin K39 OS=Leishmania major OX=5664 GN=LMJF_14_	3	20.7	341.14
49	+	3.815156918	6.07515	Q4QH70	tr|Q4QH70|Q4QH70_LEIMA Seryl-tRNA synthetase OS=Leishmania major OX=5664 GN=LMJF_11	9	19.4	53.086
50	+	1.804055711	6.06866	Q4QHI7;A0A2S1FUC9;A(	tr|Q4QHI7|Q4QHI7_LEIMA Isocitrate dehydrogenase [NADP] OS=Leishmania major OX=5664 GN	13	32	48.49
51	+	0.981654956	6.062618	E9AD27	tr|E9AD27|E9AD27_LEIMA Putative calpain-like cysteine peptidase OS=Leishmania major OX=5	3	0.7	700.25
52	+	3.262504342	6.062359	W5XL77;O62591	tr|W5XL77|W5XL77_LEIMA Putative eukaryotic initiation factor 4a OS=Leishmania major OX=56	12	33.3	45.326
53	+	1.873386	6.060165	Q4QFL8	tr|Q4QFL8|Q4QFL8_LEIMA Phosphopyruvate hydratase OS=Leishmania major OX=5664 GN=ENO	18	58.7	46.091
54	+	1.724007743	6.055041	Q4Q9A5	tr|Q4Q9A5|Q4Q9A5_LEIMA Putative 40S ribosomal protein S16 OS=Leishmania major OX=5664	5	31.5	16.687
55	+	1.271427558	5.98908	Q4Q124	tr|Q4Q124|Q4Q124_LEIMA Adenosylhomocysteinase OS=Leishmania major OX=5664 GN=LMJF_	13	36.2	47.828
56	+	2.739168752	5.98664	Q4Q1R2	tr|Q4Q1R2|Q4Q1R2_LEIMA Clathrin heavy chain OS=Leishmania major OX=5664 GN=LMJF_36_1	14	9.5	190.07
57	+	3.33305944	5.927275	Q4Q5I2	tr|Q4Q5I2|Q4Q5I2_LEIMA CCT-epsilon OS=Leishmania major OX=5664 GN=LMJF_32_1000 PE=3 S	12	28.6	59.274
58	+	1.511958875	5.924723	Q4QDQ2	tr|Q4QDQ2|Q4QDQ2_LEIMA Putative heat shock protein OS=Leishmania major OX=5664 GN=LM	31	41.7	91.803
59	+	2.314249633	5.843824	Q4QEI9	tr|Q4QEI9|Q4QEI9_LEIMA Elongation factor 1-alpha OS=Leishmania major OX=5664 GN=LMJF_1	3	5.1	49.116
60	+	2.408539719	5.820929	Q4Q4A0	tr|Q4Q4A0|Q4Q4A0_LEIMA Putative 40S ribosomal protein S3 OS=Leishmania major OX=5664 G	10	50.7	24.471
61	+	1.903078924	5.812459	E9AFL0	tr|E9AFL0|E9AFL0_LEIMA CCT-eta OS=Leishmania major OX=5664 GN=LMJF_35_3860 PE=3 SV=1	11	24.4	61.747
62	+	3.346983565	5.776036	Q868B1	tr|Q868B1|Q868B1_LEIMA 40S ribosomal protein S5 OS=Leishmania major OX=5664 GN=LMJF_1	5	41.1	21.297
63	+	4.096399278	5.768391	Q4Q9H4	tr|Q4Q9H4|Q4Q9H4_LEIMA Putative 60S ribosomal protein L7 OS=Leishmania major OX=5664 G	4	15.1	28.845
64	+	1.129129348	5.76395	Q4QF83	tr|Q4QF83|Q4QF83_LEIMA NAD-specific glutamate dehydrogenase OS=Leishmania major OX=5	23	29	115.03
65	+	1.373150619	5.7623	Q4Q2Q6	tr|Q4Q2Q6|Q4Q2Q6_LEIMA Putative ribosomal protein L3 OS=Leishmania major OX=5664 GN=L	18	48.2	47.487
66	+	1.820778732	5.761755	Q4Q9X6;Q4Q9X5	tr|Q4Q9X6|Q4Q9X6_LEIMA ATP synthase subunit beta OS=Leishmania major OX=5664 GN=LMJF	14	41.1	56.348
67	+	4.034320274	5.749895	E9AFS0;E9AFR9	tr|E9AFS0|E9AFS0_LEIMA Putative mitochondrial phosphate transporter OS=Leishmania major	7	24.3	34.661
68	+	1.928113529	5.735529	E9ADB1	tr|E9ADB1|E9ADB1_LEIMA Uncharacterized protein OS=Leishmania major OX=5664 GN=LMJF_2	15	31.6	59.966
69	+	3.304515421	5.721547	Q4Q055	tr|Q4Q055|Q4Q055_LEIMA Putative eukaryotic translation initiation factor 3 subunit 8 OS=Leish	12	20.5	82.031
70	+	2.174774221	5.716588	Q4QA19	tr|Q4QA19|Q4QA19_LEIMA PPM-type phosphatase domain-containing protein OS=Leishmania	8	19.7	44.951
71	+	3.101050785	5.682471	E9AEW4	tr|E9AEW4|E9AEW4_LEIMA Threonyl-tRNA synthetase OS=Leishmania major OX=5664 GN=LMJ	11	15.6	89.465

1	Significant	[-LOG(p-value)]	log2 FC	Majority protein IDs	Fasta headers	Unique peptides	Unique sequence coverage [%]	Mol. weight [kDa]
72	+	1.430734261	5.638192	Q4QAB9	tr|Q4QAB9|Q4QAB9_LEIMA HMG_CoA_synt_N domain-containing protein OS=Leishmania majo	13	27.1	55.255
73	+	3.170501275	5.539197	Q4Q3K8	tr|Q4Q3K8|Q4Q3K8_LEIMA Uncharacterized protein OS=Leishmania major OX=5664 GN=LMJF_3	8	26.5	33.662
74	+	2.031233337	5.531041	Q4QIM3;Q4Q1V1	tr|Q4QIM3|Q4QIM3_LEIMA Putative 40S ribosomal protein S9 OS=Leishmania major OX=5664 G	7	39.5	22.142
75	+	4.495171575	5.491022	Q4Q817	tr|Q4Q817|Q4Q817_LEIMA Putative ribosomal protein S29 OS=Leishmania major OX=5664 GN=	2	31.6	6.6828
76	+	1.387929645	5.48172	Q4QCN7	tr|Q4QCN7|Q4QCN7_LEIMA Putative 40S ribosomal protein S11 OS=Leishmania major OX=5664	3	20.6	16.312
77	+	2.180493196	5.45628	Q4QDZ1	tr|Q4QDZ1|Q4QDZ1_LEIMA Aconitate hydratase OS=Leishmania major OX=5664 GN=LMJF_18_0	17	25.6	97.491
78	+	1.366883215	5.436778	Q4QC38	tr|Q4QC38|Q4QC38_LEIMA Putative RNA helicase OS=Leishmania major OX=5664 GN=LMJF_21	8	20.5	49.487
79	+	0.994251897	5.413293	Q4QF84;Q4Q4D3	tr|Q4QF84|Q4QF84_LEIMA Putative 60S ribosomal protein L6 OS=Leishmania major OX=5664 GN	8	40	21.044
80	+	2.459424257	5.403118	E9ACG7	tr|E9ACG7|E9ACG7_LEIMA Multifunctional fusion protein OS=Leishmania major OX=5664 GN=L	10	21.8	61.899
81	+	1.614832926	5.383611	Q4Q740;Q4Q744;Q4Q74	tr|Q4Q740|Q4Q740_LEIMA Putative heat shock 70-related protein 1,mitochondrial OS=Leishma	24	42	70.608
82	+	1.410708839	5.368701	Q4QHL3	tr|Q4QHL3|Q4QHL3_LEIMA Putative ribosomal protein l35a OS=Leishmania major OX=5664 GN=	3	17.4	16.454
83	+	1.954912885	5.328869	Q4Q1M0	tr|Q4Q1M0|Q4Q1M0_LEIMA Chaperonin HSP60, mitochondrial OS=Leishmania major OX=5664	7	16.7	59.317
84	+	2.600405134	5.316454	Q4QI59	tr|Q4QI59|Q4QI59_LEIMA Uncharacterized protein OS=Leishmania major OX=5664 GN=LMJF_08	8	20.8	42.045
85	+	1.690004015	5.303079	Q4QDX9	tr|Q4QDX9|Q4QDX9_LEIMA Putative 60S ribosomal protein L10a OS=Leishmania major OX=566	8	50	24.53
86	+	1.710721505	5.293269	E9AEW1	tr|E9AEW1|E9AEW1_LEIMA Metallo-peptidase, Clan ME, Family M16 OS=Leishmania major OX=	10	24.7	54.536
87	+	1.804592185	5.284872	Q4Q7Y4;P14834;D2EAU4	tr|Q4Q7Y4|Q4Q7Y4_LEIMA Putative heat-shock protein hsp70 OS=Leishmania major OX=5664 G	29	48.5	71.652
88	+	1.569795848	5.279964	Q4QDK0	tr|Q4QDK0|Q4QDK0_LEIMA ADP/ATP translocase OS=Leishmania major OX=5664 GN=ANC2 PE=	12	41.3	35.076
89	+	2.186393958	5.273384	Q4Q259;Q9GU34	tr|Q4Q259|Q4Q259_LEIMA Elongation factor 2 OS=Leishmania major OX=5664 GN=EF2-2 PE=3 SV	39	58.8	94.132
90	+	2.975954189	5.228419	Q4Q1I3;Q4Q1I2	tr|Q4Q1I3|Q4Q1I3_LEIMA Methyltransferase OS=Leishmania major OX=5664 GN=LMJF_36_2380	4	20.4	39.939
91	+	2.520996704	5.189423	Q4Q424	tr|Q4Q424|Q4Q424_LEIMA Peptidyl-prolyl cis-trans isomerase OS=Leishmania major OX=5664	3	10.5	24.091
92	+	1.239681026	5.164075	Q4Q140	tr|Q4Q140|Q4Q140_LEIMA Putative 40S ribosomal protein S27-1 OS=Leishmania major OX=5664	4	64	9.7993
93	+	1.84510387	5.131055	E9AF09;E9AF10	tr|E9AF09|E9AF09_LEIMA Putative 60S ribosomal protein L5 OS=Leishmania major OX=5664 GN=	5	17	33.985
94	+	1.686683263	5.128364	Q4QG98	sp|Q4QG98|RL18_LEIMA 60S ribosomal protein L18 OS=Leishmania major OX=5664 GN=RPL18-A	3	16.2	22.022
95	+	1.044997407	5.015719	Q4Q5P5	tr|Q4Q5P5|Q4Q5P5_LEIMA Putative ATP-dependent RNA helicase OS=Leishmania major OX=56	18	35.9	67.008
96	+	1.573736135	5.00359	Q4QI42;Q4Q4C4;Q2531	tr|Q4QI42|Q4QI42_LEIMA Tubulin beta chain OS=Leishmania major OX=5664 GN=LMJF_08_1230	11	35.7	49.706

96	+	1.573736135	5.00359	Q4QI42;Q4Q4C4;Q2531	tr|Q4QI42|Q4QI42_LEIMA Tubulin beta chain OS=Leishmania major OX=5664 GN=LMJF_08_1230	11	35.7	49.706
97	+	3.632624588	4.988525	Q4Q253	tr|Q4Q253|Q4Q253_LEIMA Eukaryotic translation initiation factor 3 subunit L OS=Leishmania m	7	13.4	72.641
98	+	2.701224199	4.983977	E9AF44	tr|E9AF44|E9AF44_LEIMA Putative RNA-binding protein OS=Leishmania major OX=5664 GN=LM	4	17.5	30.258
99	+	1.335368386	4.979237	Q4Q5K7	tr|Q4Q5K7|Q4Q5K7_LEIMA Putative RNA binding protein OS=Leishmania major OX=5664 GN=LM	6	28.5	25.183
100	+	3.189466939	4.969603	Q9U0V9	tr|Q9U0V9|Q9U0V9_LEIMA Possible 3-ketoacyl-CoA thiolase OS=Leishmania major OX=5664 GN	7	18.6	47.402
101	+	1.67215575	4.969154	Q9U1E8;C6KJD0;P45520	tr|Q9U1E8|Q9U1E8_LEIMA Actin OS=Leishmania major OX=5664 GN=ACT PE=3 SV=1;tr|C6KJD0|	6	23.9	42.019
102	+	2.701150207	4.953829	Q4Q131	tr|Q4Q131|Q4Q131_LEIMA Diadenosine tetraphosphate synthetase OS=Leishmania major OX=	12	24	70.332
103	+	3.144821471	4.947932	Q4QC89	tr|Q4QC89|Q4QC89_LEIMA Putative 40S ribosomal protein S23 OS=Leishmania major OX=5664	4	35.7	15.935
104	+	2.415572363	4.907495	E9ADV2	tr|E9ADV2|E9ADV2_LEIMA Uncharacterized protein OS=Leishmania major OX=5664 GN=LMJF_2	10	14.8	87.066
105	+	1.256090746	4.877898	Q4Q271	tr|Q4Q271|Q4Q271_LEIMA Stress-inducible protein STI1 homolog OS=Leishmania major OX=56	10	40.8	29.012
106	+	1.038455007	4.855967	Q4Q3N3	tr|Q4Q3N3|Q4Q3N3_LEIMA Uncharacterized protein OS=Leishmania major OX=5664 GN=LMJF_	1	1	114.79
107	+	1.249160466	4.827105	Q4Q6T6	tr|Q4Q6T6|Q4Q6T6_LEIMA S-adenosylmethionine synthase OS=Leishmania major OX=5664 GN	11	29.6	43.016
108	+	2.653704502	4.814012	Q4Q7L5	tr|Q4Q7L5|Q4Q7L5_LEIMA Adenosine kinase OS=Leishmania major OX=5664 GN=LMJF_30_0880	6	22	37.1
109	+	3.088850484	4.803891	E9AD53;Q25324	tr|E9AD53|E9AD53_LEIMA Putative small GTP-binding protein Rab1 OS=Leishmania major OX=5	2	13.5	22.21
110	+	1.174194207	4.801877	E9ADB2	tr|E9ADB2|E9ADB2_LEIMA Arginyl-tRNA synthetase OS=Leishmania major OX=5664 GN=LMJF_2	17	28.5	78.249
111	+	1.990394055	4.775066	Q4QIK0	tr|Q4QIK0|Q4QIK0_LEIMA Splicing factor ptsr1-like protein OS=Leishmania major OX=5664 GN=	6	16.4	41.892
112	+	1.426839993	4.757452	A1Y2D9;A1Y2D8;P22045	tr|A1Y2D9|A1Y2D9_LEIMA Prostaglandin f2-alpha synthase (Fragment) OS=Leishmania major O	6	21.6	30.684
113	+	2.914016671	4.743757	Q4QAG8	tr|Q4QAG8|Q4QAG8_LEIMA Succinate dehydrogenase [ubiquinone] flavoprotein subunit, mito	8	19.3	66.735
114	+	4.868733369	4.742178	E9ACP3	tr|E9ACP3|E9ACP3_LEIMA Putative elongation initiation factor 2 alpha subunit OS=Leishmania	6	14.6	48.986
115	+	3.777737969	4.742071	E9AFS4	tr|E9AFS4|E9AFS4_LEIMA CS domain-containing protein OS=Leishmania major OX=5664 GN=LM	2	12.1	21.522
116	+	1.795184715	4.737669	Q4Q9V1	tr|Q4Q9V1|Q4Q9V1_LEIMA GTP-binding nuclear protein OS=Leishmania major OX=5664 GN=LM	5	27.8	24.224
117	+	1.999794593	4.674942	E9AD28	tr|E9AD28|E9AD28_LEIMA Putative calpain-like cysteine peptidase OS=Leishmania major OX=5	12	10	600.57
118	+	1.758814099	4.674333	Q4Q8E6	tr|Q4Q8E6|Q4Q8E6_LEIMA Putative glucose-regulated protein 78 OS=Leishmania major OX=566	11	20.4	71.94
119	+	1.28466394	4.656867	O97213	tr|O97213|O97213_LEIMA Putative 60S ribosomal protein L10 OS=Leishmania major OX=5664 GI	6	30	24.557
120	+	1.120235004	4.65523	Q4QEJ8	tr|Q4QEJ8|Q4QEJ8_LEIMA Uncharacterized protein OS=Leishmania major OX=5664 GN=LMJF_1	17	26.4	87.626
121	+	1.010581683	4.61941	Q4QIP1	tr|Q4QIP1|Q4QIP1_LEIMA 60S ribosomal protein L7a OS=Leishmania major OX=5664 GN=LMJF_	5	21.2	29.764
122	+	2.56166145	4.59974	Q4QIM7	tr|Q4QIM7|Q4QIM7_LEIMA Uncharacterized protein OS=Leishmania major OX=5664 GN=LMJF_	8	26.9	37.952
123	+	2.737891698	4.576905	E9AFD4	tr|E9AFD4|E9AFD4_LEIMA Putative ATP-dependent RNA helicase OS=Leishmania major OX=566	14	20.9	100.24
124	+	4.07774803	4.516661	E9AEI0;E9AEH9	tr|E9AEI0|E9AEI0_LEIMA Pyruvate kinase OS=Leishmania major OX=5664 GN=LMJF_35_0030 PE=	8	20.8	54.226
125	+	1.127162988	4.512222	Q66NE0	tr|Q66NE0|Q66NE0_LEIMA Elongation factor 1B gamma OS=Leishmania major OX=5664 GN=EF1	10	29	46.235
126	+	1.080486956	4.505882	Q4Q6K7;Q9BHF7	tr|Q4Q6K7|Q4Q6K7_LEIMA Mevalonate kinase OS=Leishmania major OX=5664 GN=LMJF_31_05	5	17	35.484
127	+	2.293287317	4.505501	Q4Q6X7	tr|Q4Q6X7|Q4Q6X7_LEIMA Valyl-tRNA synthetase OS=Leishmania major OX=5664 GN=LMJF_30	11	14.3	109.69
128	+	1.61989329	4.453024	Q4QD33;Q4QD34;Q9BJ5	tr|Q4QD33|Q4QD33_LEIMA Phosphoglycerate kinase OS=Leishmania major OX=5664 GN=PGKB	16	37.4	44.9
129	+	1.407673482	4.448195	E9ADU4	tr|E9ADU4|E9ADU4_LEIMA Putative ADP ribosylation factor 3 OS=Leishmania major OX=5664 GI	5	29.6	20.187
130	+	1.920162621	4.448177	Q4Q4U1;Q654V7	tr|Q4Q4U1|Q4Q4U1_LEIMA Dihydrolipoyl dehydrogenase OS=Leishmania major OX=5664 GN=G	8	24.4	50.577
131	+	1.039337732	4.432553	Q4QC87	tr|Q4QC87|Q4QC87_LEIMA T-complex protein 1 subunit delta OS=Leishmania major OX=5664 G	16	36.8	59.711
132	+	1.453288908	4.384561	E9AFE7	tr|E9AFE7|E9AFE7_LEIMA Putative cystathione gamma lyase OS=Leishmania major OX=5664 GN	8	27.1	44.532
133	+	1.276795738	4.36432	Q4Q3U8	tr|Q4Q3U8|Q4Q3U8_LEIMA Putative heat shock protein OS=Leishmania major OX=5664 GN=LM	9	17.2	72.042
134	+	1.725309965	4.344101	Q4QHR7	tr|Q4QHR7|Q4QHR7_LEIMA Putative eukaryotic translation initiation factor 2 subunit OS=Leish	5	12.5	52.622
135	+	1.106211312	4.304938	Q4QH17	tr|Q4QH17|Q4QH17_LEIMA Putative aminopeptidase OS=Leishmania major OX=5664 GN=LMJF_	11	23.2	57.148
136	+	2.163292051	4.298403	Q4QIQ9	tr|Q4QIQ9|Q4QIQ9_LEIMA Putative ATP-dependent DEAD/H RNA helicase OS=Leishmania maj	10	18.9	63.994
137	+	3.632057508	4.29547	P25204	sp|P25204|RS8_LEIMA 40S ribosomal protein S8 OS=Leishmania major OX=5664 GN=RPS8A PE=3	4	26.8	24.922
138	+	1.283395424	4.282685	E9ACW0	tr|E9ACW0|E9ACW0_LEIMA Putative heat shock protein DNAJ OS=Leishmania major OX=5664 G	11	39.1	43.601
139	+	2.566004576	4.242389	Q4Q9R2	tr|Q4Q9R2|Q4Q9R2_LEIMA Polyprenol reductase OS=Leishmania major OX=5664 GN=EnCR PE=3	6	20.3	34.206
140	+	2.621987695	4.228194	Q4QD56	tr|Q4QD56|Q4QD56_LEIMA Peptidylprolyl isomerase OS=Leishmania major OX=5664 GN=LMJF_	6	16.4	47.695
141	+	1.580867283	4.224294	Q4QGN9;A0A5B8Z1X6;A	tr|Q4QGN9|Q4QGN9_LEIMA Glucose-6-phosphate isomerase OS=Leishmania major OX=5664 G	7	15	67.169
142	+	0.995651645	4.203951	P69201;Q4Q165	sp|P69201|RL40_LEIMA Ubiquitin-60S ribosomal protein L40 OS=Leishmania major OX=5664 GN	4	33.6	14.682
143	+	1.613981662	4.153567	Q4QB32	tr|Q4QB32|Q4QB32_LEIMA T-complex protein 1 subunit gamma OS=Leishmania major OX=5664	18	39.9	60.327
144	+	1.933093874	4.135814	Q4QDF0	tr|Q4QDF0|Q4QDF0_LEIMA Malate dehydrogenase OS=Leishmania major OX=5664 GN=gMDH P	5	20.5	33.631
145	+	1.408869493	4.119363	Q4QHJ7	tr|Q4QHJ7|Q4QHJ7_LEIMA Putative nucleolar protein OS=Leishmania major OX=5664 GN=LMJF	8	25.2	52.685
146	+	3.390172066	4.096924	Q9U8C3;Q4QDK5	tr|Q9U8C3|Q9U8C3_LEIMA p45 (Fragment) OS=Leishmania major OX=5664 PE=2 SV=1;tr|Q4QDK	6	17.5	40.235
147	+	1.1728934	4.081328	Q9Y0F3	tr|Q9Y0F3|Q9Y0F3_LEIMA 3-hydroxy-3-methylglutaryl coenzyme A reductase OS=Leishmania m	6	16.4	45.953
148	+	1.33748305	4.065871	Q4QDW8	tr|Q4QDW8|Q4QDW8_LEIMA Putative elongation factor Tu OS=Leishmania major OX=5664 GN=	9	22.5	51.536
149	+	1.83571395	4.039312	Q4Q1R4;Q4Q1R3	tr|Q4Q1R4|Q4Q1R4_LEIMA Putative universal minicircle sequence binding protein OS=Leishma	4	51.3	12.552
150	+	2.640254224	4.017267	E9ACC0	tr|E9ACC0|E9ACC0_LEIMA Uncharacterized protein OS=Leishmania major OX=5664 GN=LMJF_02	2	5.8	31.996
151	+	2.243807419	3.979969	Q4Q5W1	tr|Q4Q5W1|Q4Q5W1_LEIMA Acetyl-CoA carboxylase OS=Leishmania major OX=5664 GN=LMJF_	16	9.9	241.13
152	+	1.099052019	3.973633	Q4QGA9	tr|Q4QGA9|Q4QGA9_LEIMA Alba domain-containing protein OS=Leishmania major OX=5664 GI	3	22.3	13.33
153	+	1.265861847	3.959731	Q4Q5U8	tr|Q4Q5U8|Q4Q5U8_LEIMA Phosphoglycan beta 1,3 galactosyltransferase 5 OS=Leishmania ma	7	7.3	123.7
154	+	1.170764548	3.952962	Q4QFY8	tr|Q4QFY8|Q4QFY8_LEIMA Putative chaperonin TCP20 OS=Leishmania major OX=5664 GN=LMJF	13	33.8	58.921
155		0.904107846	3.920483	Q4Q5J4	tr|Q4Q5J4|Q4Q5J4_LEIMA 60S ribosomal protein L18a OS=Leishmania major OX=5664 GN=LMJF_	7	44.1	20.807
156		0.885709479	3.910651	Q4QDX2	tr|Q4QDX2|Q4QDX2_LEIMA Citrate synthase OS=Leishmania major OX=5664 GN=LMJF_18_0670	1	2	50.476
157		0.938740534	3.909174	Q4QAC4	tr|Q4QAC4|Q4QAC4_LEIMA Transketolase OS=Leishmania major OX=5664 GN=LMJF_24_2060 PE	10	22.1	71.667
158	+	1.873728216	3.887315	A0A5A4RWL8;A0A5A4R	tr|A0A5A4RWL8|A0A5A4RWL8_LEIMA Phosphogluconate dehydrogenase (NADP(+)-dependent	7	22	44.485
159	+	2.107726892	3.881807	Q4Q970;Q25325	tr|Q4Q970|Q4Q970_LEIMA Heat shock protein 70-related protein OS=Leishmania major OX=566	9	17.8	70.588
160	+	1.166531695	3.842962	Q4Q1W6	tr|Q4Q1W6|Q4Q1W6_LEIMA Putative ribosomal protein L24 OS=Leishmania major OX=5664 GN	2	25	14.571
161	+	3.365788322	3.836179	Q4QDW0	tr|Q4QDW0|Q4QDW0_LEIMA Uncharacterized protein OS=Leishmania major OX=5664 GN=LMJF	11	5.6	289.99
162	+	1.843776744	3.835066	Q4VT70;Q4QCJ0;A0A5B	tr|Q4VT70|Q4VT70_LEIMA Phosphotransferase OS=Leishmania major OX=5664 GN=HK PE=3 SV=	12	38.4	51.719
163	+	1.99181399	3.820989	Q4QD53	tr|Q4QD53|Q4QD53_LEIMA Inosine-5-monophosphate dehydrogenase OS=Leishmania major C	8	20.4	55.546
164	+	1.786205146	3.80088	Q4QBF5	tr|Q4QBF5|Q4QBF5_LEIMA Putative endoribonuclease L-PSP (Pb5) OS=Leishmania major OX=5	3	22.1	16.918
165	+	1.952456244	3.777907	Q4Q6W5	tr|Q4Q6W5|Q4Q6W5_LEIMA Glutamyl-tRNA synthetase OS=Leishmania major OX=5664 GN=LM	6	12	67.619

1	Significant	[-LOG(p-value)]	log2 FC	Majority protein IDs	Fasta headers	Unique peptides	Unique sequence coverage [%]	Mol. weight [kDa]
166	+	1.8419047	3.743114	Q4QFM4	tr|Q4QFM4|Q4QFM4_LEIMA Putative kinesin K39 OS=Leishmania major OX=5664 GN=LMJF_14_	3	10.5	301.72
167	+	1.648263911	3.710243	Q4Q2W6	tr|Q4Q2W6|Q4Q2W6_LEIMA Asparagine--tRNA ligase OS=Leishmania major OX=5664 GN=LMJF	9	11.6	99.49
168		0.693071603	3.667009	Q4Q1Y2;Q4Q1Y3	tr|Q4Q1Y2|Q4Q1Y2_LEIMA Putative 40S ribosomal protein S18 OS=Leishmania major OX=5664 G	7	43.1	17.394
169	+	1.234383497	3.639172	Q4Q6Y6	tr|Q4Q6Y6|Q4Q6Y6_LEIMA Eukaryotic translation initiation factor 3 subunit 7-like protein OS=L	7	16.2	60.616
170	+	1.064270702	3.620771	Q4QDP9;Q4Q141	tr|Q4QDP9|Q4QDP9_LEIMA Putative 60S ribosomal protein L34 OS=Leishmania major OX=5664	3	19.6	19.278
171	+	1.257300715	3.586992	Q4Q7R2	tr|Q4Q7R2|Q4Q7R2_LEIMA Aspartyl-tRNA synthetase OS=Leishmania major OX=5664 GN=LMJF	7	16	62.373
172		0.875654525	3.578092	E9AEX6	tr|E9AEX6|E9AEX6_LEIMA Putative reiske iron-sulfur protein OS=Leishmania major OX=5664 GN	2	7.1	33.741
173	+	2.213458044	3.561681	E9ADR4	tr|E9ADR4|E9ADR4_LEIMA Putative ATP-binding cassette protein subfamily A,member 10 OS=L	1	0.5	207.05
174	+	1.184770054	3.561425	Q4QEW0	tr|Q4QEW0|Q4QEW0_LEIMA Citrulline--aspartate ligase OS=Leishmania major OX=5664 GN=LM	11	7.3	205.9
175	+	1.082397066	3.559084	Q4Q4U5	tr|Q4Q4U5|Q4Q4U5_LEIMA CCT-alpha OS=Leishmania major OX=5664 GN=LMJF_32_3270 PE=2 S	6	14.8	59.134
176	+	1.173316573	3.518177	E9ACH0	tr|E9ACH0|E9ACH0_LEIMA Putative long chain fatty Acyl CoA synthetase OS=Leishmania major	12	18.5	78.947
177	+	1.052606762	3.516485	Q4QFP8	tr|Q4QFP8|Q4QFP8_LEIMA Putative small myristoylated protein-3 OS=Leishmania major OX=56	3	28.7	12.936
178		0.950456362	3.488458	Q4QGC5	tr|Q4QGC5|Q4QGC5_LEIMA Tubulin alpha chain OS=Leishmania major OX=5664 GN=LMJF_13_0	10	24.6	49.759
179		1.04384783	3.468623	E9AFF2	tr|E9AFF2|E9AFF2_LEIMA Putative 60S ribosomal subunit protein L31 OS=Leishmania major OX=	2	12.8	21.26
180	+	1.829500309	3.435926	Q4Q8V7	tr|Q4Q8V7|Q4Q8V7_LEIMA Putative 60S ribosomal protein L35 OS=Leishmania major OX=5664	2	16.5	15.221
181		1.03046594	3.4318	Q4Q8H8	tr|Q4Q8H8|Q4Q8H8_LEIMA Ribonucleoside-diphosphate reductase OS=Leishmania major OX=	5	6.6	90.727
182	+	1.596317993	3.407194	Q4QF35	tr|Q4QF35|Q4QF35_LEIMA Proliferating cell nuclear antigen OS=Leishmania major OX=5664 GN	5	22.5	32.38
183	+	2.685612279	3.403584	E9AFX7;O96606	tr|E9AFX7|E9AFX7_LEIMA Polyadenylate-binding protein OS=Leishmania major OX=5664 GN=P	6	12.9	62.664
184	+	2.212776427	3.380584	Q4Q561	tr|Q4Q561|Q4Q561_LEIMA Uncharacterized protein OS=Leishmania major OX=5664 GN=LMJF_3	4	5.3	117.66
185	+	1.113355473	3.369025	Q4QFR8	tr|Q4QFR8|Q4QFR8_LEIMA Elongation of fatty acids protein OS=Leishmania major OX=5664 GN	4	17.6	32.575
186		0.8742462	3.333597	Q4QFF2	tr|Q4QFF2|Q4QFF2_LEIMA Putative ribonucleoprotein p18, mitochondrial OS=Leishmania majo	7	41.2	21.3
187	+	1.588525759	3.318572	Q4QBJ3	tr|Q4QBJ3|Q4QBJ3_LEIMA Alanine--tRNA ligase OS=Leishmania major OX=5664 GN=LMJF_22_1	12	15.7	106.32
188	+	1.522124124	3.306573	Q4Q0Q2	tr|Q4Q0Q2|Q4Q0Q2_LEIMA Uncharacterized protein OS=Leishmania major OX=5664 GN=LMJF_	6	8.5	105.31
189	+	1.626824117	3.289742	E9AFD2	tr|E9AFD2|E9AFD2_LEIMA Glycerol kinase OS=Leishmania major OX=5664 GN=LMJF_35_3080 PE	4	12.7	56.144
190	+	1.386482142	3.285671	Q4QC07	tr|Q4QC07|Q4QC07_LEIMA Putative centromere/microtubule binding protein cbf5 OS=Leishma	4	14.4	48.427
191	+	1.440738515	3.268173	Q4Q1T9	tr|Q4Q1T9|Q4Q1T9_LEIMA Putative Transitional endoplasmic reticulum ATPase OS=Leishmania	15	23.3	86.838
192		0.743382587	3.244637	Q4Q9M4	tr|Q4Q9M4|Q4Q9M4_LEIMA Succinate--CoA ligase [ADP-forming] subunit alpha, mitochondria	8	32.8	30.912
193		0.998617155	3.243886	Q4QF34	tr|Q4QF34|Q4QF34_LEIMA Phosphomevalonate kinase OS=Leishmania major OX=5664 GN=LMJ	2	4.8	49.12
194	+	2.362801807	3.237387	Q4QF36	tr|Q4QF36|Q4QF36_LEIMA Glutamine--tRNA ligase OS=Leishmania major OX=5664 GN=LMJF_15	3	5.4	66.075
195	+	1.604219301	3.227765	Q4QGX6	tr|Q4QGX6|Q4QGX6_LEIMA Uncharacterized protein OS=Leishmania major OX=5664 GN=LMJF_	3	16	27.541
196	+	1.449601833	3.207073	Q4QDS0	tr|Q4QDS0|Q4QDS0_LEIMA Prolyl-tRNA synthetase OS=Leishmania major OX=5664 GN=LMJF_1	2	2.6	81.525
197	+	1.277075644	3.176994	E9AFP0	tr|E9AFP0|E9AFP0_LEIMA Polyadenylate-binding protein OS=Leishmania major OX=5664 GN=P	12	24.4	65.35
198		0.656009298	3.156656	E9ADL4	tr|E9ADL4|E9ADL4_LEIMA Putative proteasome regulatory non-ATPase subunit OS=Leishmania	10	14.2	99.324
199	+	1.684610358	3.153697	E9AE78	tr|E9AE78|E9AE78_LEIMA Rab GDP dissociation inhibitor OS=Leishmania major OX=5664 GN=LM	3	9.7	49.792
200	+	2.842785033	3.146947	Q4Q822	tr|Q4Q822|Q4Q822_LEIMA Dihydrolipoamide acetyltransferase component of pyruvate dehydr	5	19.5	41.732
201		0.845156123	3.133478	Q4QGH2	tr|Q4QGH2|Q4QGH2_LEIMA SMP-LTD domain-containing protein OS=Leishmania major OX=566	1	2.3	79.613
202		1.031771535	3.124654	Q4Q202	tr|Q4Q202|Q4Q202_LEIMA Uncharacterized protein OS=Leishmania major OX=5664 GN=LMJF_3	4	9.2	61.14
203		0.750235341	3.117096	Q4QC12	tr|Q4QC12|Q4QC12_LEIMA Putative cytochrome c oxidase subunit VI OS=Leishmania major OX	1	7.6	19.207
204		0.900588531	3.094519	Q4Q0P9	tr|Q4Q0P9|Q4Q0P9_LEIMA Uncharacterized protein OS=Leishmania major OX=5664 GN=LMJF_3	2	9.4	30.099
205	+	1.768780117	3.084491	Q4QJA6	tr|Q4QJA6|Q4QJA6_LEIMA Dipeptidyl peptidase 3 OS=Leishmania major OX=5664 GN=LMJF_05	8	16.8	75.967
206	+	1.641426256	3.076145	Q4QFW6	tr|Q4QFW6|Q4QFW6_LEIMA Thioredoxin-like_fold domain-containing protein OS=Leishmania	4	22.1	22.328
207	+	1.768293683	3.049282	Q4QEW5	tr|Q4QEW5|Q4QEW5_LEIMA OMPdecase OS=Leishmania major OX=5664 GN=LMJF_16_0550 PE=	7	15.5	49.5
208	+	2.335883859	3.04172	Q4QJ42	tr|Q4QJ42|Q4QJ42_LEIMA Putative glutamine synthetase OS=Leishmania major OX=5664 GN=L	3	7.3	60.169
209		0.693262059	3.033402	Q4Q059;Q8I8E1	tr|Q4Q059|Q4Q059_LEIMA Protein disulfide-isomerase OS=Leishmania major OX=5664 GN=PDI	8	20.8	52.376
210	+	2.265097367	3.003141	Q4QGW6	tr|Q4QGW6|Q4QGW6_LEIMA WD_REPEATS_REGION domain-containing protein OS=Leishmani	4	4.2	122.12
211	+	1.81411179	2.996596	E9ADL3	tr|E9ADL3|E9ADL3_LEIMA C2 DOCK-type domain-containing protein OS=Leishmania major OX=	4	10.8	338.2
212	+	1.194031446	2.993141	Q4QH73	tr|Q4QH73|Q4QH73_LEIMA GRIP domain-containing protein OS=Leishmania major OX=5664 GN	6	33.6	148.13
213		0.716880578	2.974207	Q4QG44	tr|Q4QG44|Q4QG44_LEIMA Leucyl-tRNA synthetase OS=Leishmania major OX=5664 GN=LMJF_1	10	11.6	122.06
214		0.718549814	2.964609	E9ACB2	tr|E9ACB2|E9ACB2_LEIMA Putative proteasome regulatory non-ATPase subunit 6 OS=Leishmar	5	9.5	58.837
215		0.836892048	2.964156	Q4Q7N0	tr|Q4Q7N0|Q4Q7N0_LEIMA Putative 4-methyl-5(Beta-hydroxyethyl)-thiazole monophosphate	3	15.8	20.477
216		1.124819666	2.960715	Q4Q9X4;Q4Q3G4	tr|Q4Q9X4|Q4Q9X4_LEIMA 40S ribosomal protein S25 OS=Leishmania major OX=5664 GN=LMJF	3	26.7	13.046
217		1.120425478	2.940164	Q4QFW7	tr|Q4QFW7|Q4QFW7_LEIMA Putative carboxypeptidase OS=Leishmania major OX=5664 GN=LM	1	2.4	57.082
218	+	1.731091059	2.926486	E9AE98	tr|E9AE98|E9AE98_LEIMA Aspartyl putative aminopeptidase OS=Leishmania major OX=5664 GN	3	8.6	49.672
219	+	1.45544688	2.925278	Q4QJ37;Q4QJ39	tr|Q4QJ37|Q4QJ37_LEIMA Protein disulfide-isomerase OS=Leishmania major OX=5664 G	4	17.7	28.814
220	+	2.819862208	2.920531	Q4QCS8;Q4QCS9	tr|Q4QCS8|Q4QCS8_LEIMA Putative calpain-like cysteine peptidase OS=Leishmania major OX=	6	9.7	91.357
221		1.047556648	2.913768	Q4QE40	tr|Q4QE40|Q4QE40_LEIMA Diphosphomevalonate decarboxylase OS=Leishmania major OX=566	4	11.2	42.416
222	+	2.019142266	2.905599	Q4Q1R1	tr|Q4Q1R1|Q4Q1R1_LEIMA Putative poly-zinc finger protein 2 OS=Leishmania major OX=5664 G	3	20.7	14.634
223		0.729515022	2.901212	Q4QGW3	tr|Q4QGW3|Q4QGW3_LEIMA Putative 40S ribosomal protein S15A OS=Leishmania major OX=56	2	18.5	14.696
224	+	1.323426925	2.901145	Q4QCR1	tr|Q4QCR1|Q4QCR1_LEIMA Coatomer subunit beta OS=Leishmania major OX=5664 GN=LMJF_26	5	7.2	109.56
225	+	1.317675684	2.893868	E9ACL4	tr|E9ACL4|E9ACL4_LEIMA Uncharacterized protein OS=Leishmania major OX=5664 GN=LMJF_03	12	7.5	247.03
226		0.915437549	2.881412	Q4QC37	tr|Q4QC37|Q4QC37_LEIMA Uncharacterized protein OS=Leishmania major OX=5664 GN=LMJF_2	7	17.5	46.448
227	+	1.373680209	2.86614	Q4Q821	tr|Q4Q821|Q4Q821_LEIMA Vacuolar proton pump subunit B OS=Leishmania major OX=5664 GN	8	23.4	55.518
228		1.164213296	2.85813	Q4QGX0;A0A1B2BGM7	tr|Q4QGX0|Q4QGX0_LEIMA Putative lanosterol 14-alpha-demethylase OS=Leishmania major O	6	17.7	54.164
229		0.525132446	2.83043	Q4Q3T3	tr|Q4Q3T3|Q4Q3T3_LEIMA Metallo-peptidase, Clan MA(E), Family M32 OS=Leishmania major C	6	12.8	57.049
230		0.358745735	2.80314	Q4Q737	tr|Q4Q737|Q4Q737_LEIMA Reticulon-like protein OS=Leishmania major OX=5664 GN=PAPLE22	1	6.6	22.159
231	+	1.48997697	2.786349	Q4QEA3	tr|Q4QEA3|Q4QEA3_LEIMA META domain containing protein OS=Leishmania major OX=5664 GN	3	8.8	48.46
232		0.769560031	2.781293	Q9TZS4	tr|Q9TZS4|Q9TZS4_LEIMA Peroxidoxin OS=Leishmania major OX=5664 PE=2 SV=1	1	4.5	22.17
233	+	1.429404976	2.780577	Q4Q3V3	tr|Q4Q3V3|Q4Q3V3_LEIMA Succinyl-CoA:3-ketoacid-coenzyme A transferase OS=Leishmania m	7	14.9	52.551
234		0.930954109	2.774526	Q4Q8X0	tr|Q4Q8X0|Q4Q8X0_LEIMA Putative ribosomal protein L38 OS=Leishmania major OX=5664 GN=	1	12	9.4541
235		0.962442859	2.772391	Q4Q6U6	tr|Q4Q6U6|Q4Q6U6_LEIMA Uncharacterized protein OS=Leishmania major OX=5664 GN=LMJF_3	5	8.8	90.285
236		0.711983691	2.770315	Q4Q6R3	tr|Q4Q6R3|Q4Q6R3_LEIMA 5-methyltetrahydropteroyltriglutamate--homocysteine S-methyltr	6	8.4	86.109
237	+	1.429696539	2.76713	Q4QAP8	tr|Q4QAP8|Q4QAP8_LEIMA Triosephosphate isomerase OS=Leishmania major OX=5664 GN=LM	6	33.9	27.195
238	+	2.391322253	2.743119	E9AEJ6	tr|E9AEJ6|E9AEJ6_LEIMA FCP1 homology domain-containing protein OS=Leishmania major OX=	3	20.4	27.169
239		0.999030859	2.738316	Q4Q9R8	tr|Q4Q9R8|Q4Q9R8_LEIMA Pyruvate dehydrogenase E1 component subunit beta OS=Leishman	2	8.6	37.897
240		0.876685645	2.733335	Q4QBL1	tr|Q4QBL1|Q4QBL1_LEIMA Farnesyl pyrophosphate synthase OS=Leishmania major OX=5664 GI	5	16.3	40.967
241	+	1.914715007	2.731494	A0A2R4SE78;Q4Q3K1;A0	tr|A0A2R4SE78|A0A2R4SE78_LEIMA Glucose-6-phosphate 1-dehydrogenase (Fragment) OS=Lei	4	9.8	59.579
242		1.219125756	2.705965	E9AEH2;E9AFY3	tr|E9AEH2|E9AEH2_LEIMA Ribosomal protein L37 OS=Leishmania major OX=5664 GN=LMJF_33_	3	30.1	9.8354
243		0.975149459	2.699565	Q4QFB6	tr|Q4QFB6|Q4QFB6_LEIMA Uncharacterized protein OS=Leishmania major OX=5664 GN=LMJF_1	3	8.4	53.529
244		1.27441501	2.635406	Q4Q8H1	tr|Q4Q8H1|Q4Q8H1_LEIMA 40S ribosomal protein S14 OS=Leishmania major OX=5664 GN=LMJF	1	7.6	15.593
245		0.971651664	2.632824	Q4Q698;Q4Q699	tr|Q4Q698|Q4Q698_LEIMA Thiolase protein-like protein OS=Leishmania major OX=5664 GN=LM	7	18.6	46.891
246		1.005835393	2.618973	Q4Q198	tr|Q4Q198|Q4Q198_LEIMA 14-3-3 protein I OS=Leishmania major OX=5664 GN=Lm 14-3-3 I PE=3	4	18.6	29.687
247		1.058042148	2.609743	E9AD65	tr|E9AD65|E9AD65_LEIMA Oxoglutarate dehydrogenase (succinyl-transferring) OS=Leishmania	7	8.7	112.71
248		0.646726374	2.603328	O97216	tr|O97216|O97216_LEIMA Uncharacterized protein OS=Leishmania major OX=5664 GN=LMJF_04	1	2.2	75.059
249		1.162526106	2.598255	Q4QDX5	tr|Q4QDX5|Q4QDX5_LEIMA Uncharacterized protein OS=Leishmania major OX=5664 GN=LMJF_	4	8.4	77.32
250		0.83927007	2.594099	Q4Q6F6	tr|Q4Q6F6|Q4Q6F6_LEIMA Biotin/lipoate protein ligase-like protein OS=Leishmania major OX=	5	24.3	28.354
251	+	1.480100134	2.580613	Q4Q0M6	tr|Q4Q0M6|Q4Q0M6_LEIMA 2-methoxy-6-polyprenyl-1,4-benzoquinol methylase, mitochondr	3	11.1	32.012
252	+	3.114314429	2.574439	Q4Q0X8	tr|Q4Q0X8|Q4Q0X8_LEIMA Proteasome regulatory ATPase subunit OS=Leishmania major OX=5	2	7.1	45.619
253		0.903664067	2.565119	Q9NHE1	tr|Q9NHE1|Q9NHE1_LEIMA Non-specific serine/threonine protein kinase OS=Leishmania majo	3	8.2	39.749
254		1.133311353	2.558931	E9AE57;A0A5J6E2G4;A0	sp|E9AE57|FUM2_LEIMA Fumarate hydratase 2 OS=Leishmania major OX=5664 GN=FH2 PE=1 SV	7	14.8	62.602
255		0.614689253	2.534209	E9AE82	tr|E9AE82|E9AE82_LEIMA Putative GTP-binding protein OS=Leishmania major OX=5664 GN=LMJ	4	4.7	77.27
256		0.38943595	2.520783	Q4Q8I7	tr|Q4Q8I7|Q4Q8I7_LEIMA Uncharacterized protein OS=Leishmania major OX=5664 GN=LMJF_28	1	2.8	55.433
257		1.071451919	2.519869	P07382	sp|P07382|DRTS_LEIMA Bifunctional dihydrofolate reductase-thymidylate synthase OS=Leishm	3	6.7	58.688
258		1.070457407	2.516631	E9ACV1	tr|E9ACV1|E9ACV1_LEIMA Obg-like ATPase 1 OS=Leishmania major OX=5664 GN=LMJF_27_2330	5	14	44.017
259		1.054610448	2.514476	Q4QJG7	tr|Q4QJG7|Q4QJG7_LEIMA N(1),N(8)-bis(glutathionyl)spermidine reductase OS=Leishmania m	5	10.8	53.144
260		1.301100526	2.512301	Q4FX34	tr|Q4FX34|Q4FX34_LEIMA Aspartate transaminase OS=Leishmania major OX=5664 GN=asat PE=	4	12.9	45.989
261		0.823798079	2.489939	Q4QCD2	tr|Q4QCD2|Q4QCD2_LEIMA Methionine--tRNA ligase OS=Leishmania major OX=5664 GN=LMJF_	1	1.3	83.832
262	+	1.440338239	2.488785	Q4Q893	tr|Q4Q893|Q4Q893_LEIMA Putative proteasome regulatory non-ATP-ase subunit 2 OS=Leishma	3	3.4	106.05
263	+	2.441571728	2.485937	Q4Q9T0	tr|Q4Q9T0|Q4Q9T0_LEIMA Uncharacterized protein OS=Leishmania major OX=5664 GN=LMJF_2	1	4.6	36.731
264		0.996023821	2.482114	Q4Q3T2	tr|Q4Q3T2|Q4Q3T2_LEIMA Isocitrate dehydrogenase [NADP] OS=Leishmania major OX=5664 GI	1	2.6	46.335
265		1.075385678	2.480431	Q4QDQ1	tr|Q4QDQ1|Q4QDQ1_LEIMA Putative pyruvate dehydrogenase E1 component alpha subunit OS	5	15.9	42.874
266		0.810915481	2.476206	Q4Q833	tr|Q4Q833|Q4Q833_LEIMA Eukaryotic translation initiation factor 3 subunit E OS=Leishmania m	7	20.2	46.383
267		1.130845691	2.462177	Q4QAI0	tr|Q4QAI0|Q4QAI0_LEIMA Putative IgE-dependent histamine-releasing factor OS=Leishmania	2	8.8	19.419
268		1.024536087	2.448207	Q4Q3J4;Q4Q3J2;Q9U8L4	tr|Q4Q3J4|Q4Q3J4_LEIMA Malate dehydrogenase OS=Leishmania major OX=5664 GN=LMJF_34_	5	24.9	33.357
269		0.778177529	2.427985	Q4Q1D2	tr|Q4Q1D2|Q4Q1D2_LEIMA 40S ribosomal protein S24 OS=Leishmania major OX=5664 GN=S24E	3	35.8	15.77
270		1.249476346	2.397365	Q4QCE1;E9AF13	tr|Q4QCE1|Q4QCE1_LEIMA Putative 60S Ribosomal protein L36 OS=Leishmania major OX=5664	3	28.6	11.942

	Significant	[-LOG(p-value)]	log2 FC	Majority protein IDs	Fasta headers	Unique peptides	Unique sequence coverage [%]	Mol. weight [kDa]
1								
271		0.847574349	2.391044	Q9GNC1	tr|Q9GNC1|Q9GNC1_LEIMA Probable ubiquitin-conjugating enzyme e2-17 kDa OS=Leishmania	1	7.4	16.651
272		0.842529754	2.388931	Q4Q9B1	tr|Q4Q9B1|Q4Q9B1_LEIMA Putative aspartate--ammonia ligase OS=Leishmania major OX=5664	3	15.6	39.805
273		0.579359364	2.38812	Q4QGM6	tr|Q4QGM6|Q4QGM6_LEIMA Cytochrome c oxidase subunit IV OS=Leishmania major OX=5664	4	11.4	39.434
274		1.109050201	2.380971	Q4QII8	tr|Q4QII8|Q4QII8_LEIMA Putative nucleolar RNA-binding protein OS=Leishmania major OX=566	3	12.5	37.568
275		0.525243233	2.377003	Q4QC06	tr|Q4QC06|Q4QC06_LEIMA Putative ATP synthase F1 subunit gamma protein OS=Leishmania m	3	10.9	34.42
276	+	2.410453573	2.374798	Q4QCD1	tr|Q4QCD1|Q4QCD1_LEIMA Uncharacterized protein OS=Leishmania major OX=5664 GN=LMJF_	5	5.2	149.74
277		1.23313815	2.355966	Q4QGR5	tr|Q4QGR5|Q4QGR5_LEIMA Putative ornithine decarboxylase OS=Leishmania major OX=5664 G	4	7.2	77.26
278		0.755416549	2.3384	Q4Q3C1;Q66NE2	tr|Q4Q3C1|Q4Q3C1_LEIMA Elongation factor 1-beta OS=Leishmania major OX=5664 GN=eEF1B	2	9.7	25.646
279		0.45363597	2.311129	Q4Q5Y0	tr|Q4Q5Y0|Q4Q5Y0_LEIMA Putative ADP-ribosylation factor OS=Leishmania major OX=5664 GN	2	10.7	20.189
280		1.363603655	2.272103	Q4QC71	tr|Q4QC71|Q4QC71_LEIMA Putative adenylate kinase OS=Leishmania major OX=5664 GN=LMJF	5	26.8	30.06
281		1.246994941	2.268665	Q4Q2T7	tr|Q4Q2T7|Q4Q2T7_LEIMA Alba domain-containing protein OS=Leishmania major OX=5664 GN=	5	31.7	22.59
282		0.54998727	2.248132	Q4Q9N8	tr|Q4Q9N8|Q4Q9N8_LEIMA Putative 2,4-dihydroxyhept-2-ene-1,7-dioic acid aldolase OS=Leish	6	28.3	30.291
283	+	1.989686716	2.231875	Q4Q6S8	tr|Q4Q6S8|Q4Q6S8_LEIMA Putative ATP synthase, epsilon chain OS=Leishmania major OX=5664	1	6.6	20.1
284		0.792396349	2.208995	Q4QIE0;Q71S85	tr|Q4QIE0|Q4QIE0_LEIMA Superoxide dismutase OS=Leishmania major OX=5664 GN=FESODA P	4	20.4	26.074
285		1.075031841	2.19543	Q9U0W1;Q4QBC0	tr|Q9U0W1|Q9U0W1_LEIMA Acetyl-coenzyme A synthetase OS=Leishmania major OX=5664 GN	3	5.2	77.408
286		0.46847272	2.187914	Q4QA45;Q4QA46	tr|Q4QA45|Q4QA45_LEIMA Putative RNA-binding protein, UPB2 OS=Leishmania major OX=5664	2	15	18.982
287		1.143119485	2.157019	E9AC43;E9AC40	tr|E9AC43|E9AC43_LEIMA Putative long-chain-fatty-acid-CoA ligase OS=Leishmania major OX=	2	2.1	77.676
288		0.411086268	2.09705	E9ADT5;P90627	tr|E9ADT5|E9ADT5_LEIMA Cysteine peptidase C (CPC) OS=Leishmania major OX=5664 GN=LMJF	4	12.9	37.234
289	+	1.806563905	2.095269	Q4Q0J9	tr|Q4Q0J9|Q4Q0J9_LEIMA Isoleucyl-tRNA synthetase OS=Leishmania major OX=5664 GN=ILERS	5	5.7	125.76
290		1.391174175	2.092553	Q4QJJ3	tr|Q4QJJ3|Q4QJJ3_LEIMA Serine/threonine-protein phosphatase OS=Leishmania major OX=566	2	2.8	71.711
291		1.154857111	2.081857	Q4Q1J6	tr|Q4Q1J6|Q4Q1J6_LEIMA Putative developmentally regulated GTP-binding protein 1 OS=Leish	1	3.8	41.015
292		0.695639475	2.080309	Q4Q1F5	tr|Q4Q1F5|Q4Q1F5_LEIMA Dihydrolipoamide acetyltransferase component of pyruvate dehyd	2	3.9	48.75
293		1.006801882	2.077345	Q4QH32	tr|Q4QH32|Q4QH32_LEIMA mRNA (guanine-N(7)-)-methyltransferase OS=Leishmania major OX	3	4.2	117.95
294		1.231198142	2.040736	E9AEU1	tr|E9AEU1|E9AEU1_LEIMA FAD;protein FMN transferase OS=Leishmania major OX=5664 GN=LM	5	5.1	123.2
295		1.497719478	2.03393	Q4Q848	tr|Q4Q848|Q4Q848_LEIMA CS domain-containing protein OS=Leishmania major OX=5664 GN=L	5	11.1	71.276
296		0.75900621	2.023211	Q4QII7	tr|Q4QII7|Q4QII7_LEIMA RNA binding protein-like protein OS=Leishmania major OX=5664 GN=	2	9.5	35.005
297		1.277831658	2.01062	Q4Q4Z3	tr|Q4Q4Z3|Q4Q4Z3_LEIMA Putative proteasome regulatory non-ATP-ase subunit OS=Leishman	2	5.4	46.371
298		1.315503613	1.98513	E9AC56	tr|E9AC56|E9AC56_LEIMA Putative mitochondrial processing peptide beta subunit OS=Leishma	3	9.1	55.078
299		1.312020848	1.982455	Q4QGU1	tr|Q4QGU1|Q4QGU1_LEIMA Proteasome subunit beta OS=Leishmania major OX=5664 GN=LMJF	1	4.6	30.33
300		0.90001424	1.97643	E9ADY2	tr|E9ADY2|E9ADY2_LEIMA TPR_REGION domain-containing protein OS=Leishmania major OX=5	6	11.4	78.874
301		0.351227439	1.969637	Q4QE62	tr|Q4QE62|Q4QE62_LEIMA Putative translation initiation factor OS=Leishmania major OX=5664	6	10.9	80.758
302		1.066681404	1.966044	Q4Q8Z2	tr|Q4Q8Z2|Q4Q8Z2_LEIMA Uncharacterized protein OS=Leishmania major OX=5664 GN=LMJF_2	2	8.4	38.88
303		0.724898826	1.953146	Q4QHJ8	tr|Q4QHJ8|Q4QHJ8_LEIMA Putative mitogen-activated protein kinase OS=Leishmania major OX	2	7.9	46.367
304		0.481943796	1.942083	Q4Q5J8	tr|Q4Q5J8|Q4Q5J8_LEIMA RRM_8 domain-containing protein OS=Leishmania major OX=5664 GN	2	4	57.408
305		1.117813729	1.91713	Q4QAW8	tr|Q4QAW8|Q4QAW8_LEIMA Beta transducin-like protein OS=Leishmania major OX=5664 GN=L	2	4.9	60.745
306		0.74952281	1.914289	E9ADA4	tr|E9ADA4|E9ADA4_LEIMA CCT-beta OS=Leishmania major OX=5664 GN=LMJF_27_1260 PE=3 SV	11	27.8	57.885
307		0.573459471	1.907688	Q4Q2H7	tr|Q4Q2H7|Q4Q2H7_LEIMA H(+)-transporting two-sector ATPase OS=Leishmania major OX=566	3	5.2	67.735
308		1.021097187	1.898872	Q4Q5E5	tr|Q4Q5E5|Q4Q5E5_LEIMA Uncharacterized protein OS=Leishmania major OX=5664 GN=LMJF_3	3	4.4	85.948
309		0.386904458	1.897817	Q4QH45	tr|Q4QH45|Q4QH45_LEIMA 14-3-3 protein II OS=Leishmania major OX=5664 GN=Lm 14-3-3 II PE=	6	26.1	29.145
310		0.71823667	1.891335	Q4Q702	tr|Q4Q702|Q4Q702_LEIMA Putative aldehyde dehydrogenase OS=Leishmania major OX=5664 G	3	7.2	63.988
311		0.518429757	1.883307	E9AFV2	tr|E9AFV2|E9AFV2_LEIMA Cyclophilin 40 OS=Leishmania major OX=5664 GN=CYP40 PE=4 SV=1	4	12.1	38.42
312		1.490399158	1.88075	Q4Q922	tr|Q4Q922|Q4Q922_LEIMA Putative cytochrome c oxidase subunit V OS=Leishmania major OX=	3	20.9	22.29
313		1.716874345	1.878811	E9AD19	sp|E9AD19|RBSK_LEIMA Ribokinase OS=Leishmania major OX=5664 GN=LMJF_27_0420 PE=1 SV=	3	12.5	35.342
314		0.75906315	1.865576	Q9NF77	tr|Q9NF77|Q9NF77_LEIMA Putative ubiquitin-activating enzyme e1 OS=Leishmania major OX=	2	2.3	115.23
315		0.507569245	1.864421	Q4QH08	sp|Q4QH08|ASNA_LEIMA ATPase ASNA1 homolog OS=Leishmania major OX=5664 GN=LmjF11.0	2	5.6	43.935
316		0.892607984	1.857213	E9ADJ0	tr|E9ADJ0|E9ADJ0_LEIMA Putative RNA-binding protein OS=Leishmania major OX=5664 GN=LM	3	9.1	48.4
317		0.571722448	1.856264	E9AEU5	tr|E9AEU5|E9AEU5_LEIMA Putative short chain dehydrogenase OS=Leishmania major OX=5664	2	7.3	24.874
318		0.690191253	1.855572	Q4QJK0	tr|Q4QJK0|Q4QJK0_LEIMA Putative ras-like small GTPases OS=Leishmania major OX=5664 GN=L	2	13.3	21.714
319		0.724277239	1.855053	Q4QEB3	sp|Q4QEB3|GMPR_LEIMA GMP reductase OS=Leishmania major OX=5664 GN=GMPR PE=1 SV=2	4	13.4	52.031
320		0.599394623	1.854418	Q4Q2J4	tr|Q4Q2J4|Q4Q2J4_LEIMA RuvB-like helicase OS=Leishmania major OX=5664 GN=LMJF_34_3500	7	19.2	50.322
321		0.556687554	1.841575	Q4Q933	tr|Q4Q933|Q4Q933_LEIMA Proline dehydrogenase OS=Leishmania major OX=5664 GN=LMJF_26	4	10.5	63.83
322		0.48879256	1.837348	Q4Q7J9	tr|Q4Q7J9|Q4Q7J9_LEIMA Uncharacterized protein OS=Leishmania major OX=5664 GN=LMJF_36	1	4.4	29.104
323		0.576454953	1.826882	E9ADX4	tr|E9ADX4|E9ADX4_LEIMA Tryparedoxin OS=Leishmania major OX=5664 GN=TXN1 PE=1 SV=1	3	33.1	16.543
324		0.748221179	1.826481	Q4Q1X7	tr|Q4Q1X7|Q4Q1X7_LEIMA Putative 40S ribosomal protein S10 OS=Leishmania major OX=5664	2	16.7	18.65
325		1.059569318	1.807122	Q4QEI8	tr|Q4QEI8|Q4QEI8_LEIMA Elongation factor 1-alpha OS=Leishmania major OX=5664 GN=LMJF_1	2	5.1	49.058
326		0.476760588	1.792919	Q4QFR7	tr|Q4QFR7|Q4QFR7_LEIMA Elongation of fatty acids protein OS=Leishmania major OX=5664 GN	2	5.4	32.778
327		1.113416976	1.786184	Q4Q274	tr|Q4Q274|Q4Q274_LEIMA Putative PUF1 OS=Leishmania major OX=5664 GN=PUF1 PE=4 SV=1	3	8.9	61.266
328		0.377378582	1.778348	Q4Q0W8	tr|Q4Q0W8|Q4Q0W8_LEIMA Uncharacterized protein OS=Leishmania major OX=5664 GN=LMJF	4	25.6	17.423
329		0.590066485	1.762628	Q4QBS0	tr|Q4QBS0|Q4QBS0_LEIMA Putative NADH-cytochrome b5 reductase OS=Leishmania major OX=	1	2.4	31.794
330		0.645766722	1.757208	Q4Q425	tr|Q4Q425|Q4Q425_LEIMA Uncharacterized protein OS=Leishmania major OX=5664 GN=LMJF_3	1	1.4	101.09
331		0.763173575	1.750615	Q9U0V4	tr|Q9U0V4|Q9U0V4_LEIMA Uncharacterized protein L7836.08 OS=Leishmania major OX=5664 GI	2	4.9	62.726
332		0.496855297	1.750597	Q4Q8L6	tr|Q4Q8L6|Q4Q8L6_LEIMA 40S ribosomal protein S26 OS=Leishmania major OX=5664 GN=LMJF_	1	15.2	12.761
333		0.864818347	1.743615	Q4QCI1	tr|Q4QCI1|Q4QCI1_LEIMA Metallo-peptidase, Clan ME, Family M16 OS=Leishmania major OX=5	3	5.8	51.409
334		0.819344117	1.729714	E9ADC7	tr|E9ADC7|E9ADC7_LEIMA Putative proteasome regulatory non-ATP-ase subunit 3 OS=Leishma	2	7.5	37.929
335		0.605984535	1.729573	E9AFK8	tr|E9AFK8|E9AFK8_LEIMA Proteasome subunit beta OS=Leishmania major OX=5664 GN=LMJF_3	4	19.3	27.522
336		0.512074175	1.727659	Q4QE93	tr|Q4QE93|Q4QE93_LEIMA Uncharacterized protein OS=Leishmania major OX=5664 GN=LMJF_1	8	15.7	82.903
337		1.043678258	1.720698	Q4QA88	tr|Q4QA88|Q4QA88_LEIMA Poly(A)-binding protein 3 OS=Leishmania major OX=5664 GN=PABP	4	8.1	60.899
338		1.796307813	1.711055	Q4Q7P3	tr|Q4Q7P3|Q4Q7P3_LEIMA Histidine--tRNA ligase OS=Leishmania major OX=5664 GN=LMJF_30	1	3.2	52.959
339		0.580689204	1.702596	Q4Q758	tr|Q4Q758|Q4Q758_LEIMA Sphingosine-1-phosphate lyase OS=Leishmania major OX=5664 GN=	1	2	59.351
340		0.549511031	1.689903	Q4Q937	tr|Q4Q937|Q4Q937_LEIMA Putative thimet oligopeptidase OS=Leishmania major OX=5664 GN=	7	15.3	77.196
341		0.48841946	1.66905	Q4Q8Q6	tr|Q4Q8Q6|Q4Q8Q6_LEIMA Putative pantothenate kinase subunit OS=Leishmania major OX=56	5	4.4	161.57
342		1.411778377	1.667811	Q4QDK6	tr|Q4QDK6|Q4QDK6_LEIMA Putative mitogen-activated protein kinase OS=Leishmania major C	4	17.1	30.884
343		0.836685651	1.647845	Q4Q286	tr|Q4Q286|Q4Q286_LEIMA Cell differentiation protein-like protein OS=Leishmania major OX=5	1	2.8	41.112
344		0.727912493	1.643599	E9ADY9	tr|E9ADY9|E9ADY9_LEIMA Putative carnitine/choline acetyltransferase OS=Leishmania major C	1	1.9	68.602
345		0.640492813	1.63842	Q4Q1B2;P35549	tr|Q4Q1B2|Q4Q1B2_LEIMA Fibrillarin OS=Leishmania major OX=5664 GN=LMJF_36_3070 PE=3 SV	2	14.5	25.787
346		1.674660036	1.635116	E9ADT8	tr|E9ADT8|E9ADT8_LEIMA Putative high mobility group protein homolog tdp-1 OS=Leishmania	2	9.7	33.635
347		0.613202355	1.618594	Q4Q6E2	tr|Q4Q6E2|Q4Q6E2_LEIMA RanBP2-type domain-containing protein OS=Leishmania major OX=	3	0.9	547.61
348		1.139278901	1.599848	Q4QJH5	tr|Q4QJH5|Q4QJH5_LEIMA Very-long-chain (3R)-3-hydroxyacyl-CoA dehydratase OS=Leishman	1	5.8	25.167
349		0.622974064	1.593272	Q4Q1R5	tr|Q4Q1R5|Q4Q1R5_LEIMA Proteasome subunit alpha type OS=Leishmania major OX=5664 GN=	3	16	29.6
350		0.855557778	1.589203	Q4Q289;Q6YIR8	tr|Q4Q289|Q4Q289_LEIMA Proteasome subunit beta OS=Leishmania major OX=5664 GN=LMJF_	2	9.1	24.694
351		0.557374569	1.58648	Q4QGN0	tr|Q4QGN0|Q4QGN0_LEIMA Alanine aminotransferase OS=Leishmania major OX=5664 GN=ALA	1	2.4	55.015
352		0.906179088	1.580829	Q4QIH4	tr|Q4QIH4|Q4QIH4_LEIMA Putative proteasome regulatory non-ATP-ase subunit OS=Leishman	2	10.4	36.374
353		0.581432483	1.555827	Q4Q080	tr|Q4Q080|Q4Q080_LEIMA Prolyl endopeptidase OS=Leishmania major OX=5664 GN=LMJF_36_	3	4.3	78.248
354		1.918559713	1.554683	E9AFD0	tr|E9AFD0|E9AFD0_LEIMA Putative ubiquitin-activating enzyme e1 OS=Leishmania major OX=5	1	1	126.43
355		0.840596856	1.550101	Q6YIR7;Q4Q2A8;Q4Q29	tr|Q6YIR7|Q6YIR7_LEIMA Quinonoid dihydropteridine reductase QDPR (Fragment) OS=Leishma	1	4.3	21.644
356		0.303822235	1.546717	Q4QES5	tr|Q4QES5|Q4QES5_LEIMA Sucrose-phosphate synthase-like protein OS=Leishmania major OX=	3	9.9	52.454
357		0.470350421	1.537278	Q4QG67	tr|Q4QG67|Q4QG67_LEIMA Metallo-peptidase, Clan ME, Family M16 OS=Leishmania major OX=	5	10.6	57.749
358		0.452162801	1.535809	Q4QCD7	tr|Q4QCD7|Q4QCD7_LEIMA 19S proteasome regulatory subunit OS=Leishmania major OX=5664	4	10.5	54.273
359		1.555643335	1.535754	E9ABZ4	tr|E9ABZ4|E9ABZ4_LEIMA Propanoyl-CoA:carbon dioxide ligase subunit alpha OS=Leishmania r	1	2.1	73.794
360		1.277434099	1.533753	E9ACJ9	tr|E9ACJ9|E9ACJ9_LEIMA Putative 26S protease regulatory subunit OS=Leishmania major OX=5	2	6.8	44.412
361		0.471643553	1.528361	Q9U0T7	tr|Q9U0T7|Q9U0T7_LEIMA Adenylosuccinate lyase OS=Leishmania major OX=5664 GN=LMJF_04	2	4.4	53.711
362		0.525480312	1.524645	Q4QA84	tr|Q4QA84|Q4QA84_LEIMA Electron transfer flavoprotein subunit beta OS=Leishmania major C	2	14.7	28.24
363		0.732427166	1.521701	Q4QGX4	tr|Q4QGX4|Q4QGX4_LEIMA Putative pretranslocation protein,alpha subunit OS=Leishmania ma	3	6.2	53.911
364		1.04793522	1.506767	M1LHR3;M1LHQ9;Q2PD2	tr|M1LHR3|M1LHR3_LEIMA Nucleoside hydrolase-like protein (Fragment) OS=Leishmania majo	1	5.6	23.554
365		0.578204082	1.50516	E9ADY5;Q25317	tr|E9ADY5|E9ADY5_LEIMA Putative serine peptidase OS=Leishmania major OX=5664 GN=LMJF_	8	11.6	96.923
366		0.630625001	1.504637	Q4QFK7;Q4Q216	tr|Q4QFK7|Q4QFK7_LEIMA 60S ribosomal protein L40 OS=Leishmania major OX=5664 GN=LMJF_	2	18.4	17.029
367		0.803914279	1.501082	Q4Q8Q9	tr|Q4Q8Q9|Q4Q8Q9_LEIMA Proteasome subunit beta OS=Leishmania major OX=5664 GN=LMJF	2	11.7	22.463
368		0.683014176	1.500207	E9AD84	tr|E9AD84|E9AD84_LEIMA Cysteine desulfurase OS=Leishmania major OX=5664 GN=LMJF_27_1	2	6.8	47.85
369		0.735492036	1.500153	Q4QG97	tr|Q4QG97|Q4QG97_LEIMA 40S ribosomal protein S12 OS=Leishmania major OX=5664 GN=LMJF	1	6.4	15.608
370		0.433844254	1.469951	Q4QCD3	tr|Q4QCD3|Q4QCD3_LEIMA Uncharacterized protein OS=Leishmania major OX=5664 GN=LMJF_	6	3.6	248.86
371		0.455168545	1.460714	Q4QJ53	tr|Q4QJ53|Q4QJ53_LEIMA Putative 5-3 exonuclease OS=Leishmania major OX=5664 GN=LMJF_0	3	2.6	166.27
372		0.54344271	1.446854	Q4Q756	tr|Q4Q756|Q4Q756_LEIMA ADP-ribosylation factor-like protein OS=Leishmania major OX=5664	1	6.1	20.043
373		0.420726413	1.441043	Q4QH59	tr|Q4QH59|Q4QH59_LEIMA Inorganic diphosphatase OS=Leishmania major OX=5664 GN=LMJF_	2	6.5	50.993
374		0.489028882	1.440238	E9AD97;Q9TVI8;Q25305	tr|E9AD97|E9AD97_LEIMA Putative histone H1 OS=Leishmania major OX=5664 GN=LMJF_27_115	1	18.8	9.893
375		0.948715011	1.415706	Q4QFZ6	tr|Q4QFZ6|Q4QFZ6_LEIMA Ubiquitin-conjugating enzyme-like protein OS=Leishmania major O	2	15.2	16.067

1	Significant	[-LOG(p-value)]	log2 FC	Majority protein IDs	Fasta headers	Unique peptides	Unique sequence coverage [%]	Mol. weight [kDa]
376		0.624726903	1.400797	Q4Q7S1	tr|Q4Q7S1|Q4Q7S1_LEIMA Putative phosphatase 2C OS=Leishmania major OX=5664 GN=LMJF_3	3	10.2	41.732
377		0.549708437	1.400682	Q4Q4I8	tr|Q4Q4I8|Q4Q4I8_LEIMA Putative ATP-binding cassette protein subfamily F,member 3 OS=Lei	3	6	74.573
378		0.611370256	1.391572	Q4Q720	tr|Q4Q720|Q4Q720_LEIMA Putative small glutamine-rich tetratricopeptide repeat protein OS=	2	4.9	45.77
379		0.648741132	1.387892	Q4QE21	tr|Q4QE21|Q4QE21_LEIMA Aha1_N domain-containing protein OS=Leishmania major OX=5664 (	1	4.8	38.403
380		0.417948308	1.386016	Q4Q9Y1	tr|Q4Q9Y1|Q4Q9Y1_LEIMA Aldehyde dehydrogenase, mitochondrial OS=Leishmania major OX=	2	4.6	54.119
381		0.590684413	1.374857	Q4Q246	tr|Q4Q246|Q4Q246_LEIMA Proteasome subunit beta OS=Leishmania major OX=5664 GN=LMJF_	1	5.3	23.002
382		1.792479241	1.368037	Q4QG45	tr|Q4QG45|Q4QG45_LEIMA Putative proteasome regulatory ATPase subunit 2 OS=Leishmania r	2	7.1	49.289
383		0.311217817	1.367594	Q4QAA9	tr|Q4QAA9|Q4QAA9_LEIMA Putative 60S ribosomal protein L12 OS=Leishmania major OX=5664	2	26.2	17.538
384		0.373231262	1.345537	Q4QFJ8	tr|Q4QFJ8|Q4QFJ8_LEIMA Inositol-3-phosphate synthase OS=Leishmania major OX=5664 GN=IN	5	13.3	58.3
385		0.647172161	1.341642	Q4QIR7	tr|Q4QIR7|Q4QIR7_LEIMA Acetylornithine deacetylase OS=Leishmania major OX=5664 GN=LMJ	1	2.8	42.843
386		0.360879207	1.335073	Q4Q0F4	tr|Q4Q0F4|Q4Q0F4_LEIMA Putative eukaryotic initiation factor 4a OS=Leishmania major OX=56	8	14.5	84.635
387		0.485535808	1.332473	E9AEI7	tr|E9AEI7|E9AEI7_LEIMA Uncharacterized protein OS=Leishmania major OX=5664 GN=LMJF_35_	1	5	24.211
388		0.387103399	1.327608	Q4Q806	tr|Q4Q806|Q4Q806_LEIMA Putative 40S ribosomal protein S17 OS=Leishmania major OX=5664 (	2	14	16.512
389		0.364118104	1.321274	Q4QHC5	tr|Q4QHC5|Q4QHC5_LEIMA Peptidylprolyl isomerase OS=Leishmania major OX=5664 GN=LMJF	1	8.2	17.295
390		0.269522698	1.321238	Q4QF62	tr|Q4QF62|Q4QF62_LEIMA 60S acidic ribosomal protein P2 OS=Leishmania major OX=5664 GN=	1	10.8	10.998
391		0.561175995	1.315409	E9AC23	tr|E9AC23|E9AC23_LEIMA Uncharacterized protein OS=Leishmania major OX=5664 GN=LMJF_01	1	5.7	23.646
392		0.754031329	1.306395	Q4QCX2	tr|Q4QCX2|Q4QCX2_LEIMA Uncharacterized protein OS=Leishmania major OX=5664 GN=LMJF_2	1	0.9	140.56
393		1.435648078	1.304258	Q4QEK5	tr|Q4QEK5|Q4QEK5_LEIMA Putative eukaryotic translation initiation factor 4 gamma OS=Leishn	2	2.7	71.233
394		0.413861124	1.284779	E9ADI0	tr|E9ADI0|E9ADI0_LEIMA GMP_PDE_delta domain-containing protein OS=Leishmania major OX	2	13.2	22.322
395		0.717483185	1.280656	Q4QH01	tr|Q4QH01|Q4QH01_LEIMA Putative 40S ribosomal protein S21 OS=Leishmania major OX=5664	1	6.1	17.002
396		0.36067913	1.271418	Q4QFJ7	tr|Q4QFJ7|Q4QFJ7_LEIMA Putative tyrosyl-tRNA synthetase OS=Leishmania major OX=5664 GN	5	8.7	74.948
397		0.677743948	1.264518	Q4Q2C8	tr|Q4Q2C8|Q4Q2C8_LEIMA ER membrane protein complex subunit 1 OS=Leishmania major OX=	2	2.8	87.084
398		0.281137799	1.263257	Q4Q2T4	tr|Q4Q2T4|Q4Q2T4_LEIMA RuvB-like helicase OS=Leishmania major OX=5664 GN=LMJF_34_261	1	3.3	53.638
399		1.005031923	1.261533	Q4Q0M3	tr|Q4Q0M3|Q4Q0M3_LEIMA Putative NADH dehydrogenase OS=Leishmania major OX=5664 GN	1	3.4	57.375
400		0.27638641	1.261106	E9ADT0	tr|E9ADT0|E9ADT0_LEIMA Putative U-box domain protein OS=Leishmania major OX=5664 GN=L	4	8.5	66.552
401		0.383218003	1.244595	Q4Q5Z7	tr|Q4Q5Z7|Q4Q5Z7_LEIMA 2-oxoglutarate dehydrogenase, e3 component,lipoamidedehydrog	1	2.3	66.803
402		1.257622069	1.243459	Q4Q1N6	tr|Q4Q1N6|Q4Q1N6_LEIMA Uncharacterized protein OS=Leishmania major OX=5664 GN=LMJF_	1	1.9	70.227
403		0.523099372	1.231409	Q4QBG5	tr|Q4QBG5|Q4QBG5_LEIMA Mannose-1-phosphate guanyltransferase OS=Leishmania major OX	1	3.7	41.77
404		0.353859858	1.216368	E9AE86	tr|E9AE86|E9AE86_LEIMA Aminopeptidase OS=Leishmania major OX=5664 GN=LMJF_29_2240 P	4	5.1	96.388
405		0.268323436	1.212126	Q4QJF7	tr|Q4QJF7|Q4QJF7_LEIMA Uncharacterized protein OS=Leishmania major OX=5664 GN=LMJF_05	2	9.7	22.365
406		0.39226294	1.2092	Q4QA21	tr|Q4QA21|Q4QA21_LEIMA Eukaryotic translation initiation factor 5A OS=Leishmania major OX	2	13.9	17.812
407		0.337712152	1.201422	A1Y2C8;Q4Q0Z7	tr|A1Y2C8|A1Y2C8_LEIMA Zeta-crystallin/NADPH-oxidoreductase-like protein (Fragment) OS=L	1	5.8	33.029
408		0.363240401	1.190834	E9AD42	tr|E9AD42|E9AD42_LEIMA Uncharacterized protein OS=Leishmania major OX=5664 GN=LMJF_21	4	26.9	19.573
409		0.701289838	1.187999	E9ADW8	tr|E9ADW8|E9ADW8_LEIMA ANK_REP_REGION domain-containing protein OS=Leishmania maj	2	7.5	40.106
410		0.360091274	1.166189	Q4Q1S4	tr|Q4Q1S4|Q4Q1S4_LEIMA Putative nima-related protein kinase OS=Leishmania major OX=566	3	10.8	56.375
411		0.384690642	1.149089	Q4QGE5	tr|Q4QGE5|Q4QGE5_LEIMA Metallo-peptidase, Clan MA(E), family 32 OS=Leishmania major OX	3	8.5	57.033
412		0.3013904	1.141142	E9AFW9	tr|E9AFW9|E9AFW9_LEIMA C3H1-type domain-containing protein OS=Leishmania major OX=56	1	0.9	107.38
413		0.413138349	1.140153	Q4Q6X0	tr|Q4Q6X0|Q4Q6X0_LEIMA 40S ribosomal protein S26 OS=Leishmania major OX=5664 GN=LMJF	1	15.2	12.719
414		0.502197122	1.140024	E9ADX3	tr|E9ADX3|E9ADX3_LEIMA Tryparedoxin OS=Leishmania major OX=5664 GN=TXN2 PE=4 SV=1	4	34.9	17.082
415		0.517032983	1.134586	Q4QFR9	tr|Q4QFR9|Q4QFR9_LEIMA Elongation of fatty acids protein OS=Leishmania major OX=5664 GN	1	3.5	32.326
416		1.478853843	1.132976	E9ADI5;Q4QBL8	tr|E9ADI5|E9ADI5_LEIMA Putative ribonucleoside-diphosphate reductase small chain OS=Leish	1	2.6	44.142
417		0.405794775	1.12906	Q4QBY6	tr|Q4QBY6|Q4QBY6_LEIMA Putative heat shock protein DNAJ OS=Leishmania major OX=5664 G	2	6.6	36.634
418		0.611654989	1.127491	Q7YWB6	tr|Q7YWB6|Q7YWB6_LEIMA Alkyl dihydroxyacetonephosphate synthase OS=Leishmania major	5	13.2	69.579
419		0.207533026	1.107335	Q4QBU0	tr|Q4QBU0|Q4QBU0_LEIMA Putative proteasome regulatory ATPase subunit 1 OS=Leishmania	2	4.6	49.021
420		0.560553022	1.102558	Q4QI34	tr|Q4QI34|Q4QI34_LEIMA Uncharacterized protein OS=Leishmania major OX=5664 GN=LMJF_09	1	10.8	19.303
421		0.249204787	1.101236	E9AES2	tr|E9AES2|E9AES2_LEIMA Putative aldose 1-epimerase OS=Leishmania major OX=5664 GN=LMJ	3	8.6	41.427
422		0.568404602	1.094661	E9AFW0	tr|E9AFW0|E9AFW0_LEIMA Proteasome subunit alpha type OS=Leishmania major OX=5664 GN=	2	12.4	27.223
423		0.713753519	1.07977	Q4QFI0	tr|Q4QFI0|Q4QFI0_LEIMA Uncharacterized protein OS=Leishmania major OX=5664 GN=LMJF_15	2	6.6	37.718
424		0.441607427	1.076882	Q4Q2R5	tr|Q4Q2R5|Q4Q2R5_LEIMA Uncharacterized protein OS=Leishmania major OX=5664 GN=LMJF_3	2	4.3	66.779
425		0.611730713	1.066193	Q4QDN8;Q4QDN7	tr|Q4QDN8|Q4QDN8_LEIMA Plasma membrane ATPase OS=Leishmania major OX=5664 GN=H1A	1	1.5	107.02
426		0.285754795	1.060021	E9AFN7	tr|E9AFN7|E9AFN7_LEIMA 5-deoxynucleotidase OS=Leishmania major OX=5664 GN=LMJF_35_4	1	6.8	22.988
427		0.924318135	1.051552	Q4QCE4	tr|Q4QCE4|Q4QCE4_LEIMA Putative ATP-binding cassette protein subfamily E,member 1 OS=Le	3	6.4	73.976
428		0.808093635	1.012178	Q4QF32	tr|Q4QF32|Q4QF32_LEIMA Ribonucloprotein OS=Leishmania major OX=5664 GN=LMJF_15_1470	1	12.7	13.516
429		0.38705756	1.010696	E9AEK1;P39095	tr|E9AEK1|E9AEK1_LEIMA 60S ribosomal protein L30 OS=Leishmania major OX=5664 GN=LMJF_3	4	38.5	11.352
430		0.730752699	1.009365	Q4QBV0	tr|Q4QBV0|Q4QBV0_LEIMA Putative 40S ribosomal protein S15 OS=Leishmania major OX=5664	1	10.5	17.435
431		0.183778183	1.002707	Q4Q171	tr|Q4Q171|Q4Q171_LEIMA Oxoglutarate dehydrogenase (succinyl-transferring) OS=Leishmania	7	11.8	111.1
432		0.246050106	1.00254	Q4Q3F9	tr|Q4Q3F9|Q4Q3F9_LEIMA Putative importin beta-1 subunit OS=Leishmania major OX=5664 GN	2	2.5	95.615

8.5 Appendix 5: NMR data for 2M-98 metabolite

Proton NMR

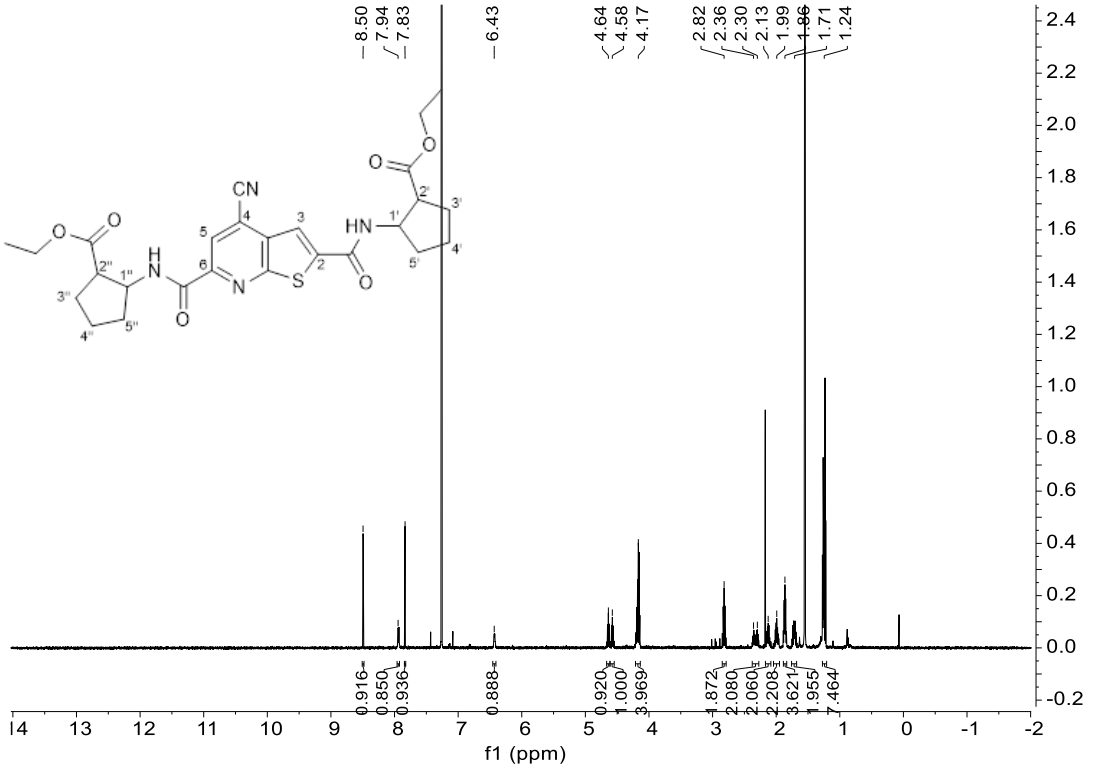

Carbon NMR

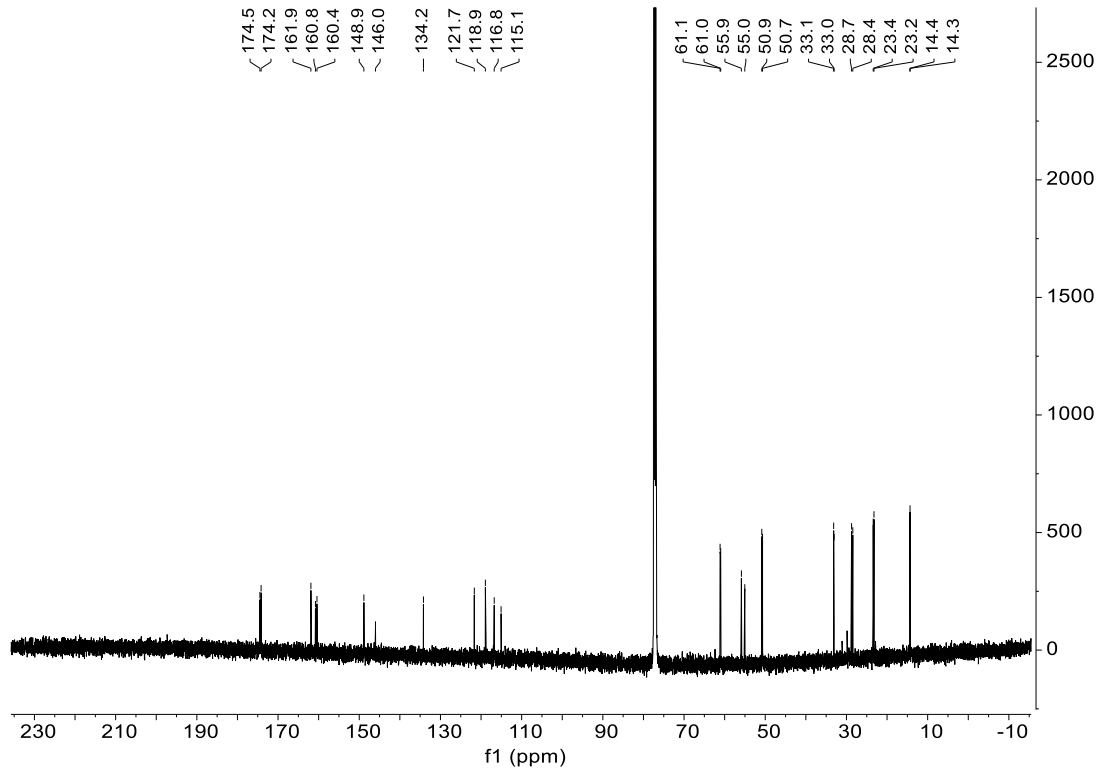

Correlated spectroscopy (COSY)

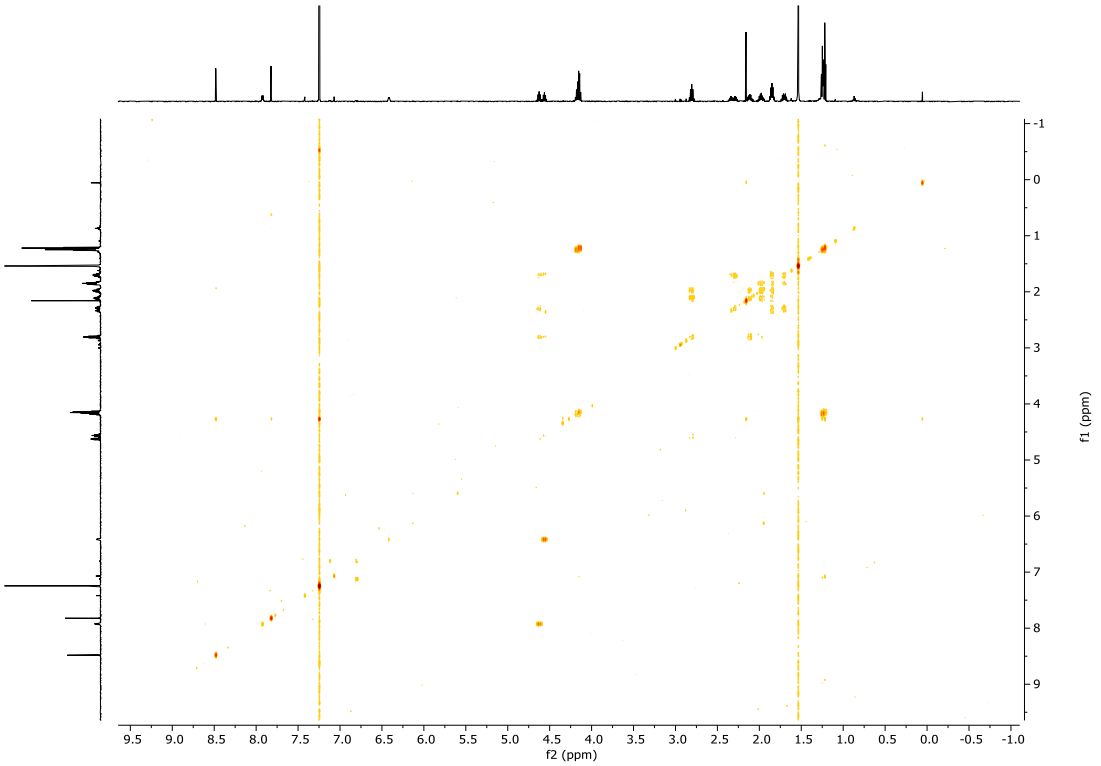

Nuclear Overhauser Effect Spectroscopy (NOESY)

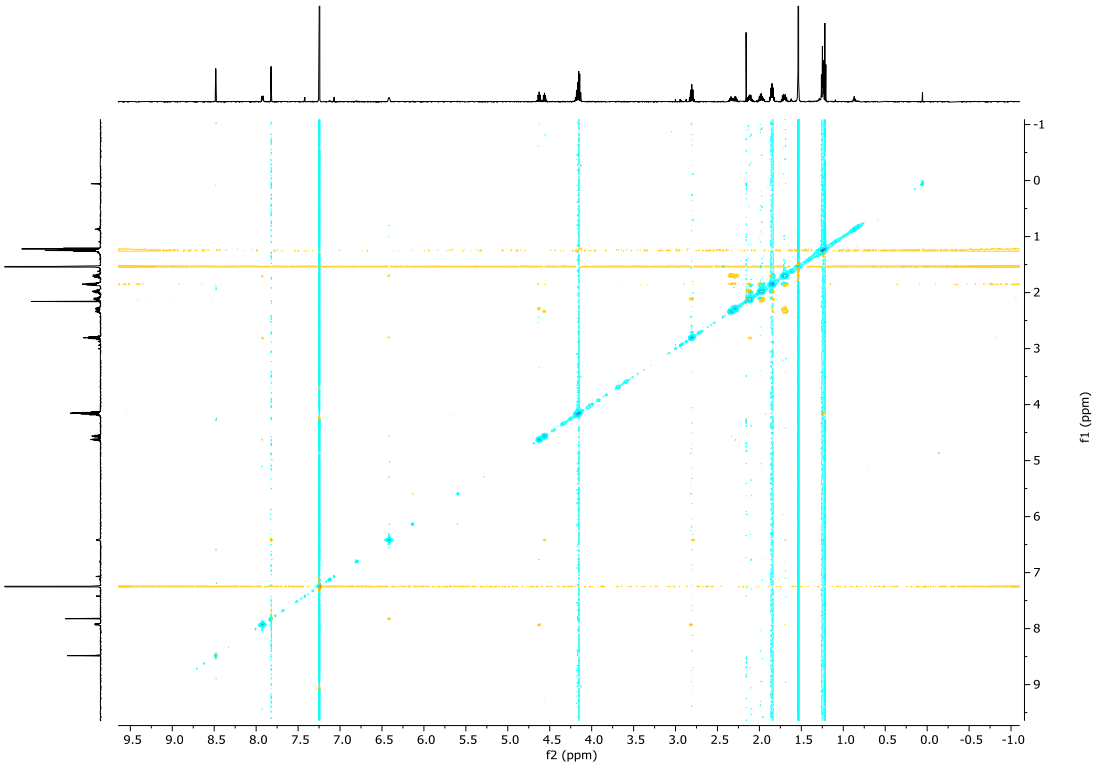

Heteronuclear Single Quantum Coherence (HSQC)

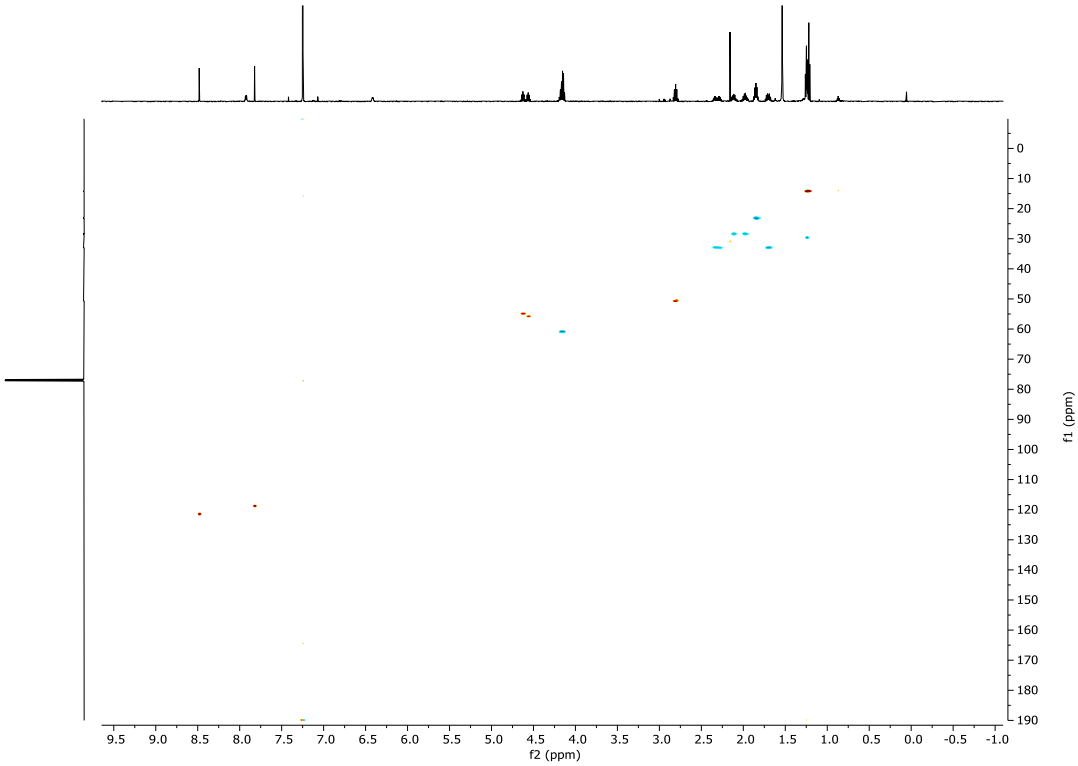

Heteronuclear Multiple Bond Correlation

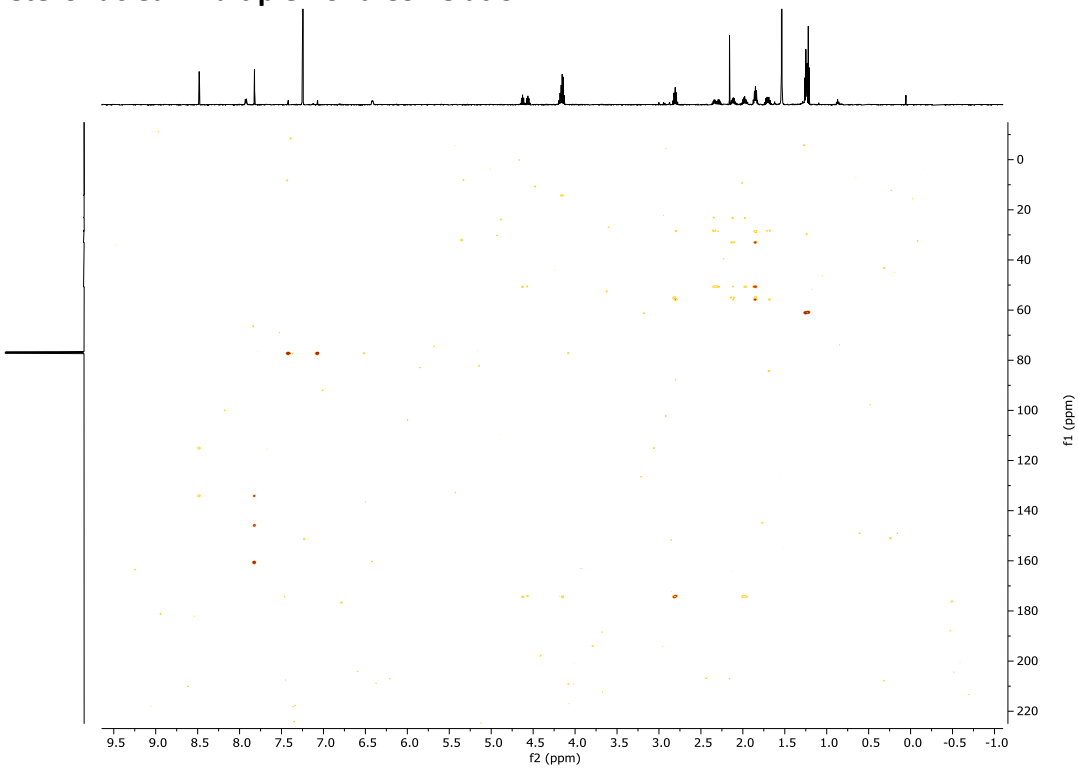

8.6 Appendix 6: NMR spectra

5-nitrothiophene-2-carbonyl chloride (**23**)

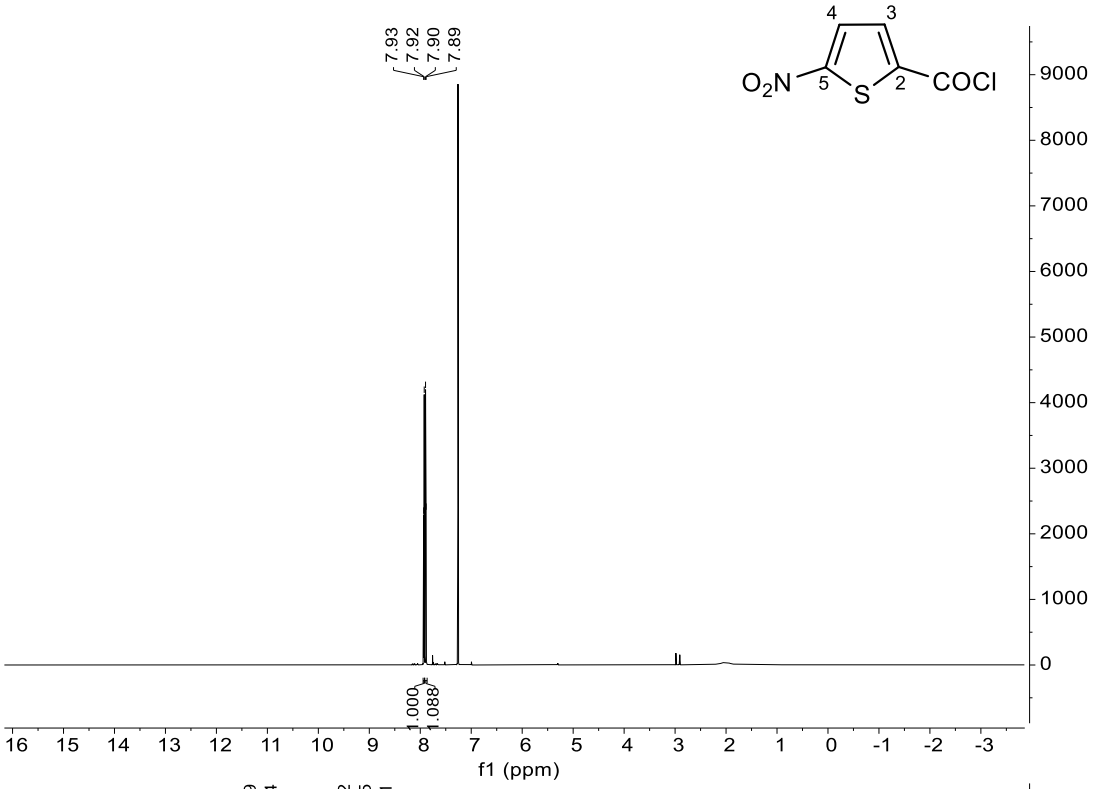

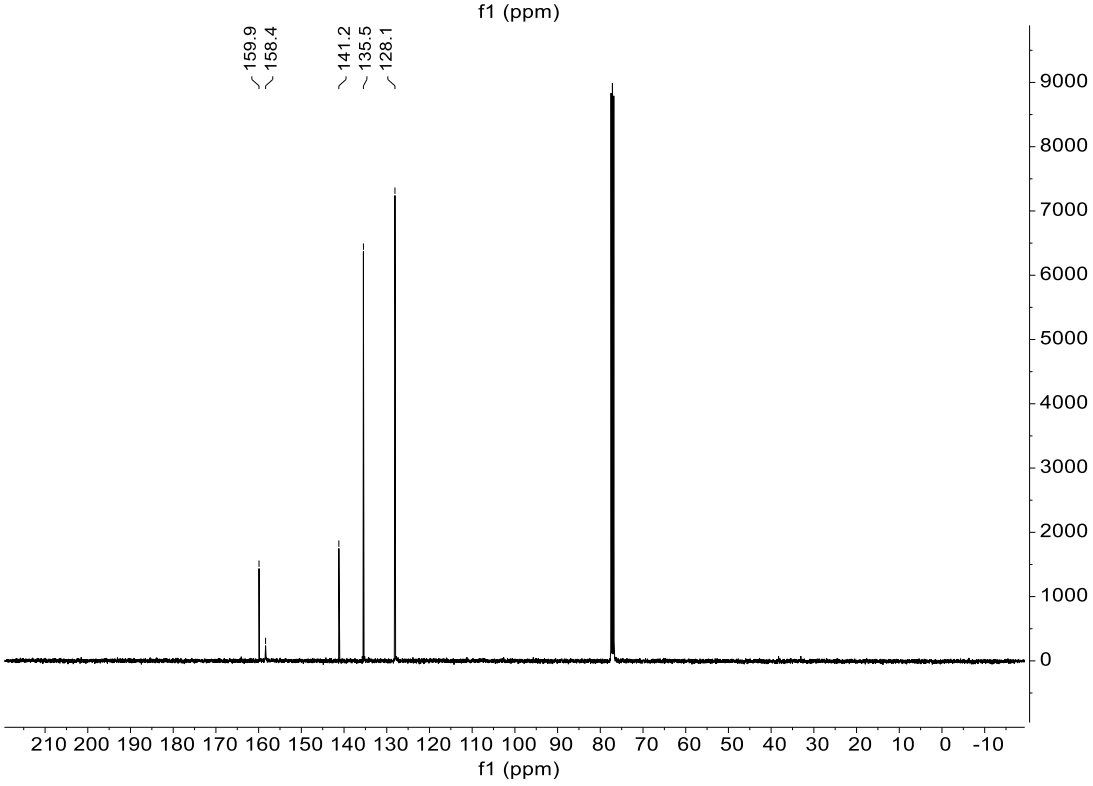

2-amino-3-cyanothiophene (**33**)

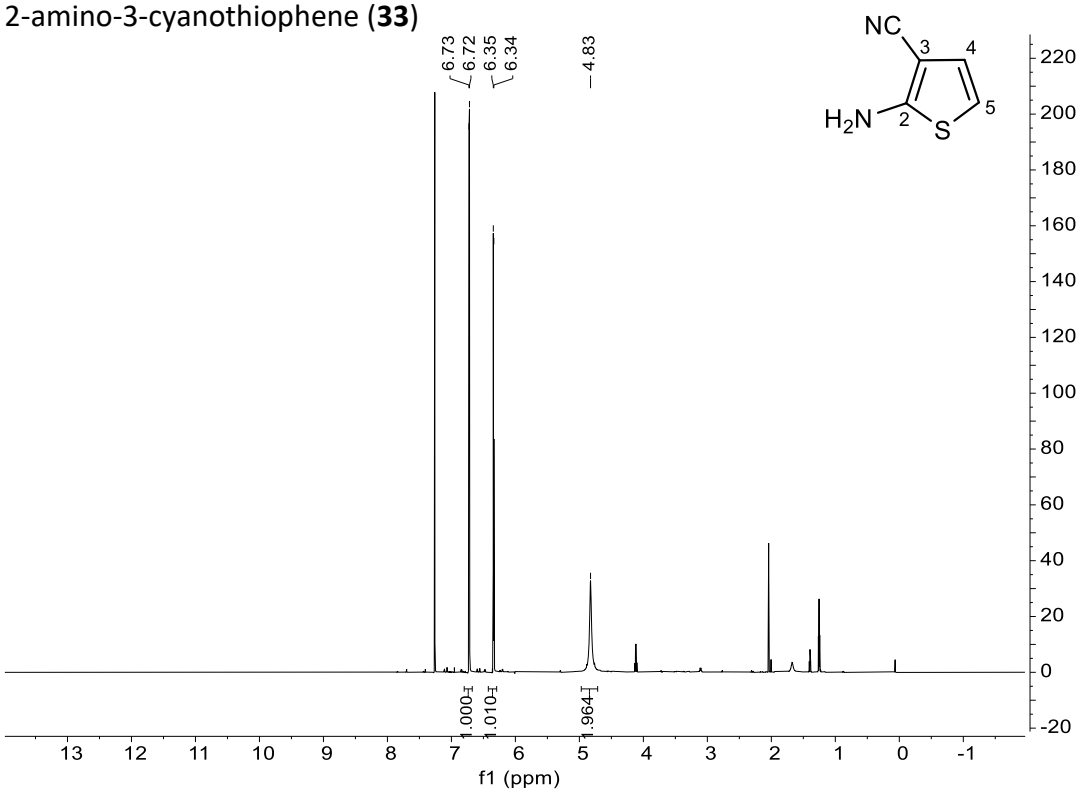

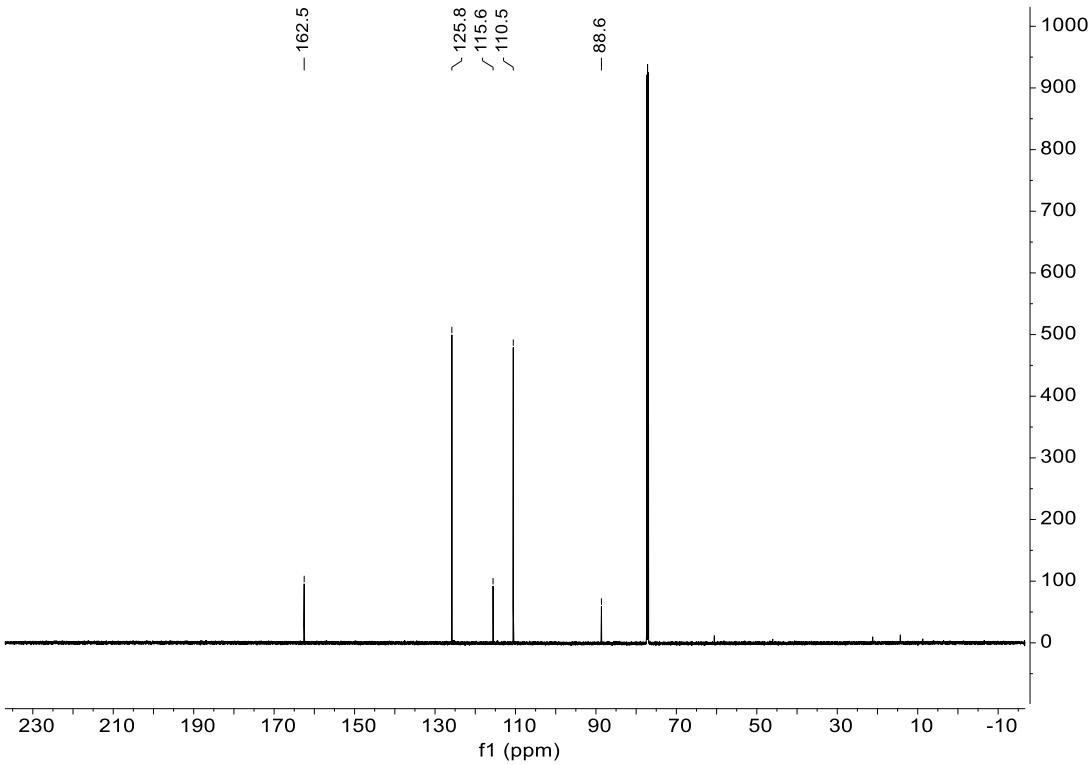

N-(3-cyanothiophen-2-yl)-5’-nitrothiophene-2’-carboxamide (**36**)

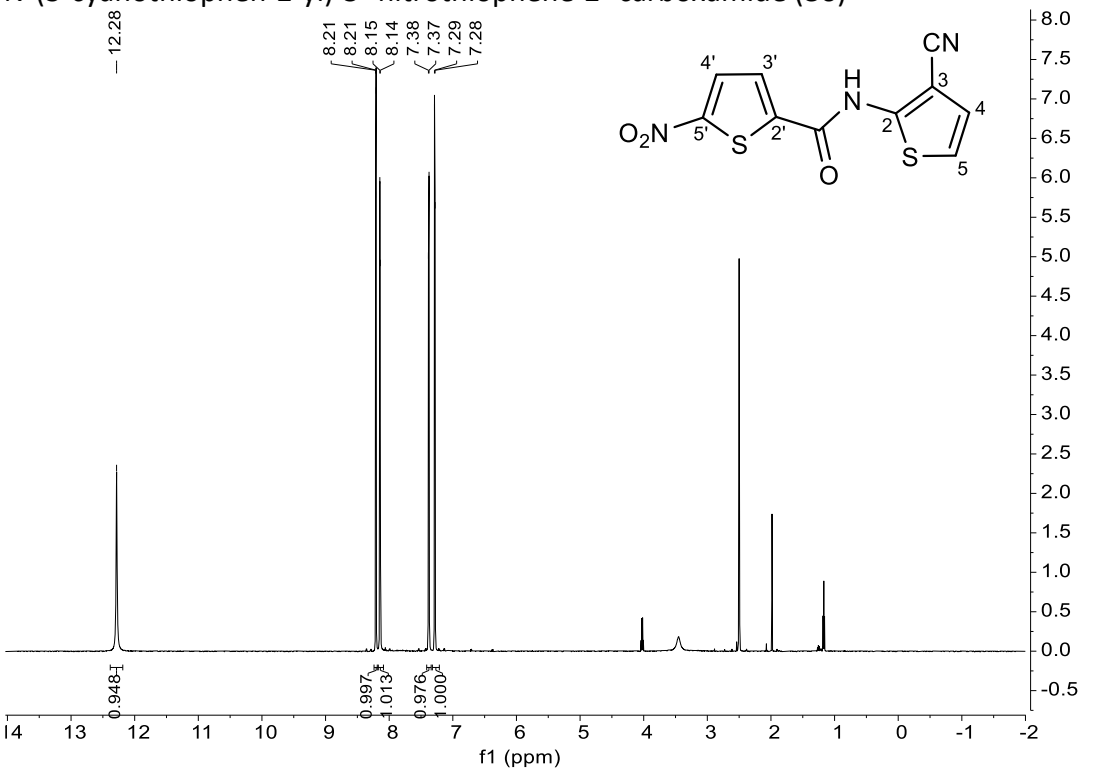

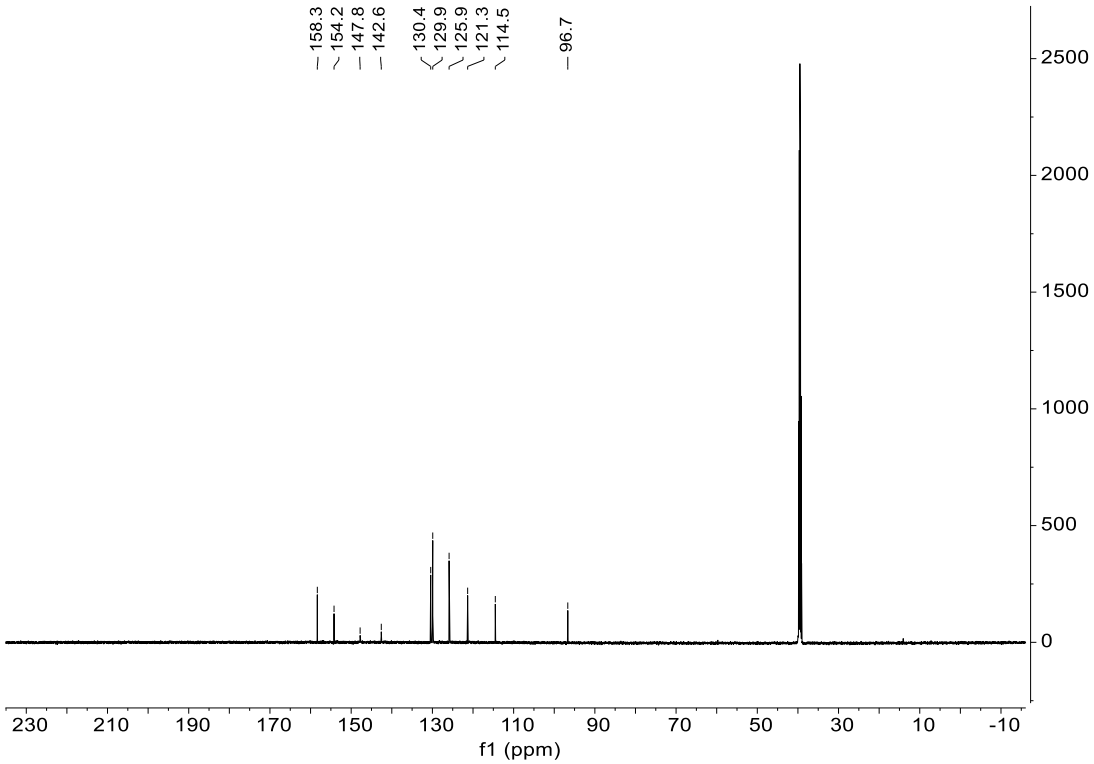

N-(3-carbamoylthiophen-2-yl)-5’-nitrothiophene-2’-carboxamide (**16**)

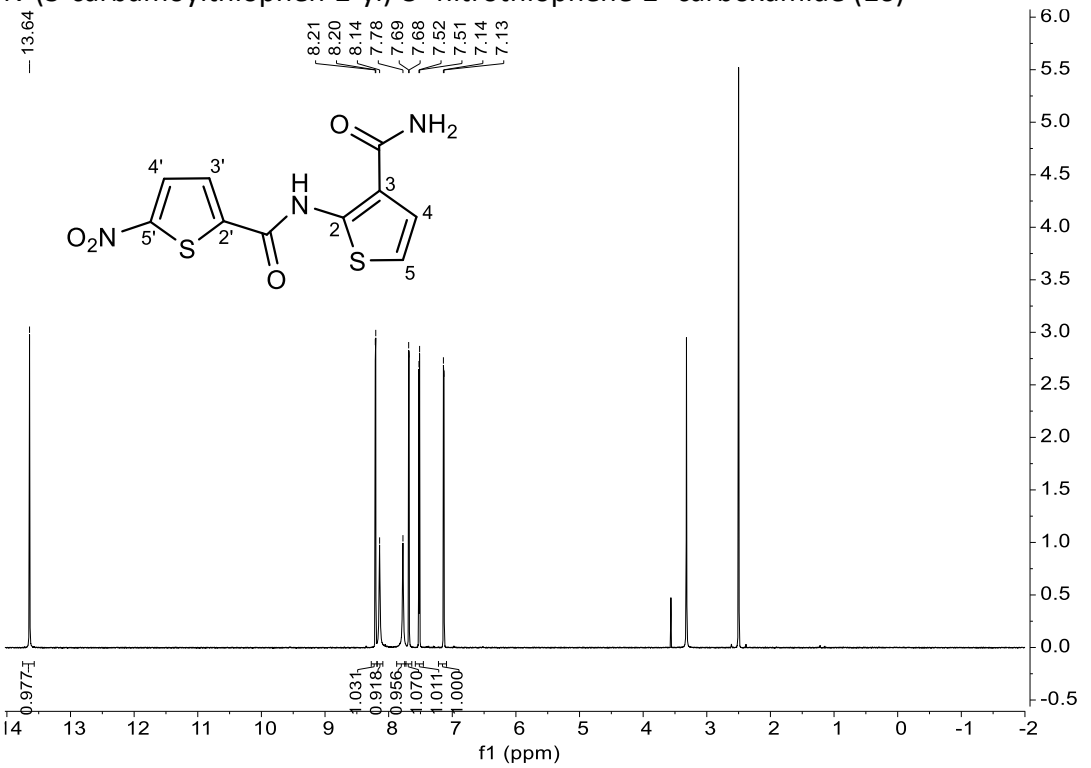

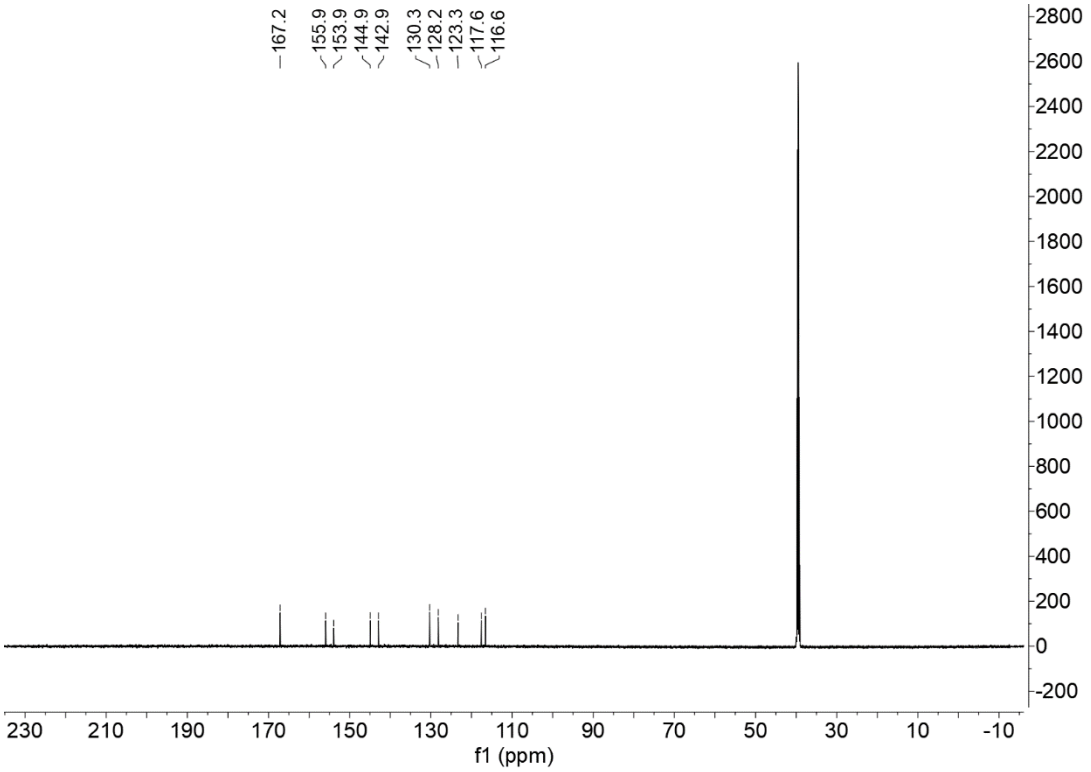

2-cyano-*N*-methylacetamide (**25**)

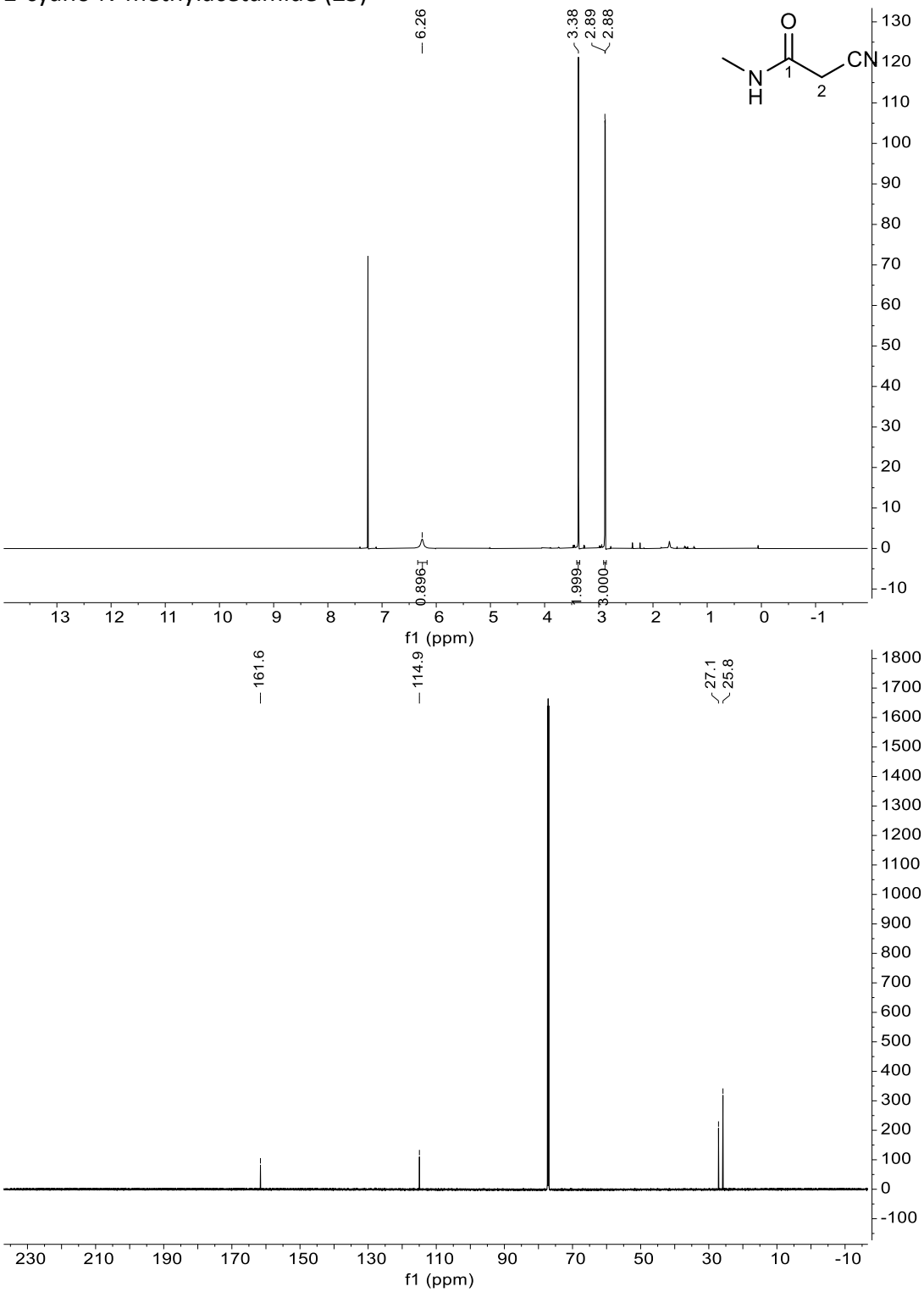

2-amino-*N*-methylthiophene-3-carboxamide (**30**)

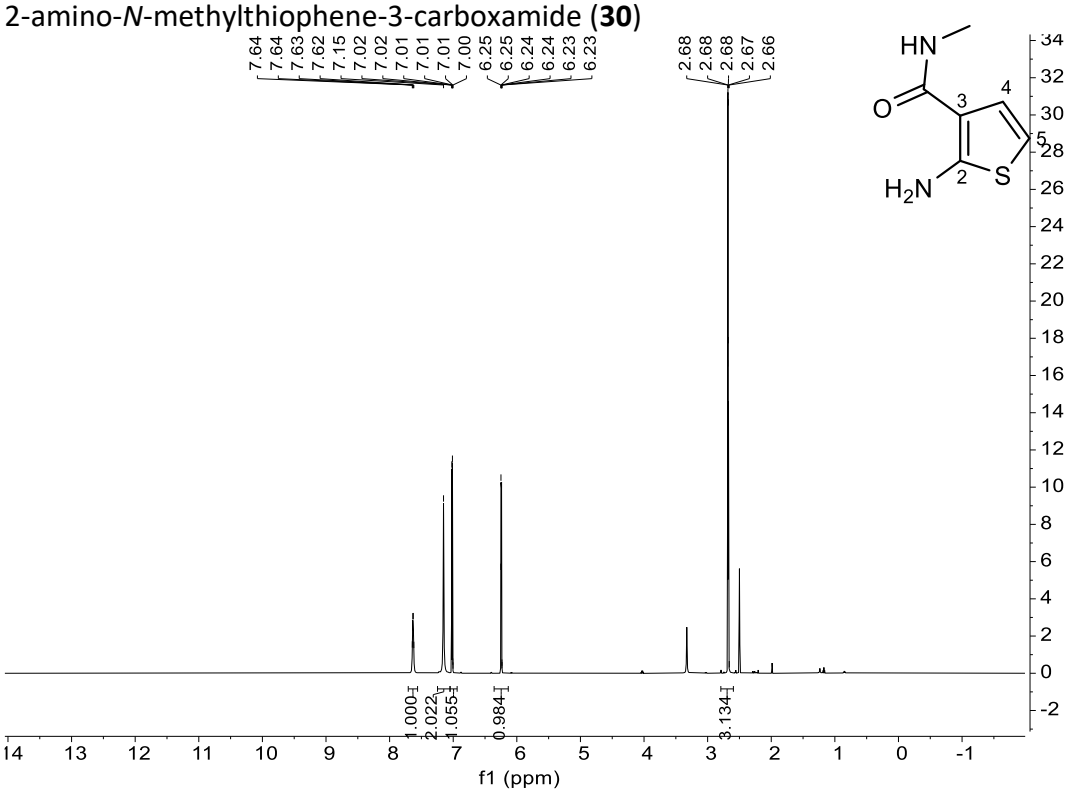

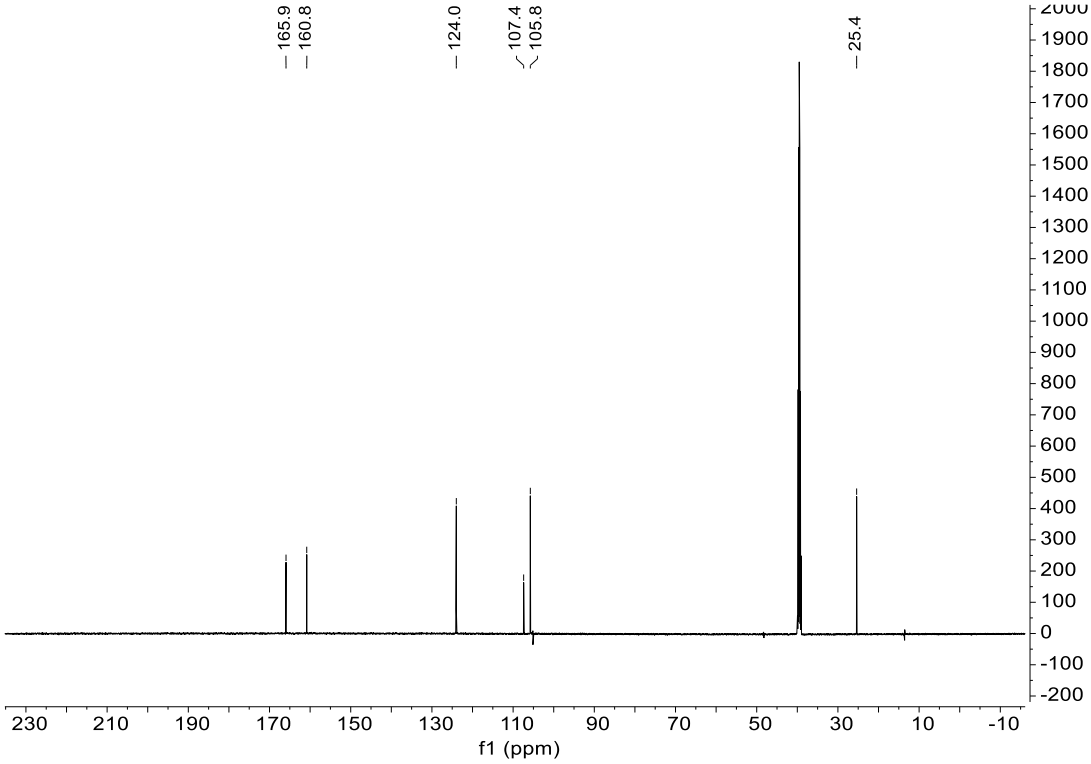

N-methyl-2-(5’-nitrothiophene-2’-amido)thiophene-3-carboxamide (**17**)

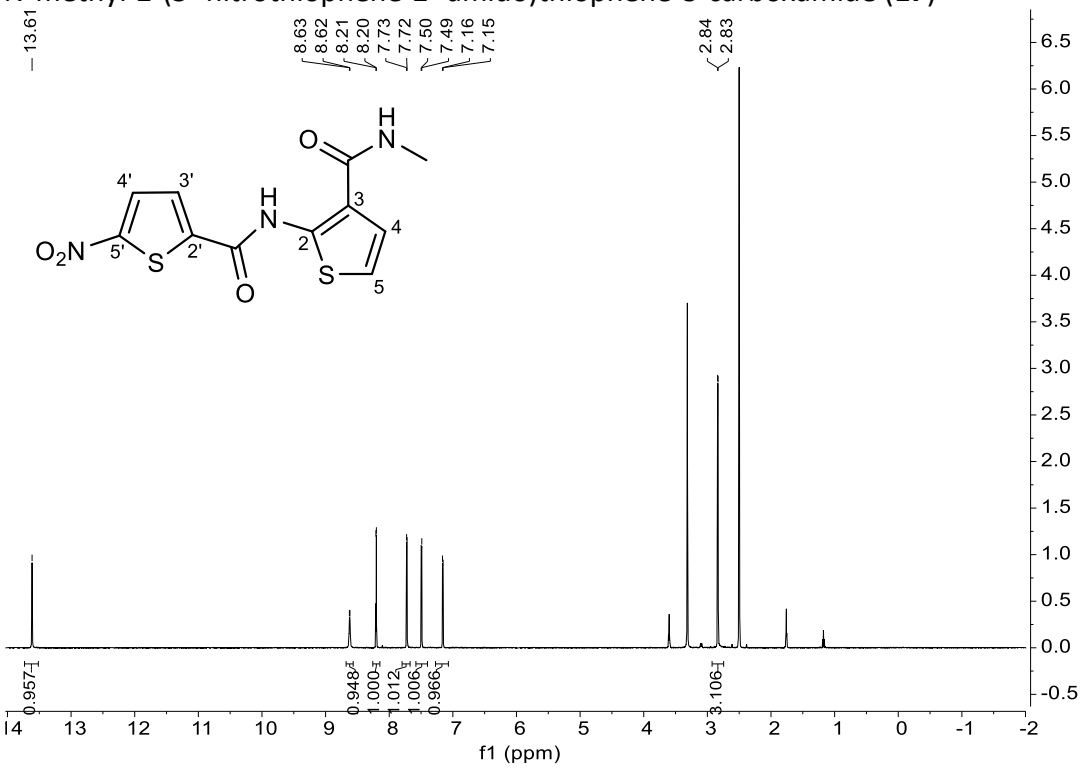

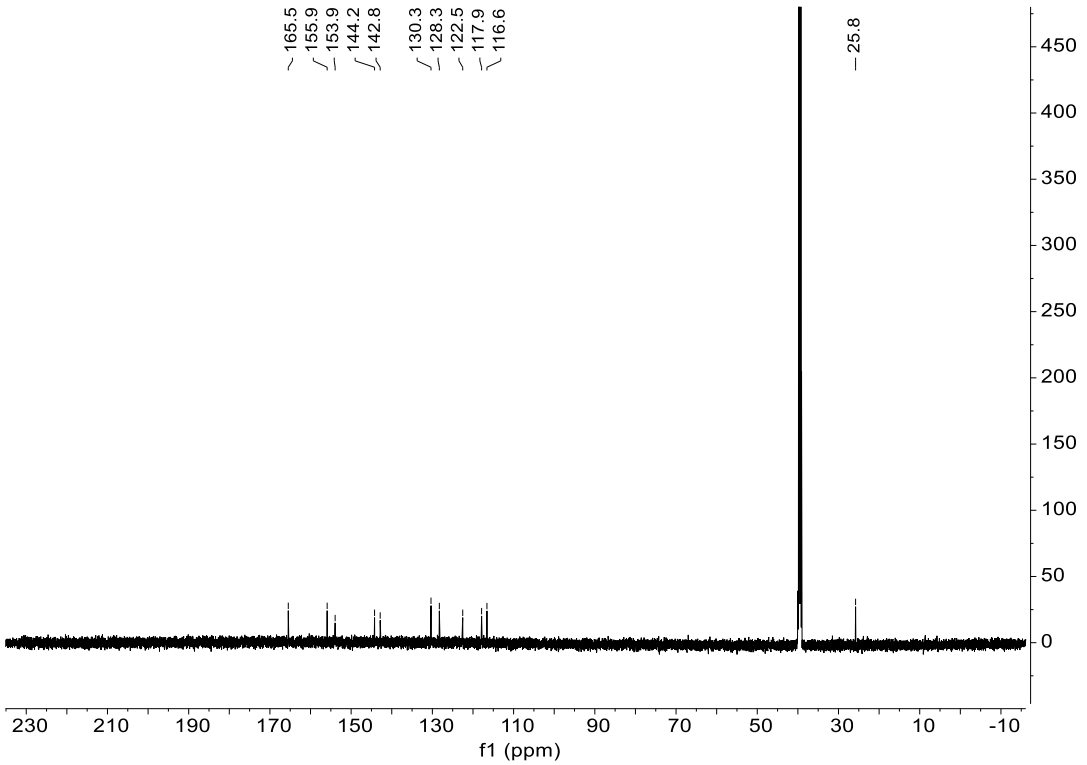

Methyl 2-aminothiophene-3-carboxylate (**31**)

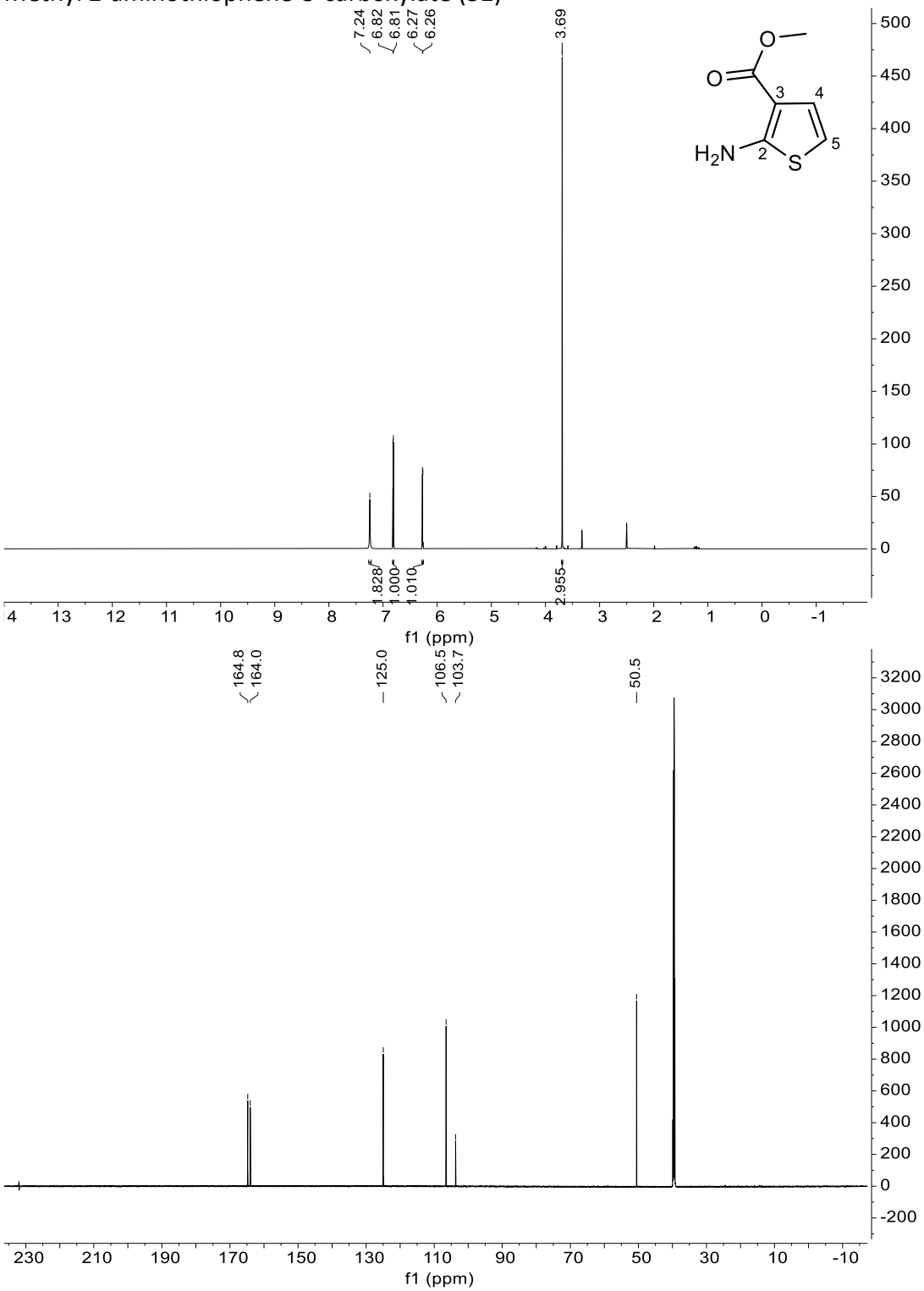

Methyl 2-(5’-nitrothiophene-2’-amido)thiophene-3-carboxylate (**34**)

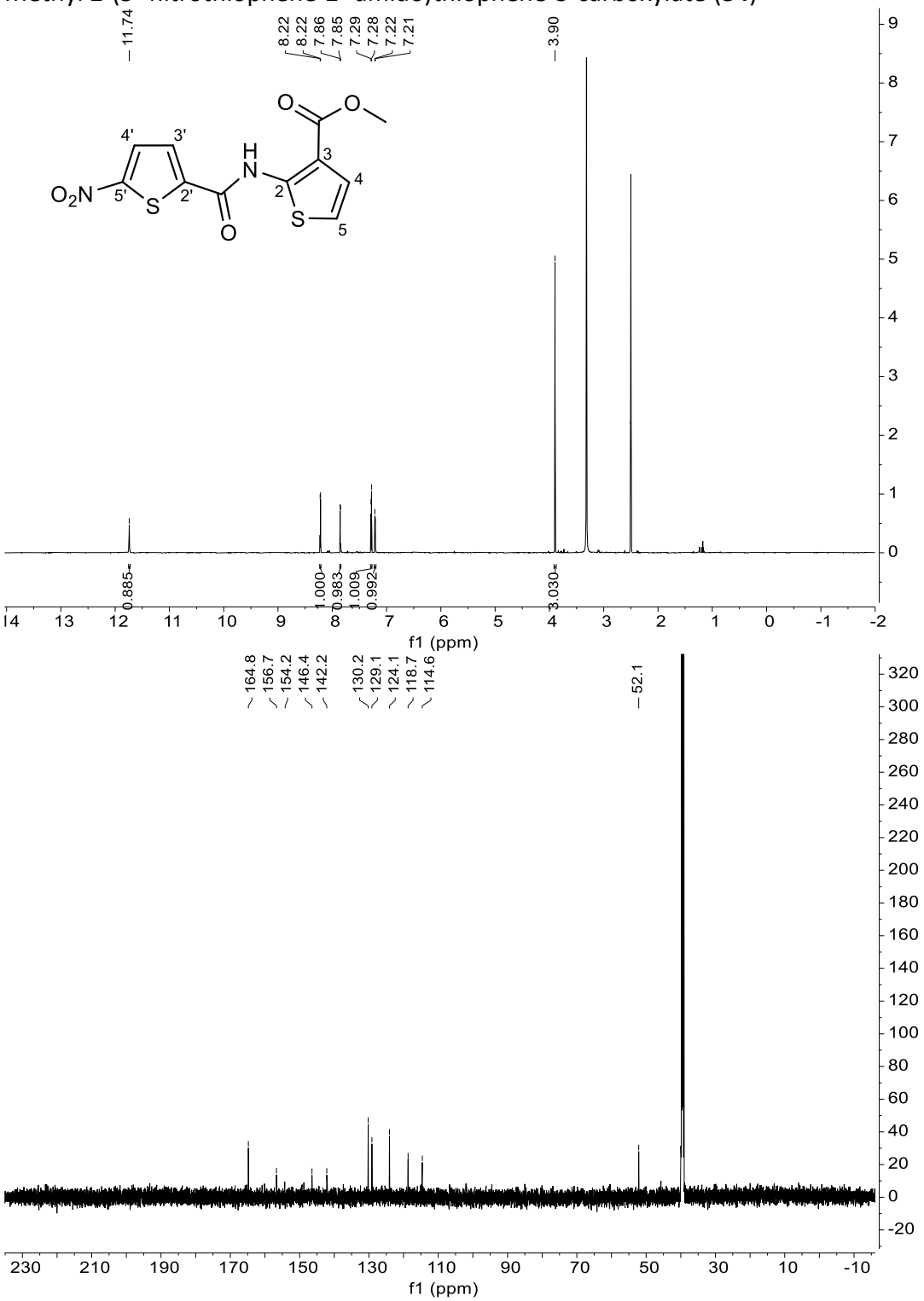

2-aminothiophene-3-ethanoate (**32**)

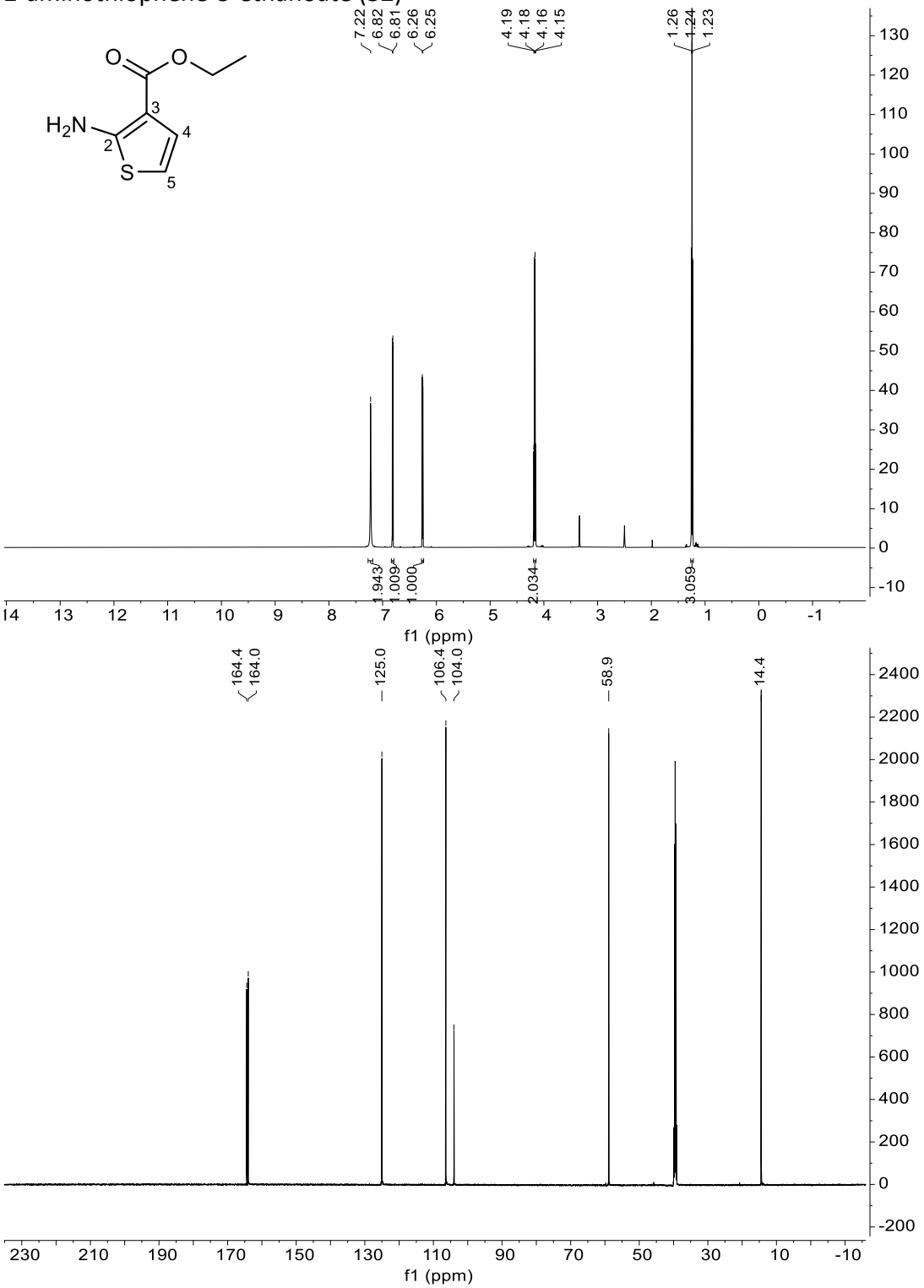

Ethyl 2-(5’-nitrothiophene-2’-amido)thiophene-3-carboxylate (**35**)

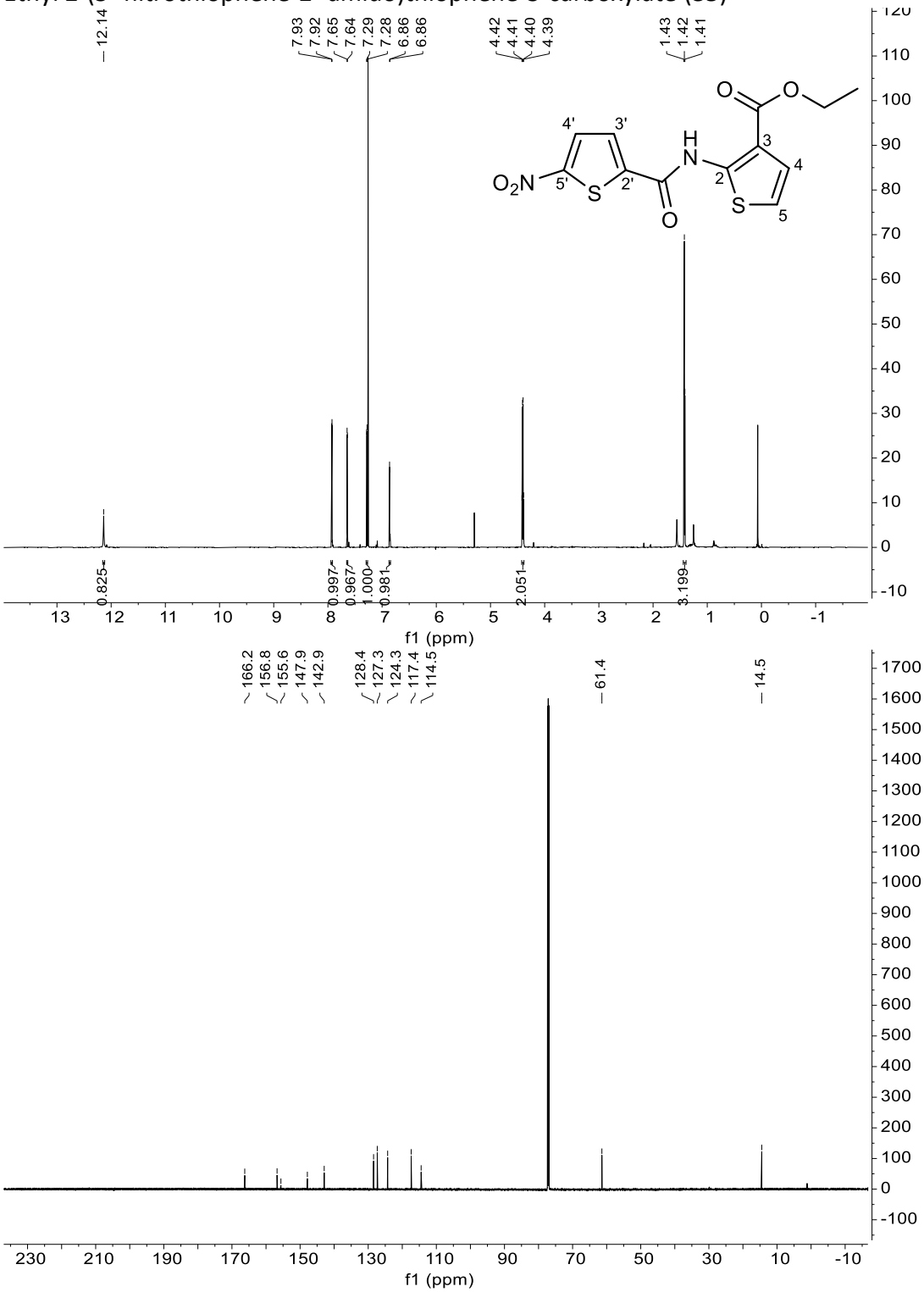

N-methyl-2-(thiophene-2’-amido)thiophene-3-carboxamide (**107**)

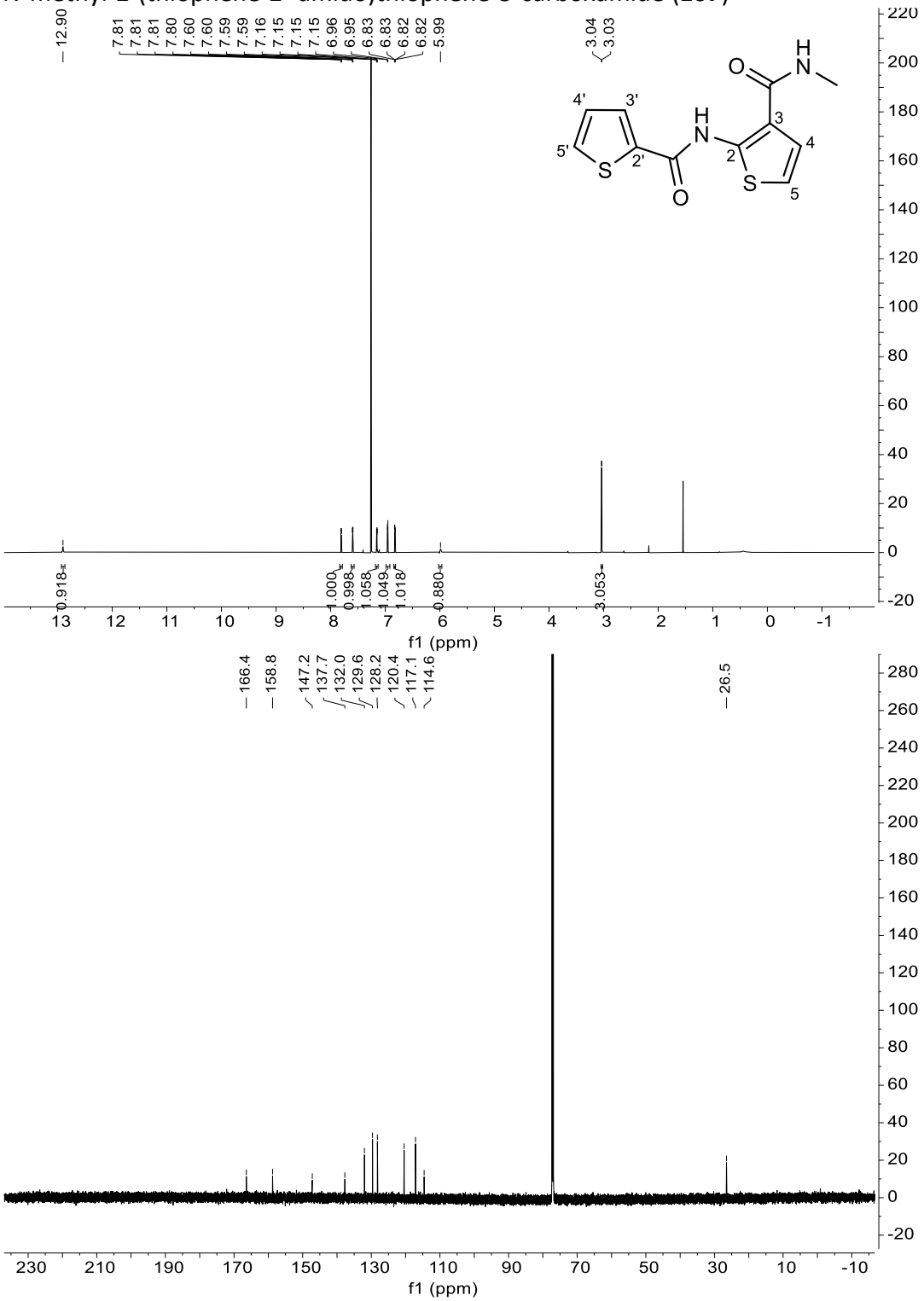

5-bromothiophene-2-carbonyl chloride (**95**)

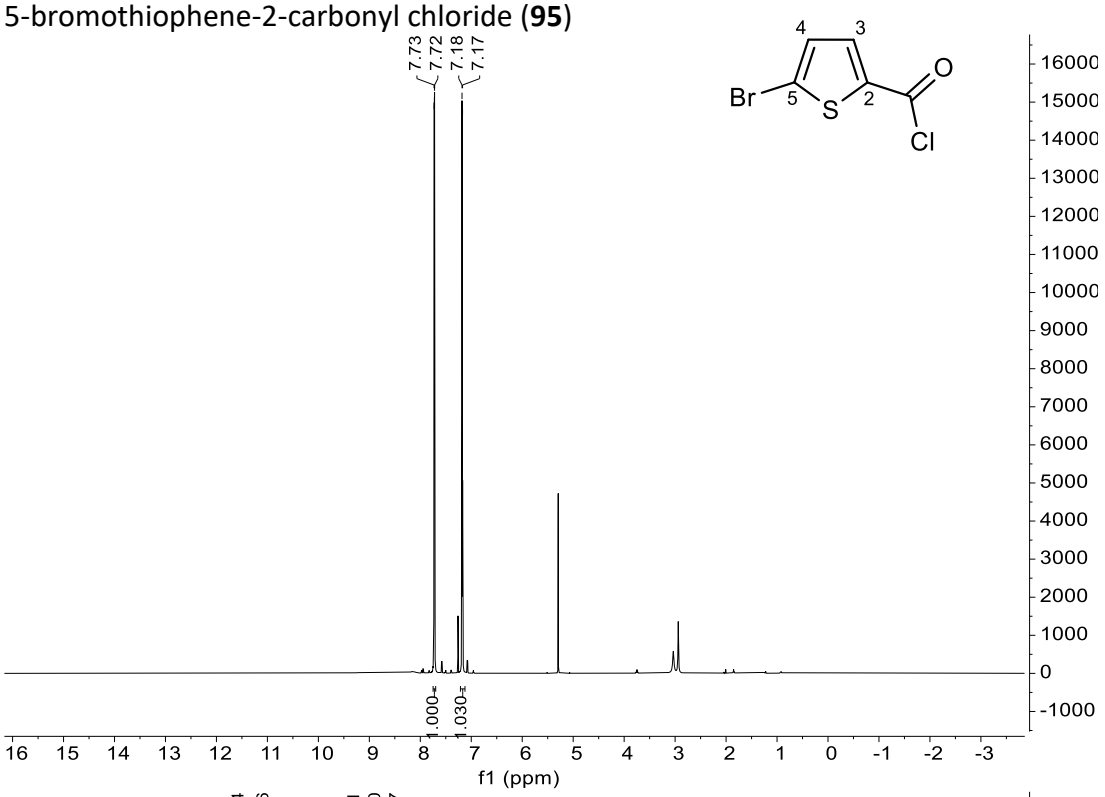

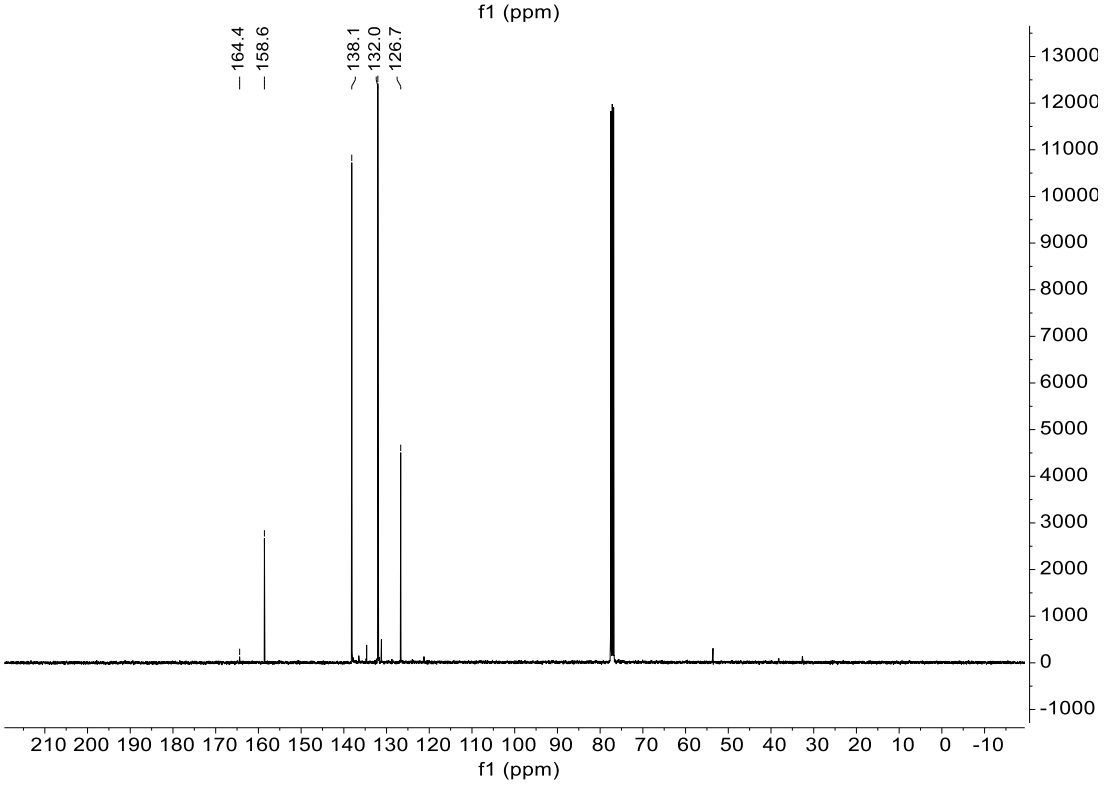

5’-bromo-*N*-[3-(methylcarbamoyl)thiophen-2-yl]thiophene-2’-carboxamide (**108**)

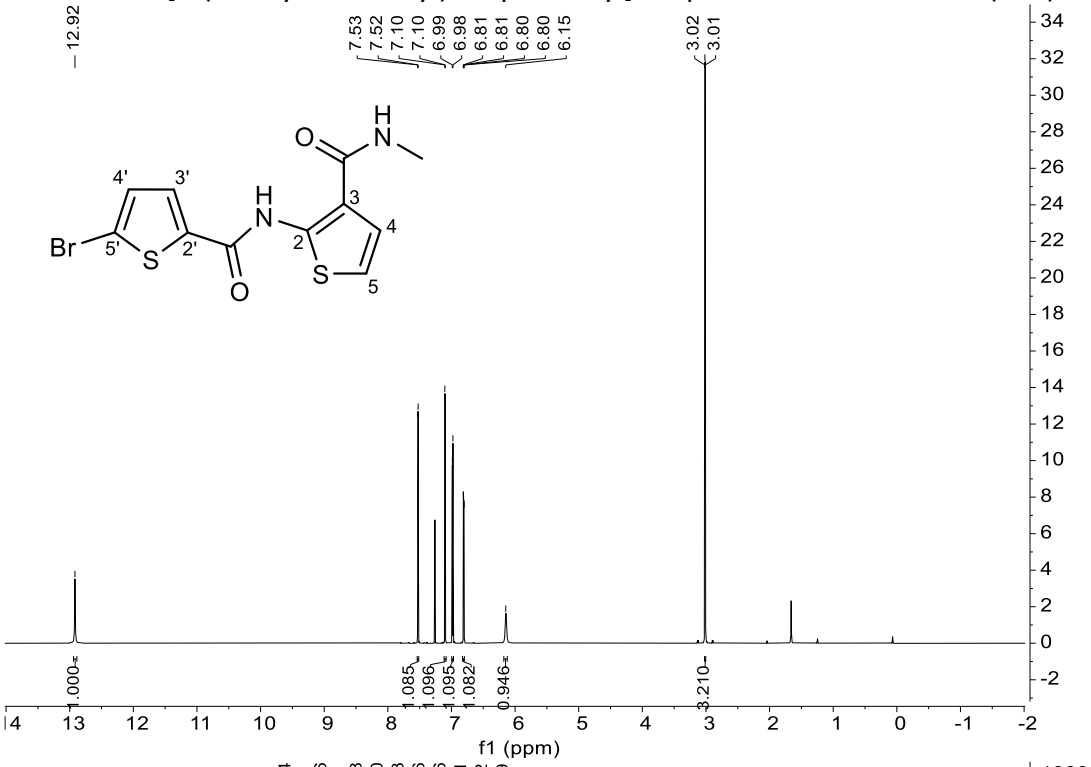

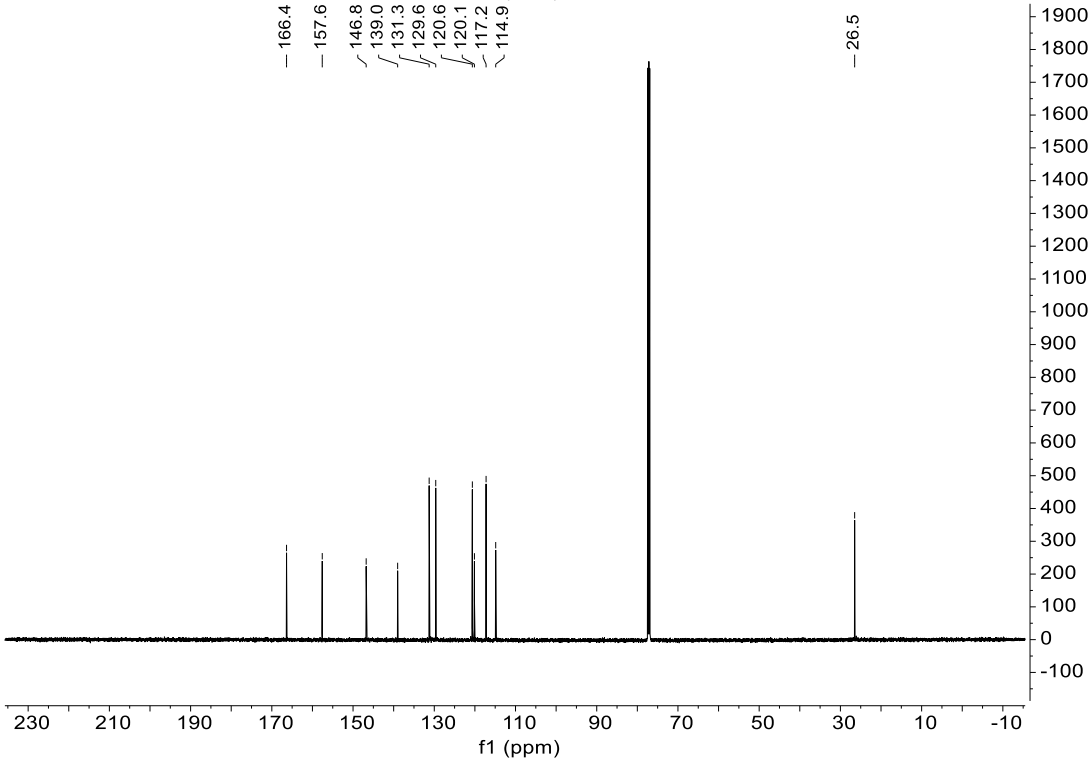

5-nitrofuran-2-carbonyl chloride (**96**)

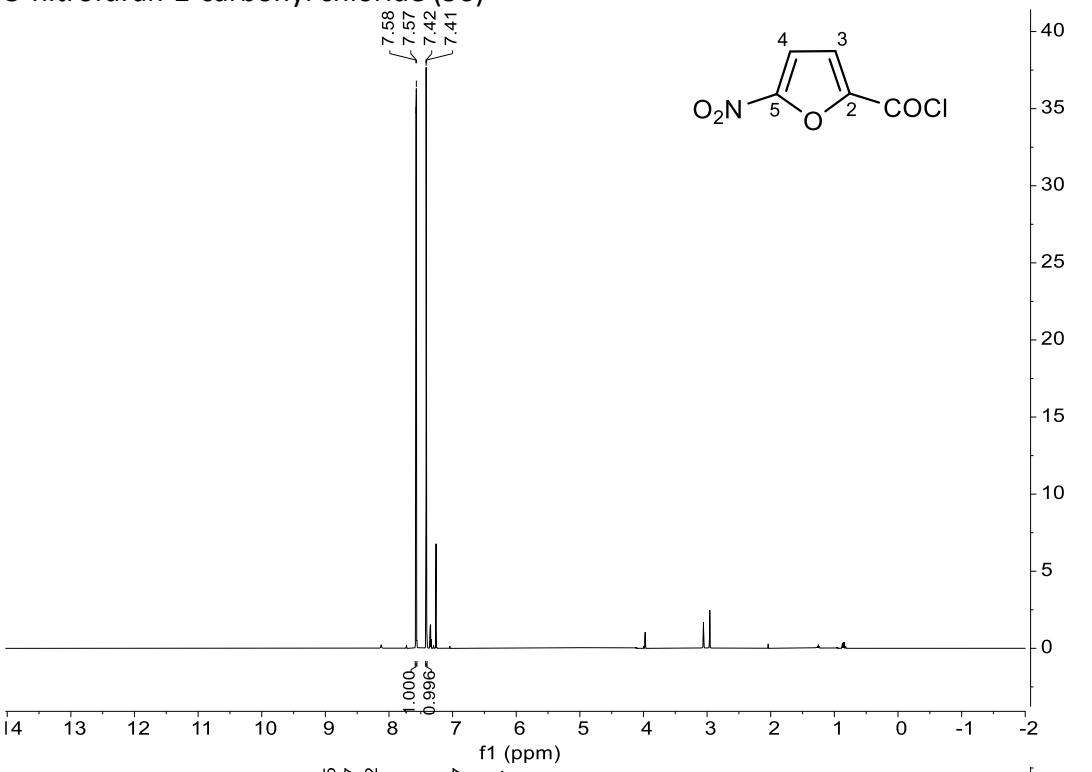

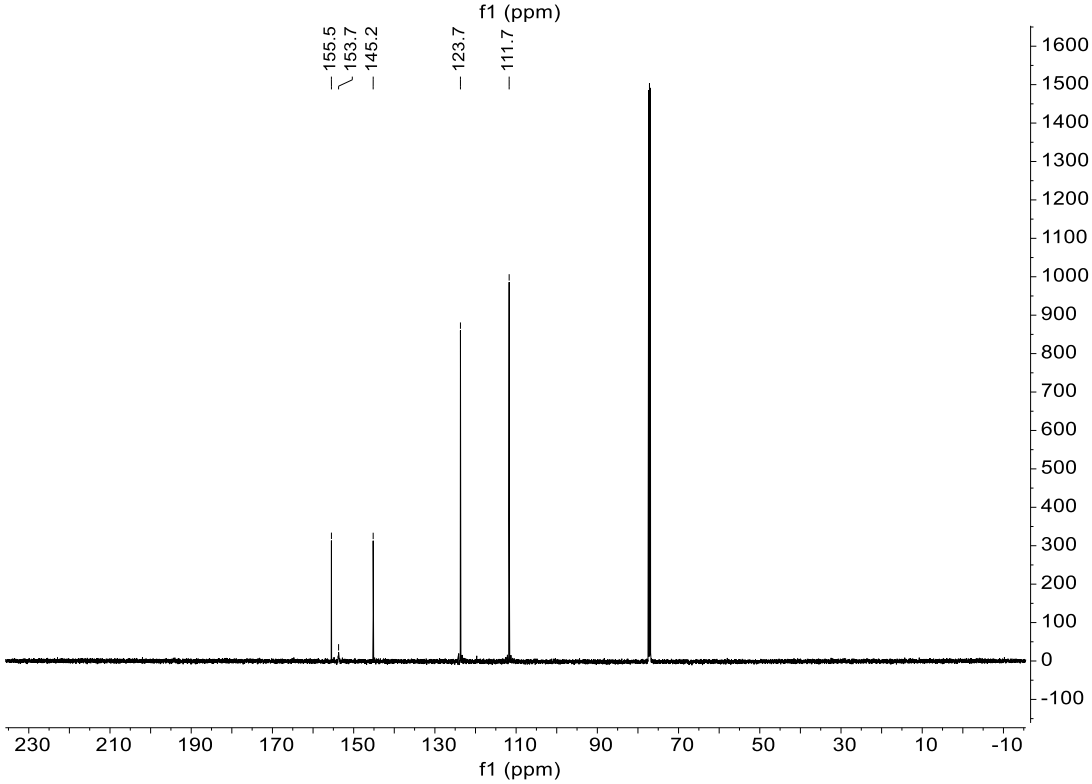

N-[3-(methylcarbamoyl)thiophen-2-yl]-5’-nitrofuran-2’-carboxamide (**109**)

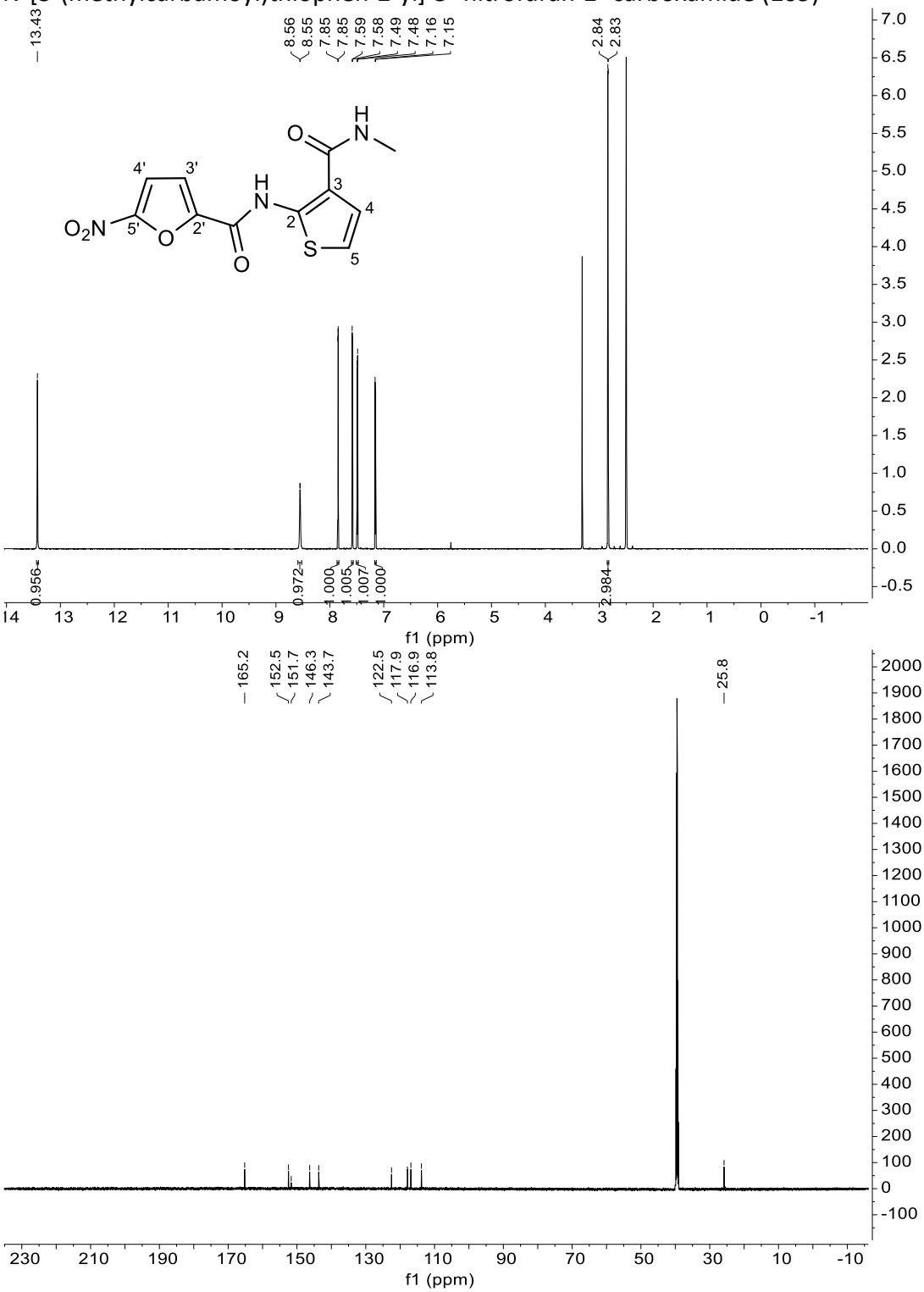

4-nitro-2-(trifluoromethyl)benzoyl chloride (**97**)

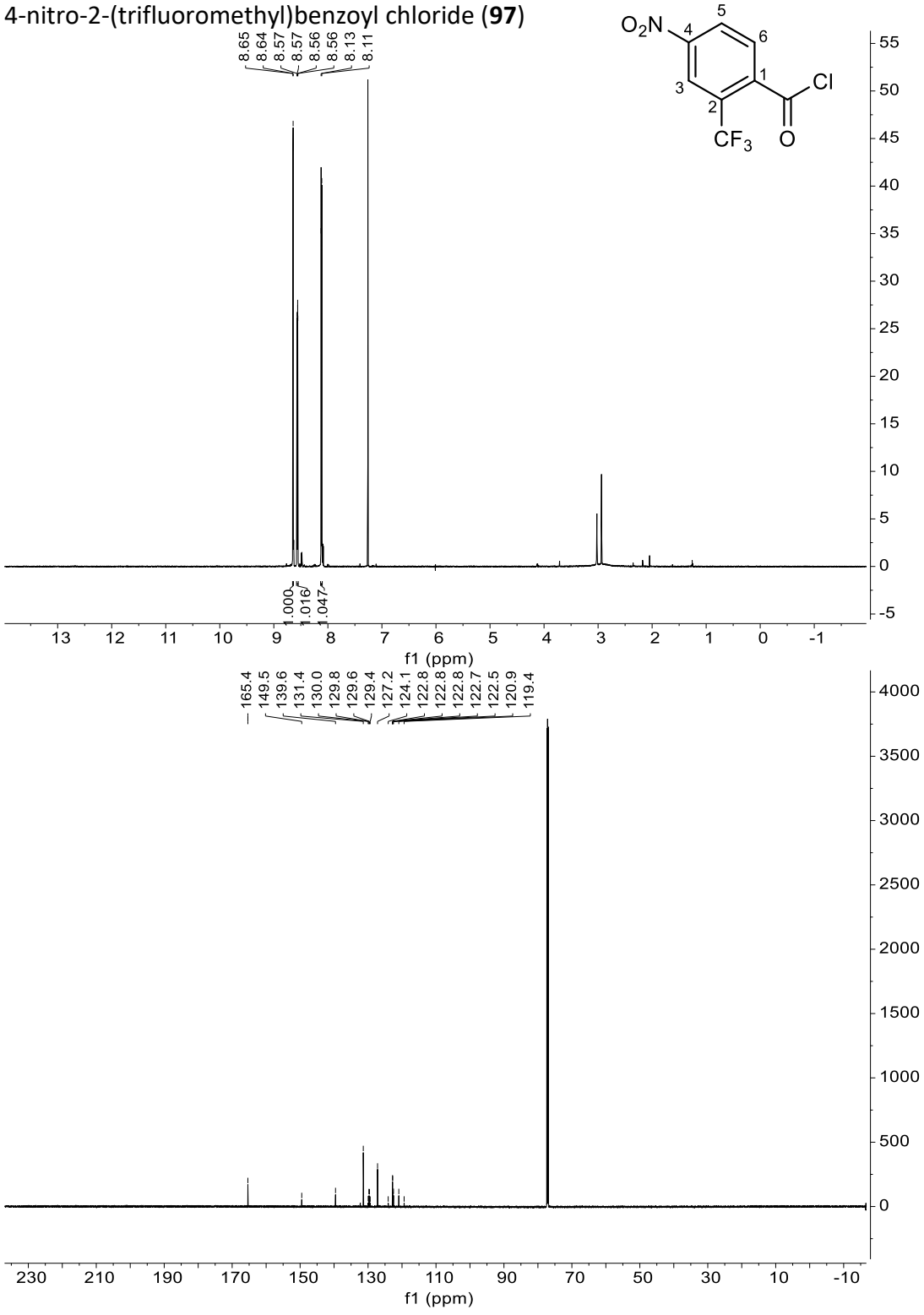

N-methyl-2-[4’-nitro-2’-(trifluoromethyl)benzamido]thiophene-3-carboxamide (**110**)

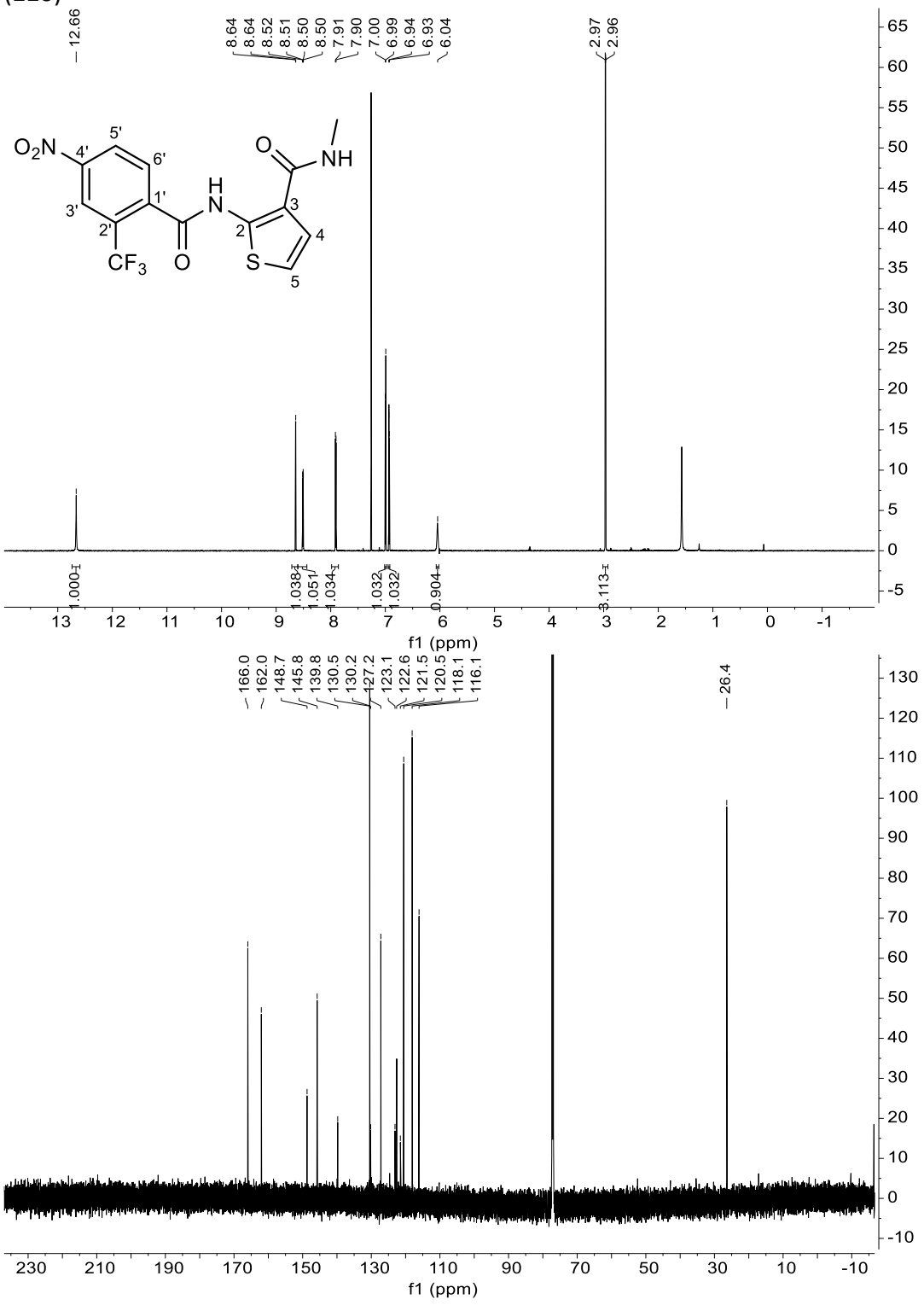

N-[3-(methylcarbamoyl)thiophen-2-yl]-1’,3’-thiazole-2’-carboxamide (**111**)

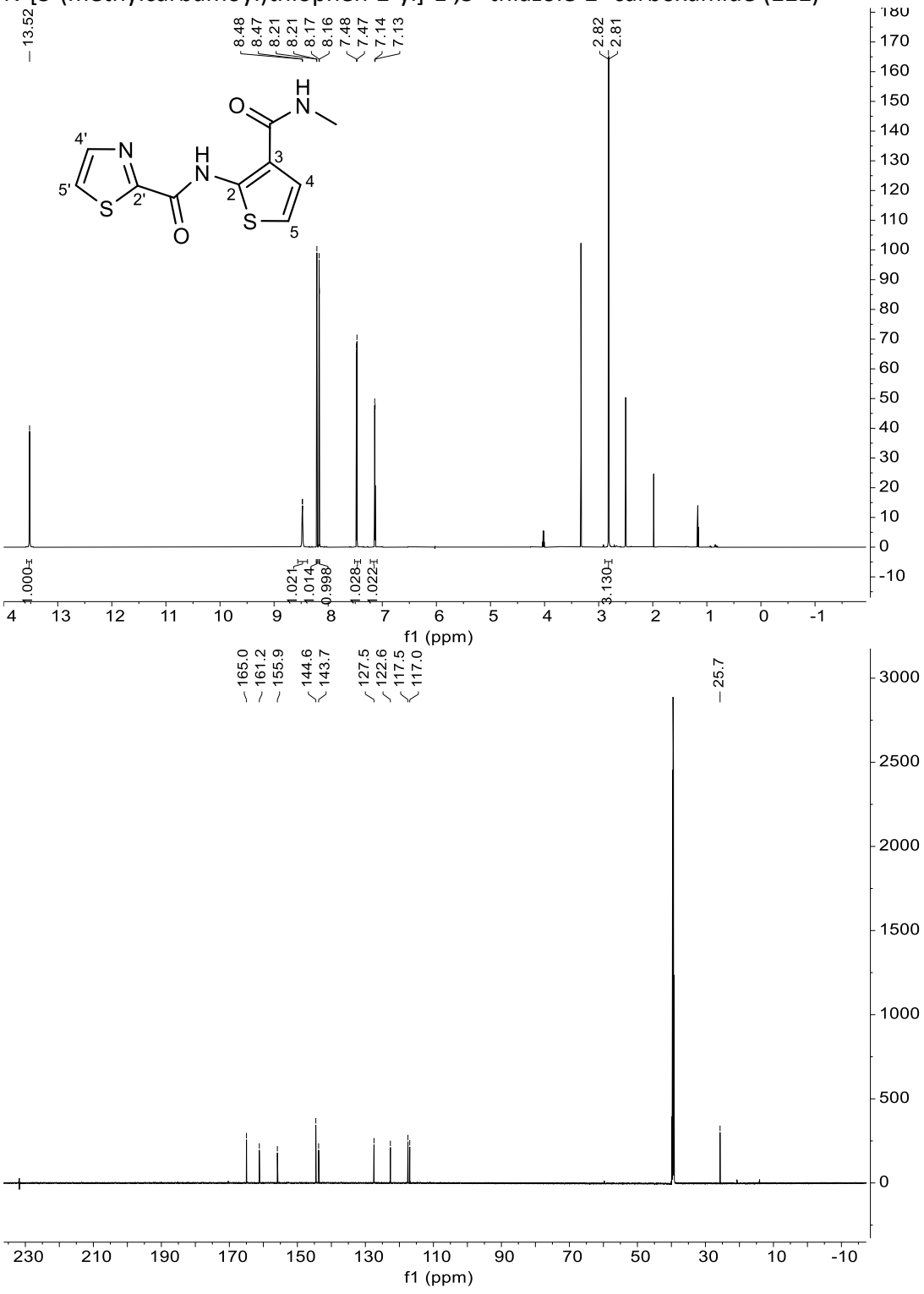

N-[3-(methylcarbamoyl)thiophen-2-yl]-1’,3’-thiazole-5’-carboxamide (**112**)

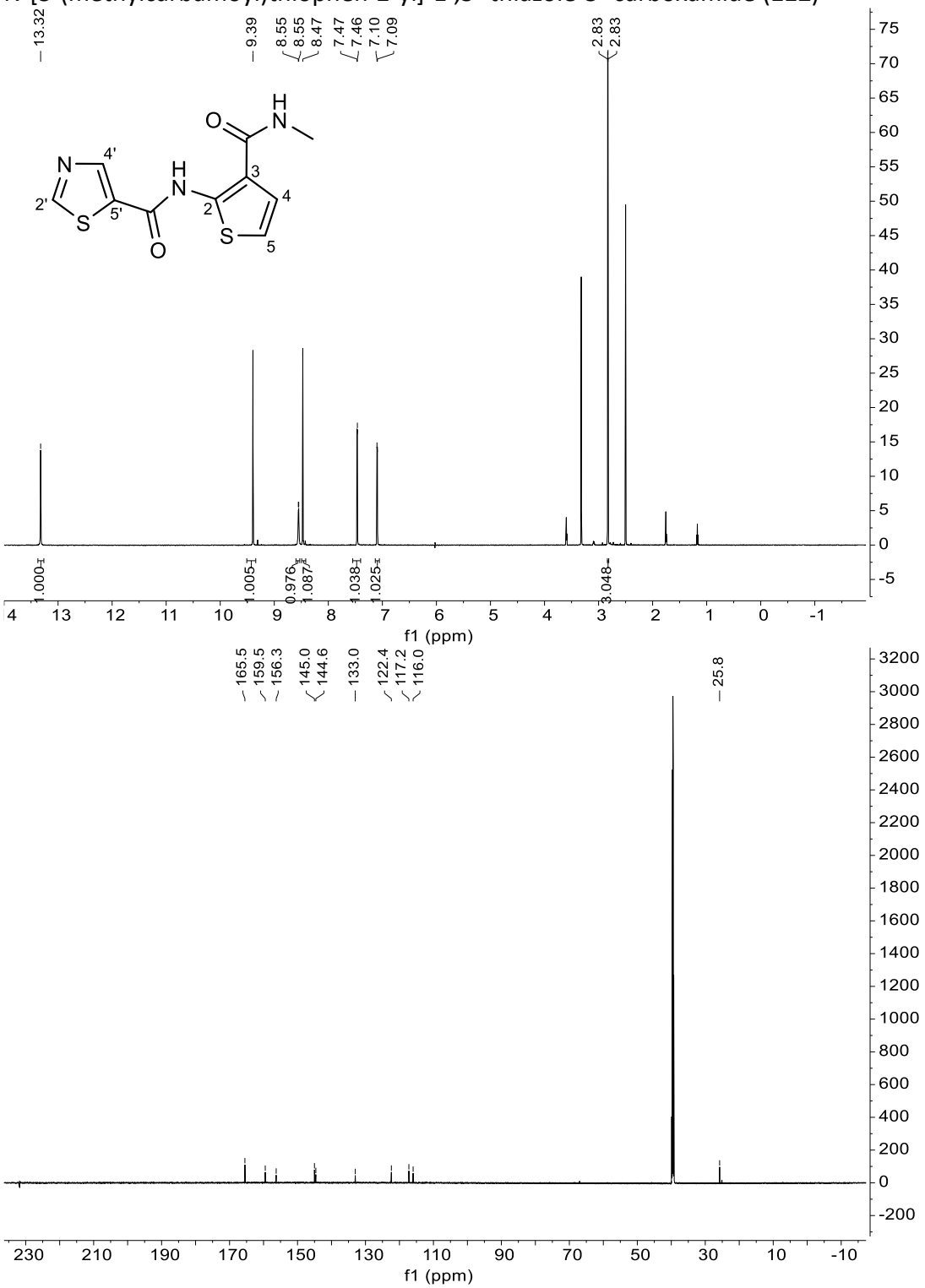

N-[3-(methylcarbamoyl)thiophen-2-yl]-1’,3’-thiazole-4’-carboxamide (**113**)

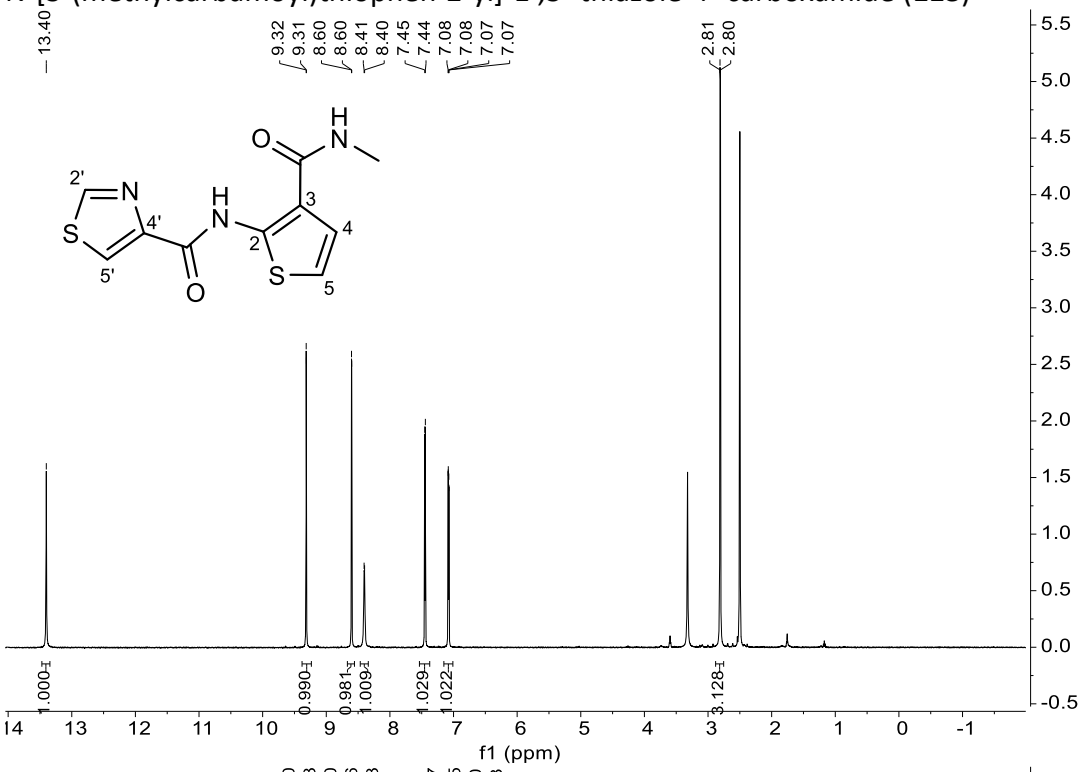

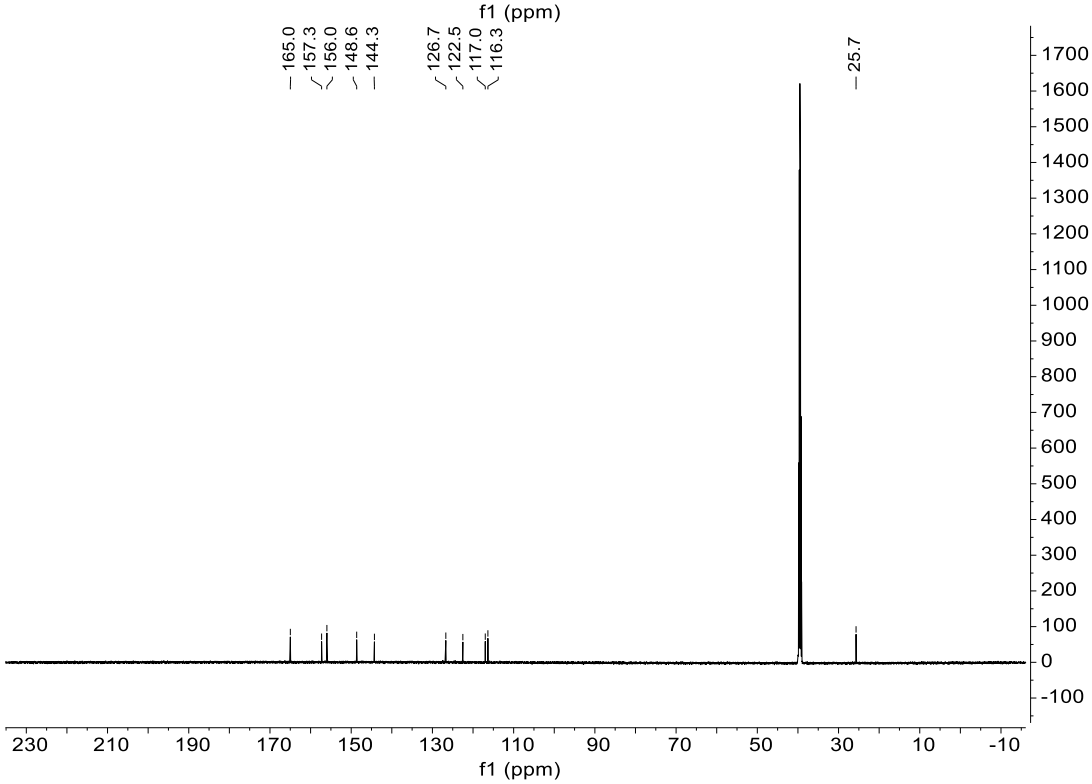

2,1,3-benzoxadiazole-5-carbonyl chloride (**101**)

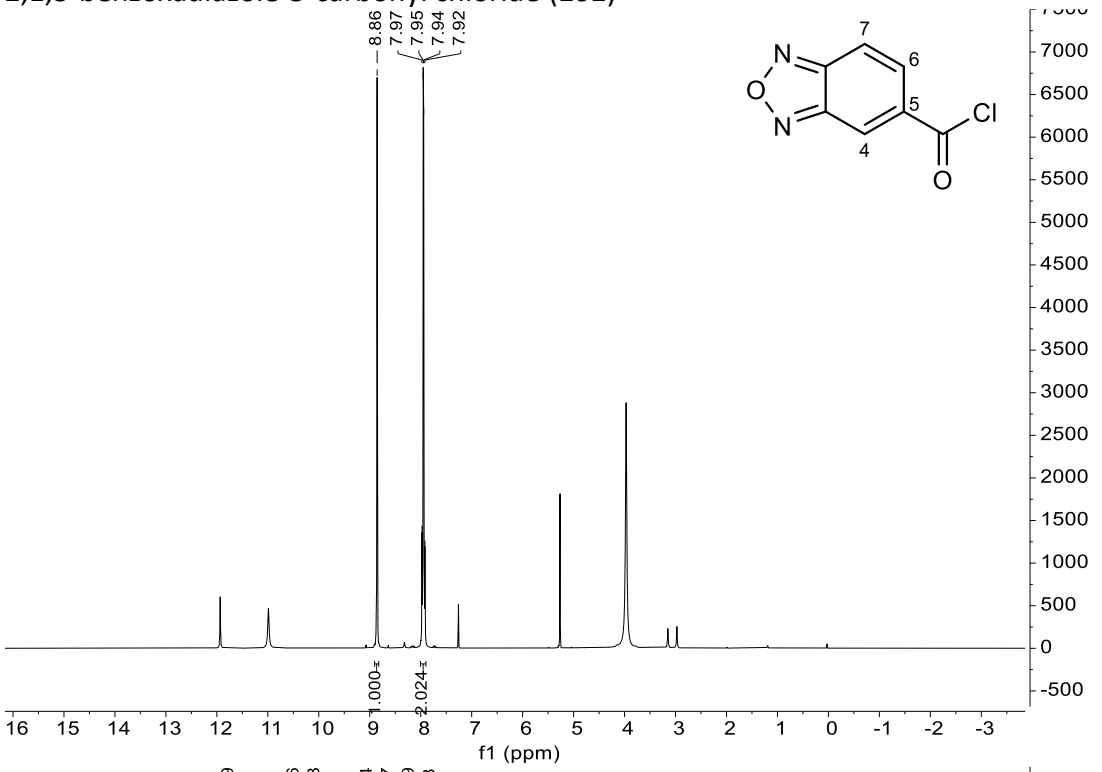

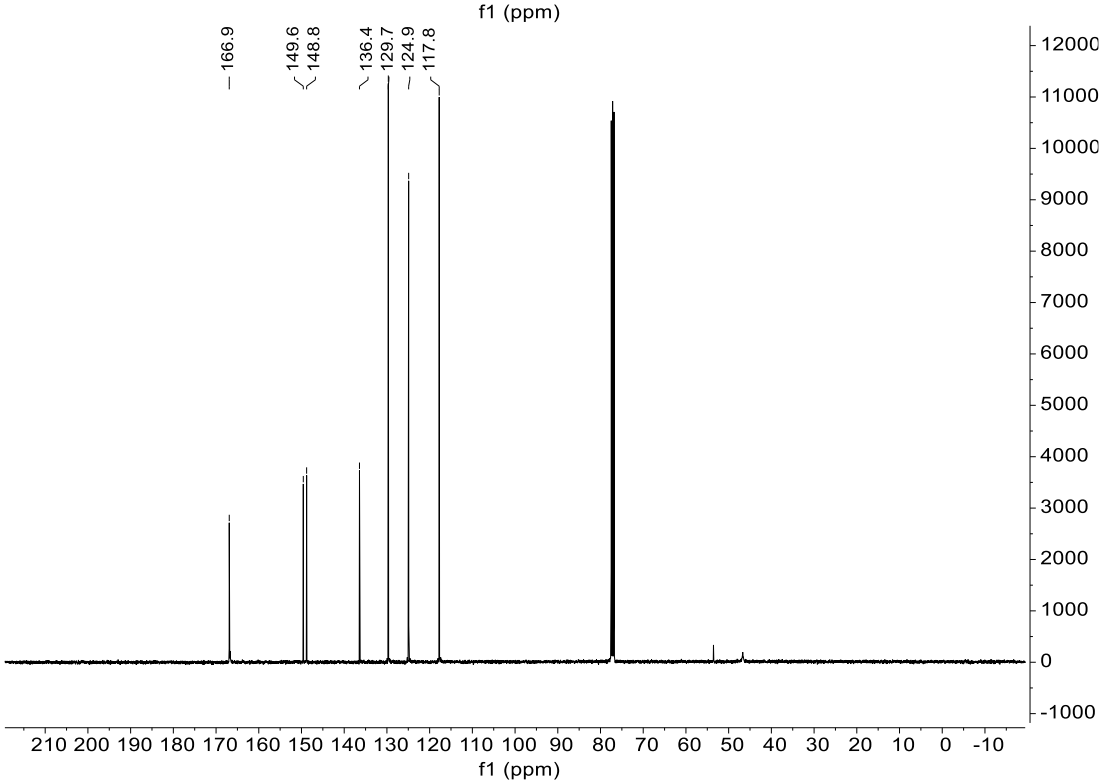

N-[3-(methylcarbamoyl)thiophen-2-yl]-2,1,3-benzoxadiazole-5’-carboxamide (**114**)

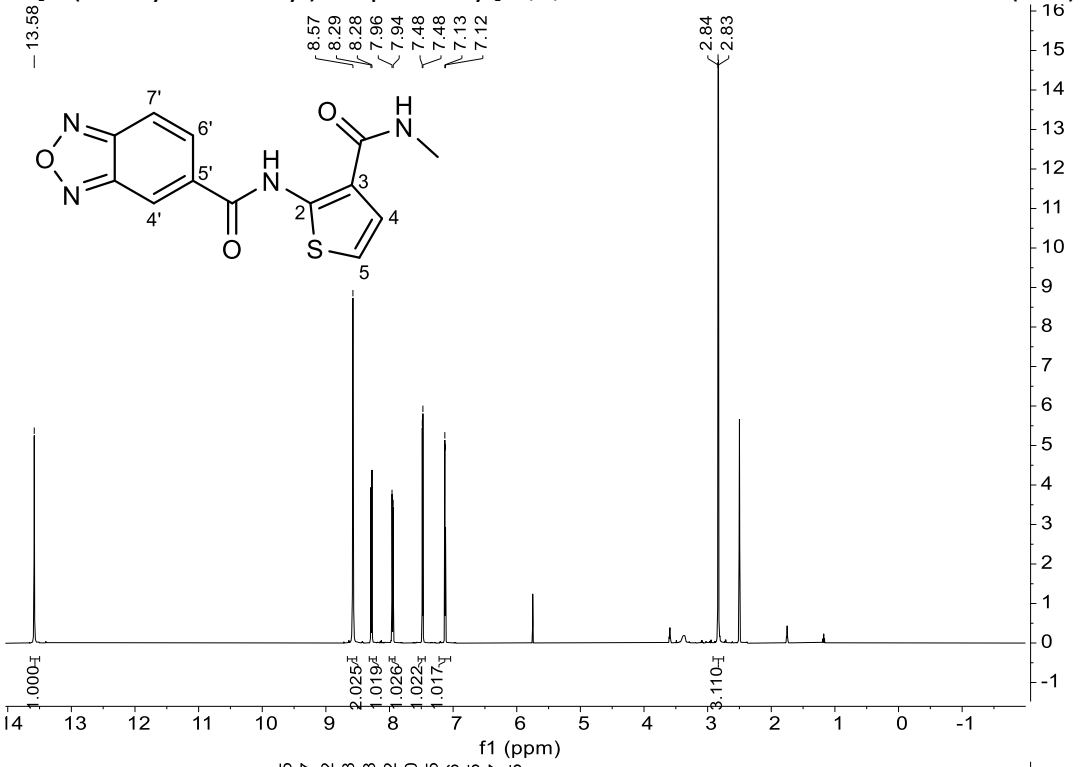

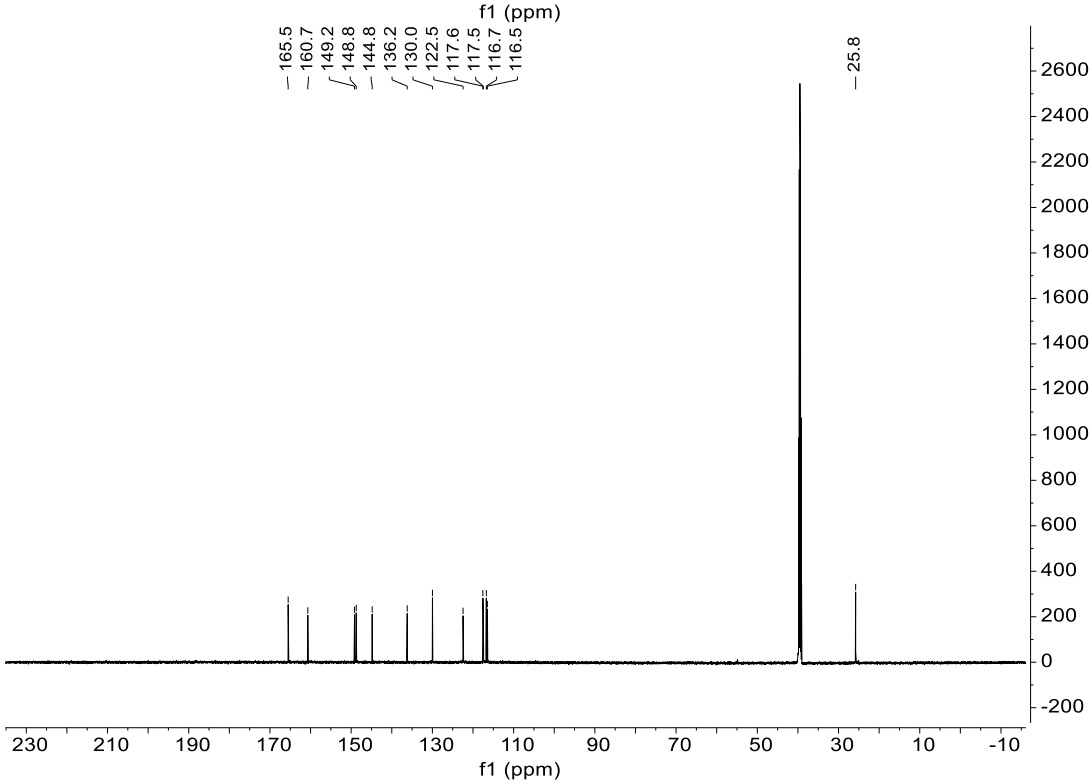

2-benzamido-*N*-methylthiophene-3-carboxamide (**115**)

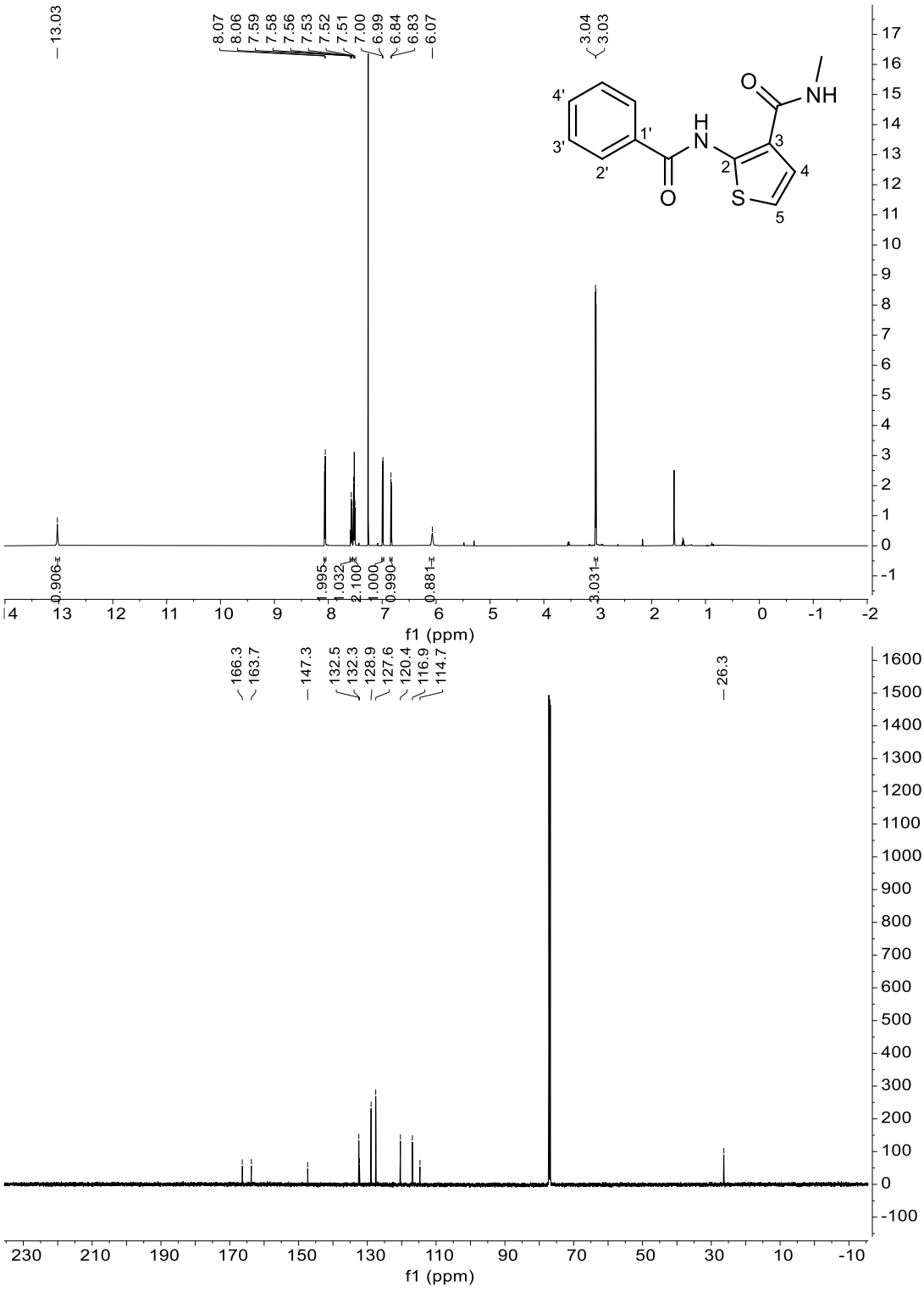

N-[3-(methylcarbamoyl)thiophen-2-yl]pyridine-4’-carboxamide (**116**)

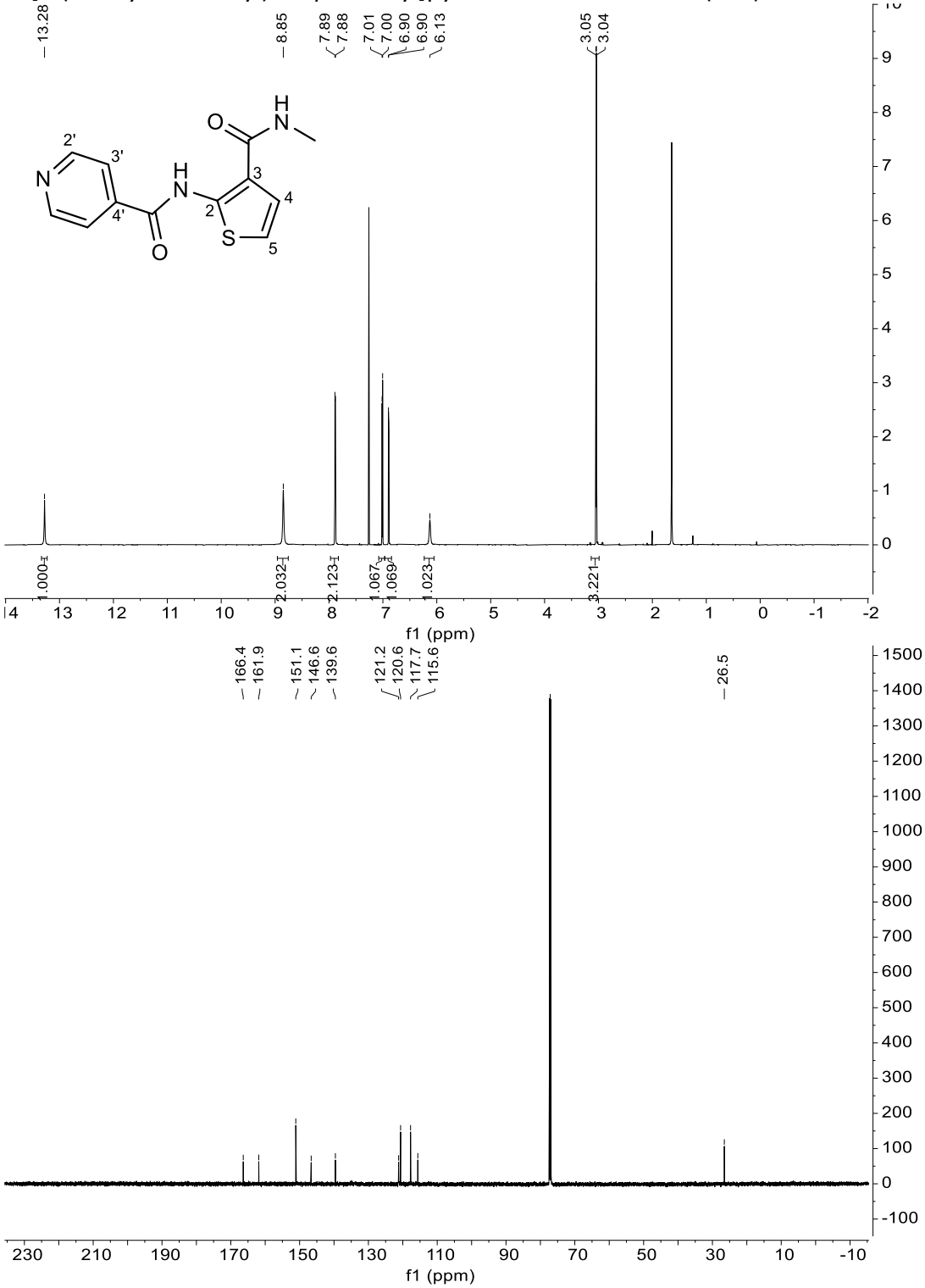

N-[3-(methylcarbamoyl)thiophen-2-yl]pyridine-3’-carboxamide (**117**)

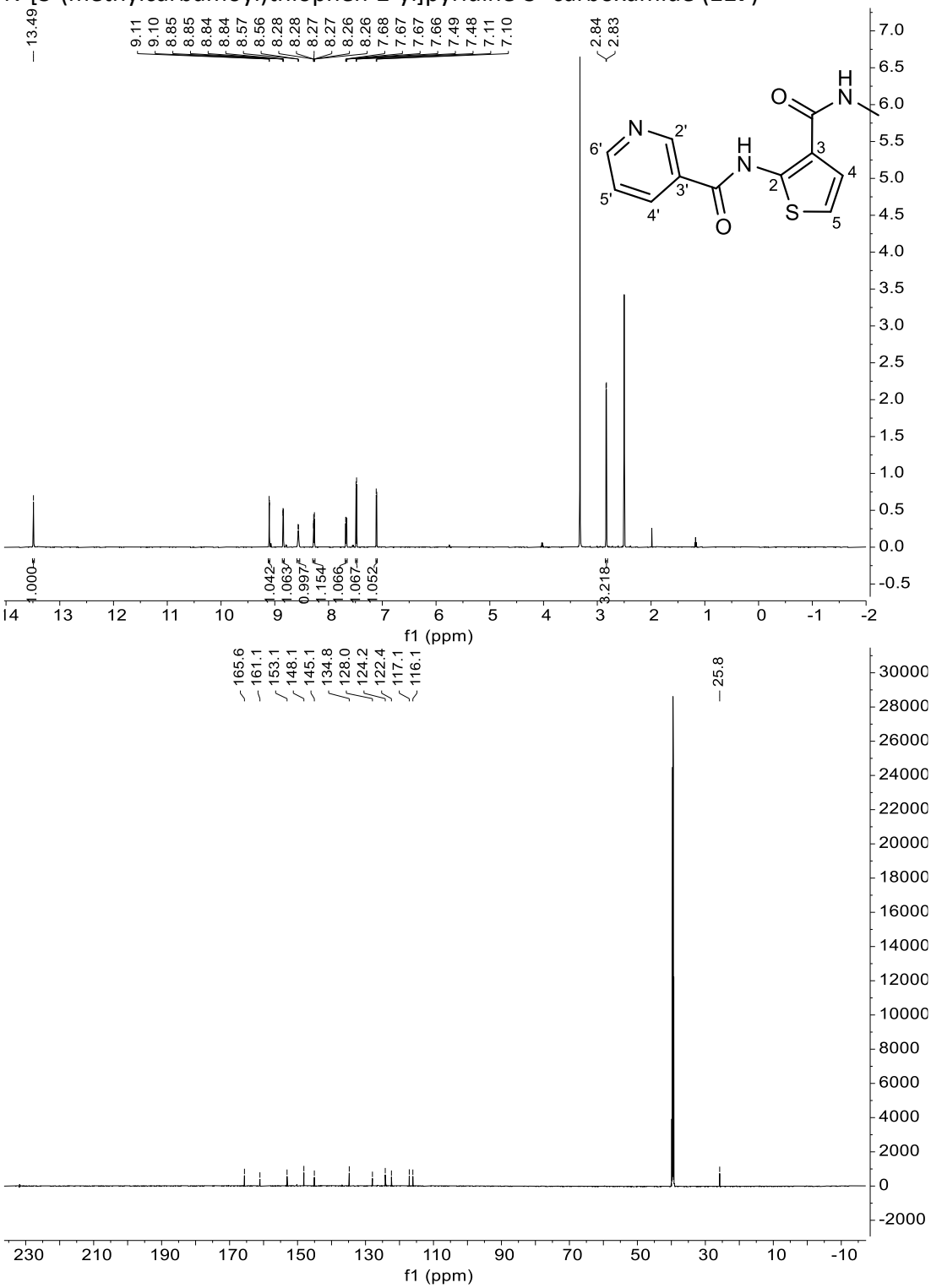

N-methyl 2-(4’-nitrobenzamido)thiophene-3-carboxamide (**118**)

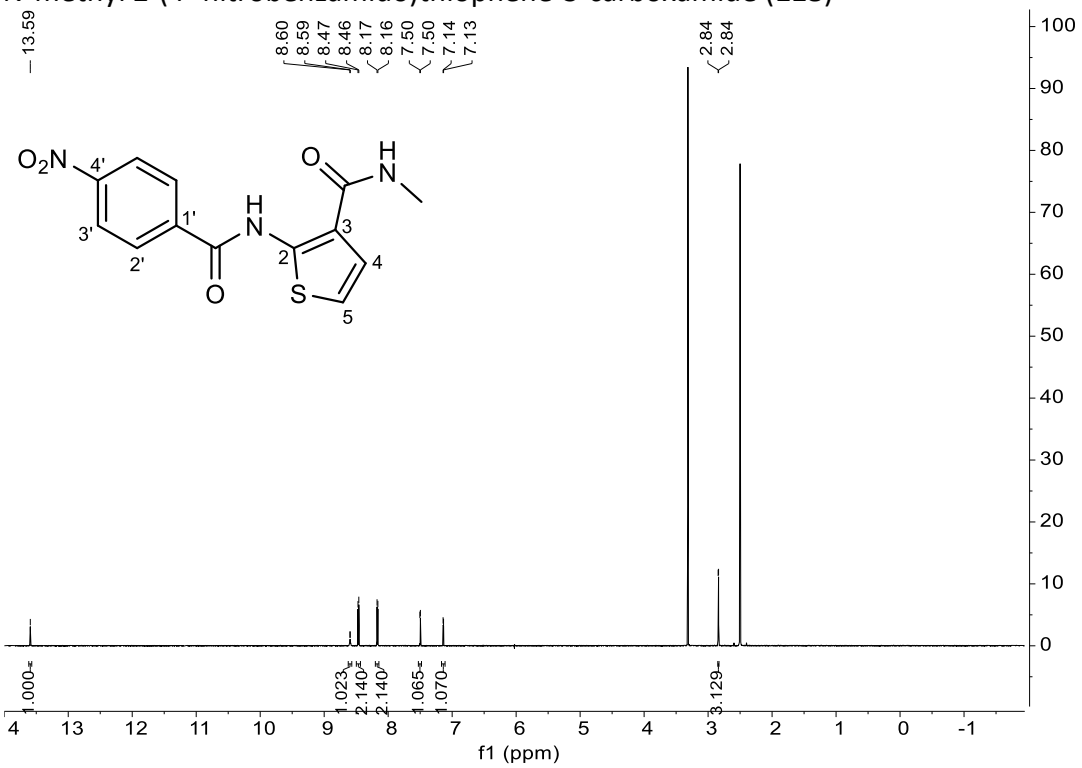

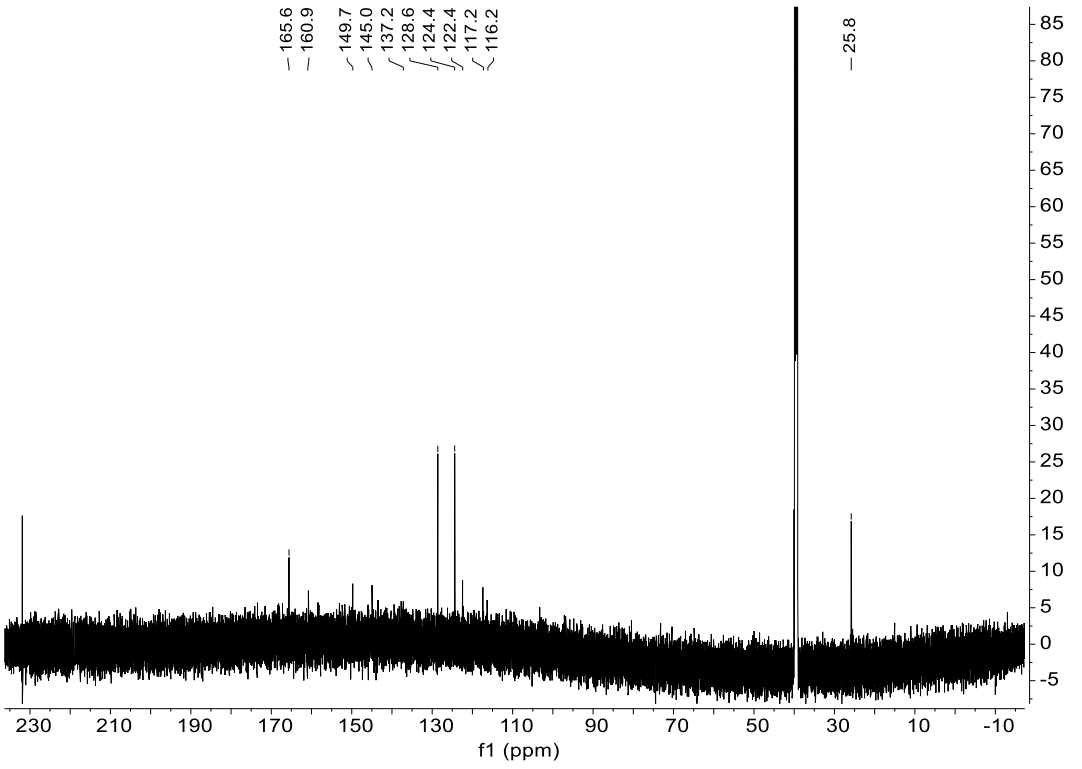

N-methyl-2-(3’-nitrobenzamido)thiophene-3-carboxamide (**119**)

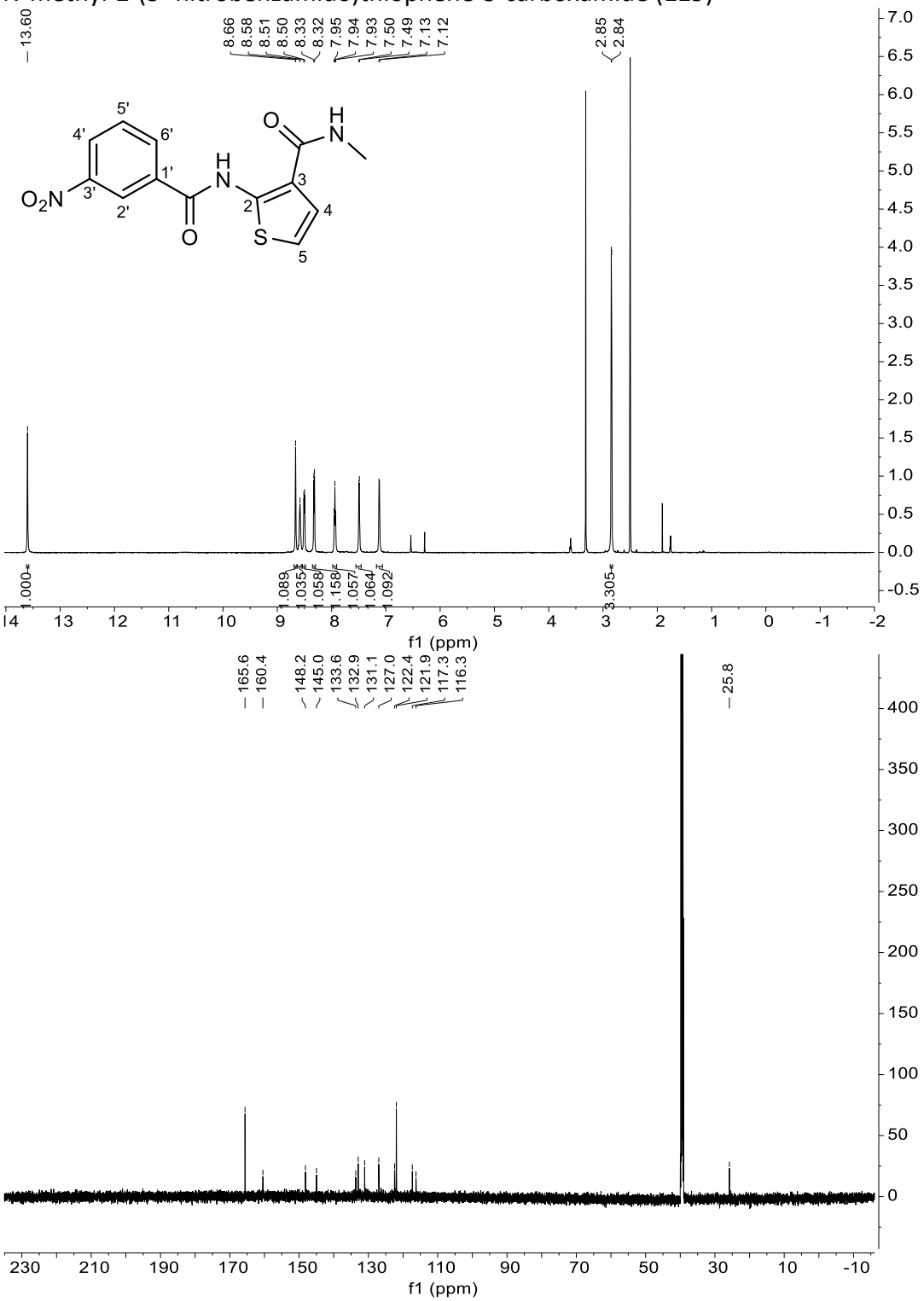

5’-amino-N-[3-(methylcarbamoyl)thiophen-2’-yl]thiophene-2-carboxamide (**120**)

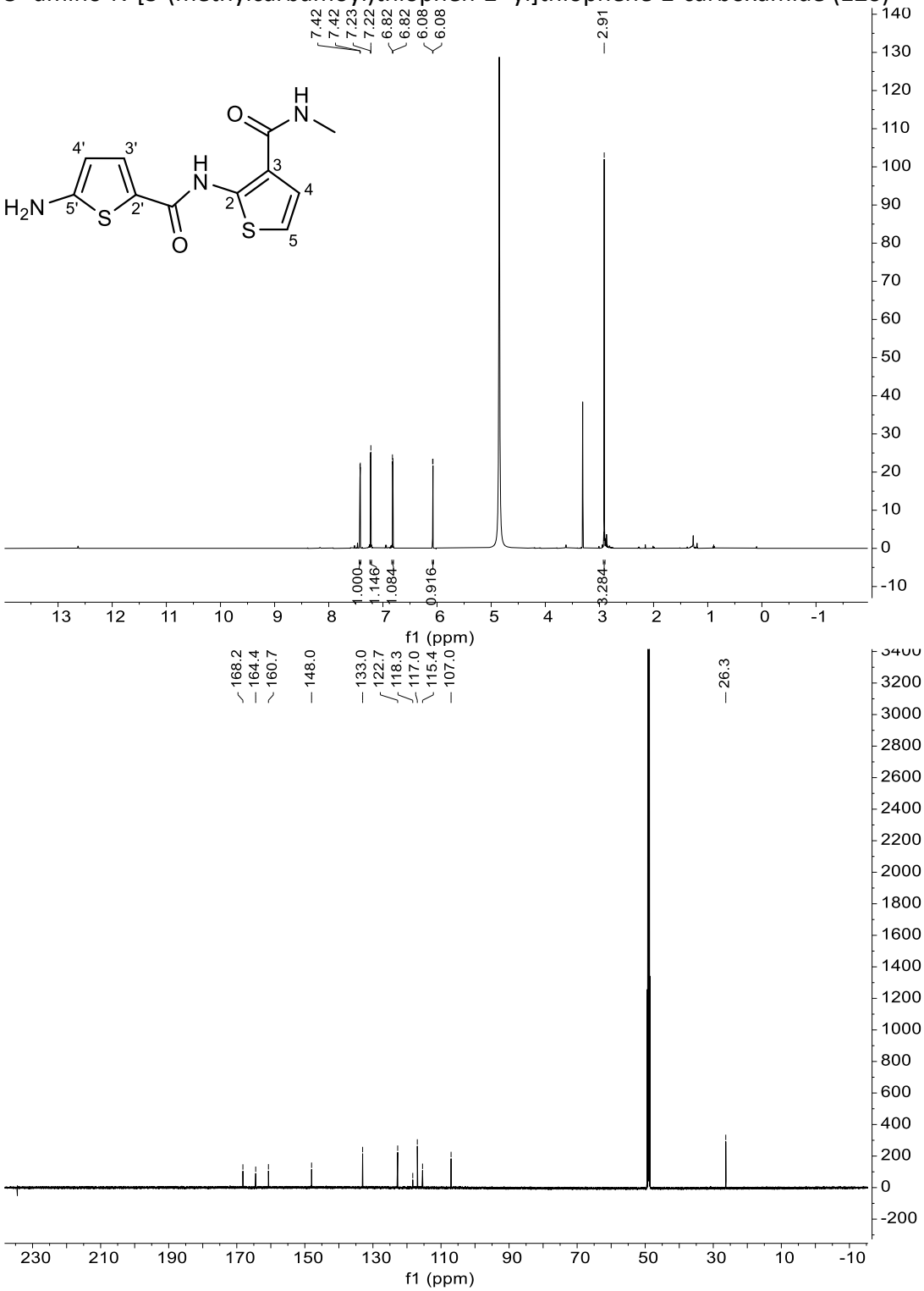

2-nitrothiazole-5-carboxylic acid (**122**)

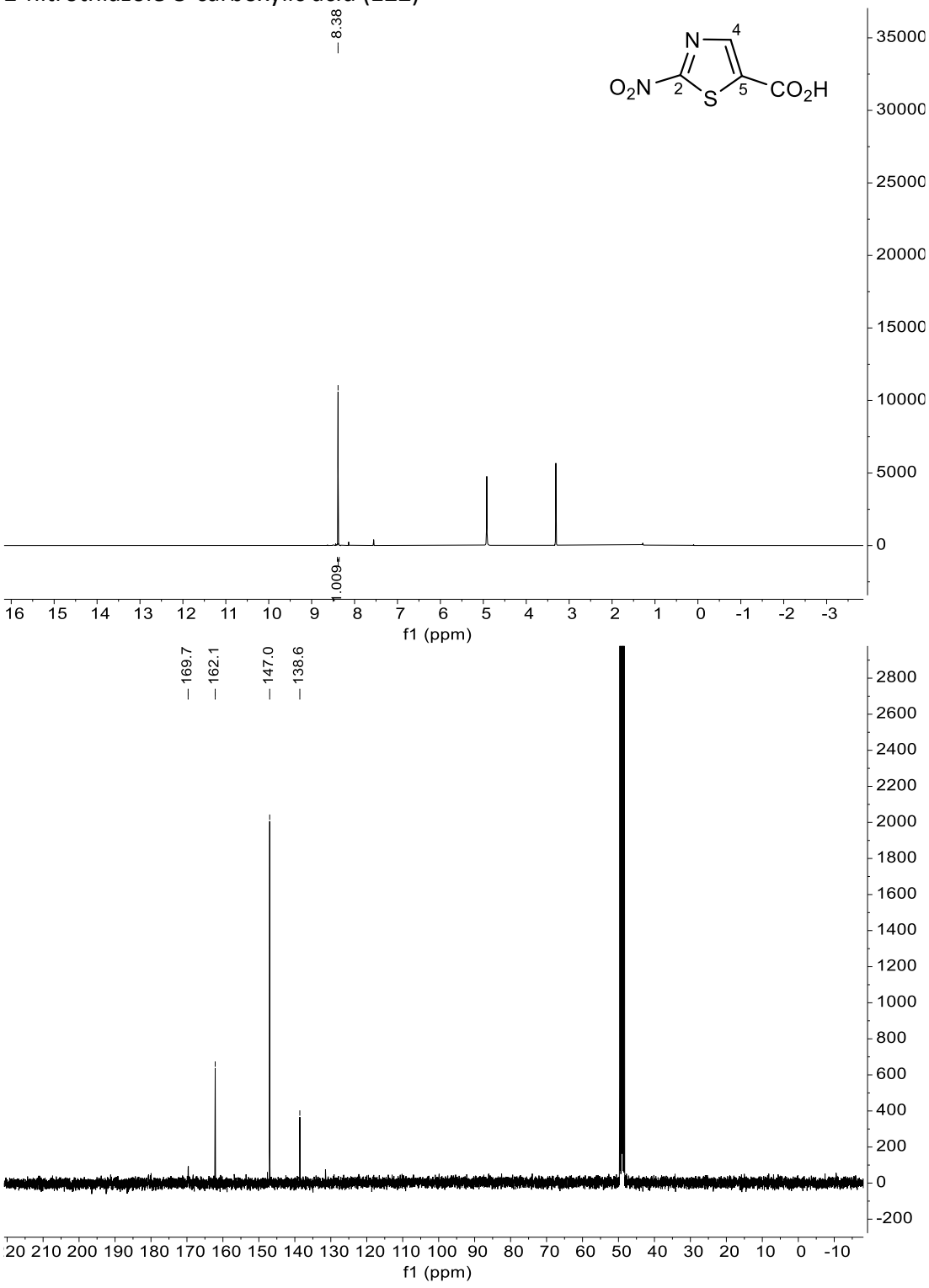

2-chlorothiazole-5-carbonyl chloride (**123**)

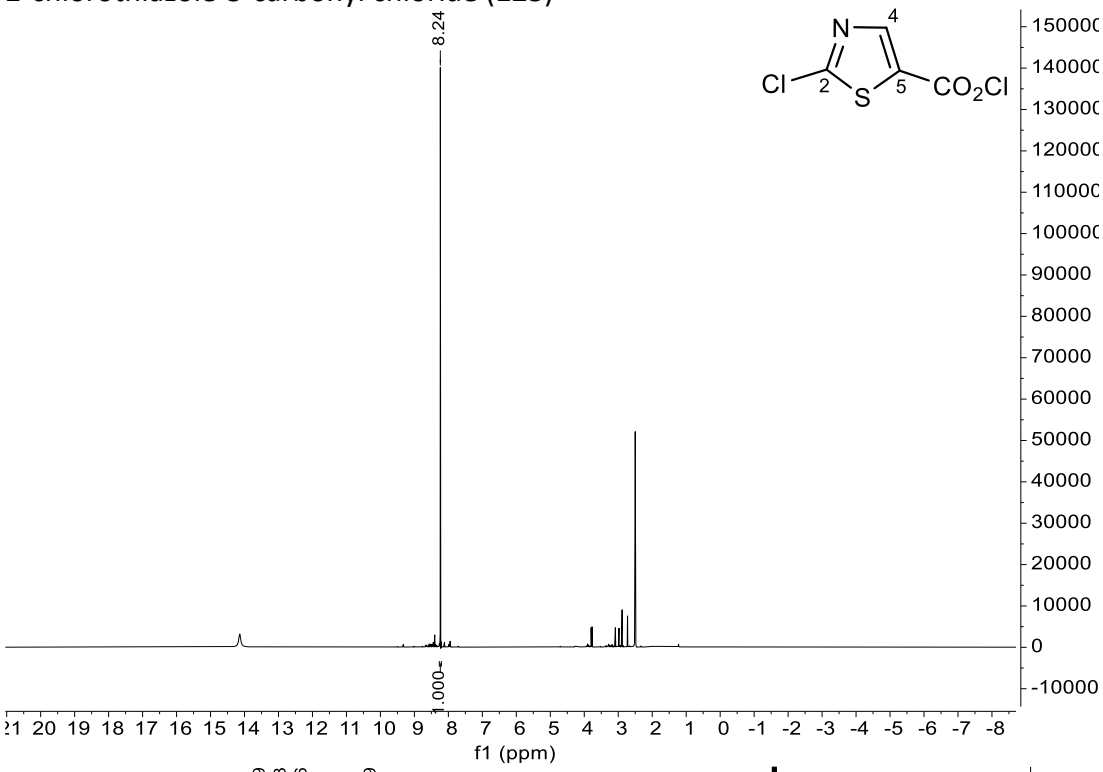

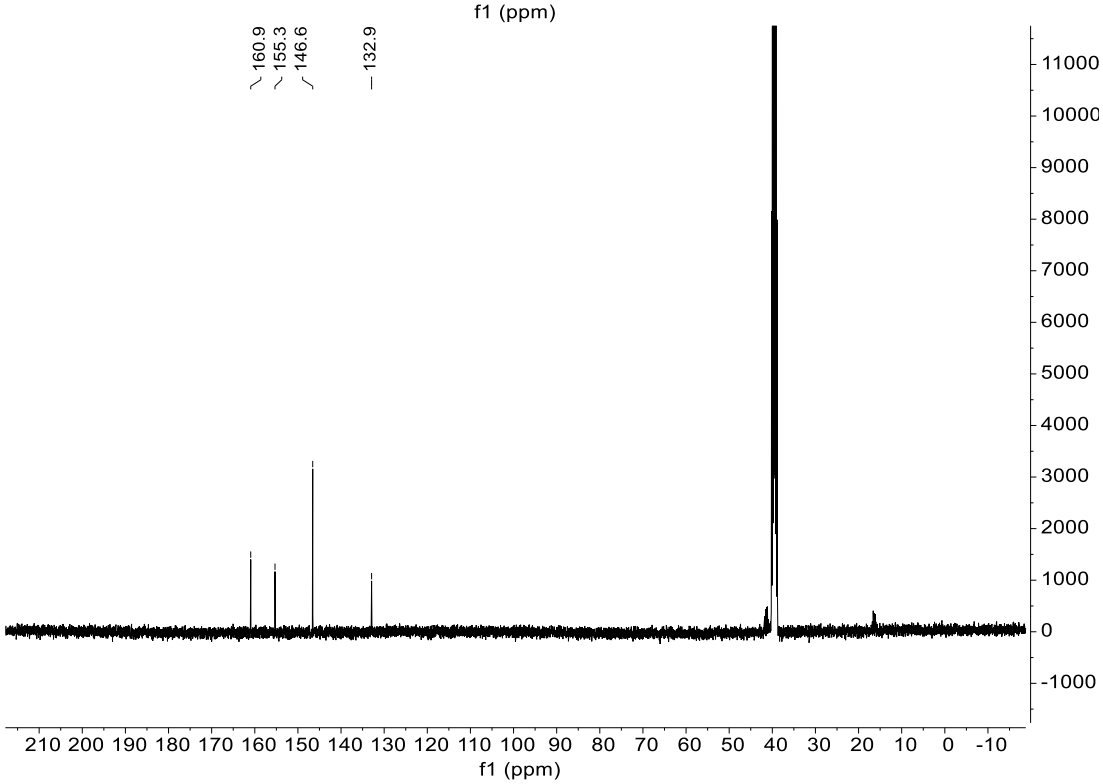

N-[3-(methylcarbamoyl)thiophen-2-yl]-2’-chloro-1’,3’-thiazole-5’-carboxamide (**124**)

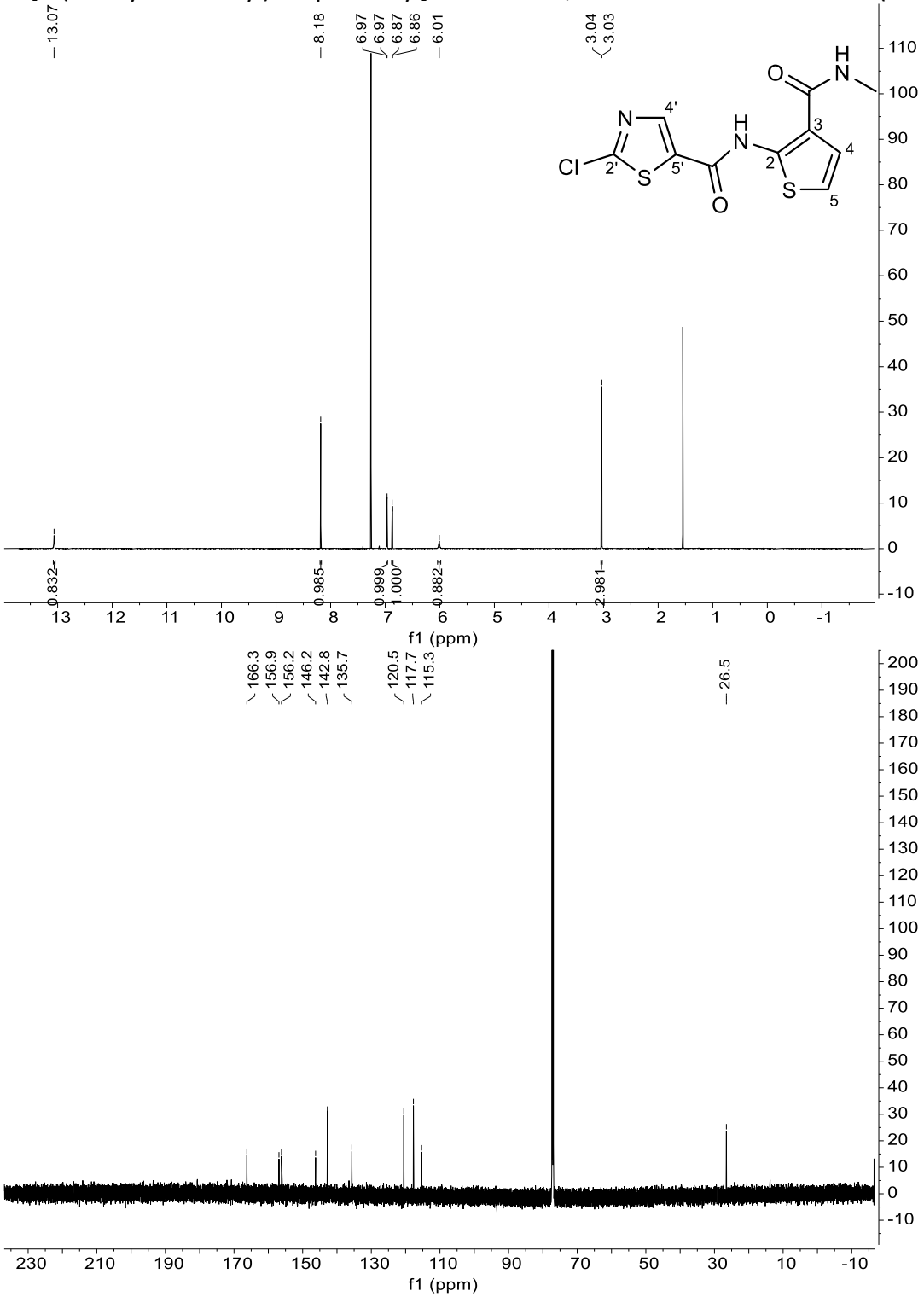

2-{[(tert-butoxy)carbonyl]amino}-1,3-thiazole-5-carboxylic acid (**126**)

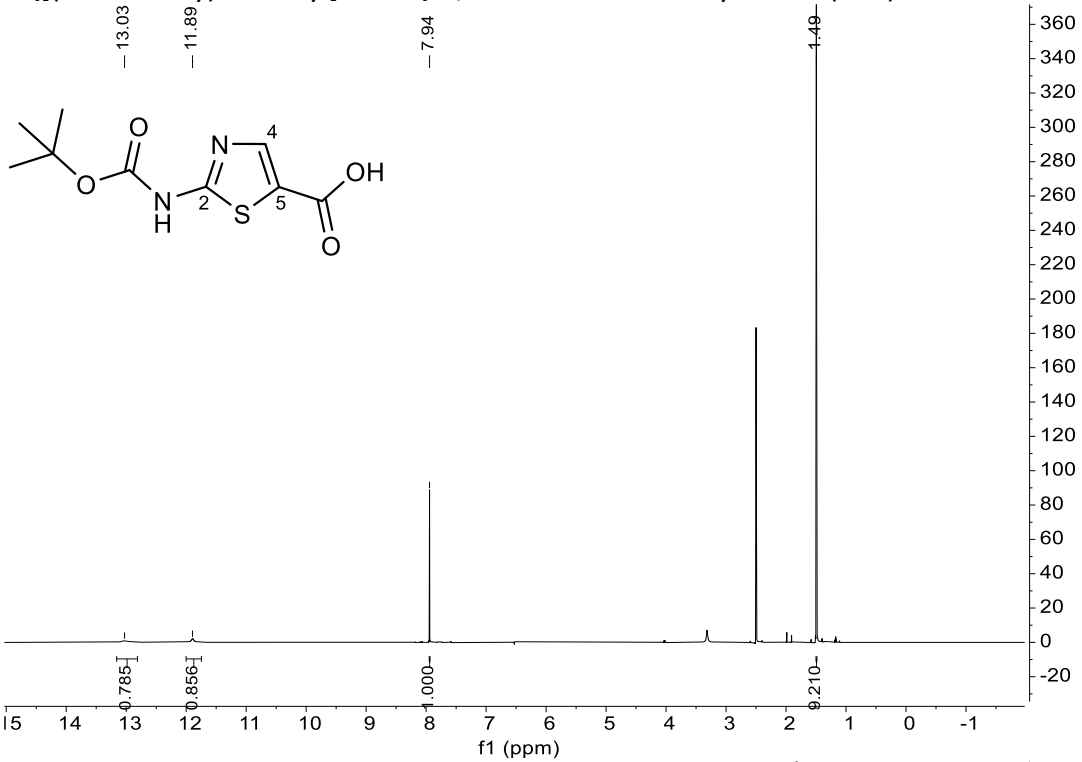

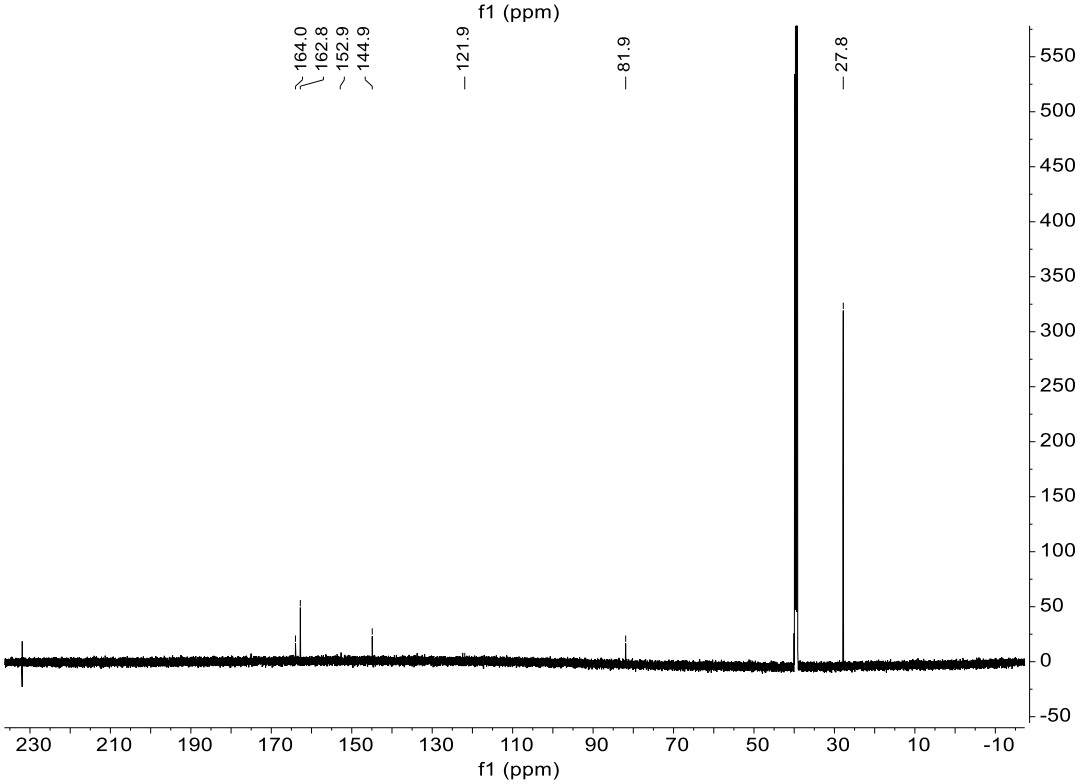

Ethyl 2-aminocyclopent-1-ene-1-carboxylate (**129**)

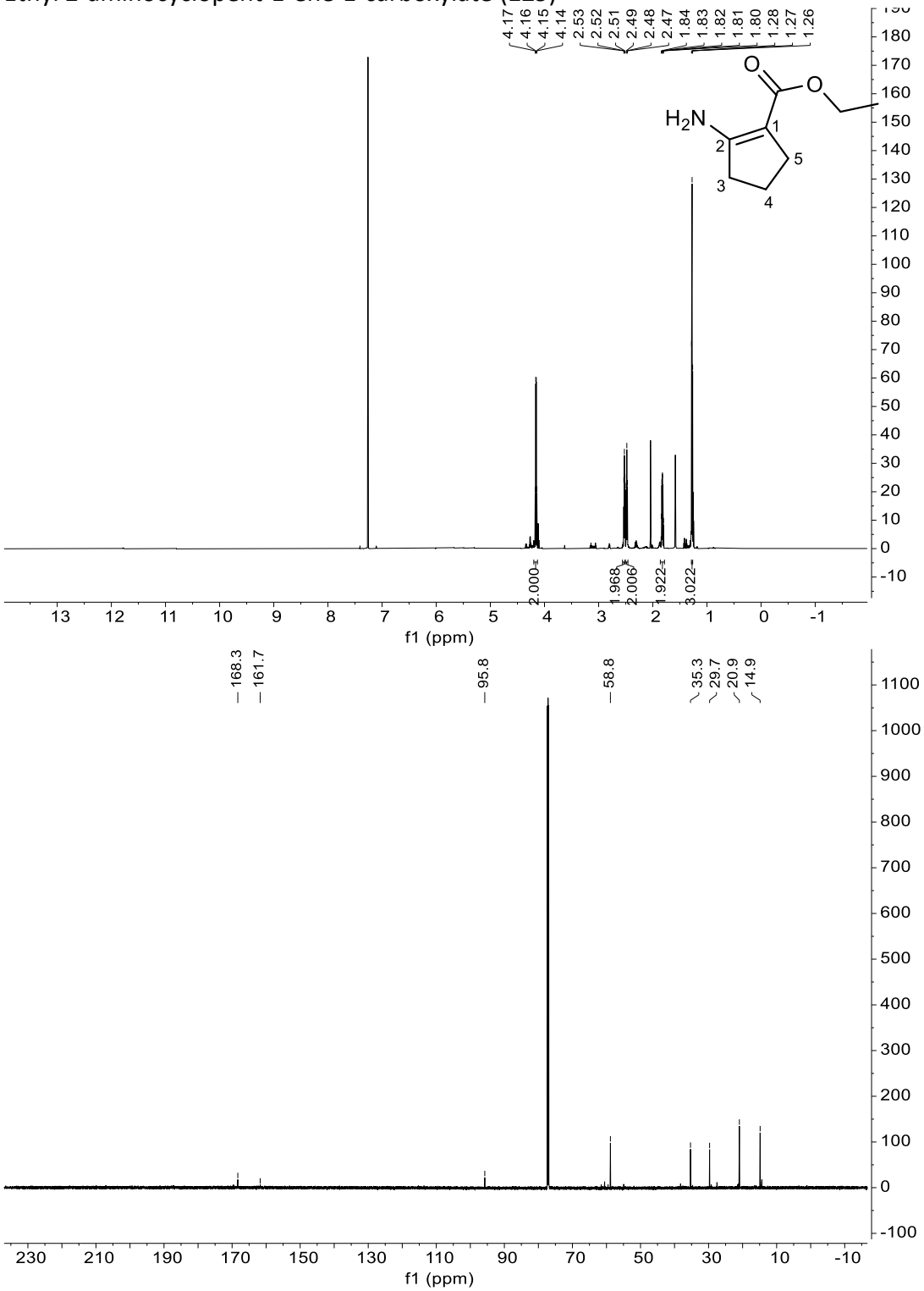

± Ethyl 2-aminocyclopentane-1-carboxylate (**130**)

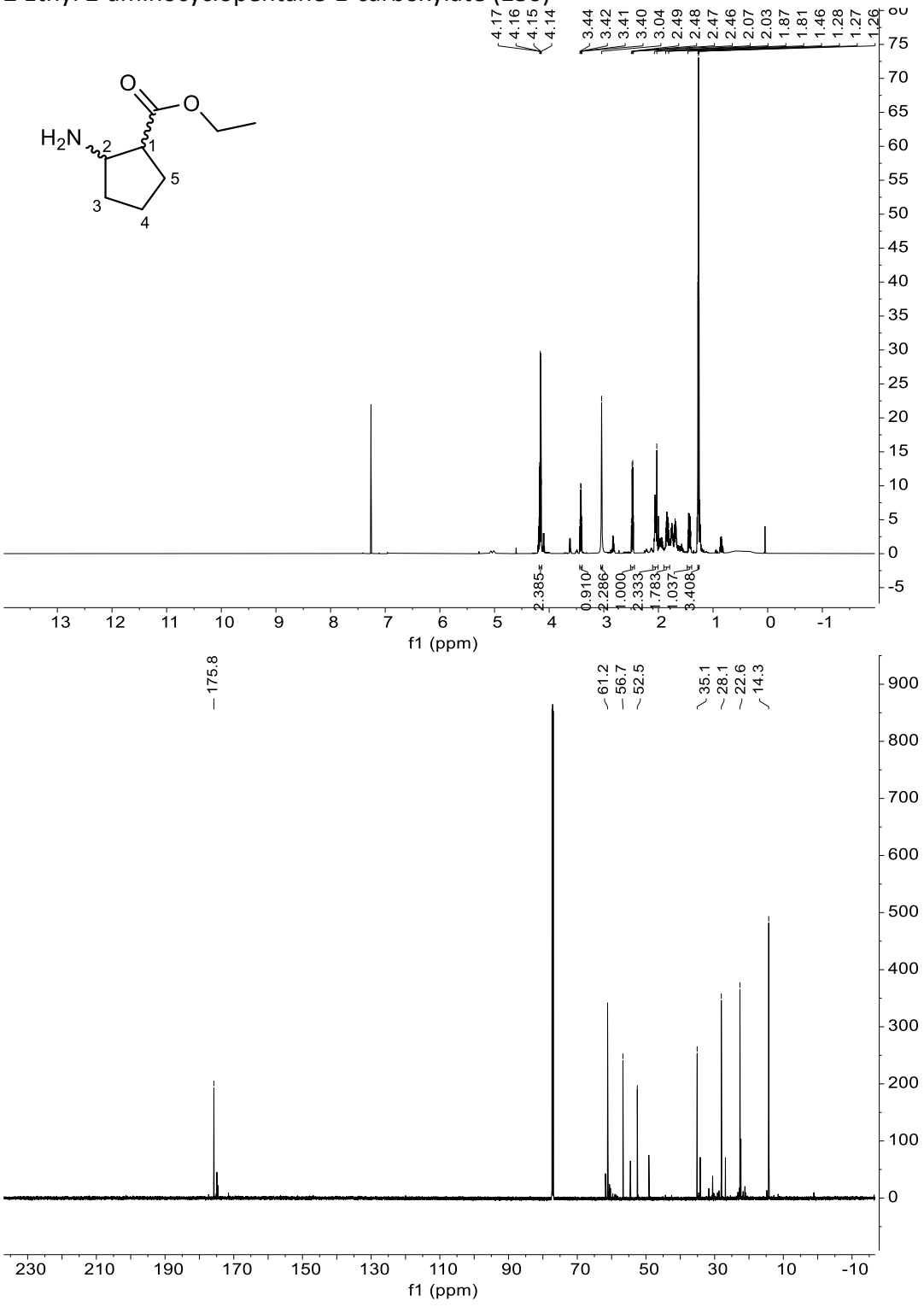

anti- Ethyl-2-(5’-nitrothiophene-2’-amido)cyclopentane-1-carboxylate (**131**)

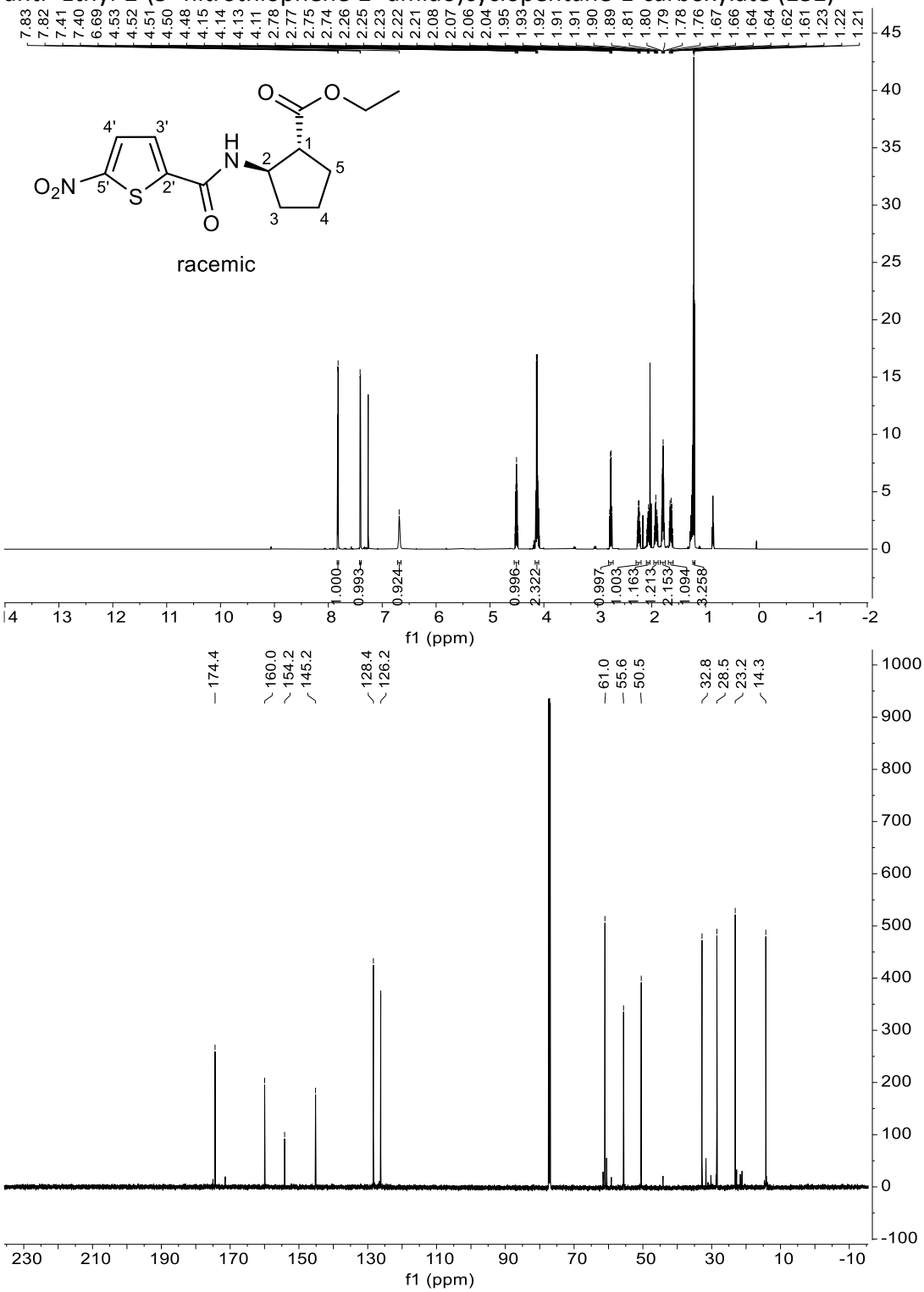

syn- Ethyl-2-(5’-nitrothiophene-2’-amido)cyclopentane-1-carboxylate (**132**)

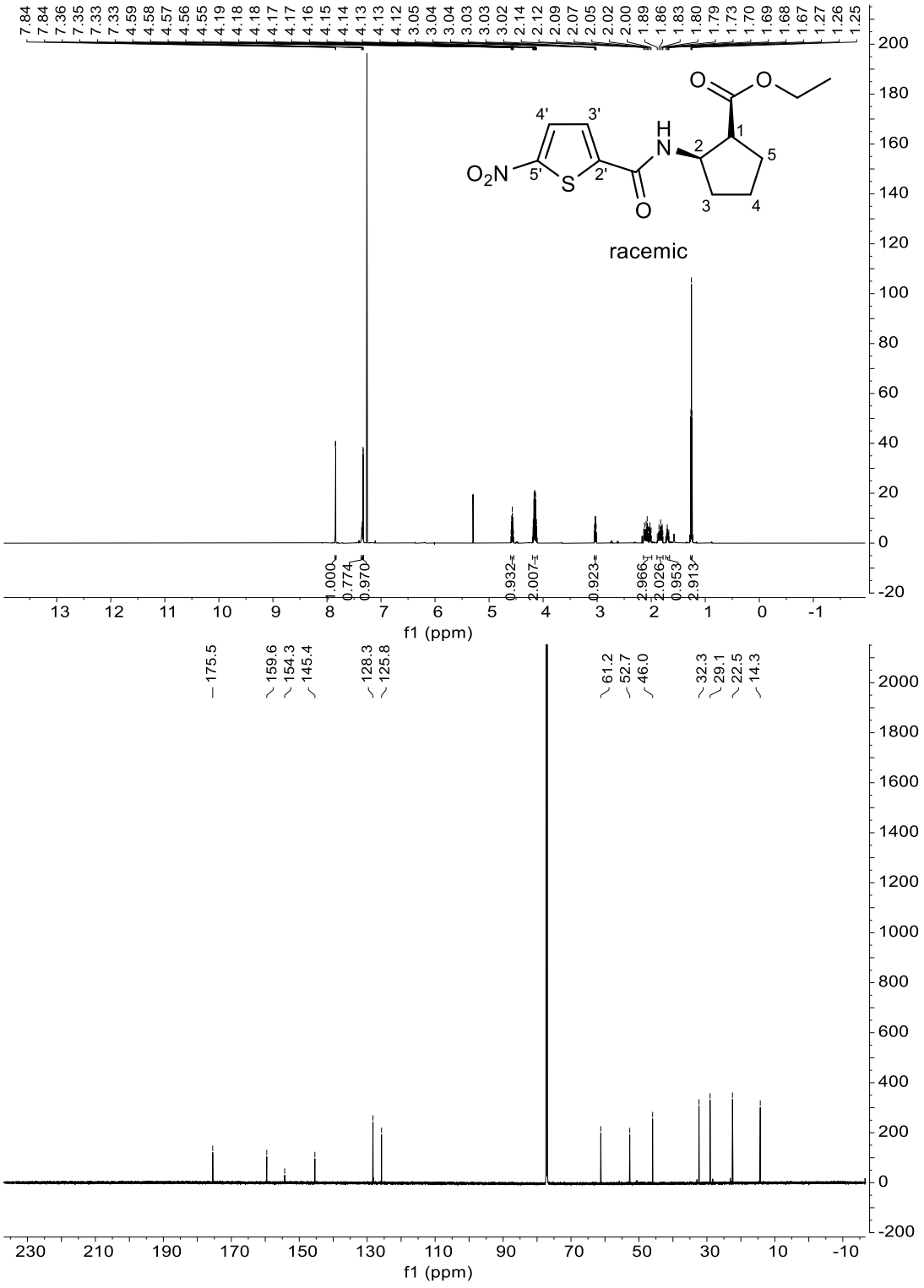

anti 2-(5’-nitrothiophene-2’-amido)cyclopentane-1-carboxylic acid (**133**)

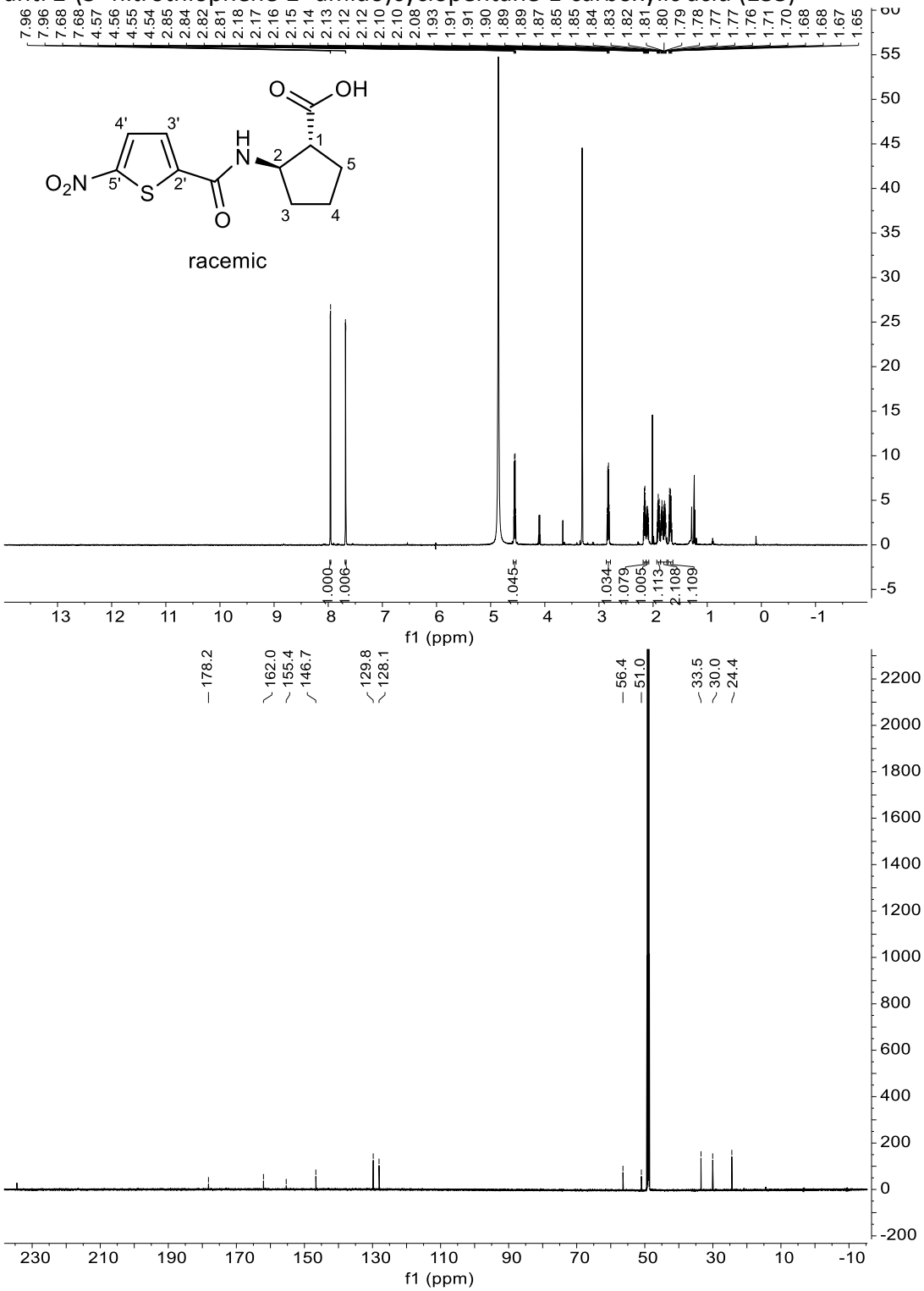

syn 2-(5’-nitrothiophene-2’-amido)cyclopentane-1-carboxylic acid (**134**)

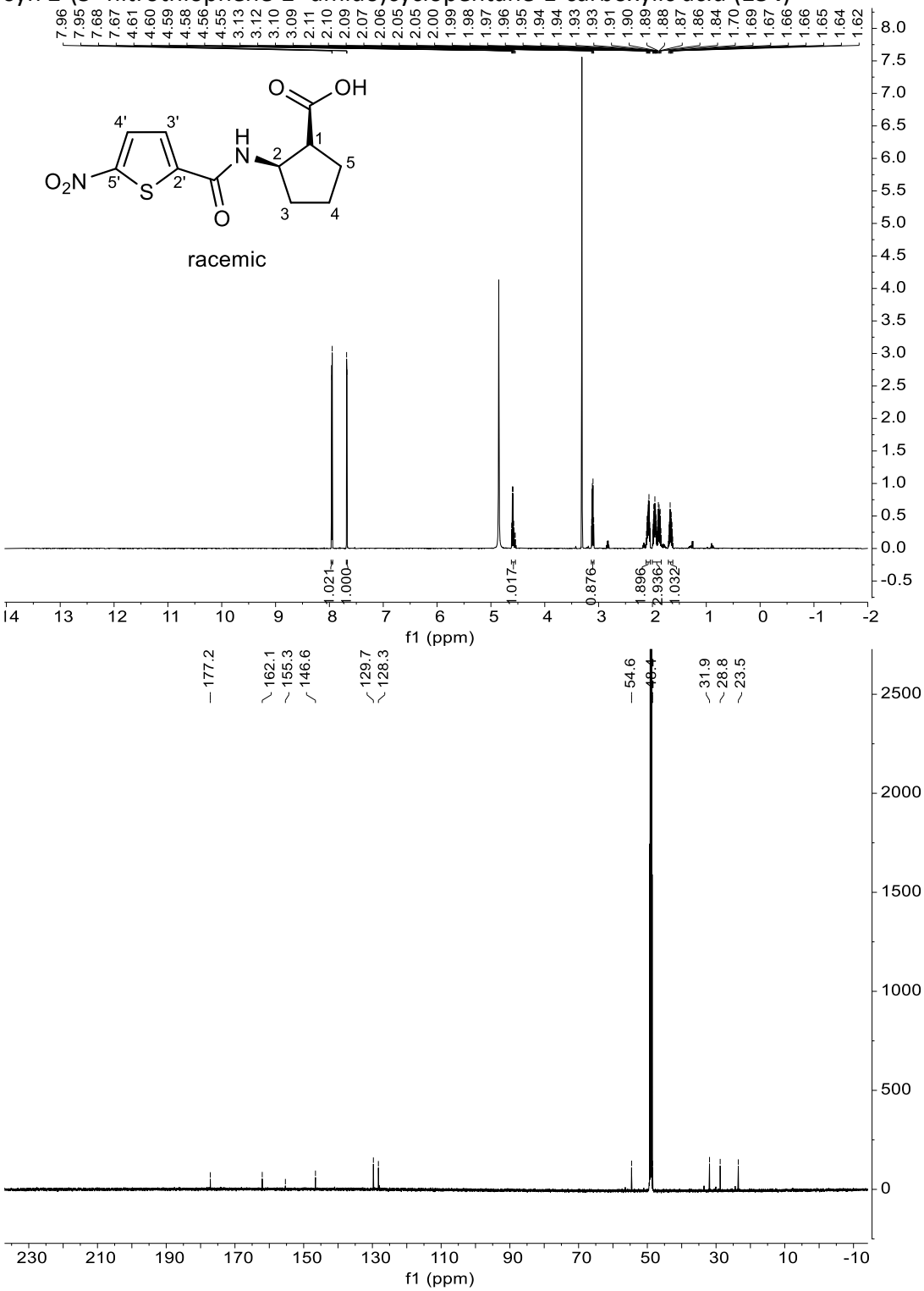

N-[± 2’-(methylcarbamoyl)cyclopentyl]-5’-nitrothiophene-2-carboxamide (**135**)

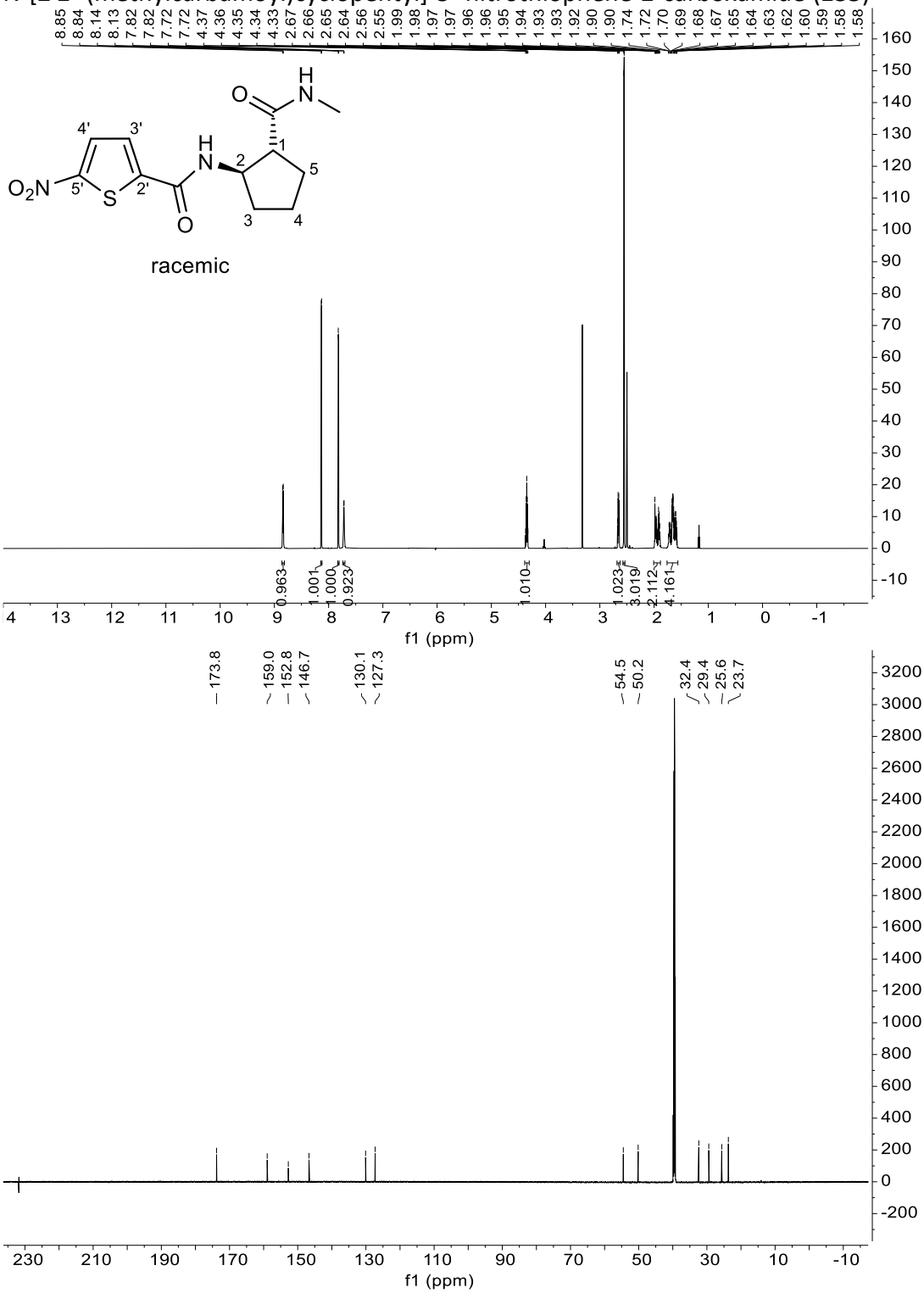

Ethyl 2-(5’-nitrothiophene-2’-amido)cyclopent-1-ene-1-carboxylate (**136**)

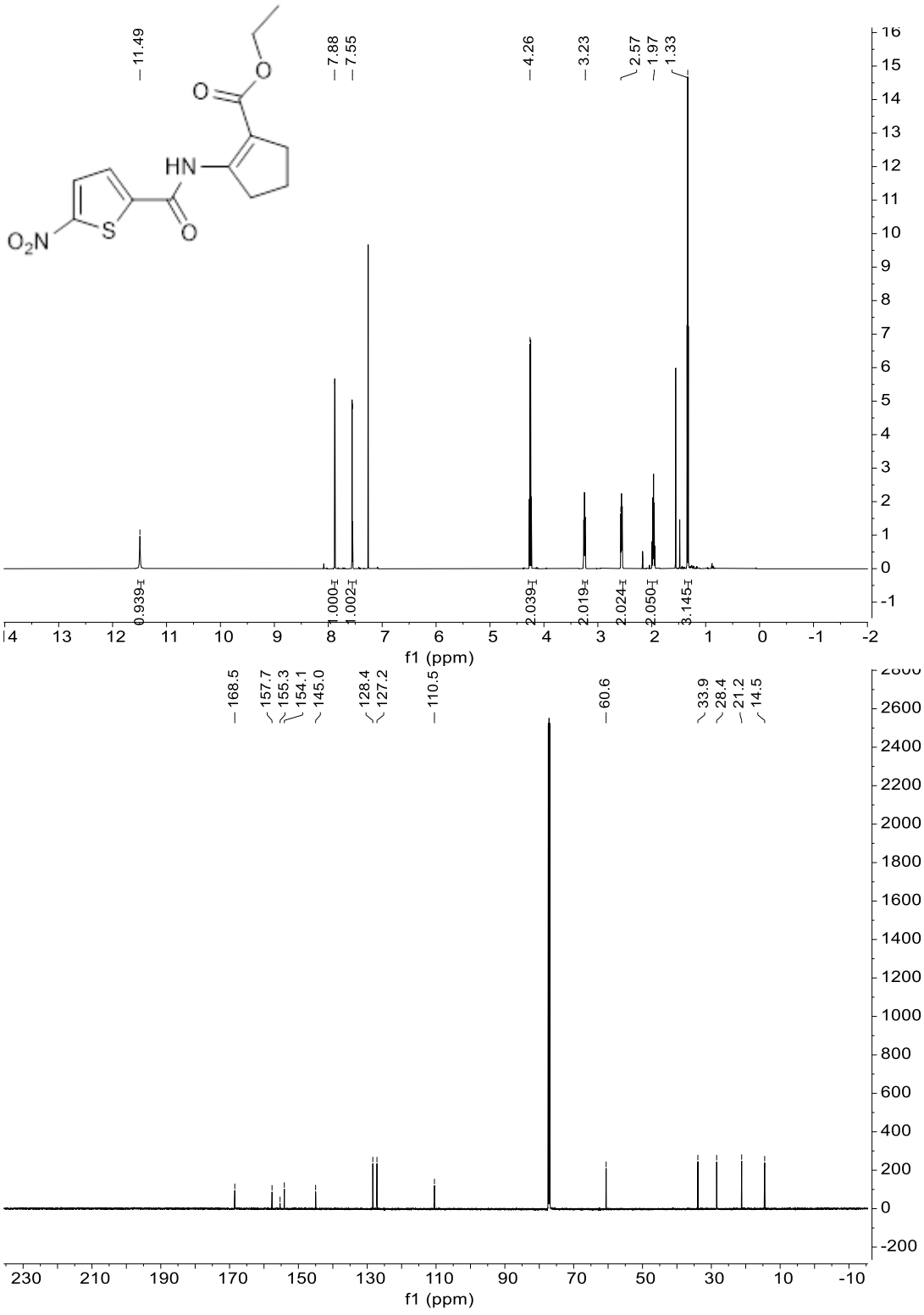

N-(2-carbamoylphenyl)-5’-nitrothiophene-2’-carboxamide (**140**)

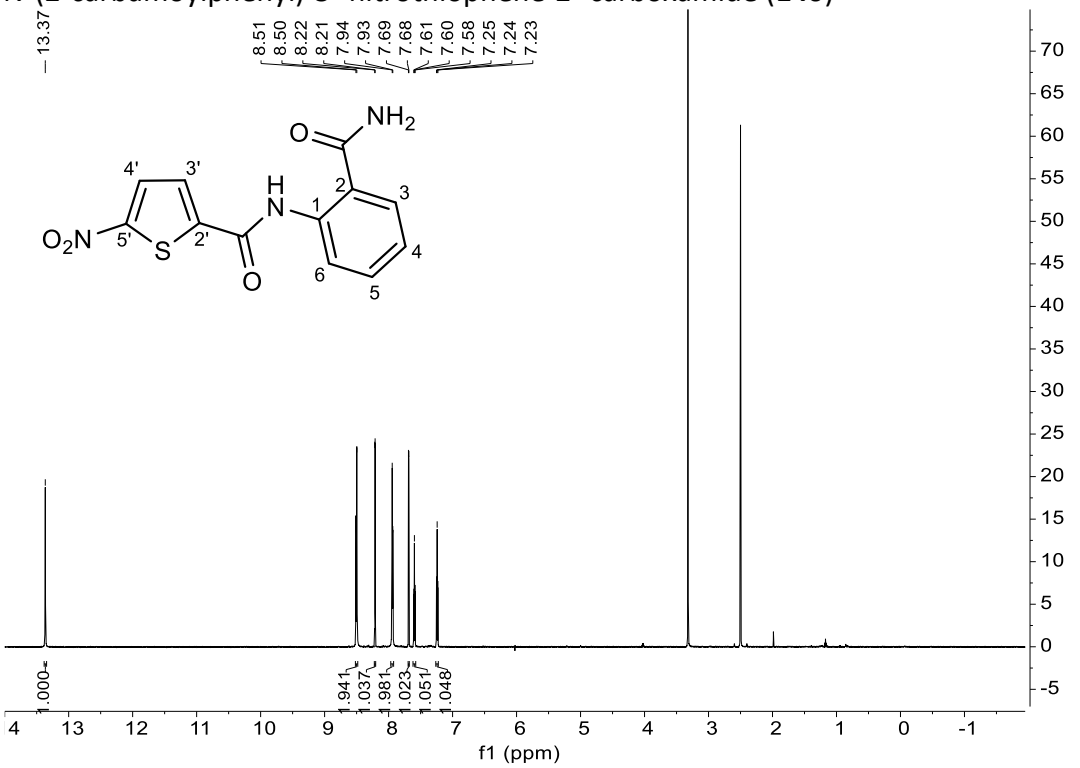

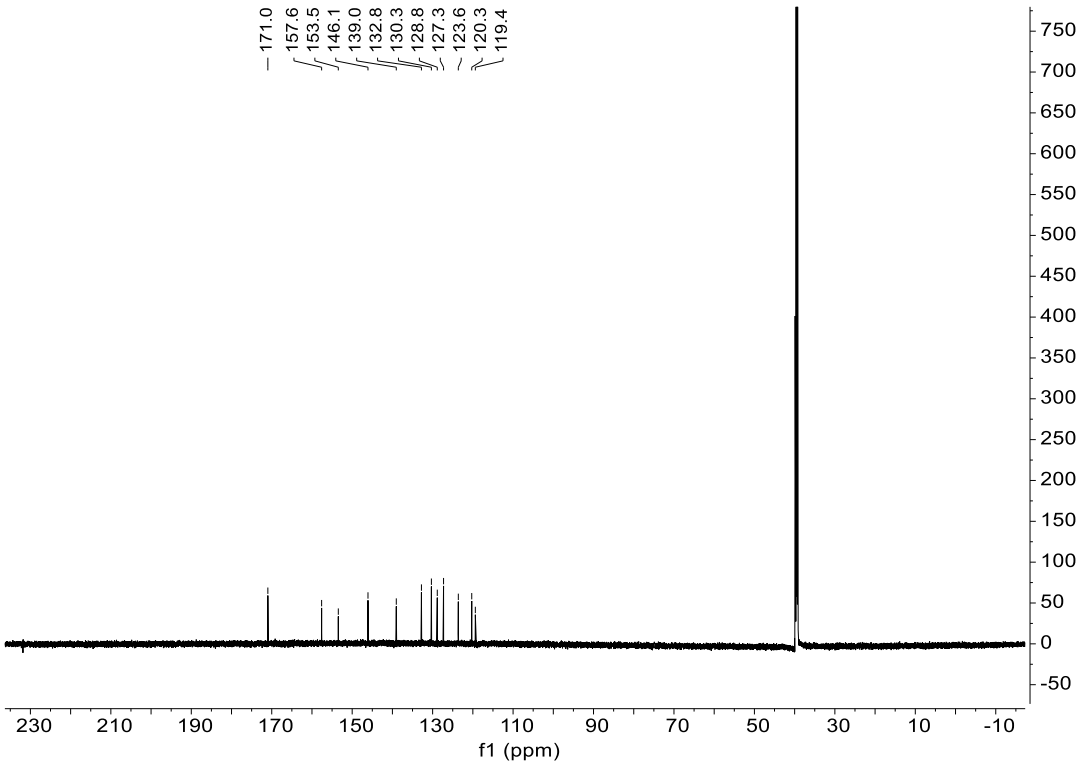

Amino-*N*-methyl-2-benzamide (**138**)

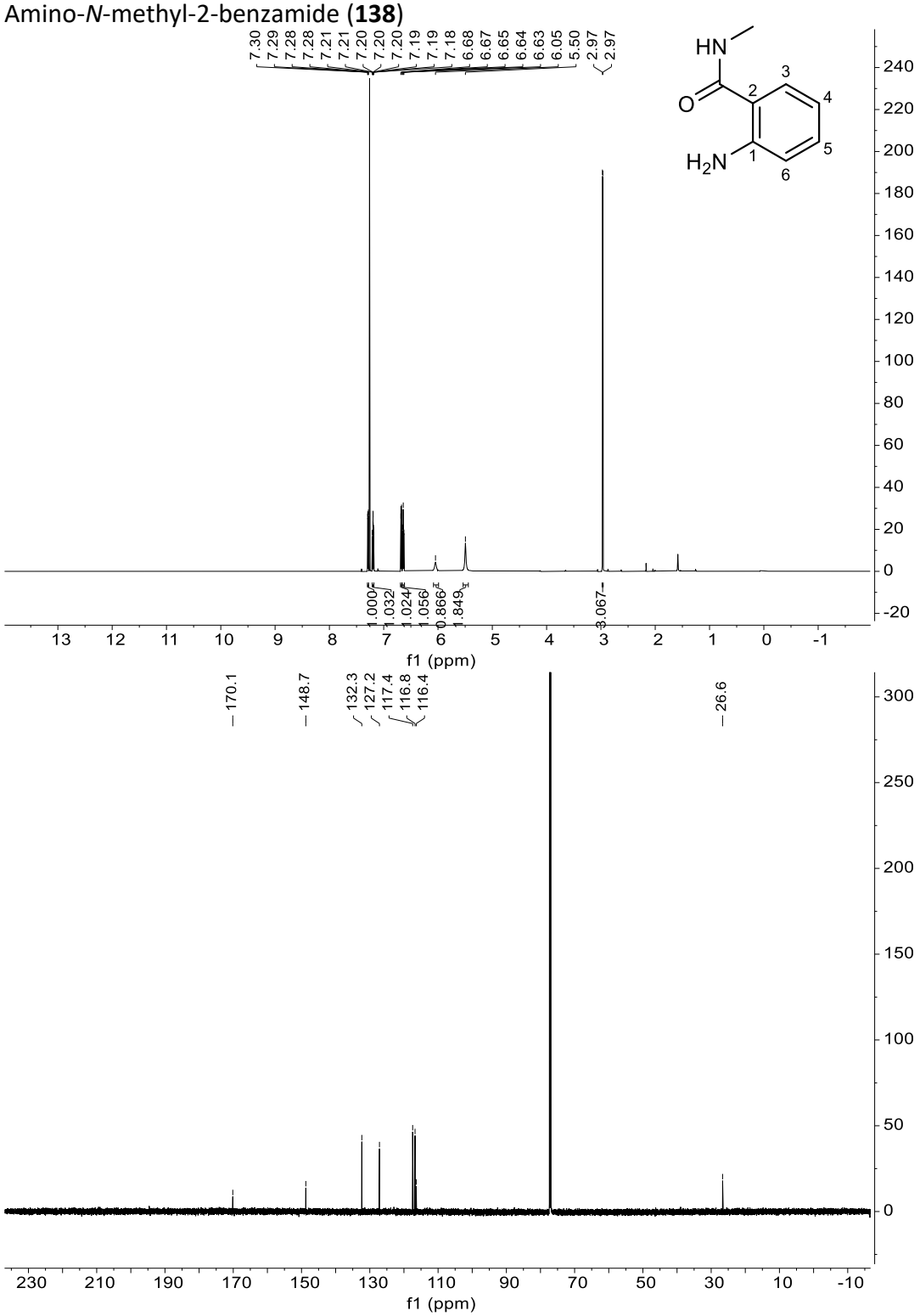

N-[2’-(methylcarbamoyl)phenyl]-5’-nitrothiophene-2-carboxamide (**141**)

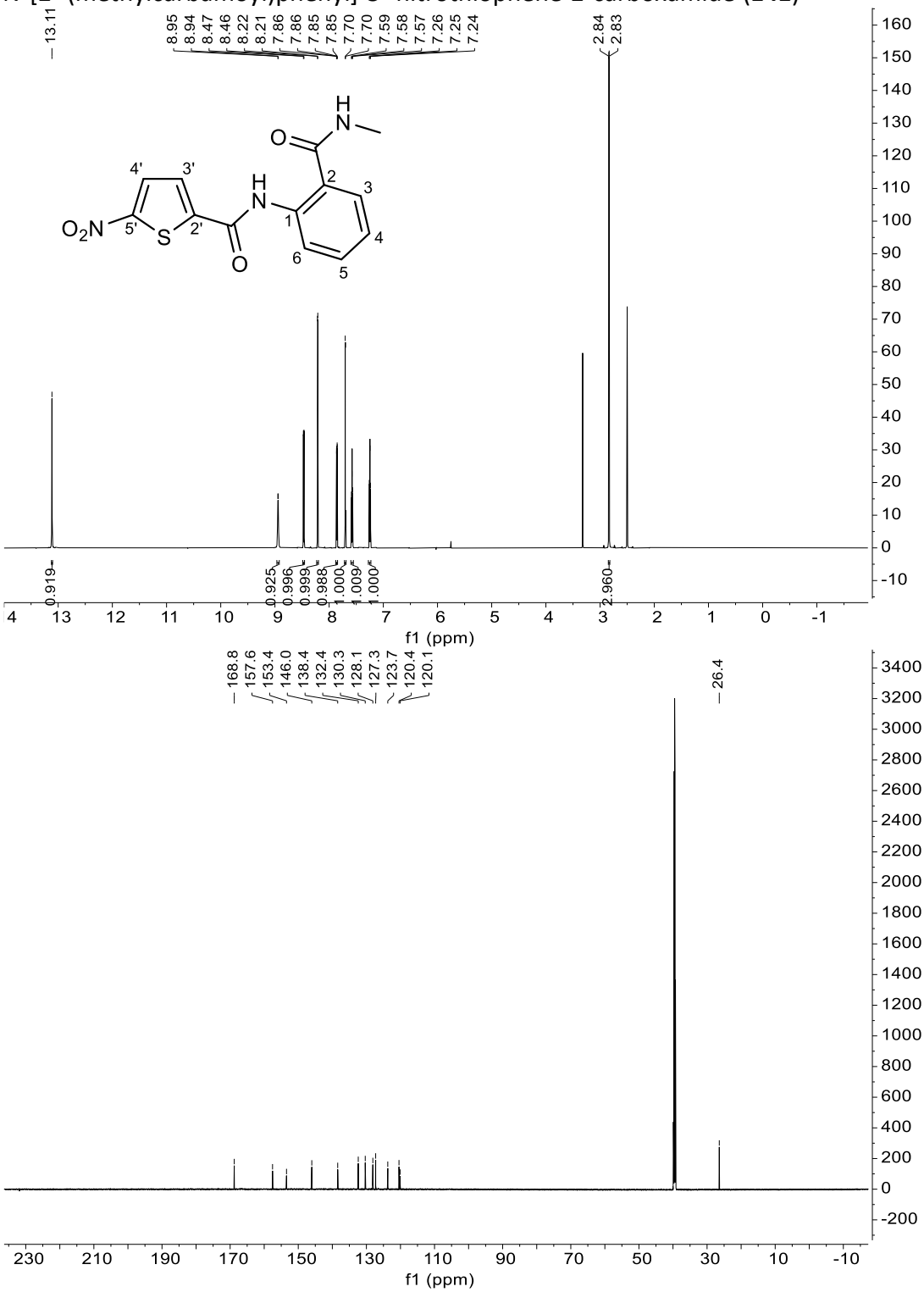

2-(5’-nitrothiophene-2’-amido)benzoic acid (**143**)

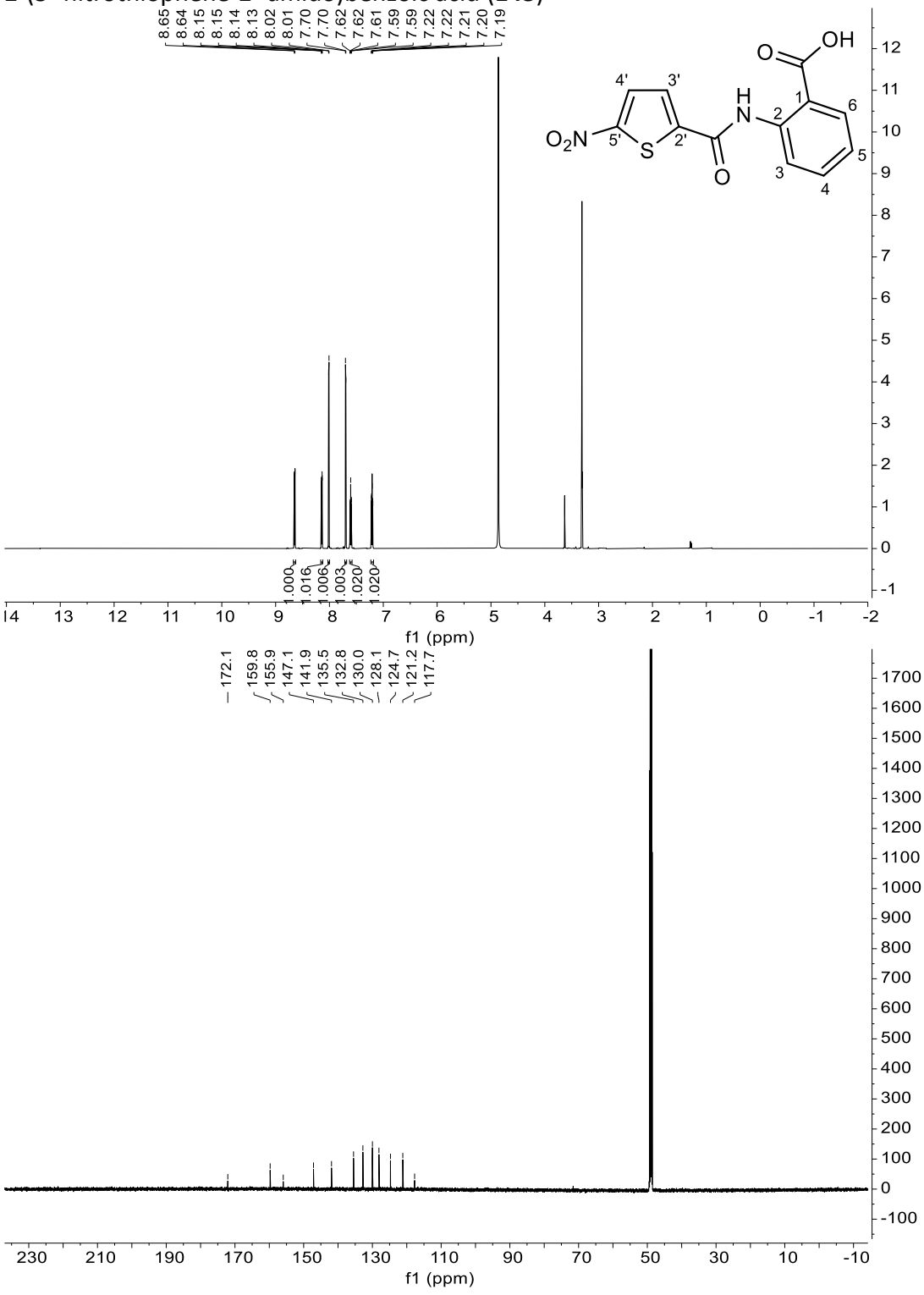

2-(5’-nitrothiophen-2’-yl)-4H-3,1-benzoxazin-4-one (**144**)

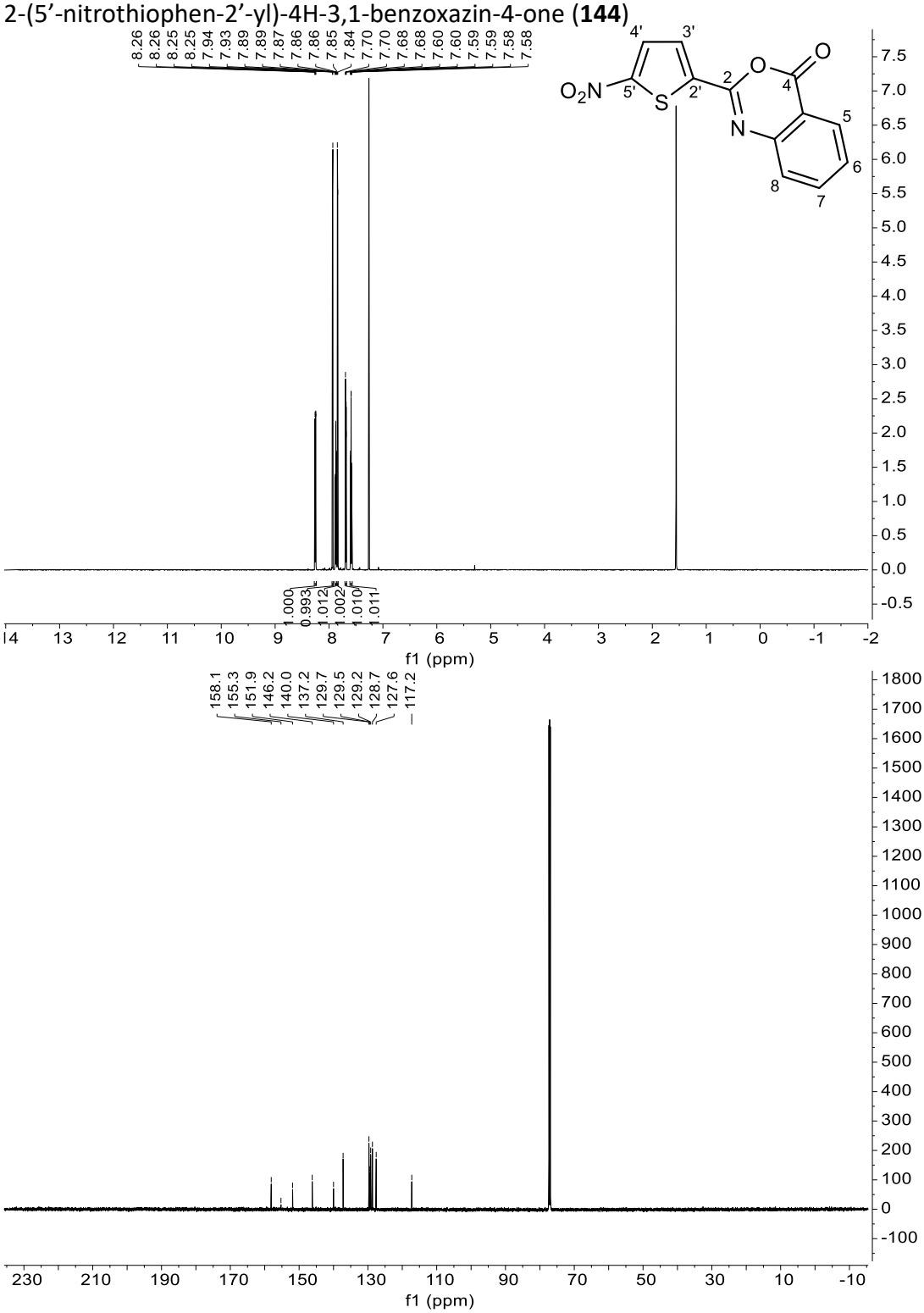

N-methyl-3-[(5’-nitrothiophen-2’-yl)amino]benzamide (**155**)

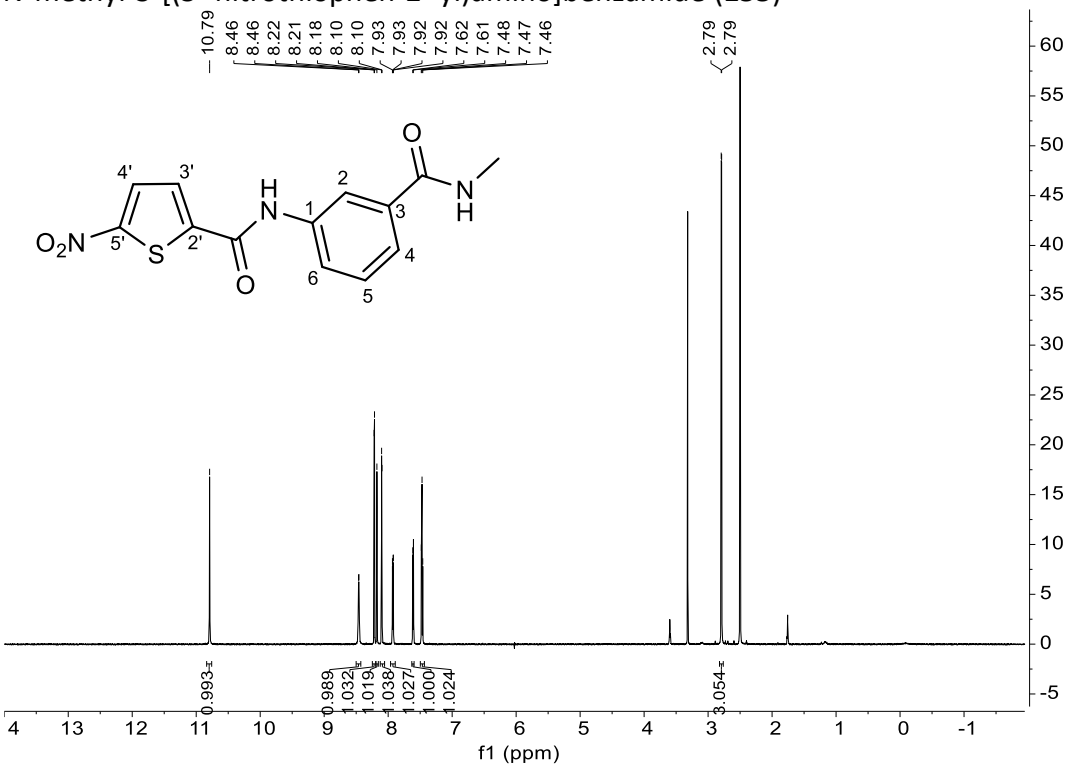

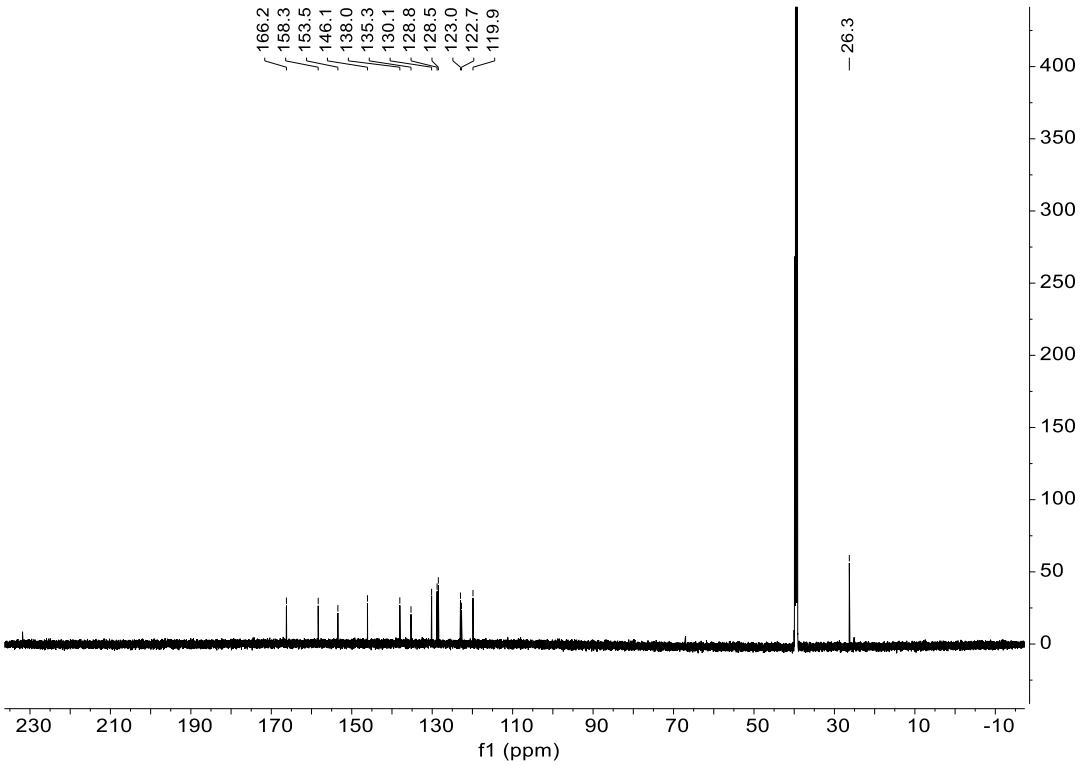

5’-nitro-*N*-phenylthiophene-2’-carboxamide (**156**)

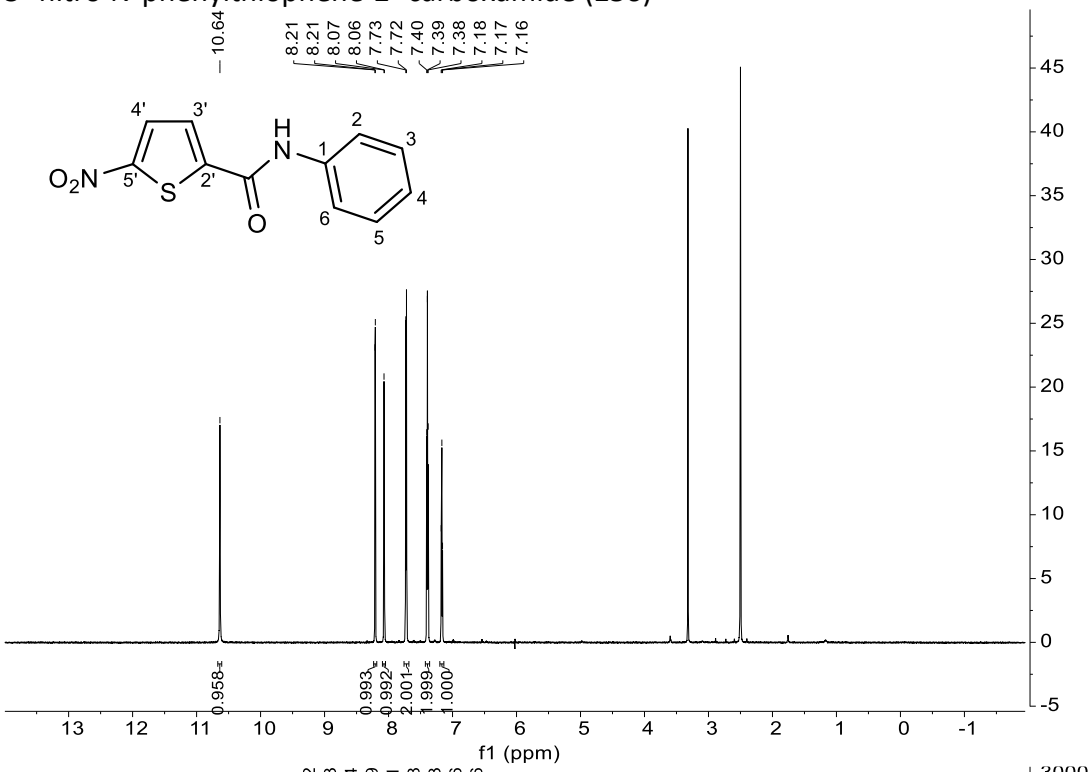

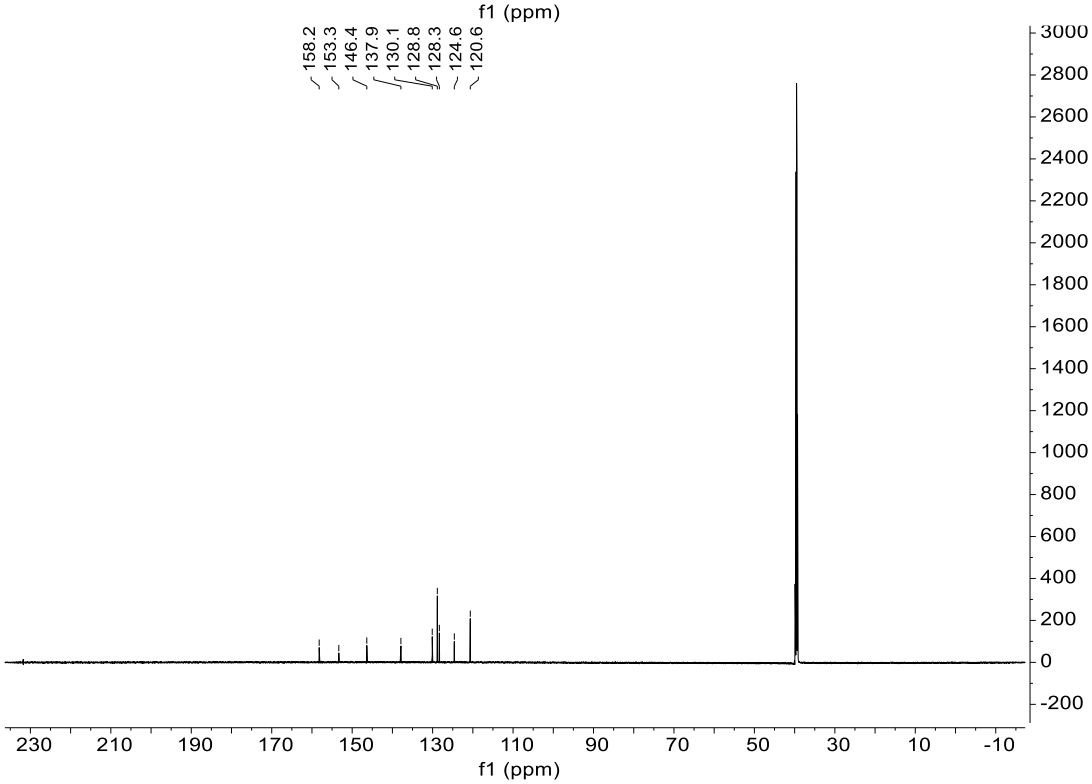

N-(2-methoxyphenyl)-5’-nitrothiophene-2’-carboxamide (**157**)

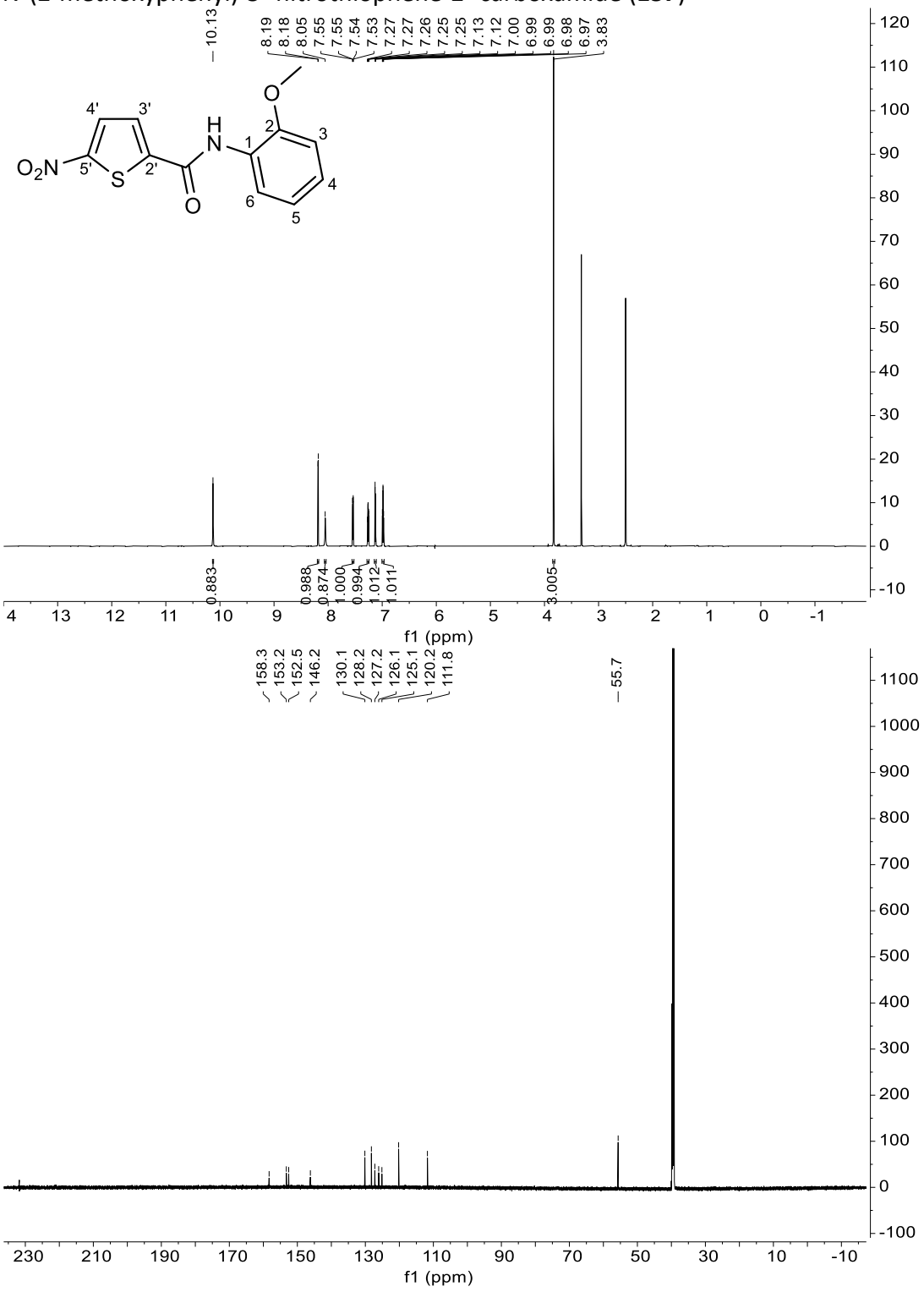

N-(3-methoxyphenyl)-5’-nitrothiophene-2’-carboxamide (**158**)

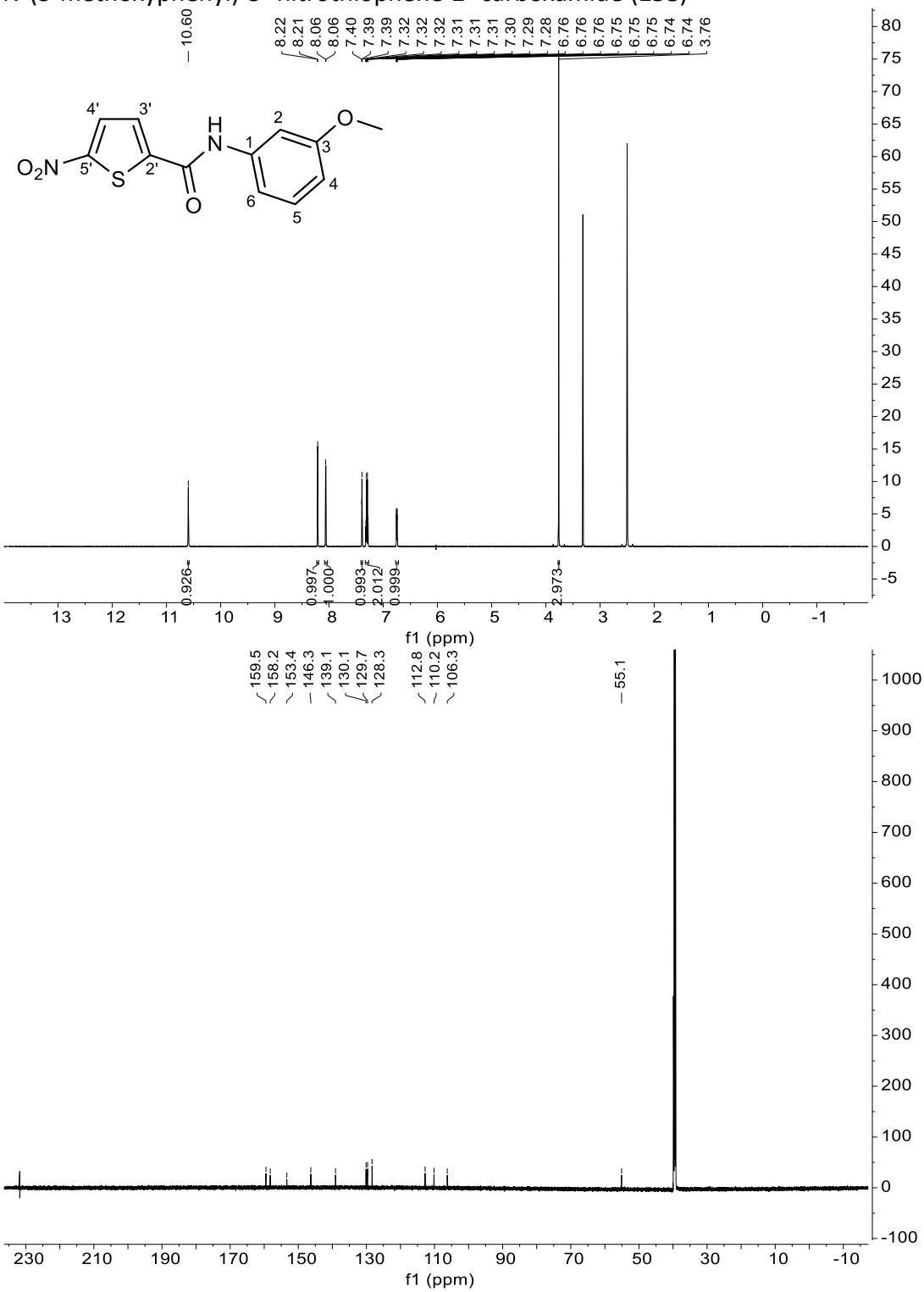

N-(4-methoxyphenyl)-5’-nitrothiophene-2’-carboxamide (**159**)

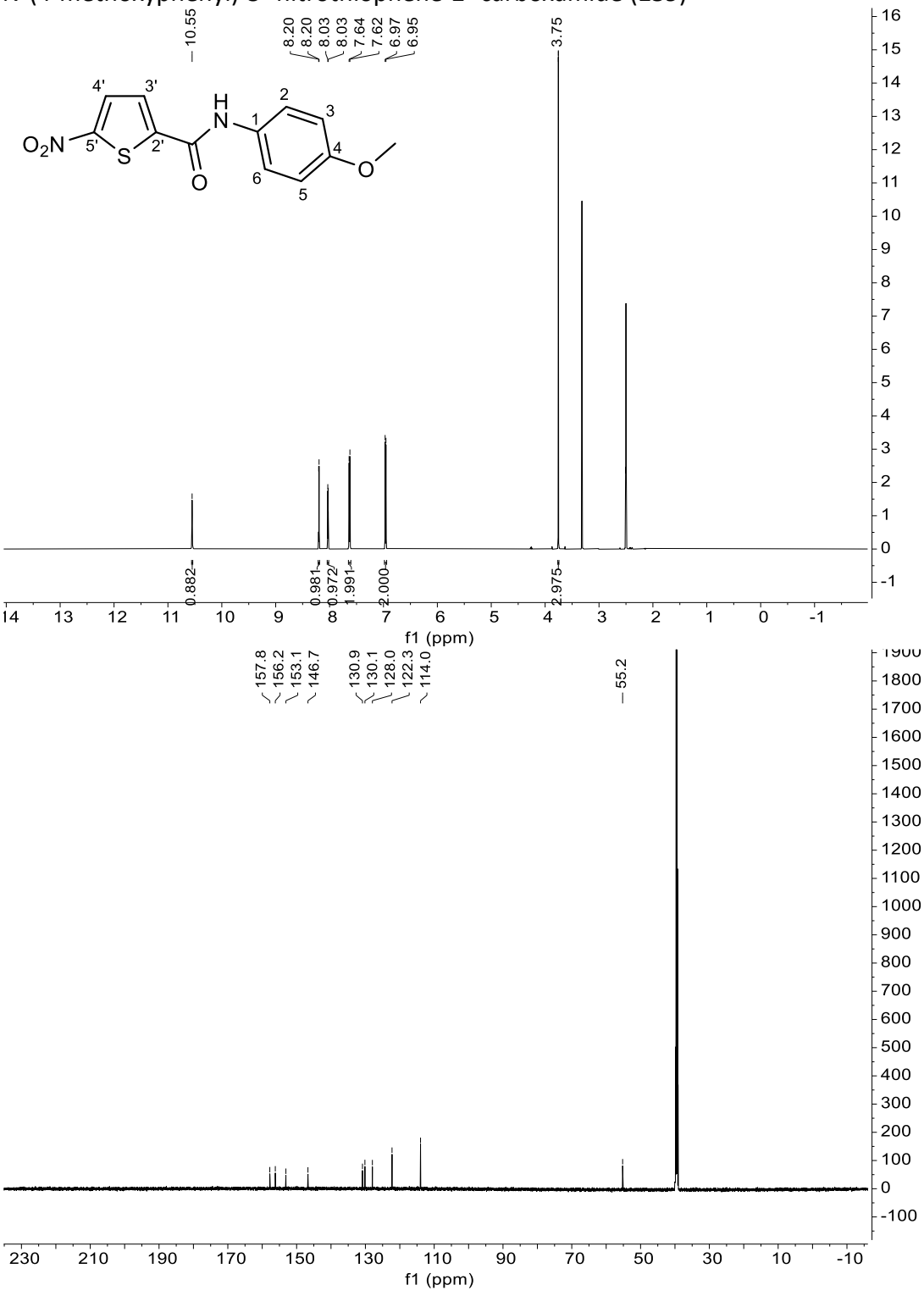

5’-nitro-*N*-[2-(trifluoromethyl)phenyl]thiophene-2’-carboxamide (**160**)

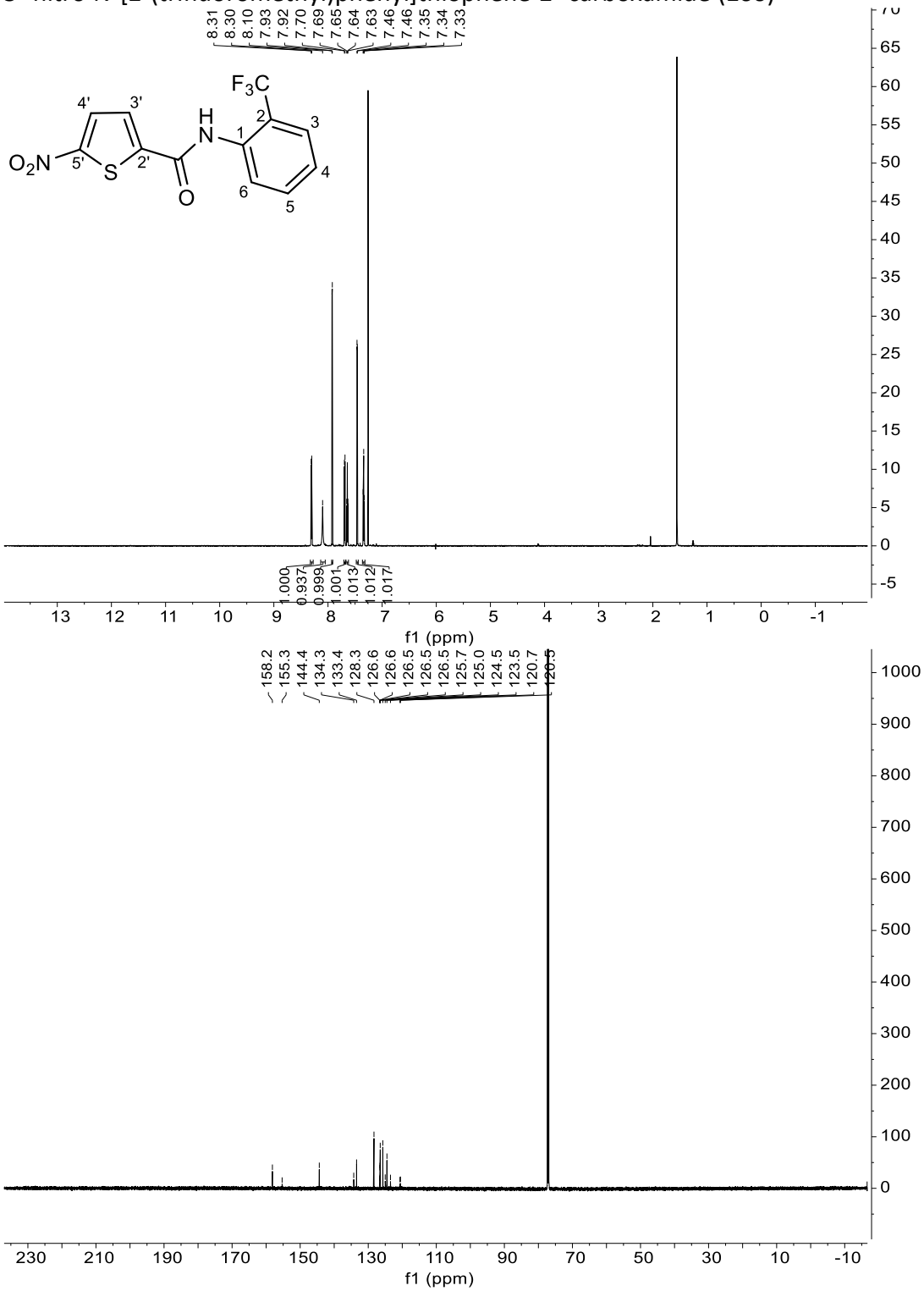

5’-nitro-*N*-[3-(trifluoromethyl)phenyl]thiophene-2’-carboxamide (**161**)

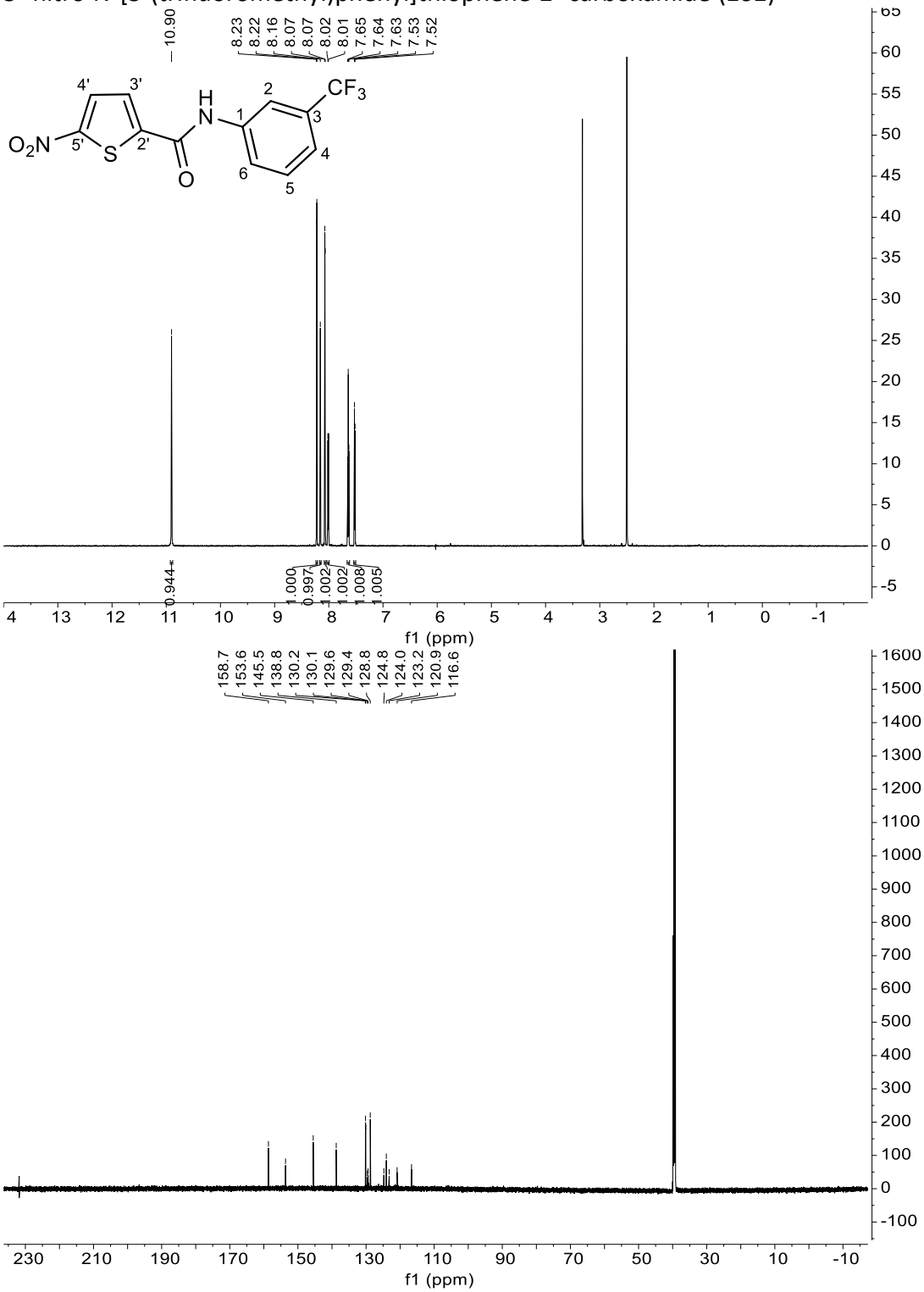

N-(2-acetylphenyl)-5’-nitrothiophene-2’-carboxamide (**162**)

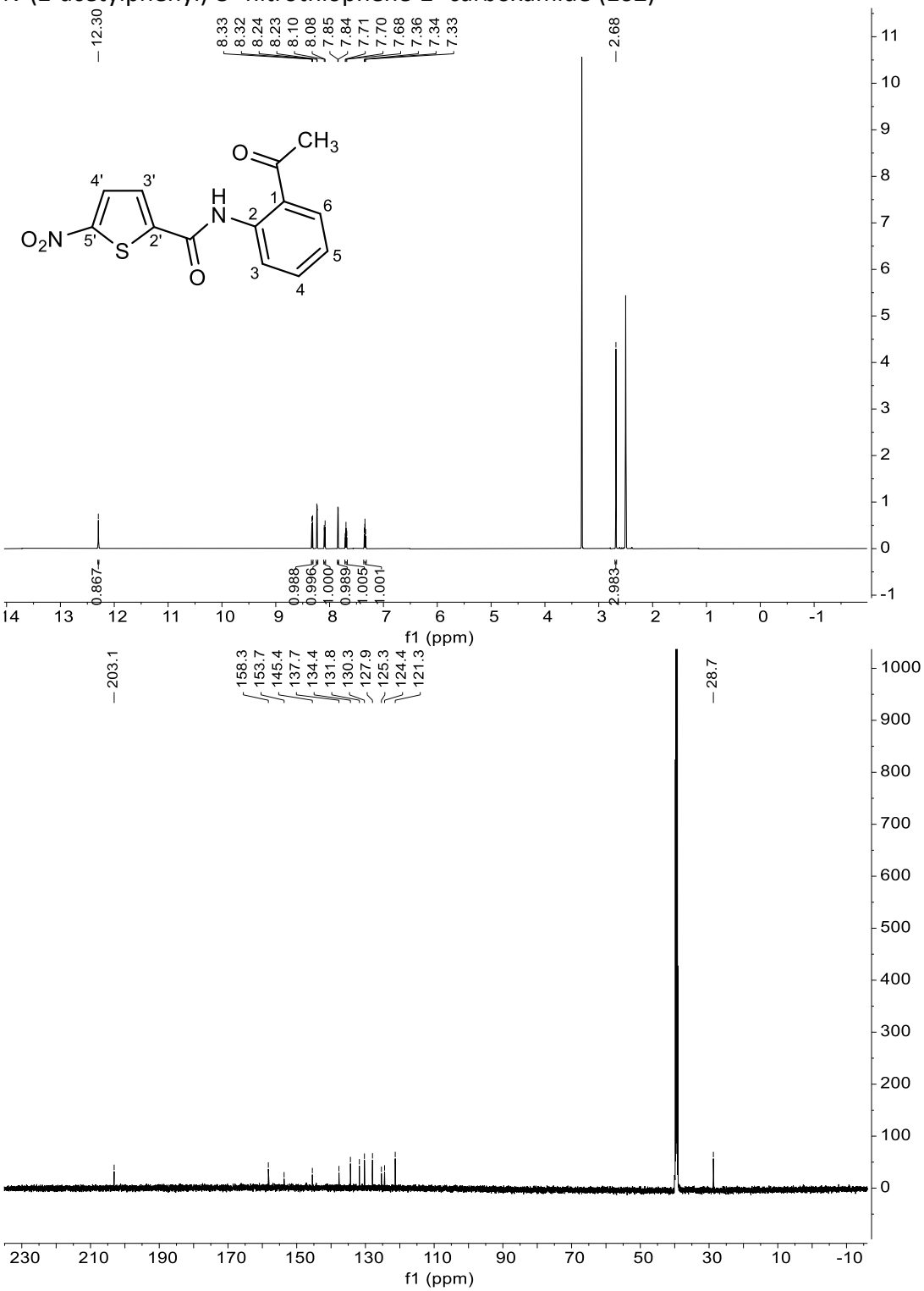

2-amino-N-dimethyl benzamide (**154**)

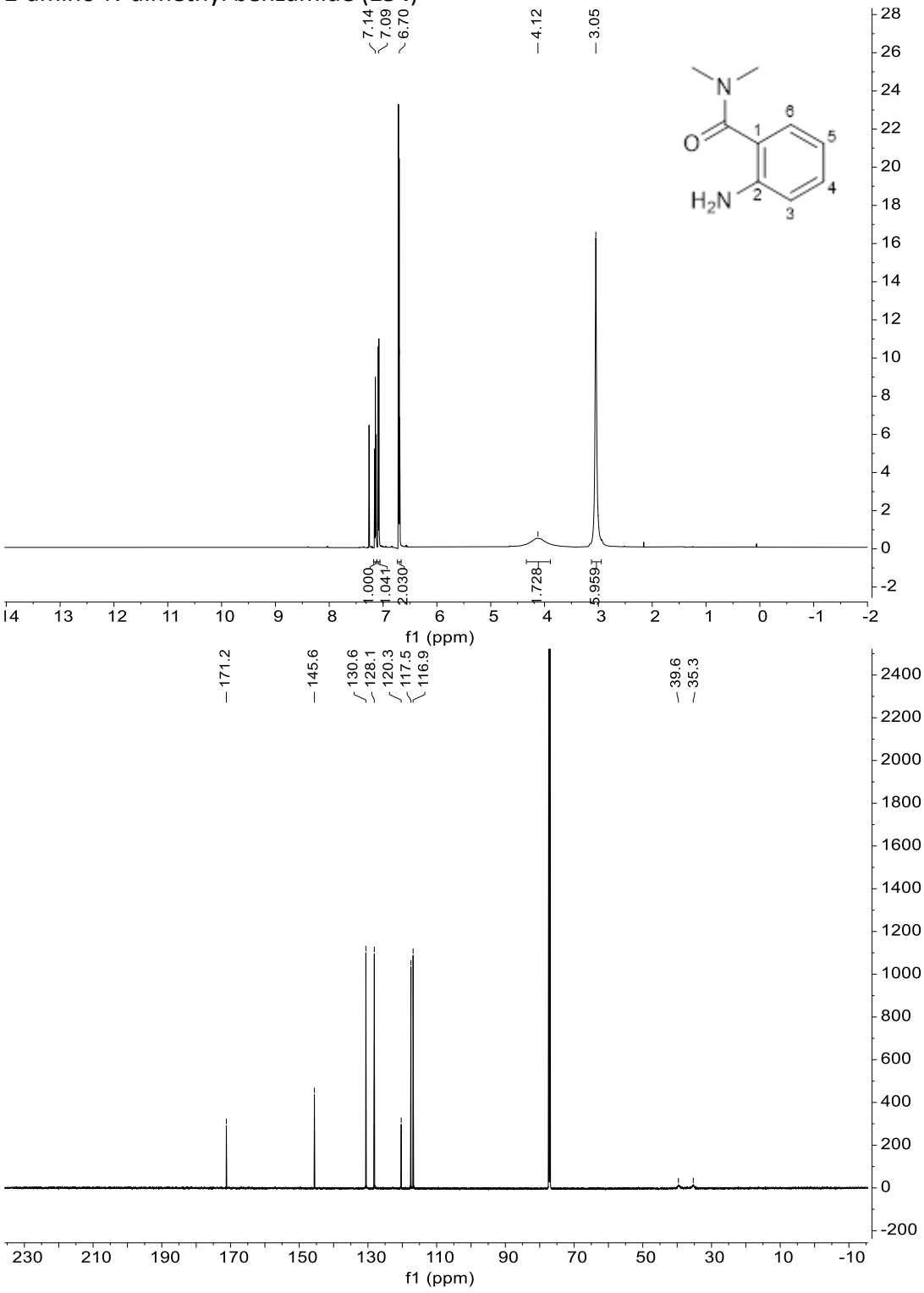

N-[2-(dimethylcarbamoyl) phenyl]-5’-nitrothiophene-2’-carboxamide (**163**)

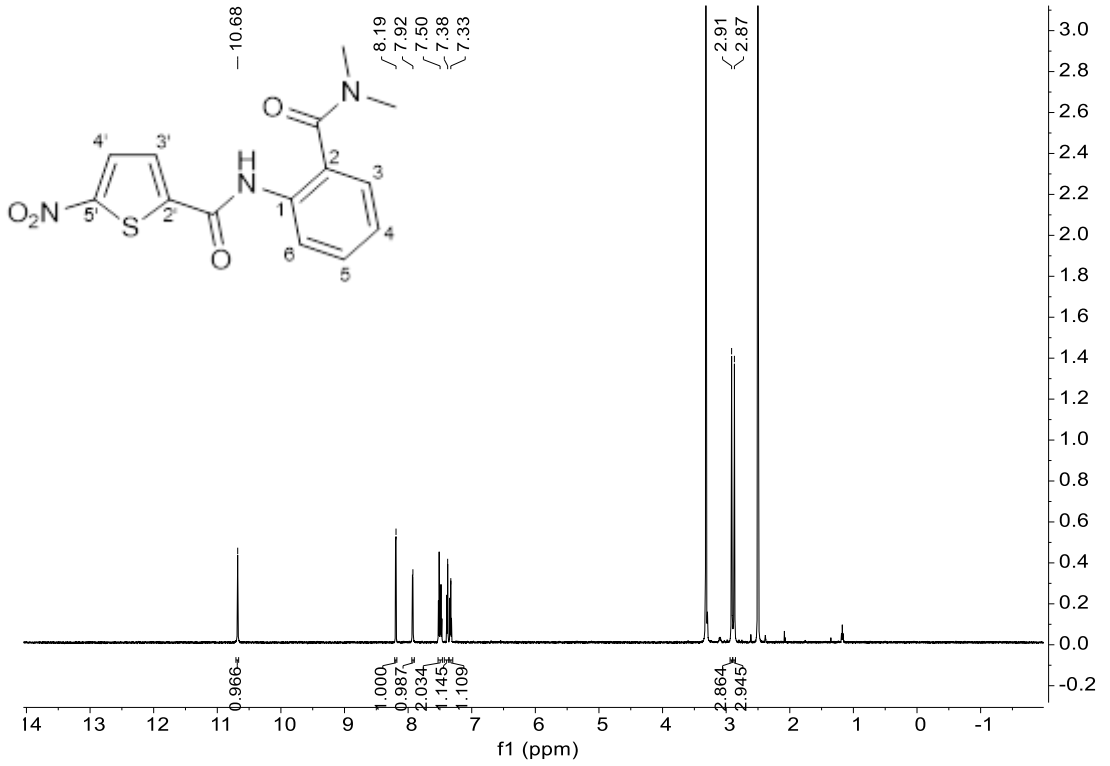

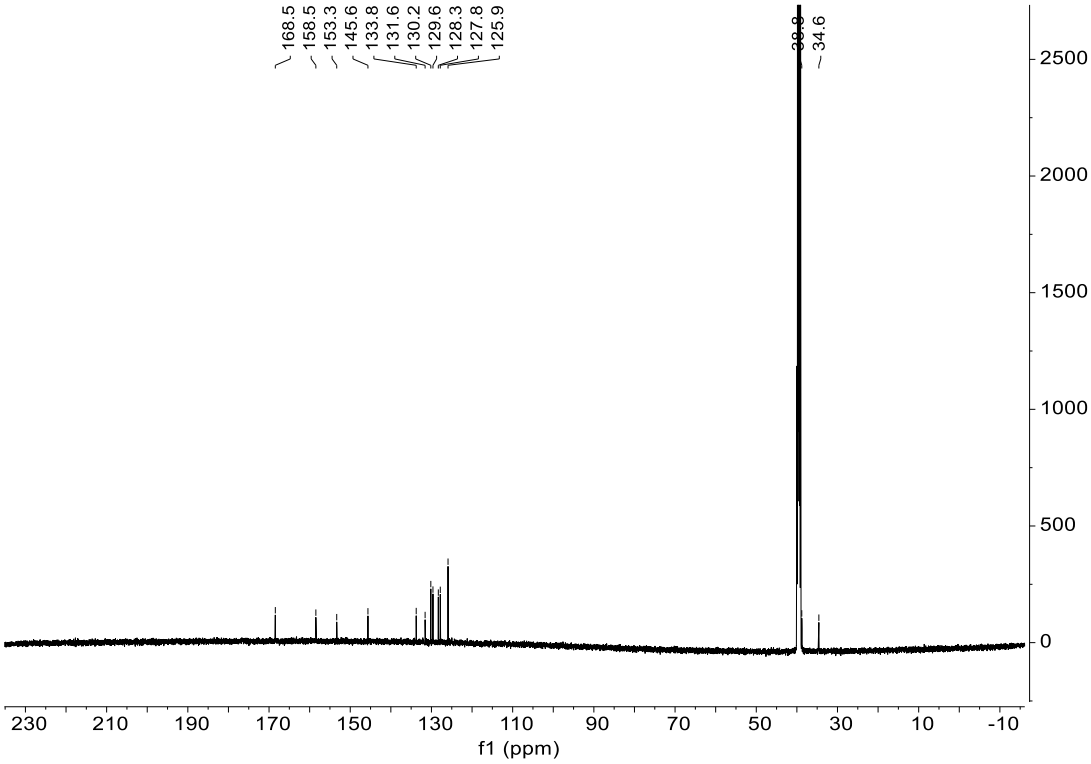

5’-nitro-*N*-[2-(tridecylcarbamoyl)phenyl]thiophene-2’-carboxamide (**164**)

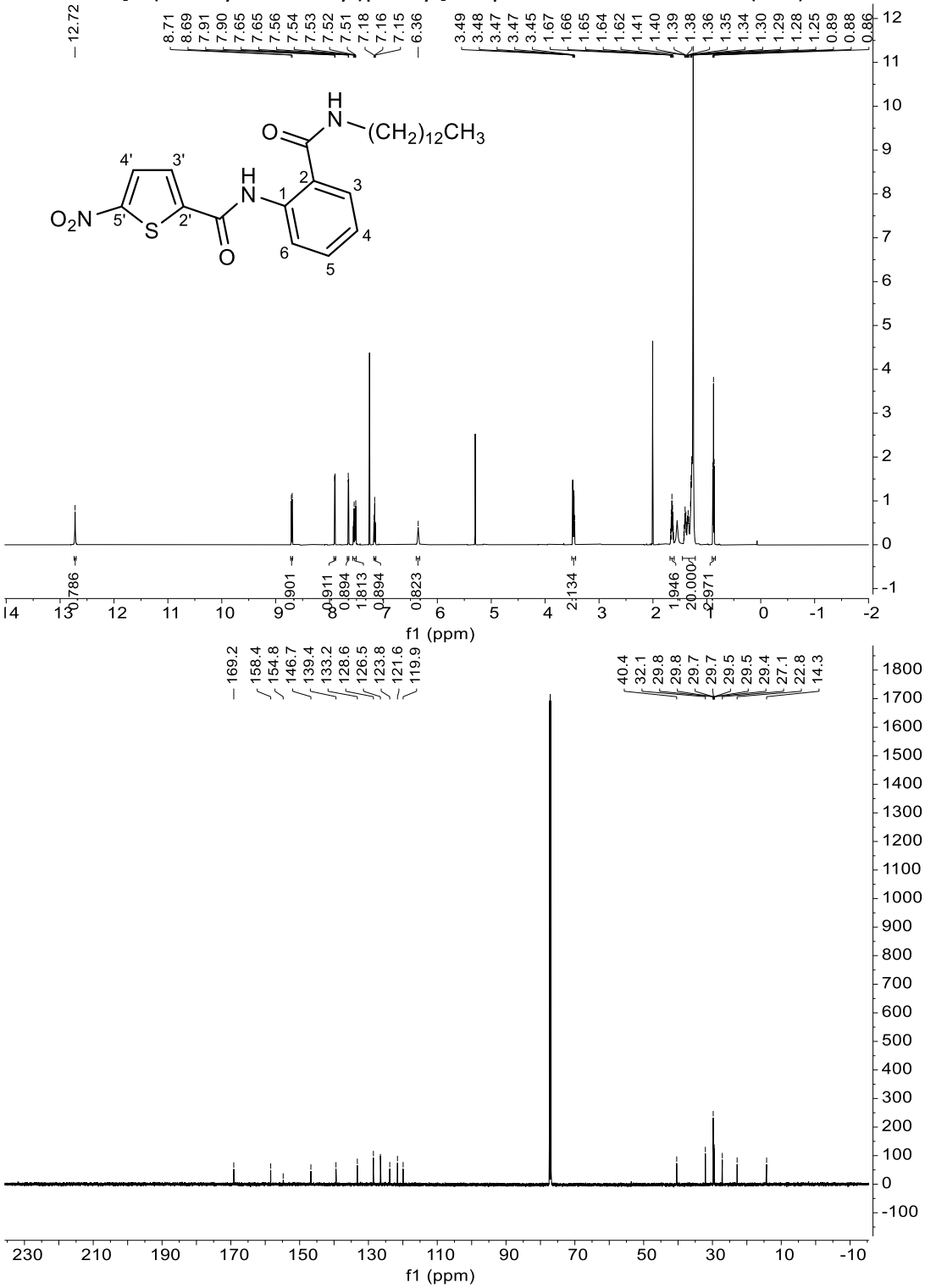

5’-nitro-N-{2’-[(propan-2-yl)carbamoyl]phenyl}thiophene-2-carboxamide (**165**)

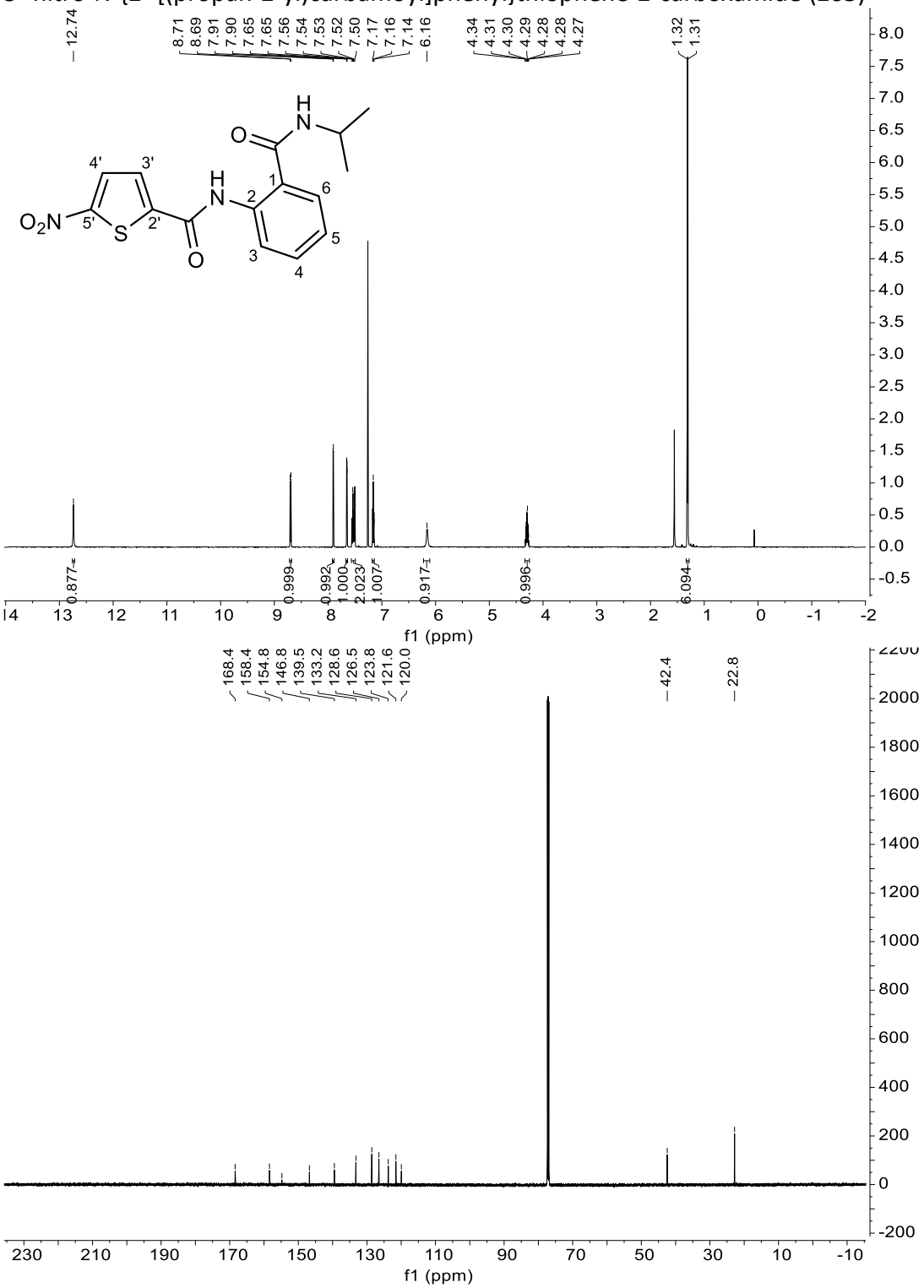

5-methyl-2,4-dihydro-1*H*-3,1-benzoxazine-2,4-dione (**175**)

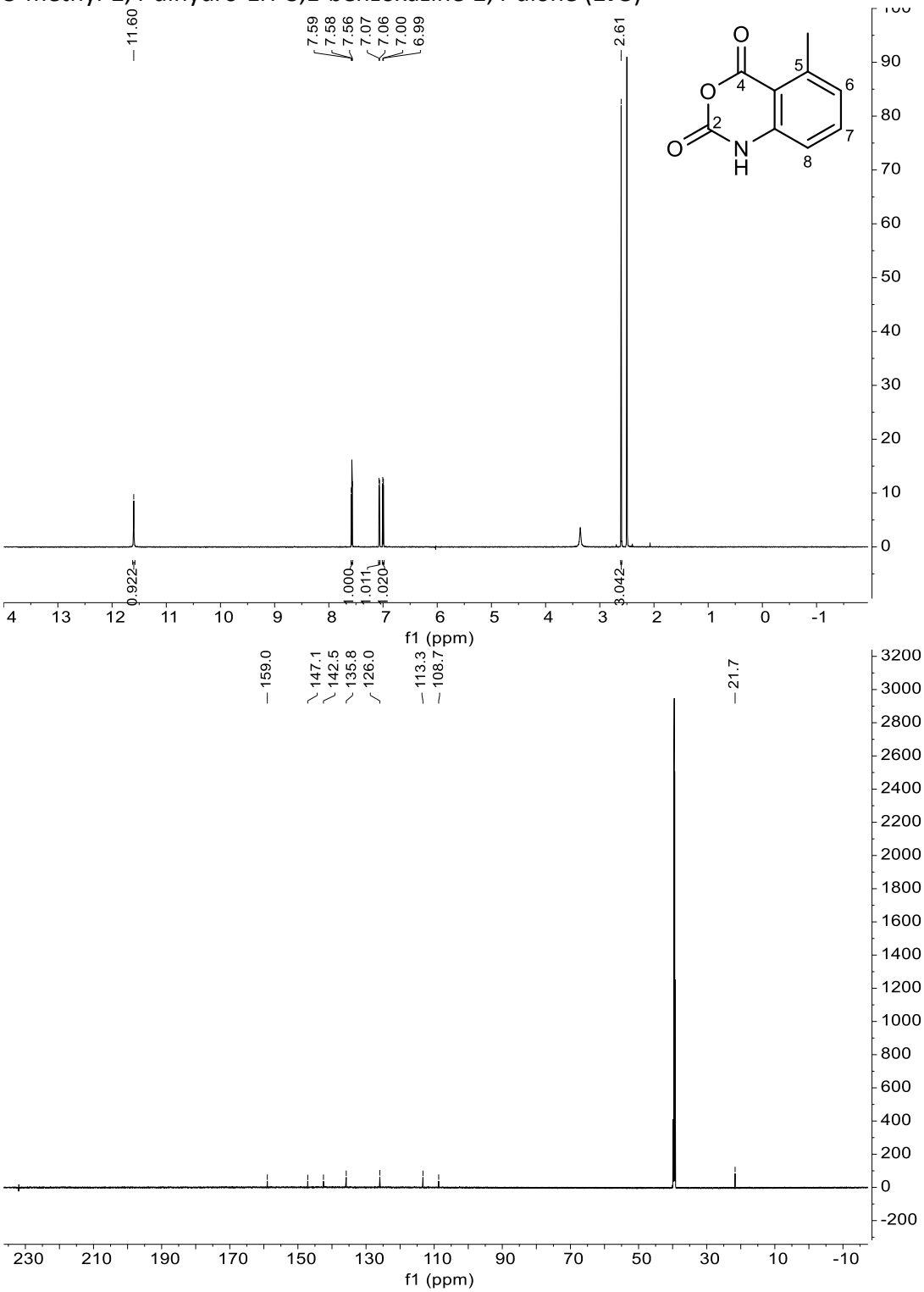

6-methoxy-2,4-dihydro-1*H*-3,1-benzoxazine-2,4-dione (**176**)

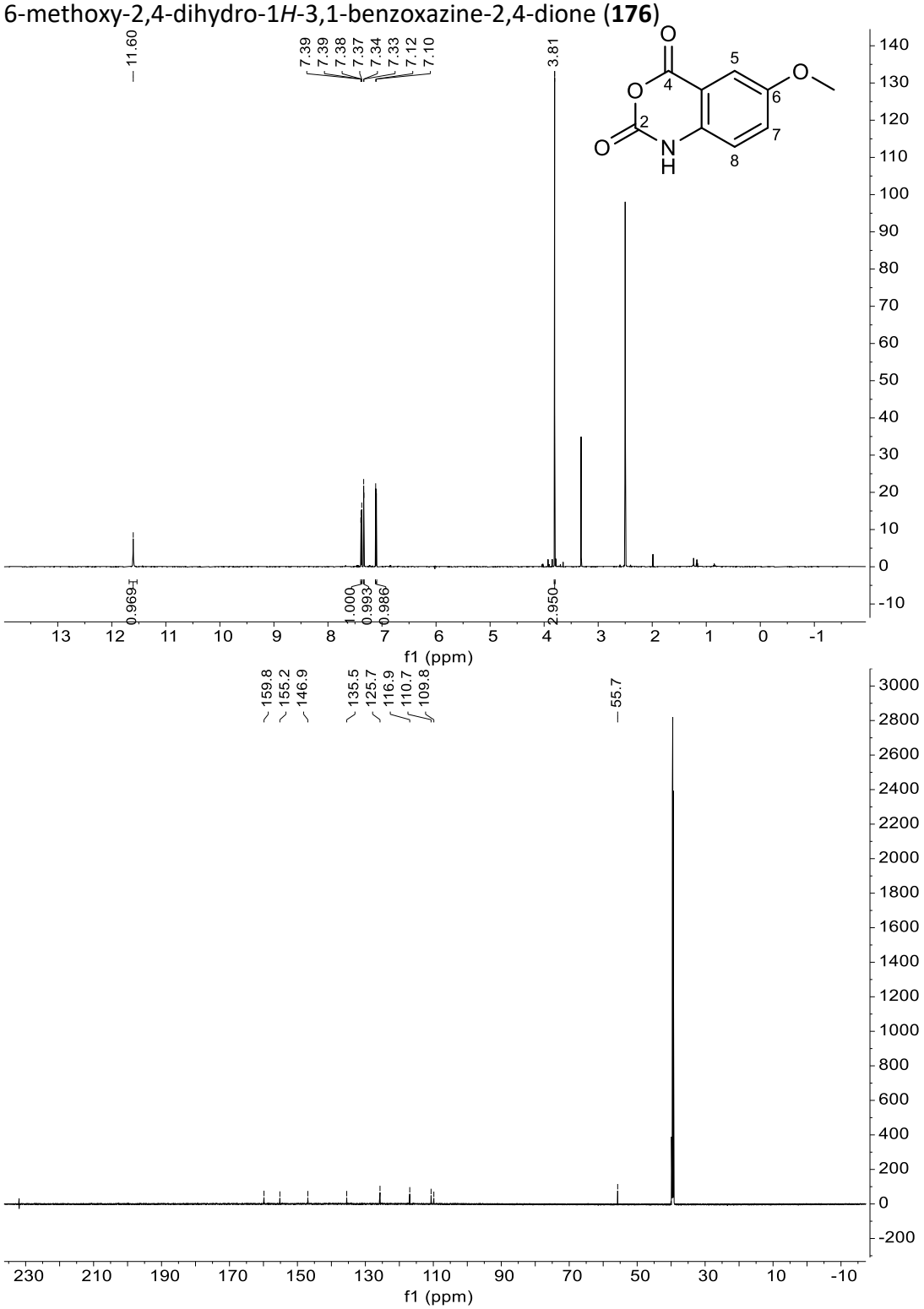

6-methyl-2,4-dihydro-1*H*-3,1-benzoxazine-2,4-dione (**177**)

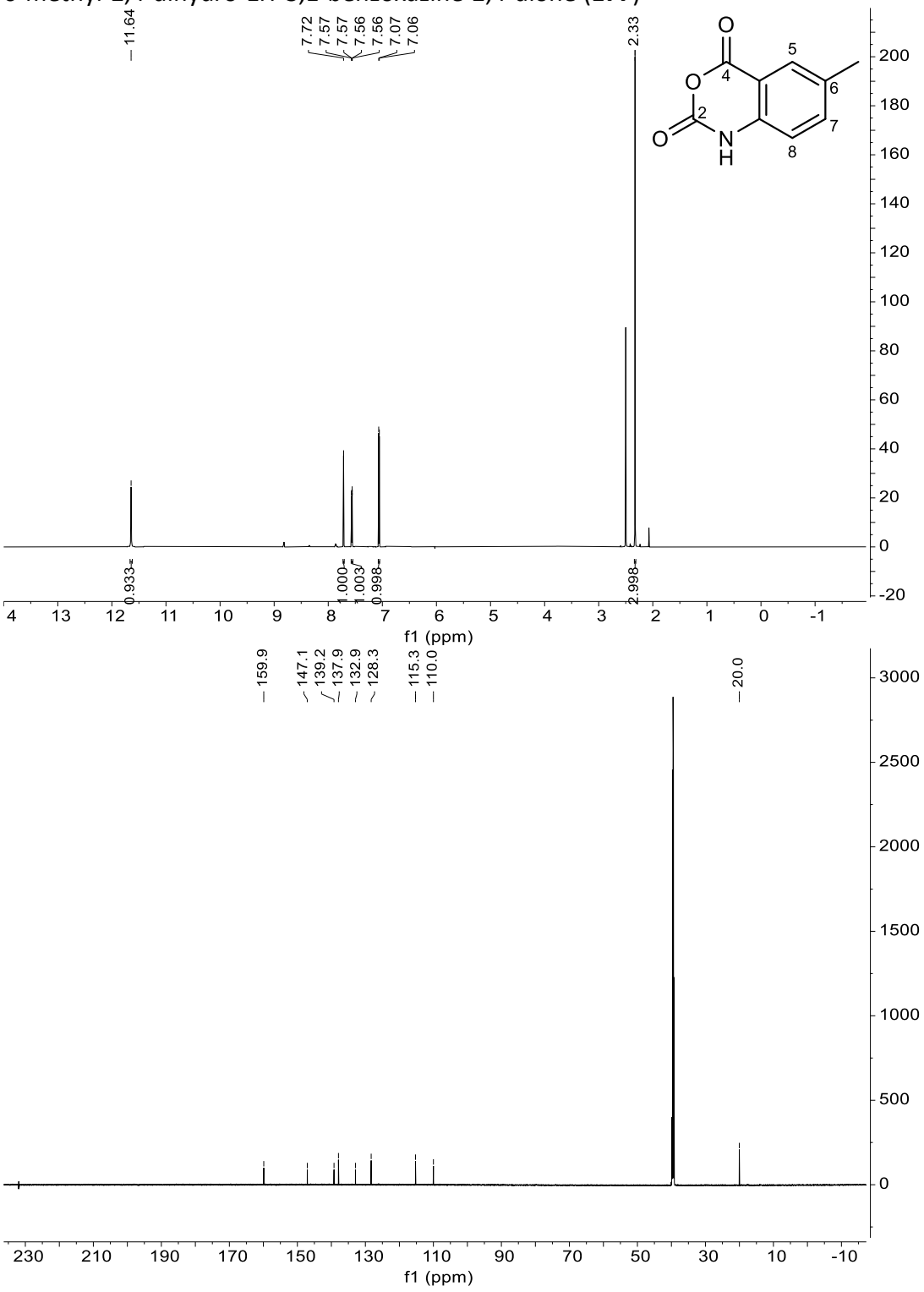

7-methoxy-2,4-dihydro-1*H*-3,1-benzoxazine-2,4-dione (**178**)

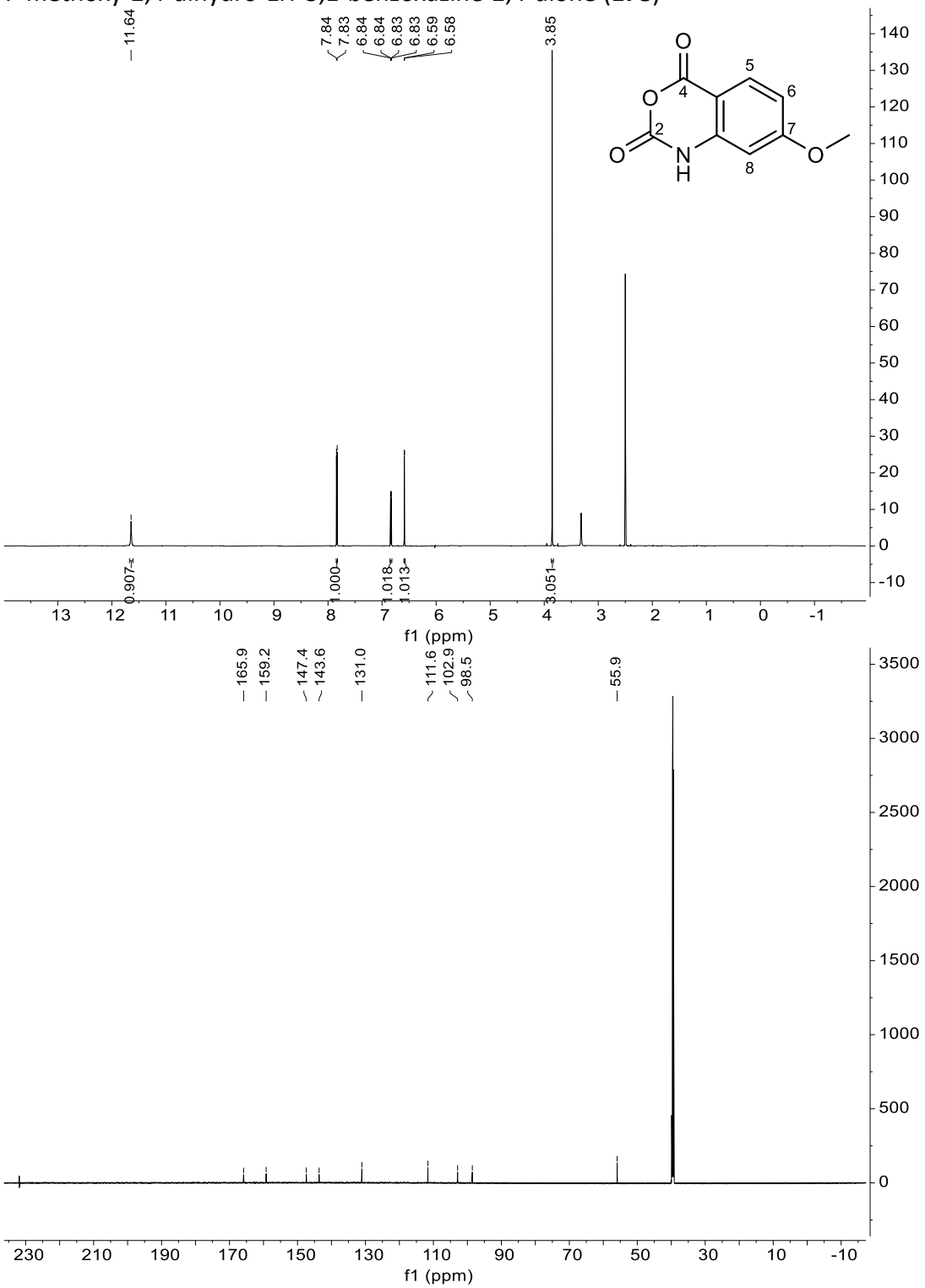

7-methyl-2,4-dihydro-1*H*-3,1-benzoxazine-2,4-dione (**179**)

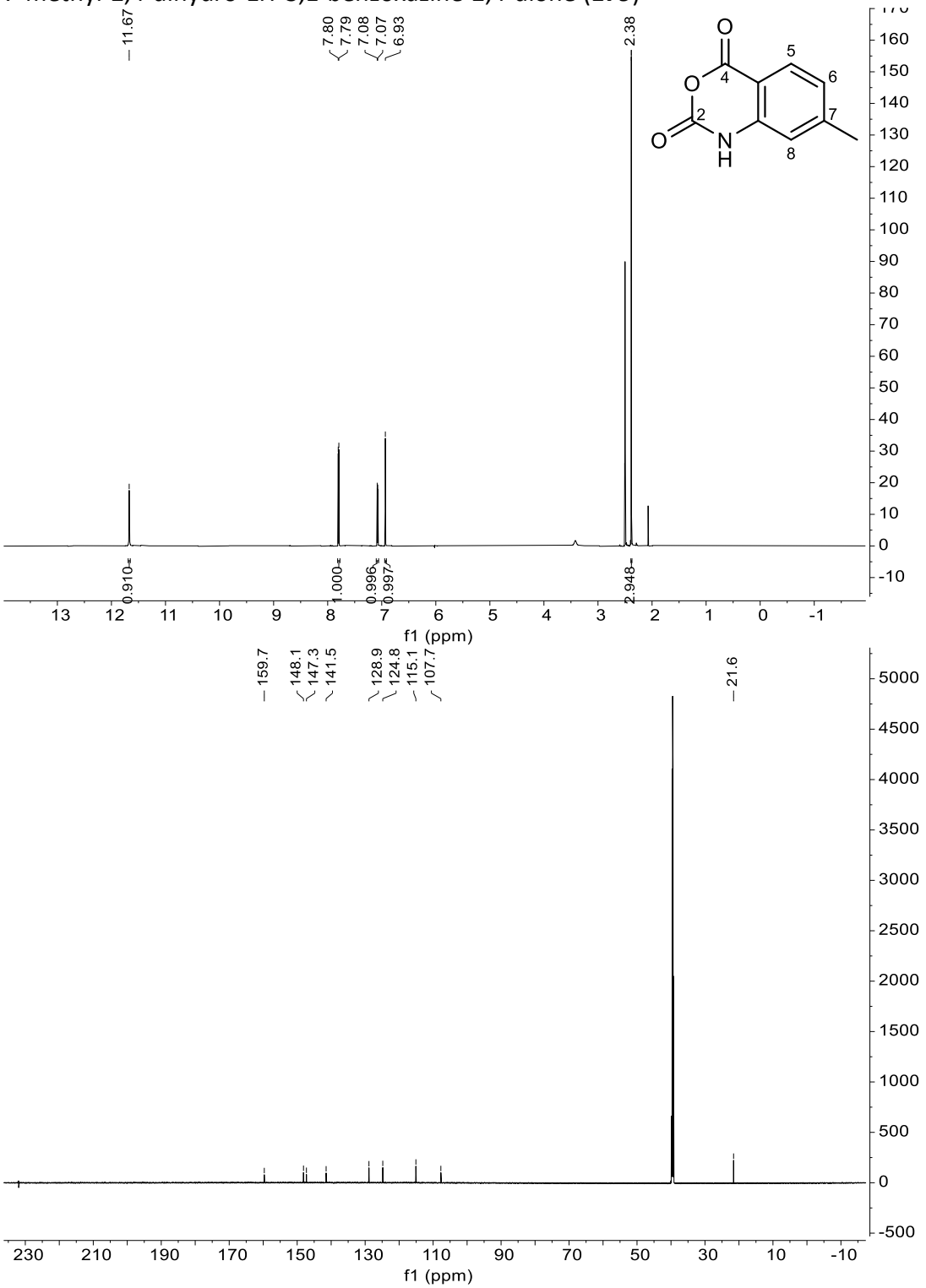

7-trifluoromethyl-2,4-dihydro-1*H*-3,1-benzoxazine-2,4-dione (**180**)

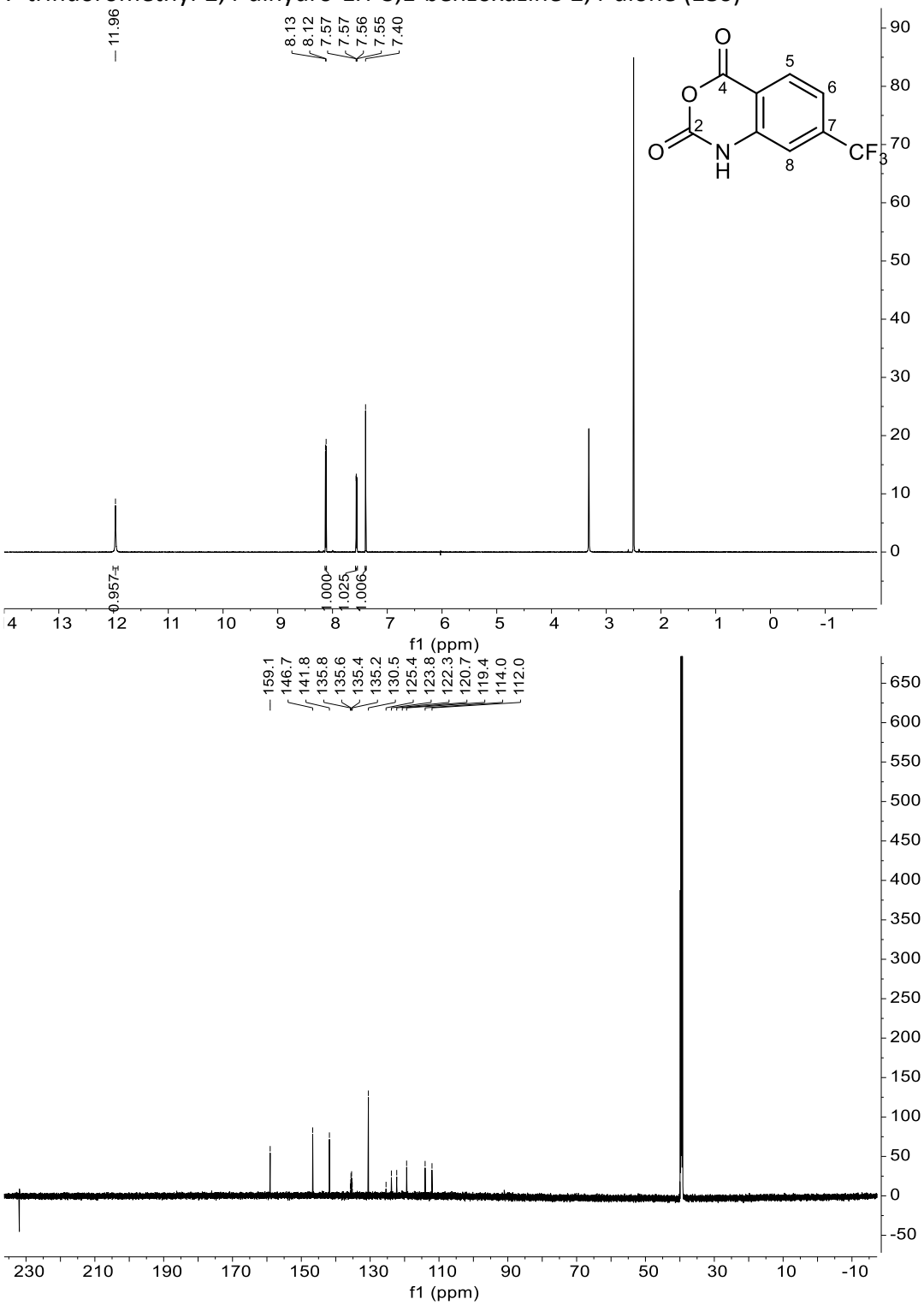

7-bromo-2,4-dihydro-1*H*-3,1-benzoxazine-2,4-dione (**181**)

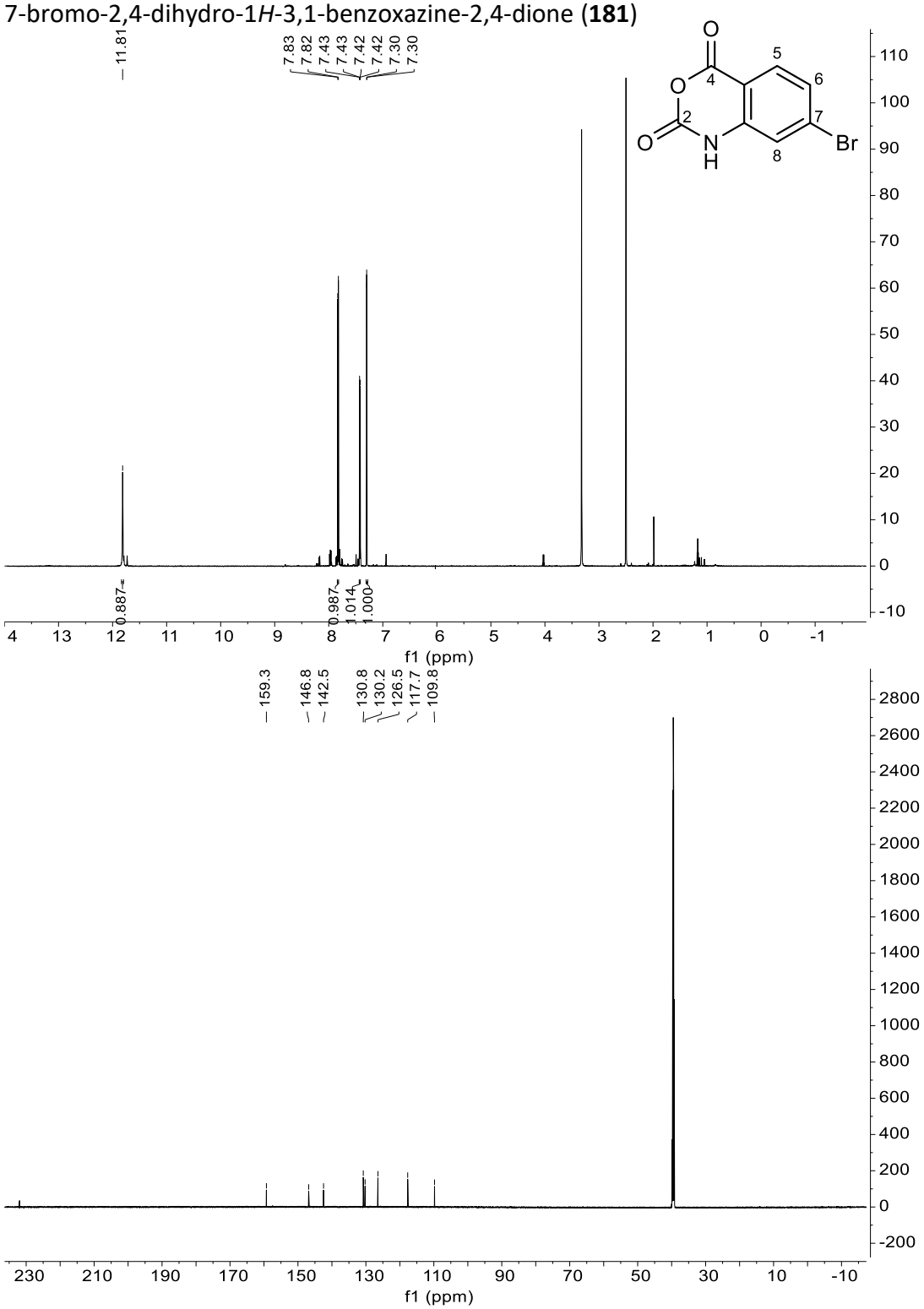

8-methoxy-2,4-dihydro-1*H*-3,1-benzoxazine-2,4-dione (**182**)

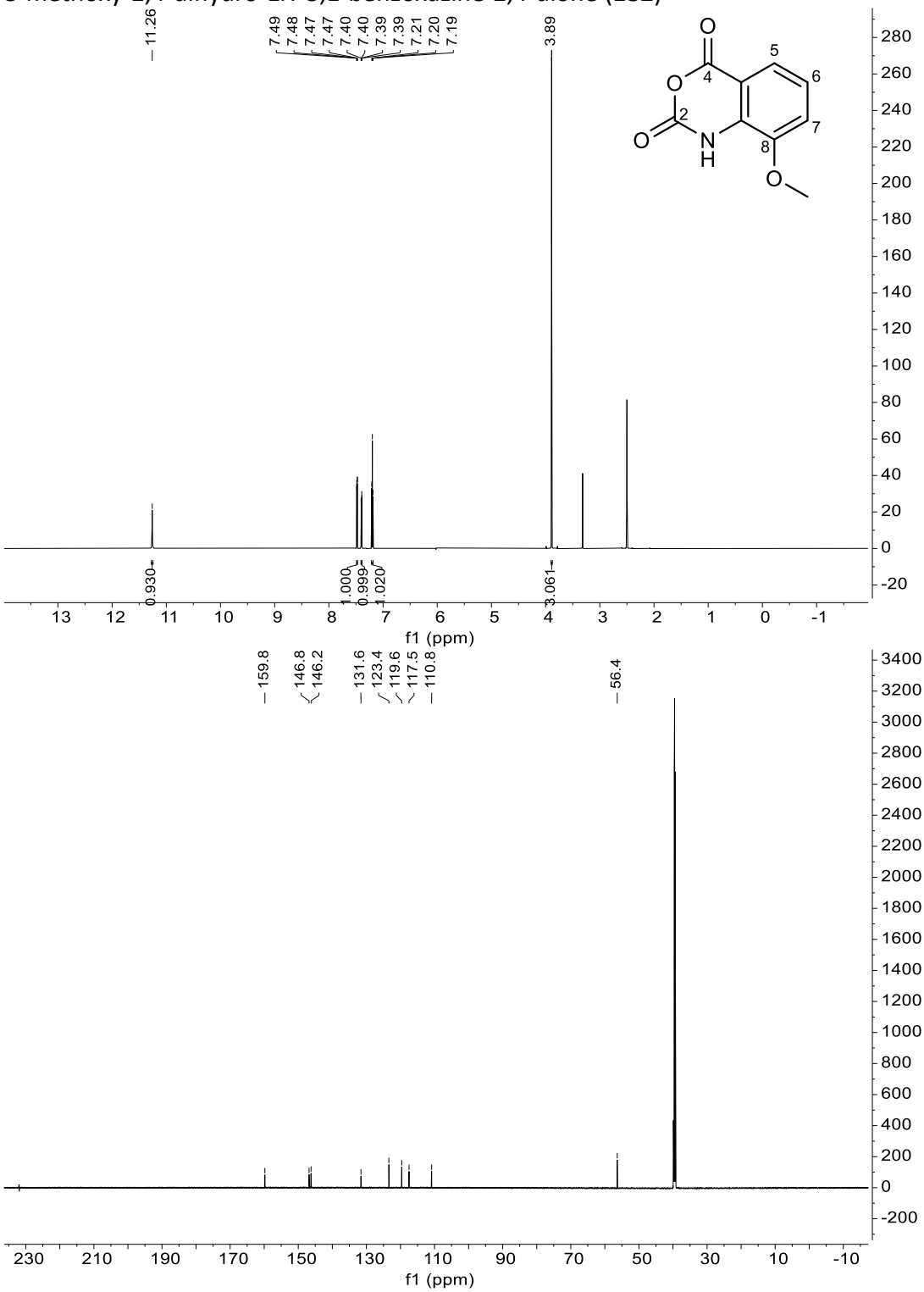

8-methyl-2,4-dihydro-1*H*-3,1-benzoxazine-2,4-dione (**183**)

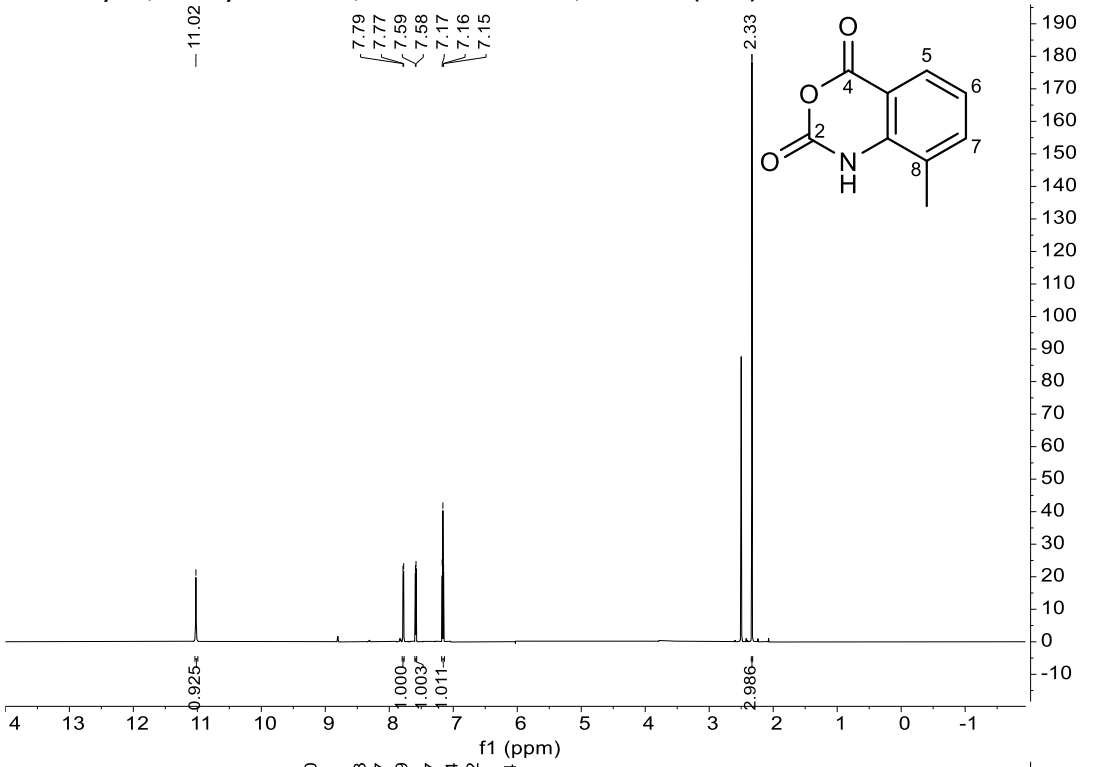

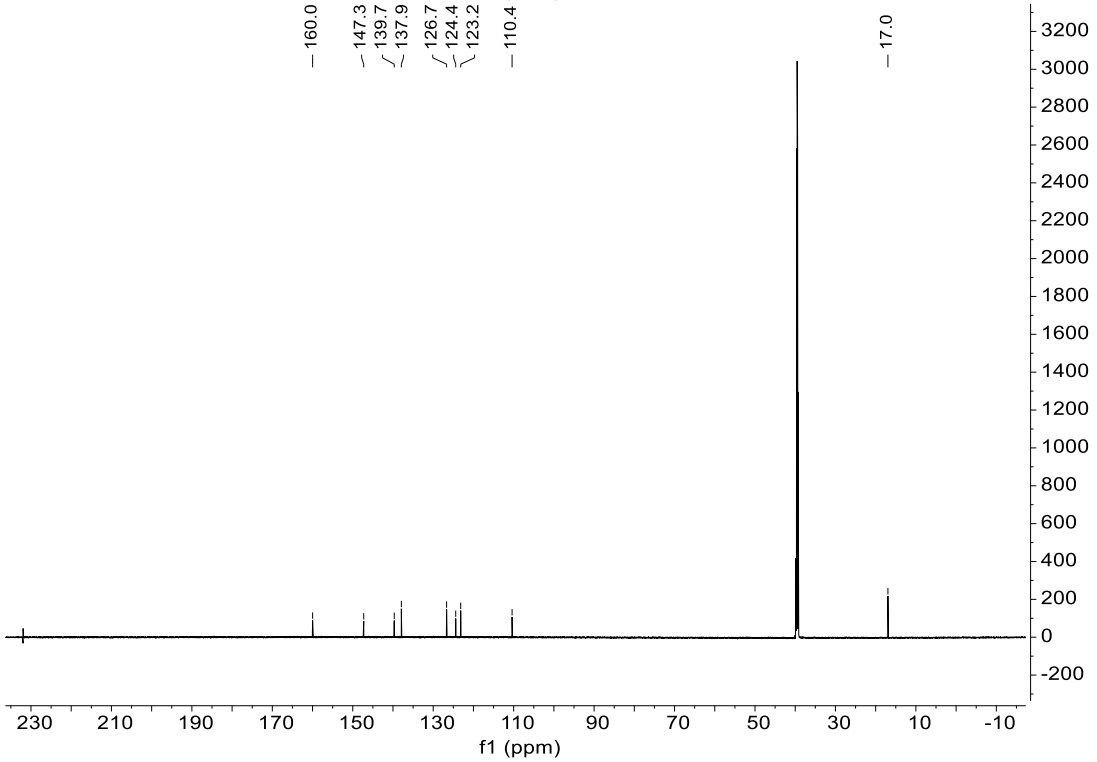

Amino-3-methyl-*N*-methyl-2-benzamide (**184**)

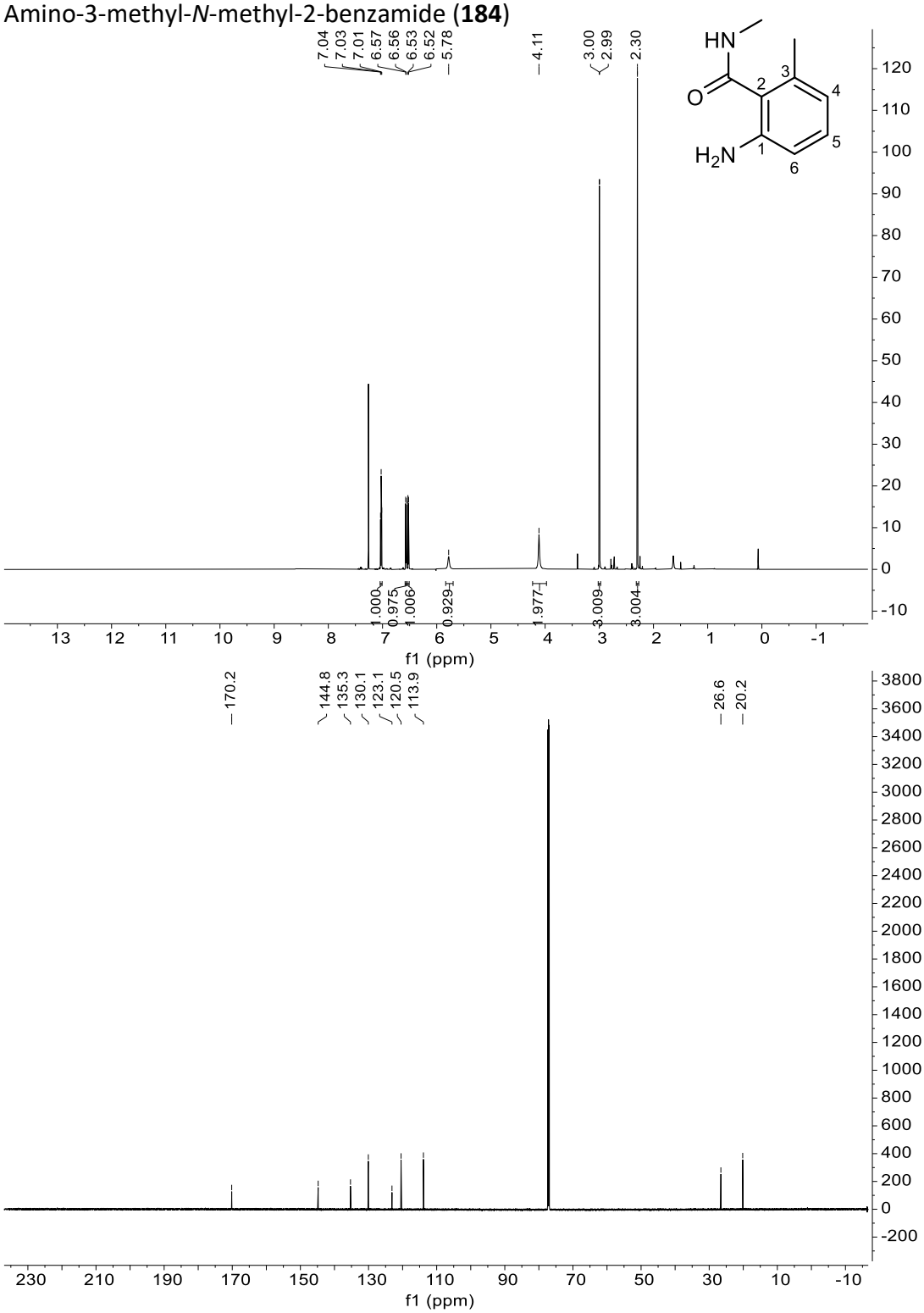

Amino-4-methoxy-*N*-methyl-2-benzamide (**185**)

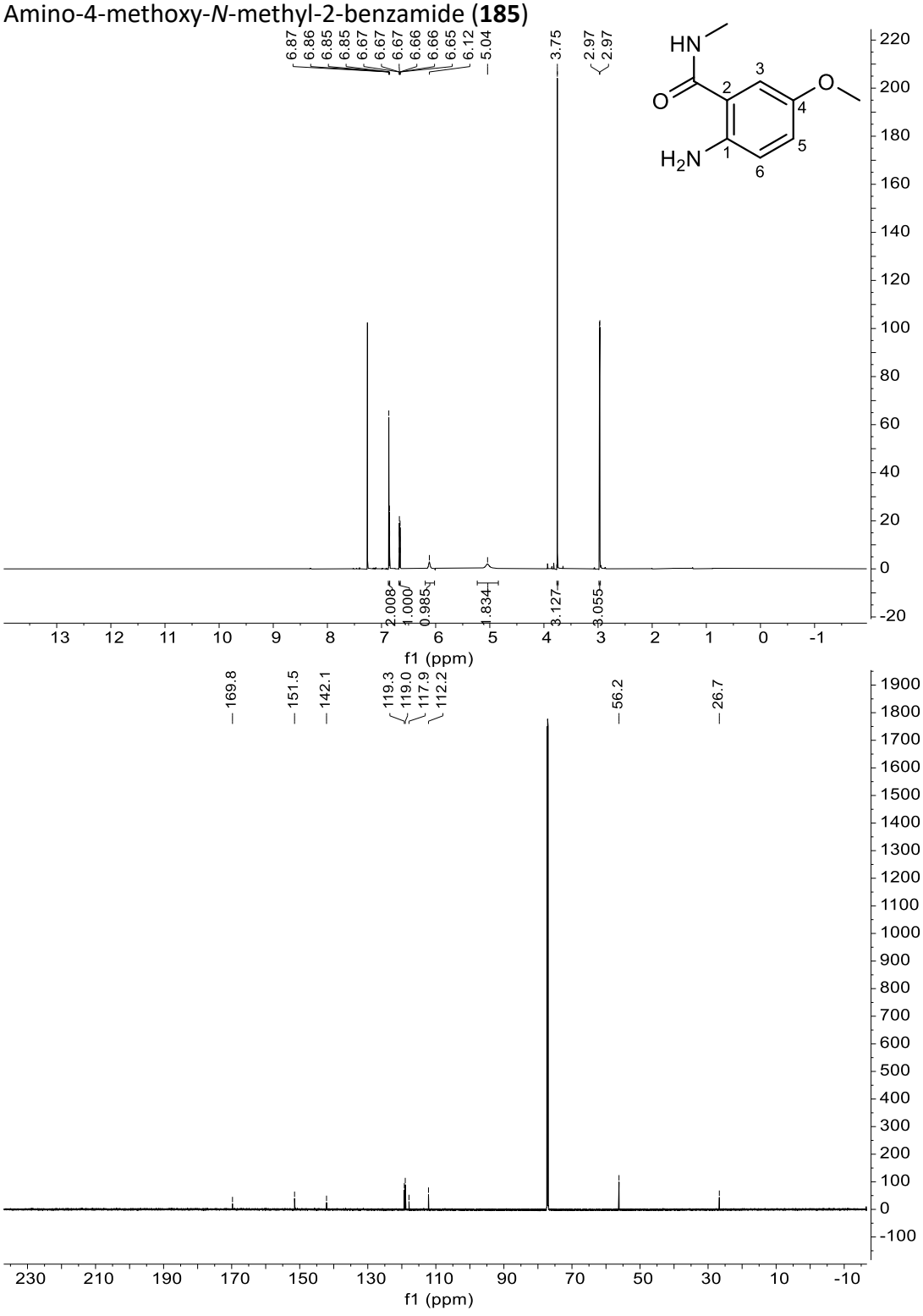

Amino-4-methyl-*N*-methyl-2-benzamide (**186**)

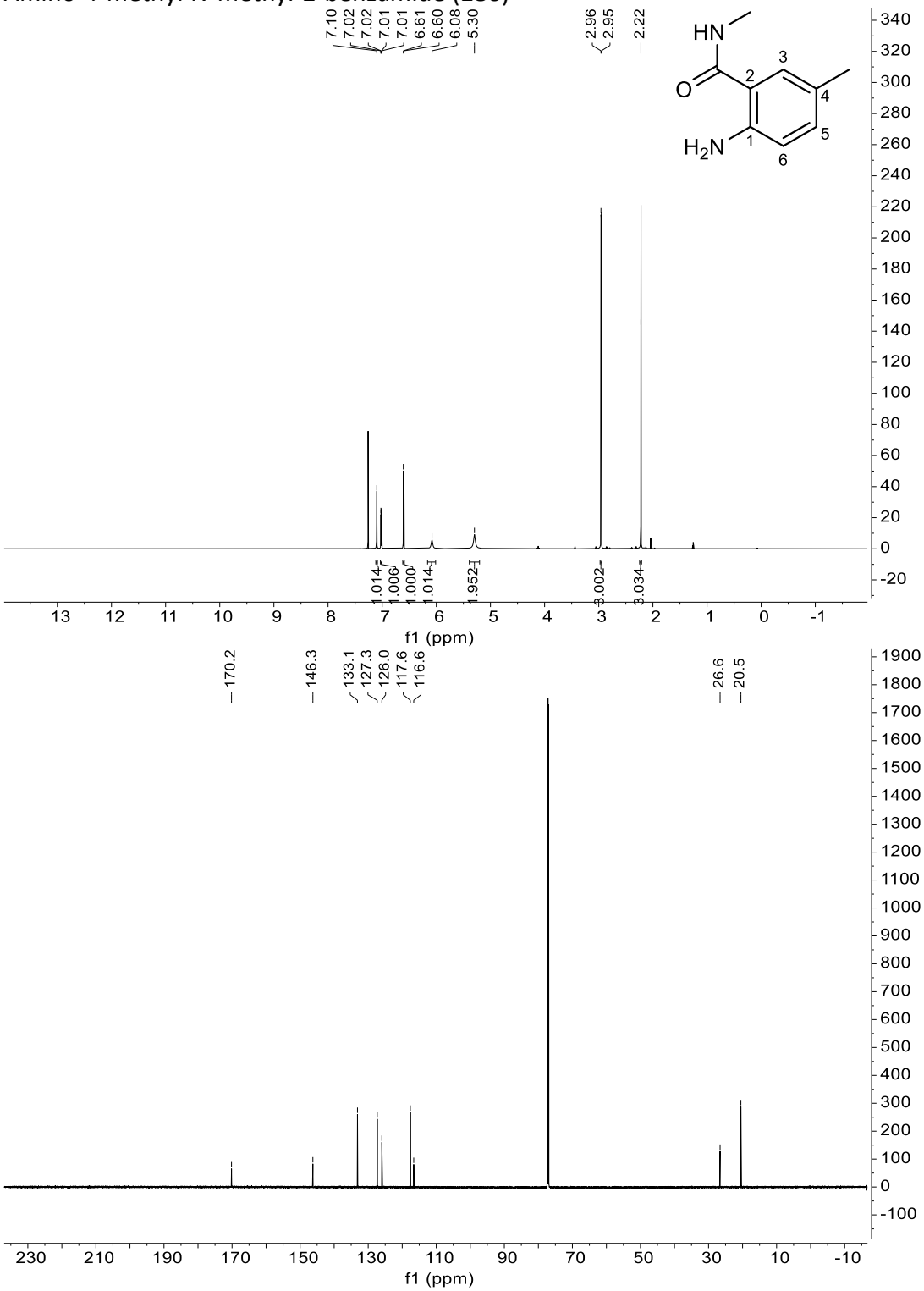

Amino-5-methoxy-*N*-methyl-2-benzamide (**187**)

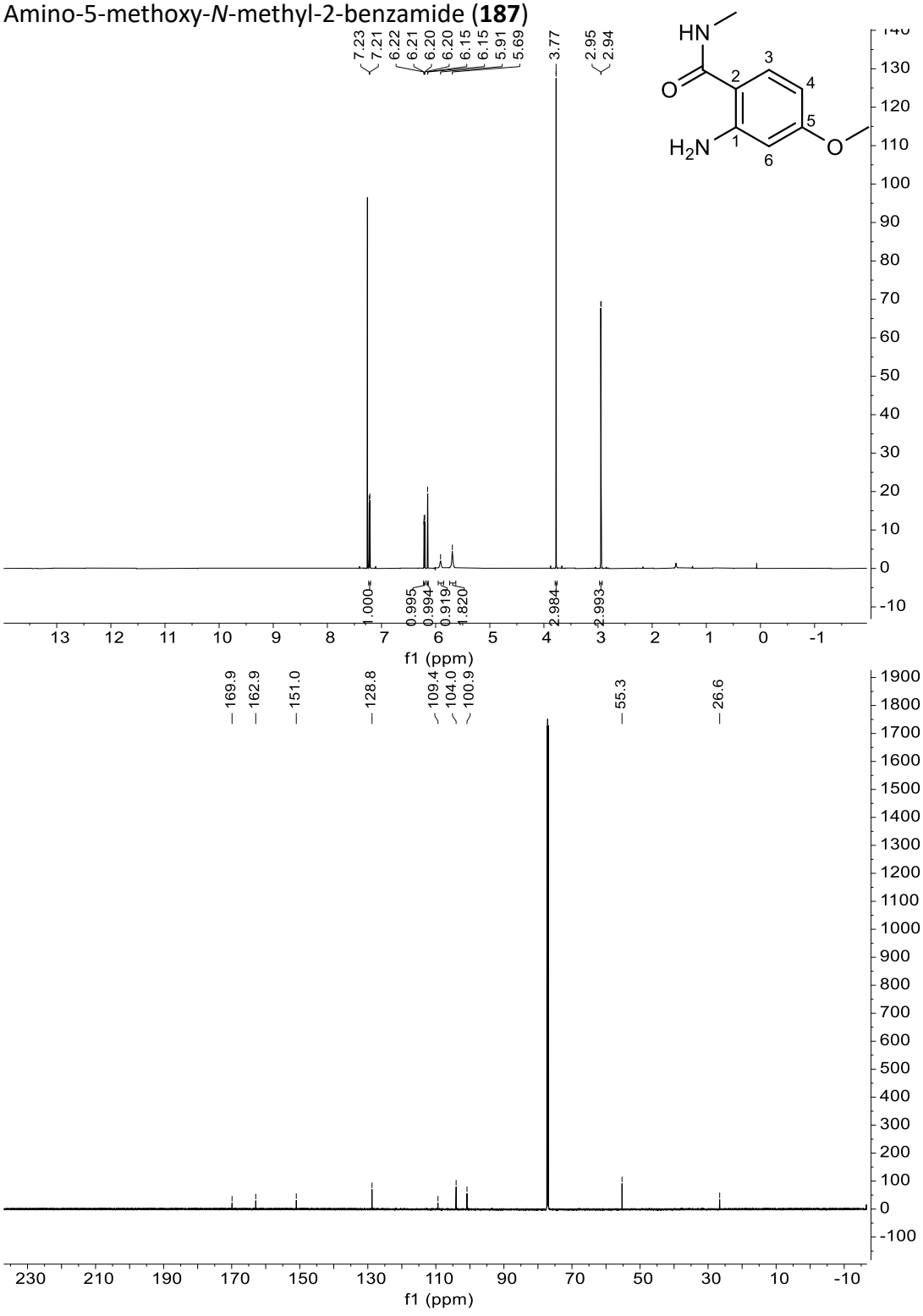

Amino-5-methyl-*N*-methyl-2-benzamide (**188**)

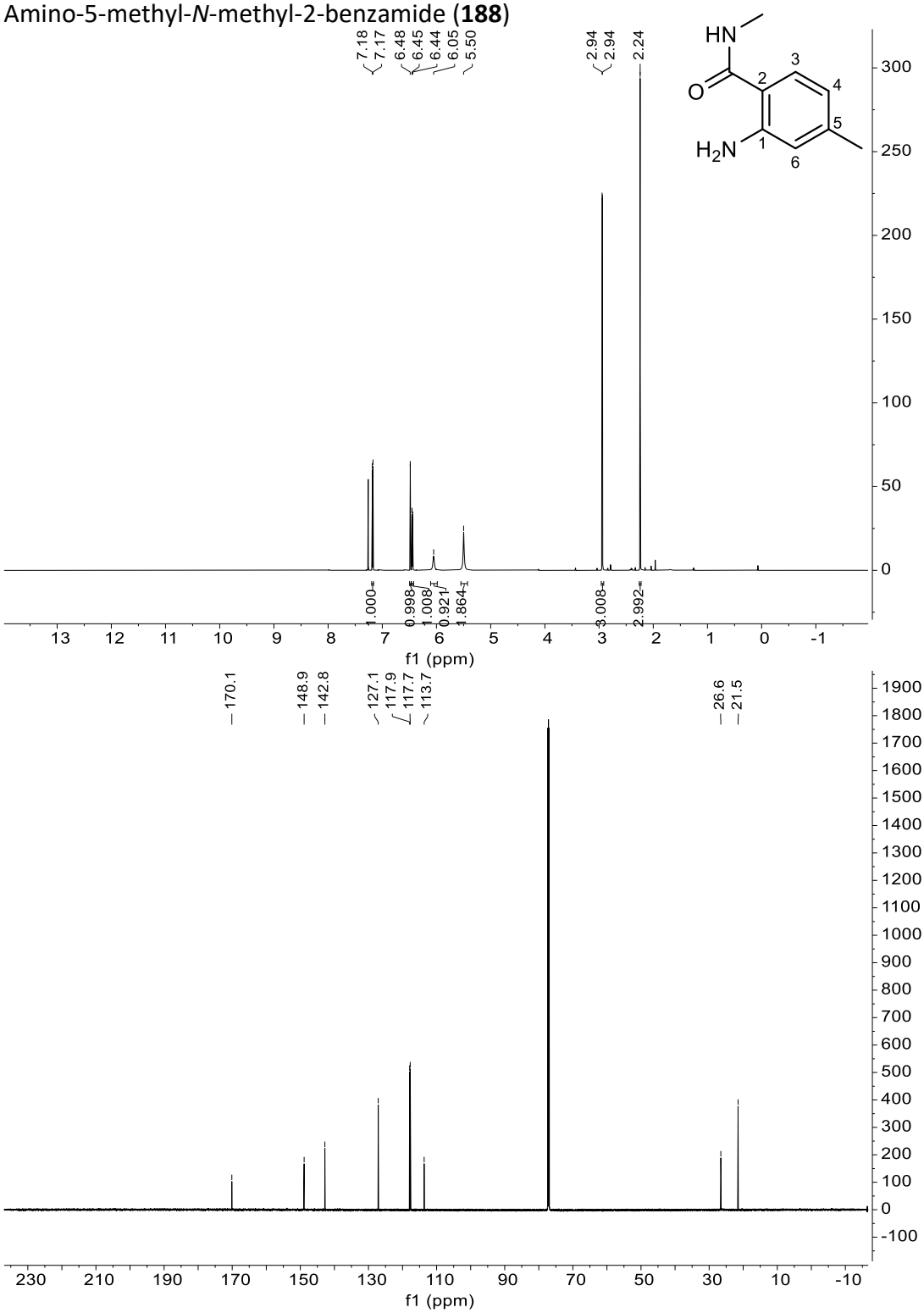

Amino-5-trifluoromethyl-*N*-methyl-2-benzamide (**189**)

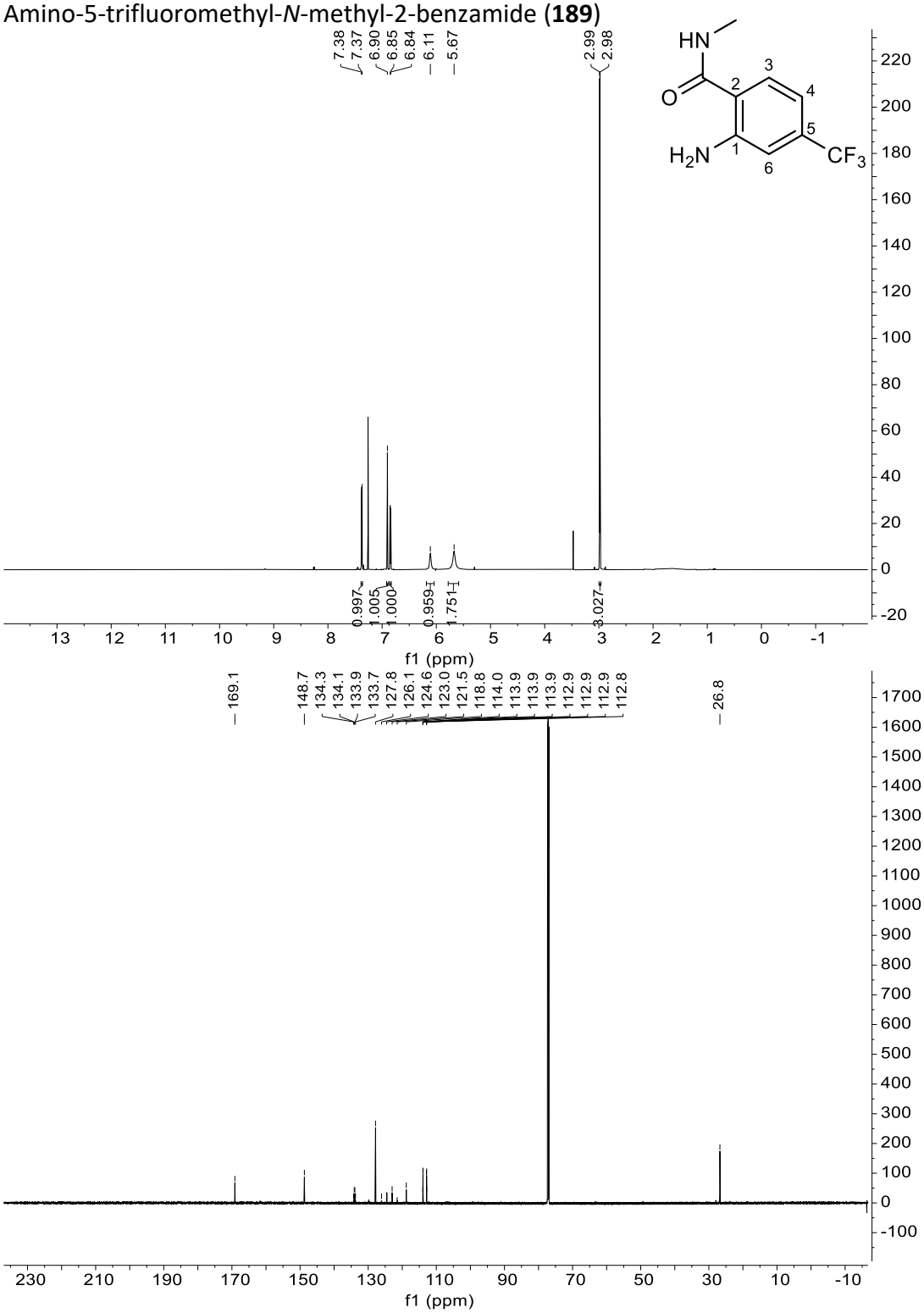

Amino-5-bromo-*N*-methyl-2-benzamide (**190**)

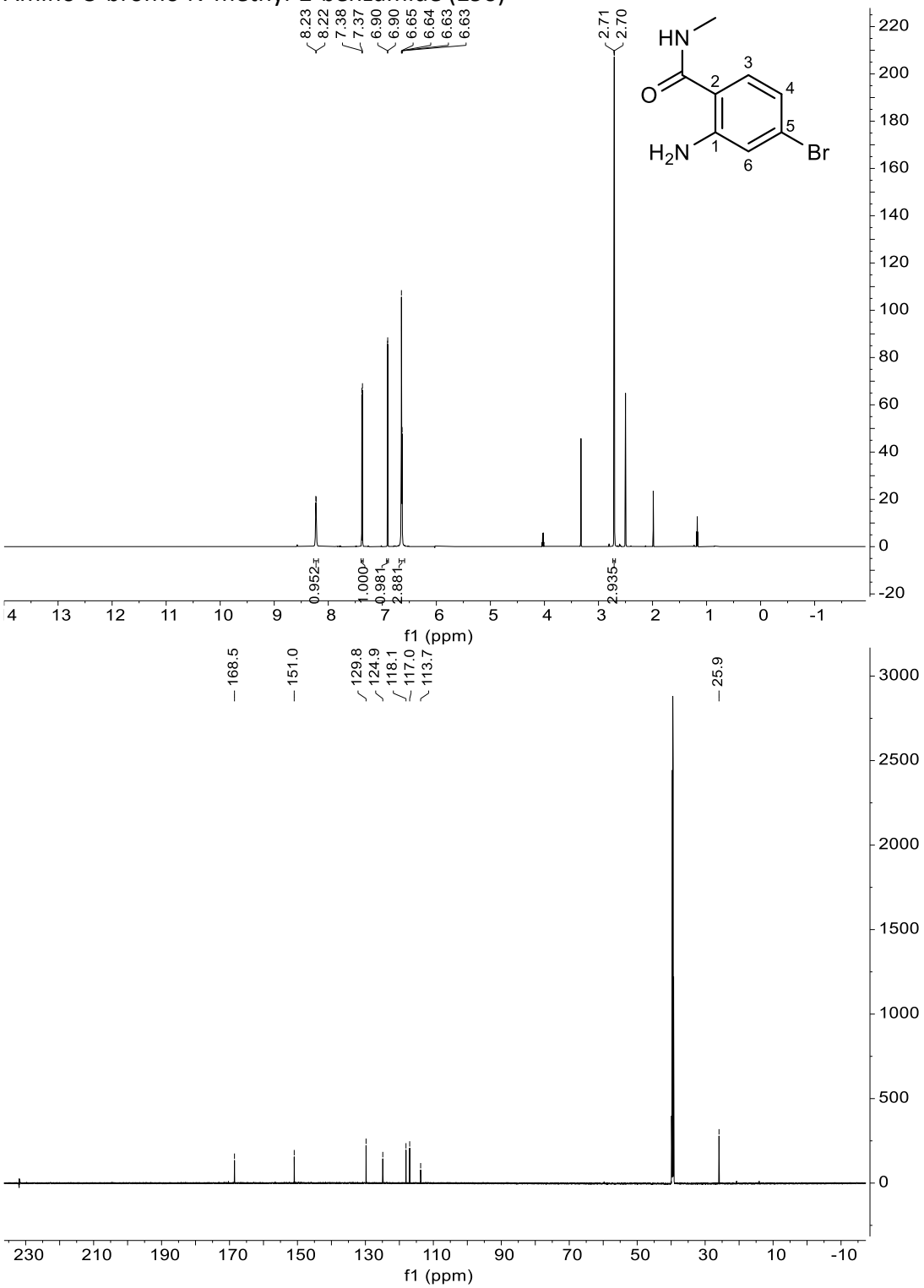

Amino-6-methoxy-*N*-methyl-2-benzamide (**191**)

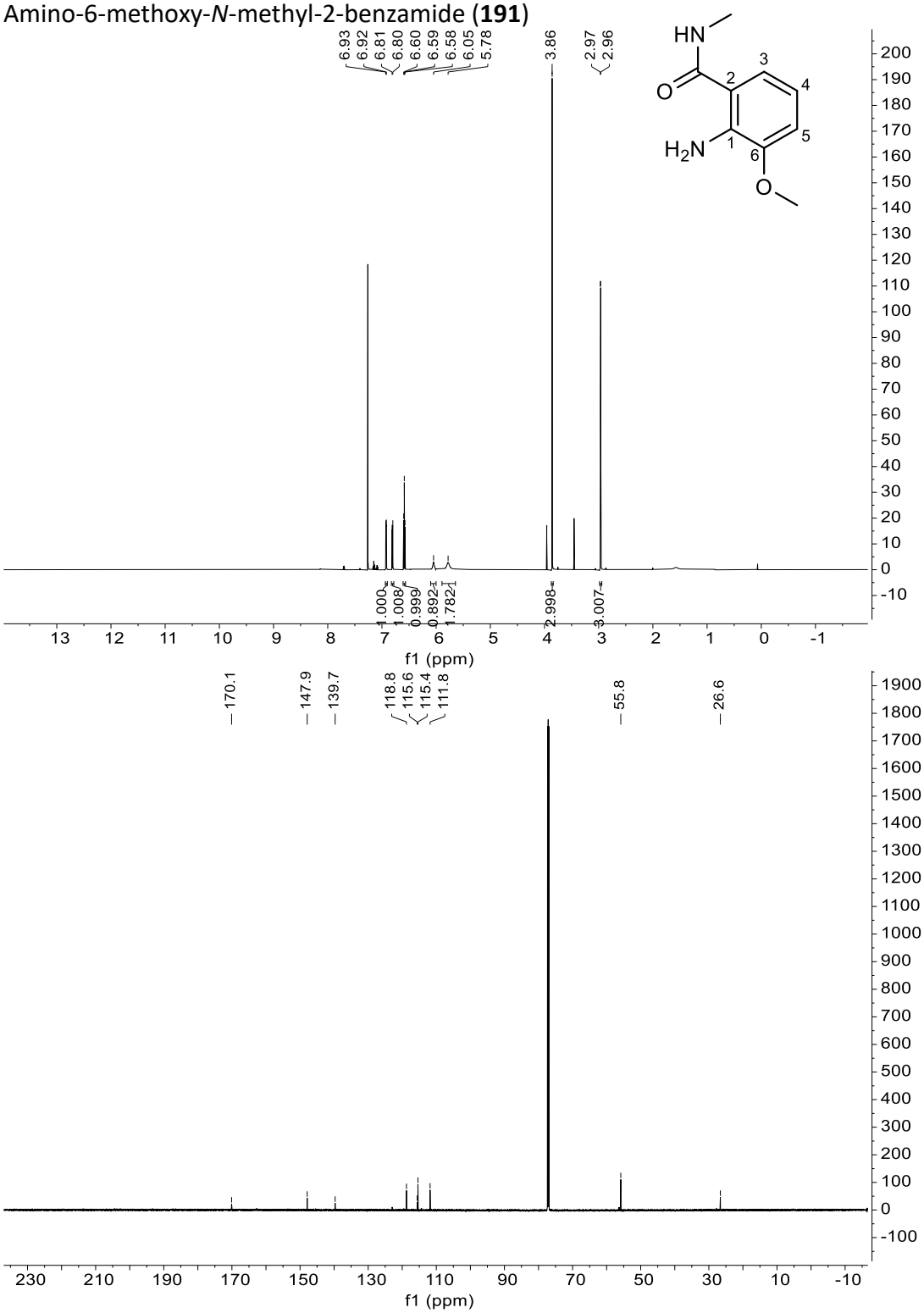

Amino-6-methyl-*N*-methyl-2-benzamide (**192**)

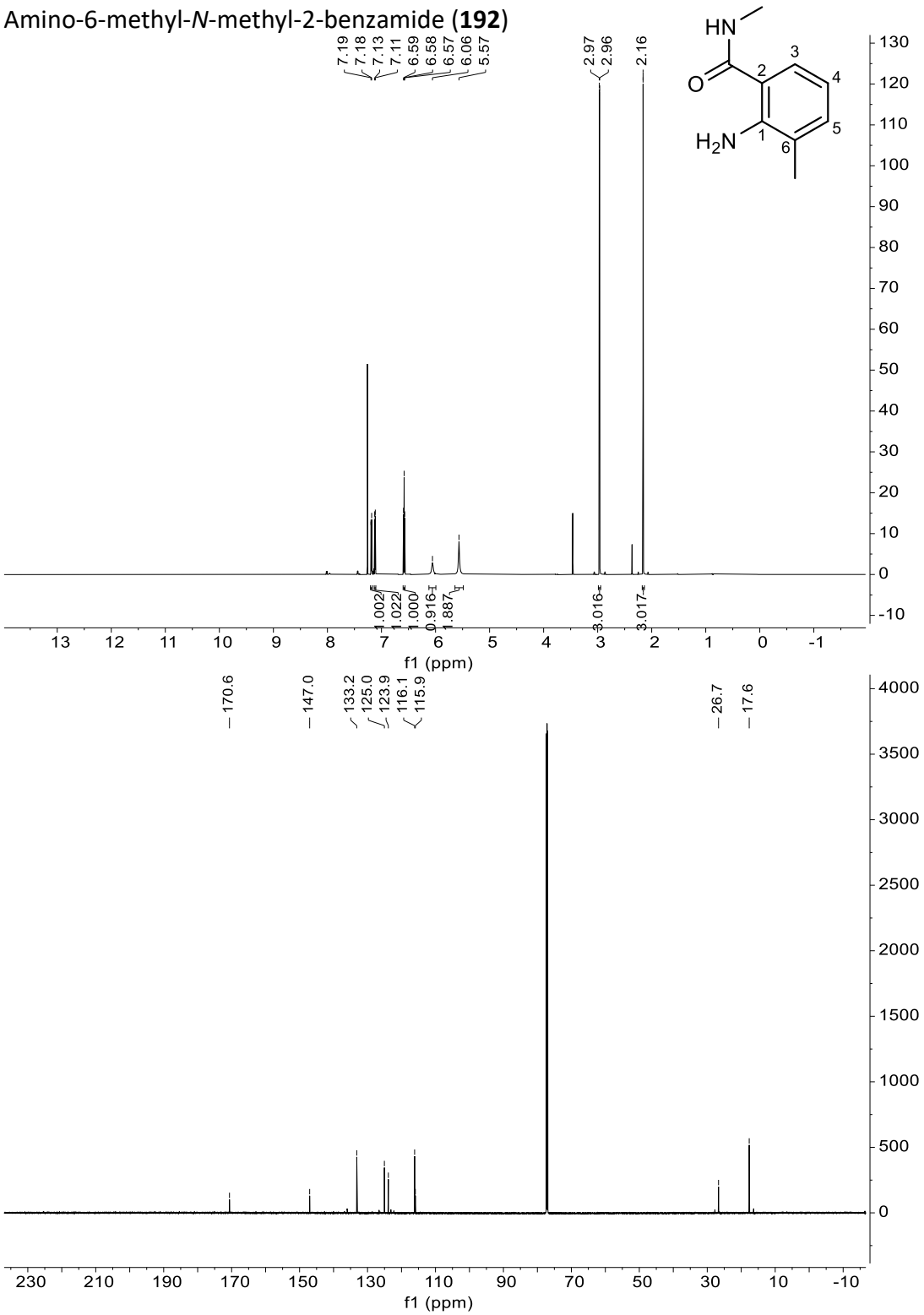

N-[3-methyl-2-(methylcarbamoyl)phenyl]-5’-nitrothiophene-2’-carboxamide (**193**)

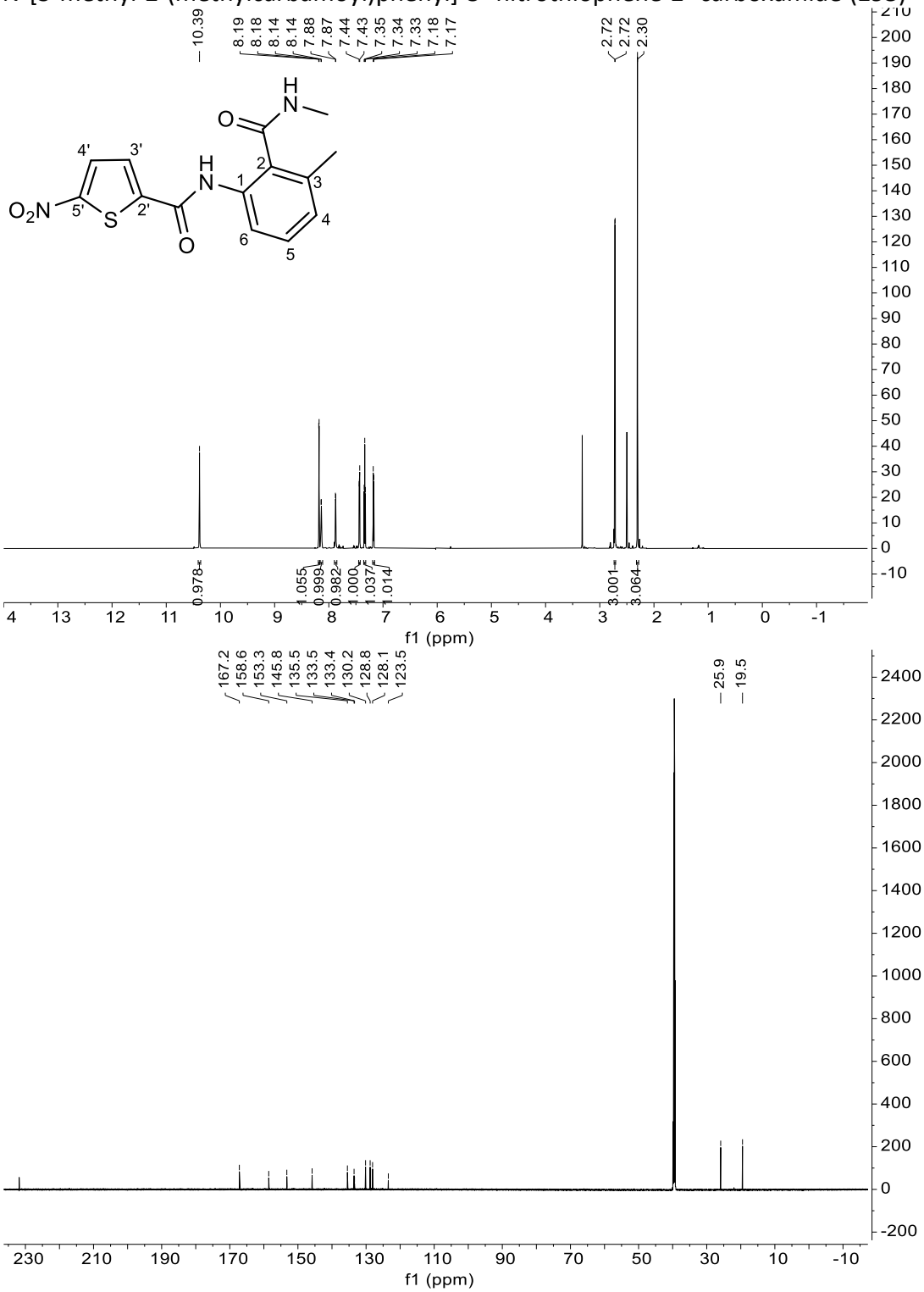

N-[4-methoxy-2-(methylcarbamoyl)phenyl]-5’-nitrothiophene-2’-carboxamide (**194**)

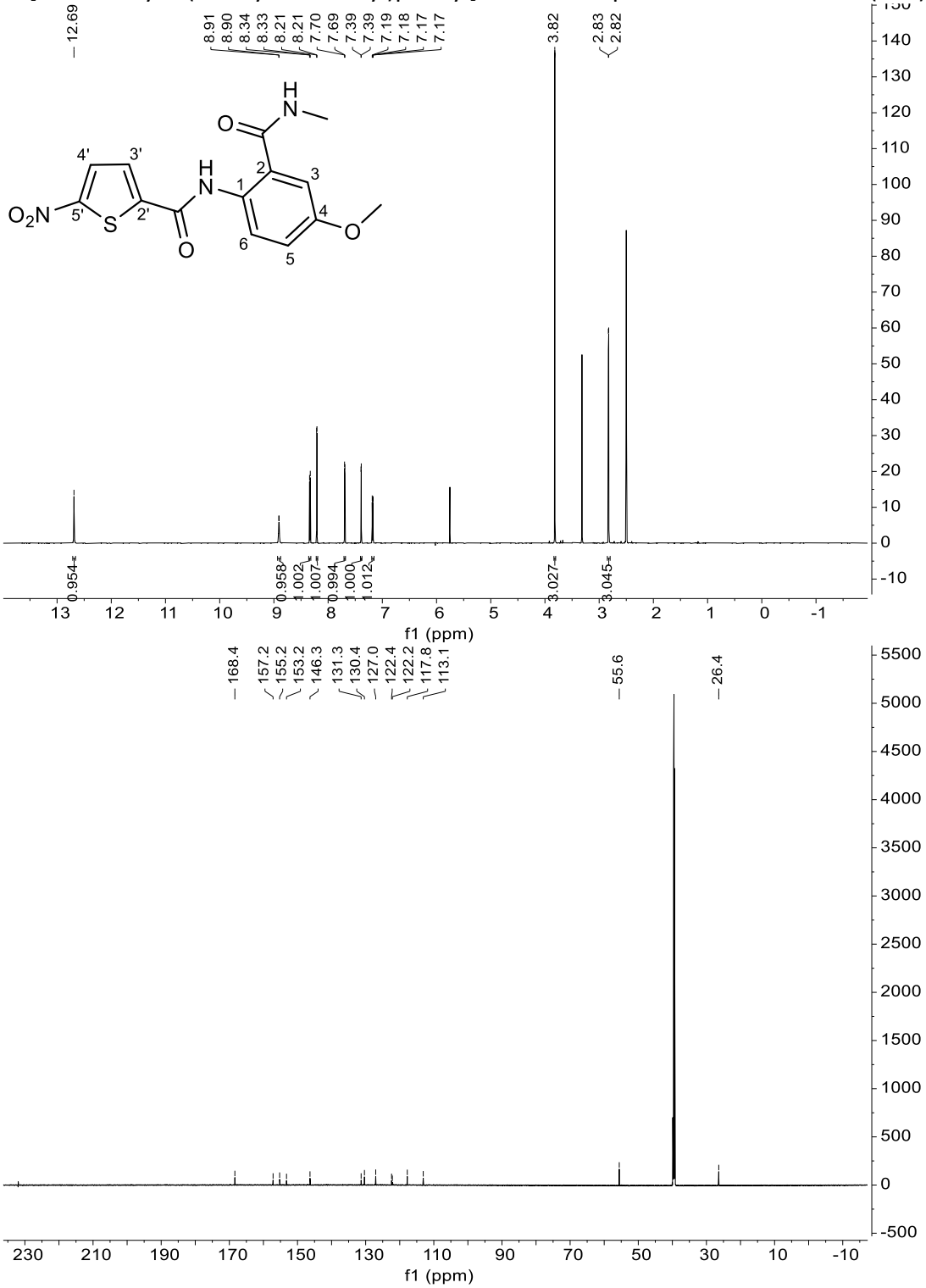

N-[4-methyl-2-(methylcarbamoyl)phenyl]-5’-nitrothiophene-2’-carboxamide (**195**)

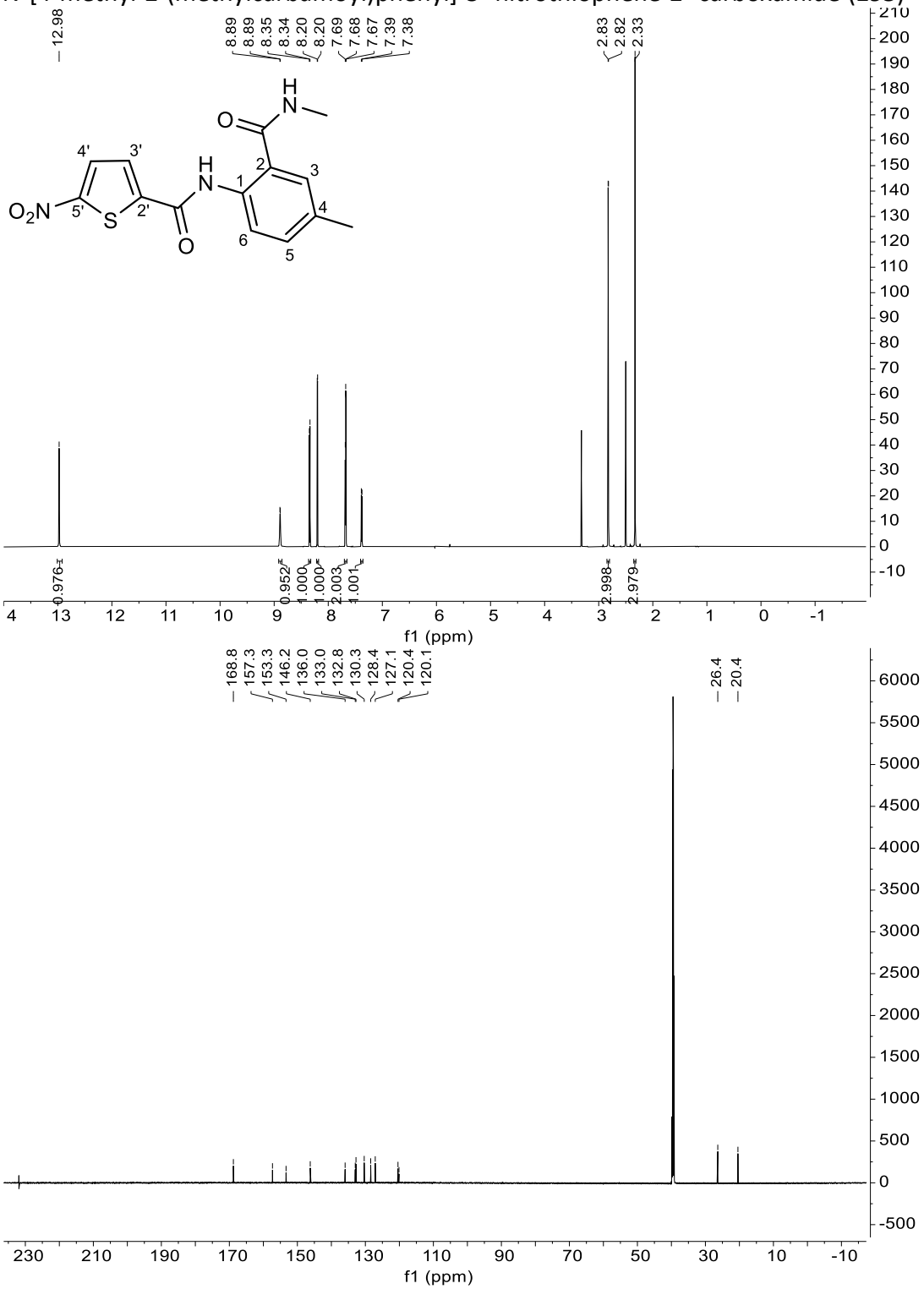

N-[5-methoxy-2-(methylcarbamoyl)phenyl]-5’-nitrothiophene-2’-carboxamide (**196**)

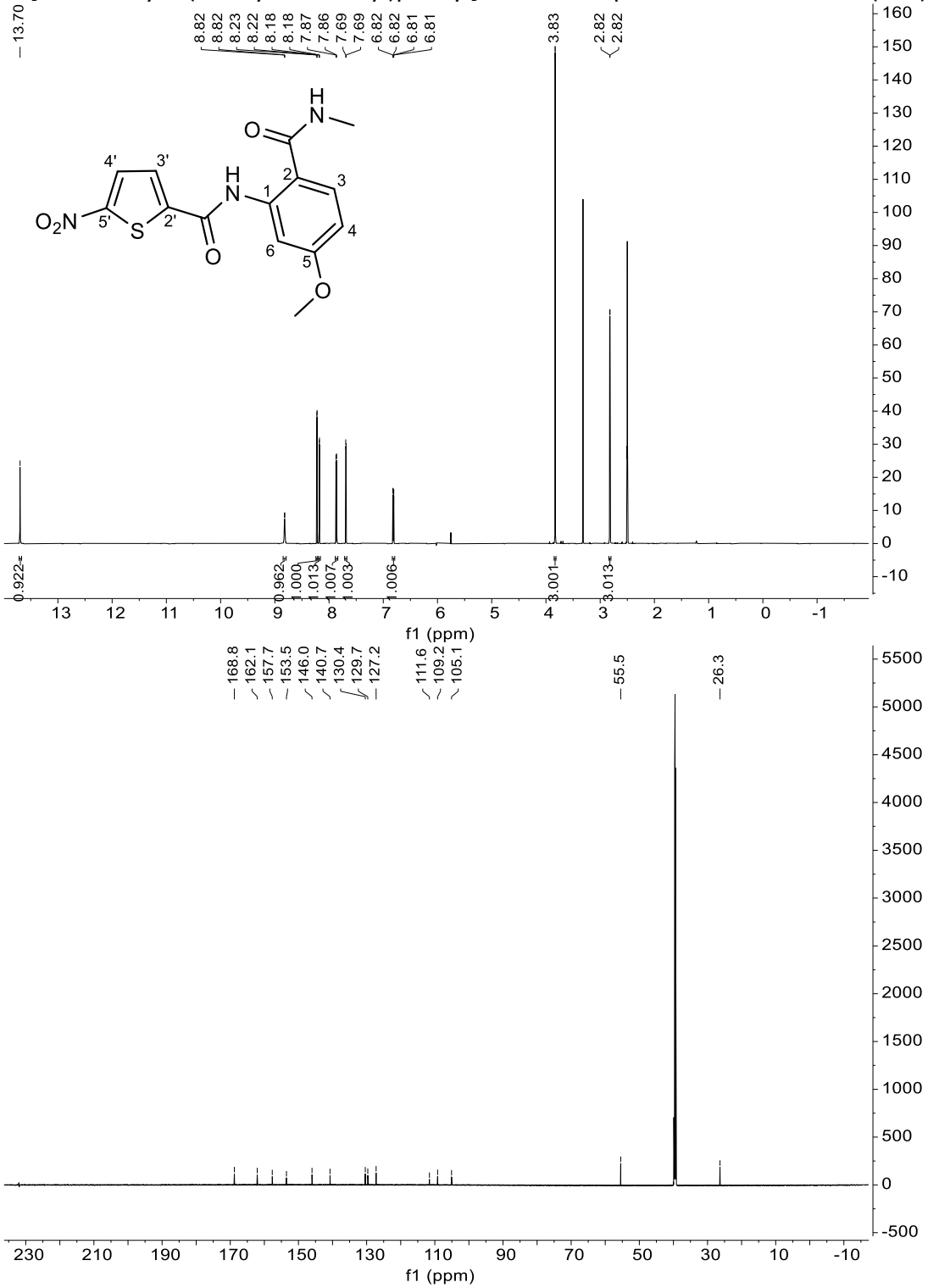

N-[5-methyl-2-(methylcarbamoyl)phenyl]-5’-nitrothiophene-2’-carboxamide (**197**)

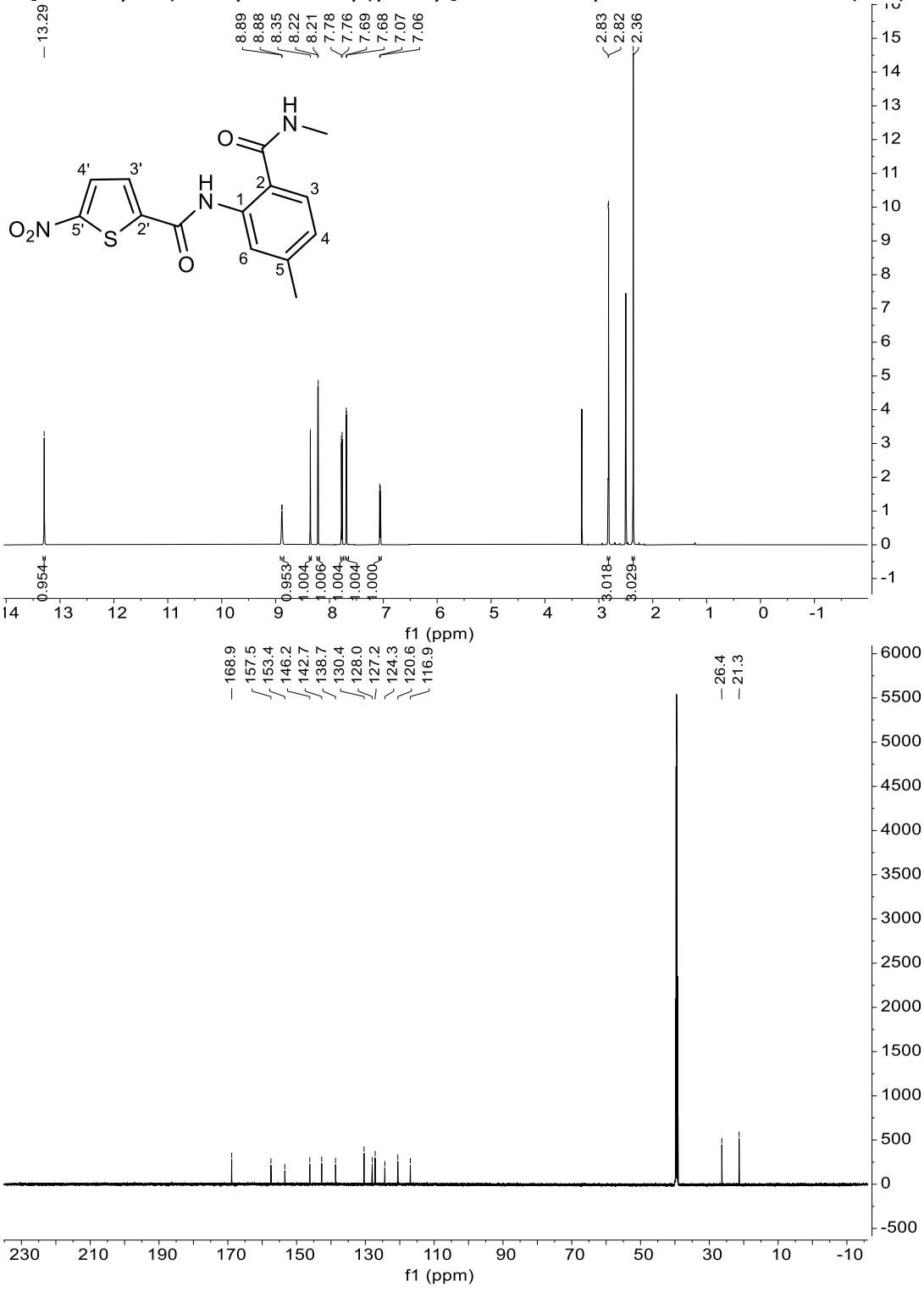

N-[2-(methylcarbamoyl)-5-(trifluoromethyl)phenyl]-5’-nitrothiophene-2’-carboxamide (**198**)

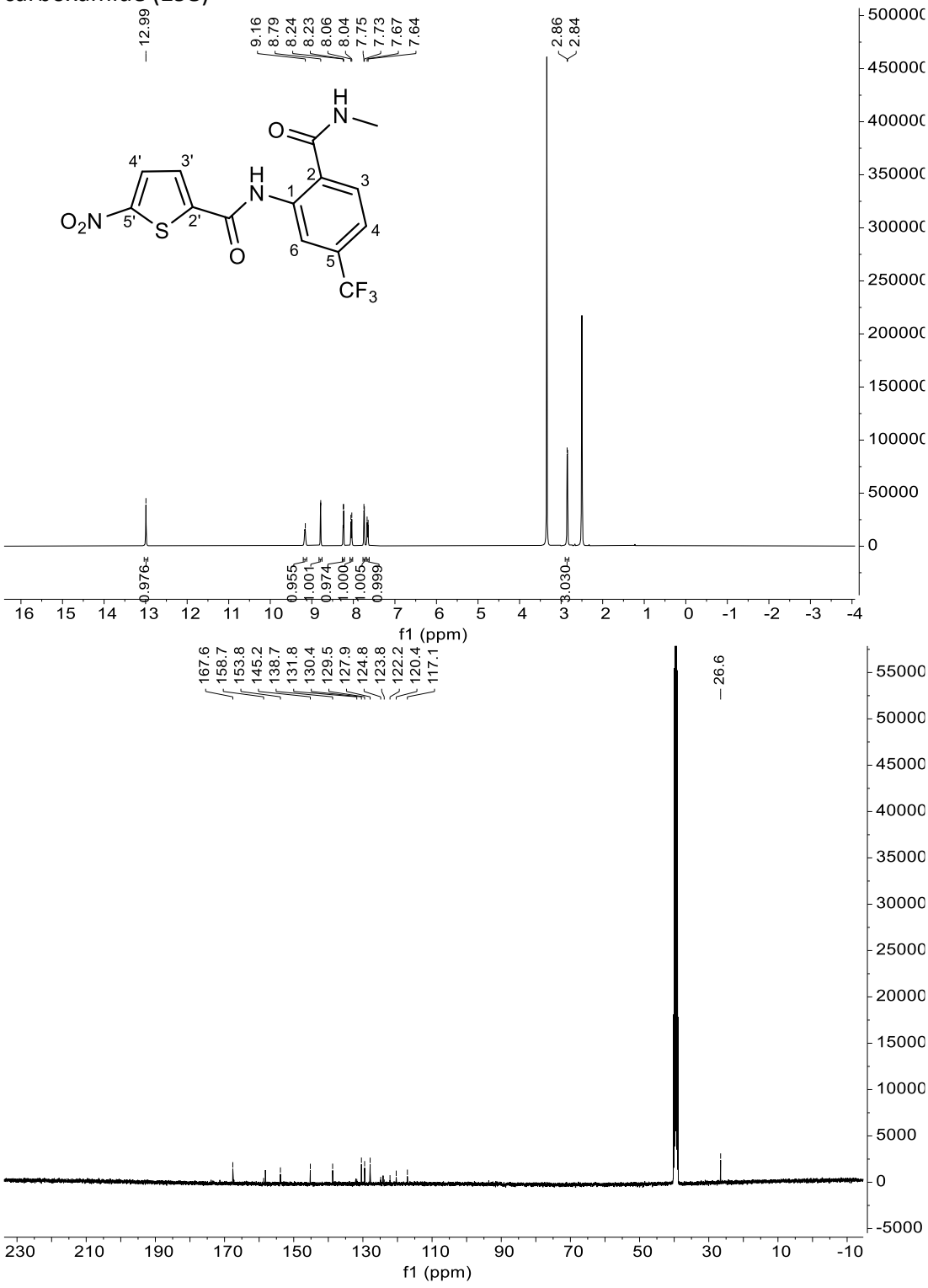

N-[5-bromo2-(methylcarbamoyl)phenyl]-5’-nitrothiophene-2’-carboxamide (**199**)

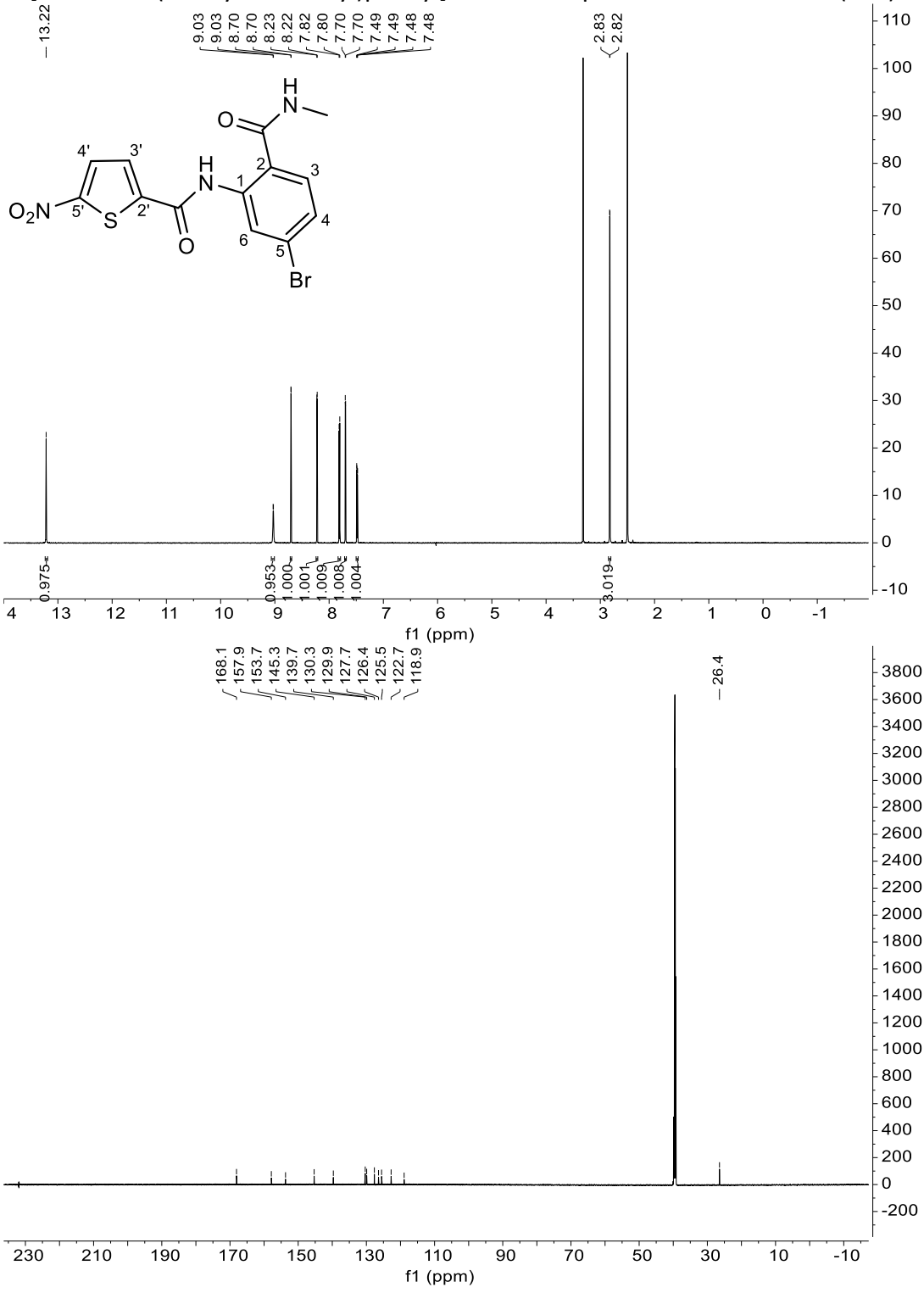

N-[8-methoxy-2-(5’-nitrothiophen-2’-yl)-4*H*-3,1-benzoxazin-4-ylidene]methanamine (**200**)

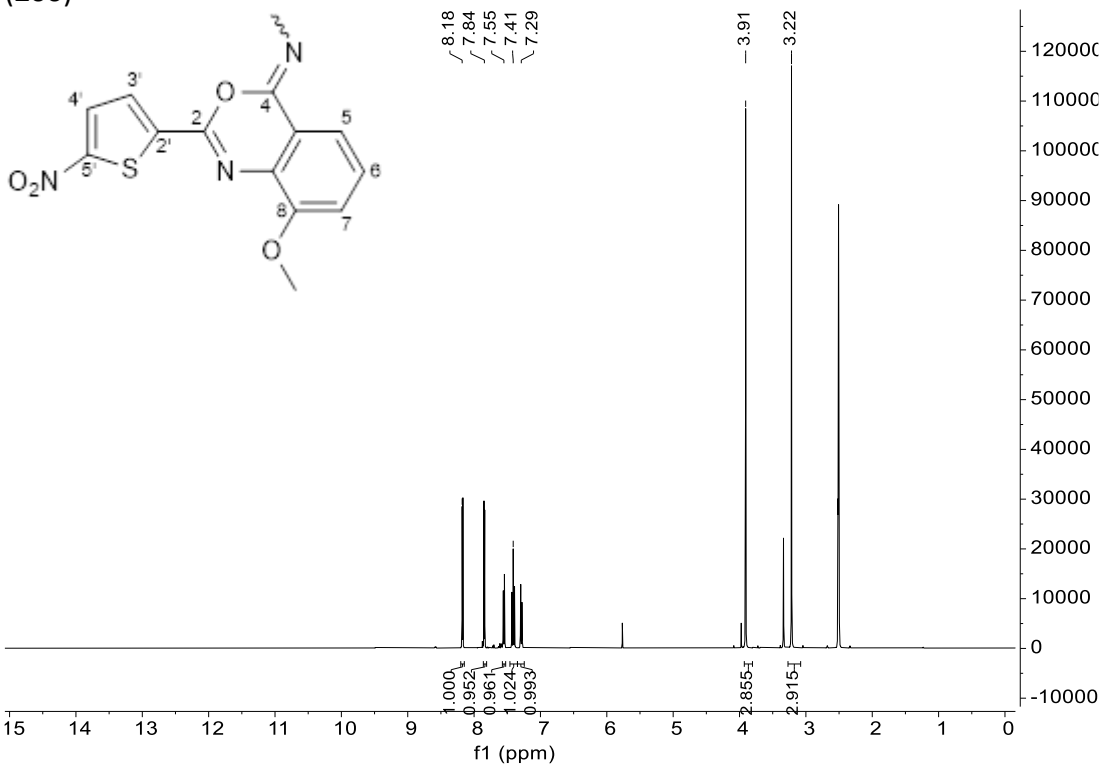

^{13}C NMR not obtained as product not soluble enough to resolve signals.

N-[8-methyl-2-(5’-nitrothiophen-2’-yl)-4*H*-3,1-benzoxazin-4-ylidene]methanamine (**201**)

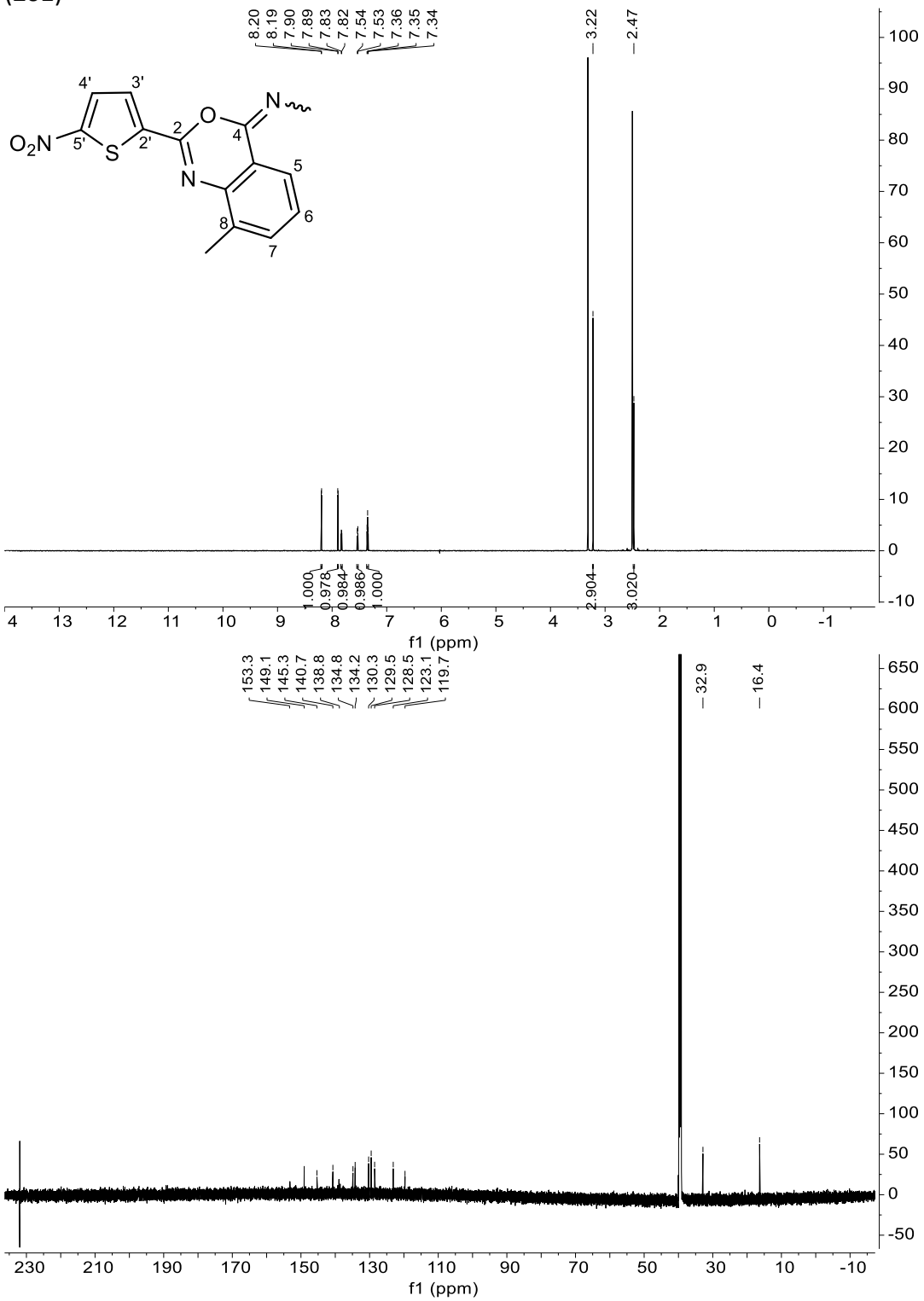

1H,2H,4H-thieno[2,3-d][1,3]oxazine-2,4-dione (**203**)

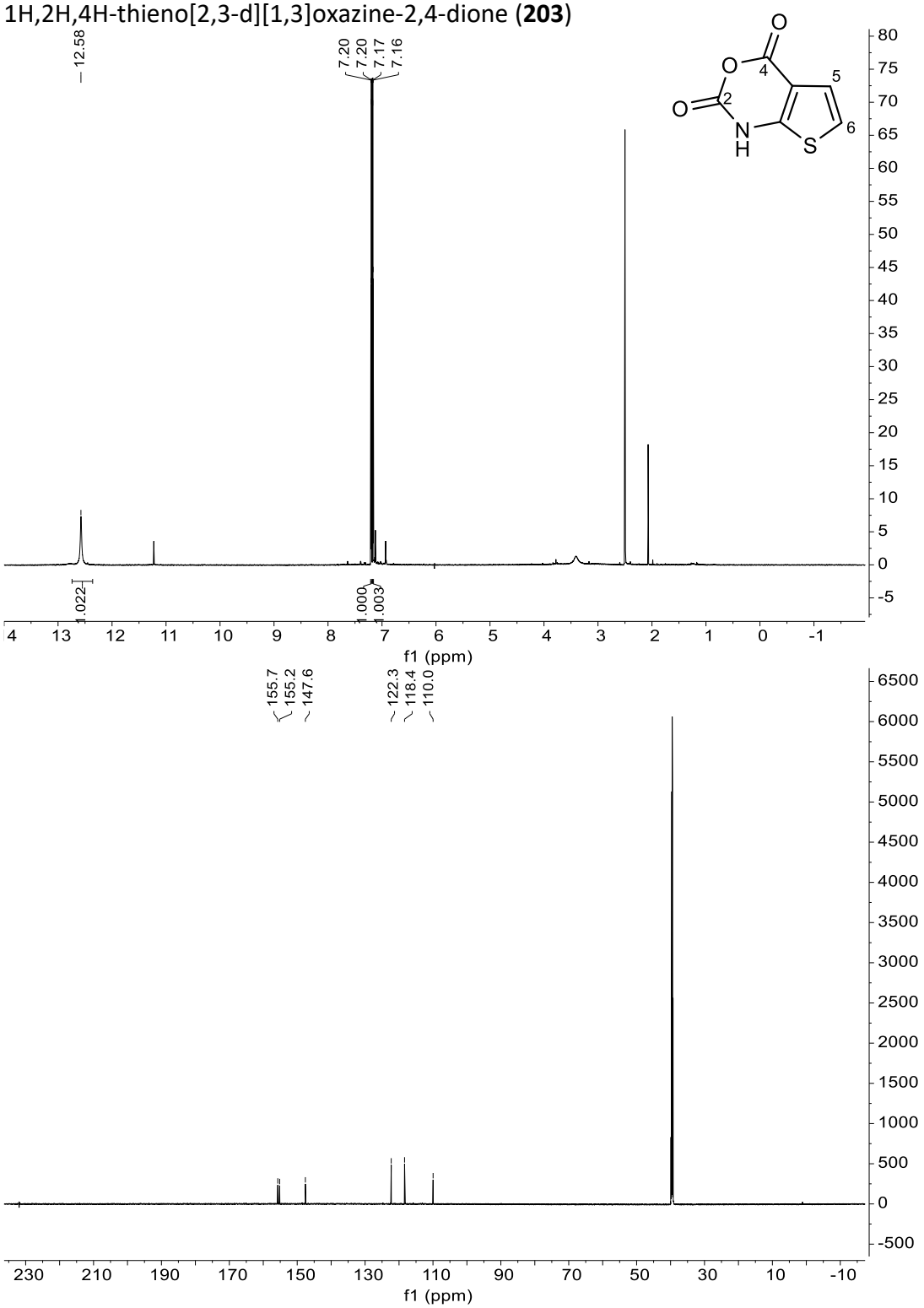

1-methyl-1H,2H,4H-thieno[2,3-d][1,3]oxazine-2,4-dione (**204**)

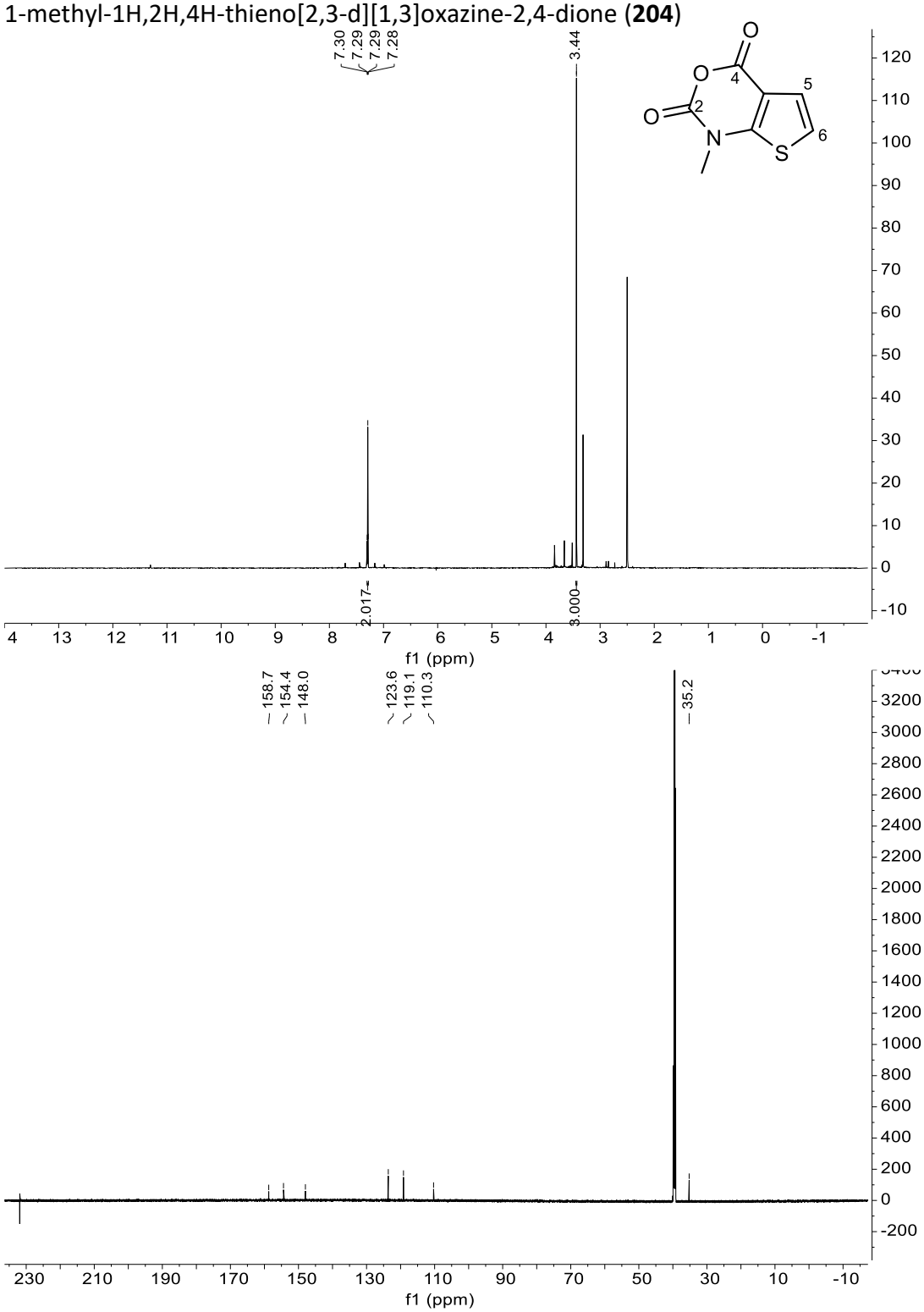

N-methyl-2-(methylamino)thiophene-3-carboxamide (**205**)

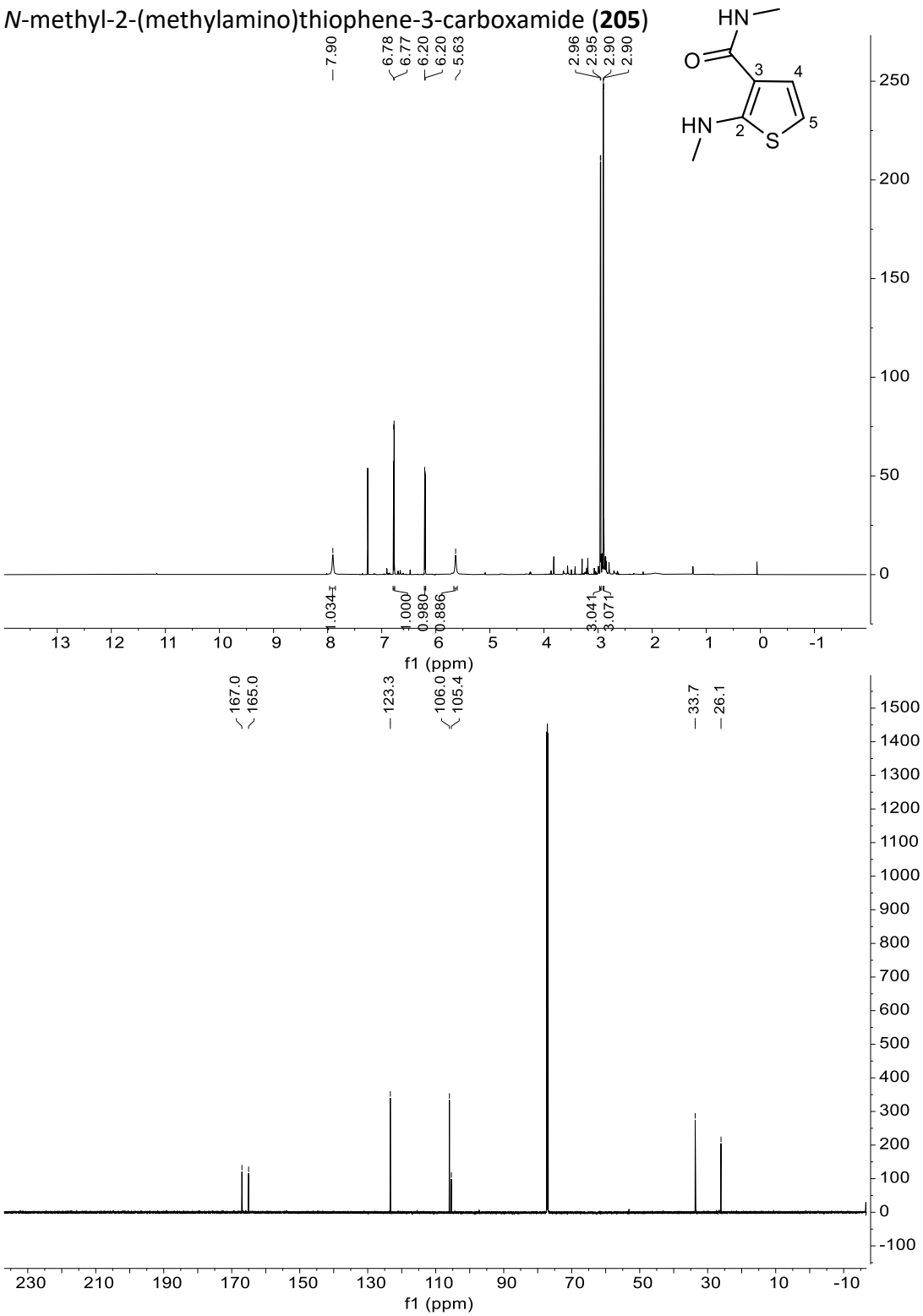

N-methyl-2-(*N*-methyl-5’-nitrothiophene-2’-amido)thiophene-3-carboxamide (**206**)

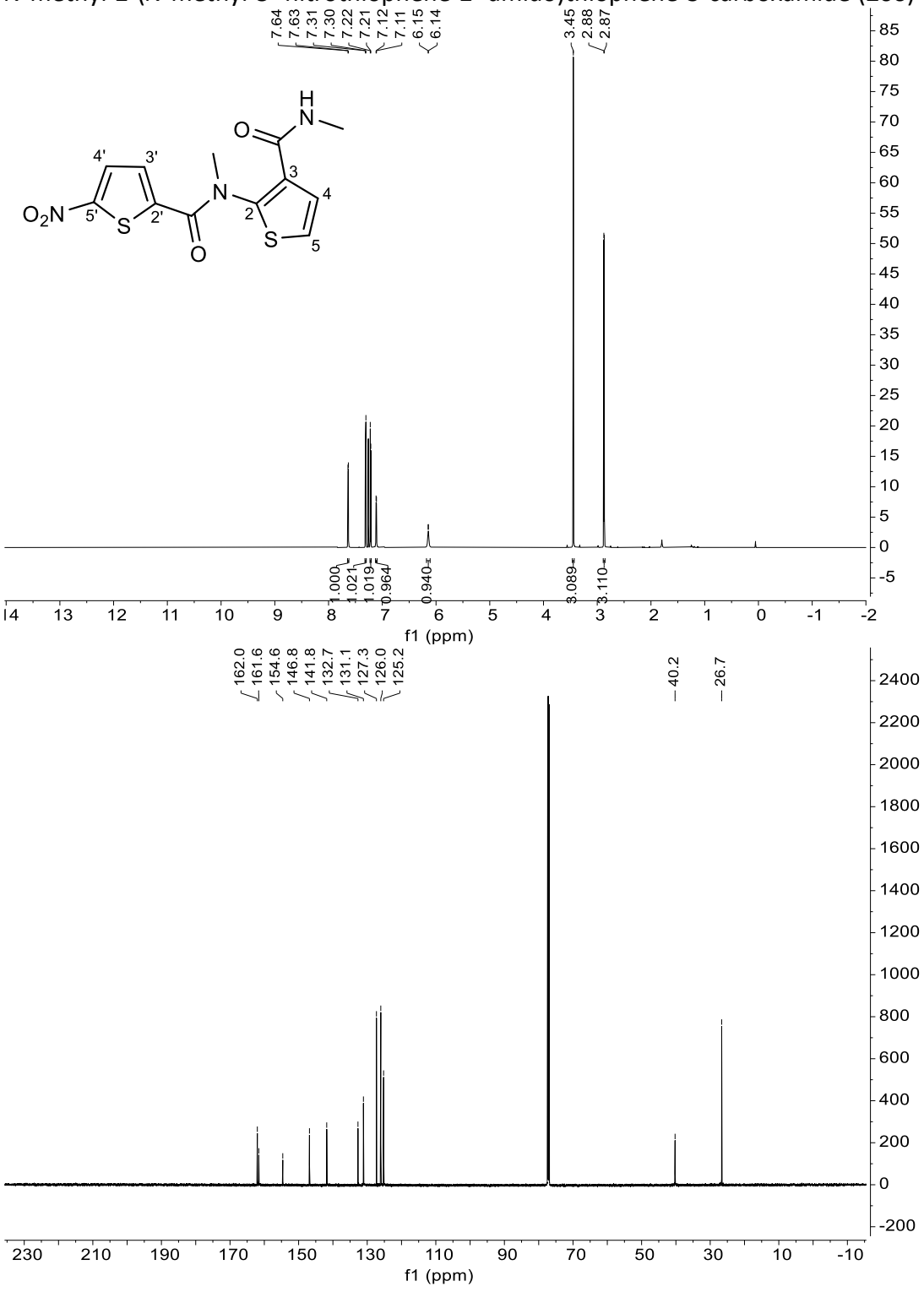

1-(5’-nitrothiophene-2’-carbonyl)-1,2,3,4-tetrahydroquinoline (**208**)

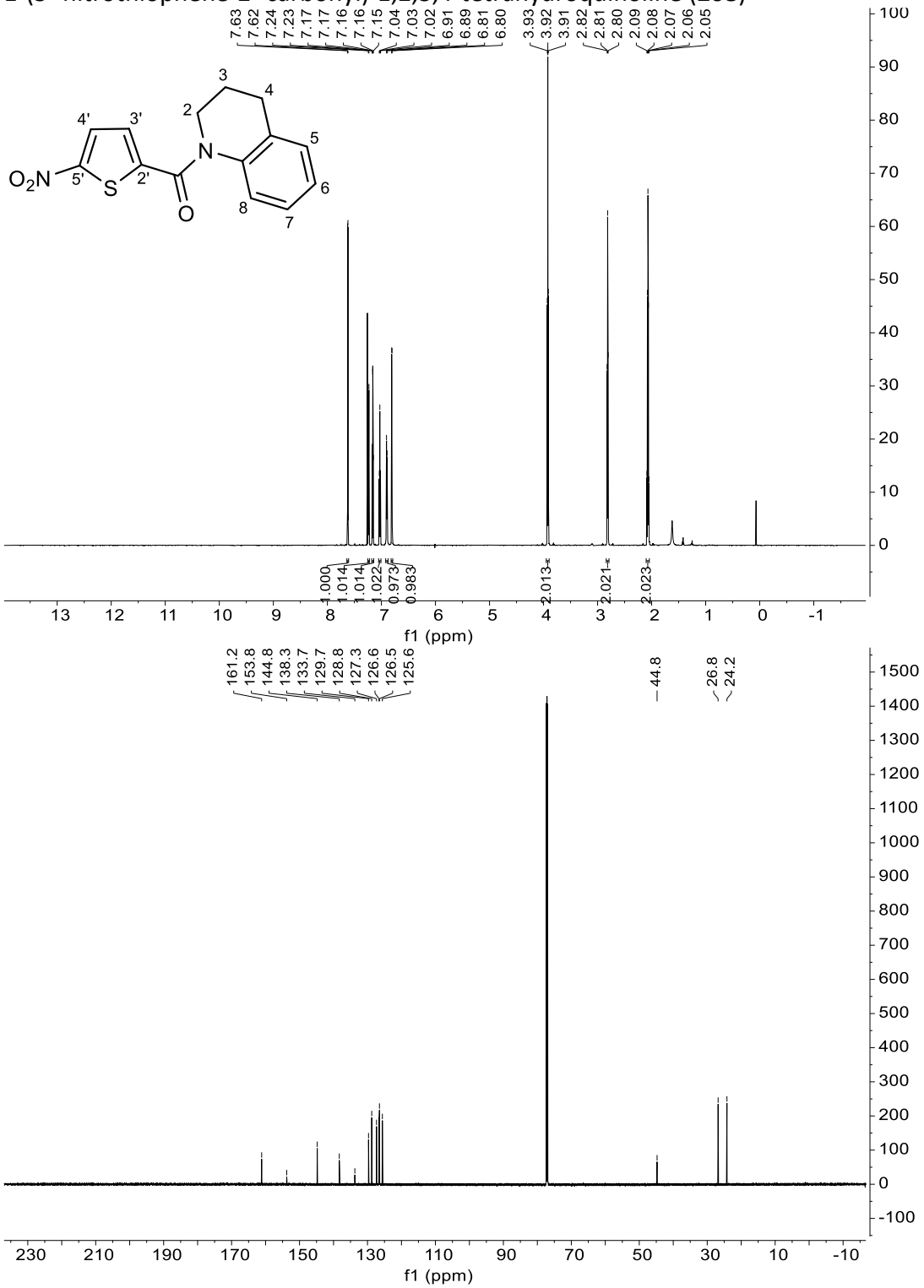

N-(2-carbamoylbenzyl)-5’-nitrothiophene-2’-carboxamide (**210**)

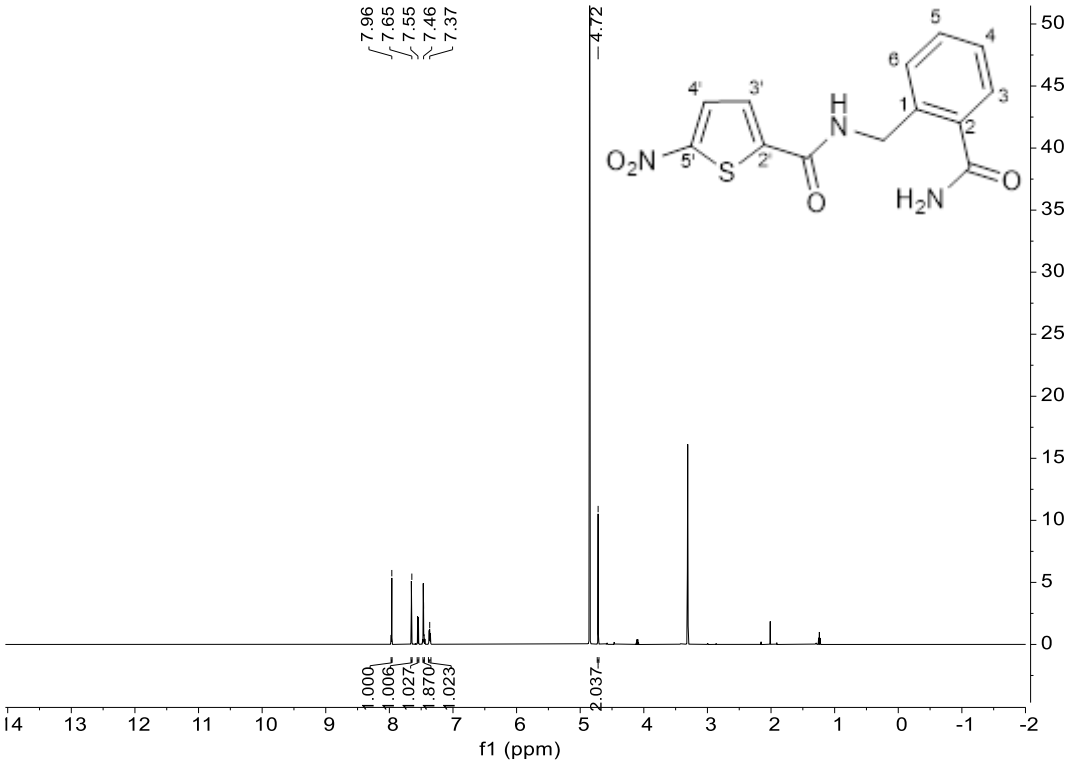

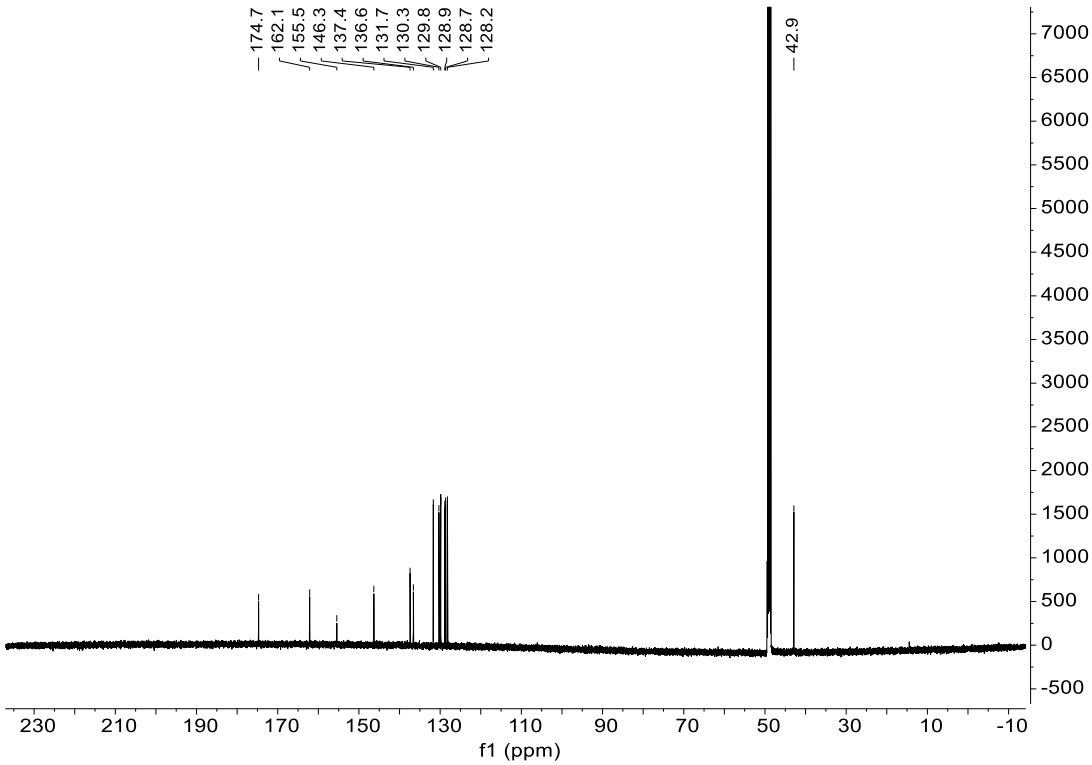

N-methyl-2-[(*E*)-[(5’-nitrothiophen-2’-yl)methylidene]amino]thiophene-3-carboxamide (**212**)

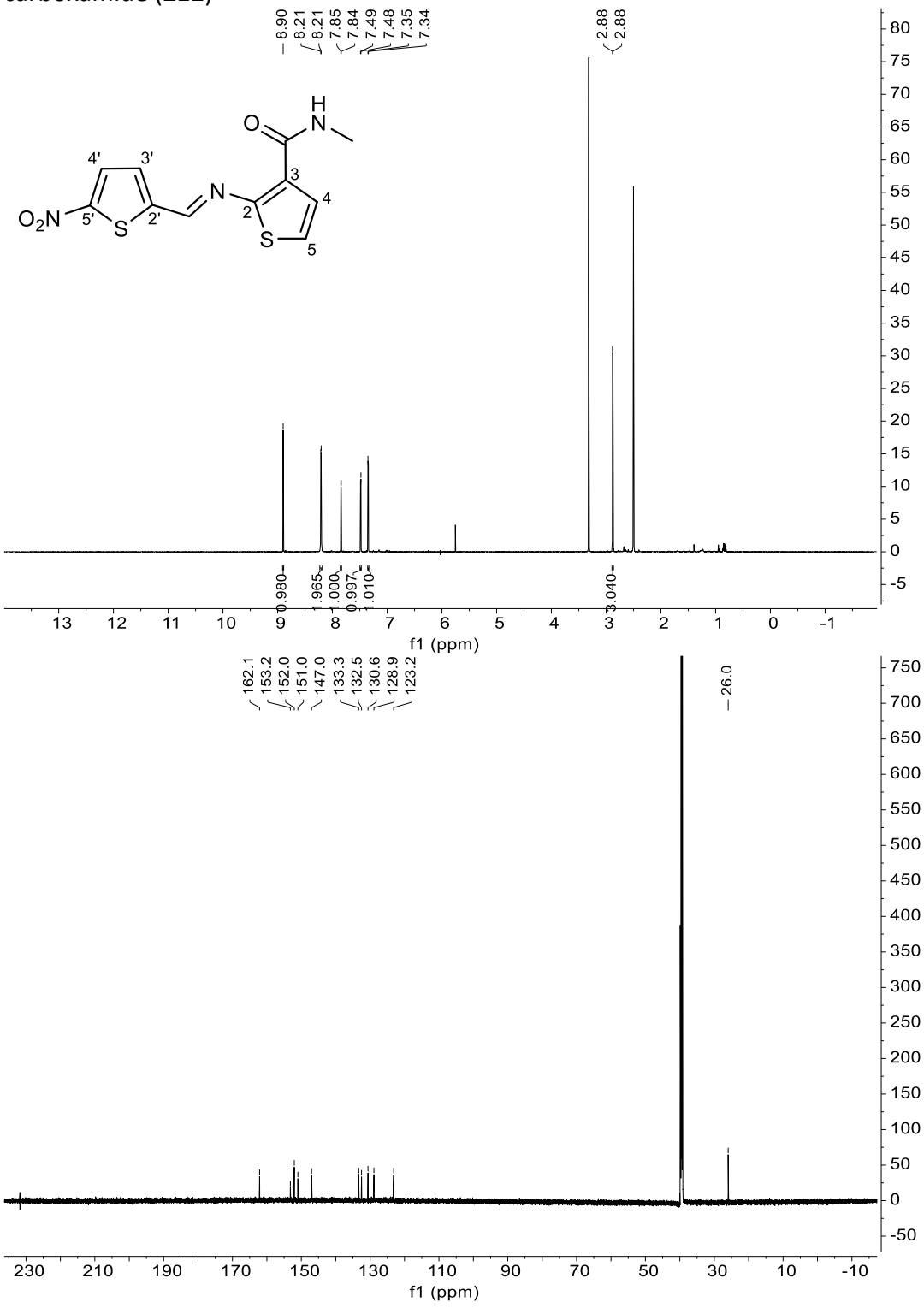

5-nitrothiophene-2-carbonyl azide (**216**)

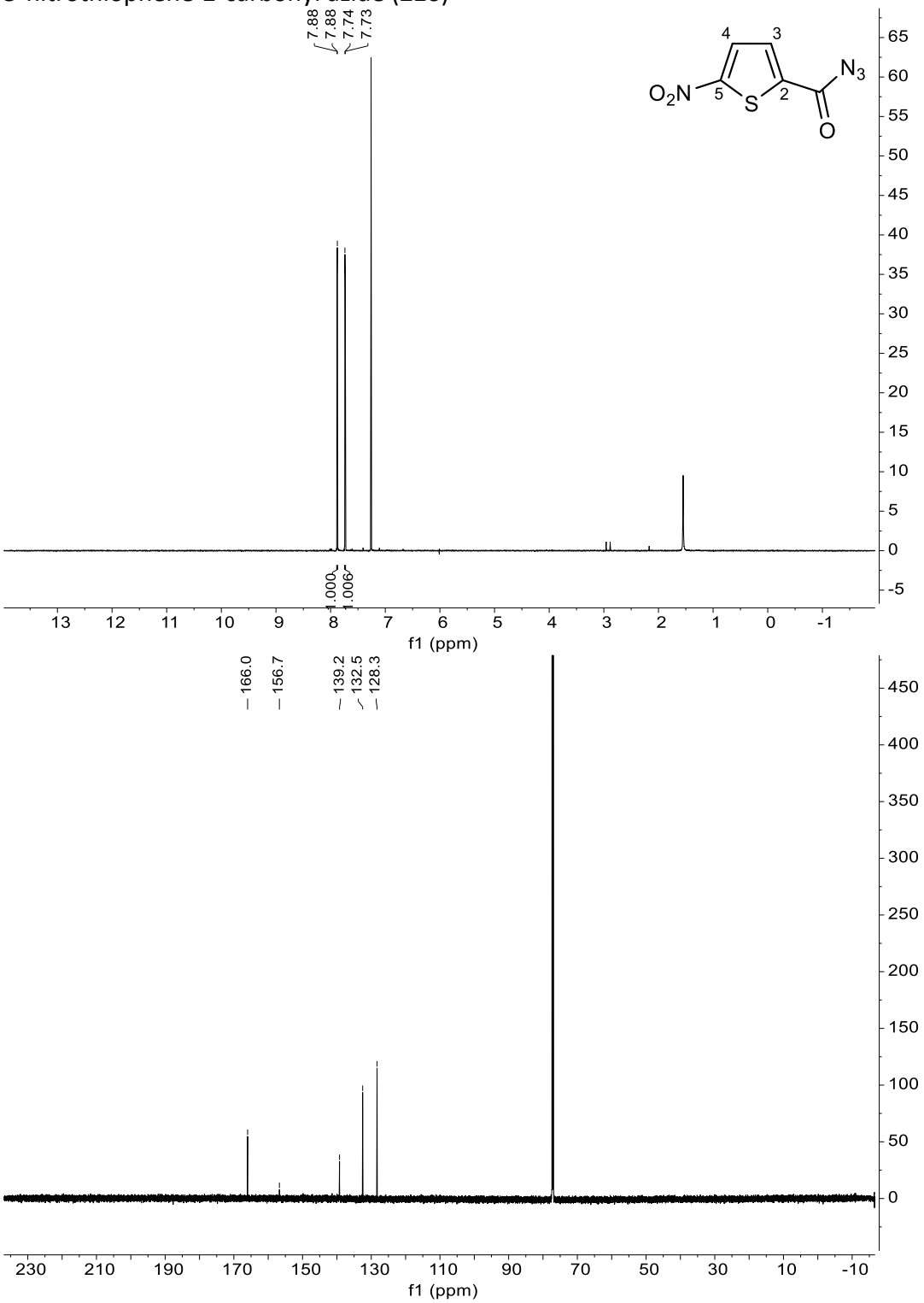

Tert-butyl *N*-(5-nitrothiophen-2-yl)carbamate (**217**)

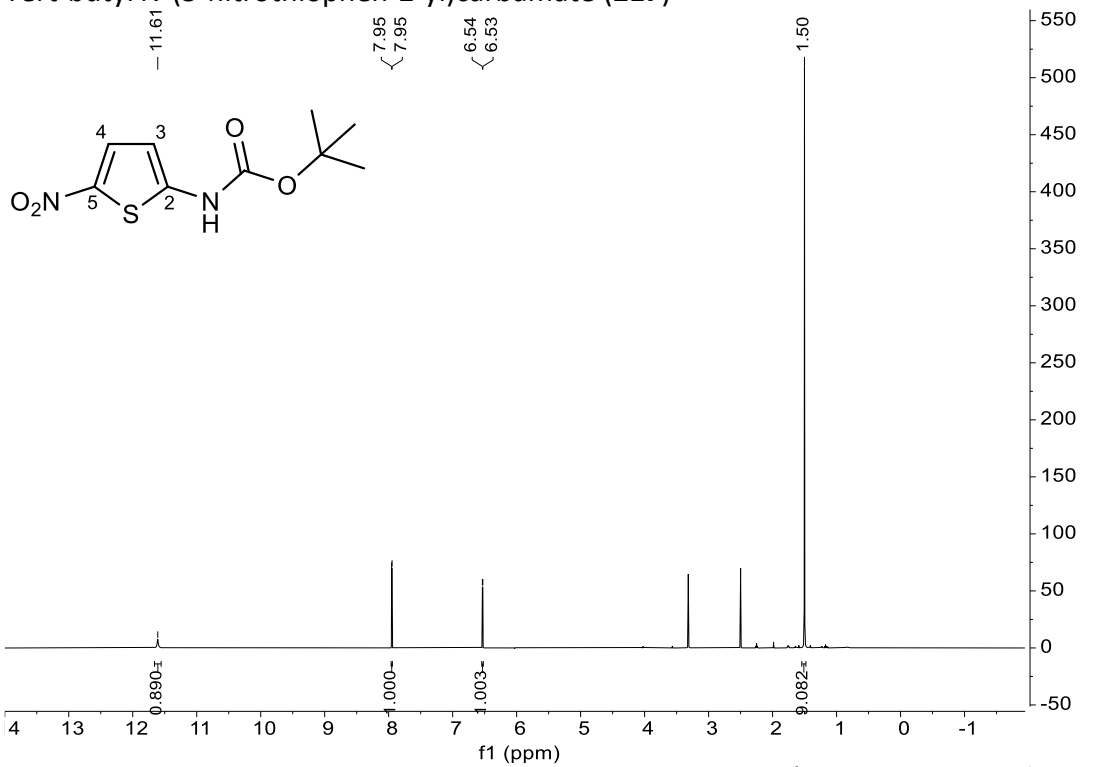

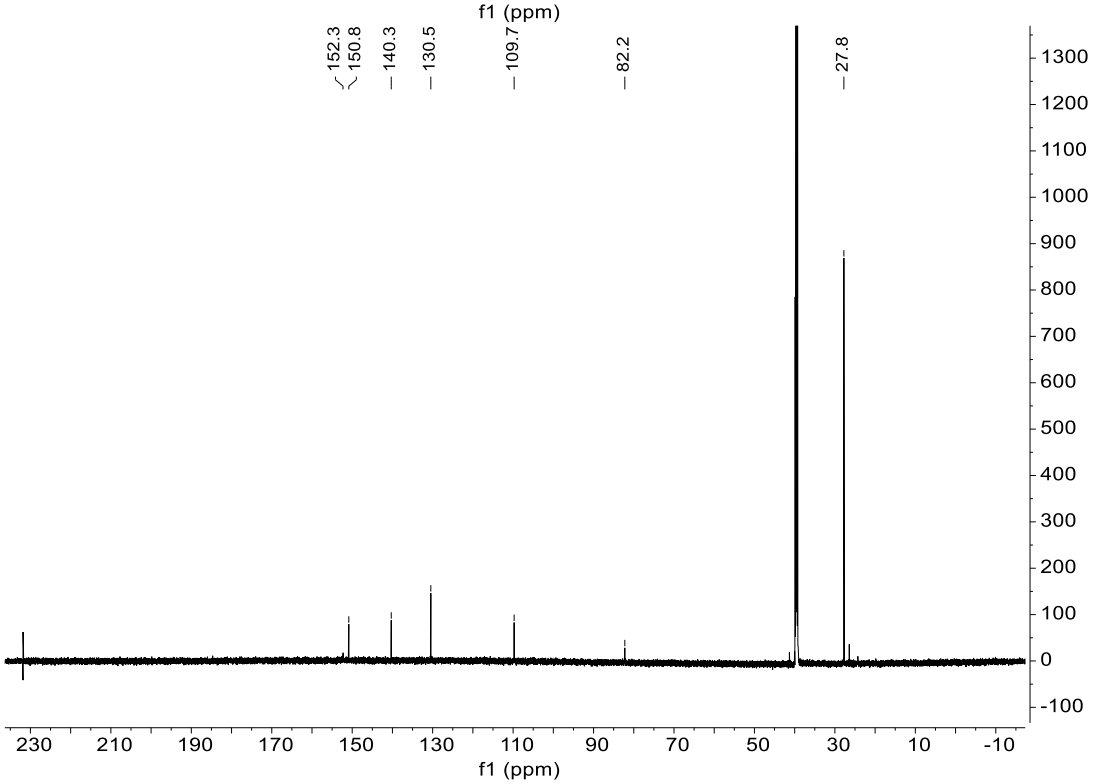

5-nitro-2-amino thiophene (**214**)

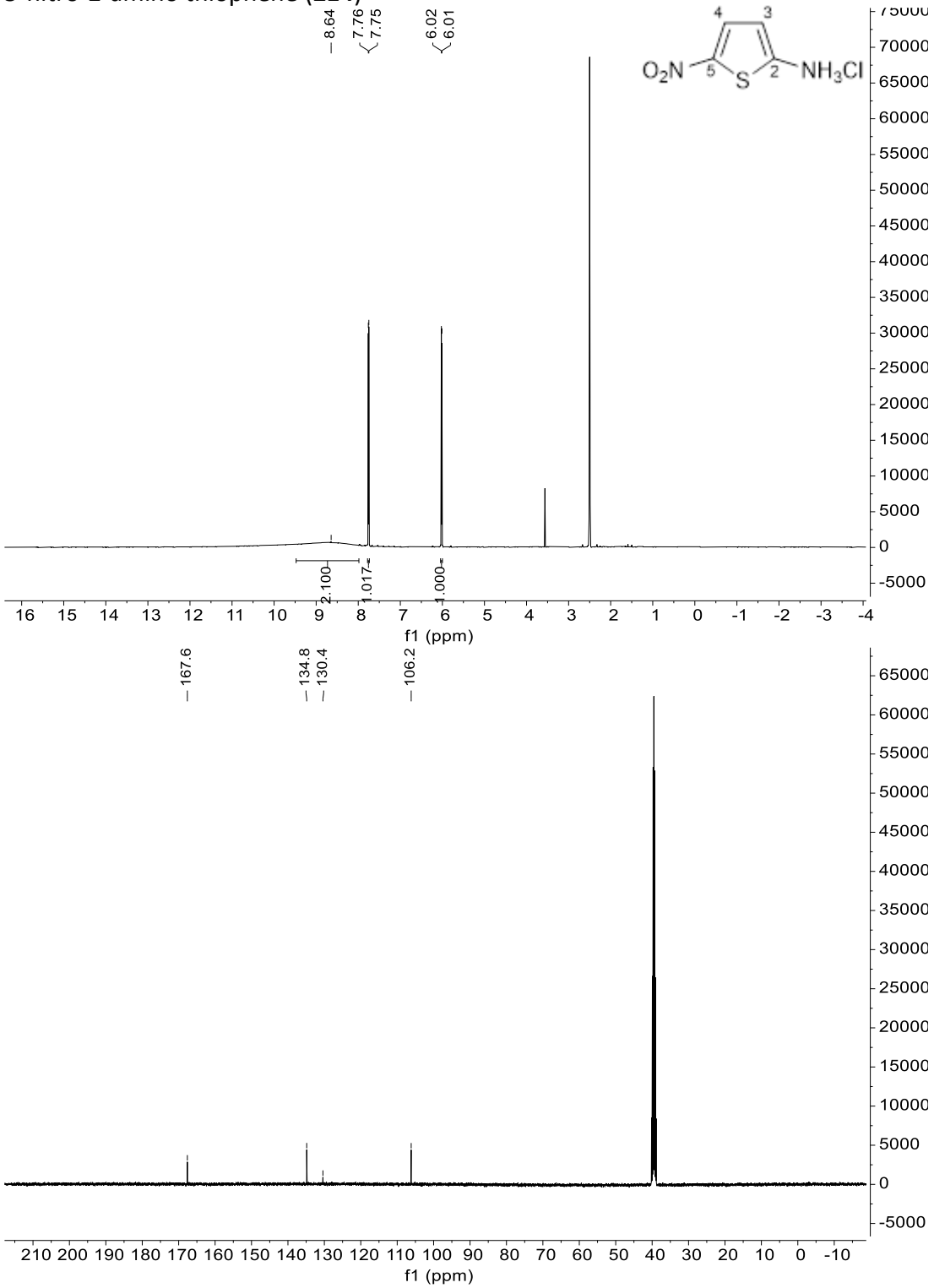

2-(methylcarbamoyl)benzoic acid (**215**)

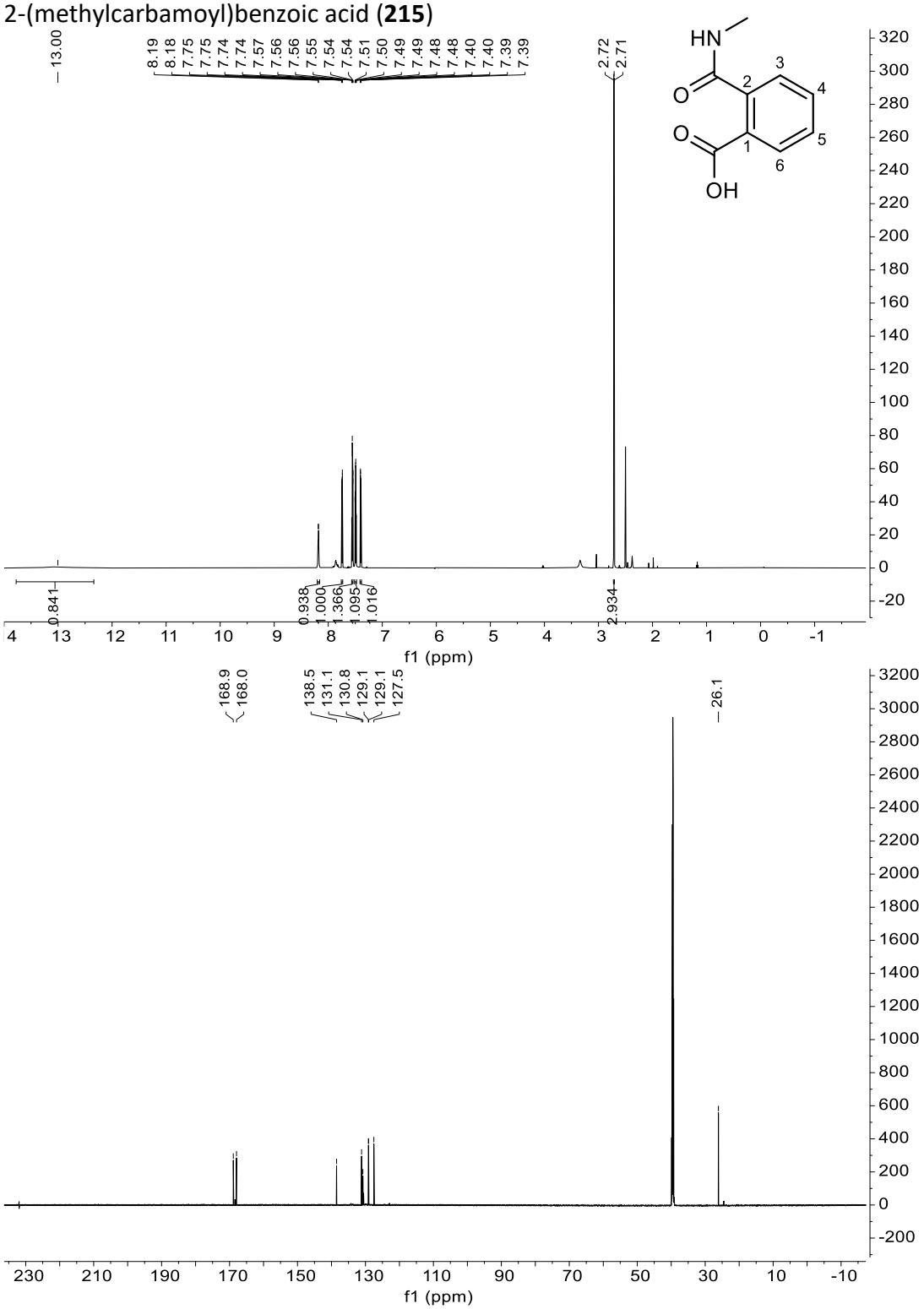

4-tert-butyl-1-methyl-2-nitrobenzene (**221**)

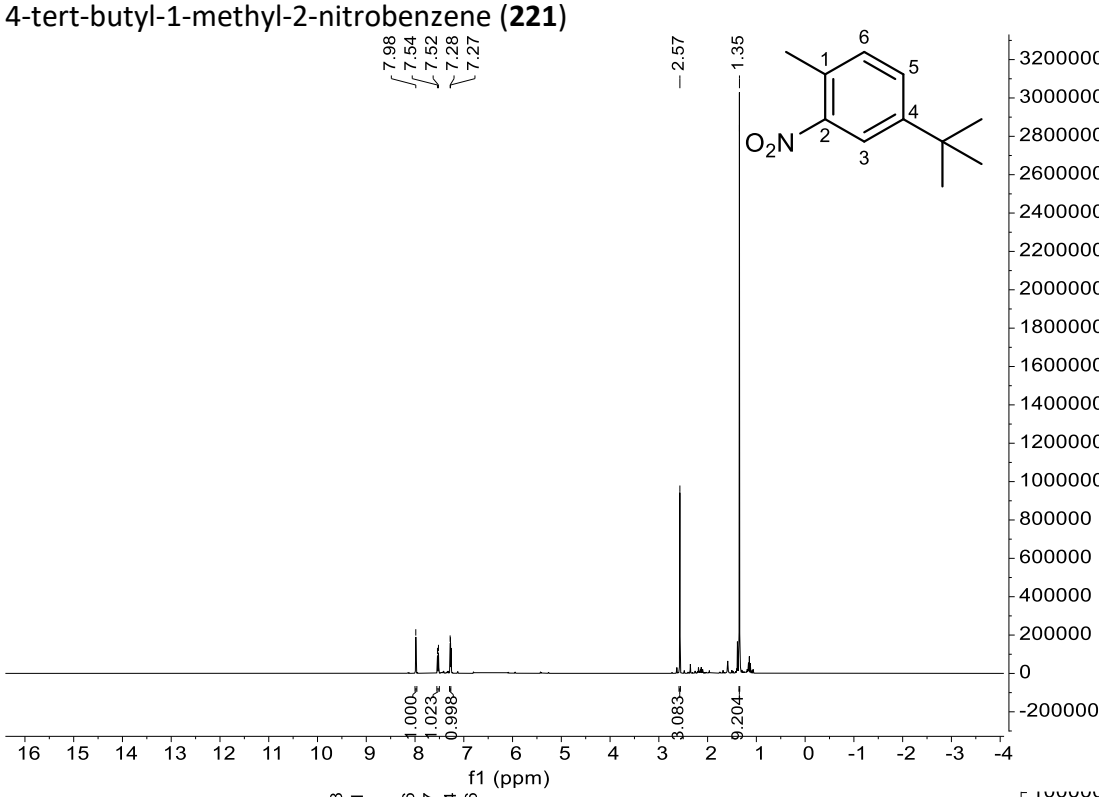

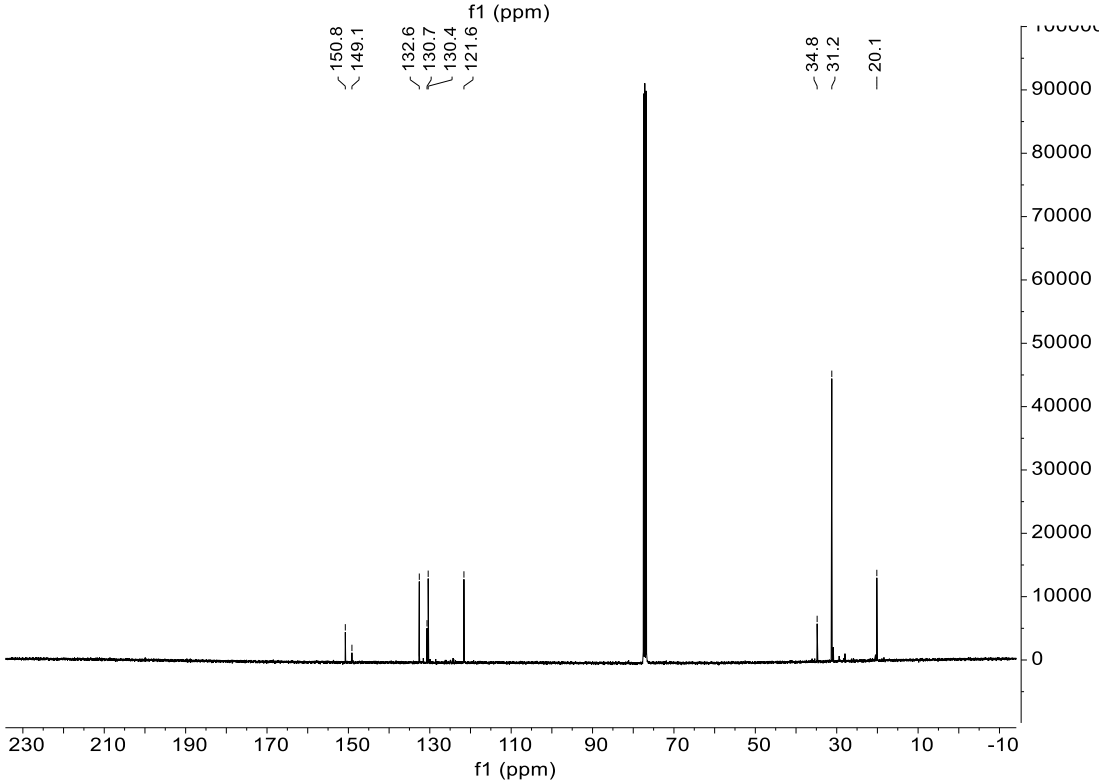

4-tert-butyl-2-nitrobenzoic acid (**222**)

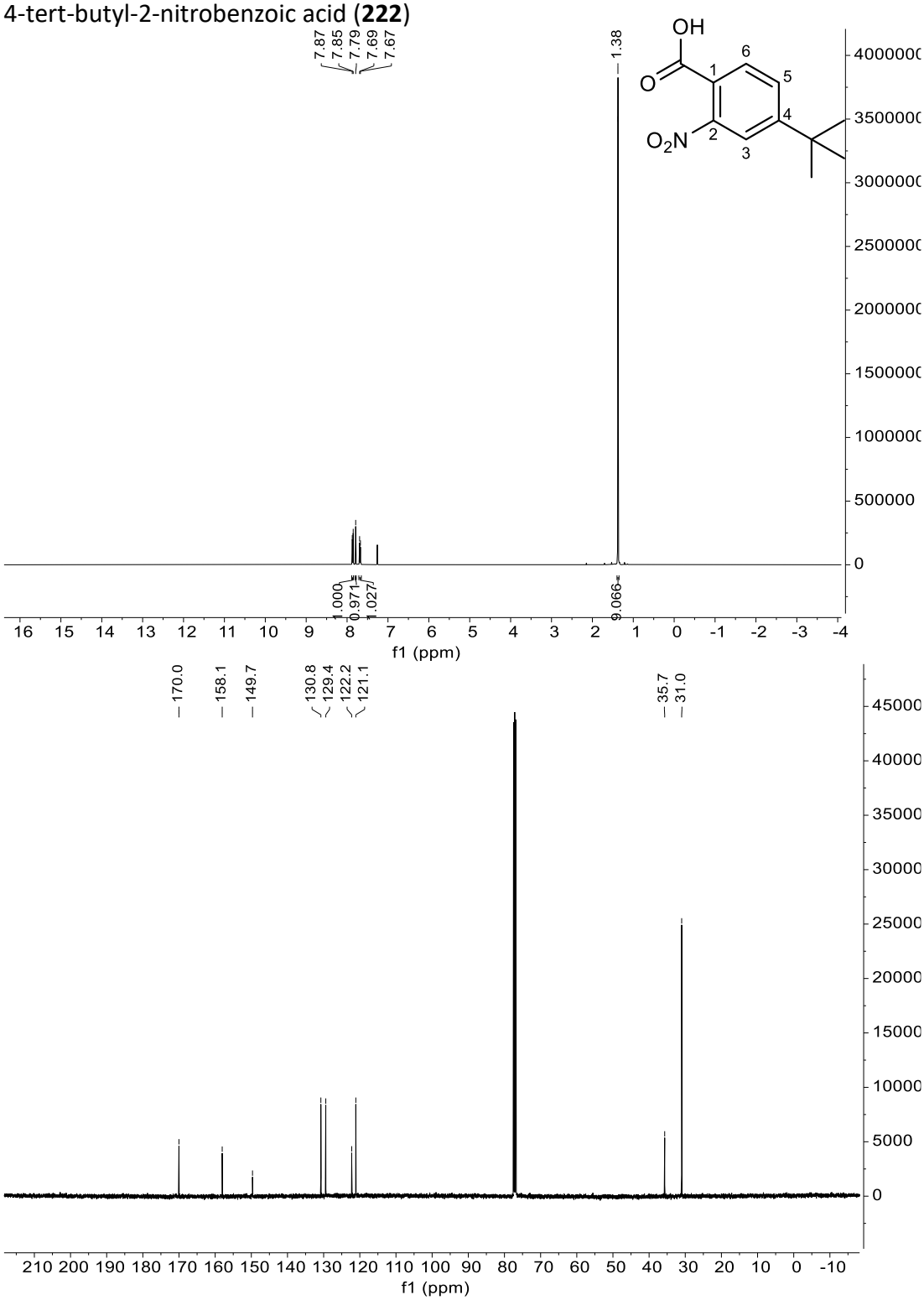

4-tert-butyl-2-nitrobenzoyl chloride (**223**)

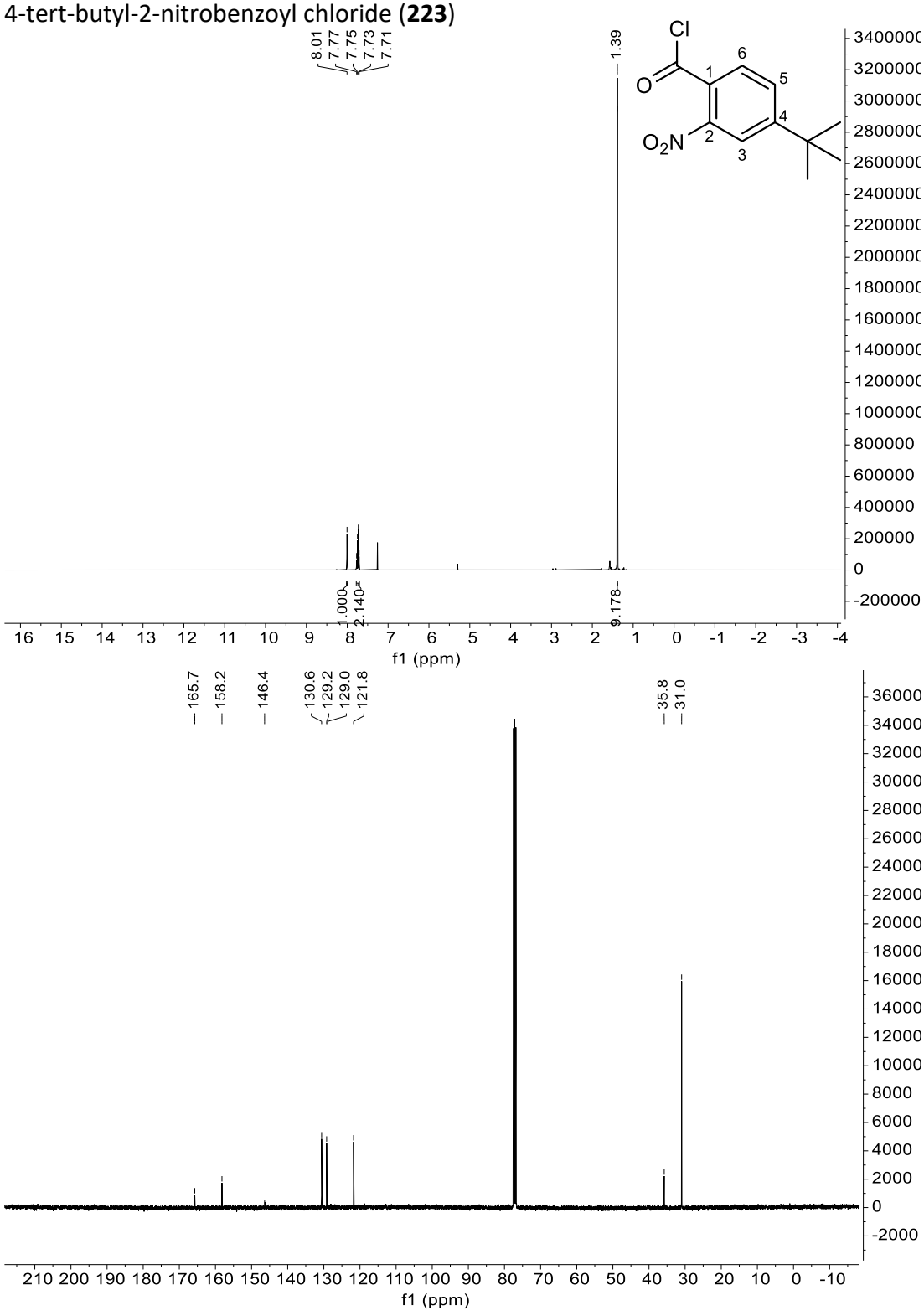

4-tert-butyl-N-methyl-2-nitrobenzamide (**224**)

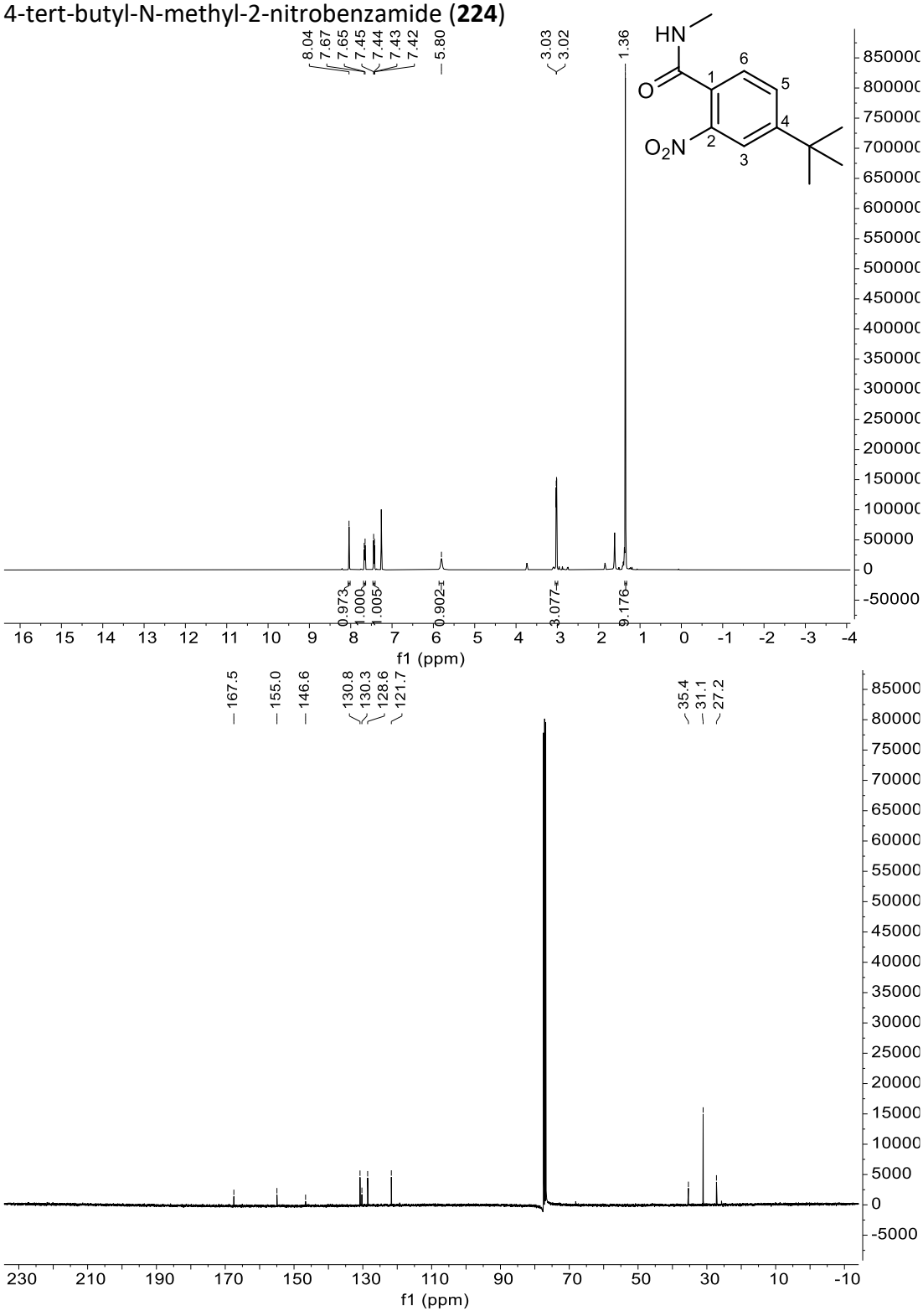

2-amino-4-tert-butyl-*N*-methylbenzamide (**225**)

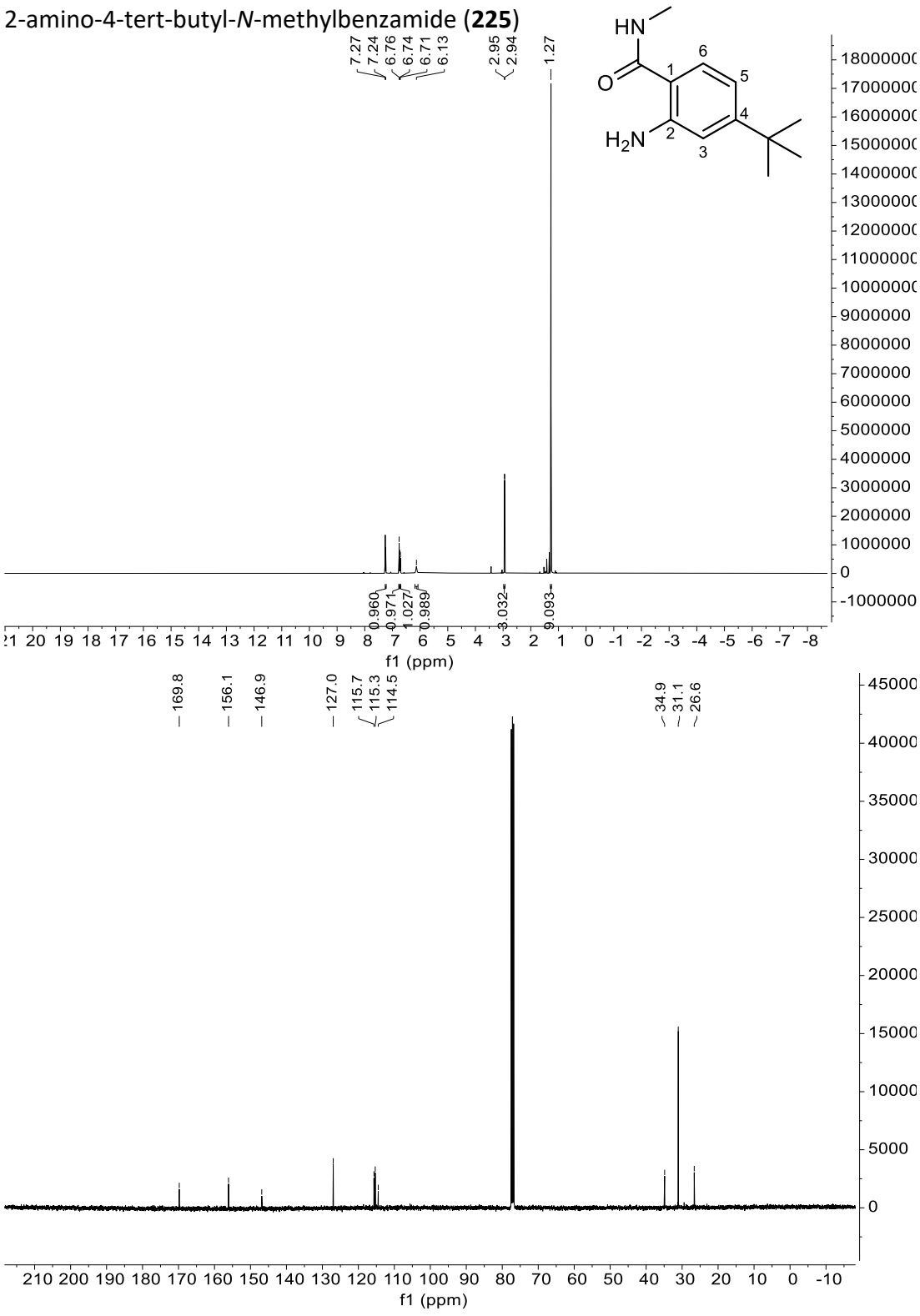

N-[5-tert-butyl-2-(methylcarbamoyl)phenyl]-5’-nitrothiophene-2’-carboxamide (**226**)

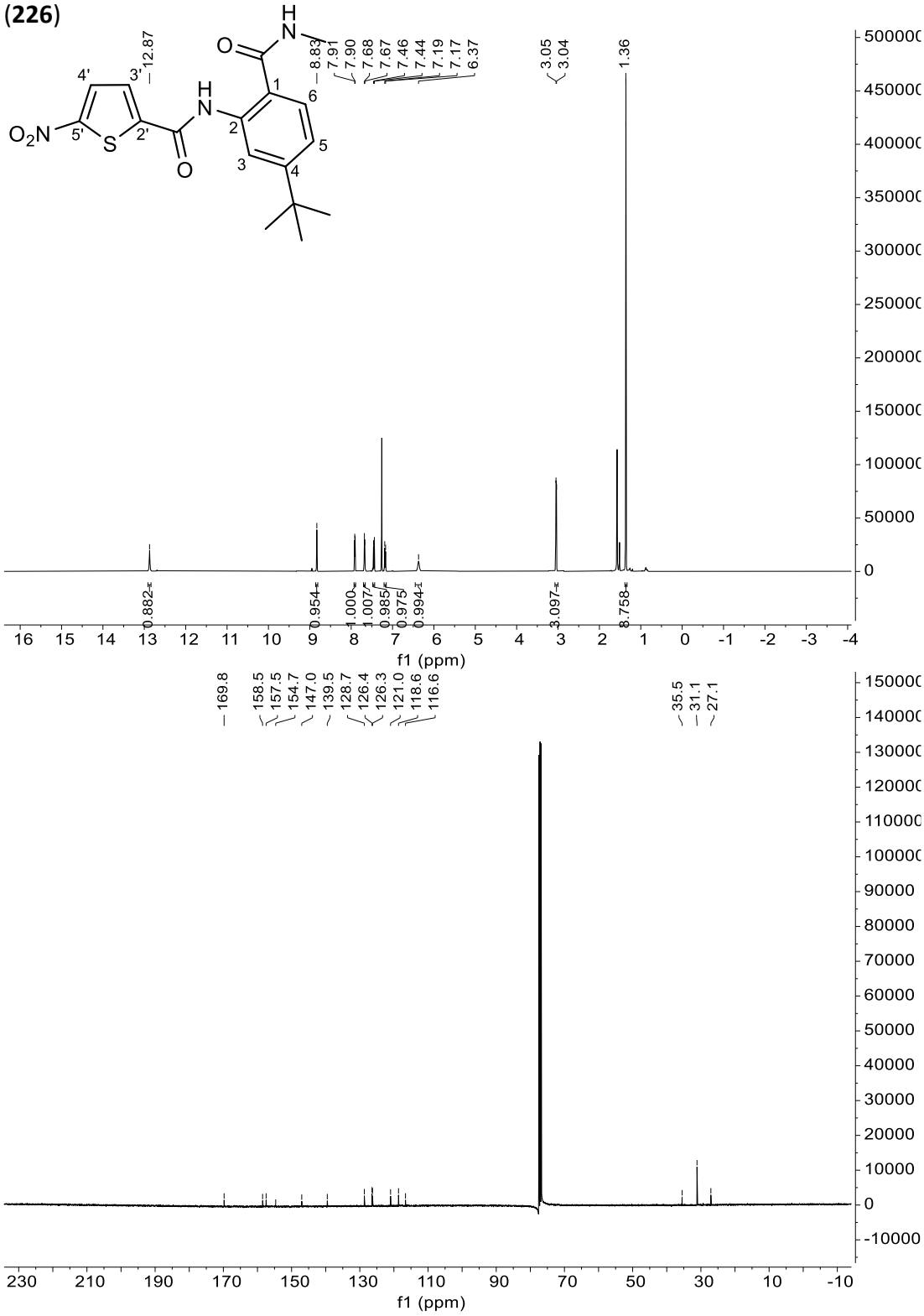

5-[2’-(2’’-methoxyethoxy)ethoxy]-2-bromo-1-nitrobenzene (**229**)

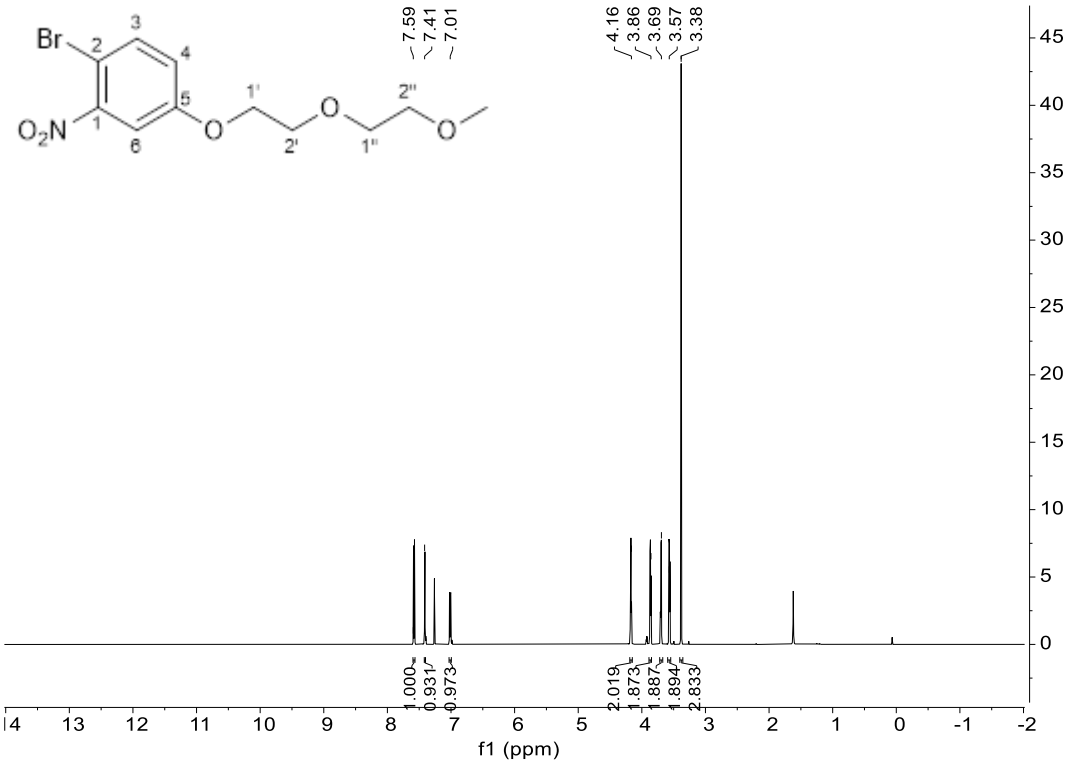

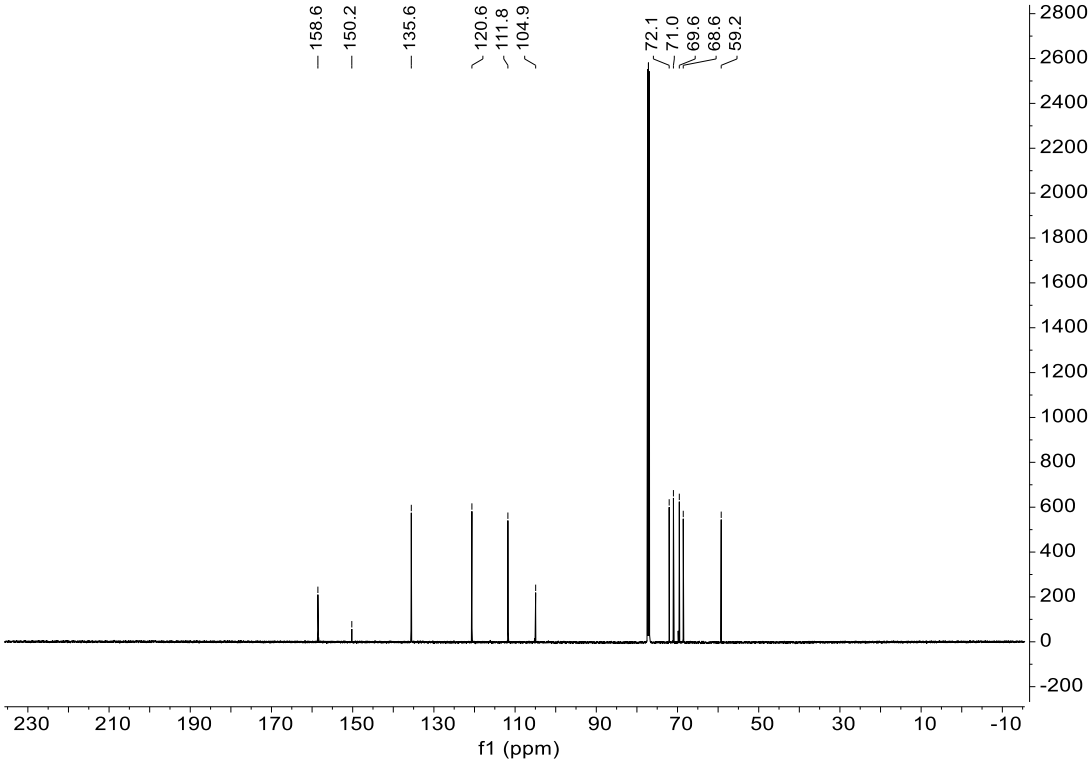

5-[2’-(2’’-methoxyethoxy)ethoxy]-2-bromo-1-aminobenzene (**230**)

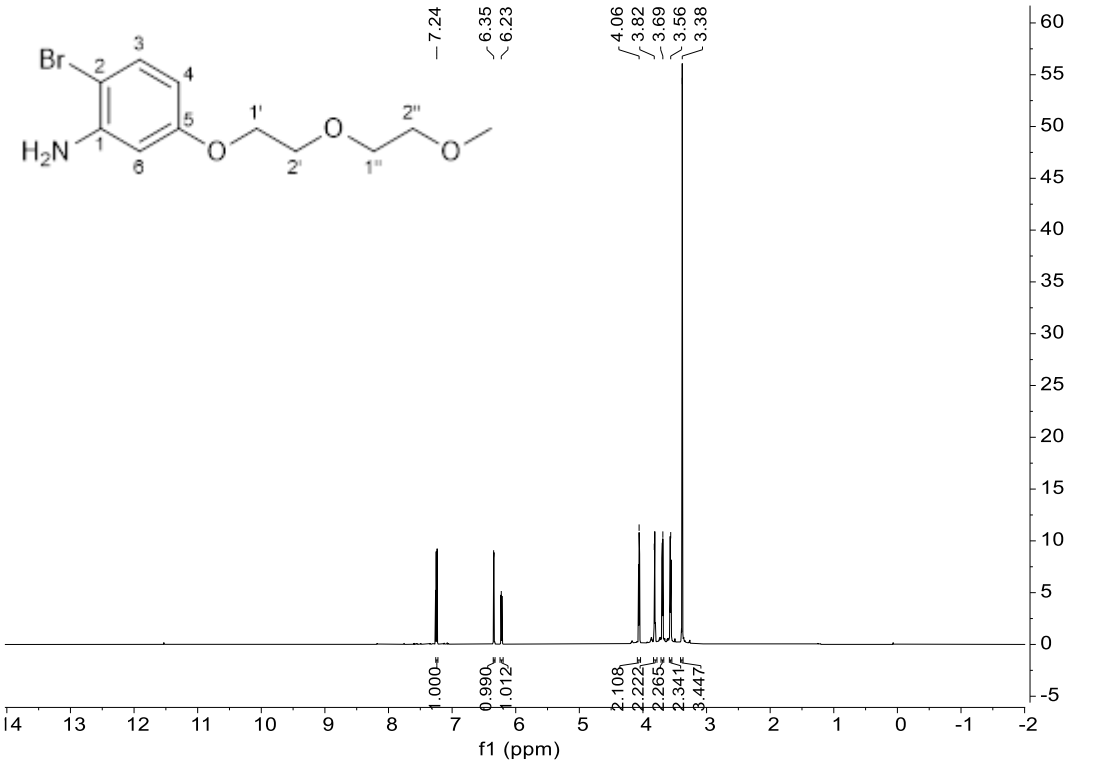

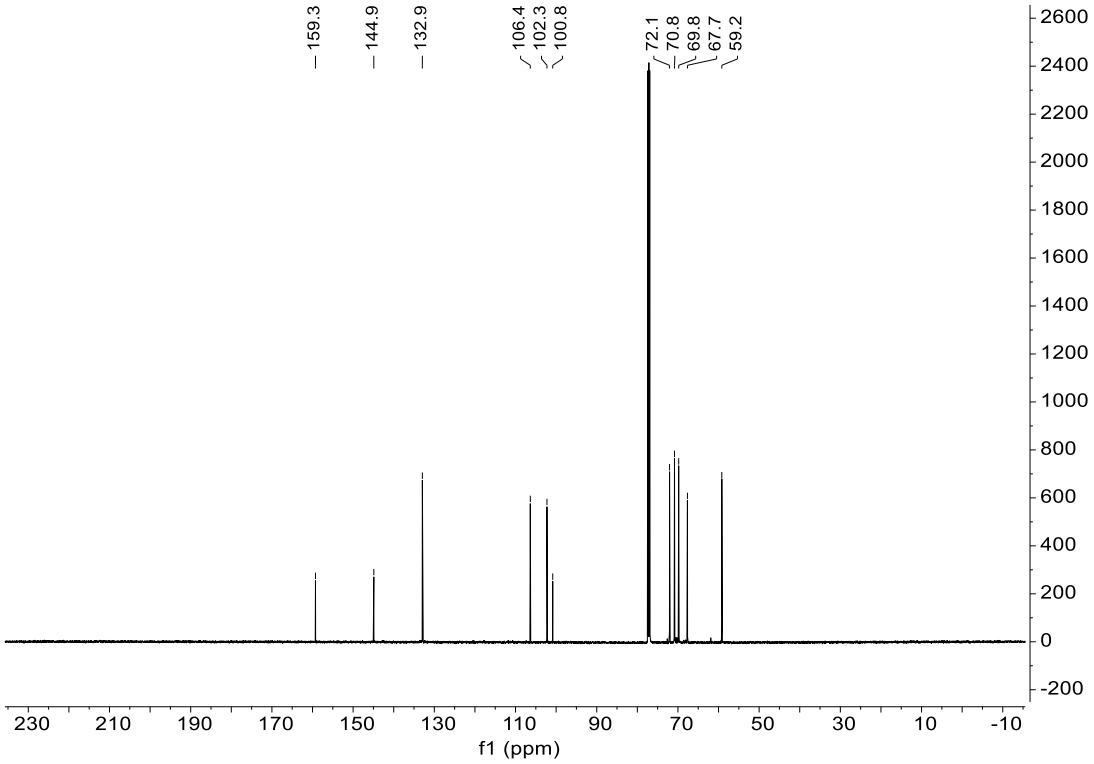

7-[2’-(2’’-methoxyethoxy)ethoxy]-3-methyl-3,4-dihydroquinazolin-4-one (**233**)

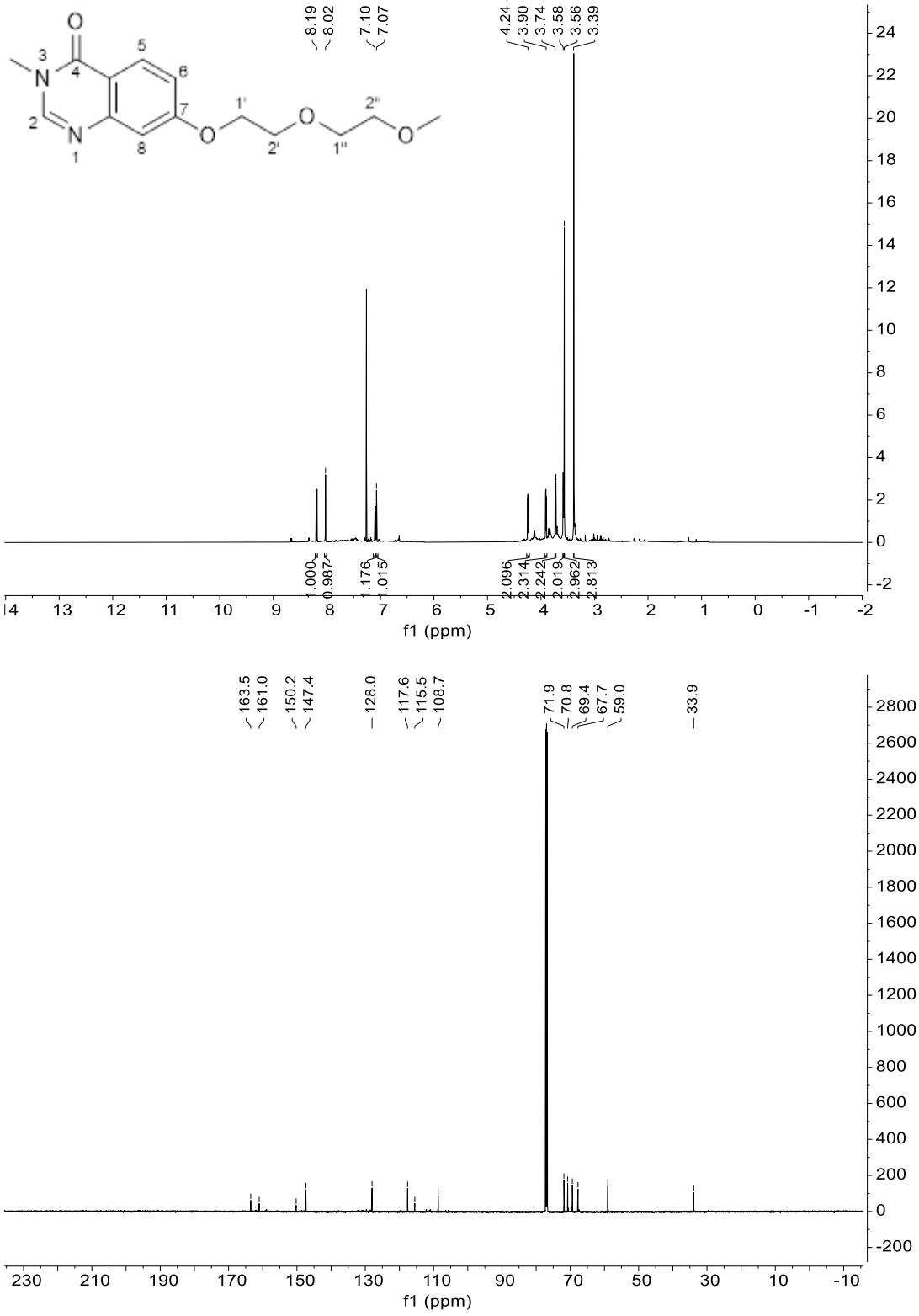

5-[2’-(2’’-methoxyethoxy)ethoxy]-2-methyl-1-nitrobenzene (**235**)

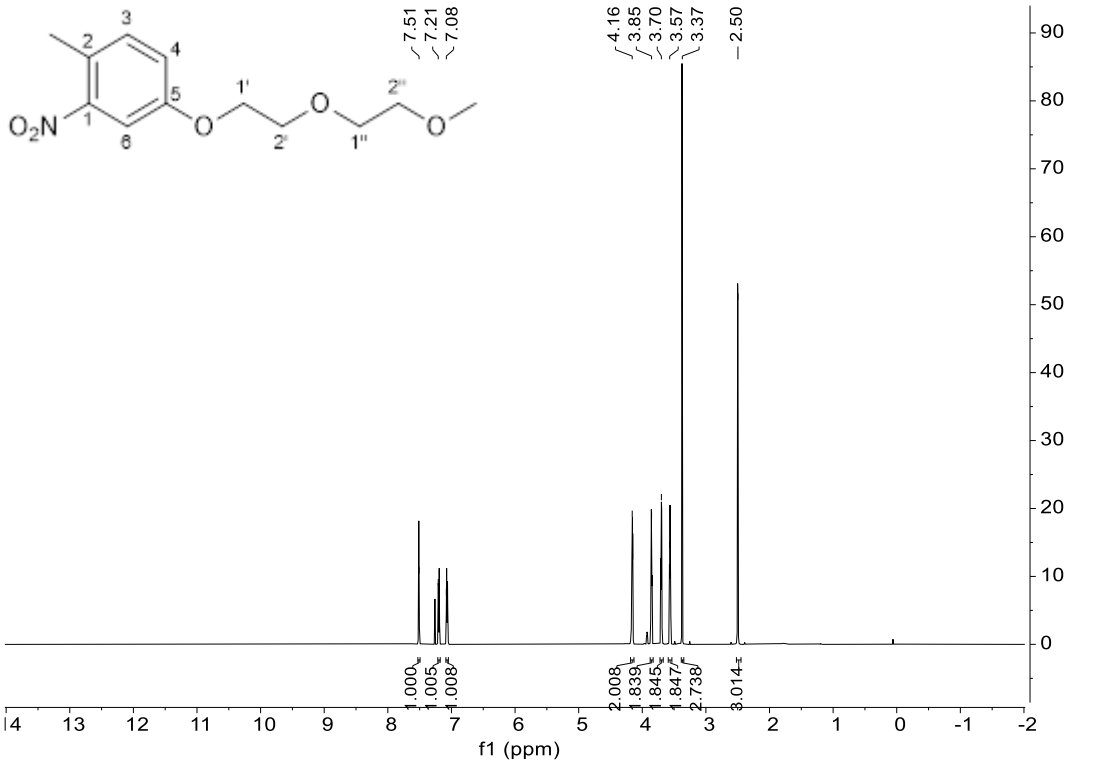

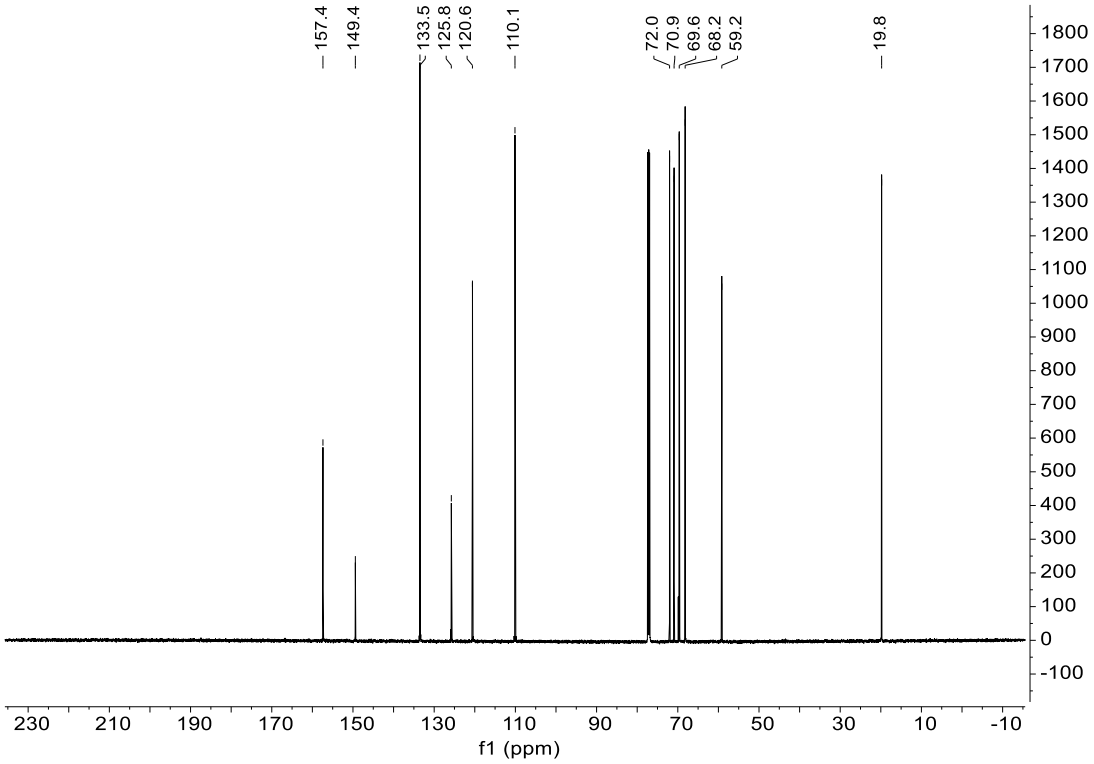

7-hydroxy-2,4-dihydro-1*H*-3,1-benzoxazine-2,4-dione (**239**)

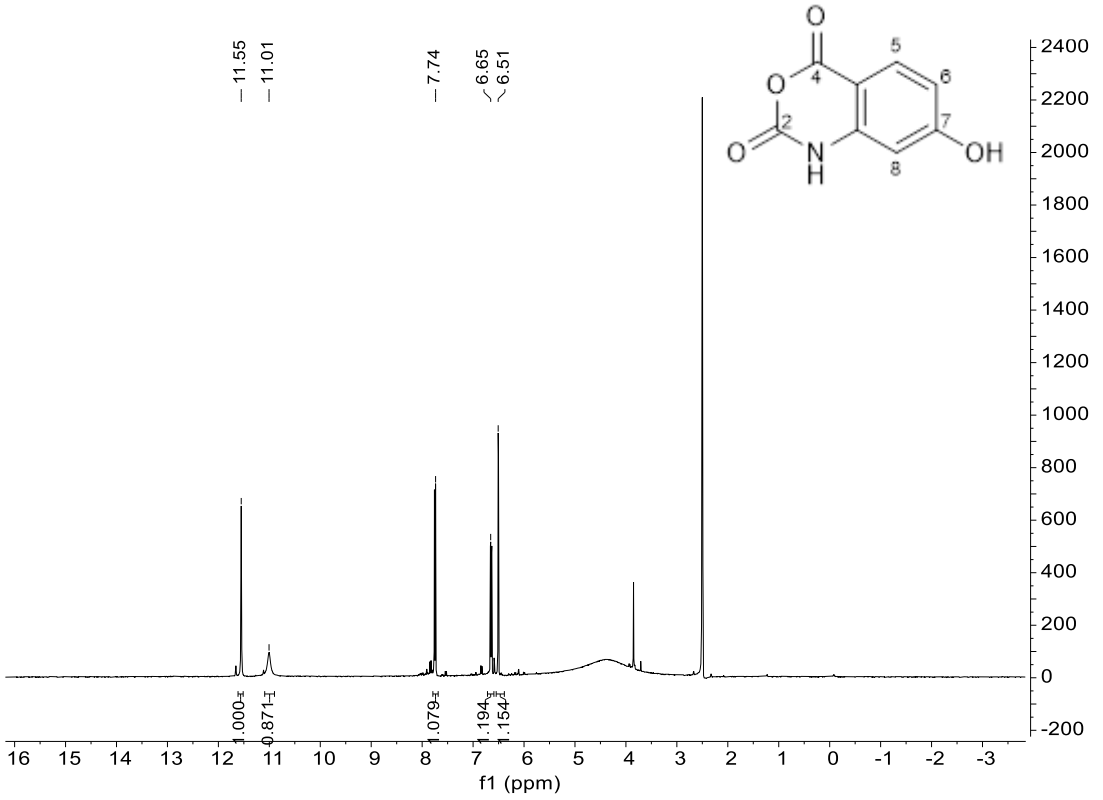

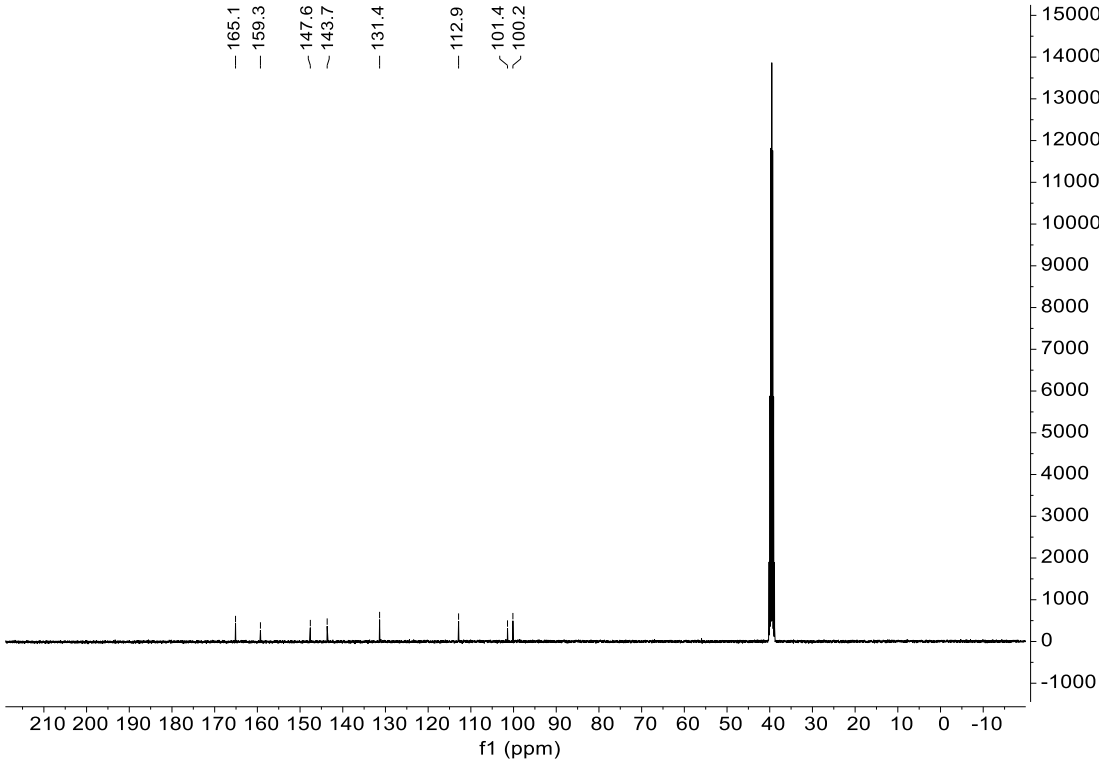

Amino-5-hydroxy-*N*-methyl-2-benzamide (**241**)

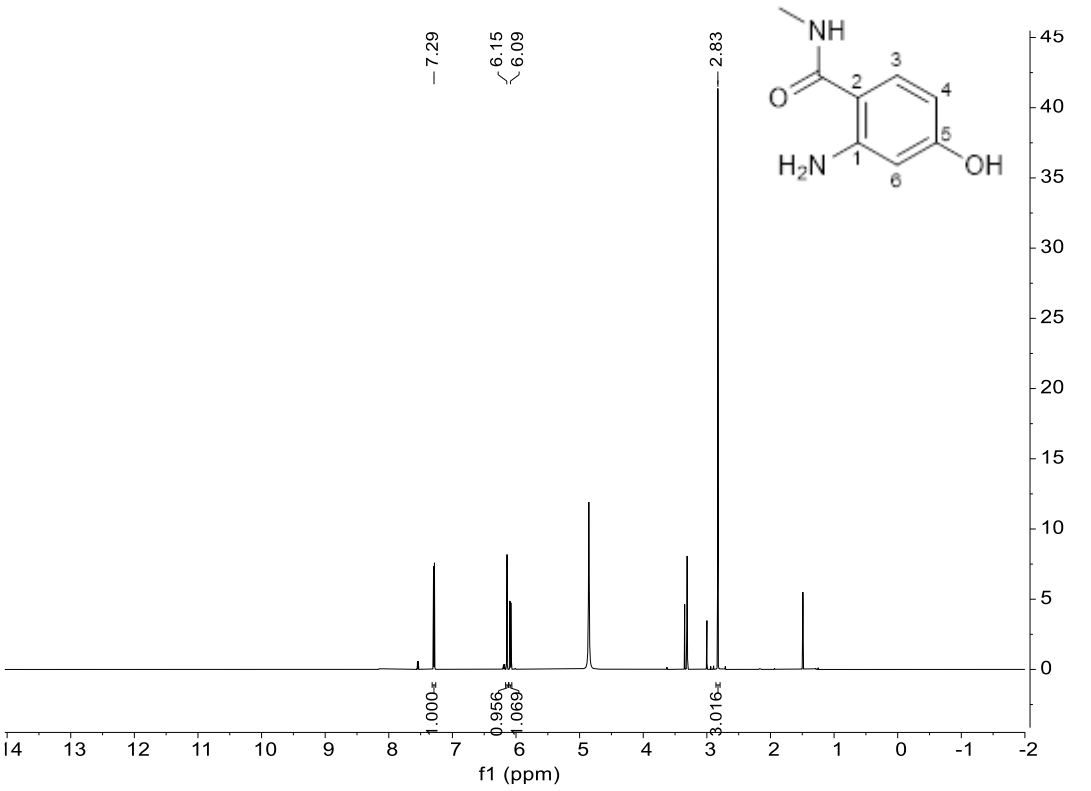

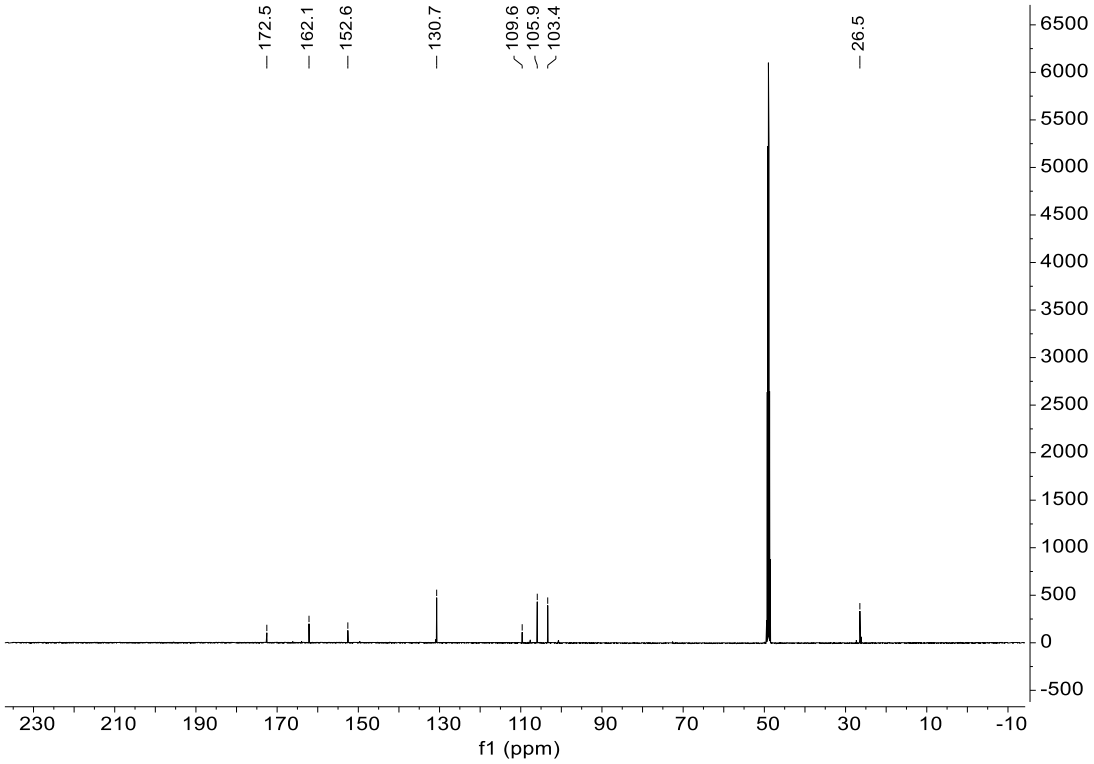

5-[2’-(2’’-methoxyethoxy)ethoxy]-1-amino-*N*-methyl-2-benzamide (**246**)

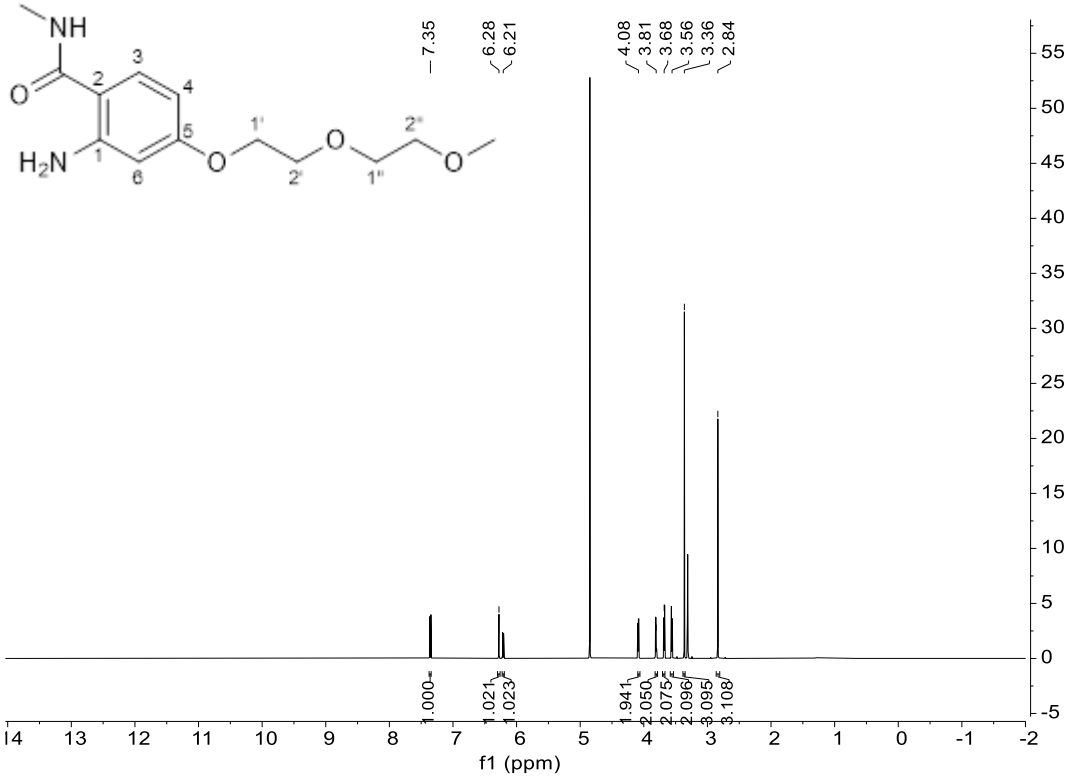

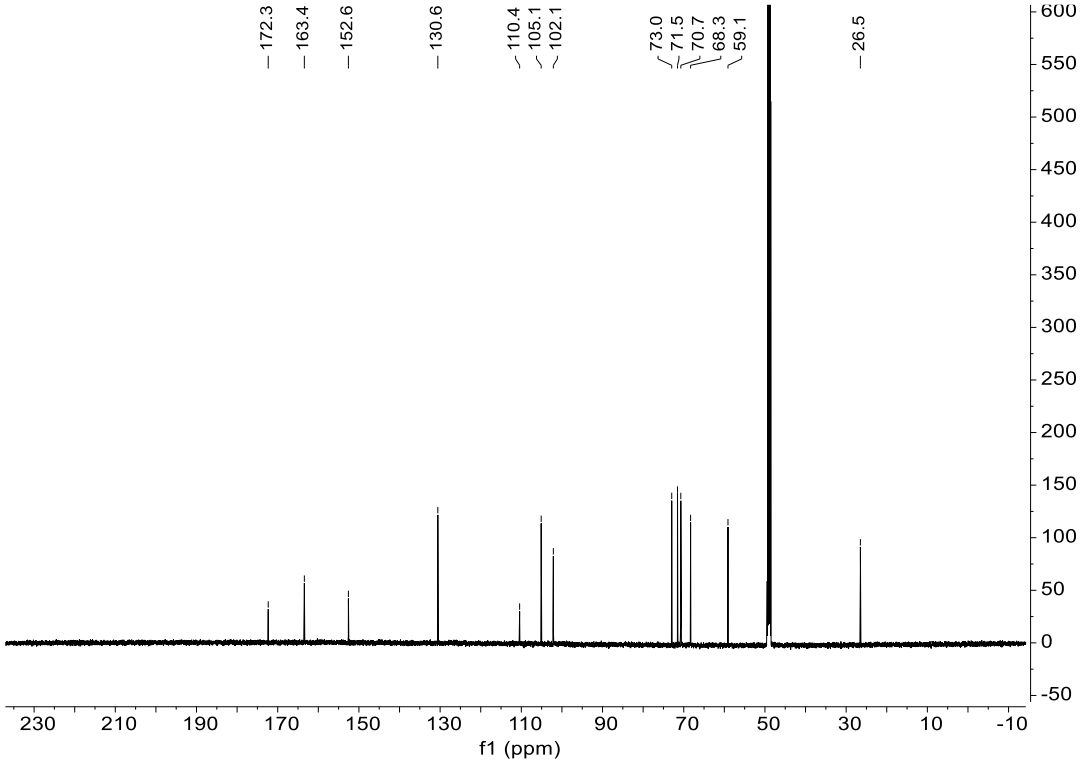

N-{5-[2’’-(2’’’-methoxyethoxy)ethoxy]-2-(methylcarbamoyl)phenyl}-5’-nitrothiophene-2’-carboxamide (**232**)

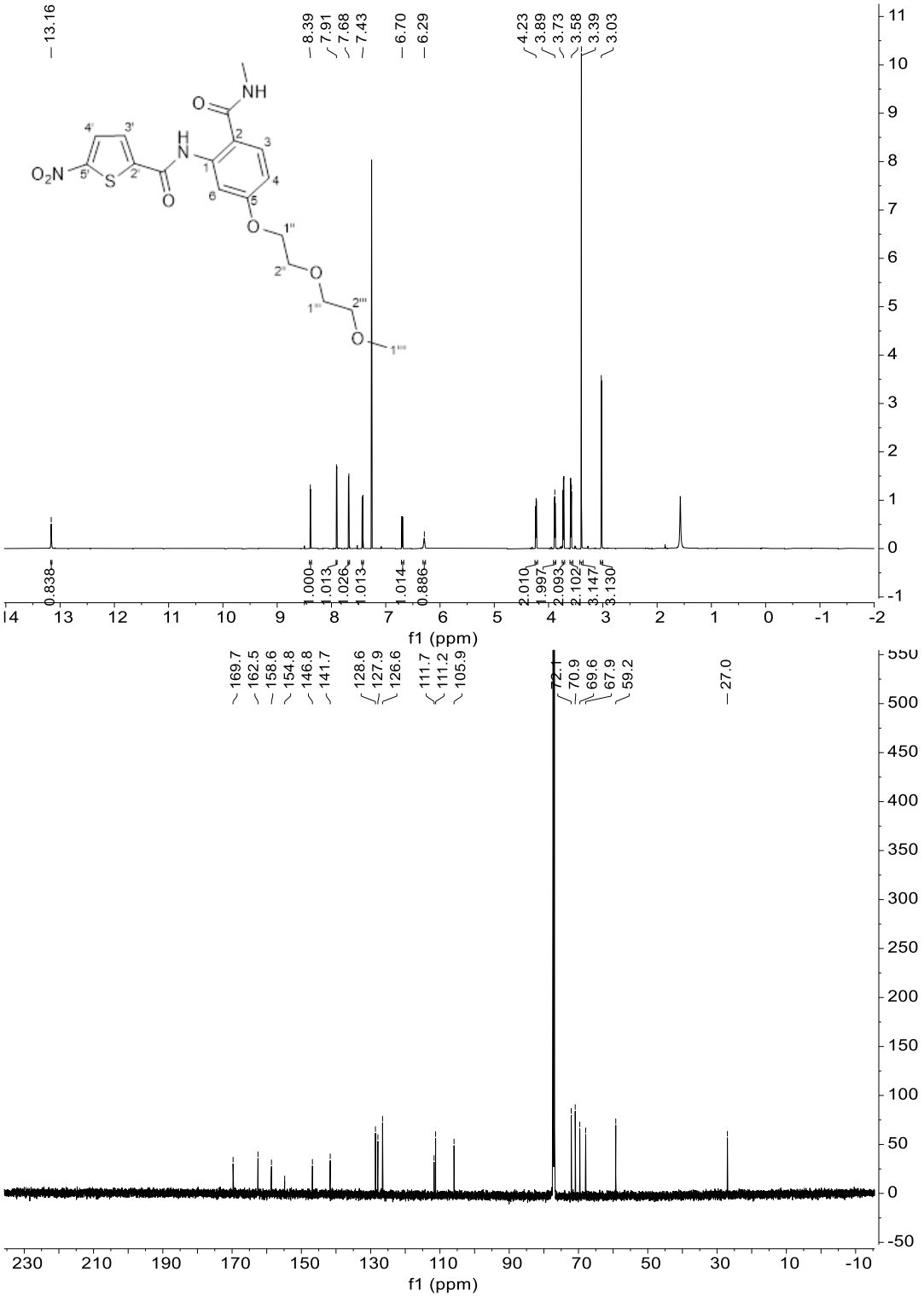

2-(2’-(prop-2’’-ynyloxy)ethoxy)ethanol (**256**)

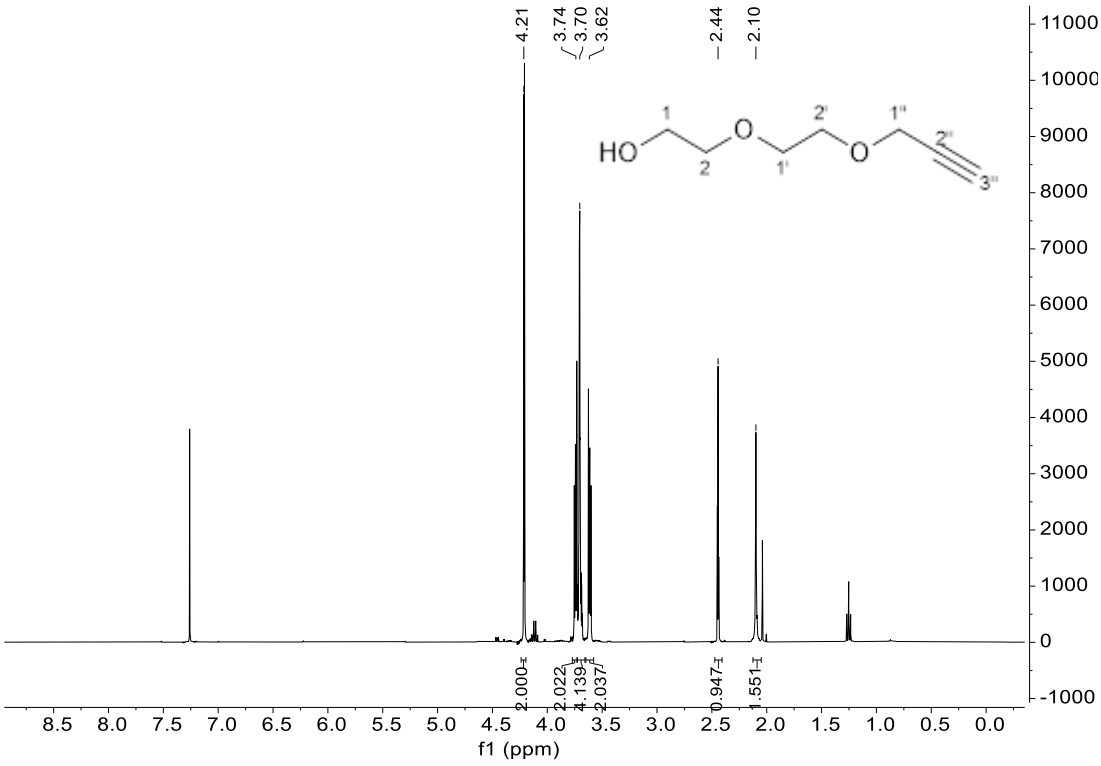

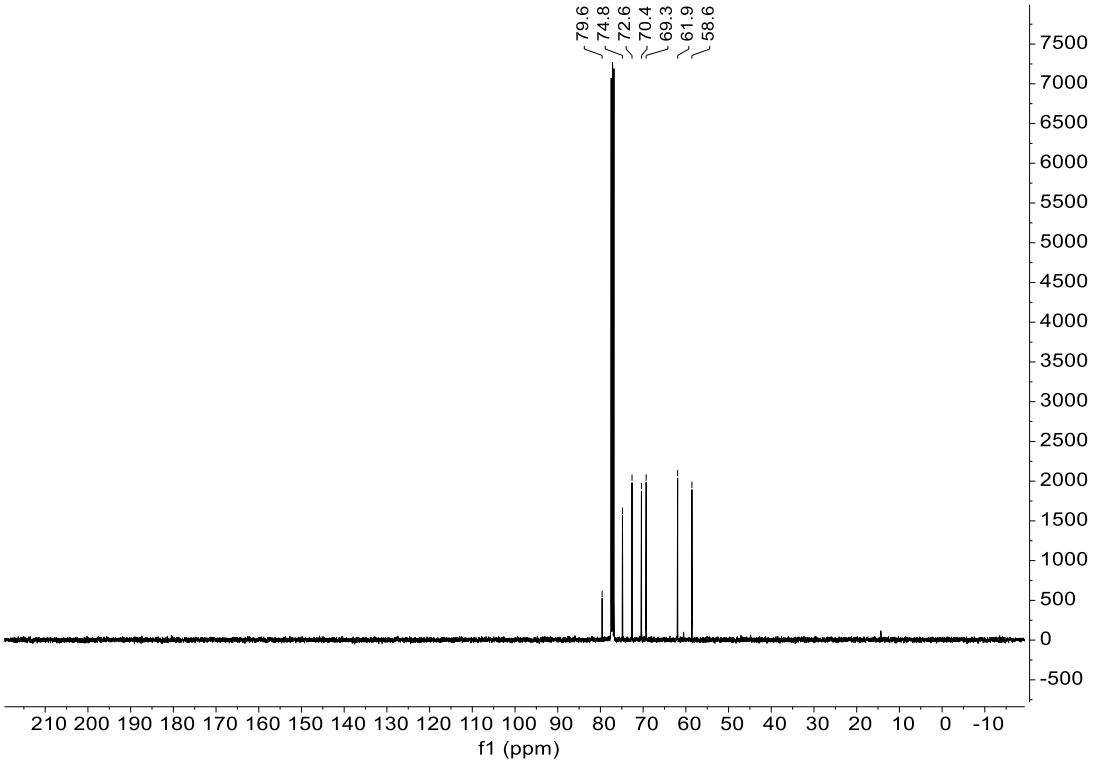

1-bromo-2-[2’-(prop-2’’-ynyloxy)ethoxy]ethane (**242**)

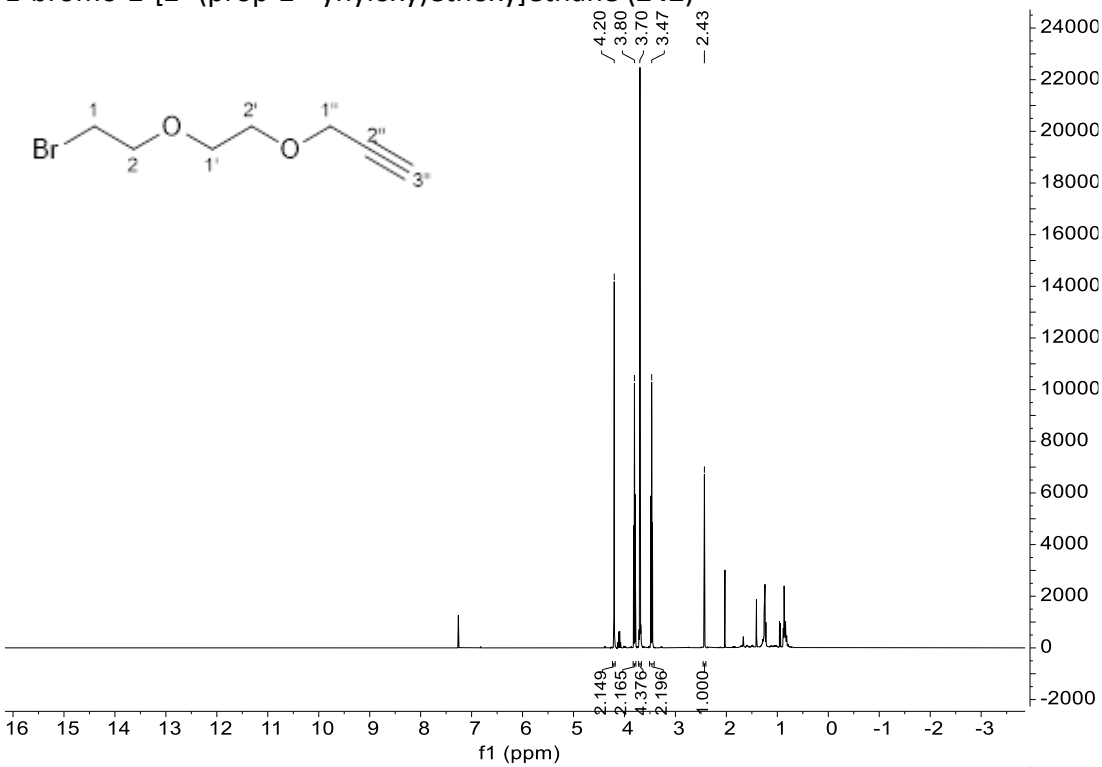

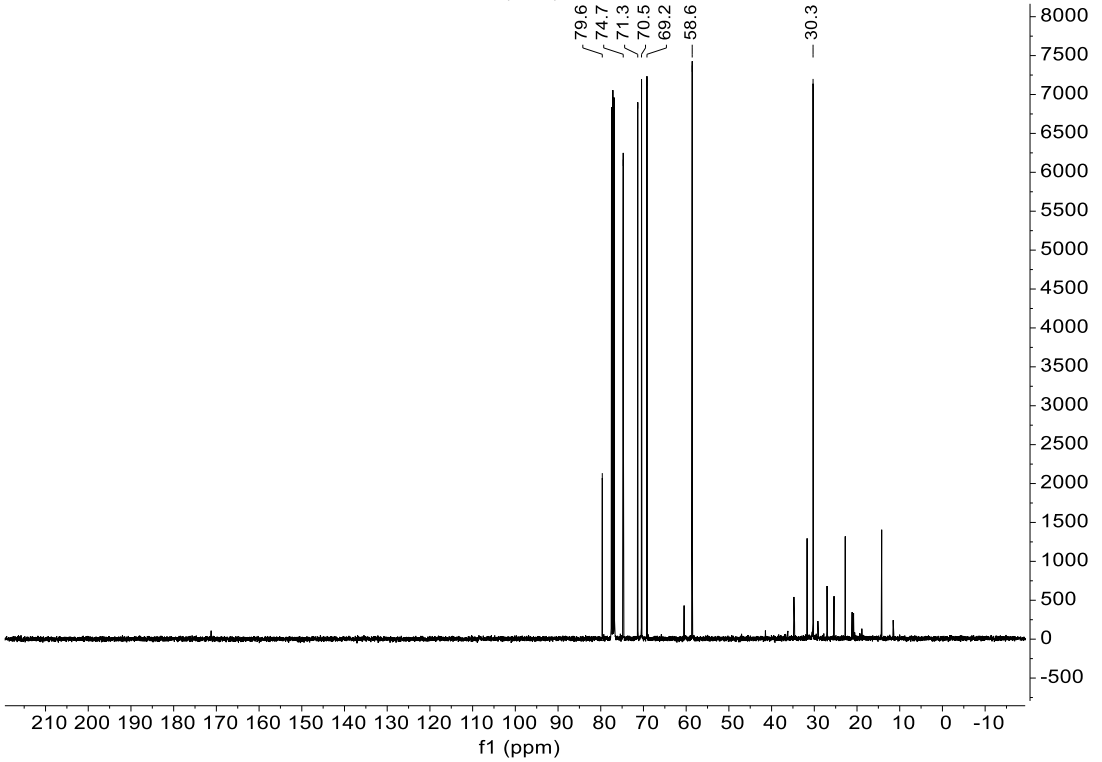

Amino-N-methyl-5-{2’-[2’’-(prop-2’’’-yn-1’’’-yloxy)ethoxy]ethoxy}-2-benzamide (**247**)

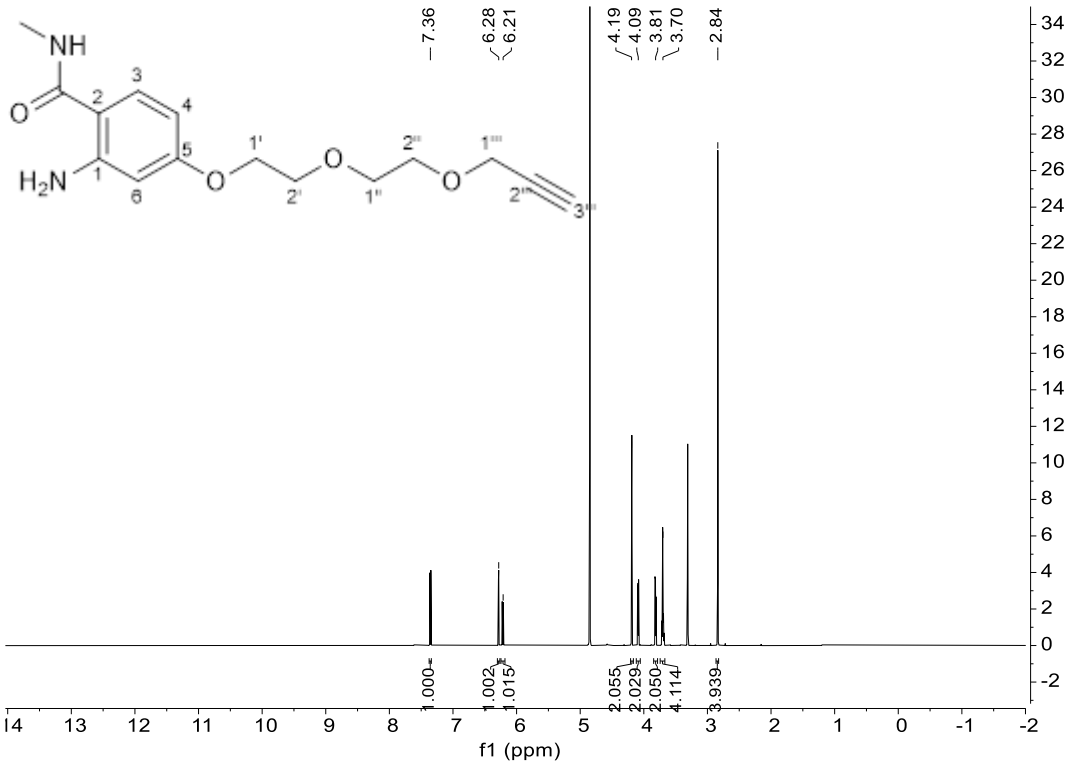

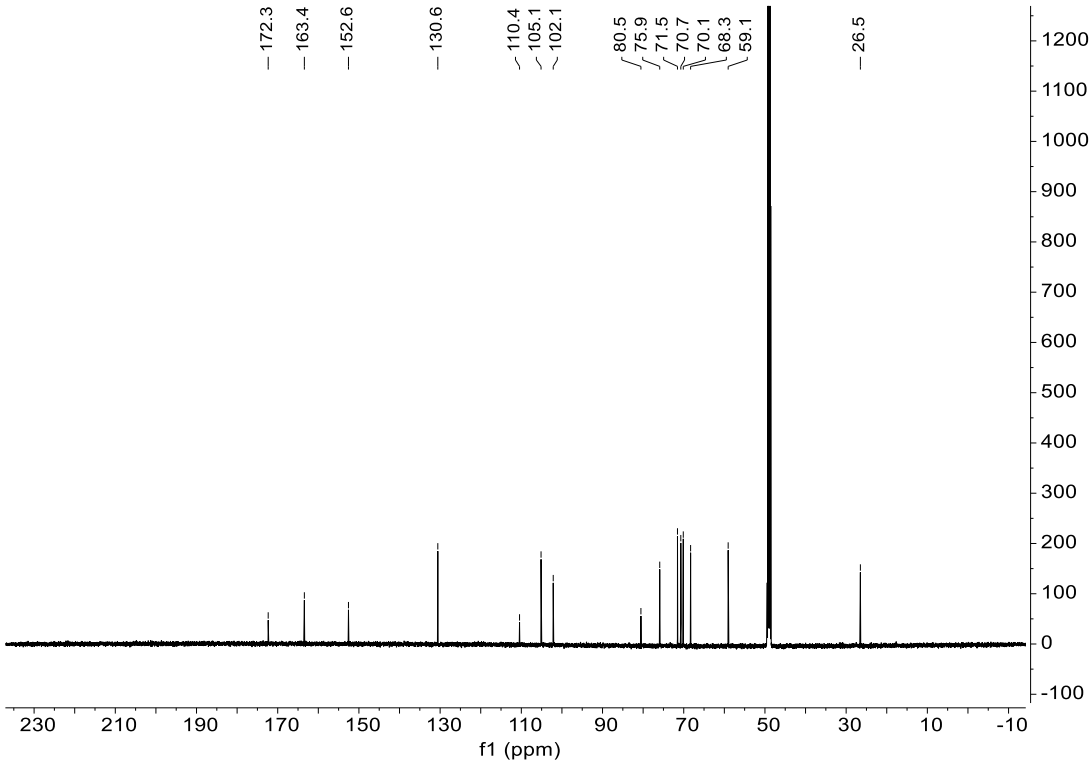

N-[2-(methylcarbamoyl)-5-{2’’-[2’’’-(prop-2’’’’-yn-1’’’’-yloxy)ethoxy]ethoxy}phenyl]-5’-nitrothiophene-2’-carboxamide (**251**)

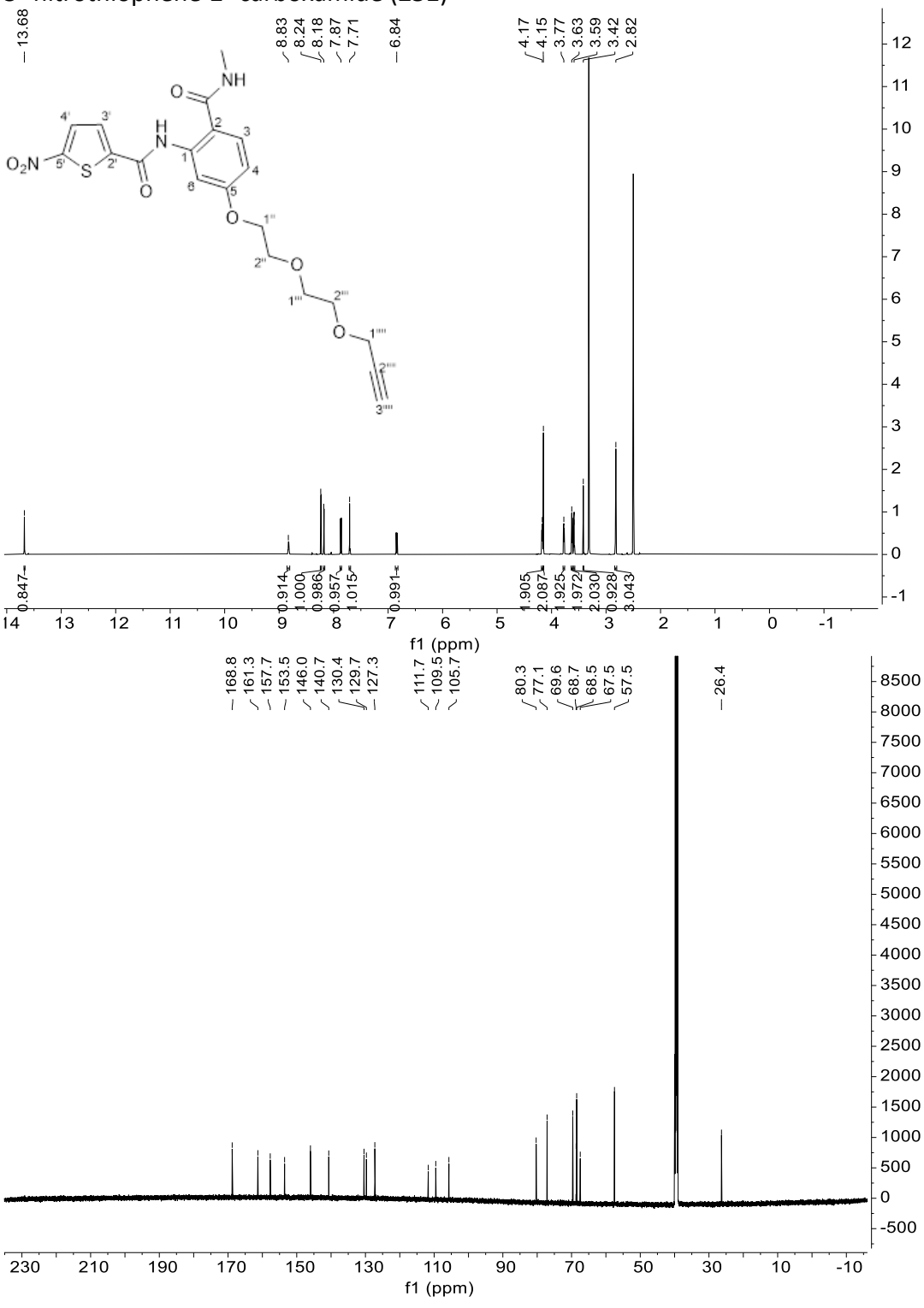

4-(2’-bromoethyl)morpholine (**243**)

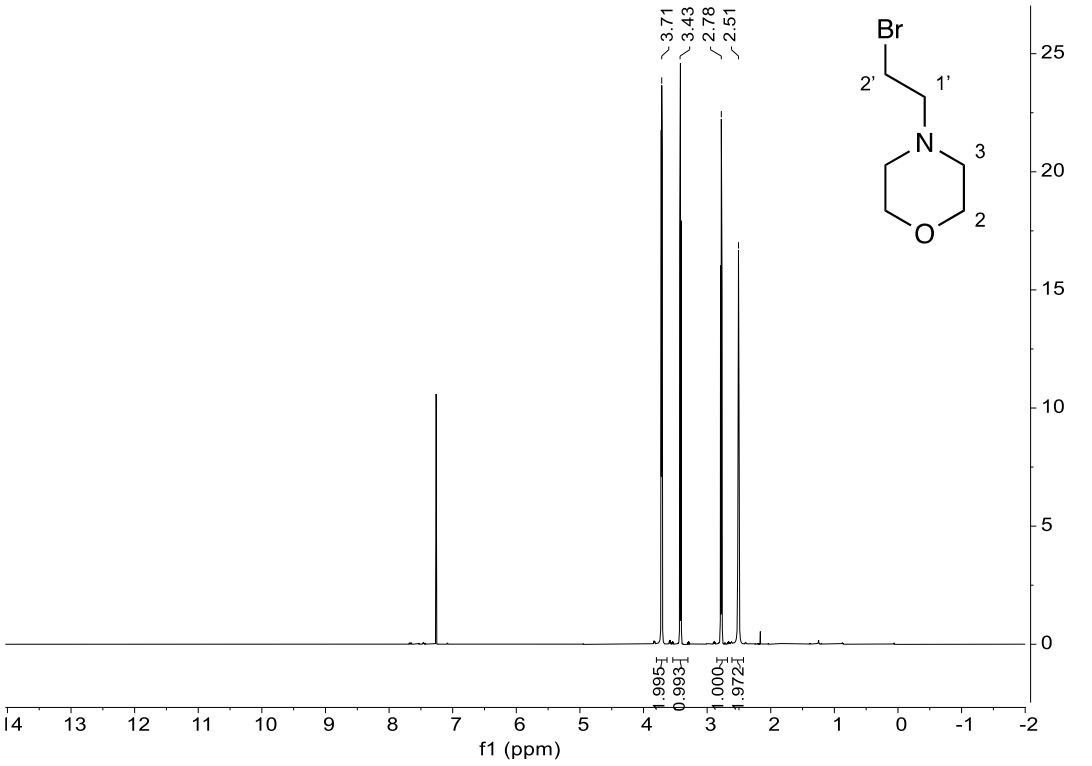

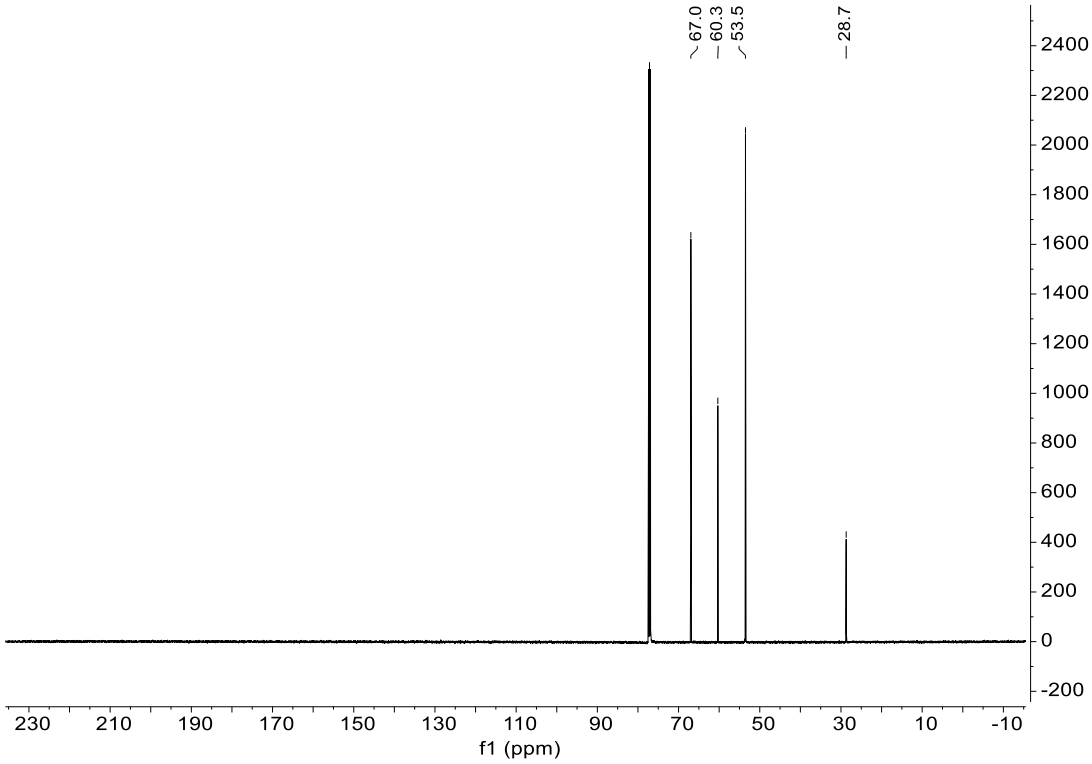

Amino-N-methyl-5-[2’-(morpholin-4’’-yl)ethoxy]-2-benzamide (**248**)

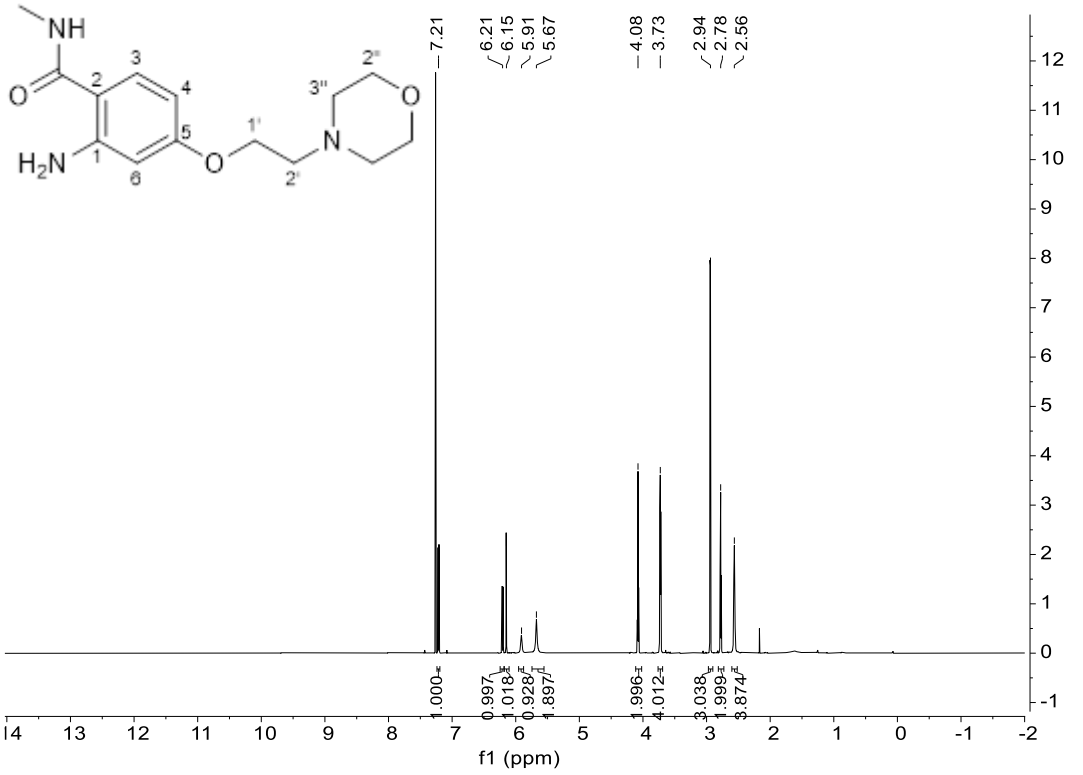

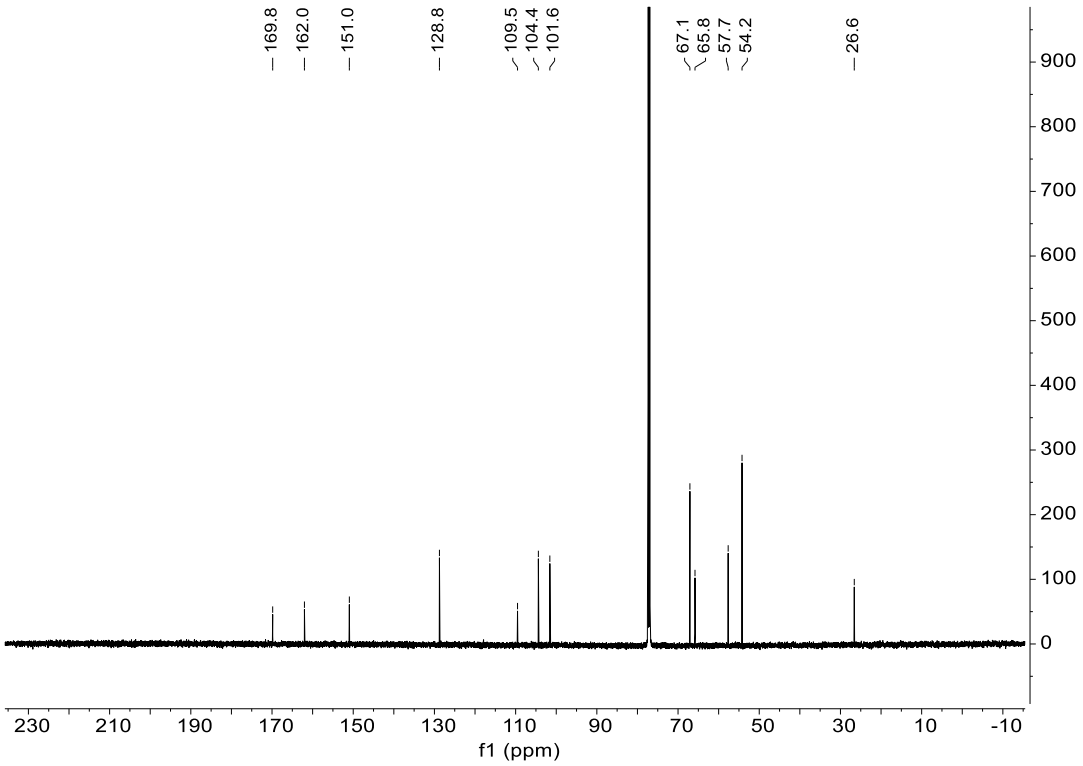

N-[2-(methylcarbamoyl)-5-[2’’-(morpholin-4’’’-yl)ethoxy]phenyl]-5’-nitrothiophene-2’-carboxamide (**252**)

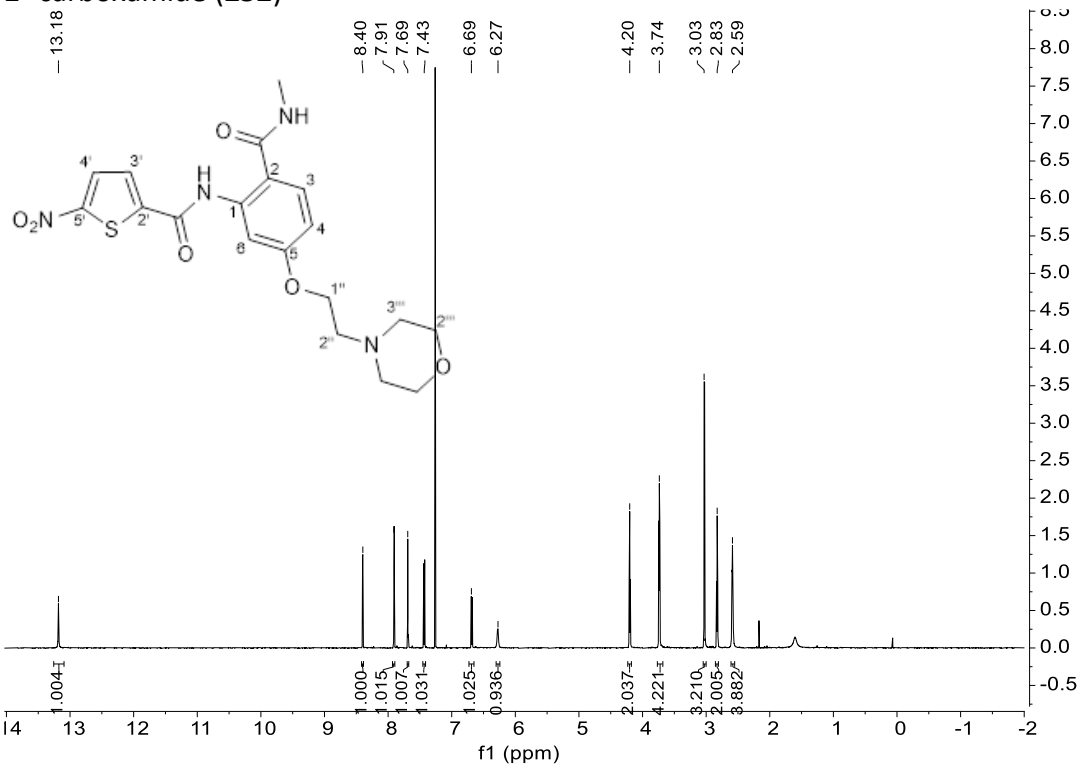

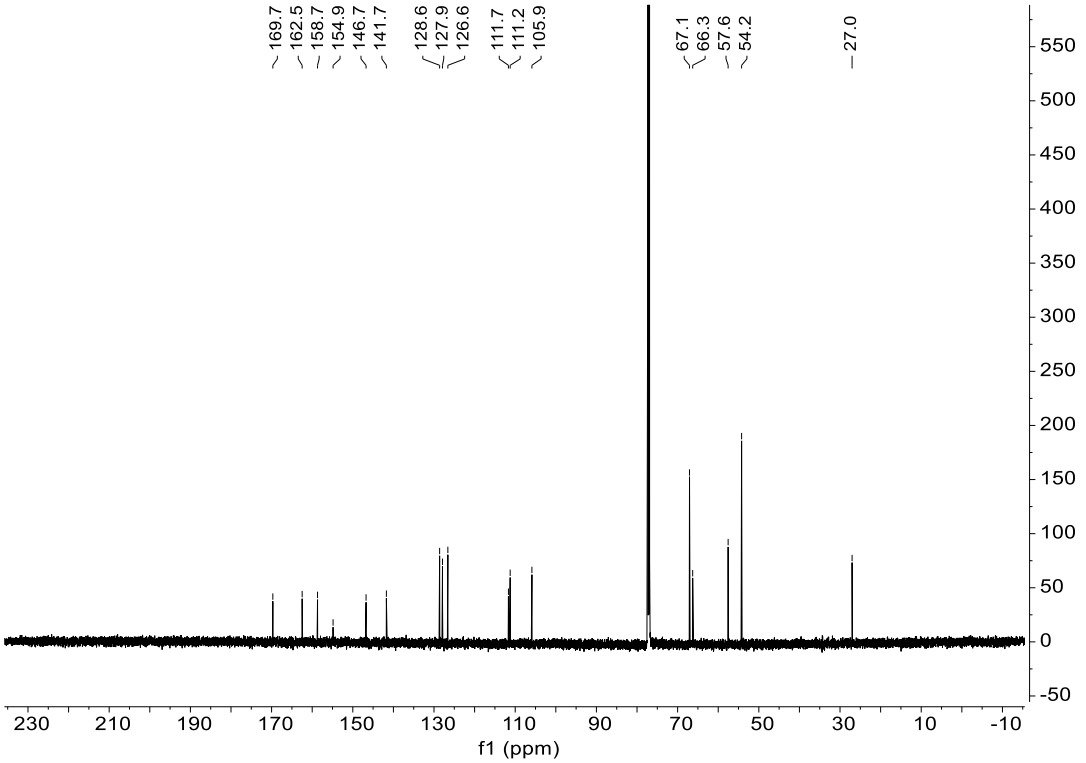

4-(3’-bromopropyl)-morpholine (**244**)

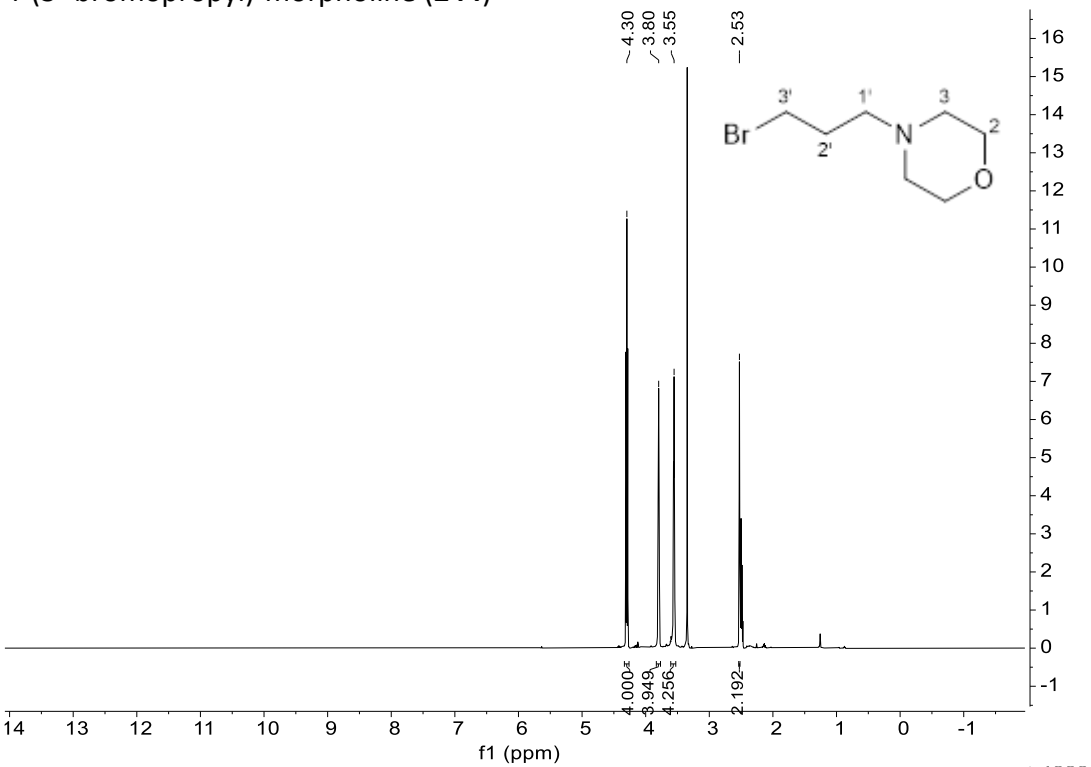

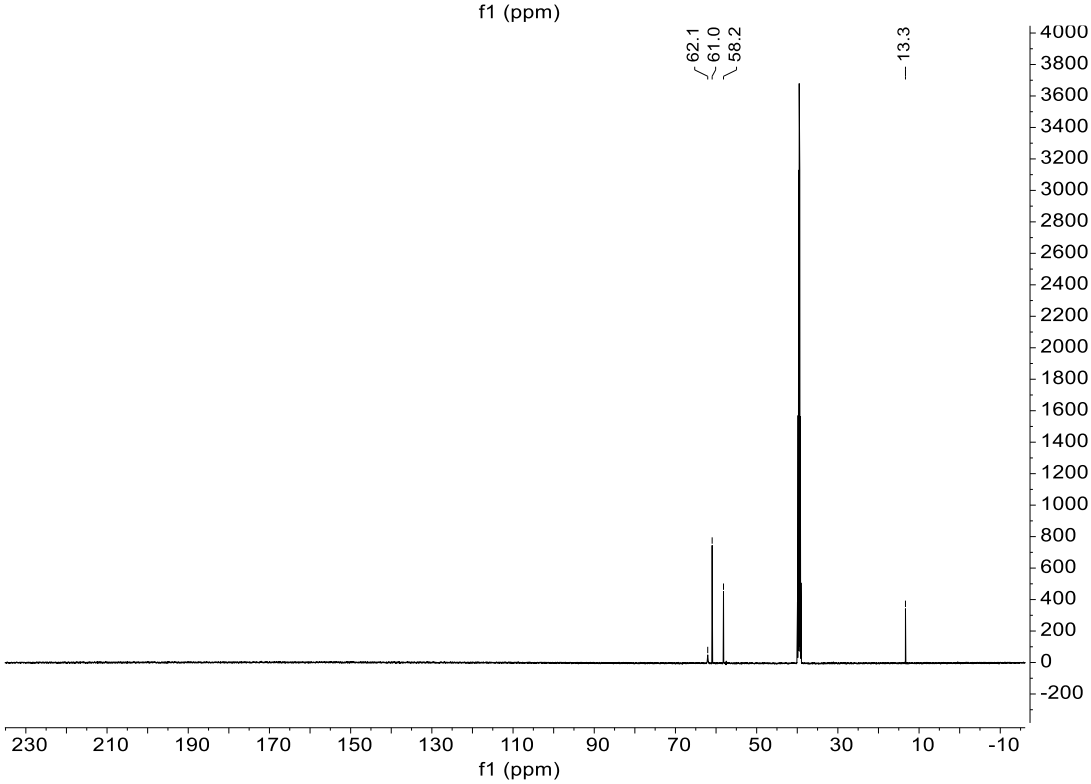

Amino-N-methyl-5-[3’-(morpholin-4’’-yl)propoxy]-2-benzamide (**249**)

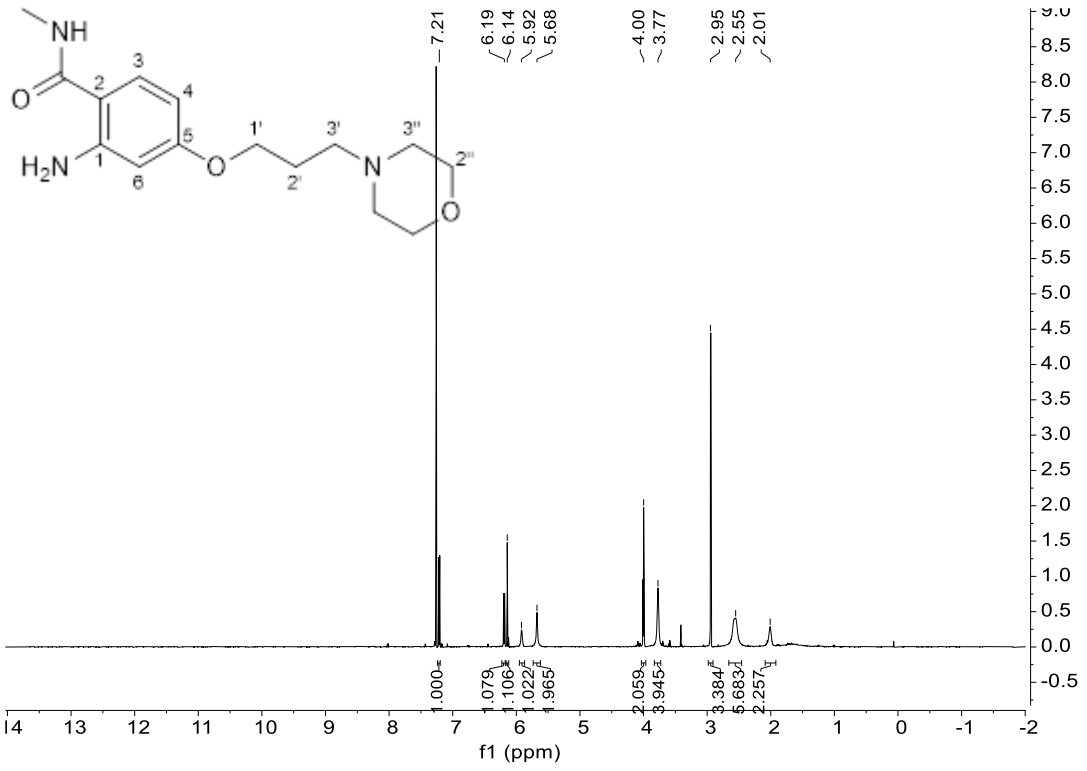

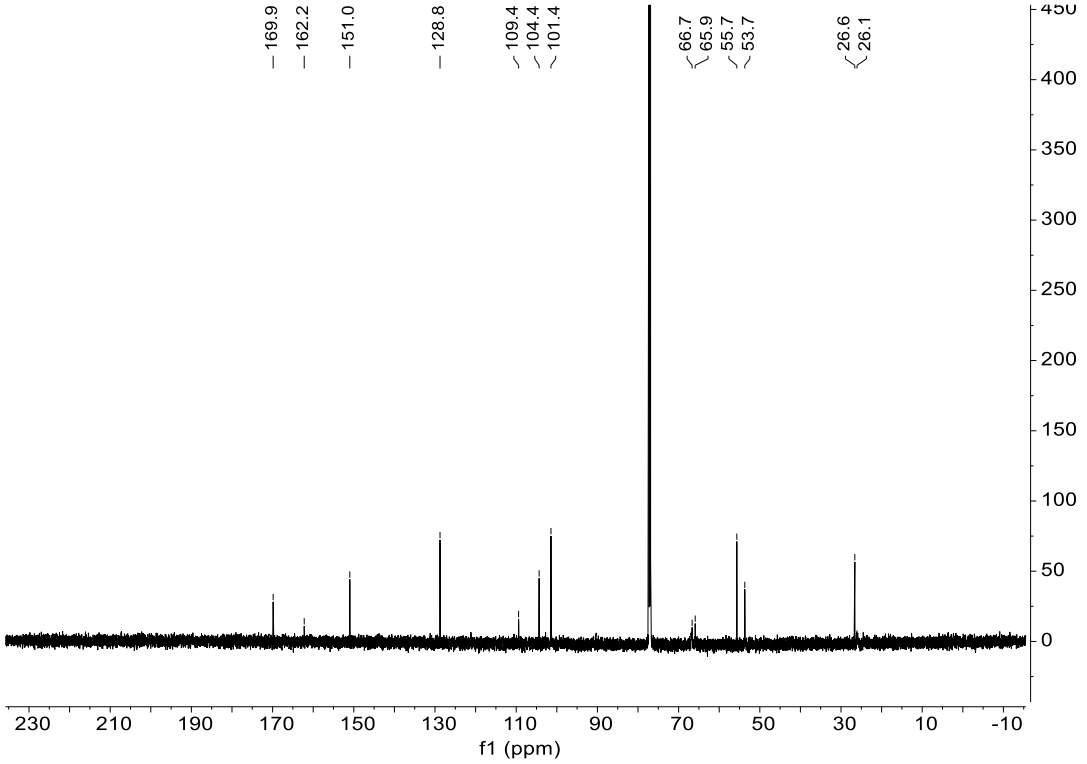

N-[2-(methylcarbamoyl)-5-[3’’-(morpholin-4’’’-yl)propoxy]phenyl]-5’-nitrothiophene-2’-carboxamide (**253**)

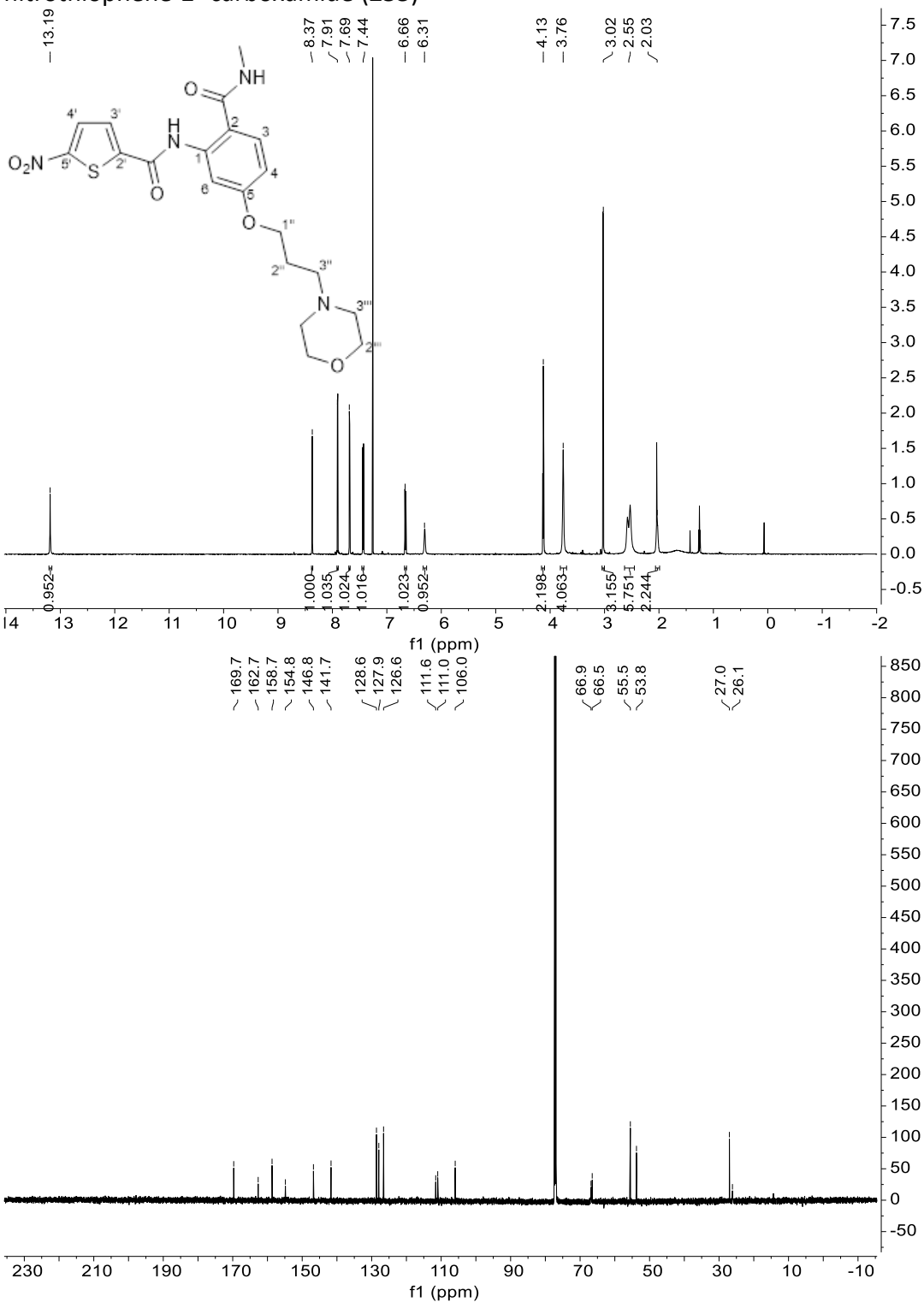

Amino-N-methyl-5-[2'-(oxan-4''-yl))ethoxy]-2-benzamide (**250**)

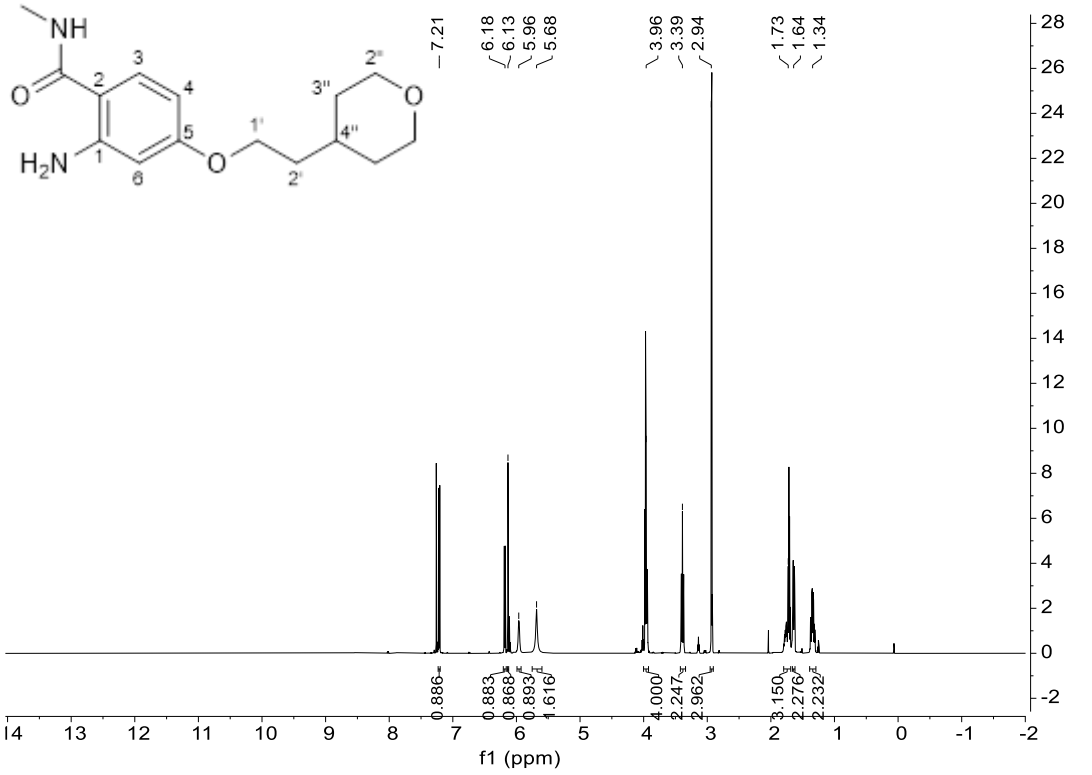

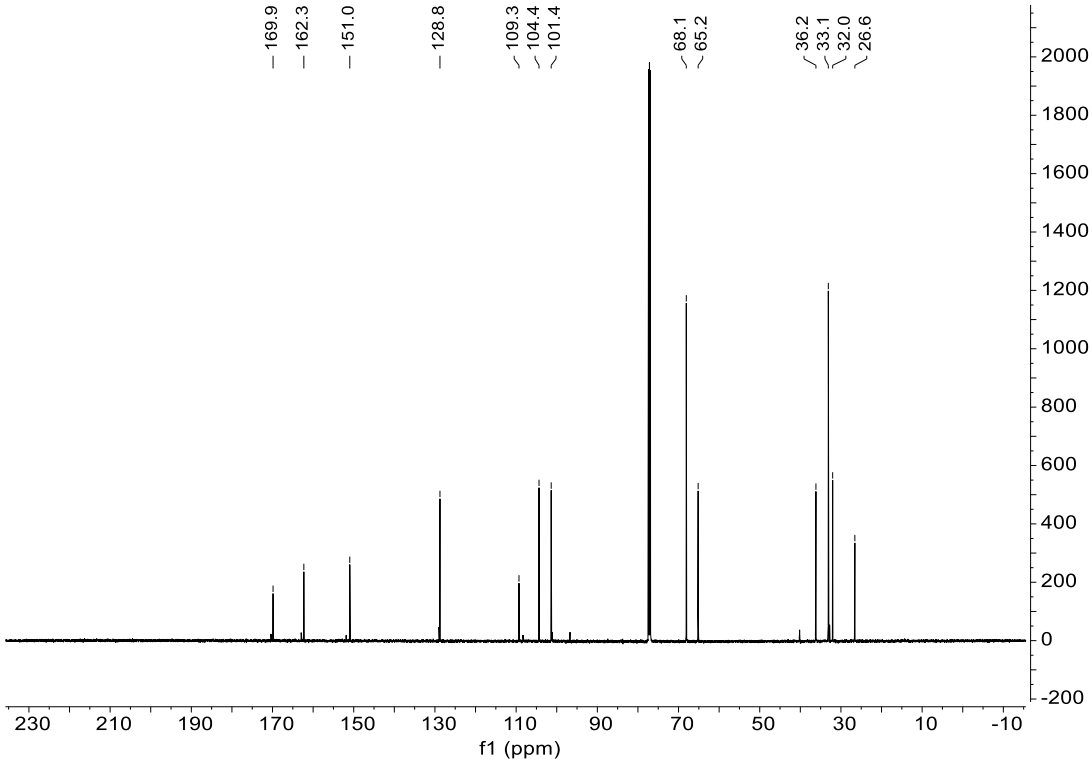

N-[2-(methylcarbamoyl)-5-[2’’-(oxan-4’’’-yl)ethoxy]phenyl]-5’-nitrothiophene-2’-carboxamide (**254**)

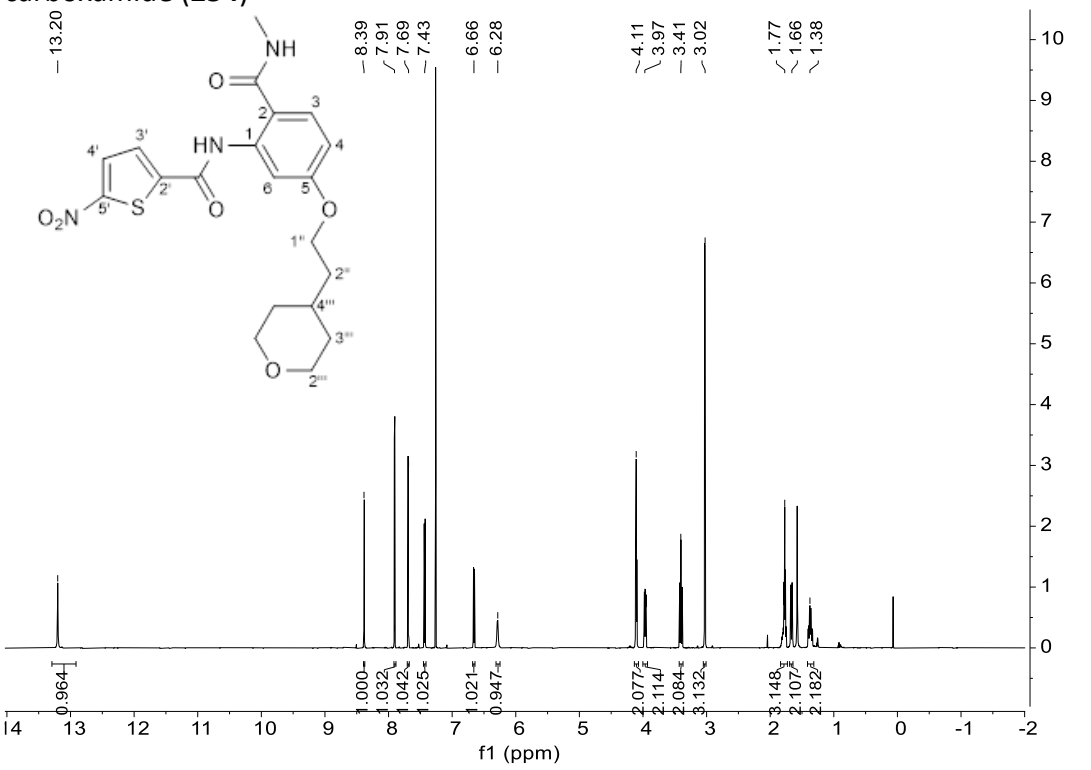

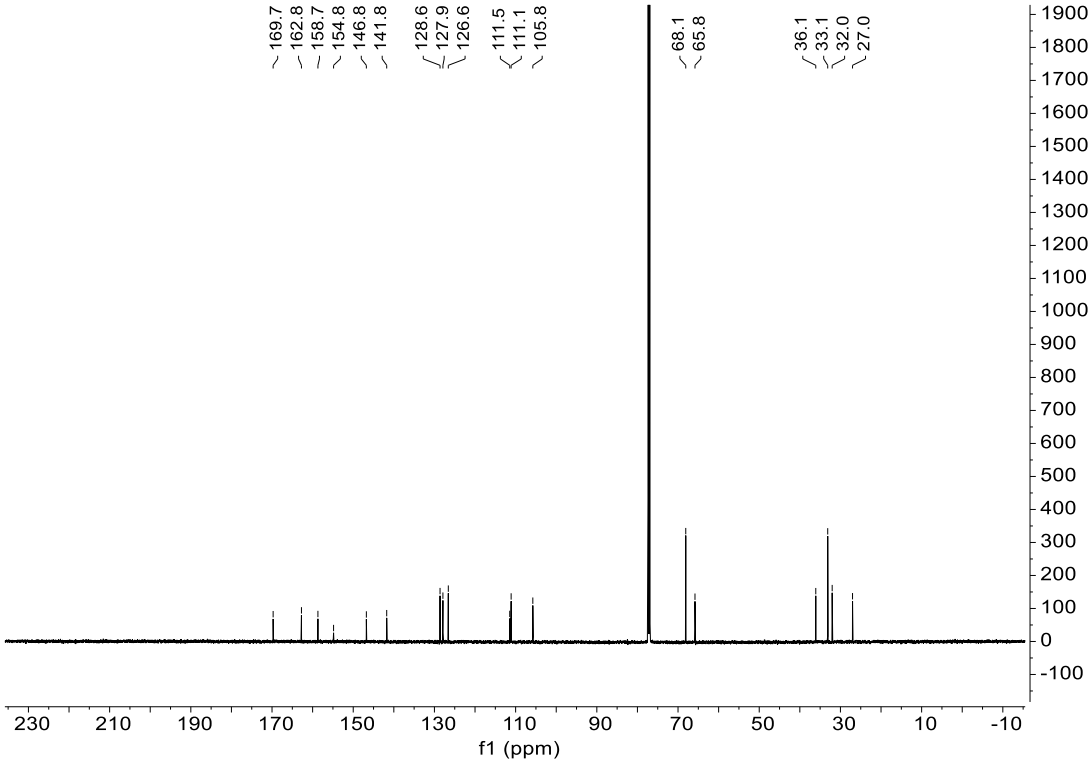

2-amino-N-methyl-4-[3’-hyrdoxypropoxy]benzamide (**269**)

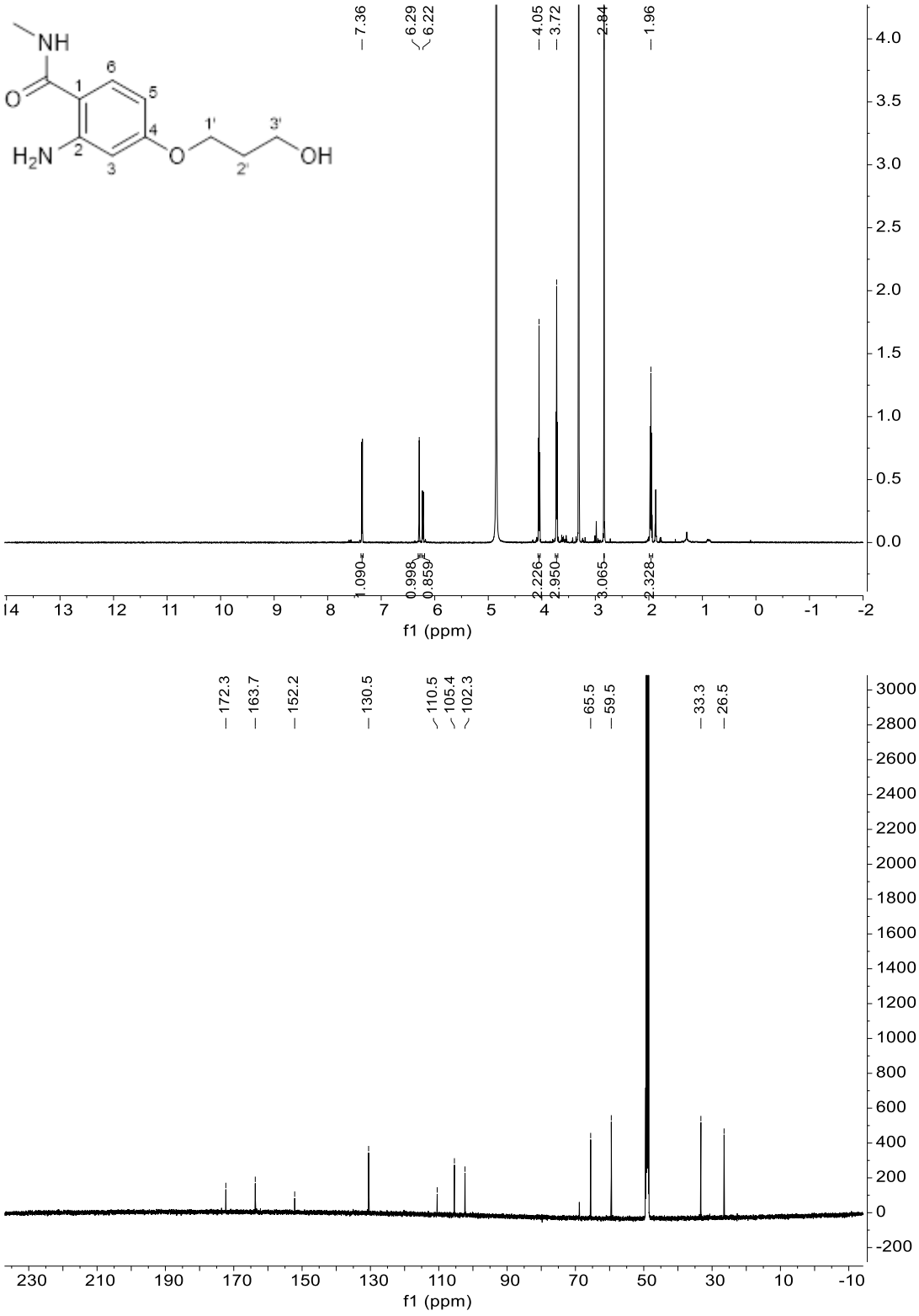

2-amino-N-methyl-4-[3’-(4’-methylpiperazin-1’-yl)propoxy]benzamide (**271**)

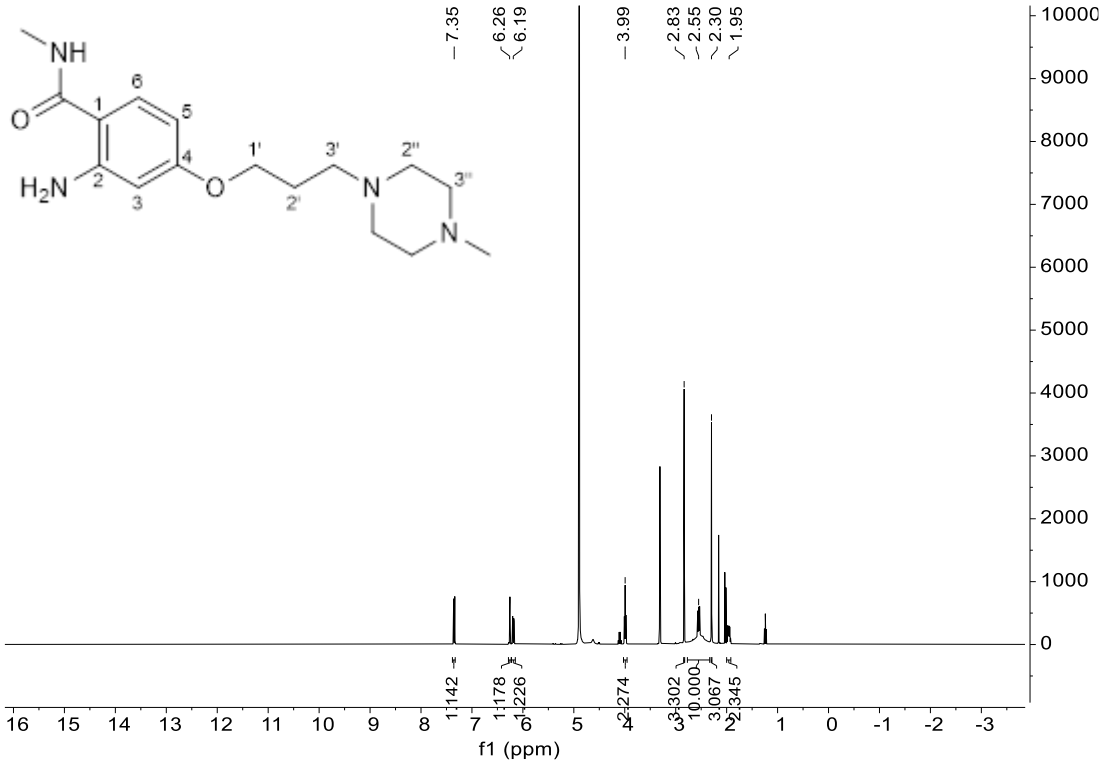

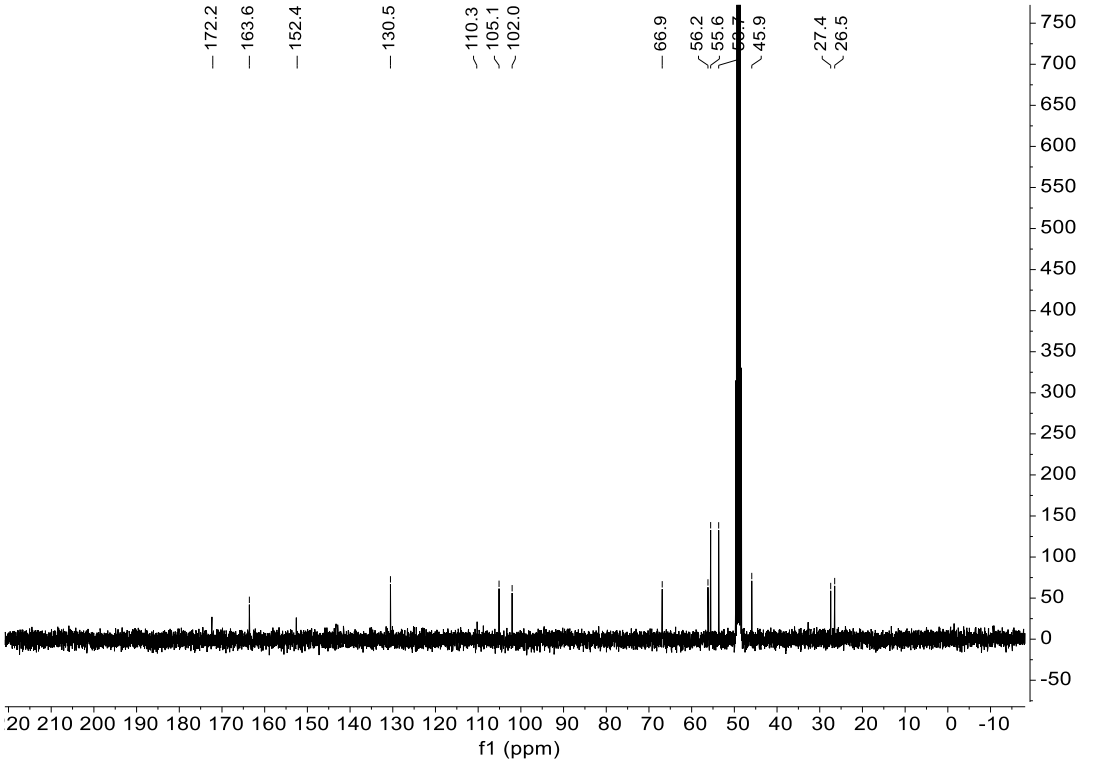

6,7-dimethoxy-2,4-dihydro-1*H*-3,1-benzoxazine-2,4-dione (**332**)

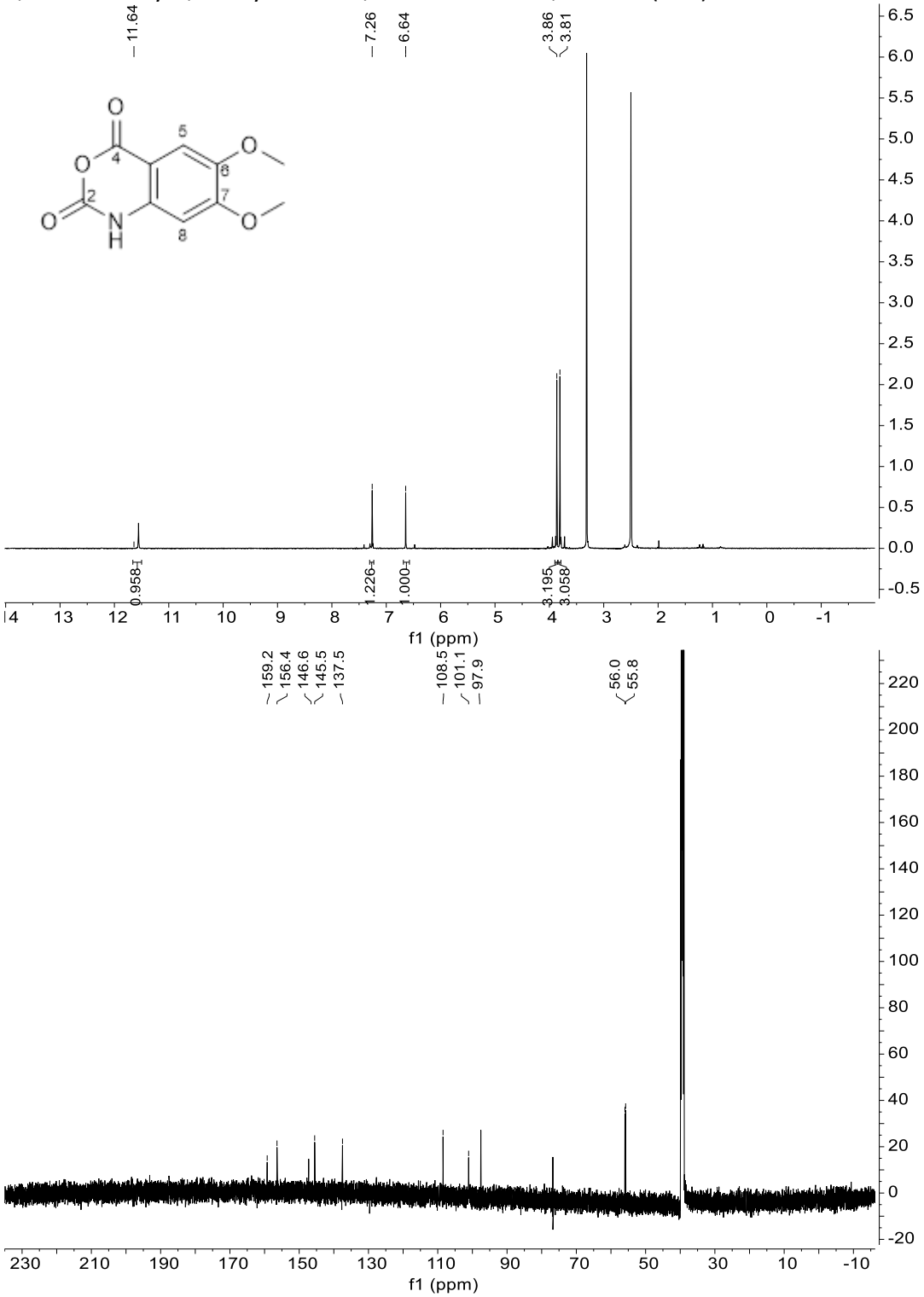

Amino-4,5-dimethoxy-*N*-methyl-2-benzamide (**333**)

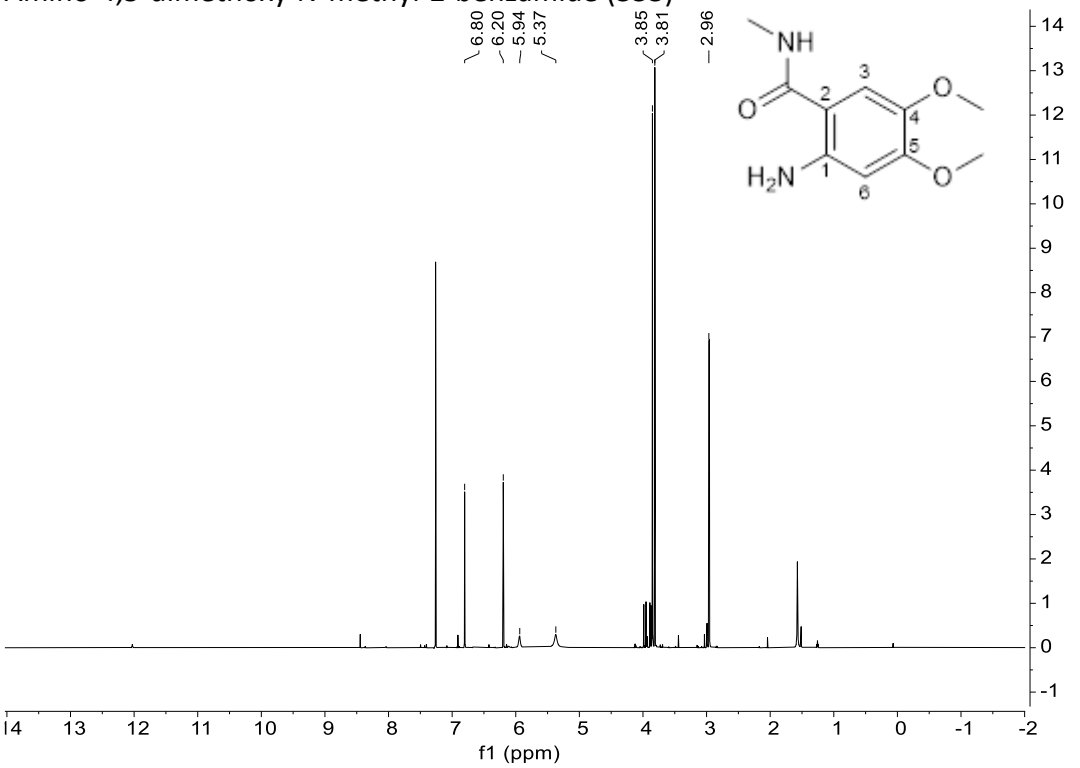

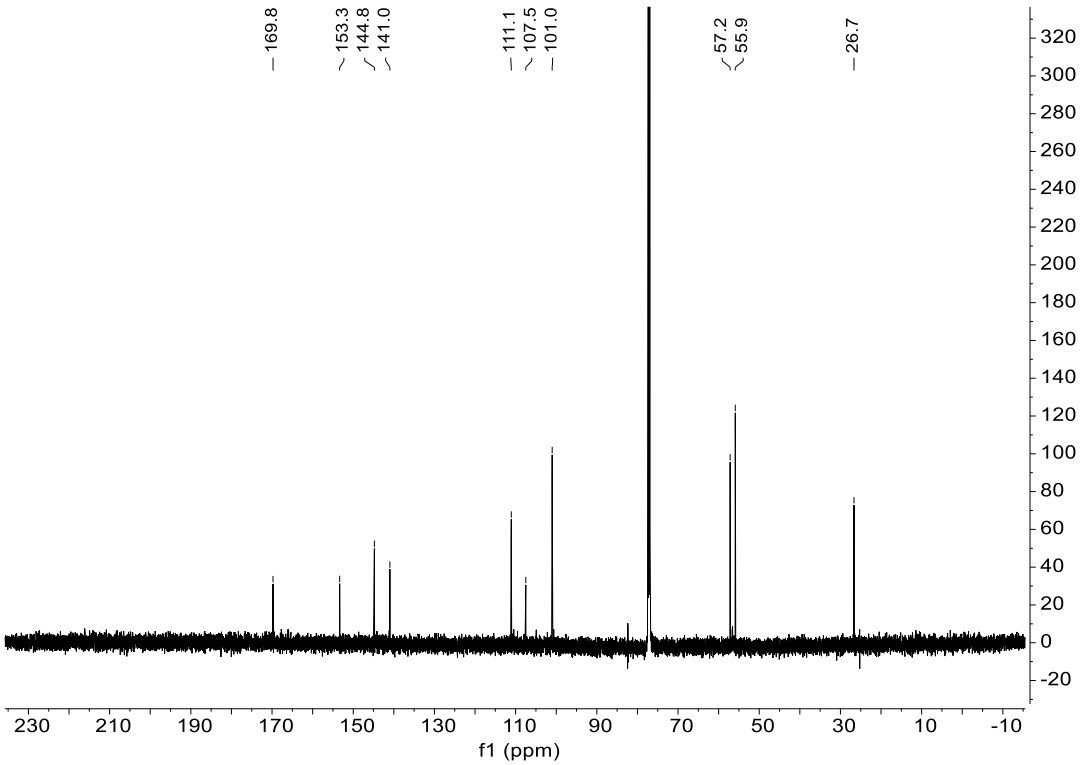

N-[4,5-dimethoxy-2-(methylcarbamoyl)]phenyl]-5’-nitrothiophene-2’-carboxamide (**334**)

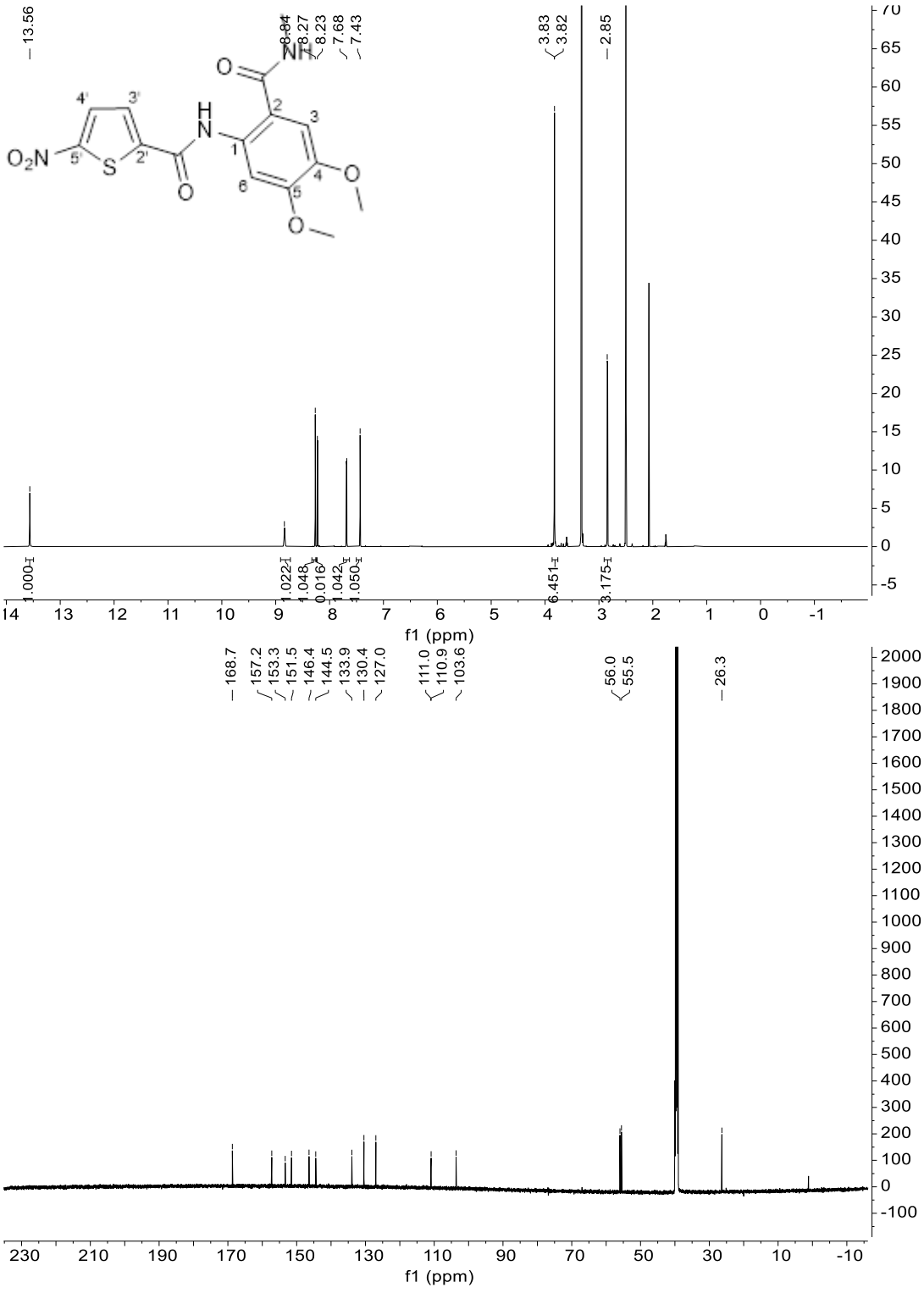

Ethyl 2-(4-cyano-6-{[2''-(ethoxycarbonyl)cyclopentyl]carbamoyl}thieno[2,3-b]pyridine-2-amido)cyclopentane-1-carboxylate (**309a**)

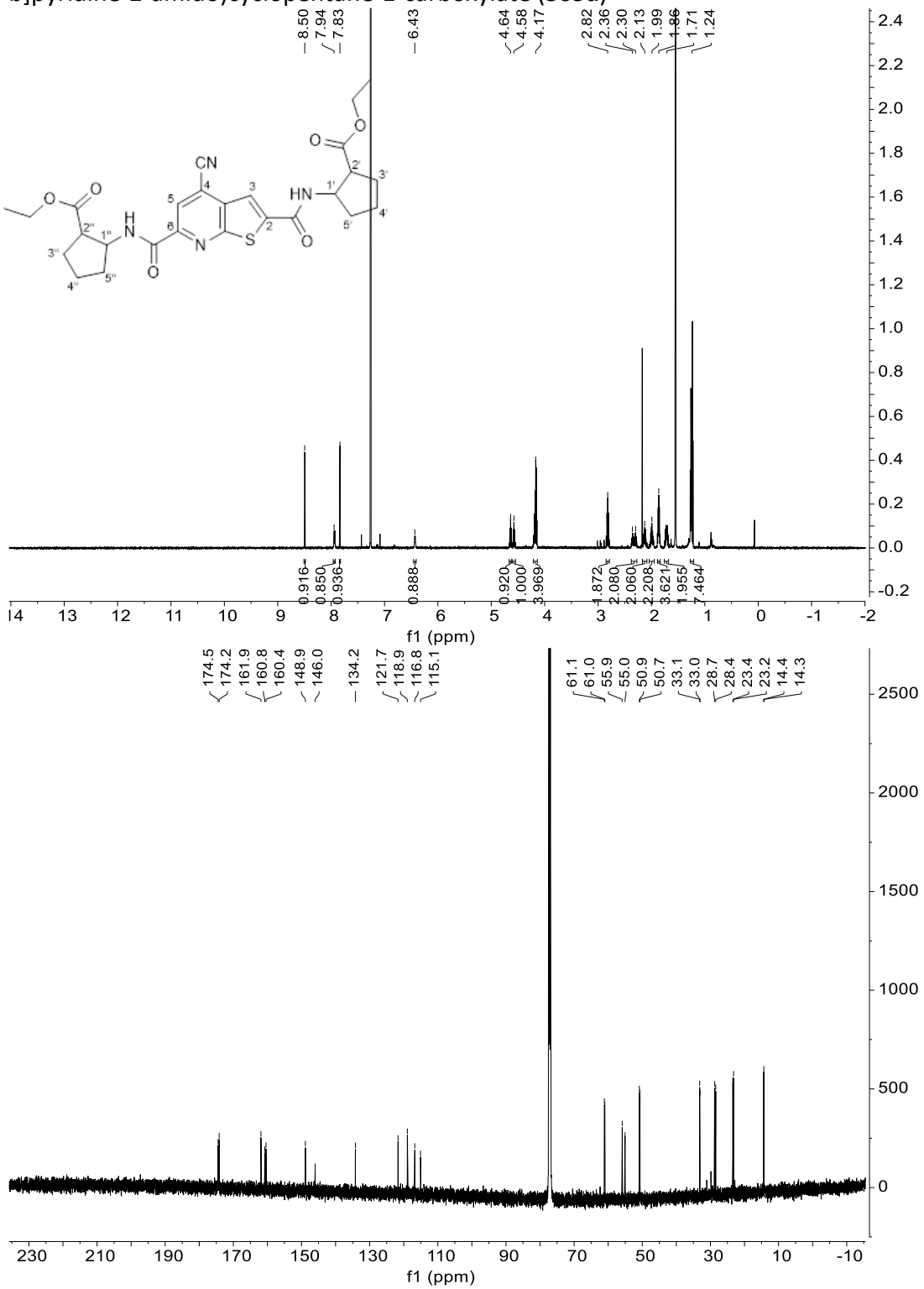

8.7 Appendix 7: Electronic supplementary information

Raw data from these studies can be found at \\prsblue02.mds.ad.dur.ac.uk\dch0pgs\VanessaLyne.